ABSTRACTS with PROGRAM

1986

The Fourteenth General Meeting of the

INTERNATIONAL MINERALOGICAL ASSOCIATION

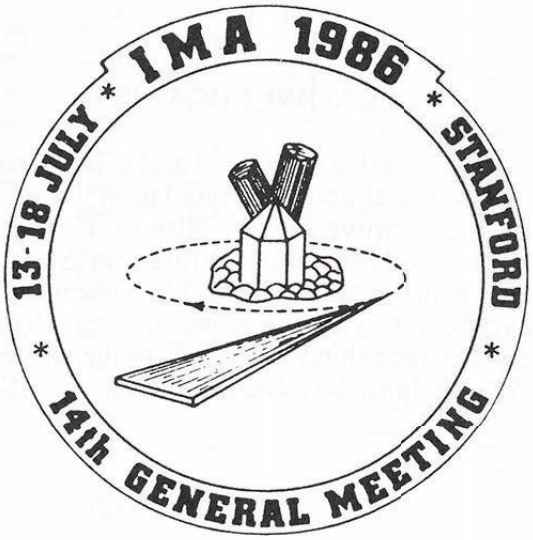

13 - 18 JULY 1986

STANFORD UNIVERSITY

Stanford, California, U.S.A.

Organizing Committee

General Chairman C. T. Prewitt
First Vice President, IMA P. J. Wyllie
MSA Representative to IMA L. W. Finger
Subcommittees:
Registration: C. T. Prewitt (Chair), G. E. Brown, Jr.
Finance: J. S. Huebner (Chair), G. E. Brown, Jr., C. T. Prewitt, P. J. Wyllie, P. Parton, G. Nord
Program: R. J. Kirkpatrick (Chair), J. D. Bass, G. E. Brown, Jr., R. C. Ewing, L. W. Finger
Publications: P. H. Ribbe (Chair), F. D. Bloss, S. Ghose, J. L. Munoz
Local Arrangements: G. E. Brown (Chair), Jr., J. F. DeMouthe, G. A. Waychunas
Field Trips: H. O. A. Meyer (Chair), G. E. Brown, Jr., R. G. Coleman, M. C. Gilbert
Publicity: L. W. Finger (Chair)

ACKNOWLEDGMENTS

The Mineralogical Society of America sponsored and subsidized this meeting, with partial financial support from the National Science Foundation, Grant No. EAR-8519299. This volume was compiled at the University of Illinois (Program Chairman, R. James Kirkpatrick) and at Virginia Polytechnic Institute and State University (Publications Chairman, Paul H. Ribbe), with assistance from Ada Simmons, Wendy Smith and Margie Strickler. The Executive Secretary of the Mineralogical Society of America, Barbara Minich, contributed a great effort behind the scenes to the success of this volume, and it is she who is responsible for soliciting the advertisements. [See disclaimer on page 39.]

For additional copies of this volume, write or telephone --

MINERALOGICAL SOCIETY OF AMERICA
1625 I Street N.W., Suite 414 Washington, D.C. 20006 (202) 775-4344

PROGRAM
for the SYMPOSIA and LECTURES
of the 14th General Meeting
of the International
Mineralogical Association

[LISTED CHRONOLOGICALLY ON PAGES 1 - 10]

▲ SCHEDULE OF SYMPOSIA AND PLENARY LECTURES

Monday, July 14

Plenary Speaker: Peter J. Wyllie, California Institute of Technology, "Progress in Experimental Petrology of Granitic Rocks" - Dinkelspiel Auditorium, 09:00

Symposia
1. Mineralogy and Geochemistry of Granites, Pegmatites, and Skarns I (T, EP) - Dinkelspiel Auditorium
2. Mineralogical Applications of Synchrotron Radiation (OC) - Terman Auditorium
3. Nucleation and Crystal Growth in Silicate Systems (C) - Campbell Auditorium
4. Ore Microscopy I (C) - Geology 320
5. Thermodynamics and Kinetics of Mineral Reactions (WG) - Materials Science 550A
6. Optical Properties of Minerals (OC) - Engineering 300

Tuesday, July 15

Plenary Speaker: Donald Brownlee, University of Washington, "Collection and Analysis of Cosmic Dust" - Dinkelspiel Auditorium, 13:30

Symposia
1. Cosmic Mineralogy (WG) - Campbell Auditorium
2. Garnet Mineralogy: Comprehensive Review (OC) - Engineering 300
3. Structural Classification of Minerals (C) - Terman Auditorium
4. Ore Microscopy II (C) - Geology 320
5. Surface Analytical Methods--Theory and Application (C) - Materials Science 550A
6. Mineralogy and Geochemistry of Granites, Pegmatites, and Skarns II (EP,T) - Dinkelspiel Auditorium

Wednesday, July 16

Plenary Speaker: Ekhard Salje, University of Cambridge, "Application of Order Parameter Theory to the Thermodynamic Properties of Phase Transitions" - Dinkelspiel Auditorium, 13:30

Symposia
1. Structural and Magnetic Phase Transitions of Minerals (C) - Engineering 300
2. Non-Crystalline Materials (OC) - Campbell Auditorium
3. Mineralogy of Metamorphic Rocks--Applications to Petrogenesis (OC) - Geology 320
4. Applied Mineralogy (C, IC) - Terman Auditorium
5. Ordering, Transformations, and Modulated Structures in Phyllosilicates (OC, A) - Materials Science 550A
6. Physics and Chemistry of Mantle Minerals I (T) - Dinkelspiel Auditorium

Thursday, July 17

Plenary Speaker: Ian Jackson, Australian National University, "The Elasticity of Mantle Minerals" - Dinkelspiel Auditorium, 13:30

Symposia
1. Physics and Chemistry of Mantle Minerals II (T) - Dinkelspiel Auditorium
2. Electron Microscopy of the Kinetics of Mineral Transformations (C) - Terman Auditorium
3. Applications of Solid-State NMR Spectroscopy to Minerals (OC) - Campbell Auditorium
4. Mineralogy and Petrology of Convergent Margin Volcanic Rocks (OC) - Geology 320
5. Recent Developments in Powder Diffraction Methods (OC,J) - Materials Science 550A

Friday, July 18

Plenary Speaker: Malcolm Ross, U. S. Geological Survey, "The Dangers of 'Asbestos' in Our Environment: Separating Fact from Fiction" - Dinkelspiel Auditorium, 08:30

Symposia
1. Environmental and Industrial Mineralogy (T) - Dinkelspiel Auditorium
2. Physics and Chemistry of Mantle Materials III (T) - Terman Auditorium
3. Defect Structures in Minerals (OC) - Materials Science 550A
4. Ore Microscopy III (C) - Campbell Auditorium
5. Layered Intrusions and Associated Ore Deposits (OC) - Geology 320

Sponsorship:
- (T) Conference Theme
- (C) IMA Commission
- (J) Joint Committee on Powder Diffraction Standards
- (WG) IMA Working Group
- (OC) Organizing Committee
- (EP) IUGS Commission on Experimental Petrology at High Temperatures and Pressures
- (IC) International Commission on Applied Mineralogy
- (A) AIPEA

▲ MINERALOGY OF GRANITES, PEGMATITES, AND SKARNS I — Monday, July 14, 1986
(CO-SPONSOR: IUGS COMMISSION ON EXPT. PETROL.) — Dinkelspiel Auditorium

Co-Chairman: S. Ayrton and G. Mahood

TIME	AUTHORS	TITLE
10:30	Mahood, G.	Waxing and Waning Magma Chambers: A Comparison of Zoning in Ignimbrites and Plutons
10:50	Ayrton, S., Bussy, F.	Mineralogical Evidence for Magma Mixing in the Mont Blanc and Elba Granites - Possible Geotectonic Implications
11:10	Zen, E-A	Magmatic-Epidote-Bearing Tonalitic Plutons in the Western Cordillera and Their Tectonic Significance
11:30	Murata, M., Itaya, T.	Sulfide and Oxide Minerals From S-Type and I-Type Granitic Rocks
11:50	LUNCH	

Co-Chairman: M. Pichavant and D. London

13:30	Pichavant, M., Manning, D. A. C.	F, B and H_2O: Effects on Phase Equilibria in Granitic Systems
13:50	Müller, P., Morteani, G.	Element Fractionation and Differentiation of the Granites of NE-Bavaria, Federal Republic of Germany
14:10	Kwak, T. A. P., Fu, M.	Distal Tin-Base Metal Skarns (Replacement Deposits)
14:30	Papike, J. J., Shearer, C. K., Jolliff, B. L., Duke, E. F., Redden, J. A., Walker, R. J., Laul, J. C.	Proterozoic Granite/Pegmatite Systems of the Black Hills, S. D.
14:50	London, D.	Petrogenesis of Rare-Element Pegmatites: Evidence From Fluid Inclusions and Phase Equilibrium Experiments
15:10	Černý, P., Ercit, T. S., Wise, M. A.	Mineralogy, Paragenesis and Geochemical Evolution of Nb, Ta-Oxide Minerals in Granitic Pegmatites

▲ MINERALOGICAL APPLICATONS OF SYNCHROTRON RADIATION — Monday, July 14, 1986
Terman Auditorium

Co-Chairman: W. A. Bassett and O. Shimomura

TIME	AUTHORS	TITLE
10:30	Bassett, W. A.	Synchrotron Radiation, Applications in Mineralogy
10:47	Shimomura, O.	Current Activity of Max80 at Photon Factory
11:04	Skelton, E. F., Elam, W. T., Webb, A. W., Schaefer, M. W., Qadri, S. B., Schiferl, D.	Ultra-High Temperature DAC Studies Using Synchrotron Radiation
11:21	Grosshans, W. A., Holzapfel, W. B.	Energy Dispersive X-Ray Diffraction in an Extended Pressure-Temperature Range
11:38	Vohra, Y. K., Brister, K. E., Weir, S. T., Desgreniers, S., Duclos, S. J., Ruoff, A. L.	Phase Transitions in the Megabar Pressure Range Using the Cornell Synchrotron Source
11:55	Ming, L. C., Manghnani, M. H.	High Pressure-High Temperature Studies with Synchrotron Radiation
12:12	LUNCH	
13:30	Zarka, A., Capelle, B.	Studies of Transitions of Quartz by Synchrotron Radiation
13:47	Parrish, W., Will, G., Masciocchi, N.	Powder Crystal Structure Refinement: An Example of the Advantages of Synchrotron X-Rays
14:04	Huang, E., Bassett, W. A., Tao, P.	Application of Synchrotron Radiation in Determining the Equation of State of Iron
14:21	Rivers, M. L., Sutton, S. R., Smith, J. V., Jones, K. W.	Trace Element Microanalysis by Synchrotron X-Ray Fluorescence

▲ MINERALOGICAL APPLICATIONS OF SYNCHROTRON RADIATION (continued)

14:38	Brown, G. E. Jr., Ponader, C. W., Jackson, W. E.	X-Ray Absorption Studies of Silicate Glasses Using Synchrotron Radiation
14:55	Calas, G., Manceau, A. Petiau, J.	Crystal Chemistry of Minerals Through X-Ray Absorption Spectroscopy
15:12	Hochheimer, H. D., Lengeler, B.	EXAFS Measurements at High Pressure

▲ NUCLEATION AND CRYSTAL GROWTH IN SILICATE SYSTEMS — Monday, July 14, 1986, Campbell Auditorium

Co-Chairman: I. Sunagawa and A. Barronnet

TIME	AUTHORS	TITLE
10:30	Kirkpatrick, R. J.	IMA 86 Crystal Growth Symposium Introduction
11:00	Lofgren, G. E.	The Role of Heterogeneous Nucleation in the Development of Igneous Rock Textures
11:30	Sunagawa, I., Tsukamoto, K., Abe, T., Nakamura, H., Kawasaki, M.	In-Situ Observation of Growth and Dissolution Processes of Silicate Crystals at Elevated Temperatures
12:00	LUNCH	
13:30	Barronnet, A.	Growth Modes of Sheet Silicates in Hydrothermal Environment
14:00	Muncill, G. E.	Non-Isothermal Crystal Growth Kinetics in the System Albite-Anorthite-H_2O at P_{H_2O} = 2 KBAR
14:20	Kuo, L.-C.	The Kinetics of Crystal Dissolution in Igneous Systems
14:40	Tsuchiyama, A.	Reaction and Digestion of Xenoliths in the Light of Melting/Dissolution Experiments
15:00	Kouchi, A., Tsuchiyama, A., Sunagawa, I.	Effect of Stirring on Crystallization Kinetics of Basalt

▲ ORE MICROSCOPY I: ORE PETROLOGY, PHYSICS AND CHEMISTRY OF ORE MINERALS — Monday, July 14, 1986, Geology 320

Co-Chairman: E. Stumpfl and B. Cervelle

TIME	AUTHORS	TITLE
10:30	Vaughan, D. J.	Sulfide Ore Minerals: Surface Properties and Electronic Structure
11:00	Cervelle, B., Malezieux, J. M.	Raman Laser Microprobe Investigation of Chromites in Polished Sections
11:20	Nakai, I., Yokoi, H., Imafuku, M., Miyawaki, R.	Crystal Chemistry of the As-Sb-S System--Synthesis of Wakabayashilite and Study of Solid Solutions by X-Ray Crystal Structure Analysis and EXAFS
11:40	LUNCH	
13:30	Craig, J. R., Vokes, F. M.	The Metamorphism of Pyrite
14:00	Hagni, R. D.	Ore Microscopy and Paragenetic Sequence of the Ores in the Southeast Missouri Lead District
14:20	Leonard, B. F., Christian, R. P.	Residence of Silver, Thunder Mountain Caldera Complex, Idaho
14:40	Bente, K.	Stabilization of Cu-Fe-Bi-Pb-Sn-Sulfides

▲ THERMODYNAMICS AND KINETICS OF MINERAL REACTIONS — Monday, July 14, 1986, Materials Sciences 550A

Co-Chairman: S. K. Saxena and L. L. Perchuk

TIME	AUTHORS	TITLE
10:30	Lasaga, A.C.	Monte Carlo Methods in Mineral Kinetics
11:00	Ganguly, J., Loomis, T. P.	Multicomponent Diffusion in Silicates and Compositional Zoning of Garnet in Natural Assemblages
11:30	Newton, R. C.	Thermodynamics of Orthopyroxene, Plagioclase and Garnet: Uncertainties Affecting Geobarometry
12:00	LUNCH	
13:30	Fuhrman, M. L., Lindsley, D. H.	An Improved, Though Still Imperfect, Solution Model for Ternary Feldspars
13:55	Saxena, S. K., Fei, Y.	Phase Equilibria at High Pressure and Temperature
14:20	Brown, M.	Reactions, P-T-t Paths and Geodynamics of Garnet-Cordierite Migmatites and Gneisses
14:45	Perchuk, L. L.	The Problems of Mineral Equilibria in Magmatic and Metamorphic Systems
15:10	Aranovich, L. Ya.	Thermodynamics of Multicomponent Solid Solutions and Geothermobarometry

▲ OPTICAL PROPERTIES OF MINERALS *

Monday, July 14, 1986
Engineering 300

Co-Chairman: F. D. Bloss and Th. Armbruster

TIME	AUTHORS	TITLE
10:30	Nassau, K.	The Physics and Chemistry of the Thirteen Causes of Color in Minerals
11:00	White, W. B.	Raman Spectra of Silicate Minerals
11:20	Armbruster, Th.	Channel Occupancy, Ordering and Optical Properties of Cordierites
11:40	Rossman, G. R.	Optical Spectroscopy of Minerals
12:00	LUNCH	
13:30	Lager, G. A.	Prediction of Refractive Indices by Point-Dipole Models
13:50	Su, S.-C., Ribbe, P. H., Bloss, F. D.	Optical Properties of Alkali Feldspars
14:10	Behmer, M.	The Use of Attenuated Total Reflection and Crystal Optics from the Polariton Point of View
14:30	Bloss, F. D.	A New, Automated Refractometer
14:50	Shankland, T. J.	Optical Absorption Spectra of Minerals and Glasses at High Temperature

*DEDICATED TO D. JEROME FISHER, PROFESSOR EMERITUS, UNIVERSITY OF CHICAGO, IMA's FIRST FULL TERM PRESIDENT, WHOSE 90th BIRTHDAY WAS JUNE 14, 1986.

▲ GARNET MINERALOGY: COMPREHENSIVE REVIEW

Tuesday, July 15, 1986
Engineering 300

Co-Chairman: K. Langer and G. R. Rossman

TIME	AUTHORS	TITLE
8:30	Newton, R. C., Geiger, C. A., Kleppa, O. J., Brousse, C.	Thermochemistry of Binary and Ternary Garnet Solid Solutions
9:00	Fursenko, B. A.	Synthesis and Stability of Unusual End Members of Silicate Garnets (Review)
9:30	Rossman, G. R.	The Hydrous Component in Garnets
10:00	COFFEE BREAK	
10:30	Takéuchi, Y.	Deviations of Garnets from Cubic Symmetry
11:00	Fuess, H., Hock, R.	Cation Distribution and Covalency in Garnets Studied by Neutron Diffraction
11:30	Amthauer, G.	Mössbauer Spectroscopy and Charge Transfer Phenomena of Garnets

▲ COSMIC MINERALOGY

Tuesday, July 15, 1986
Campbell Auditorium

Co-Chairman: R. H. Hewens and H. Takeda

TIME	AUTHORS	TITLE
8:30	Wänke, H.	Evolution of the Solar System: From Dust to Planets
9:00	Armstrong, J. T.	Mineralogy and Electron Microscopy of Refractory Inclusions in Carbonaceous Meteorites
9:20	Zolensky, M. E.	Tochilinite in C2 Carbonaceous Chondrites: A Comparison with Terrestrial Material
9:40	Xie, X.	On the Behavior of Minerals During Thermal and Shock Metamorphism of Meteorites
10:00	COFFEE BREAK	
10:30	Takeda, H.	Parent Bodies of Differentiated Meteorites
10:50	Hewins, R. H.	Stony-Iron Meteorites and Their Parent Bodies
11:10	Herzberg, C. T.	Internal Structures of the Earth and Terrestrial Planets: Constraints from High Pressure Liquidus Phase Equilibria and Bulk Planet Composition
11:30	Tomeoka, K., Buseck, P. R.	A Mineralogical Comparison of Four Hydrated Interplanetary Dust Particles
11:50	Peng, H., Chen, S., Zhuang, S., Chai, Z., Yu, Z., Liu, Z.	The Golden Ni-Fe Core in Deep-Sea Cosmic Spherule

▲ STRUCTURAL CLASSIFICATION OF MINERALS

Tuesday, July 15, 1986
Terman Auditorium

Co-Chairman: F. C. Hawthorne and J. Lima-de-Faria

TIME	AUTHORS	TITLE
8:30	Hawthorne, F. C.	A Structural Description and Classification for Oxysalt Minerals
8:55	Makovicky, E.	Archetypes, Structure-Building Principles and Classification of the Sulfosalts of As, Sb and Bi
9:20	Moore, P. B.	Cations with Lone Pairs in Mineral Chemistry
9:45	Keller, P.	Structural Classification of Oxygen Containing Minerals, Phosphates and Arsenates
10:10	COFFEE BREAK	
10:40	Lima-de-Faria, J.	The Importance of the Packing of the Structural Units on the Structural Classification of Minerals
11:05	Zemann, J.	Structural Classification of Carbonates
11:30	Liebau, F.	Classification of Silicates: Chemical, Structural, and Morphological Aspects

▲ SURFACE ANALYTICAL METHODS--THEORY AND APPLICATION

Tuesday, July 15, 1986
Materials Science 550A

Co-Chairman: G. M. Bancroft and N. Shimizu

TIME	AUTHORS	TITLE
8:30	Fyfe, W. S., Tazaki, K.	The Characteristics of Fine Particulates in Natural Systems
9:00	Shimizu, N.	Secondary Ion MASS Spectrometry (SIMS) in Analytical Mineralogy
9:30	Dillard, J. G.	Surface Chemical Characterization of Minerals and Adsorbed Species on Minerals Using X-Ray Photoelectron Spectroscopy
10:00	COFFEE BREAK	
10:30	Bancroft, G. M.	Applications of SIMS, X-Ray Photoelectron and Auger Spectroscopies for Studies of Adsorption, Leaching and Diffusion on Mineral Surfaces
11:00	Perry, D. L.	Applications of Auger and Combined Auger/X-Ray Photoelectron Spectroscopy to the Characterization of Minerals and Their Surfaces
11:30	White, A. F.	Application of XPS to Weathering in Minerals and Glasses

▲ ORE MICROSCOPY II: SULFOSALTS, PLATINUM MINERALS, AND INDUSTRIAL APPLICATIONS

Tuesday, July 15, 1986
Geology 320

Co-Chairman: E. Stumpfl and B. Cervelle

TIME	AUTHORS	TITLE
8:30	Moëlo, Y., Marcoux, E., et. Legendre, O., Makovicky, E., Karup-Møller, S.	Lillianite Homologues (Gustavite, Vikingite, Ag-Bi Rich Heyrovskyite...) From the W-As-(Pb,Bi,Ag) Occurrence of La Roche-Balue (Loire-Atlantique, France)
9:00	Moh, G. H.	Mineralogical Investigations on Franckeite-Cylindrite Intergrowths
9:20	Nakhla, F. M.	Ore Minerals Determination by Their Reflectance Parameters and Chemical Composition
9:40	Both, R. A., Stumpfl, E. F.	The Distribution of Silver in the Broken Hill Orebody
10:00	COFFEE BREAK	
10:30	Tarkian, M.	Compositional Variations and Reflectance of the Platinum Group Minerals
11:00	Hudson, D. R.	Platinum Metals in Australia - General Occurrence and Mineralogy and Recovery from Western Australian Nickel Deposits
11:20	Cornelius, M., Stumpfl, E. F.	Platinum Mineralization in Mafic-Ultramafic Rocks, Western Gneiss Terrain, W. Australia
11:40	Prichard, H. M., Tarkian, M.	Platinum Group Minerals from Two PGE-Rich Localities in the Shetland Ophiolite Complex

▲ MINERALOGY OF GRANITES, PEGMATITES, AND SKARNS II (CO-SPONSOR: IUGS COMMISSION ON EXPT. PETROL.)

Tuesday, July 15, 1986
Dinkelspiel Auditorium

Co-Chairman: M. Lagache and J. R. Holloway

TIME	AUTHORS	TITLE
8:30	Holloway, J. R., Clemens, J. D., Nekvasil, H., Rushmer, T., Vielzeuf, D., Webster, J. D.	Experimental Constraints on the H_2O Contents of Silicic Magmas
8:50	Johannes, W.	Melting in Quartz-Feld Rocks at Varying H_2O Activities
9:10	Jones, R. H., Zeng, R. S., MacKenzie, W. S.	Phase Relations in the Undersaturated Part of the System Nepheline-Kalsilite-Anorthite-Quartz at P_{H_2O} = 5 KB
9:30	Thelin, Ph.	Feldspar Phenocrysts in Granitic Rocks: A Textural Review
9:50	Lagache, M.	Trace Elements Distribution in Granitic Systems. Experimental Approach
10:10	COFFEE BREAK	
10:40	Woodhead, J. A., Silver, L. T.	U, Th, Pb, and REE Mineralogy of Granites From the Southwestern U.S.
11:00	Rundquist, D. V.	Two Main Evolutional Ranges of Granitoids and Their Mineralogy
11:20	Zharikov, V. A., Gavrikova, S. N.	Formation of Granites in the Active Margin of Aldanstanovoy Shield

▲ STRUCTURAL AND MAGNETIC PHASE TRANSITIONS OF MINERALS

Wednesday, July 16, 1986
Engineering 300

Co-Chairman: S. Ghose, J. M. D. Coey, and E. Salje

TIME	AUTHORS	TITLE
8:30	Salje, E.	Phase Transformation in Albite
8:55	Coey, J. M. D. Ghose, S.	Magnetic Phase Transitions in Silicate Minerals
9:20	Ghose, S.	Electron and Spin Ordering and Associated Phase Transitions in Ilvaite, A Mixed Valence Iron Silicate
9:45	Prandl, W.	The Spin Glass State in Garnet Mixed Crystals: New Evidence from Neutron Scattering and Macroscopic Measurements
10:10	COFFEE BREAK	
10:40	Dolino, G.	Incommensurate Phase Transitions in Quartz and $AlPO_4$
11:05	Wuensch, B. J.	Phase Transformation and Cation Distributions in Fast-Ion Conductors
11:30	McConnell, J. D. C.	Incommensurate-Commensurate Phase Transitions in Minerals

▲ NON-CRYSTALLINE MATERIALS

Wednesday, July 16, 1986
Campbell Auditorium

Co-Chairman: J. F. Stebbins and P. Richet

TIME	AUTHORS	TITLE
8:30	Carmichael, I. S. E., Christie, D. M., Ghiorso, M. S., Langmuir, C. H.	The Oxidation State of Basic Magma; Subaerial and Submarine
8:50	Richet, P.	Thermochemical Aspects of the Rheology of Viscous Liquids
9:10	Stebbins, J. F.	Atomic Motion in Molten Silicates: NMR Results
9:30	Mysen, B. O.	Structure and Properties of Iron-Bearing Silicate Melts
9:50	McMillan, P.	Raman Spectroscopy of Aluminosilicate Glasses
10:10	COFFEE BREAK	
10:30	De Jong, B.H.W.S., Veeman, W. S.	^{29}Si MAS and ^{23}Na Nutation NMR Reveal That Local Sodium Environment is Principal Difference Between Sodium Silicate Gel and Glass
10:50	Wright, A. C.	Structural Studies of Glasses Using Neutron Diffraction Techniques
11:10	Waychunas, G. A.	X-Ray Methods for Structure Determination in Non-Crystalline Materials
11:30	Brawer, S. A.	Mechanisms for Viscosity and Transport in Silicate Melts

▲ APPLIED MINERALOGY (CO-SPONSOR: ICAM)

Wednesday, July 16, 1986
Terman Auditorium

Co-Chairman: R. D. Hagni and W. Petruk

TIME	AUTHORS	TITLE
8:30	Hagni, R. D.	Collaboration of the International Mineralogical Association - Commission on Applied Mineralogy (IMA-CAM) and the International Congress on Applied Mineralogy in the Minerals Industry (ICAM)
8:35	Barbery, G.	Mineral Liberation Prediction from Ore Texture Description: Use of Mathematical Morphology
8:55	Petruk, W.	Development of an Automated SEM-IPS-IA Image Analysis System
9:15	Remond, G., Cesbron, F., Campbell, I.L., Traxel, K., Cabri, L.J.	X-Ray Spectrometry Induced By Electron (EPMA) and Proton Bombardment (micro-PIXE) Applied to Trace Element Analysis in Sulfides: Problems and Prospects.
9:35	Gabis, V., Genies, B., Ildefonse, J.P., Panis, D., Coquand, B.	Sintering of Quartzite Refractories Bonded by Boron Oxide
9:55	COFFEE BREAK	
10:25	deVilliers, J.P.R., Adendorff, K. T.	A Phase-Chemical and Crystal-Chemical Investigation of the Oxidative Lime-Roasting of Chromite Ores
10:45	Oosthuyzen, E. J.	Mineralogical Factors that Influence the Strength of Moulds Made From Chromite Foundry Sand
11:05	Hausen, D. M.	Process Mineralogy of Tungsten-Bearing Ores
11:25	Pignolet-Brandom, S., Hagni, R. D., Brandom, R. T., Vierrether, C. B., Kremser, D. T.	Reflected Light Microscopy of Pyrometallurgical Products
11:45	Szymanski, A.	Mineralogy: An Interdisciplinary Science from Electronic Technology to Biogeochemistry

▲ MINERALOGY OF METAMORPHIC ROCKS-- APPLICATIONS TO PETROGENESIS

Wednesday, July 16, 1986
Geology 320

Co-Chairman: J. M. Ferry and F. S. Spear

TIME	AUTHORS	TITLE
8:30	Bohlen, S. R.	Geobarometry and Pressure-Temperature-Time Paths of Granulites
9:00	Ferry, J. M.	Determination of the Driving Forces of Metamorphism by Measurement of Reaction Progress in Rocks
9:30	Schreyer, W.	Minerals and Mineral Assemblages of High-Pressure Metamorphic Crustal Rocks
10:00	COFFEE BREAK	
10:30	Spear, F. S.	Zoned Metamorphic Garnets and Metamorphic P-T Paths
11:00	Valley, J. W.	The Conundrum at Cascade Slide: A Petrologic/Stable Isotopic Answer
11:30	Veblen, D. R.	Mechanisms and Chemistry of Sheet Silicate Reactions in Metamorphic Rocks

▲ PHYSICS AND CHEMISTRY OF MANTLE MINERALS I: ELASTIC PROPERTIES AND SPECTROSCOPY

Wednesday, July 16, 1986
Dinkelspiel Auditorium

Co-Chairman: M. S. T. Bukowinski and S.-I. Akimoto

TIME	AUTHORS	TITLE
8:30	Jackson, I., Webb, S. L., Niesler, H.	Ultrasonic Studies of the Elasticity of Mantle Minerals
8:55	Manghnani, M. H., Webb, S. L.	Elasticity of CoO as a Function of Pressure and Temperature: Comparison with Transition Metal Oxides
9:20	Bass, J. D.	Applications of Brillouin Spectroscopy to Mineral Physics
9:45	Hazen, R. M., Finger, L. W.	High-Pressure Crystal Chemistry of Orthosilicates and Related Binary Oxides
10:10	COFFEE BREAK	
10:40	Mao, D., Bell, P.	Insitu Optical Spectroscopy of Mantle Minerals at High Pressure/High Temperature
11:05	Hafner, S. S.	High-Pressure Mössbauer Spectroscopy of Minerals
11:30	Ohsumi, K., Sueno, S., Nakai, I., Imafuku, M., Morikawa, H., Kimata, M., Nomura, M., Shmomura, O.	EXAFS Analysis Under High Pressure Using Diamond Anvil Cell

▲ ORDERING, TRANSFORMATIONS, AND MODULATED STRUCTURES IN PHYLLOSILICATES (CO-SPONSOR: AIPEA) Wednesday, July 16, 1986 Materials Science 550A

Co-Chairman: S. W. Bailey and L. Heller-Kallai

TIME	AUTHORS	TITLE
8:30	Joswig, W., Fuess, H., Takeuchi, Y.	Neutron Diffraction Studies of Hydrogen Bonding and Cation Ordering in Phyllosilicates
8:50	Giese, R. F.	Detection of Short-Range Order in Substitutionally Disordered Cation Sites of Phyllosilicates
9:10	Lipsicas, M.	Magic Angle Spinning (MAS) High Resolution NMR Spectroscopy as a Tool for Studying Short Range Order in Layer Silicates
9:30	Abbott, R. N., Jr. Burnham, C. W., Post, J. E.	Energetics of Polytypism in Di- and Trioctahedral Micas
9:50	Eberl, D. D., Srodon, J., Northrop, H.	Formation of Mixed-Layer Clays from Smectite at Low Temperature
10:10	COFFEE BREAK	
10:40	Reynolds, R. C.	Calculated X-Ray Diffraction patterns of Mixed Layer Illite-Smectites Incorporating the Effects of Different Reaction Mechanisms
11:00	Guggenheim, S.	Modulated 2:1 Layer Silicates
11:20	Price, G. D., Yeomans, J.	A Model for Polytypism and Polysomatism
11:40	Onrubia, Y., Amouric, M., Baronnet, A.	An Experimental Approach to the Conditions Required for Biotite-Chlorite Interlayering

▲ PHYSICS AND CHEMISTRY OF MANTLE MINERALS II: LATTICE AND MOLECULAR DYNAMICS, THERMODYNAMICS Thursday, July 17, 1986 Dinkelspiel Auditorium

Co-Chairman: M. S. T. Bukowinski and S.-I. Akimoto

TIME	AUTHORS	TITLE
8:30	Jeanloz, R., Knittle, E., Williams, Q., Heinz, D. L.	(Mg,Fe)SiO_3 Perovskite: The Most Abundant Mineral in the Earth
8:55	Matsui, M., Akaogi, M., Matsumoto, T.	Structural and Elastic Properties of the Ilmenite and Perovskite Phases of $MgSiO_3$, Obtained from a Computational Model
9:20	Boyer, L. L., Cohen, R. E., Mehl, M. J.	AB Initio Models for the Lattice Dynamics of Minerals at High Pressure
9:45	Bukowinski, M. S. T., Wolf	Lattice Dynamics of Orthorhombic Perovskite: Implications for Lower Mantle Modeling Efforts
10:10	COFFEE BREAK	
10:40	Akimoto, S., Yagi, T.	Application of Synchrotron Radiation to High Pressure/High Temperature Physics of Mantle Minerals
11:05	Ito, E., Takahashi, E.	The Post-Spinel and Post-Majorite Transformations and the Constitution of the Deep Mantle
11:30	Navrotsky, A.	Thermochemistry of High Pressure $MSiO_3$ and $MGeO_3$ Phases

▲ ELECTRON MICROSCOPY OF THE KINETICS OF MINERAL TRANSFORMATIONS Thursday, July 17, 1986 Terman Auditorium

Co-Chairman: N. Morimoto and C. Willaime

TIME	AUTHORS	TITLE
8:30	Boland, J. N.	Precipitation Mechanisms of Metallic Particles in Olivine
9:00	Carpenter, M. A.	Characterisation of Order/Disorder Transformations in Plagioclase Feldspars
9:30	Kitamura, M.	Phase Transformation and Mineral Behaviors of Cordierite
10:00	COFFEE BREAK	
10:30	Veblen, D. R., Bish, D. L., Schlinger, C. M.	Chemistry and Crystallography of Deep Crustal Pyroxenes
11:00	Grove, T. L., Juster, T. C.	Use of Phase Transitions and Decomposition Reactions in Pyroxenes as Cooling Rate Speedometers
11:30	Champness, P. E.	Convergent-Beam Electron Diffraction (CBD) in Mineralogy

▲ APPLICATIONS OF SOLID-STATE NMR SPECTROSCOPY TO MINERALS

Thursday, July 17, 1986
Campbell Auditorium

Co-Chairman: J. B. Higgins and A. Putnis

TIME	AUTHORS	TITLE
8:30	Putnis, A.	A Study of the Development of Short-Range Al, Si Order in Annealed Cordierite Using Magic Angle Spinning NMR
9:00	Kirkpatrick, R. J., Yang, W.-H., Carpenter, M. A.	^{29}Si NMR Spectroscopy of Plagioclase Feldspars
9:20	De Jong, B.H.W.S., Van Hoek, J., Veeman, W. S., Manson, D. V.	Gem Quality Opal CT is a ^{29}Si MASNMR Amorphous Solid
9:40	Lippmaa, E.	^{29}Si NMR Spectroscopy of Solids
10:10	COFFEE BREAK	
10:40	Oestrike, R., Yang, W. H., Montez, B., Turner, G. L., Navrotsky, A.	Applications of High Resolution NMR to Aluminosilicate Glass Structure
11:00	Yang, W.-H.	^{29}Si, ^{27}Al, ^{23}Na MASS and ^{29}Si CP/MASS NMR Spectroscopic Studies of the Reaction of Rock-Forming Silicate Minerals and Glasses with Aqueous Solution
11:20	Yesinowski, J. P., Eckert, H., Rossman, G. R.	^{1}H High Speed MAS NMR Studies of Minerals
11:40	Keefer, K. D.	The Distribution of Non-Bridging Oxygens and the Structure of Silicate Melts

▲ MINERALOGY & PETROLOGY OF CONVERGENT MARGIN VOLCANIC ROCKS

Thursday, July 17, 1986
Geology 320

Co-Chairman: R. Kay and I. Kushiro

TIME	AUTHORS	TITLE
8:30	Grove, T. L., Baker, M. B., Kinzler, R. J., Donnelly-Nolen, J. M.	Mineralogical Evidence of Magmatic Processes at Medicine Lake Highland, N. California A Convergent Margin Calc-Alkaline Volcanic System
9:00	Kay, S. M., Romick, J., Kay, R. W.	Mineralogy of Volcanic and Plutonic Rocks as a Guide to Processes in the Formation of the Aleutian Crust
9:30	Tatsumi, Y., Kushiro, I.	Origin of Subduction Zone Magmas: Experimental Approach
10:00	COFFEE BREAK	
10:30	Bacon, C. R., Druitt, T. H.	Petrologic Evidence for Recharge and Convective Mixing in the Magma Chamber of Mount Mazama Before Its Catastrophic Zoned Eruption and the Collapse of Crater Lake Caldera, Oregon
11:00	Frost, T. P., Mahood, G. A.	Basalt-Granodiorite Magma Interaction During Crystallization of the Lamarck Granodiorite, Eastern Sierra Nevada, California: Field Evidence and Rheologic Modelling

▲ RECENT DEVELOPMENTS IN POWDER DIFFRACTION METHODS (CO-SPONSOR: JCPDS)

Thursday, July 17, 1986
Materials Science 550A

Co-Chairman: P. Bayliss and R. J. Hill

TIME	AUTHORS	TITLE
8:30	Hill, R. J.	Data Collection Optimization for Rietveld Analysis
9:30	Smith, D. K., Johnson, G. G., Jr. Ruud, C. O.	Identification and Quantification of Clay Minerals in Sediments: The Penn State Clay Minerals XRPD Database
10:00	COFFEE BREAK	
10:30	McCarthy, G. J., Garvey, R. G., Mineral Subcomm.	Application of the 1986 JCPDS-ICDD Mineral Powder Diffraction File Computer Database to Mineralogical Problems
11:15	Bayliss, P.	Status of the JCPDS Mineral File

▲ ORE MICROSCOPY III: NEW METHODS AND INSTRUMENTATION

Friday, July 18, 1986
Campbell Auditorium

Co-Chairman: E. Stumpfl and B. Cervelle

TIME	AUTHORS	TITLE
10:00	Criddle, A. J.	QDF: The Quantitative Data File for Ore Minerals
10:30	Bernhardt, H.-J.	Ore Mineral Identification Using a Simple Fully Automated System
10:50	Hagni, R. D., Hagni, J. E.	Computer-Assisted Identification of Ore Minerals Using Quantitative and Qualitative Properties
11:10	Rucklidge, J. C.	Accelerator MASS Spectrometry in Geology
11:40	Cabri, L. J.	The Micro-Pixe Technique in Studies of Some Canadian Base Metal Ores

▲ DEFECT STRUCTURES IN MINERALS

Friday, July 18, 1986
Materials Science 550A

Co-Chairman: R. N. Schock and A. G. Duba

TIME	AUTHORS	TITLE
10:00	Schmalzried, H.	The Role of Point Defects in Solid Phases
10:30	Tuller, H. L.	The Use of Electrical Measurements to Determine Point Defects and Their Behavior
11:00	Wuensch, B. J.	Point Defects and Diffusion
11:30	Kohlstedt, D. L.	Role of Point Defects in High-Temperature Deformation of Olivine
12:00	LUNCH	
13:30	Brawer, S. A.	Defects in Silicate Glasses
14:00	Veblen, D. R.	Direct Electron Imaging of Extended Defects in Minerals

▲ PHYSICS AND CHEMISTRY OF MANTLE MINERALS III: THEORETICAL MODELING OF STRUCTURAL PROPERTIES AND PHASE TRANSFORMATIONS

Friday, July 18, 1986
Terman Auditorium

Co-Chairman: M. S. T. Bukowinski and S.-I. Akimoto

TIME	AUTHORS	TITLE
10:00	Miyamoto, M., Takeda, H.	Structural Studies Through Pair Potentials
10:25	Gibbs, G. V., Boisen, M. B., Jr., Finger, L. W., Lasaga, A. C.	Molecular Mimicry of Structure and Electron Density Distributions of Minerals
10:50	Louie, S. G., Cohen, M. L.	Quantum Mechanical Calculations of Structural Properties of Materials
11:15	Gordon, R. G., Hummel, H. H., Jackson, M. D.	First-Principles Theory of Some Mantle Minerals
11:40	LUNCH	

▲ MECHANISMS OF HIGH-PRESSURE PHASE TRANSFORMATIONS; DEFECTS

13:30	Poirier, J. P., Peyronneau, J., Beauchesne, S., Madon, M., Guyot, F.	Lattice Defects in Perovskites - TEM Examination and Creep Experiments
13:55	Syono, Y.	Non-Diffusive Mechanism for the Shock-Induced Phase Transition in Silicates and Oxides
14:20	Will, G., Lauterjung, J.	The Study of Time-Dependant Phenomena Shown on the Kinetics of the Pressure Induced Olivine-Spinel Phase Transition in Mg_2GeO_4

▲ LAYERED INTRUSIONS AND ASSOCIATED ORE DEPOSITS

Friday, July 18, 1986
Geology 320

Co-Chairman: Michael L. Zientek and T. N. Irvine

TIME	AUTHORS	TITLE
10:00	Emslie, R. F.	Massif Anorthosites and Layered Intrusions: Comparisons and Contrasts
10:30	Naslund, H. R., Chalokwu, C. I.	Estimation of the Trapped Liquid Composition in the Basistoppen Sill, East Greenland
11:00	Boudreau, A. E., McCallum, I. S.	Hydrothermal Transport of the PGE, An Alternative Model for the Formation of Stratobound PGE Deposits in Layered Intrusions
11:30	Zientek, M. L., Oscarson, R. L.	Textural Association of Platinum-Group Minerals, Stillwater Complex, Montana
12:00	LUNCH	
13:30	Loferski, P. J.	Multiphase Inclusions in Plagioclase from the Stillwater Anorthosites: Implications for REE Geochemistry
14:00	Weiblen, P. W.	

▲ ENVIRONMENTAL AND INDUSTRIAL MINERALOGY

Friday, July 18, 1986
Dinkelspiel Auditorium

Co-Chairman: F. Mumpton and H. U. Bambauer

TIME	AUTHORS	TITLE
10:00	Mumpton, F.	Applied Mineral Science - Alive and Well in Modern Technology
10:10	Roy, D. M.	The Role of Mineralogy in Cement Chemistry
10:40	Hill, V.	On the Mineralogy of Bauxite Deposits
11:10	Pever, D.	Clay Petrology
11:40	Schwertmann, U.	Significance of Iron Oxide Minerals in Soil Environments
12:10	LUNCH	
13:30	Bambauer, H. U., Holzapfel, T.	The Mineralogy of the Trace Element-Bearing Phases in Stack Fly Ash from Thermal Power Plants in the F. R. G.
14:00	Lee, R. J., Walker, J. S.	Application of Computer-Controlled Microscopy in Applied Mineralogy
14:30	Kirov	Zeolite Mineralogy

Schedule of

POSTER SESSIONS

and Mircocomputer Workshops

[LISTED CHRONOLOGICALLY ON PAGES 12 - 25]

▲ SCHEDULE OF POSTER SESSIONS AND MICROCOMPUTER WORKSHOP

Tuesday, July 15, 1986 13:30-17:00

1. Microcomputer Workshop
2. Mineralogy and Geochemistry of Granites, Pegmatites, and Skarns
3. Ore Mineralogy/Ore Microscopy
4. Gem Minerals
5. Garnet Mineralogy
6. Structural Classification of Minerals
7. History and Teaching of Mineralogy
8. Mineralogical Applications of Synchrotron Radiation
9. Cosmic Mineralogy

Wednesday, July 16, 1986 13:30-17:00

1. Microcomputer Workshop
2. Mineralogy of Metamorphic Rocks
3. Structural and Magnetic Phase Transitions
4. Phyllosilicate Mineralogy
5. Applied and Environmental Mineralogy
6. Thermodynamics and Kinetics of Mineral Reactions
7. Non-Crystalline and Metamict Materials
8. Optical Properties of Minerals

Thursday, July 17, 1986 13:30-17:00

1. Microcomputer Workshop
2. Mineralogy of Sedimentary Rocks
3. Amphiboles and Pyroxenes
4. Carbonate Mineralogy
5. Structure, Characterization, and Synthesis
6. Spectroscopy of Minerals
7. Computational Mineralogy
8. Mantle Mineralogy
9. Mineralogy and Petrology of Mafic and Ultramafic Rocks and Associated Ore Deposits

▲ MICROCOMPUTER WORKSHOP

Tuesday, Wednesday, and Thursday
15, 16, and 17 July, 1986
13:30 - 17:00

AUTHORS	TITLE
Boisen, M. B., Jr., Gibbs, G. V.	Interactive Programs for Studying Isometries (ISOMET) and Matrix Operations (MATOP)
Fuchs, D. R.	Database Retrieval and Card Image Display of Minerals from the Level III JCPDS Mineral Subfile
Hall, A. J.	XRD Data Processing Using the Sinclair QL
Henderson, D. M.	Some Mineralogic and Petrographic Programs for the Apple Macintosh Microcomputer
Johnson, Q.	Powder Diffraction Analysis on a PC
Kampf, A. R.	Chemical Computations
McCammon, C.	Simulation and Fitting of Mossbauer Spectra on a Microcomputer
Nickel, E. H., Fletcher, A. B.	MINFIND
Phillips, W. S., Dyar, M. D.	Program Search: A Method for Extracting Exchange Vectors from Mineral Composition Data
Smith, K. L., Smith, D. K.	POWD - Modeling Crystal Structures for X-Ray Powder Diffraction Studies. Version for the IBM PC Microcomputer
Vaughan, M. T.	Calculation of Elastic Constants from Brillouin Scattering Data

▲ POSTER SESSION: MINERALOGY AND GEOCHEMISTRY OF GRANITES, PEGMATITES, AND SKARNS — Tuesday, July 15, 1986; 14:30-17:00

AUTHORS	TITLE
Andreev, G. V.	Mineralogy and the Conditions in Synnyrite Origin
Bakumenko, I. T.	Peculiarities of Magmatic Ore Formation in Granite Pegmatites (According to Data of Inclusion Study)
Barbarin, B.; Bateman, P.C.	Origin and Evolution of Mafic Magmatic Enclaves and Mafic Rocks Associated With Some Granitoids of the Central Sierra Nevada
Bland, A. M.; Brown, M.; D'Lemos, R. S.; Power, G. M.; Topley, C. G.	Geochemistry of Granites and Related Rocks of the Channel Islands Region, Armorican Massif
Boggs, R. C.	Miarolitic Cavity and Pegmatite Mineralogy of Eocene Anorogenic Granite Plutons in the Northwestern, U.S.A.
Cerný, P.; Fryer, B. J.; Longstaffe, F. J.; Tammemagi, H. Y.	The Archean Lac du Bonnet Batholith, Manitoba: Igneous History, Metamorphic Effects, and Fluid Overprinting
Congdon, R.; Nash, W. P.	Differentiation of High-Fluorine Rhyolite, Honeycomb Hills, Utah
Czamanske, G. K.; Dillet, B.	Chevkinite, Allanite, and Sphene in High-Level Granitic Plutons Associated with Questa Caldera and the Rio Grande Rift, New Mexico, U.S.A.
Davies, A.; Perkins, W. T.; Brown, M.; Friend, C. R. L.	Geochemistry of the Late-Archaean Qôrqut Granite Complex, Southern West Greenland
Dillet, B.; Czamanske, G. K.	Tetrasilicic Mica and Alkali Amphibole in Peralkaline Granites from 26-M.Y.-Old Questa Caldera, New Mexico, U.S.A.
Duke, E. F.; Redden, J. A.; Papike, J. J.	Structural and Chemical Evolution of the Calamity Peak Layered Granite-Pegmatite Complex, Black Hills, South Dakota
Falster, A. U.	Mineralogy and Genesis of Secondary Miarolitic Cavities in Pegmatites of the Wausau Complex, Wisconsin
Fontan, F.; Fransolet, A.-M.; Keller, P.	Iron-Manganese Phosphate Associations from Pegmatites of Rwanda and Namibia
Fransolet, A.-M.	New Data and Relevant Observations on the Complex Aluminium Phosphate Associations from Li-Rich Pegmatites of the Gatumba Field, Western Rwanda

▲ TUESDAY POSTER SESSION: MINERALOGY AND GEOCHEMISTRY OF GRANITES, PEGMATITES, AND SKARNS (continued)

AUTHORS	TITLE
Grice, J. D.; Dunn, P. J.	Another New Phosphate Mineral from the Tip Top Mine, Black Hills, South Dakota
Hong, W.	A Preliminary Study on Mineralogy and Geochemistry of the Archean Granite, Anshan, Liaoning Province, People's Republic of China
Institute of Geochemistry	Rare Earth Element Geochemistry of Apatite and Sphene in Some Alkaline Intrusions From China
Jolliff, B. L.; Papike, J. J.; Shearer, C. K.; Spilde, M.	Mineral Recorders of Pegmatite Internal Evolution: Bob Ingersoll No. 1 Dike, Black Hills, South Dakota
Kawakatsu, K.; Yamaguchi, Y.	Zoning of Calcic Amphiboles From Quartz Diorite-Monzonite in Magnetite Series Granitoid Complex in the Daito-Yokota Area in Sanin Belt, Southwest Japan
Khomyakov, A. P.	Diversity of Alkaline Rock Minerals and the Problem of Quantity of Mineral Species
Lahti, S. I.	Zoning in Columbite-Tantalite Indicated by Microprobe Studies
Lumpkin, G. R.	Electron Microprobe Analysis of Feldspars and Micas from the Harding Pegmatite, Taos County, New Mexico
Martin, R. F.	Feldspar Mineralogy of Granitic Pegmatites
Massonne, H.-J.	Evidence Against the Comagmatic Character of the Devonian Granodiorite-Granite Suite of SW Nova Scotia from the Chemical Variability of Their Biotites
Neiva, A. M. R.	Geochemistry of the Granitic Rocks and Their Minerals From Serra da Estrela, Central Portugal
Olesch, M.	Normal and Inverse Zoning in Tourmalines from Pegmatites of North Victoria Land, Antarctica
Rockhold, J. R.; Nabelek, P. I.; Glascock, M. D.	Origin of Rhythmic Layering in the Calamity Peak Satelite Pluton of the Harney Peak Granite, Black Hills, South Dakota: The Role of Boron in Petrogenesis
Rønsbo, J. G.	Rare Earth Element Enrichment in Apatite from Peralkaline Undersaturated Rocks

▲ TUESDAY POSTER SESSION: MINERALOGY AND GEOCHEMISTRY OF GRANITES, PEGMATITES, AND SKARNS (continued)

AUTHORS	TITLE
Shearer, C. K.; Papike, J. J.; Scofield, N.; Walker, R. J.; Laul, J.C.	Mineralogical and Chemical Evolution of a Rare-Element Granite-Pegmatite System: Harney Peak Granite, Black Hills, South Dakota
Simmons, W. B.; Lee, M. T.; Brewster, R. H.; Wayne, D. M.	Chemical Fractionation and Evolution of the South Platte Pegmatite Suite, Jefferson County, Colorado
Sonnet, Ph.; Verkaeren, J.	Tungsten-, Tin-, and Boron-Bearing Skarns at El Hammam, Morocco
Stephenson, P. J.; Frost, M. T.; Tsambourakis, G.	Mn-Enrichment in Arfvedsonites, Biotites and Ilmenites from the Granites of Hinchinbrook Island, Queensland, Australia
Stern, L. A.; Brown, G. E., Jr.; Bird, D. K.; Jahns, R. H.; Foord, E. E.; Shigley, J. E.; Spaulding, L. B., Jr.	Pocket Mineralogy and Calculated Phase Relations of a Layered Pegmatite-Aplite Intrusive; The Little Three Mine, Ramona, CA
Swanson, S. E.	Textural and Mineralogic Zoning in the Rocklin Pluton, Western Sierra Nevada, California, U.S.A.
Tatekawa, M.	On A New Ultramicro Texture Found in the Wall Granite of the Granitic Pegmatite from Hanazono Quarry, Koseicho, Shiga Prefecture, Japan
Wang, X. J.; Černý, P.; Chackowsky, L. E.; Eby, R.	Evolution of K-Feldspar in the Red Cross Lake Pegmatitic Granite and its Pegmatite Aureole, Northeastern Manitoba, Canada
Yamaguchi, Y.	Hornblende-Cummingtonite and Hornblende-Actinolite Unmixing in Late Magmatic Stage of Koyama Calc-Alkaline Intrusive, Susa, Southwest Japan
Yang, M.	The Geochemistry of Evolution Series of Amazonite Granite and Amazonite Mineral in the Gansu Province of China
Yang, Y.; Ni, Y.; Guo, Y.	Kulanite First Found in China
Zhang, J.	Rare Element Minerals of Granitic Pegmatite in China
Zhang, R.-B.	The Preliminary Classification of China's Li-Pegmatite

▲ POSTER SESSION: ORE MINERALOGY/ ORE MICROSCOPY Tuesday, July 15, 1986; 14:30-17:00

AUTHORS	TITLE
Cai, C.; Li, Z.	Gold Minerals in China and Their Characters of the Occurrences
Chang, L. L. Y.; Wu, D.; Knowles, C. R.	Phase Relations in the System Ag_2S-Cu_2S-PbS-Bi_2S_3
Chen, D.; Lu, J.; Sun, S.; Lin, Y.; Chen, K.	A Preliminary Study on Berthierite Chashan, Guangxi, China
Chen, F.; Du, B.; Wu, Q.; Wang, D.	Molybdenite Polytypes in Molybdenum Ore Deposits of Eastern Qinling Region, Shaanxi, China
Corazza, M.; Corsini, F.; Lattanzi, P.; Tanelli, G.	Sphalerite and Arsenopyrite Compositions in Cassiterite-Polymetallic Deposits of Dachang (P. R. China)
Dickinson, C.; Pattrick, R. A. D.	Electron Microscopic Investigation of Sphalerite and Sphalerite-Chalcopyrite Intergrowths
Espahbod, M. R.	The Metallogenic Context and Mineralogical Succession of the Uranium Oxides in Iran
Frost, M. T.; Harrowfield, I. R.; MacRae, C. M.; Tsambourakis, G.	The Distribution of Silver in the Elura Pb-Zn-Ag Ore Deposit in NSW, Australia
Gaspar, O.	Textures of the Ores from Moinho Deposit, Aljustrel, Portugal, Their Genetic Significance and Implications on Beneficiation
Guo, S.; Guo, L.	A Mn- and Si-Bearing Amorphous Mineral
Harris, D. C.	The Diverse Mineralogy of the Hemlo Gold Deposit, Hemlo, Ontario
Huang, M.; Wu, G. B.; Chen, Y.; Tang, S.	Mineralogical Study of the Franckeite from the Dachang Cassiterite-Sulphide Polymetallic Ore Field Guangxi, China
Johnson, N. E.; Craig, J. R.; Rimstidt, J. D.	Structural Systematics of Tetrahedrite-Series Minerals
Karup-Møller, S.; Makovicky, E.	Mummeite, A New Member of the Pavonite Homologous Series, and the Associated Minerals from the Alaska Mine, Colorado
Kuo, T. S.	Mica as an Index Mineral to Rocks and Ores

▲ TUESDAY POSTER SESSION: ORE MINERALOGY/ORE MICROSCOPY (continued)

AUTHORS	TITLE
Lei, Y.; Lin, Y.; Yang, M.	Ullmannite in a Gold-Bearing Quartz Vein
Li, Z.	A Fundamental Law of Elements Concentrating to Form Ore Deposits--The Law of Combining Elements of Low with Higher Abundances
Luo, Z.-K.	The Tellurides in the Gold Deposits of China
Ma, F.; Sun, W.	The Constitution and Genetic Marks of Rare-Earth Minerals in the Western Ore-Area of Baiyun Ebo
Ma, X.	Fabric Characteristics and Minerogenesis of Sulfide Copper and Nickel Ore in a Deposit of Xinjiang
Moëlo, Y.	Lead-Sulfosalt Mineralogy: The State of the Art
Nakhla, F. M.	Ore Microscopy and Other Methods Adopted in Ore Mineralogy
Ren, Y.-C.	Tellurobismuthinides from Pangushan, China
Roedder, E.; Howard, K. W.	Fluid Inclusion Study of the Taolin Zn-Pb-Fluorite Deposit, PRC
Shukai, J.; Peisen, M.	Copper Deposits in Zhongtiao Mountains and Layered Intrusions
Smith, D. G. W.; de St. Jorre, L.	The Minident Data Base - Examples of Applications to the Thor Lake Rare Metal Deposits
Sun, W.; Mu, S.	The Comparative Study of β-Fergusonite in Two Different Genetic Deposit Types in the Baiyun-Ebo Mining District China
Tzepin, A. I.; Breskovska, V. V.; Borodaev, Y. S.; Mozgova, N. N.	About the Correlations of the Content of the Elements in Tetrahedrite-Tennantite Series
Wang, K.; Yang, H.	Genetic Mineralogy Study of Pyrite
Wang, S.	On the Typomorphic Peculiarites of Wolframite
Wang, Y.	The Characteristics of Galena From the Meng'en Ag-Pb-Zn Deposit and its Significance in the Study of Ore Genesis

▲ TUESDAY POSTER SESSION: ORE MINERALOGY/ORE MICROSCOPY (continued)

AUTHORS	TITLE
Wong, L.-B.; Chen, D.-Z.; Wang, P.	Mineralogy of Fankou Lead-Zinc Deposit in Northern Guangdong Province, China
Xu, G.; Shao, J.	The Discovery of Iron-Bearing Tennantite from a Certain Locality in Shanxi Province, China, and its Significance
Yue, S.	Ag-Bearing Talnakhite and its Geological Significance
Zhang, P.-S.; Tao, K.-J.	Characteristics of Fergusonite Mineral Group and Aeschynite Mineral Group in China
Zhao, X.	Characteristics of Inclusions in Some Types of Ore Deposits and Their Application to Probing into the Genesis of Ore Deposits

▲ POSTER SESSION: GEM MINERALS Tuesday, July 15, 1986; 14:30-17:00

AUTHORS	TITLE
Ghera, A.; Graziani, G.; Lucchesi, S.	Genesis of Vanadium-Bearing Beryls
Hollis, J. D.; Sutherland, F. L.	Relationships Between Colour, Crystallography and Origins of Gem Zircons in E. Australia
Kostov, R. I.	A Complex Classification of Gem Materials
Leguey, S.; Ga Gimenez, R.; Morante, M.; Medina, J. A.	Opals of Gemological Interest in the Neogene Basin of Madrid
Nogués-Carulla, J. Mª Vendrell-Saz, M.; Arbunies, M.; López-Soler, A.	Photometric Study of UV-Luminiscence of Cut Diamonds, and Its Relationship with Their Colour Classification
Ottaway, T. L.; Wicks, F. J.; Bryndzia, L. T.; Spooner, E. T. C.	Characteristics and Origin of the Muzo Emerald Deposit, Colombia
Rodionov, A. Ya	Gem Varieties of Beryl, Chrysoberyl and Phenakite Grown by Chemical Vapour Transport
Superchi, M.	New Transparent Yellow-Brown Gem Material From Mexico
Zecchini, P.; Merigoux, H.; Martin, F.	Non Destructive Identification of Gems and Man-Made Stones by I. R. Spectrometry

▲ POSTER SESSION: GARNET MINERALOGY Tuesday, July 15, 1986; 14:30-17:00

AUTHORS	TITLE
Calk, L. C.; Dodge, F. C. W.	Garnet in Granitoid Rocks of the Sierra Nevada Batholith, California
de Camargo, W. G. R.; Rechemberg, H.; Madureira F., J. B.; Kerth, W. H., Jr.	The Mössbauer Effect in the Determination of Molecular Composition of 5-Component Garnets
Kan, X.; Zhang, E.; Li, Y.	The Mössbauer Study of Pyrope-Almandite Series and its Geological Significance
Lager, G. A.; Armbruster, Th.; Rossman, G. R.; Rotella, F. J.; Faber, J.; Schultz, A. J.	Neutron Diffraction Studies in the Hydrogarnet System $Ca_3Al_2(SiO_4)_3$-$Ca_3Al_2(O_4D_4)_3$[1]
Madureira F., J. B.; de Camargo, W. G. R.	Determination of Molecular Composition of 5-Component Garnets by Graphical Procedures
Martin, F.; Zecchini, P.; Merigoux, H.	Garnet Identification by Reflective I.R. Spectrometry
Mottana, A.	Crystal-Chemical Evolution and Reliability of Garnet Analyses
Murad, E.; Wagner, F. E.	The Mössbauer Spectrum of Almandine
Otten, M. T.; Buseck, P. R.	TEM Determination of Site Occupancies in Pyrope Garnet
Stockton, C. M.; Manson, D. V.	The Chemical and Spectral Characteristics of Gem Garnets from East Africa

▲ POSTER SESSION: STRUCTURAL CLASSIFICATION OF MINERALS Tuesday, July 15, 1986; 14:30-17:00

AUTHORS	TITLE
Figueiredo, M. O.	Fundamentals of a Structural-Cum-Chemical Approach to Mineral Systematics
Hellner, E.	The Structure of Minerals in Their Inorganic Environment
Ling, W.	A Preliminary Discussion on Problems of the Study of Genetical Mineralogy
Strunz, H.	On the Classification of the Silicates
Wang, P.; Pan, Z.-L.; Wong, L.-B.; Chen, D.-Z.	An Introduction to a Handbook of "Systematic Mineralogy" in China

▲ POSTER SESSION: HISTORY AND TEACHING OF MINERALOGY Tuesday, July 15, 1986; 14:30-17:00

AUTHORS	TITLE
Prouvost, J.	Part of Scientific History in the Scientific Teaching

▲ POSTER SESSION: MINERALOGICAL APPLICATIONS OF SYNCHROTRON RADIATION Tuesday, July 15, 1986; 14:30-17:00

AUTHORS	TITLE
Calas, G.; Petiau, J.	X-Ray Absorption Studies of Sulfides and Arsenides
Finger, L. W.; Cox, D. E.	Powder Diffraction at the National Synchrotron Light Source Beam Line X13A
Fursenko, B. A.; Politov, A. A.; Tolochko, B. P.; Sheromov, M. A.	Study of Phase Transitions at High Pressures in Diamond Anvil Cell Using Monochromatic Synchrotron Radiation
Gilbert, A. E.; Sobolev, N. V.; Shatsky, V. S.; Baryshev, V. B.; Kulipanov, G. N.	Experience of Synchrotron Radiation Use For Determination of Contents and Distribution of Rare-Earth Elements in Minerals and Rocks
Stouff, P.; Boulegue, J.	Synchrotron Radiation: An Application to the Oceanic Hydrothermal Oxides
Tsukimura, K.; Sasaki, S.; Ohashi, H.	Observation of Positional Shifts Among Transition-Metal Atoms in Orthopyroxene by Synchrotron X-Ray Resonant Scattering
Yamanaka, T.; Ogata, K.; Sugiyama, K.; Tokonami, M.	Structure Determination of GeO_2 Powder Sample at High Pressure and Temperature by Synchrotron Radiation

▲ POSTER SESSION: COSMIC MINERALOGY Tuesday, July 15, 1986; 14:30-17:00

AUTHORS	TITLE
Almohandis, A. A.	Microhardness Measurements on the Largest Wabar Meteorite, Saudi Arabia
Li, Z.	Compositions of Inclusions in Chondrite Minerals in China
Lu, K.; Peng, H.; Liu, Z.; Chai, Z.; Zhuang, S.; Yu, Z.	The Discovery of Pentlandite in Deep-Sea Cosmic Spherules

▲ POSTER SESSION: MINERALOGY OF METAMORPHIC ROCKS — Wednesday, July 16, 1986; 14:30-17:00

AUTHORS	TITLE
Bakun-Czubarow, N.	Mineral Chemistry of Ilmenite-Bearing Eclogite from Mountain Czernica in the Polish Central Sudetes
Brothers, R. N.; Grapes, R. H.	Clastic Glaucophane, Lawsonite and Jadeitic Pyroxene in Franciscan Metagreywackes from Mt. Hamilton, Pacheco Pass and Panoche Pass, California
Chen, K. Y.; Sun, D. S.	Petrology of the Greenstone Belt in Gongchangling Region, Liaoning, PRC
Chihara, K.; Komatsu, M.	Jadeitites in Serpentinite Mélange of Omi-Renge Tectonic Belt in Central Japan
Chopin, C.; Klaska, R.	Metamorphism of Continental Crust at Mantle Depths: New Rock-Forming Minerals
Fed'Kin, V. V.	Evolution of Physico-Chemical Conditions of Medium-Temperature Metamorphism
Ghent, E. D.; Stout, M. Z.; Sevigny, J. H.	Metamorphism in the Mica Creek Area, Southeastern British Columbia, Canada
Grew, E. S.; Swihart, G. H.; Moore, P. B.	Serendibite, Sapphirine, and Grandidierite from the Adirondack Mountains at Johnsburg, New York, USA
Harlow, G. E.	Jadeitites and Their Fluid Inclusions from Rio Motagua, Guatemala
Huebner, J. S.; Flohr, M. J. K.; Matzko, J. J.	Origin and Metamorphism of Manganese Sediments in Melange of the Franciscan Complex, California
Labotka, T. C.; Nabelek, P. I.	Petrology of the Contact - Metamorphosed Weeks Formation, Notch Peak, Utah
Liou, J. G.; Maruyama, S.	Parageneses of Ca-Na Pyroxenes and Amphiboles from Franciscan Blueschists, Cazadero, California
Maruyama, S.; Liou, J. G.	Petrogeneses and Mineral Compositions of Franciscan Blueschists from Cazadero, California
Mitsaki-Hafner, V.	Mn-Bearing Minerals from Trikorfo Metamorphic Rocks, Thassos, Greece
Moore, D. E.; Blake, M. C., Jr.	Early Greenschist-Amphibolite Facies Metamorphism Identified in Blueschist and Eclogite Exotic Blocks of the Franciscan Complex, California

▲ WEDNESDAY POSTER SESSION: MINERALOGY OF METAMORPHIC ROCKS (continued)

Nabelek, P. I.; Labotka, T. C.; Glascock, M. G.	Chemical Changes During Contact Metamorphism of the Weeks Formation at the Notch Peak Complex, Utah
Ponader, H. B.; Liou, J. G.	Experimental Study of Rodingitization and Serpentinization
Ruendal, A. P.; Rice, J. M.	Polymetamorphism of Pelitic Rocks in the Headquarters Region, Northern Idaho
Schumacher, R.	Prograde Metamorphism of Hornblende- and Epidote-Bearing Rocks, Lower to Upper Amphibolite Facies, Central Massachusetts, USA
Sedlock, R. L.	High-Pressure Metamorphism and Uplift of Blueschist and Eclogite in the Cedros Complex, Central Baja California
Xue, J.; Chen, S.; Zhao, Y.; Ge, Y.; Ren, Y.; Zhang, H.; Ho, Y.; Pan, T.	Investigation on the Index Mineralogy of China Himalaya: The Metamorphic Silicates of Western Ali Region

▲ POSTER SESSION: STRUCTURAL AND MAGNETIC PHASE TRANSITIONS — Wednesday, July 16, 1986; 14:30-17:00

AUTHORS	TITLE
Boujida, M.; Regnard, J. R.	Relation Between Magnetic Hyperfine Field Distribution and Cation Order in Natural Hedenbergite
Feuer, H.; Schröpfer, L.; Fuess, H.	Exsolution and Phase Transition in Pyroxenes
Fuess, H.; Ballet, O.; Lottermoser, W.	Magnetic Phase Transition in the Olivines Fe_2SiO_4, Mn_2SiO_4 and Co_2SiO_4
Goss, C. J.; Putnis, A.	Changes in Lattice Parameter, Microstructure and Intrinsic Magnetic Properties with Progressive Magnetite Oxidation
Haga, N.; Ghose, S.; McMullan, R. K.; Sharma, S. K.	Anharmonicity and Structural Instability Below the Ortho-Proto Phase Transition in Enstatite, $Mg_2Si_2O_6$: A High Temperature Neutron Diffraction and Raman Scattering Study
Lawson, C. A.; Nord, G. L., Jr.	The Change from Reverse to Normal Thermoremanent Magnetization in Minerals of the Ilmenite-Hematite Solid Solution Series
Nord, G. L., Jr.; Lawson, C. A.	The Order-Disorder Transition and Transformation-Induced Domains in Ilmenite-Hematite
Redfern, S. A. T.; Salje, E.	The $I\bar{1} \leftrightarrow P\bar{1}$ Structural Phase Transition in Anorthite: Temperature Evolution of the Spontaneous Strain
Regnard, J. R.; Wiedenmann, A.; Fillion, G.	Magnetism of Pyroxenes

▲ POSTER SESSION: PHYLLOSILICATE MINERALOGY — Wednesday, July 16, 1986; 14:30-17:00

AUTHORS	TITLE
Altaner, S. P.; Bethke, C. M.	Layer Ordering in Interstratified Illite/Smectite
Amouric, M.; Parron, C.	Electron Microscopic Study of Glauconitization Process
Barabas, A. H.	The Significance of Hydrothermal Rectorite in the Cala Abajo Porphyry Copper Deposit, Puerto Rico
Boudeulle, M.; Muller, J. P.	Electron Microscopy (AEM-HREM) of Goethite from a Laterite: Twinning and Epitaxy on Kaolinite
Brearley, A. J.; Rubie, D. C.	An Experimental/TEM Investigation of the Breakdown of Muscovite at High Temperature
Chen, C.-H.; Jeng, R.-C.	Crystallinity and Chemistry of K-Micas from Metapelites of the Central Range of Taiwan
Crowley, J.; Vergo, N.	Disorder in Kaolin Minerals: Observations Using Near-Infrared Reflectance Spectroscopy
Czank, M.	HRTEM Investigation of Polytypism in Biotites
Droop, G. T. R.; Brearley, A. J.	The Disequilibrium Breakdown of Aluminous Iron-Rich Biotite at 800°C: An Experimental Kinetic and TEM Investigation
Dyar, M. D.; Hickmott, D.; Guidotti, C. V.; Cheney, J. T.	M2/M1 Ordering of Iron in Biotites from Northwestern Maine
Ferraris, G.; Mellini, M.	Serpentine and Serpentine-Like Minerals
Ferraris, G.; Mellini, M. Merlino, S.	Electron Diffraction and Electron Microscopy Study of Balangeroite and Gageite: Unit Cells, Structure Models and Petrogenetic Role
Hindman, J. R.	Ion Exchange at 40°C in Vermiculite from Libby, Montana
Mellini, M.; Zanazzi, P. F.	The T-O Layer of Lizardite: New Structure Refinements
Miúra, Y.	Serpentine-Group Minerals With and Without Chlorine in Terrestrial and Extraterrestrial Materials

▲ WEDNESDAY POSTER SESSION: PHYLLOSILICATE MINERALOGY (continued)

Nachit, H.; Monier, G.; Cregu, B. P.; Robert, J.-L.	New Experimental Data on Biotite Solid Solutions in Hydrothermal Conditions. Application to the Typology of Granitoids.
Ozawa, T.; Takahata, T.; Buseck, P. R.	A Hydrous Manganese Phyllosilicate with 12 Å Basal Spacing
Ren, D.-W.; Chen, Y.-J.; He, R.-L.	X-Ray Studies of Coarse-Grained Kaolinite from Tonstein in Pu-Bei Area, Shaanxi, China
Robert, J.-L.	Generalization of the Correlations Between Hydroxyl Stretching Frequencies and Composition of Micas: A Single Model for Biotites, Muscovite, Phengites and Lepidolites
Soboleva, S. V.; Boroutzky, B. E.	Three-Layer Biotite 3Tc from the Khibini Alkaline Massif
Volfinger, M.; Robert, J.-L.	Questions about High Chlorine Micas and Amphiboles
Walker, J. R.	Application of High-Gradient Magnetic Separation to Structural and Compositional Studies of Layer Silicates in Fine Grained Rocks
Wang, G.; Huang, Y.; Liu, W.	Discovery of 1T-Lizardite with Cyclical Twining in Kimberlite
Worden, R. H.; Droop, G. T. R.; Champness, P. E.	TEM Studies of the Pyrometamorphic Breakdown of Phengite and Chlorite
Wu, G.; Chen, S.	Mossbauer Study of Manganese Biotite from Kuiqi, China
Yu, S. C.; Jiang, W. D.	Saponite from the Coastal Range of Taiwan
Zvyagin, B. B.; Lygina, T. Z.	Palygorskite Polytypes and Their Symbolic Description

▲ POSTER SESSION: THERMODYNAMICS AND KINETICS OF MINERAL REACTIONS — Wednesday, July 16, 1986; 14:30-17:00

AUTHORS	TITLE
Bayer, G.; Wiedemann, H.-G.	Displacement Reactions in Gypsum. II
Bernardini, G. P.; Cipriani, C.; Corsini, F.; Guarini, G. G. T.; Mazzetti, G.; Poggi, L.	Evidence and Kinetics of the Homogenization Reaction in the "Allemontite" Intergrowths
Burns, R. G.; Bartels, K. S.	Defect Iron Crystal Chemistry of Fe^{2+}-Fe^{3+} Mineral Assemblages: Implications to Thermodynamic Calculations of Oxygen Fugacities
Burton, B. P.; Davidson, P. M.	Order-Disorder and Phase Separation in the Systems F_2O_3-$FeTiO_3$, $CaCO_3$-$MgCO_3$, and $CaMgSi_2O_6$-$NaAlSi_2O_6$
Cho, M.; Maruyama, S.; Liou, J. G.	The Stability of Heulandite in the System $CaAl_2Si_2O_8$-SiO_2-H_2O
Chou, I.-M.	Redetermination of Phase Equilibrium Properties in the System NaCl-H_2O to 1000°C and 1500 Bars
Cygan, R. T.	Energies and Mechanisms of Cation Diffusion in Garnets
Delmotte, L.; Guth, J. L.; Kalt, A.; Wey, R.	Conditions of Nucleation of Magadiite and Kenyaite
Duck, J. J.; Cohen, A. J.	Partition of Trace Germanium and Gallium Between Intergrown Topaz and Quartz
Fei, Y.	Heat Capacity of Minerals Relevant to the Earth's Mantle: A New Equation for the Heat Capacity of Solids
Hay, R. S.; Evans, B.	Chemically Induced Grain Boundary Migration in Calcite: A Low Temperature Solid-State Mineral Reaction Mechanism
Hovis, G. L.	Thermodynamic Properties of Alkali Feldspars
Joesten, R.	Retrieval of Grain-Boundary Diffusion Coefficients Using the Integrated Thermal History of a Contact Aureole
Lepezin, G. G.; Osorgin, N. U.	Dehydration Kinetics of Cordierites

▲ WEDNESDAY POSTER SESSION: THERMODYNAMICS AND KINETICS OF MINERAL REACTIONS (continued)

Mattioli, G. S.; Wood, B. J.	Experimental Determination of Fe_3O_4 Activity in Complex Spinels: Implications for Upper Mantle fO_2
Mizota, T.	A Small Scale Adiabatic Calorimeter for Heat Capacity Measurement of Minerals
Morimoto, N.; Sakanaka, K.; Kitamura, M.	Diffusion Coefficient of Silica in Supercritical Water
Nitkiewicz, A. M.; Kerrick, D. M.	Hydrothermal Determination of Interfacial Energies at Elevated Temperatures and Pressures
Ohmasa, M.; Sato, A.	Dehydration of Brucite to Periclase
Rao, K. R.; Chaplot, S. L.; Chaudhury, N.; Ghose, S.; Price, D. L.; Hastings, J. M.	Lattice Dynamics of Forsterite, Mg_2SiO_4: Phonon Dispersion Relations, Elastic and Thermodynamic Properties
Rebbert, C. R.; Hewitt, D. A.	Biotite Oxidation in Hydrothermal Systems: An Experimental Study
Remaut, G.; Vochten, R.	Solubility and Electrokinetic Properties of Bassetite
Skogby, H.; Annersten, H.	Kinetics of Intracrystalline Fe-Mg Distribution in Tremolite
Vochten, R. F.	Transformation of Uranite into Different Hydrated Uranium Oxides
Wang, X.; Greenwood, H. J.	A Study on the Equilibrium Grossular + Clinochlore = 3 Diopside + 2 Spinel + 4 H_2O

▲ POSTER SESSION: APPLIED AND ENVIRONMENTAL MINERALOGY — Wednesday, July 16, 1986; 14:30-17:00

AUTHORS	TITLE
Chaudhuri, J. N. B.	Mineralogy of the Slag and its Implication in the Industry
Felius, R. O.	EM-Research into the Fibrous Constituents of an Industrial Talc Powder
Gu, J.; Tang, S.	Chrysotile Asbestos from China
Li, H.	The Recent Development and Future Prospects of the Research of Minerals for Medical Applications
Li, S.	Kyanite Group Minerals - A Kind of High Alumina Refractory Materials in China
O'Hanley, D. S.; Zoltai, T.	A Semi-Quantitative Method for Distinguishing Asbestiform and Non-Asbestiform, Acicular Crystals: Data for Tremolite
de Pablo-Galán, L.	The Mineralogy and Paragenesis of Human Renal Calculii
Schwertmann, U.; Carlson, L.; Murad, E.	Environmental Effects on Iron Oxide Formation in Two Finnish Lakes
Shedd, K. B.	Crocidolite Fiber Dimensions from Mining Regions in Western Australia, South Africa, and Bolivia
Shin, S.; Suzuki, K.; Kiyozumi, Y.; Okado, H.; Noguchi, K.	Effect of Synthetic Conditions of High-Silica ZSM-5 Type Zeolite on its Catalytic Life in Methanol Conversion to Lower Olefins

▲ POSTER SESSION: NON-CRYSTALLINE AND METAMICT MATERIALS — Wednesday, July 16, 1986; 14:30-17:00

AUTHORS	TITLE
Brown, G. E., Jr.; Ponader, C. W.; Keefer, K. D.	X-Ray Absorption Study of Zirconium in Na-Zr-Silicate Glasses
Calas, G.; Petiau, J.	Local Order Around Transition Elements in Silicate Glasses and During Crystalline Nucleation: Approach by X-Ray Absorption Spectroscopy
Ewing, R. C.; Lumpkin, G. R.	High Resolution Electron Microscopy of Metamict and Annealed Zirconolite from Sri Lanka
Fritsch, E.	Vanadium Incorporation in Pure Silica Glasses: Vanadium Segregation and Tetrahedral Coordination
Greegor, R. B.; Lytle, R. W.; Chakoumakos, B. C.; Lumpkin, G. R.; Ewing, R. C.	Structural Investigation of Metamict Minerals Using X-Ray Absorption Spectroscopy
Groat, L. A.; Hawthorne, F. C.; Raudsepp, M.; McCammon, C.; Gaba, R.; Lumpkin, G. R.; Ewing, R. C.	Variation of Crystallinity/Metamictization in Natural Titanites
Imafuku, M.; Nakai, I.; Akimoto, J.; Miyawaki, R.; Sugitani, Y.; Koto, K.	Characterization of the Metamict State of Oxide Minerals by EXAFS
Jackson, W. E.; Brown, G. E., Jr., Ponader, C. W.	EXAFS Study of the Local-Coordination Environment of Potassium in Orthoclase and Albite-Orthoclase Composition Glasses
Lange, R. A.; Carmichael, I. S. E.	Density of Alumino-Silicate Liquids
Murakami, T.; Chakoumakos, B. C.; Ewing, R. C.	High Resolution Electron Microscopy of Crystalline, Partially Metamict and Metamict Zircons
Ponader, C. W.; Brown, G. E., Jr.	X-Ray Absorption Study of Ytterbium in Quenched Aluminosilicate Melts
Schlinger, C. M.	Superparamagnetic Crystalline Precipitates in Volcanic Glasses of the KBS Tuff: Mineralogy, Magnetism and Relationship to Volcanism

▲ POSTER SESSION: OPTICAL PROPERTIES OF MINERALS — Wednesday, July 16, 1986; 14:30-17:00

AUTHORS	TITLE
Chiou, J.	The Discovery of Anisotropic Transmissive Rotation Angle
Mereiter, K.; Preisinger, A.	Correlations Between Optical Properties and Crystal Structures of Uranyl Carbonate Minerals
Shinno, I.	Three Types of Photo-Luminescence in Natural Zircon
Wang, S.	On the Similarities Between Anisotropic Rotation and Reflection Rotation for Opaque Minerals
Wolfe, H. E.; Su, S.-C.; Ribbe, P. H.; Bloss, F. D.	Optical, X-Ray and Microprobe Study of Low Plagioclase Single Crystals: Discriminant Analyses of Discontinuities
Xu, Z.	A New View about the Origin of Dispersion of Biaxial Non-Opaque Minerals
Ye, D. N.	Relation Between Optical Anisoptropy Index and Orientation of Atom Groups of Mineral
Zhang, S.-Y.; Kang, W.-K.; Chang, L.-H.; Wen, M.-J.	The Principle of Multi-Use Double Variable Refractometer and its Application in the Minerals Refractive Measurement

▲ POSTER SESSION: AMPHIBOLES AND PYROXENES — Thursday, July 17, 1986; 14:30-17:00

AUTHORS	TITLE
Cannillo, E.; Ungaretti, L.; Oberti, R.; Smith, D. C.	An Updated Version of Computer Program CORANF for Determining the Site Populations and the Bulk-Mineral Chemical Composition of C2/m Amphiboles by Single-Crystal X-Ray Diffractometry and Refinement
Clowe, C. A.; Popp, R. K.; Fritz, S. J.	The Variation of Unit Cell Parameters with Ferric-Ferrous Ratio in a Hornblende
Domeneghetti, M. C.; Oberti, R.; Ungaretti, L.; Ghezzo, C.; Memmi, I.; Ricci, C. A.	Chemical Variations in the Amphiboles of an Equilibrated Amphibolite from North-Eastern Sardinia (Italy): Crystal-Chemical and Petrological Implications
Huang, W.; Wang, Y.; Zou, B.	Polytypism of $MgSiO_3$ in Natural Samples
Makino, K.; Tomita, K.	Cation Order-Disorder in Octahedral Sites (M1, M2 and M3) of Hornblendes

▲ THURSDAY POSTER SESSION: AMPHIBOLES AND PYROXENES (continued)

Molin, G. M.; Secco, L.; Dal Negro, A.; Cundari, A.; Piccirillo, E. M.	Crystal-Chemistry of Magmatic C2/c Clino-pyroxenes of Low and High Pressure Origin: Structural Distinctions
Oba, T.; Yagi, K.	The Extent of Compositional Gap Between Actinolite and Hornblende Against the Effect of Fe^{2+} Content
Rossi, G.; Oberti, R.; Dal Negro, A.; Molin, M.; Mellini, M.	Residual Electron Density at the M2 Site in C2/c Clinopyroxenes: Relationships with Bulk Chemistry and Sub-Solidus Evolution
Schumacher, J. C.	Intergrowths and Reactions Involving Ortho- and Clino-Pyriboles from Orijärvi, Southwest Finland
Shatsky, V. S.; Sobolev, N. V.; Stenina, N. G.	Exsolution Structures in Pyroxenes from Metamorphic Rocks of Kokchetav Massif (Northern Kazakhstan)
Stenina, N. G.; Shatsky, V. S.	Crystal Chemistry of Phase Transitions in Omphacites from Eclogites of Northern Kazakhstan (USSR)
Sueno, S.; Matsuura, S.	A Mineralogical Study on Two Natural Proto Amphiboles
Sykes, J.; Molin, G. M.	Structural Variations in Orthopyroxenes
Tamada, O.; Tanaka, K.	Determination of Atomic Charge of Mg and Site Ionicities in Forsterite and Enstatite by Using the Molecular Orbital Method
Tazzoli, V.; Domeneghetti, M. C.	Aluminum in Orthopyroxenes: Its Ordering in Natural and Heated Crystals
Ungaretti, L.; Oberti, R.; Cannillo, E.; Smith, D. C.	Discriminant Analysis (DA) of 400 X-Ray Refined Clinoamphiboles
Wirth, R.; Ying, Y.	Cation Distribution and Oxidation State of Iron in Glaucophane

▲ POSTER SESSION: MINERALOGY OF SEDIMENTARY ROCKS — Thursday, July 17, 1986; 14:30-17:00

AUTHORS	TITLE
Billo, S. M.	Chemical Mineralogy of Marine Evaporites
Fort, R.; Ordoñez, S.	Grain Size Analysis of Cassiterite and Related Minerals Grains of Alluvial Placer Deposits
Ordoñez, S.; Garcia del Cura, M. A.	The Origin of Sodium-Calcium Sulfate Deposits of Madrid Basin (Spain)
Qiu, C.	Characteristics of Depositional Ferromanganese Minerals in the South China Sea
Tang, X. M.; Zhan, Z. M.	On the Manganese Mineral Composition of Typical Sedimentary Manganese Carbonate Ore in China
Wang, Q.; Zhu, E.	The Assemblage and Environment of Authigenic Iron Minerals
Wang, T.; Su, G.	Glauconites in the Northern South China Sea
Zhu, E.; Li, J.	The Mineralogical Feature of Calcic Biogrnic Detritus in the China Sea

▲ POSTER SESSION: CARBONATE MINERALOGY Thursday, July 17, 1986; 14:30-17:00

AUTHORS	TITLE
Holail, H.	Deposition, Dolomitization, Silicification Paragenesis of Naqb Siwa Carbonate Sediments, Bahariya Oasis, Egypt
Konev, A. A.; Vorobyev, E. I.; Afonina, G. G.; Sapozhnikov, A. N.; Paradina, L. F.; Lapides, L. I.; Malyshonok, Yu. V.	New Natural Carbonates Along $SrCO_3$ - $BaCO_3$ Join
Kretz, R.	SEM Examination of Calcite-Dolomite Exsolution
Miyawaki, R.; Takase, J.; Nakai, I.	Crystal Chemistry of Hydrous Rare Earth Carbonate Minerals - The Crystal Structure of Tengerite
Roberts, A. C.; Sabina, A. P.; Bonardi, M.; Jambor, J. L.; Ramik, R. A.; Sturman, B. D.; Carr, M. J.	Montroyalite, A New Hydrated Sr-Al Carbonate From the Francon Quarry, Montreal, Quebec

▲ POSTER SESSION: STRUCTURE, CHARACTERIZATION, AND SYNTHESIS — Thursday, July 17, 1986; 14:30-17:00

AUTHORS	TITLE
Alberti, A.; Gottardi, G.	The Structure Geometry of Framework Silicates and the Aluminum Fraction in the Tetrahedra
Angel, R. J.; Prewitt, C. T.	Incommensurate Ordering in Mullite
Bianchi, R.; Pilati, T.; Mannucci, G.	The Crystal Structure of Grischunite
Burnham, C. W.; Post, J. E.	Positional Disorder of Cavity and Channel Cations in Mineral Structures: Influence of Local Framework Cation Configurations
Christy, A. G.	Occurrence and Stability of the Sapphirine Polytypes
Cozzupoli, D.; Grubessi, O.; Mottana, A.; Zanazzi, P. F.	Cyrilovite from Bosa (Sardinia, Italy): Structure and Crystal Chemistry
Deicha, G. A.	Inclusions in Minerals and Crystallogenesis
Dmitrieva, M. T.; Kovalenker, V. A.; Borisova, E. A.	Crystal Chemistry of Te-Bearing Fahlore
Fitzpatrick, J. J.	Pokrovskite: Its Possible Relationship to McGuinnessite and the Problem of Excess Water
Fleet, M. E.; Arima, M.	Disordered Phenacite Structures of α-$LiGaSiO_4$ and α-$LiGaGeO_4$
Foord, E. E.; Taggart, J. E.	Reassessment of the Turquoise Group: Redefinition of Planerite, $(\square)Al_6(PO_4)_2(PO_3OH)_2(OH)_8{\cdot}4H_2O$ and Aheylite, $FeAl_6(PO_4)_4(OH)_8{\cdot}4H_2O$, A New Member of the Group
Ghazi-Bayat, B.; Amthauer, G.; Schürmann, K.; Hellner, E.	Synthesis of the Mixed-Valence Iron Silicate Ilvaite
Gottardi, G.; Galli, E.; Larsen, A. O.; Mazzi, F.	Order-Disorder in Zeolites with Natrolite Framework
Hassan, I.; Buseck, P. R.	HRTEM Characterization of Scapolite Solid-Solution Series
Hochella, M. F., Jr.; Harris, D. W.; Turner, A. M.	High Spatial Resolution Scanning Auger Microscopy of Mineral Surfaces: Techniques and Applications

▲ THURSDAY POSTER SESSION: STRUCTURE, CHARACTERIZATION, AND SYNTHESIS (continued)

Huang, Y.; Zhou, X.; Li, G.; Du. S.	Mengxianminite, A New Ferro-Magnesium-Calcium-Tin-Aluminum Oxide Mineral
Kim, S. J.	Find of the True Mn^{2+} Analogue of Rancieite
Kroll, H.; Ribbe, P. H.	Quantitative Estimates of Strain in (Semi-) Coherent K- and Na-Rich Phases of Perthitic Alkali Feldspars
Lebedev, A. S.; Kargal'Tsev, S. V.; Pavlyuchenko, V. S.	Hydrothermally Grown Mg- and Fe-Tourmalines
Li, W.; Wang, Q.; Chen, G.; Sun, S.	The Crystal Structure of a New Ferric Sulphate Mineral
Ling, W.	A Preliminary Discussion on Problems of the Study of Genetical Mineralogy
Maaskant, P.	Electron Probe Microanalysis of Subsurface Phases: An Empirical Approach
Mandarino, J. A.	The Procedure for Obtaining Approval of a New Mineral Species from the Commission on New Minerals and Mineral Names, I. M. A.
Mannucci, G.; Diella, V.; Gramaccioli, C. M.; Pilati, T.	A Comparative Study of Monazite Specimens from the Alpine Region
Miller, M. L.; Ribbe, P. H.	Mg-Mn and Mg-Fe Olivines: Use of Diffraction Peak Intensities, d-Spacings and Lattice Parameters in Determining Composition and Intracrystalline Cation Distribution
Milton, C.; Vitaliano, D. B.	Moissanite, SiC: Yes or No?
Novgorodova, M. I.	Native Metals, Carbides and Carbon in Metacomatic Rocks
Peng, Z.	The Deduction of Quasicrystal Lattice and the Fractal Structure Model of Quasicrystal
Pfaffl, F. A.	Chemical Composition of Zwieselite
Post, J. E.; Turner, S.	Structure Refinement of Romanechite; Subcell and Supercell
Rice, S. B.; Vaughan, D. E. W.	Gmelinite Geochemistry and Phase Relationships
Rieder, M.; Weiss, Z.	Oblique-Texture X-Ray Photographs - A New Modification of the Powder Method

▲ THURSDAY POSTER SESSION: STRUCTURE, CHARACTERIZATION, AND SYNTHESIS (continued)

Sacerdoti, M.; Passaglia, E.	The Crystal Structure of Hydrocalumite from Montalto di Castro, Viterbo, Italy
Sarkar, S. L.	Application of APD 3600 in Quantitative Mineralogical Phase Analysis
Scambos, T. A.; Smyth, J. R.; McCormick, T. C.	Structure Refinement of a Natural High Sanidine of Upper Mantle Origin
Scandale, E.; Stasi, F.	On Satellic Type of Brazil Twins in Natural Quartz
Shoji, T.; Okaya, K.; Goto, K.; Otsuka, S.	Binocular Scanning Electron Microscope for Simultaneous Stereography
Steel, E. B.	Mineral Glass Thin Film Standards for Analytical Electron Microscopy
Wang, H.	A Mineralogical Study of Amber in the Xixia Region of Henan, P.R.C.
Wang, S.; Peng, Z.; Ma, Z.	The Crystal Structure of Qitianlingite $Fe_2Nb_2WO_{10}$
Wise, M. A.; Černý, P.	The Status of Ixiolite
Xu, B.	A New Method of Simple Identification of Zeolites
Yurimoto, H.; Sueno, S.	Mineral/Groundmass Partition Coefficients for Minerals
Zhang, H.; Xie, X.	A Study of the Existing Forms of Iron in Rutile
Zheng, M.; Kuo, T.	Cs-Geyserite at Targaja Geothermal Field, Tibet
Zhou, J.; Johan, Z.	Studying of Fine Textures of Ferrifayalite and Discussing of Oxidation of Fayalite

▲ POSTER SESSION: SPECTROSCOPY OF MINERALS — Thursday, July 17, 1986; 14:30-17:00

AUTHORS	TITLE
Affholter, K. A.; Annersten, H. S.	Mössbauer Characterization of Site Occupancies in Synthetic Allanite, $CaREEFeAl_2Si_3O_{12}(OH)$
Bernstein, L. R.; Waychunas, G. A.	EXAFS and XANES Studies of Germanium in Some Minerals and Related Substances
Cohen, A. J.	Low Temperature Hole-Trapping by Iron Ions in α-Quartz
Coy-Yll, R.; Calderon, T.; Aguilar, M.	Luminescence in Tourmaline
Hofmeister, A. M.; Xu, J.; Akimoto, S.	Thermodynamic Implications of Infrared Spectroscopy of Stishovite at Mantle Pressures
Li, D.; Peng, M.	Some New Spectroscopic Aspects of Sphalerite from China and Their Significance
Li, P.; Peng, M.	The Study on the Spectroscopy and the Color Nature of Some Gem Minerals
Lin, C.	An EHMO Study on the Crystal-Field Spectrum and g-Tensor of Cu^{2+} Ion in Turquoise
Manceau, A.; Llorca, S.; Calas, G.	X-Ray Absorption Study of Co and Ni Crystal Chemistry in Lithiophorite and Asbolane
Merigoux, H.; Martin, F.; Zecchini, P.	Observation of Inhomogenity in Cultured Quartz By I. R. Spectrometry
Muller, J. P.; Calas, G.	Paramagnetic Defect Centers in Natural Kaolinites
Peng, M.; Zheng, C.; Li, D.	The Systematical Study on Quantum Mineralogy of Piemontite from Hailand
Phillips, B. L.; Kirkpatrick, R. J.	Increased Resolution for Solid-State ^{27}Al NMR
Ping, X.; Li, D.	Application of Mineral Spectroscopy in Geology--A Case Study on Tin Deposits
Rask, J. H.; Miner, B. A.; Buseck, P. R.	Electron Energy-Loss Spectroscopy of Mn Compounds
Sanz, J.; Herrero, C. P.; Serratosa, J. M.	Tetrahedral Cation Distribution in Phyllosilicates 2:1 by ^{29}Si NMR Spectroscopy
Sharma, S. K.	High Temperature Raman Spectra of Quartz Polymorphs of GeO_2 and SiO_2

▲ THURSDAY POSTER SESSION: SPECTROSCOPY OF MINERALS (continued)

Sherriff, B. L.; Grundy, H. D.; Hartman, J. S.	Si-Al Ordering of Scapolites from ^{29}Si, and ^{27}Al, MAS NMR
Shinno, I.	Three Types of Photo-Luminescence in Natural Zircon
Solberg, T. C.; Burns, R. G.	Crystal Chemical Trends in Mössbauer Spectra of ^{57}Fe-Bearing Oxide, Silicate, and Aluminosilicate Minerals
Tyson, R. M.; Hemphill, W. R.; Theisen, A. F.	The Effect of Major and Trace Element Chemistry on the Luminescence Spectra of the Scheelite-Powellite Series
Van Moort, J. C.	Electron Paramagnetic Resonance Powder Spectra of Natural Quartzes, Especially in Relation to Gold Mineralisation
Weiss, C. A., Jr.; Kirkpatrick, R. J.	Aluminum-27 and Silicon-29 NMR Spectroscopy of Mixed-Layered Illite/Smectites
Yuan, Y.; Qui, X,; Guo, Y.	d-d Transition of Fe^{2+} Ions in Diopside

▲ POSTER SESSION: COMPUTATIONAL MINERALOGY — Thursday, July 17, 1986; 14:30-17:00

AUTHORS	TITLE
Cohen, R. E.; Mehl, M. J.; Boyer, L. L.	First Principles Calculations of the Physical Properties of Minerals as Functions of Pressure and Temperature with Spherically Breathing Ions
Doherty, M.; Price, G. D.; Parker, S. C.; Catlow, C. R. A.	Defects in Olivine: A New Approach Via Computer Simulations
Rao, K. R.; Chaplot, S. L.; Chaudhury, N.; Ghose, S.; Price, D. L.; Hastings, J. M.	Lattice Dynamics of Forsterite, Mg_2SiO_4: Phonon Dispersion Relations, Elastic and Thermodynamic Properties
Sherman, D. M.	Molecular Orbital Calculations Applied to the High Pressure Electronic Transitions of Fe(II) Minerals in the Earth's Mantle
Tamada, O.; Tanaka, K.	Determination of Atomic Charge of Mg and Site Ionicities in Forsterite and Enstatite by Using the Molecular Orbital Method
Wall, A.; Price, G. D.	Computer Modelling of Magnesium Silicate Perovskites

▲ POSTER SESSION: MINERALOGY AND PETROLOGY OF MAFIC AND ULTRAMAFIC ROCKS AND ASSOCIATED ORE DEPOSITS — Thursday, July 17, 1986; 14:30-17:00

AUTHORS	TITLE
Allen, R. L.; Roeder, P. L.	Petrological and Chemical Study of a Pyroxenitic Komatiite Sill and Basal Sulfide Lens, Munro Township, Ontario, Canada
Belkin, H. E.; de Vivo, B.; Beccaluva, L.; Macciotta, G.	Fluid Inclusion and Chemical Studies of Spinel Peridotite Xenoliths from Sardinia (Italy)
Bird, D. K.; Rose, N. M.; Manning, C. E.	Hydrothermal Alteration in Layered Gabbros of the East Greenland Tertiary Province
Garanin, V. K.; Kudryavtseva, G. P.	Mineralogy of Ilmenite from Yakutia Kimberlites
Ji, S.; Miao, P.	Copper Deposits in Zhongtiao Mountains and Layered Intrusions
Kleck, W. D.	Cavity Minerals of the Lava Flow at Lemolo Lake Quarry, Oregon
Larson, S. Å.	Igneous Layering in the Ulvö Dolerite Complex, Sweden
Lu, F.; Zhao, C.	Series and Character of Volcanic Rocks in Negari, Tibet, China
Ludington, S.	Methods for Comparing Major-Element Chemistry of Igneous Rocks
Reynolds, I. M.; Phillips, D.	An Occurrence of Mooihoekite and Haycockite in the Townlands Iron-Rich Ultramafic Pipe, Rustenburg, South Africa
Roeser, H.; Roeser, U.; Tobschall, H. J.; Schulz-Dobrick, B.	Petrology and Geochemistry of Archean Steatites from Central Brazil
Salpas, P. A.; Taylor, L. A.	Phlogopite: A Petrogenetic Indicator During Kimberlite Magmatism
Sato, H.	Chemical Composition of Orthopyroxene in the Bronzite Andesite of Goshikidai, Northeast Shikoku, Japan
Sobolev, N. V.	Rock-Forming Garnets of the Upper Mantle
Thy, P.; Moores, E. M.	Genesis and Formation of Oceanic Crust: Evidence from the Cyprus Crustal Study Project Drilling in the Plutonic Sequences of the Troodos Ophiolite

▲ THURSDAY POSTER SESSION: MINERALOGY AND PETROLOGY OF MAFIC AND ULTRAMAFIC ROCKS AND ASSOCIATED ORE DEPOSITS (continued)

Wang, F.; Wang, R.	The Characteristics of Mineral Chemistry and the Genesis of Rock-forming Minerals in the Kainozoic Basalts from Eastern China
Yu, Z.	The Occurrence of Some New Minerals in Platinum-Bearing Basic and Ultrabasic Rocks from Yan-San Region, China

▲ POSTER SESSION: MANTLE MINERALOGY — Thursday, July 17, 1986; 14:30-17:00

AUTHORS	TITLE
Cooper, E. A.; Mason, T. O.	Point Defects and Charge Transport in Fayalite and Olivine
Hirsch, L. M.; Wang, C.-Y.	Effects of Dislocations Upon the Electrical Conductivity of Olivine During High Temperature Creep Deformation
Kudoh, Y.; Ito, E.; Takeda, H.	Effect of Pressure on the Crystal Structure of Perovskite-Type $MgSiO_3$
Langer, K.; Chopin, C.	$Fe^{2+}Ti^{4+}$ Charge Transfer Between Face-Sharing Octahedra in Ellenbergerite, A New Silicate Formed at Mantle Depth
McCormick, T. C.; Smyth, J. R.	Geothermometry and Geobarometry for Kyanite Eclogites from Bellsbank and Roberts Victor Kimberlites
Rubie, D. C.; Champness, P. E.	An Experimental/TEM Study of the Olivine → Spinel Transformation with Implications for Transformational Plasticity
Sutherland, F. L.; Raynor, L. R.	The Spinel to Garnet Lherzolite Mantle Transition Beneath Eastern Australia, in Relation to a Hot Tasmanian Geotherm

ABSTRACTS

for the Symposia and Poster Sessions

of the 14th General Meeting

of the International

Mineralogical Association

[LISTED ALPHABETICALLY BY THE FAMILY NAME OF THE FIRST AUTHOR ON PAGES 41 - 284]

This meeting was supported in part by the National Science Foundation of the United States of America under Grant No. EAR-8519299.
"Any opinions, findings, and conclusions or recommendations expressed in this publication are those of the authors and do not reflect the views of the National Science Foundation, the International Mineralogical Association, or the Mineralogical Society of America." The abstracts printed herein were not reviewed.

ABSTRACTS

of papers submitted to the quadrennial meeting of the

International Mineralogical Association

Stanford University, Stanford, California, USA -- 13-18 July 1986

NOTE: Abstracts marked • had to be retyped; some were subjected to minor editorial revision.

ENERGETICS OF POLYTYPISM IN DI- AND TRIOCTAHEDRAL MICAS

ABBOTT, RICHARD N., Jr., Dept. of Geology, Appalachian State Univ., Boone, NC 28608, USA; BURNHAM, CHARLES W., Dept. of Geological Sciences, Harvard Univ., Cambridge, MA 02138, USA; POST, JEFFREY E., Dept. of Mineral Sciences, Smithsonian Institution, Washington, DC 20560, USA

Coulombic energies of model mica structures calculated using WMIN (Busing, 1981) are compared to assess the effects of Al/Si ordering, $OH^- \rightleftharpoons F^-$ exchange, and $2M_1$ vs 1M polytypism on the stabilities of dioctahedral and trioctahedral micas. These simplified structure energies depend only on unit cell geometry, atomic coordinates, and the formal charge assigned to each atom.

Unit cell geometries and atomic coordinates for the trioctahedral models were taken from structure refinements of coexisting 1M and $2M_1$ biotites (Takeda and Ross, 1975). The two polytypes differ significantly only in the stacking of layers. Two compositions were modelled for each polytype: $KMg_3AlSi_3O_{10}F_2$ and $KMg_3AlSi_3O_{10}(OH)_2$. In the latter model H was placed such that the O-H bond is normal to (001) with length 0.9Å (Giese, 1984).

The unit cells and atomic coordinates for the dioctahedral models were taken from a structure refinement of $2M_1$ muscovite (Richardson and Richardson, 1982). The 1M polytype was fabricated using the same structure stacked in the 1M fashion. Again two compositions were modelled: $KAl_2AlSi_3O_{10}F_2$ and $KAl_2AlSi_3O_{10}(OH)_2$. The model O-H bond lies 15° from (001) and directed toward the alkali cavity with length 0.9Å (Giese, 1984).

Calculations were carried out assuming local Al/Si ordering consistent with the principle of Al-avoidance and assuming all tetrahedral sheets have the same composition with Al:Si = 1:3. With these constraints there are 4 possible ordered arrangements for 1M polytypes and 8 for $2M_1$ polytypes (Abbott, 1984).

The calculations show the following: (1) For trioctahedral OH^- micas, the 1M polytype is roughly 1.75 kj/anion more stable than $2M_1$. (2) For the trioctahedral F^- micas, the energy difference is about 91 kj/anion in favor of 1M. (3) For dioctahedral OH^- or F^- micas the $2M_1$ polytype is 1.2 to 2.1 kj/anion more stable than 1M. (4) For a given polytype and octahedral sheet structure, various Al/Si ordered arrangements have slightly different energies, such that: (5) For $2M_1$ polytypes, the lowest energy arrangements (space groups $P2_1/n$, $P2_1$ and $P2_1/c$) maximize the closest interlayer Al-Al separation, while (6) for 1M polytypes, the lowest energy arrangement (space group $P2_1$) maximizes the closest intralayer Al-Al separation. The order of energies for different Al/Si ordered arrangements is the same as that predicted by independent means by Abbott (1984).

Because our models were based on refined structures of Al/Si disordered micas, energies were calculated assuming identical Al-O and Si-O tetrahedral distances. Atomic coordinates for the 1M-trioctahedral Al/Si ordered arrangements were adjusted by DLS refinement to test the influence of more realistic tetrahedral Al-O and Si-O bond lengths. These had a pronounced effect on the absolute energies but no effect on the relative energies, thus not affecting our conclusions.

F^- has a large stabilizing influence on the trioctahedral 1M polytype, though the 1M polytype is also favored for OH^- trioctahedral micas. The favored dioctahedral mica polytype is $2M_1$, and $F^- \rightleftharpoons OH^-$ exchange has little or no influence. Substitution of F^- for OH^- is thus much more important for trioctahedral than for dioctahedral micas. Given the difference in the position of the H in dioctahedral vs trioctahedral sheets, this result is reasonable because K^+-H^+ repulsion will be much greater in the latter. Al/Si ordering on tetrahedral sites has little influence on polytype energies. The principal factor determining the relative energies of 1M vs $2M_1$ polytypes appears to be the configuration of the octahedral layer, probably through its influence on distortions in the tetrahedral layers.

Abbott, R.N.,Jr. (1984) Can. Mineral. 22, 659-667.

Busing, W.R. (1981) U.S. Nat'l Technical Info. Service, ORNL-5747.

Giese, R. (1984) Reviews in Mineralogy 13, 105-144.

Richardson, S.M. and J.W. Richardson, Jr. (1982) Am. Mineral. 67, 69-75.

Takeda, H. and M. Ross (1975) Am. Mineral. 60, 1030-1040.

MOSSBAUER CHARACTERIZATION OF SITE OCCUPANCIES IN SYNTHETIC ALLANITE, $CaREEFeAl_2Si_3O_{12}(OH)$

AFFHOLTER, K.A.*, Dept. of Geological Sciences, VPI&SU, Blacksburg, VA 24061, USA ; ANNERSTEN, H.S., Inst. of Geology, Box 555, Uppsala, SWEDEN. *Now at N.M. Museum of Natural History, P.O. Box 7010, Albuquerque, N.M. 87194, USA.

Site occupancies of iron in seven synthetic end-member allanites, $A_2M_3Si_3O_{12}(OH)$ (A = Ca, REE; M = Fe, Al), and a natural allanite have been analyzed by ^{57}Fe Mossbauer spectroscopy. Substitution of REE^{3+} into the A site of the allanite structure is compensated by simultaneous substitution of ferrous iron in the M(3) site. Distortion of this site is found to be sensitive to compositional changes giving rise to large variations of the ferric iron quadrupole splittings with different compositions. The allanites with REE = La, Ce, La-Ce, Sm, Gd, Dy, and Yb were synthesized hydrothermally (P = 5.5 kbar, T = 450°C to 650°C) with an approximate NNO buffer (i.e., the buffering effect from the Rene 41 pressure vessel).

As indicated by the Mossbauer parameters, iron in the synthetic allanites occurs in both the ferric and ferrous states. The absorption pattern having the smallest isomer shift (0.34-0.38 mm/s) is assigned to ferric iron. The extremely large quadrupole splitting suggests this cation is situated in a very distorted site, and thus ferric iron can be assigned to the M(3) site in allanite in agreement with earlier suggestions. Relatively large variations in the quadrupole splittings for the different compositions are observed for the ferric iron pattern. This indicates distortion of the M(3) site, in agreement with observed dramatic variations of the M-O distances in the M(3) polyhedra of epidote group minerals with changes in composition. In the natural allanite a second ferric iron pattern is observed. It has a considerably smaller quadrupole splitting which assigns this pattern to either the M(1) or M(2) sites.

Two ferrous iron patterns are resolved in the synthetic REE allanites (except La). One pattern with isomer shifts varying from 1.04 to 1.08 mm/s indicates an FeO_6 octahedra. This absorption pattern may be assigned to any of the M-sites, probably the M(3) site since the small splittings are indicative of a fairly distorted site, comparable to the M(2) site in orthopyroxene.

The second ferrous iron pattern is characterized by large isomer shift values (1.17 mm/s (Yb-allanite) to 1.30 mm/s (La-Ce-allanite)) approaching the values found for this cation in the large dodecahedron in silicate garnets. Since the isomer shift may be correlated with the size of the coordination polyhedra, this pattern is assigned to either of the large A sites (A1 or A2). This feature may reflect the increasing isomer shift with the increasing ionic radii of the REE substituted into the A site in the synthetic allanites. No ferrous iron is found in La allanite, suggesting the A site is too large to accommodate iron, La being the largest REE in this investigation. On the other hand, Yb allanite, having the REE with the smallest radius, shows ferrous iron in the smallest A site polyhedra. In fact, the structural formula obtained from the site assignments and area ratios of the absorption doublets in the Mossbauer spectra, indicate that the Yb is in the M site instead of the A(2) site. This observation is further supported by the lack of a Yb(A2)-OH stretching band at 3181 cm^{-1} in the infrared spectra of this sample.

APPLICATION OF SYNCHROTRON RADIATION TO HIGH PRESSURE/HIGH TEMPERATURE PHYSICS OF MANTLE MINERALS

AKIMOTO, S., Inst. for Solid State Physics, University of Tokyo, Minato-ku, Tokyo 106, Japan; YAGI, T., Res. Inst. for Iron, Steel and Other Metals, Tohoku University, Sendai 980, Japan

In order to study the behaviors of materials under high pressure and temperature, x-ray diffraction study gives us the most fundamental and important information. It gives us knowledge of the equations of state (P-V-T relations) of each phase, the locations of the phase boundary between two polymorphs in P-T space, and the crystal structures of high-pressure polymorphs. Recently, synchrotron radiation (SR) methods are beginning to replace classical x-ray methods in high pressure/high temperature *in-situ* x-ray observation. We can expect to perform high quality x-ray diffraction study in a short exposure time by using SR. For the past three years, a multiple-anvil type x-ray system called MAX 80 constructed at the SR facility in Japan (called Photon Factory) has been fully used for solving the problems related to the earth's mantle. A few examples of the application of MAX 80 system to mantle minerals are presented.

Equilibrium Phase Boundary Equilibrium phase boundary for the olivine-spinel transformation in Fe_2SiO_4 and for the garnet-perovskite transformation in $CaGeO_3$ was determined. *In-situ* measurements with an energy dispersive x-ray diffraction system enabled us to carry out dynamical observation of the transformation. In these measurements, a mixture of the low-pressure phase and the high-pressure phase was kept at the desired P-T condition and the relative stability of these two phases was determined by observing the change in diffraction intensities of two phases. For Fe_2SiO_4 the olivine-spinel transformation pressure was determined as $P(GPa) = 2.71 + 2.58 \times 10^{-3}\ T(°C)$ between 800° and 1200°C. For $CaGeO_3$ the equilibrium phase boundary between the garnet and perovskite phases was determined as $P(GPa) = 6.9 - 8 \times 10^{-4}\ T(°C)$ between 900 and 1100°C. The negative P-T slope definitely established in the present study is in reasonable agreement with the value, -2.3×10^{-3} GPa/°C, that was calculated from the thermochemical data on the enthalpy of transformation. Since the pressure values used in the present measurements are based on the NaCl pressure scale, the phase boundaries determined in this work are recommended as reliable pressure fixed points at elevated temperatures.

Bulk Modulus and Thermal Expansivity Accurate determination of the equations of state of majorite (garnet/pyroxene solid solutions with the garnet structure) were carried out using SR methods. The samples studied are pure pyrope, 58 % enstatite 42 % pyrope solid solution, pure almandine and 25 % ferrosilite 75 % almandine solid solution. It was found that the bulk modulus of majorite is a little smaller than that of the pyrope or almandine endmember. Thermal expansion of pyrope and 58 % En-garnet was also measured at 6 GPa. It was found that thermal expansion does not show a significant change neither with composition nor with pressure in these garnets. Thermal expansion data on Fe_2SiO_4 spinel at 6 GPa are also presented. By comparing the present data with those taken at atmospheric pressure using high-temperature four-circle diffractometer, it is emphasized that the reliable thermal expansion data of a high-pressure phase must be taken at pressure conditions where that phase is thermodynamically stable.

THE STRUCTURE GEOMETRY OF FRAMEWORK SILICATES AND THE ALUMINUM FRACTION IN THE TETRAHEDRA

ALBERTI,A., GOTTARDI,G., Istituto di Mineralogia e Petrologia, Università di Modena, Via S. Eufemia 19, 41100 Modena, Italy.

Alberti and Gottardi (1985) showed that the average Al content in a zeolite as deduced from interatomic distances via Jones' curve (1968) is sistematically lower (ca 5%) than the Al content given by the chemical analysis, if the (Si,Al) distribution is disordered; on the contrary the agreement is satisfactory in the case of an ordered distribution. They attributed this systematic error in the bond length relative to framework oxygen atoms having static disorder due to the disordered (Si,Al) distribution, and showed that this error, and the related underestimation of Al content, increases: a) when the T-O-T angle increases; b) when the (Si,Al) distribution in the T sites is completely random; c) when, in a T-O-T bond, the disordered oxygen sites do not lie in the bond plane. Considering an initial Al content of 25%, a completely disordered (Si,Al) distribution could produce a calculated Al content of 24% with a T-O-T angle of 120°, and only 13% with a T-O-T angle of 180°.

Starting from this result a computer program has been written assuming that:

1. the "Loewenstein rule" is true
2. the Si-Al substitution does not change the coordinates of the tetrahedral cation
3. the coordinates of a framework oxygen given by the X-ray structure refinement correspond to the center of gravity of the sites occupied by the oxygen atom upon Al substitution in the tetrahedral positions. The oxygen sites have been weighted according to their occupancies
4. the sites occupied by the disordered oxygen have been calculated assuming the Si-O distance/Si-O-Si angle relationship given by Hill and Gibbs (1979) for the silica polymorphs

$$d(Si\text{-}O) = 1.526 - 0.068 \sec(Si\text{-}O\text{-}Si)$$

and the Al-O distance/Al-O-Si angle relationship

$$d(Al\text{-}O) = 1.699 - 0.044 \sec(Al\text{-}O\text{-}Si)$$

obtained by regression analysis on a large number of experimental data
5. the Al content in a tetrahedron is determined as the one giving a calculated mean T-O distance equal to the one obtained by the X-ray refinement. The total content is the average of the four Al fractions contributed by the four tetrahedral bonds.

With these assumptions, the Al content has been calculated for many framework silicates: the differences between the Al content calculated with this method and with Jones' relationship in a single tetrahedron are between -2% and +10%. For the whole structure of a disordered zeolite, the Al content calculated with this method is normally in good agreement with the chemical value, and nearly 5% higher than the Jones' value. The results for disordered alkali-feldspars are less satisfactory, probably because of the inadequacy of the relationship used to calculate (Si-O) distance.

Alberti,A., Gottardi,G. (1985) Zeolites - Synthesis, Structure, Technology and Application. pp 255-261. B.Drzaj, S.Hocevar, S.Pejovnik (eds.) Elsevier
Jones,J.B. (1968) Acta Cryst. B24, 355
Hill,R.J., Gibbs,G.V. (1979) Acta Cryst. B35, 25

PETROLOGICAL AND CHEMICAL STUDY OF A PYROXENITIC KOMATIITE SILL AND BASAL SULFIDE LENS, MUNRO TOWNSHIP, ONTARIO, CANADA

Allen, R.L. & Roeder, P.L., Dept. of Geological Sciences, Queen's University, Kingston, Ontario, K7L 3N6, CANADA

Dee's Sill is a layered pyroxenitic komatiite that varies in composition from a basal peridotite to an upper gabbro and contains a massive-sulfide lens on the basal contact. The sill was first described by N.T.Arndt (Ph.D, Univ. of Toronto, 1975) and is located in west-central Munro Township near the stratigraphic base of the Munro Formation in the Abitibi Greenstone Belt (2.7Ga). The sill is intruded between andesite and basalt in a series of flows with the following stratigraphic sequence: felsite, andesite, Fe-rich tholeiitic basalt, peridotitic komatiite and pyroxenitic komatiite.

The sill has been serpentinized and metamorphosed from prehnite-pumpellyite to lower greenschist grade, thus, all the original olivine and some of the pyroxene has been replaced by mainly lizardite. The recognition of olivine and altered pyroxene is based upon igneous textures and replacement mineralogy.

The sill occurs as three comagmatic lobes, separated by a 'pillar' of basalt and post-intrusive faults, and has a strike-length of 400m. It is petrologically layered, with gradational contacts separating layers. An apophysis from the top of the sill and local discordance with the surrounding extrusives demonstrate its intrusive origin, otherwise it is remarkably similar to Fred's Flow (Arndt; Can. J. Earth Sci., 1977), a layered pyroxenitic komatiite several kilometers

to the northeast. Thirty-five samples have been used to establish a columnar section across the thickest part of the sill (110m), including the massive-sulfide lens. Whole-rock chemistry and electron-microprobe analyses have been used to help document the chemical and mineralogical variation across the sill.

The **bottom chill zone** is less than one meter thick with 20-45% skeletal olivine microphenocrysts, euhedral chromite (1%), fine-grained alteration products and a MgO content of 17wt% (anhydrous). Above this is 10-30m of **peridotite** containing 60-75% serpentinized euhedral olivine, 15-20% anhedral, magnesian salite, 1/2-2% euhedral chromite and groundmass. This grades into 5-10m of **pyroxene peridotite** containing 40-50% serpentinized euhedral olivine, 5-15% serpentinized euhedral pyroxene, 20-30% anhedral salite, 1% chromite and groundmass. This in-turn grades into 3-5m of **pyroxenite** containing 35-60% serpentinized euhedral pyroxene, 0-10% embayed serpentinized olivine, anhedral augite, sphene and groundmass. The petrological and chemical variation continues from the ultramafic part of the sill into 20 to 65 meters of **gabbro** (the major unit at the top of the sill) which has 35-50% sub-euhedral plagioclase, 25-40% subhedral calcic augite, sphene, quartz and groundmass. The MgO content of the sill reachs a minimum in the gabbro (4-7% MgO), then increases along with Cr_2O_3 and NiO through the top of the gabbro and the marginal zone to the upper chill zone. Numerous quartz veinlets and a high silica content in the upper gabbro and the marginal zone are believed to be post-magmatic. The **marginal zone** is 2-6 meters thick and contains medium- to course-grained pyroxene phenocrysts that are often well aligned as spinifex. The pyroxene are skeletal and have composite mineralogy: a tube-like core, now replaced by lizardite + chlorite, lined inside and outside by augite. The marginal zone grades into a narrow (<1m) **upper chill zone** containing skeletal olivine, aluminous augite, chromite, groundmass and 17% MgO. Chlorite-filled amygdules occur near the upper contact and are typically surrounded by a layer of small chromite grains that are sometimes concentrated on one side of the amygdule. These may represent flotation of the chromite grains by gas bubbles. Layering in the sill is attributed to olivine and pyroxene crystallization and settling, and pyroxene accumulation at the roof (Kinzler & Groves; Am. Min., 1985), from an aphyric pyroxenitic magma, as represented by the chill zone.

The **massive-sulfide lens** (1 X 4m) occurs in a depression of the basal contact. The bottom contact of the sulfide lens is abrupt and pinches-out laterally. Sulfides decrease gradually upward into the peridotite, from matrix-textured ore, to intercumulus and disseminated sulfides. Near the bottom of the lens, sulfide surrounds serpentinized olivine-spinifex blades. The sulfide lens is predominately pyrrhotite with minor pentlandite, chalcopyrite, violarite, chromite and magnetite. It is composed mainly of iron and sulfur with sulfide concentrates having 1-2% Ni, 100-3500ppm Cu and 900-2000ppm Co. Below the sulfide lens and laterally along the sill's contact are found massive-sulfide spheroids (1-30mm diam.) with similar sulfide mineralogy and composition. The larger of these blebs are surrounded by large dendritic chromite grains with magnetite and sulfide inclusions. These distinctive chromite grains are only found beside the sulfide blebs and are believed to have at least partially crystallized from a sulfide-oxide melt, similar to certain chromites at Kambalda (Woolrich, Cowden & Giorgetta; Econ. Geol., 1981). It is believed that the sulfide blebs and the massive-sulfide lens represent the early separation of a sulfide-oxide melt from the pyroxenitic komatiite magma of the sill.

MICROHARDNESS MEASUREMENTS ON THE LARGEST WABAR METEORITE, SAUDI ARABIA

ALMOHANDIS, A.A., Dept. of Geology, King Saud University, Riyadh, Saudi Arabia.

This paper presents microhardness measurements on the largest meteorite specimen (2200 kg) ever found on the Arabian Peninsula near the main Wabar crater in the Empty Quarter, Saudi Arabia. The meteorite was discovered by the Arabian American Oil Company, ARAMCO in 1965 (Aber crombie, 1966). The meteorite is presently exhibited in front of the college of science, King Saud University at the new campus in Dirayah, Riyadh, Saudi Arabia.

The meteorite is an ablation-sculpted low cone, 156 cm x 110 cm with a thickness of 50 cm at the apex. It is dark gray in colour, mildly weathered, and has patches of remnant fusion crust.

The dominant metallographic structure of the meteorite is massive areas of kamacite containing small grain boundary schreibersites and rhabdites. The metallographic description and chemical analyses (Buchwald,1975; Clarke et al., 1981) indicate that the meteorite is typical of IIIA medium octahedrite.

The microhardness of the kamacite was measured using Vickers Company instrument in the laboratory of Department of Mineral Sciences, Smithsonian Institution, Washington, D.C., U.S.A. A grid of 37 impressions arranged in 4 horizontal rows was made on kamacite. This grid was measured immediately after it was completed then remeasured one day later.

The average VHN found for the first measurement was 208.5R + 12 and for the second measurement was 207.1R + 11. The kamacite in this meteorite has well-developed Neumann lines which are slightly deformed, so this kamacite has undergone some stress but not enough to produce an episolon structure.

REFERENCES

Abercrombie, T.J.(1966) Saudi Arabia, National Geographic, 129 (1): 1-53.

Buchwald, V.F. (1975) Handbook of Iron Meteorites, University of California Press, Berkeley, 1488 pp.

Clarke, R.S., Jr., Jarosewich, E. and Almohandis, A.A. (1981) Composition and metallography of two recently recovered Wabar meteorite specimens. Meteoritics, 16, P.303.

LAYER ORDERING IN INTERSTRATIFIED ILLITE/SMECTITE

ALTANER, Stephen P. and BETHKE, Craig M., Department of Geology, University of Illinois, Urbana, IL 61801

Layer arrangement in interstratified illite/smectite (I/S) has often been described mathematically using Markov statistics. This statistical theory provides the basis for modeling X-ray diffraction (XRD) patterns of interstratified clays (e.g., Reynolds, 1980), as well as the basis for studies of the thermodynamic and kinetic properties of I/S. According to this application of Markov theory, illite and smectite layers are arranged along the c* crystallographic axis and form MacEwan crystallites. Illite layers center on anhydrous interlayers; smectites span hydrous interlayers. Markov coefficients describe interactions between illite and smectite layers within MacEwan crystallites; layer ordering depends on the values of these terms.

Nadeau et al. (1985) used a transmission electron microscope (TEM) study to provide an alternative description of layer ordering in I/S. Their study showed that I/S is composed of "fundamental particles" of varying sizes. These particles are smaller than the MacEwan crystallites inferred from XRD studies. Nadeau et al. proposed that the surfaces of fundamental particles are hydrated, so that accumulations of particles behave as MacEwan crystallites. In this theory, illite layers fall across interlayers within particles, whereas smectite layers center on the hydrated region between particles. Layer ordering results from the size distribution of fundamental particles.

Many mineralogists believe that the fundamental particle concept contradicts the Markov description of layer ordering. We used a stochastic technique to test the relationship between these theories. By building MacEwan crystallites according to Markov theory and analyzing the size distributions therein, we synthesized particle size distributions.

Our calculated distributions for randomly interlayered and short-range ordered I/S agree quantitatively with distributions measured by Nadeau et al. This suggests that both Markov theory and particle size distributions describe correctly the layer ordering in most I/S. Our calculated distributions do not match TEM observation for I/S with long-range ordering; Markov theory seems to describe poorly this type of I/S.

REFERENCES

Reynolds, R. C. (1980) Interstratified clay minerals: in Crystal Structures of Clay Minerals and their X-ray Identification, Brindley, G. W. and Brown, G., eds., Min. Soc., London, 249-303.

Nadeau, P. H., Wilson, M. J., McHardy, W. J. and Tait, J. M. (1985) The conversion of smectite to illite during diagenesis, evidence from some illitic clays from bentonites and sandstones: Min. Mag., 49, 393-400.

ELECTRON MICROSCOPIC STUDY OF GLAUCONITIZATION PROCESS

AMOURIC M. and PARRON C., CRMC2, Campus de Luminy, case 913, 13288 Marseille cedex 09, France

Classically, according to previous X-ray diffraction and chemical data, the dominant mineral in glauconite pellets is an iron-rich, mixed-layer mineral, structurally similar to interstratified illite-smectite. Thus glauconite should be a mixture of high-charge mica-like layers and low-charge, smectite-like layers (Hower, 1961 ; Burst, 1958a). So, to document eventual interstratificiation phenomena in glauconite minerals and to produce further information about the glauconitization process, HRTEM has been carried out on glauconite microstructures.

Pellets, the purest in glauconite, were electromagnetically separated and very thin slices of these pellets were prepared by means of ultramicrotoming and ion-thinning techniques. One-dimensionnal images were mainly analysed, showing the characteristic 00ℓ basal lattice fringes of the main mineral phases present and their relation (Amouric and Parron, 1985).

About the structure, typical glauconite appears to have a characteristic mica architecture (d(00ℓ)~10Å). The polytypic behaviour (1M and 1Md) of this dioctaedral mica is similar to that of a trioctahedral one (Appelo, 1978). The $2M_1$ polytype, though rare, is demonstrated here for the first time.

The texture of the glauconite pellets is characterized by a "spindle-arrangement" of the mica crystallites. These spindles form the automorphous lamellae of evolved glauconite grains revealed with SEM (Odin, 1975). In the spindles, glauconite crystallites are always well-contrasted, exhibit a regular structural organization, show clearly individualized forms with growth steps and important lateral developments. These features indicate a phase which develops through a layer growth mechanism.

Inside the lamellae, a mineralogically unidentified layered phase "(X-phase)" with d(00ℓ)~12.5 Å genetically precedes the appearance of glauconite crystallites. Indeed, the X-phase shows all characteristics of a progressive destabilization to an amorphous product (A). This amorphous product (A) generally marks a front of lateral evolution between the X-phase and the well-structured mica phase. The observed X-phase may correspond to the nontronitic-phase reported during the glauconitization process by many authors (Wermund, 1961 ; Velde, 1976).

The occurence of a gel-like material, often surrounding the composite glauconite-X phase lamellae, suggests that the X-phase may previously crystallize from this gel.

Lastly it appears clearly that glauconite crystallites are never interlayered with other phases.

To sum up, the present study reveals that glauconitization constitutes an evolutionary process in which the earliest stage comprises the formation, -probably from a gel-, of a ~ 12.5 Å phase and its subsequent destabilization. Then, crystallization of pure glauconite occurs at the expense of 12.5 Å phase. These observations well support the "neoformation theory" about the glauconitization process (Millot, 1970 ; Odin, 1975 ; Odom, 1976).

Amouric M. et Parron C. (1985).Clays and Clay Miner., vol. 33, 6, 473
Appelo C.A.J. (1978), Thesis, Univ. Amsterdam
Burst J.F. (1958a), Amer. Miner. 43, 481
Hower J. (1961), Amer. Miner. 46, 313
Millot G. (1970), Geology of Clays, Springer Verlag, New York
Odin G.S. (1975), Thesis, Univ. Paris
Odom, I.E. (1976), Clays and Clay Miner. 24, 232
Velde B. (1976), Miner. Mag. 40, 753
Wermund E.G. (1961), Bull. Amer. Assoc. Pet. Geol. 45, 1667

MÖSSBAUER SPECTROSCOPY AND CHARGE TRANSFER PHENOMENA OF GARNETS.

AMTHAUER,G., Institute of Geosciences, University of Salzburg, 5020 Salzburg, Austria.

Most of the Mössbauer work done on silicate garnets deals with ^{57}Fe, which is found to occupy all the three crystallographically different cation positions of the garnet structure: the eightfold coordinated X-, the sixfold coordinated Y-,and the fourfold coordinated Z-site. Only a few Mössbauer investigations are performed on ^{119}Sn in andradites $Ca_3Fe_2^{3+}Si_3O_{12}$ and show, that Sn is fourvalent and in the Y-positions.As indicated by typical values of the isomer shift and the quadrupole splitting Fe^{3+} occupies the Y-sites and in the case of silicon deficiency also the Z-sites. The distribution of Fe^{3+} between the Y- and Z-positions is temperature dependent; at high temperatures the distribution is more disordered. The Fe^{3+}-exchange starts above ca. 600 °C. In synthetic hydroandradites, where Si^{4+} is replaced by H^+, Fe^{3+} is completely ordered in the octahedral sites.
There is general agreement, that Fe^{2+} occupies the X- and Y-sites as revealed by two different quadrupole doublets with characteristic Mössbauer parameters.However, in natural Ti-rich garnets an additional quadrupole doublet is observed the interpretation of which is still problematic. On the basis of its Mössbauer parameters and general crystal chemical arguments it was assigned on the one hand to $Fe^{2+}(X)$ $Fe^{3+}(Z)$ electron delocalization (Schwartz et al.,1980) on the other hand to Fe^{2+} at the Z-positions (Amthauer et al.,1977). Recent studies on Ti-andradites hydrothermally synthesized at low oxygen fugacities (Amthauer et al.,1985) support an assignment of this doublet to Fe^{2+} at the Z-positions, because in these synthetic garnets the X-sites are completely filled by Ca^{2+}. Additional evidence for this interpretation is found in the optical absorption spectra of Ti- and Fe-rich garnets and their temperature dependence.
Below 20 K andradite as well as almandine $Fe_3^{2+}Al_2Si_3O_{12}$ show the presence of magnetic ordering in their Mössbauer spectra (Murad, 1984; this work).From these spectra the signs of the quadrupole interaction can be determined and compared to those measured at ambient temperature in an applied magnetic field.

References:
Amthauer,G., Annersten,H., Hafner,S.S.(1977)Phys Chem Min 1,399
Amthauer,G., Fehr,K.T., Huckenholz,H.G., Kühberger,A. (1985) Fortschr Miner 63,7
Murad,E.(1984) Amer Miner 69,722
Schwartz,K.B., Nolet,A., Burns,R.G.(1980) Amer Miner 65,142

MINERALOGY AND THE CONDITIONS OF SYNNYRITE ORIGIN

ANDREEV G.V., Geological Institute, Ulan-Ude, 670015, USSR

A new rock named synnyrite was found in the Synnyr plutonic plug in North TransBaikalia in the late sixties. The Synnyr plug has an isometrical form in the plan. Its cross dimensions vary from 23 to 26 km. The plug has concentric-zoned structure. A stock of pulaskites and hedrumites is exposed in the central part of the plug. It is surrounded by a pipe-lake body formed by nepheline and pseudo-leucitic syenites and synnyrites. Body thickness varies from 3.5 km to 12 km. Three synnyrite bodies were found within the internal zone of the pipe-lake body on the contact with hedrumites: Malumninsky, Three Heads and Ushmunsky. Cross dimensions of these bodies are correspondingly equal to 7.0 and 2.7 km, 5.5 and 0.5 km, 1.5 and 0.9 km.

By appearance synnyrites are grey, light-grey and dark-grey, sometimes with a violet tint. Rock texture is massive, fluidal and gneisslake. Rock structure is dactyloscopic and micropegmatitic, sometimes hypidiomorphic. The main minerals are orthoclase, kalsilite, nepheline, biotite and piroxene. Magnetite, sphene, apatite and others were established as accessory ones.

The following peculiarities of the main minerals are shown. The orthoclase does not usually contain an albite component. Kalsilite is represented by a homogeneous potassium variety. Nepheline is characterized by a very high content of potassium component. The specific features of contents are typical for biotites and pyroxenes.

The fine melt inclusions are found in the minerals of synnyrites and pseudo-leucitic syenites. Their homogenization temperstures are 1100-1050 in pseudo-leucite, 1250-1150 in pyroxene, 1080-1020 in nepheline. The given figures indicate that the formation of rocks considered took place as a result of the crystallization of the high temperature melt. The pressure value is determined by different methods. It is 900-1300 atmospheres. The high content of potassium oxide up to 20.42 % (average 18%) is a distinctive feature of the chemism of synnyrites.

INCOMMENSURATE ORDERING IN MULLITE

ANGEL, R.J. & PREWITT, C.T., Dept. Earth & Space Sciences, State University of New York, Stony Brook, NY 11794-2100, USA.

Mullite is an aluminosilicate with variable composition $Al_2[Al_{2+2x}Si_{2-2x}]O_{10-x}$, $0<x<1$. This compositional variation is based upon the exchange $O^{-2} + 2Si^{+4} = 2Al^{+3}$ which introduces oxygen vacancies into the structure, and is accomodated by the development of a superstructure which is incommensurate relative to the average structure. The X-ray diffraction pattern of mullite therefore consists of maxima at Bragg positions, which arise from the average structure, together with pairs of satellites which are associated with the incommensurate modulation.

The average structure of a member of the mullite solid solution has been determined by refinement of X-ray diffraction data to a higher spatial resolution than previously achieved. The general features of the average structure identified by previous workers (eg. Burnham 1964) are confirmed; the structure may be derived from that of sillimanite by the removal of some oxygens from the structure, coupled with transfer of tetrahedrally co-ordinated atoms into a new site. In addition, the use of higher order temperature factors for two of the oxygen sites has enabled the small displacements of these atoms associated with Al/Si ordering on the tetrahedral sites to be identified.

Intensity data has also been collected for the satellite reflections, which occur around $1/2\underline{c}^*$ Bragg positions with a wave vector $\underline{q}=0.30\underline{a}^*$. Analysis of this data by Patterson synthesis has shown it to be incompatable with various anti-phase domain models for mullite proposed by other workers (Saalfeld 1979, Nakajima & Ribbe 1981, Yla-Jaaski & Nissen 1983). The satellite intensities were also analysed in terms of the Heine & McConnell (1984) theory of the origin of incommensurate structures in insulators. The plus and minus Patterson functions (McConnell & Heine 1984) identify the symmetries of the two component structures as those suggested by McConnell & Heine (1985). One component has the Al/Si ordering scheme of sillimanite, and also contains small displacements of tetrahedral and co-ordinating oxygen atoms. The other component has the symmetry of andalusite and iota-alumina, and orders oxygens and vacancies, as well as redistributing atoms between the two types of tetrahedral sites.

This study therefore confirms the general nature of the ordering schemes in mullite proposed by McConnell and Heine (1985). The stability of the mullite defect solid solution is thus due to the interaction of an oxygen/vacancy ordering scheme with two different Al/Si ordering schemes.

Burnham, C.W. (1964) CIWY, 63, 223-228.
Heine, V., & McConnell, J.D.C. (1984) J.Phys. C17, 1199-1220.
McConnell, J.D.C., & Heine, V. (1984) Acta Cryst. A40, 473-482.
McConnell, J.D.C., & Heine, V. (1985) Phys. Rev. B31, 6140-6142.
Nakajima, Y., & Ribbe, P.H. (1981) Amer. Mineral. 66, 142-147.
Saalfeld, H. (1979) Neues Jb. Miner. Abh. 134, 305-316.
Yla-Jaasaki, J., & Nissen, H-U. (1983) Phys. Chem. Min. 10, 47-54.

THERMODYNAMICS OF MULTICOMPONENT SOLID SOLUTIONS AND GEOTHERMOBAROMETRY

ARANOVICH, L.Ya., Institute of Experimental Mineralogy, USSR Academy of Sciences, Chernogolovka, Moscow distr., 142432, USSR.

Based on thermodynamic treatment of experimental phase equilibria and natural metamorphic assemblages, the analytical representation of the activity-composition relations has been obtained for

garnet $[Ca,Mg,Fe]_3(Al,Cr)_3Si_3O_{12}$(Gr),

cordierite $[Mg,Fe]_2Al_4Si_5O_{18} \cdot n(H_2O,CO_2)$(Cor),

orthopyroxene $[Fe,Mg,Al](Al,Si)O_3$(Opx) and

biotite $K[Mg,Fe,Al]_3(Al,Si)_4O_{10}(OH,F)$(Bi).

The values of corresponding energetic parameters are given in the table. Using these parameters the internally consistent set of geothermometers and geobarometers has been derived which includes:

Geothermometers	ΔG° for 1 exchangeable g/at. of Fe-Mg
Gr - Bi	- 7997 + 5.818T - 0.038P(bar)
Gr - Cor	- 6134 + 2.668T - 0.035P
Gr - Opx	- 4766 + 2.654T - 0.023P
Bi - Opx	- 3232 + 3.164T - 0.015P
Geobarometers	**ΔG° for 1 net-transfer g/at. of Mg**
Gr + Cor + Sil + Qz	6 - 4.596T + 0.638P
Opx + Cor + Sil + Qz	1817 - 5.452T + 0.575P
Gr + Opx	1018 + 0.431T + 0.078P
Gr + Opx + Cor + Qz	- 1205 - 0.961T + 0.255P
Gr + Opx + Sil + Qz	- 1811 + 0.856T + 0.063P
Opx + Cor + Qz	- 6670 - 4.176T + 0.531P

The applications of the geothermobarometers in question are shown for some metapelites and ultrabasic xenoliths.

THERMODYNAMIC PARAMETERS OF SOLID SOLUTIONS AND COMPONENT REACTIONS (in calories)

GARNET

$W_{CaMg} = W_{MgCa} = 3300 - 1.5T$; $W_{FeMg} = W_{FeMn} = W_{MgMn} = 0$

$W_{CaFe} = -1178 + 0.89T$; $W_{FeCa} = 1067 - 5.2T$

Uvar + Pyr = Gros + Knor

$\Delta G^\circ = 29229 - 11.88T$

Uvar + Alm = Gros + Fe - Knor

$\Delta G^\circ = 25575 - 10.40T$

CORDIERITE

$Mg_2Al_4Si_5O_{18} + H_2O = Mg_2Al_4Si_5O_{18} \cdot H_2O$

$\Delta G^\circ = -11451 + 27.125T$

$Mg_2Al_4Si_5O_{18} + CO_2 = Mg_2Al_4Si_5O_{18} \cdot CO_2$

$\Delta G^\circ = -3835 + 25.29T$

BIOTITE

OH - Phl + F - Ann = F - Phl + OH - Ann

$\Delta G^\circ = -4905 - 6.438T - 0.049P$

OH - Phl + 1.5 OH-Sid = OH - Ann + 1.5 OH - Ist

$\Delta G^\circ = 2418 - 2.117T$

ORTHOPYROXENE

$W_{FeMg} = -2372 + 1.688T$

$W_{MgAl} = -1237$

$W_{FeAl} = -7212 + 1.340T$

CHANNEL OCCUPANCY, ORDERING AND OPTICAL PROPERTIES OF CORDIERITES

ARMBRUSTER, TH., Lab. chem. miner. Kristallogr., University of Bern, Freiestr. 3, CH-3012 Bern, Switzerland

Cordierite with the simplified formula $(Mg,Fe)_2Al_4Si_5O_{18}$ possesses a tetrahedral framework structure. Striking is the presence of cavities (ca. 4 Å in diameter) which are connected by narrow bottle necks (ca. 2.6 Å in diameter) to form endless channels. The optical variation of this mineral is caused by chemical and structural reasons.

a) Effect of Si, Al-ordering

Two cordierite modifications are structurally established: high-cordierite (SPG: P6/mcc, Z=2) and low-cordierite (SPG: Cccm, Z=4). High-cordierites possess a random Si, Al-distribution within the bottle neck forming rings of tetrahedra. In contrast, low-cordierites show a well ordered distribution. Characteristic of high-cordierites are growth zoning and sectors, resembling a twinning pattern.

Synthetic hexagonal Mg-cordierite reveals $n_a = 1.5291$, $n_c = 1.5244$, whereas low-cordierite with the same chemical composition has $n_a = 1.5253$, $n_b = 1.5237$, $n_c = 1.5214$, $2V_x = 88^\circ$ (Armbruster and Bloss 1981). If cordierite crystallizes as high-cordierite and subsequently transforms to low-cordierite a sector twinning pattern may remain.

b) Effect of Mg, Fe, and Mn in octahedral coordination

Optical variation due to different Mg, Fe, Mn amounts can only be studied in Na-poor, degassed samples. With increasing Fe, Mn-content the refractive indices and the birefringence increase (Selkregg and Bloss 1980). A Fe-cordierite (degassed) has $n_a = 1.568$, $n_b = 1.558$, $n_c = 1.550$, $2V_x \approx 85^\circ$.

c) Effect of Na incorporation

Charge deficit due to $Be^{2+} \rightarrow Al^{3+}$, $Al^{3+} \rightarrow Si^{4+}$ and $Li^{+} \rightarrow$ (Mg, Fe, Mn) partial substitution is mainly responsible for Na which balances the charges and centers the six-membered rings of tetrahedra. Degassed Na-bearing cordierites have higher refractive indices than Na-poor degassed crystals with the same Mg, Fe, Mn-content in octahedral coordination (Selkregg and Bloss 1980, Armbruster and Irouschek 1983). In addition, the optic axial angle of Na-rich crystals is significantly lower than of Na-poor ones.

d) Effect of volatiles in the structural cavities

Cordierites which are nearly identical in the parameters discussed under a) - c) may still show different optical properties due to varying amounts and ratios of multiple volatiles in the structural cavities. Most important in natural samples is the H_2O content. While the refractive indices increase with H_2O content, the optic axial angle decreases significantly and the birefringence increases slightly (Armbruster and Bloss 1982).

Volatiles with electron density distributions close to a sphere (e.g. noble gasses) cause similar optical effects as water (Armbruster 1985). Volatiles with anisotropic shape (e.g. rod-shaped molecules: CO_2, N_2) lead to an increased refractive index in the direction of prefered "rod alignment" and thus cause a high optic angle and birefringence (Armbruster 1985). CO_2-rich cordierites are of special importance in granulite facies rocks.

ARMBRUSTER, TH. (1985) Phys. Chem. Minerals, 12, 233-245.

ARMBRUSTER, TH. and BLOSS, F.D. (1981) Contrib. Miner. Petrol., 77, 332-336.

ARMBRUSTER, TH. and BLOSS, F.D. (1982) Amer. Mineral., 67, 284-291.

ARMBRUSTER, TH. and IROUSCHEK, A. (1983) Contrib. Miner. Petrol., 82, 389-396.

SELKREGG, K.R. and BLOSS, F.D. (1980) Amer. Mineral., 65, 522-533.

MINERALOGY AND ELECTRON MICROSCOPY OF REFRACTORY INCLUSIONS IN CARBONACEOUS METEORITES

ARMSTRONG, J. T., Div. of Geological and Planetary Sciences, California Institute of Technology, Pasadena, CA 91125, USA

Carbonaceous chondrites contain some of the most primitive, least altered materials that formed at the beginning of solar system history. Important constituents of many of these meteorites are mm- to cm-sized inclusions called CAIs that contain refractory Ca-, Al-rich phases. A number of these phases are similar to those calculated to be the first major oxides to have condensed from the cooling solar nebular gas. A variety of isotopic anomalies are observed in these inclusions including excesses of the daughter products of short-lived radionuclides, such as ^{26}Al, suggesting that CAIs were isolated very early in solar system history and never rehomogenized isotopically with later formed materials.

The major phases found in CAIs include hibonite, spinel, anorthite, melilite and Ti-rich fassaite pyroxene. Accessory minerals include perovskite, diopside, wollastonite, grossular, nepheline, sodalite and hercynite/pleonaste. Spinel, hibonite and pyroxene are distinguished from their terrestrial analogues by the relatively high amounts of V_2O_3 (0.3-3% by wt.) that they typically contain. Fassaitic pyroxenes in CAIs differ from terrestrial in containing ~75% of Ti as Ti^{+3}. Hibonites in CAIs are distinguished by exhibiting strong coupled substitution of $Mg^{+2}+Ti^{+4}$ for $2(Al^{+3},V^{+3})$ and by the preferential location of V^{+3} and Ti^{+3} in the trigonal bipyramidal sites in the crystal (Ti^{+3} in this site apparently giving rise to the unique blue color of these hibonites, e.g. 1). Ti^{+3}/Ti^{+4} in hibonites has recently been shown to be a useful oxygen cosmobarometer for the formation of CAIs [2].

Also contained in CAIs are small (μm- to mm-sized) complex aggregates of very fine-grained opaque minerals known as Fremdlinge [3]. Recent detailed analytical and electron microscope studies of these assemblages indicate that they were the first solid phases to form in CAIs and that their unique mineralogy places significant constraints on the possible mechanisms of formation and cooling of CAIs [e.g. 4-7]. Many of the phases in Fremdlinge are found nowhere else in meteorites and some have no terrestrial analogues. The rather bizarre nature of Fremdlinge led some investigators to suggest that they formed in the interstellar medium, but recent isotopic investigations suggest that these objects formed in the solar nebula during early solar system history [8].

The major phases found in Fremdlinge include Pt-rich NiFe metal (typically Ni_2Fe-Ni_3Fe), OsRuRe and PtIr alloys, coulsonite (FeV_2O_4)-magnetite solid solutions, Ni-poor pentlandite, Ru-bearing pyrhottite and troilite, molybdenite, whitlockite and chlorapatite. A variety of accessory and trace phases have been identified including scheelite, heazlewoodite, WS_2, NiPt alloys, Ni_5P_2 and Ni_4 (Ge,Sn)(S,Te). Fremdlinge are often found surrounding by narrow rims of fine-grained, V-rich fassaitic pyroxene (up to 15% V_2O_3), and diffusive reaction of Fremdlinge with neighboring spinels forming coulsonite-pleonaste solid solutions is sometimes observed.

Some Fremdlinge appear texturally and mineralogically to be unequilibrated, while others show strong evidence of secondary reequilibration [4,5,7]. Recent studies indicate that many sulfide-rich Fremdlinge formed by in-situ sulfidization of metal-magnetite Fremdling precursors [5,7]. The mineralogy of primary Fremdlinge suggest that these objects formed by aggregation of material formed, prior to incorporation in CAI, by different processes that included oxidation and reduction both at high and low T, thus requiring turbulent mixing processes in the early nebula. Maximum T and minimum cooling rates of CAIs after Fremdling incorporation, as estimated from observed phase assemblages and compositional gradients in Fremdlinge, are at best only marginally in accord with those calculated for the major oxide and silicate phases [4,7]. The formation and survival of Fremdlinge in CAIs remains a formidable enigma in the understanding of early solar nebula processes.

Refs.: [1] Ihinger and Stolper, Earth Planet. Sci. Lett., 1986, in press. [2] Live et al., Lunar Planet. Sci. (LPS) XVII, 488, 1986. [3] El Goresy et al., Proc. Lunar Sci. Conf. 9th, 1279, 1977. [4] Armstrong et al., Geochim. Cosmochim. Acta 49, 1001, 1985. [5] Armstrong et al., LPS XVI, 15, 1985. [6] Armstrong et al., Meteoritics 20, 603, 1985. [7] Armstrong et al., LPS XVII, 13, 1986. [8] Hutcheon et al., LPS XVI, 384, 1985.

MINERALOGICAL EVIDENCE FOR MAGMA MIXING IN THE MONT BLANC AND ELBA GRANITES - POSSIBLE GEOTECTONIC IMPLICATIONS.

AYRTON S. & BUSSY F., Inst. de Minéralogie, Collège propédeutique University of Lausanne, 1015 Dorigny, Switzerland.

In a comparative study between the Upper Paleozoic (probably Permian) Mt. Blanc and Upper Tertiary (Miocene) Elba granites, identical features indicating the mixing of magmas are conspicuous. These are namely:

-the abundance of dark fine-grained dioritic enclaves in both granites, suggesting the coexistence of two distinct magmas.

- the spherical or ellipsoidal form of the enclaves depending on whether the granite has an isotropic or fluidal structure, as well as common lobate outlines, pointing to liquid coexistence of two magmas with different viscosities.

- the invariably fine grain-size of the enclaves and the presence of acicular apatite indicate that thermal equilibrium was not established between the two magmas, and that the dioritic magma cooled rapidly in contact with the other. Immiscibility phenomena are therefore not considered in these occurrences.

- mixing related to this coexistence is mainly visible in the enclaves, which contain : (1) all the constituent minerals of the granite, as megacrysts relative to the fine-grained matrix of the enclave, sometimes saddling the interface; (2) metasedimentary xenoliths identical to others within the granite; (3) "enclaves-within-enclaves" or "internal enclaves" of granitic or dioritic composition. Up to 3-4 fine-grained enclaves may be imbricated, the enclosed enclave being systematically more basic than the enclosing lithology.

Mineralogical analysis of the enclaves confirms: (1) the igneous origin of the enclaves; (2) the foreign and granitic origin of the megacrysts (= xenocrysts), as they are identical to the mineral constituents of the granite; they almost all present signs of disequilibrium with the matrix of the enclave: quartz ocelli with reaction rims of biotite and alkali feldspar, spotted plagioclases, rounded alkali feldspars; they show a stage of final crystallisation in equilibrium with the enclave: poecilitic margins of the quartz grains, calcic shell of the plagioclases whose core has the composition of those of the granite, rapakivi envelope of the alkali feldspars with big or small oriented plagioclases. Only the biotites appear to have completely reequilibrated.

In the granite, indications take the form of small calcic plagioclases similar to those in the enclave and crystals of plagioclase and alkali feldspar with features identical to those of the megacrysts in the enclaves. The granite is itself the product of mixing, whose homogeneous nature is a reflection of the efficiency of the process. Mixing probably occurred at several stages of the magmatic evolution of these plutons (especially the Mt Blanc), repeatedly involving previously hybridized and variably differentiated magmas.

Geochemical analysis under way appears to confirm this view.

The same features exist in the vast majority of granitoids from any geological period, and within virtually any geological context: the Mt. Blanc granite may be related to the waning stages of the Variscan cycle or to the embryonic manifestations of Alpine events, and was not emplaced near a continental margin. The Elba granite, which intruded the Ligurian-Toscan nappe pile, appears to be the result of mantle-related magmatism, which produced the "Etruscan Swell" during the terminal stages of the Appenine orogeny. Magma mixing is evident in the Mesozoic batholiths of the American cordilleras, and in island arcs. Rapakivis, which are good indicators of the mixing of magmas, formed at different times during the history of the Earth, mainly but perhaps not exclusively at the beginning and at the end of orogenic events, or between orogenic cycles.

Clearly, mantle-derived basic liquids play an important role in the genesis and evolution of granitoids, most of which are probably of crustal origin.

PETROLOGIC EVIDENCE FOR RECHARGE AND CONVECTIVE MIXING IN THE MAGMA CHAMBER OF MOUNT MAZAMA BEFORE ITS CATASTROPHIC ZONED ERUPTION AND THE COLLAPSE OF CRATER LAKE CALDERA, OREGON

BACON, C. R., U.S. Geological Survey, Menlo Park, CA 94025, USA; DRUITT, T. H.*, NATO Postdoctoral Fellow, U.S. Geological Survey, Menlo Park, CA 94025, USA

The 6845±50-BP climactic eruption of Mount Mazama vented ~50 km^3 of magma, dominantly homogeneous rhyodacite (RD; 70.4±0.3% SiO_2) followed by subordinate andesite and mafic-cumulate scoriae (60.5 to 51.4% SiO_2). We will show that the most silicic RD erupted from the Llao Rock vent ~200 yr before caldera formation and that climactic RD pumice contains admixed magma compositionally distinct from the parent of earlier RD. The magma chamber either (1) contained zoned RD underlain by mixed RD and all of the zoned RD vented in the Llao eruption, or (2) was recharged with mafic magma shortly before the Llao eruption, causing convective mixing and homogenization of the silicic volume.

Mount Mazama consists mainly of andesite and dacite erupted between ~400 and 50 ka. Calcalkaline basalt and andesite, and minor tholeiite, were erupted from nearby vents throughout Mazama's history. Rhyodacite flows (71.6-70.4% SiO_2) were emplaced between ~30 and ~20 ka, probably from a contiguous chamber beneath Mazama. The Llao Rock zoned eruption vented RD pumice (72.2-70.0% SiO_2) at 7015±45 BP and RD lava with andesitic inclusions. The Cleetwood RD flow (70.7-70.0% SiO_2) erupted later and was still hot when the climactic eruption started. Climactic deposits, in order of eruption, are: RD fall deposit, welded RD ignimbrite, and zoned ignimbrite.

Climactic scoriae are of two chemical types characterized by different trace element abundances exemplified by Sr content. High-Sr scoriae (HS) occur beneath low-Sr scoriae (LS) in the zoned ignimbrite and are rare constituents of the fall deposit. Minor and trace element data show that LS and HS originated from different calcalkaline basalt parents. Low-Sr inclusions occur in 20-30 ka RD, and HS in Holocene RD. Variable proportions of pl ± opx ± cpx ± hb ± ol ± mt ± il ± ap account for 30-70 wt% of scoriae, many of which are cumulates; RD contains up to 12% pl + opx + cpx ± hb + mt + il + ap ± zc. High-Sr scoriae have hb>px, and Sr-rich pl and glass; LS have hb<px, and Sr-poor pl and glass. Partly melted granitoid blocks (GR) are common in upper zoned ignimbrite. Fe-Ti oxide Ts (Stormer 1983; Andersen and Lindsley 1985) are: preclimactic RD 850-880°C; Cleetwood RD and all climactic RD pumices 880°C; HS 880-890°C; LS 890-915°C; GR 940-975°C. Scoria glass composition (61.4-72.0% SiO_2) vs. oxide T plots suggest Ts for some ol-rich, il-free scoriae of >935°C. Low-Sr scoriae and preclimactic RD fO_2 was ~0.4 log units lower than HS and climactic pumice. Scoria crystal content increases and glass SiO_2 decreases with increasing T. Glass compositions show that magmas were derived mainly by fractional crystallization, and that differentiated preclimactic RD was not derived from climactic-composition RD but from LS magma.

Inferred T and compositional gradients imply mafic cumulates formed in a floored chamber, and silicic magma formed by buoyant rise of residual liquid. Ages of inclusion-bearing RD and the eruptive sequence suggest: (a) zoned RD overlay LS magma and cumulates in the early chamber; (b) recharge with HS magma, that ponded between LS and RD, <20 ka; (c) convective overturn of RD and mixing with ≤12% HS magma to produce climactic RD. Reversely zoned pyroxenes in climactic, Cleetwood, and late Llao RD but not in other RD support (c). Recharge may have occurred many times, leading to steady-state conditions of zoned RD overlying convectively mixed RD long before the Llao eruption; all zoned RD would have vented in the Llao eruption. Alternatively, the Llao eruption may have taken place during or shortly after a recharge event that destroyed stable zonation. If this is the case, the caldera-forming event took place <200 yr after recharge.

*now at Dept of Geology, University of Liverpool, Liverpool L69 3BX, UK

Andersen DJ and Lindsley DH (1985) EOS 66 no. 18 416
Stormer JC Jr (1983) Am Mineral 68 586-594

PECULIARITIES OF MAGMATIC ORE FORMATION IN GRANITE PEGMATITES (ACCORDING TO DATA OF INCLUSION STUDY)

BAKUMENKO I.T., Institute of Geology and Geophysics, Siberian Branch of the Academy of Sciences of the USSR, Novosibirsk, 630090, USSR

Thermobaric and fluid modes of granite pegmatite formation has been reconstructed by the study of a crystallized melt and associated fluid inclusions of magmatic step. Granite pegmatites of two types connected with rest magmas of granite massifs and anatectic melts obtained at metamorphism have been studied with O.N.Kosukhin and V.P.Chupin as co-authors (1,2).

Among chamber pegmatites of rest origin the crystallization step of weakly mineralized small non-industrial bodies is characterized by the highest temperature (above 650°C). Magmatic zones of pegmatites of useful ore formation are of low temperature. Topaz- and quartz-bearing pegmatites poor in fluor form at 650-600 °C, and those reach in fluor with piezoquartz and fluorite form at 600-550 °C. A magmatic step termination temperature of "miarolitic" pegmatites, intermediate between rare-metal and chamber ones, with coloured tourmalines is even lower (down to 520-500 °C). Irrespective of absolute values, a temperature difference between the beginning of peripheral aplitic zone crystallization and the termination of crystallization of rest magmas in central pegmatoid-block zones and cavities of magmatic step is constant (about 50-80 °C). The crystallization temperature ranges are much wider in external zones than in internal ones.

According to the measurements by V.P.Chupin (2), among the pegmatites of anatectic origin the pegmatite formations connected with granulitic facies metamorphism are characterized by the highest temperature (above 820 °C), and micaceous pegmatites are of the lowest temperature (640 °C). Other pegmatites of amphibolite facies occupy an intermediate position.

An increase in fluid pressure in melts crystallized at lower temperatures is typical of both rest and anatectic pegmatites. Water predominates in the fluide of rest chamber pegmatites, its content being varied from 3 to 10 wt% at a fluid pressure of 0.8-1 to 4-5 kbar. The melt crystallization temperature decreased further in miarolitic pegmatites in the result of accumulation of fluxing components. Water pressure in this case is lower than in chamber pegmatites, and CO_2 content in fluide is somewhat higher, which is typical only of high-temperature varieties of chamber pegmatites. In contrast to rest magmas, those of anatectite-pegmatite crystallize under more high-pressure conditions (5-9 kbar) and contain carbon dioxide in a higher concentration up to its predomination in high-temperature melts.

REFERENCES

1. I.T.Bakumenko Magmatic step of granite pegmatite formation (according to data of inclusion study). Mineralogicheskii zhurnal N 5, 1983, s.62-71, "Naukova dumka", Kiev.
2. O.N.Kosukhin, I.T.Bakumenko, V.P.Chupin Magmatic step of granite pegmatite formation. Trudy IGiG, vyp.476, "Nauka", Siberian Branch of the Academy of Sciences of the USSR, Novosibirsk, 1984, s.136.

MINERAL CHEMISTRY OF ILMENITE-BEARING ECLOGITE FROM MOUNTAIN CZERNICA IN THE POLISH CENTRAL SUDETES

BAKUN-CZUBAROW, N., Institute of Geological Sciences, Polish Academy of Sciences, Zwirki i Wigury 93, 02-089 Warszawa, POLAND

In the Polish Central Sudetes common eclogites occur in thin lithostratigraphic layers within granite gneisses. The eclogites are slightly differentiated in their basaltic chemical composition, modes, textures and fossil geothermic gradients of equilibration.

The ilmenite-bearing eclogite from Mountain Czernica differs distinctly from all the other Sudetic eclogites in its mineralogy and chemical composition. Such iron and titanium rich rocks are also extremely rarely found among the eclogites occurring in gneisses.

The main minerals of the Czernica eclogite are pyroxene symplectite, garnet and clinoamphiboles. Apatite, relict omphacite, biotite symplectite, light mica, ilmenite, rutile, titanite and zoisite occur in subordinate quantities or as accessories. Quartz and kyanite are lacking. Main microscopic features of the eclogite are: xenomorphic garnets full of inclusions of all the other minerals, common and almost complete replacement of omphacite by pyroxene-plagioclase symplectite, abundance of titanium minerals with primary titanite, ilmenite and ilmenite-rutile mosaic intergrowths.

The eclogite minerals were studied by means of electron microprobe in Geophysical Laboratory Carnegie Institution of Washington.

Garnets are extremely iron and calcium rich varietes among the other Sudetic eclogites. They display chemical zoning with Fe increasing and Mg decreasing outwards. The composition of garnets ranges within the following limits: from 45 to 55 mol % of almandine, from 30 to 38 mol % of calcium molecule and from 8 to 21 mol % of pyrope. Omphacites occurring in the form of armoured relics contain on average 30 mol % of jadeite, 3 mol % of acmite and about 5 mol % of eskolaite. From among clinoamphiboles occurring in both the forms as inclusions in garnets and as separate bigger blasts two varietes can be distinguished: primary karinthines being tschermakitic or pargasitic hornblende with distinct predominance of Mg over Fe in formulae and secondary subsilicic ferroan alumino-pargasites with Fe dominating over Mg. Pargasites also display very high content of tetrahedral Al, about 2.5 Al a.f.u. Gradual transitions between the two clinoamphiboles within separate blasts have also been observed. Ilmenite occurring in separate grains as well as in mosaic intergrowths with rutile possesses about 6 mol % of geikielite, 1 mol % of pirophanite and 5 mol % of hematite.

Two successive stages can be distinguished in metamorphic history of the Czernica eclogite:

(1) Eclogite stage: A lamprophyre being a product of highly fractionated tholeiitic magma was transformed into eclogite with garnet-omphacite-karinthine paragenesis with subordinate amounts of ilmenite, rutile, titanite and white mica; the only lamprophyre mineral stable was most likely apatite. The peak conditions of eclogite metamorphism estimated by means of garnet-clinopyroxene, garnet-amphibole, ilmenite-clinopyroxene geothermobarometers and jadeite barometer were 720 ± 30°C at minimum 15 kbars of total pressure. At the turn of this stage common symplectitization of omphacite took place.

(2) Post-eclogite stage: An decrease of total pressure and increase of water pressure caused the partial replacement of eclogite minerals by secondary clinoamphibole.

THE MINERALOGY OF THE TRACE ELEMENT-BEARING PHASES IN STACK FLY ASH FROM THERMAL POWER PLANTS IN THE F.R.G.

BAMBAUER, Hans Ulrich and Thomas HOLZAPFEL, Institut für Mineralogie, Westf. Wilhelms-Universität, 4400 Münster, Federal Republic of Germany

In power plants of the F.R.G. bitoumeneous coal is burned by two different combustion furnace systems: in dry bottom furnaces with burning-temperatures between 1100 - 1300 °C and in slag tap furnaces with burning-temperatures between 1300 - 1650 °C. The annual production of fly ash by these power plants actually amounts together about 5 Mill. tons. About 0.5 % of these solid residuals passes the pollution control devices (so-called "stack fly ash") and is emitted to the atmosphere.

It is well known that stack fly ash from slag tap furnace combustions have 2 - 5 times higher concentrations of many metal and trace elements (e.g. Zn, Pb, Cd) than stack fly ash from dry bottom units.

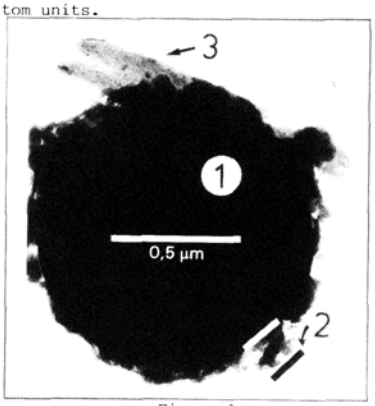

Figure 1

Earlier chemical analysis of trace element contents in unburned coal and coal fly ash showed significant enrichment of nearly all trace elements in the finely grained fly ash with a mean enrichment factor of about 10.

Figure 1 : typical glassy stack fly ash particle
1 = glassy alumosilicatic matrix
2 = "surface layer" (about 30 - 100 nm thick)
3 = crystalline "surface nodule" (anhydrite)

Up to now only few informations are available about possible independant trace element phases or alternative bonding of trace species in different components of stack fly ash. Data about composition and homogenity of the sub-micron ash particles are mostly lacking.

Our investigation on these topics were carried out for six different stack fly ashes from power plants with dry bottom and slag tap furnaces. The analyses were performed mainly with SEM,(S)TEM, EDS and LAMMA (Laser Micro-Mass Analyzer). Additional information about size distribution ahd crystalline phases of the stack fly ash was obtained by SEM-linked image analyzer resp. by XRPD-analysis.

Our results show that most particles are alumosilicatic glassy balls (Fig. 1) with diameters between 0.02 and some few tenth of microns. Part of the trace elements are bound in the glassy matrix (e.g. V, Cr, Mn, Co, Ni, Cu, Zn, As, Mo, Ag, Cd, Sn, Pb). Many fly ash particles are coated with surface layers or (crystalline) surface nodules which mainly consist of Ca-sulfates, Ca-phosphates and some Cl-bearing phases. In these surface phases we found Li, F, Sc, Ti, V, Cr, Mn, Fe, Co, Ni, Cu and Zn but we could not detect f.ex. Ga, Ge, As, Se, Mo, Cd, Sb, Hg or Tl. Beside glassy particles which may contain crystalline phases like mullite, quartz, hematite and magnetite there exist two different types of coky particles one of which is a trace element absorber (e.g. for As, Zn, Sn, Tl).

The trace element analysis of single micron- and sub-micron particles proved inhomogenity of the particle compositions but yielded no remarkable differences in trace element concentrations between micron- and sub-micron particles. We found in stack fly ash from dry bottom and slag tap furnaces only a slight enrichment for some elements (e.g. V, Cr, Zn, Co, Ni) with decreasing particle diameter.

APPLICATIONS OF SIMS, X-RAY PHOTOELECTRON AND AUGER SPECTROSCOPIES FOR STUDIES OF ADSORPTION, LEACHING AND DIFFUSION ON MINERAL SURFACES

BANCROFT, G. M., Department of Chemistry, University of Western Ontario, London, Ontario, Canada N6A 5B7

SIMS (Secondary Ion Mass Spectroscopy), X-ray Photoelectron Spectroscopy (XPS) and Auger Spectroscopy have become extremely useful for following surface chemical processes on minerals in considerable detail. The adsorption and chemical reactions of heavy metal (Pd, Hg, Au, Pt) complexes on sulphide minerals such as pyrite (FeS_2) is first discussed. Surface sulphide groups are shown to be necessary for initial adsorption of metal complexes. After the initial adsorption, Au(III) and Pd(II) species are reduced to the metals, while Pt(II) is not.[1,2]

The reduction is auto-catalyzed via an electrochemical process, and SEM and Auger photographs show the growth of the metals on the sulphides. Such adsorption/reduction could play an important role in the deposition of these metals in natural systems.

The leaching of titanite ($CaTiSiO_5$) will then be examined using XPS and SIMS. Titanite has been proposed as the ceramic component of the glass-ceramic host for the immobilization of nuclear fuel reprocessing wastes.[3-4] Central to this proposal is the argument that titanite can be in thermodynamic equilibrium with a range of groundwaters. Our experimental evidence for this thermodynamic argument is presented based on SIMS depth profiles of natural and synthetic titanites after leaching in deionized water, Ca^{2+}/Si^{4+} doped solutions and pure D_2O. From the absence of leaching in equilibrium solutions and evidence of titanite regrowth on adjacent mineral surfaces leached within the titanite stability field, it is concluded that the thermodynamic approach is valid under these conditions. Selective leaching of rare earths, and D diffusion into the titanites are also monitored by SIMS.

1. G. E. Jean and G. M. Bancroft, Geochimica and Cosmochimica Acta, 49, 979-987 (1985).
2. M. Hyland, G. M. Bancroft and N. S. McIntyre, to be published.
3. P. J. Hayward, F. E. Doern, E. V. Cecchetto and S. L. Mitchell, Can. Mineral., 21, 611-623 (1983).
4. G. M. Bancroft, J. B. Metson, S. M. Kanetkar and J. D. Brown, Nature, 299, 708-710 (1982), and to be published.

THE SIGNIFICANCE OF HYDROTHERMAL RECTORITE IN THE CALA ABAJO PORPHYRY COPPER DEPOSIT, PUERTO RICO

Arthur H. Barabas, Department of Geology, MS 24, California State University, Fresno, Fresno, California 93740

Rectorite, a regularly interstratified smectite-white mica, is widespread both in the hydrothermally altered, low-potassium tonalite host of the Cala Abajo porphyry copper deposit (Rio Vivi district, west central Puerto Rico) and in nearby altered wall rocks of similar bulk composition. It contains essential K, Mg, and Fe and approximately 30-35 % expandable layers. Rectorite constitutes an intermediate stage in the transformation of plagioclase to white mica by metasomatic additions of K, Mg, and H and removal of Ca and Na ions. It forms directly from plagioclase (Ca-rich zones first) or from the inital alteration products of plagioclase (dioctahedral smectite and epidote). The rectorite association defined here comprises rectorite and Fe-rich smectite in plagioclase and chlorite, pyrite (typically > 1 volume %), rutile, and magnetite in ferromagnesian sites. Rocks containing the association form a mappable unit developed between propylitically altered wall rocks to the southwest and porphyries with the white mica-rich, rectorite-poor alteration associated with the Cala Abajo ore zone. Rectorite also occurs in some rocks with advanced argillic alteration.

At room temperature, both two-phase aqueous fluids and saturated brines occur in fluid inclusions (Types I and II, respectively). For Type I inclusions homogenization temperatures are typically 310-340° C and salinities are 2.4 to 8.6 wt. % equivalent NaCl. For Type II inclusions, halite dissolution temperatures (T_S), which range from 270 to greater than 600° C, are generally greater than homogenization temperatures (230-310° C). The corresponding salinities (36 to greater than 77 weight percent NaCl equivalent) for Type II inclusions indicate that suspended halite crystals were present during trapping. Trapping temperatures of 320-385° C are inferred from T_S measurements for those Type II inclusions believed to have trapped brine without halite. Pressures of 70-535 bars correspond with these temperatures. If the temperature of rectorite stability is coincident with that of pyrophyllite, as most occurrences suggest, the isochores for the Type I inclusions suggest trapping at maximum temperatures of 310-360 ° C and pressures of 50-570 bars. Although their relative ages are not known, the P-T conditions appear to have been similar for the trapping of both Type I and II fluids.

ORIGIN AND EVOLUTION OF MAFIC MAGMATIC ENCLAVES AND MAFIC ROCKS ASSOCIATED WITH SOME GRANITOIDS OF THE CENTRAL SIERRA NEVADA.

Bernard BARBARIN* and Paul C. BATEMAN
U.S. Geological Survey, 345 Middlefield Road, Menlo Park, CA 94025
(*French Government Visiting Postdoctoral Fellow)

Petrographic, modal, mineralogical, chemical, and isotopic data obtained from five plutons in the central Sierra Nevada impose constraints that indicate a general model for the origin and evolution of mafic magmatic enclaves (mafic inclusions), associated mafic rocks, and enclosing granitoids. The model consists of two contrasting, but temporally overlapping, mechanisms: one mechanism produces bulk compositional diversity, whereas the other produces mineralogic similarity, isotopic equilibration, and similar chemical affinities between the various types of rocks.

In the first mechanism, a mantle-derived mafic component mixes with a felsic crustal component to create hybrid magmas, which then fractionate to produce the different facies of the granitoid plutons. When contrasting rheological conditions inhibit mixing of the mafic and felsic components, mingling occurs and leads to the formation of mafic magmatic enclaves. Late surges of mafic magma mix with evolved granitic magma to produce the hybrid magma of the mafic dikes. Coarse-grained mafic-rich rocks represent mechanical segregations of mafic minerals and accessory phases from evolved granitic magma. Mafic magmatic enclaves commonly are included in these segregations. Similar segregations can also be derived from the mafic magma and produce enclaves unusually rich in mafic minerals.

In the second mechanism (which operates concurrently with the first mechanism, but is dominant in later stages of crystallization), diffusive processes induce uniform mineral compositions and similar chemical affinities in the enclaves, host granitoids, and mafic-rich rocks. However, mafic dikes that were emplaced during late stages of crystallization of the granitoid magmas and cut across foliations, have not equilibrated with the other rocks.

This model is consistent with most available data for the central Sierra Nevada batholith and with data from calc-alkaline granitoid plutons elsewhere. Variations from one pluton to another are primarily related to proportions of the two components involved in the mixing process and to the relative efficiency of the two contrasting mechanisms.

Mineral liberation prediction from ore texture description: use of mathematical morphology

G. Barbery
Head, Mining and Metallurgy Department
Laval University, Québec, Canada G1K 7P4

Mineral liberation prediction is a most important subject in the application of ore mineralogy to ore processing. Particles produced by fragmentation of multiphase materials exhibit a distribution of composition which should be predicted, if mineralogical information is to be used in process design, process assessment, process simulation and optimization.

Various authors in the past have attempted such an approach, but their methods were mostly unrealistic in either the description of ore texture, or in the definition of particle shape after breakage, or in the assessment of the relationship between texture and breakage.

A new approach is presented, which makes use of the following elements:
- texture modelling and model calibration using image analyzers. The covariance function of texture is taken as descriptor,
- particle generation modelling and model calibration using image analyzers. The covariance function of particles resulting from breakage is taken as descriptor.
- independance of texture and breakage is assumed in a first approach (pure transgranular hypothesis).

Under well defined conditions (stationarity and isotropy of the geometric stochastic processes describing texture and breakage, convexity assumption for particles), the principles of integral geometry enable to predict, for a biphasic material, particle composition distribution, and thus "liberation".

Various examples are given, for texture and for particle generation. Since the model can predict particle composition distribution, typical "washability" or "separability" curves can be calculated, and model calibration, especially for texture, can

thus be carried out using laboratory physical separations. Examples are given for various materials (magnetic taconites grinding, pyrite in gold ores), which break according to the pure transgranular hypothesis.

New developments are presented for the generalization of the model to materials that do not fulfill the pure transgranular hypothesis. Bitextural materials that retain most of the simplicity of the model, and yet enable to cope with preferential breakage are presented for coal applications.

GROWTH MODES OF SHEET SILICATES IN HYDROTHERMAL ENVIRONMENT

BARONNET, A., Centre de Recherche sur les Mécanismes de la Croissance Cristalline, Campus de Luminy, case 913, 13288 Marseille cedex 09, France

An increasing amount of information is now available on growth modes of sheet silicates in ordinary aqueous or hydrothermal solutions [1,2], as well as on their topology during "solid-state" transformations from silicate precursors [e.g. 3,4]. Arrested 2D-nucleation or spiral growth mechanisms of the basal faces of some natural clay minerals including kandites, sericite and chlorite crystallites [5,6] from hydrothermal metasomatic deposits, hydrothermal veins and metamorphic rocks have been reported by use of the high resolution microtopographic methods of TEM. If some correlations between growth mechanisms and environmental conditions were found, such interesting studies did not provide a complete picture of the possible growth modes of such minerals in response to time and/or to changes of the thermodynamic and kinetic parameters of the environment.

Micas, with their extended stability fields [7] and the now available possibility to nucleate and grow them hydrothermally as monocrystals under almost fully controlled growth conditions [2,8], may serve as prototypes to understand the general growth behaviour of other planar sheet silicates.

Low temperature (<400°C) nucleation phenomena of dioctahedral micas (muscovite, paragonite, phengite) as seen by TEM [9] resemble those encountered in paracrystalline growth : single or a few layer thick, ~100 Å wide, equant or lath-shaped, sheet units coalesce readily edge-to-edge and to a lesser extent by piling up one on top of the other to form sheet clusters. The mutual arrangement of such sheet units combine in parallel, twin and less frequently turbostratic positioning, thereby forming a disordered stacking sequence. At this stage, such clusters are similar to those found in sedimentary illite [10] and at the very start of low temperature synthesis of trioctahedral smectites [11]. During the piling up of very thin muscovite/illite sheets, incorrect match of full and empty alkali sites at the interface may be regarded as responsible for expansibility properties of such aggregates which mimic some ordered or disordered illite-smectite intergrowths as indicated by XRD [12]. At lower supersaturation, solution-mediated ripening takes place so that misoriented and smallest component sheets in the core of clusters dissolve and feed the rim which grows invards and outwards to form a defective "monocrystal".

At higher temperature (>450°C), hydrothermally-nucleated dioctahedral micas display the conventional behaviour under decreasing supersaturation : formation of discrete nuclei with few propensity to aggregate followed by 2D-growth and further on, eventually by spiral growth of their basal faces while the crystals ripen.

At any growth temperature, the clustering ability of all trioctahedral micas (phlogopite, biotites, lepidolites, etc) remains low. Therefore, the disordered structure of phlogopite and biotite is as-grown and not caused by clustering of subunits. For these micas, the density and strengths of screw dislocations that produce spirals on basal faces are larger than in dioctahedral micas [2]. They also grow more frequently complex polytypes than they do from the latter micas.

On any mica, monomolecular steps are rough and behave one-dimensionally whilst bunched two-or three-molecular steps are fully polygonized and behave like microfacets. The latter and higher steps are usually unstable and split into trains of monomolecular steps. Such trains are made of equispaced single or pairs of steps, but never of triplets. HREM examinations of the as-grown basal face profiles confirm that the minimum height of such steps is 10 Å and that the interlayer sheet actually limits the {001} faces [13].

The growth modes of lateral (010) and {110} faces are fairly sensitive to departures from equilibrium. At low supersaturation, those faces are smooth, with occasional thick steps, and round off near the edges. Since bundles of perfect dislocations mainly screw in character outcrop sometime on such lateral faces, spiral growth is possible. At increasing supersaturation rates, those faces become first stepped parallel to (001). Then, skeletal crystals are produced which are similar in form to biotites crystallized in some quench volcanic rocks but also to some platy clay minerals from weathering environments.

An extensive number of single crystal phlogopite growth experiments in KOH aqueous solutions, using the thermal gradient method, shows that : 1) the kinetics of lateral faces as a function of supersaturation combines the effects of surface and volume diffusions, 2) from chemical zoning phenomena, the existence of a boundary layer close to these faces is highly probable for tetrahedrally-coordinated ions, 3) from extremely low dissolution entropies of the mica [14] and surprisingly low diffusivities of some IV-coordinated cations across the boundary layer, the growth unit of the mica is probably larger than the tetrahedra. Similar experiments in Ni-and Cr-doped hydrothermal solutions produce self-stressed phlogopite nuclei with exotic growth forms : conical shaped sheets evolving as delicate mica roses, cylindrical packets made by piling up of curved mica sheets. These results illustrate the great sensitivity of the growth modes of the planar sheet silicates in response to changes of temperature, kinetic as well as chemical parameters under hydrothermal conditions. A similar approach would be needed to understand the growth modes of cylindrical or rolled, and corrugated sheet silicates.

[1] BARONNET, A. (1975). Fortschr. Mineral. 52, 203
[2] BARONNET, A. (1980). Current Topics in Materials Science, vol. 5, 447
[3] VEBLEN, D.R., and BUSECK, P.R. (1979). Science, 206, 1398
[4] VEBLEN, D.R., and BUSECK, P.R. (1980). Amer. Mineral., 65, 599
[5] SUNAGAWA, I. and KOSHINO, Y. (1975). Amer. Mineral., 60, 407
[6] SUNAGAWA, I., KOSHINO, Y., ASAKURA, M. and YAMAMOTO, T. (1975). Fortschr. Mineral., 52, 217
[7] HEWITT, D.A. and WONES, D.R. (1984). In : "Micas", MSA Edit., chap. 7, 201
[8] BARONNET, A. (1984). Fortschr. Mineral., 62, 187
[9] BARONNET, A. (1982). Estrud. Geol. 38, 185
[10] GUVEN, N. (1974). Mineral. Mag., 39, 788
[11] DECARREAU, A. (1983). Sci. Geol., 74, 191
[12] NADEAU, P.H., WILSON, M.J., McHARDY, W.J. and TAIT, J.M. (1985). Mineral. Mag., 49, 393
[13] AMOURIC, M. and BARONNET, A. (1983). Phys. Chem. Minerals, 9, 146
[14] BARONNET, A., AMOURIC, M., CHABOT, B. and CORNY, F. (1978). J. Crystal Growth, 43, 255

APPLICATIONS OF BRILLOUIN SPECTROSCOPY TO MINERAL PHYSICS

BASS,J. D., Dep't of Geology, University of Illinois, Urbana, IL 61801, USA

The elastic properties of minerals, especially high-pressure polymorphs of silicates and oxides, provide a powerful constraint on the mineralogy and structure of the Earth's interior. However, single-crystal samples recovered from high-pressure experiments are usually very small and therefore unsuitable for elasticity measurements by conventional techniques such as ultrasonic interferometry. A technique based on the Brillouin scattering phenomenon provides a way of measuring the elastic moduli of exceedingly small (<100 μm) single-crystal samples, thereby greatly expanding the range of samples that can be characterized.

Brillouin scattering refers to the interaction of light with thermally generated elastic waves, or acoustic phonons. By measuring the change in frequency of light scattered from a single crystal sample, one obtains the velocity of sound in a specific crystallographic direction. For example, with an optically isotropic material and a 90° scattering geometry the measured frequency shift, Ω, yields an acoustic velocity, v, by the relation $v=(\Omega/\Omega_o)c\cdot(\sqrt{2}\ n)^{-1}$, where c is the speed of light in vacuum and n is the refractive index. The main advantages of the technique result from the fact that it is optical in nature. Exceedingly small samples, similar to those used for single-crystal X-ray diffraction, can be characterized. Also, acoustic velocities can be easily measured in an arbitrary number of crystallographic directions by simply changing the orientation of the sample on a goniometric device. As adapted for use in the Earth sciences, mainly by Weidner and co-workers, the advantages of Brillouin spectroscopy have been optimized by configuring the experimental apparatus in a similar way to 4-circle X-ray diffractometry.

To date, many geologically important phases have been characterized by Brillouin spectroscopy, including garnets, pyroxenes, and high-pressure phases such as silicate spinels and ilmenites. The results now at hand indicate that a transition from olivine to a modified spinel (β-phase) structure yields a much larger increase in acoustic velocity than is indicated at 400 km depth on the basis of seismological studies. Other mineralogical components that do not undergo phase changes at this depth are required to dilute the effect of the olivine to β phase change if the 400 km discontinuity is to be explained by this transition. Approximately 40% olivine is appropriate. The velocity structure of the transition region (400-670 km) is best fit with a mineral assemblage containing more Ca-rich pyroxene and garnet than are presumed in more olivine-rich compositional models. Thus the 400 km discontinuity may represent a compositional boundary. The elastic properties of majorite, a garnet-structure high-pressure form of pyroxene, is of primary importance in further refining our understanding of mantle composition.

Until recently the Brillouin scattering technique has been limited to studies of transparent samples. The development of Fabry-Perot interferometers with increased contrast and resolution have permitted high-quality Brillouin spectra to be obtained from opaque materials, and in particular from surface waves excited on metals. These technical advances have opened new classes of materials that may be studied by Brillouin spectroscopy.

SYNCHROTRON RADIATION, APPLICATIONS IN MINERALOGY

BASSETT, W.A., Department of Geolgocial Sciences, Cornell University, Ithaca, New York 14853

An electron beam bent by a strong magnet emits electromagnetic radiation with unique properties that make it desirable for a large variety of techniques useful in the study of Earth materials. When beam energy and flux are sufficiently large and the bending magnet sufficiently strong,

X-rays are produced having very high intensities over a wide range of wavelengths,

The divergence of the X-ray beam is very small compared with that from a conventional source,

The radiation is polarized,

The radiation arrives in very short pulses of extremely high intensity and short duration.

These attributes of synchrotron radiation not only allow considerable expansion and acceleration of older and more conventional X-ray methods, but also open the way to applications not otherwise practical. Some of the most important methods being applied to problems in the Earth sciences are as follows:

High-pressure/high-temperature X-ray diffraction

EXAFS (extended X-ray absorption fine structure)

XANES (X-ray absorption near edge structure)

Powder diffraction structure analysis

X-ray microprobe analysis

X-ray radiography

Other techniques potentially useful in the Earth sciences are:

Single crystal studies with superior signal-to-noise ratio

X-ray topography

Low angle scattering

Dichromatic radiography

There are currently three synchrotron laboratories in the U.S. that provide X-rays:

SSRL (Stanford Synchrotron Radiation Laboratory)

CHESS (Cornell High Energy Synchrotron Source)

NSLS (National Synchrotron Light Source at Brookhaven National Laboratory)

Application for time on these sources is made by submitting a proposal to one the facilities. The proposal is then judged by peer review. Other major synchrotron sources exist throughout the world.

The potential for the study of Earth materials by synchrotron radiation is just beginning to be realized.

DISPLACEMENT REACTIONS IN GYPSUM. II .

BAYER, G., Institut für Kristallographie, ETH-Zürich, CH-8092 Zürich, Switzerland, WIEDEMANN, H.-G., Mettler Instrumente AG, CH-8606 Greifensee, Switzerland

Displacement reactions may generally occur between solid reaction partners, between solids and melts or solutions, or between solids and vapors. They involve the exchange of atomic constituents and are of importance also in the formation of minerals. The reaction products are formed in situ on, or within the solid starting phases.

The present investigations are concerned with displacement reactions which occur when gypsum, $CaSO_4 \cdot 2H_2O$, is brought into contact with aqueous solutions of different salts. These reactions lead to the formation either of a Ca-compound or of a sulfate of lower solubility than gypsum. The reaction products are formed in situ within the gypsum crystal surface and grow further as long as the salt solution has access to it; they may show preferential orientation in certain cases (1). The reactions can be observed and followed directly by microscope when cleavage plates of $CaSO_4 \cdot 2H_2O$ are used. The gypsum plates were placed on microscope slides having a round cavity in the center. By use of a syringe the salt solutions were introduced into this cavity, below the cleavage plates. Thereby it was possible to follow the displacement reaction on one

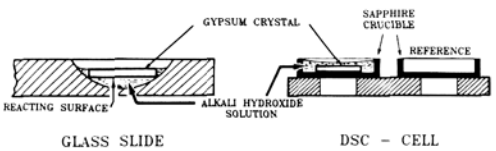

Fig. 1 Experimental set-up for microscopic and DSC-investigations

side of the cleavage plate which was essential for reasons of light transmission and focussing (Fig. 1). For simultaneous thermomicroscopic/DSC-measurements the microscope hot stage FP 84 and the Mettler Thermosystem FP 800 were used.

Gypsum cleavage plates were reacted with solutions of different alkali salts (MeOH, MeF, Me_2CO_3, $(Me, H)_3PO_4$, Me_2WO_4) and with chloride or nitrate-solutions of Sr, Ba and Pb. The nucleation and crystallization of some of these reaction products could be followed and recorded in relation to time, temperature and concentration of the salt solutions. As an example Fig. 2 shows the reaction kinetics between gypsum and NaOH as derived from thermogravimetric measurements. The results presented in this paper will be concerned with the formation of barite and scheelite by displacement reactions.

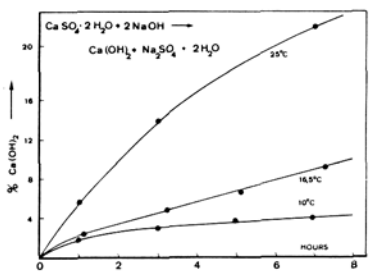

Fig. 2. Effect of temperature and time on the formation of $Ca(OH)_2$ on gypsum cleavage plate immersed in 2 molar NaOH

1) BAYER, G. and WIEDEMANN, H.-G.: Displacement reactions in gypsum. I . Thermochim. Acta (1986), in print

STATUS OF THE JCPDS MINERAL FILE

BAYLISS, P., Department of Geology and Geophysics, University of Calgary, Calgary, Alberta, Canada T2N 1N4

The 1986 issue of the *Mineral Powder Diffraction File* has just been published; however, now is the time to start to prepare for the next issue in about six years time.

The first aim of the file is to have powder data of every valid mineral species. There are about 120 minerals that are not in the *Mineral Powder Diffraction File* that were described before 1974 and are considered species by Fleischer (1983). My estimate is 60 valid, 10 amorphous and 50 questionable. Of the 60 valid species, meagre data are available for 30 of them. Should the Mineral File contain this meagre data?

There are about 140 minerals that are not in the *Mineral Powder Diffraction File* that were described in the 1974 to 1984 period and are considered species by Fleischer (1983, 1984, 1985). My estimate is 25 amphiboles and 35 others with no data, 20 with meagre data, and 60 did not make the editorial system. The synthetic equivalent of about 25% of new minerals are already in the Inorganic Powder Diffraction File. The Mineral File contains 20 mineral species not recognised by Fleischer and 50 unnamed minerals. The Mineral File contains 25 minerals that were rejected by I.M.A., which includes 8 minerals that were redescribed after rejection. However, Fleischer (1983) contains 30 minerals rejected by I.M.A. Should these data, unnamed minerals, and doubtful minerals be dropped from the Mineral File?

At present there are about 100 minerals without a unit cell and probably another 100 minerals with an incorrect cell. How to spell names is a problem because there are about 90 differences between Fleischer (1983) and Embrey & Fuller (1980) as follows: 30 umlaut, 15 Russian transliteration, 5 American-English, 10 anglization, and 20 others. A problem occurs when I.M.A. adopts different nomenclature to AIPEA, *e.g.* imogolite. The present Mineral File acknowledges many scientists who have pointed out errors; however, your comments and advice will be greatly appreciated.

THE USE OF ATTENUATED TOTAL REFLECTION AND CRYSTAL OPTICS FROM THE POLARITON POINT OF VIEW

BEHMER, M., Inst. f. Mineralogie u. Kristallographie d. Universität Wien, Dr.-Karl-Lueger-Ring 1, A-1010 Wien, Austria

An experimental technique that allows the observation of dispersion branches of bulk polaritons (=BP) in solids, such as minerals, by ATR-spectroscopy has been first shown in 1974 /1/2/. The important fact is that the ATR-crystal and the sample are in direct optical contact. In this case the x-component of the wave vector of incident electromagnetic radiation (IR-radiation), which is used to study bulk polaritons, is given by: $k_x = \omega/c\ n_1 \sin\alpha$, where n_1 denotes the refractive index of the ATR-crystal outside the sample and α the angle of reflection. A comprehensiv description of the method is given in /3/4/. The polariton point of view is as follows. The canonical momentum $\hbar k$ of an elementary exication in solids, such as bulk polaritons, and the energy $\hbar\omega$ of incident radiation must be of the same order of magnitude. This provides the condition: $k_{BP} = k_x$ or $\omega/c\ n(\omega) = \omega/c\ n_1 \sin\alpha$, between the two medias at the plane of contact. With the help of /5/ $k_{BP} = \omega/c\ n(\omega)$ it is possible to convert the crystal optic into the relevant Brillouin zone scheme of solids. The expression $n(\omega)$ denotes the square root of the frequency dependent dielectric constant (e.g. the dielectric function of crystalline matter). The dispersion relation $\omega = \omega(k)$ of bulk polaritons splits areas with perfect and reduced reflection /3/. The measurements of ATR-spectra with variable angle of reflection α and variable refractive indices n_1 of ATR-crystals are used for determining this boundary-line experimentally. Fig.1 shows typical ATR-spectra obtained from ZnS c, cf. /6/. A KRS5-hemicylinder ($n_1 = 2.38$) was used as ATR-crystal. The polariton dispersion takes place in the spectra by a frequency shift to higher frequencies of the upper edge of the IR-reststrahlen band. The measured $\omega = \omega(k)$-diagramm originating from bulk polaritons in ZnS is given in Fig.2. Areas with perfect re-

THE USE OF ATTENUATED TOTAL REFLECTION AND CRYSTAL OPTICS FROM THE POLARITON POINT OF VIEW
BEHMER, M.

flection have been hatched. The dashed and dotted lines in Fig.2 correspond with the dispersion line of incident radiation under the angle 25° and 45° (n_1 = constant). The reflectivity becomes perfect at the frequency, where the dispersion line of incident radiation crosses the dispersion relation of bulk polaritons.

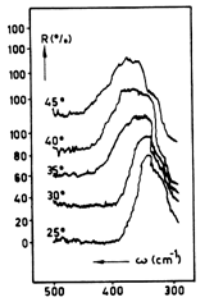

Fig.1: ATR-spectra of ZnS c, ATR-crystal KRS5.

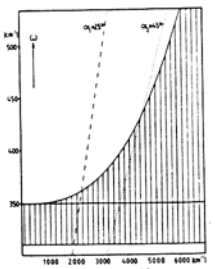

Fig.2: Measured dispersion branch of ZnS c.

References

/1/ FALGE, H.J., OTTO, A., and SOHLER, W., Phys. Stat. Sol. (b) 63, 259 (1974)
/2/ NITSCH, W., FALGE, H.J., and CLAUS, R., Z. Naturforsch. 29a, 1011 (1974)
/3/ CLAUS, R., MERTEN, L., and BRANDMÜLLER, J., Light Scattering by Phonon-Polaritons, Springer Tracts in Modern Physics 75, (1975)
/4/ BORSTEL, G., FALGE, H.J., and OTTO, A., in Springer Tracts in Modern Physics 74, (1974)
/5/ BORN, M., and HUANG, K., Dynamical Theory of Crystal Lattices, Oxford, (1954)
/6/ BEHMER, M., Fortschr. d. Min. 62, Beiheft 1, 16 (1984)

FLUID INCLUSION AND CHEMICAL STUDIES OF SPINEL PERIDOTITE XENOLITHS FROM SARDINIA (ITALY)

BELKIN, H.E., MS 959, U.S. Geological Survey, Reston, VA 22092, USA; DE VIVO, B., Centro Studio Geocronologia e Geochimica Formazioni Recenti, CNR, Dipart. di Scienze della Terra, Citta Univers., P.le A. Moro 5, 00100 Roma, Italy; BECCALUVA, L., Dipart. di Scienze della Terra, Univ. di Napoli, S. Marcellino 10, 80138 Napoli, Italy; MACCIOTTA, G., Ist. di Petrografia, Univ. di Parma, via Gramsci 9, 43100 Parma, Italy.

Spinel peridotite xenoliths commonly occur in Pliocene-Quaternary alkaline to subalkaline volcanic rocks that crop out in Sardinia (Italy). A study of their fluid inclusions and mineral and whole-rock chemistry has been used to place constraints on their origin and history of ascent. Fluid inclusions have been examined by microthermometric techniques using a CHAIXMECA heating and freezing stage; XRF and microprobe analyses have been performed on the xenoliths and constituent minerals, respectively.

The host rocks are a series of fissural lavas, alkaline to subalkaline in affinity associated with lesser amounts of intermediate and differentiated products in some areas. The xenoliths are small, 1 to 3 cm, and were found in alkali basalt, basanite, hawaiite and trachybasalt. Most xenoliths are harzburgites or lherzolites although dunites, wehrlites and pyroxenites are found. The harzburgites and lherzolites are characterized by a protogranular texture, a large and variable grain size (1 mm to 1 cm), and a typical four-phase assemblage: olivine (70 to 80 vol. %, Fo ~ 90, unzoned), orthopyroxene (15 to 20 vol. %, En ~ 90, unzoned), clinopyroxene (4 to 10 vol. %, emerald green color, Wo 45-50 En 46-50 Fs 3.5-5, zoned with rims higher in Mg and Ca and lower in Al and Na) and chromian spinel (1 to 2 vol. %, Cr/(Cr+Al) = 0.14-0.46). Kink bands in olivine and orthopyroxene and rare narrow exsolution lamellae of clinopyroxene from orthopyroxene are present. A reaction selvage that locally surrounds interstitial lobate-shaped spinels suggests subsolidus reaction. The application of various geothermometers based on the equilibration of clinopyroxene/orthopyroxene pairs give values that range from 920 to 1050°C. The spinel peridotite xenoliths are chemically and mineralogically similar to other xenoliths that represent fragments of the uppermost subcontinental mantle randomly sampled by their host magmas.

Fluid inclusions containing essentially pure CO_2 and various proportions of silicate glass have been found in orthopyroxene, clinopyroxene and olivine and represent the trapping of two immiscible fluids. Most of these inclusions are secondary because they occupy healed fractures that sometimes cross-cut each other and also cross grain boundaries. A few high density inclusions appear to be primary but show partial decrepitation phenomena. The temperature of homogenization (Th) of vapor (V) and liquid (L) CO_2 ranges from -40° to +31°C (95% Th V + L → L; 5% Th V + L → V) and yields a CO_2 density that ranges from 1.11 to 0.18 g/cm^3. Most densities are between 0.60 and 0.80 g/cm^3. The frozen inclusions melt in a very narrow temperature range with an equilibrium melting temperature = ~-56.6°C; this suggests essentially pure CO_2. If a trapping temperature of 1000°C for a pure CO_2 system is assumed, the trapping pressure would be between 0.5 kb and 10 kb. For an average media (rock or magma) density of 2.8 g/cm^3, the inclusions would be trapped at depths from 2 km (0.18 g/cm^3 CO_2) to 37 km (1.11 g/cm^3 CO_2). The CO_2 fluid inclusions represent a separate volatile phase ascending with the magma that was continuously trapped (along with silicate melt) by intragranular fracturing. Although the inclusions appear to show a continuum from high to low CO_2 density, the mode represents trapping at 9 to 17 km and may indicate a common fracturing event during ascent. Another cluster of inclusions with densities equivalent to trapping at 2 to 3 km may represent residence in a shallow magma reservoir.

STABILIZATION OF CU-FE-BI-PB-SN-SULFIDES

BENTE, K. Mineralogisch-Kristallographisches Institut der Universität Göttingen, Goldschmidtstr. 1, D-3400 Göttingen

Phase stabilizations and stabilization phenomena are importent for the solution of problems of phase synthesis and the interpretation of mineral stabilities. For metastabilities and stabilizations the following reasons are to be suggested: replacements of atoms (ions), aqueous (hydrothermal) conditions, heterogeneous nucleation and extreme conditions as high temperatures and pressures. For the verification of these suggestions the investigation of Cu-Fe-Bi-Pb-Sn-sulfides are chosen, because extensive data sets of there structures and thermodynamics are known. Therefore direct correlations between stabilization phenomena of these phases are to be expected.

Results of such investigations are presented in respect to atom (ion) replacements by Fe in Cu-Bi-sulfides, especially for CuS (covellite), Cu_5FeS_6 (idaite), $Cu_4Bi_5S_{10}$, $(Cu,Fe)Pb_6Sb_2Bi_4S_{16}$ (kobellite) and for the solid solution series between FeS_2 and CuS_2 and for Sn-Pb-disulfides. Basing on spectroscopic, thermodynamic and structural data the crystalgeometric conditions for the stabilization by Fe are characterized as necessary but the electronic interactions between the metal atoms (ions) Fe and Cu as sufficient conditions. In many cases the stabilization by atom (ion) substitution can be replaced or completed by aqueous (hydrothermal) solutions respectively precipitations. This is valid especially for the stabilization of phases, which are stable at high pressures and temperatures under dry conditions as $(Pb,Sn)S_2$ and $(Cu,Fe)S_2$. Phase stabilization by hetro-

geneous nucleation was tested for simple Pb-Bi-compounds by means of epitaxy on NaCl. Comparable with Sc_2S_3 and precipitated Bi_2S_3 from aqueous solutions, these compounds, stabilized by epitaxy, are suggested to show more or less ordered NaCl-type structures with metal vacancies.
The results are discussed in respect to mineral phase associations, especially for phase decay reactions and intergrowths of sulfides.

EVIDENCE AND KINETICS OF THE HOMOGENIZATION REACTION IN THE "ALLEMONTITE" INTERGROWTHS.

BERNARDINI,G.P., Dept.of Earth Sciences; CIPRIANI,C., Mineralogical Museum; CORSINI,F., Dept.of Earth Sciences; GUARINI,G.G.T., Dept.of Chemistry; MAZZETTI,G., Mineralogical Museum; POGGI,L., Dept.of Earth Sciences.
The University of Florence, I-50121 Florence, ITALY.

Natural "allemontite" samples show characteristic exsolution textures having no counterpart in synthetic (As,Sb) compounds(1).

In the present report, on the grounds of annealing and thermoanalytical experiments performed on natural samples, an hypothesis about their mechanism of formation is advanced taking into account kinetic evidence and thermodynamic considerations.

Thermoanalytical curves allowed the determination of the temperature range in which the two phases originally present in the samples, namely As or Sb and stibarsen, reacted to form a homogeneous solid solution. Such a "homogenization" reaction was investigated by obtaining TTT plots with increasing temperature (2), as exemplified in Fig.1. The same figure shows the textural evolution of the myrmekitic-type intergrowth suggesting a diffusional mechanism for the transformation. This was proved by performing the kinetic analysis of isothermal runs at different temperatures in the range 420°-520°C. Typical X-ray diffraction patterns of the quenched products of the annealing experiments have the shape of the ones reported in Fig.2 for the 480°C experiment. From the relative heights of the 102 reflections of one reactant and of the product, the extent of change was evaluated. The time necessary to complete the transformation at the various temperatures was deduced from intensities ratios vs. time plots. As expected such data were well fitted by equations typical of diffusion controlled transformations (3).

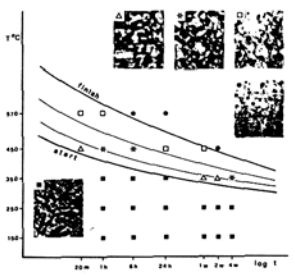

Fig.1

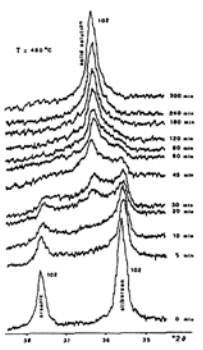

Fig.2

From an evaluation of heat and entropy of activation, the latter resulted to have a negative value indicating low transformation probability. This information, coupled with considerations about the change in equilibrium position with temperature, based on the thermoanalytical determination of the heat of reaction, led to consider that the unmixing of the solid solution is not achieved in synthetic studies because of the low probability of the rate determining step of the overall transformation.

REFERENCES.
1) Bernardini,G.P., Cipriani,C., Corsini,F. & Mazzetti,G., 1984. Il sistema "naturale" As-Sb: risultati preliminari. Rend.SIMP, 39, 649-656.
2) Putnis,A. & McConnell,J.D.C., 1980. Principles of Mineral Behaviour. Blackwell, Oxford.
3) Brown,M.E., Dollimore,D. & Galwey,A.K., 1980. in Comprehensive Chemical Kinetics, 22, 74. Bamford,C.H. & Tipper,C.F.H. eds., Elsevier, Amsterdam.

ORE MINERAL IDENTIFICATION USING A SIMPLE FULLY AUTOMATED SYSTEM

BERNHARDT, H.-J., Mineralogisch-Petrographisches Institut
2000 Hamburg, Germany

The spectral reflectances of ore minerals offer a powerful basis for their microscopic identification. Nevertheless this method is not as yet widely applied. Two reasons for this are: 1. The expense of commercially available microscope photometers and 2. the lack of a combined on line measuring and identification procedure. Consequently a simple system has been designed for the specific requirements of ore mineral identification.

The commonly used continuous interference filter, prism- or grating-monochromator, is replaced by 16 homogeneous interference filters (SCHOTT PIL 0.5) representing the wavelength 400 to 700 nm in steps of 20 nm. These filters are mounted on a movable slide. They are driven into the ray path of the microscope by means of a stepping motor. The use of homogeneous interference filters instead of a common continuous monochromator has several advantages: 1. The wavelengths are unchangeably fixed and identical within the entire filters; therefore just a very simple memechanism for the movement is needed. 2. High transmittances (40-50 %) are combined with narrow bandwidths (FWHM: 9-12 nm).

The system is controlled by a HP-75C handheld computer wich is connected to a printer, a micro cassette drive, a RS-232 interface, a digital voltmeter and a stepping motor control, using the HP-interface-loop. After data aquisition of both standard and sample curve, the spectral reflectances as well as colour values are calculated, the curves are plotted and may be smoothed. The measurement of one spectral curve requires about 100 seconds.

The described system is attached to a photometer (ZEISS MPM equipped with a photomultiplier), which was originally designed for manual use. Tests revealed, that the transmitted light intensity is strong enough to combine this monochromatizing device with a simple - less sensitive - photometer like that developed by TARKIAN et al.(1975).

Special coding made it possible to store all reference spectra on one micro data cassette. After a preselection phase using colour values in order to exclude as many minerals as possible, the measured curve of the unknown mineral is compared with the reference curves of the remaining minerals. Result is a list of possible minerals and values indicating the degree of similarity between unknown and reference mineral (same procedure as in BERNHARDT 1982). The time required for one identification is between 1 and 15 minutes, depending on the number of comparisons.

The RS-232 interface is used to connect the above system to a larger and faster computer (HP-9816) in order to store the measured spectral curves and to enter the data to the general microscopic opaque mineral identification and information system (MOMI). Here quantitative data, qualitative observations and chemical properties are used for identification.

References

BERNHARDT,H.-J. (1982) Ein einfaches Verfahren für die Erzmineral-Diagnose mittels Reflexionsspektren.- N.Jb.Miner.Mh., H.6, 241-247.

TARKIAN,M. STUMPFL,E.F. & MATTHIES,H. (1975) A new miniphotometer for teaching and routine work in ore microscopy.- Miner.Mag., 40,97-103.

EXAFS AND XANES STUDIES OF GERMANIUM IN SOME MINERALS AND RELATED SUBSTANCES

BERNSTEIN, Lawrence R., 380 Willow Road, Menlo Park, CA 94025 USA; WAYCHUNAS, Glenn A., Center for Materials Research, Stanford University, Stanford, CA 94305 USA

Germanium displays diverse geochemical behavior, being concentrated in such disparate materials as coal, iron meteorites, sphalerite deposits, copper sulfide deposits, and iron oxides and hydroxides (Bernstein, 1985). The recently opened Apex Mine in southwest Utah (Bernstein, 1986) extracts Ge from limonite, goethite, and hematite that contain as much as 0.7 wt. percent Ge, though the nature of the Ge in this material has remained unknown.

To gain a better understanding of the crystal and solution chemistry of Ge, high resolution EXAFS and XANES fluorescence spectra were obtained at the Stanford Synchrotron Radiation Laboratory (SSRL) on powdered samples and an aqueous solution.

Near-edge (XANES) spectra for several materials are shown in Figure 1. All of the spectra show a smooth, sharp initial edge, with no pre-edge features. The position of the edge crest appears to be most influenced by the type of ligand and the coordination number: highly covalently-bonded ligands (Ge,As,S,P) produce lower energies than more ionically-bonded ligands (O,OH), while tetrahedral coordination (GeO_2 with quartz structure, aqueous Ge, plus all the compounds in Figure 1a except GeS) produces lower energies than octahedral coordination (all the other compounds). In stottite, $FeGe(OH)_6$, octahedrally-coordinated hydroxyl groups produce the highest observed edge-crest energy.

Materials containing Ge in regular or nearly-regular octahedral coordination (stottite, hematite, limonite) have a distinct feature at about 11135 eV. In GeO_2 (rutile structure) and possibly in GeS, which both contain Ge in distorted octahedral coordination, this feature is split. Materials containing tetrahedrally coordinated Ge have one or more features at energies less than 11135 eV, apparently dependent upon the particular ligand.

The EXAFS results have led to several new conclusions. In particular: (1) Ge(IV) substitutes for Fe(III) in hematite and probably in limonite from the Apex Mine; (2) the dilute, neutral aqueous solution contains Ge chiefly as $Ge(OH)_4$; and (3) the Cu-Fe-Ge-As-Zn sulfides renierite and germanite contain Ge(IV) in regular or nearly regular tetrahedral coordination. In the germanian hematite from the Apex Mine (0.7 wt. percent Ge), six nearest-neighbor oxygen atoms are at about 1.87 Å, and 4 second-neighbor iron atoms are at about 2.90 Å; these figures comform well to the expected values for Ge(IV) in the octahedral Fe(III) crystallographic site of hematite.

References

Bernstein, L.R. (1985) Germanium geochemistry and mineralogy. Geochimica et Cosmochimica Acta, v. 49, p. 2409-2422.

Bernstein, L.R. (1986) Geology and mineralogy of the Apex germanium-gallium mine, Washington County, Utah. U.S. Geological Survey Bulletin 1577, 9 p.

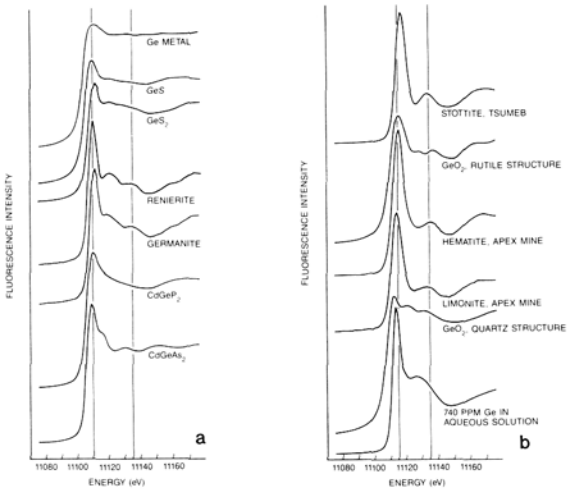

Figure 1. K-edge spectra for Ge.

THE CRYSTAL STRUCTURE OF GRISCHUNITE

BIANCHI,R.,PILATI,T.,C.N.R.Centre c/o Dept.of Physical Chemistry,University of Milan;MANNUCCI,G.,Earth Science Dept.,University of Milan,I-20133 Milan,Italy

On a fragment of type material,kindly supplied by Prof.S.Graeser,the structural determination of grischunite,a new arsenate mineral from Falotta,Graubünden, has been carried out by X-ray diffraction. The unit cell data a=12.855(2),b=13.497(2),c=12.047(1)Å ,space group Pcab ,Z=4 are in agreement with the previously published data by Graeser et al.(1).

For determining and refining the structural data,of 2393 independent reflections which have been collected using a Nonius CAD-4 diffractometer,1739 for which $I > \sigma(I)$ have been considered;an empirical absorption correction according to Walker and Stuart ... was also applied. The structure was solved by direct methods,using the MULTAN routine,and refined by least squares: the final R index is 0.036.

Of the three non-crystallographically equivalent sites containing transition metals,one has shorter distances with the adjacent O atoms (average 2.090(2)Å,against 2.189(2),and 2.230(2)Å,respectively).The Ca and Na atoms in the structure essentially occupy two additional (different) positions ,with average Me-O distances 2.548 and 2,503 Å,respectively;for sodium,the equivalent B (1.89 $Å^2$ against 0.7 $Å^2$ for all the other metal atoms) indicates a partial occupancy of the Na site.All these reasons give evidence for changing the proposed formula $(Ca,Na)(Mn^{2+},Fe^{3+})_2(AsO_4)_2$ to a new one,i.e.$NaCa_2Mn^{2+}Fe^{3+}(AsO_4)_3.2H_2O$,with about one-half of Mn substituted by Fe in the position with short Me-O distances;the presence of water has also been ascertained by examining the difference Fourier map.The agreement with the analytical data reported by Graeser et al.(2) is improved,and the mineral seems to be more related to the alluaudites.

(1) Graeser,S.,Schwander,H.,& Suhner,B.,Schweiz.min.petr.Mitt. 64,1-10 (1984)

• CHEMICAL MINERALOGY OF MARINE EVAPORITES

BILLO, S.M., Department of Geology, King Saud University, ad-Dir'iyah, Riyadh, Saudi Arabia

Quantitative studies on the course of crystallization during evaporation of sea water reveal that the sequence of deposition of early evaporite minerals consists of calcium carbonate, calcium sulfate, and halite, successively. The order of deposition depends on temperature, mineral solubilities, and concentration of the various ions. Most ancient marine evaporite deposits are mineralogically similar to the preceding sequence. The Permian Castile Formation in the Delaware Basin of Texas and New Mexico is a classic example of a totally interrupted marine evaporite sequence consisting of gypsum or anhydrite and halite with basal interlaminated carbonate layers. Recent studies on the mineralogy and trace element distribution of Castile evaporites using differential thermal analysis (DTA) and atomic absorption spectrophotometry, in addition to elaborate computer programming, have confirmed positive correlation with the established resolution of the type section of the Castile Formation into parallel and independent time-series of halite, calcium sulfate, calcium carbonate, organic matter, magnesium, strontium, potassium and iron for depicting the changing climatic patterns in the region.

HYDROTHERMAL ALTERATION IN LAYERED GABBROS OF THE EAST GREENLAND TERTIARY PROVINCE

BIRD, D. K.; ROSE, N. M.; MANNING, C. E., Dept. of Geology, Stanford University, Stanford, CA, 94305, USA;

Gabbroic intrusions exposed in the East Greenland Tertiary igneous province represented heat sources for large-scale hydrothermal circulation systems during the initial stages of the opening of the North Atlantic Ocean. Investigations of the Skaergaard intrusion, related large gabbroic dikes (Macrodikes), and the Nordre Aputiteq and Kruuse Fjord layered gabbros indicate that the style and complexity of alteration within and near each intrusion is closely linked to its size and its magmatic and structural history during emplacement and cooling.

The Skaergaard intrusion and the Macrodikes were emplaced off the main axis of rifting and experienced simple cooling histories. At the Skaergaard intrusion, hydrothermal alteration consists of discreet fracture events that record successively lower alteration temperatures during the cooling of the pluton. Alteration conditions span upper amphibolite to zeolite facies of metamorphism. Calcic amphiboles ranging in composition from actinolite to pargasitic hornblende are the most common vein-filling minerals in the Layered Series (LS) and Marginal Border Group (MBG). Five vein types have been identified based on mineral assemblages and paragenetic relations. The earliest hydrothermal veins are <1-2 mm. wide, continuous for tens of meters and occur with frequencies between 0.2 to >1.5 (LS) and 1.4 to >20 fractures/meter (MBG). Mineralization in these veins is similar to upper amphibolite facies metamorphic assemblages found in metabasaltic rocks, containing calcic amphiboles, clino- and orthopyroxenes, biotite, talc, ilmenite, magnetite, chlorite and Ca-plagioclase. Based on vein pyroxene compositions and maximum dehydration temperatures of calcic amphiboles, the earliest veins formed at >500° to 750°C and <925° to 960°C. The other four vein types are much less abundant and formed later in the cooling history of the Skaergaard hydrothermal system. As a group, late veins contain lower amphibolite, greenschist and subgreenschist facies mineral assemblages and commonly show alteration halos with widths greater than or equal to those of the fractures themselves. Mineralization in later veins is typically characterized by two calcic amphiboles (with a gap in the Al^{IV} contents) coexisting with salite, albite, quartz, prehnite, epidote, calcite, titanite, pyrite and Ca-zeolites. The lower abundance of the late vein types is consistent with a decrease in the fracture-controlled permeability of the intrusion with decreasing temperature.

Veins in the Upper Border Group of the Skaergaard intrusion are more abundant than in the Layered Series and are filled predominantly by epidote and minor amounts of garnet, prehnite, alkali feldspar, calcite or quartz. Thermodynamic analysis of epidote-garnet and epidote-prehnite vein assemblages suggest formation at 350° to 450°C and <300°C, respectively. Intrusion of the Basistoppen Sheet, a differentiated gabbroic sill, into the Upper Border Group gabbros during late stage cooling of the Skaergaard intrusion may, in part, be responsible for the extensive fractures and hydrothermal fluid circulation at <350°C that led to the abundant epidote mineralization above the Sandwich Horizon.

Hydrothermal alteration of the large (0.1 to >1 km wide) layered gabbroic dikes near the Skaergaard intrusion (Macrodikes) consists primarily of hornblende + chlorite + talc veins, with later serpentine mineralized fractures (Bird et al., 1985). Fractures are more common in areas of abundant basalt xenoliths and near the Macrodike contacts. As in the Layered Series of the Skaergaard intrusion, epidote- and prehnite-filled veins are uncommon and occur only in late-stage fault zones.

In contrast to the Skaergaard and Macrodike gabbros, the Nordre Aputiteq and Kruuse Fjord intrusions show evidence for more complicated magmatic histories. In these intrusions, sub-solidus hydrothermal fluid circulation produced abundant, superimposed alteration events within and near fractures and cavities over a wide temperature range. Secondary mineralization at Nordre Aputiteq is concentrated in the leucocratic tops of layered gabbro units that probably crystallized from episodic magma pulses and consists of metasomatic mineral assemblages that form reaction zones between unaltered gabbro and mineralized miarolitic cavities that are up to 10 cm in diameter. Alteration in the cavities is characterized by an early assemblage plagioclase + pyroxene + hornblende that is partially replaced by epidote-bearing assemblages that may include salite, albite, prehnite, actinolite, chlorite, zeolites and sericite. Thermodynamic analysis of coexisting phases suggests that prehnite-bearing assemblages formed at <350°C and sericite-bearing assemblages at <300°C.

The earliest stages of hydrothermal alteration in the Kruuse Fjord gabbro consist of veins mineralized by hornblende, biotite, magnetite and clinopyroxene similar to the high temperature vein systems in the Layered Series of the Skaergaard intrusion. In many veins the early minerals are replaced, overgrown or crosscut by prehnite, chlorite, albite, titanite, epidote and actinolitic hornblende.

The overall nature of aqueous solution - gabbro interaction in the Kruuse Fjord and Nordre Aputiteq intrusions differs significantly from that of the Layered Series of the Skaergaard intrusion and the Macrodikes. In the latter, extensive fracturing of the gabbros is associated with amphibolite facies vein mineral assemblages that sealed the fractures to further fluid flow and chemical reactions. Lower temperature epidote- and prehnite-bearing assemblages are virtually absent. In contrast, the Kruuse Fjord and Nordre Aputiteq gabbros contain extensive and paragenetically complex Ca-Fe^{3+}-Al silicate alteration that appears to be related to the complex structural and magmatic histories of these intrusions.

Bird, D. K., Rosing, M. T., Manning, C. E. and Rose, N. M., 1985, Geologic field studies of the Miki Fjord area, East Greenland: Bull. Geol. Soc. Denmark, v. 34, p. 219-236.

GEOCHEMISTRY OF GRANITES AND RELATED ROCKS OF THE CHANNEL ISLANDS REGION, ARMORICAN MASSIF

BLAND, A.M., Dept. of Geology and Physical Sciences, Oxford Polytechnic, OX3 OBP, UK; BROWN, M., School of Geological Sciences, Kingston Polytechnic, KT1 2EE, UK; D'LEMOS, R.S., Dept. of Geology and Physical Sciences, Oxford Polytechnic, OX3 OBP, UK; POWER, G.M., Dept. of Geology, Portsmouth Polytechnic, PO1 3QL, UK; TOPLEY, C.G., Dept. of Geology and Physical Sciences, Oxford Polytechnic, OX3 OBP, UK

The Channel Islands region is defined to include the main Channel Islands of Jersey, Guernsey, Sark and Alderney and the La Hague area of the Cotentin, west of Cherbourg, France. The Upper Proterozoic – Lower Palaeozoic granitic rocks of the region may be divided into two groups. The older group comprises foliated bodies of predominantly quartz dioritic composition which have been emplaced into basement gneisses on Guernsey, Sark, Alderney and La Hague, and are of considerable volumetric importance. The second group comprises the younger granitic complexes which are exposed on Jersey, La Hague and Guernsey and which range in age from very late Precambrian to Ordovician. They are associated with calc-alkaline diorite and gabbro intrusions and were probably generated in a convergent plate tectonic setting.

The geochemistry of the foliated quartz dioritic rocks is assessed using a data base of over 200 new analyses. Their overall geochemical character is calc-alkaline and the suite as a whole exhibits a coherent chemical pattern consistent with a volcanic arc origin; for example, on the Rb v. (Y+Nb) discriminant diagram the quartz diorites plot across the Volcanic Arc Granite field. However, systematic variations in trace element contents do exist on both a local and a regional scale and may be assigned to fluctuations in the proportion of restite to melt, fractionation, contamination by country rocks and deformation and metamorphism. The geological and geochemical evidence together with available isotopic data point to the conclusion that these quartz diorite intrusions represent a single important episode of Upper Proterozoic calc-alkaline igneous activity related to the site of a former active continental margin.

The whole-rock trace element geochemistry of the younger granitic complexes of the Channel Islands region varies systematically with geographical position from north-west to south-east.

On Guernsey, the St. Peter Port layered hornblende gabbro – bojite intrusion is the first of the younger complexes and is followed by the Bordeaux Diorite Complex and associated granodiorite group and inhomogeneous suite of diorites (Brown, M., et al., 1980. Mineral. Mag. London, 43, 919-929). Unpublished isotopic work has not given a precise age for the Complex. Geochemical data are also available for the Cobo granite (Rb/Sr age 496±12 Ma) and the L'Ancresse granodiorite. In La Hague, Cambro-Ordovician sediments are everywhere in tectonic contact with the underlying Northern Granites. The main components of the complex are: meladiorite - leucodiorite agmatite, which also occurs as blocks and rafts in the Houffet granodiorite; the La Becchue quartz diorite; the St. Germain and Ecuty granites (Rb/Sr age 528±10 Ma); and the Cap de la Hague granodiorite (Rb/Sr age 496 Ma). On Jersey, 3 granite complexes have been emplaced into the Brioverian Jersey Shale Formation and the Jersey Volcanics. The North-west Granite Complex comprises 3 lithologically different granite types dated by Rb/Sr at 465±10, 438±17 and 426±14; and is associated with an early gabbro-diorite complex. The South-west Granite Complex is also comprised of 3 granite types: porphyritic granite, which is the least evolved geochemically (Rb/Sr age 550±12 Ma); microgranite, which is possibly related to the porphyritic granite by fractionation (Rb/Sr age 527±7 Ma); and coarse granite (Rb/Sr age 483±13 Ma)(Bland, A.M., 1985. Unpubl. PhD thesis, Oxford Polytechnic).

The younger granitic complexes of the Channel Islands region are calc-alkaline. Using trace element discriminant diagrams such as Rb v. SiO_2, Nb v. SiO_2, Y v. SiO_2 and Rb v. (Y+Nb) reveals that these rocks have a similar chemistry to Volcanic Arc Granites. The Rb/Zr v. Y diagram shows a trend of data from 'Normal Continental Arcs' to 'Mature Continental Arcs', but in the Channel Islands region this relates to distance from the supposed trench. There is no systematic variation either in age or in initial $^{87}Sr/^{86}Sr$ of the complexes to the south-east, but within complexes younger rocks have higher initial $^{87}Sr/^{86}Sr$. In a regional context which uses the geophysical data from the Channel and the High T - Low P metamorphic belts of Cadomian age in N. Brittany (e.g. St. Malo), the younger granitic complexes are related to a south-east subducting plate margin of late Precambrian to Ordovician (?) age.

A NEW, AUTOMATED REFRACTOMETER

BLOSS, F. Donald, Department of Geological Sciences, Virginia Polytechnic Institute and State University, Blacksburg, VA 24061, USA

A new scientific instrument, called the Bloss Automated Refractometer or BAR (patent pending), will scan the surface of a polished thin section and measure the principal refractive indices at each *x,y* point of a user-specified grid where a nonopaque solid occurs. Simultaneously, for anisotropic crystals, it will determine the orientation of their optical indicatrix, whether uniaxial or biaxial. Crystals as small as 0.4 mm in diameter with refractive indices in the 1.100 to 2.000 range are currently measurable, but capability of measuring smaller grains is under development. If applied to the uncovered polished surface of (a) a medium- or coarse-grained thin section of rock, ceramic, or concrete, (b) an epoxy mount of organic crystals or fibers, or (c) a cross-section through an optical fiber or bundle thereof, the BAR will ultimately determine for each nonopaque phase in (a) or (b): (1) their relative proportions; (2) average cross-sectional area; (3) a petrofabric analysis for each anisotropic phase, including biaxial phases; (4) preferred dimensional orientations within the plane of the thin section; and (5) the principal refractive indices (plus $2V$ if biaxial) and their range of variation. Eventually, the BAR will also print an enlarged map showing grain or fiber boundaries plus the refractive indices it measured at points along this grain or fiber cross-section. To enhance this last capability attempts are being made to increase the precision of the BAR's measurements of refractive indices from (*ca.*) 0.0005 to 0.0001 or less.

A complete set of measurements at a single point may require 60 seconds, or more, for a biaxial crystal, but much less for uniaxial and particularly isotropic crystals. However, neighboring points on the same biaxial crystal will also require much less than 60 seconds. A complete modal analysis and petrofabric analysis on a polished section, if the BAR measures 1000 points, might require as much as 15 or so hours. However, once started, the BAR will work unattended. The ability of the BAR to determine the refractive indices of opaque grains and to operate at wavelengths beyond the visible is being explored, particularly in respect to polished ore and coal specimens.

MIAROLITIC CAVITY AND PEGMATITE MINERALOGY OF EOCENE ANOROGENIC GRANITE PLUTONS IN THE NORTHWESTERN, U.S.A.

BOGGS, RUSSELL C., Department of Geology, Eastern Washington University, Cheney, WA 99004, USA.

Epizonal anorogenic granite plutons were emplaced near the western margin of North America during early Eocene time (45 to 55 m.y.a.)(part of the Challis episode). Details of the tectonic setting of these plutons has not been worked out but likely represents an area of incipient back-arc rifting. The plutons are found in a belt which extends southeasterly from north-central Washington across to near Missoula, Montana and then southward to the vicinity of Idaho City, Idaho.

The mineralogically most studied of these plutons are the Golden Horn batholith in north-central Washington (Boggs, 1980, 1984, Dunn, 1976) and the Sawtooth batholith in south-central Idaho which represent the two major types of anorogenic granite found in this area. The Golden Horn batholith consists of four rock types, 1) peralkaline arfvedsonite, 2) border (alaskitic arfvedsonite), 3) hypersolvus biotite, and 4) subsolvus biotite granites (Stull, 1969, Boggs, 1984). Each of these granites contains a characteristic suite of minerals. The most important minerals of these suites are (in approximate sequence of formation):

- Arfvedsonite granite - arfvedsonite, microcline, pyrochlore group, titanite, quartz, zircon, acmite, euxenite, albite, polylithionite, okanoganite, zektzerite, bastnaesite group, chevkinite, fluorite, allanite, astrophyllite, elpidite, gagarinite, monazite, siderite.
- Arfvedsonite granite (sogdianite pegmatite association) - acmite, microcline, quartz, sogdianite, zektzerite, polylithionite, bastnaesite, synchysite, Ca-Y-silicate.
- Border granite (rare-earth mineral association) - arfvedsonite, microcline, magnetite, quartz, kainosite, chlorite, acmite, gadolinite, allanite, titanite, zircon, albite.
- Border granite (calciohilairite association) - microcline, quartz, albite, fluorite, acmite, chlorite, calciohilairite.
- Biotite granites - ferro-hornblende, zircon, orthoclase, quartz, anatase, titanite, albite, epidote, prehnite, laumontite

The Sawtooth batholith is a peraluminous granite and typical minerals of this peraluminous suite include (in approximate sequence of formation):

- Beryl pockets - zinnwaldite, quartz, microcline, albite, hematite, beryl var. aquamarine, spessartine, bertrandite, and fluorapatite.
- Topaz pockets - zinnwaldite, quartz, microcline, fluorite, masutomilite, topaz, spessartine, hematite, albite, cassiterite, muscovite.
- Helvite pockets - quartz, microcline, albite, helvite, topaz.
- Carpholite pockets - Quartz, microcline, topaz, albite, carpholite group mineral.

Other plutons known to contain pegmatites or miarolitic cavities include the Lolo pluton near Missoula, Montana (quartz, fluorite), the Dismal Swamp pluton southwest of the Sawtooth batholith (quartz, topaz, beryl?), the Crags pluton north of Challis, Idaho (quartz, feldspars, beryl, topaz), and the Castle Peak stock in north-central Washington (quartz, beryl). About 50 other plutons either known or assumed to belong to this series are known to occur in Idaho (Bennett, 1980) and other plutons not now recognized as belonging to this series are probably present in northeastern Washington, northern Idaho and southern British Columbia, Canada.

References

Bennett, E.H. (1980) Granitic rocks of Tertiary age in the Idaho batholith and their relation to mineralization. Economic Geology, 75, 278-288.

Boggs, R.C. (1980) Okanoganite, a new rare-earth borofluorosilicate from the Golden Horn batholith, Okanogan County, Washington. American Mineralogist, 65, 1138-1142.

Boggs, R.C. (1984a) Mineralogy and geochemistry of the Golden Horn batholith, northern Cascades, Washington. Ph.D. Dissertation, University of California, Santa Barbara, California, 188 pp.

Dunn, P.J., Rouse, R.C., Cannon, B. and Nelen, J.A. (1977) Zektzerite: a new lithium sodium zirconium silicate related to tuhualite and the osumilite group. American Mineralogist, 62, 416-420.

Stull, R.J. (1969) The Geochemistry of the southeastern portion of the Golden Horn Batholith, northern Cascades, Washington. Ph.D. thesis, University of Washington, Seattle, Washington, 127pp.

GEOBAROMETRY AND PRESSURE-TEMPERATURE-TIME PATHS OF GRANULITES

BOHLEN, STEVEN R., Dept. of Earth and Space Sciences, State University of New York, Stony Brook, New York 11794, USA

Quantitative assessment of the tectonic events resulting in the formation of granulites requires knowledge of the P-T-time path for such terrains. P-T-time information for granulites requires accurate and precise thermometry and barometry. Recently several barometers have been calibrated experimentally for metaluminous and peraluminous rocks in order to determine the pressures of granulite formation. These include:

fay + qtz = ferrosilite, Bohlen and Boettcher, 1981
il + sill + qtz = alm + ru, Bohlen et al., 1983a
fay + an = garnet(Gr_1Alm_2), Bohlen et al., 1983b
il + an + qtz = garnet(Gr_1Alm_2) + ru, Bohlen and Liotta, 1986
herc + qtz = alm + sill, Bohlen et al., 1986

From these experiments and appropriate thermochemical data, other barometers can be calibrated:

ferrosilite + an = garnet(Gr_1Alm_2) + qtz, Bohlen et al., 1983b
sph + an = gross + ru + qtz, Essene and Bohlen, 1985
il + gross + qtz = alm + sph, Essene and Bohlen, 1985

Peak metamorphic pressures determined using the above equilibria in 30 upper amphibolite ($T < 650^oC$) and granulite ($T = 700-825^oC$) facies terrains range from 6-10 kbar with a clustering (22 of 30) of P at 7.5 $\pm$ 1 kbar. Also peak pressures for upper amphibolite facies terrains (12 terrains, P = 6.0 - 8.5, ave. = 7.3 kbar) are similar to those for granulites (18 terrains, P = 6.2 - 10.0, ave. 7.9 kbar). Especially for cases of paired upper amphibolite - granulite terrains, it is evident that amphibolites are distinguished from granulites by the latter's higher metamorphic temperatures but not higher pressure.

In 13 of the 18 granulite terrains, retrograde metamorphic P-T paths can be determined from compositionally zoned garnet rim compositions and the equilibria above. For garnet closure temperatures of 550 - 625°C, the inferred dP/dT retrograde paths are 2 - 8 bar/°C for all of the terrains. The same retrograde dP/dT is inferred regardless of the other Mg-Fe minerals (or lack thereof) with which the requisite barometric assemblage coexists. Therefore the zonation in the garnet cannot be caused by simple exchange with other mafic minerals. This implies that the barometric assemblages remained in equilibrium during the initial stages of retrogression and that granulite terrains cool initially

(200 - 250°C below peak T) without appreciable decreases in P.

The inferred peak metamorphic conditions for many granulite terrains occur in the sillimanite stability field but within 0.0 - 1.0 kbar of the kyanite-sillimanite boundary. The peak conditions are consistent with common occurrences of coarse, blocky sillimanite. Given the nearly isobaric path for initial retrogression, the lack of abundant retrograde kyanite in granulites implies that the cooling rate was rapid in comparison with conversion of sillimanite to kyanite.

In contrast with upper amphibolite terrains, peak and retrograde pressure data suggest that granulite terrains are formed by heating of magmas intruded beneath or into a given terrain rather than by increased heating from increased burial. These data along with thermal modeling (Wells, 1980) imply that heating occurred before and during loading and that the maximum pressures attained by granulites during the entire P-T-time path are equal, or close, to the inferred "peak" pressures, otherwise kyanite would be far more common in granulites. Magmatic heating of the lower crust before and during tectonic loading followed by initial, nearly isobaric cooling (an anti-clockwise P-T-time path as plotted on a P-T diagram) insures a long period of equilibration within the sillimanite field during prograde metamorphism. The anti-clockwise P-T path inferred for granulites contrasts sharply with the clockwise paths (loading before appreciable heating), inferred by Spear and Selverstone (1983) and England and Thompson (1984) for thrust- and fold-belt terrains metamorphosed to greenschist and amphibolite facies, that imply rapid, nearly isothermal decompression prior to and after the thermal maximum.

Peak pressure data and data on initial retrograde P-T paths for most granulite terrains are consistent with an anti-clockwise P-T-time path that in turn results from a significant contribution of magmatic heat during metamorphism. This implies that magmatic heating plays the critical role in the development of granulite terrains. Nappe/thrust style tectonics in the absence of appreciable magmatic heating can apparently only generate conditions appropriate for greenschist and amphibolite facies metamorphism. The ponding of magmas at the base of the crust might account additionally for the "double" thickness of crust inferred in granulite terrains. Different amounts of magmatic heating explain the variable average geothermal gradients (30-50°C) inferred for granulites.

INTERACTIVE PROGRAMS FOR STUDYING ISOMETRIES (ISOMET) AND MATRIX OPERATIONS (MATOP)

BOISEN, M. B., Jr., Dept. of Mathematics and GIBBS, G. V., Dept. of Geological Sciences, Virginia Polytechnic Institute & State University, Blacksburg, VA 24061

ISOMET is an interactive FORTRAN program that calculates matrix representations of point and space group operations (isometries) with respect to a user selected basis given the pertinent geometric information about the operation. It will compose two such operations, give the resulting matrix representation and describe the operation geometrically (the axis, rotation angle, screw component etc.). Also, given the matrix representation of a space group operation, ISOMET will give a geometrical analysis of the operation and will give the matrix representation of that space group operation with respect to a new origin and basis.

MATOP is an interactive FORTRAN program that performs basic matrix and vector operations in 3-space. It is designed to facilitate calculations in nonorthogonal bases. It performs the basic operations of multiplication, similarity transformation and matrix inversion. The vector operations of inner product, cross product and multiplication by a matrix (from a list of up to 15 matrices that are based on user input) are included.

The original versions of these programs were written to support the exercises and examples in our book "Mathematical Crystallography" written as the text for the MSA short course of the same name given at the 1985 GSA meetings. The source codes for these programs have been written so that the methods for performing the various operations as presented in the book are followed step by step.

PRECIPITATION MECHANISMS OF METALLIC PARTICLES IN OLIVINE

BOLAND, J.N., CSIRO, Division of Geomechanics, P.O.Box 54, Mount Waverley, Victoria, Australia, 3149.

The high temperature stability of iron and nickel bearing olivines (nominally Fo_{90}) relative to changes in the oxygen partial pressure (or oxygen fugacity, f_{O2}) of the surrounding gas has been studied using analytical electron microscopy. At f_{O2} values close to and below the phase boundary for the reduction of stoichiometric wustite (FeO) to metallic iron, the natural olivine samples also underwent a reduction reaction. The first detectable metallic phase was nucleated heterogeneously along dislocations in the (I00) and (00I) subboundaries. Although the (I00) subboundaries contained a high density of dislocations with I00 Burgers vector, the nucleation sites for the precipitation reaction were restricted to 0I0 and 00I dislocations. Furthermore, these nucleation sites seemed to coincide with the location of ledges in the (I00) subboundaries.

From the theory of heterogeneous nucleation, the rate of nucleation at dislocations is proportional to the square of the Burgers vector. The dominant Burgers vectors in olivine are b_I= I00, b_2 = 00I and b_3 = 0I0 and their respective magnitudes are 0.476nm, 0.599nm and1.023nm. Hence b_3-type dislocations would be expected to be the most effective nucleation site, followed by b_2 and b_I-type dislocations. The observations of the metallic precipitate distribution in reduced olivine support this model. In polycrystalline samples, the effects of grain boundaries on the reduction reaction are clearly evident. Larger micron-size metallic precipitates nucleate heterogeneously and grow at the grain boundaries. Again, this behaviour is predicted from the theory. The preferential grain boundary precipitation depletes the adjacent olivine matrix of the active cations iron and nickel creating a precipitation-free-zone (PFZ) along the boundaries.

The composition of the metal precipitates is a function of the oxygen fugacity. At a value of f_{O2} defined by the iron-wustite phase boundary the precipitates are nickel-rich with compositions as high as $Ni_{80}Fe_{20}$. Under extreme reducing conditions generated by passing CO-gas over the samples, the composition changes to Ni_4Fe_{96} -such a composition represents the complete removal of the iron and nickel contents in the olivine.

The kinetics of the reduction reaction was studied at 1300°C using single crystals of San Carlos olivine. From an analysis of the precipitate composition, distribution and growth (see Fig.), it is found that the rate of migration of the reduction-reaction-front is much slower than expected from a simple cationic diffusion model for the process. The rate of the reaction may be correlated, at least numerically, with the diffusivity of oxygen, but the actual atomic transport steps in the overall reduction process are more complex (Boland and Duba, 1985; Schmalzried,1984).

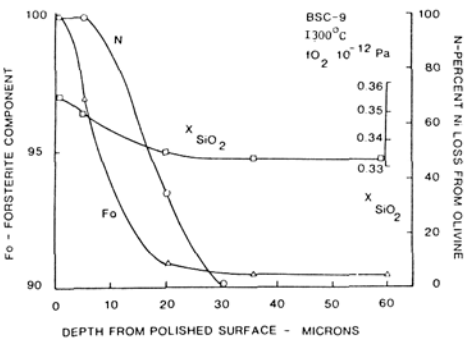

Fig. Results derived from the analytical electron microscopy showing the composition of the metallic precipitates (N) and the matrix olivine (Fo) as a function of depth from the gas-mineral interface.

References:

Boland,J.N. and A.Duba, Defect mechanisms for the solid state reduction of olivine. In: Point Defects in Minerals, Ed. R.N. Schock, Geophys. Monogr. 3I, AGU Washington, I985, pp 2II-225.

Schmalzried,H., Oxide solid solutions and its internal reduction reaction.Ber.Bunsenges.Phys.Chem.88, II86-II9I (I984).

THE DISTRIBUTION OF SILVER IN THE BROKEN HILL OREBODY

BOTH, R.A., Dept. of Geology and Geophysics, University of Adelaide, Adelaide, South Australia, 5000; STUMPFL, E.F., Institute of Mineralogy and Petrology, Mining University, A-8700 Leoben, Austria.

The Broken Hill lead-zinc-silver orebody was famous in the late 19th century and early 20th century for spectacular enrichments of silver in the oxidized zone. Silver has continued to be an important by-product from the primary ore, yet little attention has been given to its mode of occurrence.

The orebody consists of a series of lenses in metasediments and metavolcanics of the Early Proterozoic Willyama Supergroup. The ore is generally regarded as a submarine exhalative deposit that underwent complex deformation and granulite facies metamorphism (e.g. Plimer, 1984).

An electron microprobe study has been made of tetrahedrite and galena from 63 typical ore samples from the 4 mines of the Broken Hill orebody and representing the 5 principal "lenses" or "lodes" (B lode, A lode, 1 lens, 2 lens and 3 lens). The mode of occurrence of silver has been further studied by investigations on lead concentrates.

Terahedrite is rare in samples from B and A lodes and occurs as minute inclusions within galena. It is more common in 1 lens and common in 2 and 3 lenses and varies in form from minute inclusions to relatively coarse grains.

The tetrahedrites show an extremely wide range in composition, with individual analyses ranging from 0.06 to 50.88 wt% Ag. The majority of analyses lie between 1 and 25 wt% Ag.

The galenas show a range in silver content from below the detection limit (approximately 100 ppm) to a maximum of 1810 ppm for individual analyses.

Previous geochemical studies have shown a tendency for lenses of the Broken Hill orebody to have characteristic chemical compositions, evident in both the ore and individual minerals, but the silver data on tetrahedrite and galena (Figure 1) show only limited evidence of this. The silver content of tetrahedrite shows a wide range in all lenses. The galena data show some indication of differentiation between lenses, with generally low silver values in B lode, intermediate values in A lode, 1 lens and 2 lens, and higher values in 3 lens.

Areal analyses using the electron microprobe of representative lead concentrates from the Broken Hill orebody have shown that the main silver-bearing minerals are galena, tetrahedrite and pyrargyrite. This finding contrasts with the occurrence of silver in the Mount Isa lead-zinc-silver ore, where silver-rich tetrahedrite (freibergite) accounts for most of the silver (Riley, 1974).

References:

PLIMER, I.R., 1984: The mineralogical history of the Broken Hill Lode, N.S.W. J. Geol. Soc. Aust. V. 31, pp 379-402.

RILEY, J.F., 1974: The tetrahedrite-freibergite series, with reference to the Mount Isa Pb-Zn-Ag orebody. Mineral. Deposita, V. 9, pp 117-124.

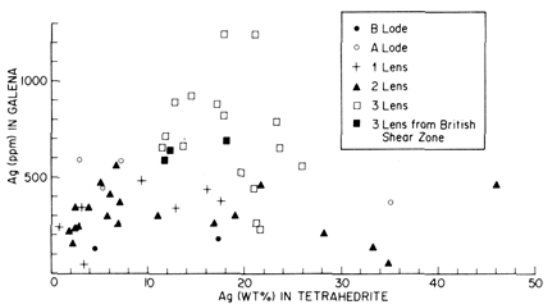

Figure 1: Silver content of galena vs silver content of tetrahedrite. Points represent mean values for samples.

ELECTRON MICROSCOPY (AEM-HREM) OF GOETHITE FROM A LATERITE : TWINNING AND EPITAXY ON KAOLINITE.

BOUDEULLE, M., Lab. de Minéralogie-Cristallographie, UA CNRS 805, Université de LYON, 69622 VILLEURBANNE CEDEX ; MULLER, J.P., Lab. de Minéralogie-Cristallographie, UA CNRS 09, Université PARIS VI-VII, 75230 PARIS, FRANCE.

Laterites result from intense weathering of rocks under humid tropical climate. The alteration products are mainly *kaolinite*, *hematite*, *goethite* and *gibbsite*.

In the course of a petrologic, mineralogic and geochemical analysis of a laterite sequence from Cameroon (MULLER and BOCQUIER, 1986), special attention has been paid to the morphology and inter-relationships of goethite with the other minerals.

The objectives of this study are to provide more informations about two interesting features. (i) star-shaped twinning ; (ii) epitaxy upon kaolinite, and to consider their significance as potential indicators of nucleation and crystal growth conditions.

Transmission electron microscopy and diffraction combined with X-Ray energy dispersive spectrometry have been carried out both on air-dried suspensions and ultra-thin sections of embedded material.

Star-shaped twins, with angles at about 60° between the individuals, correspond to (021) twinning. Their formation can be discussed in terms of bidimensional nucleation and cation disorder. Epitaxy of goethite upon kaolinite is now well documented. The orientation relationships are :

Goethite	Kaolinite
(100)	(001)
[010] (9.95 Å)	[200] (10.32 Å)
[003] (9.06 Å)	[010] (8.95 Å)

According to the 3-fold symmetry of kaolinite octahedral layer, goethite acicular crystals expand along the equivalent three directions, even forming twins.

Electron diffraction patterns suggest that a transitional structure with a definite atomic arrangement, an interphase, develops between the two minerals. This fact would contribute to a better understanding of the extensive atomic substitution (Al-Fe) in both compounds.

J.P. MULLER and G. BOCQUIER (1986), GEODERMA, in press.

HYDROTHERMAL TRANSPORT OF THE PGE, AN ALTERNATIVE MODEL FOR THE FORMATION OF STRATABOUND PGE DEPOSITS IN LAYERED INTRUSIONS.

BOUDREAU, A. E., and **McCALLUM, I. S.**, Department of Geological Sciences, AJ-20, University of Washington, Seattle, WA 98195

Several lines of evidence suggest that the stratabound platinum-group element (PGE) -rich zones of the Bushveld and Stillwater Complexes, which are characterized by unusually coarse textures, relatively abundant halogen-bearing and hydrous phases, a variety of exotic minerals (*e.g.*, graphite) and, in the case of the Merensky Reef, high temperature fluid inclusions, are the result of fluid transport of the PGE: 1) The secondary dunites/hortonolites of the Bushveld Complex, which are generally thought to have been the result of recrystallization by hot, silica-poor fluids, contain the highest reported grades of PGE in rocks from the Complex, and illustrate that late-stage fluids can remobilize and concentrate the PGE, particularly Pt and Pd. 2) Volcanic condensates from Hawaii are known to be unusually enriched in the noble metals. 3) Ultramafic rocks, which make up the footwall of the ore zones, typically have higher PGE abundances than do basaltic or more silicic rock types. If the PGE, particularly Pt and Pd, were initially present primarily with interstitial sulfides in the ultramafic footwall rocks, then they could be readily transported by late-stage fluids migrating through the crystal pile.

The high Cl content of halogen-bearing phases from the PGE zones of both the Stillwater and Bushveld Complexes suggests that Cl is the dominant complexing agent for the PGE. Consider the exchange of a divalent metal, M^{++}, between silicate melt and vapor:

$$\underset{\text{melt}}{MO} + \underset{\text{vapor}}{2NaCl} = \underset{\text{vapor}}{MCl_2} + \underset{\text{melt}}{Na_2O}$$

for which, the equilibrium constant is

$$K_e = \frac{[a(MCl_2)_{vapor}][a(Na_2O)_{melt}]}{[a(MO)_{melt}][a(NaCl)_{vapor}]^2}$$

It is thus apparent that, for a divalent metal complexed as a neutral chloride species, the concentration of the metal in the vapor phase is proportional to the square of the Cl activity (as NaCl) in the vapor, if all other activities remain unchanged. If the PGE are carried predominantly as Cl complexes, then one would expect to see a correlation between the PGE content of the sulfide and the Cl concentration of coexisting halogen-bearing phases. This appears to be true for two PGE zones from the Stillwater Complex. Apatite associated with the PGE-poor sulfides of the Picket Pin deposit of Anorthosite zone II contains considerably less Cl than does the apatite associated with the J-M Reef of Olivine-bearing zone I (fig. 1). Although the complexing behavior and relative solubilities of the PGE at high temperatures is unknown, the high (Pt + Pd)/Ir ratio of these ores is consistent with a hydrothermal origin because 1) At low and moderate temperatures, Pt and Pd are known to be more soluble in Cl-complexing aqueous fluids than is Ir, and 2) Ir is known to be partitioned into olivine and thus would be less available for transport.

We suggest that Cl-rich aqueous fluids exsolving during the solidification of the cumulus pile incorporated the PGE and base metals, which may have been originally preconcentrated in minor interstitial sulfide phases during the initial formation of the cumulate sequence. Horizons marked by major lithologic discontinuities due to influxes of more primitive magma are likely stratigraphic traps to the upward migration of these fluids, as they may define a horizon above which the cumulate sequence has not yet reached vapor saturation. Fluids reaching this horizon must redissolve and cause partial melting and/or recrystallization of existing cumulates, and can result in the precipitation of the PGE-sulfides. A variety of features, *e.g.* rounded and embayed cumulus plagioclase grains associated with the J-M Reef, are consistent with this interpretation.

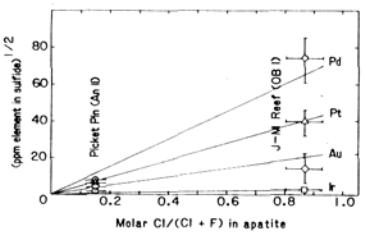

Figure 1. Comparison of metal concentration in sulfide vs. Cl content of apatite from two PGE zones from the Stillwater Complex.

RELATION BETWEEN MAGNETIC HYPERFINE FIELD DISTRIBUTION AND CATION ORDER IN NATURAL HEDENBERGITE

BOUJIDA, M., and REGNARD, J.R., DRF/Service de Physique/MDIH, CEN Grenoble 85 X - F38041 Grenoble cedex

Hedenbergite is a monoclinic chain silicate of the pyroxene group with nominal composition $CaFeSi_2O_6$. In the monoclinic $M_2Si_2O_6$ structure, the M cations (M = Fe, Mg, Mn, Ca, Na) occupy two non equivalent positions M1 and M2. Ca^{2+} and Na^{+} ions occupy preferentially the M2 sites which are strongly distorted sites having eighfold coordination. Ferrous and magnesium ions are located in octahedral M1 sites which form continuous zig-zag chains parallel to the c axis. The distances between nearest neighbouring Fe^{2+} within a chain is about 3.06 Å and much smaller than the distances of about 7.8 Å between Fe^{2+} ions located on neighbouring chains. From this arrangement a special type of quasi one-dimensional magnetic behavior can be expected. In order to study the magnetic properties of hedenbergite when both Fe^{2+} and Mg^{2+} (non magnetic) occupy the M1 octahedral sites, we use a natural sample of hedenbergite from Elba. The analysis of this sample using atomic absorption spectrophotometry leads to the formula $Ca_{0.96}Mg_{0.19}Fe_{0.82}Mn_{0.02}Si_2O_6$. The above formula indicates that the zig-zag chains of M1 sites are occupied by about 80 % of Fe^{2+} and 20 % of Mg^{2+} ions.

The inverse powder susceptibility can be approximated above T = 100 K by a Curie-Weiss law $1/\chi = T - \theta_p/C$. The positive value of the paramagnetic Curie temperature $\theta_p = +21$ K indicate dominant ferromagnetic exchange interactions. The Curie constant C corresponds to an average effective moment $\mu_{eff} = 5.43$ B.M. which is characteristic of Fe^{2+} with a large orbital contribution to the moment. The antiferromagnetic ordering temperature defined by the inflection point of $\chi = f(T)$ below the maximum is 23 ± 1 K. The magnetization M has been measured at T = 4.2 K as a function of external fields up to B_o = 15 T. $M(B_o)$ exhibits an inflexion point at a critical field $B_c \approx 40$ T. Such behaviour is characteristic for a metamagnetic transition, where the antiferromagnetic ordering changes directly to a parallel spin alignment. These magnetic measurements are consistent with the magnetic structure-type obtained by neutron diffraction characterized by ferromagnetic alignment of the moments inside each zig-zag M1 chain and antiferromagnetic alignment of the moments of neighbouring chains [1]. In this natural hedenbergite, the moments inside a zig-zag chain of M1 sites are parallel and aligned in the a-c plane forming an angle of 45° with the a axis.

The Mössbauer spectra recorded in the paramagnetic region ($T > T_N$) can be fitted with a single quadrupole doublet attributed to Fe^{2+} in the M1 sites. The magnetic ordering temperature obtained by Mössbauer spectroscopy is $T_N = 29 \pm 2$ K. The higher apparent magnetic ordering temperature measured by Mössbauer spectroscopy may be attributed to relatively slow spin fluctuations in the quasi one-dimensional chains. The Mössbauer spectra registered at 4.2 K and 1.5 K are best fitted by a distribution of hyperfine fields $P(B_{hf})$ which can be related to the various Fe^{2+}-Mg^{2+} nearest neighbour configurations surrounding a Fe^{2+} probe ion within the zig-zag chain of M1 sites. Assuming that distributions of isomer shift (IS) and quadrupole interaction (QS) are negligible, we used a method described by Varret [2] which is based on a discrete distribution $P(B_{hf})$ of hyperfine magnetic fields. A satisfactorily fit was obtained when the distribution was simulated by six Fe^{2+} magnetic hyperfine patterns in which IS and QS were constrained to be equal. The magnetic hyperfine field values lie between 14 and 19 T. The maximum of the $P(B_{hf})$ distribution obtained at about $B_{hf}^{max} = 17$ T is significantly smaller than the value $B_{hf} = 18.8$ T measured for Fe^{2+} in synthetic $CaFeSi_2O_6$ [3]. The observed small values of the hyperfine fields can be attributed to an important anisotropic orbital contribution to the hyperfine field in agreement with magnetic measurements. The discrete fitted distribution (6 values of B_{hf}) can be explained by considering all the possible Fe^{2+}-Mg^{2+} configurations up to second cation neighbours surrounding the Fe^{2+} probe. However the relative weights of the 6 components seem to indicate that we are not in presence of a random distribution of Fe^{2+} and Mg^{2+} in M1 sites. Future work is envisaged with EXAFS to determine the proportion of Fe^{2+} and Mg^{2+} in nearest-neighbour positions to an iron in a M1 site on the zig-zag chains of this natural hedenbergite.

[1] A. Wiedenmann and J.R. Regnard, Sol. St. Comm. 57, 499-504 (1986).
[2] F. Varret, Proc. Int. Conf. Appl. Mössbauer effect Jaipur 1981, 129-140.
[3] J.M.D. Coey and S. Ghose, Sol. St. Comm. 53, 143-145 (1985).

AB INITIO MODELS FOR THE LATTICE DYNAMICS OF MINERALS AT HIGH PRESSURE

BOYER, L. L., Condensed Matter Phys. Branch, Naval Research Laboratory, Washington, DC 20375-5000, USA; COHEN, R. E., Postdoctoral Research Associateships, Washington, DC 20418; MEHL, M. J., Condensed Matter Phys. Branch, Naval Research Laboratory, Washington, DC 20375-5000, USA

In recent years it has been demonstrated that calculations based on local density approximations (LDA) to density functional theory provide reliable electronic ground state energies for solids in general. For crystalline solids it is possible to calculate these "total energies" with no additional approximations beyond LDA, i.e., with no shape-approximations imposed on the self consistent potential or charge density. Having the total energy for a given material as a function of the positions of the nuclei is sufficient to determine both the static and vibrational pressure for any volume or structure we choose. Thus, in principle, reliable predictions of equations-of-state of complex minerals at high pressures are possible using LDA. In practice, calculations which are exact within LDA are limited by the large amount of computing required to relatively simple systems and a small number of structural distortions. To obtain sufficient information to determine the lattice dynamics, and, hence the vibrational pressure would in general, require accurate total energies for a very large number of structural distortions.

Fortunately, simplifying approximations are available for minerals having closed shell electronic structures which reduce the computational labor by several orders of magnitude. For a variety of halide materials remarkably good results are achieved, following the method of Gordon and Kim (1), by rigidly overlapping free ion densities (2). But for oxides it is necessary to include the stabilizing effect of the crystal potential on the O^{-2} ion (3). In a recent publication (4) we showed that a potential induced breathing (PIB) model based on the Watson sphere construction accounts for the violation of the Cauchy relations among elastic constants, in alkaline earth oxides, and plays a significant role in the splitting of the longitudinal and transverse mode frequencies. More recently we

AB INITIO MODELS FOR THE LATTICE DYNAMICS OF MINERALS AT HIGH PRESSURE

BOYER, L.L., et al.

have applied this model to study the statics and dynamics of more complex structured oxides such as $BaTiO_3$, (perovskite) corundum, rutile, quartz and stishovite. In addition, exact LDA calculations using a linearized augmented plane wave basis have been carried out for some of the simpler halides and oxides for detailed comparisons with the PIB model. In this report we review the current status of simplified models based on LDA for predicting static and dynamic properties of halides and oxides.

(1) R.G. Gordon and Y.S. Kim, J. Chem. Phys. 56, 3122 (1972).
(2) L.L. Boyer, Ferroelectrics 35, 83 (1981).
(3) A.J. Cohen and R.G. Gordon, Phys. Rev. B 14, 4593 (1976).
(4) L.L. Boyer, M.J. Mehl, J.L. Feldman, J.R. Hardy, J.W. Flocken and C.Y. Fong, Phys. Rev. Lett. 54, 1940 (1985).

• MECHANISMS FOR VISCOSITY AND TRANSPORT IN SILICATE MELTS

BRAWER, S.A., AT&T Bell Laboratories, Murray Hill, NJ 07974

Microscopic mechanisms for viscous flow and transport in silicate melts will be discussed. The mechanisms have been deduced from molecular dynamics computer simulations of silicate and fluoroberyllate liquids. (The structure of stimulated fluoroberyllate melts is the same as that of computer-simulated silicates of comparable composition.) It is observed that well-defined defects exist in the simulated liquids, in the form of overcoordinated Si and O ions. All diffusion takes place at defect sites. This mechanism provides a ready explanation for the observation that the viscosity of highly polymerized silicate melts decreases with increasing pressure. A spin model, due to G.H. Fredrickson and H.C. Andersen, is described, which models transport as the cooperatively hindered motion of defects. The behavior of the model has been determined from computer stimulations. The model exhibits non-Arrhenius temperature dependence of the average relaxation time and a broad distribution of relaxation times, both of which are similar to properties of silicate melts. Experimental consequences of these results are explored.

• DEFECTS IN SILICATE GLASSES

BRAWER, S.A., AT&T Bell Laboratories, Murray Hill, NJ 07974

A brief review is presented of defects in silicate glasses. The ideal structure of silicate glasses, at ambient pressure, has each silicon tetrahedrally coordinated by oxygen, and each oxygen either 2-fold coordinated by silicon (bridging oxygen) or having only one silicon neighbor (non-bridging oxygen). Deviations from this ideal structure are defects. Several defects have been well characterized by electron spin resonance, notably by J. Frieble and D. Griscom. These include the E' center (oxygen vacancy) and the peroxy linkage (oxygen-oxygen pair). Also described is recent work by Stathis and Kastner, in which defects in vitreous silica were excited by sub-band-gap radiation. The proposal by F. Gallener that planar 3-fold rings explain certain sharp Raman bands in vitreous silica is described. Computer simulations of silicate and fluoroberyllate liquids always contain defects in the form of 5-fold silicon and 3-fold oxygen. The nature of such defects in silica is described. These defects are thermally excited in silica and are predicted to be virtually nonexistent in coventional silica glass. The number of defects is expected to increase rapidly with the number of non-bridging oxygens, and to be a significant presence in less polymerized glasses. Several experimental results seem to be consistent with the presence of a few percent of overcoordinated silicon and oxygen in glasses with more than one non-bridging oxygen per silcon.

AN EXPERIMENTAL/TEM INVESTIGATION OF THE BREAKDOWN OF MUSCOVITE AT HIGH TEMPERATURE

BREARLEY, A.J., and RUBIE, D.C., Dept. of Geology, Manchester University, Manchester M13 9PL, U.K.

In many experimental kinetic studies, finely-crushed (powdered) mineral samples together with large quantities of fluid have been used as the starting materials. In high-porosity aggregates of this type, surface nucleation of product phases is common with subsequent unconstrained growth into the fluid-filled pore spaces. Mass transport through the pore fluid is rapid so that interface processes are generally rate-controlling. In contrast, rocks undergoing metamorphism are likely to have a low porosity, making the applicability of kinetic data from such studies to natural systems inappropriate.

To investigate the mechanisms and kinetics of a dehydration reaction under conditions of low porosity and low fluid content, samples of a quartz-muscovite schist have been run, both dry and with added H_2O (1 wt %), at temperatures of 720°C and 760°C, at 1 kbar, for times up to 5 months. These conditions significantly overstep the equilibrium temperature (~560°C) for the reaction of muscovite + quartz to K-feldspar + aluminosilicate + H_2O. At 760°C, in samples with added H_2O, oriented corundum needles with associated layers of melt ~0.2 μm wide develop in muscovite paralliel to (001) within a few hours. Subsequently (<2 weeks), muscovite becomes completely pseudomorphed by an extremely fine-grained aggregate by the reaction

muscovite + quartz → melt + sillimanite + mullite

(fig. 1a). As this reaction is metastable below ~5 kbar, both the melt and the mullite are regarded as metastable phases. In samples which were initially dry at 760°C, large muscovites become pseudomorphed in <5 months by an equilibrium assemblage consisting of volumes of K-feldspar, 3-4 μm across, enclosing oriented sillimanite + minor biotite with grain sizes up to 0.3 μm (fig. 1b). The orientation relationship between the product phases is $(001)_{biot}$ ~//$(13\bar{1})_{ksp}$ ~//$(100)_{sill}$ and $[100]_{biot}$//$[114]_{ksp}$//$[001]_{sill}$. However, small muscovites are pseudomorphed by melt + sillimanite + mullite.

Evidently the initial presence of H_2O caused disequilibrium by enhancing the kinetics of metastable melting reactions relative to the kinetics of the reaction forming K-feldspar + sillimanite + H_2O, in accordance with the Ostwald step rule. This demonstrates that the rapid development of equilibrium among minerals in the presence of H_2O cannot always be assumed.

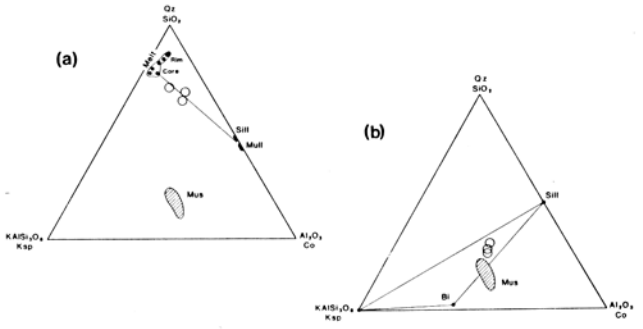

Fig. 1. Compositions of phases in muscovite pseudomorphs reacted at 760°C for 5 months (Fe and Mg components have been ignored as concentrations are low in all phases except biotite). The range of original muscovite compositions is indicated by the cross-hatched area. Bulk analyses of pseudomorphs, obtained using a defocussed electron beam, are shown as open circles.

(a) Water initially present. Melt compositions vary from the core to the rim of pseudomorphs as indicated. The bulk composition of the pseudomorphs is much richer in SiO_2 than the original muscovite.

(b) Sample initially dry. Pseudomorph bulk compositions are only slightly enriched in SiO_2 relative to the original muscovite.

CLASTIC GLAUCOPHANE, LAWSONITE AND JADEITIC PYROXENE IN FRANCISCAN METAGREYWACKES FROM MT HAMILTON, PACHECO PASS AND PANOCHE PASS, CALIFORNIA

BROTHERS, R.N., Dept. of Geology, Auckland University, Auckland, New Zealand; GRAPES, R.H., Joint Mineral Sciences Research Laboratory, Victoria University, Wellington, New Zealand

Clastic grains within Franciscan metagreywackes include plagioclase, quartz, white mica, chlorite, sphene, pumpellyite, lithic fragments, jadeitic pyroxene, lawsonite and glaucophane. The neometamorphic (non-clastic) mineral assemblage contains albite, quartz, calcite, aragonite, lawsonite, glaucophane, chlorite, white mica, sphene and pumpellyite.

A detrital origin for the pyroxene and some lawsonite and glaucophane is indicated by textural relationships and mineral chemistry. Clasts of these three minerals are distinguished from the neometamorphic assemblage, in the first instance, by having larger grain sizes and deformational features including bending, cracking and optical strain polarisation. Large strain-polarised grains of jadeitic pyroxene have inclusions of strained lawsonite or glaucophane, but none of these minerals has been seen growing across boundaries between adjacent clasts in the metagreywackes. In contrast, neometamorphic lawsonite forms small unstrained tablets grown across the margins of large clasts (e.g. pyroxene, plagioclase, quartz) and also totally surrounded by microcrystalline quartz-albite-chlorite-white mica in recrystallised matrices of the metagreywackes. Similar textural relationships are shown by authigenic glaucophane as discrete prisms or as dark coloured prismatic outgrowths on large clasts of pale glaucophane. In many cases where jadeitic clasts are in contact with greywacke matrix or detrital quartz, the pyroxenes are deeply embayed and replaced by fine-grained mixtures of albite+chlorite+quartz; as a general rule, within the scale of a thin-section, such replacements are most pronounced where neometamorphic lawsonite is also well developed.

The impure jadeite has highly variable compositions within single grains in all occurrences. Back-scattered electron imaging shows that, where enclosed within an albite clast, the pyroxene often consists of mineral islands in irregular shapes separated by albite or quartz (see figure sketched from photographs); concentrations of chlorite flakes indicate the outline of the original pyroxene grain. In this setting, two distinct compositional microdomains may be identified within the original grain boundary (see figure): pyroxene islands enclosed by clast albite have variable, but generally low, Jd contents; pyroxene islands surrounded by quartz have higher contents of Jd. These textures and compositions suggest retrograde equilibration of low Jd pyroxene+albite (the pre-deposition mineralogy of the clast) to high Jd pyroxene+quartz either prior to or during the Franciscan metamorphic event. Back-scatter studies also show that detrital lawsonite has Fe-enriched cores and sharply defined Fe-depleted rims which have compositions characteristic of neometamorphic lawsonite.

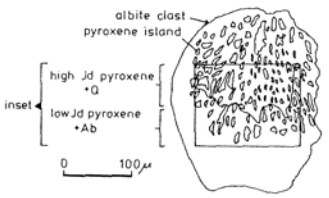

X-RAY ABSORPTION STUDY OF ZIRCONIUM IN NA-ZR-SILICATE GLASSES

BROWN, G.E., JR., PONADER, C.W., Department of Geology, Stanford University, Stanford, CA 94305, USA, KEEFER, K.D., Sandia National Laboratory, Albuquerque, NM, 87185 USA

Zirconium is commonly present in trace amounts in natural silicate melts and is a major component in some technologically important glasses, serving as a toughening and nucleating agent. In neither case is much know about the structural environment of Zr. This study was carried to out to provide such information. Observed variations in the coordination number of Zr with Na_2O/ZrO_2 ratio in several of the glasses studied suggest models for the bonding of Zr in silicate melts which may be applicable to more general silicate compositions.

Three compositions were studied in which the Na_2O/ZrO_2 ratio varied from less than to greater than one: ZNS-5: 13.0 Na_2O, 15.0 ZrO_2, 72.0 SiO_2, ZNS-6: 17.3 Na_2O, 17.3 ZrO_2, 65.3 SiO_2, and ZNS-10: 23.1 Na_2O, 17.4 ZrO_2, 59.5 SiO_2 (in mole %). Transmission EXAFS for Zr were collected at the Stanford Synchrotron Radiation Laboratory on bending-magnet line I-5 using Si(400) monochromator crystals. The data were analyzed, using monoclinic ZrO_2 as a model compound, by least-squares fitting of the fourier-filtered, back-transformed and k^3-weighted chi function. Zr in glass ZNS-5 was found to have an average coordination of 6.9 oxygens at 2.12 A. In glass ZNS-6 the coordination number is smaller but the bond lengths are similar, 6.1 and 2.11 A, respectively. Glass ZNS-10 appears to have a lower coordination number, 5.2, than the other glasses although the average bond length is the same as that found in ZNS-6, 2.11 A. The range of bond lengths in all three glasses appears to be significantly narrower than that found in zircon (2.13-2.27 A) and ZrO_2 (2.05-2.28 A) based on the width of the Zr-O peak in the radial distribution functions and the width of the main line in the K-edge (Fig 1). Zr in smaller amounts in aluminosilicate glasses has also been shown to have a coordination number of approximately 6 and an average Zr-O distance of 2.10 A (Ponader and Brown, 1984; Petiau, *et al.*, 1984).

These coordination numbers are consistent with those predicted on the basis of local charge balance and bond strength considerations in the three glass compositions. For glass ZNS-6, ($Na_2O = ZrO_2$ in mole %), if the non-bridging oxygens are assumed to be bonded to two 6-8 coordinated Na atoms plus one 4-coordinated Si atom, a Zr coordination of 6 oxygens is predicted based on Pauling bond strength arguments. For glass ZNS-5, ($Na_2O > ZrO_2$), some of the non-bridging oxygens should have more than two Na atoms bonded to them, resulting in a higher average Zr coordination than in glass ZNS-6. The third glass ZNS-10, ($Na_2O < ZrO_2$), is predicted to have some non-bridging oxygens with fewer than two Na atoms and one Zr bonded to them resulting in a smaller coordination (perhaps 4-5 coordination) than in glass ZNS-6. In addition, there should be some non-bridging oxygens in ZNS-10 with the same local environment as in glass ZNS-6 resulting in 6-coordinated Zr atoms. Therefore, glass ZNS-10 is predicted to have Zr with an average coordination of ~5 which is consistent with the EXAFS analysis. These proposed structural models are also consistent with the variations in widths (ΔE) of the main K-edge features for the 3 glasses: ΔE(ZNS-6)=2.1eV, ΔE(ZNS-5)=2.3eV, ΔE(ZNS-10)=2.75eV (Fig. 2). A broadening of the K-edge is expected when the absorber, Zr, is located in different types of environments.

Study supported by DOE, Basic Energy Sciences Program and, in part, by NSF Grants EAR-8016911 and EAR-8513488.

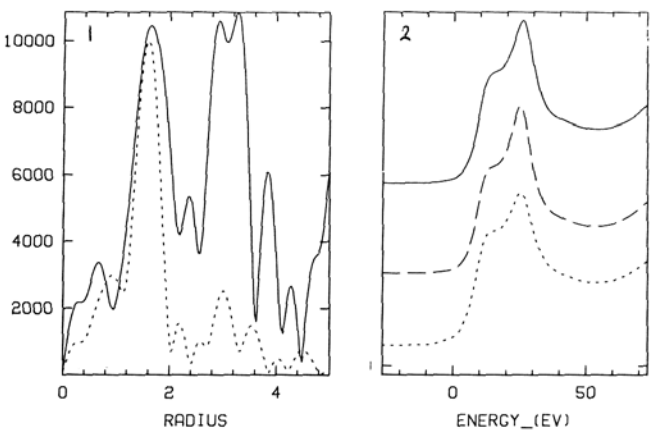

Fig. 1. Radial distribution functions for zircon (solid) and ZNS-5 (dotted).
Fig. 2. K-edge spectra for ZNS-5 (solid), ZNS-6 (dashed) and ZNS-10 (dotted).

REFERENCES

Ponader, C.W. and Brown, G.E., Jr. (1984), EOS, Trans. of the Amer. Geophys. Union, 65(45), 1140.

Petiau, J., Calas, G., Dumas, T., and Heron, A.M. (1984) EXAFS and Near Edge Structure III, Hodgson, K.O., Hedman, B., and Penner-Hahn, J.E., eds., Springer-Verlag, 291-296.

X-RAY ABSORPTION STUDIES OF SILICATE GLASSES USING SYNCHROTRON RADIATION

BROWN, G.E., JR., PONADER, C.W., AND JACKSON, W.E., Dept. of Geology, Stanford University, Stanford, CA 94305, USA

X-ray absorption spectroscopy is a relatively old method that has recently gained renewed interest and wide-spread application as an element-specific structural probe because of the availability of high intensity, tunable, synchrotron radiation sources. One of the key advances in the mid-seventies that led to its current importance was the development of a single-scattering theory that allowed the extended fine-structure beyond the main absorption edge (the EXAFS) to be interpreted in terms of the number and type of backscattering atoms surrounding the absorber, their distance from the absorber, and their relative degree of disorder. The near-edge fine structure, referred to as NEXAFS, has been described as a multiple-scattering phenomenon, but there is not yet an adequate theory that can be used to reliably interpret NEXAFS spectra. The position and intensity of near-edge features are sensitive to coordination geometry and oxidation state and contain important bonding information. Both types of spectroscopy are currently being used to provide unique structural data on cation environments in amorphous materials including oxide and aluminosilicate glasses of geochemical importance. This paper will review some of these results, compare structural information from EXAFS analysis of silicate glasses with that from other spectroscopic methods, correlate these results with predictions from recent molecular dynamics simulations, and discuss some of the limitations of the method caused by positional disorder in amorphous materials.

To date, several dozen x-ray absorption studies of oxide glasses have been reported. In most of these studies the problem of determining phase shifts and back-scattered amplitudes of the scattered photoelectron wave is handled by using crystalline model compounds containing the same absorber as the glass in a similar structural environment; the refined phases and amplitudes from the crystals are used in fitting distances and coordination numbers to a model which reproduces the observed glass EXAFS spectrum. For certain elements (M) such as K and Ca in complex aluminosilicate glasses, EXAFS spectroscopy is the only direct structural method that provides distances and coordination numbers, unlike x-ray radial distribution analysis (*e.g.* Taylor and Brown, 1979) where the range of M-O distances and interferences by O-O and T-T distances (O = oxygen, T = tetrahedral cation - Si or Al) make characterization of local alkali cation environment difficult. Recent EXAFS studies of the local coordination environments of Na (McKeown *et al.*, 1985a), K (Jackson *et al.*, 1986), and Ca (Boek *et al.* 1983; Binstead *et al.*, 1985) in aluminosilicate glasses and crystalline analogues such as albite, microcline, and anorthite have shown these cations to occupy sites in the glasses with distances and coordination numbers of 2.6 A and 6.5 oxygens, 2.9 A and 8.9 oxygens, and 2.6 A and 7 oxygens, respectively, in close agreement with their local geometry in the crystalline analogues. In contrast, comparison of Ca K-edge EXAFS and NEXAFS spectra of titanite and diopside composition glasses and their crystalline analogues indicates differences in glass and crystal Ca environments.

EXAFS and NEXAFS studies of Al (McKeown *et al.*, 1985b) and Mg (this study) environments in silicate glasses pose special problems because of the soft nature of the x-rays at the energies of these edges, which necessitates the use of ultra-high vacuum photoemission methods. Nonetheless, we have obtained useful structural information for these elements in silicate glasses which indicates that they occupy tetrahedral environments in the compositions studied. More recently we have initiated other EXAFS studies of the structural environments of trace amounts of selected transition metal, rare earth, and actinide elements in silicate glasses. Selected results will be discussed.

Study supported by NSF Grants EAR-8016911 and EAR-8513488

REFERENCES

Binsted, N., Greaves, G.N., and Henderson, C.M.B. (1985) Contrib. Mineral. Petrol. 89, 103-109.

Boek, H.P., Brown, G.E., Jr., and Waychunas, G.A. (1983) EOS, Trans. Amer. Geophys. Union 64, 868.

Jackson, W.E., Brown, G.E., Jr., and Ponader, C.W. (1986) (this volume)

McKeown, D. A., Waychunas, G. A., and Brown, G. E., Jr. (1985a) J. Non-Crystal. Sol., 74, 325-348.

McKeown, D. A., Waychunas, G. A., and Brown, G. E., Jr. (1985b) J. Non-Crystal. Sol., 74, 349-371.

Taylor, M. and Brown, G.E., Jr. (1979) Geochim. Cosmochim. Acta, 43, 61-75.

REACTIONS, P-T-t PATHS AND GEODYNAMICS OF GARNET-CORDIERITE MIGMATITES AND GNEISSES

BROWN, M., School of Geological Sciences, Kingston Polytechnic, Penrhyn Road, Kingston upon Thames, KT1 2EE, UK

Reaction textures can provide two kinds of information useful to petrologists; this is because the slowness of the reaction kinetics results in both reactant and product solid phases being preserved. Such textures are common in relatively dry high-grade rocks, especially those which have experienced rapid decompression. First, study of the minerals in these textures can provide insight into the process of re-equilibration during reaction. Second, information can be obtained from a study of mineral compositions and relationships in such textures which may constrain part of the P-T-t path followed by the rock. The reactants may preserve, through zoning or included mineral phases, evidence of the earlier metamorphic history, while the reaction texture reflects one particular P-T point on the P-T-t path. Frequently, in rocks which exhibit reaction textures, more than one reaction is frozen in and more than one P-T point may be determined. If the stability relations of the particular reaction which has been frozen in have been determined, either by experiment or by calculation, then it may be possible to obtain information on the physical conditions at which the reaction was proceeding. Compositional zoning is common in minerals in these situations, for example in garnet which frequently undergoes reaction during decompression. Often, two adjacent minerals exhibit zoning, especially at their common boundaries, and the assumption is sometimes made that the compositions of the cores were in equilibrium and can be used to determine temperature at the start of the reaction, while edge compositions reflect final equilibration and, therefore, some lower temperature during continued uplift. The information gained from study of rocks with reaction textures can constrain parts of P-T-t paths followed by metamorphic terrains. The P-T-t paths can be used to constrain possible geodynamic processes and models and, therefore, to place constraints on possible tectonic settings for the development of metamorphic belts.

The first example is from the South Armorican Metamorphic Belt in France, a paired blueschist terrain/migmatite terrain. Pelitic migmatites vary from stromatic types developed syn-D1 (metatexites) to schlieric types developed syn-D2 (diatexites), the more extensive anatexis during D2 reflecting decompression melting. The migmatites carry abundant garnet (homogeneous core areas surrounded by retrograde rims produced during reaction to Crd and Bt + Pl) with very rare inclusions of biotite but more common inclusions of plagioclase and quartz, and infrequent but ubiquitous kyanite relics in plagioclase, although sillimanite is the widespread Al-silicate. Textural relations between and mineral chemistries of ferro-magnesian phases in the diatexites suggest that two discontinuous reactions which produced cordierite and additional continuous compositional changes have been overstepped as a result of decrease in P during high-grade metamorphism and anatexis. Early P-T conditions were $P = 10 \pm 2$ kbar at T greater than 700°C and late P-T conditions, during which garnet and biotite were partially replaced by cordierite, were $P = 5 \pm 0.5$ kbar at T = 715°C with $X(H_2O)$ around 0.6. The P-T-t path so defined, reflecting adiabatic decompression, results from processes, presumably related to stretching and crustal thinning, in the facing plate at a subducting margin during the Ligerian orogeny. The diatexites represent material which has risen more rapidly and from greater depth than the stromatic migmatites as a result of diapirism concomitant with stretching. Such diapiric amplification induces a strong decompression that is registered in the mineral parageneses. The high thermal gradients apparently represented in terrains of this type are due to the fact that the amplification of gravity instabilities is a process which evolves faster than heat conduction.

The second example is a garnet-orthopyroxene-cordierite gneiss from the late-Archaean – early-Proterozoic Sharyzhalgay Complex, USSR which exhibits evidence for overstepping two reactions during rapid uplift. The reactions are Grt + Qtz to Pl + Opx, which forms an early corona structure, and Grt + Opx (lower Al) to Crd + Opx (higher Al) in a symplectite which replaces both garnet and early pyroxene. Mineral assemblage stability data, mineral compositions and zoning patterns together with P-T data derived from various published geothermobarometers indicate that the uplift P-T-t path passed through the following approximate P-T points: 6 kbar/750°C; 4 kbar/700°C; and, 3 kbar/600°C. A diapiric model related to magma emplacement under granulite facies conditions is proposed.

COLLECTION AND ANALYSIS OF COSMIC DUST

BROWNLEE, D.E., University of Washington, Seattle, Washington

Submillimeter extraterrestrial particles, debris from comets and asteroids, are accreted by the Earth at a rate of 10,000 tons a year. Particles larger than 100 μm usually melt during atmospheric entry and form the "cosmic spherules" that have been collected from deep sea sediments for over a century. Particles smaller than 50 μm are not as strongly heated and commonly survive as "micrometeorites", particles that experience no melting. Micrometeorites are currently collected in the stratosphere with NASA U2 aircraft.

The spheres are not as pristine as micrometeorites but their larger mass is important for certain analytical investigations. Detection of the cosmogenic isotopes ^{26}Al, ^{53}Mn and ^{10}Be and measurement of nonterrestrial oxygen isotope ratios in the spheres is proof of their extraterrestrial origin. The most common spheres have chondritic elemental abundances and are composed of olivine, magnetite and glass. A small fraction of the spheres contain unmelted relict grains usually forsterite, enstatite or sulfide. Trace element studies of the relict grains provides a means of comparing the particles with established meteorite types. The relict grain composition, the bulk elemental composition of the totally melted spheres and oxygen isotopic composition all indicate that most of the spheres are derived from a parental material similar to C2 carbonaceous chondrites. In addition to silicate spheres, "iron" spheres are also found. The iron spheres contain magnetite, wustite and metal. In some cases the metal phase is composed almost entirely of platinum group elements in chondritic proportions.

The micrometeorites are comparatively pristine but small. They are being investigated by essentially all techniques that can be applied to nanogram samples. Many lines of evidence indicate that the particles are extraterrestrial but the most straightforward is their high abundance of cosmic ray tracks that can be directly imaged in small mineral grains with the TEM. Most of the particles are fine grained and have chondritic elemental compositions. Most of the particles with nonchondritic compositions are dominated by a single phase, usually olivine, pyroxene or sulfide. The chondritic particles are of two basic types, those composed of hydrated silicates and those composed of entirely anhydrous phases. Many of the hydrated particles appear to be related to CI/CM carbonaceous chondrites. The anhydrous particles are a unique type of material that has not been observed in the form of conventional meteorites. They are the most porous and finest grained meteoritic materials known. There is a strong likelihood that the porous anhydrous particles are cometary.

POSITIONAL DISORDER OF CAVITY AND CHANNEL CATIONS IN MINERAL STRUCTURES: INFLUENCE OF LOCAL FRAMEWORK CATION CONFIGURATIONS

BURNHAM, CHARLES W., Dept. of Geological Sciences, Harvard University, Cambridge, MA 02138, USA; POST, JEFFREY E., Dept. of Mineral Sciences, Smithsonian Inst., Washington, DC 20560, USA

Cations that occupy sites in cavities or channels in mineral structures frequently exhibit large apparent thermal parameters that extrapolate with decreasing temperature to non-zero values at 0°K. Various authors have attributed this behavior to positional disorder caused by more than one chemical species on the cavity site, by response of the cavity cation to varying local electrostatic fields arising from different framework cation distributions, or by other less obvious factors. Using electrostatic energy minimization techniques (program WMIN, Busing, 1981) and short-range repulsive potentials obtained from MEG calculations, we have examined the influence of varying local framework cation distributions on minimum-energy cavity cation positions in several mineral systems: high albite, hollandites with 1/2 and 2/3 filled tunnel sites; A-site occupied edenite and richterite amphiboles. Preliminary results of these calculations have been reported by Post and Burnham (1983), Post and Burnham (1984), and Docka et al. (1980).

Minimum energy positions for cavity cations have been calculated assuming fixed oxygen frameworks with varying ordered arrangements of octahedral or tetrahedral cations. Different arrangements are modelled by altering cation charges and cation-anion repulsive parameters. Oxygen frameworks have the fixed symmetry of the base structures, but the effective symmetry is lowered and in some cases the unit cells are doubled, tripled, or quadrupled to permit appropriate ordered distributions of octahedral or tetrahedral cations. Electrostatic energies are then minimized by varying the coordinates of the cavity cations.

The Na cations in high albite take up differing positions depending on the local distribution of Al and Si in tetrahedral sites. Calculations for all distributions not violating Al-avoidance yield a distribution of Na positions that explains well the observed quarter-atom Na positions and thermal parameters of previous structure refinements. When calculations are made using the framework determined at 1090°C (Prewitt et al., 1976), the new distribution of Na minimum-energy positions easily explains the observed changes in Na quarter-atom positions and thermal parameters from room temperature to high temperature. We argue, therefore, that in high albite all reasonable local Al/Si distributions occur, and the hypothesis of a domain structure is unnecessary to explain Na behavior.

Calculated Ba positions in half filled hollandite tunnels vary, depending on octahedral Ti/Al distribution, from the nominal 4/m special position up to 1.0Å parallel to and 0.6Å perpendicular to the tunnel axis, with the larger perpendicular displacements associated with smaller parallel displacements for energetically less favorable Ti/Al arrangements having Al's in adjacent edge-sharing octahedra. Calculated K positions in the two-thirds filled cases vary from the special position in response to differing Ti/Mg cation distributions up to 0.7Å parallel to and 0.55Å perpendicular to the tunnel axis. Again energetically less favorable Ti/Mg distributions (Mg's in adjacent edge-sharing octahedra) lead to tunnel cation displacements with larger perpendicular components. Comparison of Sr versus Ba and Na versus K shows that, for a given octahedral cation distribution, smaller tunnel cations are consistently displaced further from the 4/m site.

Edenite substitution in a tremolite base structure ($\square^A + Si^T \rightleftharpoons Na,K^A + Al^T$) leads to minimum energy A-site positions displaced 0.61 to 0.73Å from the conventional 2/m equipoint for Na and 0.41 to 0.61Å for K, with slight differences between OH^- and F^- structures and Al substitutions into T1 versus T2. Richterite substitution ($\square^A + Ca^{M4} \rightleftharpoons Na,K^A + Na^{M4}$) leads to displacements ranging from 0.06 to 0.72Å depending on K versus Na in the A-site, OH^- versus F^-, and the distribution of Na and Ca in the four nearest equidistant M4 sites. Displacements of the minimum energy A-site position will be off symmetry elements unless the local environment is symmetric, in which case the displacement will be within m or along 2 depending on that local symmetry.

Since the positional disorder of cavity cations is a predictable response to framework cation configurations, no significant additional configurational entropy contributions need be added to those already present due to framework cation disorder.

Busing, W.R. (1981) U.S. Nat'l. Technical Info. Serv., ORNL-5747
Docka, J.A., et al. (1980) GSA Abstr. with Prog. **12**, 414
Post, J.E. and C.W. Burnham (1983) GSA Abstr. with Prog. **15**, 663
Post, J.E. and C.W. Burnham (1984) GSA Abstr. with Prog. **16**, 625
Prewitt, C.T. et al. (1976) Am. Mineral. **61**, 1213-1225

DEFECT IRON CRYSTAL CHEMISTRY OF Fe^{2+}-Fe^{3+} MINERAL ASSEMBLAGES: IMPLICATIONS TO THERMODYNAMIC CALCULATIONS OF OXYGEN FUGACITIES

BURNS, R.G. and BARTELS, K.S., Department of Earth, Atmospheric & Planetary Sciences, Massachusetts Institute of Technology, Cambridge, MA 02139, USA

Several mineral assemblages used to assess oxygen fugacities of igneous and metamorphic rocks comprise iron-bearing phases having variable stoichiometries. Such defect chemistries have been demonstrated in recent Mossbauer spectral measurements of a variety of Fe^{2+}-Fe^{3+} silicates, including garnets,[1] ilvaites,[2] aenigmatites,[3] fayalites,[4] and ferruginous micas.[5] The applicabilities of oxygen-buffering reactions such as

$$3Fe^{2+}_2SiO_4 + O_2 = 2Fe_3O_4 + 3SiO_2 \quad (1)$$
fayalite — magnetite — quartz

$$KFe^{2+}_3Si_3AlO_{10}(OH)_2 + O_2 = KAlSi_3O_8 + Fe_3O_4 + H_2O \quad (2)$$
annite — sanidine — magnetite

$$3Na_2Fe^{2+}_5TiSi_6O_{20} + 2O_2 = Fe_3O_4 + 3Fe_2TiO_4 + 6NaFe^{3+}Si_2O_6 + 6SiO_2 \quad (3)$$
aenigmatite — magnetite + ulvospinel solid-solution — aegerine — quartz

are questionable when the fayalite is "ferrifayalite",[4] the annite is ferric biotite,[5] the magnetite is cation deficient,[6] and the aenigmatite contains appreciable amounts of Fe^{3+}.[3] The problem is complicated further by our observations that identical rock-types having similar mineral assemblages contain phases with different stoichiometries. For example, annite at its type-locality in the Cape Ann granite near Rockport, Massachusetts is ferric-rich biotite and coexists with nearly stoichiometric fayalite plus magnetite. Granites from Mourne Mountain (Ireland), however, contain Fe^{3+}-biotite, non-stoichiometric magnetite and "ferrifayalite," whereas the Pikes Peak (Colorado) granite contains Fe^{2+}-annite coexisting with "ferrifayalite" and cation-deficient magnetite. These results suggest that reactions such as

$$3[(Fe^{2+}_a Fe^{3+}_b \square_c)_2SiO_4] + O_2 \rightarrow 2[Fe_{3-d}O_4] + 3SiO_2 \quad (4)$$

or

$$2[K(Fe^{2+}_x Fe^{3+}_y \square_z)_3Si_3AlO_{10}(OH)_2] + 3SiO_2 \rightarrow 3[(Fe^{2+}_a Fe^{3+}_b \square_c)_2SiO_4] + 2KAlSi_3O_8 + 2H_2O \quad (5)$$

and

$$[K(Fe^{2+}_x Fe^{3+}_y \square_z)_3Si_3AlO_{10}(OH)_2] + O_2 \rightarrow [Fe_{3-d}O_4] + KAlSi_3O_8 + H_2O \quad (6)$$

need to be evaluated, and not the idealized ones expressed by equations 1-3. That equation 1 is an inadequate representation of the fayalite-magnetite-quartz (FMQ) buffer is suggested by observed discrepancies between the numerous experimentally determined equilibrium boundaries and the curves calculated from thermodynamic data for the reaction assuming stoichiometry of the pure fayalite and magnetite.[7]

With a view to determining coefficients a, b, c, d in equation 4, we are conducting Mossbauer spectral, electron microprobe, and electron microscopy measurements of magnetite, fayalite, and "ferrifayalite" on specimens equilibrated in a gas-mixing furnace at controlled oxygen fugacities bounded by the magnetite-hematite (MH), fayalite-magnetite-quartz (FMQ), and iron-quartz-fayalite (IQF) buffers. Preliminary results, for example, indicate that the Mourne Mountain granite crystallized at a higher temperature on the FMQ buffer than did the Cape Ann granite.

1. K.B. Schwartz, D.A. Nolet, and R.G. Burns, Amer. Mineral., 65, 142-153 [1980].
2. D.A. Nolet and R.G. Burns, Phys. Chem. Minerals, 4, 221-234 [1979].
3. J. -B. Choi and R.G. Burns, GSA Abstr. Indianapolis, 15, 543 [1983].
4. M.W. Schaefer, Amer. Mineral., 70, 729-736 [1985]. 5. M.D. Dyar and R.G. Burns, Amer. Mineral., 71, in press [1986].
6. L.S. Darken and D.W. Gurry, J. Amer. Chem. Soc., 68, 799-810 [1946].
7. R.J. Arculus, Ann. Rev. Earth Planet. Sci., 13, 75-95 [1985].

ORDER-DISORDER AND PHASE SEPARATION IN THE SYSTEMS Fe_2O_3-$FeTiO_3$, $CaCO_3$-$MgCO_3$, AND $CaMgSi_2O_6$-$NaAlSi_2O_6$

BURTON, B. P. and Davidson, P. M. National Bureau of Standards, Gaithersburg, MD. 20899.

Thermodynamic models that include anisotropy of solution properties (ordering is favored in one crystallographic direction but phase separation is favored in another) can account for phase relations of the systems Fe_2O_3-$FeTiO_3$, $CaCO_3$-$MgCO_3$, and $CaMgSi_2O_6$-$NaAlSi_2O_6$. These models predict phase diagram topologies and systematics for excess heats of mixing that are at least qualitatively consistent with experiment. In the simplest case, a two-parameter model yields the symmetrical prototype diagram of Fig. 1; asymmetric diagrams require three or more parameters. Modifications and assumptions for specific systems are elaborated below.

Fe_2O_3-$FeTiO_3$: Chemical interactions are assumed to favor ordering $\parallel$ to c-hex and phase separation $\perp$ c-hex. Magnetic interaction parameters are required to model the Neel transition in Fe-rich solutions, and the magnetic degree of freedom enters the model as an additional component [Burton (1985) Am. Min. 70, 1027-]. It is predicted that magnetic ordering significantly reduces the solubility of Ti in Fe-rich solutions, Fig. 2.

$CaCO_3$-$MgCO_3$: Ordering $\parallel$ c-hex + phase separation $\perp$ c-hex is assumed, but strong asymmetry in the tendency for phase separation (a third parameter) is required to produce a stability field for two calcite-structure phases, Figs 3. Note that two distinct phase diagram topologies are possible.

$CaMgSi_2O_6$-$NaAlSi_2O_6$: M1-M1 and M2-M2 interactions ($\parallel$ c-mono) are assumed to favor ordering and M1-M2 interactions are assumed to favor phase separation ($\perp$ c). Thus, a third parameter is required to allow different degrees of long range order on M1 and M2 sites, and a fourth is required to produce an asymmetric phase diagram (Figs. 4). Order parameters for M1 and M2 sites are equal only at ØK and the critical temperature for ordering of omphacite, consistent with space group symmetry. Note that Fig 4b shows a stability field for coexisting ordered phases.

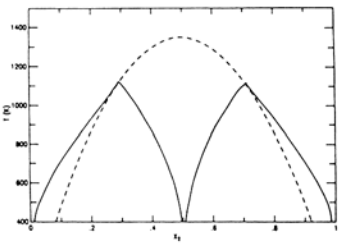

Figure 1.

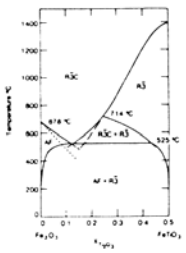

Figure 2.

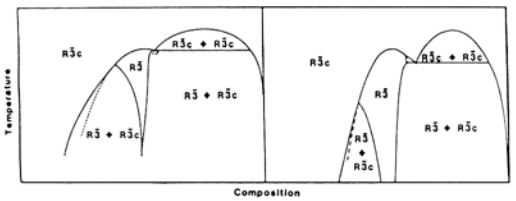

Figure 3a

Figure 3b

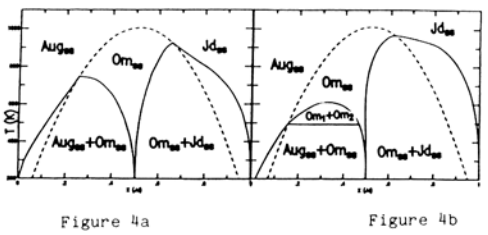

Figure 4a

Figure 4b

THE MICRO-PIXE TECHNIQUE IN STUDIES OF SOME CANADIAN BASE METAL ORES

CABRI, L.J., Mineral Sciences Laboratories, Canada Centre for Mineral & Energy Technology, 555 Booth Street, Ottawa, Ontario, CANADA K1A 0G1

The Micro-PIXE (Particle Induced X-ray Excitation) analytical technique has been used as a proton microprobe to determine trace elements in sulfide minerals ("thick-target PIXE") from base metal sulfide ores. The proton microprobe is an in situ non-destructive trace-element technique which has usually been used with an energy dispersive detector. Accurate derivation of element concentrations from observed X-ray yields can be obtained by using recent developments in modelling the X-ray production in thick targets, and combining these developments with least-squares codes for fitting multi-element spectra. Satisfactory calibration is obtained using synthetic sulfide standards. Typical minimum detection limits for elements from Se (44) to Sn (50) in minerals such as chalcopyrite, pyrite, pyrrhotite and sphalerite range from < 5 to about 20 ppm.

A major problem in many base metal sulfide ores is the precise determination of the distribution of silver among silver minerals (100-20 wt.% Ag), silver-containing minerals (1-20 wt.% Ag) and silver-bearing minerals (< 1 wt.% Ag) (Cabri et al., 1984). The silver concentration of the last may be within the detection limits of an electron microprobe for some minerals such as galena (up to 0.9 wt.% Ag, Chen & Petruk, 1980), and chalcopyrite (up to 0.29 wt.% Ag, Harris et al., 1984). However, the electron microprobe is not sufficiently sensitive for most minerals under consideration.

The Micro-PIXE technique has been applied to sulfides from a wide range of Canadian base metal ores (Brunswick Mining & Smelting, Geco, Kidd Creek, Mattagami-Norita and Nanisivik). As expected, the trace-element concentrations within individual deposits variably reflect the larger scale mineral and metal zonation. Chalcopyrite, galena, pyrite and sphalerite were all determined to be silver-bearing minerals. For example, in samples from Kidd Creek, 90% of 38 chalcopyrite samples contain > 10-12 ppm Ag, and Ag content varies to 0.16 wt.%; similarly, 35% of 37 sphalerite samples contain > 12-13 ppm Ag, varying up to 300 ppm Ag. For Brunswick Mining & Smelting, 10 chalcopyrite samples have Ag contents ranging from 28 to 106 ppm and 62% of 40 sphalerite samples contain > 9-13 ppm Ag, varying up to 54 ppm Ag. The silver content of pyrite, on the other hand, is generally lower, being just above or below detection levels of 4 to 9 ppm. However, the total amount of contained Ag in pyrite may be significant since, for example, pyrite constitutes 59 wt. % of the mill tailings at Brunswick Mining & Smelting (Petruk & Schnarr, 1982).

Other trace elements determined are As, Se, Cd, In and Sn in sphalerite; Zn, As, Se, In and Sn in chalcopyrite; and Cu, Co, Zn, As, Se and Sn in pyrite. Data for pyrrhotite are sparse, but Cu, Ni, Co, As, Se and Ag have been determined on a few samples.

References:

Cabri, L.J., Harris, D.C. & Nobiling, R. (1984): Trace silver analysis by proton microprobe in ore evaluation. In Precious Metals: Mining, Extraction, and Processing, Proceeding AIME, 93-100.

Chen, T.T. & Petruk, W. (1980): Mineralogy and characteristics that affect recoveries of metals and trace elements from the ore at Heath Steele Mines, New Brunswick. CIM Bull., 73, No. 823, 167-178.

Harris, D.C., Cabri, L.J. & Nobiling, R., (1984): Silver-bearing chalcopyrite, a principal source of silver in the Izok Lake massive sulfide deposit and its confirmation by electron and proton microprobe analyses, Canadian Mineral., 22, 493-498.

Petruk, W. & Schnarr, J.R. (1982): An evaluation of the recovery of free and unliberated mineral grains, metals and trace elements in the concentrator of Brunswick Mining and Smelting Corp. Ltd., CIM Bull., 74, 833, 132-159.

• GOLD MINERALS IN CHINA AND THE CHARACTERISTICS OF THEIR OCCURRENCES

CAI Changjin and LI Zhixiang, China National Gold Company, 46 Dongsi Xidajie, Beijing, People's Republic of China

According to the record from about 160 deposits, gold minerals discovered in China include gold, electrum, kustelite, platinum-palladium-bearing gold, platinum, cupric gold, aurian palladium, platinum gold, osmium-bearing cuproaurite, calaverite, sylvanite, petzite, kostovite, etc. The new gold minerals discovered first in China are α-goldmalgamite, γ-goldamalgam, weishanite, tetraauricupride and liujiyinite. The major economic gold minerals are gold and electrum; the less important include kustelite and gold tellurides. The gold minerals mentioned above occur mainly in the following types of gold deposits. (Gold minerals found in different deposits are of a somewhat different nature.)

(A) Deposits occurring in magmatites, their contact zones and wall rocks: (1) Deposits in ultrabasic rocks and their contact zones. The gold minerals include gold, electrum, kustelite, tetraauricupride, γ-goldamalgam, weishanite, and the metallic compounds of gold and platinum metals. (2) Deposits in intermediate-acidic intrusives and their contact zones. The main gold mineral is electrum, with gold, kustelite and calaverite, and liujiyinite (occasionally observed). (3) Deposits in volcanic, subvolcanic rocks and their wall rocks. In these, the gold minerals are electrum, kustelite, calaverite, petzite and sylvanite.

(B) Deposits occurring in sedimentary rocks: (1) Deposit in carbonate rocks. The gold minerals are gold and electrum with a considerable proportion of micro-gold and submicro-gold. (2) Deposits in fine elastic rocks and clay rocks. The mineral is gold, which is mostly micro-gold and submicro-gold.

(C) Deposits occurring in various kinds of metamorphic rocks: (1) Deposits in slate and sandy slate. The mineral is gold. (2) Deposits in Archean metamorphic greenstone series, in which gold, electrum, kustelite, petzite, sylvanite and calaverite were found, and kostovite occasionally.

(D) The gold minerals in various kinds of placer deposits are mainly gold and electrum, and sometimes kustelite, tetraauricupride, Au-Hg metallic compounds are found.

(E) The gold minerals in the oxidation zone include gold, electrum, kustelite, calaverite and petzite.

CRYSTAL CHEMISTRY OF MINERALS THROUGH X-RAY ABSORPTION SPECTROSCOPY

CALAS,G; MANCEAU,A; PETIAU,J., Lab. Minéralogie-Cristallographie, UA CNRS 09, Universités Paris 6 et 7, 4 place Jussieu, 75252 PARIS CEDEX 05, FRANCE.

Taking advantage of the high intensity of synchrotron radiation sources, X-ray absorption spectroscopy (XAS) is increasingly used for studying the local atomic structure of amorphous materials or imperfectly organized minerals (phyllites), and in complex multicomponent systems, because its chemical selectivity. XAS in fact present distinct regions of the spectra, concerned by different physical processes:

- edge spectroscopy, within 10-20 eV around the threshold energy. The corresponding electronic transitions involve localized empty states and inform about the parameters influencing the electronic state of the absorbing atom (oxydation state, site symmetry, covalence..).
- X-ray Absorption Near Edge Structure (XANES) concerns an intermediate range of energy (10 to 70 eV above the threshold), where multiple scattering processes have to be taken into account. A recently developped quantitative treatment allows to derive structural parameters describing the local symmetry, including bond angles and interatomic distances.
- Extended X-ray Absorption Fine Structure (EXAFS) includes the oscillations from 50-80 eV above the threshold, interpreted as arising from single scattering of the ejected photoelectron by the surrounding atoms. The widely used formalism gives access to partial radial distribution functions, but the information is limited to the 2-3 nearest atomic shells.

The studies already made on minerals concern various types of problems: electronic states of mineral components and crystal chemistry of minor components (short range order) and intracrystalline cationic distribution (medium range order) including charge compensation or discrete heterogeneous repartition ("clustering").

1. Electronic structure of mineral components.

In some cases as in 3d-transition elements, the first empty bound states give information on crystal-field effects. It is in fact possible, under good spectral resolution, to separate the various electronic levels, and to correlate these values to those determined from optical absorption spectra or calculated by the

CRYSTAL CHEMISTRY OF MINERALS THROUGH XAS.
CALAS G. et al.

MS Xα theory. In semiconducting minerals, these edge spectra give access to localized partial density of states in the conduction band.

2. Crystal chemistry of minor components in minerals.

Comparison of edges corresponding to distinct crystal chemical parameters has lead to a fingerprint approach, allowing the study of elements in various media (crystals, gels, glasses). This approach is particularly useful in diluted crystals, where no other technique can be applied, although some caution must be taken to ensure that there is no perturbation from "solid state effects" when comparing to more concentrated references. This can include determination of oxidation states, coordination number or site distorsion.

3. Intracrystalline cationic distribution.

Irregularities in the distribution of atoms in minerals are not easy to highlight by conventional structural methods, particularly for minor and trace elements. This information is of great importance to recognize various formation conditions or to model more realistic partition coefficients. Some evidences are given by EXAFS for such irregularities concerning as well homovalent subtitutions (Ni/Mg) as heterovalent (Cr/Mg). In case of multisite distribution, EXAFS may help also do discuss the actual location of the studied element, with some insight on charge compensation processes (although neighbour elements as Al and Si cannot be separated).

The rapid development of techniques associated with XAS increases greatly the possibility to use it in Mineralogy. It is now possible to study very dilute systems down to 100 ppm, to work under high P-high T conditions with a diamond cell, to have access to kinetic processes through dispersive XAS or to study materials surfaces and solid-solid or solid-gas interfaces by Refl-EXAFS. Associated with the present development of fully dedicated storage rings, these technical progresses will greatly fill the gap between phase determination and the physicochemical properties of minerals.

LOCAL ORDER AROUND TRANSITION ELEMENTS IN SILICATE GLASSES AND DURING CRYSTALLINE NUCLEATION: APPROACH BY X-RAY ABSORPTION SPECTROSCOPY.

CALAS, G.; PETIAU, J., Lab. Minéralogie-Cristallographie, UA CNRS09, Universités de Paris 6 et 7, 75230 PARIS CEDEX 05, FRANCE.

The atomic selectivity of X-ray Absorption Spectroscopy (XAS) is an essential property for the study of minor components in silicate glasses. Transition elements play contrasted roles in geochemical systems: differenciated magmas are typically enriched in Zr or U owing to their low mineral/liquid distribution coefficients. The behaviour of other elements like Ni or Cr is markedly different as they are trapped in the first crystallizing phases such as olivins and spinels. It is therefore important to see how the local atomic environment influences the geochemical properties. The relation of transition elements with the tetrahedral framework is an especially important unanswered question. This puts in evidence the two observation scales necessary to describe the insertion of the element inside the glass matrix: the definition of the coordination atomic shell ("short range order") and the order beyond it ("medium range order"). Short range order may be studied by the three techniques covered under the general term of XAS, namely edge spectroscopy, X-ray Absorption Near Edge Structure (XANES) and Extended X-ray Absorption Fine Structure (EXAFS). The information can be compared to the results deduced from other spectroscopic techniques (optical absorption, Mossbauer effect..). The medium range organization around the studied element cannot be easily studied by neutron or X-ray scattering because of its low concentration and the complexity of the pair distribution function in multicomponent glasses. On the contrary EXAFS gives access to partial pair distribution functions even in diluted systems.

1. Short range order.

The K-edge structure has a rich information content, especially concerning the first transitions which can be interpreted in terms of localized electronic states. A specific feature occurs at energy lower than the threshold and characterizes transitions towards partially occupied d-states. It gives a direct access to the oxidation state and the coordination number. For example, in the case of Ti4+, this feature is interpreted as proving low coordination numbers and non-centrosymmetric sites. A change towards octahedral symmetry occurs during the crystalline nucleation process. EXAFS analysis of the oxygen coordination shell confirms these results and indicates a narrow radial distribution. A general tendency for low coordination numbers and well-defined cation-oxygen distances is observed for transition elements incorporated in silicate glasses.

2. Medium range order.

Only weak contributions of the further atomic shells are observed in EXAFS spectra of silicate glasses because destructive interferences result from wide interatomic distances distributions. However they inform about the rigidity of the connection between the polyhedra. The degree of disorder in the linking of the polyhedra seem to be concentration dependent. There is nearly no contribution of further atomic shells in concentrated glasses, on the contrary to dilute systems. It has been observed, for instance, in Mn-containing silicate glasses. Titanium K-edge EXAFS in silicate glasses show the contribution of a Si(Al) shell, defining a mean Ti-O-Si angle of around 120°. Crystalline nucleation may be followed through the evolution of the surrounding of the glass components as Ti or Zr which play a special role in this process. In glasses of cordierite composition, titanium progressively enters Al_2TiO_5 crystals, a phase which remains during the crystallization of the glass. On the contrary zirconium environment shows an evolution characterized by an intermediate stage before the crystallization of the final Zr-containing phase, tetragonal ZrO_2. These transient sites induce the further crystallization of high-quartz, and may explain why TEM shows that these crystals grow without any definite structural relations with zirconia crystals.

X-RAY ABSORPTION STUDIES OF SULFIDES AND ARSENIDES.

CALAS,G: PETIAU,J., Lab. Minéralogie-Cristallographie, UA CNRS 09, Universités Paris 6 et 7, 75230 PARIS CEDEX 05, FRANCE.

Synchrotron radiation allows high-resolution X-ray absorption spectroscopy (XAS) at the absorption edges of both cations and anions constituting multicomponent sulfides and arsenides. With the same experimental device, XAS gives access in fact to two different types of information. In the lower energy range, the edge structure is mainly related to the electronic structure of the absorbing atom and gives experimental constraints on the nature of the first empty states. At energies higher than 50-80eV above the edge, the Extended X-ray Absorption Fine Structure (EXAFS) gives a direct information on the atomic structure around the absorbing atom. The process is described as the single scattering of free photoelectrons by the surrounding atoms. In the intermediate energy range the spectral features constitute the X-ray Absorption Near Edge Structure (XANES). XANES may be interpreted either in the reciprocal or in the direct space. In the first case it is directly related to the partial density of states in the band structure. In the second case it is viewed as the result of multiple scatterings of the photoelectrons by the atoms in a small cluster, giving some insight on the geometrical organization around the absorbing element.

1. Electronic structure.

K-edge spectroscopy gives local p-projected density of states. The final states are actually perturbed by the presence of the core hole created by the absorption process. However in the compounds which exhibit a metallic character -and to a lesser extent in semiconducting compounds- a partial screening of the core hole occurs. This allows to consider the same electronic configuration in initial and final states. The metal and ligand contributions to the band structure are illustrated by the case of niccolite NiAs. In this compound Ni and As K-edges can be correlated by considering that the thresholds of both edges correspond to the bottom of the conduction band which derives from both metal and ligand. The absorption feature which occurs on the nickel K-edge at an energy lower than the threshold corresponds to states of primarily d-symmetry, although with some p-character on account of their significant intensity. The absence of this feature on the As K-edge indicates that the d-p mixing only concerns states localized on nickel. In chalcopyrite the comparison among iron and copper K-edges gives the participation of both elements to the conduction band. The results are in accordance to MSXα band structure calculations, up to 20 eV above the absorption edge. Edge spectroscopic studies have also been conducted on MX2-type compounds in order to follow

the evolution of the electronic structure as a function of the S-As substitution in the marcasite-löllingite series. Information is obtained about site distorsions, metal-ligand and metal-metal bonding and about the energy position and localization of the first empty states.

2. Local atomic structures.

XANES and EXAFS are useful tools to understand better the structural organization around major or minor components. The influence of the atomic structure is illustrated by the XANES of Cu and Fe in chalcopyrite: the same atomic surrounding for these two atoms gives similar XANES. The same structure is also observed in sphalerite and enargite. A simplified treatment of the photoelectron multiple scattering gives a relation between the energy position of the absorption maxima and the interatomic distances in such cases where the local geometry is the same. This is particularly useful to study the insertion of minor components in a crystalline structure, as in Fe-containing sphalerites. The similar shape of XANES at iron and zinc edges proves that the iron site keeps the original symmetry. However Fe-S distances are found to be significantly larger than Zn-S distances. The presence of iron impurities induces a local adaptation of the site which is different from the mean site of the lattice. EXAFS gives an independent way to study this local effect and confirms XANES observations.

By taking into account the development of fluorescence detection techniques, which allow to study elements at more dilute content (100 ppm), as well as soft X-ray spectroscopy which gives access to sulfur K-edges, XAS will greatly develop in the forthcoming years. This concerns mainly the study of minor components of chemically complex sulfides and sulfosalts through EXAFS and XANES. Edge spectroscopy is perhaps more limited by the need of calculations concerning the electronic empty levels in the minerals.

GARNET IN GRANITOID ROCKS OF THE SIERRA NEVADA BATHOLITH, CALIFORNIA

CALK, L. C., and DODGE, F. C. W., U.S. Geological Survey, 345 Middlefield Road, Menlo Park, CA 94025, USA

Magmatic garnet is a conspicuous though rare constituent of some of the granitoid rocks of the central Sierra Nevada batholith. Other than in a silicic biotite tonalite from the well-known Sherman Thomas heat-flow borehole at the extreme western margin of the batholith, garnet is restricted to a few leucocratic granites and to some aplites and pegmatites. Usually less than one percent of the mineral is present. Outcrops containing visible garnet seldom extend over a few tens of square meters, with the exception of several square kilometers of exposure of a garnet-bearing pluton near the middle of the batholith, the granite of Dinkey Dome. Most garnet occurs as disseminated, euhedral or subhedral crystals as large as 3 mm; crystals as large as 10 mm are found in pegmatites. It is included in quartz, plagioclase, or K-feldspar, or may occur along grain boundries of these minerals. Other minor accessory minerals commonly found in garnet-bearing rocks are apatite, zircon, muscovite, biotite, and sillimanite. Inclusions of these minerals are rarely present in garnet.

Compositions of garnets from 10 localities, 6 in granitoid rocks and 4 in pegmatites, were determined by electron microprobe. Mineral formulae were calculated using a computer program that first allocates enough Al to the tetrahedral site to make $Si + Al^{IV} = 6$ and then assigns sufficient iron to Fe_2O_3 to make $Fe^{+3} + Al^{VI} + Cr + Ti = 4$. These compositions were then used to calculate end members. The Sierran garnets are predominantly almandine-spessartine with minor amounts of pyrope, although almandine-rich garnet of the tonalite from the borehole has a high pyrope content (14 mole percent). Garnets in granites contain more than 45 mole percent almandine plus skiagite, whereas those in aplites and pegmatites contain more than 50 percent spessartine.

Two factors have led to magmatic garnet formation. Almandine-spessartine or spessartine garnets of silicic granites, aplites, and pegmatites have crystallized in response to increase in concentration of Mn relative to Fe in highly differentiated melts. More Fe-rich garnet, found in magnetite- free silicic tonalite, formed in response to relatively low oxygen fugacity prevailing during magmatic crystallization. Other modes of origin for these garnets, such as physical contamination of granitic magmas by metasedimentary impurities or metamorphism of the plutonic rocks, do not seem likely.

THE MOSSBAUER EFFECT IN THE DETERMINATION OF MOLECULAR COMPOSITION OF 5-COMPONENT GARNETS

CAMARGO, W.G.R.de; RECHEMBERG, H.; MADUREIRA Fº, J.B.; KERTH JR. , W.H.; Institute of Geosciences and Institute of Physics,University of São Paulo, São Paulo, SP, Brazil

In a previous communication (W.G.R.de Camargo et al., "A Mathematical Approach for Determination of Molecular Composition of Transparent Spinels" - 9th European Crystallographic Meeting, Torino , Italy, 1985), a mathematical treatment was introduced for determination of molecular composition of 4-component transparent spinels, by using the physical properties of mineral samples.

In the present paper the same mathematical procedure is being used for 5-component garnets, but now introducing the Mossbauer effect, which may indicate the Fe^{++}/Fe^{+++} ratio = K and consequently the ratio between the Fe-bearing garnets (almandite/andradite).

Table 1 - Physical constants and chemical composition of garnet end-members:

		D	n	Δd(A)	composition
Almandite	(alm)	4.318	1.830	0.766	$Fe_3Al_2Si_3O_{12}$
Andradite	(and)	3.859	1.887	0.649	$Ca_3Fe_2Si_3O_{12}$
Grossular	(gr)	3.594	1.734	0.693	$Ca_3Al_2Si_3O_{12}$
Pyrope	(py)	3.582	1.714	0.781	$Mg_3Al_2Si_2O_{12}$
Spessartite	(sp)	4.190	1.800	0.745	$Mn_3Al_2Si_3O_{12}$

D=specific gravity, n=index of refraction, Δd=interplanar spacing difference: Id(420) garnet - d(10$\bar{1}$1) quartz|.

Considering x=%(alm), y=%(and), z=%(gr), t=%(py) and u=%(sp), the following equations may be derived:

$$D_x x + D_y y + D_z z + D_t t + D_u u = 100\, D_s \quad (1)$$

$$n_x x + n_y y + n_z z + n_t t + n_u u = 100\, n_s \quad (2)$$

$$\Delta d_x x + \Delta d_y y + \Delta d_z z + \Delta d_t t + \Delta d_u u = 100 \Delta d_s \quad (3)$$

$$x + Y + z + t + u = 100 \quad (4)$$

$$i = x/y \quad (5)$$

D_s, n_s, Δd_s = physical constants of analysed sample.

Replacing u=100-(x+y+z+t) in the equations (1), (2), (3), the system takes the form below:

$$(D_x-D_u)x+(D_y-D_u)y+(D_z-D_u)z+(D_t-D_u)t = 100(D_s-D_u) \quad (6)$$

similar equation in n (7)

similar equation in Δd (8)

and again replacing x=iy in the equations (6), (7), (8), we have:

$$\left[(D_x-D_u)i+(D_y-D_u)\right]y+(D_z-D_u)z+(D_t-D_u)t = 100\,(D_s-D_u) \quad (9)$$

similar equation in n (10)

similar equation in Δd (11)

In the chemical formula of almandite:

1 mole almandite —— 3 ion grams Fe^{++}
x moles almandite —— n ion grams Fe^{++} $\quad x = n/3 \quad (12)$

and thus, for andradite:

1 mole andradite —— 2 ion grams Fe^{+++}
y moles andradite —— m ion grams Fe^{+++} $\quad y = m/2 \quad (13)$

Dividing (12) by (13)

$$i = x/y = \frac{n/3}{m/2} = \frac{2n}{3m} = \frac{2}{3} K$$

$K = (Fe^{++}/Fe^{+++})$ may be obtained through the Mossbauer spectroscopy, a ratio between Fe^{++} and Fe^{+++}.

As a consequence, the system of equations may reach the following final configuration:

$$2/3\left[(D_x-D_u)K+(D_y-D_u)\right]y+(D_z-D_u)z+(D_t-D_u)t = 100(D_s-D_u)$$

$$2/3\left[(n_x-n_u)K+(n_y-n_u)\right]y+(n_z-n_u)z+(n_t-n_u)t = 100(n_s-n_u)$$

$$2/3\left[(\Delta d_x-\Delta d_u)K+(\Delta d_y-\Delta d_u)\right]y+(\Delta d_z-\Delta d_u)z+(\Delta d_t-\Delta d_u)t = 100\,(\Delta d_s-\Delta d_u)$$

which solve the molecular composition of 5-component garnets.

AN UPDATED VERSION OF COMPUTER PROGRAM CORANF FOR DETERMINING THE SITE POPULATIONS AND THE BULK-MINERAL CHEMICAL COMPOSITION OF C2/m AMPHIBOLES BY SINGLE-CRYSTAL X-RAY DIFFRACTOMETRY AND REFINEMENT.

CANNILLO, E., UNGARETTI, L., OBERTI, R., Centro Studio Cristallografia Strutturale C.N.R., 27100-Pavia, Italy; SMITH, D.C., Muséum National d'Histoire Naturelle, 75005-Paris, France.

Least-squares refinement of X-ray diffraction data (XRef) can directly provide reliable chemical information only in suitable circumstances, i.e. when the site population is composed of: a) two atomic species having a large differences in their atomic number (e.g. Mg,Fe; Al,Fe; Ca,Na; K,Na); b) two atomic species having a large and precisely known difference in their mean bond lengths (e.g. Si,Al; Mg,Al; Fe^{2+},Fe^{3+}). When dealing with more chemically-complex site populations (3 or more atomic species present in a single site, e.g. Mg,Al,Fe^{2+},Fe^{3+},Ti) more sophisticated procedures are required. These exploit well-founded crystal-chemical constraints or assumptions and, when available, partial independent chemical information to transform the XRef results - mainly the mean atomic number (m.a.n.) and the mean bond length (m.b.l.) of each site - into site populations, and thence into an electrically-balanced chemical composition.

A preliminary approach in this direction (computer program CORANF) was successfully applied to alkali- and sodic-calcic-amphiboles from high-P metamorphic rocks (Ungaretti et al., 1981a, Proc. XI Gen. Meet. I.M.A., 82-110; 1981b, Bull. Minéral., 104, 400-412; 1983, Bull. Minéral., 106, 645-672); the bulk-mineral chemical compositions determined in this way were in very good agreement with the available EMP analyses and the site populations were consistent with the observed m.a.n. and m.b.l. values.

However, with calcic amphiboles in particular, some inconsistencies appeared between the chemical analyses by XRef and EMP and between the observed and calculated m.b.l. and this prompted a reappraisal of the original CORANF procedure. This has been made possible by the large increase in the number of refinements now available (over 400) for a wider range of amphibole compositions.

Some crystal-chemical assumptions used by the original CORANF lose their general validity: e.g. ordering of Al^{VI} at the M2 site is not always complete since in some pargasites significant Al also enters the M3 site, and additional substitutions in the T2 site are not prohibited since in richterites Ti can substitute for Si. More importantly, the m.b.l. for the same cation occupying the same site showed large variations in amphiboles approaching different end-member compositions, such that it is no longer valid to assume a fixed m.b.l. for a specific cation in any amphibole composition.

Over 70 amphibole crystals which yielded unambiguous site population assignments on the basis of integrating the XRef and EMP results were selected for applying least-squares procedures. A new set of equations was thus derived which allowed the calculation of the m.b.l. values of the tetrahedral (Si, Al) and octahedral (Mg, Al, Fe^{2+}, Fe^{3+}, Ti) cations for any end-member composition. For instance, Mg in the M1 site shows a m.b.l. of 2.056, 2.078 and 2.101 A respectively in richterite, glaucophane and tschermakite; similar variations also occur in the other sites , though to a lesser extent in the tetrahedral sites.

The updated version of CORANF consists of 4 successive steps: 1) a selected number of observed diffraction intensities is used to obtain a preliminary estimate of the atomic coordinates, site populations and scale factor which are used to start the refinement; 2) at the end of the refinement the final A and M4 site-occupancies and the T1-O and T2-O m.b.l. are used to approximately determine the amphibole composition in terms of the end-member solid solution; 3) the corresponding m.b.l. values are calculated; 4) the new m.b.l. values are employed in the old system of equations and applied to the XRef results to furnish the octahedral and tetrahedral site populations.

This version of CORANF can now be confidently applied to the whole of Na-Ca-Mg-Fe-Al-Si amphibole compositional space. In the case of significant amounts of other elements being present CORANF will produce less exact results but even rough independent estimates of K and Ti (which mainly affects the CORANF procedure) can be handled by the program markedly improving the site population assignment.

THE OXIDATION STATE OF BASIC MAGMA; SUBAERIAL AND SUBMARINE

I.S.E.CARMICHAEL, University of California, Berkeley, CA 94720, D.M.CHRISTIE, Lamont-Doherty Geological Observatory, Palisades, New York, 10964, M.S.GHIORSO, University of Washington, Seattle, WA,98195, and C.H.LANGMUIR, Lamont-Doherty Geological Observatory, Palisades, New York, 10964

The experimental calibration of oxygen fugacity, temperature and ferric/ferrous ratios in natural silicate liquids (Sack et al. 1980; Kilinc et al. 1983) can be used to derive values of oxygen fugacity for glassy lavas, both subaerial and submarine. Although oxygen fugacity is strongly temperature dependent, the relative oxygen fugacity, namely the difference between the calculated value for any lava, and that of a synthetic buffer such as Ni-NiO (NNO), at the same temperature(1200°C) is not; lavas are therefore plotted in terms of delta NNO.
Analyses of Fe_2O_3 and FeO for over 80 handpicked mid-ocean ridge basalts give relative oxygen fugacities that are 2-3 log units more reducing than NNO, and thus are among the most reduced terrestrial lavas yet found. Irrespective of their tectonic or geographic setting, or bulk composition, these submarine glasses cluster close to the values found for the upper levels of the Skaergaard intrusion by Sato and Valenza(1980). Subaerial glassy lavas, such as those of Kilauea, typically undergo subaerial reduction by SO_2 degassing (Anderson and Wright,1972) but nevertheless are only 1 log unit below NNO. Alkali-rich lavas are more oxidising, and may extend to 3 log units above NNO. In almost all cases the sulphur redox state shows more variation than the iron redox state in basic magmas.
We suggest that the iron and sulphur redox couples, dissolved in the liquid, act as self-regulating internal oxygen reservoir, and can constrain a cooling liquid to the constant relative oxygen fugacity observed in well characterised liquid lines of descent. If the partial molar volume of Fe_2O_3 in natural silicate liquids is very compressible, then magmas equilibrating at great depth with a solid assemblage of low oxygen fugacity would have a higher iron redox state than those equilibrating with shallow mantle sources. The redox states of magmas, ascending isochemically, could therefore be a crude indicator of the depth of their source regions.

CHARACTERISATION OF ORDER/DISORDER TRANSFORMATIONS IN PLAGIOCLASE FELDSPARS

CARPENTER, M.A., Dept. of Earth Sciences, University of Cambridge, Downing St., Cambridge CB2 3EQ, England

A large number of annealing experiments have been completed on crystals of plagioclase feldspars, with compositions between $\sim An_{30}$ and $\sim An_{75}$, in a systematic attempt to bracket the various possible order/disorder transformations which can occur in this solid solution. Under dry annealing conditions, significant changes in the state of order can be achieved experimentally in run times of days at ~1300°C, weeks at 1100-1300°C and months at 1000-1100°C. Below ~1000°C changes in ordering can be induced if water is present, requiring days at ~1000°C, weeks at ~900°C and months at ~800°C ($P_{H_2O} \sim 1$kb). In order to characterise these structural changes, however, single crystal diffraction information is required. Distinctions can then be made between the $C\bar{1}$, $P\bar{1}$, $I\bar{1}$ and e structures. Of particular significance for the state of order are the presence or absence and sharpness or diffuseness of reflections at h+k = odd, ℓ = odd positions of the reciprocal lattice. In the present experiments changes in structural state have been followed by examining electron diffraction patterns obtained from crushed fragments of small quantities of experimental products.

Structural changes of the type $C\bar{1} \rightarrow I\bar{1}$, $I\bar{1} \rightarrow C\bar{1}$, $C\bar{1} \rightarrow e$, $e \rightarrow I\bar{1}$ and $I\bar{1} \rightarrow e$ have been followed, though not always to completion, using natural crystals as starting materials. Since both ordering and disordering have been induced the positions of $C\bar{1} \rightleftharpoons e$, $C\bar{1} \rightleftharpoons I\bar{1}$ and $e \rightleftharpoons I\bar{1}$ equilibria can be constrained. The most striking result is a marked difference between the ordering behaviour of crystals with compositions on either side of the $C\bar{1} \rightleftharpoons I\bar{1}$ transition line; the fields of e ordering have been split into e_1 and e_2 to signify this difference (Fig. 1). In the composition range $\sim An_{50}$-An_{70} the sequence of structural changes with falling temperature appears to be $C\bar{1} \rightarrow I\bar{1} \rightarrow e_1$. In the composition range $\sim An_{30}$-An_{50} the sequence is $C\bar{1} \rightarrow e_2$; although the temperature of this transition has not been well constrained, it must be below ~750°C (Fig. 1).

The suggestion that the incommensurate (e) plagioclase structure may have a true field of stability relative to the $I\bar{1}$

structure (at $\sim An_{30}$-An_{50} and $T \leq 800^{\circ}C$) is consistent with recent calorimetric measurements of the enthalpies of ordering. It may also prompt some reanalysis both of the equilibrium phase relations of the albite-anorthite system and of the way that crystals of intermediate compositions evolve in nature. An important but unresolved issue, however, is the thermodynamic character of these order/disorder transformations. If the $C\bar{1} \rightleftharpoons I\bar{1}$ and the $C\bar{1} \rightleftharpoons e$ transformations are second order then the $e \rightleftharpoons I\bar{1}$ transformation may be first order.

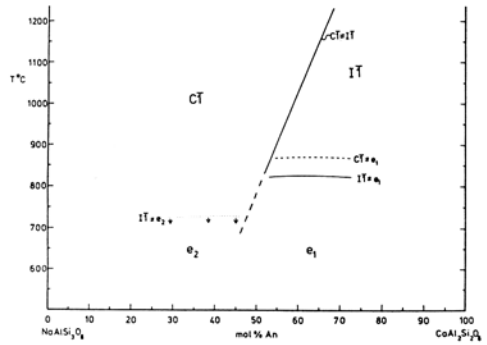

Fig. 1. Boundaries of stability fields for different ordered structures in the plagioclase feldspar solid solution, as determined from dry and hydrothermal annealing experiments. Solid lines represent transformations which have been reversed. Note that no attempt has been made to show positions for the peristerite, Huttenlocher and Bøggild miscibility gaps.

MINERALOGY, PARAGENESIS AND GEOCHEMICAL EVOLUTION OF Nb,Ta-OXIDE MINERALS IN GRANITIC PEGMATITES

ČERNÝ,P.,Dept. of Earth Sciences,University of Manitoba,Winnipeg, MB R3T 2N2; ERCIT,T.S.,Mineral Sciences Div., National Museum of Natural Sciences,Ottawa,ON K1A 0M8; WISE, M.A., Dept. of Earth Sciences, University of Manitoba, Winnipeg, MB R3T 2N2, Canada.

Since the early nineteen sixties, oxide mineralogy of Nb and Ta in granitic pegmatites has been expanded by some 25 new species; our understanding of the crystal chemistry of most of the"classic" mineral groups has considerably improved; progress has also been achieved in the study of Nb,Ta-bearing parageneses and in the documentation of their geochemical evolution. In contrast, experimental work on mineral stabilities and equilibria, and chemical modelling of the same are underdeveloped.

Most of the new mineral species belong to late hydrothermal alteration products that replace the common Nb,Ta-carriers, particularly in the most fractionated complex pegmatites (rankamaite, alumotantite,natrotantite,etc.). However,many new end-members were added to the existing series and groups(manganotapiolite,foordite, stibiobetafite,etc.),and some crystallochemically "independent" species were found as well (petschekite,liandratite).

On the columbite-tantalite-tapiolite $A_8B_8O_{24}$ quadrilateral, compositional data show narrow geochemical gaps along the Nb-rich and Fe-rich sidelines, and a well-defined crystallochemical gap between columbite-tantalite and ferrotapiolite. Coexisting columbite-tantalite + tapiolite pairs from different localities correlate well,suggesting only limited variability in $\underline{a}(O_2)$ in the parent environment. Manganotapiolite, known so far from a single occurrence, seems to be metastable. Structurally,most columbites-tantalites are disordered to intermediate; high degree of order is rare,and found predominantly in manganotantalite. The frequencies of different structural states in tapiolite are difficult to estimate, as disorder and Mn substitution have very similar effects on unit cell dimensions of ferrotapiolite.

The wodginite group, $A_4B_4Ta_8O_{32}$,consists today of MnSn, FeSn, MnTi and $Mn_{0.5}Ta$ end-members with extensive substitutions in the A and B sites,although there is a geochemical gap between titano-wodginite and tantalowodginite. Disordered wodginites closely approach the chemistry and symmetry of most ixiolites which show incipient ordering and slight monoclinic distortion of their (ideally) orthorhombic structure. However, wodginite analogs of Sc- and W-rich ixiolites have not yet been found, and at least some of the wolframoixiolites represent heterogeneous mixtures.

Compositional variability in the pyrochlore-betafite-microlite group $A_{2-m}B_2O_6(O,OH,F)_{1-n}\cdot pH_2O$ was expanded by new Y, Bi, Sb and Cs bearing members,although the status of some of them is questionable. Parabariomicrolite, a closely related OH-rich rhombohedral derivative was discovered, and the first natural occurrence of the inverse pyrochlore structure was found in another derivative, cesstibtantite.

In the rare-element class of granitic pegmatites, the paragenesis of the Nb,Ta-oxide minerals is characterized by Y-bearing species in the rare-earth pegmatite type, and by the common ferromanganoan minerals ($\pm$Ti, Sn) in the beryl-bearing, albite, and albite-spodumene pegmatites. The greatest variety of species, and the most advanced fractionation leading to depletion in Fe,Mn and crystallization of Al,Ta-, Sn,Ta-, Na,Ta- and Li,Ta-oxide minerals, are found in the spodumene, petalite and amblygonite subtypes of the complex pegmatite type. In contrast, the lepidolite subtype is dominated by microlite, with negligible manganocolumbite and Y-bearing minerals.

Nb,Ta-bearing mineral populations from diverse types of rare-element pegmatites suggest that both the Ta and particularly the Mn enrichment trends are promoted by high $a(F_2)$. Except for a few cases in which an overall Mn enrichment is due to an anomalous Mn-rich composition of parental granitic melts, extreme Mn and Ta fractionation is typical of lepidolite ($\pm$ topaz bearing) pegmatite type.

Electrostatic energy calculations indicate that columbite-tantalite should crystallize with about equal ease in any degree of order-disorder, but the distribution of structural states displays diverse preferences among natural mineral populations. Some of them may be explained by differences in nucleation and crystallization rates, but others seem to be controlled by crystallochemical factors.

THE ARCHEAN LAC DU BONNET BATHOLITH, MANITOBA: IGNEOUS HISTORY, METAMORPHIC EFFECTS, AND FLUID OVERPRINTING.

ČERNÝ, P., Dept. of Geological Sciences, University of Manitoba, Winnipeg, MB R3T 2N2 Canada; FRYER, B.J.,Dept. of Geology,Memorial University,St.John's, NF A1B 3X5 Canada; LONGSTAFFE,F.J.,Dept. of Geology,University of Alberta,Edmonton,AB T6G 2E3 Canada; TAMMEMAGI,H.Y., RE/SPEC Ltd.,Calgary,AB T3A 0X9 Canada.

The Lac du Bonnet batholith is located in southeastern Manitoba, in the English River Subprovince of the Archean Superior Province of the Canadian Shield. It displays a complex intrusive and tectonic evolution, in part combined with the effects of aqueous fluids at different stages of consolidation. It exemplifies many problems encountered in the study of extensive potassic batholiths typical of Precambrian Shields.

The batholith is emplaced along a subvertical fault contact between the Bird River greenstone belt and a tonalitic gneissic terrane. It is situated over a prominent downwarping of the intermediate discontinuity (20 to 26 km) and a slight upwarping of the Moho (32 to 30 km),in the same direction from the tonalitic terrane to the greenstone belt. The batholith has subvertical contacts, sharp intrusive against the greenstone belt but diffuse into the tonalitic gneiss. The layering and foliation in the greenstone belt is gently reoriented by the intrusion but the gneissic terrance appears undisturbed.

The batholith consists of five major phases: (a) gneissic hornblende-biotite tonalite, (b) gneissic porphyritic hornblende-biotite granodiorite, (c) undeformed to gneissic leucogranite, (d) late-tectonic equigranular to porphyroblastic biotite granite, and (e) late-tectonic porphyroblastic biotite granodiorite. The biotite granite (d) constitutes about 85% of the surface exposure of the batholith; the tonalite (a) and the late granodiorite (e) are very minor components. Biotite granite ((d) is accompanied by sparse allanite-bearing pegmatite,but swarms of gadolinite-type Y,REE,Be,Nb,Ta,Ti-bearing pegmatites surround the leucogranite (c) bodies. Enclaves of the greenstone-belt schists are locally abundant within the biotite granite (d), aligned subparallel to the nearest batholith margins.

The five major phases chemically define specific areas on variation diagrams (Rb-Sr,Rb-Ba,Li-Mg,Li-SiO_2,Ca-Y,Ca-Sr,Al-Ga, K/Rb-Rb,K/Ba-Ba). Internal fractionation trends are indicated by some phases but no obvious links are in evidence among the different rock types. Also, there is no correlation of the average degree of fractionation with the intrusive sequence of the five phases. The REE signature is very similar in most phases: LREE-enriched (Ce_N 80-130, Ce_N/Yb_N 14-50) with mild negative Eu anomalies. Only the leucogranite (c) is HREE-enriched (Ce_N/Yb_N 3-6.5) with strong negative Eu anomaly. The mean whole-rock $\delta^{18}O$ values are remarkably consistent for all five phases (+7.8 - +8.4). The Rb-Sr isochron age of the biotite granite (d) is 2603 ± 97 Ma (R_i 9.7007 ± 0.0036); the leucogranite (c) data are disturbed, yielding 2550 ± 190 Ma (R_i 0.700 ± 0.030)(±2δ).

The intrusive style of the batholith is controlled by the adjacent regional fault which channelled the consecutive intrusions, and which deformed early members during episodic movements. The tonalite (a) is probably not an inherent member of the batholith but it may represent enclaves of diapiric tonalite domes exposed in close vicinity. The early and late granodiorites are very close to the biotite granite (d), thus the petrogenetic interpretation can be focussed at the biotite granite (d) and leucogranite (c).

The isotopic relationships limit the possible source role of supracrustals or ancient crust to <25% of total protolith, unless huge volumes of LILE-depleted lower crust are invoked. However, low-percentage melting of tonalitic sources would generate prominent negative Eu anomalies that are conspicuously absent. At present, very short-lived felsic volcanic lithologies seem to be a likely source, at least from the geochemical point of view.

Extensive porphyroblastesis of K-feldspar in the biotite granite is accompanied by remarkable disturbance of $\delta^{18}O$ (+6.6 - +11.0), depletion in LREE and HREE (at constant Eu), Ti,Zr,Hf,Th, and P,and slight enrichment in K and Ga. Major components and Rb-Sr isotopic ratios are not affected. Massive flow of CO_2-rich aqueous fluids channelled along zones of weakness appears to be responsible. The silicic leucogranite (c) is somewhat remote from composition of its parent melt, as a high proportion of volatiles and rare elements separated into its pegmatite aureole. Shearing and recrystallization of the leucogranite compounded the geochemical disturbances suffered during emplacement and crystallization. The porphyroblastic biotite granite (d) and leucogranite (c) cannot be interpreted by aid of crystal/melt equilibria alone.

RAMAN LASER MICROPROBE INVESTIGATION OF CHROMITES IN POLISHED SECTIONS

CERVELLE, B., Lab. Minéralogie-Cristallographie, Universités Paris 6 et 7, associé au CNRS, 4 place Jussieu, 75252 Paris Cedex 05, France. MALEZIEUX, J.M., Lab. Minéralogie, USTL 1, 59655 Villeneuve d'Ascq Cedex, France.

This study was undertaken thanks to the possibility of using a Raman Laser Microprobe (MOLE) (1). It concerns, on the one hand, synthetic spinels belonging to the following series : $MgAl_{2-x}Cr_xO_4$; $FeAl_{2-x}Cr_xO_4$; $Mg_{1-x}Fe_xAl_2O_4$; $Mg_{1-x}Fe_xCr_2O_4$; $Mg_{1-x/2}Fe_{x/2}Al_{2-x}Cr_xO_4$; and, on the other hand, natural chromites with the general formula $(Mg, FeII)(Cr,Al,FeIII)_2O_4$ collected from ultramafic rock samples.

The specimens synthetized from the constituent oxides in a solar furnace, and the natural ores were mounted in resin and polished. The Raman spectra obtained from areas of about 1μm² indicate that the vibrational behaviour for those spinels may be interpreted, on the one hand, in terms of 1-mode or 2-modes comportments (2). The 1-mode comportment, expressed by a sliding frequency of the high-frequency bands, is essentially related to the trivalent cations content. This type of behaviour allows to correlate the frequency of the highest frequency band (mode A_{1g}) with the ratio Cr+FeIII / Cr+Al+FeIII (fig. 1). Consequently, a Cr^{3+} signature in spinels of different compositions consists of the location of the high-frequency Raman band, which varies from 760 cm^{-1} for the Al-rich end member to 680 cm^{-1} for the Cr-rich end member (3).

The 2-modes comportment, which concerns the synthetic samples only, results in the appearance of the low-frequency bands for the highly aluminous and magnesian terms.

On the other hand, additional vibrational modes are present in the Raman spectra of Cr-rich spinels. This behaviour can be explained by the distortion of the structure Fd3m into F$\bar{4}$3m induced by the chromium substitution (4), resulting in the splitting of the T_{2g} and E_g modes.

Besides the problem of interpreting the vibrational behaviour of solid solutions such as chromites, the Raman Laser Microprobe allows to obtain "in situ" mineral spectra from areas very similar in size to those analyzed with an electron microprobe.

It constitutes a valuable complement to the micro-spectrometric methods of general use in mineralogy.

(1) DHAMELINCOURT P. (1979). Etude et réalisation d'une microsonde moléculaire à effet Raman. Thesis, USTL, 59655 Villeneuve d'Ascq Cedex, France. (2) BARKER A.S. Jr, SIEVERS A.J., (1975). Reviews of Modern Physics, 47, suppl. 2, 3-168.
(3) MALEZIEUX J.M. et al. (1983). Tschermaks Mineral. Petrol. Mitt., 32, 171-185. (4) CERVELLE B. et al. (1984). Bull.Mineral., 107, 627-634.

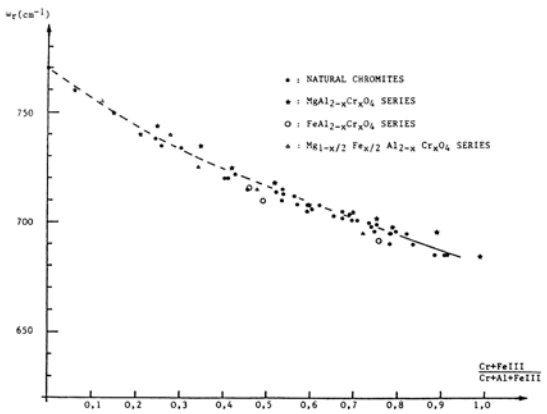

FIGURE 1 : Correlation between the frequency of the highest frequency Raman band and the ratio Cr+FeIII/Cr+Al+FeIII in natural and synthetic chromites.

CONVERGENT-BEAM ELECTRON DIFFRACTION (CBD) IN MINERALOGY

CHAMPNESS, P.E., Dept. of Geology, Manchester University, Manchester, M13 9PL, U.K.

In conventional selected-area electron diffraction (CSAD) a parallel, defocussed beam of electrons is used to form a diffraction pattern that consists of sharp spots. The spatial resolution is limited by spherical aberration to ~0.5 μm. In CBD a strong upper objective pole-piece or a mini-lens is used to form a convergent electron beam. The resulting diffraction pattern consists of discs, the diameter of which depends upon the convergence angle, α. The spatial resolution of the technique is determined by the diameter of the probe, together with any beam broadening that takes place in the specimen. Probe sizes <50 Å are available in modern TEM/STEM instruments.

In addition to the normal geometric information that is available from CSAD patterns, the diffraction discs in CBD contain 3D crystallographic information that allows the point group and space group of the specimen to be determined, often from a single pattern. This arises because the strong dynamic scattering of electrons leads to the breakdown of Friedel's Law. Thus, far from being the poor relation of X-ray and neutron diffraction that it was once considered to be, electron diffraction is, in many ways, superior to these techniques.

The detail in the CBD pattern is of two kinds (a) diffuse fringes that are confined to the zero-order diffraction maxima and vary with the thickness of the specimen and (b) fine lines (HOLZ lines) that are insensitive to crystal thickness and occur both inside and outside the discs. If the electron beam is exactly along a zone axis, the symmetry of the zero order zone (type (a) detail) belongs to one of the ten projection diffraction groups (two-dimensional point groups). Each projection diffraction group contains several possible diffraction groups. In most cases the diffraction group can be uniquely determined from the symmetry of the whole pattern and the HOLZ symmetry of the zero order beam. From the diffraction group, possible point groups can be determined. CBD patterns taken down a number of prominent zone axes (and sometimes only one) will identify the point group.

Use of a convergent beam leads to significant excitation of HOLZ (higher order Laue zone) reflections. The diameters of the HOLZs can be used to determine the repeat of the zone axis parallel to the electron beam. Thus it is possible to identify polymorphs and determine the unit cell dimensions. The HOLZ maxima may also be indexed and used to determine the lattice type and to identify glide planes perpendicular to the electron beam. Glide planes and screw axes can also be identified from 'lines of dynamic absence' in the zero order rows in the diffraction pattern.

CBD has been used to identify stacking variants in nigerites, Sn-Zn-Al oxides. The six-layer structure has been confirmed to have space group P3m1 or P31m (Bannister et al., 1947) and a new 8-layer Sn-poor structure, which is finely intergrown with the 6-layer structure, has been shown to be C2/m or C2/c. A 24-layer variant is also present.

The space group of the $MgGeO_3$ clinopyroxene structure has been confirmed to be C2/m (Ozima and Akimoto, 1983) and CBD has been used to identify the orthopyroxene $MgGeO_3$ that is intergrown with it. These phases have been found in charges of Mg_2SiO_4 composition synthesised in the olivine field and then reacted in the spinel field. Both phases were undergoing an oriented transformation to spinel.

Bannister, F.A., Hey, M.H., and Stadler, H.P. Mineral. Mag. 28, 129-136 (1947).

Ozima, M. and Akimoto, S-I., Amer. Mineral. 68, 1199-1205 (1983).

Phase Relations in the System Ag_2S-Cu_2S-PbS-Bi_2S_3

Luke L. Y. Chang, Department of Geology, University of Maryland, College Park, Maryland 20742, U.S.A., Daqing Wu, Institute of Geochemistry, Academia Sinica, Guiyang, Guizhou, People's Republic of China, and Charles R. Knowles, Idaho Geological Survey, Moscow, Idaho 83843, U.S.A.

The formation of sulfbismuthides and the extents of solid solutions in the system Ag_2S-Cu_2S-PbS-Bi_2S_3 were studied at 500°C using sealed and evacuated capsule methods. In the system Ag_2S-Cu_2S-Bi_2S_3, two new phases were found. $Ag_2Bi_4S_7$ was identified to be a benjaminite-type phase, and $AgCu_5Bi_6S_{12}$ is comparable in composition with reported (Pb,Ag,Bi)$Cu_4Bi_5S_{11}$. A new phase, $Cu_{0.55}Pb_{5.61}Bi_{2.08}S_9$, was also found in the system Cu_2S-PbS-Bi_2S_3, and its x-ray powder diffraction data match well with those of aschamalmite. In the system Ag_2S-PbS-Bi_2S_3, the previously reported lillianite-pavonite series was observed.

Ten solid solutions were recognized in the system Ag_2S-Cu_2S-PbS-Bi_2S_3. With "x", "y", "z", and "n" representing substitutions of Ag+Bi=2Pb, Ag=Cu, and Bi=Cu, and interstitial addition of Cu, respectively, the pavonite, benjaminite, $Cu_3Bi_5S_9$ and $CuBi_3S_5$ solid solutions can be expressed as:

$$Ag_{1-(x+y)}Cu_{y+(n+1)z}Pb_{2x}Bi_{3-(x+z)}S_5,$$

$$Ag_{3.52-(x+y)}Cu_{y+(n+1)z}Pb_{2x}Bi_{6.83-(x+z)}S_{12},$$

$$Ag_yCu_{3-(x+y)+(n+1)z}Pb_{2x}Bi_{5-(x+z)}S_9, \text{ and}$$

$$Ag_yCu_{1-(x+y)+(n+1)z}Pb_{2x}Bi_{3-(x+z)}S_5$$

with $0<x<0.36$, $0<x<1.54$, $0<x<0.50$, and $0<x<0.10$, $0<y<0.36$, $0<y<0.64$, $0<y<0.70$, and $0<y<0$ 2, $0<z<0.56$, $0<z<1.43$, $-0.21<z<0.16$, and $0<z<0.08$, and n=2, respectively. The lillianite solid solution extends from $Pb_{2.8}Bi_{2.1}S_6$ to $Pb_{1.56}Ag_{0.68}Cu_{0.20}Bi_{2.67}S_6$, whereas the range of the heyrovskyite solid solution is limited. In the $AgBiS_2$ solid solution, the amount of Cu varies inversely with the amount of Pb, and the solid solution decreases in range with increasing PbS content. The wittichenite solid solution has a range from Cu_3BiS_3 to $Cu_{2.5}Ag_{0.5}BiS_3$ and can not accommodate any detected amount of PbS. The bismuthinite-aikinite solid solution is restricted to the system Cu_2S-PbS-Bi_2S_3. Solid solution based on $Cu_{0.55}Pb_{5.61}Bi_{2.08}S_9$ extends to $Ag_{0.76}Cu_{1.31}Pb_{3.18}Bi_{3.18}S_9$.

MINERALOGY OF THE SLAG AND ITS IMPLICATION IN THE INDUSTRY

CHAUDHURI, J. N. B., Suprova Research Laboratories, 27A, Raja Basanta Ray Road, Calcutta 700 026, India.

The high metal-content and the vast reserve (Chaudhuri,1986) of old polymetallic dump slag around the Harz Mountains (FRG) make its study imperative for industrial re-utilization. Not only could this solve the problem of increasing envirometal pollution but it could also meet at least a part of the country's increasing demand for base metal. The upgrading of the slag through proper processing techniques, however, requires a thorough knowledge of its mineralogy. The author has carried out mineralogical studies of the samples from Langelsheim, Lauthental and Sieber near the Harz Mountains and achieved the following promising result:

Based on the Niggli values (al, c, fm), the present slag is classified as a Pb-Zn slag. The initial temperature of the melt (slag), computed from η-T curve (WINTERHAGER & KAMMEL, 1961) as well as from the interpolated liquidus section of the system "FeO" - CaO - SiO_2 (SCHAIRER, 1942) laid around 1150° C.

The silicate phase is characterized (71-85%) by the presence of the frequently occurring coarse-grained mixed crystals of fayalite and willemite (= zinc fayalite containing up to 13% ZnO). As in the naturally occurring roepperite of Sterling Hill (Mn, Fe, Mg, Zn)$_2SiO_4$ with 10% ZnO, the zinc fayalite (>60 μm) of the Harz slags shows isomorphous emplacement of Fe^{2+} (0.74 Å) through Zn^{2+} (0.74 Å) and Mg^{2+} (0.66 Å). Sporadic inclusions of Ca^{2+} (0.99 Å), Ba^{2+} (1.34 Å) and Al^{3+} (0.51 Å) in the fayalite lattice may result in a subtitution mixed crystal (≤60 μm) analogous to the formula (Fe, Zn, Mn, Mg, Ca, Ba, Al)$_2$ (Al, Si)O_4 and thus evidence for the partially fast cooling process in the slag. The process of isomorphous emplacement in the subordinate silicate phase like monticellite, melilite and pyroxene leads to a Zn-content of up to 6% ZnO. Further silicate phases like barian-orthoclase (hyalophane) and α-celsian (both>60 μm) include the major part of the total Ba-content (5.96% BaO), only 4% of which is confined in fayalite, monticellite, melilite etc.. The presence of Ba-melilite was established for the first time in the polymetallic dump slags of the Harz Mountains. The hyalophane is characterized by the coupled substitution of (K^+ + Si^{4+}) through

MINERALOGY OF THE SLAG AND ITS IMPLICATION IN THE INDUSTRY
CHAUDURI, J. N. B.

(Ba^{2+} + Al^{3+}). As in fayalite, the $Al^{\cdots}$ in hyalophane is respresented both in the cation and $(SiO_4)^{4-}$ -anion complex simultaneously.

The high concentration of zinc (3.76-11.39%) is contained mainly in sphalerite and wurtzite (11%) and in spinels (9.6 - 15.4%). The euhedral spinels consist of fine-grained (30 - 40 μm) mixed crystals of magnetite-franklinite and gahnite-herzynite(BATCHELOR & KINNAIRD, 1984), which frequently show a characteristic zoning. Wurtzite represents the isomorphous presence of FeS in sphalerite ($\leq$60 μm), which might have been caused by the reduction in the wurtzite-sphalterite transformation temperature (1020° C + 5° C). Cenospheres of pyrrhotite (12 - 15 μm) or troilite (?) occur frequently in association with galena, white metal and bornite in the matte and contain 10-30% Zn. Copper and lead (apart from its presence in the silicate phase) can be found mostly in the sulphide phase of the matte and have concentrations like 0.39 - 0.92% CuO and 0.76 - 1.89% PbO respectively.

The result shows that like the naturally occurring ores(ERGUNALP & WEBER, 1985), the dump slags of the Harz Mountains show high Zn -content, which might be recovered by a combined pyro- and hydrometallurgical (COLUSSI & MERIANI, 1980) method. In a manner similar to the use of slags for construction purposes (EMERY, 1975) in the USA, the Ba-Bearing fayalite might not only be used as flux material for ray-absorbing heavy concrete, but they could also serve for refractory purposes, as in the case of olivine.

BATCHELOR, R. A. & KINNAIRD, J. A., (1984): Min. Mag., 48, 425-429
CHAUDHURI, J. N. B., (1986): Sci. & Cult., 52 (1), 19-21
COLUSSI, I. & MERIANI, S. (1980): Int. I. Miner. Process., 7, 43-55
EMERY, J. J. (1975): CIM Bull, 68, (764), 60-68
ERGUNALP, D. & WEBER, H. (1985): Erzmetall, 38, 238-242
SCHAIRER, J. F., (1942): J. Am. Ceram. Soc., 25, 241-274
WINTERHAGER, H. & KAMMEL, R., (1961): Erzmetall, 14 (7), 318-328

•A PRELIMINARY STUDY OF BERTHIERITE FROM CHASHAN, GUANGXI, CHINA

CHEN Dianfen, LU Jun, SUN Shuqiong, LIN Yuejing and CHEN Keqiao, Institute of Mineral Deposits, Chinese Academy of Geological Scienes, Beijing, People's Republic of China

The berthierite occurs in Vein No. 28 at Chashan, Guangxi, China. The vein is about 3600 m in length with an average thickness of about 1 m, occurring in middle-upper Devonian limestone. It is rich in Sb, Pb, Zn, W, Ag, etc. and has a very complex mineralogical composition. Besides antimony minerals such as berthierite, stibnite and antimony, there are galena, sphalerite, arsenopyrite, pyrite, woliramite, scheelite, freibergite, bournonite and jamesonite. The predominant mineral assemblages include pyrite-arsenopyrite, galena-sphalerite, berthierite-stibnite and quartz-stibnite. The decrepitation temperatures of the ore minerals are 265-210, 203-187, 202-180 and 124-120°C, and the homogenization temperatures of gangue mineral quartz and fluorite range from 300-100°C.

Berthierite occurs as columnar and acicular idiomorphic crystals. The crystals are about 100-300 μ in length with a width of about 20-30 μ. It has strong bireflectance and reflection pleochroism (Table 1). The color indices of berthierite are calculated with light source of equal energy S_E (Table 2). So far as we know, these data are the most complete and precise ones available. The chemical formula is calculated as $Fe_{0.93\text{-}1.07}Sb_{2.2\text{-}2.17}S_4$ with trace amounts of As, Sn and Bi. The strongest lines in the X-ray diffraction pattern are: 3.6405(100), 3.1643(80), 2.9901(80), and 2.5996(80). The cell dimensions are a = 11.46, b = 14.04, and c = 3.74 Å. The Mossbauer spectrum of berthierite consists of one symmetrical doublet. The parameters are (at 298 K): δ = 0.788-0.822 mm/s, Δ = 2.66-2.727 mm/s. Mossbauer study suggests that iron, located in distorted octahedra, are divalent and are connected with $(SbS_2)^-_2$ by ionic bonding. This is in agreement with the crystal structure of berthierite reported by Buerger and Hahn (1955).

Table 1. The reflectivity and bireflectance of berthierite (%).

λ(nm)	405	436	480	526	546	589	622	644	656	700
R_{γ} // c	44.5	45	43.9	42	41	40.4	39.2	38.9	38.5	37.5
R_{β} // b	38	36.8	36.2	35.5	35.8	35	35.2	35.2	34.6	33.5
R_{α} // a	30.7	30	29.5	27.5	28.2	30.3	30.7	30.4	30.6	30.5
$\Delta R_{\gamma-\beta}$	15.8	20	17.9	16.8	13.5	14.3	10.8	10	10.7	11.3
$\Delta R_{\beta-\alpha}$	19.2	20.3	20.4	22.5	23.7	14.4	12	14.6	12.3	11
$\Delta R_{\gamma-\alpha}$	36.7	40	37.9	41.7	37	28.6	21.7	22.9	20.5	22.2

Table 2. Color indices (S_E) of berthierite.

R_{vis} (%)		x	y	λ_d (nm)	Pe
R_{γ}	41	0.3233	0.3255	481	0.0377
R_{β}	35.5	0.3299	0.3392	517	0.0146
R_{α}	31.6	0.3359	0.3315	-501	0.011

CRYSTALLINITY AND CHEMISTRY OF K-MICAS FROM METAPELITES OF THE CENTRAL RANGE OF TAIWAN

CHEN, CHAO-HSIA and JENG, RUEY-CHANG, Central Geological Survey, Ministry of Economic Affairs, P. O. Box 968, Taipei, Taiwan, R. O. C.

The Central Range of Taiwan consists of a late Paleozoic to Mesozoic basement and a Cenozoic cover sequence; the former is a metamorphic complex collectively termed the Tananao Schist, and the latter is a slate belt. Metapelites including argillite, slate, phyllite, and black schist are widespread in the Central Range. Metamorphic grade increases generally eastward in the middle part, southward in the northern part, and northward in the southern part of this mountain range.

A total of 235 loose metapelite powder samples from the Central Range have been diffracted by Cu Kα radiation. The relative peak intensities at ∿ 8.9°, 17.8°, and 19.8°2θ were measured and their ratios (designated by $R_{(8.9/19.8)}$, $R_{(17.8/19.8)}$ and $R_{(8.9/17.8)}$) calculated; the half-height peak width at ∿8.9°2θ (designated by $Hb_{8.9}$, in °2θ) was also measured. Diffractograms were inspected for peak resolutions at ∿ 25.2° and 25.6° and at ∿ 34.6° and 35.0°. The crystallinities of K-mica and chlorite are supposed to be good, fair, or poor depending on whether these adjacent peaks are well separated, slightly separated, or not separated.

A linear relationship exists between $R_{(8.9/19.8)}$ and $R_{(17.8/19.8)}$, which is related to the degree of preferred orientation of mica flakes and the development of slaty cleavage in metapelite. A plot of $R_{(8.9/19.8)}$ vs. $R_{(8.9/17.8)}$ shows a probable phase transformation at $R_{(8.9/19.8)}$= ∿ 1.8, below which illite and mixed-layer illite/smectite of poor crystallinity predominate, whereas above $R_{(8.9/19.8)}$=1.8 2M micas of better crystallinity predominate. Instead of being fixed at a certain $Hb_{8.9}$ value, the lower greenschist facies boundary determined by $R_{(8.9/19.8)}$, $Hb_{8.9}$ and peak resolutions varies from 0.21° to 0.24° of the $Hb_{8.9}$ value. The boundary encloses the Tananao Schist as a metamorphic core. Prehnite-pumpellyite and greenschist are the two major facies in the Central Range where the metamorphic grade bears a close relationship with the age and burial depth of strata.

K-micas in 18 metapelite samples from the Central Cross-Island Highway have been analyzed by electron microprobe. Average of 16 to 32 analyses was taken to represent the composition of K-mica in each sample. The plots of Al^{iv} vs. Al^{vi}, Mg vs. Al^{iv}, (Na+K) vs. Al^{iv}, and Na vs. K reveal specific fields of distribution of K-micas from different geologic environments. Chemistry of K-micas from both the slate belt and the Tananao Schist of the Central Cross-Island Highway indicates a low greenschist facies metamorphism; the chemistry of micas from metapelite of the Yuantoushan area indicates a sillimanite grade metamorphism. At constant Al^{iv}, micas from the slate belt have lower Mg and (Na+K) but higher Al^{vi} than micas from the Tananao Schist, which might imply lower P,T in the former than that in the latter. A decrease in Na and increase in K of micas from the slate belt to the Tananao Schist along the highway is evident. The control of the Na/K ratios of the $(K,Na)Al_3Si_3O_{10}(OH)_2$ crystalline solutions by the activity ratio of paragonite to muscovite and the Na^+/K^+ ratio of thermal fluid in association with the mica is significant and noteworthy.

•MOLYBDENITE POLYTYPES IN MOLYBDENUM ORE DEPOSITS OF EASTERN QINLING REGION, SHAANXI, CHINA

CHEN Fugeng, DU Benceng, Laboratory of Shaanxi Bureau of Geology and Mineral Resources, Xi'an, Shaanxi; **WU Qingzhou, and WANG Dinxia,** The 13th Brigade of Shaanxi Bureau of Geology and Mineral Resources, Xi'an, Shaanxi, The People's Republic of China

Three polytypes of molybdenite $2H_1$, $2H_1+3R$ and 3R were found in five molybdenum ore deposits in the Eastern Qinling region, Shaanxi, China. The relative proportions of $2H_1$ and 3R in the $2H_1+3R$ polytype may be estimated by comparing the clearness of rhombohedron spots regularly appearing in hexahedron spots on an electron diffraction pattern. Among more than 200 molybdenite crystals studied, the $2H_1$ and $2H_1+3R$ polytypes are dominant with $2H_1$ more than $2H_1+3R$, whereas only two crystals of 3R polytype were observed.

Two types of $2H_1$ polytype were distinguished: primary $2H_1$ and secondary $2H_1$. The former was formed by direct crystallization from hydrothermal fluids and the latter was formed through the recrystallization of 3R caused by the loss of impurities due to changes of T-P conditions and chemical properties of the media.

The $2H_1+3R$ polytypes in this area are rich in impurity elements, which exist mainly in the form of mechanical mixtures in molybdenite. Increase of temperature, decrease of PH value, increase of oxygen fugacity, and stress tend to facilitate the loss of impurities from 3R polytype and result in a favorable condition for the transformation of 3R to secondary $2H_1$.

The spatial distributions of different polytypes in these ore deposits can be satisfactorily explained in terms of the mechanism of the formation of secondary $2H_1$ polytype and the effects of physical and chemical conditions of the media on the crystallization as well as the recrystallization of molybdenites.

•PETROLOGY OF THE GREENSTONE BELT IN GONGCHANGLING REGION, LIAONING, PRC

CHEN Kuang-Yuan and SUN Dai-Sheng, Beijing Graduate School of Geology, People's Republic of China

The greenstone belt in Gongchangling region consists of volcano-sedimentary rocks metamorphosed to greenschist and to epidote-amphibolite facies dated 31.40-31.45 m.y., being surrounded on both sides by Proterozoic granites dated 21.00-21.35 m.y. and 18.15-19.52 m.y., respectively, and occupying an area of outcrop only about 3.27% of the latter. It can be divided into four recurring cycles composed of 10 rock units with seven banded iron horizons (Fe1-Fe7).

Volcanics of each cycle pass from ultramafic or mafic rocks at the base through intermediate to acid rocks at the top. The ultramafics are peridotitic, pyroxenitic and basaltic komatiites altered to talc, tremolite and magnesio-hornblende schists with relict amygdaloidal, polygonal jointing, dendritic, plate and random spinifex, porphyritic, corrosion, cumulate and devitrified textures and structures typical of komatiites. Their MgO content reaches 28.74-25.42, 20.56-14.44, 9.61-8.22 (wet) and 30.46-27.05, 21.38-14.87, 9.80-8.31 (dry), respectively, with K_2O < 0.64-0.65, TiO_2 < 0.60-0.61 mostly (wt %). The mafics are low-potassic tholeiitic volcanics and subvolcanics of the island arc type altered to amphibolitic rocks with relict diabasic, gabbro-diabasic and tuffaceous structures. The intermediate to acid rocks are keratophyric to quartz-keratophyric tuffaceous and crystal tuffaceous layers altered to amphibole, biotite and muscovite leptites. All of them belong to ortho-metamorphic rocks.

Sediments are mainly colloidal, being ferro-aluminous, ferro-silicic and silicic and typical of BIF, metamorphosed to parametamorphic schists, banded iron ores and quartzites with well-preserved relict colloidal structure as well as bedding in addition to secondary graded bedding. Carbonate sediments are rare, found only occasionally as single lenses of banded calcite marble and sideroplesite nodules or interbands in schists.

The third type of metamorphic rocks is transitional ortho-parametamorphic rocks in which the volcanic and sedimentary materials appear in alternative bands or intermingled with each other in quartz-banded amphibolite and leptite, epidote-banded marble, riebeckite quartzite, quartz-chlorite banded oligoclase schist, almandite-biotite banded riebeckite albite schist, etc. They occur where and when volcanic eruption is passing to sedimentation.

The variations of TFe (wt %) and f (%) of some indicative rock-forming minerals are 10.56-23.65, 30.31-76.04 for biotite, 7.76-26.09, 19.00-66.50 for chlorite; 25.07-31.67, 84.09-95.19 (alm. mol. 71.90-93.60%) for almandite; 29.40-33.56, 82.25-93.80 for grunerite, respectively. They are inversely proportional to the distance of country rock from banded iron ore bed and proportional to the rise of grade of iron ore. Corresponding values for greenalite, stilpnomelane, cummingtonite, arfvedsonite and riebeckite are 30.15, 66.03; 29.80, 76.19; 24.47, 70.77; 27.61, 93.85; 25.40, 97.92, respectively, being all indicators of high grade ore of BIF.

References

[1] Chen, K.Y., Sun, D.S., et al. (1983) Komatites from Gongchangling Iron Mine, Northeastern China. J. Chengdu Coll. Geol. 1.
[2] Chen, K.Y., Sun, D.S., et al. (1984) Genetic mineralogy of Gongchangling Iron Mine. Minerals and Rocks, 4, 2.
[3] Chen, K.Y., Sun, D.S., Yin, H.A. (1986) Genetic Mineralogy and Prospecting Mineralogy. Zhongqing Press, Zhongqing, P.R.C.

JADEITITES IN SERPENTINITE MÉLANGE OF ŌMI-RENGE TECTONIC BELT IN CENTRAL JAPAN

CHIHARA,K. and KOMATSU M., Dep. of Geology and Mineralogy, Niigata University, Niigata (950-21), JAPAN

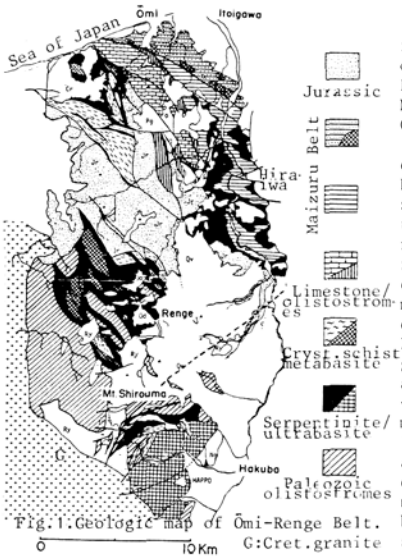

Fig.1.Geologic map of Ōmi-Renge Belt. G:Cret.granite

Jadeitites occur as tectonic inclusions in serpentinite melange of Ōmi-Renge Tectonic Belt surrounding Hida Metamorphic massif in Central Japan.

Ōmi-Renge Belt occupies the north-east part of Hida marginal tectonic zone, where the following tectonic slices are intruded by serpentinite (from west to east): 1) continental margin sediments and fore-arc basin olistostromes of mid-late Paleozoic age: 2)blue-and greenschists(320-360 Ma) and metamorphic rocks(350-600Ma),3) Akiyoshi-type, middle Carboniferous to late Permian limestone and adjacent olistostromes. The incipient tectonic mixture of Ōmi-Renge belt is indicated by a serpentinite mélange which may have formed before the end of the Triassic. The mixture as a whole, overthrusts middle Permian sedimentary-metaophiolite terrain(Maizuru belt in the easternmost area. The mixture is , in turn, overthrust by Hida gneiss-granite complex in the west(Figs. 1 and 2).

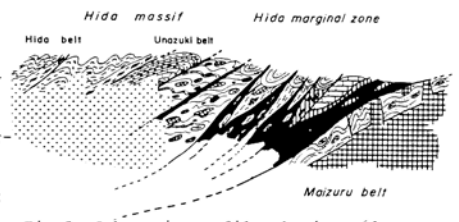

Fig.2. Schematic profile showing mélange.

Each serpentinite mélange contains various tectonic blocks, which are different in separate serpentinite bodies. Among them, Hiraiwa serpentinite body contains various blocks such as jadeitite, meta-carbonate, albitite, rodingite, clinozoisite rock: Omi serpentinite melange contains jadeitite, metagabbro, amphibolite, albitite, garnet amphibolite, chert, meta-carbonate rock, metabasalt; adjacent narrow serpentinite bodies contain also jadeitic rocks. As a whole, jadeitite inclusions are dominant only in the serpentinite mélange in the eascern area.

Jadeitite blocks are surrounded metasomatic Na-amphibole zone (in some cases by nyboitic and Na-richteritic) between the host serpentinite.

Jadeitites are nearly monomineralic and composed of nearly pure jadeite crystals. Their color is variable; dark and pale green, blue-green, lavender, cobalt blue, and white. The minerals contain minor components(Table 1). Dark green color is attributable mainly to ureyite molecule, lavender to charge transfer.

Table 1. Color and minor components of jadeitites from Kotaki and Ōmi areas

	white	lavender	pale green	pale blue	green	dark green
Cr_2O_3	0.00-0.06	0.00-0.06	0.00-0.01	0.03	0.00-0.03	0.91-1.61 (Wt.%)
FeO*	0.04-0.22	0.04-0.38	0.05-0.36	0.74-0.97	0.39-0.83	0.64-1.08
MgO	0.00-0.59	0.05-0.14	0.00-1.45	1.73-1.75	0.69-0.97	0.56-0.97
CaO	0.01-0.59	0.18-0.35	0.04-1.96	2.11-2.56	0.62-1.34	0.71-1.10
TiO_2	0.00-0.05	0.00-0.04	0.00-0.08	0.32-0.57	0.00-0.03	0.23-1.09

• THE DISCOVERY OF ANISOTROPIC TRANSMISSIVE ROTATION ANGLE

CHIOU Juhguo, Chengdu College of Geology, Chengdu, Sichuan, People's Republic of China

A theoretical analysis has been undertaken that made the author deem: the refractive index, the transmissive speed of light, the reflectivity and the absorbing coefficient of principal transmissive direction of an anisotropic transparent or translucent mineral are unequal, so those would result in the inequality of their principal transmissivity and transmissive amplitude. Retardation and phase difference must be produced because of the inequality of principal refractive index and transmissive speed, after the two principal transmissive components had propagated through the thin section, most of the resultant anisotropic transmissive vibrations are elliptical. Only a few of them are linear (planar) with special retardation (0 or 1/2 nλ) or phase difference (0 or nπ). The direction of the longer axis of the resultant anisotropic ellipses and the linear vibrations would not coincide with the incident linear polarized light, and would rotate an angle, the angle should be existed, it might be called anisotropic transmissive rotation angle (r'aβ) or anisotropic transmissive apparent rotation angle (r'a). The optical properties are tested and verified with a photomultiplier microphotometer by the author.

The following transmissive optical properties and parameters which were discovered by the author have been tested, established and measured:

1. Anisotropic transmissive rotation angle (r'aβ) and anisotropic transmissive apparent rotation angle (r'a) of some anisotropic transparent and translucent minerals. 2. Principal transmissivity (T) of some anisotropic transparent and translucent minerals. 3. Anisotropic transmissive ellipticity (θτa) of anisotropic transparent and translucent minerals. 4. Dispersion symbol of anisotropic transmissive rotation (Dr'a) of some anisotropic transparent and translucent minerals. 5. Anisotropic transmissive sign (Ts) of some anisotropic transparent and translucent minerals.

These transmissive optical properties and parameters important to mineral identification, to a theoretical explanation of internal reflection of anisotropic transparent and translucent minerals under crossed nicols, and to a theoretical study of crystal optics and others.

THE STABILITY OF HEULANDITE IN THE SYSTEM $CaAl_2Si_2O_8$ - SiO_2 - H_2O.

CHO, Moonsup, MARUYAMA, S. and LIOU, J.G. Department of Geology, Stanford University, Stanford, CA 94305

Heulandite associated with quartz constitutes a mineral assemblage characteristic for the zeolite facies, together with laumontite-quartz and analcime-quartz (Coombs et al., 1959). A depth zonation of heulandite to laumontite in thick burial volcanigenic sequences suggests that the upper stability of heulandite may be governed by a univariant reaction,

$$\underset{\text{heulandite}}{CaAl_2Si_7O_{18}\cdot 6H_2O} = \underset{\text{laumontite}}{CaAl_2Si_4O_{12}\cdot 4H_2O} + 3\ \underset{\text{quartz}}{SiO_2} + 2\ \underset{\text{water}}{H_2O} \qquad (1).$$

The reaction (1) has been bracketed through reversal experiments at: 155±6°C, 1000 bars; 175±6°C, 1500 bars; and 180±8°C, 2000 bars (Fig. 1). The entropy and volume changes of this reaction are very small unlike the common dehydration reactions, and result in not only extremely slow reaction rate but also large uncertainties in the thermodynamic calculations. Thus, experiments with long duration up to approximately 10 months have been conducted to overcome the kinetic problems. Reaction reversibility was established by determining the growth of one assemblage at the expense of the other, which was demonstrated by both XRD and SEM studies. The SEM observation of reaction textures indicates that the dissolution of heulandite is controlled by surface reaction processes. The standard molal entropy of heulandite was estimated to be 783.7±11.3 J/mol.K from the experimental brackets. Predicted standard molal Gibbs free energy and enthalpy of formation of heulandite are -9722.28±6.3 kJ/mole and -10524.27±9.6 kJ/mole, respectively.

The present experimental results on the reaction (1) are combined with the previous experimental data on Ca-zeolites to establish the P-T relations in the system $CaAl_2Si_2O_8$ - SiO_2 - H_2O. The results are summarized in Fig. 1. Heulandite together with laumontite, stilbite, quartz and H_2O defines an invariant point, which is located approximately at 600 bars and 140°C. Heulandite, which is stable between the stability fields of stilbite and laumontite, can occur only at pressures higher than that of the invariant point, at the condition of $P_{H_2O} = P_{total}$. However, substitution of Na and/or K for Ca, and variations in SiO_2, H_2O contents, and P_{H_2O}/P_{total} ratio may significantly affect the P-T stability of end-member heulandite. Nevertheless, the experimentally-determined P-T relations are consistent with those deduced from natural parageneses. The direct transition from stilbite to laumontite without the heulandite zone may be favored at lower P/T geothermal area (e.g., Tanzawa Mountains, Japan), whereas the regional distribution of stilbite through heulandite to laumontite may be typical in burial sequence with higher P/T gradient (e.g., New Zealand).

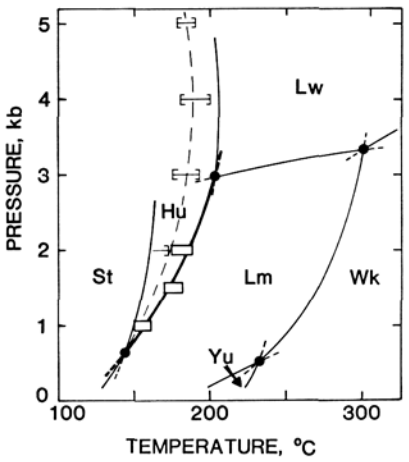

Fig. 1. A P_{fluid} - T diagram showing the relationship among Ca-zeolites in the system $CaAl_2Si_2O_8$ - SiO_2 - H_2O. Open boxes represent the uncertainty ranges in the equilibrium pressures and temperatures of the reaction (1) determined in this study. Brackets indicate the experimental brackets of the stilbite (St) - laumontite (Lm) reaction determined by Liou (1971a). The equilibrium dehydration curves relating laumontite, wairakite (Wk), yugawaralite (Yu), lawsonite (Lw) and heulandite (Hu) are also shown (from Nitsch, 1968; Liou, 1971b; and Zeng and Liou, 1982).

REFERENCES

Coombs, D.C., Ellis, A.J., Fyfe, W.S. & Taylor, A.M., 1959, The zeolite facies, with comments on the interpretation of hydrothermal syntheses. Geochim. Cosmochim. Acta, 17, 53-107.

Liou, J.G., 1971a, Stilbite-laumontite equilibrium. Contr. Mineral. Petrol., 31, 171-177.

Liou, J.G., 1971b, P-T stabilities of laumontite, wairakite, lawsonite and related minerals in the system $CaAl_2Si_2O_8$-SiO_2-H_2O. J. Petrol., 12, 379-411.

Nitsch, K.H., 1968, Die Stabilitat von Lawsonit. Naturwissenschaften, 55, 388.

Zeng, Y. & Liou, J.G., 1982, Experimental investigation of yugawaralite - wairakite equilibrium. Am. Mineral., 67, 937-943.

METAMORPHISM OF CONTINENTAL CRUST AT MANTLE DEPTHS : NEW ROCK-FORMING MINERALS

CHOPIN C., ER 224, E.N.S., 46 rue d'Ulm, 75005 Paris, France
KLASKA R., Inst. f. Mineralogie, Ruhr-universität Bochum, F.R.G.

Unusually high pressures are recorded by a coherent coesite-bearing terrane now exposed over at least 50 km^2 (at most 400 km^2) in the Dora Maira massif, a continental crustal unit of the internal Western Alps. Coesite relics are preserved as inclusions within garnet, kyanite, omphacite and jadeite in various lithologies, essentially metapelite and eclogite (Chopin 1986). Besides, a wealth of new rock-forming minerals occurs for common bulk-rock compositions. The most rewarding lithology is a layer of highly magnesian, quartz-rich metapelite with the assemblage quartz-phengite-talc-kyanite-garnet (90 to 98 mol% pyrope). Pyrope porphyroblasts may locally reach 10 to 20 cm in diameter; they contain numerous inclusions among which the new mineral ellenbergerite (Chopin et al. 1986) and, in other outcrops, six additional new silicates and phosphates.

Ellenbergerite, $(Mg,Ti,Zr,\square)_2Mg_6Al_6Si_6Si_2O_{28}(OH)_{10}$, space group $P6_3$, has a unique structure with single chains of face-sharing octahedra with one third vacancies along the 6_3 axes, and pairs of face-sharing octahedra linked by edge-sharing to form octahedral double chains along the 2_1 axes, all interconnected by SiO_4 tetrahedra. Phosphorus incorporation, mainly through the SiAl=PMg substitution, may have such an extent that over 4 of the 8 Si atoms can be replaced by P, which leads to a new phosphate with ellenbergerite structure; space group $P6_3mc$ results from disorder in the octahedral double chains; a = 12.27 Å, c = 4.95 Å. Considerable solid solution toward silicate is also present in a Li-bearing Mg-phosphate with still uncertain formula; space group $P6_3mc$, a = 12.38 Å, c = 5.04 Å. The pyrope megacrysts also contain : - a polymorph of wagnerite, $Mg_2PO_4(F,OH)$ with space group $P2_1/n$; - a polymorph of magnesian dumortierite, space group $P6_3mc$, a = 11.7 Å, c = 4.75 Å, which has again the ellenbergerite structure, with BO_3 groups replacing two $SiO_3(OH)$ tetrahedra on the three-fold axes ; - magnesiostaurolite, with 80 to 95 mol% of the Mg-end-member i.e. nearly twice as much as the most magnesian natural staurolite so far recorded. New minerals are not restricted to these magnesian rocks as shown by the occurrence of the new phosphate $Ca_2Al(PO_4)_2(OH)$, probably isostructural with goedkenite, in the pyrope-bearing layer and in common metapelites of the enclosing series as well.

Petrologic evidence suggests that this crustal fragment underwent temperatures in the range 700-800°C and minimum pressures well in excess of 25 kbar, which may even reach 35 kbar according to preliminary experimental work on ellenbergerite stability. The combination of these typical mantle pressures with rather low temperatures and with the chemical variety of upper crustal rocks results in a new mineralogical landscape. Striking features are the existence of solid solutions between the silicate and phosphate realms, and the repeated occurrence among the new minerals of the dense ellenbergerite structure.

Chopin C. (1986) Phil. Trans. R. Soc. London, in press
Chopin C. et al. (1986) Contr. Mineral. Petrol. 92 , in press

REDETERMINATION OF PHASE EQUILIBRIUM PROPERTIES IN THE SYSTEM NaCl-H_2O TO 1000°C AND 1500 BARS

CHOU, I-MING, 959 National Center, U.S. Geological Survey, Reston, VA 22092, USA

Phase equilibria in the system NaCl-H_2O were recently determined by Bodner and others (1) to 1000°C and 1500 bars using synthetic fluid inclusions formed by healing fractures in quartz in the presence of the two coexisting fluids at various pressures and temperatures. In that study, salinities of the vapor-saturated liquids at P and T were determined by using the measured temperatures of halite dissolution (T_h) in the halite-bearing inclusions in each sample and by using the halite solubility equation in (2). As figure 1 shows, the extrapolation in (2) to higher temperatures (dashed line) considerably underestimates the solubility of halite, and the recent data (3) (solid line in fig. 1) require a modification of the phase diagram reported in (1).

The new phase diagram (fig. 2) is considerably different from that given in (1). In this modification, a correction of 7°C for the systematic error in T_h reported in (1) was applied, and the halite solubility equations in (3) and (2) were used for T_h greater than 430°C and less than 430°C, respectively. The new phase diagram not only minimizes the discrepancy between the data given in (4) and in (1) at 550°C (see fig. 2) but also provides satisfactory explanations for the peculiar DTA signals at higher temperatures and at pressures below 500 bars, including the sharp reversal in the dP/dT slope of the "halite liquidus" and the "peak-splitting" phenomenon (figs. 7, 8 in (5)). This revision is quite significant for the interpretation of the high-temperature fluid inclusion data.

References:
(1) Bodnar, B. J., et al. (1985), Geochim. et Cosmochim. Acta, 49, 1861-1873. (2) Potter, R. W., II, et al. (1977), J. Research U.S. Geol. Survey, 5, no. 3, 389-395. (3) Chou, I. M., et al. (in press), Abstr. In EOS for 1986 Spring AGU. (4) Urusova, M. A. (1975), Russian J. Inorganic Chem., 20, 1717-1721. (5) Gunter, W. D., et al. (1983), Geochim. et Cosmochim. Acta, 47, 863-873. (6) Sourirajan, S., and Kennedy, G. C. (1962), Am. Jour. Sci., 260, 115-141. (7) Urusova, M. A. (1974), Russian J. Inorganic Chem., 19, 450-454. (8) Urusova, M. A., and Ravich, M. I. (1971), Russian J. Inorganic Chem., 16, 1534-1535. (9) Keevil, N. B. (1942), Am. Chem. Soc. Jour., 64, 841-850. (10) Benrath, A., et al. (1937), Zeitschr. Anorg. u. Allg. Chemie, 231, 285-297.

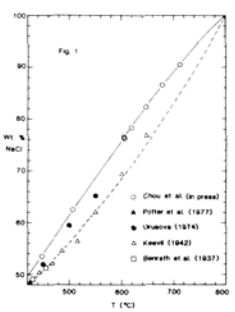

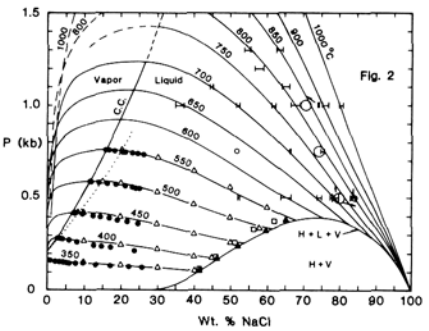

Fig. 1. Solubilities of halite in vapor-saturated liquids determined at temperatures above 420°C. The solid and dashed lines are based on the equations given in (3) and (2), respectively.

Fig. 2. Isothermal (P-X) projections of the coexisting phases in the system NaCl-H_2O obtained from redetermination of the synthetic fluid inclusion data (1) (horizontal bars and open circles) and data from the literature. The horizontal bars are at the contoured temperatures; the open circles indicate data at intermediate temperatures, the size of the symbols representing compositional range. The critical curve (C.C.) and its dashed extrapolation is from (6). The dotted curve is the critical curve from (7). The halite solubility curve (H + L + V) is constructed from the P-T data of (6) and the T-X data of (3). Also shown are the liquid composition data from (6) (solid circles and squares) and from (4), (7) and (8) (triangles). The squares and solid triangles are for halite-saturated liquids at 350°, 400°, 450°, 500° and 550°C.

OCCURRENCE AND STABILITY OF THE SAPPHIRINE POLYTYPES.

CHRISTY, A.G., Dept. of Earth Sciences, University of Cambridge, Downing Street, CAMBRIDGE CB2 3EQ, United Kingdom.

Sapphirine, composition approximately $Mg_7Al_{18}Si_3O_{40}$, is a mineral characteristic of high-grade metamorphic rocks of suitably Mg- and Al-rich chemistry. Two polytypically related structural variants, one monoclinic and one triclinic in symmetry, have been found in nature to date, and the aim of the present work is to investigate the relationship between stacking order in this mineral and such factors as variations in its chemistry, cation ordering, and particularly its pressure and temperature of crystallization. To this end, a variety of samples have been examined, both of natural sapphirines and of synthetic materials in the $MgO-Al_2O_3-SiO_2$ system, the latter produced both by sintering of an oxide mixture at 1 bar, 1425°C, and under various P-T conditions from a gel of the appropriate composition according to the method of Hamilton and Henderson (1968, Min.Mag.36,pp.832-8).

Observational work has largely consisted of a combined high-resolution imaging and diffraction study conducted on the Philips EM6G and JEOL JEM 100CX electron microscopes.

In addition to this, characterisation of the sapphirines and any associated phases has also involved chemical analysis by electron microprobe, and some X-ray powder diffractometry, particularly of the synthetic samples.

Structurally, sapphirine shows certain resemblances to the pyroxene and pyroxenoid groups of minerals. The stoichiometry may be written $^{(6)}M_{16}{}^{(4)}T_{12}O_{40}$, where M is (Al,Mg) with some Fe^2 and T is (Al,Si) with some Fe^3. There is a significant range of M^2T^4-M^3T^3 substitution.

The tetrahedral cations are linked through oxygens to form open-branched vierer chains running parallel to the monoclinic z direction; the octahedral cations are linked into edge-sharing ribbons 3-4 octahedra wide in the y direction and also extended indefinitely parallel to the chains. These structural components are interconnected in an analogous fashion to the 'I-Beam' subunits of the pyroxenes and amphiboles. The possibility of stacking variation is introduced as a result of there being a choice of two possible positions for the branches on each tetrahedral chain relative to those of its neighbours, it being possible to regard the structure between chains as a stack of 7Å-wide (010) slabs, each mapped onto the next by a stacking vector of a/2 + b/2 ± c/4 (monoclinic axes of Moore, 1969, Am.Min.54,pp.31-49). Alternation of the signs of successive c components gives the 2M polytype whose structure was originally refined by Moore, whereas keeping the stacking vector constant produces the 1Tc polytype in either of two twin orientations.

In this respect, sapphirine is closely analogous to wollastonite, and it appears reasonable to model its energetics using a modification of the Axial Next-Nearest Neighbour Ising (ANNNI) approach, such as that applied to the calcic pyroxenoids in Angel et al.(1985, Act.Cryst.B41,pp.310-319), in which the free energy differences between stacking sequences are seen as arising from differences in the interaction energies between neighbouring layers, whose signs are dependent on there relative disposition. However, whereas in the case of wollastonite, six polytypes are known to occur naturally, suggesting that several such interaction parameters are likely to be of significant magnitude, and important in controlling the stacking, this does not appear to be the case for sapphirine. Here, periodicities other than 1- or 2-layer have not been observed, except as weak diffraction maxima lying on streaks in patterns taken from a couple of specimens showing marked disorder. Intergrowth of 1Tc and 2M sequences on a scale of tens of Ångstrom to 1000Å has been seen in HRTEM work, and deduced from X-ray work, on both natural and synthetic samples. This suggests either that the kinetics of stacking equilibration may be very slow, or that the most energetically favourable mode of stacking may be determined by local variations in the cation distribution, and hence heavily dependent on the chemistry of the sapphirine and the extent and nature of its cation ordering, over a wide range of P-T conditions.

THE VARIATION OF UNIT CELL PARAMETERS WITH FERRIC-FERROUS RATIO IN A HORNBLENDE

CLOWE, C.A., POPP, R.K., and FRITZ, S.J. Department of Geology, Texas A&M University, College Station, TX, 77843

A natural metamorphic hornblende has been annealed over a range of oxygen fugacities to determine equilibrium ferric-ferrous ratios and the resulting unit cell dimesions. The original hornblende composition based on 23 O's is Si-6.50, Al(IV)-1.50, Al (VI)-0.87, Mg-2.22, Fe(2+)-1.56, Fe(3+)-0.44, Mn-0.04, Ti-0.09 Ca-1.78, Na-0.41, K-0.10. Experiments were conducted at 700°C in air at 1 atm, as well as hydrothermally at 650°C, 1 kbar at oxygen fugacities defined by the MH, FMQ, and CCH_4 oxygen buffers, for times up to 12 days. Ferric-ferrous ratios were determined, with a precision of ±0.02, using the single dissolution technique of Fritz and Popp (Am. Mineral., 70, 961-968, 1985). Unit cell parameters were obtained by least-squares refinement of powder X-ray diffraction data obtained using synthetic CaF_2 as an internal standard.

	days	a	b	c	β	R**
air	0.02	9.786(8)	18.091(28)	5.316(8)	104.90(9)	0.47
MH	4	9.811(2)	18.069(4)	5.320(1)	105.00(2)	0.30
MH	8	9.813(2)	18.068(5)	5.320(1)	105.04(3)	0.31
FMQ	12	9.836(2)	18.070(4)	5.319(1)	105.03(2)	0.18
CCH_4	4	9.846(2)	18.055(7)	5.315(2)	105.04(2)	0.16
CCH_4	8	9.848(4)	18.044(13)	5.315(2)	105.03(4)	0.15
*CCH_4	4	9.841(3)	18.066(11)	5.312(3)	105.04(4)	0.14

** molar $Fe^{3+}/(Fe^{3+} + Fe^{2+})$
* run represents air annealed sample rerun at CCH_4

Variation in ferric-ferrous ratios is presumed to result from the dehydroxylation equilibrium

$$Fe^{2+} + OH^- = Fe^{3+} + O^{2-} + \tfrac{1}{2}H_2.$$

It is assumed that equilibrium is achieved in the hydrothermal runs because ferric-ferrous ratios are independent of run times, and because the same final ratio is obtained regardless of the starting value (e.g. the final CCH_4 run listed above). Similarily, unit cell parameters for a given buffer are independent of run duration and starting composition. In all these experiments, there is no evidence for decomposition, based on X-ray and optical examination, and thus the chemical composition of the amphibole should remain constant, except for gain or loss of H_2.

Of the unit cell edges, only a shows significant variation with ferric-ferrous ratio. There is a suggestion of an increase in b with increasing Fe^{3+} content, but given the large standard errors for the air annealed sample, all values are equal well within two standard errors, and most are equal within one. The value of a sinβ (the unit repeat across facing double chains) decreases linearly with increasing Fe^{3+}, and is described by the equation

$$a \sin\beta = 9.531 - 0.164R \qquad r = -0.979$$

Colville et al. (Am. Mineral., 51, 1727-1754, 1966) have shown that for clinoamphiboles in which the content of the (M4) site remains constant, the value of b is related to the occupancy of M(2), whereas a is related to the overall occupancy of M(1), M(2), and M(3). The decreasing value of a sinβ for these amphiboles is considered to result from replacement of Fe^{2+} by the smaller Fe^{3+}. Without knowledge of the M(2) site populations, the apparent constancy of b cannot be explained unambiguously, but speculation is possible. Crystal structure refinements of two amphiboles with chemical compositions very close to that used in these experiments were tabulated by Hawthorne (Canad. Mineral., 21, 173-480, 1983). Both of those amphiboles have M(2) occupied only by Al, Mg, and Fe^{3+}. Therefore, an increase in total Fe^{3+} should not have an effect on b unless additional Fe^{3+} displaces Al from M(2). Whether significant changes in site populations are achieved for the temperature and run times used here awaits further crystallographic investigation. Based on the results of longer runs at the MH buffer, Clowe et al. (EOS, 67, #7, p.86, 1986) concluded that ferric-ferrous ratios equilibrate much more rapidly than the rate at which decomposition reactions occur, but how such rates compare to the rate of intracrystalline site-exchange reactions is unknown.

MAGNETIC PHASE TRANSITIONS IN SILICATE MINERALS

COEY, J.M.D., Physics Departmant, Trinity College, Dublin 2 Ireland, GHOSE, Subrata, Department of Geological Sciences, University of Washington, Seattle, WA 98195, USA.

A body of data on magnetization, susceptibility, Mössbauer spectra, magnetic neutron scattering and specific heat now exists for the main structural families of iron-rich silicate minerals which allows a fairly complete picture to be established of the magnetic phase transitions which occur in iron end-members. For magnetic purposes, silicate minerals are best described in terms of the structural units occupied by the magnetic cations: Since iron is forty times as abundant in the crust as all other magnetic cations together it is the arrangement of Fe^{2+} and Fe^{3+}, normally in octahedral sites, that is relevant. We review here the main features of magnetic order in sheet, ribbon, chain and group silicates. Their magnetism is characterized by relatively strong exchange coupling within the edge or corner-sharing octahedral units, and a weaker antiferromagnetic coupling between them.

Sheets of edge-sharing octahedra are found in phyllosilicates. The trioctahedral ferrous end- members minnesotaite (2:1 layer) and greenalite (1:1 layer) order as planar antiferromagnets below 17 and 28 K, respectively. The principal Fe^{2+}-Fe^{2+} exchange coupling via a ~90° Fe-O-Fe bond is positive with J~2 K. Interplane interactions are about 20 times weaker and of opposite sign. A spin flop occurs in fields of order 0.1 T, giving ferromagnetic-type hysteresis. The easy-plane anisotropy of these ferrous silicates is explained by an effectively trigonal crystal field which stabilises the orbital singlet ground state. Dioctahedral ferric phyllosilicates have antiferromagnetic nearest-neighbour exchange with J~-1 K, but the magnetic order depends on the cation distribution; ferripyrophyllite, which has a strong M2 site preference, orders antiferromagnetically below T_N = 18 K, whereas nontronite, which has more random occupancy of 2/3 of the octahedral sites by Fe^{3+}, exhibits spin freezing with no long-range magnetic order only below T_f = 2 K. Relatively small amounts of Fe^{3+} suffice to destroy the ferromagnetic alignment in the plane of the common iron-rich trioctahedral minerals biotite and chlorite; spin freezing occurs below about 5 K, depending on the composition and cation distribution. Monte Carlo simulations show that spin vortices tend to form around the ferric pairs. However, once the ferromagnetic state is stabilized by an applied field, the sample never reverts to the spin glass state at any point around the hysteresis loop.

The main features of magnetic order in phyllosilicates carry over to inosilicates of the amphibole and pyroxene groups, where the metal cation sites form ribbons. Grunerite orders magnetically below 47 K in a structure with ferromagnetic ribbons, coupled antiparallel by weaker antiferromagnetic interactions. The spin flop occurs in 1.2 T. Between 47 and 8 K, the ferrous moments on all four sites are aligned parallel to b, but below 8 K the M1 and M4 moments cant away from the axis. (A similar spin canting found in fayalite is attributed to competing anisotropy on the two ferrous sites). The magnetic structure of the alkalai amphibole crocidolite is similar to that of grunerite, the ferric iron being coupled parallel to its ferrous neighbours in the ribbons. T_N is 30 K. Ribbons in pyroxenes are narrower: orthoferrosilite, where both M1 and M2 sites are occupied by Fe^{2+} has T_N = 45 K. Moments lie along b. Only M1 sites are occupied by ferrous iron in Hedenbergite, which has T_N = 38 K, and a magnetic structure of ferromagnetic chains, coupled antiferromagnetically to their neighbouring chains. Acmite is the ferric equivalent of hedenbergite, and here the iron chains are antiferromagnetic with T_N = 7 K.

Ilvaite is a ribbon silicate with a structure different to that of pyroxene. It has the highest Néel point yet measured in a silicate (118 K), and its magnetic structure consists of ferromagnetis A-site ribbons, coupled antiparallel to their neighbours. Ferrobustamite and deerite also order magnetically in the liquid helium temperature range.

Of the group silicates which order magnetically, Babingtonite has T_N = 24 K. In the groups of four edge-sharing octahedra, the two ferrous ions are coupled parallel, but they are approximately antiparallel to the ferric ions.

Finally, in the olivine group, M1 sites form chains, but M2 sites form planes. Both are occupied by Fe^{2+} in fayalite (T_N=65 K), but in kirschsteinite only M1 is filled and $T_N \lesssim 1$K

LOW TEMPERATURE HOLE-TRAPPING BY IRON IONS IN α-QUARTZ

COHEN, A. J., Dept. of Geology and Planetary Science, University of Pittsburgh, PA 15260, USA

All natural and synthetic quartz known to the author contains aluminum, iron and titanium trace impurity. Thus, amethyst, rose and smoky quartz all contain varying amounts of these three impurities. Amethyst contains mainly Fe^{3+} iron in excess of the Al^{3+} present. Rose quartz contains Ti^{3+} and mainly Fe^{3+} iron. In massive form the Al^{3+} is in large excess of the Ti^{3+} and Fe^{2+}. In smoky quartz the Al^{3+} is always in excess of the titanium and total iron (1). Smoky quartz cooled to liquid N_2 temperature or below develops a band characteristic of amethyst quartz (2,3). Recently Meyer et al. (4) studied optically detected magnetic resonance of the $[AlO_4]^\circ$ center in smoky quartz at 1.6°K. They found that bands at 1.96eV(A_1) and at 2.85eV(A_3) were associated with the center. They showed that a band at 2.33eV that they labeled A_2 was not associated with the $[AlO_4]^\circ$ center. It is suggested in this work that this band is associated with the Fe^{4+} center and that the A_2 absorption band is no longer present in smoky quartz at 1.6°K. It is further suggested that the A_2 center will be present in quartz at temperature of 77°K or below only when Fe^{2+}, Fe^{3+}, and Ti^{3+} ions are essentially absent. It may be virtually impossible to find natural quartz or produce synthetic quartz fulfilling these conditions of purity. Appearance of an absorption band at 2.30eV upon cooling synthetic smoky quartz to 77°K was first reported by Halperin and Ralph (5). The significance of this band went unnoticed until explained by Cohen (3). Van Den Brom and Vogler (2) produced the same band in natural smoky quartz by applying an electric field at low temperature. They were the first to attribute this band to charge transfer between Fe^{3+} and a trapped hole - namely the same band as found in amethyst quartz. These authors reported no change in the band between 8° and 80°K. Table 1 lists the peaks of gaussian bands and their widths at one-half the maximum absorption coefficient ($W_{½}$) for the A_2 band in smoky quartz at room temperature and the "A_2" band of Meyer et al. (1984) at 1.6°K. This "A_2" band has a similar peak position in eV and $W_{½}$ to the Fe^{4+} band found at room temperature and that found on cooling smoky quartz to 77°K. It is felt that Meyer et al. found no relationship between the A_2 and the $[AlO_4]^\circ$ center because the former was no longer present as such but had been transformed into a center interacting with the interstitial Fe^{3+} present. Adekeye and Cohen (6) have shown that the dichroic ratios of the Fe^{4+} band and the A_2 band in the basal plane of quartz are almost identical, 1.56 and 1.53 respectively in similar orientations, which indicates that the populations are nearly equal and that the Fe^{4+} center may be formed from the A_2 center by furnishing an electron to the trapped-hole of the A_2 center.

Table 1. Comparison of Gaussian Absorption Bands in α-quartz.

Band	Orientation	Temperature °K	Peak in eV	$W_{½}$ in eV	f
A_2*	π	R.T.	2.55(1)	0.85(1)	
A_2**	π	R.T.	2.60(1)	0.83(1)	
A_2*	σ	R.T.	2.45(1)	0.87(1)	
A_2**	σ	R.T.	2.55(1)	0.87(1)	
"A_2"*	π	1.6	2.33±0.05(4)	0.57±0.05	(4)
$Fe^{4+}(\theta)$**	π	R.T.	2.27(3)	0.64(3)	0.025(3)
$Fe^{4+}(\theta)$**	$\sigma_{\parallel a_2}$	R.T.	2.30(3)	0.61(3)	0.025(3)
$Fe^{4+}(\theta)$**	$\sigma_{\perp a_2}$	R.T.	2.26(3)	0.60(3)	
Fe^{4+}**	π	8.4	2.32±0.02(2)	0.83±0.03(2)	
Fe^{4+}*	π	77	2.30(3)	0.44(3)	
Fe^{4+}*	α	77	2.30(3)	0.56(3)	

*synthetic quartz **natural quartz

(1) Partlow, D.P. and Cohen, A.J. (1986), Optical Studies of Biaxial Aluminum-Related Color Centers in Smoky Quartz. Am. Mineral. In Press. (2) Van Den Brom, W.E. and Vogler, J. (1974), Electromodulated Absorption in Smoky Quartz. Physics 75A 245-267. (3) Cohen, A.J. (1985), Amethyst Color in Quartz, The Result of Radiation Protection Involving Iron. Am. Mineral. 70, 1180-1185. (4) Meyer, B.K., Lohse, F., Spaeth, J.M. and Weil J. G. (1984), Optically Detected Magnetic Resonance of the $[AlO_4]^\circ$ centre in crystalline Quartz. J. Phys. C: Solid State Phys. 17, L31-L36. (5) Halperin, A., and Ralph, J.E. (1963), Optical Studies of Anisotropic Centers in Germanium-Doped Quartz. J. Chem. Phys. 39, 63-73. (6) Adekeye, J.I.D. and Cohen, A.J. (1986), Correlation of Fe^{4+} Optical Anisotropy, Brazil Twinning and Channels in the Basal Plane of Amethyst Quartz. Applied Geochemistry 1, In Press.

FIRST PRINCIPLES CALCULATIONS OF THE PHYSICAL PROPERTIES OF MINERALS AS FUNCTIONS OF PRESSURE AND TEMPERATURE WITH SPHERICALLY BREATHING IONS

COHEN, RONALD E., National Research Council--NRL Associate; MEHL, MICHAEL J.; BOYER, LARRY L.; All at: Dept. of the Navy, Naval Research Laboratory, Code 4684, Washington, D.C. 20375-5000

The physical properties of minerals can now be calculated fairly accurately from first principles without the input of any experimental data. These models are first principles models in the sense that no fitting to measured properties or other empirical data are used. Only the values of universal constants, such as Planck's constant and atomic masses, are necessary. First principles calculations can give predictions of physical properties of solids under extreme conditions which are difficult or impossible to obtain in the laboratory. They also help us understand the behavior of minerals with known properties.

Spherically symmetric charge relaxation in response to the long-range electrostatic potential (PIB: Potential Induced Breathing) has been shown to be very important for the static and dynamic properties of high symmetry oxides such as those in the B1 and B2 structures (Boyer et al., 1985). These electron gas-type models are now being tested on more complex crystal structures such as corundum (Al_2O_3) and rutile (TiO_2). The cohesive energy is calculated with no adjustable parameters, and the dependence of the ion self-energies on the site potentials gives a many-body contribution to the energy. Preliminary results for corundum at P=0 give V=84.8 Å^3, c/a=2.59, x(O)=0.30, z(Al)=0.36, compared with experimental values of 84.9, 2.73, 0.31 and 0.35. The static equation of state is within a fraction of a percent of experiment. For rutile, the calculated values are V=59.2 Å^3, c/a=0.73 and u(O)=0.31, compared with 62.4, 0.64 and 0.31.

The internal energy of a crystal is represented within PIB by:

$$\Phi = \frac{1}{2}\sum_{\substack{ll' \\ kk'}} \frac{z_k z_{k'}}{|\mathbf{r}(l_k) - \mathbf{r}(l'_{k'})|} + \sum_{lk} S_k(P(l_k)) + \frac{1}{2}\sum'_{\substack{ll' \\ kk'}} \phi_{kk'}(P(l_k), P(l'_{k'}), |\mathbf{r}(l_k) - \mathbf{r}(l'_{k'})|);$$

where the z's are the formal valences of the atoms, R is the distance between an atom pair, $\phi_{kk'}$ is the short-range potential between an atom pair and S_k is the self energy of an atom. The self-energy and the pair potentials are functions of the charge density which in turn are functions of the long-range Madelung potential at the atom site. Minimization of the energy represented by the above equation is not the same as the iterative site potential matching which has been used in most of the modified electron gas (MEG) type models for oxides and silicates.

At present, atomic wave-functions are calculated within a Watson sphere with a charge opposite to the ionic valence with local density theory. The self-energy is calculated from the Thomas-Fermi formulation of the kinetic energy and the local denity exchange and correlation functionals. Pair potentials are calculated by overlapping the atomic charge densities and calculating the energy of a uniform electron gas with density appropriate to each point in space. The Thomas-Fermi kinetic energy is used in the self-energy since the same formulation is used in the overlap and atomic parts.

Many improvements to the model are being considered, including better density functionals and better approximations to the charge density of atoms in crystals. Full linearized augmented plane wave (LAPW) calculations are being used to better understand charge densities in oxides.

The dynamical properties of the model are complicated by macroscopic electric fields, and will be discussed.

DIFFERENTIATION OF HIGH-FLUORINE RHYOLITE, HONEYCOMB HILLS, UTAH.

Roger Congdon and W.P. Nash, Department of Geology and Geophysics, University of Utah, Salt Lake City, Ut 84112-1183

The Honeycomb Hills, located in west-central Utah, consist of pyroclastic deposits and domal flows of highly evolved, fluorine-rich rhyolite erupted 4.7 Ma ago. Concentrations of trace elements exhibit systematic variations correlative with sequence of eruption. Earliest erupted pyroclastic units contain highest amounts of incompatible elements such as Rb (2000ppm), Li (344), Cs (76), Be (80 typical, up to 1400) and U (17). Incompatible elements decline in concentration upward through the pyroclastic sequence and into overlying domal rhyolites, reaching lowest levels in the last flows erupted (fig. 1). Conversely Zr, Hf, Sr, Ba, Y, and all REE increase in concentration in younger eruptive products. LREE enrichment and depletion factors (fig. 2) are consistent with those for other high-silica rhyolite systems, but HREE are systematically and uniformly depleted in more evolved volumes of magma (fig. 3). The lavas contain abundant phenocrysts (35-50% by volume) of sanidine, oligoclase-albite, quartz, fluorbiotite, and fluortopaz set in a groundmass of the same minerals or glass containing up to 2.3% F. Sanidine, fluorbiotite and fluortopaz occur also as megacrysts up to 8 cm in diameter. Accessory minerals include fluorapatite, zircon, LREE-fluorite, euxenite(?) and a HREE niobate. Fractionation of these phases explains the overall depletion in REE in the most highly evolved liquids.

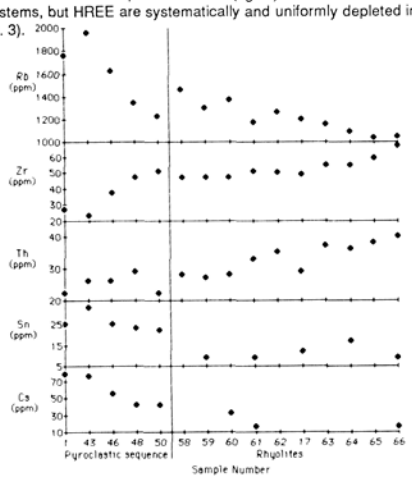

Figure 1. A plot of select trace elements vs. stratigraphic position. Rocks to left are most evolved, to right are least evolved (dome center).

Initial pyroclastic eruptions were accompanied by preferential loss of water versus fluorine from the magma as shown by increased fluorine contents of biotite in post pyroclastic flows. Fugacity ratios of H_2O/HF for the fluid phase decline by an order of magnitude from (log) 2.5 to 1.5 between pyroclastic eruptions and domal flows. Temperatures of eruption were approximately 600°C as determined by two-feldspar thermometry. Flow to the surface of these cool, crystal-rich lavas, must have been facilitated by high F contents which serve to reduce viscosity. High phenocryst contents may indicate residence time at considerable depth followed by rapid rise to the surface. Evidence for an ascent on the order of 5 km/year includes large (0.5 m) sandstone xenoliths.

Metamorphic xenoliths indicate that these lavas may have originated from anatexis in a metapelite source region at least 6.5 km below the surface based on local stratigraphy. Other indicators, such as high Sn (up to 30 ppm), Rb and F values point to a possible pegmatitic origin.

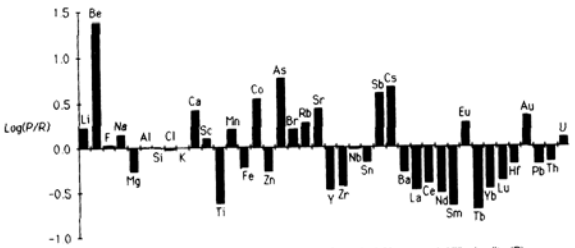

Figure 2: Enrichment factors. The log of a typical Honeycomb Hills rhyolite (R) divided into a more highly evolved pyroclastic rock (P) from the same source.

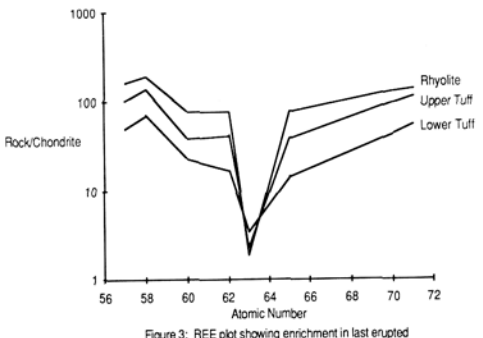

Figure 3: REE plot showing enrichment in last erupted magma. Lower tuff is most highly evolved.

POINT DEFECTS AND CHARGE TRANSPORT IN FAYALITE AND OLIVINE

COOPER, E. A. and MASON, T. O., Dept. of Materials Science and Engineering, Northwestern University, Evanston, IL 60201, USA

Electrical property measurements at elevated temperature (900-1200°C) were employed in the study of point defect structure and electron conduction mechanism in fayalite and various olivine compositions. The Seebeck coefficient, which has not been previously reported for high iron compositions, is particularly useful in establishing the conduction mechanism. The issue of M1 vs. M2 site occupancy can be resolved by combining conductivity, Seebeck, and Moessbauer results.

Synthetic polycrystalline fayalite and olivine were prepared by hot isostatic pressing of sol-gel derived powders. This synthesis route allows for atomic scale homogenization and also achieves high densities. A grain growth stabilization anneal was performed prior to electrical property measurements. A four thermocouple steady state technique (described previously [1]) was chosen over the variable gradient technique. Both Seebeck coefficients and four point conductivity can be measured simultaneously with this apparatus.

A new technique for determining site occupation of iron, based upon a combination of conductivity and Seebeck coefficient, will be presented. Results for the fayalite-forsterite solid solution will be compared with results in spinel systems.

From oxygen partial pressure variations of the electrical properties, the defect structure of fayalite and olivine can be inferred. Our results will be compared with previous results and models for the defect structure(s) of this solid solution.

Reference:
1. Trestman-Matts, A., Dorris, S. E., and Mason, T. O., "Measurement and Interpretation of Thermopower in Oxides", J. Am. Ceram. Soc., 66 [8] 589-92 (1983).

This work is supported by the National Science Foundation under Grant No. EAR-8409666.

SPHALERITE AND ARSENOPYRITE COMPOSITIONS IN CASSITERITE-POLYMETALLIC DEPOSITS OF DACHANG (P.R.CHINA)

CORAZZA, M., CORSINI, F., LATTANZI, P. & TANELLI G.
Dipartimento di Scienze d. Terra, via La Pira 4, Firenze, Italy

The Dachang district (Guangxi) is the second largest producer of Sn of China, and an important source of Zn, Cu, Sb and several other metals (Tanelli & Lattanzi, 1985).

The two major mines in the district are the cassiterite-sulfide mine of Changpo, and the Zn-Cu-skarn deposit of Lamo, both represented by stockwork and massive mineralizations hosted within Upper Devonian thermometamorphic limestones and, at Changpo, quartzites, in close proximity of Cretaceous granitic intrusions.

Apart from the much greater abundance of Sn at Changpo, the main mineralogy of the two deposits is fairly similar, and it is in particular characterized by the widespread coexistence of iron sulfides, arsenopyrite, sphalerite and stannite, which represent potential useful indicators of the ore-forming environment (Scott 1983; Shimizu & Shikazono, 1985).

Textural relationships involving the above minerals are complex and sometimes ambiguous. Arsenopyrite may appear markedly replaced by sphalerite and/or pyrrhotite, which in turn is often altered to pyrite/marcasite. Elsewhere, the textures between arsenopyrite, sphalerite and iron sulfides may be interpreted as "mutual boundary". Stannite, less common than the above minerals, occurs as oriented intergrowths within sphalerite.

At both Changpo and Lamo, sphalerite is mostly associated with pyrrhotite (monoclinic and/or hexagonal), and its FeS content is fairly homogeneous, averaging 20.2±1.0 mol% at Changpo, and 20.8 ±1.7 mol% at Lamo. The few samples associated with pyrite show a more variable, and in average lower, FeS content (Changpo: 14.8 ±2.8 mol%; Lamo: 14.2±5.0 mol%). Cd and Mn contents are in general below 0.5 wt%.

Application of the geothermometer of Nakamura & Shima (1982; see also Shimizu & Shikazono, 1985) for coexisting stannites and sphalerites from Changpo gives temperature in the order of 300-350°C.

Arsenopyrite composition is quite variable at both Changpo (31.4 to 35.9 at% As) and Lamo (30.6 to 35.3 at% As). Most samples are characterized by very high As contents, requiring quite high temperatures (>500°C for the As-richest composition) and/or very low sulfur fugacities in the forming environment. In general, the least As-rich compositions are associated with pyrite, and the most As-rich with pyrrhotite. Co, Ni, Cu and Sb contents are always below 0.5 wt%.

The sulfur fugacity-temperature fields defined by the FeS content of sphalerite and, respectively, by the As content of coexisting arsenopyrite, overlap only for few samples, demonstrating that, in general, the two minerals are not in chemical equilibrium, even where mutual boundary textures can be observed.

The lack of sulfur-buffering equilibrium assemblages at Changpo and Lamo precludes the application of arsenopyrite and sphalerite compositions for precise temperature and sulfur fugacity estimates. However, combining the textural and chemical data, it can be suggested that sulfide deposition started with arsenopyrite formation at temperatures as high as 500°C, and continued down to less than 300°C (formation of monoclinic pyrrhotite); the sulfur fugacity-temperature conditions, initially confined below the arsenopyrite/pyrrhotite + liquid sulfidation curve, moved eventually into the stability field of pyrite.

REFERENCES
Nakamura Y & Shima H. (1982) - Abstr. Joint Mtg. SMGJ-AMPEG-MSJ
Scott S.D. (1983) - Mineral.Mag. 47, 427
Shimizu M. & Shikazono N. (1985) - Mineral.Deposita 20, 314
Tanelli G. & Lattanzi P. (1985) - Mineral.Deposita 20, 102

PLATINUM MINERALIZATION IN MAFIC-ULTRAMAFIC ROCKS, WESTERN GNEISS TERRAIN, W. AUSTRALIA

CORNELIUS, M.; STUMPFL, E.F. Institute of Mineralogy and Petrology, Mining University, A-8700 Leoben, Austria.

The Western Gneiss Terrain (WGT; Gee, 1979) represents the westernmost part of the Yilgarn Block; its dimensions are approx. 1000 km in N-S and 20-450 km in E-W direction. In contrast to the granite-greenstone terrains in the east the WGT is dominated by metamorphic belts of schists and gneisses of sedimentary origin (Sm-Nd ages: 2.9 to 3.6 b.y); these have been intruded by granitoids. A number of small mafic and ultramafic bodies occur within the paragneisses (Harrison, 1986); important localities include New Norcia, Coates, Kondinin and Bridgetown-Yornup. In contrast to the considerable interest which the Yilgarn greenstone belts have attracted in recent years, the mafic-ultramafic complexes of the WGT have received little attention so far. We report first results of a project incorporating new field and drillcore evidence, petrography, mineral and whole-rock chemistry, REE and PGE distribution patterns, and sulfide and platinum mineralogy.

At New Norcia, W.A., a sequence of gabbro- norites, olivine gabbro-norites and harzburgites has been drilled to 350 m below surface. The ultramafic unit is largely altered to tremolite-serpentinite which is chemically characterised by chondritic Al/Ti ratios pointing towards a rather primitive magma.

In the gabbro-norite, sulfide-rich zones carrying major pyrrhotite, pentlandite and minor chalcopyrite and pyrite, occur with a quartz-biotite-chlorite association, similar to that described from the Merensky Reef (Ballhaus and Stumpfl, 1986). Platinum and palladium minerals have been discovered in a sulfide band in the gabbro-norite; sulfides in olivine gabbro-norite and in harzburgite frequently contain palladium minerals. So far, michenerite (PdBiTe), majakite (PdNiAs) and sperrylite ($PtAs_2$) have been identified; the Pd minerals occur preferentially in sulfides. Sperrylite is confined to silicates close to the sulfide-silicate contact; its grainsize ranges from 5 to 150 µm (average 50 µm). The size of the palladium minerals varies from 1 to 40 µm (average about 10 µm). Quartz and biotite aggregates frequently occur with the sulfides. The mode of occurrence of platinum minerals within silicates and sulfides suggests fractionation of the PGE such as observed in the Merensky and Stillwater Reefs, and complex

PLATINUM MINERALIZATION IN MAFIC-ULTRAMAFIC ROCKS, WESTERN GNEISS TERRAIN, W. AUSTRALIA

CORNELIUS, M.; STUMPFL, E.F.

poly-phase transport mechanisms. The association of PGM and sulfides with hydrous silicates (biotite, chlorite) and quartz points towards participation of a fluid phase in platinum mineralization. Chondrite normalized REE analyses in samples with high sulfide content reveal approximately chondritic abundances with light to strong enrichment of the LREE and/or light enrichment of the HREE. Possible links of mineralizing processes and REE patterns are under investigation.

Chondrite normalized precious metal patterns (Au/Ir = 1-2; Fig. 1) resemble those of komatiites rather than those of differentiated layered igneous complexes.

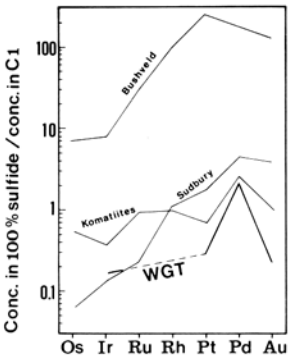

Fig. 1: Schematic PGE distribution pattern in ultramafic rocks from New Norcia (WGT); Sudbury, Komatiite and Bushveld trends for comparison.

Ballhaus, C.G., Stumpfl, E.F., 1986, Sulfide and platinum mineralization in the Merensky Reef. Evidence from hydrous silicates and fluid inclusions. Subm. to Contrib.Min.Petrol.

Gee, R.D., 1979, Structure and tectonic style of the Western Australian Shield. Tectonophysics, v.58, 327-369.

Harrison, P.H., 1986, The mineral potential of layered igneous complexes within the Western Gneiss Terrain. West.Autralia Geol. Survey Ann.Rept. (in press).

LUMINESCENCE IN TOURMALINE

COY-YLL,R., Dept. of Crystallography and Mineralogy, Universidad Complutense,28040 Madrid,SPAIN;CALDERON, T., Dept. of Geology, La Rabida,Huelva,SPAIN;AGUILAR, M., Inst. of Solid State Physics,CSIC,Madrid,SPAIN

The tourmaline mineral group provides an interesting system in which effects due to magnetic exchange coupling(Mattson and Rossman,1984) and thermal conductivity at low temperatures(Lawless and Pandey,1984) have been studied at some extent. Indeed, the tourmaline crystal structure has been intensively studied for several years.Recently,the structural refinement of a (Li,Mn)Al-tourmaline has been reported by Nuber and Schmetzer(1984).Single-crystal Raman spectra of both pink and green tourmalines have been discussed elsewhere (Alvarez and Coy-Yll,1978).

In this short-note attention is paid to the luminescent features of two distinct colored tourmalines:a pale-pink crystal which appears to be closely related to the elbaite pole, and a deep-blue specimen which lies near to the schorl pole. Several sections cut perpendicularly to the c-axis were used for either thermoluminescence(TL) or photoluminescence(PL) experiments.Samples were heated up to 500°C in search for TL.Following each TL run the sample was allowed to cool and then heated again to obtain the black-body background. Readouts were perfomed at vacuum as well as at nitrogen atmosphere.A heating rate of 10°C s^{-1} was used.PL data were obtained at 77K.

The pink specimen shows a natural TL which consits of three broad glow-peaks centered at 210,310,and 360°C.The natural TL from the blue specimen includes six well-resolved glow-peaks,which appear at 160,170, 185,280,300 and 380°C.After exposing the samples to β-radiation(the total dose was $\sim$ 3000 rad)and heating up again some salient features regarding the intensity, broadening and position of the second glow-peaks were seen.The irradiation effects in both tourmalines preclude the existence of a simple relationship among the temperatures at which both unradiated and radiated samples give a TL signal.Samples heated at nitrogen atmosphere enable us to detect a number of gas-induced TL peaks.These peaks are not well-resolved.They occur usually at temperatures below 300°C.Their appareance could be related to the own ability of tourmaline in trapping the gases present in the environment(Saito et at.,1984).But it is not yet completely understood whether a such ability can be reactivated to some extent by either sample preparation or thermal-induced changes in the crystal structure.Calderon and Coy-Yll (1982) have reported the existence of an irreversible transition at 360°C (Δ H=0.1 cal/g).

By setting the output monochromator at 620nm,the region at which emission of Mn^{2+} in elbaite has been already reported(Calderon and Coy-Yll,1982),the present pink specimen shows an excitation spectrum with two main bands centered at 410nm and 457nm.The observation of greatest interest is that the 410nm band (the $^6A_{1g} \rightarrow {}^4E_g, {}^4A_{1g}$ transition in octahedrally-coordinated Mn^{2+})shows an unexpected broadening effect.In fact, such an effect has not been observed in neither Mn-doped calcite(Aguilar and Osendi,1982)nor Mn-doped forsterite(Green and Walker,1985).This feature might be related to impurity-defect complexes in tourmaline crystal structure.As will be discussed in a subsequent paper,tourmaline displays a rather complicated PL process since it is possible to excite in some complexe bands and observe Mn^{2+} emission.After X-ray exposure the latter appears to be annihilated.

Aguilar,M.;Osendi,MI(1982).J.Luminescence 27,365
Alvarez,M.A.;Coy-Yll,R.(1978).Spectrochim.Ac.34A,899
Green,G.R.;Walker,G.(1985).Phys.Chem.Minerals 12,271
Calderon,T.;Coy-Yll,R.(1982).J.Chem. 18,217
Lawless,W.N.;Pandey,R.K.(1984).Solid State Comm 51,833
Nuber,B.;Schmetzer,K.(1984).N.Jb.Miner.Mh. 7,301
Mattson,S.M.;Rossman.G.R.(1984).Phys.Chem.Minerals 11,225
Saito,K.;Alexander,EC.;Dragon,J.C.(1984).Geophys Res 84 7891

CYRILOVITE FROM BOSA (SARDINIA, ITALY): STRUCTURE AND CRYSTAL CHEMISTRY.

COZZUPOLI D., GRUBESSI O., MOTTANA A., Dipartimento di Scienze della Terra, Università "La Sapienza", 00100 Roma, ITALY; ZANAZZI P.F. Dipartimento di Scienze della Terra, Università di Perugia, 06100 Perugia, ITALY.

The crystal structure of the cyrilovite from Bosa (Sardinia,Italy), a new locality for this rare mineral, has been refined in the $P4_12_12_1$ space group to a R value of 0.053 for 907 observed reflections.

The structure, confirming and refining that of the other end-member of the solid solution series, wardite (Fanfani et al., Mineral.Mag. 37, P.598, 1970), consists of sheets of Fe^{3+}-centered octahedra sharing vertices to form a square net, in the center of which the 8-fold coordinated Na^+ ion is located. The Na-Fe-O sheets are linked together by PO_4 distorted tetrahedra and by hydrogen bonds. The unit cell parameters of cyrilovite (a= 7.318(2), c= 19.277(7)Å, V= 1032.3(4)$Å^3$, c/a= 2.634) are substantially greater than those of wardite, accounting for the greater dimensions of the octahedrally coordinated cation. The chemistry of the Bosa cyrilovite is close to the end-member $NaFe_3(OH)_4(PO_4)_2 \cdot 2H_2O$, with a limited solid solution of Al for Fe^{3+} and of Ca for Na. Both these substitutions lie in the known range, although the latter may imply a yet poorly known possibility of vacancies in the 8-fold coordinated sites. The IR spectra show the presence of Al substituting for Fe in the form of additional weak bands (cf. Tarte et al., Bull. Minéral., 107, p.745, 1984), but they are inconclusive as far as the Ca for Na substitution is concerned.

THE METAMORPHISM OF PYRITE

CRAIG, James R., Dept. of Geological Sciences, Virginia Polytechnic Institute and State University, Blacksburg, Virginia 24061, USA;
VOKES, Frank M., Geologisk Institutt, Universitetet i Trondheim - Norges Tekniske Høgskole, 7034 Trondheim, Norway

Pyrite, FeS_2, the most abundant, widespread, and one of the most refractory of sulfide minerals, is nearly ubiquitous in metamorphosed stratabound sulfide deposits where it ranges from the dominant to a minor consitituent. The physical and chemical response of pyrite to changing thermal and stress conditions is important to the mineralogy and the textural features found in many stratabound ores in regionally metamorphosed terranes. The high physical strength of pyrite, which is maintained through the thermal range of most metamorphosed deposits results in pyrite generally remaining rigid while other sulfide minerals, as well as many silicate and carbonate gangue phases, deform in response to stress. Consequently, pressure shadows, which host softer phases such as chalcopyrite and sphalerite, commonly develop adjacent to pyrite grains. At low temperatures pyrite deforms by brittle fracture (cataclasis) , but at high temperatures it may undergo ductile deformation by dislocation flow.

During isochemical metamorphism the common pyrite-pyrrhotite assemblage, nearly regardless of ratio, serves as the most important buffer for the activity of sulfur and for the FeS contents of sphalerite. As temperature rises during prograde metamorphism, pyrite and pyrrhotite reequilibrate with resultant breakdown of pyrite and development of more sulfur-rich pyrrhotite. This results in the destruction of many small early-formed pyrite grains. In contrast, as temperature drops during retrograde metamorphism, pyrrhotite gives up sulfur which is then available for the growth of pyrite as new crystals or as overgrowth on crystals that survived the prograde phase. The primary controls on the quantity of pyrite consumed and/or regrown are the initial ratio of pyrite and pyrrhotite and the temperature range over which equilibrium is maintained between the two minerals. Although many details of prograde processes are obscured by retrograde reequilibration, it appears that the net result of the metamorphic episode on these minerals is the production of fewer, but larger, pyrite crystals than were initially present. The amount of pyrite grown during the retrograde phase can be estimated if one knows the pyrite/ pyrrhotite ratio and the temperature range over which there was equilibration during cooling. Thus if an ore mass has a pyrite/ pyrrhotite ratio of 1/1 at 600°C and the pyrite and pyrrhotite continue to equilibrate on cooling down to 300°C, there is sufficient sulfur release from the pyrrhotite to form 5% of the total amount of pyrite finally present If the initial ratio of pyrite to pyrrhotite is 1/4 at 600°C, cooling under the same conditions results in 18% of the final pyrite having formed as a result of sulfur loss from the pyrrhotite, and if the initial ratio of pyrite to pyrrhotite is 1/9, such cooling could create 34 % of the pyrite.

Growing pyrite crystals may incorporate inclusions of sulfides (including small pyrite grains), oxides, silicates, and carbonates which may yield information on the pressures, temperature, or relative timing of growth. Many porphyroblasts display crudely concentric patterns of inclusions developed during growth. Rotation of pyrite crystals during their growth may result in the development of "snowball" textures incorporating various inclusions. In contrast, rotation after growth results in abrasion and the rounding of initially euhedral crystals.

(This work supported by NATO grant 85/0218 and a Mining and Minerals Resources and Reserch Allotment grant to VPI & SU)

QDF: THE QUANTITATIVE DATA FILE FOR ORE MINERALS

CRIDDLE, A.J., Department of Mineralogy, British Museum (Natural History), Cromwell Road, London SW7 5BD, U.K.

In 1977, when the first issue of the QDF was published it was envisaged by the Commission on Ore Microscopy (COM) as the first step in the development of an international repository of quantitative data for the ore minerals. In card form, it consisted of 204 cards for 155 minerals. It was intended that later issues would include new data and, where appropriate, retain or replace cards from the first issue. In other words, the QDF was not designed to be static in content, nor, necessarily, in format. Underlying its production was the recognition by the COM of a major impediment to the usefulness of the ore microscope - the lack of definitive optical data for mineral identification. Specular reflectance values, at near-normal incidence, of the ore minerals, were seen as the answer to the problem. Many attempts had been made since the 1920's to utilise this property, photovisually and photometrically. It was not, however, until the 1960's and 1970's that microscope-photometers sufficiently sensitive for the job were developed. Fortuitously, the same period saw the development of the electron microprobe. For the first time it became possible, as a matter of routine, to obtain reliable compositional and optical data for the same grain of an ore mineral. QDF 1 was a compilation of such data with, where possible, confirmatory X-ray data. Many of the cards it contained were incomplete in some, or all, of the characteristic properties, nevertheless, it became accepted as a valuable data-base in those laboratories equipped for quantitative ore microscopy, and is still used as the basis for many identification schemes, including several computerised schemes.

The second issue reflects the progress that has been made in all aspects of quantitative microscopy since 1977. In particular, microscope-photometers, equipped with small computers, now enable reflectance curves for a mineral to be obtained in a fraction of the time it takes to determine its composition with the electron microprobe. This has meant that more complete data for many more species were available for inclusion in the second issue. Of the 420 data sets in QDF 2, more than 85% contain full visible-spectrum data (about the same percentage include compositional and X-ray data). The increased size of the file determined that, unlike the first issue, it should be produced as a book. It is organised alphabetically by mineral name, with one page per data-set. The format differs from the first, and allows space for the inclusion of more quantitative optical data. These reflectance and reflectance-derived data are used as the basis of three keys for access to the file for the purpose of mineral identification. They are unusual in containing, for some minerals, more than one set of data. In this, they illustrate the effect that compositional and structural variation can have on the reflectance spectrum of a mineral.

The objectives of the COM in compiling this issue were to provide characteristic data in an easily accessible form for as many ore minerals as possible. The species coverage was to be such that the file would be useful to the practising ore microscopist as well as satisfying the needs of any modern course in ore microscopy. These objectives will be discussed: the background to the production of this, and future issues will be reviewed; and the advantages of using quantitative techniques in the teaching of ore microscopy will be considered. Examples from the QDF will be used to illustrate these points. Other examples will be used to demonstrate the effectiveness of the file as an aid to mineral identification.

Criddle, A.J. & Stanley, C.J. (eds.) (1986): Commission on Ore Microscopy: *IMA/COM Quantitative Data File for ore minerals (second issue)*. Trustees of the British Museum (Natural History), London.

Henry, N.F.M. (ed.) (1977): Commission on Ore Microscopy: *IMA/COM Quantitative Data File (first issue)*. Applied Mineralogy Group, Mineralogical Society, London.

DISORDER IN KAOLIN MINERALS: OBSERVATIONS USING NEAR-INFRARED REFLECTANCE SPECTROSCOPY

CROWLEY, James and VERGO, Norma, U.S. Geological Survey, Reston, VA

Near-infrared reflectance spectra (0.8 to 2.5 μm) were recorded for 25 kaolin mineral powder samples, including ordered kaolinite, disordered kaolinite, dickite, nacrite, and halloysite. The spectra permit distinction between ordered and disordered kaolinite (fig. 1), and between each of the three kaolin polytypes (fig. 2).

Previous x-ray diffraction study has demonstrated that disorder in kaolinite involves defects in the positions of vacant octahedral sites (Plaçon and Tchoubar, 1977). This results in kaolinite-like and dickite-like layers within the scattering domains of disordered kaolinite. Mid-infrared spectra for disordered kaolinite show incipient dickite absorption bands superimposed on weakened kaolinite bands (Barrios et al, 1977). Corresponding incipient dickite bands also occur in near-infrared spectra at positions indicated by arrows A and B, fig. 1 and 3, respectively. Disordered kaolinite spectra appear similar to spectra for physical mixtures of ordered dickite with ordered kaolinite, suggesting that the percentage of each layer type in an unknown sample may be inferred by comparison with spectra for a set of reference mixtures. Following this approach, we have estimated the proportion of dickite component in each of the disordered kaolinite samples. The reference mixtures were prepared using similar particle-size fractions of the end-member components in order to minimize differential spectral absorption caused by particle-size differences.

Halloysite exhibits turbostratic stacking (no alignment in the a-b plane) because of its interlayer water sheet. Halloysite spectra show broadened OH absorption bands in the 1.4- and 2.2- μm-wavelength regions, probably related to variable hydrogen bond lengths between surface hydroxyl groups and interlayer water (figs. 1 and 3). The intense 1.9 μm feature seen in halloysite spectra is characteristic of molecular water. Preliminary results indicate that the intensity of the 1.9 μm band is diminished in dehydrated halloysite; however, the other bands remain almost unchanged and do not resemble the narrower bands seen in spectra for disordered kaolinite and disordered dickite. Apparently, the interlayer hydrogen bonds formed in dehydrated halloysite maintain a broad energy distribution. This is consistent with x-ray diffraction (XRD) data, which show that dehydrated halloysite retains its turbostratic character.

Figure 3 shows detailed spectra in the 1.4-μm-wavelength range for the three kaolin polytypes. The spectrum for nacrite differs from the others in that its 1.41 μm band is split into two components, including a major band near 1.40 μm and a side band near 1.41 μm (arrow C, fig. 3). Although the nacrite appeared to be nearly pure from XRD analysis, the splitting suggests that the sample is a mixture of nacrite and dickite layer types. If reference mixtures for calibration are used as outlined above, the shape of this composite absorption band potentially should provide a useful indicator of nacrite-dickite mixture proportions.

In conclusion, near-infrared spectra for disordered kaolin minerals provide important structural information. Spectra can be used to estimate the proportions of dickite-like and kaolinite-like layers in a sample, and may be suitable for analyzing some polytype mixtures for which XRD data give ambiguous results. Portable field instruments can be used to record near-infrared reflectance spectra, and from spectral variations it should be possible to map the distribution of kaolin polytypes in mineral deposits. In conjunction with experimental evidence, such data may ultimately provide insight into the geological and geochemical conditions controlling polytype occurrence.

OPPOSITE: KO: Ordered kaolinite, KD: Disordered kaolinite, H: Halloysite, N: Nacrite, D: Dickite. Sample localities: Dickite, NMNH #106242, Genesee Tunnel, Red Mountain, Colo.; Halloysite, NMNH # 106237, Ind.; Ordered kaolinite, Murfreesboro, Ark.; Disordered kaolinite, Ga.; Nacrite, Nayarite, Mexico.

Barrios, J., Plançon, A., Cruz, M.I., and Tchoubar, C., 1977, Qualitative and quantitative study of stacking faults in a hydrazine treated kaolinite--Relationship with the infrared spectra: Clays and Clay Minerals, vol. 25, p. 422-429.

Plançon, A., and Tchoubar, C., 1977, Part II. Nature and proportions of defects in natural kaolinites: Clays and Clay Minerals, vol. 25, p. 436-450.

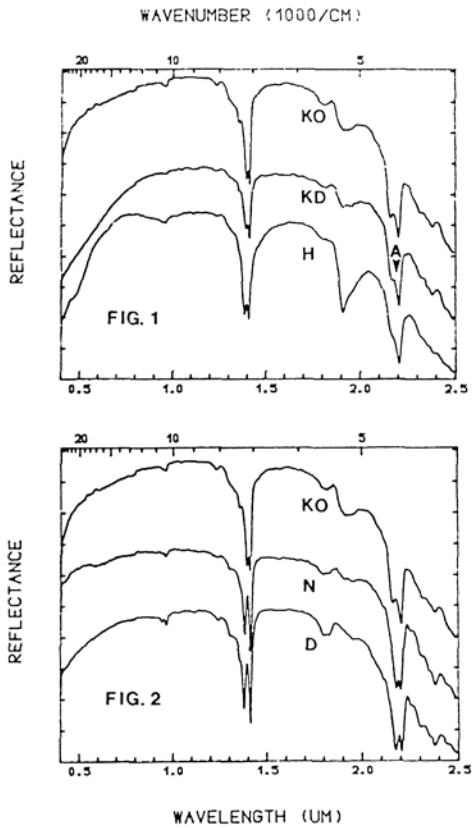

FIG. 3

ENERGIES AND MECHANISMS OF CATION DIFFUSION IN GARNETS*

CYGAN, RANDALL T., Geochemistry Division, Sandia National Laboratories, Albuquerque, NM 87185, USA

A fundamental understanding of cation diffusion processes in silicate minerals can be obtained by examining the interactions of ions associated with point defects in the silicate lattice. The migration of a cation from an occupied crystallographic site to an appropriate vacancy will require a specific amount of energy to overcome the energy barrier created by the local association of ions along the diffusion pathway. This migration energy, along with the defect formation energy, are linked to the macroscopic activation energies obtained from Arrhenius plots (log D versus 1/T) of experimental diffusion data.

Cation migration energies can be derived by evaluating the Coulombic, short-range repulsive, and van der Waals interactions for ions in a crystal lattice which has been modified for simulating the appropriate diffusion mechanism. By examining the change in lattice energy for the modified lattice as a function of the cation position along the diffusion pathway, one can obtain a reasonable approximation of the cation migration energy. These rigid ion model calculations ultimately rely on reasonable short-range energy parameters for the pair-wise ionic interactions and a suitable lattice energy minimization computer program.

Migration energy calculations, performed for the diffusion of the major divalent cations (Mg, Mn, Fe, and Ca) of the distorted cubic site in each of the endmember silicate garnets, provide useful insights for determining the most favorable diffusion mechanism. Simulations of the vacancy and interstitial mechanisms for each of these garnet phases suggest that the vacancy mechanism is the preferred process for cation diffusion. Use of transition state theory, combined with knowledge of the shape of the migration energy potential well, allows for the determination of the diffusion frequency factor (Arrhenius pre-exponential term). Ultimately, the migration energy and frequency factor can be utilized to predict absolute diffusion coefficients for an extrinsic diffusion process such as is the case for garnets in metamorphic terranes. The results of the transition state theory harmonic calculations, along with a Debye frequency analysis, are presented in the accompanying Arrhenius plot for the case of Mg diffusion in pyrope garnet. Also included in this plot are recent experimental diffusion data for the Mg-Mn-Fe garnets. The discrepancy between the slopes of the theoretical diffusion curves and the experimental data can be attributed to the effect of polarization processes which were neglected in the migration energy calculations using a rigid ion approximation. However, the theoretical frequency factors agree with those obtained from the most recent experimental diffusion studies.

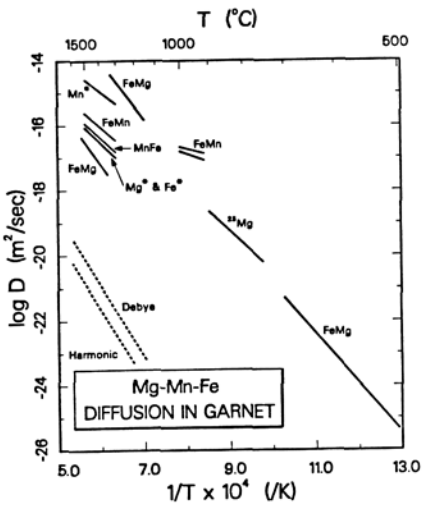

*This work was supported by the U. S. Department of Energy under contract DE-AC04-76DP00789.

CHEVKINITE, ALLANITE, AND SPHENE IN HIGH-LEVEL GRANITIC PLUTONS ASSOCIATED WITH QUESTA CALDERA AND THE RIO GRANDE RIFT, NEW MEXICO, U.S.A.

CZAMANSKE, Gerald K., and DILLET, Brigitte, U.S. Geological Survey, 345 Middlefield Road, Menlo Park, CA 94025 U.S.A.

We have obtained 18-element electron-microprobe analyses for chevkinite-perrierite (C), allanite, (A), and sphene (S) from 9 discrete plutons: southern--Lucero Peak (LP) and Rio Hondo (RH); south caldera ring fracture--Bear Canyon (BC), Sulfur Gulch (SG), and Red River complex (RR); and intracaldera--Cabresto Lake (CL), Rito del Medio (RM), Canada Pinabete (CP), and Virgin Canyon (VC). This coherent data set of 32 C, 53 A, and 134 S analyses provides a basis for studying: (1) the relation of mineral chemistry and zoning to whole-rock chemistry and structural setting, (2) elemental-substitution schemes within each mineral phase, and (3) elemental distribution between the three phases.

S ranges from a conspicuous phase (max 1.1 vol%; to 4 mm long) in samples containing 65.8 to 73.2 wt% SiO_2 (values normalized to 100% anhydrous) from RH, RR, and CL, to a minor phase in rocks containing 74.4 to 77.1 wt% SiO_2 from LP, RH, BC, SG, RM, CP, and VC. A is a minor phase in samples containing 71.6 to 77.1 wt% SiO_2 from LP, RH, BC, SG, CL, CP, and VC, whereas C is sparse in samples containing 71.2 to 77.9 wt% SiO_2 from BC, SG, RM, CP, and VC.

Sawka *et al.* (Geology, v. 12, p. 131-134) found a consistent pattern of REE depletion from cores to rims of zoned S and A in a Sierra Nevada granite. As might be expected for shallower emplacement levels, relations at Questa are more complex. Zoning trends of major elements and REE's in S and A typically differ from grain-to-grain, and REE concentrations and chondrite-normalized patterns within the same sample or pluton may differ significantly.

Despite these complexities, the phase assemblage (S+A+C) and the major-element and REE chemistries of S, A, or C typically reflect significant peculiarities of plutons or individual samples. For example: (1) S in the peralkaline and later-metaluminous phases at VC contains, respectively, uniquely low (less than 0.1 cation) and high (approx 1.0 cation) Al, and of the three intrusive phases within the pluton, only the later metaluminous contains A. (2) At similar host-rock SiO_2 content, zoning trends in S can be characterized by LREE enrichment (RR, RM, VC), relatively uniform REE depletion (LP, SG), strong HREE depletion (RH), or HREE enrichment (CP). (3) S in the only magnetite-free CP sample is strongly depleted in Fe, La, and Ce in comparison with that in magnetite-bearing samples with similar SiO_2 and Al_2O_3 contents, and the rock contains S+A rather than S+C. (4) At similar host-rock SiO_2 content, La/Nd in A may range from 1 to 2 (CP, VC), 5 to 13 (LP, CL), or 18 to 37 (RH).

Although no examples of well-zoned C have been found, C chemistry is dominated by the expected substitution of REE+Y+Th+U for Ca (correlation coefficient r, -0.98). Good correlations are also found for Fe versus Ca (-0.89), Fe versus Mn (-0.92), and La versus Nd (-0.84). The latter correlation, also found for A ($r_{La/Nd}$, -0.92), reflects rotation of the REE patterns around Ce, which remains relatively constant. For A, such rotation causes La and Nd contents to range from 0.58 to 0.11 and 0.017 to 0.19 cations, respectively, in the carapace aplite of SG. Also characteristic of A are correlations of REE+Y versus Ca (-0.79), Fe versus Al (-0.97), Fe versus Ti (0.87), and Al versus Ti (-0.83); there is no correlation of Fe with Mn in A. S is characterized by good correlations of REE+Y versus Ca (-0.94) and Fe versus Mn (0.92), as well as of Fe versus Al (0.81) and Ti versus Al (0.88), if the aberrant VC examples are excluded; there is no correlation of La with Nd.

We believe that the complexities revealed by our data reflect variations in the type, number, and sequence of crystallization of REE-bearing phases, as well as microenvironments of crystallization. They may bear significantly on commonly used crystallization-fractionation models for trace elements.

HRTEM INVESTIGATION OF POLYTYPISM IN BIOTITES

CZANK, M., Mineralogisches Institut, Olshausenstr. 40, D-2300 Kiel, F. R. Germany

The structure of biotite (tri-octahedral layer silicate), ideally $K(Mg,Fe)_3[AlSi_3O_{10}](OH, F)_2$ is formed by tetrahedral-octahedral-tetrahedral (T-O-T) layers which are bonded together by sheets of 12-fold coordinated K^+ (or Na^+). In the 1M polytype with $c_o \simeq 10$A the T-layers that are connected by O-layers are shifted by $a_o/3$ with respect to each other, while T-layers connected by K^+ are roughly mirror images of one another. In respect to the pseudehexagonal symmetry of the T-layers, they also can be stacked with relative shifts of $\sim a_o/3$ along each of the pseudohexagonal axes and with relative rotations of ± 60°, ± 120°, and 180°. There are six simple theoretically possible polytypes: 1M, $2M_1$, $2M_2$, 2O, 3T, and 6H that have 1, 2, 3, and 6 T-O-T layers, respectively, within the translation period c_o' [1]. For natural and synthetic biotites the 1M, $2M_1$, and 3T polytypes are relatively common; the $2M_2$ and 2O are very rare; and 6H has not been observed. Various complex polytypes (up to $c_o' = 25c_o$) that are formed by periodic combinations of the three most common basic polytypes and which are mostly triclinic (Tc) have been described [2, 3]. Pandey et al. [3] proposed spiral growth around single screw dislocations for the complex polytypes. Additionally, using stacking fault energy calculations, they showed that only a few of the almost infinite number of possible polytype structures can be expected.

This HRTEM study was performed on natural, optically homogeneous biotites (BI) from Orijärvi, Finland with an average composition:
$(K_{.73}Na_{.11}\square_{.16})(Mg_{2.57}Fe^{2+}_{.22}Al_{.16}Ti_{.03}\square_{.02})(Si_{3.01}Al_{.99})O_{10}(OH)_2$
that was calculated from electron microprobe analyses. The BI coexists with complex pyribole and Zn-rich spinel and is structurally inhomogeneous. In addition to various stacking sequences which repeat only a few times, complex polytypes with $c_o' = 1$, 2, 8, 13, 17, 18, 19, 23, 24, and (!) $115c_o$ were observed. Some of these polytypes occur more than once, and with different stacking combinations (e. g., three different sequences with $c_o' = 17c_o$). The polytypic sequence with 115 layers repeats itself 12 times. The following polytypes were characterized: 1M, $2M_2$, 8Tc, 13M, 13Tc, 17Tc, 18Tc, and 19M, and of these the 13M, 13Tc, 17Tc, and 19M to our knowledge have not been previously observed or proposed. The $2M_2$ and 18Tc should be the energetically least favorable [3].

Additionally randomly occurring intercalated "chlorite" (CH) layers in the BI were observed; however, in a few places repetition of the sequence 4 BI + 1 CH was found. Intercalated CH layers that are present within the polytypes, generally do not disturb the polytypic sequence, which suggests that they may have grown after the polytypes were formed. Rare transformations of BI layers to CH layers were also found.

From the chemical composition only ~81% of the crystals can be cast as ideal K- or Na-biotite. The non-ideal components (e. g., octahedral Al) are possible sources of distortion in the T-O-T layers. In such distorted T-O-T layers the T-layers are more probably stacked other than the 1M type. In fact, we observed that on the average, which includes the complex polytypes, every fifth T-O-T layer is stacked differently in the studied BI. Qualitative EDS measurements suggest that the more ordered 1M parts of the BI grains are slightly richer in Fe and lower in Al than the more disordered parts. Consequently, the growth of both the rare and new polytypes may have been controlled by compositional variations.

References

[1] Smith, J. V. & Yoder, H. S. (1956) Mineral. Mag. 31, 209-235.
[2] Rieder, M. (1971) Z. Kristallogr. 132, 161-184.
[3] Pandey, et al. (1982) Phys. Chem. Minerals. 8, 268-278.

GEOCHEMISTRY OF THE LATE-ARCHAEAN QÔRQUT GRANITE COMPLEX, SOUTHERN WEST GREENLAND

DAVIES, A., Dept. of Geology and Physical Sciences, Oxford Polytechnic, OX3 0BP, UK; PERKINS, W.T., Dept. of Geology and Physical Sciences, Oxford Polytechnic, OX3 0BP, UK; BROWN, M., School of Geological Sciences, Kingston Polytechnic, KT1 2EE, UK; FRIEND, C.R.L., Dept. of Geology and Physical Sciences, Oxford Polytechnic, OX3 0BP, UK

Isotopic and geochemical data from mid-Archaean (c. 3,000 Ma) calc-alkaline orthogneisses in West Greenland support a petrogenetic model involving a two-stage melting process in which the first-stage mantle-derived melts had a short crustal residence. In contrast, late-Archaean granites (post-2,800 Ma) derived by anatexis of continental crust are less volumetrically important although common and form an important component of the late-Archaean history of the Godthåbsfjord-Isukasia region of southern West Greenland.

The sequence of events in this region during the mid-Archaean includes tectonic interleaving of slices of the older Amîtsoq gneisses and Malene supracrustal rocks; the syntectonic intrusion of the voluminous tonalitic-granodioritic-trondhjemitic-granitic Nûk magmas, precursors of the Nûk gneisses; metamorphism which reached granulite facies in parts of the region; and a complex series of late-Archaean (post-2,800 Ma) events which may include, in different parts of the region, a second interleaving event, ductile deformation in linear belts, the development of domes and synforms, retrogression under amphibolite facies conditions, and the production of local and regional volumes of granitic magmas by multiple anatexis dated at 2,750 Ma, 2,610 Ma and 2,500 Ma (see Robertson, S., 1984. Geol. Soc. Newsletter, 13, 18-19). This contribution is concerned with the last and most voluminous granite-producing event, the Qôrqut granite complex (Brown, M., et al., 1980. J. geophys. Res., 86, 10,617-10,632).

The Qôrqut granite complex (Qgc) is comprised of 3 groups of granites: leucocratic granites which often contain biotite schlieren or thin lamellae and which represent locally-derived anatectic melts; polyphase homogeneous grey biotite granites which represent further-travelled anatectic melts; and, aplogranite – granite-pegmatite sheets derived from residual liquids. It has a 3-dimensional structure consisting of a lower zone dominated by leucocratic granites and partially-melted enclaves; an intermediate zone of innumerable gently-dipping grey granite sheets of various types and enclave horizons; and, a border or distal zone at the sides or ends of the complex, with an upper zone in the mountain peaks which represents the roof, dominated by aplogranite – granite-pegmatite sheets which cut previously-sheeted country rocks.

New isotopic data on Amîtsoq gneisses adjacent to the Qgc and on the leucocratic granites are consistent with magma generation from a mixed source of depleted, partially reset Amîtsoq gneisses and Nûk gneisses at c. 2,480 Ma. This contrasts with evidence for an enriched source for similar age granites to the north-east (see Robertson, S., 1984. J1 geol. Soc. London, 141, 1076). The geochemical characteristics of the Qgc are illustrated using a data base of over 150 analyses. There is no rational geochemical variation with height in the 1,500 m exposed section through the Qgc. The zones within the Qgc developed contemporaneously within a confined segment of magmatic activity centred on the fjord Qôrqut, the complex being emplaced as a series of discrete magma pulses each of which had moved a variable distance since separation from a melting zone, the trace element chemistry reflecting liquid-crystal interactions during melting and crystallization (Perkins, W.T., 1984. Unpubl. PhD thesis, Oxford Polytechnic). Multi-element variation diagrams and trace element discriminant diagrams such as Rb, Nb and Y v. SiO_2 and Rb v. (Y+Nb) show that the granites of the Qgc have affinities with modern post-collision types. Detailed differences, such as much lower HREE contents, reflect source chemistry.

Granites and granite-pegmatites of broadly similar age occur to the north and east of the main Qgc outcrop (Robertson, S., 1983. Rapp. Grønlands geol. Unders., 115, 56-59; Baadsgaard, H., et al., 1985. Rapp. Grønlands geol. Unders., 125, 48-51). Recently, crustal thickening by thrusting and folding in the interval post-granulite facies metamorphism – pre-Qgc has been identified as a major feature of late-Archaean tectonics in the Godthåbsfjord-Isukasia region of southern West Greenland. Thus the common syn- to post-tectonic granites probably represent syn- to post-collisional granite magmatism related to crustal thickening.

INCLUSIONS IN MINERALS AND CRYSTALLOGENESIS

DEICHA,G.A., CNRS, Université P.& M.Curie, Tour 26(5E) 4 place Jussieu, F75252 PARIS Cedex 05, France

Scanning electron microscopy(SEM) bridges the gap between knowledge of ultimate crystalline structures and visual aspects of materials from the Lithosphere, as they appear in the light of petrographical microscopes. The scanning electron microscope does not require the preparation of thin sections(1): observation on its screen can simply deal with rough fractures of fresh broken pieces from rocks, gangues and any other material. Fragments, selected under a magnifying-glass, are studied and mounted with help of a binocular. Far beyond the power of photonic optics, SEM shows in such micromounts a broad variety of intra-crystalline, as well as inter-granular cavities. Such cavities display important differences in size, shape, mutual relations, frequencies; they appear to be, more or less closely, linked to all kinds of discontinuities in the material. It is sometimes easy to relate individual cavities and also whole systems of them, to the nucleation, growth, alteration or dissolution of involved minerals and aggregates. SEM fractographies, obtained in the course of such investigations, give a new approach to the understanding of crystallogenesis, especially related to architectural details in the micrometer range of magnitude. For instance, primary growth lacunae often require magnifications going from $\times 10^3$ to over $\times 10^5$. In some of the intergranular joints, the pores can number over 10^4 per mm^2, matching already quoted frequencies of over 10^6 per mm^3 as regards fluid inclusions, observed since decades by ultramicroscopy (dark field) in felspars of granites and milky quartz.

Confrontation of informations gathered from natural samples and SEM investigations on artificial products of synthesis, ranking from diamond to hydrohalite, helps to understand the effects of the crystallogenetic disequilibrium on the formation and evolution of intra-mineral and inter-granular cavities.

Symposia topics of the General Meeting of IMA will allow to discuss questions related to this problem, in considering undercooling in molten silicate systems, supersaturation of geochemical solutions in pegmatite formation as well as in metamorphism and ore deposits.

The open meeting of the Commission of History and Teaching of Mineralogy also offers an opportunity to survey the status of inclusion thermobarogeochemistry (after N.P.ERMAKOV), in the past and present, within universities and mining schools programmes. The open meeting of the Working Group Inclusions in Minerals is partly intended to sum up the fluctuating relationship between cavities and their filling, be it gaseous, liquid, vitreous or microcrystalline (2). Some of the other IMA commissions and working groups could also contribute to widen the interdisciplinary discussion about the disequilibrium as a fundamental crystallogenetic factor.

On a broader basis, the knowledge of the behaviour of microscopic, as well as submicroscopic, cavities in the materials of the Lithosphere is also of value to the development of other Earth Sciences, as has been shown at the last sessions of the International geological Congress (Moscow 1984) and of the International Congress of Geography (Paris-Alpes 1984).

(1) DEICHA, G.A. - Cristallogenèse minerale et cavités des matériaux de la Lithosphère. Comité des Travaux Historiques et Scientifiques (CTHS), Bulletin de la Section des Sciences, VII, 130 p. XXX pl. La Documentation Française, 29 quai Voltaire, Paris 1984.

(2) NAUMOV, V.B. - Inclusions in Minerals. 60 p. V.I.Vernadsky Institut, Academy of Sciences, Moscow, 1985.

^{29}Si MAS AND ^{23}Na NUTATION NMR REVEAL THAT LOCAL SODIUM ENVIRONMENT IS PRINCIPAL DIFFERENCE BETWEEN SODIUM SILICATE GEL AND GLASS

DE JONG, B.H.W.S., Smitweld, P.O.Box 253, 6500DJ Nijmegen, the Netherlands and VEEMAN, W.S., Department of Physical Chemistry, University of Nijmegen, 6525ED Nijmegen, the Netherlands.

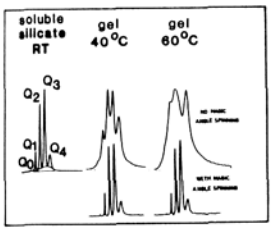

Lack of spectral resolution prevents complete description of silica constitution in a glass. To bracket this constitution in a glass, the speciation of silica has been determined in a soluble sodium silicate (viscosity 144cp (20°C), analysis dry weight 24.76 mole %Na_2O, 75.24 mole%SiO_2, pH 12.4). This solution was subsequently converted to a gel by heat treatment at different temperatures, and to a glass by melting at 1300°C. Finally the glass was redissolved at 40°C maintaining the same ratio between fluid and solid. The FTNMR spectra of Figure 1 show line broadening associated with the conversion from soluble silicate to gel, with as most notable feature the increase in Q_4 intensity of the 60°C heat treated sample. Magic angle spinning shows this apparent high Q_4 concentration to be spurious, and that no silica condensation has yet occurred. MASNMR spectra in Figure 2 of succesively heated samples reveal silica condensation between 60 and 80°C, and a fairly pronounced transition between 400 and 600°C. The latter is caused by crystallization of a mixture of cristobalite and sodium silicates. From 80°C up, the NMR spectra remain qualitatively similar with as most notable feature the apparent increase in Q_4 of the glass spectrum. Redissolution of the sodium silicate glass was carried out for 120 hours in a closed container at 40°C, with as fluid triply distilled water. After 2 hours the pH did rise to 12.5 identical to that of the original soluble silicate. A FTNMR spectrum of this solution is shown in Figure 3. This spectrum looks qualitatively similar to that of the starting solution suggesting a memory retention of the original structural elements by the glass structure. It is here again notable that the Q_4 concentration is very small in comparison to that observed for the glass. It is also clear from this experiment that the hypothesis by Lentz(1967) concerning retention of structural elements between a glass and its dissolution products is incorrect.

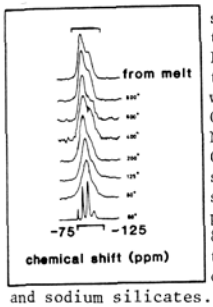

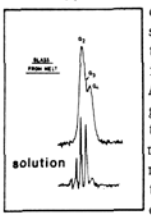

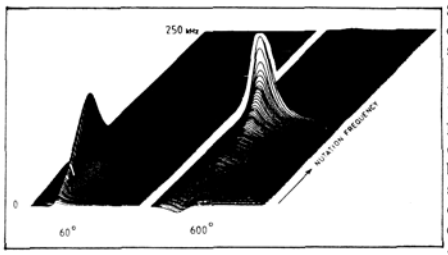

Spectacular are the differences of local sodium environments between gel and solid as revealed by ^{23}Na nutation NMR. As shown in Figure 4, the sodium environment in the 60° heat treated gel consists of a small broad electric field gradient, suggestive of a wide variety of environments, in contrast to the spectrum at 600°C, which shows a narrow large electric field gradient. The former environment is typical for a hydrated sodium atom, the latter for an anhydrous sodium atom associated with Si-O bonds. This interpretation is also in accordance with Q distribution calculations which show that not all sodium atoms can be associated with Si-O bonds in silica gel. The sensitivity of ^{23}Na nutation NMR spectroscopy to local variations in sodium environment shows great promise in elucidating such environments in poorly crystalline materials as zeolites, clays, or beta aluminas.

GEM QUALITY OPAL CT IS A ^{29}Si MASNMR AMORPHOUS SOLID

DE JONG, B.H.W.S., Smitweld P.O.Box 253, 6500DJ Nijmegen, the Netherlands; VAN HOEK, J., VEEMAN, W.S., Dept. Physical Chemistry, University of Nijmegen, Toernooiveld, 6525ED Nijmegen, the Netherlands; MANSON, D.V., Gemmological Inst.of America, 1660 Stewart Street, Santa Monica, Ca 90404, USA

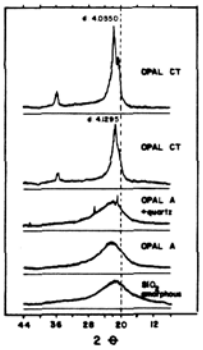

Opal consists of approximately monodisperse, 1500-3000 Angstrom spheres of silica occuring in a wide variety of geologic settings(Frondel, 1962; Iler, 1979; Gauthier, 1985). X-ray diffraction experiments on opal from sedimentary basins reveal solid state transitions from amorphous to crystalline, the various stages being designated opal A, opal CT, and opal C. The diffraction pattern of opal A and CT are shown in Figure 1. The final stage in burial metamorphism of opals is indicated by the presence of quartz. As such opal and its various transition stages function as stratigraphic markers in sedimentary basins (Flörke 1956; Graetsch et al., 1985; Kastner, 1979). As only three stages can readily be distinguished as a function of burial depth by X-ray diffraction, it seemed likely that additional stages in the solid state transition between amorphous and crystalline opal could be characterized by ^{29}Si MASNMR, hence providing a refined stratigraphic marker. In addition study of opals in their various transition stages might shed light on the nature of amorphous solids, and the relation between amorphous-crystalline pairs, a subject receiving increasingly more attention.

^{29}Si MASNMR spectra of nine natural opals and one synthetic one were collected using standard NMR techniques. Characteristic spectra of opal A and CT are shown in Figure 2. Additional data are shown in Table 1. The observed chemical shifts indicate that all detectable silica occurs as Q_4, and that less condensed silica species characteristic of silanol groups do not occur. Comparison of ^{29}Si MASNMR spectra of opal with those of vitreous silica, silica gel, and various silica polymorphs, shows that the opal spectrum resembles that of vitreous silica most. The peak chemical shift from -109.5 ppm for vitreous silica to -111.6 ppm for opal indicates an average Si-O-Si angular change from 146.8 to 150.1 degrees. Our spectra also show that the ^{29}Si MASNMR spectrum of opal CT does not resemble in peak position nor in line width that of cristobalite, nor can be constructed by addition of the cristobalite and tridymite NMR spectrum. As such it is unlikely that the opal CT diffraction pattern in Figure 1 should be intepreted as being caused by Debye broadening of cristobalite microcrystallites.

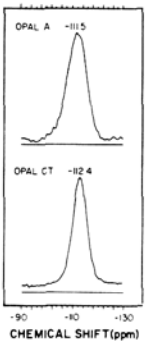

Our ^{29}Si MASNMR results indicate that all opals are amorphous and that the diffraction pattern of opal CT is not due to Debye line broadening caused by reduction of cristobalite or tridymite-like crystallites. If, as ascerted by Taylor and Brown(1979) vitreous silica is tridymite-like, the structural elements in opals should consists primarily of six membered rings, hence falling in a class of Porai-Koshits rather than Zachariassen amorphous solids.

Table 1. Proton and ^{29}Si chemical shifts, Full Width at Half Maximum(FWHM), FF Si free induction decays (FID), and weight percent water in opals in temperature steps.

Sample	Description	^{29}Si shift[1] (ppm)	H shift[2] (ppm)	FWHM (ppm)	FID	wt-105°C	H_2O(wt%) 105-500°C	500-1000°C
1	Opal A [3]	-111.8	-1.8	nd	5009	nd	nd	nd
2	Opal CT	-111.9	-1.7	6.2	5340	1.74	7.0	0.01
3	Opal CT	-112.4	-1.7	5.8	8502	0.58	4.4	3.8
4	Opal A	-111.5	-1.8	8.9	5656	nd	nd	nd
5	Opal A	-111.5	-1.9	8.0	13592	2.04	4.6	0.27
6	Opal A-qtz	-111.4	-1.7	9.2	2772	2.04	2.9	0.24
7	Opal CT	-111.8	-1.8	7.2	7940	1.08	7.5	0.23
8	Opal A	-111.5	-1.9	8.6	10658	2.68	4.1	0.01
9	Opal A-qtz	-110.6	nd	8.8	11188	nd	nd	nd
10	Opal A-qtz [4]	-111.9	nd	5.6	6274	nd	nd	nd
11	Opal A-qtz [5]	-111.4	nd	nd	82	nd	nd	nd
12	Opal A [6]	-107.0	nd	11.0	2500	nd	nd	nd

[1] Relative to TMS, proton shifts relative to TMS: benzene 7.3 ppm, H_2O 4.8-4.7 ppm, N in opal 5.5 ppm. [2] Relative to benzene [3] Opal A is x-ray amorphous, Opal CT has some diffraction structure in between tridymite and cristobalite [4] Sample 10 is sample 6 after heat treatment for 24 hours at 300°C [5] Sample 11 is the same as sample 6 but run on Bruker cxp 300 [6] synthetic opal

CONDITIONS OF NUCLEATION OF MAGADIITE AND KENYAITE

DELMOTTE L., GUTH J.L., KALT A., WEY R., Ecole Nationale Supérieure de Chimie de Mulhouse, France.

Two hydrous sodium silicates, magadiite $Na_2Si_{14}O_{29},9H_2O$ and kenyaite $Na_2Si_{22}O_{45},10H_2O$ were found in lake beds at Lake Magadi, Kenya (EUGSTER, 1967). Very few occurences were reported later in some african and north-american alkaline lakes. LAGALY et al. (1975, 1983) were able to synthesize them. Both are layered silicates but so far their structure remains unsolved.
We were investigating conditions of crystallization of high silica zeolites. Accordingly we selected operating conditions suited to that goal.
All experiments were carried out in steel bombs with Teflon lining of 75-cc capacity. Charges consisting of 30 g of a 3.3×10^{-1} N sodium hydroxide solution (or a mixture of NaOH and tetrapropylammonium hydroxide) and 2.14 g of precipitated amorphous silica, Merck (16.5 % H_2O) were heated to 170°C (± 1°C) at a rate of 17°C per minute, allowing the final temperature to be reached in less than 10 minutes.Runs ranged from one hour to 14 days, then the bombs were quenched. The solid phases were identified by optical microscopy, scanning electron microscopy and X-Ray diffraction. pH, sodium and silica contents of mother liquor were measured.
Magadiite is the first crystalline species to appear ant it remains the most abundant for 3 days. Nevertheless after 2 days kenyaite is clearly visible and it peaks after 4 days. In turn silicalite (which does not crystallize in the absence of tetrapropylammonium hydroxide), cristobalite and finally quartz are formed, with overlapping fields of existence. Quartz is obtained pure for runs lasting more than 8 days.
Crystallization of magadiite and kenyaite is associated with a minimum of pH, sodium and silica content in the mother liquor. While these species are dissolving, pH, sodium and silica concentrations rise gradually. When the supersaturation level of the subsequent phase is reached, this one nucleates. In the same way formation of magadiite and kenyaite is obviously related with initial supersaturation. If the heating rate is lowered, dissolution of amorphous silica is less rapid. With a rate as low as 0.7 °C per minute the temperature of 170 °C is reached in more than 3 hours and magadiite and kenyaite are observed no more. The first phase to appear is either silicalite or cristobalite.
Clearly magadiite and kenyaite are intermediate phases which obey Ostwald's phase rule. Their high nucleation rate demands a high supersaturation level which can be achieved by fast initial heating. This conclusion was confirmed when other amorphous silicas where used as starting reactants. Aerosil 200 (Degussa) dissolves readily in alkaline solutions whereas dissolution of silica precipitated by hydrolysis of tetraethylsilicate is more difficult. With the former, magadiite is favoured but neither magadiite nor kenyaite could be obtained with the latter.
In conclusion, nucleation of magadiite and kenyaite requires high supersaturations which may be difficult to meet in nature. This probably accounts for the rare occurence of these silicates.

REFERENCES

BENEKE, K. and LAGALY G. (1983) American Mineralogist, 68, 818-826
EUGSTER, H.P. (1967) Science, 157, 1177-1180
LAGALY, G. BENEKE, K. and WEISS A. (1975) American Mineralogist, 60, 642-649

A PHASE-CHEMICAL AND CRYSTAL-CHEMICAL INVESTIGATION OF THE OXIDATIVE LIME-ROASTING OF CHROMITE ORES

De VILLIERS, J.P.R., ADENDORFF, K.T., Council for Mineral Technology, Randburg, 2125, SOUTH AFRICA.

The lime-roasting of chromite ores is considered as an alternative to the conventional soda-ash process for the production of chromium chemicals. The variable oxidation state of chromium provides a mechanism for the preferential extraction of chromium to the exclusion of aluminium, magnesium, and iron. In order to optimize extraction, characterization of the phases produced and examination of the phase relations in the system CaO-Cr oxide-SiO_2 under oxidizing conditions are essential.

The phase-chemical investigation revealed the existence of two phases, which exhibited extensive solid-solution behaviour. A solid solution of Ca_2SiO_4 and $Ca_3(CrO_4)_2$ containing pentavalent chromium was found to be in equilibrium with liquid at high temperatures. A mechanism of coupled substitution with vacancy formation is proposed, viz

$$Ca^{2+} + 2Si^{4+} \rightarrow \square + 2Cr^{5+}$$

which forms the solid solution $Ca_{4-x}Si_{2-2x}Cr_{2x}O_8$ where x is 0 to 1. The formation of this solid solution causes the stabilization of β-Ca_2SiO_4 by chromium under oxidizing conditions. The second phase, $Ca_5Cr_{3-x}Si_xO_{12}$, which is the chromium analogue of silico-carnotite, $Ca_5P_2SiO_{12}$, a common constituent in phosphate slags, was also found to be in equilibrium with the melt. This phase was examined by single-crystal X-ray-crystallographic techniques, and the presence of both hexavalent and tetravalent chromium was indicated by the site-occupancy refinement of a $Ca_5Cr_2SiO_{12}$ crystal. The formation of this solid solution therefore involves substitution of Cr^{4+} by Si^{4+}.

The phase chemistry of mixtures of lime and chromite was examined above 850°C in air. The phases $Ca_5Cr_3O_{12}$ and $Ca_3(CrO_4)_2$ were produced as relatively pure phases, since the valency of chromium is higher than three, which excludes divalent and trivalent ions from these phases. Other phases that formed were brownmillerite, i.e. $Ca_4Al_2Fe_2^{3+}O_{10}$, containing residual chromium, calcium chromite, i.e. $Ca(Cr,Fe,Al)_2O_4$, spinel, sesquioxide, and a chromium hauyne, $Ca_4Al_6CrO_{16}$. The addition of CaF_2 as a flux accelerated the roasting reactions, and these took place at lower temperatures, resulting in a higher yield. The chromium-containing phase in this case was a fluorapatite, $Ca_5(CrO_4)_3F$, containing pentavalent chromium.

A 1:1 ratio of chromite to lime was found to be the optimum ratio to yield a product that includes $Ca_5Cr_3O_{12}$, brownmillerite, and MgO. The substitution of 7 per cent CaF_2 for some CaO resulted in improved kinetics and the formation of Cr-apatite, brownmillerite with a low Cr content, and MgO. The apatite, like $Ca_5Cr_3O_{12}$, can be preferentially leached with dilute acid, leaving a residue low in chromium. Chromite-lime mixtures richer in lime, resulted in increased acid consumption, and chromite-rich mixtures caused refractory phases such as calcium chromite, spinel, and sesquioxide to form. The latter phases are insoluble in acid and would cause excessive amounts of chromium to be lost.

RARE EARTH ELEMENT GEOCHEMISTRY OF APATITE AND SPHENE IN SOME ALKALINE INTRUSIONS FROM CHINA

DI Zhou-Ling, Institute of Geochemistry, Academia Sinica, Guiyang, Guizhou, People's Republic of China

In alkaline rock, apatite and sphene are very ubiquitous accessory minerals. We collected them from alkaline syenite, monzonite, aegirine syenite, pyroxene monzonite and carbonate glimmerite from five different alkaline intrusions. The rare earth element (REE) contents of whole rock are analyzed by plasma spectroscopy, apatite and sphene by X-fluroscope. REE contents in alkaline rocks studied by us that are not very high generally range from 148.72 to 440.71 ppm, but in carbonate glimmerite there is an exception, the REE content increases sharply to more than 0.2 %. As well known, apatite and sphene in alkaline rock are two major minerals can accommodate a great amount of REE, ΣREE contents of 9 apatite and 6 sphene are respectively 4752.49-15904.9 and 9740.84-32111.3 ppm, tens or hundreds tims the host rocks. There are two positive correlation between REE contents of host rock (R) and apatite (A) as well as host rock and sphene (S). The two regression equations and correlation coefficient are listed as lollows:

$A=6953.88+4.366R$, $r_{A-R}=0.88$, $n=9$

$S=-3336.93+72.51R$, $r_{S-R}=0.81$, $n=6$

In each pair of apatite and sphene, REE content of the former is always lower than the later. Either the host rocks or the pairs of minerals are particulary rich in light REE and show the same steep chondrite-normalised partterns. There are some common features about the REE distribution in each sample: (1) Apatite is a rich light REE mineral. In the pair of apatite and sphene, it can be seen that LREE / HREE or $(La/Y)_N$ ratio of the former is more than the later and REE partituon coefficient values also show that LREE are preferentially accommodated by apatite relative to sphene; (2) Comparing the chondrite-normalised plots only sphene has a weak peak at Ce with δ_{Ce}= 1.10-1.12 and apatite shows a obvious valley at Eu. Eu depletion that has not been observed in the host rock also appeares in the plot of sphene but the extent of it are smaller than them of apatite; (3) In heavy, middle and light REE composition triangular plot, it always showed that apatite is rich in LREE, sphene rich in MREE and their host rock relatively rich in HREE, although all the dots concentrated near LREE apex.

ELECTRON MICROSCOPIC INVESTIGATION OF SPHALERITE AND SPHALERITE-CHALCOPYRITE INTERGROWTHS

DICKINSON, C., PATTRICK, R.A.D., Dept. of Geology, Manchester University, Manchester M13 9PL, U.K.

Different textural varieties of sphalerite from stratiform, stratabound and vein deposits have been subjected to optical, microprobe and TEM investigations. The TEM work with an EDS analytical facility has been used to provide information on the causes of optical and composition variations in sphalerite and on chalcopyrite-sphalerite intergrowths.

Sphalerites from vein deposits with dark bands enriched in trace elements (Cu, Fe, Sb, Ag, Pb) often contain areas of orientated precipitates (~200 Å). However similar bands in collomorphic seafloor sulphides high in trace elements have no visible inclusions suggesting the accommodation of these elements in the ZnS lattice.

Low Fe vein sphalerite contains opaque zones. The TEM showed that these zones are due to pervasive symplectic intergrowths of digenite in the sphalerite. This is probably a post-depositional feature related to the introduction of late Cu-rich fluids into favourably orientated permeable zones in the ZnS.

Investigation of collomorphic sphalerites from the Navan Pb + Zn deposit revealed the ZnS to be totally recrystallized and twinned with galena particles concentrated along the twin planes. Small spheroidal particulate sphalerite (~50 μm) from Navan has opaque cores with overgrowths of transparent Fe-poor ZnS. These cores are rich in Cu, Pb, Ag and Sb and TEM analysis showed them to be an amorphous intergrowth of ZnS and sulphosalt-like compositions. It is possible these cores represent original exhalative particles on which later sphalerite grew from fluids permeating the ore pile.

Low Fe vein sphalerite, which has undergone limited replacement by chalcopyrite, has been examined. Chalcopyrite particles (~0.2 μm) in the sphalerite are sometimes surrounded by haloes rich in Cu_2S. These chalcopyrite particles are nuclei for dendritic chalcocite growths along cleavage planes, although isolated, faceted Cu_2S dendrites also occur. Bornite particles (~0.2 μm) are present and are surrounded by coronas of digenite particles. These textures are due to the action of the later Cu-rich solutions with the ZnS and the lack of FeS in the sphalerite inhibiting more extensive chalcopyrite formation.

Analysis of sphalerite containing chalcopyrite disease revealed many particles of Cu-Fe-sulphides with 'apparent' compositions between $CuFeS_2$ and Cu_2S. The relevance of these as possible stages in the formation of chalcopyrite disease is being investigated

SURFACE CHEMICAL CHARACTERIZATION OF MINERALS AND ADSORBED SPECIES ON MINERALS USING X-RAY PHOTOELECTRON SPECTROSCOPY

DILLARD, J. G., Department of Chemistry, Virginia Polytechnic Institute and State University, Blacksburg, VA 24061, USA

The chemical characteristics of mineral surfaces play an important role in adsorption reactions involving gases and liquids, in processing treatments associated with mineral separation, and in nucleation phenomena related to the deposition and formation of new solid phases. A more complete and accurate description of the fundamentals of reactions on minerals is aided by detailed knowledge of the mineral surface chemistry. In this presentation the use of x-ray photoelectron spectroscopy (XPS) to obtain information on the chemical composition, the concentration, the chemical state, and coordination geometry of surface elements will be discussed with special emphasis on transition metal species. The availability of such information is important for the description and the development of models to represent processes at mineral surfaces.

The determination of surface chemical properties may be accomplished using x-ray photoelectron spectroscopy (XPS) also referred to as Electron Spectroscopy for Chemical Analysis (ESCA). In this method a soft x-ray impinges on a solid sample and the kinetic energy of photoejected electron is measured. Because soft x-rays are used in the photoemission process, electrons from the core levels of elements can be ejected. Using x-rays of a known energy, the binding energy (ionization energy) of the electrons can be evaluated from the expression: BE = hν-KE, where BE is the binding energy of a particular core level electron in an element, hν is the x-ray photon energy, usually Mg Kα (1254 eV) or Al Kα (1486 eV), and KE is the electron kinetic energy. The binding energy results permit an identification of the elements present and in some instances the oxidation state of the element is indicated. The binding energies for the oxidation states of sulfur are sufficiently unique to permit identification of chemical states as shown:

Sulfur Component	BE (eV)
S^{2-}	162.5
S_8	163.9
SO_3^{2-}	166.7
SO_4^{2-}	168.8

For transition metal containing minerals the binding energy results and the shape of core photoelectron peaks often reveal information on the chemical state of the elements present. Multiple ionization processes induce charge transfer phenomena associated with metal ions and non-metal anions (ligands) in the solid, and give rise to photopeaks called shake-up satellites. In the case of cobalt, nickel, and copper, the state of these satellite features aids in the identification of the chemical nature of the metal. For example, examination of Co 2p spectra in the figure reveal that satellite features(*) are present in Co(II) oxides but are absent in Co(III) compounds. In copper(II) materials, shake-up satellite transitions appear, but satellites are not detected in Cu(I) compounds. For solids containing Ni(II) it is possible to distinguish octahedral, tetrahedral, and square planar coordination geometry from detailed studies of shake-up satellite structure.

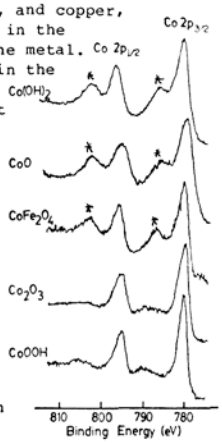

Other photoionization phenomena, including multiplet splitting, x-ray induced Auger processes, and valence band photoelectron spectra, which provide additional induced Auger processes, and valence band photoelectron spectra, which provide additional surface characterization information will be presented.

TETRASILICIC MICA AND ALKALI AMPHIBOLE IN PERALKALINE GRANITES FROM 26-M.Y.-OLD QUESTA CALDERA, NEW MEXICO, U.S.A.

DILLET, Brigitte, and CZAMANSKE, Gerald K., U.S. Geological Survey, 345 Middlefield Road, Menlo Park, CA 94025 U.S.A.

We have studied the association alkali amphibole (AA)-tetrasilicic mica (TSM)-acmite-biotite in early-crystallized peralkaline rims of the resurgent granitic intrusions of Virgin Canyon and Canada Pinabete. These peralkaline rims are interpreted as unerupted equivalents of the peralkaline Amalia Tuff, whose eruption formed Questa caldera.

AA occurs both as phenocrysts (to 1 mm long) and as small (0.1 mm) grains in the groundmass of the peralkaline granites ($(Na_2O+K_2O)/Al_2O_3$=0.96-1.00; 75.9-77.4 wt% SiO_2). It is primary (sometimes enclosed in K-feldspar phenocrysts) and typically zoned, displaying shabby-looking brown richteritic cores, surrounded by clear-blue rims of magnesio-arfvedsonite. AA chemistry shows a fractionation trend from katophorite through richterite to magnesio-arfvedsonite, representing a prolonged period of crystallization. The chemistry of a strongly zoned AA grain is shown in structural formulae (1) and (2), which are keyed to the figure. Near-end-member arfvedsonite is found in the most differentiated, marginal facies of the Virgin Canyon peralkaline granite (77.4 wt% SiO_2; 12.0 wt% Al_2O_3).

TSM occurs either (1) enclosed in AA phenocrysts as single or multiple laths (to 0.1 mm across) in different orientations or (2) as aggregates of laths (to 0.05 mm across) associated with AA, biotite, acmite, manganoan ilmenite, and magnetite. Unlike the only other known natural occurrence, which has been described from Le Mont-Dore (Massif Central), France, the Questa TSM is not Mn-rich and shows a coupled substitution of 1.15 to 1.92 Mg cations with 1.37 to 0.56 (Fe^{2+}+Mn) cations (correlation coefficient r, -0.93). The relation between Al(IV) and the octahedral cations is shown in the figure below and by structural formulae (3) and (4). Within a given sample, TSM in aggregates contains more Al(IV), and thus has fewer octahedral vacancies, than TSM enclosed in AA. The most SiO_2-rich samples of peralkaline granite contain TSM with the highest content of Si cations and the most octahedral site vacancies, and so TSM in aggregates is interpreted to have formed at an earlier stage than TSM enclosed in AA. TSM chemistry may also have been influenced by the AA host.

The occurrence and composition of igneous AA and TSM at Questa are compatible with experimental data indicating stability at low pressure and high temperature in environments in which the activities of Na, K, and Si are large relative to that of Al. The chemical evolution of the amphiboles may reflect decreasing oxygen fugacity as well as decreasing temperature.

(1) $(K_{0.16}Na_{0.76})(Na_{1.19}Ca_{0.81})(Mg_{2.77}Fe^{2+}_{0.77}Mn_{0.49}Fe^{3+}_{0.80}Ti_{0.05})(Si_{7.61}Al_{0.39})O_{22}F_{2.0}$

(2) $(K_{0.22}Na_{0.49})(Na_{1.88}Ca_{0.12})(Mg_{1.35}Fe^{2+}_{1.41}Mn_{0.48}Fe^{3+}_{1.47}Ti_{0.06}Al_{0.08})(Si_{7.83}Al_{0.17})O_{22}(OH_{1.0}F_{1.0})$

(3) $(K_{0.90}Na_{0.04})(Mg_{1.53}Fe_{0.95}Mn_{0.15}Ti_{0.12})(Si_{3.30}Al_{0.70})O_{11}(OH_{0.7}F_{1.3})$

(4) $(K_{0.91}Na_{0.04})(Mg_{1.92}Fe_{0.44}Mn_{0.12}Ti_{0.05}Al_{0.09})(Si_{3.60}Al_{0.40})O_{11}(OH_{0.4}F_{1.6})$

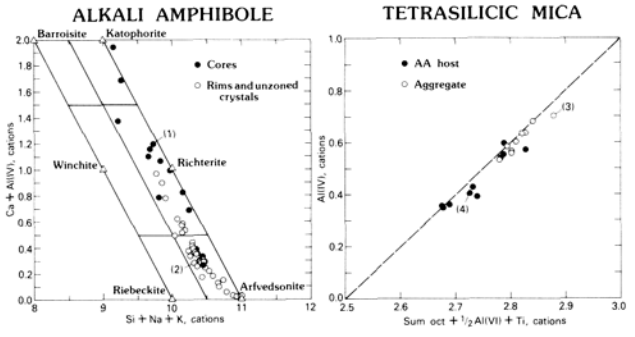

CRYSTAL CHEMISTRY OF Te-BEARING FAHLORE

DMITRIEVA, M.T., KOVALENKER, V.A., and BORISOVA, E.A., Institute of Ore Deposits, Mineralogy and Geochemistry, Academy of Sciences of the USSR, 109017 Moscow, USSR

Tellur-bearing variety of fahlores - goldfieldite $(Cu,Fe)_{12-x}(Te,As,Sb)_4S_{13}$ belongs to realm of very rare minerals, because its formation is possible only in the narrow interval of physical and chemical parameters: combination of highly oxidative environment which ensure stability for positively charged ion Te^{4+} and high activity Sb-goldfieldites and As-goldfieldites were studied by X-ray and electron microprobe analyses. Studies of chemistry of goldfieldite and Te-bearing fahlore from the USSR deposits (Volcanic belts of Middle Asia, Caucasus, Far Eart) and Bulgaria (Central Srednegorie) resulted in conclusion, that along with previously known tetrahedrite-goldfieldite isomorphic series there is tennantite-goldfieldite mineral series in the earth as well, The data available on the chemistry of goldfieldite and Te-bearing fahlore reveal very typical for these minerals enrichment in bismuth, mutual substitutions of which with Te, Sb and As are complicated and unambiguous.

The X-ray investigation confirmed the isomorphous substitution of Sb and As for Te. The isomorphism can be proved with confidence in As-goldfieldite due to substantial difference in ionic radii between Te^{4+}(0.89) and As^{3+}(0.69). The isomorphism in Sb-goldfieldite is less detectable. Unit cell parameters for As-goldfieldite with composition $(Cu_{22.2}Fe_{1.22})(Te_{6.02}As_{2.08})S_{13}$ A_o = 10.341±0.005 A against A_o = 10.21 A for tennantite (ASTM - 11-102), for Sb-goldfieldite with composition $(Cu_{20.64}Fe_{0.3}Zn_{2.09})_{23.03}(As_{1.87}Te_{1.47}Sb_{3.87})_{8.21}S_{26}$ A_o = 10.333 ± 0.005 against A_o = 10.35 A for tetrahedrite.

The structure of synthetic powder analog of goldfieldite has been refined by Kalbskopf (1973) but he hadn't at his disposal the single crystal of goldfieldite and structure was refined through measurements of only 31 powder lines.

In our study the structure of Te-tetrahedrite (A_o= 10.333 ± 0.005 A, space group J43m) has been refined using single crystal to final R-value of 0.07. Although good crystals are very rare, it was possibly to find a suitable one. Intensities data of 360 reflections have been collected on a 4-circle diffractometer "Syntex" (graphite monochromator, MoK_j-radiation).

The structure was found to be a cation deficient model of tetrahedrite structure, which was studied by Pauling and Neuman (1934), Belov and Pobedimskaja (1964), Wuensch (1964), Makovicky (1979) et al.

The refinement revealed Cu-vacancies formation due to the replacement of Sb^{3+} and As^{3+} by Te^{4+} .

DEFECTS IN OLIVINE: A NEW APPROACH VIA COMPUTER SIMULATIONS.

DOHERTY, M. and PRICE, G.D., Depts Chemistry and Geological Sciences, University College London, UK; PARKER, S.C., Dept Chemistry, Univ. Bath, UK; and CATLOW, C.R.A., Univ. Keele, UK.

Defects in olivine are of fundamental geological importance because they determine the rheology of the upper mantle of the Earth. It is therefore essential that the behaviour and defect properties of olivine be understood if mantle dymanics and plate tectonic processes are to be successfully described. Olivine is stable under ambient conditions and there is a large body of data on the defect properties of both pure Mg_2SiO_4 and iron bearing olivines. Nevertheless, considerable uncertainty remains concerning the detailed nature of the point defects present in forsterite, the mechanisms involved in cation and anion diffusion, the rate determining process involved in the creep of olivine and the effect of pressure on all of these phenomena. In an attempt to resolve these problems, we are using computer simulation techniques to model and predict not only the perfect lattice properties of forsterite, but also its defect properties and their behaviour as a function of pressure. An atomistic approach is used, based on the classical Born model of a solid, in which potential functions represent the interactions between the ions in the crystal. We have investigated a wide range of potentials and have used the set of potentials that best reproduce the perfect lattice properties of forsterite to calculate the energetics of various vacancies, interstitials, and related Schottky and Frenkel defects. We have further determined the lowest energy path ways and activation energies for vacancy, interstitial and interstitialcy diffusion of Mg in forsterite. These results are in excellent agreement with those obtained by or inferred from experiment. The transferability of these potentials means that having sucessfully been used to model the behaviour of defects in forsterite, they can be used to predict the diffusion and defect properties of the higher density polymorphs of Mg_2SiO_4, which are the major phases in the transition zone of the mantle. Because of the high pressures needed to synthesise these phases, computer simulations seem to offer one of the better ways of studying these polymorphs.

INCOMMENSURATE PHASE TRANSITIONS IN QUARTZ AND $AlPO_4$

DOLINO, G., Laboratoire de Spectrométrie Physique, (USTMG/CNRS), B.P. 87, 38402 Saint-Martin-d'Hères, France.

Since its discovery by Le Chatelier in 1888, the α-β phase transition of quartz has been the subject of many studies which have revealed the main physical and geological properties of this first order phase transition occuring around 846 K.

In 1980, however, a new phase, existing in a small temperature range of 1.4K, was discovered in between the classical α and β phases by thermal expansion measurements. Other macroscopic properties (heat capacity, birefringence, elastic constants ...) also show large effects due to the existence of this intermediate phase.

However the most interesting features are found by investigations of the microscopic structure of this phase : as predicted by a theoretical study, neutron and X-ray diffraction revealed the existence of sattelite peaks in the close neighbourhood of the usual lattice Bragg peaks. The position (and the intensity) of these satellites are strongly temperature dependent, showing that this new modulation is incommensurate with the lattice. Direct observations by electron microscopy show the existence of a triangular structure due to the superposition of 3 modulation waves at 120°.A different structure with a single modulation wave induced by the application of uniaxial stresses, has been observed in diffraction experiments with neutron and synchrotron radiation.

As in most other incommensurate phase interaction between the modulation wave and defects occurs in quartz, as evidenced by optical observations.

On the dynamical side, the study of lattice vibrations by inelastic neutron scattering shows that the α-β transition is induced by a "soft mode" corresponding to alternate rotation of SiO_4 tetrahedra. However the minimum frequency of this soft mode does not occur at the Brillouin zone center, but is slightly shifted along <100> directions, leading to the existence of an intermediate incommensurate phase. This shift of the minimum is probably due to a gradient interaction between the soft mode and a transverse acoustic mode -(similar phenomena are also found in isomorphous $AlPO_4$).

It is quite probable that many other incommensurate phases can be found in minerals either displacive as in quartz or due to composition modulations.

CHEMICAL VARIATIONS IN THE AMPHIBOLES OF AN EQUILIBRATED AMPHIBOLITE FROM NORTH-EASTERN SARDINIA (ITALY): CRYSTAL-CHEMICAL AND PETROLOGICAL IMPLICATIONS.

DOMENEGHETTI, M.C., OBERTI, R., UNGARETTI, L., Centro di Studio per la Cristallografia Strutturale del C.N.R., 27100-Pavia, Italy; GHEZZO, C., MEMMI, I., RICCI, C.A., Dipartimento di Scienze della Terra, Università di Siena, Italy.

A body of mafic and ultramafic amphibolites derived from previous granulite assemblage outcrops within the migmatites of the metamorphic basement of North-Eastern Sardinia (Italy).

The crystal-chemistry of the amphiboles present in one of these metamorphic rocks composed by more than 98 vol.% of amphibole associated with chlorite and spinel and very rare relics (gar and cpx) of the pre-existing granulite paragenesis has been studied by X-ray single-crystal diffractometry (XRef) and by microprobe analysis.

Notwithstanding that the amphiboles show an apparent textural equilibrium, a continuous range of amphibole compositions has been determined by XRef in several single-crystals present in a rock volume of less than 1 cm^3 and by microprobe analysis of a thin section not showing evidence of intracrystalline zoning.

All the amphibole crystals showed very similar pale-green colour; when mounted on a single-crystal X-ray diffractometer variations in the ratios of selected intensities allowed the recognition of crystal-chemical differences; on this basis 8 crystals representative of the compositional range were used for data collection and refinement; the conventional R factors were around 1.5%, the e.s.d. of bond lengths and of the mean atomic number were $\pm$ 0.001 A and $\pm$ 0.05 electrons respectively.

The site population and the chemical composition have been deduced by the CORANF computer program (Cannillo et al., this meeting); one of the crystals used for X-ray data collection has been successively analyzed, as a check, with a WDS microprobe, fully confirming the CORANF results.

All the refined amphiboles have C2/m space group; the M4 site is always occupied by Ca, with minor amounts of Fe^{2+} (0.11 - 0.17 a.p.f.u.). The main crystal-chemical differences concern the tetrahedral sites (Al^{IV} = 0.95-1.61 a.p.f.u.), the M2 site ($R^{3+} = Al^{VI}+Fe^{3+}+2Ti$ = 0.64-1.06 a.p.f.u.), the A site (Na+K = 0.31-0.55 a.p.f.u.), and the $Fe^{2+}/(Fe^{2+}+Mg)$ and $Fe^{3+}/(Fe^{3+}+Fe^{2+})$ ratios (0.24-0.31 and 0.14-0.29, respectively). However the amphibole compositions (Fig. 1 a,b; squares indicate calcic end-members) are characterized by identical Al^{IV}/R^{3+} (=1.5), $R^{3+}/(Na+K)_A$ (=2) and accordingly $Al^{IV}/(Na+K)_A$ (=3) ratios, i.e. the amphiboles have compositions along the A join tremolite and $NaCa_2Mg_3Al_2Si_5Al_3O_{22}(OH)_2$ (un-named end-member:*).

The mean unit cell volume of the refined amphiboles is 909.3 $\pm$ 0.5 A^3, i.e. the quite large chemical and geometrical differences do not affect significantly the unit cell volume, due to balancing effects amongst the multiple isomorphous substitutions occurring in these amphiboles.

Microtexture, mineral composition and petrochemistry suggest that the early assemblage was essentially composed by gar + cpx $\pm$ pla ; the Na content of the amphiboles can be ascribed either to a Na-bearing mineral phase or to a Na-rich fluid. The different amphibole compositions can be considered as the result of the reaction of different proportions of the early mineral phases; in fact the Al content and the $Fe^{2+}/(Fe^{2+}/Mg)$ ratio reach their extreme values when the amphiboles are adjacent to gar (Fe,Al-rich) and cpx (Mg-rich) relics respectively.

The lack of chemical homogeneization between adjacent amphibole crystals of widely different compositions can be explained by the rather low T of the retrograde metamorphism ($\sim$ 650 °C) inadequate to allow the mobilization of Al and Si from the tetrahedral sites; the rearrangement of the complex pattern of the isomorphous substitutions amongst the different amphibole crystals was probably further prevented by the marked similarity of their unit cell volumes.

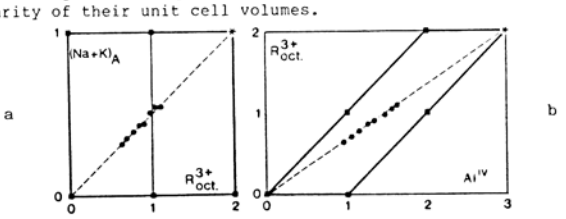

THE DISEQUILIBRIUM BREAKDOWN OF ALUMINOUS IRON-RICH BIOTITE AT 800°C: AN EXPERIMENTAL KINETIC AND TEM INVESTIGATION.

DROOP, G.T.R. and BREARLEY, A.J., Dept. of Geology, The University, Manchester, M13 9PL. England.

The breakdown reaction of natural aluminous iron-rich biotite in pelitic xenoliths under pyrometamorphic conditions (~800°C) has been recently investigated by TEM (Brearley, 1986 in prep). The biotite exhibits only limited evidence of transformation by the reaction: biotite = K-feldspar + hercynitic spinel + magnetite over a period of approximately four days (estimated from heat flow data for the intrusion).

In order to investigate the mechanisms and kinetics of this reaction more extensively, an experimental and TEM study has been carried out using cores of a well-characterised biotite schist as a starting material (initial grain size = 0.1-0.5 mm). This technique has the advantage of preserving the spatial relationships between the phases and furthermore, should mean that the experimental reaction mechanism closely approaches that in nature. The compositions of the biotites in both naturally and experimentally reacted samples are similar and enable direct comparisons to be made.

All the experiments have been performed at 800°C and 1kb in hydrothermal cold-seal pressure vessels using QFM buffer assemblage to control fO_2. Several experimental runs of between one day and 8 weeks duration have been carried out in order to examine the evolution of the reaction microstructure as a function of time. All the run products have been studied by light microscopy and transmission electron microscopy (TEM).

In the optical microscope the reaction is characterised by the progressive darkening of the biotite and the development of small areas of extremely fine-grained reaction products. TEM observations show that darkening of the biotite is attributable to the development of numerous, unoriented, spherical particles of magnetite (<300Å) which occur over wide areas of biotite. This microstructure is exactly analogous to that observed in the natural examples of this reaction (Brearley, 1986).

In addition to magnetite, significantly larger hercynitic spinel crystals (0.2-1 microns) are found which appear to have nucleated on planar defects on $(001)_{biot}$. The orientation of the hercynite in its early stages of growth is strongly controlled by the crystallography of the biotite, the two phases having the orientation relationship $(001)_{biot}$ // $(111)_{sp}$: $[010]_{biot}$ // $[110]_{sp}$.

It is probable that the two phases initially have a semi-coherent interface, but lose coherency as the spinel coarsens. The hercynite has an unusual elongate growth morphology parallel to $(001)_{biot}$, a factor which is controlled by enhanced diffusion rates within the basal plane of the biotite. The hercynite is always associated with volumes of a melt phase which, as the reaction proceeds develop as rims around the spinel. Once this stage in the transformation is reached, the restriction on growth of the spinel is removed and it tends towards a more characteristic cubic growth form.

The reaction proceeds preferentially at localised centres within the biotite where orthopyroxene also develops as a reaction product coexisting with spinel and melt. In runs of short duration (<1 week) the pyroxene is oriented relative to the biotite with $(001)_{biot}$ ~// $(001)_{pyx}$: $[130]_{biot}$ // $[100]_{pyx}$. This orientation relationship is rapidly lost as the melt fraction increases, and in runs of over 1 week pyroxene is usually only found as elongate lathes within the glass phase.

Even after the longest runs carried out to date (2 months) areas of biotite are still present which show no or limited evidence of transformation. These regions occur adjacent to biotite which has reacted very extensively and in some cases a gradational boundary is observed over 2-3 microns between untransformed and completely reacted biotite.

The compositions of all the phases have been studied in detail by analytical electron microscopy. The earliest spinel to nucleate (excepting magnetite) has an M/(M+F) = 0.05-0.17 and coexists with a peraluminous melt and biotite with M/(M+F)= 0.4-0.45. The spinel appears to have a metastable composition because it becomes progressively more magnesian as a function of run time. After runs of two months duration the spinels have M/(M+F) ratios of between 0.23 and 0.26. The same observation also holds for the compositions of the orthopyroxenes, which in short runs are exceptionally aluminous (16-20% wt% Al_2O_3) and have M/(F+M) ratios identical to the coexisting biotite. In longer runs the compositions of these two phases diverge, the orthopyroxene becoming slightly more Mg-rich and significantly less aluminous (8-10 wt% Al_2O_3).

PARTITION OF TRACE GERMANIUM AND GALLIUM BETWEEN INTERGROWN TOPAZ AND QUARTZ

DUCK, J. J. and COHEN, A. J., Dept. of Geology and Planetary Science, University of Pittsburgh, PA 15260. USA

Eight specimens of intergrown topaz and quartz were analyzed for germanium and gallium by the modified methods of Schneider and Sandell, and Culkin and Riley, respectively (1,2). Three specimens were quartz overgrown on euhedral yellow or pink topaz crystals from Ouro Preto, Minas Gerais, Brazil. Another specimen from Brazil has topaz partially enclosing the quartz. Two specimens were smoky quartz intergrown with colorless topaz from the Urals and Nertschinsk, USSR. One specimen was smoky quartz intergrown with blue topaz from Usakos, Namibia which contained minute tourmaline crystals on its surface. The last specimen was colorless topaz enclosing small euhedral smoky quartz crystals from Tres Barras, Minas Gerais, Brazil. Partition coefficients (K_d) were determined for the above samples and these results are compared in an attempt to correlate to observed order of crystallization with variation in the K_d.

The major cause of high trace germanium content in topaz compared to quartz is the presence of isolated silica tetrahedra in topaz and the three-dimensional structure of the silica tetrahedra in quartz. It is suggested that gallium substitution will occur at two sites in topaz; first, substitution for the aluminum in octahedral coordination and second, substitution for the silicon in tetrahedral coordination.

Increased substitution of germanium in the tetrahedral silicon sites is believed to favor gallium substitution for silicon in order to reduce compression and tension in the unit cell of quartz and possibly topaz.

(1) Schneider, W.A. and Sandell, E.B. (1954), Photometric Determination of Traces of Germanium After Carbon Tetrachloride Extraction, Mikrochimica Acta, 2, 263-268.
(2) Culkin, F. and Riley, J.P. (1958) The Spectrophotometric Determination of Gallium in Rocks and Minerals. Analyst 83, 208-212.

STRUCTURAL AND CHEMICAL EVOLUTION OF THE CALAMITY PEAK LAYERED GRANITE-PEGMATITE COMPLEX, BLACK HILLS, SOUTH DAKOTA

DUKE, E.F., REDDEN, J.A., and PAPIKE, J.J., Inst. for the Study of Mineral Deposits, S.D. Sch. of Mines & Tech., Rapid City, SD 57701, USA

The Calamity Peak granite-pegmatite complex (~1 km^2) displays many of the structural, textural, and compositional features of the larger Harney Peak granite dome (~100 km^2)[1,2]; thus it provides a model for the evolution of mid-Proterozoic granite systems of the Black Hills region, including their mode of emplacement, chemical variations, and wall-rock interactions. The initial intrusion is inferred to have been a flat-lying discordant sheet intruded into steeply dipping mica schist country rock (Fig.); however, an arcuate sheet, concave downward, cannot be ruled out. New magma pulses (possibly several hundred) were successively emplaced along the hanging-wall contact of earlier pulses, as indicated by truncations of early layers, creating a composite layered structure. Differential upward movement of the central part of the complex resulted in doming accompanied by new intrusive pulses. Growth of the dome caused plastic deformation of overlying country rocks and molded foliation into a concordant attitude in much of the hanging wall.

In the present structure, contacts and internal layering define a dome that is partly concordant with the country rocks; discordancy is evident at the apparent floor of the pluton, which is exposed in the core of the dome, and on the side opposite the regional dip. Coarse layering is defined by alternating pegmatitic and aplitic layers 0.5-2.0 m thick. The aplites are in turn layered on a scale of 1-10 mm due to modal variations of tourmaline, quartz, and feldspar. Textural differentiation of the coarser layers may have resulted from segregation of initially homogeneous magmas into pegmatitic (upper) and aplitic (lower) components during crystallization as proposed by Jahns and Tuttle[3]. The layered series is cut by successive stages of fracture-filling bodies and aplite dikes.

Perthite, muscovite, and biotite compositions show systematic variations between mapped portions of the complex. Rb and Cs content of both perthite and micas are high in the layered series and early fracture fillings and drop to low values in later fracture fillings. Sr and Ba in perthite are low except in late perthite-rich zones.

Metamorphic mineral assemblages in wall rocks grade from staurolite - andalusite to sillimanite - K-feldspar within 600 m south of the contact, demonstrating that the pluton imposed an abnormally high thermal gradient. Whole-rock analyses of mica schist wall rocks collected along a 1600-m traverse parallel to bedding indicate twofold enrichments in Rb (425 ppm), Cs (95 ppm), and F (0.21 wt.%) adjacent to the pluton contact, whereas K remains relatively constant (~3.5 wt. %). The Rb and Cs halos extend 30-40 m from the contact compared with 5 m for F; hence the element dispersion halos are comparable to those observed around individual Black Hills zoned pegmatites[4].

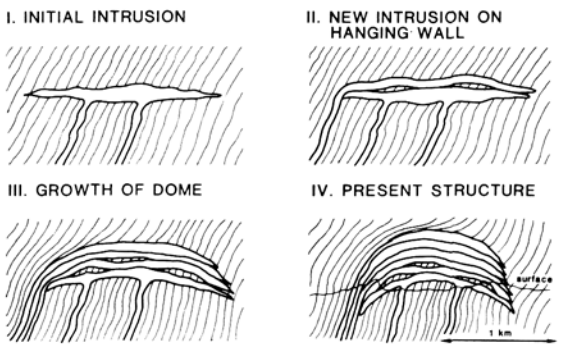

References.
(1) Kupfer, D.H., 1963, U.S.G.S. Bull. 1142E, p. 1-23. (2) Duke, E.F., et al., 1985, EoS, v. 66, p. 396. (3) Jahns, R.H., and Tuttle, O.F., 1963, M.S.A. Spec. Paper 1, p. 78-92. (4) Shearer, C.K., et al., 1986, Am. Min. (Jahns Vol.), in press.

M2/M1 ORDERING OF IRON IN BIOTITES FROM NORTHWESTERN MAINE

DYAR, M. D., Div. of Geol. and Planet. Sci., Caltech, Pasadena, CA, 91106 USA; HICKMOTT, D., Dept. of Earth, Atmos. and Planet. Sci., M.I.T., Cambridge, MA 01239 USA; GUIDOTTI, C. V., Dept. of Geology, Univ. of Maine, Orono, ME, 04469 USA; and CHENEY, J. T., Dept. of Geology, Amherst College, Amherst, MA 01022 USA.

Octahedral cation ordering in micas has been studied in the past by using either observed differences in mean M-O, OH, F bond lengths or refinements based on scattering powers of cations. However, the technique of Mossbauer spectroscopy is even better suited to accurate characterization of Fe site populations; two Fe^{2+} doublets corresponding to M1 and M2 octahedral sites in biotite can consistently be resolved in spectra. In this study a suite of 31 biotites from the Rangeley quadrangle area in northwestern Maine has been analyzed by electron microprobe and Mossbauer spectroscopy; Fe^{2+}/Fe^{3+} and Fe^{2+} M2/M1 ratios were determined for samples from a systematic range of metamorphic grades (garnet through sillimanite) and mineral assemblages.

Biotites were handpicked from the rocks and then ground to powders (by hand) while mixed with sugar and acetone. Samples were run on the Mossbauer spectrometer at M.I.T. through the courtesy of Roger G. Burns, and data were processed at M.I.T. and Caltech using a Gauss non-linear regression method for curve-fitting. A typical Mossbauer spectrum is shown below; Fe^{2+} M1 and M2 peaks are designated on the plot. In a few spectra (such as this one) it was also possible to resolve two additional doublets corresponding to Fe^{3+} M1 and M2; those M2/M1 ratios range from 2.0 to 1.25 with large errors. However, Fe^{2+} peaks are larger and have less error; M2/M1 ratios are accurate within ± about 10%.

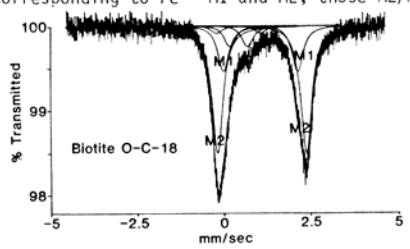

Large variation among Fe^{2+} M2/M1 ratios was observed; no sample had the expected 2:1 site occupancy ratio expected from a random distribution of Fe in a unit cell. M2/M1 ratios ranged from a low of 0.64 for a ksp+sill zone sample to a high of 3.40 for a low st grade biotite. Average M2/M1 values and Mg/Mg+Fe numbers for biotites from each grade are plotted here. There is a general trend of decreasing M2/M1 (increasing site disorder) from st to sill grade which is intuitively reasonable; higher temperature should favor increasing randomness. However, the M2/M1 trends also might reflect variations in Mg number if Mg has a strong preference for the smaller M1 site. In such a scenario, Mg enrichment from gn to st grade would cause the M1 site to be filled by Mg (causing apparent Fe^{2+} enrichment in M2). At higher grades (as sill replaces chte in the limiting assemblage with bio - gn - st) Mg content decreases and Fe^{2+} can occupy more of the M1 site. It is impossible to determine from the Mossbauer data if Mg is ordering (and all the other cations are randomly distributed among the rest of the sites) or if Fe alone is ordered, or if all the cations in the structure are ordered. However, it is clear that there must be at least one major cation in the structure which has a distinct site preference for M1 or M2. Given the magnitude of the observed variation in Fe site distribution, probably either Fe (in M2) or Mg (in M1) is ordered. Scatter in the ordering systematics can be attributed to other compositional effects, retrogradation, and the presence of occasional late stage chlorite. In conclusion, octahedral cation ordering appears to be a function of both grade change and bulk compositional effects.

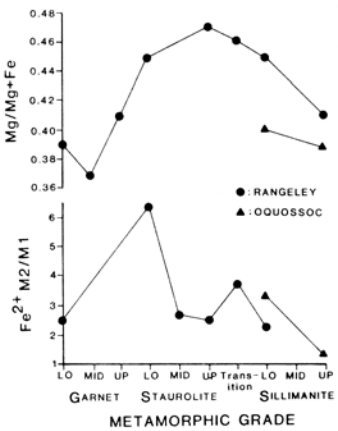

FORMATION OF MIXED-LAYER CLAYS FROM SMECTITE AT LOW TEMPERATURE

EBERL, D. D., U. S. Geological Survey, Mail Stop 404, Federal Center, Denver, CO 80225, USA; SRODON, J., Institute of Geological Sciences, Polish Academy of Sciences, 31-002 Krakow, Senacka 3, Poland; NORTHROP, H. R., U. S. Geological Survey, Mail Stop 963, Federal Center, Denver, CO 80225, USA

It is well-known that smectite reacts to form mixed-layer illite/smectite when it has been heated during burial or contact metamorphism. This reaction, or family of reactions, involves substantial alteration or complete dissolution of smectite 2:1 layers. Reaction by this mechanism may take hundreds, thousands, or millions of years to yield a substantial percentage of illite layers, with the kinetics of the reaction depending on temperature and on chemical environment. It is possible, however, to form illite/smectite from smectite at low temperatures (30°, 60°, and 90° C) in a matter of days if smectite is subjected to wetting and drying cycles in the presence of a potassium mineral. The formation of illite layers by the latter mechanism involves no substantial alteration in 2:1 layer chemistry; rather, illite-layer formation is related to a rearrangement of existing 2:1 layers into more stable configurations around potassium ions that have been dehydrated by drying. This reaction is relatively insensitive to changes in temperature and chemical environment, although the presence of calcium chloride does decrease the rate of illitization. The percentage of illite layers formed by wetting and drying is proportional to the number of wetting and drying cycles, with most of the illite layers forming during the first 20 cycles, and to the layer charge of the original smectite, with this relation more closely obeyed by montmorillonites than by beidellites. The reaction also is influenced by the type of K-mineral present (eg. microcline, muscovite, phlogopite, glauconite, or illite), and by the K-mineral/smectite ratio of the system. Illite/smectite formed from smectite by wetting and drying sometimes can be distinguished from illite/smectite formed by burial diagenesis by examining the fixed potassium content of the illite layers.

Another method for forming illite layers from smectite at low temperature is by treating smectite with high pH solutions (e.g. 0.5 N KOH), with or without wetting and drying cycles. Under these conditions, smectite reacts readily to form illite layers by chemical alteration of the 2:1 layers. A substantial change in 2:1 layer chemistry is indicated by an increase in cation-exchange capacity for the smectite layers, by an increase in fixed cation content for the illite layers, and by a significant change in oxygen isotope ratios for the 2:1 layers.

A third method for the rapid formation of mixed-layer clay from smectite is by wetting and drying montmorillonite in the presence of a mineral containing cations that can enter into octahedral coordination. Under these conditions, cations dissolved from the mineral can migrate into vacancies in octahedral sheets. Negative charge on 2:1 layers thereby is neutralized, and smectite interlayers collapse to pyrophyllite-like spacings (approximately 9.2 Å) according to the Hofmann-Klemen effect. For example, when Na-montmorillonite (Kinney) is subjected to 11 wetting and drying cycles with magnesite at 60° C, the clay reacts to form a discrete pyrophyllite-like phase (001 = 9.2 Å), plus mixed-layer clay. Finally, smectite can react to form mixed-layer chlorite/smectite under surface conditions by precipitation of aluminum and magnesium hydroxide pillars in interlayer space.

These experiments indicate that the smectite structure is labile at low temperatures. It can react to form mixed-layer clay if subjected to wetting and drying cycles in the presence of either a potassium mineral, or a cation that can enter into octahedral coordination. Smectite also will react in high pH solutions (with KOH) to form illite/smectite.

• MASSIF ANORTHOSITES AND LAYERED INTRUSIONS: COMPARISONS AND CONTRASTS

EMSLIE, Ronald F., Geological Survey of Canada, 601 Booth St., Ottawa, Ontario, Canada K1A OE8

Despite the restricted bulk composition range of rock assemblages constituting anorthosite massifs, comparison of many of their characteristics with those of mafic layered intrusions provides important insights into aspects of their origin, intrusion mechanisms, and crystallization. In particular, origins that require parent magmas of massifs to be solely or largely of crustal derivation become very difficult to defend.

The large size of many anorthosite massifs is one of their most imposing features. Next to the Bushveld complex, Proterozoic anorthosite massifs rank among the largest basic intrusions in the Earth's crust. Some of the larger examples include: Lac St. Jean, Quebec - 20,000 km^2, Kunene, Angola - 17,000 km^2, Harp Lake, Labrador - 10,000 km^2, Nain, Labrador - 10,000 km^2.

The limited age range (~0.9 to 1.7 Ga) for Proterozoic massifs is clearly one of their most distinctive features and contrasts with large mafic intrusions which evidently have no such time-related occurrence in the geological record. Where unequivocal geological evidence exists, anorthosite massifs occur in cratonic settings like large layered mafic intrusions. Spatially, there are regional concentrations of large massifs, notably in the eastern Canadian Shield, but worldwide, they are probably not rarer than mafic intrusions of comparable size.

Troctolite, norite, their leucocratic variants and anorthosite comprise the major components of most massifs. Persistently coarse and very coarse grain sizes are particularly common in anorthositic compositions whereas troctolitic and noritic cotectic crystallization products are often medium to coarse grained. Plagioclase megacrysts larger by a factor of 2 to 10 than groundmass plagioclase may occur sporadically in all other rock types. Adcumulate textures and modal compositions almost exclusively characterize most units of massifs.

Commonly, large massifs contain masses of essentially homogeneous rocks together with variable quantities of modally layered rocks which may grade into each other locally or have intusive contacts. Modal layers are most common in troctolitic compositions, less common in noritic compositions and rare in anorthosite. Modally-graded layers, cross-bedded layers and scour-and-fill structures have been described from massifs and may occur at different sclales. Weak to strong planar plagioclase lamination frequently occurs in conjunction with, and subparallel to, modal layers.

Cognate xenoliths are recognized in many massifs. Many commonly these are anorthosite or leuconorite compositions and accordingly are most easily recognizable in troctolitic or leucotroctolitic host rocks. Megacrysts of highly aluminous orthopyroxenes occur within xenoliths and provide the strongest evidence of an earlier crystallization interval of the magmas at depth, prior to intrusion to higher crustal levels.

Plagioclase compositions in massifs rarely are more calcic than about An_{70} or much more sodic than about An_{40}. The range An_{65-45} embraces the majority of massif plagioclases. Olivines are typically Fo_{65-55}, but range from about Fo_{70-40}. Orthopyroxenes En_{70-55} are most common with extremes from about En_{75-45}. Large parts of some massifs, or entire smaller massifs may have ranges of less than 10 mole percent An in plagioclase and Mg/Mg+Fe in mafic silicates. Considering the size of massifs, the restricted compositional ranges of the mineral constituents are in marked contrast to the total ranges observed in large mafic layered intrusions.

Although mineral composition ranges in typical massifs are relatively narrow, certain correlations are apparent: olivine-bearing rocks tend to have associated more calcic plagioclase than orthopyroxene-bearing rocks in the same massif; more magnesian olivine and orthopyroxene tends to be associated with more calcic plagioclase. These are characteristics expected of products of fractionated basic magmas. Olivine and orthopyroxene compositions imply that parent liquids had Mg/Mg+Fe in the range 0.43 to 0.28, too low to have been primary mantle melts but consistent with fractionated mantle melts. Other evidence of fractionation lies in intermediate Ca/Ca+Na in plagioclase, relatively low Ni and Cr contents of olivines and orthopyroxenes, high Sr contents in plagioclase, and LREE-enriched whole rock compositions.

The best known ore deposits associated with massif anorthosites are concentrations of ilmenite and titaniferous magnetite. The former are typically associated with noritic assemblages whereas the latter tend to occur more commonly in troctolitic associations. Sulfide mineral assemblages tend to be poor in Ni and richer in Cu. Chromite and PGE mineralizations are notably absent from massif anorthosite associations. These features are all in accord with crystallization from evolved basic magmas but not with crustal melts unless the crustal source materials had highly specialized compositions.

Although stratiform intrusions form portions of massif complexes, as a whole the complexes themselves do not have an overall definable stratigraphy. This may be regarded as evidence that massifs were not intruded as large volumes of mainly liquid magma. The forms and internal structures of massif complexes appear to have little in common with lopolithic, funnel, sill, or sheet-like forms common to mafic intrusions; the differences may be accounted for by contrasting fluid properties of their respective magmas.

THE METALLOGENIC CONTEXT AND MINERALOGICAL SUCCESSION OF THE URANIUM OXIDES IN IRAN

ESPAHBOD, M.R., Uranium Exploration Division, A E O I, Ave Kargar, Tehran, Iran

The metalliferous areas in Iran are essentially limited to the major Alpine movements which could be subdivided in three principal metallogenic provinces. One is the volcanic belt with parallel - stretching to Zagros thrust fault, the second is Alborz range (mostly north western and eastern part) and the third is Central part of Iran. Also, some metallogenic subareas are distinguished in south east Zagros as well as Jaz murian depression. The uranium oxides are observed in extreme north western part of Central Iran (Baitche Bagh copper mine). The uranium spherolites have been occurred as small pitchblende veins with coffinite minerals due to multistage epigenitic processe, associated with Cu,Ni,Co,Bi,Au,Ag minerals amongst which chalcosite, smaltite, skutterudite, safflorite, rammelsbergite, Tennantite, Erythrite, Bismuthinite together with chalcopyrite and small quantity of native gold are predominant. In Talmessi-Meskani area (part of Anarak metallogenic district), the uranium oxides have been occurred in the form of pitchblende and para pitchblende together with coffinite in andesite porphyrite. The seven fold parageneses, say Cu,Ni,Co,U,Bi,Ag,Au providing a range of the mineral assemblage which are manifested as a mineralogical succession and geochemical halos. The uranium oxides are mostly associated with chalcosite, chalcopyrite, Algodonite, Domeykite, malachite, lavendulanite, Rammelsbergite, Annabergite, safflorite, Erythrite etc.

Equally, the uranium oxides as uraninite and pitchblende spehero-lites are observed in Albite metasomatism Episyenites of the BAFQ-CHADORMALU metallogenic district.

In eastern Alborz the uranium oxides in the form of sooty varities are observed in pyritized ignimbritic rhyolites.

REFERENCE :

BARIAND, P. (1963). Contribution a la mineralogical de l IRAN: Ph,D. These, Unive, Paris, Faculte des science.

BARIAND, P. (1965). Preliminary metallogenic map of IRAN. Geol survey. Report No. 7,44 P.

ESPAHBOD, M.R. (1978). Preliminary investigation in Anarak region (radioactive propection). 11 page internal report. Persian text.

KURBANOV, R. (1972) Prospecting for hard minerals in the Anarak area of Central IRAN. Technoexport Moscow, USSR.

HIGH RESOLUTION ELECTRON MICROSCOPY OF METAMICT AND ANNEALED ZIRCONOLITE FROM SRI LANKA

EWING, R.C. and LUMPKIN, G.R., Dept. of Geology, University of New Mexico, Albuquerque, NM 87131, USA

Radiation effects in zirconolite from Sri Lanka have been examined using HRTEM. Sri Lankan zirconolites are x-ray and electron diffraction amorphous. An alpha-recoil dose of more than 10^{26} alpha-events/m^3, equivalent to ~2 displacements per atom (dpa), has accumulated over the 550 m.y. age of the specimen. The composition approximates $Ca_{.7}Th_{.3}Zr_{1.0}Ti_{1.6}Fe_{.2}Mg_{.2}O_7$.

Metamict and annealed (in air at 1100°C for 2 hrs.) samples were examined using a JEOL 2000FX TEM operated at 200 keV. Grains of metamict zirconolite give electron diffraction patterns consisting of diffuse rings with "equivalent" d-spacings of 0.305 and 0.185 nm. Based on crystal structure refinements of synthetic (Gatehouse et al., 1981) and natural zirconolites and EXAFS/EXANES spectroscopy on metamict and annealed material from Sri Lanka, the diffuse rings can be related to the mean bond lengths. We interpret the 0.305 nm ring to be representative of M-M and/or O-O distances in the metamict structure. Similarly, the 0.185 nm ring represents the M-O distances. High resolution, phase contrast images display a pattern of random contrast similar to calculated images of random network structures thicker than 0.3-0.6 nm. Typical lattice fringes were not observed in any of these images. There was no evidence of crystallinity in more than 100 grains that were examined. Approximately 10 percent of the grains contained subspherical microvoids ranging from 100 to 400 nm in diameter.

HRTEM images and corresponding electron diffraction patterns of the annealed sample are interpreted as the monoclinic ($d\bar{d}$) zirconolite polytype twinned at the unit cell scale (White et al., 1984). The maximum thickness of untwinned material is on the order of 6-7 nm. Most twins consist of (010) and (110) lamellae resulting from t-type layers within the ($d\bar{d}$) matrix. Twinning due to incorporation of m-type layers was also observed. A few lamellae were found to have a three layer repeat ($\underline{c}$ = 1.69 nm) consistent with the orthorhombic (t^3)zirkelite polytype. Lattice dimensions of the monoclinic ($d\bar{d}$) polytype are $\underline{a}$ = 1.22 nm, $\underline{b}$ = 0.72 nm, $\underline{c}$ = 1.12 nm, and β = 101°. X-ray diffraction data refined in space group C 2/c give lattice dimensions of $\underline{a}$ = 1.244(1) nm, $\underline{b}$ = 0.7298(7) nm, $\underline{c}$ = 1.145(1) nm, and β = 100.4(2)°.

Polycrystalline grains were also found in the annealed sample. They give electron diffraction patterns consisting of spotty rings with d-spacings and intensities similar to the fluorite structure type. Nearly identical patterns result from electron beam heating of metamict zirconolite. HRTEM images show 0.36 nm lattice fringes which, in some areas, change to a higher order (n = 3) superstructure with a repeat of 1.08 nm.

Results of this study indicate that zirconolite from Sri Lanka is completely metamict at a dose of over 10^{26} alphas/m^3. Electron diffraction patterns give diffuse rings consistent with M-O, M-M, and O-O distances. HRTEM images are consistent with a random network structure of corner and/or edge linked polyhedra under the experimental conditions employed (0.12 nm maximum resolution, thickness > 0.3-0.6 nm).

Heating of metamict zirconolite produces initially a disordered fluorite type structure which appears to transform to highly twinned monoclinic zirconolite at high temperature (1000-1200°C).

White, T.J., Segall, R.L., Hutchinson, J.L., and Barry, J.C. (1984). Polytypic behaviour of zirconolite. Proceedings of the Royal Society of London, A 392, 343-358.

Gatehouse, B.M., Grey, I.E., Hill, R.J., and Rossell, H.J. (1981), Zirconolite, $CaZr_xTi_{3-x}O_7$; structure refinements for near-end-member compositions with x = 0.85 and 1.30. Acta Crystallographica, B37, 306-312.

This work supported by the U.S. Department of Energy, Office of Basic Energy Sciences under Grant #DF-FG04-84ER45099 (RCE).

MINERALOGY AND GENESIS OF SECONDARY MIAROLITIC CAVITIES IN PEGMATITES OF THE WAUSAU COMPLEX, WISCONSIN

Falster, Alexander U., Mineralogical Research, 920 McIntosh St., Wausau, Wisconsin 54401, USA

The Wausau Complex is a peralkaline intrusion consisting of the Stettin, Wausau, Rib Mountain and Ninemile plutons. The complex is of proterozoic age and is exposed in Marathon County, Wisconsin. Pegmatite bodies of modest size are abundant.

Four distinct types of miarolitic pegmatites, characterized by zoning (contact, wall, intermediate, pocket and core zones), have been recognized, among these one type is remarkable for a distinct solution-etched zone directly below the primary miarolitic cavitity: Quartz of the medium grained quartz-feldspar intergrowth has been selectively removed and in the resulting voids (average dimension 5 mm) a distinctive mineral assemblage of Ti-oxides, cheralite, zircon-II, fluorapatite, ilmenite, hematite, quartz-II, K-feldspar-II and several other minerals formed.

It appears that in pegmatites of this type a gradual escape of pegmatitic fluid occurred, instead of the explosive degassing so evident in other pegmatite types in the Wausau Complex. Evidently, the pegmatitic fluids escaping from the primary pocket corroded the Ti-rich (up to 3.2 weight percent TiO_2) biotite near the pocket zones, dissolved most of the quartz in the graphic granite surrounding the primary pocket, and, while recirculating through these secondary cavities, deposited the characteristic mineral assemblage. Primary miarolitic cavities of the pegmatites in the Wausau Complex are commonly poor in Ti-oxides but rich in minerals bearing Fe, Be, and REEs. Thus the source of the Ti-oxides appears to be in the Ti-bearing biotite, but the REEs, P, Be, and Zr seem to have been contributed by the primary pockets.

EVOLUTION OF PHYSICO-CHEMICAL CONDITIONS OF MEDIUM-TEMPERATURE METAMORPHISM

FED'KIN,V.V. Institute of Experimental Mineralogy USSR Academy of Sciences, 142432 Chernogolovka Moscow district, USSR

The present abstract lists the results of five year studies on thermodynamic regime of metapelite and calc-silicate complexes with respect to evolution of metamorphism. The detailed studies on compositions of coexisting minerals, their zoning, composition of inclusions and direct contacts enable employment of chemical inhomogeneity of the rock-forming minerals as an indicator of physico-chemical metamorphic conditions. The obtained experimental data on exchange equilibria and development of new mineralogical geothermometers/geobarometers provided information on changes in thermodynamic parameters of metamorphism (T,P and regime of volatile components) during crystal growth of rock-forming minerals, namely: garnet, staurolite, cordierite etc.

Based on these data, the regularities regarding evolution of metamorphic processes in metapelite and calc-silicate complexes of shields and fold belts have been deduced. Throughout fold belt formation P-T conditions of metamorphism range from 0.5 - 1.0 to 7-8 kbar and 400-450 to 600-650°C, respectively, at the prograde stage and from 5-7 to 2-3 kbar and then to 0.2-0.5 kbar as well as 650-700 to 550-580°C and then to 400-470°C, respectively, at its retrograde stage. Thus, ancient geothermal gradients are somewhat inconsistent with one another at different stages of fold belt formation. They correspond to higher pressures at early stages of geosynclinal regime and to higher temperatures and relatively lower pressures at its final stages. By changes in compositions of coexisting minerals and mineral inclusions in the cores and rims of large grains can the shift in a geothermal gradient in the same samples from individual metamorphic complexes (Northern Pamirs, Tien Shan) be

traced.

The mineral assemblages of metamorphic complexes of granulite facies-amphibolite facies shields (e.g. Aldan) provide no information on prograde transformations due to high rates of chemical reactions at high grade metamorphism. The mineral equilibria involving hydrous- and carbonate-bearing phases enable estimation of the fluid regime of metamorphism(H_2O, CO_2). Partial water pressure of amphibolitic metamorphism in the fold belts was not greater than 1.5-2.0 and only in places (the Ukranian Carpathians) reached the value of 5 kbar. This was ensured by experimental data on granite melting involving different H_2O contents in the melt. Partial pressure of CO_2 is also low; not greater than 0.5-0.7 kbar.

The obtained physico-chemical regularities, along with geological and structural-tectonic evidence might shed light on the possible relationship between thermodynamic regime of metamorphism and geological history of some crustal areas

HEAT CAPACITY OF MINERALS RELEVANT TO THE EARTH'S MANTLE: A NEW EQUATION FOR THE HEAT CAPACITY OF SOLIDS

FEI,YINGWEI, Department of Geology, Brooklyn College, Brooklyn, N.Y.11210 and Department of Earth and Environmental Sciences, Graduate School, CUNY, New York, N.Y.10036

A new expression for the heat capacity of solids is proposed here. This equation is useful a) for fitting the measured low-temperature heat capacity data on crystals and b) for determining heat capacity at high temperatures without violating the limit set by Petit and Dulong. The proposed equation is

$$C_p = 3Rn(1 + k_1T^{-1} + k_2T^{-2} + k_3T^{-3}) + (A + BT)T$$

where R and n are gas constant and the number of atoms in the chemical formulae, respectively. A and B are calculated from thermal expansion coefficient and isothermal bulk modulus data. The k's are determined by fitting the measured low-temperature heat capacity data.

The heat capacity for 24 minerals relevant to the Earth's mantle has been calculated by the proposed equation. The errors possibly resulting from experimental measurements or extrapolations of the thermal expansion coefficient and bulk modulus are carefully examined.

EM-RESEARCH INTO THE FIBROUS CONSTITUENTS OF AN INDUSTRIAL TALC POWDER

FELIUS, R.O., Inst. of Earth Sciences, State University Utrecht, P.O. Box 80.021, 3508 TA Utrecht, the Netherlands.

A sample of industrial talc powder with fibers was collected from a raw material supply in the Netherlands. Some powder of the sample was dispersed in alcohol. A droplet of the dispersion was put on a copper grid with a holey carbon film. The grid was mounted either on a double tilt stage for examination in a Philips EM 420 with a spherical aberration constant C_s=2.0 mm, or on a single tilt stage for examination in a JEM 200C, equiped with a standard Link System Si X-ray detector.

TEM-, HRTEM-images and SAED-patterns were made at 120 kV with the EM 420. The JEM 200C was used for TEM-images and SAED-patterns at 200 kV as well as for EDS-analyses at 100 kV. The SAED-patterns were gauched with either gold as an internal standard or TlCl as an external standard.

The thus obtained SAED-patterns are in good agreement with those computed from the cell parameters of respectively talc [1], anthophyllite [2] and tremolite [3] or with the superimposed reciprocal lattices of anthophyllite and talc [4].

The TEM-images and their corresponding SAED-patterns show three fibrous morphology types with the following mineralogical compositions: talc ribbons with a strong elongation // a-axis and recumbent on (001); anthophyllite ribbons with a strong elongation // c-axis and lying upon (100); ribbons of anthophyllite, epitaxial intergrown with various amounts of talc with $(100)_{anth.}$ // $(001)_{talc}$; long hairlike crystallites of anthophyllite, elongated // c-axis, recumbent upon any face and sometimes epitaxial intergrown with minor talc; splintery laths of intergrowths of anthophyllite + talc ± tremolite.

Extra reflections and striations // b*-axis around the reflections in the SAED-patterns of anthophyllite and the corresponding HRTEM-images show the presence of at least single, triple and quadruple pyroxene chains inbetween the amphibole chains. These chain width errors are hold responsible for both the fibrous morphology of the anthophyllite and its ribbonlike, hairlike or splintery cleavage [5].

With many thanks to ing. J. Pieters of the Dept. of Molecular Cell Biology, State University Utrecht, for operating the microscopes.

[1] M. Akizuki & J. Zussmann (1978): The Unit Cell of Talc. Min. Mag., vol. 42, pp. 107-110.

[2] D.R. Veblen & C.W. Burnham (1978): New Biopyriboles from Chester, Vermont: I Descriptive Mineralogy. Am. Mineral., vol. 63, pp. 1000-1009

[3] M. Ross, W.L. Smith & W.H. Ashton (1968): Triclinic Talc and associated Amphiboles from Gouverneur Mining District, New York. Am. Mineral., vol. 53, pp. 751-769.

[4] R.L. Virta (1985): The Phase Relationship of Talc and Amphiboles in a fibrous Talc Sample. Report of Investigations/United States Dept. of the Interior, Bureau of Mines; 8923.

[5] D.R. Veblen (1980): Anthophyllite Asbestos: Microstructures, intergrown Sheet Silicates, and Mechanisms of Fiber Formation. Am. Mineral., vol. 65, pp. 1075-1086.

• SERPENTINE AND SERPENTINE-LIKE MINERALS

FERRARIS, G., Dip. Scienze della Terra University, via S. Massimo 24, 10123 Torino, Italy and MELLINI, M., C.N.R., C.S. Geologia Strutturale, via S. Maria 53, 56100 Pisa, Italy

The well-known chemical variability of serpentine minerals does often point out an actual mineralogical complexity. For instance, high silica and low silica analyses can be interpreted in terms of the inophite and antigorite polysomatic series. In fact, the two series oppositely deviate in composition from the ideal $Mg_3Si_2O_5(OH)_4$ (S module), by addition (antigorite) or removal (inophite) of silica.

By alternating X modules $[Mg_6Si_2O_3(OH)_{14}H_2O]$ and S modules, carlosturanite S_5X and the other S_mX inophites are obtained (Am. Mineral. 70, 773); they have Si/Mg ratio given by [2(m+1)]/[3(m+2)]. Carlosturanite seems to be a widespread serpentinite mineral and, until now, four different findings of this serpentine-like mineral are known, from low grade metamorphic environments.

On the other hand, antigorite, that is, the most abundant serpentine mineral occurring in higher grade serpentinites, can be described in terms of a polysomatic series with exceeding silica content. To describe antigorite, we shall adopt a two-modules polysomatic series, instead of the three-modules series proposed by Spinnler (Ph.D. Thesis 1985, Arizona State Univ.). In such a way we can avoid too strict dependence upon a poorly known structure model. Our modules are still S and T, with T having the talc composition $Mg_3Si_4O_{10}(OH)_2$. The opposite polarity of the tetrahedral layer shall be expressed by S^+ and S^-, respectively. The whole series $S_m^+ S_m^-$,T, has a variable Si/Mg ratio given by [2(m+m'+2)]/[3(m+m'+1)]. When $m \rightarrow \infty$, the ideal S serpentine composition is obtained from both series.

A unified approach to the title minerals can be obtained by introducing, besides polytypism, the concepts of polysomatism and of secondary structure. By secondary structure we mean the structural modifications ruled by symmetry operators other than the 3D space group operators; namely, the cylindrical and polygonal periodicities found for the chrysotile family. On the whole, the following distinction can be made.

(a) Minerals with different primary structures

lizardite inophite antigorite

These minerals are chemically and structurally different; polytypes are possible.

(b) Minerals with different secondary structures

chrysotile parachrysotile polygonal serpentine

These minerals do not differ in chemistry or primary structure; polytypes are possible. Furthermore, a third level structure has been found for chrysotile based on rod close packing of fibers.

ELECTRON DIFFRACTION AND ELECTRON MICROSCOPY STUDY OF BALANGEROITE AND GAGEITE: UNIT CELLS, STRUCTURE MODELS AND PETROGENETIC ROLE.

FERRARIS, G., Dipartimento di Scienze della Terra, Universita' di Torino, Italy; MELLINI, M., Centro di Geologia Dinamica e Strutturale dell'Appennino, C.N.R., Pisa, Italy; MERLINO, S., Dipartimento di Scienze della Terra, Universita' di Pisa, Italy.

Electron diffraction and transmission electron microscopy (TEM) investigations were carried out on the fibrous minerals balangeroite and gageite. The studies indicated for balangeroite a monoclinic cell with $a_m \cong b_m \cong 19.4$ Å, c_m (unique axis) = 9.65 Å, γ_m = 91.1°; two polytypic modifications were found for gageite: gageite 2M, monoclinic, isostructural with balangeroite, cell dimensions $a_m \cong b_m \cong 19.4$ Å, c_m = 9.84 Å, γ_m = 90.5°, and gageite 1Tc, triclinic, unit cell dimensions $a_t \cong b_t \cong 14.1$ Å, c_t = 9.84 Å, $\alpha_t \cong \beta_t \cong 88.6°$, γ_t = 86.9°.

Chemical (Dunn, 1979; Compagnoni et al., 1983) and physical data pointed to the presence of four-repeat silicate chains (T), running in the channels of the octahedral framework described by Moore (1969) and placed on both sides of the Moore's octahedral walls (O) to give rise to composite TOT modules, interconnected through octahedral bundles. The corresponding ideal crystal chemical formula is $M_{42}O_{26}(OH)_{40}(Si_4O_{12})_4$, with M denoting cations in octahedral coordination, mainly magnesium in balangeroite and manganese in gageite.

The monoclinic and triclinic structural arrangements may be described as consisting of equivalent layers, with translation periods a_m and c_m, the width of the layers being $b_o = b_m/2$. Adjacent layers are related by the vector $t_1 = -a_m/2 + b_o + c_m/3$ or the vector $t_2 = -a_m/2 + b_o - c_m/3$. The layer sequence $t_1 t_2 t_1 t_2 \ldots$ is realized in the monoclinic modifications, whereas the sequence $t_1 t_1 t_1 \ldots$ (or $t_2 t_2 t_2 \ldots$) is realized in the triclinic modification. The symmetry properties of the two arrangements, the peculiar features of their diffraction patterns, the appearence of diffuse spots in various patterns, are discussed and explained on the basis of the OD theory.

Finally TEM evidence for the replacement of chrysotile for balangeroite by retrograde metamorphism is given, and the role of that mineral in the metamorphism of ultramaphites is discussed.

REFERENCES

Compagnoni, R., et al. (1983) - Am. Mineral., 68, 214-219.

Dunn, P.J. (1979) - Am. Mineral., 64, 1056-1058.

Moore,P.B. (1969) - Am. Mineral., 54, 1005-1017.

DETERMINATION OF THE DRIVING FORCES OF METAMORPHISM BY MEASUREMENT OF REACTION PROGRESS IN ROCKS

FERRY, J. M., Department of Earth and Planetary Sciences, The Johns Hopkins University, Baltimore, MD 21218 USA

Introduction

Metamorphic mineral reactions are driven by one or a combination of factors: (1) heat added to or extracted from rock; (2) P-V work performed on rock by its surroundings or *vice versa*; (3) chemical interaction between rock and fluids that are out of equilibrium. The relative importance of the factors may be quantitatively assessed for suites of rock samples by measurement of the progress of the metamorphic reactions.

Theory

The total amount of heat involved during a reaction is:

$$Q = \Delta\bar{H}^{P,T}\xi \qquad (1)$$

where $\Delta\bar{H}^{P,T}$ is the enthalpy of reaction and ξ is measured reaction progress. $Q>0$, heat added to rock; $Q<0$, heat extracted from rock; $Q = 0$, adiabatic metamorphism.

The total amount of P-V work involved during a reaction is:

$$W = -P\Delta\bar{V}^{P,T}\xi \qquad (2)$$

where $\Delta\bar{V}^{P,T}$ is the volume of reaction. $W>0$, work performed on rock by its surroundings; $W<0$, *vice versa*.

If rock is infiltrated by n moles fluid (with X_i^o mole fraction i) and they are out of equilibrium, the relationship between n and progress of the resulting reaction is:

$$n = (\nu_i\xi - X_i^f\xi\Sigma\nu_j)/(X_i^f - X_i^o) \qquad (3)$$

where X_i^f is the mole fraction i in the fluid after reaction, ν_i is the stoichiometric coefficient of i in the reaction, and ν_j is the stoichiometric coefficient of each volatile species (including i) that participates in the reaction. $n>0$, metamorphism driven by chemical interaction of rock with at least n moles fluid; $n = 0$, metamorphism in the absence of fluid-rock interaction.

The cumulative result for more than one reaction in a rock is the sum of Q, W, and n values for individual reactions.

The progress of metamorphic reactions in suites of rock samples may be measured by the change in mode of a reactant or product mineral and/or by the change in the composition of reactant or product mineral solid solutions.

Results and Applications

Most prograde metamorphic reactions are characterized by $\Delta\bar{H}^{P,T}$ and $\Delta\bar{V}^{P,T} > 0$; prograde metamorphism therefore typically is driven by rocks' absorption of heat from their surroundings and by their performing P-V work on their surroundings. The most surprising result is that prograde metamorphism of many rock types in a wide range of metamorphic regimes is also driven by the chemical interaction of rocks with externally-derived fluid that they are out of equilibrium with (i.e., $n>0$). Mineral reactions in contact and regionally metamorphosed impure carbonate rocks are almost universally driven by interaction with aqueous fluids. The active metamorphism of carbonate-cemented sandstones of the Salton Trough is caused by reaction of rock with the geothermal fluids. Contact metamorphism of pelitic rocks in some instances is driven by infiltration of rock by CO_2-rich fluids. Regional metamorphism of sulfidic schists may be caused by interaction of rock with low-S CH_4-H_2O-CO_2 fluids. The amount of fluid involved (n, equation 3) typically is in the range 0.1-5 rock volumes.

A further application of equation (3) is characterization of the flow pattern and flow mechanism of chemically reactive fluids through rocks during metamorphism. In one regional metamorphic terrane in south-central Maine, U.S.A., for example, the time-integrated fluid flux through impure carbonate rocks increased monotonically with increasing grade of metamorphism from 0 to 3 rock volumes. More fluid, however, flowed through rocks while they were under low-grade conditions than under high-grade conditions. Because increasing grade correlates with time, more fluid flowed through rocks at early times in the metamorphic event than at late times. On an outcrop scale fluid flow through some map units was highly channelized. The channelways have been identified as individual lithologic layers that acted as metamorphic aquifers. Surrounding less permeable layers acted as metamorphic aquitards and aquicludes. In contrast, fluid flow through other map units appears to have been relatively pervasive. A linear correlation between the amount of heat absorbed by rocks during metamorphism (Q, equation 1) and the amount of fluid that interacted with them (n, equation 3) suggests that flowing fluids may be an important transport agent of heat during regional metamorphism.

EXSOLUTION AND PHASE TRANSITION IN PYROXENES

FEUER, H., SCHRÖPFER, L., FUESS, H. Institut für Kristallographie und Mineralogie der Universität Frankfurt, Federal Republic of Germany

Exsolution mechanisms and phase transitions in the subsolidus region of quadrilateral pyroxenes were studied by X-ray and electron diffraction at elevated temperatures. The preparation of the synthetic samples is described elsewhere (Schröpfer, 1985). The chemical composition was determined by energy dispersive X-ray analysis. The nomogram of Turnock et al., 1973 using the lattice parameters was applied, too. Microtextures in both synthetic and natural samples from the Ballachulish intrusion (Scotland) were examined by transmission electron microscopy (TEM) in order to elucidate the thermal history.

Precession photographs were taken at temperatures between 700 and 1050°C using a modified single crystal heater. A heating stage was employed in a JEOL JEM 100B microscope and calibrated in the temperature range 400 - 950°C. Sample contamination and temperature gradients introduced considerable uncertainties.

Phase transition in pigeonite

Pigeonite (pig) transforms from a high- (C2/c) to a low- ($P2_1/c$) temperature structure upon cooling. The temperature of this displacive transformation (500-1000°C) depends on the chemical composition (Prewitt et al., 1971) and gives rise to antiphase domains related by 1/2 (a+b). Ion thinned specimens of composition $En_{70}Wo_9Fs_{21}$ and $En_{40}Wo_{18}Fs_{42}$ were heated in the TEM and monitored by their diffraction pattern. The transition is indicated by vanishing of b-type reflections (h+k = odd). Deviations from experimental X-ray results reveal the difficulties of temperature calibration in TEM.

Exsolution

(X-ray) A discontinuous change of the lattice constants for a pig crystal of $En_{64}Wo_{10}Fs_{26}$ at (925 + 15)°C indicates the transformation from low to high pig. In the same temperature range augite (aug) is exsolved parallel (001) and (100) simultaneously.

At constant temperature the aug lamellae parallel (001) grow at the expense of those parallel (100) as a function of time. This is mirrored by the change of the X-ray intensities.

(TEM) A finescale microtexture in pig intergrown with orthopyroxene was identified by HRTEM (200kV). This periodic modulation consists of s-shaped platelets oriented approximately parallel (101) and gives rise to satellite reflections. Lattice images of the platelets are identical with those of lamellar aug exsolution parallel (001) in pig and thus suggest a C-centred structure (aug) for the precipitates. A micro-analytical confirmation of the chemical composition is not available due to their small size (average 5nm).

In addition to these observations of microstructures in synthetic pyroxenes some mineral samples were studied. Aug from Ballachulish monzodiorite exsolves pig parallel (001) and (100). The interfaces are not exactly parallel to the crystallographic planes. The (001) lamellae exhibit an extremity bending to (100) direction which forms an obtuse angle with the (001) stem position. Similar observations were reported by Kitamura et al. (1981) in a Bushveld aug. They propose a morphology change at a certain temperature where the best fitting plane between pig and aug changes from (001) to (100). At present such a model cannot be established from our experiments.

Kitamura M, Yasuda M, Morimoto N (1981) Proc. Japan Acad. 57, Ser B: 183 - 187

Prewitt C T, Brown G E, Papike J J (1971) Proceed. Sec. Lun. Sci. Conf. Vol.1 : 59 - 68

Schröpfer L (1985) Phys. Chem. Minerals 12 : 49 - 54

Turnock A C, Lindsley D H, Grover J E (1973) Synthesis and unit cell parameters of Ca-Mg-Fe pyroxenes. Am Mineral 58 : 50 - 59

FUNDAMENTALS OF A STRUCTURAL-CUM-CHEMICAL APPROACH TO MINERAL SYSTEMATICS

FIGUEIREDO, M.O., Centro de Cristalogr. e Mineralogia, IICT, Al.Afonso Henriques, 41-4ºE, 1000 Lisboa Portugal

In a detailed historical review H. STRUNZ grouped modern mineral classifications into three categories (Procd. 27th IGC, 10, 65/112, 984): chemical-morphological, chemical-structural and genetic-geochemical. It is therefore undeniable that minerals are chemical entities, but the growing interest on mineral physics has enhanced structural features and the extensive knowledge of the crystal structures of most minerals has even brought about the idea of taking the classification of crystal structure-types as a guide-line for mineral systematics. However, such an extreme position seems questionable for two main reasons. Firstly, when dealing with naturally-occurring, crystalline compounds, chemical constitution and crystal structure are indivisible parts of the same reality which also embraces thermodynamic features like the pressure/temperature stability domain; and, secondly, a few natural inorganic solid phases, for long recognized as minerals, are para-crystalline or even amorphous. In fact the state of bonding and the crystal structure-type of a crystalline mineral jointly determine its bulk physical properties, chemical tolerance (isomorphism) and thermodynamic compliance (stability and polymorphism). Furthermore, the local concentration of available chemical components strongly conditions the stable mineral assemblages (parageneses).

What seems advisable in the present state of the Science of Mineralogy is to systematize minerals according to a structural-cum-chemical classification system which must allow the proper inventory in descriptive mineralogy (particularly for teaching purposes) and the easy coding, searching and retrieving of mineralogical data by the use of computers.

The convenience of a mixed approach to mineral systematics was previously emphasized (M.O. Figueiredo, "The interplay of chemical and structural data in the classification of minerals", abstract, 9th European Cryst. Meet., Torino, Italy, 1985).

Based on the definition of "mineral" as "any naturally-occurring inorganic solid phase", a double-entry classification system is now devised according to the following scheme. The chemical entry contemplates the complexity of the mineral as a substance - element or compound - and, for these, the chemical nature of both structural fractions. The cationic fractal (Teilstruktur Kationen, TSK for short) is subdivided into lithiophyllic, chalcophyllic and siderophyllic in accordance with the geochemical trend, and the anionic fractal (Teilstruktur Anionen, TSA) into halogens, oxygen (including OH) and chalcogens (including arsenic and antimony). The structural entry considers first the physical state of the mineral (amorphous or crystalline). For the crystal structure-types, subsequent classification stands on the rank of the structural units - monoatomic in eutactic arrays (in the sense of M. O'Keeffe, 1977, Acta Cryst., A33, 924-927) and multiatomic in condensed arrays, these further subdivided into polycationic, polyanionic and polymeric - and on the internal dimensions of the structure type, that is, the dimensionality of the linkage pattern or bond assemblage (0-D for groups, 1-D for chains, 2-D for sheets and 3-D for frameworks) or else, of the configuration of the bulk TSK in eutactic structural arrangements.

A project on the application of these principles to the implementation of a microcomputer data-base system for minerals - MINDAT - will be described. The present state of the data bank on sulfides and sulfosalts will be briefly reported.

POWDER DIFFRACTION AT THE NATIONAL SYNCHROTRON LIGHT SOURCE BEAM LINE X13A

FINGER, L.W., Geophysical Laboratory, Washington, DC 20008 USA; COX, D.E., Physics Department, Brookhaven National Laboratory, Upton, NY 11973, USA

This white radiation beam line is equipped with a triple-axis spectrometer for a wide range of powder diffraction experiments. The first axis consists of two goniometers with a vertical axis (θ_M-$2\theta_M$) carrying a horizontal scattering arm about 2 m in length mounted on air pads. The scattering arm supports a moveable sled on which is mounted a 4-circle diffractometer with horizontal sample (θ_S-$2\theta_S$) and analyzer (θ_A-$2\theta_A$) axes for scattering experiments in the vertical plane. To facilitate safe alignment and positioning of samples, the first axis contains an automated goniometer head with computer control over rotations and translations.

With this instrument three different kinds of powder experiment can be conducted. The first involves a monochromatic beam and an analyzer crystal, which serves as a very narrow "angular" receiving slit. The d-spacing of this perfect crystal can be chosen to optimize the scattering angle at which the focussing minimum occurs. For general work a Ge (111) monochromater and Ge (220) analyzer appear to be most useful. At a wavelength of 1.3 A, the focussing minimum is observed for 2θ approximately 20° with a full-width at half-maximum (Γ) of roughly 0.015° (about a factor of 10 smaller than for a conventional diffractometer). It is possible, therefore, to resolve very small deviations from an ideal symmetry. Figure 1 demonstrates the resolution obtained for a synthetic zeolite. In this case, sample effects limit Γ to 0.04°; however, the right hand peak can be seen to be a doublet. With peak fitting techniques, the separation is found to be 0.036°. The high resolution and peak-to-background ratio (≈3000:1 for (111) of CeO_2) make the apparatus extremely useful for determination and refinement of crystal structures from powder data.

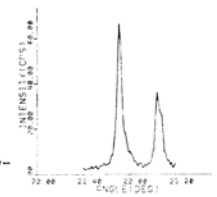

Figure 1

A second type of experiment involves energy-dispersive diffraction with a solid-state detector, an arrangement particularly useful for analysis of samples with limited x-ray access, such as a diamond anvil cell. Because there may be a large pressure gradient in the sample area, the apparatus includes computer controlled slits that permit the incident beam to be as small as 10 μm. As the beam size is diminished the relative volume of diamond to that of the sample in the incident beam increases. As a result the signal-to-noise ratio is decreased. Furthermore the background is highly curved, which complicates the extraction of diffraction peaks. An aperture of 100 μm in the diffracted beam path enhances the signal-to-noise ratio by a factor of 5, which makes it possible to analyze small volumes of material with low scattering power. Figure 2 illustrates the enhancement obtained for gold at 300 kbar. The P/B was increased from 1.5 to 5.1. Note the effect on the peak at 28 keV.

The third type of experiment involves energy-dispersive diffraction with a crystal analyzer. This technique has much higher resolution than the solid-state detector at a reduced intensity and longer counting times.

Beam time on the facility described in this abstract will be available for general users in the near future. Interested individuals should contact the authors regarding details of submission of proposals.

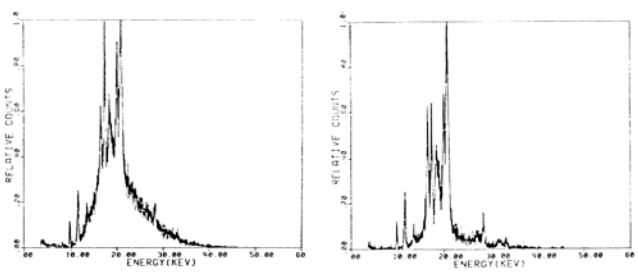

Fig. 2a. Large Aperture. 2b. Small Aperture.

POKROVSKITE: ITS POSSIBLE RELATIONSHIP TO MCGUINNESSITE AND THE PROBLEM OF EXCESS WATER

FITZPATRICK, J. J., U.S. Geological Survey, Denver, CO 80225, USA

Pokrovskite ($Mg_2(CO_3)(OH)_2 \cdot 0.5H_2O$) was originally described by Ivanov et al. in 1984. At that time, this mineral had been found at several North American localities, but no descriptions were published then or since.

Pokrovskites from four North American localities have been investigated in this study: Sonoma Co., Calif.; Jackson Co., N.C.; Montgomery Co., Md.; and Baltimore Co., Md. All occurrences are within ultramafic bodies of dunite or serpentinite, and associated minerals are other hydrous magnesium carbonates and silicates. Material from three of the four occurrences was examined in detail to characterize chemistry, thermal behavior, optics, IR spectral characteristics, and crystallography.

Chemical analyses (Table I) yield varying values for H_2O^+. Heating at 110°C for 10 hours fails to dislodge any of this water, indicating that it is in some way bound into the structure. High values for total iron in the North Carolina material suggest that an Mg-Fe solid solution series is possible. The highly similar cell parameters of rosasite family members and pokrovskite (Table II) suggest that pokrovskite is a member of that family. Its compositional and apparent structural similarity to mcguinnessite, $(Mg,Cu)_2(CO_3)(OH)_2$, lead to questions regarding the nature of the reported excess water in pokrovskite. A recent refinement of the structure of rosasite (J. Szymański, CANMET, oral comm., 1986) indicates no likely site for this water. Although there is no doubt that this water is present, from both chemical analysis and TGA data, the question of whether or not it is essential to the structure remains open. Dehydration experiments currently being conducted will determine if pokrovskite is equivalent to end-member mcguinnessite.

References

Erd, R. C., Cesbron, F. P. Goff, F. E., and Clark, J. R., 1981, Mcguinnessite, a new carbonate from California. Min. Record, v. 12, no. 3, p. 143-147.

Ivanov, O. K., Yu. A. Malinovskii, and Yu. V. Mozherin, 1984, Pokrovskite, $Mg_2(CO_3)(OH)_2 \cdot 0.5H_2O$, a new mineral from the Zlatagorskaya layered intrusive, Kazakhstan, Zapiski Vses. Mineralog. Obsh., v. 113, no. 1, p. 90-95.

Jambor, J. L., 1976, Studies of basic copper and zinc carbonates: three powder X-ray data for zincian, malachite, rosasite, and cobalt analogues. Geol. Sur. of Can., Paper 76-1C, p. 97-105.

TABLE I Chemical Analyses of Pokrovskites

	Kazakhstan* USSR	Montgomery Co. Md.	Sonoma Co. Calif.	Jackson Co. N.C.
CaO	0.39	0.24	0.07	0.61
MgO	50.80	51.73	45.9	44.93
MnO	1.02	1.76	2.8	0.45
FeO	---	2.23	2.1	6.97
Fe_2O_3	1.90 (total Fe)	0.56	2.45	3.82
CO_2	28.78	30.1	29.8	29.1
H_2O^-	0.44	0.06	0.56	0.06
H_2O^+	16.72	14.3	16.2	14.3
H_2O^{+**}	---	14.3	16.2	14.5

* Ivanov et al. (1984)
** Re-analyzed after holding sample at 110°C for 10 hours

TABLE II Lattice Parameters for Pokrovskites

	Rosasite[1]	Mcguinnessite[2]	Pokrovskites USSR[3]	Montgomery Co Md.[4]	Jackson Co N.C.[4]
a	9.344	9.398	9.43	9.348	9.360
b	12.069	12.011	12.27	12.180	12.158
c	3.392	3.379	3.395	3.378	3.400
β	90.48°	93.28°	96.6°	96.01°	95.45°
V(Å^3)	382.5	380.8	390.1	382.5	385.1

[1]Jambor (1976); [2]Erd et al. (1981); [3]Ivanov et al. (1984); [4]this study

DISORDERED PHENACITE STRUCTURES OF α-$LiGaSiO_4$ and α-$LiGaGeO_4$

FLEET, M.E. and ARIMA, M., Dept. of Geology, University of Western Ontario, London, Ontario N6A 5B7, Canada

α-$LiGaSiO_4$ and α-$LiGaGeO_4$ have disordered phenacite (Be_2SiO_4) crystal structures, with analogous structural formulae of $(Li,Si)_2Ga_4$ and $(Ga,Ge)_2Li_4$, respectively.

Ga- and Ge-substituted eucryptite compositions have been crystallised using a lithiumvanadomolybdate flux and cooling over the temperature interval 1000 to 600°C at 1°/h. Prismatic single crystals have maximum dimensions of 0.4x0.8 mm (α-$LiGaSiO_4$), 0.1x0.4 mm (α-$LiAlGeO_4$), and 0.3x4 mm (α-$LiGaGeO_4$). Crystal structures were determined by refinement of X-ray reflection data ($2\theta \leq 80°$, Mo Kα) in space group $R\bar{3}$:

Column of tetrahedra parallel to c

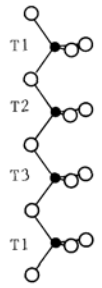

site	Tetrahedral site occupancies phenacite	α-$LiGaSiO_4$	α-$LiGaGeO_4$
T1	Si	Ga	Li
T2	Be(I)	Li,Si	Ga,Ge
T3	Be(II)	Li,Si	Ga,Ge
	α-$LiGaSiO_4$		α-$LiGaGeO_4$
a	13.6392(7)Å		13.9357(6)Å
c	9.0948(5)		9.2957(4)
<T1-O>	1.778Å (Ga-O)		1.944Å (Li-O)
<T2-O>	1.671 (Si-O)		1.771 (Ge-O)
	1.987 (Li-O)		1.821 (Ga-O)
<T3-O>	1.678 (Si-O)		1.774 (Ge-O)
	1.946 (Li-O)		1.820 (Ga-O)
R (%)	8.1		5.6

The present study has confirmed the network-forming role of Li in the crystal structures of Ga- and Ge-substituted eucryptite compositions. In fact, LiO_4 tetrahedra are only slightly distorted from ideal geometry. The disorder of Si and Li in the T2 and T3 positions of α-$LiGaSiO_4$ was unexpected but may be attributed to spatial accommodation within the network. Study of flux-grown $LiAlGeO_4$ and $LiAlSiO_4$ compositions is in progress.

IRON - MANGANESE PHOSPHATE ASSOCIATIONS FROM PEGMATITES OF RWANDA AND NAMIBIA.

FONTAN, F., Laboratoire de Minéralogie, Université de Toulouse, Allées Jules-Guesde 39, F-31400 Toulouse, France; FRANSOLET, A.-M., Institut de Minéralogie, Université de Liège, Bât. B18, Sart Tilman, B-4000 Liège, Belgium; KELLER, P., Institut für Mineralogie und Kristallchemie, Universität Stuttgart, Pfaffenwaldring 55, D-7000 Stuttgart 80, Fed. Rep. Germany.

New chemical analyses on Fe-Mn phosphates from the Buranga and the Nyiramuganza pegmatites, Rwanda, have been performed. On the basis of both all presently available chemical data and the petrographic relationships, we can portray the evolution sequences of these phosphate associations, where the relatively large variation range of the Fe/Mn ratio in the major phosphates is certainly in connection with the fractionation degree of the pegmatites and implies several generations of the $Li(Fe,Mn)PO_4$ phases. From a general point of view, the results are similar with those, which are known so far from other pegmatites. However, owing to the detailed investigation, some typical associations and a few mineralogical aspects have to be pointed out and are compared with other phosphate occurrences in African pegmatites.

Concerning the well-known oxidation sequence, triphylite → ferrisicklerite → heterosite, it seems that the incipient replacement of the mother phase by ferrisicklerite is always characterized by similar relationships showing exsolution lamellae of ferrisicklerite within triphylite, whereas the textural relationships between ferrisicklerite and heterosite are less regular. If we consider the chemical bulk composition of the three zones, mainly consisting of triphylite, of ferrisicklerite, and of heterosite respectively, from various pegmatites (Buranga and Nyiramuganza, Rwanda; Tsaobismund and Harmonie, Namibia), we systematically observe in increase in the CaO, Na_2O, K_2O, and H_2O (wt %) contents. A particular attention has been drawn about the geochemical behaviour of Zn in this sequence.

The hypothesis on several generations of alluaudites s.l. within a pegmatite tends to be confirmed (Fransolet, 1977; Fransolet et al., 1986). We have investigated Al-rich alluaudite (wyllieite ?) in close association with triphylite, as well as alluaudite s.s., rimming the masses of ferrisicklerite-heterosite in the Buranga mine. Additionally we have detected graphic-like structures showing arrojadite grains armoured by Al-bearing alluaudite. An oxidation sub-sequence of alluaudite frequently occurs. We have observed it by both chemical and optical analyses. In several cases, the alluaudite aggregates show replacement processes (pseudomorphs) mainly by phosphosiderite, and also by landesite s.l. to a certain extend.

References:

Fransolet, A.-M., 1977, Le problème génétique des alluaudites. Bull. Soc. fr. Minéral. Cristallogr.100, 348-352.

Fransolet, A.-M., Keller, P. and Fontan, F., 1986, The phosphate mineral associations of the Tsaobismund pegmatite, Namibia. Contrib. Mineral. Petrol. (in press).

REASSESSMENT OF THE TURQUOISE GROUP: REDEFINITION OF PLANERITE, $(\square)Al_6(PO_4)_2(PO_3OH)_2(OH)_8 \cdot 4H_2O$ AND AHEYLITE, $FeAl_6(PO_4)_4(OH)_8 \cdot 4H_2O$, A NEW MEMBER OF THE GROUP

FOORD, EUGENE E., and TAGGART, JOSEPH E., U.S. Geological Survey, Box 25046, Denver Federal Center, Denver, CO. 80225, USA

The mineral species turquoise and additional known and newly defined or redefined members of the turquoise group have been studied in detail to resolve existing problematical mineralogical aspects: the structural formula, variable chemistry, oxidation states of iron present, site occupancies, IR-spectral characteristics, and X-ray diffraction properties.

Currently, turquoise (Cu-Al), faustite (Zn-Al), chalcosiderite (Cu-Fe), and coeruleolactite (Ca-Al) are accepted as valid species members of the turquoise group. Planerite ($\square$-Al), and aheylite (Fe-Al) have been accepted by the IMA and are discussed here. The general structural formula for the group is shown to be: $A_1B_6(PO_4)_{0-2}(PO_3OH)_{0-2}(OH)_8 \cdot 4H_2O$ where A = $\square$, Cu, Fe, Ca, Zn and B = Al, Fe, Cr. A ferrous-ferric, $FeFe_6(PO_4)_4(OH)_8 \cdot 4H_2O$ member exists (A. Mucke, written commun., 1984), but the name has not been approved by the IMA CNMNMN. (Zn-Fe), (Ca-Fe) and ($\square$-Fe^{3+}) members may exist in nature, and should be looked for.

Planerite was originally described in 1862 by R. Hermann, from the Gumeshevsk copper mines in the Ural Mountains, U.S.S.R. He defined it as containing ferrous iron, but analyses of six planerite samples from the Gumeshevsk area (one entered into the collections of the British Museum in 1864) show that the mineral is characterized by having the A site vacant or nearly so. A structural formula for the recently established holotype specimen R9710 (USNM) calculated on the basis of 6 Al atoms and 8 (OH) groups is: $(\square_{0.98}Cu_{0.02})_{\Sigma 1.00}Al_6(PO_4)_{2.11}(PO_3OH)_{1.96}(OH)_8 \cdot 3.96H_2O$. Cell data are: a 7.505(2)A, b 9.723(3)A, c 7.814(2)A, α 111.43°, β 115.56°, γ 68.69°, V = 464.2(1)A^3, Z = 1. D_m = 2.68(5) g/cm^3, D_c = 2.71 g/cm^3. Thermogravimetric analyses indicate three discrete weight loss events: (1) 170-200°C (H_2O), (2) 280-300°C (OH), and (3) 340°C (PO_3OH). Data for turquoise show only two weight loss events: (1) 220°C (H_2O) and (2) 325°C (OH). Mössbauer spectroscopy studies of three planerites from Gumeshevsk indicated that what little iron was present was ferric and not ferrous. Charge balance in planerite is maintained by protonation of two of the four phosphate groups. The possible presence of hydronium (H_3O^+) substituting into the A site has not been ruled out, but even this could account for a maximum of only half of the loss of divalent cations.

Aheylite is defined as the ferrous-iron-dominant (A site) member of the turquoise group. The mineral occurs associated with cassiterite, pyrite, quartz, sphalerite, variscite type L, variscite type M, wavellite, and vivianite in ore samples from the Mira Flores vein system, District of Huanuni, Dept. of Oruro, Bolivia. Individual spheres of aheylite are as much as 2 mm across and are very pale blue green to light blue green. The botryoidal spheres are made up of euhedral radiating and concentric aggregates of crystals as much as several microns in maximum dimension. Cell data are: a 7.408(2)A, b 9.891(1)A, c 7.627(2)A, α 110.94°, β 115.05°, γ 69.89°, V = 460.3(9)A^3, Z = 1. The calculated structural formula is: $(Fe_{0.46}Zn_{0.40}\square_{0.14})_{\Sigma 1.00}Al_6(PO_4)_{3.72}(PO_3OH)_{0.28}(OH)_8 \cdot 4.10H_2O$.

A 'half-empty' planerite-aheylite gave: $(\square_{0.50}Fe^{2+}_{0.35}Zn_{0.15})_{\Sigma 1.00}Al_6(PO_4)_{3.07}(PO_3OH)_{1.00}(OH)_8 \cdot 4.01H_2O$. Mössbauer spectroscopy indicated that the iron present is all ferrous.

'Coeruleolactite' from General Trimble's mine, East Whiteland Township, Chester County, Penna., is a planerite-turquoise with the A site nearly half-filled with Cu and minor Zn. Individual 4-10μ-sized euhedral crystals compose botryoidal encrustations associated and mixed with L-type variscite, wavellite, rare matulaite, gibbsite, cacoxenite, goethite, and limonite. Cell data for the material are: a 7.529(9)A, b 9.951(10)A, c 7.782(10)A, α 112.51°, β 116.54°, γ 68.57°, V = 468.4(8)A^3, Z = 1.

Compilation of available superior analyses for members of the turquoise group indicate the existence of continuous solid-solution series between the various end-members. Purity of the 16 completely analyzed members of the turquoise group was checked by SEM, electron microprobe, TGA, and X-ray diffraction methods. only a very small amount of what is currently termed turquoise actually contains Cu as the principal constituent of the A site. Planerite and cation-deficient turquoise are more common than currently recognized.

True planerites may be easily distinguished from other members of the turquoise group by (1) color and (2) X-ray diffraction characteristics.

GRAIN SIZE ANALYSIS OF CASSITERITE AND RELATED MINERALS GRAINS OF ALLUVIAL PLACER DEPOSITS.

FORT,R.,Inst. Geología Económica. CSIC. Fac. de Geología. Univ. Complutense. MADRID 28040 (Spain); ORDOÑEZ,S.,Dto de Petrología. Fac.de Geología. Univ.Complutense.MADRID 28040, (Spain)

Size analysis were made using twenty bulk samples of ancient (Quaternary) and present day alluvial deposits related with a cassiterite-ilmenite stockwork in monzonite granites, vein-like quartz-cassiterite on shales and arkoses with very scarce cassiterite-ilmenite deposits. The minerals were separated from the sized fractions by use of heavy liquids and magnetic separator methods. The weights of the original size fractions (light minerals) and the weights of separed heavy minerals were the bases for the size-distributions presented here. The weights of heavy minerals fractions are measured microscopically, with density and performing shape corrections.

Theoretical considerations about cumulative curves of heavy minerals and related light minerals (quartz) may be made on Hydraulic Equivalence Values (H.E.V.):

	1	2		1	2
Cassiterite	0.93	0.58	Andalucita	0.11	0.06
Ilmenite	0.58	0.39	Apatito	0.22	0.15
Monacite	0.63	0.42	Turmalina	0.17	0.11
Anatase	0.40	0.27	Zircon	0.58	0.39

1- Stokes Law. 2- Impact Law

The results of an averange of size distributions showed that actual values are not in agree with theoretical considerations supported by H.E.V. Standad desviation values are related with primary ore types (stockwork or vein-like)(fig. 1) and median size values are related with the size of primary ores (fig. 2). It was the result of a scarce evolution of hydrodinamic features of sediments on a ephemeral stream network.

The size analysis of this detrital heavy minerals suggest that the sedimentological data can be useful in designing recovery processes and interpreting nature and primary ore origin of many placer deposits.

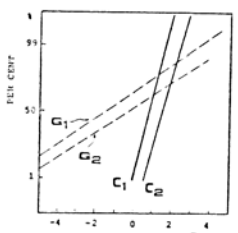

Q_1- Quartz from Vein-like
Q_2- Quartz from stockwork
C_1- Vein-like cassiterite
C_2- Storkwork cassiterite

Fig. 1

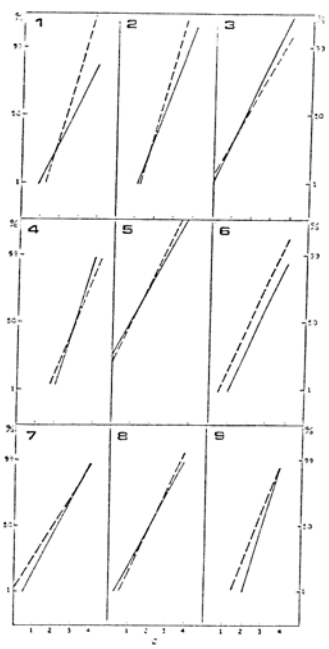

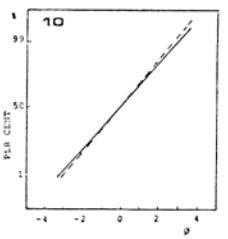

Fig. 2- 1-Anatase, 2- Andalucite, 3- Apatite, 4-Zircon, 5- Black tourmaline, 6- Green tourmaline, 7- Cassiterite, 8- Ilmenite 9- Monazite, 10- Quartz.

---- Modern Alluvium —— Ancient Alluvium

NEW DATA AND RELEVANT OBSERVATIONS ON THE COMPLEX ALUMINIUM PHOSPHATE ASSOCIATIONS FROM LI-RICH PEGMATITES OF THE GATUMBA FIELD, WESTERN RWANDA.

FRANSOLET, A.-M., Inst. of Mineralogy B18, University Liège, Sart Tilman, B-4000 LIEGE, Belgium.

The existence in the Buranga mine of oxidized triphylite associated with montebrasite, as well as the variable Al contents in the alluaudites s.l., has prompted us to carry on a detailed investigation of the Al-rich phosphate associations occurring both in the Buranga and in the Rusororo pegmatites in order to compare finally their hydrothermal alteration and weathering processes with those, which are known for the Fe-Mn phosphate associations. As the mineral identification and the interpretation of the petrographic textures are more fastidious than in the case of the Fe-Mn phosphates, it has been decided to present some relevant mineralogical problems, encountered at the outset of this investigation.

The wet chemical analyses and the X-ray diffraction control, systematically performed on minerals of the amblygonite-montebrasite series occurring in this pegmatite field, show that, when a content of 0.2 wt% Na_2O is chemically determined, an impurity appears on the powder pattern. Owing to a specimen from Buranga with up to 2.05 wt% Na_2O, the additional phase turns out to be identified as lacroixite. By combining both the microprobe technique and the wet chemical analyses, it can be demonstrated that lacroixites from Buranga and Rusororo contain Li and OH. The idealized formula for the Buranga lacroixite, which occurs as minute exsolved grains in montebrasite with a chess-board texture, is $(Na_{0.8}Li_{0.2})AlPO_4(F_{0.6}OH_{0.4})$; for the Rusororo mineral, intimately associated with berlinite in a polygranular texture, both replacing montebrasite, the formula is $(Na_{0.6}Li_{0.4})AlPO_4(F_{0.6}OH_{0.4})$.

The substitutions Na Li and F OH in lacroixite are discussed implying comparisons with the amblygonite-montebrasite series, and particularly with natromontebrasite. The low contents of the transition metal cations detected in lacroixite are also compared with these detected in the other major Al phosphates. Some comments are made about the very restricted substitution of Fe for Al in these phosphates from the two pegmatites, such as montebrasite, trolleite, brazilianite, augelite, and bertossaite, in contrast with the possible complete solid solution known as far, for instance, in the wardite-cyrilovite series or in the variscite-strengite series occurring in near-surface weathering environments.

It seems that the excess of Fe, Mn, and Mg precipitates as scorzalite and/or as wyllieite within the masses of montebrasite and of trolleite. The oxidation of wyllieite, $Na_2Mn(Fe^{2+}Al)(PO_4)_3$ as bottle green specks rimmed by scorzalite in trolleite, into brown rosemaryite, $NaMn(Fe^{3+}Al)(PO_4)_3$, which finally is deeply altered into a mixture of pink variscite, yellow brown childroeosphorite, and cryptomelane, represents a short sequence of the evolution in the Al phosphate associations, which can serve as a first reliable element for the comparison with the evolution of the Fe-Mn phosphate associations.

VANADIUM INCORPORATION IN PURE SILICA GLASSES: VANADIUM SEGREGATION AND TETRAHEDRAL COORDINATION

FRITSCH, E., Lab. Mineralogie-Cristallographie, T16-26, 4, Place Jussieu, 75230 Paris Cedex 05, France. Present address: Gemological Institute of America, 1660 Stewart Street, Santa Monica, CA 90404, USA

Past studies have suggested that vanadium is octahedrally coordinated in a variety of multicomponent glasses. No attempt has been made to describe its structural behavior in pure silica glass, and such information is needed to indicate how high-valence cations — V^{4+} and possibly Ti^{4+} — enter the strongly covalent glassy silica framework.

A series of well characterized silica glasses have been prepared in air with vanadium contents ranging from 100 to 700 ppm weight. Chemical analyses show the coexistence of V^{4+} and V^{5+}, which are in roughly equivalent proportion for dopant concentrations of 400 to 700 ppm.

X-ray Absorption Near Edge Structure (XANES) demonstrates that all the vanadium in silica glass is tetrahedrally coordinated. For V^{4+}, this contrasts with the coordination as observed in the usual vanadyl complex.

Electron Spin Resonance (ESR) and optical absorption results obtained on blue samples of V-doped silica glasses have been interpreted in terms of interaction between V^{4+} and V^{5+}. In contrast with multicomponents glasses, vanadium impurity is not dispersed, but rather is segregated in small clusters. Long range InterValence Transfer (IVT) occurs, enhancing the d-d transitions and creating two strong absorption bands in the near infrared at 10800 and 8600 cm^{-1}. Similarly, as temperature is increased, the ESR spectra exhibits a characteristic change from localized spins at 7K to electron delocalization at 300K and more.

In conclusion, the high-charge ions V^{4+} and V^{5+} strongly polarize the oxygen ligands in SiO_2 glass and therefore, compete with the Si-O covalent bonding. Minimizing the interaction energy leads to the formation of clusters containing chains of at least three vanadium ions of both valence states. This is the first time that such a charge transfer mechanism has been described for trace vanadium in glasses. This phenomenon could also be of interest in studies of coloration in some vanadium-bearing minerals.

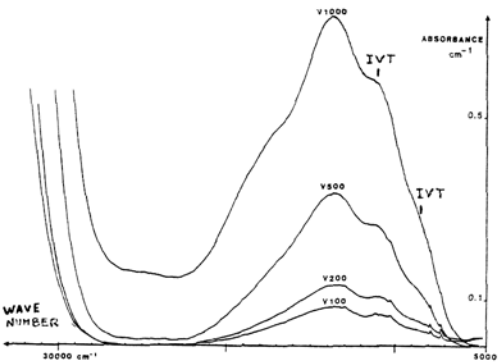

Optical absorption spectra of vanadium doped silica glasses showing the two InterValence Transfer (IVT). V100 = 110 ppm wt. V; V200 = 150 ppm wt. V; V500 = 265 ppm wt. V; V1000 = 710 ppm wt. V.

ESR spectrum of V1000 at 6K. Hyperfine structure is still hindered by delocalization.

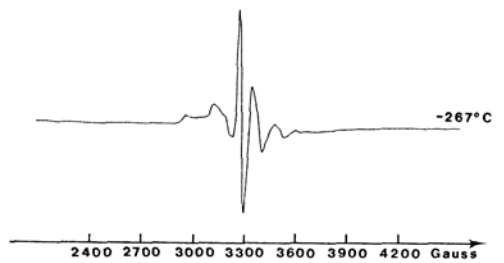

THE DISTRIBUTION OF SILVER IN THE ELURA Pb-Zn-Ag ORE DEPOSIT IN NEW SOUTH WALES, AUSTRALIA

FROST, M.T., HARROWFIELD, I.R., MacRAE, C.M., and TSAMBOURAKIS, G., CSIRO Division of Mineral Chemistry, P.O. Box 124, Port Melbourne, Victoria 3207, Australia.

The deposit is situated in a Devonian sequence of sandstones and siltstones that accumulated in the Cobar trough. Elura mineralization occurs at the northern end and the orebody itself is a discrete, crudely elliptical, vertical pipe-like body with maximum dimensions of 210 by 115 m. At the top the orebody divides into two and is oxidized completely above the 98 m depth. Mining commenced in the early 1980s with reserves of 27 million tonnes that contain 5.6% Pb, 8.6% Zn and 135 ppm Ag.

The ore consists of a complex assemblage of sulphides (galena, sphalerite, pyrite, pyrrhotite, chalcopyrite, arsenopyrite and freibergite), siderite and silicates (1). A central core, consisting of pyrrhotite rich ore, is surrounded by two pyrite-rich and pyrrhotite-poor zones, the outer of which is siliceous.

Detailed studies reveal that there is considerable variation in texture and mineralogical composition and that there is a relationship between texture and the minor and trace elements of the sulphides. Bulk Ag from 63 ore samples varies from 729 to 22 ppm. High Ag values are found in the upper regions in the siliceous or pyritic ore. There is a general decrease in Ag with depth and the pyrrhotitic ore at any level contains relatively lower levels of Ag. Mineralogically there are the following three main factors, illustrated in the accompanying figure, which account for this variation.

(1) The Ag content of galena. Electron microprobe methods were developed which enabled Ag and other elements (e.g., Sb, As, Mn, Cu) to be analyzed in sulphides with detection limits down to 10 ppm. Silver content varies from over 1400 to less than 20 ppm in a coupled substitution with Sb. Low Ag

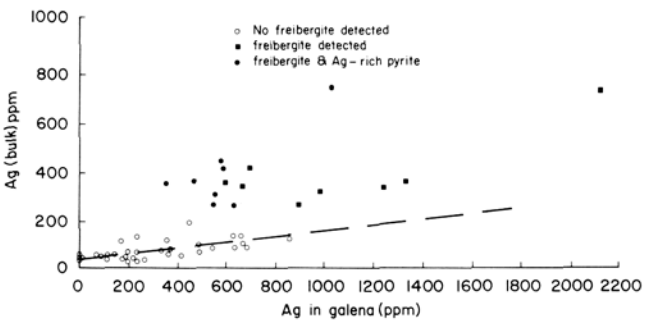

contents occur in galena associated with the pyrrhotite ore and at depth.

(2) The Ag content in pyrite. The texture of pyrite and the abundance of impurities varies considerably. Several thousand point analyses revealed that Ag, As, Sb, Cu and Mn occur in a zoned pyrite in significant proportions (e.g., mean Ag values in pyrite in the siliceous ore of the upper orebody sometimes exceed 300 ppm). Very low levels of Ag and other minor elements occur in texturally distinct pyrite that is either associated with pyrrhotite or found at depth.

(3) Freibergite content. Small (<0.2%) amounts of freibergite (16 to 21 wt.% Ag) are present in the upper parts of the ore body.

Automatic SEM-based methods have been developed to measure the proportions of minor arsenopyrite, chalcopyrite and freibergite. Analysis so far suggests that their abundances are not correlated and the factors which control the occurrence of freibergite are not those that control As and Cu-mineralization.

(1) Schmidt, B.E., 1980. Geology of the Elura Ag-Pb-Zn deposit, Cobar District, N.S.W. MSc Thesis, ANU, Canberra.

The work has been supported by Electrolytic Zinc Pty Ltd.

BASALT-GRANODIORITE MAGMA INTERACTION DURING CRYSTALLIZATION OF THE LAMARCK GRANODIORITE, EASTERN SIERRA NEVADA, CALIFORNIA: FIELD EVIDENCE AND RHEOLOGIC MODELLING

FROST, T.P., U.S.G.S., 345 Middlefield Rd., Menlo Park, CA 94025, and Dept. of Geology, Stanford University, Stanford, CA 94305, USA; MAHOOD, G.A., Dept. of Geology, Stanford University, Stanford, CA 94305, USA

Evidence of magma interaction resulting in both hybridization and mingling is preserved in a diverse suite of gabbroic to intermediate rocks associated with the compositionally zoned hornblende-biotite Lamarck Granodiorite of the eastern Sierra Nevada, California. Ellipsoidal mafic inclusions (50.1-52.5% SiO_2) formed by quenching of small amounts of high-alumina basalt magma in granodiorite magma early in its cooling history, when crystallinity and viscosity were relatively low. Discrete synplutonic intrusions of hornblende gabbro through hybridized mafic granodiorite (48.2-63.5% SiO_2) crosscut regional trends in foliation and compositional zoning in the host pluton (58.0-71.2% SiO_2). The intrusions are preserved because they were emplaced when the granodiorite magma was largely crystallized and its viscosity was extremely high. Local partial melting of crystals entrained in the felsic magma lowered its viscosity upon attaining thermal equilibrium with the intrusions. Where compositional contrasts between intrusion and host granodiorite are large, mingling dominated; contacts are sharp and abundant mafic inclusions derived from the intrusion are present in the granodiorite. Where the host is relatively mafic (58-62% SiO_2) or where the local-scale proportion of mafic magma is large, the contact is an extensively hybridized zone as wide as 200 m with both hybrid schleiren and inclusions. Unhybridized intrusions have compositions similar to the ellipsoidal inclusions, whereas hybridized intrusions have silica contents as high as 63.5%. Linear least-squares correlation coefficients between major oxides and SiO_2 for inclusions, mafic intrusions, hybrids, and granodiorite with less than 65% SiO_2 are greater than 0.92, with the exception of Na_2O and K_2O, which supports a magma interaction model. Late magmatic replacement of hornblede by biotite and deuterically altered plagioclase are evidence for alkali mobility. Linear trends on variation diagrams support a mixing origin for the suite, but the linear trends can be reproduced by fractional crystallization as well. Least-squares coefficients are not as high for magmas with greater than 65.0% SiO_2, suggesting that fractional crystallization is the dominant process in producing the more silicic part of the suite.

The mafic intrusions locally contain coarse-grained hornblende gabbro inclusions with compositions indicative of cumulate origin that were entrained from deeper crustal levels.

Mafic schleiren are present throughout the granodiorite. Those spatially associated with mafic intrusions have compositions that lie on the linear trends for the inclusions, intrusions, and hybrids. Mafic schlieren some distance from the intrusions have compositions that indicate they are localized accumulations of mafic minerals.

Late diorite dikes intruding the nearly crystallized granodiorite heated, mobilized, and entrained residual melt of granite-minimum composition. Quenching of the diorite magma upon reaching thermal equilibrium with the granite melt in the dikes formed pillows in a manner analogous to the inclusions in the granodiorite. Intrusion of the composite dikes to higher levels in the pluton was permitted by the lowering of viscosity of the aplite by release of latent heat of the diorite magma upon crystallization.

Whether interacting magmas mix or mingle is a function of the heat contents and mass fractions of the end members. We have modelled the viscosities of the interacting magmas upon reaching thermal equilibrium, accounting for major-element compositions, heats of fusion, heat capacities of liquids and crystals, and a range of initial temperatures, crystallinities, crystal sizes, and magma water contents. The results of the modelling suggest that dry basalt and granite-minimum melts near their liquidi can hybridize at nearly all proportions. Mafic and felsic magmas with crystallinities and water contents typical for the upper crust are likely to hybridize only if the compositional difference between host and injected mafic magma is less than 10% SiO_2 or the mass fraction of mafic magma is greater than 0.5. Hybrids predicted under these conditions are tonalites or mafic granodiorites. Thermally equilibrated mixtures of granite and intermediate magmas have high viscosities due to the high intrinsic viscosities of the endmembers and the lower heat contents of intermediate magmas, as compared to basalt magma. These results suggest that rocks with greater than 65% SiO_2 are products of crystal fractionation of mafic to intermediate magmas, which may themselves be hybrids, and that the full range compositions in calc-alkaline suites is unlikely to be strictly a product of magma mixing between basalt and granite-minimum melts.

DATABASE RETRIEVAL AND CARD IMAGE DISPLAY OF MINERALS FROM THE LEVEL III JCPDS MINERAL SUBFILE

D. R. Fuchs, Aleph Enterprises, PO Box 213, Livermore, California 94550, USA

The new JCPDS Level III Mineral Subfile in digital format contains all the information present on the traditional JCPDS card. We have developed a system that will search this database on an IBM PC or AT using information input by the user. It is possible for the user to enter data for density, crystal system and the presence or absence of one or more elements and get a list of all the minerals in the file that meet these criteria. Other search parameters can also be used, either alone or in combination with other data to limit the number of minerals in the final list. One possible example of such use would be to search for all minerals that have a density between two limiting values, are cubic, and contain one or more elements. It is also possible to locate a given mineral by just specifying the JCPDS number or the mineral name.

Once a possible species is located it is possible to display the complete data for that JCPDS entry on the screen in a format very similar to that used for the JCPDS cards. The graphics display of the data includes greek letters, diacritical marks, etc. just as one would see them in the JCPDS mineral book or on the JCPDS cards, making it both easy to find various parameters for a given species and to read and interpret them once found.

Both the searching capability and the card display aspects of the system will be demonstrated and problems submitted by attendees are welcome.

THE CHARACTERISTICS OF FINE PARTICULATES IN NATURAL SYSTEMS

FYFE, W.S., and K. TAZAKI, Dept. of Geology, University of Western Ontario, London, Canada N6A 5B7

The understanding of surface adsorption processes which is fundamental to aquatic chemistry depends heavily on the nature of fine particles. Particles with sizes in the 100 A range are commonly produced by weathering and biological processes. Examples will be drawn from clay precursors, and mineral products formed by bacteria and algae. For characterization high resolution TEM is essential. The stability of such ultrafine materials is difficult to understand in terms of conventional treatment of their chemical potential. Surface complexing, particularly by organic molecules may be indicated and may be involved in the processes linking transitions from simple ions, to complexes, to clusters (nucleii), to crystals. Understanding the nature and distribution of such materials in natural systems is essential to the understanding of sorbtion processes as for example in nuclear waste disposal.

MAGNETIC PHASE TRANSITION IN THE OLIVINES Fe_2SiO_4, Mn_2SiO_4 AND Co_2SiO_4.

FUESS, H., BALLET, O., LOTTERMOSER, W., Institut für Kristallographie und Mineralogie der Universität Frankfurt, Federal Republic of Germany

The silicates of Fe, Mn and Co with the olivine structure type (space group Pnma) order antiferromagnetically at low temperatures. The magnetic spin structures and their evolution with temperature from 4.2K to the Néel temperature T_N were determined by neutron diffraction measurements on single crystals. The two crystallographic sites M1 and M2 show quite different behaviour. Whereas the spins on M2 are parallel to one crystallographic axis a canting angle between the spin direction on M1 and the crystallographic axes is observed. The magnetic moments on the two sites have different values.

The magnetic structure in Fe_2SiO_4 has spins parallel to $\vec{b}$ (M2) and a canting away from $\vec{b}$ is observed which is essentially inclined towards $\vec{a}$. This canting angle subsists over the whole temperature range below T_N = 65.3K but shows a continuous decrease in value. The magnetic moments are almost equal at 4.2K but they decrease with increasing temperature and the moment of M1 is smaller than that of M2 over the whole temperature range (Lottermoser et al. 1986). Additional Mössbauer measurements in the antiferromagnetic state support these results (Lottermoser, 1986). The interpretation of the neutron data for Mn_2SiO_4 revealed spins parallel to the $\vec{a}$ - axis for M2 and canting angles with components along $\vec{b}$ and $\vec{c}$ for M1. With increasing temperature the canting angle diminishes and the spins are parallel to $\vec{a}$ at about 20K. The magnetic structure remains collinear between 20K and T_N = 47.1K. Neutron powder diffraction on solid solutions of $(Mn,Fe)_2SiO_4$ demonstrated that the order type of fayalite dominates for compositions up to 50% Fe.

Co_2SiO_4 is antiferromagnetic with spins parallel to $\vec{b}$ for M2. A canting on M1 is observed for the temperature range 4.2K to T_N = 49.5K. Bulk magnetization measurements on single crystals by Treutmann and Wacker (1985) demonstrate a pronounced anisotropy for all three compounds in the antiferromagnetic range. These measurements are compared with a theoretical simulation of the magnetization measurements. The simulation is based on a self consistent calculation in the mean field approximation of the less energetical configuration of classical moments under the relevant magnetic field.

The anisotropy field appears to contribute drastically to the essential features of these curves. The simulation reproduces the magnetization curves and the differences in the magnetic moments of M1 and M2 well for Fe_2SiO_4. The simulation also agrees with the neutron diffraction results. The calculations for Mn_2SiO_4 and Co_2SiO_4 are in progress.

Lottermoser W (1986) Thesis, University Frankfurt

Lottermoser W, Müller R, Fuess H (1986)
Journ. Magn. Mag. Mater., in press

Treutmann W, Wacker K (1985) Personal communication

CATION DISTRIBUTION AND COVALENCY IN GARNETS STUDIED BY NEUTRON DIFFRACTION

FUESS, H., HOCK, R., Institut für Kristallographie und Mineralogie der Universität Frankfurt, Federal Republic of Germany

Neutron diffraction is a powerful tool for the investigation of the cation distribution among different crystallographic sites in minerals due to differences in the scattering power of neighbouring elements. In addition the magnetic moments of neutrons allow an investigation of the magnetic properties of solids. We investigate natural and synthetic garnets in order to determine the cation distribution, the magnetic structure and the magnetization density.

In natural garnets the tetrahedral position is occupied by silicon. The analysis of the occupation of the remaining two cation positions is achieved by a refinement of the scattering length. The refined value is then compared with the chemical composition and the actual site distribution is derived. Chemical analysis is carried out by energy dispersive methods using a transmission electron microscope. Additional Mössbauer spectra are recorded in order to determine the Fe^{2+}/Fe^{3+} ratio.

Two garnets are completely analysed (Pieper et al., 1983)

hessonite from Auerbach (Germany)

$\{Ca_{2.87}Fe''_{0.13}\}[Al_{1.61}Ti_{0.07}Fe'''_{0.28}Ca_{0.04}](Si_3)O_{12}$

and pyrope from Trebnitz (CSSR)

$\{Mg_{2.23}Ca_{0.38}Fe''_{0.45}\}[Al_{1.80}Cr_{0.11}Fe'''_{0.04}Ti_{0.01}](Si_3)O_{12}$

Powder data for samples of grossulare, andradite, almandine and caldierite were recorded. Data evaluation for the determination of cation distribution and of the magnetic order of caldierite is in progress.

Magnetic structures of the rare earth iron garnets were extensively studied by neutron diffraction. The magnetization density of yttrium iron garnet $\{Y_3\}[Fe_2](Fe_3)O_{12}$ revealed a considerable amount of uncancelled spins on the oxygen position (Bonnet et al., 1979) a direct proof of a magnetic superexchange between Fe in octahedral and tetrahedral positions which are coupled antiferromagnetically via oxygen. Furthermore magnetic density is found between Fe (tet) and oxygen which is a sign of a considerable contribution of covalent bonding between these atoms whereas no such effect is observed in the Fe(oct)-O bond. The magnetic form factors for the two Fe-ions differ considerably. They are compared with theoretical values for Fe^{3+}. Measurements on terbium and erbium iron garnet revealed magnetization density on the oxygen position, too. This indicates that the superexchange mechanism should be similar in the ferrimagnetic garnets between rare earths cations and iron.

Bonnet M, Delapalme A, Fuess H, Becker P (1979)
J. Phys. Chem. Sol 40, 863 - 879

Pieper G, Fuess H, Töpel-Schadt J, Amthauer G (1983)
N. Jb. Miner. Abh. 147, 197 - 159

AN IMPROVED, THOUGH STILL IMPERFECT, SOLUTION MODEL FOR TERNARY FELDSPARS

FUHRMAN, M. L., AND LINDSLEY, D. H., Department of Earth and Space Sciences, SUNY, Stony Brook, NY 11794, USA

An important first step toward a ternary feldspar model was made by Ghiorso (CMP 87, 282-296), who used the experimental data of Seck (N. Jb. Min. Abh. 115, 315-345; CMP 31, 67-86) to evaluate Margules parameters for the An-Or join and for ternary interaction. His model is quite successful for a number of feldspar relations but nevertheless has some drawbacks: (1) it predicts unrealistically high temperatures for many natural and synthetic ternary feldspars, (2) its data base is synthesis experiments (none reversed), (3) a rigorous formulation would require (at least) two equations of state for feldspars - one each for monoclinic and for triclinic feldspars, and (4) Ghiorso's model also lacks volume data for ternary feldspars.

Eventually feldspar solution models must use at least two equations of state, but for now we adopt the form of Ghiorso's model with the following changes: (1) We obtain ternary excess volumes from the data of Kroll et al. (Am. Min. 71, 1-16) and Newton et al. (GCA 44, 933-941); (2) we use the model of Haselton et al. (Am. Min. 68, 398-413) for the Ab-Or join; (3) we use Seck's data but omit the 650°C experiments, because these had the largest residuals and were least compatible with the other experiments in Ghiorso's model; (4) we adjusted the compositions of a few of Seck's experiments within his analytical uncertainty to allow slightly more ternary solution. These changes eliminate excess entropies for An-Or and the ternary; our model has three adjustable parameters (Table 1) compared with the six of Ghiorso. The overall success of our model is permissive evidence that Seck's 750-900° experiments approached equilibrium.

Table 1. Solution Parameters. WG = WH - T*WS + P*WV.

Parameter	Reference	WH (J)	WS (J/K)	WV (J/bar)*
W(OrAb)	Haselton et al.	27320	10.3	0.394(±.017)
W(AbOr)	Haselton et al.	18810	10.3	0.394(±.017)
W(AbAn)	Newton et al.	28226	0	0
W(AnAb)	Newton et al.	8471	0	0
W(OrAn)	This work	52468.2(±496.7)	0	0
W(AnOr)	This work	47396.4(±235.7)	0	-0.120(±.040)
W(OrAbAn)	This work	8700.4(±897.2)	0	-1.094(±.125)

*Fitted to the volume data of Kroll et al. and of Newton et al.

The convention for Margules parameters (Table 1) is that of Ghiorso and other workers; it is opposite to that used by Haselton et al., J. B. Thompson and others. The general form of our activity expressions is identical to that of Ghiorso, except that we include the excess volume in the Margules parameters, and we give the ternary interaction terms, which were omitted from Ghiorso's activity expressions. Activities are obtained from Ghiorso's equations (16,17,18) except that the last term ($W_V PXX$) in each is replaced by the ternary: $W_{OrAbAn}[X_{Or}X_{An}(1-2X_{Ab})]\}/RT\}$, (a_{Ab}); $W_{OrAbAn}[X_{An}X_{Ab}(1-2X_{Or})]\}/RT\}$, (a_{Or}); $W_{OrAbAn}[X_{Or}X_{Ab}(1-2X_{An})]\}/RT\}$, (a_{An}).

Other two-feldspar thermometers obtain temperature by setting the activities of $NaAlSi_3O_8$ equal in both phases. A ternary solution model permits calculation of three temperatures for a given two-feldspar pair. A powerful test of a ternary model is its ability to give congruent and reasonable temperatures for a variety of two-feldspar pairs. Temperatures from our model and two other thermometers are shown in Table 2. To obtain our temperatures, we allow the compositions of the phases to vary from those reported by up to 2 mole percent, an amount probably within analytical error. Our model and thermometer use parameters for Ab-An and Ab-Or identical to those of Haselton et al.; differences between the temperatures stem from our explicit terms for An-Or and the ternary parameter, which are implicitly zero in the Haselton thermometer. A major use of our model may be to test whether a given two-feldspar pair was in equilibrium.

TABLE 2. Temperature (°C)

Sample			Haselton	Ghiorso	Ab*	An*	Or*
Johannes expt.	800°	1 Kbar	783	805	734	735	734
" "	"	"	862	819	781	769	772
" "	650°	"	580	-	636	637	684
Hildreth Bishop Tuff	720°	(oxides)	708	622	676	671	650
" " "	780°	"	812	761	783	778	749
Ewart ignimbrite	750°	(oxides)	871	689	807	776	705
Sybille Syenite (Laramie Anor.Comp.)			1298	>1200	918	920	927

*Our thermometer, one temperature for each equilibrium.

•SYNTHESIS AND STABILITY OF UNUSUAL END MEMBERS OF SILICATE GARNETS (REVIEW)

FURSENKO, B.A., Institute of Geology and Geophysics, Novosibirsk 630090, U.S.S.R.

The complex composition of natural silicate garnets of general formula $A_3B_2Si_3O_{12}$ causes a great number of different minerals, the end members of garnet solid solutions, to be evolved. Some of these end members are rare and occur only as minor impurities. These "unusual" garnets are not present in the pure state, which reflects specific "unusual" conditions of their formation. Numerous garnet systematics and possibility to determine stability and physical properties of solid solutions from the properties of end members stimulate experiments on synthesis and stability of such "unusual" garnets.

In recent years, some mixed-valence garnets were synthesized at elevated pressures, e.g., blythite $Mn^{2+}{}_3Mn^{3+}{}_2Si_3O_{12}$ [1], calderite $Mn^{2+}{}_3Fe^{3+}{}_2Si_3O_{12}$ [2], and skiagite $Fe^{2+}{}_3Fe^{3+}{}_2Si_3O_{12}$ [3]. To be formed they need rather specific (narrow) redox conditions, as was shown in detail for calderite [2] first synthetized by Coes in 1955.

Cr in garnets was shown to be an indicator of high pressures. $Mn_3Cr_2Si_3O_{12}$, $Fe_3Cr_2Si_3O_{12}$ [4], and knorringite $Mg_3Cr_2Si_3O_{12}$ [5-7] were synthesized at pressures above 50-60 kbar. The lower pressure limit of the knorringite stability field remains to be refined. According to Irifune [6] (synthesis from oxides), its dP/dT slope is positive; whereas, Turkin and Doroshev [7], using the method of univariant reactions, found dP/dT to be slightly negative.

The very unusual non-cubic garnets of composition $4ASiO = A_3(ASi)Si_3O_{12}$ become stable at pressures exceeding 100-120 kbar. Until recently only one silicate garnet of this type, $Mn_3(MnSi)Si_3O_{12}$, was synthesized at 120 kbar [8]. Recently, the non-cubic garnet $Mg_3(MgSi)Si_3O_{12}$ was synthesized at a pressure of 180-200 kbar and temperature above 1800°C [9,10]. Similar to $MnSiO_3$, its stability field is between pyroxene phase at low pressures and ilmenite phase at high pressures. These garnets are characterized by octahedral coordination of 1/4 of the Si atoms which occupy together with A^{2+} the B sites of garnet structure. Some impurities such as Fe[Fe/(Fe+Mg) = 0.25] and/or Al (more than 5 mol %) stabilize the cubic garnet with Si in the B sites as it takes place in natural and synthetic majorite and in synthetic solid solutions between $MgSiO_3$ and pyrope. The octahedral coordination of Si in garnets is also possible when Na^+ substitutes for a part of the A^{2+} cations as was indicated first by Sobolev et al. [11]. Some of such "alkaline" garnets have been synthesized by Ringwood [12]. It seems to be interesting to study in more detail the stability region of these garnets and their solid solutions, because they can play an important role in the upper mantle [13].

References

[1] Fursenko, B.A. (1982) Doklady AN SSSR, 268, 421-424.
[2] Lattard, D. and Schreyer, W. (1983) Contrib. Mineral. Petrol., 84, 199-214.
[3] Karpinskaya, T.B., Ostrovsky, I.A. and Yevstigneeva, T.L. (1982) Izv. AN SSSR, ser. geol. N 9, 128-129.
[4] Fursenko, B.A. (1981) Bull. Mineral., 104, 418-422.
[5] Ringwood, A.E. (1977) Earth Planet. Sci. Letters, 36, 443-448.
[6] Irifune, T., Ohtani, E. and Kumazawa, M. (1982) Phys. Earth Planet Interiors, 27, 263-272.
[7] Turkin, A.I., Doroshev, A.M. and Malinovsky, I.Yu. (1983) In: "Silicate systems at high pressures." Novosibirsk, 5-24.
[8] Akimoto, S. and Syono, Y. (1972) Am. Mineral., 57, 76-84.
[9] Sawamoto, H. and Konzaki, M. (1985) Abstr. 1st Sov.-Jap. Symp. Phase Trans. High Pressure Temperature (Sept. 3-13), USSR, 48-50.
[10] Kato, T. and Kumazawa, M. (1985) Nature, 316, 803-805.
[11] Sobolev, N.V. and Lavrent'ev, Yu.G. (1971) Contrib. Mineral. Petrol., 31, 1-12.
[12] Ringwood, A.E. and Major, A. (1971) Earth Planet. Sci. Letters, 12, 411-418.
[13] Moore, R. and Gurney, J. 91985) Abstr. Conf. Native Elements in Meteorites and Continental Lithosphere, pt. IV, Novosibirsk, 25-26.

STUDY OF PHASE TRANSITIONS AT HIGH PRESSURES IN DIAMOND ANVIL CELL USING MONOCHROMATIC SYNCHROTRON RADIATION

FURSENKO B.A., Institute of Geology and Geophysics, Novosibirsk 630090, USSR; POLITOV A.A., TOLOCHKO B.P. Institute of Solid State Chemistry, Novosibirsk 630091, USSR; SHEROMOV M.A., Institute of Nuclear Physics, Novosibirsk 630090, USSR

The white polychromatic beam of synchrotron radiation (SR) is widely used in high pressure experiments in diamond anvil cells (DAC) combined with energy dispersive X-ray diffraction (EDXRD). We test an alternative technique using monochromatic radiation and position sensitive detector (PSD).

Our experiments were carried out on a SR beam of VEPP-4 storage ring at the Institute of Nuclear Physics (Diffraction Cinema Station) [1]. Monochromatic radiation was obtained by reflection from the (111) plane of silicon crystal ($\Delta\lambda/\lambda = 10^{-3}$). A PSD of the resolution 100 μm was used [2]. This technique allows a pressure displacement of reflexes to be recorded with greater accuracy than by EDXRD although the exposure time increases. The use of PSD allows a large part of diffractogram to be recorded at once and phase transitions to be observed in real time as with EDXRD.

The DAC used was described in [5]. The sample was 200-300 μm in diameter and 50 μm thick. No use of pressure-transmitting liquid in our experiments resulted in some broadening of peaks. Figs 1 and 2 present the results for well known substances AgJ [3] and KJ [4]. The wavelength of monochromatic radiation is 0.69 Å, accumulation time from 60 to 300 s. Additional reflexes in Fig.1 are due to the gasket (Fig.1c) and may be subtracted from the resulting pattern.

For AgJ an attempt was made to depressurize quickly the high-pressure phase B1 (NaCl type) and to follow the back-transition dynamics through an intermediate tetragonal phase into initial wurtzite one. We failed to record the intermediate phase under these conditions, which indicates that our exposure time of 60 s

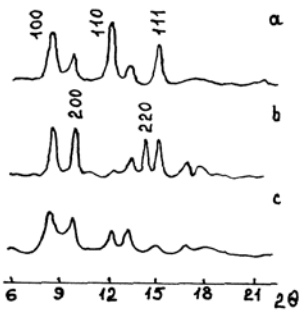

Fig.1. X-ray diagrams of KJ: a) phase B2 at P ≥ 2.0 GPa; b) phase B1 at 10^{-4} GPa; c) gasket without sample.

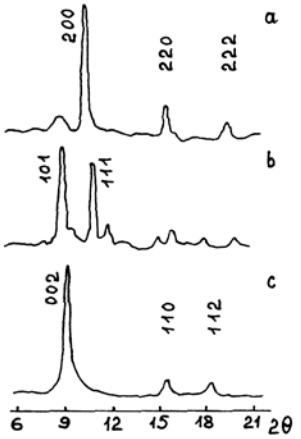

Fig.2. X-ray diagrams of AgJ: a) phase B1 at P ≥ 0.29 GPa; b) tetragonal phase at 0.29 > P > 0.24 GPa; c) hexagonal phase at P < 0.24 GPa.

is too long to detect this process. To reduce the recording time it is necessary to increase the monochromatic beam intensity. The use of a focusing monochromator and focusing mirror is planned, which will allow the intensity to be increased by 2-3 orders.

1. Mezentsev N.A. et al. (1983) Preprint of Inst. Nucl. Phys. N 83-156, Novosibirsk. 2. Baru S.E. et al. (1978) Nucl. Instr. Meth., v.152, 195. 3. Moor M.J. and Kasper J.S. (1968) J. Chem. Phys., v.48, 2446-2450. 4. Piermarini G.I. and Weir C.E. (1962) J. Res. Natl. Bur. Stand., Ser. A Phys. Chem., v.66A, N 4, 325-331. 5. Fursenko B.A. et al. (1984) Pribori i tekhnika eksper. N 5, 174-178.

SINTERING OF QUARTZITE REFRACTORIES BONDED BY BORON OXIDE

GABIS,V.+, GENIES,B.++, ILDEFONSE,J.P.+, PANIS,D.+, COQUAND,B.+
+ Lab. Minéralogie Appliquée, ESEM, Université d'Orléans, F-45067 ORLEANS cedex 2(FRANCE)
++ Centre de Recherche Cl.Delorme, L'AIR LIQUIDE - 78350 JOUY EN JOSAS(FRANCE)

Sintering is a process by which fine particles, in direct contact with each other, form a dense solid body when heated to a suitable temperature. Sintering processes in ceramics fall into three main classes :

- Solid state self sintering - Bonding of particles of a single phase occurs by a transport of matter to the points of contact and the growth of necks between the powder particles. No subsidiary phase appears.

- Solid state reaction sintering - Bonding of particles results from the growth of a secondary interstitial phase. This phase occurs at high temperature by a solid state reaction between powder particles and additives. It acts as a cement.

-Liquid phase sintering. A viscous liquid is formed at high temperature and gives birth to thin liquid films between particles serving as a bond for the body. Moreover, the liquid may sometimes dissolve a limited amount of the primary solid and generate new solid phases by precipitation. It results in a solid skeleton which strengthens the ceramic body.

A prominent example of liquid phase sintering is given by quartzite refractories bonded by boron oxide. Two kinds of experiments were performed. Quartz particles mixed with boron oxide and heated at different temperatures in an electric furnace. And compact quartzite + B203 linings sintered with an oxygen-propane burner, the back part of the lining remaining cold. This last procedure has been choosen to reproduce what happens in industrial furnaces like those used in foundry. The temperature was progressively raised to 1600°C and maintened for 30 minutes.

Mineralogical composition and microstructure of sintered linings were investigated with X-ray diffraction, scanning electron microscopy, density and porosity measurements. It was found that cristobalite is the only phase present at the hot face, and that quartz is present a few millimeters below this surface. The amount of quartz raises gradually when looking at deeper and deeper. Borosilicate glass is also present and its amount depends on the depth. Experiments performed with quartz powder + 1 % B203 show that cristobalite appears already at about 1000°C. It cannot be the result of a solid state polymorphic transformation. But it is possible to connect cristobalite genesis to the borosilicate liquid present between quartz particles. This liquid results from an eutectic melting at about 475°C and its amount increases when temperature raises. This corresponds to a certain limited solubility of quartz in the liquid. So that, when local saturation is achieved, cristobalite precipitates according to the Ostwald rule.

At 1600°C, direct transformation of quartz to cristobalite is quite possible. So that, we can assume there are two kinds of cristobalite at that temperature. One of them corresponds to a solid state reaction, the other one to a precipitation from a silica saturated liquid.

Other experiments were performed at 1400°C with sintered refractory in contact with molten grey cast iron. After some hours, the hot face exhibits tridymite along with cristobalite. Obviously, tridymite results from a polymorphic transformation of residual quartz. On the whole, four silica forms can be distinguished in the front part of the quartzite refractory lining, when maintained at 1400°C : starting quartz; stable tridymite; metastable cristobalite precipitated from a borosilicate liquid, and also issued from a solid state transformation of quartz during sintering at 1600°C; and dissolved silica.

After runs with molten iron cast, at 1400°C, two orthosilicates were also observed at the front face of the ceramic body : fayalite Fe2SiO4 and tephroite (Mn, Fe)2SiO4. Both result from a chemical reaction between silica and molten alloy.

Liquid phase sintering is thus a complex process. Many reactions occur : polymorphic transformations, eutectic melting, solution and precipitation. Moreover, sintering continues as long as hot molten alloys are side by side with the refractory lining. And it is only after a long time that the starting raw powder becomes a monolithic rigid body.

MULTICOMPONENT DIFFUSION IN SILICATES AND COMPOSITIONAL ZONING OF GARNET IN NATURAL ASSEMBLAGES

GANGULY, J., and LOOMIS, T. P., Dept. of Geosciences, University of Arizona, Tucson, AZ 85721, USA

We present a general review of the theory of diffusion fluxes in multicomponent ionic crystals, and a comparative analysis of diffusion and related data in olivine, pyroxene, and garnet to develop an understanding of the influence of crystal-chemical parameters on cation diffusion. We also discuss the potential problems with some of the experimental techniques for the measurement of diffusion data, explore techniques for high resolution measurement of diffusion profiles in diffusion-couple experiments, and illustrate retrieval of tracer diffusivities from multicomponent diffusion profiles by numerical simulation. Finally, we address the problem of the development of compositional zoning in natural garnet, and the time-scale of some geologic processes that can be constrained by the time required for the (observed or inferred) diffusional relaxation of zoned garnet.

It is shown that in some cases, failure to recognize compositional effects on tracer diffusion coefficients could lead to significant error in the retrieval of $\tilde{D}$ (inter-diffusion coefficient) from D^* (tracer-diffusion) values, and vice versa, using the Darken or Manning formulations, and in the extrapolation of diffusion coefficient as functions of composition. The tracer diffusivity of an atom usually increases with the increase in the dimension of the host sublattice in a given mineral group. However, for binary diffusion in silicates, $\tilde{D}$ may be approximated very well by an empirical relation $\log \tilde{D} = X_j \log D_i^*(X_i \to 0) + X_i \log D_j^*(X_j \to 0)$, where the tracer coefficients are for the specified dilute solutions.

Analyses of the available diffusion data in silicates suggest that the observed discontinuous change in the activation energy of diffusion as a function of temperature is, in some cases, an artifact of experimental problems, especially due to the use of sintered powders, and not due to any change of volume diffusion mechanism. It seems unlikely that there is any change of mechanism in the volume diffusion of divalent cations in garnet and olivine in temperature ranges 1400-750°C and 1400-1000°C, respectively.

The results of numerical simulation suggest that zoning in natural garnets in low to medium grade metapelites is a consequence of Mn-Fe fractionation during the continuous growth of garnet in the assemblages garnet-biotite-chlorite. The simulated growth zoning profiles in the assemblage garnet-biotite-sillimanite show a reversal of Fe-zoning that has developed in the lower grade. Also lower pressure of metamorphism leads to the crystallization of relatively homogeneous garnets. As will be shown by illustrative examples, these numerical simulations of growth zonings can serve as basis for interpretations of kinetic and growth processes that have been responsible for the observed zoning profiles in natural garnets in metapelites.

•MINERALOGY OF ILMENITE FROM YAKUTIA KIMBERLITES

GARANIN, V.K., KUDRYAVTSEVA, G.P., Department of Mineralogy, Faculty of Geology, Moscow State University, 119899, Moscow, U.S.S.R.

A composite study of ilmenite made it possible to reveal two genetic sources of this mineral in kimberlites. Ilmenite of xenogenous origin in the form of nodules is the product of disintegration of deep-seated rocks of ultrabasic and basic composition. Ilmenite from the groundmass of kimberlite crystallizes from the kimberlite magma itself. The great diversity of deep-seated ilmenite rocks causes a considerable variety in composition and properties. Three stages of deep-seated formation of ilmenite rocks have been established. The earliest is connected with the evolution of garnet rocks in the series peridotite ($p > 4GPa$, $t > 1200°C$) - eclogites ($p < 2$ GPa, $T \sim 950$-$850°C$). During the next stage the variegated series of ilmenite diopsidites is crystallized ($p = 3.8$-1.5 GPa, $t = 1200$-$1145°C$). Peculiar high-ferruginous garnet-ilmenite aggregates ($T = 950°C$) are the most recent ilmenite rocks. These rocks are the source of ferromagnetic ilmenite nodules with a high content of the hematite component.

The regularity of composition and property changes of ilmenite from every rock type have been shown, and the PT-parameters of crystallization of the latter have been determined. The differences in ilmenite composition from different kimberlite pipes and kimberlite fields showing the peculiarity of the chemical composition and structure of the deep-seated zones of the Earth have been established. On the basis of thermomagnetic analysis of ilmenite, an effective method of study of the horizontal and vertical zonation of kimberlite pipes has been worked out. It is suggested to use the non-uniformity of ilmenite as a mineralogical criterion of estimation of kimberlite productivity.

The composition of ilmenite from the kimberlite groundmass is naturally changed from high-Mg (MgO > 5 wt %) chromous ilmenite in productive pipes to low-Mg manganous ilmenite in pipes with low productivity. There are differences in composition of ilmenite from kimberlite rocks of different stages of intrusion. Besides, the rocks of more recent stages (less deep-seated) contain ilmenite enriched by manganese (up to 6 wt % MnO). The order of crystallization of the groundmass minerals when PT-parameters are lowered is the following: high-magnesian olivine (Fo 90%) + high-titanian chromospinel → magnesian olivine (Fo from go to 92%) + high-magnesian ilmenite → chromian titanomagnetite → perovskite + rutile → magnetite.

TEXTURES OF THE ORES FROM MOINHO DEPOSIT, ALJUSTREL, PORTUGAL, THEIR GENETIC SIGNIFICANCE AND IMPLICATIONS ON BENEFICIATION

GASPAR,O.,Laboratório da D.G.G.M., P-4465 S. Mamede de Infesta

Textures and parageneses of Aljustrel ores are very complex ones and a systematic caracterization closely linked with detailed geological reconnaisance of mineralised structures has been made since 1978, aiming the beneficiation of ores with contents of 45% S, 40% Fe, 2-3% Zn, 0,5-1% Pb, 0,8 g/t Au and 30 g/t Ag.

Particular attention was given to the distribuition of Ag, As, Au, Bi, Cd, Co, Hg, Sb and Sn in major and minor phases: pyrite, sphalerite, galena, arsenopyrite, bournonite, tetrahedrite, tennantite, kobellite, stannite, cassiterite, pyrrohtite, marcasite, boulangerite, glaucodot, gudmundite, aikinite, horobetsuite, meneghinite, betechtinite, enargite, plagionite, mackinawite and magnetite.

Analogies between textures of Aljustrel ores wich are in connection with a lower Carboniferous submarine felsic explosive vulcanism and mineralization processes taking place in the sea today have been drawn.

Complex and very fine intergrowths, lateral and vertical variations of textures and ore composition make the beneficiation by flotation very difficult imposing a crushing to $K_{80} = 30$ um.

Ore microscopy has been applied to check the processing efficiency of a pilot ore dressing plant of 1,5 tonnes/hour of semi-differential concentrates of Cu, Zn and Pb, and at the bench scale in the development of flow sheets for ore types having various grain sizes and Cu-Zn-Pb grades as well.

•INCLUSIONS IN MINERALS FROM YAKUTIA KIMBERLITES: METHODS OF INVESTIGATION AND NEW DATA

GARANIN, V.K., KUDRYAVTSEVA, G.P., BUTKUNOV, A.I., Department of Mineralogy, Faculty of Geology, Moscow State University, 119899, Moscow, U.S.S.R.

The results of a study of mineral inclusions in xenocrystals (garnet, olivine, zircon, spinellides, and ilmenite) are given in this paper. In garnets, polymineral sulphide nodules of the chalcopyrite-pyrrhotite-pentlandite association, spinellides (chrome-spinellides, hercynite), clinopyroxene, olivine, ilmenite, acicular inclusions of chrome-spinellides, rutile and ilmenite, as well as compound hydrocarbonic inclusions have been diagnosed. Sulphides are present in all genetic varieties of garnets. Inclusions of other minerals have only been found in some garnets, the composition of syngenetic minerals regularly changing depending on the garnet paragenesis.

Polymineral sulphide aggregates, chrome-spinellides, garnet, clinopyroxene and ilmenite have been found in olivine. Special features of the composition of the host mineral and its inclusions makes it possible to consider them as peridotites of the Mg and Mg-Fe series. In zircon sulphides, titaniferous chrome-spinellides, olivine, clinopyroxene and inclusions of minerogenic media of hydrous carbonate composition have been diagnosed. There are no garnet inclusions in zircon. Most zircons (including those with gem properties from the Mir pipe) are genetically connected with spinel peridotites. As the most widespread inclusions in chrome-spinellides are olivine and garnet, it is possible to classify these mineral associations as peridotite.

In ilmenite, syngenetic polymineral sulphide nodules of the djerfischerite-chalcopyrite-pentlandite-pyrrhotite association, garnet, clinopyroxene as well as epigenetic inclusions of Cr-Ti-spinellides (decay products of solid solutions) have been found. The special features of the host mineral and its incluions show that they are genetically related to two types of paragenesis: the peridotite and the pyroxenite ones. The PT-crystallization conditions of different mineral parageneses of garnet, olivine, zircon, spinellides and ilmenite have been specified. These composition peculiarities of minerals from diamondiferous parageneses have made it possible to specify the conditions of diamond formation and to suggest new mineralogical criteria for the estimation of kimberlite productivity.

SYNTHESIS OF THE MIXED-VALENCE IRON SILICATE ILVAITE

GHAZI-BAYAT, B., Institute of Mineralogy, University of Marburg, 3550 Marburg, FRG; AMTHAUER G., Institute of Geosciences, University of Salzburg, 5020 Salzburg, AUSTRIA; Schürmann, K., Institute of Mineralogy, University of Marburg, 3550 Marburg, FRG; HELLNER, E., Institute of Mineralogy, University of Marburg, 3550 Marburg, FRG.

Ilvaite $CaFe_2^{2+}Fe^{3+}[Si_2O_7/O/(OH)]$ is a sorosilicate occuring in two polymorphs: a monoclinic low-temperature phase ($P2_1/a$) and an orthorhombic high-temperature phase (Pnam). With regard to Mössbauer spectroscopy syntheses have been made under hydrothermal conditions in order to obtain pure phases in relation to different oxygen fugacities.

Using a constant water vapor pressure of 2 kbars we could determine a relative stability field of ilvaite as a function of temperature and oxygen fugacity (cf. Figure 1). In contrast to Gustafson (1974) we could not synthesize ilvaite as a stable phase using an Fe/Fe_3O_4 buffer. All synthesized ilvaites (stable phases) are related to oxidizing buffer systems like Ni/NiO and Fe_2O_3/Fe_3O_4. At oxygen fugacities controlled by the Fe_2O_3/Fe_3O_4 buffer we could synthesize pure ilvaites between 330 and 370°C. At oxygen fugacities controlled by the Ni/NiO buffer we obtained ilvaites as stables phases at temperatures between 430°C and 480°C sometimes together with small amounts of hedenbergite and magnetite.

SYNTHESIS OF THE MIXED-VALENCE IRON SILICATE ILVAITE
GHAZI-BAYAT, B., et al.

All synthesized ilvaites are monoclinic with a ß-angle between 90.20° and 90.34°. Sometimes they occur under the microscope as small euhedral, black crystals up to a size of 25 microns. Mössbauer spectra of the synthetic ilvaites exhibit typical parameters sometimes with low traces (<1%) of magnetite.

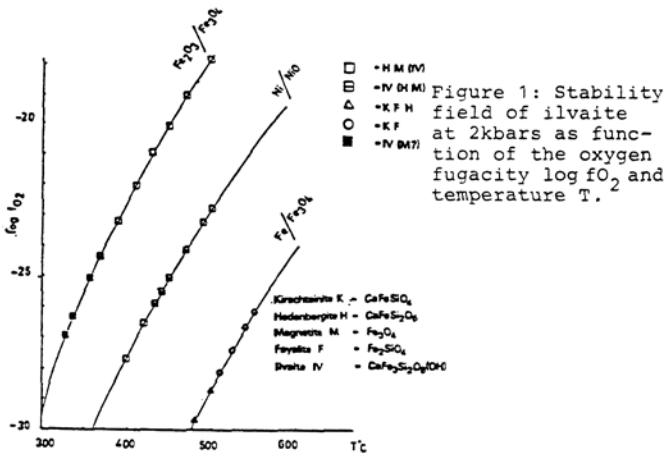

Figure 1: Stability field of ilvaite at 2kbars as function of the oxygen fugacity log fO_2 and temperature T.

Gustafson, W.I. (1974) J.Petrol 15, 455

METAMORPHISM IN THE MICA CREEK AREA, SOUTHEASTERN BRITISH COLUMBIA, CANADA

GHENT, E.D., STOUT, M.Z., and SEVIGNY, J.H., Department of Geology and Geophysics, University of Calgary, Calgary, Alberta T2N 1N4, Canada

The Mica Creek area of British Columbia (Lat. 52°N, Long. 118°W) is underlain by Late Precambrian metasedimentary rocks with smaller amounts of metabasites. Metamorphic grade ranges from upper garnet zone to K-feldspar-sillimanite zone and the succession of isograds in pelitic rocks is: staurolite-kyanite; staurolite out; sillimanite; muscovite-quartz-K-feldspar-sillimanite; and K-feldspar-sillimanite. In metabasites, garnet plus clinopyroxene appears just upgrade from the sillimanite isograd. Abundant migmatite appears near the staurolite out isograd. Trondhjemite pegmatites occur throughout the area, but are most prominent within units of metapsammites and amphibolites. Abundant granitic intrusions occur near the K-feldspar-sillimanite isograd. The granites are peraluminous with biotite-muscovite and rare garnet. They are rarely foliated and appear to have been intruded late in the metamorphic episode.

The age of the metamorphism is Late Mesozoic. The metamorphic rocks have been thrust eastward and are now in fault contact (along the Purcell Fault) with lower pressure (staurolite out at the kyanite-sillimanite isograd) Lower Paleozoic to Late Precambrian rocks of the Western Rocky Mountains. To the west, the rocks are in fault contact with lower pressure (staurolite stable with sillimanite) metamorphic rocks of the Blue River area.

Temperatures have been estimated for 65 samples of metasedimentary rocks using the garnet-biotite Fe-Mg exchange thermometer (Ferry and Spear calibration). For samples below the sillimanite isograd, these temperature estimates are in reasonable agreement with other geothermometers based upon mineral equilibria and with oxygen isotope thermometry. For samples above the sillimanite isograd, the estimated temperatures show a wide scatter and many are too high to be consistent with muscovite-quartz-plagioclase stability.

Temperatures estimated for samples of metabasite using the clinopyroxene-garnet Fe-Mg exchange thermometer generally do not agree with temperatures estimated from nearby garnet-biotite temperature estimates, unless the Thompson calibration is used. Temperatures estimated from the empirical garnet-hornblende Fe-Mg exchange thermometer of Graham and Powell disagree with many garnet-clinopyroxene temperature estimates for the same samples. At lower metamorphic grades, garnet-hornblende temperature estimates agree well with garnet-biotite temperature estimates for closely spaced samples.

Based upon limited experimental diffusion data for minerals and crystal chemical reasoning, one would predict that the closure temperatures for Fe-Mg exchange in mineral pairs would be, in order of decreasing temperature, garnet-clinopyroxene, garnet-hornblende, and garnet-biotite.

Pressure estimates for metapelites using garnet-plagioclase-aluminum silicate-quartz barometry agree reasonably well with pressure estimates for metabasites based upon clinopyroxene-garnet-plagioclase-quartz barometry. Barometers based upon TiO_2 activity and $CaMgSi_2O_6$ activity for metasedimentary and metabasite mineral assemblages can be tested for consistency in the Mica Creek rocks.

Estimates of H_2O fugacity using muscovite-quartz-plagioclase-aluminum silicate equilibria suggest that fluids were dominantly composed of H_2O. Fluid inclusion studies on the same samples show that the densest fluid inclusions give isochores which pass through the P-T estimates based upon mineral equilibria. These dense inclusions are H_2O-rich which is consistent with estimates of fluid composition based upon mineral equilibria. Lower density fluid inclusions of different composition can be used to constrain the P-T uplift path of these rocks.

Oxygen isotope studies on metapelitic rocks suggest that the quartz has undergone little modification of its protolith oxygen isotope composition during metamorphism. There is no significant change in oxygen isotopic composition with metamorphic grade, i.e., toward lighter isotopic values as has been reported from other metamorphic terranes.

GENESIS OF VANADIUM - BEARING BERYLS

GHERA, A.; GRAZIANI, G.; LUCCHESI, S., Dip. Scienze della Terra, Università "La Sapienza", P. le A. Moro 5, 00185 Roma, ITALY

The genesis of vanadium - bearing beryls has been studied with respect to their bulk crystal chemical composition and the paragenesis of the mineral inclusions.

The content of minor elements in numerous brasilian (Salininha) and zambian samples has been investigated evidencing a particularly high magnesium content besides the presence of the chromophorous element (vanadium). Similar inclusions were recognized by optical observations and electron microprobe analyses in these specimens: calcite, talc, phlogopite, quartz and carbonate or hydroxyapatite. Moreover the Salininha samples are characterized by the presence of dolomite and sporadic corundum.

The paragenesis of all these inclusions suggests similar P - T formational conditions referable to metasomatic activities set on dolomitic limestones.

Such hypoteses are also supported by considerations on the geochemical rôle of vanadium which, for the examined samples, might derive from bitouminous sediments.

ELECTRON AND SPIN ORDERING AND ASSOCIATED PHASE TRANSITIONS IN ILVAITE, A MIXED VALENCE IRON SILICATE

GHOSE, Subrata, Mineral Physics Group, Department of Geological Sciences, University of Washington, Seattle, WA 98195, USA

Ilvaite is a black mixed valence iron silicate mineral, which shows considerable thermally activated electron delocalization between Fe^{2+} and Fe^{3+} ions in octahedral sites, reminiscent of the situation in magnetite. The various electronic, crystallographic and magnetic phase transitions in ilvaite have been studied by x-ray and neutron diffraction, ^{57}Fe Mössbauer resonance, electrical resistivity, magnetic susceptibility and specific heat measurements. The crystal structure of ilvaite, $Ca(Fe^{2+},Fe^{3+})Fe^{2+}Si_2O_8(OH)$ consists of double chains of octahedra running parallel to the c axis containing Fe^{2+} and Fe^{3+} (A sites) with half as many larger Fe^{2+} octahedra (B sites) attached above and below, cross-linked by $[Si_2O_7]$ groups and Ca^{2+} ions in seven-fold coordination. The activation energy of electron delocalization: Fe^{2+} (A) $\rightleftarrows$ Fe^{3+} (A) is 0.13eV as determined from electrical resistivity measurements in single crystals parallel to c.[1] The bulk of the electron ordering takes place at around 380K as indicated by a broad peak in the specific heat curve, followed by a crystallographic phase transition from orthorhombic ($Pnam$) to monoclinic ($P2_1/a$) symmetry at 343K.[4,5] In the orthorhombic phase, the Fe^{2+} and Fe^{3+} ions are disordered in the A sites, whereas in the monoclinic phase, the Fe^{2+} ions are mostly ordered in Ao and Fe^{3+} ions in Am sites. With further decrease in temperature, the electron ordering continues down to 5K[2,3]. Simultaneously, the molar susceptibility $K_{||}$ rotates continuously in the ab plane down to 90K.[5] Two phase transitions from paramagnetic to antiferromagnetic at 120 and 40K are found by magnetic susceptibility, specific heat and Mössbauer measurements.[1,4,5] The magnetic structure determined by powder neutron diffraction at 80K indicates ferromagnetic coupling of Fe^{2+} and Fe^{3+} spins in a single octahedral chain, which are antiferromagnetically coupled to those in the adjacent edge-sharing single chain, whereas Fe^{2+} spins on B sites are disordered; at 5K, spins on B sites are ordered as well with all spins pointing parallel and antiparallel to the b axis.[2] Mössbauer spectra between 150 and 4.2K indicate a pseudotetragonal local symmetry at both Fe^{2+} sites with a $^5A_1$ orbital singlet ground state, further confirmed by single crystal magnetic susceptibility measurements.[1,4]

1. Coey, J.M.D., J. Allan, Kan Xuemin, N. Van Dang, and S. Ghose (1984): J. Appl. Phys. 55, 1963-1965.
2. Ghose, S., A. W. Hewat, and M. Marezio (1984) Phys. Chem. Minerals, 11, 67-74.
3. Ghose, S., P. K. Sen Gupta, and E. O. Schlemper (1985) Amer. Mineral. 70, 1248-1252.
4. Ghosh, D., T. Kundu, S. Dasgupta, and S. Ghose (1986) Phys. Chem. Minerals. (to be published).
5. Robie, R. A., H. T. Evans, Jr., and B. S. Hemingway (1986) J. Geophys. Research (to be published).

MOLECULAR MIMICRY OF STRUCTURE AND ELECTRON DENSITY DISTRIBUTIONS OF MINERALS

GIBBS, G. V. and BOISEN, M. B., Jr., Virginia Polytechnic Institute & State University, Blacksburg, VA 24061; FINGER, F. W., Carnegie Institution of Washington, Geophysical Laboratory Washington, D.C. 20008; LASAGA, A. C., Yale University New Haven, CT 06511

As the bond lengths and angles of the disiloxy ($SiOSi$) bond in siloxane molecules are similar to those in silicates, molecular orbital (MO) calculations on hydroxyacid molecules with disiloxy bonds can be used to study the bonding in silicates. For example, near Hartree-Fock MO calculations on $H_6Si_2O_7$ have reproduced the bond lengths and angles for the silica polymorphs. They have also provided insight into the wide range of $SiOSi$ angles, the bulk modulus, and the defects of vitreous silica. Similar calculations on hydroxyacid molecules containing first- and second-row X-cations yield XO bond lengths that match those in chemically similar silicates and oxides. These results can be extended to oxides containing main-group X-cations for the remaining four rows of the periodic table by applying a formula $R = 1.39p^{-0.22}$ based on a bond strength parameter $p = s/r$ where s is the Pauling bond strength of an XO bond and r is the row number of the X-cation. The bond lengths calculated with this formula mimic the Shannon bond lengths for oxides within 0.05Å on average.

Total electron density maps of the silica polymorphs and periclase are successfully mimicked by those of chemically similar molecules allowing for a calculation of bonded radii of the atoms comprising an XO bond for first- and second-row X-cations. It was found that the bonded radius of the oxide ion is not constant (it increases systematically with the ionicity of the XO bond), that the change in XO bond length is shared equally between the bonded radius of the cation and oxide ion as one cation is replaced by another and that bonded radii are highly correlated with X-cation crystal radii.

The ability of MO calculations to mimic the static and dynamic properties of a mineral like α-quartz implies that the forces that govern the structure and properties of the mineral are similar to those that govern the structure and properties of a molecule like $H_2Si_2O_7$. Using total energy surfaces calculated for the molecule, a computational model of the structural energy of α-quartz was developed. By minimizing the energy with respect to its structural variables, the atomic coordinates of the mineral were reproduced within 0.02Å on average. Not only did the calculations yield a bulk modulus of 0.394 megabars in agreement with the observed value, but they yield an equation of state that models that observed up to 5 kilobars. The success of these calculations bodes well for the development of new computational models for mimicking the structures and properties of minerals, using energy surfaces derived for carefully selected molecules.

DETECTION OF SHORT-RANGE ORDER IN SUBSTITUTIONALLY DISORDERED CATION SITES OF PHYLLOSILICATES

GIESE, R. F., Dept. of Geological Sciences, State University of New York at Buffalo, 4240 Ridge Lea Road, Amherst, NY 14226, USA

Classical single crystal diffraction techniques can not adequately treat structures which are less than perfectly ordered. In a crystal structure refinement, disorder is often indicated by partial occupancy of a crystallographic site, as required by the space group or as indicated by the electron density at the site and the distance to coordinating atoms. Having determined that two or more atoms are occupying the same crystallographic site, it is not clear whether the apparent disorder is the result of a complete segregation of the different atom types (as in a twinned crystal) or whether there is short range ordering in domains.

A number of techniques, both experimental and computational, have been developed to identify short range order and even to indicate what the structure might be in the domains. The phyllosilicates are relatively simple to model because they can be treated as two-dimensional patterns. Two attempts have been made to identify the short range order of cation substitutions, both based on minimizing the electrostatic potential energy of the crystal.

The possible short range patterns in the octahedral sites of biotites containing different valence cations have been examined by 1) randomly filling the sites with cations for a chosen chemistry and 2) rearranging the cations to minimize deviations from the electrostatic valence rule. The resulting patterns of divalent, trivalent, and vacant sites are very distinctive, and form domains with dimensions of a few to tens of unit cells.

A more complex model has been used to study muscovite and the possible arrangements of Si and Al in the tetrahedral sites. Here, the electrostatic energy was calculated for a number of randomly chosen distributions of the two cations over all the sites in the unit cell. All the tetrahedral sites were treated as independent. The lowest energy (most stable) arrangements were numerous, suggesting that there is little advantage for the two cations to order, either long range or short range. A similar treatment of margarite showed a strong energetic preference for one particular cation arrangement, that which corresponds to the ordered structure observed in the mineral.

EXPERIENCE OF SYNCHROTRON RADIATION USE FOR DETERMINATION OF CONTENTS AND DISTRIBUTION OF RARE-EARTH ELEMENTS IN MINERALS AND ROCKS

GILBERT A.E., SOBOLEV N.V., SHATSKY V.S., Institute of Geology and Geophysics, BARYSHEV V.B., KULIPANOV G.N., Institute of Nuclear Physics, Novosibirsk 630090, USSR

Results of determination of rare-earth elements (REE) by the method of X-ray fluorescence analysis (XFA) using synchrotron radiation (SR) both non-destructively and with chemical separations of REE as a group in rock specimens are presented. Some possibilities are also considered to study REE distribution in mineral grains by scanning with a SR beam.

The most important properties of SR beams for REE analysis are as follows: high intensity combined with sharp directivity and continuous spectrum allowing the monochromatic excitation retunable in a wide energy range (30 to 100 keV) to be realized, and natural SR polarization which reduces 10 or more times the background of Compton scattering of exciting radiation on a specimen with the detection direction optimized. SR was used from the VEPP-4 storage ring of the Institute of Nuclear Physics (Novosibirsk) 1 .

Standard specimens (SS) of rocks ST-1A, SGD-1A and SS SG-1A with the addition of 100 ppm of REE were used to determine detection and reproducibility limits of the results of REE analysis by the non-destructive XFA-SR method. The typical values of the detection limits for the detector counting rate of 10^4 Hz and exposure time of 10^3 s are as follows:
La - 0.2 ppm, Pr - 0.15 ppm, Nd - 0.17 ppm, Sm - 0.2 ppm, Ho - 0.25 ppm, Er - 0.33 ppm 2 .

To test the method potentiality a specimen of xenolite of cataclastic lherzolite from the kimberlite pipe "Udachnaya" poor in REE was analyzed. Detection limits of non-destructive determination were 0.08 to 0.12 ppm, the chemical pre-separation allowed the detection limit to be reduced down to 4.4 - 6.8 ppb. The results of REE determination agree with the data obtained by the neutron activation analysis.

A possible use of SR in studying the REE distribution in single mineral grains is considered. A grain of garnet from the kyanite-garnet-muscovite schists of Northern Kazakhstan was used as a sample. Fig.1 shows the distribution of petrogenic elements determined by a JXA-5A microprobe. Fig.2 shows the REE distribution in the same grain obtained by scanning with a SR beam.

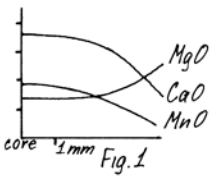

Fig.1

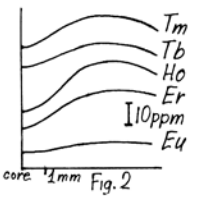

Fig.2

Because of the absence of standards close in composition to the garnet under study the values obtained are not to be scaled absolutely, but they clearly indicate the non-uniformity of REE distribution in the garnet grain. The analysis of the data obtained shows that when the measuring time is 1 s per point it is possible to obtain REE distribution maps with an error of 30% and 10% for the contents of 2 ppm and 20 ppm, respectively.

1. Baryshev V.B., Kulipanov G.N., Skrinsky A.N. Review of X-ray Fluorescent Analysis Using Synchrotron Radiation. Proc. Int. Cong. SRI-85, Stanford, 1985. Nucl. Instr. and Meth., 1986 (in print).

2. Gilbert A.E., Kozmenko O.A., Baryshev V.B., Zolotarev K.V., Kulipanov G.N. On the possibility of synchrotron radiation use for determination of concentrations and distribution of rare-earth elements in samples of rocks. Zhurnal analiticheskoi khimii, USSR, 1986 (in print).

FIRST-PRINCIPLES THEORY OF SOME MANTLE MINERALS

GORDON, ROY G., HUMMEL, HARRY H. and JACKSON, MARK D., Department of Chemistry, Harvard University, Cambridge, MA 02138

The modified electron gas (MEG) theory is extended to include polarization (partial covalency) in mainly ionic crystals, such as oxides. Valence-shell electrons of the oxide ion are shifted slightly in the direction of neighboring cations such as Si^{4+}. These polarizations amount to average electron displacements of about 10% of the bond length. X-ray diffraction data on α-quartz are better explained by this polarized charge density, than by conventional crystallographic analysis which assumes spherical charge densities around the nuclei. Polarization is also important in describing the bent Si-O-Si bonds in α-quartz and α-cristobalite, as well as the very high compressibilities of these lattices.

Predictions are made of possible post-stishovite high-pressure phases of silica. Three phases were found to have energies extremely close to stishovite in the megabar pressure range: $CaCl_2$ (which is a slight orthorhombic distortion of the stishovite lattice), α-PbO_2, and a defect NiAs structure in which alternate unit cells in the A-direction have cation vacancies. The energies of these four phases are so close that vibrational thermal effects and a more refined treatment of polarization may be required to distinguish them. Four other possible post-stishovite phases were considered, but found to be significantly less stable than the four mentioned above: CaF_2, ZrO_2, anatase, and brookite.

The structures and energies of several magnesium silicate phases were also calculated by the same theoretical methods. The pressure-induced transitions of Mg_2SiO_4 from olivine to spinel and $MgSiO_3$ from ilmenite to perovskite were found to be quite sensitive to the polarization model. The perovskite $MgSiO_3$ is found to have an orthorhombic distortion from cubic, and the amount of distortion increases slightly with pressure.

CHANGES IN LATTICE PARAMETER, MICROSTRUCTURE AND INTRINSIC MAGNETIC PROPERTIES WITH PROGRESSIVE MAGNETITE OXIDATION.

GOSS,C.J. and PUTNIS,A., Dept. of Earth Sciences, University Cambridge, Downing St., Cambridge. CB2 3EQ. U.K.

The aim of this study is to correlate the observed changes in magnetic properties (saturation magnetisation, remanence and coercive force) with phase transformations, lattice parameter variations and microstructure for the iron oxide series: magnetite-maghemite-hematite. The study involves a systemmatic study of changes in properties at ambient temperature for a single magnetite type.

The starting material is a synthetic magnetite prepared by a colloidal technique and consists of octahedral grains of edge length 350-450Å. Oxidation was carried out in air (atmospheric pressure) for fixed times at temperatures from 200°C to 1000°C. Such material is very similar to that used by the tape recording industry and is of the same size as single domain remanence carriers in rocks.

The unit cell of the original material is 8.398Å consistent with accepted values for magnetite. Infra-red studies show the presence of OH- ions and weight losses of 1% are observed on low temperature oxidation. The original material has a reduced saturation magnetisation due to a combination of the effects of finite crystallite size and the replacement of iron ions by H+ ions (thus disrupting the spin alignment). The starting material can therefore be defined as a hydrogen ferrite $Fe_{3-x}H_xO_4$ or hydrous magnetite $Fe_3O_4.H_2O$.

Low temperature oxidation (200°C) produced a single phase spinel of composition intermediate between magnetite and maghemite; a spinel solid solution, $Fe_{3-x}O_4$. Higher temperatures (500°C) produced the fully oxidised spinel phase, maghemite. Decreases in unit cell parameter consistent with expected values were observed. Oxidation was thought to take place by the simultaneous removal of H^+ ions and the oxidation of Fe^{2+} to Fe^{3+}. This retains charge balance and creates the necessary vacancies required for maghemite, $Fe_8[Fe_{40/8}[]_{8/3}]O_{32}$, without a removal of iron or addition of oxygen mechanism. High resolution transmission micrographs show the grains to be single phase at these stages.

At temperatures above 600°C the presence of hematite was detected but traces of the spinel phase remained until temperatures of 800°C (15 min. annealing) and 900°C (5 min.) had been reached. At these temperatures the unit cell parameter of the spinel phase co-existing with hematite was observed to increase. The spinel solid solution phase formed on initial oxidation was thought to break down on further oxidation to form hematite and magnetite, which subsequently fully oxidizes to hematite.

Evidence in support of these conclusions has been obtained from high resolution electron microscopy and a systemmatic study of the changes in magnetic properties. The oxidation mechanism proposed here is expected to operate in nature on fine-grained or precipitated magnetites in wet environments.

ORDER-DISORDER IN ZEOLITES WITH NATROLITE FRAMEWORK

GOTTARDI G. & GALLI E., Ist. di Mineralogia, Università di Modena, Italy; LARSEN A.O., Norsk Hydro, 3901 Porsgrunn, Norway; MAZZI F., Dip. Scienze della Terra, Università di Pavia, Italy.

Until now the minerals with the natrolite framework were natrolite, mesolite and scolecite, plus tetranatrolite, the disordered counterpart of natrolite. The status of gonnardite was uncertain, because no single crystals suitable for X-ray work were available, and because some authors believed it to be a disordered form of thomsonite (1) on the basis of cell dimensions, while others (2) emphasized its similarity with tetranatrolite on the basis of powder pattern and IR spectra. One of us (A.O.L.) found fine crystals of gonnardite in a syenite pegmatite in a larvikite of the Vevja quarry, Tvedalen, Norway. X-ray single crystal analysis and refinement was performed down to a residual of 3%. Gonnardite too has the natrolite framework with a disordered (Si,Al) distribution, and the only cation site already known for natrolite, where Na is always dominant over Ca. So there is no real difference between tetranatrolite and gonnardite, the former being Ca-poorer than the latter. If the chemical formulae of all tetranatrolites and gonnardites analyzed so far are considered, it is evident that a solid solution series exists nearly from the formula of mesolite to that of natrolite, without any gap, and with a Si:(Si+Al) ratio somewhat lower than 60%, on the average. So the (Si,Al) disorder in the framework and the substitution of Na by Ca are reciprocally conditioned. To recognize this mutual influence one has to remember that in fully or partially ordered natrolites the maximum number of Ca-atoms per 80 oxygens is 0.5 (3), a value reached when the zeolite is paragenetically associated with mesolite, which has the same framework and 5.66 Ca per 80 oxygens in its stoichiometric formula. For natrolite, there are also some other analyses (4) corresponding to higher Ca-contents, but they need confirmation. In gonnardite-tetranatrolite the Ca-content per 80 oxygens may rise continuously from zero to 5.4 (1). The situation is fairly similar to that of alkali feldspars, which give a high temperature phase with (Si,Al) disorder and full (Na,K) substitution, and a low temperature phase with (Si,Al) order and a limited (Na,K) substitution; the similarity is only crystallographic, because there is no evidence that gonnardite-tetranatrolite crystallized at a temperature higher than natrolite and/or mesolite.

The water content in gonnardite is higher than in natrolite; this is explained by supposing that each Na is surrounded by 2 water molecules (and by 4 framework oxygens) in the same fashion as in natrolite, but each Ca is surrounded by 3 more water molecules, so that there is a positive correlation between Ca- and H_2O-content. The extra water sites of gonnardites are probably occupied also in paranatrolite, the little known superhydrated phase of tetranatrolite.

References

(1) Hey M.H.: Miner.Mag. 23 (1932): 51-125.
(2) Gottardi G. & Galli E.: Natural Zeolites. Springer Verlag, Heidelberg (1985), p.72.
(3) Alberti A., Pongiluppi D. & Vezzalini G.: N.Jb.Miner. Abh. 143 (1982): 231-248.
(4) Hey M.H.: Miner.Mag. 23 (1932): 243-249.

STRUCTURAL INVESTIGATION OF METAMICT MINERALS USING X-RAY ABSORPTION SPECTROSCOPY

GREEGOR, R.B. and LYTLE, R.W., The Boeing Company, Seattle, WA 98124, USA; CHAKOUMAKOS, B.C., LUMPKIN, G.R., and EWING, R.C., Department of Geology, University of New Mexico, Albuquerque, NM 87131, USA

Titanium in the octahedral B-sites of several metamict Nb-Ta-Ti oxides (AB_2O_6 type: aeschynite-(Y)(blomstrandine), euxenite; $AA'B_2O_7$: zirconolite; $A_2B_2O_6$: pyrochlore, betafite) have been investigated using x-ray absorption spectroscopy. These minerals contain U and Th which during their decay emit ~ 5 MeV alpha particles which, along with the ~0.1 MeV recoil-nuclei, cause damage to the crystalline structure by causing atomic displacements. After many decay events ($>10^{26}$ alphas/m^3) the recoil tracks overlap and the original structure becomes aperiodic and produces a diffraction pattern consistent with that of a glass. The extended x-ray absorption fine structure (EXAFS) and the x-ray absorption near edge structure (XANES) are well suited for the study of aperiodic structures and allow the determination of coordination number, bond length, disorder, and chemical environment around specific atoms.

Because of high intensity and tunability, the x-ray absorption measurements were made at the Stanford Synchrotron Radiation Laboratory (SSRL). The results for the XANES measurements of Ti at the B-site for the minerals in the metamict state are shown in Figure 1. All of the spectra in Figure 1 are remarkably similar in appearance, showing a pre-edge feature followed by a steep absorption edge with a doublet at the top of the absorption rise. In Figure 2 the XANES of Ti at the B-site for the same set of minerals after annealing to the crystalline phase (blomstrandine 510°C 52 hr, euxenite 1100°C 60 hr, zirconolite 1100°C 2 hr, pyrochlore and betafite 1000°C 1 hr) show a considerably different set of XANES spectra. These spectra resemble those for the synthetically produced crystalline counterparts of the respective minerals. The spectra for the metamict samples of Figure 1 resemble spectra for structures having corner sharing Ti octahedra such as titanite, neptunite and astrophyllite. This suggests that one effect of the metamictization process is to change edge-sharing TiO_6 polyhedra to corner-sharing geometries. Such a transition implies an increase in structural disorder, lowering of average coordination number and average bond length at the Ti site, with an increase in the Ti-M separation and inter-octahedral angle resulting in increased molar volume. These implications are in general agreement with the EXAFS measurements and other studies on radiation induced swelling.

This research was supported by DOE, Office of Basic Energy Sciences. The synchrotron beam time was provided by SSRL.

FIGURE 1. XANES FOR METAMICT MINERALS

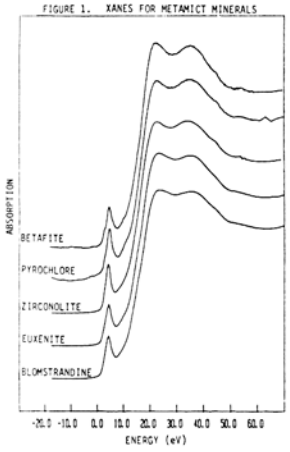

FIGURE 2. XANES FOR ANNEALED MINERALS

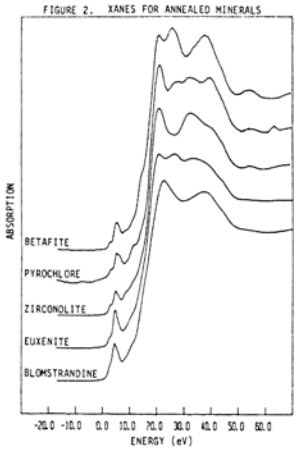

SERENDIBITE, SAPPHIRINE, AND GRANDIDIERITE FROM THE ADIRONDACK MOUNTAINS AT JOHNSBURG, NEW YORK, USA

Grew, Edward S., Department of Geological Sciences, University of Maine, Orono, Maine 04469, USA; Swihart, George H., and Moore, Paul B., Department of Geophysical Sciences, University of Chicago, Chicago, Illinois 60637, USA

Serendibite at Larsen and Schaller's (1932) main locality occurs in a 1.5 x 0.3 m pod exposed in situ between K-feldspar (Kfs) rock and marble, in cm-thick rinds on blocks of Kfs rock, and in a 4-cm thick vein in the Kfs rock. The pod is zoned as follows (SW to NE): (1) Kfs rock (2) scapolite (Scp) - diopside (Di) ± phlogopite (Phl) (3) serendibite (Srd)-Di-Phl ± Scp, (4) Phl, and (5) marble. The zonal sequence in the rinds is 1-2-3-4 and in the vein, 1-2-3-2-1. The Kfs rock consists of mm-sized microperthite and minor biotite, tourmaline (Tur), Scp, apatite, Di, plagioclase (Pl), grossular (Grs), spinel (Spl), and Srd. The marble contains calcite (Cal), dolomite, and forsterite (largely serpentinized). Cal, Spl, pargasite (Prg), Tur, sinhalite (Snh), Pl, grandidierite (Gdd), and sapphirine (Sap) appear locally in zone 3, and Grs, in zones 2 and 3. Textures suggest that Srd broke down by reactions such as: Srd ->Tur + Cal ± Spl, Srd ± Di -> Prg + Tur + Cal, or Srd ± Snh -> Gdd + Prg + Cal as CO_2-H_2O-bearing fluids were introduced; Na may have come from Scp or Phl. In one sample, Sap occurs in a matrix of Cal, Di, Phl, and Scp on the outside of Tur overgrowths resulting from Srd breakdown. Representative electron microprobe analyses (in weight %) are for Srd, SiO_2 - 26.1, Al_2O_3 - 35.6, FeO - 0.9, MgO - 15.9, CaO - 13.8, Na_2O - 1.3, Sum - 93.6; Gdd, SiO_2 -21.7, Al_2O_3 - 53.5, FeO - 0.2, MgO - 14.0, Sum - 89.4; and for Sap, SiO_2 - 12.8, Al_2O_3 - 67.0, MgO - 19.8, Sum - 99.6. The serendibite rocks resulted from boron enrichment in skarns developed metasomatically between the Kfs rock and marble (and somehow also within the Kfs rock itself) under granulite-facies conditions estimated from Bohlen et al (1985) to be 720-740°C, 6.5-8 kbar. Breakdown of Srd to Gdd, Tur, Prg, and Sap probably also occurred under these granulite-facies conditions during a later stage of the metasomatic process. A $^{11}B/^{10}B$ ratio near 4.05 for Srd probably excludes marine evaporite as a source for the boron. References : Bohlen, S.R., Valley, J.W. and Essene, E.J. (1985) J. Petrol. 26, 971-992; Larsen, E.S. and Schaller, W.T. (1932) Amer. Mineral. 17, 457-465.

ANOTHER NEW PHOSPHATE MINERAL FROM THE TIP TOP MINE, BLACK HILLS, SOUTH DAKOTA.

Grice, J.D., Mineral Sciences Division, National Museum of Natural Sciences, Ottawa, Ontario, Canada K1A 0M8, DUNN, P.J., Dept. of Mineral Sciences, Smithsonian Institution, Washington, D.C. 20560, U.S.A.

The Tip Top mine, near Custer, South Dakota, occurs in one of many phosphate-rich pegmatites, geologically related to the Harney Peak granite. The Tip Top pegmatite consists largely of quartz, perthite, albite, beryl, muscovite, tourmaline and triphylite-lithiophylite. It has been mined intermittently since 1938 for feldspar, mica and beryl.

Over 50 phosphate minerals have been identified in this deposit, 8 of which are new mineral species: jahnsite, robertsite and segelerite (Moore *et al.* 1974, Amer. Mineral.), fransoletite (Peacor *et al.* 1983, Bull. Minéral.), tinsleyite (Dunn *et al.* 1984, Amer. Mineral.), tiptopite (Grice *et al.* 1985, Canad. Mineral.), ehrleite (Robinson *et al.* 1985, Canad. Mineral.) and a new "whiteite-like" species briefly described here.

Grice, Dunn and Ramik have recently made an IMA submission (Feb., 1986) describing a new "whiteite-like" mineral. It occurs as yellow, bipyramidal crystals measuring 1.5x0.5x0.5 mm. The clear crystals have a dull lustre and often are deeply etched. It is associated with other secondary phosphate minerals, montgomeryite, englishite, roscherite, robertsite-mitridatite and tiptopite on a matrix of quartz and beryl. The new mineral is monoclinic, possible space groups $P2/a$ or Pa with a 14.842(a), b 6.97(1), c 10.109(4)Å and β 112.59(5)°. The X-ray powder diffraction pattern is indistinguishable from whiteite. Noting the paucity of iron in the associated phosphate minerals the mineral was analyzed. Its chemical formula $CaMnMg_2Al_2(PO_4)_4(OH)_2 \cdot 8H_2O$ differs from whiteite $CaFeMg_2Al_2(PO_4)_4(OH)_2 \cdot 8H_2O$ and jahnsite $CaMnMg_2Fe_2(PO_4)_4 \cdot 8H_2O$. With Z=2 D(calc)=2.637 which agrees well with D(Meas)=2.63(2) g/cm^3. Optically the "whiteite-like" mineral is biaxial positive, with α 1.580(1), β 1.584(1), γ 1.591(1), $2V$(meas) 81(5)° and $2V$(calc) 75°. A faint, concentric colour banding of pale green to colourless does not have a corresponding chemical variation within the limits of the electron microprobe.

VARIATION OF CRYSTALLINITY/METAMICTIZATION IN NATURAL TITANITES.

L.A. Groat, F.C. Hawthorne, M. Raudsepp, C. McCammon and R. Gaba, Earth Science/Physics Departments, University of Manitoba, Winnipeg, Manitoba, Canada, R3T 2N2; G.R. Lumpkin and R.C. Ewing, Geology Department, University of New Mexico, Albuquerque, New Mexico 87131, U.S.A.

Natural titanites show significant variation in crystallinity due to varying degrees of metamictization. We have examined sixteen natural titanites showing a wide range of crystallinity to document the effect of these variations on their physical and chemical properties. X-ray diffraction patterns show very variable resolution, particularly at high angle, decreased resolution and intensity resulting presumably from loss of diffraction coherence with increasing metamictization; infrared spectra show very variable resolution, particularly in the Si-O principal vibration region (1200-800cm^{-1}), that parallels the trends shown in the X-ray diffraction patterns. Resolution of both techniques is also a function of sample grinding time, as serious degradation of the diffraction patterns and infrared spectra occurred with increased grinding times. Electron microprobe analysis sums systematically decrease with decreasing crystallinity, correlating with the corresponding decrease in sample density, and Mössbauer spectra show increasing Fe^{2+}/Fe^{3+} with decreasing crystallinity.

X-ray precession photographs show spot sizes that increase with decreasing crystallinity. The crystal structures of four titanites were refined in space group C2/c, both before and after annealing at 1000°C for 6 hours. The most notable result was the correlation of the thermal parameters with the degree of crystallinity as estimated from the powder X-ray and infrared methods. This presumably reflects the increased positional disorder in the more metamict sample structures. Examination of the most metamict sample by transmission electron microscopy shows distinct mottled diffraction contrast, presumably resulting from overlapping α-recoil tracks; the electron diffraction patterns are sharp, but with diffuse diffraction halos suggesting aperiodic areas. Annealing seems to restore the structure, but for the different experimental methods used, the increase in resolution is not uniform.

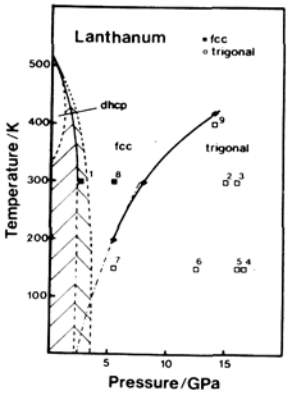

Figure 2: Phase boundaries of the dhcp-fcc and the fcc-trigonal transitions in lanthanum. The numbers mark the sequence of the measurements. The range of dhcp-fcc bistability from ref. 1 is shaded.

trigonal distortion. The present data (full line) for this second order phase transition agree well with earlier data from resistivity measurements (dash-dotted line, (2)).

These and other data will be discussed as examples for future applications of this technique.

(1) B. Merkau and W.B. Holzapfel, Physica B (in press)
(2) H. Balster and J. Wittig, J. Low. Temp. Phys. 21, 377 (1975)

ENERGY DISPERSIVE X-RAY DIFFRACTION IN AN EXTENDED PRESSURE-TEMPERATURE RANGE

GROSSHANS, W.A. and HOLZAPFEL, W.B., Fachbereich Physik, Universität-GH-Paderborn, D-4790 Paderborn

The high photon fluxes of synchrotron radiation allow for reasonable recording times in high pressure X-ray diffraction even with small samples and weak scatterers as well as for kinetic studies of phase transitions. A spectrometer system with complete remote control for simultaneous recording of X-ray diffraction and ruby fluorescence spectra will be discussed. The remote control allows for X-ray data collection, for all adjustments, for changes in pressure and for its determination without removing the high pressure cell from the diffractometer.

Diamond anvil cells with miniature heaters and thermcouples for measurements at temperatures up to 600 K as well as with liquid nitrogen cryostats for temperatures down to 100 K and pressures up to 50 GPa have been used with this setup.

The accuracy of this system has been tested with measurements of the lattice parameters on silver up to 40 GPa with nitrogen as pressure transmitting medium. The scattering of the data gives an accuracy in the specific volume of about 0.3 %. As an example for studies of phase diagramms, figure 1 presents data for lanthanum. The dhcp-fcc phase boundary resulted from kinetical studies (1), where the volume fraction $\zeta(t)$ of the transformed material was measured and fitted to an Avrami equation $\zeta(t) = 1-\exp(-(t/\tau)^n)$ with n=1. The solid line corresponds to the "thermodynamic" transition pressure in a model of homogeneous nucleation, neglecting local stresses. The hatched area illustrates the large hysteresis of this transition. The upper bound of the bistability range (broken line) is close to earlier data for the transition pressure (2). The rhombic symbols in figure 1 represent the onset of the

MINERALOGICAL EVIDENCE OF MAGMATIC PROCESSES AT MEDICINE LAKE HIGHLAND, N. CALIFORNIA, A CONVERGENT MARGIN CALC-ALKALINE VOLCANIC SYSTEM

GROVE, T.L., BAKER, M.B., KINZLER, R.J., Dept. Earth, Atm. and Planet. Sci., Mass. Inst. of Tech.,Cambridge, MA 02139; DONNELLY-NOLAN, J.M., U.S. Geological Survey, 345 Middlefield Road, Menlo Park, CA 94025

Mineralogical evidence has played a key role in constraining geochemical modelling and interpretation of the magmatic processes which operated in the Medicine Lake volcanic system to produce calc-alkaline series lavas. The mineral assemblages in the basalt to andesite series are consistent with the crystallization of mantle-derived high-alumina basalt (HAB) parent magma at shallow crustal levels (1 to 2 kbar) accompanied by assimilation of a silicic crustal component. Partly melted silicic xenoliths which have been preserved in varying stages of digestion provide samples of the material which has been assimilated. The changing mineral assemblages in these inclusions record the progress of the assimilation process.

The Giant Crater-Chimney Crater flow on the south side of Medicine Lake is compositionally zoned from HAB (48 wt.% SiO_2, 18% Al_2O_3, 10% MgO, 9% FeO) to basaltic andesite (BA, 53% SiO_2, 6.5% MgO, 7% FeO). The least evolved HAB lavas contain olivine (Fo_{89-87}) and plagioclase (An_{86-80}) microphenocrysts (1 to 4 modal %). The intermediate HAB lavas are nearly aphyric, and the most evolved BA lavas contain glomerocrysts of olivine (Fo_{85-70}) and plagioclase (An_{84-69}) and abundant xenocrysts of quartz, sodic plagioclase (An_{29-39}) and Fe-rich orthopyroxene (En_{54-60}).

Silicic xenoliths from the Giant Crater and other Holocene lava flows are granitic in composition and have granophyric to hypidiomorphic textures indicating a mixed subvolcanic silicic plutonic to pre-volcanic "Sierran" plutonic source for the assimilated material. The least melted silicic inclusions contain partly melted biotite, which breaks down to orthopyroxene, magnetite, ilmenite and a volatile-rich glass. In the more highly melted inclusions, biotite has disappeared and orthopyroxene, magnetite and ilmenite remain with alkali ($Or_{50}Ab_{46}$) and plagioclase (An_{20-40}) feldspar and quartz. The

MINERALOGIC EVIDENCE OF MAGMATIC PROCESSES AT MEDICINE LAKE
GROVE, T.L., et al.

partial melt in these inclusions is alkali, FeO and TiO_2 rich (65% SiO_2, 16% Al_2O_3, 6% Na_2O, 6% K_2O, 4% FeO, 1% TiO_2) and highly enriched in incompatible trace elements. Highly melted inclusions contain dominantly quartz and an alkali-rich melt depleted in FeO and TiO_2. Plagioclase and alkali feldspar are present in reduced proportion. The phase disappearance sequence described above is consistent with melting under low pressure, hot and dry conditions (Naney,1983,AJS,283,993). Under equilibrium conditions plagioclase should be the last mineral to melt in these inclusions, but quartz is more abundant than feldspar in the residual mineral assemblage. Quartz is residual because its dissolution rate is slower than the dissolution rates of feldspars.

The combined fractional crystallization and assimilation process (AFC) which generates andesite from HAB proceeds by low pressure olivine + plagioclase crystallization accompanied by progressive assimilation of partial melts of silicic xenoliths. Phenocryst compositions and proportions in lavas and troctolitic cumulate inclusions (35% oliv: 65% plag by wt.) are similar to experimentally determined phase proportions for this HAB at low pressure (Grove et al.,1982,CMP,80,160). The early part of the HAB to BA trend shows an increase in FeO, TiO_2, and incompatible elements which is caused by fractional crystallization of oliv + plag, back mixing of fractionated liquid and selective assimilation of melts of the silicic xenoliths. The latter part of the trend is generated by continued fractionation accompanied by bulk assimilation of the highly melted xenoliths.

Ratios of assimilation/fractionation (R) estimated for the HAB to BA trend are high (R>1), and are inconsistent with simple heat budget calculations for AFC at shallow crustal levels (R=0.3). The high R values can be reconciled, if heat and mass transfer are decoupled. Field evidence indicates that large volumes of basalt are present. A small amount of crystallization of the large volume of basalt supplies heat to drive the AFC process. A small fraction of the total volume of basalt magma is contaminated by silicic melt. Such a process is consistent with the relative volumes of erupted material (uncontaminated HAB = 9 km^3, contaminated BA = 0.2 km^3) and relative rates of thermal (10^{-4} cm^2/sec) vs chemical (10^{-8} cm^2/sec) diffusion.

USE OF PHASE TRANSITIONS AND DECOMPOSITION REACTIONS IN PYROXENES AS COOLING RATE SPEEDOMETERS

GROVE, T.L., and JUSTER, T.C., Dept. of Earth, Atm. and Planet. Sci., Mass. Inst. of Tech., Cambridge, MA 02139 USA

Pyroxenes may contain a submicroscopic record of phase transitions which can be used to infer the thermal history of the sample in which the crystal formed. An interpretation of this submicroscopic textural record is useful for both estimating the sample's temperature-time path and for interpreting the temperature recorded in pyroxene geothermometers. Transmission electron microscopy (TEM) has been used to characterize pyroxenes produced in dynamic crystallization experiments carried out at controlled cooling rates and pyroxenes from lava flows, dikes and sills where thermal histories can be inferred. The submicroscopic textures allow calibration of cooling rate over the range of >1000°C/hr to 0.01°C/hr, rates that are appropriate for the cooling of small igneous bodies. Pyroxene compositions which are useful for cooling rate speedometry span the range of Wo_5 to Wo_{45}. This study has been restricted to pyroxenes with Mg# (=Mg/(Mg+Fe^{2+})) in the range 0.70 to 0.80. Pyroxenes with this range of Mg#s are common in volcanic and plutonic rocks, and an understanding of the significance of their submicroscopic textures has broad application.

A schematic equilibrium phase diagram for a section through the pyroxene quadrilateral at Mg#=0.75 (Fig. 1) has been constructed using the data of Lindsley et al. (1983,JGR,88,A887), Huebner (1982,Rev. Min.7,213) and Tullis and Yund (1979,Am. Min.64,1063). This diagram serves as a base for constructing TTT (Time-Temperature-Transformation) diagrams. On the TTT diagram the beginning of the transformation is represented as a C-shaped curve. The shape of the curve is controlled by the interplay of diffusion rate and nucleation rate (or initial wavelength for spinodal decomposition), and the nose of the curve occurs at the temperature for which diffusion rate is rapid and nucleation or initial wavelength is optimal. Our laboratory and natural experiments have been used to position the C-shaped curves in Figs. 2 and 3. The TTT diagram for Wo_5 (Fig.2) contains a field for decomposition of pigeonite to pigeonite + augite by either spinodal decomposition or homogeneous nucleation. The nose of this curve is placed using TEM observations of cooling rate experiments and lunar samples (Grove,82,Am. Min.67,251), and is consistent with observations of Carpenter (1978,P. Chem. Min.2,237). The pigeonite > orthopyroxene transition produces homogeneously-distributed lamellar precipitates on (100) of a high-Ca phase. This transition has been observed in pigeonite from the Great Connecticut dike, and the cooling history estimated for this sample is used to position the C-curve. Two C-curves for spinodal decomposition to augite + pigeonite in Wo_{30} and Wo_{42} are shown in Fig.3. The curve for Wo_{30} is from Grove (1982) and the Wo_{42} curve is inferred from TEM observation of augites in a 4m thick lava flow at Medicine Lake, N. Calif. The beginning of decomposition is very sensitively controlled by the position of the coherent spinodal in this part of composition space (Fig.1). Hence, Ca-rich augites decompose to two-phase assemblages only at slow cooling rates.

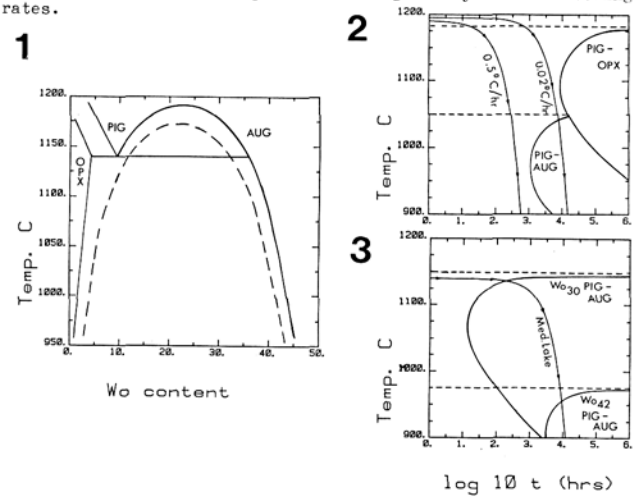

• CHRYSOTILE ASBESTOS FROM CHINA

GU Jiexiang and TANG Suren, Department of Non-Metallic Mines Engineering, Wuhan University of Technology, Hubei, People's Republic of China

The major industrial chrysotile deposits in China may be classified according to mode of occurrence, into two types, i.e., ultrabasic rock type and carbonatite type. Using various methods of X-ray diffraction, studies for 73 samples from seven major chrysotile deposits are made. It is shown that there are six varieties of chrysotile in China, including clino-chrysotile, ortho-chrysotile, Dc type chrysotile, para-chrysotile, povlen-clinochrysotile and povlen-orthochrysotile. The characteristic of each variety of chrysotile is as follows: Typical d values are $d(202) < 2.45$ Å and $d(203) = 2.09$ Å (weak) for 2Mc1, while $d(202) \cong 2.52$ Å and $d(203) = 2.34$ Å (strong), for 2Orc1. The 201 reflection on a rotation photograph, intensity of reflection for 2Orc1 is very strong and is weak for 2Mc1, when l is odd, reflection of 2Orc1 is separated into $+l$ and $-l$ while reflection of 2Orc1 is only a spot, when l is even. Meanwhile, the author discovered that the chrysotile deposit in Jilin, which contains mainly ortho-chrysotile (over 70%) and relatively more para-chrysotile, is a rare and special chrysotile deposit in the world.

MODULATED 2:1 LAYER SILICATES

GUGGENHEIM, S., Dept. of Geological Sciences, University of Illinois at Chicago, Chicago, Il. 60680, USA

A modulated layer silicate is defined as a layer silicate with a periodic perturbation occurring in the structure. Although a prominent sublattice approximating a normal type of 2:1 structure (e.g., talc, mica) occurs, the overall structure is more complicated. These complications usually involve tetrahedral connections across the interlayer region and discontinuities in the tetrahedral sheets. However, in order to maintain two dimensional character, a continuous or nearly continuous octahedral sheet is a requirement; therefore, sepiolite and palygorskite type minerals are not discussed. Members of this subgroup include zussmanite (Lopes-Vieira and Zussman, 1969), ganophyllite/eggletonite (Eggleton and Guggenheim, 1986), stilpnomelane (Eggleton, 1972), minnesotaite (Guggenheim and Eggleton, 1986) and bannisterite (Threadgold, 1979).

MODULATED 2:1 LAYER SILICATES

GUGGENHEIM, S.

Modulated 2:1 layer silicate structures may be divided generally into two groups, forming tetrahedral sheet discontinuities that are either island-like (zussmanite, stilpnomelane, bannisterite) or strip-like (ganophyllite, minnesotaite). Bannisterite is complex but more closely approximates island-like structures. A plot of the average radius size of the tetrahedral cations (r_t) vs the average radius size of the octahedral cations (r_o) shows the distribution of structures with respect to tetrahedral/octahedral (T/O) sheet misfit. Theoretical approximations (ignoring the effects of temperature and pressure) may be made delineating where an ideal tetrahedral sheet is equal in lateral size to an ideal octahedral sheet. It is evident that T/O sheet misfit is a geometrically limiting factor for stability. For relatively small differences in component sheet lateral dimensions, a limited corrugation of the T/O sheet interface allows for a continuously varying structural adjustment. It is likely that distortions of the octahedral anion arrangement located at strip or island edges contribute also to the relief of T/O sheet misfit. Compared to octahedra confined between opposing tetrahedra, these octahedra have additional coordinating anions not linked to tetrahedra; several tetrahedra have inverted apices and are not attached to octahedra. In at least one case (ganophyllite), cation ordering contributes greatly to reducing misfit.

The r_t vs r_o plot may be used as a predictive tool both to identify new modulated 2:1 layer silicates and to aid in establishing the nature of the perturbation. Based on their plotted positions, parsettensite and gonyerite are identified as new members of the group. Electron diffraction data are presented to confirm this conclusion. Gonyerite represents the first known modulated chlorite structure whereas parsettensite appears to be a variation of the stilpnomelane structure with smaller island-like regions. The nature of the modulations are discussed.

References

Eggleton, R.A. (1972) The crystal structure of stilpnomelane. Part II. The full cell. Mineralogical Magazine 38, 693-711.

Eggleton, R.A., and Guggenheim, S. (1986) A re-examination of the structure of ganophyllite. Mineralogical Magazine, in press.

Guggenheim, S. and Eggleton, R.A. (1986) The crystal structures of minnesotaite. Canadian Mineralogist, in press.

Lopes-Vieira, A. and Zussman, J. (1969) Further detail on the crystal structure of zussmanite. Mineralogical Magazine 37, 49-60.

Threadgold, I. (1979) Ferroan bannisterite-a new type of layer silicate structure. Seminar on Broken Hill. Mineralogical Society of New South Wales and the Mineralogical Society of Victoria.

•AN Mn- AND Si-BEARING AMORPHOUS "MINERAL"

GUO Shiqin, and GUO Lihe, Institute of Mineral Deposits, Chinese Academy of Geological Sciences, Beijing, People's Republic of China

At the contact zone between manganese ore and trachyte in the Wafanzi manganese deposit, a kind of Mn and Si-bearing amorphous mineral was recognized. It is a product of low temperature hydrothermal solutions, just like opal. It is red-brown in color with various tones. The refractive index is 1.4600-1.4796, and specific gravity 2.571-2.810. Silica and manganese oxide make up its major components with the average weight percentages being 41.7% and 29.69%, respectively. Its water content is over 10%. Moreover it contains minor amounts of such elements as Fe, Al and Ca. Its color tone depends on its iron and manganese contents: it becomes darker with increasing iron and manganese.

The "mineral" occurs in veinlet form on the site of manganese ore at the contact zone. The width of the veinlet is less than 1 mm. It is associated with jacobsite, rhodonite, garnet, epidote, brucite, apophyllite and some other minerals and also contains a lot of tiny inclusions of jacobsite.

In spite of its stable chemical composition, the mineral shows no crystal structure; therefore, there are no sharp diffraction peaks in its X-ray diffraction pattern. When the sample is heated to and then kept at 380°C for one hour, no crystal phase is observed. When the temperature reaches 950°C, braunite appears. When it is below 380°C, the infrared spectrum also shows an amorphous structure. At 950°C, the Si-O vibrations of the sample are obviously split, implying the appearance of a new phase - braunite. The infrared spectrum reveals the existence of a major phase, which may be an amorphous aluminosilicate.

HIGH-PRESSURE MÖSSBAUER SPECTROSCOPY OF MINERALS

HAFNER, S.S., Institute of Mineralogy, University of Marburg, 3550 Marburg, West Germany

Mössbauer spectroscopy is a sensitive method for studying the local electronic state and chemical bonding of certain atoms in minerals. Since more than two decades, attempts have been made to use the Mössbauer effect for measuring possible dependency of the electronic state on pressure. Three different high-pressure devices have been employed thus far. (i) The pioneering apparatus of Debrunner et al. (1) used steel anvils, the direction of the gamma rays being perpendicular to the axis of the pistons of the press. The absorber area using this device is, however, very small, requiring a high density of the particular isotope for the effect. Drickamer et al. (2) studied a large number of synthetic iron compounds, mainly enriched in ^{57}Fe to 70% or more at pressures up to about 200 kbar. (ii) Huggins et al. (3) used diamond anvils, the gamma rays passing through the anvils. They measured absorbers at pressures of 500 kbar and higher under quite hydrostatic conditions. With this apparatus, the gamma rays pass through the anvils. The area of the absorber is about 10^{-4} cm^2. With a special technique, samples could be heated simultaneously with a laser at 1000°C and higher. (iii) Another method (4) uses anvils of B_4C which allow absorber areas of 0,2 cm^2. Approximately 80% of the gamma rays are absorbed by the anvils. The range of pressures at the absorber is limited to about 100 kbar. Pressures can be calibrated precisely by measurement of the resistance of a thin metallic wire passing through the sample. The temperature of the absorber can be raised and regulated up to at least 300°C by heating the anvils. Using a clamp device, absorbers can be held under pressure at 5 K.

All three techniques suffer from a reduced resonant absorption effect because of small size of sample (i, ii), strong colimation (i, ii), and/or high absorption of the gamma rays by the anvils (ii, iii). However, high pressure studies on a routine basis can be made in the pressure range of 0-60 kbar at 5 and 300-600 K, yielding high quality spectra. For ^{57}Fe, the amount of natural Fe in the mineral sample should be approximately 1 mg in a sample of approximately 10 mg. High-pressure spectra e.g. of ^{57}Fe and ^{119}Sn of natural iron-, and tin-bearing minerals can be studied under well-controlled conditions of pressure and temperature, yielding resonant absorption effects exceeding 5% and without experimental broadening of linewidth, e.g. using B_4C anvils. However, applications to significant mineralogical problems have been scarce until now.

Application of the B_4C technique showed that the dependence of isomer shifts and quadrupole splittings e.g. of Fe^{2+}, Fe^{3+} at the various sites in silicates are generally small. Results and conclusions known up to date will be demonstrated.

(1) P. Debrunner et al. Rev. Sci. Instr. 37, 1310 (1966).
(2) H.G. Drickamer et al. Science 163, 885 (1969).
(3) F.E. Huggins et al. Carnegie Institution of Washington Year Book 74, 405 (1975).
(4) J.S. Schilling et al. Rev. Sci. Instr. 45, 1353 (1974).

ANHARMONICITY AND STRUCTURAL INSTABILITY BELOW THE ORTHO-PROTO PHASE TRANSITION IN ENSTATITE, $Mg_2Si_2O_6$: A HIGH TEMPERATURE NEUTRON DIFFRACTION AND RAMAN SCATTERING STUDY

HAGA, N. and GHOSE, Subrata, Mineral Physics Group, Department of Geological Sciences, University of Washington, Seattle, WA 98195, U.S.A.; McMULLAN, R. K., Chemistry Department, Brookhaven National Laboratory, Upton, NY 11973, U.S.A.; SHARMA, S. K., Hawaii Institute of Geophysics, 2525 Correa Road, Honolulu, HI 96822, U.S.A.

The first order phase transition from orthoenstatite to protoenstatite occurs at approximately 1263K. We have carried out high temperature neutron diffraction and Raman scattering experiments on orthoenstatite single crystals up to 1245K to determine anharmonic thermal vibrations and structural instability below the ortho-proto phase transition. Neutron refinements of the orthoenstatite structure at 298, 730, 1000, 1200 and 1245K using harmonic and anharmonic thermal vibration parameters up to 4th rank tensors indicate pronounced anharmonic thermal vibration of the Mg(2), followed by O3A, O3B, O2A, O2B, O1A, O1B and Mg(1) atoms, whereas those for SiA and SiB atoms are not significant. The thermal vibration parameters increase with temperature, showing pronounced non-linearity above 700K. A similar non-linearity is also observed for the frequencies of strong Raman bands, which decrease with temperature, whereas the line-widths increase with temperature. The libration amplitudes of the SiA and SiB tetrahedra and the corresponding chain-kinking angles (O3-O3-O3) increase markedly with temperature. The SiB chain kinking angle and some of the Mg-O bond lengths show critical behavior in the 1200-1245K range, indicating signs of the impending phase transition.

COLLABORATION OF THE INTERNATIONAL MINERALOGICAL ASSOCIATION-COMMISSION ON APPLIED MINERALOGY (IMA-CAM) AND THE INTERNATIONAL COUNCIL FOR APPLIED MINERALOGY

Richard D. Hagni, Department of Geology and Geophysics, University of Missouri-Rolla, Rolla, Missouri 65401, USA

Only very recently has the significance of applied mineralogy in the minerals and various other industries received sufficient attention. As its importance became better recognized in the 1970's, several organizations were formed to sponsor papers in applied mineralogy. The Process Mineralogy Committee of AIME was organized in 1978 and met in 1979 in New Orleans. Additional national organizations were subsequently formed in South Africa, France, and Canada. As these organizations prospered, it was recognized that there was a need to form an international organization to promote and stimulate the exchange of ideas, methods, and applicatons of mineralogy. The first International Congress on Applied Mineralogy in the Mineral Industry (ICAM) was organized and convened in Johannesburg, South Africa in June, 1981. During that ICAM meeting, the International Committee (later changed to Council) on Applied Mineralogy was formed to guide the future of ICAM. Subsequently, the International Mineralogical Association, recognizing a similar need, organized the Commission on Applied Mineralogy (IMA-CAM).

During the second triennial meeting of ICAM, which was held February, 1984 in Los Angeles, California, representatives from IMA-CAM and the International Council for Applied Mineralogy met to discuss areas of mutual interest and possible means of collaboration. Those discussions resulted in the agreement that both groups would continue to exist and hold separate meetings, and that the two organizations would co-sponsor symposia or sessions on topics of mutual interest at subsequent IMA and ICAM meetings.

It was agreed that the initial co-sponsored symposia would be held at the Stanford, California meeting of IMA. Toward this end, two sessions have been organized: 1) "Applied Mineralogy" in which ICAM is the lead organization, and 2) "Surface Analytical Methods" for which IMA-CAM is the lead organization.

It is anticipated that these two joint symposia will form the foundation for future valuable, informative, and successful collaboration between IMA-CAM and the International Council for Applied Mineralogy. Subsequent collaboration for joint sessions is planned for the third ICAM in Orléans, France in July, 1987.

ORE MICROSCOPY AND PARAGENETIC SEQUENCE OF THE ORES IN THE SOUTHEAST MISSOURI LEAD DISTRICT

HAGNI, Richard D., Department of Geology and Geophysics, University of Missouri-Rolla, Rolla, Missouri 65401, USA

The ore deposits of the Southeast Missouri Lead District, the world's largest lead producing district, are composed of lead, zinc, copper, iron, cobalt, and nickel sulfides, copper-arsenic sulfosalts, together with the non-sulfide gangue minerals, dolomite, quartz, calcite, dickite, and bitumen. Those ore and gangue minerals have been introduced into the host Upper Cambrian Bonneterre Formation, which consists of dolomite and shaly dolomite in the vicinity of the ore deposits, where favorable structural conditions were associated with favorable sedimentary facies. The minerals were deposited by replacement of the host carbonate rock and by deposition of crystals that line the vugs.

Observations of the sequence in which the minerals were superimposed upon each other within the vugs, the ore microscopic study of the fine-grained disseminated and massive ores, and the interpretation of the open space filling, replacement, and exsolution textures, has provided an understanding of a general paragenetic sequence that is applicable to all of the ore deposits in the district, although not all portions of the sequence are everywhere present.

The first stage in the paragenetic sequence is that of the deposition of the disseminated iron and iron-nickel sulfide association of pyrite, marcasite, and bravoite that was deposited by replacement of the host dolomite and shaly dolomite.

The second stage of ore deposition is characterized by local, early massive bornite-chalcopyrite replacements of dolomite that contain small amounts of the cobalt-nickel thiospinels, iron, cobalt and nickel disulfides, nickel arsenide, copper-arsenic sulfosalts, and copper sulfides. The minerals found in this association include bornite, chalcopyrite, fletcherite, nickelean carrollite, pyrite, bravoite, vaesite, cobaltian pyrite, gersdorffite, tennantite, enargite, digenite, anilite, chalcocite, djurleite, covellite, and blaubleibender covellite. Most of these minerals are very uncommon in the Southeast Missouri ores and they are absent from most other Mississippi Valley-type districts.

During the main disseminated, massive, and colloform sulfide ore deposition stage, chalcopyrite was deposited largely before sphalerite, sphalerite mainly before galena, galena before, during and after colloform pyrite and marcasite. The fluids ranged in temperature from 137°C to 82°C with a salinity of about 23 wt % NaCl equivalent.

Vug-lining crystals were deposited following the main ore stage. Sparry dolomite was repetitively deposited and leached. Earlier formed octahedral galena was partially leached. Cubic galena, quartz, and other sulfides were deposited. Millerite was deposited and altered to an association of polydymite, siegenite, and vaesite.

The last stage involved deposition of calcite and minor dickite, marcasite, chalcopyrite, pyrite, bravoite, and bitumen from fluids that were less saline and cooler.

The sulfide minerals were repetitively deposited. Nine periods of chalcopyrite deposition have been distinguished, five periods of sphalerite, seven periods of galena, and many periods of pyrite and marcasite.

The lengthy paragenetic sequence for the ore deposits, the repeated deposition of each of the ore and gangue minerals, and the distinct fluctuations for most of the minerals even within a single period of deposition are characteristic of the ore deposits in the Southeast Missouri Lead District and for all Mississippi Valley-type deposits. These features result from a lengthy time of ore deposition, a pulsating introduction of the ore fluids, fluctuations in the fluid physico-chemical character and concentrations of chemical constituents during the deposition of a given period of deposition, the local dissolution of previously deposited minerals and redeposition of those constitutents elsewhere, and the admixture of fluids of supergene and perhaps magmatic hydrothermal origins with connate brines.

COMPUTER-ASSISTED IDENTIFICATION OF ORE MINERALS USING QUANTITATIVE AND QUALITATIVE PROPERTIES

HAGNI, Richard D., Department of Geology and Geophysics, University of Missouri-Rolla, Rolla, MO 65401, USA; HAGNI, John E., Scientific Computer Systems Inc., P.O. Box 783, Arlington, VA 22216-0783, USA

Previous systems for the identification of ore minerals utilizing properties determined with the reflecting microscope have not been adequate because of one or more of the following reasons: 1) they have relied mostly upon qualitative properties, 2) they require measurements of ore mineral properties utilizing equipment that is not available in most laboratories, 3) they are based upon a single property or two, 4) they are inflexible in that they require determinations for most or all of the specified properties, and 5) they do not utilize today's available technology.

In order to provide a modern ore mineral identification system, a microcomputer program, ORE.ID, has been written which rapidly searches a data base consisting of the principal identification properties for 649 ore minerals. Although the data base includes quantitative and qualitative properties, searches may be performed on any or all of the properties.

The quantitative data base includes average Vickers hardness number and reflectance. The semi-quantitative and qualitative data base includes Talmage hardness, strength of anisotropism, color and tint shown by the ore mineral, and the colors and tints of the internal reflections. Information from the International Mineralogical Association-Commission on Ore Microscopy (IMA-COM) quantitative data card file have been utilized where available. Most of the additional data were compiled from the literature, but some were measured or determined in the Ore Microscopy Laboratory at the University of Missouri-Rolla (UMR) and others were approximated using graphs and known properties. The entry of the seven data items or portions of those data for an unknown ore mineral into the program causes the computer to search the data base and to find those minerals for which data matches occur.

Although the principal purpose of the program is to narrow the possible minerals for a given unknown to a small number that can then be compared more closely to those in standard descriptive texts, in many instances the program provides an immediate selection of a single most probable mineral. This is largely the result of a feature of the program that displays the number of data matches for each of the possible minerals. The display

of the chemical components for each computer-selected possible mineral also helps to further identify the unknown mineral. The search range can either be widened for each of the identification properties to find a larger list of ore minerals if the initial search did not find likely minerals, or the search range can be narrowed for a repeated search of the data base to find a smaller, more select list of possible ore minerals. Previously entered data can be conveniently retained for repeated searches.

ORE.ID is an evolving program and several new features have recently have been or are being added. Data for 78 platinum-group minerals have been added to the data base. The program is being reorganized to search on the basis of chemical composition rather than simply print the chemical constitutents for those minerals found to match the input data. Quantitative color values for 107 ore minerals from the IMA-COM data card file and calculations of x, y, Y, λ_d, and Pe from literature reflectance values for about 300 additional ore minerals are currently being added to the program to extend its use to those individual whose laboratories are equipped to measure those values.

The program will operate on any microcomputer that will run dBase II and has a memory of at least 64K. The program runs on an IBM PC and an IBM XT in the Ore Microscopy Laboratory at the University of Missouri-Rolla and on a Heathkit H-100 (Zenith Z-100) at Scientific Computer Systems, Inc.

The microcomputer program provides a marked advancement for the practicing economic geologist in comparison to ore mineral identification systems that involve charts, tables, cards, and punched cards. ORE.ID is rapid, easy-to-use, flexible, utilizes most of the properties commonly determined for ore minerals, searches a data base consisting of a very large number of minerals, and is available from the authors.

XRD DATA PROCESSING USING THE SINCLAIR QL

Hall, A. J., Department of Applied Geology, University of Strathclyde, GLASGOW, Scotland.

A computerised X-ray diffraction technique has been developed using the Sinclair QL microcomputer. The technique is now in regular use, both in research and teaching, for mineral identification and quantification. The QL with its 128K memory and good resolution colour graphics, provides an inexpensive, rapid and very versatile method of presenting and interpreting XRD profiles.

A Philips diffractometer is interfaced to an ITT.XTRA PC which is programmed to collect and store XRD profiles on floppy disc. Interfacing of the ITT and QL permits transfer of data to the QL cartridge or disc.

XRD profiles are plotted on a 400 x 100 pixel window on the QL screen. Four other windows carry instructions or information. Variable horizontal scaling (0-100°2θ) and vertical intensity scaling (absolute, normalised or log) permits versatile presentation of profiles which can be labelled or superimposed for comparison. A peak search routine based on stored data for one hundred common minerals is particularly valuable for unscrambling mixtures. Stored profiles or JCPDS data, unlimited in number in theory, can be loaded from cartridge and displayed on the QL screen within minutes. A FACIT colour plotter provides high quality hard-copy.

The QL was selected because of its low cost (~$750), its portability and the easy-to-use superbasic language. XRD is the best method of mineral identification and XRD users need no longer be tied to the XRD laboratory; XRD data can be interpreted where convenient - in the office, at home or in the field.

JADEITITES & THEIR FLUID INCLUSIONS FROM RIO MOTAGUA, GUATEMALA

HARLOW, George E., Department of Mineral Sciences, American Museum of Natural History, New York, NY 10024-5192

Jadeite rock (jadeitite) occurs as blocks in tectonized serpentinite along the north side of the Motagua Fault in Guatemala, particularly along Rio La Palmilla and between the villages of Palmilla and Usumatlan. Jadeitite occurs in mixed jadeitite-albitite "fields" but is most conspicuous as stream boulders. The fields "outcrop" as badly-weathered rubble-strewn white mounds in weathered serpentinite and manifest roughly concentric zoning from outer serpentinite to chlorite schist to rimming albitite. Rim zones are pierced by veins of acicular actinolite with crystals up to 10 cm long. The serpentinite rim zones are also decorated with mammillary hydromagnesite. Jadeitites are composed of jadeitic pyroxene with variable amounts of white mica (usually paragonitic) and albite with minor titanite, zoisite, apatite, and zircon. "Retrograde" reactions, replacing jadeite and paragonite as rims and fracture fillings, have produced analcime, albite, blue amphibole (baroisitic) and occasional natrolite and zoisite. Reaction zones progressively replace jadeitite with albitite that frequently shows sheared textures. Textures in jadeitite range from sheared granular aggregates, to sub-centimeter wheat-sheaf pyroxene intergrowths, to multi-centimeter prismatic crystals filling brittle fractures. Pyroxene compositions trend from pure/nearly-pure jadeite through rimming omphacite to occasional late-stage diopside; acmite and hedenburgite contents are usually low ($\leq$12 mol % ea) and rarely there is significant ureyite ($NaCrSi_2O_6$) content (up to 35 mol %) in association with fragmented chromite.

Particularly important questions relative to jadeitite petrology are the conditions of formation and metastability, both with respect to intrinsic parameters, P + T, and to the chemical activities of fluids, Na^+, SiO_2, etc. The reactions that are invoked in formations are:

Albite = Jadeite + Quartz (1)

or Albite + Nepheline = Jadeite (2)

Retrograde reactions are controlled by:

Jd-pyroxene + Fluid = Analcime + Na-amphibole (3)

and Analcime + Quartz = Albite (4)

Because of the lack of substantiated nepheline in any occurrence or suggested protolith, equation (1) has been preferred, but lack of quartz in jadeitites may permit equation (2) to be important. Variation of SiO_2 activity, particularly its decrease, is ascribed to absorption by the ultramafic as a reactant during serpentinization, particularly where olivine is greater than pyroxene. Unfortunately, reactions 1 and 2 are poorly constrained experimentally at low T (≈300° C?) where brittle deformation is recorded in several jadeitites.

A potentially useful indicator is abundant fluid inclusions in coarse jadeite from Guatemala. Preliminary results show the following: 1) The inclusions are usually 2 phase (fluid + smaller gas bubble, constant ratio), usually elongated along the c-axis, and appear to be a mix of primary, pseudo-seconday and secondary. 2) All inclusions freeze at -5.6° to -5.7° C which yields a NaCl equivalent solute concentration in H_2O of 8.7 wt.%. If the fluid is related to sea water involved in serpentinization, these data give slightly more than twice the original fluid salinity and suggest a low local water to rock ratio (≈1:1). The fluid composition is consistent with a Na-rich metasomatic/hydrothermal origin for jadeitization. 3) Homogenization temperatures range from 260° to 283° C, which can define a lower limit of an envelope in which jadeitization occurs. Using the constructions of isochores of Bodnar and Roedder (1980), extrapolation for the observed inclusions to 500° C (an upper limit used by some authors) yields a minimum bracketing P between 2.0 and 2.6 kbar (compared to a minimum 14 kbar for eq. 1, 8.5 kbar for eq. 2 and 11 kbar for eq. 3)

Obviously these inclusions have too low a density to be consistent with data for equations 1 to 3. They represent a uniform fluid with very little dispersion in density sampled ubiquitously during crystallization and later events, and it is doubtful that they could have uniformly leaked during ascent. Obviously more inclusions need to be examined and better constraints established, but a low T and P model for jadeitization must be scrutinized seriously. Fluid inclusion measurements on jadeitite albite and regional albitites are underway to attempt to constrain their formational conditions and relationship to jadeitites.

THE DIVERSE MINERALOGY OF THE HEMLO GOLD DEPOSIT, HEMLO, ONTARIO.

HARRIS, D.C., Geological Survey of Canada, 601 Booth Street, Ottawa, Ontario K1A 0E8

The Hemlo gold deposit, discovered in 1982, is located near the northeast shore of Lake Superior, 35 Km east of Marathon adjacent to the Trans-Canada Highway 17. The deposit of Archean Age occurs at the contact between felsic metavolcanics and pelitic metasediments. The deposit consists of several mineralized zones with the main zone extending 2900 m in length, 2500 m down dip and ranges in thickness from 3 to 45 m. This zone contains at least 70 million tonnes of ore with an average grade of 7.6 grams Au per tonne. Three properties covering portions of the deposit have been brought into production.

The gold ore is substantially enriched in Mo, Sb, As, Hg, Tl, V and Ba and contains a diverse assemblage of minerals. The most common ore minerals are pyrite, molybdenite, stibnite, tetrahedrite – tennantite, native gold (up to 22% Hg), sphalerite (up to 27% Hg), zinckenite, realgar, cinnabar and aktashite. Minor to trace ore minerals are aurostibite, boulangerite, bournonite, twinnite, geocronite, chalcostibite, native antimony, jamesonite, gudmundite, ullmannite, berthierite, stibarsen, native arsenic, arsenopyrite, orpiment, gersdorffite, pararealgar, dufrenoysite, baumhauerite, seligmannite, coloradoite, tvalchrelidzeite, barian tomichite, parapierrotite, routhierite, ilmenite, magnetite and chromite.

The gangue minerals are principally quartz, barite, sericite, vanadian muscovite (up to 8.5% V203), rutile (with as much as 5.6% V203, 6.5% Sb203, 2.3% W02) and barian microcline (with up to 16.6% BaO). Other minor accessory minerals are tourmaline, titanite, phlogopite-biotite, microcline, albite, hornblende, cafarsite, lewisite, allanite, monazite, grossular, vesuvianite and scheelite.

HRTEM CHARACTERIZATION OF SCAPOLITE SOLID-SOLUTION SERIES

HASSAN, Ishmael and BUSECK, Peter R., Depts. of Geology and Chemistry, Arizona State University, Tempe, AZ., 85287, USA

Scapolite, a common volatile-bearing framework aluminosilicate mineral, forms a solid-solution series between $Na_4[Al_3Si_9O_{24}]Cl$ (marialite = Ma) and $Ca_4[Al_6Si_6O_{24}]CO_3$ (meionite = Me) [1]. The general features of the average structures of scapolites are well known [2,3,4]. The two established space groups based on X-ray studies are I4/m for Ma and Me [2,3,4] and $P4_2/n$ for intermediate members [3,4]. The reflections from scapolite may be classified into two groups: strong type-a with (h+k+l) even and weak type-b with (h+k+l) odd, the latter being forbidden for I4/m but allowed for $P4_2/n$. Antiphase domains are observable only with type-b reflections [5,6]. They were interpreted as arising from either ordering of Cl and CO_3 [5], or from Al/Si ordering between the T2 and T3 sites in samples that contain little Cl [6]. Electrostatic energy calculations for a 37.5% Me indicate that Na is adjacent to Cl and Ca to CO_3; moreover short-range order of Na_4Cl and Ca_4CO_3 clusters is favorable and might give rise to antiphase domains [7]. We report here the discovery of ordering of such clusters as well as short-range ordering of the same types of clusters.

Electron diffraction patterns and corresponding high-resolution transmission electron microscope (HRTEM) images have been obtained for a number of crystal orientations ([001], [100], [110], [011], [111], [021], [120], among others) of specimens with Me = 39.5%(ON70) and 79.6%(ON47). Sharp 'b' reflections were observed for both specimens; however, they are absent in some crystals of the 79.6% Me, indicating local variations in composition and/or ordering. For both specimens, additional (type-c) reflections with 00l, l = odd, and with hko, h+k = odd, were observed. These violate the existence of the 4_2 screw axis and the n glide plane, respectively. Based on similar observations it was concluded that P4 or P4/m are the space groups since reasonable structures can be derived starting with I4/m [5]. The 'c' reflections do not disappear on tilting and therefore are unlikely to be caused by double diffraction. The displacement vector R = ½[111] across the APBs observed by [5] indicates the non-equivalence of (1/4,1/4,1/4) and (3/4,3/4,3/4) sites and therefore excludes I4/m and $P4_2/n$ as the correct space groups [5].

Some images show different contrast on alternating rows giving rise to half-spacings. In the following projections they occur between the following type of planes:

[110] : (111) and (222); (100) and (200)
[012] : (021) and (042); (100) and (200)
[120] : (001) and (002); (210) and (420).

It is difficult to see this alternating contrast in other projections because the 'b' and 'c' reflections are very weak compared to the strong 'a' reflections, as shown by optical diffractograms.

Through-focus, through-thickness image simulations were done for two structural models. Model 1 is based on the X-ray structure [2] whereas model 2 is based on the same ordered Al-Si framework, but with Na_4Cl and Ca_4CO_3 ordered at (1/4,1/4,1/4) and (3/4,3/4,3/4) respectively. The experimental images could only be matched with the simulated images based on model 2, indicating that ordering of Na_4Cl and Ca_4CO_3 clusters gives rise to the weak 'b' and 'c' reflections. The intensity of the 'b' reflections is at a maximum where the ratio $Cl:CO_3$ is 1:1 and it decreases towards Ma and Me [4].

We also observed darker and brighter dots over the positions of the clusters, suggesting the presence of short-range ordering of Na_4Cl and Ca_4CO_3 types of clusters. This chaotic ordering should give rise to diffuseness and not the sharp 'b' and 'c' spots.

The scapolite samples were provided by courtesy of Professor Dennis M. Shaw, McMaster University. This work is supported by NSF grants EAR-8408169; microscopy was done at the ASU HREM facility which is supported by NSF and ASU.

[1] Evans,B.W., Shaw,D.M.& Houghton,D.R., Contr.Min.Petr. 24 (1969) 293.
[2] Levien,L.& Papike,J.J., Am. Min. 61 (1976) 864.
[3] Papike,J.J.& Zoltai,T., Am. Min. 50 (1965) 641.
[4] Lin,S.B.& Burley,B.J., Tsch. Min. Petr. Mitt. 20 (1973) 28.
[5] Phakey,P.P.& Ghose,S., Nature Phy. Sci. 238 (1972) 78.
[6] Oterdoom,W.H.& Wenk,H.R., Contr.Min.Petr. 83 (1983) 330.
[7] Chamberlain,C.P.,Docka,J.A.,Post,J.E.& Burnham,C.W., Am.Min. 70 (1985) 134.

PROCESS MINERALOGY OF TUNGSTEN-BEARING ORES

HAUSEN, D. M., Chief Process Mineralogist, Newmont Exploration Limited, P. O. Box 310, Danbury, Connecticut, 06813, USA

Applications of process mineralogy to the exploitation of tungsten ores range diversely from early exploration leading to the development of mineralized target through a variety of metallurgical test work and pilot plant studies, to the trouble-shooting of mine and plant production. These include the following:

(1) Quantitative evaluation of tactite mineralogy by x-ray diffraction to establish the relative favorability of various tactites of diverse mineralogic composition.
(2) A rapid XRD method is described for the determination of end member garnet compositions of the andradite-grossularite series, pertinent to the favorability assessment of tactite composition for tungsten mineralization.
(3) Identification and textural examination of tungsten-bearing minerals and potential by-products in gangue matrices.
(4) Extraction and precipitation of tungsten as synthetic scheelite and ammonium paratungstate, $5(NH_4)_2O.12WO_3.7H_2O$.
(5) Differential thermal analysis of ammonium paratungstate in oxidizing, reducing and neutral atmospheres, as a guide to phase transformations intermediate to the production of "blue oxide" reduced oxides of tungsten.

Stability ranges for the various intermediate tungstates and oxides of tungsten have been determined and compared for various atmospheres as a guide to production methods.

A STRUCTURAL DESCRIPTION AND CLASSIFICATION FOR OXYSALT MINERALS.

HAWTHORNE, F.C., Department of Geological Sciences, University of Manitoba, Winnipeg, MB R3T 2N2 CANADA.

There are ~2500 oxysalt minerals involving most elements of the periodic table, and the structural description and classification of these minerals is one of the more fundamental problems in current mineralogy. Some mineral groups (silicates, aluminofluorides, phosphates) have been structurally classified according to the polymerization of a specific type of coordination polyhedron. Recently, it has been proposed that structures may be ordered or classified according to the polymerization of those coordination polyhedra with higher bond-valences (Hawthorne, 1983, 1985); this essentially extends and generalizes previous schemes to consider the polymerization of different types of coordination polyhedra, and expresses the associated crystal-chemical ideas in the language of bond-valence theory (Brown, 1981). Thus far, this approach has been used within the bounds of specific mineral stoichiometries, whereby the primary division of classification has been the general stoichiometric form of the mineral, with the development of a structural description and classification occurring within each chemical group. The desirability of a scheme in which the primary groupings are structural rather than chemical has been stressed by Lima-de-Faria (1983) and Hawthorne (1983), and sufficient structural information is available to set up such a scheme. Here I consider oxysalt minerals with triangular, tetrahedral and octahedral coordination of small highly-charged ($\geq$2+) cations, a family that includes carbonates, borates, selenites, arsenites, antimonites, sulphates, chromates, phosphates, arsenates, vanadates, silicates, aluminofluorides, oxides and hydroxides. Structures are described and ordered according to their basic heteropolyhedral cluster, or fundamental building block, and the way in which this cluster polymerizes to form the structure module, a complex anionic polyhedral array whose excess charge is balanced by the presence of large low-valence cations. This results in the following classes of structures (Lima-de-Faria, 1983; Hawthorne, 1985): (i) unconnected polyhedra; (ii) finite clusters; (iii) infinite chains; (iv) infinite sheets; (v) infinite frameworks. These descriptions are particularly useful for loosely packed and highly hydrated minerals, the structures of which often resist adequate description in terms of such traditional concepts as close-packing.

I.D. Brown (1981): Structure & Bonding in Crystals, II, 1-30, Academic Press, N.Y.
F.C. Hawthorne (1983): Acta Crystallographica, A39, 724-736.
F.C. Hawthorne (1985): American Mineralogist, 70, 455-473.
J. Lima-de-Faria (1983): Garcia de Orta, Series Geologia, Lisboa, 6, 1-14.

CHEMICALLY INDUCED GRAIN BOUNDARY MIGRATION IN CALCITE: A LOW TEMPERATURE SOLID-STATE MINERAL REACTION MECHANISM

HAY, R. S. and EVANS, B. (Both at: Dept. of Earth and Planetary Sciences, M.I.T., Cambridge, MA, 02139)

The term chemically induced grain boundary migration (CIGM) usually describes solid-solution formation behind a moving grain boundary in metals systems at temperatures where (lattice diffusion)/(grain boundary diffusion) ratios are small. The force driving boundary migration must come from part of the energy reduction accompanying solid-solution formation in the crystal volume swept by the boundary. In geologic systems, CIGM may be important in a number of different situations: 1. During grain growth of a monophase aggregate, trace elements may be incorporated or exsolved by CIGM. A chemical driving force resulting from the mixing or unmixing of these trace elements in the lattice could therefore be partly responsible for grain growth. 2. CIGM may contribute to solid-solution formation in a polycrystalline aggregate in a manner analogous to metals systems. 3. CIGM may be relevant to general heterogenous mineral reactions, where atomic species are exchanged in stoichiometric proportions along an advancing interphase boundary during growth of a new phase.

Lab experiments on calcite bicrystals and Yule marble show that CIGM is efficient at solid-solution formation at temperatures where (lattice diffusion)/(grain boundary diffusion) ratios are small. For CIGM to cause cation exchange in the calcite lattice, it must involve boundary diffusion of the substituting species down the boundary, segregation of this species at the boundary, and detachment of the segregated species from the boundary and incorporation of it into the lattice when the boundary migrates. Stoichiometry requires that the mole flux of the substitutional species along the boundary be balanced by an equal and opposite Ca mole flux along the boundary to a Ca sink.

CIGM kinetics must involve boundary migration and boundary diffusion kinetics, coupled to CIGM chemical free energy reduction. It is also possible that boundary migration and boundary diffusion are coupled to each other. If a faster migrating boundary removes more (or less) boundary segregated cations per unit time, potential gradients driving diffusion of this species down the boundary are made larger (or smaller), so boundary diffusion rates are changed. Additionally, if boundary diffusion rates couple with the boundary migration process to change CIGM rates, as suggested by one proposed mechanism for CIGM, a feedback loop between boundary migration rate and boundary diffusion rate results. Also, at temperatures near the melting point, CIGM is not observed, presumably because lattice diffusion is a more efficient transport process. High lattice diffusion rates may therefore inhibit CIGM.

To learn about the CIGM mechanism in calcite, we studied temperature dependence, and the correlation between boundary migration velocity and cation concentraion left in the crystal. To measure temperature dependence, slabbed and polished samples of the same calcite bicrystal were annealed for 2 days with a Sr saturated $CaCO_3$-Li_2CO_3 melt at temperatures from 680°C to 840°C. To measure correlation of migration velocity with cation concentration, similarly prepared samples were annealed in the presence of the same Sr saturated melt in a heat stage at 700°C, and the boundary position was photographed insitu in an optical microscope in transmitted light. Samples from both sets of experiments were examined in an optical microscope, serially sectioned, and then examined in an SEM-EM with mass contrast sensitive backscattered electron imaging and a digital image processor. Sr concentrations were also measured analytically in spot mode.

Results of the experiments were: 1. Grain boundary migration velocities had a broad maximum at a temperature of about 750°C, and decrease below 700°C and above 800°C for the bicrystal studied. 2. Sr concentration averaged about 3 mol% at the bicrystal surface and had a weak temperature dependence, although Sr solubility in calcite increases from 40% to 80% in the temperature range studied. Therefore, disequilibrium between μ_{Sr}(melt) and μ_{Sr}(crystal) increases with temperature during CIGM in calcite. 3. Boundary migration velocities determined from positions measured insitu with time show a strong correlation exists between boundary migration velocity and cation concentration in the crystal volume swept by the boundary.

HIGH-PRESSURE CRYSTAL CHEMISTRY OF ORTHOSILICATES AND RELATED BINARY OXIDES

HAZEN, R. M. and FINGER, L. W., Geophysical Laboratory, Carnegie Institution of Washington, Washington, DC 20008, USA

High-pressure crystal structures are completed for 20 minerals with the garnet, olivine, scheelite or spinel structures. Bulk crystal compression in these minerals is closely related to volume changes of constituent cation-anion polyhedra.

High-pressure structures of garnets ($\underline{A}_3\underline{B}_2Si_3O_{12}$), including pyrope and grossular to 60 kbar (Hazen and Finger, 1978) and almandine, andradite, and pyrope to 200 kbar (in progress), reveal that bulk crystal compression is similar to that of the 8-coordinated A cation polyhedron, which is the largest and most compressible polyhedron. Compression of A-O bonds ranges from about $2.5x10^{-4}$ $kbar^{-1}$ for Mg-O to $3.0x10^{-4}$ $kbar^{-1}$ for Ca-O bonds. Aluminum- and ferric iron-oxygen bonds in 6-coordinated B sites shorten by about $1.6x10^{-4}$ $kbar^{-1}$ and are less compressible than A-O bonds. Compression of silicon tetrahedra, the least compressible garnet polyhedra, are about $1.0x10^{-4}$ $kbar^{-1}$.

Seven binary oxides with the scheelite (ABO_4) structure, including $CaWO_4$, $CaMoO_4$, $PbWO_4$, $PbMoO_4$, $CdMoO_4$ (Hazen et al., 1985), $BiVO_4$ (Mariathasan et al., 1986) and $LaNbO_4$ (Mariathasan et al., 1985) have been studied by high-pressure x-ray techniques. As in garnets, larger 8-coordinated A units compress more than tetrahedra; bulk crystal compression is similar to that of A polyhedra. An unusual variety of 8-coordinated cations in scheelites, from Na^{+1} in $NaIO_4$ to Ge^{+4} in $GeSiO_4$, results in the wide range in observed bulk moduli of scheelite-type compounds. Compression of WO_4, MoO_4, and other BO_4 tetrahedra is significantly less than that of 8-coordinated polyhedra, with B-O bond compressibilities less than $1.5x10^{-4}$ $kbar^{-1}$.

High-pressure structures of forsterite (Hazen and Finger, 1980), fayalite (Hazen, 1977) and monticellite (in progress), as well as the olivine isomorph, chrysoberyl (Hazen, in review), reveal a more complex relationship between polyhedral compression and olivine crystal compression. As in garnets and scheelites, bulk compression of olivine is similar to that of the larger cation polyhedra - divalent Mg, Fe or Ca octahedra in the silicates studied here - while the silicon tetrahedron is relatively rigid. Unlike the garnets and scheelites, however, olivines have extremely anisotropic compression, with the orthorhombic a axis significantly less compressible than b or c. This anisotropy results from the concentration of rigid SiO_4 tetrahedra in distinct (100) planes. These "layers" of tetrahedra constrain compression along a in silicate olivines. This behavior contrasts with that of chrysoberyl, $BeAl_2O_4$, in which the Al octahedra and Be tetrahedra have similar compressibilities. Chrysoberyl compression is close to isotropic because tetrahedra do not restrict octahedral compression parallel to a.

Three spinel-type A_2BO_4 compounds have been studied at high pressure. Nickel silicate spinel (Finger et al., 1979) behaves much like other orthosilicates, with octahedral Ni-O bonds much more compressible than tetrahedral Si-O bonds. Changes in relative sizes of octahedra and tetrahedra lead to an increase in the only variable position parameter, u (oxygen is at position u,u,u), with increasing pressure. In spinel ($MgAl_2O_4$; Finger et al., 1986), the Mg-O tetrahedral bonds are more compressible than octahedral Al-O bonds, thus causing a decrease in u with pressure. In contrast, octahedra and tetrahedra in magnetite (Fe_3O_4; Finger et al., 1986) have the same compressibility; the structure simply scales with pressure and u is unchanged.

In all of these orthosilicates and related binary oxides the bulk crystal compression is similar to that of the largest cation polyhedron, which is usually the most compressible polyhedron as well. Silicon or other cation tetrahedra, which account for less than 5% of the total crystal volume in these compounds, are relatively small and rigid structural units that are surrounded by larger and more compressible polyhedra and, consequently, do not have a major effect on crystal molar volume or bulk modulus. The distribution of rigid tetrahedral units may, however, restrict the compression of larger polyhedra in certain directions, thus causing large compression anisotropies.

Finger,L., R.Hazen, A.Hofmeister (1986) Phys.Chem.Min. in press.
Finger,L.W., R.M.Hazen and T.Yagi (1979) Amer.Mineral. 64, 1002.
Hazen,R.M. (1977) Amer.Mineral. 62, 286.
Hazen,R.M. and L.W.Finger (1978) Amer.Mineral. 63, 297.
Hazen,R.M. and L.W.Finger (1980) Carnegie Inst.Wash.Yb. 79:364.
Hazen,R., L.Finger, J.Mariathasan (1985) J.Phys.Chem.Sol. 46:253.
Mariathasan,J., L.Finger, R.Hazen (1985) Acta Cr. B41:179.
Mariathasan,J., R.Hazen, L.Finger (1986) Phase Trans. in press.

THE STRUCTURE OF MINERALS IN THEIR INORGANC ENVIRONMENT.

HELLNER, E., Inst. for Mineralogy, Philipps-Universität, D-3550 Marburg, Germany-West.

A systematic description and classification of inorganic structure types (including Minerals) is proposal. It is based on the descripton of point configurations occupied by atoms (Bauverbände). A point configuration is a set of equivelent points derived from one point by all symmetry operations of a space group. The point configurations are described by invariant lattice complexes and coordination polyhedra. Symbols for lattice complexes have been proposed by C. Hermann (1960), modified and completed by Fischer, Burzlaff, Hellner & Donnay (1973) and reported in I.T. for Crystallography 1983 (Fischer & Koch). The coordination polyhedra are symbolized according to Donnay, Hellner, Niggli (1966). Structure types of different orders will be given as examples for the I-, P-, F-, Y**-, S-, $^{\pm}$Y, Q- and C-families. In addition there exist structure types belonging to heterogenous families, e.g. [I+W] for ß-W, [D+T'] for the Laves phase and Argyrodite, [Y(3l)+D$\underline{x}$] for ß-Mn and the ionic conductor $RbAg_4J_5$. Structure types and families are called homoetypic, if single atoms are replaced by polyhedral arrangements of atoms; e.g. P[6o] in exists in CaB_6, I_{222}[6o] exists as framework in garnet, hydrogarnet, Hg_3TeO_6, $(NH_4)Fe(CN)_6 \cdot 1{,}5\ H_2O$ and in $RhBi_4$. For the description of the 2-dimensional Bauverbände the hexagonal closed-packed net, the graphite net, the Kagomênet and the nets N[43^{2}43] and N[6434] are used. They enable to symbolize the olivine structure, layer structures, the $CuAl_2$ structure, but also brookite, Pyroxenes, amphiboles and feldspars.

References:

Donnay,J.D.H., Hellner, E. & Niggli, A.: Symbolism for lattice complexes. Revised by a Kiel Symposium. Z. Krist., 123, 255-262 (1966).

Fischer, W., Burzlaff, H., Hellner, E. & Donnay, J.D.H.: Space Groups and Lattice Complexes. NBS 134, HS Department of Commerce (1973).

Fischer, W. & Koch, E.: Lattice Complexes. I.T. for Crystallography, 819-848 (1983).

Hermann, C.: Zur Nomenklatur der Gitterkomplexe. Z. Krist. 113, 142-154 (1960).

SOME MINERALOGIC AND PETROGRAPHIC PROGRAMS FOR THE APPLE MACINTOSH MICROCOMPUTER

HENDERSON, D.M., Dept. of Geology, University of Illinois, Urbana, IL 61801, USA.

The ease of use, high resolution of screen and printer, versatility, compactness and portability combine to make the Macintosh microcomputer especially attractive for educational purposes. However, its radically different operating system and graphics processing inhibit easy portability of programs from other computers to Macintosh. As a consequence, there are relatively few mineralogic and petrographic programs widely available and ready for use on Macintosh. The programs briefly described below may help in correcting the aforementioned problem. They are available to all interested users.

The programs being demonstrated are self-standing ones written in FORTRAN77. They include the following. DNORM computes Barth and CIPW rock norms from chemical analyses of rocks; it also produces output for several kinds of triangular diagrams. MINALS computes endmember components and formulae from chemical analyses of rockforming minerals. ACAMAR computes chemical compositions of rocks from mineral modes. DISTANG computes interatomic distances and angles for mineral structures from cell parameters and atom position coordinates; the design is intended to ease finding edge lengths and angles of coordination polyhedra. Some other programs (in FORTRAN) will also be made available to participants of the Microcomputer Workshop.

INTERNAL STRUCTURES OF THE EARTH AND TERRESTRIAL PLANETS: CONSTRAINTS FROM HIGH PRESSURE LIQUIDUS PHASE EQUILIBRIA AND BULK PLANET COMPOSITION

HERZBERG, C.T., Dept. Geological Sciences, Rutgers University, New Brunswick, New Jersey, 08903, U.S.A.

The development of high pressure technology in Japan has made it possible to acquire experimental data on melting phase equilibria in mantle systems to pressures of 20 GPa, corresponding to a depth of over 600 kilometers in the Earth. E. Ohtani pioneered the use of the MA8 cubic anvil in his studies of the fusion curves of fayalite and forsterite; the latter was determined to 15 GPa, a four fold increase in the pressure of previous determinations. The success of these early experiments in the late 1970s and early 1980s set the stage for melting experiments in more complex systems, and the results have been instrumental in the testing and development of a petrological theory on the structure of the Earth and its terrestrial companion planets.

The fusion curve of forsterite has provided thermodynamic constraints for determining the liquidus temperatures of a wide range of compositions, such as mantle peridotite and various assumed bulk planet compositions. As for all fusion curves, the slope dT/dP becomes reduced with increasing pressure, but it has an average value of about 40°C/GPa. This compares with a slope of about 130°C/GPa for the solidus of upper mantle spinel and garnet lherzolite determined to 5 GPa in many laboratories. A theoretical analysis of the topology of these phase relations lead Herzberg (1983) to conclude that the solidus and liquidus must converge or meet closely in T-P space in the 10 to 15 GPa range for a fertile garnet lherzolite composition. Where this occurs, the initial melt along the solidus is not a basalt, but rather an ultrabasic melt having the same or similar composition as that of garnet lherzolite itself (eg., 40 % MgO). It was predicted that at yet higher pressures, liquidus olivine must be replaced by pyroxene or garnet. The experimental results of Takahashi and Scarfe (1985), Takahashi (1986), Scarfe and Takahashi (1986), Kato and Kumazawa (1986) and Herzberg (1986) have corroborated the prediction of the convergence, and have shown that olivine is replaced by majorite as the liquidus phase at high pressures for lherzolite compositions.

These phase equilibria have provided new constraints on the origin of upper mantle lherzolite. Although many if not most samples have experienced multistage partial melting and olivine accumulation throughout Earth history, it was suggested by Herzberg and O'Hara (1985) that upper mantle lherzolite was originally formed as the solidification product of an ultrabasic initial melt during the primary differentiation event. The major element composition of the Earth's upper mantle is constrained completely by high pressure liquidus phase relations, and bears no resemblance to any proposed bulk Earth composition. However, if indeed the bulk Earth is chondritic in composition, the restriction of mass balance would require that the lower mantle and possibly part of the transition zone be the complementary residuum, enriched in CaO, Al2O3, and SiO2. It is emphasized that melting during this primary differentiation event was regulated by the anhydrous solidus; a magma ocean model wherein large degrees of partial melting occurred in excess of the solidus is not required by the experimental data. A version of this theory was originally advanced by Kumazawa and Fukao (1978).

It is demonstrated that the internal structure of any terrestrial planet can be deduced from these phase equilibria and estimates of the planet's bulk composition. Based on estimates of the latter in Basaltic Volcanism of the Terrestrial Planets, the following predictions have been made:

MERCURY: UPPER MANTLE - much less MgO than lherzolite (ie., spinel websterite); LOWER MANTLE - either dunite & spinel wehrlite or harzburgite & pyroxenite.
VENUS: same as the Earth
MOON: UPPER MANTLE - spinel websterite; LOWER MANTLE - pyroxenite & dunite.
MARS: UPPER MANTLE - websterite to lherzolite; LOWER MANTLE - spinel wehrlite.

STONY-IRON METEORITES AND THEIR PARENT BODIES

HEWINS, ROGER H., Dept. of Geological Sciences, Rutgers University, New Brunswick, N.J. 08903, USA

The common stony-iron meteorites, mesosiderites and pallasites, share a number of geochemical characteristics with the HED basaltic achondrites (howardites-eucrites-diogenites) and IIIAB iron meteorites. Oxygen isotopic data indicate derivation of all of these from a common nebular reservoir (1). The compositions of metal in IIIAB irons and pallasites are very similar and similar to mesosiderite metal (2-4). These similar charactistics permit but do not require a common parent body. Textures and mineral compositions indicate very different thermal histories, however.

Pallasites may have formed at a core-mantle interface. Pallasite olivine assemblages were thoroughly equilibrated at high temperature, although metallic phases in IIIAB irons (and pallasites) have recorded relatively high cooling rates for the low temperature range, currently estimated at about 300°/m.y. (5). If IIIAB irons represent its core, the achondrite parent body would have a radius of only about 20 km (8,5). Mesosiderites are polymict breccias, with the silicate fraction ranging from virtually unequilibrated to partly equilibrated. They probably originated by low velocity accretion of a core fragment onto a differentiated asteroid (7, 10). Mesosiderites have a prolific development of the low temperature ordered NiFe phase tetrataenite and estimated cooling rates are extremely low, on the order of 1°/my (6,7). In strong contrast to the IIIAB case, the mesosiderite cooling rate is equivalent to the depth of at least 40 km in a body with a radius of 400 km (8,7). The mesosiderite and now disrupted pallasite-IIIAB parent bodies therefore appear totally incompatible.

The HED achondrites could be derived from Vesta, an asteroid of radius approximately 280 km, because visible-infrared spectra of its surface match the meteorite light curves (9). No regions of Vesta's surface have yet been observed to be stony-iron or iron, and Vesta appears to be a fairly intact differentiated body. It appears highly unlikely that mesosiderites, pallasites and IIIAB irons could be derived from Vesta. These arguments suggest at least three possible parent bodies for the stony-iron/achondrite meteorites, Vesta, the IIIAB body and the mesosiderite parent. This is consistent with the spectral identification of two classes of asteroid, S-type (metal-olivine-pyroxene) and A-type (olivine-rich) as collisional remnants of differentiated bodies (11, 12). Melting to produce achondrites and irons, and hence stony-iron mixtures, was common in the inner solar system.

References

1. R.N. Clayton et al., 1986, Lunar Planet. Sci. XVII, 141.
2. E.R.D. Scott, 1977, Min. Mag. 41, 265-272.
3. J.T. Wasson et al., 1974, Geochim. Cosmochim. Acta 38, 135-149.
4. G.E. Harlow et al., 1982, Geochim. Cosmochim. Acta 46, 339-348.
5. C. Narayan and J.I. Goldstein, 1985, Geochim. Cosmochim. Acta 49, 397-410.
6. R.S. Clarke Jr. and E.R.D. Scott, 1980, Am. Mineral. 65, 624-630.
7. R.H. Hewins, 1983, PLPSC 14th, J. Geophys. Res. 88, B257-266.
8. P.E Fricker et al., 1970, Geochim. Cosmochim. Acta 34, 475-491.
9. M.J. Gaffey, 1983, Lunar Planet. Sci. XIV, 231-232.
10. J.T. Wasson and A.E. Rubin, 1985, Nature 318, 168-170.
11. M.J. Gaffey, 1985, Lunar Planet. Sci. XVI, 258-259.
12. J.F. Bell et al., 1984, Bull. Am. Astron. Soc. 16, 708-709.

DATA COLLECTION OPTIMIZATION FOR RIETVELD ANALYSIS

HILL,R.J., Division of Mineral Chemistry, CSIRO, PO Box 124, Port Melbourne, Victoria 3207, AUSTRALIA

In the Rietveld method for the analysis of powder diffraction data the entire pattern is calculated using a model for the positions of the peaks (the unit cell parameters), their intensities (the atomic positional and thermal parameters, preferred orientation, etc.) and their widths and shapes, together with a description of the background. The calculated pattern is then compared with the observed step profile, point by point, and the model parameters are adjusted by least-squares methods.

As in the case of single-crystal studies, a number of critical decisions must be made prior to the collection of the raw step intensities in order to ensure the best possible outcome of the refinement. These are, in particular: (i) the wavelength to be used, (ii) the beam collimation, (iii) the range of diffraction angles to be scanned, (iv) the angular distance between steps, and (v) the counting time / monitor setting at each step.

The wavelength is determined by the complexity of the pattern (i.e., the size and symmetry of the unit cell); the collimation system depends on source size and take-off angle (in the case of X-ray data), and/or the beam divergence required; the upper limit of diffraction angles is dictated by the effective scattering power of the constituent atoms and the 'crystallinity' of the sample. The effect of these factors on peak overlap, width, shape and asymmetry, and the ratio of peaks to parameters is well known. However, the selection of appropriate values for the step interval in 2θ and the counting time, T, at each step is not as straightforward; they are usually chosen more by tradition or by pressure of time than by a consideration of their possible effect on the results of the analysis. Indeed, Rietveld analyses have been published with step widths and maximum step intensities ranging over more than two orders of magnitude.

Since each measured step intensity is used in the Rietveld method, the number of 'observations', N, can be made arbitrarily large (independent of the number of Bragg reflections) by decreasing the step interval. It is, however, the intensities of the Bragg peaks that are the fundamental quantities in the structure analysis, not the step intensities themselves. The precision of peak intensity measurement is improved by increasing N or T, but only to the point where counting variance becomes negligible in relation to other sources of error; further increases provide no additional structural information.

The Figure provides a schematic representation of the variation in Rietveld agreement indices and parameter esd's as a function of step intensity and width. The optimum intensity is only a few thousand counts. If significantly larger intensities are measured the accuracy of the structural parameters is not improved (i.e., time is wasted) and the usual weighting scheme based on counting variance becomes inappropriate (i.e., the parameter esd's no longer reflect their accuracy). In the case of step width, the optimum value is approximately half the minimum full-width at half-maximum of well-resolved peaks. Smaller steps provide little or no improvement in parameter accuracy (especially when step intensities are large) and, at the same time, introduce severe serial correlation between adjacent steps in the profile.

In practice, it is the combination of N and T chosen for the experiment that is of greatest importance. If the pattern has many overlapping peaks, N should be large to provide adequate resolution and T should be correspondingly small to reduce serial correlation. In fact, a given level of Rietveld precision can be achieved more efficiently by the use of large N and small T than by combinations of small N and large T; the implications of these restrictions for 'real-time' data collection are noteworthy.

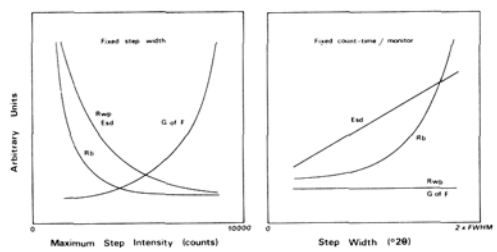

ON THE MINERALOGY OF BAUXITE DEPOSITS

HILL, V.G., International Bauxite Association, Kingston 5, Jamaica (W.I.); BLACKWOOD, D.A. Jamaica Bauxite Institute, Kingston 6, Jamaica (W.I.)

The major bauxite deposits occur in eight identifiable provinces which are tectonically stable regions subjected to intensive tropical weathering and the accumulation of the products. The mineralogy of the resultant bauxite reflects the effects of host rock petrology and the geochemistry of the environment.

The mineralogy of bauxite is critical to its efficient processing to alumina. Among the essential minerals, the relative content of the aluminium ore minerals (gibbsite, boehmite and diaspore) determine the basic Bayer digestion conditions, while the abundance and characteristics of the iron minerals (hematite versus aluminian goethite) determine the sizing of the major equipment on the red side of the plant and the mud separation circuit in particular. These techno-economic considerations permit the grouping of commercial bauxites into basic types depending on their processing characteristics and consequent variations on the red side of the Bayer plant. Among the varietal minerals, quartz versus kaolin and to a lesser extent rutile versus anatase determine the incremental increase in soda consumption per tonne of alumina produced. The phosphate minerals, apatite and crandallite, and lithiophorite affect liquor purity and so their control is required in order to ensure product purity. The organics present affect liquor productivity and so the control of their species and concentration in the liquor are also important.

The quantitative determination of the modal mineralogy is important for the efficient processing of bauxites, but these need to be correlated with traditional assay parameters since these provide a well-defined background against which comparisons can be made. Traditional wet chemical assays, XRF, XRD and SEM data are used to demonstrate the critical differences between the bauxite types identified and serve as a basis for their quantitative comparisons. The implications of mineralogy and bauxite types in the exploitation and handling of the ore are also discussed.

ION EXCHANGE AT 40°C IN VERMICULITE FROM LIBBY, MONTANA

Hindman, James R., Formerly with Construction Products Division, W.R. Grace & Co., P.O. Box 609, Libby, MT 59923. Current address: Salt Lake City Research Center, U.S. Bureau of Mines, 729 Arapeen Drive, Salt Lake City, UT 84108, USA

The effects of ion exchange in vermiculite from Libby, Montana, were examined for 26 cations at 40 degrees Celsius. Electron microprobe analysis of vermiculite from this locality indicates considerable variation in exchageable site ion content with a typical formula for this material being:

$$(K\ Na\ Ca\ Mg\ H_2O)(Mg\ Fe^{+2}\ Mn\ Fe^{+3}\ Ti)(Si\ Al\ O)(OH\ F)$$
$$1.09\ .02\ .22\ .39\ 2.78\ 3.96\ 1.03\ .02\ .43\ .17\ 5.66\ 2.34\ 20\ 3.88\ .12$$

At equilibrium with 1 molar solutions the amount of ion replacement varied for each of the 4 exchageable cations. Potassium was replaced in a range of 0.2-18 meq/100gm; sodium 0.4-2 meq/100gm; calcium, 20-48 meq/100gm; and magnesium, 10-29 meq/100 grams of vermiculite.

The x-ray diffraction powder pattern of vermiculite from Libby generally contains the following reflections: 14.4 (100), 12.6 (50), 12.1 (76) and 10.1 (5). Ion exchange produces a change in some or all of these major reflections. The resulting set of 26 powder patterns reveal similarities based on the coordination number of the exchanging cation with respect to water molecules and apical oxygen. Reflections in the ranges of 14.0-14.6, 12.2-12.6, and 11.5-12.1 Angstroms were present in samples exchanged with cations generally assuming 6-fold coordination. The reflection at 10.1-10.3 Angstroms was intensified by exchange with monovalent cations preferring 12-fold coordinaion, and became absent in the case of monovalent cations which assume 6-fold coordination. A reflection which was not observed in untreated vermiculite, d = 10.9-11.3 Angstroms, appeared as the most intense reflection observed in material exchange by Be(+2), Cu(+2), Cd(+2), Sr(+2), Pb(+2), and Na(+1). It was also present in patterns of Rb(+1) and Cs(+1) exchange vermiculite.

Anomalous data for both ion exchange and x-ray diffraction was observed for vermiculite treated with Cr(+3), Fe(+3) and Cu(+2). It is assumed that this data reflects further oxidation of ferrous iron in the vermiculite structure by these ions. Taken as a whole, the data obtained in this study suggests that the structure of Libby vermiculite contains at least two arrangements of atoms in the ion exchageable layers which have not been observed in crystal structure studies of magnesium vermiculite. This would contradict the interpretation that the reflections between 10 and 14 Angsroms originally used to classify Libby material as hydrobiotite are the result of mixed layers of biotite and vermiculite.

EFFECTS OF DISLOCATIONS UPON THE ELECTRICAL CONDUCTIVITY OF OLIVINE DURING HIGH TEMPERATURE CREEP DEFORMATION

HIRSCH, L. M., and C.-Y. WANG, both at: Dept. of Geology and Geophysics, University of California, Berkeley, CA 94720, USA

For geophysical studies of solid-state deformation, diffusion and electrical conduction, it is important to understand the role that tectonic stresses and the defects they produce may have upon the physical properties of mantle minerals. We investigated the possibility that stress-induced dislocations may affect the electrical conductivity of olivine. The electrical conductance of single crystals of San Carlos olivine has been measured during creep deformation in the temperature range of 1610-1725 K, under controlled oxygen fugacity and under uniaxial stresses of 60 to 140 MPa. Three different orientations of the specimens were selected such that in each case the predominant slip planes were at 45 degrees to the compression axis. Sample conductance was measured in the same direction as the applied stress by use of an impedance measuring assembly employing a 10 kHz, 1 Volt AC source. The general behavior of the specimens in response to the load may be summarized as follows: The total change of conductance resulting from deformation is found to be strongly dependent upon the total strain. Upon the application of the load, specimens which experienced appreciable strain exhibited a continuous increase in conductance. Plots of the conductance normalized by the conductance prior to loading versus elapsed time display a small downward concavity without large changes of their curvatures. No change in the phase angle of the impedance was detected in any of the experiments. The specimens which showed no significant deformation also showed negligible change in conductance. The specimens which experienced the greatest strains exhibited the largest changes in normalized conductance. The conductance changes resulting from deformation are not recovered during high temperature annealing in the absence of load. No significant difference in the relative behavior of the conductance of specimens deformed at different oxygen fugacities (within the olivine stability field) was detected.

Measured conductance is related to the intrinsic conductivity through a geometric factor given by the ratio of the cross-section area to the length of the specimen. It is calculated that the geometrical shape changes during deformation are the predominant causes for the observed changes in conductance, and consequently, the deformation produced in these experiments has caused little change in the intrinsic electrical conductivity of olivine. The dislocation structures observed in our deformed specimens are relatively homogeneous and compatible with previous investigations. The predominant character of dislocations in the plane parallel to the electric field was screw, while edge segments lie perpendicular to the electric field. However, the dislocation network was mobile, and consequently, no particular character of the dislocations can necessarily be assigned greater significance. Since the electrical conductivity of a solid is normally dominated by the most mobile of the charged majority defects, the present results suggest that, under the conditions explored here, (1) the generation and movement of dislocations and other defects associated with plastic deformation does not significantly affect the carrier concentration in olivine, and (2) the mobility of the defect responsible for conduction in olivine is not significantly perturbed by dislocation effects, or that these effects do not exist. In addition, the results suggest that the electrical conductivity of the upper mantle would not be significantly affected by lateral variations in tectonic stresses. The implication of the present results is that the defects which control the motion of the dislocations which lead to plastic deformation are independent of the defects controlling conduction. This conclusion would place sizable constraints upon the possible defect reactions which occur in olivine. However, as we have only examined cases where screw dislocations were in the plane of the electric field, these conclusions are tentative. Additional experimentation employing different electrode configurations is required in order to resolve this ambiguity.

EXAFS MEASUREMENTS AT HIGH PRESSURE

HOCHHEIMER, H.D., Max-Planck-Institut für Festkörperforschung, D-7000 Stuttgart 80, FRG; LENGELER, B., KFA Jülich, FRG

The analysis of the extended X-ray absorption fine structure (EXAFS), which shows up above the absorption edges of atoms in molecules, liquids and solids, has developed into a reliable method for the determination of the short range order around the absorbing atom. EXAFS is caused by an internal electron interference effect. The superposition of the outgoing photoelectron wave with parts backscattered from the neighboring atoms leads to a modulation of the matrix element of the transition probability with the electron energy. Periodicity and amplitudes of EXAFS reflect the parameters of the local geometrical structure e.g. bond lengths and coordination numbers.
The EXAFS-part $\chi(k)$ of the absorption coefficient is given by

$$(1) \qquad \chi(k) = \sum_j A_j(k) \exp(-2\sigma_j^2 \cdot k^2) \sin(2R_j \cdot k + \alpha_j(k))$$

The summation is carried out over all coordination shells j. The amplitude $A_j(k)$ contains information about N_j, the number of identical atoms in the scattering shells j at the distances R_j and about the backscattering amplitude characteristic for the scattering atom. The exponential in eq. 1 is a Debye-Waller factor and describes the disorder (dynamical (thermal) or static (structural)) with mean square relative displacements σ_j^2. $\alpha_j(k)$ is the scattering phase, consisting of the phase shift due to the potential of the scattering atom and the phase shift of the central atom. k is the wavevector connected with the kinetic energy of the photoelectron. The method most widely used to separate the different contributions in eq. 1 consists in a Fourier transformation of $\chi(k)$ into real space. Each term of the sum of eq. 1 attributed to scattering atoms in a distance R_j, shows up as a peak in the magnitude of the Fourier transform F(r). Knowing the values of the phase term $\alpha_j(k)$ the distance R_j can be obtained from the positions of the peaks in $|F(r)|$. The height of these peaks is characterized by $A_j(k) \cdot \exp(-2\sigma_j^2 \cdot k^2)$. Measurements of a reference system of known structure which contains the same atoms as the sample of interest, represent the best way to gain information about the phase term and the backscattering amplitude. That is one of the reasons that EXAFS is an excellent tool to obtain information about structural changes of samples under high pressure. Here the sample at zero pressure is the reference substance and the change of coordination number and distance due to a high pressure modification can be determined with respect to the known zero pressure modification. Other facts which have generated the interest in high pressure EXAFS experiments are the following:

a) In the case of (first order phase transformations the cell dimensions of the lattice is obtained from X-ray diffraction pattern. But especially when atoms with small and high atomic number are present, it is nearly impossible to obtain information about the positions of the light atoms. In these cases EXAFS yields the additional information about the arrangement of the light atoms surrounding the heavy ones.
b) In cases where the atomic arrangement of the sample is disordered (amorphous solid, liquids etc.) the X-ray diffraction will fail, whereas EXAFS still can be used to study the arrangement in the disordered state.

In the last years several EXAFS measurements at high pressures were carried out and different types of high pressure cells were used.
To obtain EXAFS data of good quality we have designed a high pressure cell with large Be-windows (1x10 mm^2). The cell can be used up to ∿10 kbar with liquid or gas as pressure medium. Measurements were carried out at the storage ring DORIS at Hamburg, and RbCN was used as a sample for the study.
The EXAFS-part and the near edge structure, which also contains information about the structure of the sample, change around 5.8 kbar due to a phase transition to a new structure of RbCN stable at pressures above 5.8 kbar. The high pressure phase has a CsCl-type structure whereas at pressures below 5.8 kbar a NaCl-type structure is found.
Using the known value of the C-N distance and the lattice parameter of the zero pressure as well as the one of the high pressure modification, we can calculate the Rb-(C/N) distance for the different orientations of the CN^- molecules. A comparison of these values and the Rb-(C/N) distances determined from the EXAFS yields the following results:
In the NaCl-type structure the CN^- molecules are oriented in the (100) as well as in the (111) direction. In the CsCl-type structure all CN^- are oriented along the (111) axis. Furthermore we observe a large "damping" of the EXAFS-signal which is due to a large disorder of the Rb-atoms and the libration of the CN^- molecules. This result is in agreement with neutron diffraction measurements on KCN. Furthermore, EXAFS-measurements on Cr doped with Ge are reported.

HIGH SPATIAL RESOLUTION SCANNING AUGER MICROSCOPY OF MINERAL SURFACES: TECHNIQUES AND APPLICATIONS

HOCHELLA, M.F., Jr., Dept. of Geology, Stanford University, Stanford, CA 94305, USA; HARRIS, D.W. and TURNER, A.M., Physical Electronics Laboratories, Perkin-Elmer Corporation, 1161-C San Antonio Rd., Mountain View, CA 94043, USA

The analysis of mineral surfaces has lead to important insights about weathering and dissolution phenomena (see, e.g., Berner et al., 1985, and references therein) and partitioning reactions between minerals and aqueous solutions (see, e.g., Brule et al., 1980, and references therein). The technique most commonly used for these studies is x-ray photoelectron spectroscopy (XPS). However, despite its many attributes, current XPS instrumentation typically lacks sufficient lateral resolution for the study of individual grains in rocks and compositionally inhomogeneous surfaces. On the other hand, scanning Auger microscopy (SAM) provides near-surface analysis with submicron lateral resolution. Although there are problems with analyzing nonconducting materials with Auger spectroscopy, state-of-the-art instrumentation and refined charge reduction and elimination techniques have recently allowed us to collect high quality Auger spectra on mineral surfaces with lateral resolution typically well below 1.0 μm, and in some cases below 0.1 μm. The objectives of this study are 1) to develop the Auger technique to the point where it can be used routinely to quantitatively analyze mineral surfaces with high lateral resolution (Hochella et al., 1986a), and 2) to use the techniques developed to gain further insight into important surface related phenomena in the earth sciences (Hochella et al., 1986b).

Technique development. Beam and sample conditions have been found which minimize charging and sample degradation problems on most mineral surfaces while allowing for the collection of Auger spectra with acceptable S/N. An accelerating voltage of 3 keV and beam currents below 10 nA, resulting in beam current densities less than a few amps/cm^2, are used. The sample is titled with respect to the primary beam to increase the backscattered and secondary electron emmision efficiency. Finally, the beam is rastered and/or defocused whenever possible and the vacuum level is maintained as high as possible. Although the surface of carbonates still break down under the beam even with these precautions, we have successfully performed high lateral resolution SAM on many oxides, silicates, and sulfides.

SAM spectra taken from different faces of albite single crystals suggest that the depth of Auger analysis is sufficient to measure representative bulk compositions from relatively clean surfaces of crystalline silicates. We have shown that very light ion sputtering, used to eliminate thin contaminant surface layers due to air exposure and/or solvent residues, should not affect semi-quantitative chemical analysis. We have also shown that elements as light as Li and Be can be detected with SAM in minerals that contain them as major components (e.g. spodumene and beryl).

As a part of this study, we are also developing Auger quantitative analysis methods specifically for minerals. To this point, we have carefully measured Auger peak-to-peak heights from 15 silicate electron microprobe standards and a number of oxides and sulfides. We have determined that Auger intensities for silicates do not vary directly with elemental concentration, emphasizing the need for more than the commonly used Auger sensitivity factors for semi-quantitative analysis.

Applications. We have identified three principle areas for the application of SAM to geologic research. They include surface analysis requiring high lateral resolution, the identification of submicron grains in rocks, and high resolution line scans across solid-solid interfaces. The following are examples from these 3 areas.

We have recently used high resolution SAM to measure the near-surface composition of 5 to 50 μm sulfide grains in the gold bearing ore from the Carlin Mine, Nevada. The gold in the unoxidized portion of the ore body is highly disseminated and is rarely observed directly. The nature of the gold and its distribution in the host rock is very important to the understanding of the petrogenesis of the deposit and for developing the most efficient and highest yielding method of metallurgical extraction (Bakken and Einaudi, 1986). Experimental and field evidence suggested that the gold might be located on sulfide grain surfaces. We have shown with SAM that this is not generally the case, and that other models for gold association must be sought.

Using SAM to identify minerals requires that the near-surface composition of the grain be representative of its bulk composition. When this is the case, we have shown that SAM can identify submicron (down to approximately 0.5 μm) grains without the need for ultra-thin sectioning and analytical electron microscopy (AEM).

We have also used SAM to measure cation diffusion profiles between a spessartine and almandine garnet couple (see Loomis et al., 1985, and Hochella et al., 1986b). It is important to understand chemical diffusion within garnets because it is a critical factor in controlling compositional zonation which can be used to help interpret the history of metamorphic rocks that contain them. Diffusion modelling for garnets requires accurate measurements of experimental diffusion distances. For the garnet couple which we studied, the diffusion distances are estimated to be only approximately 0.1 μm. SAM line scans show apparent diffusion distances which are 2 to 3 times shorter than those indicated by equivalent line scans taken with the electron microprobe.

References:

Bakken B.M. and M.T. Einaudi, Proc. Sym. Gold '86, Toronto, (in press).

Berner R.A., G.R. Holdren, and J. Schott, Geochim. Cosmochim., 49, 1657 (1985).

Brule D.G., J.R. Brown, G.M. Bancroft, and W.S. Fyfe, Chem. Geol., 28, 331 (1980).

Hochella M.F., D.W. Harris and A.M. Turner, Am. Mineral., 71 (in press).

Hochella M.F., A.M. Turner and D.W. Harris, Scan. Electron Micro., 1986 (in press).

Loomis T.P., J. Ganguly and S. Elphick, Contri. Mineral. Petrol., 90, 45 (1985).

THERMODYNAMIC IMPLICATIONS OF INFRARED SPECTROSCOPY OF STISHOVITE AT MANTLE PRESSURES

HOFMEISTER, A.M., XU, J., Geophysical Laboratory, 2801 Upton St. N.W., Washington DC 20008, USA: AKIMOTO, S., Institute for Solid State Physics, The University of Tokyo, Tokyo 106, JAPAN

Mid-infrared (IR) spectra of synthetic stishovite taken at quasi-hydrostatic pressures from 1 atm to 320 kb generated by a megabar diamond-anvil cell (DAC) possess three strong bands, one weak band and one shoulder whose frequencies gradually increase with pressure from the 1 atm values of 838, 582, ~460, 763, and 1050 cm^{-1} respectively. No peaks were found below 400 cm^{-1} from stishovite samples of up to 20μm thickness, either in a DAC or in an IR microscope. The number of IR modes observed equals that predicted for the rutile structure ($3E_u + 1A_{2u}$), if the shoulder is the longitudinal optic (LO) component of $^1Eu^1$. The absorption data are also consistent with unpolarized reflection spectra taken of stishovite powder in an IR microscope, in that the reflection spectrum is dominated by the 3 E_u bands with LO-TO (transverse optic) positions of 1020-833, 610-576, and 520-476 cm^{-1}. The four TO peak positions compare favorably with those predicted by Striefler and Barsch (1976: JGR, vol. 81, p. 2453) as 812, 552, 503, and 609 cm^{-1} from a rigid ion model, but are closer to those predicted from rutile powder spectra as 861, 538, 443 and 772 cm^{-1} from:

$$\nu_s = \nu_r(d_s^3\mu_s/d_r^3\mu_r)^{1/2} \quad (1)$$

where μ is the reduced mass and d is the interatomic separation.

Mid-IR absorption and reflectance spectra of natural stishovite exhibit not only the 3 E_u bands but also have strong peaks at 664 and 760 cm^{-1} that override the A_{2u} band. Lack of excess bands near 800-900 cm^{-1} rules out silica glass as a contaminant. The strong IR bands at 600-800 cm^{-1} are characteristic of $(SiF_6)^{2-}$ bands, as are some of the excess Raman bands observed at 400-500 cm^{-1} by Hemley, Mao and Chao (1986, Phys. Chem. Min., in review). Dissolution of the Coconino Sandstone matrix by HF acid probably caused surface contamination of natural stishovite with $(SiF_6)^{2-}$, that may be charge compensated with K^+ leached from feldspar.

Our 1 atm IR positions, Raman data of Hemley et al. (1986), and acoustic velocities of Weidner et al. (1982: JGR vol. 87, p. 4740) were used to calculate heat capacity (C_v) from Kieffer's model (1979: Rev. Geophys. Space Phys. vol. 17 p. 35). The three inactive frequencies were estimated as 726, 400 and 231-143 cm^{-1} by applying eq. (1) to rutile INS data of Traylor et al. (1971: Phys. Rev. vol. 3, p. 3457). The density of states $g(\nu)$ was approximated by nine different combinations of isolated Einstein oscillators and optic continua, each with 3 or 4 different lower cutoffs that serve to "bracket" the estimated inactive modes. Agreement for all models with experiment was poor ($\pm$50%) below 200 K. From 300 to 1000 K, only one model for $g(\nu)$ resulted in calculated C_v that was within 4% of experiment. This model is not entirely consistent with Keiffer's approach in that the LO component at ~1000 cm^{-1} was ignored and one of the modes (A_{2g}), separated as an Einstein oscillator, is a rotation rather than an Si-O stretch. Kieffer's model does not calculate C_v accurately for stishovite because it has a limited number of optic modes (18) that are widely distributed over frequency, and possibly because the B_{1g} mode could depend strongly on temperature as in rutile.

The frequencies of all bands increase with pressure such that ν depends linearly on P up to about 160 kb, whereas ν depends linearly on volume (V) and ln ν depends linearly on ln V over the entire range of measurements. (A bulk modulus B_T of 3.06 Mb and dB_T/dP of 3.2 were used to calculate V(P).) Both $d(\ln \nu)/d(\ln V)$ and $d\nu/dV$ are constant because V and ν change only slightly (~10%) over 360 kb, and because a small amount of scatter exists. Whether the mode Gruneisen parameters $\gamma_i = d\ln(\nu_i)/d(\ln V)$ are constant, or decrease by about 10% over 360 kb cannot be determined without stronger constraints on dB_T/dP. The IR TO modes at 836, 763, 580, and 476 cm^{-1} (E_u^1, A_{2u}, E_u^2 and E_u^3) have γ_{io}'s of 1.00, 0.80, 1.98, and 0.94, respectively. The lowest γ_i is expected to occur for A_{2u} because only this mode involves motions of Si and O along the c axis, which is the least compressible according to Weidner et al. (1982). Low γ_i's are expected for E_u^1 because this mode does not alter the close packing, and for E_u^3 because this mode does not involve stretching of nearest neighbor Si-O bonds. The largest γ_i is expected for E_u^2 because this mode involves stretching of O nearest Si. The LO component of E_u^1 at 1011 cm^{-1} has a γ_i of roughly 1.2 $\pm$ 0.2, which suggests that the LO components of the other IR modes are likely to have values of γ_i similar to that of their TO components. The average of the mode IR γ's is 1.23 $\pm$ 0.2, which is reasonably close to $\lambda_{th} = VB_T\alpha/C_v$ of 1.46 $\pm$ 0.06 at 700 K and 1 atm.

DEPOSITION, DOLOMITIZTION, SILICIFICATION PARAGENESIS OF NAQB SIWA CARBONATE SEDIMENTS, BAHARIYA OASIS, EGYPT

HOLAIL, H., Dept. of Geosciences, Purdue University, West Lafayette, IN 47907, USA

The lower part of the Campanian Naqb Siwa sediments (Bahariya Oasis, Egypt) are composed of dolostones hosting chert nodules and lenses as well as cavity filling of secondary quartz and calcite. The allochems suggest that the limestones formed in marine peritidal environments, while the low Na and Sr contents suggest stabilization of limestones in the presence of fresh water.

There are two textural varities of dolostones: (1) fine to medium grained and (2) medium grained. The fine to medium grained dolostones, composed of unzoned 0.04 - 0.3 mm dolomite crystals with traces of former presence of evaporites, represent penecontemporaneous dolomitization of carbonate sediments in upper intertidal environments. The medium dolostones consist of 0.5 mm dolomite crystals that shows textural and compositional zoning with cloudy centers and clear rims, concentric luminescent zoning, and low Na and Sr contents. These dolostones formed by early diagenetic replacement of limestones due to dilution of marine pore water by fresh water.

The evaporite molds most frequently appear as nodules and as isolated lenses or in aggregates which are lined with traces of gypsum and now are filled with partially dolomitized chert. The latter consists of cryptocrystalline and microcrystalline silica enclosing different sizes of dolomite rhombs. A later stage of silicification in the form of microscrystalline and mesocrystalline silica seems to have precipitated as cement or replacing the dolomite rhombs. Under cathdoluminescence the silica is dark, indicating formation in a low-temperature diagenetic environment.

A possible sequence of six diagenetic events are suggested by the interrelations of the various authogenic replacements. These events are: (1) deposition of carbonate evaporite nodules, (2) recrystallization, (3) early stage of silicification and formation of chert nodules instead of evaporate nodules, (4) dolomitization of carbonate sediments and partially dolomitization of chert nodules, (5) late stage of silicification as pore-space filling and replacing the dolomite rhombs, and finally (6) calcitization and corrosion of chert nodules boundaries.

RELATIONSHIPS BETWEEN COLOUR, CRYSTALLOGRAPHY AND ORIGINS OF GEM ZIRCONS IN E. AUSTRALIA.

HOLLIS, J.D.: SUTHERLAND, F.L., Division of Earth Sciences, The Australian Museum, 6-8 College St., Sydney, Australia, 2000.

Large 'gem' zircons derived from alkaline volcanics in E. Australia show colours and crystal forms distinct from acid granite zircons. They are mostly xenocrysts, probably brought up from crustal alkali syenites and nepheline syenites, but some euhedral types are cognate with trachytes. The fission track ages on the zircons (0-70 Ma) reflect annealing during transport in the volcanics, but help guide thinking on the ultimate age and provenance of the source rocks.

Surveys of crystal forms show distinctive trends, partly reflecting evolution of forms during cooling and changing melt compositions during fractionation. Data are presented on crystals from Elsmore, New South Wales, Lake Bullenmerri, Victoria and Boat Harbour, Tasmania. There is some relationship between crystal types and colours, with certain crystal groups having distinct colours. A crystal classification scheme is illustrated.

Elsmore shows:

1. Pale Group (colourless, yellow brown, orange),predominantly aByZ forms with significant BY_3, aByZp and aBY_3.
2. Scarlet Group (scarlet, orange, brownish red),predominantly aBcyZ forms with significant aByZ, aBcYZ and aBYZ.
3. Brown-orange Group (pale to deep), predominantly aByZ with significant ByZ.
4. Umber Group (to orange brown), BcyZ predominant with many BcZ.
5. Mauve-orange (to colourless), aBY_3 and aBYZ predominant.
6. Abraded Group (mauve orange-brownish orange) BY predominant, some BY_3. Alluvial types date at 41 Ma compared to euhedral types of 30 Ma in pyroclastics.

Bullenmerri shows:

1. Pale group, BY forms predominant.
2. Yellow brown Group, B and BY forms dominant.
3. Pale green Group, B and BY forms dominant.

Boat Harbour has a single group (colourless, orange, scarlet) mostly BY tending to BY_3. They come from a 26 Ma olivine melilitite host, which also contains xenoliths of nepheline syenite.

Most zircon crystallisation trends commence with ABZ-BZ (highest temperatures and alkalinity, Pupin) forms, then trend to ABYZ before progressing right to BY. This left curve is widespread in large zircons and may relate to decreasing alkalinity before increase in alkalinity at lower temperatures.

The frequent relationship between colour and crystal form groupings suggest trace elements control colour centres and crystallography. Temperature and alkalinity may be less important than previously supposed.

The zircons probably largely crystallised from Tertiary-Mesozoic hot spot magmas and,in some cases (low U), from highly undersaturated deep source magmas.

Chart for common zircon forms. Downward progression from 110 (Y) to 100(Z) prisms. Left to right progression through 211 (A), through 101(B) to 301(C) pyramids. Lower case indicates minority form.

A	Ab	AB	aB	B	Bc	BC	bC	C
AY	AbY	ABY	aBY	BY	BcY	BCY	bCY	CY
AY_3	AbY_3	ABY_3	aBY_3	BY_3	BcY_3	BCY_3	bCY_3	CY_3
AYZ	AbYZ	ABYZ	aBYZ	BYZ	BcYZ	BCYZ	bCYZ	CYZ
AyZ	AbyZ	AByA	aByZ	ByZ	BcyZ	BCyZ	bCyZ	CyZ
AZ	AbZ	ABZ	aBZ	BZ	BcZ	BCZ	bCZ	CZ

EXPERIMENTAL CONSTRAINTS ON THE H_2O CONTENTS OF SILICIC MAGMAS

HOLLOWAY, John R., CLEMENS, J.D., NEKVASIL, H., RUSHMER, T., VIELZEUF, D., and WEBSTER, J.D., Depths of the Earth, Inc., Depts. of Chemistry and Geology, Arizona State University, Tempe, AZ 85287, USA

The rheology, temperature, texture, ascent mechanism and emplacement history of silicic magmas depends more on their H2O content than any other single variable. In this paper we present the results of recent published and unpublished experimental work aimed at estimating the H2O content of silicate melt in representative magmas of the S-, A-, topaz rhyolite-, and I-types.

Methodolgy: In most of the studies we present, the method consists of two steps. The first is to deduce the crystalization sequence observed in a rock. To do this accurately requires that the rock has undergone no secondary recrystalization. The second step is to experimentally determine, or to calculate the P, T, and XH2O conditions which reproduce the observed sequence. In doing experiments, it is very helpful if crystallization temperature and oxygen fugacity have been independently estimated from the mineral assemblage.

Examples: **S-type.** The H2O content of the Violet Town volcanics was estimated by Clemens and Wall (1984) used results of melting experiments at 2 and 5 Kbar because geobarometry indicated the phenocryst assemblage crystallized at about 3.5 Kbar. The observed crystallization sequence showed biotite to crystallized after plag, which requires >2.5 wt% H2O, and biotite also crystallized after garnet, which can only occur at <4.5% H2O. Finally, the biotite indicates liquidus T >830°C, in agreement with thermometry.

A-type. Colllins et al. (1982) describe the Watergums Granite as a high level pluton emplaced in an almost wholly molten state. Clemens et al. (1986) experimentally determined the phase equilibria in this composition as a function of melt H2O content at a total P of 1 kbar. Oxygen fugacity was controlled very near that of the quartz-fayalite-magnetite buffer because that assemblage is observed in the rock. The melting experiments indicate that the initial crystallization T was >830°C and may have been >900°C. Comparison of observed and experimental crystallization sequences place the minimum melt H2O content at 2.2 to 2.4 wt%. Comparison of plag compositions suggests a melt H2O content of >2.4% during plag crystallization just below 900°C. Miarolitic cavities indicate fluid saturation (4.3%) late in the crystallization sequence, within the biotite field, suggesting that the initial melt H2O content was near the minimum estimate of 2.4%.

EXPERIMENTAL CONSTRAINTS ON THE H_2O CONTENTS OF SILICIC MAGMAS
HOLLOWAY, J.R. et al.

Variations in total P of 100% would have little effect on these conclusions.

Topaz-rhyolite. Burt et al.(1982) describe topaz rhyolites as lithophile element and fluorine-enriched lavas, and suggest that they are geochemically similiar to A-type granites. Webster, et al. (1985) experimentally studied a very fresh, glassy sample of a topaz rhyolite at total P of 0.5, 1, and 2 kbar over a wide range on melt H2O contents. Their results, when compared to the crystallization sequence observed in the lava, suggest a minimum total P of 1.2 kbar for the phenocrysts. At this P the minimun H2O content of the melt was about 4 wt%, and crystallization began at <750°C.

I-type. The mineral assemblages found in most I-types often exist over wide ranges of P, T, and XH2O, making it difficult to make precise estimates of their melt H2O contents. Rushmere et al. (1985) obtained preliminary data on the phase relations of the Kadoona Dacite, and I-type lava from SE Australia. Their 10 Kbar experiments require a minimum melt H2O content of 4 wt% at the time of biotite crystallization (900°C), but comparison of the amount of melt at that point with the groundmass volume shows that 4% H2O yields too little melt, so either the P was lower or the H2O content higher. However, uncertainties in the restite content of the rock subject this estimate to large uncertaintity.

Conclusions. Within the limits of the current estimates, their appears to be little difference in melt H2O content between magma types. Work is currently underway to use the thermodynamic model of Nekvasil & Burnham (1986) to more precisely estimate melt H2O contents.

References: Burnham,C.W., and Nekvasil,H.(1986) Am. Mineral.,Jahn's Vol., in press. Burt,D.M., Sheridan,M.F., Bikun.,J.V.,and Christiansen,E.H.(1982)Econ. Geol. 77 1818-1836. Clemens,J.D., Holloway,J.R., and White, A.J.R.(1986) Am. Mineral., Jahn's Vol., in press. Clemens, J.D., and Wall, V.J.(1984) Contrib. Mineral. Petrol. 88 354-371. Rushmer, T., Holloway, J.R., and Wyborn, D.(1985) EOS 66 1130. Webster, J.D., holloway, J.R., and Hervig, R.L.(1985) EOS 66 1130.

A PRELIMINARY STUDY ON MINERALOGY AND GEOCHEMISTRY OF THE ARCHEAN GRANITE, ANSHAN, LIAONING PROVINCE, PEOPLE'S REPUBLIC OF CHINA

Hong Wenxing
Institute of Geochemistry, Academia Sinica, Guiyang, Guizhou Province, Peoples Republic of China

The mineralogy and geochemistry of the Archean granite in Anshan, Northeast China have been studied with the following major results.

On the basis of the U-Pb isochron study for accessory minerals (zircon, apatite, sphene, allanite and garnet) and the whole rock Rb-Sr and Pb-Pb isochron dating, the isotopic age of the granite is 2.8 G.a., one of the oldest ages known in China up to date.

The petrographic types of the Archean granite are mainly assigned to potash-feldspar granite, monzonitic granite and granodiorite, and the petrochemical type belongs to potash series granite.

For trace elements, the contents of Ba, Sr, Zr, Cl, Ca, Ti and REE are higher in the Archean granite than in the younger ones formed after Paleozoic. About 15 species of accessory minerals have been recognized yet in Anshan Archean granite, including Fe-, Ca-, and Ti-bearing minerals (magnetite, apatite, garnet and sphene), Zr(Hf)-bearing mineral (zircon) and REE mineral (allanite). The Archean granite contains much less accessory minerals in comparison with the granites formed later than Paleozoic.

REE content in the granite ranges from 119 to 409 ppm with an average of 369 ppm, which is much higher than the average REE contents for granites in southern China and southern Xizang. The REE distribution patterns are rightly declined V-shape curves, displaying negative Eu anomaly (δEu=0.46---0.72) and with $(La/Yb)_N$ ranging from 22 to 60.

THERMODYNAMIC PROPERTIES OF ALKALI FELDSPARS

HOVIS, GUY L., Dept. of Geology, Lafayette College, Easton, PA 18042, USA

Thermodynamic K-Na mixing properties, as well as thermodynamic properties related to Al-Si ordering, have been determined for alkali feldspars via a combination of solution calorimetric, x-ray diffraction, heat capacity, and phase equilibria techniques. Five alkali feldspar ion-exchange series have been studied to date, four with topochemically monoclinic Al-Si distributions, the other a low albite - microcline series.

Solution calorimetric experiments conducted on four of the series indicate that enthalpies of K-Na mixing are maximized at values increasing from 1.2 to 1.9 kcal/mol from the most disordered to the most ordered series. Furthermore, maximization of the enthalpy of mixing changes toward increasingly sodic compositions as ordering increases (see figure). Volumes of mixing are also asymmetric toward sodic compositions for all topochemically monoclinic series, but have the opposite asymmetry for low albite - microcline. However, statistical differences between symmetric and asymmetric models for volume are very small. In either case the magnitudes for volumes of mixing are distinctly greater for the triclinic series than for the topochemically monoclinic ones.

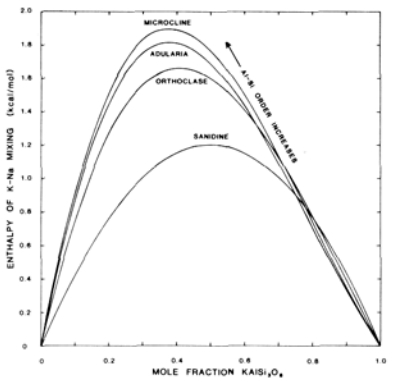

Free energies of K-Na mixing for the most ordered and the most disordered of the topochemically monoclinic series, determined from molten salt - alkali feldspar ion-exchange equilibria, are positive, similar in value to each other, and asymmetric toward sodic compositions (Hovis, Delbove, and Roll, 1983). They are lower in magnitude than those measured previously for topochemically triclinic feldspars (Delbove, 1975). Entropies of K-Na mixing for these three series, calculated from the free energy data by entering enthalpies and volumes of mixing as knowns, are positive, but asymmetry appears to vary with the degree of Al-Si order. Excess entropies for the more disordered of the two series differ slightly from those based on low-temperature heat capacity measurements (Haselton, Hovis, Hemingway, and Robie, 1983), which produce values that are greater in magnitude and more symmetric with respect to composition than the latter. This difference is close to the combined uncertainties in the data but could be interpreted as being due to the presence of short-range order in these minerals. Entropies of mixing for both of the topochemically monoclinic series are less than the calculated value for low albite - microcline.

Calorimetric data for end-member feldspars indicate that enthalpy increases with Al-Si disorder between T1 and T2 tetrahedral positions, and that the slope for enthalpy with Z (an ordering parameter defined as twice the difference of the mole fractions of Al in the T1 versus the T2 site; Thompson, 1969) is slightly greater at sodic than at potassic compositions. The slope for potassium feldspar calculated from the end-member values of just three topochemically monoclinic series agrees well with the previously reported value based on more extensive measurements (Hovis, 1974). Interestingly, enthalpies associated with the interchange of Al and Si between T1o and T1m tetrahedral sites in topochemically triclinic feldspars appear to be very small or nonexistent for both potassic and sodic feldspars. The same appears to hold for volume properties.

APPLICATION OF SYNCHROTRON RADIATION IN DETERMINING THE EQUATION OF STATE OF IRON

HUANG, E., BASSETT, W.A., and TAO, P., Dept. of Geol. Sci., Cornell University, Ithaca, NY 14853, USA

The equations of state of bcc and hcp iron have been determined in a high-temperature/high-pressure diamond anvil cell using synchrotron radiation as X ray source. Four isothermal runs were carried out at 25, 150, 300, and 450°C. Gold was used as pressure calibrant throughout the runs. The equation of state of the bcc iron was determined at pressures up to 13.0 GPa at each temperature. The bulk moduli, K_o, of bcc iron determined by fitting the compression data to the Birch-Murnaghan equation (Fig. 1) have values of 171, 175, 171, and 176 (± 7) GPa at 25, 150, 300, and 450°C, respectively. The first derivative of bulk modulus, K_o', was assumed to be 4 in each case. The result at room temperature is in excellent agreement with that obtained by the conventional X ray diffraction method (Wilburn & Bassett, 1978). The effect of temperature on the K_o value of the bcc iron is not significant when the uncertainties in the experiment are considered.

The equation of state for hcp iron was determined on the basis of compression data from 14.0 to 24.0 GPa. By fitting the Birch-Murnaghan equation to the compression data (Fig. 2), the bulk modulus for hcp iron was estimated to be 210 ± 12 GPa with $K_o' = 2$ at room temperature. The molar volume for the hcp iron is estimated to be 6.66 ± 0.03 cm^3/mole at room temperature. The results are reasonably consistent with those reported by Takahashi et al. (1968) and Jephcoat et al. (in press). Since the bulk moduli of the bcc iron are not found to change significantly with temperature in this experiment, the bulk moduli of the hcp iron at high temperatures are assumed to be the same as that determined at 25°C. The average volume thermal expansion coefficient of the hcp iron is 3.0 (± 0.4) x 10^{-5} $°C^{-1}$ below 450°C (Fig. 2). The measurement at 450°C is considered to be less accurate because of the possibility of alloying between iron and gold at this higher temperature.

Jephcoat, A.P., H.K. Mao, and P.M. Bell, The static compression of iron to 78 GPa with rare gas solids as pressure-transmitting media, J. Geophys. Res., in press.

Takahashi, T., W.A. Bassett, and H.K. Mao, Isothermal compression of the alloys of iron up to 300 kilobars at room temperature: iron-nickel alloys, J. Geophys. Res., 73, 4717-4725, 1968.

Wilburn and Bassett, Hydrostatic compression of iron and related compounds: an overview, Am. Mineral., 63, 591-596, 1978.

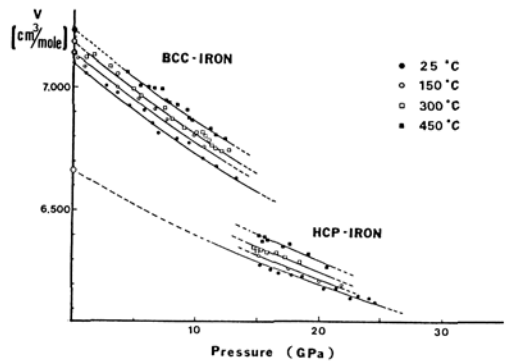

Figure 1

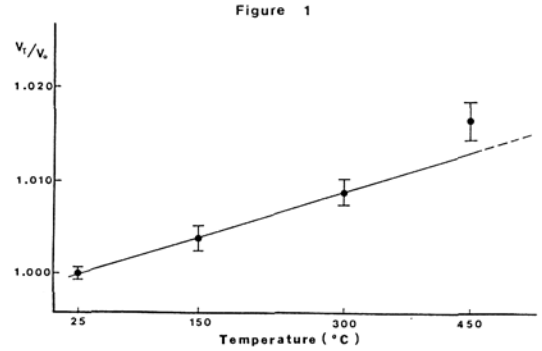

Figure 2

•MINERALOGICAL STUDY OF THE FRANCKEITE FROM THE DACHANG CASSITERITE-SULPHIDE POLYMETALLIC ORE FIELD, GUANGXI, CHINA

HUANG Minzhi, WU Gong Bao, CHEN Yuchan and TANG Shaohua, Institute of Mineral Deposits, Chinese Academy of Geological Sciences, Beijing, People's Republic of China

The franckeite from Dachang occurs in the NE-trending fractures in the marles and mega-lenticular limestone on the outer flank of the upper veinlet-type tin ore bodies in the Changpo ore deposit. The particular mineral is present in the form of thin tabular aggregates within the coarsely cyrstalline calcite veins. The evolutionary sequence of minerals in the veins is: cassiterite, quartz → pyrite, marmatite, stannite → franckeite, teallite → zenkenite. The duration of precipitation of calcite is relatively long, starting from the late stage of the formation of sulphides and ending with the formation of franckeite. The uniform temperature of calcite ranges from 128°C to 326°C, with a mean temperature of 221°C. The $\delta^{13}C$ value is -8.3%, the $\delta^{18}O$ value is +15%, and the $\delta^{18}O$ H_2O is +4.93%. The explosion temperature of franckeite is 180°C, the $\delta^{34}S$ value is -3.1%.

The formula of the particular mineral is $Fe_{0.93}[(Pb_{5.92}Ag_{0.17})Sn_{2.03}]_{8.12}Fe_{0.93}Sb_2S_{14.01}$. Its chemical composition and X-ray powder pattern indicate this mineral belongs to a "normal" franckeite of the lead-rich end members. Its crystal incoherent structure is composed of two sets of non-share crystal lattices; i.e., of natural penetration of three layers of pseudo-tetragonal lattice (T) and one layer of three layers of pseudo-hexagonal lattice (H), with its superstructure being of the 8c type. The Mossbauer spectroscopic study of ^{119}Sn shows that Sn and Fe occur in the mineral in the form of Sn^{4+} and Fe^{2+} with no Sn^{2+} and Fe^{3+} being seen. The crystal-chemical formula is: $[(Pb_{0.732}Sb^{3+}_{0.086}Sn^{4+}_{0.083}Fe^{2+}_{0.078}Ag^{+}_{0.021})_{1.000}S]\cdot 0.366\ [(Sn^{4+}_{0.459}Sb^{3+}_{0.440}Fe^{2+}_{0.101})_{1.000}S_2]$.

The formation of the lead-rich franckeite-teallite association represents a specific sulphur activity and a lower oxygen fugacity. The concentration of metallic ions in the liquid ranges from the (Pb + Ag)/Sn ratio equal to 3 to the $SnS_2/(FeS + Sb_2S_3)$ ratio equal to 2, suggesting a more alkaline reducing environment. The ore-containing fluid represents a moderate- and low-temperature hydrothermal solution formed by a mixture of post-granitic-magmatic hot water with meteoric water. The ore-containing elements, such as Pb and S, came from a mixed source of magma and surrounding rocks.

• MENGXIANMINITE, A NEW FERRO-MAGNESIUM-CALCIUM-TIN-ALUMINUM OXIDE MINERAL

HUANG Yunhui, ZHOU Xiuzhong, LI Gejing, Institute of Mineral Deposits, Chinese Academy of Geological Sciences, Beijing, People's Republic of China and DU Shaohua, Yichang Institute of Geological and Mineral Resources, Chinese Academy of Geological Sciences, Yichang, Hubei, People's Republic of China

A new Fe^{2+}-Mg-Ca-Sn-Al oxide mineral, mengxianminite, was found in a vein associated with hsianghualite, liberite, phlogopite, fluorite, chrysoberyl, spinel, taaffeite, nigerite, hoegbomite, bromellite, phenacite, eucryptite, cassiterite, microlite, apatite, etc. This vein occurs in the contact metamorphic tactite which formed from the contact of granite and dolomite. The mineral usually occurs as brownish-green tabular masses with a glassy luster and uneven fracture, locally forming minute veinlets. Its grain size is 0.02-0.05 mm in diameter and 0.5 mm in length with perfect (010) and (100) cleavage. Specific gravity is 3.85, and H_v (Kp/mm^2) = 606-946/762, H_M = 6.16. Optical biaxial negative 2V = 76°. Extinction angle $N_g c$ = 2-5°, N_g = 1.788, N_p = 1.766, N_m = 1.788. Elongation is positive.

Chemical compositions of two grains, analyzed by electron microprobe, are: MnO 1.18, 1.17; FeO 6.46, 6.52; CaO 7.93, 7.74; SiO_2 0, 0.51; Al_2O_3 44.53, 41.55; MgO 4.97, 5.57; Na_2O 1.89, 1.91; TiO_2 0, 0; F_2O 0, 0.12; SnO_2 29.47, 30.31; ZnO 3.60, 3.57; Nb_2O_5 0.09, 0.20; BaO 0.07, 0; Total wt % = 100.18, 99.17. Its chemical formula is $(Fe,Mn)_2(Ca,Na)_3Mg_2(Sn,Zn)_5Al_8O_{29}$.

The dominant lines of the X-ray powder diffraction pattern are: 2.8134(80), 2.6178(60), 2.3742(100), 1.4247(100), 1.2319(50). The single crystal studies by the Weissenberg method show it probably belongs to the orthorhombic system, a = 5.678 ± 0.001, b = 9.906 ± 0.002, c = 30.84 ± 0.003, ß = 90°.

This new mineral is named mengxianminite to honor the late Professor Meng Xianmin, a brilliant geologist and mineralogist.

POLYTYPISM OF $MgSiO_3$ IN NATURAL SAMPLES

HUANG WANKANG, Institute of Geochemistry, Academia Sinica, Guiyang, Guizhou Province, People's Republic of China; WANG YENGUO and ZOU BENSAN, Institute of Metal Research, Academia Sinica, Shenyang, P.R.C.

The polymorphic transformation of ortho-enstatite and clino-enstatite in five natural samples has been investigated by HRTEM. The observed pyroxenes were selected from two meteorites--Jilin chondrite and Qingzhen enstatite chondrite, two mantle rocks in basalts--spinel- and garnet-lherzolite and one Alpine ultramafic massif in Dazuka, Tibet.

I. Meteorite CLEN in enstatite possesses the field of any multiple of 9Å wide, twinning and high concentration. Compared with the criteria of CLEN formation suggested by Buseck P.R.(1975), the CLEN in Jilin and Qingzhen chondrites were produced by conversion of PEN. Smyth J.R.(1974) suggested that if PEN is quenched in a few seconds or less, twinned CLEN will result, while slower cooling rates will allow a slower ordering process to form significant amounts of OREN. So Jilin chondrite with dominant OREN would be formed at a slower cooling rate than Qingzhen chondrite which possesses 30-50% CLEN with OREN and CLEN alternating frequently. As experiment shows that the concentration of OREN could rise slowly in expense of CLEN in the range 655°-975°C (Smyth, 1974), Qingzhen chondrite preserving primary features of PEN to CLEN conversion is thought not to suffer obviously later thermo-metamorphism. From this, a reasonable suggestion could be derived: the meteorite containing considerable amounts of CLEN produced by conversion of PEN would undergo light or no metamorphism during its forming history.

2. CLEN in the mantle rocks The characteristics of CLEN in enstatite from spinel- and garnet-lherzolite fall in the field of 2n9Å only (2,4,6 and 8*9Å) without twinning. These features imply that CLEN was produced by shear deformation of OREN. Two mechanisms for OREN to CLEN transformation due to shearing have been proposed by former researchers. One is a macroscopic shear of 18.3° on (100) parallel to I0011, the other is a shear of 13.3°.

A picture of I012I structure image of enstatite from spinel-lherzolite shows the details of transformation in the partial dislocation region, in which the calculated value of Burgers vector is H_2-H_1=2.7Å=0.8C Sin40.24°. This is matched in 0.83C, i.e. the angle of shear is 13.3°. Thus, the mechanism of 13.3° shear angle has been approved in structure image.

The spinel- and garnet-lherzolit are formed under the upper mantle at ~1000°C, 15-22Kb and 1100°C, ~40Kb, respectively. Their temperatures were not lower than 1000°C after they were involved in basalts. It means that OREN to CLEN transformation in the mantle rocks took place under high temperature, instead of moderate to low temperatures as suggested by Buseck(1975).

Under this temperature/pressure condition of spinel-lherzolite, the formation of CLEN from OREN requires 2-3 kilobars of shear strength (Riecker R.E.,1967). As having tabular-granuloblastic texture, it is assumed that OREN to CLEN transformation in garnet-lherzolite might be produced in higher shear stress.

According to experimental results of Raleigh, C.B. (1971), OREN should transform to CLEN only at a strain rate of $10^{-6}sec^{-1}$ in the range 1000°-1200°C. That is much higher than a reasonable geologic strain rate of 10^{-13} -$10^{-15}sec^{-1}$, but close to the strain rate for volcanism and seismism.

3. OREN to CLEN transformation in Alpine ultrabasic rocks

CLEN transformed from OREN in harzburgite, Dazuka massif is different from that in meteorite in having no (2n+1)9Å field width and lower concentrations, and also different from that in mantle rocks in twinning appearring. Because many features show that the massif was under constant action of tectonic compression during its forming history, CLEN in the Dazuka massif should be produced by shearing.

On the assumption of a reasonable geologic strain rate of 10^{-13}-$10^{-15}sec^{-1}$, OREN to CLEN transformation only occurred at low temperature in the Dazuka massif (≤650°C). It is likely that the polymorphic transformation took place during emplacement of the massif, while it was basically consolidated.

REFERENCES
Buseck P.R. (1975) Am. Mineral., 60, 771-784.
Raleigh C.B. (1971) J.Geophy. Res., 76, 4011-4022.
Riecker R.E. (1967) Geol. Soc. Amer. Bull., 78, 1048-1054.
Smyth J.R. (1974) Am. Mineral., 59, 345-352.

PLATINUM METALS IN AUSTRALIA - GENERAL OCCURRENCE AND MINERALOGY AND RECOVERY FROM WESTERN AUSTRALIAN NICKEL DEPOSITS

HUDSON, D.R., CSIRO Division of Minerals and Geochemistry, Private Bag, PO Wembley, Western Australia 6014.

Australia has a vast, but largely unrealized potential for the discovery and production of platinum group elements (PGE). The western half of the continent is underlain by Precambrian rocks and includes two well-exposed, Archean granite-greenstone cratons, the Yilgarn and Pilbara Blocks. Komatiite-associated Ni sulfide deposits and numerous partly-dismembered layered gabbros, several of which contain significant Ni-Cu sulfide mineralization, occur within the cratons and are potential hosts for PGE mineralization. Proterozoic gabbros occur within the Kimberley and Pilbara regions of Western Australia and in central Australia, but to date, like the Archean gabbros, only minor PGE mineralization has been reported.

Early PGE production in Australia was based on recovery of osmiridium from mainly alluvial deposits derived from ultramafic rocks in northwest and southern Tasmania. The deposits produced some 900 kg to 1965, but in recent years production has been meagre. There have, in addition, been numerous reports of minor occurrences of platinum group minerals (PGM) associated with gold and base metal mining in eastern Australia.

Hudson and Horwitz (1986) have recently identified PGM and gold in samples taken from outcrop loaming and drainages along 10 km of strike of an Archean sedimentary horizon in the Pilbara. The PGM are dominantly alloys of iridium, osmium and ruthenium, but minor platinum-containing alloys also occur.

Australia's most significant PGE production has come as a consequence of the mining of Western Australian komatiite-associated nickel sulfide ores. Mining commenced in 1967 and to June 1980 the Kambalda deposits had produced 400 thousand tonnes of nickel metal; current production is about 40 thousand tonnes of metal per year. An estimate of the average composition of Kambalda ore (ppb in 100% sulphide ore) has been given by Hudson and Donaldson (1984) as Pt

1630, Pd 2104, Os 537, Ir 293, Rh 240, Ru 1070, Au 1721, and Ag 5710. The total PGE (kg) contained in mined ore can be calculated for the period 1967-1986 (and for current production rates): eg, Pt 7200 (448), Pd 9350 (584), etc. At current production rates, the contained PGE has a value of about $US20 million per year.

Mineralogical studies of PGM in heavy mineral residues from the gold-recovery gravity circuit of the Kambalda nickel mill (Hudson and Donaldson, 1984) and studies of ore samples from a number of geological environments within the nickel deposits (Hudson, 1986) have indicated the following discrete phases: Pt - sperrylite, moncheite; Pd - sudburyite, stibiopalladinite, palladoarsenide, michenerite, testibiopalladite, merenskyite; Ir - irarsite. Sperrylite is the most abundant PGM, and occurs within massive sulfide ores, particularly those that are chalcopyrite-rich; its distribution is believed to reflect primary magmatic processes. Palladium minerals occur predominantly in sulfide veins within the footwall rocks or in association with post-ore hydrothermal veins and porphyries; they are believed to have formed by late-magmatic or post-magmatic processes.

Although no accurate estimate has been made of the ratio of PGE in discrete phases relative to that contained in solid solution or as submicroscopic grains in ore sulfides, it is believed that a significant percentage of Pt occurs as sperrylite, some of which can be recovered as a separate concentrate. Discrete Pd minerals are rare within the main ore zones and little scope exists for the recovery of a separate heavy mineral concentrate.

Hudson, D.R., 1986, Platinum group minerals from the Kambalda nickel deposits, Western Australia, Econ. Geol. (in press).

Hudson, D.R. and Donaldson, M.J, 1984, Mineralogy of platinum group elements in the Kambalda nickel deposits, Western Australia: In sulphide deposits in mafic and ultramafic rocks, Buchanan, D.L., and Jones, M.J., eds (London: IMM, p 55-61).

Hudson, D.R., and Horwitz, R.C. 1986, Mineralogy and geological setting of a new occurrence of platinum group minerals between Roebourne and Karratha, Western Australia. CSIRO Division of Mineralogy and Geochemistry Research Review 1985 (in press).

ORIGIN & METAMORPHISM OF MANGANESE SEDIMENTS IN MELANGE OF THE FRANCISCAN COMPLEX, CALIFORNIA

HUEBNER, J. Stephen, FLOHR, Marta J. K., and MATZKO, John J.
U.S. Geological Survey, Reston, Virginia 22092

Of many small Mn-rich lenses associated with layered chert, the Buckeye Mine best preserves metamorphic ore. Here are found rhodochrosite, the Mn-oxides hausmannite and braunite, and the silicates caryopilite (Mn-serpentine), chlorite, gageite, and taneyamalite in <10-mm layers and fragments of disrupted layers that contain 1-3 minerals. These minerals are analogues of minerals found in carbonate (siderite), oxide (magnetite and hematite) and silicate (greenalite, chamosite, howeite) facies of iron formation. Unlike iron formation, however, the orebody is enclosed in massive white chert with nearby rhythmic red (ferruginous, radiolarian) and green chert, all contained in volcanogenic metagraywacke incipiently metamorphosed at blueschist-facies grade.

The bulk composition of the orebody can be modelled by the quaternary system MnO-SiO_2-CO_2-O_2. Rhodochrosite, hausmannite, braunite, and caryopilite have nearly end-member compositions, as does gageite except for minor MgO and FeO (see Table). Most nonquaternary components are in chlorite, taneyamalite, and vitreous material. Minor components include ZnO (<0.3 wt%) and NiO ($\leq$0.5%) in gageite, NiO ($\leq$ 1.6%) in chlorite, and V_2O_3 in braunite, serpentine, and taneyamalite. Barite, apatite, and fragments of layers are in veins. Despite the marine origin, the only possible major signature of seawater remaining in the deposit is Mg, in chlorite.

Vitreous material occurs as sedimentary laminations, interstitial masses in recrystallized rhodochrosite, and fragments of disrupted layers. Completely isotropic materials have compositions similar to chlorite. Some partly devitrified material has a composition similar to gageite. The textural diversity of silicates enables us to propose a sequence of devitrification and recrystallization from isotropic material to well-foliated masses. However, although both clay-like and coarsely crystalline caryopilite are seen, no isotropic material of this composition was found. It is unlikely that manganese was introduced into volcanic glass by a process that preserved its non-crystalline state. More likely, these materials are relics of gel-like Mn-rich sediments. We also suggest that, to preserve these relics, little or no aqueous fluid was present during metamorphism.

On the basis of the blueschist-facies minerals lawsonite and glaucophane in the graywacke, the ore assemblages rhodochrosite + braunite and rhodochrosite + hausmannite, and the absence of pyroxmangite and tephroite, Huebner (1967, Ph.D. Thesis, Johns Hopkins University) concluded that the ore was metamorphosed at 550K, 6000 bars, fCO_2 = 400 bars, and log fO_2(bar) = -14 and that this oxidation state was far higher than that of the surrounding metagraywacke. We propose that this high fO_2, like the relic vitreous material, is preserved because during metamorphism the lens remained isolated from fluids in the surrounding country rock.

The origin of orebodies like the Buckeye hinges upon the kinetics of sedimentation and fluid transport. Deposition of manganese and white chert was sufficiently fast that clastics are absent, the number of radiolaria is less in ore than in the surrounding red chert, and a terrigenous chemical signature is absent. We favor an origin in which most free water and marine salts were excluded by the same processes that formed the vitreous material and chemical sediments. Crystallization of hydrous silicates consumed any free water that was present in the lens. If a barrier was necessary to maintain a dry lens, the surrounding dense white chert would serve as such a barrier.

Electron Microprobe Analyses of Mn-Silicates and Vitreous Material (Vit Mat) Expressed As Cations Per 20-Cation Formula Unit

	Gageite	Vit Mat	Caryopilite		Taneyamalite		Chlorite		Vit Mat	Vit Mat
	B50	B50	B45	B24	B38	B24	B38	B84	B84	B50
Si	5.53	5.64	8.82	8.93	9.50	9.89	6.70	6.80	7.42	6.02
Al^{iv}	.00	.00	.00	.00	.10	.00	1.30	1.20	.58	1.98
Al^{vi}			.02	.23	.87	.35	1.98	2.00	1.84	1.98
Ti	.00	.00	.00	.02	.13	.04	.00	.00	.00	.00
V^{+3}	.00	.00	.00	.00	.20	.00	.02	.00	.01	.00
Mg	.75	.70	1.81	.71	2.04	1.81	8.07	9.01	7.50	6.62
Fe^{+2}	.05	.07	.10	.44	.63	1.61	.54	.29	.28	.23
Ni	.00	.00	.06	.02	.01	.02	.00	.01	.00	.04
Mn^{+2}	13.65	13.55	9.18	9.64	5.74	5.53	1.32	.61	2.33	3.11
Zn	.02	.04	.00	.02	.01	.04	.02	.02	.00	.02
Ca	.00	.00	.00	.00	.02	.02	.05	.03	.02	.00
Na	.00	.00	.00	.00	.76	.68	.00	.01	.01	.00
*	89.76	89.57	88.54	88.01	91.84	92.28	86.55	85.58	87.97	86.15

* Sum as oxide weight percent. K, Cl sought but not found.

CHARACTERIZATION OF THE METAMICT STATE OF OXIDE MINERALS BY EXAFS

IMAFUKU, M., NAKAI, I., AKIMOTO, J., MIYAWAKI, R.,and SUGITANI, Y., Dept. of Chemistry, The University of Tsukuba, Ibaraki 305 Japan; KOTO, K.,
Institute of Scientific and Industrial Research, Osaka University, Ibaraki, Osaka 567 Japan

INTRODUCTION

Although a number of studies have been made to understand metamict minerals[1], the causes of loss of crystal structure and nature of the metamict state have not yet been clearly understood. Metamict minerals are X-ray amorphous, which has been a serious obstacle to the study of these minerals. Since EXAFS is an ideal method for obtaining direct structural informations of amorphous substances. We have applied the technique to characterization of the metamict state, especially around Zr, Y and Nb atoms; so far only one report of EXAFS analysis of metamict minerals is seen[2].

EXPERIMENTAL

X-ray absorption measurements were made with synchrotron radiation at BL-10B in Photon Factory, Tsukuba, Japan. Samples used were metamict gadolinite, crystalline gadolinite, naegite (metamict: a variety of zircon), crystalline zircon, intermediate type green zircon, annealed green zircon (crystalline), samarskite and some of their crystalline speeimens. IR and Mössbauer spectra were also measured.

RESULTS AND DISCUSSIONS

Fig. 1 shows the K absorption spectra. Fourier transforms (FT) of the EXAFS oscillations, $k^2\chi(k)$, are shown in Fig. 2 (phase shift has not been corrected). The 1st peaks at about 1.7 Å and 1.6 Å of crystalline zircon and ZrO_2, respectively, are assigned to Zr-O bonds, and the strong 2nd peaks at about 3.3 Å are due to Zr-Zr interaction. The 1st peaks of the intermediate and metamict zircon are at about 1.46 and 1.55 Å, respectively (Fig. 2(c),(d)) 0.1-0.2 Å shifted to shorter distances and the former is 0.1 Å shorter than that of ZrO_2. Zr is coordinated by (4+4) and 7 oxygen atoms in zircon and ZrO_2, respectively. These observations suggest that the local environment around the Zr atom in the metamict state and that in the crystalline state are different: the coordination

CHARACTERIZATION OF THE METAMICT STATE OF OXIDE MINERALS BY EXAFS
IMAFUKU, M., et al.

number may be 7 or less in the former. The 1st peaks of crystalline and annealed green zircon are in good agreement with each other suggesting recovery of the structure of the latter. The metamict specimens show remarkable decrease in intensity of the 2nd peaks, indicating loss of the long range order found in the crystalline state. Similar results were obtained for gadolinite and samarskite. Therefore, the metamict state is characterized by disordered state of the second coordination sphere.

1) e.g. E.R. Vance and B.W. Anderson (1972) Mineral. Mag., 38, 605.
2) R.B. Greegor et al. (1984) Springer Proc. Phys., 2, 343.

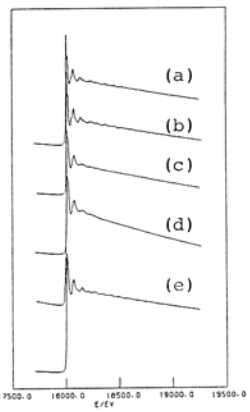

Fig. 1. X-ray absorption spectra.

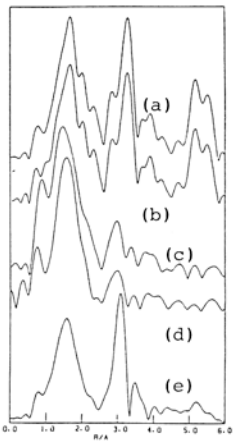

Fig. 2. Fourier transforms of $k^2\chi(k)$.

(a): zircon (b): annealed zircon (c): intermediate zircon
(d): a naegite (metamict zircon) (d): ZrO_2(baddeleyite)

THE POST-SPINEL AND POST-MAJORITE TRANSFORMATIONS AND THE CONSTITUTION OF THE DEEP MANTLE

ITO, E. and TAKAHASHI, E., Institute for Study of the Earth's Interior, Okayama University, Misasa, Totti-ken, 682-02 JAPAN

In order to clarify the nature of the 670 km discontinuity and the mineralogy and chemistry of the lower mantle, phase equilibria in the systems MgO-FeO-SiO_2 and $CaSiO_3$-$MgSiO_3$-Al_2O_3 and the natural peridotite have been investigated in the pressure range 10 to 27 GPa and at temperatures to 1600°C, using a uniaxial split-shpere type ultrahigh pressure apparatus (USSA-5000).

The spinel solid solution of $(Mg_{1-x}Fe_x)_2SiO_4$ ($x<0.3$) dissociates into the assemblage of perovskite and magnesiowustite at pressures higher than 23 GPa with a negative Clapeyron slope. It is highly likely that the dissociation would be responsible to the 670 km discontinuity. It should be also noted that the dissociation is completed in a quite narrow pressure interval and would make the discontinuity very sharp.

In the system $CaSiO_3$-$MgSiO_3$-Al_2O_3, the stability of majorite expands rapidly towards the $CaSiO_3$-$MgSiO_3$ join up to 18 CPa, which, however, is drastically reduced owing to the stabilization of $MgSiO_3$ ilmenite (at 1200°C) or perovskite (at 1600°C) at pressures above 22 GPa. It is also suggested that relatively CaO-rich and Al_2O_3-rich phases can coexist with the perovskite at pressures higher than 24 GPa. The experimental results indicate that the majorite would be an important constituent in the transition zone and the dissociation of majorite into the perovskite-bearing assemblage could also contribute to the 670 km discontinuity. In contrast to the case of spinel, however, the dissociation of majorite requires a fairly large pressure interval (~4 GPa).

The phase equilibria of the natural peridotite are consistent to those observed in above two systems. The volumetric constitution of the peroditic mantle is suggested as following: β or γ phases (~50 %), majorite (~45%), and cpx (~5%) in the transition zone and Mg-rich perovskite (≳70%), magnesiowustite (~20%) and others (the CaO-rich and Al_2O_3-rich phases) (≲10%).

THE ELASTICITY OF MANTLE MINERALS

JACKSON, I. Research School of Earth Sciences, Australian National University, Canberra, A.C.T., Australia

The most definitive information concerning the constitution of the Earth's deep interior is contained in models of the spatial variation of elastic wave velocities and attenuation derived by inversion of seismological data. The interpretation of such information, in terms of chemical composition, mineralogy, temperature and the microstructure of mantle rocks, is dependent upon laboratory measurements (preferably reinforced by theoretical understanding) of the elastic and anelastic properties of appropriate materials under controlled and relevant conditions. This 'calibration' of the seismological probe is the ultimate goal of much contemporary research in mineral physics/petrophysics.

Attention is therefore necessarily focussed on the achievement in the laboratory of the closest possible simulation of the conditions of seismic wave propagation in the Earth's mantle. Thus one seeks to measure elastic/anelastic properties of upper mantle minerals (and rocks) and high-pressure phases representative of the deeper mantle, under appropriate P-T conditions (to ~100 GPa, 3000 K), and preferably at seismic frequencies (≲1 Hz). These demanding conditions cannot possibly be simultaneously satisfied by any single laboratory technique. However, these criteria are being met individually, and in useful combinations, by the application of a wide variety of experimental methods which yield complementary information concerning the elastic/anelastic properties of minerals and rocks. The complementarity will be illustrated by emphasis of special advantages associated with the use of each of these techniques. Examples include the precision and pressure capability of ultrasonic pulse interferometry; access to high temperatures via resonance methods; investigation of the ultrahigh pressure regime by shock and static compression; the opportunity to study microcrystals (e.g. of high-pressure phases) by Brillouin scattering or thermal diffuse scattering of X-rays; and access to the seismic frequency band via sub-resonant methods.

The current state of our knowledge of the elastic properties of minerals, deriving from the application of these various techniques, will be reviewed. The elastic moduli and their pressure and temperature derivatives have been measured mainly by ultrasonic methods for all of the major upper mantle minerals - with the exception of clinopyroxene for which the derivatives are yet to be determined. For the known high-pressure phases, the single-crystal elastic moduli have now been measured by Brillouin spectroscopy under ambient conditions on synthetic microcrystals for most of the end-members (coesite and stishovite, β- and spinel phases of Mg_2SiO_4, and the ilmenite phase of $MgSiO_3$). Similar data for the garnet- and perovskite-structured phases of $MgSiO_3$ may be anticipated in the near future.

In parallel with the experimental work on the elasticity of minerals (and their structural analogues) there has been significant progress in the elucidation of the structural and compositional factors which control crystal elasticity. At a qualitative level, polyhedral models have provided insight into persistent trends evident among the elastic moduli of structurally related phases. More fundamentally, *ab initio* methods, in which short-range interatomic forces are calculated from appropriate electronic wavefunctions, have been successfully applied in the modelling of the crystal structures and elastic moduli of complex minerals.

These advances provide the basis for more informed interpretation of seismological velocity-depth models than has previously been possible. Recent analyses of the constitution of the mantle will be reviewed. Despite the additional constraints provided by the new data, there remains a range of acceptable composition/temperature models. In particular, the relative contributions of phase transformations and compositional changes to the velocity/density structure of the transition zone remain to be unambiguously established.

These analyses also focus attention upon the inadequacies of the current mineral elasticity dataset and therefore upon important directions for future work. The principal limitations are the absence of single-crystal elastic moduli for the garnet (majorite) and perovskite phases of $MgSiO_3$ and for the various high-pressure solid solutions, and the total lack of pressure and temperature derivatives for high-pressure phases. Another important shortcoming of the present dataset is the virtual absence of laboratory information concerning wave velocities and attenuation at seismic frequencies - which precludes definitive interpretation of the zone of low velocities and high attenuation commonly observed in the upper mantle.

ULTRASONIC STUDIES OF THE ELASTICITY OF MANTLE MINERALS

JACKSON, I., WEBB, S.L., and NIESLER, H. Research School of Earth Sciences, Australian National University, Canberra, ACT, Australia

Improved techniques have been developed for measurement of the pressure dependence of single-crystal elastic moduli by ultrasonic pulse interferometry. These new techniques combine greater accuracy in the measurement of elastic wave travel times (resulting from subtraction of the transducer-bond phase-shift contribution) with the extended pressure capability (3 GPa) of a liquid-medium piston-cylinder apparatus. These developments provide not only for more reliable determination of first pressure derivatives of elastic moduli than has previously been possible, but also for qualitatively different experiments in which second pressure derivatives may now be measured on relatively incompressible silicates and oxides.

These methods have been applied in the study of two suites of minerals - the B1 oxides (MgO, MnO and $Fe_{0.95}O$) and the major upper mantle silicates (olivine - both Fo_{90} and Fa, bronzite and pyropic garnet). The following features and applications of the data will be emphasized:

(i) Precise ultrasonic determination of the bulk modulus K and its pressure derivatives (K' , K" etc.) allows the calculation via an assumed equation-of-state of isothermal, adiabatic or shock compression curves. For example, comparison of calculated and observed shock compression curves for MgO suggests that the Birch-Murnaghan equation (third-order Eulerian finite strain) adequately describes the compression to pressures well beyond 100 GPa.

(ii) The measured bulk modulus of $Fe_{0.95}O$ is in excellent agreement with previous determinations from ultrasonic wave propagation and static and shock compression experiments, but is significantly lower than the value inferred for stoichiometric FeO from bulk modulus-molar volume systematics. Normal pressure dependence is observed for C_{11} and C_{12} (and hence K) for both MnO and $Fe_{0.95}O$. C_{44} on the other hand displays a markedly anomalous pressure dependence for each of these oxides. By analogy with similar anomalies at low temperature, the pressure-induced softening of C_{44} is attributed to magnetoelastic interactions which become progressively more important as the paramagnetic → antiferromagnetic transition is approached.

(iii) The lack of any evidence for softening of the shear modulus C_{55} for fayalite (Fe_2SiO_4) in the pressure interval 0–3 GPa suggests that the olivine → spinel transition probably does not proceed under hydrostatic conditions via the martensitic mechanism proposed by Poirier.

(iv) Measurements of the pressure dependence of the single-crystal elastic moduli C_{ij} of bronzite confirm the unusually large first pressure derivatives measured by Frisillo and Barsch for the compressional and off-diagonal moduli and hence for the bulk modulus K. However, the negative second pressure derivatives are also found to be unusually large in magnitude, so that the first pressure derivatives decrease progressively with increasing pressure towards more normal values. Some insight into the anomalous pressure dependence of the elastic moduli is provided by consideration of a polyhedral model of the pyroxene structure.

EXAFS STUDY OF THE LOCAL-COORDINATION ENVIRONMENT OF POTASSIUM IN ORTHOCLASE AND ALBITE-ORTHOCLASE COMPOSITION GLASSES

JACKSON, W.E., BROWN, G.E., JR., PONADER, C.W., Dept. of Geology, Stanford University, Stanford, CA 94305, USA

Alkali cations such as K and Na play important charge-balancing roles in many naturally-occurring aluminosilicate minerals, glasses, and melts. Variation in Na/K ratios can have a significant effect on physical properties such as the melting temperature of feldspars and the viscosity and conductivity of alkali-feldspar composition melts. Yet, little is known about the structural environments of these cations in glasses and melts or how variations in local environment might affect properties.

As part of an effort to understand structure-property -composition relationships in aluminosilicate glasses and melts, we have carried out the first extended x-ray absorption fine structure (EXAFS) study of the local coordination environment of K in selected glasses and crystalline model compounds along the $NaAlSi_3O_8$-$KAlSi_3O_8$ join. The results of this study are combined with results from our recent EXAFS study of Na environments in selected glasses within the Na_2O-Al_2O_3-SiO_2 system (McKeown et al., 1985). Both are related to the mixed-alkali effect (Isard, 1968; Hayward, 1976).

Fluorescence EXAFS data for K were taken during a dedicated run at the Stanford Synchrotron Radiation Laboratory on bending -magnet line I-5 using Si(111) monochromator crystals and a He atmosphere around the beam path and sample to minimize air absorption of the soft K x-rays. The samples studied included the glass compositions Ab_{50}-Or_{50} and Or_{100} and low microcline which was used as a model for phase shift and back-scattered amplitude information needed in fitting the glass data.

Assuming the K-environment in low microcline to have nine nearest oxygen neighbors at an average K-O distance of 2.97 A (Brown and Bailey, 1964), K in the Or_{100} glass was found by least-squares fitting of the fourier-filtered, back-transformed, and k^3 weighted chi function to have an average coordination of 8.9 oxygens at a distance of 2.93 A (see Fig. 1). K in the Ab_{50}-Or_{50} glass was found to be coordinated by approximately 12 oxygens at an average distance of 3.0 A. The Na cation in glasses near the Ab_{100} composition is thought to have about 7 nearest oxygen neighbors at an average distance of 2.60 A and does not show much variation in environment with Na/Al ratio (McKeown et al., 1985). The estimated accuracies of the coordination numbers (N) and distances are 20% and 0.1 A, respectively. Despite the large uncertainty in N-value and its dependence on the N-value of K assumed in low microcline, all attempts at modeling the glass data suggest a larger potassium coordination in the mixed-alkali glass than in the pure end-member glass. This proposed structural variation can be correlated with the observed variation in some physical properties of mixed-alkali feldspar glasses; however, it does not lead to a general structural explanation for the mixed-alkali effect. The results of our study contrast with and, perhaps, complement recent attempts to explain the mixed-alkali effect in aluminosilicate glasses in terms of speculated changes in Al-coordination and non-bridging oxygen content (Hayward, 1977). Additional K-, Na-, and Al-EXAFS data for mixed-alkali glasses are needed for evaluating such speculations and for formulating a structural explanation of the mixed-alkali effect.

Study supported by NSF Grant EAR-8513488

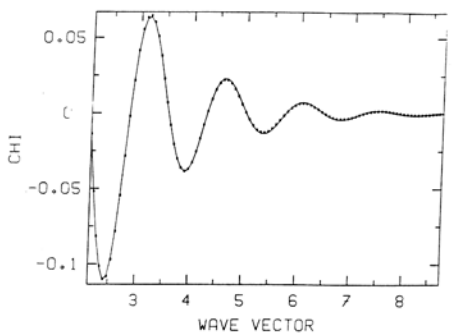

Figure 1
Example of least-squares fit of model chi function (dotted line) with back-transformed chi function (solid line) for Or_{100} glass in which K-O distance and N-value are varied and with phase and backscattered amplitude information taken from low microcline with known K-O distance and N-value.

REFERENCES

Brown, B.E. and Bailey, S.W. (1964) Acta Crystallogr. 17, 1391-1400.
Hayward, P.J. (1976) Phys. Chem. Glasses 17, 54-61.
Hayward, P.J. (1977) Phys. Chem. Glasses 18, 1-6.
Isard, J.O. (1968) J. Non-Crystal. Sol. 1, 235-261.
McKeown, D.A., Waychunas, G.A., and Brown, G.E., Jr. (1985) J. Non-Crystal. Sol. 74, 325-348.

$(Mg,Fe)SiO_3$ PEROVSKITE: THE MOST ABUNDANT MINERAL IN THE EARTH

JEANLOZ, Raymond, KNITTLE, Elise, WILLIAMS, Quentin, Dept. Geology and Geophysics, University of California, Berkeley, CA 94720, USA; HEINZ, D.L., Dept. Geophysical Sciences, University of Chicago, Chicago, IL 60637, USA

The dominant minerals of the upper mantle, olivine, pyroxene and garnet, all transform to the orthorhombically distorted perovskite structure (± an oxide) at pressures exceeding 20-25 GPa (200-250 Kbar) and temperatures above 1300 K. New synthesis experiments confirm that silicate perovskite is stable to pressures exceeding 100 GPa (1 Mbar). Also, the properties of $(Mg,Fe)SiO_3$ perovskite and perovskite-rich assemblages at high pressures and temperatures are in close agreement with the seismologically observed properties of the lower mantle. Hence, silicate perovskite is likely to be the dominant phase of the lower mantle, and to make up ~ 45 percent of the entire planet.

In-situ X-ray diffraction at room temperature shows that the compression of silicate perovskite is well represented to over 100 GPa by an eulerian finite-strain isotherm. The resulting bulk modulus and its pressure derivative are K_0 = 265 GPa and K_0' = 4.0 at zero pressure. According to our data, there is no evidence for any variation in the structural distortion (b/a = 1.032, c/a = 1.044) either to ultrahigh pressure or to elevated temperatures (~ 900 K, maximum). The thermal expansion coefficient, measured by X-ray diffraction at zero pressure, attains a high-temperature value of $\alpha \cong 4x10^{-5}$ K^{-1} above 500 K. The temperature dependence of α can be expressed by the Grüneisen formalism, with γ_0 = 1.8 and θ_0 = 530 K for the zero-pressure Grüneisen parameter and Debye temperature.

FTIR spectra have been collected to 27 GPa (at room temperature) to document the effect of pressure on the vibrational modes of $MgSiO_3$ perovskite. The highest infrared absorption mode, located at 800 cm^{-1} at zero pressure, is due to an SiO_6 (octahedral) stretching vibration. This vibration and the lower frequency external or mixed vibrations increase by about 2.6 cm^{-1}/GPa with pressure. The average of the mode-Grüneisen parameters for the mid-infrared bands ($\overline{\gamma} \cong 1.4$) is somewhat lower than, but compatible with, the value of γ_0 derived from the thermal expansion measurements. These values provide an experimentally-based estimate for the adiabatic geothermal gradient across the lower mantle: $(\partial T/\partial z)_s \cong 0.38$ K/km.

The melting temperature of $(Mg,Fe)SiO_3$ perovskite, measured by quantitative laser-heating experiments between 25 and 60 GPa, is found to be at 3000-3200 K. No pressure-dependence is found, implying that the volume change on melting is near zero. According to microprobe analyses, iron is partitioned out of the perovskite, thus suggesting that the melt is denser than the coexisting solid at high pressures. These results provide an upper limit for the geotherm through most of the lower mantle ($\lesssim$ 3200 K), and support the idea that iron-enriched melts may sink in the Earth's deep mantle.

COPPER DEPOSITS IN THE ZHONGTIAO MOUNTAINS AND LAYERED INTRUSIONS

JI Shukai, Institute of Geological Sciences of Shanxi, 32 Wuchen Road, Taiyuan, Shanxi, and MIAO Peisen, Regional Geological Survey Brigade of Shanxi, 58 Yianghao, Yuci, Shanxi, People's Republic of China

[By title only.]

RETRIEVAL OF GRAIN-BOUNDARY DIFFUSION COEFFICIENTS USING THE INTEGRATED THERMAL HISTORY OF A CONTACT AUREOLE

JOESTEN, RAYMOND, Department of Geology and Geophysics, The University of Connecticut, Storrs, CT USA

Wollastonite reaction rims on chert nodules in marble from the Christmas Mts (Texas) contact aureole thicken from 4.5mm @ 102m from the gabbro to 7mm @ 80m, 30mm @ 49m and 53 to 79mm @ 2 to 13m. Polygonal matrix wollastonite grains coarsen from 0.011mm @ 102m to 0.053mm @ 46m and 0.2-0.3mm within 20m of the contact, while scattered wollastonite porphyroblasts appear @ 30m and coarsen to impingement with a diameter of 1.07mm @ 12m. Quartz in nodule cores coarsens from 0.0075mm @ 102m to 0.28mm @ 49m, 0.56mm @ 9.5m and 1.06mm @ 2m.

Kinetic models for normal grain growth (Joesten, 1983) and for layer thickening (Fisher, 1978) set a function of the square of the grain diameter or layer thickness equal to the product of a material constant and a temperature-time integral that includes the Arrhenius function for the diffusion coefficient. The time index for non-isothermal diffusion-controlled mineral growth is the temperature-time integral evaluated along T-t curves for the thermal history of the natural experiment. The thermal history of the aureole is obtained using a numerical model for a cylindrical intrusion, radius=823m, that matches maximum temperatures in the contact aureole of 600°, 940°, 1000°, and 1030°C @ 115, 23, 13 and 0m by convection for 700yr followed by crystallization and cooling. The log of the T-t integral varies linearly with distance from the gabbro, with a slope proportional to activation energy and an intercept proportional to the material constant.

A plot of the log of the square of the grain diameter of wollastonite and quartz against distance from gabbro yields temperature-dependent grain-boundary diffusion coefficients for oxygen in wollastonite and quartz (TABLE 1).

Grain diameter of impingement wollastonite varies linearly with the radius of spherical wollastonite nodules that ceased growth on comsumption of the quartz core, implying that coarsening coincided in time with wollastonite rim growth. Grain-boundary cross-section of the wollastonite aggregate decreased by 2 orders of magnitude during layer growth. Coupling of the kinetics of coarsening of impingement wollastonite with diffusion-controlled growth of wollastonite rims yields temperature-dependent grain-boundary diffusion coefficients for CaO, and SiO_2 in wollastonite (TABLE 1).

Because the value of the grain-boundary diffusion coefficient (D) and boundary width (δ) cannot be determined separately, they appear either as a product or ratio in TABLE 1. Diffusion coefficients derived from analysis of grain-coarsening and layer growth in the Christmas Mts contact aureole satisfy the diffusion-compensation relations for grain-boundary diffusion of oxygen and cations based on laboratory experiment.

TABLE 1

O, SiO_2	$D/\delta = 4.035x10^{-1}$ [m/s]	exp (-210/RT)	[kJ/mole]
O, $CaSiO_3$	$D/\delta = 9.333x10^{-4}$ [m/s]	exp (-180/RT)	[kJ/mole]
CaO, $CaSiO_3$	$\delta D = 8.457x10^{-9}$ [m^3/s]	exp (-245/RT)	[kJ/mole]
SiO_2, $CaSiO_3$	$\delta D = 2.014x10^{-10}$ [m^3/s]	exp (-245/RT)	[kJ/mole]

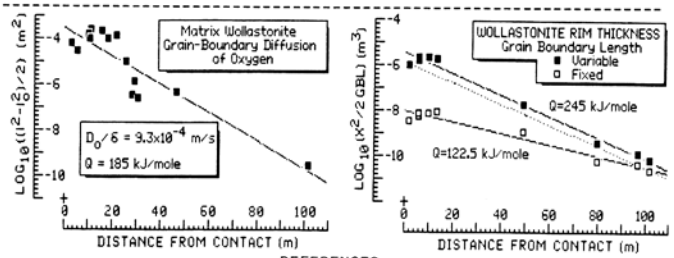

REFERENCES

Fisher, G.W., 1978, Rate laws in metamorphism: Geochim. Cosmochim. Acta, v.42, p.1035-1050.

Joesten, R., 1983, Grain growth and grain boundary diffusion in quartz from the Christmas Mountains (Texas) contact aureole: Am. J. Sci., v.283-A (Orville Vol.), p.233-254.

Joesten, R., 1985, A diffusion-compensation relation for normal grain growth and grain-boundary diffusion of oxygen in oxides: J. Am. Ceram. Soc., v.68, C62-C64.

MELTING IN QUARTZ-FELD ROCKS AT VARYING H_2O ACTIVITIES

JOHANNES, W., INSTITUT FÜR KRISTALLOGRAPHIE UND PETROGRAPHIE UNIVERSITÄT HANNOVER, WELFENGARTEN 1 3000 HANNOVER 1, FRG

There are reliable data on the beginning of melting temperatures and compositions of partial melts in the alkali-feldspar granite system Qz-Ab-Or at H_2O saturation. For a more pronounced interpretation of the formation of migmatites and S-type granites systematic information are needed concerning a) the influence of plagioclase compositions and of reduced water pressures on beginning of melting temperatures and b) the development of H_2O-undersaturated partial melts at hypersolidus conditions.

The increase of solidus temperatures is shown to be small with increasing An content of plagioclase in the tonalite system Qz-Ab-An-H_2O and very small in the granite system Qz-Or-Ab-An-H_2O. Especially in granites having Ab-rich plagioclases the beginning of melting temperatures are (at the same water pressure) almost identical with those of the alkali-feldspar granites. The influence of increasing An content in plagioclase upon increase of solidus temperatures has been overestimated in the past.

The solidus temperatures of tonalites are as low as 700° C (at $P_{H2O} \geq 4$ kbars). This is less than 50°C above the solidus temperatures of granites suggesting that tonalites and tonalite migmatites might very well be of anatectic origin.

Calculated as well as experimentally determined solidus temperatures are shown for various pressures and water activities. The data demonstrate that melts produced at low H_2O activities ($a_{H2O} < 0.5$) can be intrusive and need not to be "overheated".

If limited amounts of free water are available in rocks of granitic composition during high-grade metamorphism melting begins at water saturated solidus temperatures and continuous with formation of water-undersaturated melts. If magmas containing H_2O-undersaturared melts move upwards isothermally, the amount of melt is increasing and crystallization starts at relatively low pressures. This mechanism explains the intrusion of high-level granitic plutons from deeper parts of the continental crust.

STRUCTURAL SYSTEMATICS OF TETRAHEDRITE-SERIES MINERALS

JOHNSON, N.E., CRAIG, J.R., & RIMSTIDT, J.D. Department of Geological Sciences, Virginia Polytechnic Institute and State University, Blacksburg, VA 24061 USA

Tetrahedrite-series minerals are the most common of sulfosalt minerals, occurring in a great many ore deposits which formed under widely varying conditions. Its ability to tolerate a large range of substitutions, both in type and amount, has led some to describe it as a "sulfide amphibole" (Sack & Loucks (1985)). As in the case of amphiboles, a sound knowledge of the structure of tetrahedrite and how this structure varies with composition is of prime importance in understanding how and why it occurs with such great diversity. The structure of tetrahedrite was originally solved by Matchatschki (1928) who described it as a derivative of the sphalerite structure. More recent research (Koch & Hellner (1981), Nyman & Hyde (1981)) has related it to the sodalite structure. The second approach, using a geometric analysis of the framework similar to that done for sodalite, (Depmeier (1984)), allows for the explanation of several observed compositional peculiarities in tetrahedrite-series minerals.

The structure of tetrahedrite is viewed as a three-dimensional framework of corner connected $M(1)S_4$ tetrahedra (where M(1)= Cu, Fe, Zn, Cd, Hg) forming a series of "cages". These cages are filled with $SM(2)_6$ octahedra (where M(2)= Cu, Ag, □) which, when connected to the framework sulfur atoms, produce a tetrahedrally truncated tetrahedron or Laves polyhedron (Belov & Pobedimskaya (1969)). The truncated corners are capped with XS_3 pyramids (where X= Sb, As, Bi, Te). Lone pairs on the X cation extend away from the pyramid and into adjacent cages. Rotations of the framework tetrahedra about their $\bar{4}$ axes correlate strongly with tetragonal distortions of the tetrahedra, and with the M(2) and X cations, indicating that analogous to sodalite, the tetrahedrite framework expands or contracts depending on the size of the cage filling polyhedron.

The well-documented antipathetic relationship between silver and arsenic appears to result from the opposite rotational effects that these two elements impose on the framework, a view in agreement with the findings of Johnson & Burnham (1985). The limit of two atoms per formula unit of iron, zinc, cadmium and mercury (Charlat & Lévy (1974), Johnson et al. (1986)) substituting into the six tetrahedral sites can be explained by the ordering of these cations into the framework so that non-CuS_4 tetrahedra do not share corners, which results in an "iron-avoidance principle" analogous to the aluminum avoidance in sodalite.

Belov, N.V. & Pobedimskaya, E.V. (1969): Covelline (klockmanite), chalcocite (acanthite, stromeyerite, bornite), faherz. Sov. Phys. Cryst. 13, 843-847.

POWDER DIFFRACTION ANALYSIS ON A PC

JOHNSON, Q., Materials Data, Inc., P.O. Box 791, Livermore, CA 94550, USA

MICRO-PEAK and MICRO-ID, programs for x-ray powder diffraction analysis, run on IBM-PC and compatible microcomputers. MICRO-PEAK is designed to process digital diffraction data acquired by manual or automation systems and to prepare, among other things, graphical plots of spectra and a listing of diffraction peaks and intensities for use by MICRO-ID. MICRO-ID is an extremely fast and effective search/match system which identifies the diffraction pattern by comparison to standard patterns.

MICRO-PEAK operates on a raw diffraction spectra consisting of starting angle and step size plus raw intensities. It provides the user the ability to plot original raw data and also provides interactive commands to allow modification and plotting of modified data. Plots are displayable as both raw data and after a moving-average smoothing. Optional background subtraction and alpha-2 stripping are provided. Peak finding can be conducted in an automatic and/or manual mode. Additional peaks found manually can be entered into a final list of peaks to be used by MICRO-ID. A "zoom" command allows magnified image processing. Split-screen and overlay displays are useful for comparison of different patterns. Addition, subtraction or comparison with standard patterns are possible. A typical split-screen pattern which shows a portion of an actual diffractometer scan of Al2O3 compared with a simulated scan using MICRO-POWD is shown in Fig. 1.

MICRO-ID is a search/match program which can be used as a stand-alone program or as a companion to MICRO-PEAK. This program uses subfiles of the JCPDS database to provide rapid phase identification from powder diffraction data. For example, using the MINERALS Subfile of the JCPDS database (consisting of over 3200 standard patterns), a typical search runs well under one minute and often less than ten seconds. Results are generally equal to or better than those obtained on main-frame search/match programs. Comparison of the unknown pattern to matched standards is possible.

Both programs run best on a computer equipped with at least 512K of memory and a hard disk. A graphics card is required for MICRO-PEAK and a printer is recommended for both programs.

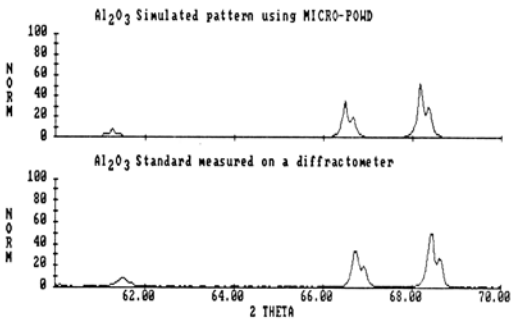

Fig. 1. Split-screen using "zoom" shows how well simulated pattern matches actual measured pattern. Note slight two theta difference due to error in measured pattern.

STRUCTURAL SYSTEMATICS OF TETRAHEDRITE-SERIES MINERALS
JOHNSON, N.E., CRAIG, J.R. & RIMSTIDT, J.D.

Charlat, M. & Lévy, C. (1974): Substitutions multiples dans la série tennantite-tétraédrite. Bull. soc. franç. Minéral. Crist. 97, 241-250.

Depmeier, W. (1984): Tetragonal tetrahedral distortions in cubic sodalite frameworks. Acta Cryst. B40, 185-191.

Johnson, M.L. & Burnham, C.W. (1985): Crystal structure refinement of an arsenic-bearing argentian tetrahedrite. Amer. Mineral. 68, 220-226.

Johnson, N.E., Craig, J.R. & Rimstidt, J.D. (1986): Systematics of compositional variations in tetrahedrite. Can. Mineral. (in press).

Koch, E. & Hellner, E. (1981): The frameworks of sodalite-like structures and of tetrahedrite-like structures. Zeit. Krist. 154, 95-114.

Matchatschki, F. (1928): Formel und Kristallstruktur des Tetraedrites. Norsk Geol. Tidsskr. 10, 23-32.

Nyman, H. & Hyde, B.G. (1981): The related structures of α-Mn, sodalite, Sb_2Tl_7, etc. Acta Cryst. A37, 11-17.

Sack, R.O. & Loucks, R.R. (1985): Thermodynamic properties of tetrahedrite-tennantites: constraints on the interdependence of the Ag⇔Cu, Fe⇔Zn, Cu⇔Fe and As⇔Sb exchange reactions. Amer. Mineral. 70, 1270-1289.

(This work supported by a Mining and Minerals Resources Research grant to VPI & SU)

MINERAL RECORDERS OF PEGMATITE INTERNAL EVOLUTION: BOB INGERSOLL NO. 1 DIKE, BLACK HILLS, SOUTH DAKOTA

JOLLIFF, B.L., PAPIKE, J.J., SHEARER, C.K., SPILDE, M., Inst. for the Study of Mineral Deposits, S.D. Sch. of Mines & Tech., Rapid City, SD 57701, USA

The Bob Ingersoll No. 1 Dike is an internally zoned, rare-element pegmatite enriched in Li, B, Be, Nb, Ta, Sn, and F, located in the Precambrian core of the southern Black Hills, 2 km north of the Harney Peak Granite near Keystone, South Dakota. The pegmatite consists of six zones: (1) a thin, fine-grained border zone of quartz-albite-muscovite-tourmaline, (2) a continuous wall zone 1 to 4 m thick, of cleavelandite-quartz-muscovite; (3) a perthite-quartz-cleavelandite 1st intermediate zone, forming a thick hood in the upper part of the pegmatite; (4) a quartz-cleavelandite-amblygonite-montebrasite 2nd intermediate zone, irregularly distributed in upper parts of the pegmatite; (5) a 3rd intermediate zone of dominantly quartz-cleavelandite, forming a discontinuous shell around the core, thicker in lower parts of the pegmatite; and (6) a core of quartz-cleavelandite-lepidolite. The pegmatite is an inclined and flattened funnel-shaped dike, approximately 25 x 33 m in plan near the top and at least 80 m deep.

The main objective of this work is to examine major and accessory minerals for trends of compositional variation that indicate the sequence of crystallization and record the progressive differentiation of the pegmatite that led to extreme rare-element enrichments. Minerals specifically investigated include tourmaline, muscovite, lepidolite, apatite, Nb-Ta-Sn oxides, and feldspars.

Examples of trends of compositional variation from the border of the pegmatite to its core are compared for several of the minerals in the figure below. The particular differentiation indices are selected as examples to show general trends of progressive differentiation. Variations, particularly between the wall zone and the core, such as increasing Li+Al(Y-site) in tourmaline, decreasing Rb/Cs in mica, and increasing Ta/(Ta+Nb) in Nb-Ta oxides reflect the general compositional evolution of the pegmatite during crystallization. These trends are in accord with previous work on other pegmatites[1,2]. The spread of data across intermediate zones suggests overlap in timing of crystallization, and may reflect differentiation caused by variable partitioning between coexisting silicate melt and exsolving supercritical aqueous fluid. Border zone values may reflect contamination and rapid, disequilibrium crystallization. The large compositional ranges of wall zone minerals, e.g. tourmaline and apatite, reflect variations that correlate with position relative to the outer contact of the pegmatite. Perthites of the 1st intermediate zone show a range of variation in rare-alkali enrichment (Rb/Cs from ~35 to 1.0) that correlates to position within the zone and suggests crystallization from the outer contacts inward and from the top of the dike downward. Compositional variations that correlate to vertical position in the pegmatite suggest differentiation related to the upward movement of aqueous fluid through silicate melt. Elevated contents of B, F, P and Li probably extended silicate melt-aqueous fluid miscibility beyond values of typical igneous rocks[3]. Crystallization of minerals that removed these elements from the melt in part governed the timing of aqueous fluid exsolution, and through the consequential effects on melt structure, contributed to the deposition of rare-element enriched mineral assemblages.

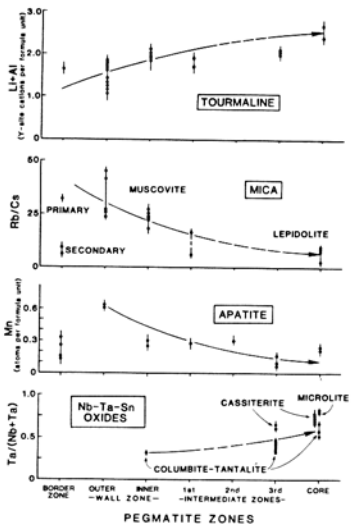

References.
(1) Černý, P., et al., 1985, Can. Min., 23, 381-421. (2) Foord, E.E., 1976, Ph.D. Thesis, Stanford University, 326 p. (3) London, D., 1986, Am. Min., 71, in press.

PHASE RELATIONS IN THE UNDERSATURATED PART OF THE SYSTEM NEPHELINE-KALSILITE-ANORTHITE-QUARTZ AT P_{H_2O} = 5 KB

JONES, R.H., Dept. of Geology, Manchester University, Manchester, M13 9PL, U.K.; ZENG, R.S., Institute of Geology, Academia Sinica, Beijing, China; MACKENZIE, W.S., Dept. of Geology, Manchester University, Manchester M13 9PL, U.K.

An experimental study of the phase relations in the silica undersaturated part of the residua system has been carried out both without anorthite and with up to 10% of anorthite present. The field of leucite is considerably reduced with increase in water pressure and disappears at about P_{H_2O} = 8 kb, both in the anorthite-bearing system and the anorthite-free system: leucite and kalsilite cannot accommodate any significant amount of calcium in their structures under the conditions we have used.

In the anorthite-free system there is a eutectic between kalsilite, nepheline and K-feldspar at $Ne_{25}Ks_{51}Q_{24}$ and in the 10% plane of the anorthite-bearing system there is a piercing point on the boundary separating the phase volumes of plagioclase, kalsilite and nepheline which projects on to the plane Ne-Ks-Q at a slightly more nepheline-rich composition than $Ne_{25}Ks_{51}Q_{24}$.

Plots of analyses of Cenozoic volcanic rocks containing normative leucite, from the Chayes' RKNFSYS, show an unexpectedly high concentration near $Ne_{23}Ks_{55}Q_{22}$. Low pressure phase relations in the residua system cannot explain this concentration of liquid compositions but at pressures of water of 5 kb or more fractional crystallization is likely to produce liquids in this region of the diagram from the evidence provided by the experimental systems.

NEUTRON DIFFRACTION STUDIES OF HYDROGEN BONDING AND CATION ORDERING IN PHYLLOSILICATES

JOSWIG, W., FUESS, H., Institut für Kristallographie und Mineralogie der Universität Frankfurt, F.R. Germany
TAKEUCHI, Y., Mineralogical Institute, University of Tokyo, Hongo, Tokyo 113, Japan

Neutron diffraction experiments were performed on single crystals of micas, brittle micas and chlorite minerals in order to elucidate structural details in phyllosilicates.

The special advantage of neutron diffraction over X-rays is the location of hydrogen positions and the distribution of neighbouring elements.

In the chlorite mineral penninite the hydrogen bonding scheme between the talc sheet and the brucite sheet was established with high precision. The three hydrogen bonds are of almost equal strength (O····O : 2.915, 2.916, 2.906Å) and are slightly bent. They may be classified as medium. A partial cation order is observed in the brucite sheet indicated by the refined neutron scattering lengths and bond distances. No ordering is found for octahedral and tetrahedral cations of the talc sheet (Joswig et al., 1980).

The neutron diffraction refinement of clintonite proved the incorporation of ferric iron in the tetrahedral site despite an excess of aluminium. This result is supported by direct evidence from a Mössbauer study (Joswig et al., 1986).

General conclusions concerning the orientation of the inner OH-dipole can be drawn from the result of neutron diffraction studies. It was demonstrated that the angle between the OH-dipole and the (001) plane is a direct function of the occupation of the octahedral sites. This angle amounts to about 12° for a vacant M(1) position (muscovite, margarite [dioctahedral part]) whereas a value of about 90° is observed for M(1), M(2) and M(3) sites completely filled with identical or similar cations (phlogopite, clintonite, penninite). Occupation by distinctly different cations (e.g. Li^+) will produce intermediate values (margarite [trioctahedral part]). An X-ray investigation of dickite revealed an OH-dipole parallel to the (001) plane (within the accuracy of X-ray data). This result is explained by the absence of repulsion from neighbouring hydrogen which is only present in a 2 : 1 layer structure (Joswig and Drits, 1986).

Joswig W, Fuess H, Rothbauer R, Takeuchi Y, Mason S (1980) A neutron diffraction study of a one-layer triclinic chlorite (penninite). Amer. Mineral., 65, 349 - 352

Joswig W, Amthauer G, Takeuchi Y. A neutron diffraction and Mössbauer spectroscopic study of clintonite (xanthophyllite) Amer. Mineral., in press

Joswig W, Drits V A (1986) The orientation of the hydroxyl groups in dickite by X-ray diffraction. N. Jahrb. f. Miner. 19 - 22.

CHEMICAL COMPUTATIONS

KAMPF, A. R., Mineralogy Section, Natural History Museum of Los Angeles County, 900 Exposition Blvd., Los Angeles, CA 90007, USA

The calculation of a mineral's chemical formula, density, or Gladstone-Dale chemical refractive energy, while mathematically simple, can be quite tedious if conducted manually. This program accepts chemical analytical data, either as oxide or element weight percentages. The amount of each element in the formula can be computed based upon the number of atoms of any single element or combination of elements. From this calculated formula, and inputed values for the cell constants and the number of formula units in the unit cell, the density can be calculated. For chemical data input as oxides, the program calculates the Gladstone-Dale chemical refractive energy and can utilize the Gladstone-Dale relationship to predict the density or average refractive index, or to compute the compatibility index. This program is written in IBM Advanced BASIC.

• THE MOSSBAUER STUDY OF PYROPE-ALMANDITE SERIES AND ITS GEOLOGICAL SIGNIFICANCE

KAN Xuemin, ZHANG Enlin, and LI Yirong, Institue of Geochemistry, Academia Sinica, Guiyang, Guizhou Province, People's Republic of China

The Mossbauer spectra of the pyrope-almandite series are characterized by a single doublet from ferrous ions at the dodecahedral sites, and the dependences of their Mossbauer parameters on the temperatures and on the chemical compositions were reported (1,2). Particularly, it was pointed out that the ferrous doublets of some pyropes show asymmetric peak heights (2,3). This paper is devoted to the studying of the dependences of the asymmetries on the geological environments in which the samples were found.

Sixteen samples were studied at room temperature with a constant acceleration Mossbauer spectrometer. The results show that the isomer shifts and quadrupole splittings of ferrous iron in the pyrope-almandite series are very stable and hardly dependent on the changes in chemical compositions from pyrope to almandite. Therefore, it is probably unreasonable to attribute the asymmetry of the ferrous doublet to the next nearest neighbor effect.

In opposition to the stable isomer shift and quadrupole splitting, the doublet asymmetries vary with chemical compositions and with geological environments. The typical spectra with different asymmetries are shown in Figure 1. The line widths of high velocity peaks are always slightly narrower than that of the low velocity and have more intensive heights. If Y_π and Y_σ represents the peak height of the low and high velocity, respectively, the asymmetry of the ferrous doublet, AS, is defined as:

$$AS = 2\,\frac{Y_\sigma - Y_\pi}{Y_\sigma + Y_\pi}$$

Although there is a tendency for some samples with high amounts of Cr and low amounts of Fe to have higher AS values, no regular relations between AS and the chemical compositions were found. On the other hand, it was found that the AS values of the samples we studied can be divided into three ranges that are respectively related to the different geological environments as in the following:
AS = (23±2)%, for pyropes from kimberlite related to the production of diamond;
AS = (16±1)%, for pyropes from the mantle-derived xenoliths;
AS = (6±3)%, for almandites from metamorphic rocks.

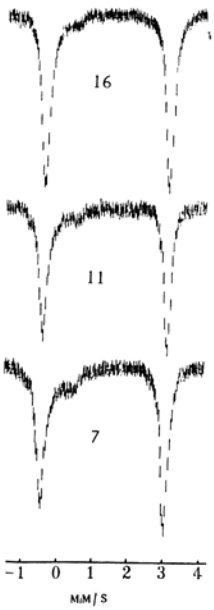

Figure 1. Mossbauer spectra of pyrope and almandite. No. 7, pyrope from kimberlite; No. 11, pyrope from the mantle-derived xenolith; No. 16, almandite from metamorphic rock.

REFERENCES: [1] Lyubutin, I.S., Belyaev, L.M. and Dodokin, A.P. (1970) Kristallografiya, 15, 1249 (in Russian). [2] Amthauer, G., Annersten, H. and Hafner, S.S. (1976) Z.Kristal., 143, 14. [3] Ying Yupu, Li Zhe and Hu Jiarui (1982) Scientia Sinica (Ser. B), XXV, 9, 989.

MUMMEITE, A NEW MEMBER OF THE PAVONITE HOMOLOGOUS SERIES, AND THE ASSOCIATED MINERALS FROM THE ALASKA MINE, COLORADO.

KARUP-MØLLER,S., Institute of Mineral Industry, Technical University of Denmark, 2800 Lyngby, Denmark.
MAKOVICKY,E., Institute of Mineralogy, University of Copenhagen, 1350 Copenhagen, Denmark.

New ore material from the Alaska mine and the adjacent Acapulco adit yielded an Ag-Bi rich sulfosalt assemblage associated with chalcopyrite, pyrite, sphalerite, galena, tetrahedrite, quartz and barites. Mummeite is columnar, present in random orientation, associated with chalcopyrite and small amounts of ourayite or heyrovskyite and patches of decomposed schapbachite. In other samples from the deposit the following minerals have been identified: cosalite, ourayite, pavonite, aikinite and neyite. The original high-temperature phase exsolved on cooling into an intimate intergrowth of thin, alternating lamellae of two chemically close phases, mummeite and cuproplumbian mummeite.

The two phases in subparallel intergrowth are both monoclinic, space group C2/m or Cm and unit cell parameters respectively equal to a 13.47(1), b 4.06(1), c 21.63(1)Å, β 92.9(1)° and a 13.48(1), b 4.06(1), c 21.72(1)Å, β 93.9(1)°. They represent the 8'th member of the pavonite homologous series and differ from each other by the degree of Cu-for-Ag, 3Cu-for-1Bi and 2Pb-for-(Ag+Bi) substitution, the ideal unsubstituted formula being $Ag_{3.5}Bi_{7.5}S_{13}$ (Z=2), i.e. $M_{11}S_{13}$. In a typical example, the overall composition of mummeite before exsolution was $Ag_{2.84}Cu_{1.09}Pb_{1.39}Bi_{6.37}S_{13}$ whereas that for the mummeite exsolution lamellae is $Ag_{3.03}Cu_{0.63}Pb_{1.10}Bi_{6.50}S_{13}$ and that for cuproplumbian mummeite $Ag_{2.47}Cu_{1.83}Pb_{1.68}Bi_{6.01}S_{13}$. Up to 15 at.% of ideal (Ag+Bi) contents and up to 6.6 at.% of ideal Bi were found substituted respectively by Pb and Cu in cuproplumbian mummeite with the metal to sulphur ratio reaching $M_{11.99}S_{13}$.

The find of mummeite and of another presently studied pavonite homologue (N=9) in the material from the Acapulco adit as well as the recently published or announced data on synthetic and natural phases (Dr. W.G.Mumme) make the pavonite homologous series the most complete sulphosalt series with N assuming all values form 2 to 9.

The second occurrence of the rare mineral neyite was found in the material from the Alaska mine where it is associated with aikinite, Ag-Bi containing galena, sphalerite and chalcopyrite. Space group is C2/m (or Cm, C2), a 37.55(1), b 4.07(1), c 41.83(1)Å, β 96.3(1)°. From microprobe analyses the empirical atomic ratio can be expressed as $Ag_{6.5}Cu_{8.8}Pb_{23.2}Bi_{31.5}S_{80}$.

Zoning of Calcic amphiboles from quartz diorite-monzonite in magnetite series granitoid complex in the Daito-Yokota area in Sanin Belt, southwest Japan.

Kazuya Kawakatsu and Yoshiaki Yamaguchi
Department of Geology, Shimane University, Matsue 690, Japan

Small masses of quartz diorite-monzonite are the earlist intrusion of the Daito-Yokota granitoid complex of late Cretaceous-Paleogene age, in the Sanin Belt, southwest Japan. The masses have been intruded by granodiorite-granite the complex. The solidification of the compex is believed to have been taken place at a shallow level under a condition of high oxygen fugacity. The complex is a representative of those of megnetite series granitoids and magnetite has been mined from the weathered outcrops of the quartz diorite-monzonite (Ishihara, 1977; Czamanske et al., 1981). Back-scattered electron observation and microprobe analysis were made on selected specimens from the quartz diorite-monzonite, in which mafic silicate phase comprises dominantly calcic amphibole.

Amphibole developes interstitially in strongly euhedral form, together with quartz, alkali feldspar and magnetite, among zoned euhedral plagioclese. In general, magnetite occurs texturally associated with amphibole on the rim. Amphibole is strongly zoned from magnesio-hornblende through actinolitic-hornblende to actinolite toward rim. Compositional variation of amphibole shows Fe decrease and Mg increase toward rim. Substitution of Al^{IV} for Si is mainly compensated by substitution of Al^{IV}, Fe^{3+} and Ti in octahedral sites. There is a characteristically small Al^{VI} content and Fe^{3+} is the dominant octahedral trivalent cation. This characteristically small Al^{VI} content and Fe^{3+} is the dominant octahedral trivalent cation. This characteristic feature of the compositional variation is responsible to a condition of low pressure and high oxygen fugacity, as explained in the Finnmarka complex (Czamanske and Wones, 1973) and some porphyry copper-generating intrusions (Mason,1978; Chivas,1981).

Amphibole crystal is usually divided into three different domains along zoning; 1) Brownish core of magnesio-hornblende composition, 2) Pale greenish region of composition changing toward actinolitic-hornblende, 3) Oscillatory-zoned region, in which oscillatory-zoning develops outward largely along c-axis of amphibole. The composition of the oscillatory-zoned region is usually ranging from actinolitic-hornblende to actinolite, but this region often contains zones of magnesio-hornblende.

Composition of two feldspars associated with the oscillatory-zoned region indicates low equilibration temperature for the minimum solidus temperature. Amphibole in the oscillatory-zoned region may have been produced under subsolidus condition in the presence of a fluid phase exsolved in the latest magmatic stage. Most of magnetite is considered to have crystallized in this stage. No systematic gap in composition between hornblende and actinolite is found in this region . This may be due to the fast growth of the oscillatory-zoned region.

Reference

Chivas,A.R. (1981) Contrib, Mineral. Petrol., 78,389-403.
Czamanske,G.K. and Wones,D.R. (1973) J.Petrol., 14,349-380.
Czamanske,G.K. et al. (1981) J.Geophys.Res., 86,10431-10469.
Ishihara,S. (1977) Min. Geol., 27,293-305.
Mason,D.R. (1978) Econ.geol., 73,878-890.

MINERALOGY OF VOLCANIC AND PLUTONIC ROCKS AS A GUIDE TO PROCESSES IN THE FORMATION OF THE ALEUTIAN CRUST

KAY, S. MAHLBURG, ROMICK, J., KAY, R.W., Dept. Geol. Sciences, Cornell University, Ithaca, NY 14853

The mineralogy of arc volcanic and plutonic rocks in the oceanic part of the Aleutian arc gives insight into the processes occurring in the construction and modification of arc crust by providing information on the conditions under which magmas crystallize, and the type and extent of mixing at different crustal levels.

The depth of crystallization and the amount of mixing of less-crystallized and more-crystallized magmas can explain a spectrum of andesitic tholeiitic to calc-alkaline volcanic rocks (Kay and Kay, 1985). Evidence for mixing in the extreme calc- alkaline lavas consists of disequilibrium mafic assemblages consisting of high-Al amphibole, Cr poor and rich clinopyroxene and Ni poor and rich olivine which show both reverse and normal zoning. In contrast, simple mafic assemblages dominated by clinopyroxene and olivine showing normal zoning suggest that mixing is less important in the tholeiitic lavas. Mixing is of intermediate importance in transitional calc-alkaline rocks which have low-Al amphibole, clinopyroxene and orthopyroxene showing limited reversed zoning, and in transitional tholeiitic rocks which have normally zoned orthopyroxene and clinopyroxene and groundmass pigeonite. The occurrence of amphibole as a phenocryst phase indicates that both mixing and crystallization occurs at greater depth in the calc-alkaline series.

Compositions of feldspars and opaques in these lavas support conclusions drawn from the mafic mineralogy. Feldspars in the tholeiitic lavas are generally normally zoned and their AN contents decrease (AN62-38) with whole rock SiO_2 contents (51-64%). In contrast, plagioclase in extreme calc-alkaline dacites shows a wide compositional variation (AN38-88) and irregular zoning patterns. Plagioclases in the transitional calc-alkaline volcanic rocks are also complexly zoned but show a smaller range of AN contents than the extreme calc-alkaline rocks.

The mineralogy of the calc-alkaline ashes are similar to the calc-alkaline dacites suggesting that they represent the most siliceous mixing end member in the calc-alkaline series. All of these ashes contain amphibole. One group contains low-Al amphibole (6-8% Al_2O_3), magnetite and plagioclase with < AN60. A second group has high-Al amphibole, clinopyroxene, orthopyroxene, magnetite and plagioclase with compositions as high as AN92. A third group has both assemblages suggesting that mixing has occurred just prior to eruption.

The chemistry of the shallow-level calc-alkaline plutons (i.e., Hidden Bay on Adak Island, Citron 1980) is similar to that of the volcanoes but their minerals crystallized at lower temperature. Clinopyroxene, orthopyroxene, amphibole and biotite initially increase in Fe, but become more Mg-rich with increasing whole rock FeO/MgO ratio. This reversal coupled with low $\delta^{18}O$ (Perfit et al. 1979, Citron 1980) indicates that final crystallization conditions in the pluton were highly oxidizing and water-rich. Exsolved titanomagnetite is the only oxide phase. Relative to the volcanics, the pyroxenes are characterized by low Al, Na and Ti. Most amphibole replaces pyroxene and has lower Al contents (<5.5% Al_2O_3) than that in the volcanics. Pargasitic amphibole occurs in a border zone diorite. Biotite occurs in all plutonic units and often replaces the other mafic phases. Plagioclase AN contents exceed AN 60 in only two analyzed gabbros. Evidence for mixing in the plutons is largely obliterated by subsolidus equilibration.

THE DISTRIBUTION OF NON-BRIDGING OXYGENS AND THE STRUCTURE OF SILICATE MELTS*

KEEFER, K. D., Sandia National Laboratories, Albuquerque, NM 87185, USA

Many attempts have been made to describe the structure of silicate melts and its influence on the properties of the melt, and most have met with limited success. Flory-Huggins theory has been applied but is useless for the highly siliceous melts of interest to geologists because of its failure to account for ring closures. Various thermodynamic approaches use the effective degree of polymerization as a parameter, but in most cases, there is no evidence for the O^{2-} these theories usually predict.

The structure of silicate melts can be described by the distribution of non-bridging oxygens among the silicate tetrahedra in the melt; that is, the fraction of tetrahedra having 0, 1, 2, etc. non-bridging oxygens. This distribution changes with the field strength of the network modifier cation which has contributed the non-bridging oxygen. This effect is readily seen in crystalline silicates in which low field strength cations (such as potassium) form silicates with few non-bridging oxygens per tetrahedron whereas high field strength cations (such as lithium) form silicates with highly unpolymerized tetrahedra.

This species distribution can change while preserving the total number of non-bridging oxygens; thus melts having the same average degree of polymerization can have very different structures and properties. If, at a constant degree of polymerization, non-bridging oxygens tend to associate on the same tetrahedron, large regions having few non-bridging oxygens will be formed. Such systems, then, will tend to phase separate, as tetrahedra with widely differing number of non-bridging oxygen don't mix readily.

There have been major advances in the past few years in the theory of disordered systems and of critical phenomena. Fractal geometry, for example, has provided a quantitative description of certain random structures. Percolation theory has shown that nearest neighbor interaction can yield long range (thousands of site) correlations. These theories are readily applied to systems such as silicate melts in which connectivity is well defined and only local interactions exist. Although, in many cases, analytic results are unobtainable, computer simulation may be used to model processes such as percolation. Since long range forces are not considered, very simple interaction potentials suffice which makes it practical to simulate very large systems of particles.

Thus, the description of a silicate melt in terms of the distribution of non-bridging oxygens is a very powerful tool. The general trends of this distribution are easily deduced from crystal chemistry. Such a distribution can be measured experimentally using techniques such as NMR and Raman spectroscopies and can predict long range correlation in disordered systems. Theories exist which can predict both thermodynamic properties such as phase separation and activity curves when such a distribution is known.

*This work performed at Sandia National Laboratories supported by the U.S. Department of Energy under contract number DE-AC04-76DP00789.

STRUCTURAL CLASSIFICATION OF OXYGEN CONTAINING MINERALS. PHOSPHATES AND ARSENATES

KELLER, P., Institut für Mineralogie und Kristallchemie, Pfaffenwaldring 55, 7000 Stuttgart-80, F. R. G.

The proposed structural classification is developed on the basis of the model of closest packing of spheres, where the coordination of anions is especially considered (KELLER, 1982;1985). The most important features of the new classification scheme are:

(i) The scheme is valid for all crystal structures in which cations and anions are distinguishable. It is not restricted to any particular coordination polyhedra or to special linkages of coordination polyhedra, e.g. dense-packed structure types.

(ii) The complete classification scheme is theoretically determinable.

(iii) The required structural parameters are easily determined for most classification stages. If complicated topological parameters have to be used, they are so strongly restricted by the foregoing classification procedure that it is a solveable task.

(iv) The result of classification procedure are consequent sequences of related crystal structures.

(v) The classification is useful for complete crystal structures, but also for restricted parts of structures like the arrangements of coordination polyhedra of cations or like the "fundamental building blocks".

The basic relation of the proposed classification is

$$D - CF + LF + OF = 0 \quad ,$$

where D = dimensionality, CF = coordination factor, LF = linking factor, and OF = orientation factor. The value of dimensionality is determined by the extent of arrangements of linked coordination polyhedra in crystal structures. It is D = 3, D = 2 and D = 1 for unlimited arrangements in three, two and one dimension, respectively. For insular structures is D = 0. The value of CF is determined by the mean coordination number of cations (CN) and the ligand-cation-relation of the chemical formula (ß). It is CF = CN - ß. The value of LF depends on the coordinationnumbers of ligands. The orientation factor includes data about the orientation of linking elements.

According to the structural importance of the given parameters, crystal structures are subsequently divided into "classes", (divisions"+"subdivisions"), and ("groups"+"subgroups") by the values of D, CF and LF, respectively. Geometrically isomorphous structures of each "subgroup" can be divided into different "types" by topological parameters which are included in OF and partly in LF. Finally, isostructural minerals should be combined in "families".

The crystal structures of phosphates and arsenates are among the most exciting in the mineral kingdom. Coordination polyhedra of cations with different coordination numbers and numerous ligand combinations (O^{2-} and OH^- ions, H_2O) may be linked contemporaneously by vertices, edges and faces to complicated arrangements, often stabilized by a complex system of hydrogen bonds. A classification scheme of phosphates and arsenates will be presented in detail, to demonstrate the efficiency of the proposed classification.

KELLER, P. (1982) Kristallchemische Größen zur Klassifikation der oxidischen Minerale. Fortschritte Miner. 60, 27 - 29

KELLER, P. (1985) Structural classification of oxygen containing minerals. Ninth European Crystallographic Meeting, Torino. Abstracts of papers, 440

DIVERSITY OF ALKALINE ROCK MINERALS AND THE PROBLEM OF QUANTITY OF MINERAL SPECIES

KHOMYAKOV, A.P. Laboratory of Mineralogy, Institute of Mineralogy, Geochemistry and Crystal Chemistry of Rare Elements, Moscow, 113127, USSR.

The problem of limited quantity of mineral species in the Earth's crust against the background of an astronomically large number of theoretically possible combinations of chemical elements has been actively discussed by A.E. Fersman and his followers. It is again attracting attention nowadays in view of the sharply accelerated pace of discoveries of new minerals. For example, 12, 22 and 54 new minerals were discovered in the Khibina and Lovozero alkaline massifs (Kola peninsula) in the periods of 1890-1941, 1950-1969 and 1970-1985 respectively.

Agpaitic nepheline syenites composing only a minute part of igneous rocks as a whole exceed the rocks of any other formation in diversity of minerals (over 500 species). This is due to a number of factors, two of which are determinant: 1) extremely high alkalinity of agpaitic magmas causing simultaneous concetration in those of approximately half of the elements of the periodic table; 2) extraodinary variety of cationic and anionic motives and their combinations in crystal structures of alkaline minerals.

Alongside with petrogenic O, Si, Al, Na, K, Ca, Fe, Mg, Mn, Ti about 30 other elements (Li, Be, Sr, Ba, B, Ce, Y, Zr, Nb, P, Th, U, Ag, Tl, Cu, Zn, Sn, Pb, As, Sb, Mo, W, Co, Ni, F, S, Cl, C, H) form their own minerals in Khibina, Lovozero and similar Ilimaussaq intrusion (S. Greenland), a considerable number of minerals being fairly complex in composition. Proceed from calculation of the practically possible combinations of the above elements the number of expected minerals in alkaline rocks is approximately estimated as $n \cdot 10^4 - n \cdot 10^5$ species.

Plenty of independent structure types in vast families of Ti-, Nb-, Zr- and Be-silicates with common type formula $Na_xM_ySi_pO_q$ may serve as an illustration of diversity of alkaline minerals crystal structures. Atoms of Na within the structure of these compounds have a wide range of coordination numbers (4-9) and corresponding polyhedra. The Na-O polyhedra are capable of joining each other by the tops, ribs, faces forming diverse structural motives including chains, columns, layers, nets (each of several topologically different variants). A set of M-O and Si-O fragments is still more complex and diverse in the structures. They occur as single and paired octahedra and tetrahedra or form diverse rings, chains, bands, layers and frameworks. The combinations of Na-, M- and Si-O motives are not less numerous than the motives are diverse, variety of MSiO-combinations increasing sharply with polymerization degree of M-O and Si-O fragments.

Available data show that the number of various cationic and anionic motives and their combinations in the structures of all main classes of minerals is quite comparable to the number of elements in the periodic system. This permits to advance a hypothesis of the absence of a natural limit to the quantity of mineral species, the number of which in the Earth's crust can be evaluated to be at least 1 or 2 orders higher than the number of currently known minerals (about 3000). One can forecast surely further considerable expansion of the System of minerals owing at least to Na- and K-representatives.

FIND OF THE TRUE Mn^{2+} ANALOGUE OF RANCIEITE

KIM, Soo Jin, Dept. of Geological Sciences, Seoul National University, Seoul 151, Korea

Rancieite and birnessite problem is one of the controversial subjects. Although Chukhrov et al. (1979) and Perseil and Giovanoli (1979) insist that rancieite and birnessite are identical, my previous (1979) and this work show that the manganese oxide minerals of formula $R^{2+}_{2-2x}Mn^{4+}_{5+x}O_{11}(OH)_2.nH_2O$ fall into two families : the rancieite family have n approximately 3, the birnessite family have n 1.5 or less. In both families, R^{2+} may be predominantly Ca (rancieite) and Mn^{2+} (Mn^{2+}-rancieite) in the natural minerals ; in birnessite sensu stricto Na is dominant ; Mg and K may be present as minor constituents. Although both families have similar layer structure which consists of edge-shared MnO_6 octahedral layer and sheet of water molecules and hydroxyl ions (Giovanoli et al., 1970), two structures have significant difference in the arrangement of their manganese octahedral frameworks (Potter and Rossman, 1979) as evidenced by infrared spectra.

The Mn^{2+} analogue of rancieite was named "takanelite" for the sample from Japan by Nambu and Tanida (1971) and approved by I.M.A. However, it turned out from this work that "takanelite" is not the true Mn^{2+} analogue of rancieite. The true Mn^{2+} analogue of rancieite was firstly discovered from the Janggun mine, Korea. It shows characteristic XRD pattern different from that of rancieite. Chemistry of rancieite and its Mn^{2+} analogues shows distinct isomorphous series between Ca- and Mn^{2+}-end members. "Takanelite" should theoretically be the same as the Mn^{2+} analogue of this study but differs in its XRD patterns. "Takanelite" has the same XRD pattern as that of rancieite. This can not be expected on the crystal-chemical viewpoint, considering $r_{Ca^{2+}}$=0.99 and $r_{Mn^{2+}}$=0.80Å. X-ray examination of "takanelite" preserved at the Smithsonian Institution shows that it is rancieite admixed with todorokite and nsutite. Now that the true Mn^{2+} analogue of rancieite has been discovered, it is reasonable that "takanelite" should be discredited and a new name should be given to the true Mn^{2+} analogue in this study.

The Mn^{2+} analogue of rancieite is brownish to dark grey with distinct anisotropism, metallic luster, H. 2½-3, sp. gr. 2.91. In reflected light, light grey to grey, no reflection pleochroism, distinct anisotropism with brownish grey, grey to dark grey, parallel extinction, no internal reflection, low reflectance. Chemical analysis gave MnO_2 74.01, Fe_2O_3 0.26, MnO 10.42, CaO 3.64, MgO 0.59, K_2O 0.33, $H_2O(+)$ 11.50 = 100.75, leading to the idealized formula $Mn^{2+}_{2-2x}Mn^{4+}_{5+x}O_{11}(OH)_2.3H_2O$ with x≒0.30 ; Z=2, a 7.562, c 14.476Å ; strongest lines 7.25(s), 3.619(w), 2.451(m), 1.429(m)Å. IR spectra show absorption bands at 3440(m), 1635(m), 1070(w), 670(vw), 570(vs), 510(vs), and 460(vs) cm^{-1}. DTA curve shows endothermic peaks at 190°, 610°, 790°, and 920°C. Heating at 200°C for 24 hours, 7.25Å line shifted to 6.90Å.

Mn^{2+} analogue of rancieite occurs as massive or colloform bands in the nsutite-rich manganese oxide ores in the supergene oxidation zone of rhodochrosite deposits at the Janggun mine, Korea. It has also been identified from the manganese oxide ores at the Anson Betts mine, Plainfield, Ma., U. S. A.

Chukhrov, F. V. et al. (1979), Intern. Geol. Rev., 23, 115-123.
Giovanoli, R., Stähli, E. and Feitknecht, W. (1970), Helv. Chim. Acta, 53, 453-456.
Kim, S. J. (1979), J. Geol. Soc. Korea, 16, 105-113.
Nambu, M. and Tanida, K. (1971), J. Japan Assoc, Miner. Petro Econ. Geol., 65, 1-15.
Perseil, E. A. and Giovanoli, R. (1979), Colloques Intern. du C.N.R.S. No 289 - La Genèse des Nodules de Manganèse, 369-377.
Potter, R. M. and Rossman, G. R. (1979), Am. Miner, 64, 1199-1218.

IMA 86 CRYSTAL GROWTH SYMPOSIUM - INTRODUCTION

KIRKPATRICK, R. JAMES, Dept. of Geology, University of Illinois, 1301 W. Green St., 245 Nat. Hist. Bldg., Urbana, IL, 61801

Igneous processes from magma generation to final crystallization, including wall-rock interaction, xenolith incorporation and digestion, fractional crystallization, and magma mixing usually involve phase transformations between crystals and melt. The processes by which these phase transformations occur are usually grouped under nucleation, crystal growth and dissolution. The study of these processes has been a major direction of research in petrology for about the last 15-20 years.

The main objectives of this symposium are to bring together important recent work on these three processes and outline directions of future research in this field.

For silicate materials the macroscopic processes involved in crystal growth and dissolution include the reaction at the crystal-melt interface, diffusion in the melt and crystal, heat transfer, and convection in the melt. There is now a considerable body of knowledge about crystal growth and dissolution rates and crystal morphologies for geologically interesting materials and also a reasonably good theoretical base for understanding the interface reactions, diffusion, and heat transfer. This work has provided major advances in interpreting the origin of textures of igneous rocks and the conditions under which these rocks crystallize. There are, however, few data and a poor theoretical base for understanding crystal growth when there is significant convective transport in the melt.

There are also reasonably good experimental data for how and why nucleation occurs in geologically interesting silicate melts, but the theoretical base (i.e., classical nucleation theory) appears to be unable to quantitatively explain the observations. New theories of both homogeneous and heterogeneous nucleation appear to be needed.

Important directions of future research, in addition to better understanding nucleation and convection-influenced crystal growth and dissolution, include application of existing theory and experimental understanding to plutonic igneous rocks of all types, understanding the rates and mechanisms of the processes by which magma is generated in the crust and mantle, understanding the interaction of magma with wall-rock and xenoliths, and modeling of magma chamber processes including the interaction of all physical and chemical processes (i.e., convection and heat flow, crystallization kinetics, and crystal settling).

This introductory talk will emphasize petrographic and experimental observations which remain poorly understood within the context of present day theory.

^{29}Si NMR SPECTROSCOPY OF PLAGIOCLASE FELDSPARS

KIRKPATRICK, R. JAMES, YANG, WANG-HONG, Dept. of Geology, University of Illinois, Urbana, IL, USA, 61801; CARPENTER, MICHAEL A., Dept. of Earth Sciences, Cambridge University, Cambridge, UK CB2 3EQ

Although the plagioclase feldspars are among the most studied minerals, many aspects of their complex structures are still unresolved. Many of these problems are related to local structure, rather than the average structure obtainable by diffraction methods. ^{29}Si NMR spectroscopy is well suited to examine these problems, because it is sensitive to the local structural environment of Si.

^{29}Si MASS NMR spectroscopy of a series of well purified and characterized set of natural and laboratory heated plagioclase feldspars (Carpenter et al., G.C.A., 49, p. 947, 1985) yields the following major conclusions. 1) The ^{29}Si chemical shifts of the best resolved sites [T1 (0Al) and T1 (1Al)] vary no more than ±1 ppm between An0 and An89, and the spectra are best interpreted by assuming that the positions of all of the non-Q^4 (4Al) sites do not vary significantly with composition (Fig. 1). 2) The spectrum of Val Pasmeda An100 contains resolvable signal from the eight Q^4 (4Al) Si sites of $P\bar{1}$ plagioclase (Fig. 2), and the spectrum of celsian contains resolvable signal from the two Q^4 (4Al) Si sites of an I2/c feldspar. 3) In $P\bar{1}$ and $I\bar{1}$ An-rich samples Ab solid solution in An occurs by substitution of Si onto sites occupied by Al in ordered An100, with Si preferring T2 to T1 sites and probably clustering near Na atoms substituting for Ca. 4) The spectra of homogeneous samples with apparent $I\bar{1}$ average symmetry (An 78-98) are best interpreted as indicating that they have local $P\bar{1}$ symmetry. 5) The spectra of single phase "e"-plagioclases are best interpreted as indicating that these phases are not composed of alternating lamallae of Ab and An but have a more complicated incommensurate modulated structure that is probably different in "e_1"-and "e_2"-plagioclases. 6) Difference spectra for ordered and disordered samples of the same composition indicate which Si sites appear and disappear upon disordering. These sites are different for "e_1"- and "e_2"-plagioclases.

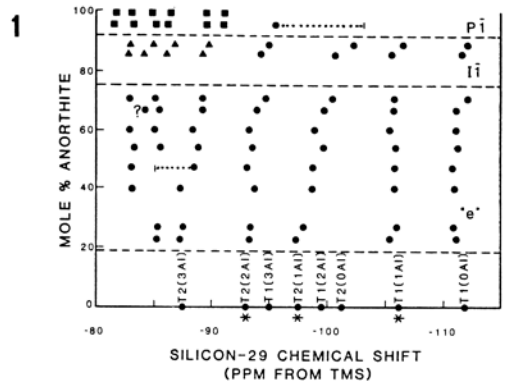

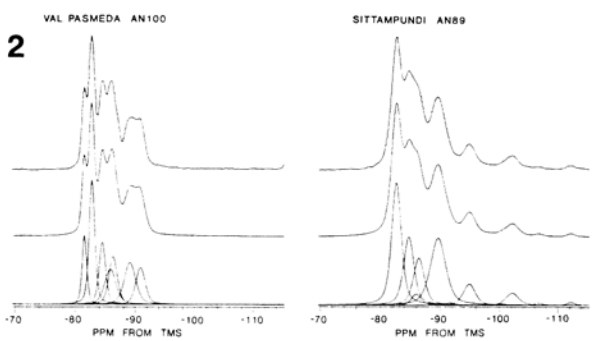

PHASE TRANSFORMATION AND MINERAL BEHAVIORS OF CORDIERITE

Masao KITAMURA, Department of Geology and Mineralogy, Faculty of Science, Kyoto University, Sakyo, Kyoto, 606 JAPAN

Cordierite [$(Mg,Fe)_2Al_4Si_5O_{18}\cdot nH_2O$] occurs in two polymorphic forms: high-temperature hexagonal form (P6/mcc) and low-temperature orthorhombic form (Cccm). The former (or indialite) has been found in nature only in two localities [1,2], while the low-temperature form is common in nature. The transformation between two forms is associated with the Al/Si ordering among the tetrahedral sites. In the present paper, recent transmission electron microscopic (TEM) and analytical TEM (AEM) studies on the phase transformation and mineral behaviors of cordierite are reviewed.

Order of transformation : The constraint of the group theory [3] indicates that the order-disorder transformation of cordierite is of the first order. The AEM study of the texture of natural cordierite derived from indialite also suggested the first order transformation by a nucleation-growth process [2]. A metastable process of the transformation other than the nucleation-growth was also reported. During this process, modulated textures constrained by symmetry of high-temperature form appear [4]. The twin formed through the metastable behavior is a real (110) one. In the nucleation-growth process, not real (110) twin but pseudo twin relation results in, where the twin individuals are related by one of the operations of the six-fold rotation axis of indialite [2].

Phase relation : A tentative phase diagram of Mg-Fe cordierite [2] was published by AEM examination of natural cordierite. The details of the phase diagram have been determined by hydrothermal synthesis and AEM [5]. In the diagram, indialite is stable around 700°C in an intermediate composition of Mg and Fe, resulting in an azeotropic relation between cordierite and indialite.

Formation of trilling : The trilling is a characteristic radial twin of cordierite which has been found in natural and synthetic cordierites. Two interpretations for the formation process of the trilling have been proposed: the growth process [6] and transformation process [7]. The trilling of cordierite in hornfels consists of growth sectors [8]. The TEM study on the trilling showed an existence of intrasector pseudo twin in the (001) sectors and intersector pseudo twin among the prism sectors. These pseudo twins suggest a complex formation process including both growth and transformation: (1) indialite first nucleated and cordierite overgrew as the prism sectors, forming the trilling, (2) the (001) sectors grew as indialite and transformed to cordierite.

[REFERENCES]

[1] Miyashiro,A.,Iiyama,T.,Yamasaki,M. and Miyashiro,T. Amer. J. Sci., **253**, 185-208 (1955).
[2] Kitamura,M. and Hiroi,Y., Contr. Min. Petr., **80**, 110-116 (1982).
[3] Putnis,A., Contr. Min. Petr., **74**, 128-131 (1980).
[4] McConnell,J.D.C., Mineral. Mag., **38**, 1-20.
[5] Yamada,H.,Kitamura,M. and Morimoto,N., 1984 meeting of Sannko Gakkai of Japan (abstract).
[6] Venkatesh,V., Amer. Mineral., **39**, 636-646 (1954).
[7] Zeck,H.P., J. Petrol., **13**, 367-380 (1972).
[8] Kitamura,M. and Morimoto,N., 1983 meeting of Japan Min. Soc. (abstract)

CAVITY MINERALS OF THE LAVA FLOW AT LEMOLO LAKE QUARRY, OREGON; Wallace D. Kleck, 3358 Marigold Circle, Costa Mesa, CA, 92626, USA

The Lemolo Lake quarry is next to Lemolo Lake and is located in the High Cascade Mountains about thirty miles north of Crater Lake, Oregon. Exposed in the quarry is a lava flow which contains a suite of magmatic minerals as euhedral crystals in gas formed cavities.

The flow contains normally zoned plagioclase (An73 to An55), 64 percent; clinopyroxene (Wo37En45Fs18 by microprobe), 28 percent; olivine (normally zoned from Fo79 to Fo72 by microprobe), 4.8 percent; metal oxides, 2.8 percent. By XRF analysis the rock contains SiO2, 52.50 percent; Al2O3, 18.20 percent; TiO2, 1.25 percent; Fe2O3, 2.00 percent; FeO, 6.64 percent; MnO, 0.19 percent; CaO, 8.99 percent; MgO, 6.43 percent; K2O, 0.85 percent; Na2O, 2.55 percent; P2O5, 0.40 percent. The rock can be classified as a high-alumina, basaltic andesite.

The cavities in the rock are the typical gas formed cavities observed in lava flows. These cavities normally contain a coating of minerals averaging about 2 mm thick. These cavity minerals are estimated to compose about one percent of the rock; they are euhedral and typically have well formed crystal faces.

The presence of principle and subsidiary surfaces in many cavities prove that a liquid was the source for most of the cavity minerals. The zoning of the plagioclase from An73 in the rock to An0 in the cavities and the nature of the minerals in the cavities indicate that the cavity liquid was derived from a final residuum of the rock magma.

The following minerals occur in the cavities of the lava flow at the Lemolo Lake quarry (idenity/approximate percentage in the cavities/composition/general information):

plagioclase/77%/it occurs as normally zoned crystals which range from An60 to An0 (by optical properties) /it occurs as tabular to equidimensional, euhedral crystals; some crystals are up to 4 mm in maximum dimension but average about 1 mm.

orthopyroxene/8%/single crystals are generally unzoned but range between Wo0En66Fs34 and Wo12En47Fs41 (Ca, Fe, and Mg by microprobe)/crystals are commonly flattened on {010}; it is commonly altered brick red, dull black, or rarely to acmite; crystals are up to 2 mm on c but average about 0.5 mm.

clinopyroxene/2%/?ferroaugite (by optics)/it occurs as small yellowish-green, columnar crystals; crystals are less than 1 mm in maximum dimension.

acmite/<1%/Fe+3 0.7-0.8 per formula unit (by optics) /crystals are yellow and acicular to bladed; it commonly occurs on ilmenite or as a replacement of orthopyroxene.

horndbende/<<1%/100Mg:(Mg+Fe)=85 (Mg and Fe by microprobe)/it occurs as blunt, stubby, dark-brown crystals which average about 1mm on c; it occurs primarily in the base of the flow.

ilmenite/6%//it occurs as splendent crystals which are tabular on {0001}; crystals are commonly cavernous on one or more faces; they average about 1 mm on a and are rarely up to 3 mm.

magnetite/<1%//it occurs as corroded, rounded octahedrons which are dull black or red; crystals are normally less than 1 mm on a.

pseudobrookite/<<1%/Mg, 1.8%; Fe, 31% (by microprobe)/it occurs as deep-red, submetallic, tabular crystals which average about 1 mm on c; it occurs primarily in the oxidized base of the flow.

apatite/2%/F is greater than 0.9 per formula unit (by optics)/crystals are acicular, colorless, transparent and are in some places cavernous; crystals are up to 3 mm on c.

tridymite/1%//it occurs as thin tabular to wedge shaped crystals which are colorless and transparent; most crystals are less than 1 mm on a.

cristobalite/3%//it commonly occurs as aggregates less than 1 mm with some {111} or {100} recognizable.

?zircon/<<1%//it occurs as pink, prismatic crystals which are less than 0.1 mm on c.

ROLE OF POINT DEFECTS IN HIGH-TEMPERATURE DEFORMATION OF OLIVINE

KOHLSTEDT,D.L., Dept. of Materials Science and Engineering, Cornell University, Ithaca, NY 14853, USA

At temperatures in excess of three-quarters of the melting point and at the relatively low stress levels which are of geologic interest, point defects directly control the creep of many minerals. Under these conditions, the strain rate is proportional to the self-diffusion coefficient of the slowest species which, in turn, is proportional to the concentration of the appropriate point defects. Because the concentrations of point defects in multicomponent silicates such as olivine can be systematically changed by varying the partial pressure of oxygen, activity of a component oxide phase, and dopant concentration (as well as temperature and total pressure), the dominant mechanism of deformation can be determined by measuring the strain rate as a function of these thermodynamic parameters.

In this diffusion-controlled creep regime, deformation processes can be divided into two catagories: (i) For coarse-grain rocks, the creep rate is controlled by climb of dislocations which requires lattice diffusion and/or short-circuit diffusion along dislocations. (ii) For fine-grain materials, creep occurs by direct diffusional transport of matter through the lattice and/or along grain boundaries, so that the creep rate is determined by the slowest ionic species diffusing via its fastest path.

To identify the dominant deformation mechanisms in single crystals, the creep behavior of naturally occurring San Carlos olivine has been studied as a function of the thermodynamic parameters. (i) Temperature: In marked contrast to observations for many materials, the activation energy for creep of olivine single crystals is significantly (at least 25%) larger than the activation energy for diffusion of the slowest species. For olivine, the diffusivities of oxygen and silicon are substantially smaller than those of magnesium and iron; however, there remains some controversy as to whether oxygen or silicon diffuses more slowly. (ii) Oxygen partial pressure: Over the entire stability field, the creep rate increases as the oxygen partial pressure to about the one-sixth power. (iii) Component oxide activity: The creep rate increases with increasing pyroxene activity raised to approximately the one-half power. For charge neutrality conditions involving octahedral cation vacancies and electron holes, the latter two observations are not consistent with the behavior of the concentration of vacancies or interstitials of either oxygen or silicon. Thus, a simple diffusion-controlled, dislocation creep model cannot explain the high-temperature creep response of olivine single crystals. Instead, it has been suggested that the dependence of creep rate on oxygen partial pressure and pyroxene activity reflects contributions from the concentrations of both jogs and the appropriate point defects. Likewise, the activation energy for creep is composed of two terms, one for formation of charged jogs and the other for diffusion of the slowest species. One charged jog-point defect pair that is consistent with most of the experimental creep results involves motion of positively charged jogs along dislocations at a rate which is limited by diffusion of oxygen via a vacancy mechanism.

The primary dopant used to affect the strength of olivine has been a water-derived defect. In the presence of water at a given oxygen fugacity, temperature, and stress, the creep strength of single crystals is reduced by a factor of about two at 300 MPa total pressure, due to an increase in the rate of dislocation climb. Although this defect is evidenced by strong IR absorption in the OH stretching band, its rapid diffusivity and the marked correlation of its concentration with hydrogen fugacity suggest that it moves through the olivine lattice as a hydrogen ion. The precise nature of the point defect responsible for the water-weakening effect, however, has not yet been identified.

Investigations of the dominant mechanisms of creep in fine-grain olivine have largely been carried out in high-pressure deformation apparatuses to prevent disaggregation along grain boundaries due to stresses arising from thermal expansion anisotropy. Because of complexities related to jacketing samples, the dependence of creep rate on oxygen fugacity and oxide activity have not yet been measured. However, the dependence of creep rate on stress, grain size, and temperature reveals the following: (i) Under wet conditions, diffusional creep is rate-limited by mass transport of one of the ionic species along grain boundaries. (ii) Under dry conditions, the diffusional creep is rate-limited by lattice diffusion of iron and magnesium; thus, under these conditions, the primary path for the transport of oxygen and silicon must be along the grain boundaries. These results indicate that water-derived defects directly affect the ionic diffusivities in olivine. Consequently, the concentrations of point defects directly influences the creep rate in both the dislocation climb and the diffusional creep fields.

NEW NATURAL CARBONATES ALONG $SrCO_3$ - $BaCO_3$ JOIN

KONEV A.A., Institute of the Earth Crust of the Siberian Branch of the USSR Ac.Sci., Irkutsk, USSR; VOROBYEV E.I., AFONINA G.G., SAPOZHNIKOV A.N., PARADINA L.F., LAPIDES L.I., MALYSHONOK Yu.V.; A.P.Vinogradov Institute of Geochemistry of the Siberian Branch of the USSR Ac.Sci., Irkutsk, USSR

Till recent years a limited isomorphism between $SrCO_3$ and $BaCO_3$ in natural conditions has been known. Maximum Sr in $BaCO_3$ was 11 mole % and Ba in $SrCO_3$ - 3 mole % [1]. But at the same time, complete solid solutions on the $SrCO_3$-$BaCO_3$ join have been synthesised at high T and P [2,3].

Authors have discovered and investigated new minerals of intermediate compositions and thus have proved a complete isomorphism between $SrCO_3$ and $BaCO_3$ in natural paragenesises. The latter occur among benstonite carbonatites from the Murun alcaline massif of the Aldan shield.

The table presents compositions of some studied carbonates.

N	Mas.% SrO	BaO	CaO	CO_2*	Σ	Mole % $SrCO_3$	$BaCO_3$	$CaCO_3$	Σ
1	55.09	7.20	6.47	30.76	99.53	76.61	6.77	16.62	100
2	54.80	14.20	2.32	29.20	100.72	79.60	14.20	6.20	100
3	45.41	17.42	6.15	29.10	98.08	66.20	17.20	16.60	100
4	18.10	56.50	0.66	24.60	99.86	31.50	66.40	2.10	100
5	4.00	72.50	-	22.70	99.20	7.50	92.50	-	100

*Calculated to give C = Sr+Ba+Ca.

1 Ca,Ba-strontianite - an exsolution phase in Sr,Ba-calcite; 2 Ca,Ba-strontianite - in Sr-witherite-4; 3 Ca,Ba-strontianite - product of exsolution of benstonite (occurs with baritocalcite and Sr-witerite-4); 4 Sr-witherite; 5 witherite - product of exsolution of Sr-witherite-4.

Sr-witherite with 1/3 $SrCO_3$ and 2/3 $BaCO_3$ is the most interesting one. This composition corresponds to minimum temperature of transition (745°C) between rhombohedral and orthorombic solid solutions $SrCO_3$ - $BaCO_3$ in the subsolidus region. That suggests the high temperature nature of early carbonatite minerals: benstonite, Sr,Ba-calcite and Sr-witherite. However, the Sr-witherite formation is likely to be connected with special conditions of additional heating: the mineral was found only in xenoliths of quartz-benstonite carbonatites in charoit rocks.

During the reduce of temperature the sequence of transformations and exsolutions of these high temperature carbonates took place. In particular, benstonite transformated into Ca,Ba-strontianite and barytocalcite, while Sr-witherite - into Ca,Ba-strontianite and witherite.

DTA curve for Sr-witherite gives endothermic peak at 770°C. The cooling at 920°C as a starting point gives the exothermic peak at 730°C. This indicates, that a polimorph change of the mineral is reversible (transfer from orthorombic into rhombohedral modification and vice versa). The transition temperature obtained is lower than that for strontianite (929°C) and witherite (811°C).

IR spectrum of Sr-witherite confirms disordered distribution of Sr and Ba over cation positions.

According to the data on monocrystal X-ray study Sr-witherite has orthorombic lattice; its space group being Pmcn. Volume of its elementary cell and parameter "a" exactly correspond to those estimated for $Sr_{0,32}Ba_{0,66}CO_3$; parameter "b" is less by 0,015 Å, and" c" is bigger by 0,016 Å than corresponding parameters expected for the mineral of the above composition.

References

1. Speer J.A. In: Rev.miner.VII.Carbonates mineralogy and chemistry.Michigan,1983,p.145-190.
2. Cork J.M., Gerhard S.L. Am.Miner.,1931,16,p.71-77.
3. Chang L.L.V. J.Geol.,1965,v.73,p.346-368.

A COMPLEX CLASSIFICATION OF GEM MINERALS

KOSTOV, R.I., Institute of Applied Mineralogy, Bulgarian Academy of Sciences, G.S. Rakovski Str. 92, 1000 Sofia, Bulgaria

Up till now gem materials have been classified mainly according to their physical properties (hardness, color, clearness), minerals taken as a basis. A lot of other gem materials, such as amorphous and organic materials, both natural and synthetic have been intensively studied recently, so that the variety of gem objects requires a new complex classification.

The first gemmological (and mineralogical) systematics have been attributed to the medieval scholars al-Kandi and al-Biruni (A.A. Laemmlein, 1963). The contemporary physico-technological systematics of gem materials are based on that of K.E. Kluge (1860) and they are adopted in most of the textbooks of gemmology (M. Bauer, 1896; G.F.H. Smith, 1912; A.E. Fersmann, 1923, 1954; R. Webster, 1962; E.Y. Kievlenko et al., 1972; A.I. Tsurupa, 1974; I. Sunagawa, 1982; A.N. Platonov et al., 1984; etc.). Genetic classifications are proposed by S.H. Ball (1922), B.Y. Merenkov (1936), M. Superchi (1980), I. Sungawa (1982) and J.P. Samsonov and A.P. Turingue (1984), the last one based on a genetic-formational principle. The classifcations of A. Eppler (1912), L. Bragg (1958) and H. Bank (1965, 1973) are considered mineralogical-crystallochemical (crystallostructural). A mineralogical-morphological point of view was suggested by I. Kostov (1973).

Synthetic gems and treated material are usually classifed as natural analogues, their growth mechanism substituting for the genetic origin (for example see K. Nassau and J. Nassau, 1980; I. Sunagawa, 1982). Amorphous materials of biogems are artificially grouped aside. No attention has been paid to the aesthetic, art and historical values of the gem materials.

The proposed complex seven component classification of gem materials aims to bring together their morphological, art, genetic, optical, crystallochemical, historical and utilization status (by using the initial letters a MAGOCHU system), each status divided into specific groups and subgroups. The MAGOCHU system allows computing of the great variety of gem materials and objects. Despite their economic significance (ES), no specific economic value status has been included, because in fact gems are priceless.

MORPHOLOGICAL STATUS	1-crystal; e-elongated, i-isometric, t-tabular; t-twins 2-monomineral aggregate 3-polymineral aggregate 4-phenocrystals in rock 5-monomineral rock 6-polymineral rock 7-amorphous Z-zonal, sectorial, tectonic features
ART STATUS (technology)	R-raw material D-designed F-faceted G-gemma; c-cameo, i-intaglio J-jewelled (type of metal) U-unique masterpieces (number of gems) V-variety W-weight (size)
GENETIC STATUS (locality)	E-extraterrestrial; m-meteoritic, l-lunar L-lithospheric; i-intrusive, e-effusive, m-metamorphic incl. metasomatic and impact, p-pegmatitic, h-hydrothermal, w-weathering, a-alluvial, s-sedimentary B-biospheric; p-plant, i-invertebrate, v-vertebrate, c-complex H-humanospheric
(firm-producer, growth)	S-synthetic; n-nature analogue, m-man-made new material, i-imitation, r-recultivated, t-treated, c-cultivated
OPTICAL STATUS (colour)	T-transparent; m-monochromatic, p-polychromatic, o-other O-opaque I-iridescent, with inclusion etc. Q-quality
CRYSTALLOCHEMICAL STATUS	C-crystalline; i-inorganic, o-organic
HISTORICAL STATUS	X-non-crystalline; i-inorganic, o-organic P-prehistoric, primitive A-ancient M-medieval, Renaissance N-new (XIX-XX c.)
UTILIZATION STATUS	CR-crown regalia RU-religious use PJ-personal jewel (incl. cloth) DO-decorative objects SS-social sign MC-museum collection; s-state, p-private TU-therapeutic use ES-economic significance SR-scientific research

EFFECT OF STIRRING ON CRYSTALLIZATION KINETICS OF BASALT

Akira Kouchi*, Akira Tsuchiyama** and Ichiro Sunagawa***

* Institute of Low Temperature Science, Hokkaido University, Sapporo, 060 Japan.
** Department of Geology and Mineralogy, Kyoto University, Sakyo, Kyoto, 606 Japan.
*** Institute of Mineralogy, Petrology and Economic Geology, Tohoku University, Aoba, Sendai, 980 Japan.

Although the importance of flow (or convection) in magmas for crystallization kinetics has been implicitly realized, no attempt has been made to examine this effect experimentally. We present here the results of experiments demonstrating that stirring affects the crystal morphology, nucleation density, partitioning of minor elements and texture.

Isothermal crystallization experiments on basalt (olivine tholeiite, 1921 lava of Kilauea; liquidus~1210°C) have been carried out using an infrared heating furnace. Flow (or convection) is present in the case of a (dynamic experiment), but not in the case of b (static experiment). A series of experiments were performed by changing the supercooling, duration and rotation rate.

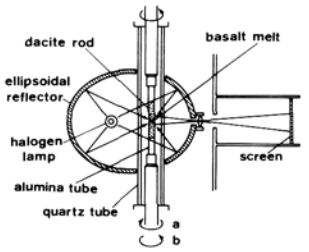

When stirring was not applied, the results agreed well with previous experiments. But when stirring was applied and a flow of Reynolds number=10^{-3}~$^{-4}$ was present, considerably different results were obtained, especially in respect to the nucleation rate and the morphology of crystals. At ΔT=25°C essentially similar results were obtained on the nucleation rates and morphologies of crystals in both static and dynamic experiments. However, at supercoolings larger than 45°C, nucleation density increased drastically in dynamic experiments reaching up to ten times as large as that in static experiments. Crystals of plagioclase and clinopyroxene took small acicular morphology regardless of ΔT in dynamic experiments, in contrast to marked changes in morphology with ΔT in static experiments, and hyalopilitic textures were formed. A TTT-diagram shows that the nucleation incubation time is shorter in dynamic experiments than in static experiments.

The thickness of the diffusion boundary layer, δ, of the static experiments is larger than that of dynamic experiments, and the δ decreases with an increase of rotation rate. No compositional difference in major elements was found in plagioclase and clinopyroxene produced in both static and dynamic experiments. However, minor element concentrations, e.g. Mg in plagioclase and Ti, Al in clinopyroxene, were found to increase with both ΔT and flow velocity.

All these results imply that chemical diffusion in the melts did not but interface kinetics did play an important role in the dynamic experiments. It is suggested that hyalopilitic texture commonly seen in natural basalt is mainly due to flow in magma.

The details of this study will be published elsewhere(1).

Reference
(1)Akira Kouchi, Akira Tsuchiyama and Ichiro Sunagawa. Effect of stirring on crystallization kinetics of basalt:texture and element partitioning. Contrib. Mineral. Petrol. in press

SEM EXAMINATION OF CALCITE-DOLOMITE EXSOLUTION

R. Kretz
Department of Geology, University of Ottawa,
Ottawa, K1N 6N5, Canada

Calcite crystals in marble of the Grenville province (Canadian Precambrian Shield) commonly contain lamellae, rods, and very small particles of dolomite, which have evidently exsolved from Mg-calcite. The dolomite microcrystals are oriented with crystal axes coincident with those of the calcite host. In some rocks the dolomite microcrystals occur dominantly as lamellae, 10 to 60 microns (μ) thick, which lie parallel to (0001), in agreement with O-lattice theory (Grover and Kubanek 1983). In other rocks, the microcrystals occur dominantly as rods, 10 to 60 μ in diameter and 50 to 500 μ long. The rods usually lie in the cleavage plane of calcite, parallel to the long diagonal (i.e. parallel to $\bar{a}$) or in other directions, and in places they form radiating patterns. Very small microcrystals (1 to 3 μ in diameter) occur abundantly in certain places.

The observed distribution of dolomite within crystals of calcite was evidently determined by nucleation kinetics. Initially, when temperature slowly declined from about 650°C, the Gibbs free energy change for the exsolution reaction (ΔG) was small, and relatively few nuclei were created. Transfer of Mg and Ca by diffusion was adequate to enable microcrystals to grow in response to falling temperature. The very small microcrystals evidently nucleated at a lower temperature, in response to an increase in ΔG resulting from a marked decrease in the rate of Mg-Ca exchange diffusion in calcite. Hence two pulses of nucleation occurred during slow cooling of the calcite crystals.

Grover, J. and Kubanek, F. 1983. Amer. J. Sci., 283-A, 514-539.

QUANTITATIVE ESTIMATES OF STRAIN IN (SEMI-)COHERENT K- AND Na-RICH PHASES OF PERTHITIC ALKALI FELDSPARS

KROLL, H. Institut für Mineralogie, Westfälische Wilhelms-Universität, D-4400 Münster, West Germany, and RIBBE, P.H. Department of Geological Sciences, Virginia Polytechnic Institute and State University, Blacksburg, VA 24061, USA

Strain may result from structural coherency between intergrown K- and Na-rich phases that have exsolved from what was once a single, homogeneous feldspar crystal at some higher temperature. Yund & Tullis discussed coherent exsolution in considerable detail (*Rev. in Mineral. 2*, II ed., 1983). Using the a vs. $(b{\cdot}c)$ plot devised by Bernotat (1982 -- see figure), we have deduced a quantitative measure of strain by defining 100% strain of a high sanidine (HS) in association with an unstrained analbite (AA) to mean that $(b{\cdot}c)_{HS} = (b{\cdot}c)_{AA}$. Likewise, 100% strain of a low albite (LA) in association with unstrained low microcline (LM) means that $(b{\cdot}c)_{LA} = (b{\cdot}c)_{LM}$. Thus the a dimension of the hypothetical strained HS is:

$$a = \text{Volume}_{HS}/(b{\cdot}c)_{AA} \sin\beta_{HS} = 8.797 \text{ Å}, \text{ where } (b{\cdot}c)_{AA} = 91.49 \text{ Å}^2.$$

The similar LA reference point for the Na-rich side of the strain diagram is

$$a = 7.930 \text{ Å}, \text{ where } (b{\cdot}c)_{LM} = 93.62 \text{ Å}^2.$$

Using the equations of the straight-line segments that fit the a vs. $(b{\cdot}c)$ data for the unstrained LA-LM and AA-HS cation exchange series of Kroll et al. (*Am. Mineral. 71*, 1986), the following give a "strain index" (S.I.), in percent:

$$\text{for the K-rich side -- } \quad S.I. = 3391.84 + 67.960a - 42.516(b{\cdot}c),$$

$$\text{for the Na-rich side -- } \quad S.I. = 1028.00 + 193.88a - 28.472(b{\cdot}c).$$

A strain index was calculated for each data point in the figure, and regression analyses were used to find coefficients for the following equations that express S.I. in terms of the d-spacings for the $\bar{2}01$, 060 and $\bar{2}04$ diffraction peaks:

$$\text{for the K-rich side -- } \quad S.I. = 3165.74 + 156.080d_{\bar{2}01} - 982.033(d_{060}{\cdot}d_{\bar{2}04}).$$

$$\text{for the Na-rich side -- } \quad S.I. = 270.37 + 474.866d_{\bar{2}01} - 575.721(d_{060}{\cdot}d_{\bar{2}04})$$

Stewart's (1975) caution that non-binary components (B, Fe^{3+}, NH_4^+, etc.) may mimic strain effects is important, but the effects of the common substituents are relatively small, amounting to about +1.5% in S.I. per mol % anorthite in solid solution in the Na-rich phase and about -2.0% in S.I. per mol % celsian in the K-rich phase.

QUANTITATIVE ESTIMATES OF STRAIN IN (SEMI-)COHERENT K- AND Na-RICH PHASES OF PERTHITIC ALKALI FELDSPARS . . . continued.

KROLL, H. and RIBBE, P.H.

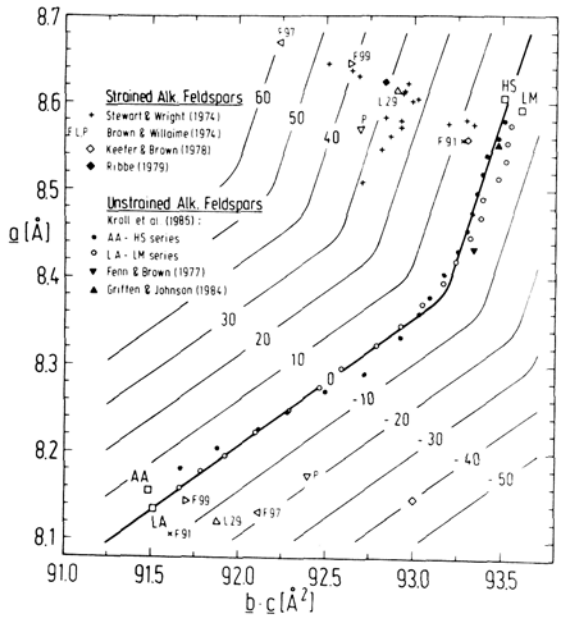

EFFECT OF PRESSURE ON THE CRYSTAL STRUCTURE OF PEROVSKITE-TYPE $MgSiO_3$

KUDOH,Y.[1], ITO,E.[2], TAKEDA,H.[1], 1;Mineralogical Institute, Faculty of Science, University of Tokyo, Tokyo, JAPAN, 2;Institute for Study of the Earth's Interior, Okayama University, Misasa, Tottori, JAPAN

Perovskite-type $MgSiO_3$ was predicted by Reid and Ringwood as one of the important mineral phases in the earth's lower mantle [1]. The crystal structure of perovskite-type $MgSiO_3$ was first determined by Yagi et al. [2] and Ito and Matsui [3] as distorted rare-earth, orthoferrite-type structure. Diminution of such distortion from ideal cubic perovskite at high pressure was suggested by Yagi et al. [2].

This paper reports the effect of pressure on the crystal structure of perovskite-type $MgSiO_3$ investigated with single-crystal X-ray diffraction method using a diamond anvil high pressure cell.

The specimen used was a single crystal of perovskite-type $MgSiO_3$ synthesized by Ito [4], having the size of approximately 50 μm in diameter. For high pressure experiment, an Inconel 750X plate 0.25 mm thick was used as gasket. The pressure fluid medium was a 16:3:1 mixture of methanol:ethanol:water [5]. The pressure calibration was made with the ruby fluorescence method [6].

The unit cell dimensions were obtained with a least-squares procedure applied to sin 2θ values of 11-15 reflections measured on a four-circle single-crystal diffractometer. Based on the observed cell volumes at 14, 40, 67 and 96 kbar and cell volume at room pressure reported by Ito and Matsui [3], the parameters Ko and Ko' in the Murnaghan-Birch equation of state were calculated. The values Ko = 2.20 Mbar and Ko' = 4.7 were obtained.

X-ray diffraction intensities were measured at pressures of 40, 67 and 96 kbar by four-circle single crystal X-ray diffractometer with graphite monochromated MoKα radiation. The fixed-φ scan mode [7] was adopted for the intensity collections. The results of observed variation of bond lengths and angles with pressure, compressibilities of coordination polyhedra are presented and discussed.

Reference

[1] Reid,A.F. and Ringwood, A.E. (1975). J. Geophys. Res. 80, 3363-3370. [2] Yagi, T. Mao,H.K. and Bell, P.M. (1978). Phys. Chem. Minerals 3, 97-110. [3] Ito,E. and Matsui, Y. (1978). Earth Planet. Sci. Lett. 38, 443-450. [4] Ito,E. and Weidner,D.J. (1986). to be submitted, Geophys. Res. Lett. [5] Fujishiro,I., Piermarini,G.J., Block,S. and Munro,R.G. (1982). High Pressure Res. Ind. AIRAPT Conf., 8th, 1982, p.608. [6] Barnett, J.D., Block,S., and Piermarini, G.J.(1973). Rev. Sci. Instrum. 44, 1-9. [7] Finger,L.W., King,H. (1978). Am. Mineral. 63, 337-342.

THE KINETICS OF CRYSTAL DISSOLUTION IN IGNEOUS SYSTEMS

KUO, LUNG-CHUAN, Exploration Research and Development Division, Conoco Inc., Ponca City, OK 74603, USA

Crystal dissolution in high-temperature silicate melts is controlled by reaction at crystal-melt interface and/or by mass transport across a boundary layer in the melt next to the crystal. In most igneous systems in which crystals and melts have distinctly different compositions, mass transport is the dominant mechanism for dissolution.

The mass transport is driven by diffusion and/or convection in the melt. For the diffusion-controlled dissolution (molecular diffusion) the dissolution rate (in length/time) is inversely proportional to the square root of time, whereas the operation of both diffusion and convection (natural convection) may lead to a steady-state dissolution with a constant dissolution rate. Convection can be further enhanced by rotating the crystal in a melt (forced convection), and dissolution is controlled by diffusion if the dissolution rate is proportional to the square root of the angular velocity of crystal rotation. These conditions can also be distinguished by the correlation between dissolution rates and apparent binary diffusion coefficients derived from the concentration gradients in the boundary layers.

Dissolution kinetics of olivine, pyroxenes, feldspars, quartz, garnets, and spinels has been investigated experimentally in a variety of natural and synthetic basaltic melts at both atmospheric and elevated pressures. The dissolution rates increase with increasing superheating but decrease with increasing pressure at constant superheating. Differential dissolution among minerals in a given melt can be correlated with their degrees of disequilibrium with respect to that melt composition at the experimental temperature and pressure. When the crystal is fixed within the melt, the dissolution is controlled by molecular diffusion before the onset of convection (and therefore the onset of steady-state dissolution), whereas a steady-state dissolution is achieved instantaneously when crystals are allowed to move freely in the melt. Rotation of crystals up to 360 rpm yields constant dissolution rates 2 to 3 times that for steady-state dissolution under otherwise identical conditions. The diffusion controlled dissolution typically results in subrounded (and, in some cases, embayed), smooth crystal morphologies with dissolution rates being independent of crystallographic orientation.

Resorbed morphologies displayed by many igneous minerals indicate dissolution events during magmatic evolution. Data on dissolution rates can therefore be used to constrain the length of time for such events. Impact melting of some lunar troctolite and olivine xenocrysts typically lasts less than 1 hour. Partial resorption with euhedral overgrowth at the rims of some plagioclase phenocrysts in mid-oceanic ridge basalts, perhaps due to magma mixing, can be developed in a few to a few tens of days. Alkali basalts carrying spinel peridotile xenoliths ascend through the lithosphere at velocities of up to the order of 10 km/hr.

Data on dissolution kinetics are also essential for quantitative modelling of the contamination of magmas by country rocks and xenoliths. Meter-sized blocks of quenched crust of a lunar magma ocean may sink back to the bottom, thereby modifies, both petrologically and geochemically, the close-system differentiation of that magma ocean. Such modelling is of potential importance in further understanding the origin and petrologic characteristics of terrestrial layered intrusives. The time-dependent variations of silica, potassium, rare earth, and strontium isotopic contents in basaltic magmas due to the dissolution of felsic xenoliths have been formulated as a function of size, mass fraction, and composition of the xenoliths and

THE KINETICS OF CRYSTAL DISSOLUTION IN IGNEOUS SYSTEMS

KUO, LUNG-CHUAN

the temperature of the magma. These results show preferential potassium contamination due to its high diffusivity and large deviation from equilibrium.

Contamination due to dissolution is likely to be more effective in more fluid magmas (for example, komatiitic, kimberlitic, pegmatitic, and carbonatitic magmas) because of the higher diffusivities of components. In addition, if the dissolving mineral species have high degrees of disequilibrium with respect to these melts, interface-controlled dissolution may be involved or even become dominant. Faceted crystal morphologies resulting from the interface-controlled dissolution in a variety of non-silicate compositions have been observed. Systematic studies on dissolution kinetics at elevated pressures are valuable for modelling the behavior of xenolith dissolution at depth. In particular, significant difference in the dissolution of eclogite versus peridotite, if occurred, may affect the population of these rocks in erupted alkali basalts and kimberlites and, consequently, the interpretation of the constitution of the upper mantle.

MICA AS AN INDEX MINERAL TO ROCKS AND ORES

KUO Tsung Shan, Institute of Mineral Deposits, Chinese Academy of Geological Sciences, Ban Wan Zhuang, Beijing, People's Republic of China

In the last five years the author has collected about 100 mica samples from granite bodies and ore deposits, mainly in Nanling, SE China, investigated with reference to 200 mica studies in China and approximately 6000 data. The study aims to determine whether mica can be used as an index mineral in ore prospecting. The research shows that various micas associated intimately with characteristic kinds of rocks and ores. The rare element contents of micas are generally high in Ce, La, Cr, Zn, Li, and Ba and very low in Cd and Bi. Rare micas are usually high in F. The examples are:

For rocks

In the normal alkaline-earth granites both muscovite and biotite are fairly constant in chemical and physical properties. The color of biotite is controlled by the percent of TiO_2, FeO, and Fe_2O_3 and in the formula:

$X_2Y_4 - 6Z_8O_{20}(OH,F)_4$, $Al^{iv} > 2$ in biotite (ß,γ ≅ 1.63-1.64) and $Al < 2$ in muscovite (ß,γ ≅ 1.58-1.59), but biotite in hornblende-biotite granite has ß,γ = 1.65-1.66; $Al = Al^{iv}$.

In granitic pegmatites muscovite is usually high in Li, Rb, Cs, and F. A Cs-mica (a new species submitted to IMA) occurs at Nanping, Fujian Province, with Cs_2O = 0.23%, F > OH,

$(Cs_{0.78}K_{0.21}Ca,Na)_{1.01}(Al_{1.78}Li_{0.10}Mg,Fe^{2+},Fe^{3+})_{2.1}(Si_{3.04}Al_{0.96})_4O_{10}(F,OH)_2$

located in the central part of the zoned pegmatite, associated with pollucite, quite like muscovite but with higher D and more brittle ß,γ ≅ 1.600, -2V = 40°.

In Mg-rich rocks such as dolomite, basic and ultrabasic xenoliths in eclogite, kimberlite, etc., all with phlogopite as accessory which, in the kimberlite, Menying, Shandong Province, shows reverse absorption with 0.43 Fe^{3+} in tetrahedral coordination (Mossbauer effect).

In alkaline miarolitic granite the Quichi Granite in the suburb of Fuchow, Fujian Province, has developed miaroles, with myrmikitic alkaline feldspar and accessories of riebeckite and aegirine, in the miaroles. Quichiite, a new species (submitted to CNMMN, IMA), occurs in the zone around xenoliths in the granite. It contains Al_2O_3 5.45, MnO 8.20, Li_2O 1.19, and F 4.8%, with formula $(K_{1.89}Na_{0.08}Rb_{0.04})_{2.01}(Fe^{2+}_{2.54}Mn_{1.14}Li_{0.78})(Fe^{3+}_{0.37}Mg_{0.50}Ti_{0.28})_{5.61}(Si_{6.38}Al_{1.05}Fe^{3+}_{0.57})_8O_{20}[F_{2.51}(OH)_{1.51}]_{4.02}$, a tetraferrilithiomontdorite.

For ores

In niobite-bearing granites in albitized granite at Bo Lo County, Guangdong Province, there occurs rubidozinnwaldite, $(K,Rb,Na)_{2.04}(Li,Al,Fe^{2+},Fe^{3+})_{5.54}(Si,Al)_8O_{20}(F,OH)_{3.8}$ with Rb_2O 1.54, Li_2O 3.28, 7 .16%, and Nb 337 ppm in the mica.

In albitized granite from Suchow, Jiangsu Province, there occurs zincian siderophyllite, with Li_2O 1.50, MnO 0.94, ZnO 0.40, F 4.60%, and Nb 859 ppm in the mica.

In biotite granite from Tung Po, Hunan Province, zinnwaldite is found in the W-, Sn-, Mo-, Bi-, and Be-mineralized part, with Li_2O 1.96, Rb_2O 0.86 and F 4.60%.

Be-bearing stockwork marble is found also in Tung Po where beryllium margarite occurs in the central part of the veinlets and associated with tourmaline and fluorite. The formula is $Ca(Al,Li)_2[(Al,Be)_2Si_2](O,OH)_{10}(OH,F)_2$, with BeO 1.33%.

In the Sn-, Cu-, Re-, V-, Cr-, and Fe-deposits, the micas associated with the ores contain the relevant elements 10-100 times those in the micas of barren rocks, as Sn 200-1000, Cu 400-750, REE 1000 ppm, V_2O_5 1.8-4.5%, Cr_2O_3 3.4-8.6%. The phlogopite in the Jungjiu iron ore, Jiangsu Province, is nearer near to the iron ore, the higher the iron content and the higher the refractive index.

References

[1] Kuo, Tsung Shan et al.(1983) Acta Petrologica Mineralogica, 2, 260.
[2] Hayama (1959) J. Geol. Soc. Japan, p. 21.
[3] Young, Y.C., personal communication.
[4] Chen, W.Y. (1981) The 9th Lab. Guangdong Province, October.
[5] Woo, S.B. (1978) Bull. Inst. Mineral Deposits, July.

DISTAL TIN - BASE METAL SKARNS (REPLACEMENT DEPOSITS)

KWAK, T.A.P., and MINHU, Fu, Department of Geology, LaTrobe University, Bundoora, Victoria, Australia 3083

Distal Tin (-Base Metal) skarns (replacement deposits) consititute the economically most important Sn skarns along with a few examples of (exo-) greisen Sn skarns. Known examples include the Renison, part of the Mt. Bischoff and Cleveland, the Queen Hill-Severne and Razor Back deposits, Tasmania, Australia; the Doradilla deposit, N.S.W., Australia; Changpo, Bali, Longtonshan deposits, Dachang, Guangxi, P.R.C.; parts of the Geiju deposits, Yunnan, P.R.C. and possibly part of the stratiform Sn-deposits in Billiton Is., Indonesia. None are known in North and South America, Africa, or Europe although some poorly described cassiterite-sulphide bodies in the U.S.S.R. appear to be similar. These are probably part of the ore type commonly called cassiterite-sulphide type deposits known in the U.S.S.R.

[At this juncture, 13 characteristics were described by the authors. *Ed.*]

The reason that distal Sn skarns have generally not received the attention such economically important deposits deserve is the fact that they are relatively rare. This is because they need a fairly unique set of conditions to form. Specifically, (a) a carbonate unit is needed which occurs within the outer aureole of the pluton, (b) a suitable source (pluton) is also needed but most importantly, (c) suitable permeability must be available. In areas where suitable carbonate units do not occur within the inner aureole region (e.g. Renison), distal skarn genesis is easier to envision than in areas where such units occur throughout the area of the aureole (Changpo). This may well be caused by high permeability and sufficiently rapid ore solution flow being present so that the fluids leave the site of potential proximal skarn genesis. Also, for a large deposit to form, perhaps permeability in host rocks must be limited in area so that large volumes of ore fluid are focused on a relatively small distal area.

PETROLOGY OF THE CONTACT - METAMORPHOSED WEEKS FORMATION, NOTCH PEAK, UTAH.

LABOTKA, Theodore C., Dept. of Geological Sciences, Univ. of Tennessee, Knoxville TN 37996-1410; NABELEK, Peter I., Dept. of Geology, Univ. of Missouri-Columbia, Columbia MO 65211.

Thin-bedded, micaceous limestones of the Upper Cambrian Weeks Formation, were intruded and contact-metamorphosed by the Middle Jurassic Notch Peak Stock in west-central Utah at a depth of 4 to 6 km. Unmetamorphosed rocks consist of calcite + quartz + muscovite + dolomite + plagioclase. At a distance of about 2500 m from the contact, phlogopite became abundant as a result of the reaction muscovite + 8 dolomite + 3 quartz + 4 H_2O = chlorite + phlogopite + 8 calcite + 8 CO_2. Most rocks contain the assemblage phlogopite + calcite + quartz, although tremolite is locally found. Gross recrystallization occurred at the diopside isograd where phlogopite + calcite + quartz broke down to form diopside + K-feldspar. Wollastonite replaced calcite + quartz in rocks as far as 2000 m from the stock. Idocrase commonly occurs in wollastonite-bearing rocks, and the diagnostic assemblage at the highest grade of metamorphism is calcite + diopside + wollastonite + idocrase + K- feldspar. Additional minerals include sphene and, in some samples, scapolite. As yet, there is no direct information on the temperature of metamorphism based on mineral equilibria, but heat-conduction models indicate that the maximum temperature was ~600±20° C. The stability of wollastonite and idocrase at temperatures less than this indicate that the fluid phase had $X_{CO2} \leq 0.05$. Some high-grade samples lost as much as 23 wt% CO_2 during metamorphism, indicating that as much as 9 rock-volumes of H_2O flooded portions of the aureole. Previous studies on adjacent rock units indicate that the fluid was derived from the stock; convection of thefluid probably perturbed the temperature field, and the wollastonite isograd represents an infiltration front. The large salient in the isograd on the north side of the stock reflects a channel through which the convecting fluid escaped.

PETROLOGY OF THE CONTACT - METAMORPHOSED WEEKS FORMATION, NOTCH PEAK, UTAH.

LABOTKA, T. C., and P. I. NABELEK

The occurrence of scapolite and NaCl-saturated fluid inclusions indicate that the fluid was hypersaline. The alkali feldspars contain a high proportion of Ba, as much as 13% BaO, and the bulk composition of the high-grade rocks contain as much as 1500 ppm Ba in excess of the unmetamorphosed value, corrected for volume loss (see Nabelek et al., this volume). The portion of the stock adjacent to the Weeks Formation is also enriched in Ba. Thus the infiltrating briny fluid appears to have redistributed some minor elements that occur in feldspar near the contact with the stock.

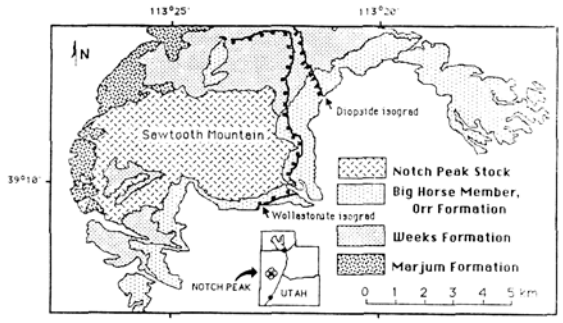

TRACE ELEMENTS DISTRIBUTION IN GRANITIC SYSTEMS. EXPERIMENTAL APPROACH.

LAGACHE M. Dept of Geology, ER 224, Ecole normale supérieure 46 rue d'ulm; 75230 Paris Cedex 05, FRANCE.

Trace elements partition laws in granitic systems roughly follow Goldschmidt's rules. A further interpretation of the present analytical data requires an experimental approach in order to improve our knowledge of the pressure, temperature and chemical environment dependance of partition coefficients. The experiments can also be used to calculate thermodynamic properties of the solid phases.

Aqueous fluids play a prominent part in late and post magmatic phenomena. The purpose of this paper is to study equilibria between hydrothermal solutions and alkali feldspars and plagioclases.

1. Alkali feldspars

Partitioning of a monovalent trace element between an alkali feldspar (pure end member or solid solution) and a hydrothermal solution. Example of Rb partitioning.

Binary systems. Partitioning of a trace element proceeds according to an ion exchange reaction of the type:
$MAlSi_3O_8 + tA \rightleftarrows MA + tAlSi_3O_8$; $MAlSi_3O_8$ is an alkali feldspar, where M is the alkali major element, A is the anion in the solution.

The distribution of M and t is given by the ratio

$$D_M^t = \frac{n_t}{n_M} \cdot \frac{N_M}{N_t}$$

n_t and n_M = mole fractions of the feldspars tF and MF. N_t and N_M : mole fractions of the salts tA and MA.

It can be shown that the distribution of a trace element of the same valence as the major element (homovalent) is a function of the ratio between the size of the structural site available and the size of the element. In the case of Rb, D = 0,04 for albite (Ab) and 0,42 for K feldspar (KF) at 650°C, 1,5 kbar. Those partition coefficients are not temperature dependent.

Ternary system. Partitioning of a trace element t between intermediate members of the series of alkali feldspars and hydrothermal solutions can be described by the relationship :

$$D^t_{Na,K} = n_{Na} D^t_{Na} + n_K D^t_K$$

The distribution of t depends essentially on the departure from ideality of the host solid solution. Knowing the thermodynamic properties of the three binary systems Ab-KF, Ab-RbF and KF-RbF it is possible to calculate $D^t_{Na,K}$. The calculations are performed according to the model of Kohler. The presence of a positive deviation from ideality of the alkali feldspars solid solution results in an enhanced acceptance of the trace element (Rb) in the intermediate members of the solid solution. This result is confirmed by experiments.

2. Plagioclases

Partitioning of a trace element between a plagioclase (pure end member Ab or An, or solid solution) and a hydrothermal solution. Example of Sr partitioning.

Binary systems. Partitioning of a divalent trace element proceeds according to the following equilibrium reaction :

$$2\ NaAlSi_3O_8 + SrCl_2 \rightleftarrows 2\ NaCl + SrAl_2Si_2O_8 + 4\ SiO_2$$

$$CaAl_2Si_2O_8 + SrCl_2 \rightleftarrows CaCl_2 + SrAl_2Si_2O_8$$

The distribution of Sr is given by :

$$D^{Sr}_{Na} = \frac{n_{Sr}}{(n_{Na})^2} \cdot \frac{(N_{Na})^2}{N_{Sr}} \quad \text{and} \quad D^{Sr}_{Ca} = \frac{n_{Sr}}{n_{Ca}} \cdot \frac{N_{Ca}}{N_{Sr}}$$

Partitioning of Sr between Ab and solution clearly depends on the total concentration of chlorides in the fluid (heterovalent exchange).

Sr is largely concentrated in Ab (D = 10) and less concentrated in An (D = 0,4) than in the solution at 600°C, 1,5 kbar. The partition coefficient of Sr in Ab is temperature dependent.

The thermodynamic functions of the three binary systems Ab-An, Ab-SrF and Ab-SrF have been measured. For Ab-An and Ab-SrF we observe a quasi ideal solid solution for a molar fraction of Ab greater than 0,50. An-SrF varies as does Ab-Kf : the solid solution can never be considered as ideal.

Ternary system. The model of Kohler predicts a quasi exponential decrease of the distribution of Sr from Ab to An. The experimental results are consistent with the model which is then as valid for heterovalent exchanges as for homovalent exchanges.

3. Applications to granitic systems. Examples.

PREDICTION OF REFRACTIVE INDICES BY POINT-DIPOLE MODELS

G.A. LAGER, Department of Geology, University of Louisville, Louisville, KY 40292

The local electric field at lattice site k in a crystal may be written as[1]

$$F(k) = E + \sum_{k'} L(kk')\, M^{(n)}(k')/\varepsilon_o \nu \qquad (1)$$

where the summation is over all k' sites within the unit cell. $M^{(n)}(k')$ is the multipole at site k' and can be an intrinsic property of a molecule or ion or be induced by an electromagnetic field. The superscript n denotes the order of the multipole (e.g., monopole for n=0, dipole for n=1, etc.). L(kk') refers to the components of the Lorentz-factor tensor and is related to the interaction between neighboring multipoles along different crystallographic directions. E is the macroscopic field, ε_o is the permittivity of a vacuum and ν is the unit-cell volume. If the ion in a polarized state is represented by a point dipole at its center and the electronic polarizability $\alpha(k')$ is assumed to be isotropic, i.e., independent of the direction of the electric field, then

$$M^{(1)}(k') = \varepsilon_o \alpha(k') F(k') \qquad (2)$$

and

$$F(k) = E + 1/\nu \sum_{k'} L(kk')\alpha(k')F(k'). \qquad (3)$$

In his classic study of the birefringence of calcite and aragonite, Bragg[2] considered anisotropy in the dipole-dipole interactions but assumed isotropic polarizabilities for calcium and oxygen. Fawcett[3] and Bolton et al.[4] improved on Bragg's

[1]Cummins, P.G., D.A. Dunmur, R.W. Munn and R.J. Newham (1976). Acta Cryst. A32, 847-853.
[2]Bragg, W.L. (1924). Proc. R. Soc. London, Ser A 105, 370-386.
[3]Fawcett, W. (1963). Proc. Phys. Soc. 82, 33-46.
[4]Bolton, H.C., W. Fawcett and I.D.C. Gurney (1962). Proc. Phys. Soc. 80, 199-208.

model by allowing for the anisotropic polarizability of oxygen in the structures of rutile and anatase and brookite (TiO_2), respectively. Oxygen atoms in each structure are coordinated to three titanium atoms arranged in a near-planar configuration. In each case, the polarizability parallel to the plane defined by the titaniums was greater than that perpendicular to the plane. The birefringence could not be explained assuming an isotropic polarizability for oxygen. Bolton and McIntyre[5] carried out essentially the same analysis for α-quartz with similar results. Unfortunately, the introduction of anisotropic polarizabilities in the point-dipole model is not always possible, even for relatively simple structures, because of the limited amount of optical data. For an ion in a general position, the number of independent non-zero elements of the polarizability tensor will be at least equal to the number of optical parameters (refractive indices and extinction angles). More recently, Pohl[6] has developed a least-squares method based on Eq. (3). The Lorentz-factor tensor is calculated from crystal-structural data using a two-dimensional transformation (planewise summation) rather than a direct summation of dipoles within a spherical or rectangular cavity (e.g., ref. 2-4). This has the advantage of insuring a quick and regular convergence of the lattice sums. If the electronic polarizabilities are known or can be estimated, Eq. (3) becomes a system of linear equations in F(k') which can be solved for F(k). Components of the dielectric constant tensor (squares of the refractive indices) can then be determined from the electric fields and electronic polarizabilities. The lattice sums calculated in Eq. (3) can also be used to refine polarizabilities by minimizing the function

$$\sum_{i=1}^{3} [K_{ii}(\alpha_1,\ldots\alpha_n)-K_{ii}^{obs}]^2 \qquad (4)$$

where $K_{ii}(\alpha_1,\ldots\alpha_n)$ expresses the dielectric constant tensor as a function of the electronic polarizabilities and K_{ii}^{obs} represents the experimentally-determined dielectric constants.

[5]Bolton, H.C. and P.N. McIntyre (1968). Proc. Phys. Soc., Ser 2 1, 889-894.
[6]Pohl, D. (1978). Acta Cryst. A34, 574-578.

Neutron powder diffraction data for hydrogrossular were complicated by the presence of small shoulders associated with each reflection in the profile (see fig.). These shoulders, which could not be detected in high-resolution Guinier x-ray films (λ= 1.9359A), probably reflect a compositional gradient involving deuterium. Fair agreement with observed data was obtained for a model with $(SiO_4):(O_4D_4)$=2:1, a=12.00A and atomic parameters from Basso et al.[3] (see fig.). However, this model could not be refined because of poor sample quality.

Time-of-flight single-crystal data were collected for a low-water hydrogrossular (0.16 wt% H_2O) at 20K to corroborate infrared measurements completed on the same material. Although negative density corresponding to the H-position determined by Basso et al.[3] was located in a difference Fourier map, inclusion of this position in the least-squares refinement produced no significant change in the agreement factor.

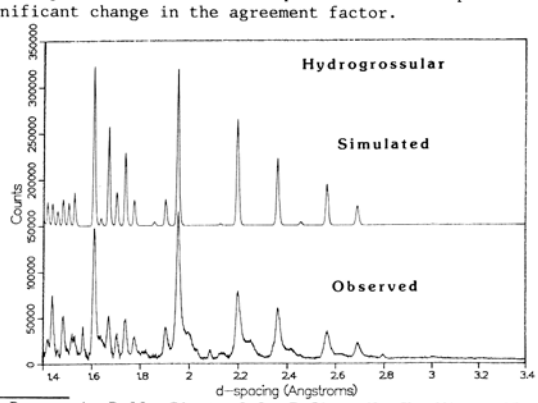

[3]R. Basso, A. Della Giusta & L. Zefiro, N. Jb. Miner. Mh. H.6, 251 (1983)

NEUTRON DIFFRACTION STUDIES IN THE HYDROGARNET SYSTEM $Ca_3Al_2(SiO_4)_3$-$Ca_3Al_2(O_4D_4)_3$[1]

LAGER, G.A., Department of Geology, University of Louisville, Louisville, KY 40292, USA; ARMBRUSTER, Th., Labor. für chem. und miner. Kristallographie, University of Bern, Bern, Switzerland; ROSSMAN, G.R., Division of Earth and Planetary Sciences, California Institute of Technology, Pasadena, CA 91125, USA; ROTELLA, F.J., IPNS Program, Argonne National Laboratory, Argonne, IL 60439, USA; FABER, J., Material Science and Technology Division, Argonne National Laboratory, Argonne, IL 60439, USA; SCHULTZ, A.J., Chemistry Division, Argonne National Laboratory, Argonne, IL 60439, USA.

Time-of-flight neutron powder diffraction data have been collected for $Ca_3Al_2(O_4D_4)_3$ [C_3AD_6] at 300K, 200K and 100K and for hydrogrossular [$Ca_3Al_2(SiO_4)_2(O_4D_4)$] at 300K. C_3AD_6 was synthesized hydrothermally at 478K and 200 bars from tricalcium aluminate. Sample preparation for hydrogrossular consisted of hydrothermal treatment of C_3AD_6 and amorphous SiO_2 (2 months, 623K, 500 bars) with periodic grinding and mixing in a N_2 atmosphere to achieve homogeneity. With the introduction of Si in the garnet framework, the characteristically sharp x-ray diffraction lines for C_3AD_6 became diffuse and broadened.

The C_3AD_6 data were refined using a Rietveld profile analysis modified for spallation pulsed neutron sources. Unit-cell and atomic parameters are tabulated below for each temperature:

T°K	a(Å)	O(x,y,z)	D(x,y,z)
300	12.5695(1)	0.0289(2), 0.0522(1), 0.6402(1)	0.1519(1), 0.0909(1), 0.7980(2)
200	12.5530(1)	0.0283(1), 0.0524(1), 0.6399(1)	0.1515(1), 0.0908(1), 0.7987(2)
100	12.5389(1)	0.0284(1), 0.0525(1), 0.6402(1)	0.1523(1), 0.0898(1), 0.7996(1)

Interatomic distances at 300K are significantly different than those reported by Foreman[2] who used a combination of x-ray and neutron powder data. Distances (Å) in the oxygen (deuterium) tetrahedron are 3.244(2.584) and 3.057(1.948) at 300K versus 3.242(2.573) and 3.052(1.944) at 100K. The O-D distance (0.908) remains essentially constant as a function of temperature.

[1]Research supported by NSF Grant EAR-8205605 (GAL)
[2]D.W. Foreman, J. Chem., Phys. 48, 3037 (1968)

ZONING IN COLUMBITE-TANTALITE INDICATED BY MICROPROBE STUDIES

LAHTI, SEPPO I., Geological Survey of Finland, 02150 Espoo, FINLAND

A large number of columbite-tantalite crystals (81) collected from 47 pegmatite dykes in the Eräjärvi area in southern Finland were analysed with microprobe. Because the chemical analyses (three to six determinations / crystal) indicate substantial variation in composition, twenty crystals showing very large (Nb, Ta) and (Fe, Mn) substitution were studied more closely. The distribution of the heavy elements, Ta and Nb, in the mineral was determined using backscattered electron images. The variation in Fe, Mn and minor elements was established with X-ray beam line profiles.

Microprobe determinations show that the crystals are often zoned (normal and oscillatory zoning) or characterized by various replacement textures. The zoned or inhomogeneous crystals are usually derived from the border or wall zone, whereas the homogeneous crystals from the intermediate zone, albite-rich replacement bodies and fracture fillings.

With some exceptions the extreme (Fe, Mn) and (Nb, Ta) substitution is 0-30 at % in individual crystals. Microprobe analyses indicate that majority, i.e. 70-80 % of the crystals from the wider dykes and 30-40 % of the crystals from the narrower dykes show minute (at the most 5 at. %) substitution of Fe by Mn and Nb by Ta within a crystal. This kind of small-scale variation in composition is obviously often due to normal zoning.

In oscillatory zoned crystals the oscillations occur as separate, narrow zones (often 1-50 μm in width) parallel to the simple crystallographic planes or as broader zones (50-150 μm in width) often consisting of a group of narrow zones closely similar in composition. The contacts are sharp or, in some crystals gradual. The width of one particular zone is usually constant, but marked variations can be observed between the different structural planes. Although the zones are usually

ZONING IN COLUMBITE-TANTALITE INDICATED BY MICROPROBE STUDIES

LAHTI, SEPPO I.

planary, irregular curvy zones were observed in some of the crystals studied.

The composition of the zones of six oscillatory zoned crystals studied varies largely. The difference in (Nb, Ta) and also in (Fe, Mn) substitution is between the nearby zones some at. %, but the extreme difference in substitution between the zones may be as high as 15 at. %. From the inner to outer zones the sequence often seems to display a trend towards a greater Ta content, whereas the Fe/Mn ratio varies largely.

The columbite crystals may exhibit corroded inclusions of columbite-tantalite crystallized earlier. If the replacing columbite exhibits irregular oscillatory zoning or if both of the phases are zoned, the texture may be very complex. The compositional variation between the different phases can be large. In general, Ta seems to have been enriched during the replacement processes. The extreme difference in (Fe, Mn) and (Nb, Ta) substitution varies substantially between the various parts of a crystal, and it may even be 40 at. %.

DENSITY OF ALUMINO-SILICATE LIQUIDS

R.A. LANGE and I.S.E. CARMICHAEL, Department of Geology & Geophysics, University of California, Berkeley, CA 94720

Currently, there is controversy in the literature about the effect of composition on the partial molar volume of Al_2O_3 in multicomponent silicate liquids. To address this issue, we have measured the densities of liquids up to 1600°C in the systems $CaO-Al_2O_3-SiO_2$, $Na_2O-CaO-Al_2O_3-SiO_2$, $MgO-Al_2O_3-SiO_2$, $CaO-MgO-Al_2O_3-SiO_2$ and $CaO-MgO-SiO_2$ using the double-bob Archimedean method. In conjunction with density measurements made in our lab on the system $Na_2O-Al_2O_3-SiO_2$, these data form a comprehensive set which eliminates the contribution of interlaboratory errors to the uncertainty of the partial molar volume of Al_2O_3. The results of these data allow the density of liquids along the plagioclase join to be calculated. These data can also be combined with ultrasonic measurements made in our lab to obtain dV/dP for plagioclase and diopside liquids at 1 atmosphere.

$Fe^{2+}Ti^{4+}$ CHARGE TRANSFER BETWEEN FACE-SHARING OCTAHEDRA IN ELLENBERGERITE, A NEW SILICATE FORMED AT MANTLE DEPTH

LANGER, K., Inst.Min.Krist.,Techn.Universität, D 1000 Berlin, Germany, FRG; CHOPIN, C., E.R. 224, Ecole Normale Supérieure, 75005 Paris, France

Ellenbergerite, $[Mg_{1/3},(Ti,Zr)_{1/3},\square_{1/3}]_2\ [Mg_6,(Al,Mg)_6]\ Si_6(Si,P)_2\ O_{28}(OH)_{10}$, occurs as mm-sized purple inclusions in pyrope megacrysts (CHOPIN et al. 1986) formed at about 700°C, $\geq$ 28 kbar in coesite-bearing metapelites of the Dora Maira massif, Western Alps (CHOPIN 1984). The dense structure (CHOPIN et al.1986) space group $P6_3$, consists of single chains of face-sharing octahedra on the 6_3 axes and of pairs of face-sharing octahedra linked by egde-sharing to form octahedral double chains on the 2_1 axes, all interconnected by $(Si,P)O_4$ tetrahedra. The mineral is strongly pleochroic and colour-zoned with ω colourless and ε colourless to deep violet.

Six crystals extracted from three different pyrope megacrysts were oriented by means of single crystal rotation photographs and embedded to produce 24 to 150 µm thick slices parallel to [0001]. The σ- and π-spectra ($\vec{E}||\omega$ and $\vec{E}||\varepsilon$, respectively) were obtained in the range 34000-5000 cm^{-1} on a total of 27 various spots, 15.6 µm in diameter, using a microscope spectrometer (LANGER and FRENTRUP 1979). Microprobe analyses were performed on the same spots.

The σ-spectra are featureless, except for an UV edge near 34000 cm^{-1} where the edge is defined as the wavenumber at which $\alpha = \log(I_o/I)/t = 200\ cm^{-1}$ (1 % transparency of a slice 100 µm thick. On the other hand, the π-spectra display, beside the UV edge near 32500 cm^{-1}, a broad band centered in the range 18500 to 19500 cm^{-1}, depending on crystal and spot measured. The strong intensity of the band is correlated with colour intensity of the measured spot. The band shapes are very close to those of single Gaussian bands, as shown by the close correspondence of integral intensities, J,calculated, as $J = (\pi/2)^{1/2} \cdot \Delta\tilde{\nu}_{1/2} \cdot \log(I_o/I)_{max}$, and planimetrically measured. Some π-spectra show at the low energy wing of the former, strong band a very weak shoulder or asymmetry near 14000 cm^{-1}.

The large half width, $5660 \leq \Delta\tilde{\nu}_{1/2} \leq 7500\ cm^{-1}$, and the strict polarization of the 19000 cm^{-1}-band is indicative of MM charge transfer. Indeed, the linear absorption coefficients, $\alpha_{[cm^{-1}]}$, or integral absorption coefficients, $A_{[cm^{-2}]} = J/t$, are positively correlated with [c], the [Fe]·[Ti] concentration product, as obtained from the microprobe analyses (concentration = no.of ions per formula unit), e.g. $\alpha_{[cm^{-1}]} = -25 + 12241 \cdot ([Fe]\cdot[Ti])$ with correlation coefficient r = 0.974. Therefore, the 19000 cm^{-1}-band is interpreted by FeTi charge transfer transitions in face-sharing octahedral single chains on the 6_3 axes. The oscillator strength, $f_{\parallel} = 1.877\ (A_{\parallel} \cdot V)\cdot([c]\cdot n_{da})^{-1}$ (SMITH and STRENS 1976) calculated with this interpretation, $f = 645\cdot10^{-4}$, is in support of the FeTi charge transfer origin of the band.

The lack of the band in the σ-spectra proves that there is no charge transfer between face-sharing pairs of the octahedral double chains on the 2_1 axes. The fact that only one single FeTi band is displayed in the π-spectra indicates that Mg(Fe), Ti, and □ are ordered within single octahedral chains because such ordering results in only one Mg(Fe)-Ti distance, 2,73 Å, whereas in case of disorder two distances, 2.73 and 2.48 Å, and, hence, two bands would exist.

LITERATURE
CHOPIN, C. (1984), Contrib.Min.Petrol.86, 107-118. CHOPIN, C., KLASKA, R., MEDENBACH, O., DRON, D.(1986), Contrib.Min.Petrol.in press.LANGER, K., FRENTRUP,K.R. (1979), J.Microscopy 116, 311-320. SMITH, G., STRENS, R.G.J.(1976) in STRENS, R.G.J.ed. "The Physics of Minerals and Rocks", Wiley, New York, 583-612

IGNEOUS LAYERING IN THE ULVÖ DOLERITE COMPLEX, SWEDEN

Sven Åke Larson, Sveriges Geologiska Undersökning, Kungsgatan 4, S-411 19 Göteborg, Sweden.

The Ulvö dolerite complex, central east Sweden (K/Ar age c. 1215 Ma) are layered intrusions exhibiting a varity of primary structures and minerals (Larson,1980). The dolerites can be traced as sheet like (width c. 250 m) circular lopolithic bodies with diametres of 40-100 km. The dolerite magma was of alkali olivine basaltic affinity with a major mineral content of labradoritic plagioclase, augitic pyroxene, hornolitic-hyalosideritic olivine, Fe-Ti oxides, biotite and subordinate apatite. In spite of the slight thickness excellent rhythmic layering (compositional and grain size), cryptic layering, igneous lamination, trough layering, slumping and discordant layering are present. Cryptic layering and field evidence suggest a multiple intrusive emplacement at an estimated depth of 2-3 km. Convective currents and 'stable' density stratification have influenced the nucleation and cooling of the magma. Three zones can be distinguished within the central lopolith. The lower zone (LZ) is a result of an early magma surge which is partly mixed with a later magma pulse. This zone represents a stable density stratification (cooling from below and heating from above). The rhythmically layered zone (Rz) includes that part of the magma which has mainly been influenced by convective currents and now presents rhythmic layering on the scale of c. 1 to 150 centimetres. The upper zone (Uz) is equal to that part of the magma which crystallized from the roof of the intrusion and downwards. The rhythmic layering of oxides in Rz caused a compaction of the crystal mush, especially in melanocratic layers, resulting in less intercumulus liquid. Thus, ulvite was formed in melanocratic layers but oxidation and exsolution resulted in ilmenite formation in mesocratic layers. The crystallization is likely to has taken place at T=1020°C; $-\log f_{O_2} = 10.2$ and the equilibrium conditions was T = 850-900°C; $-\log f_{O_2}$=13.5-14.2, reflecting the subsolidus exsolution of ilmenite (Buddington & Lindsley, 1964). The V_2O_3content of titaniferous magnetite is up to 1.2 weight % and the Cr_2O_3 content is up to 1.4 weight %. A unite cell edge of 8.39 Å and 8.47 to 8.49 Å was recorded for magnetite and ulvite respectively. The ulvite

content in magnetite$_{ss}$ is 0-13 mole %. The 'high grade' ore (>50 vol. % oxides) can be found within Rza layers usually not exceeding 0.5 metres in thickness. The most favorable conditions for magnetite$_{ss}$ concentrations prevailed within the central lopolith outcropping on the islands of Ulvöarna and Trysunda (Fig.1).

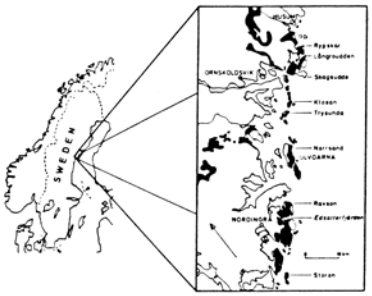

Fig.1. The location of the dolerite (black) area.

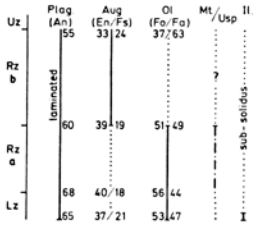

Fig.2. Cumulus (line) and intercumulus (dots) minerals in a section through the lopolith.

References
Buddington,A.F.& Lindsley,D.H., 1964: Iron-Titanium Oxide Minerals and Synthetic Equivalents. J.Petrol.,5,pp.310-357.
Larson,S.Å.,1980: Layered Intrusions of the Ulvö dolerite complex, Ångermanland, Sweden. Geologiska Institutionen, Publ.A 36, Univ. of Gothenburg.213p.

MONTE CARLO METHODS IN MINERAL KINETICS

LASAGA, A.C., Dept. of Geology and Geophysics, Yale University, New Haven, CT 06511, USA

There is much current research on the rates of mineral-melt and mineral-fluid reactions and their mechanisms. Recent work on metamorphic dehydration and decarbonation reactions, for example, has found different reaction mechanisms including intergranular diffusion control and surface control as well as various growth textures. The silicate melt research has focused on crystal growth while the low temperature geochemical work has emphasized dissolution. Unfortunately, we need to understand complete rate laws that include equilibrium as the final point.

We have recently begun to unify the kinetic treatment of these mineral reactions by the powerful Monte Carlo methods. Monte Carlo simulations model crystal growth and dissolution as a stochastic process in which microscopic rate constants for individual atomic events are replaced by probabilities. Crystal growth or dissolution is simulated by choosing surface sites at random and performing the elementary processes of precipitation, dissolution, and surface diffusion with frequencies proportional to the probabilities of each event. Monte Carlo parameters are further constrained by use of the kinetic theorem of microscopic reversibility. The effect of the stress field around dislocations is incorporated by decreasing the bond energy by the amount of strain energy introduced into the bonds.

The Monte Carlo calculations were used to predict the details of etch pit formation in mineral-water reactions as well as the morphology of the etch pits. The predictions of etch pit formation based on the analytic theory have been compared with the undersaturation levels observed in natural solutions. These calculations show that minerals like quartz, forsterite, and enstatite may exhibit a variety of etch pit formation (types and absolute number of etch pits) depending on the value of ΔG between the solution and the mineral. The critical undersaturation for etch pit formation observed in Monte Carlo dissolution surfaces agrees nicely with the critical value predicted by earlier simpler theories. This critical value also agrees with field observations on quartz in natural soils.

The Monte Carlo simulations can be used to predict the growth rate and dissolution rate as a function of the deviation from equilibrium, $\Delta\mu$. The Monte Carlo simulations incorporate many more factors than the early theories could possibly tackle. The growth and dissolution behavior of crystals is found to be extremely assymetric with respect to solution saturation ($\Delta\mu/kT$). At extremely high undersaturations, the dissolution rate approaches a constant in agreement with experiment. At high supersaturations, the growth rate increases exponentially. Near saturation, the region of most interest in natural applications, the growth/dissolution rate is a more complex function of the saturation state.

The deviation from equilibrium necessary to initiate dissolution or growth is strongly dependent on the surface free energy, and on the configuration of the surface. Comparing Monte Carlo results with the classical 2-dimensional nucleation growth theories, the latter predict too great a region of essentially zero rate, a prediction that has also caused disagreement with experiment. The Monte Carlo results suggest that there may be an intrinsic problem with the numerical approximations in the 2-dimensional nucleation theory.

The presence of dislocation-induced steps forms the physical basis for the BCF theory of crystal growth. Close to equilibrium, the BCF theory predicts a rate given by $R = A\,\Delta\mu^2$. The Monte Carlo results validate the BCF theory although the simplifications inherent in the BCF equation lead to non-trivial differences in the exponents. In general, the Monte Carlo exponents predict a growth rate that obeys $R = A\,\Delta\mu^{2.7-2.9}$ which modifies the BCF predictions. The exponents obtained in the Monte Carlo results are in good agreement with our own recent experimental data on mineral growth at high temperatures.

THE CHANGE FROM REVERSE TO NORMAL THERMOREMANENT MAGNETIZATION IN MINERALS OF THE ILMENITE-HEMATITE SOLID SOLUTION SERIES

LAWSON, CHARLES A. and NORD, GORDON L., JR., 959 National Center, U.S. Geological Survey, Reston, VA 22092, USA

The phenomenon of self-reversed thermoremanent magnetization (TRM), where a sample cooled from above its Curie temperature in an applied magnetic field acquires a TRM antiparallel to that field, occurs in intermediate compositions of the ilmenite-hematite (Ilm-Hem) solid solution series. Ishikawa and Syono (1963) recognized that only samples that have cooled through the order-disorder transition (see companion abstract by Nord and Lawson) are able to acquire reverse TRM. It was also shown that samples that originally acquired a reverse TRM would acquire a normal TRM after an appropriate heat treatment. Ishikawa and Syono's model for the acquisition of reverse TRM requires not only that the bulk of the sample be ordered but also the presence of a second phase that has the following properties: 1) it is disordered, 2) it is more iron-rich than the bulk of the sample, 3) it has a higher Curie temperature than the bulk of the sample, and 4) it is coupled antiferromagnetically to the ordered, bulk portion of the sample. They called this second phase the "x-phase". More recently, we have used transmission electron microscopy (TEM) to directly observe microstructures in samples that acquire reverse TRM (Lawson et al., 1981). We found that transformation-induced, cation-ordered domains are present and are surrounded by disordered domain boundaries. In our model, the disordered domain boundaries are the "x-phase", and indeed can satisfy the first three necessary properties of the "x-phase". In addition, we hypothesized that a minimum threshold volume of domain boundaries must be present in a sample in order for it to acquire a reverse TRM. The fourth property of the "x-phase", that of being antiferromagnetically coupled to the ordered regions, is neither supported nor disputed by our data and remains an implicit assumption of all models explaining reverse TRM.

In our present study, we have synthesized single-phase samples of the composition Ilm70-Hem30 using a controlled-oxygen-fugacity furnace, with T=1300°C and log fO2=-5.70. Samples were

THE CHANGE FROM REVERSE TO NORMAL THERMOREMANENT MAGNETIZATION IN MINERALS OF THE ILMENITE-HEMATITE SOLID SOLUTION SERIES
LAWSON, CHARLES A. and NORD, GORDON L., JR.

quenched from the synthesis temperature in liquid nitrogen and cooled to room temperature in approximately 10-15 seconds. Quenched samples acquire a strong reverse TRM, and results of the Lowrie-Fuller test indicate that this remanence is carried by single-domain or pseudo-single-domain carriers. TEM images show that these samples have a well-developed cation-ordered domain structure (domains approximately 100 nm), with many disordered domain boundaries. In contrast, a quenched sample that has been annealed for 240 hours at 900°C (below the 1000°C order-disorder transition for Ilm70-Hem30) acquires a much less intense normal TRM, with the Lowrie-Fuller test indicating multidomain magnetic behavior. The cation-ordered domains in this sample are very large (>> 1000 nm), and relatively few domain boundaries remain.

Using the two samples described above as examples of two possible end members (in terms of scale of microstructures and behavior of remanence), we are currently performing a series of annealing experiments (at temperatures below the order-disorder transition) on the quenched Ilm70-Hem30 samples. These experiments will allow us to monitor the systematic changes in magnetic properties for this composition as a function of annealing time and temperature. In addition, we will be able to follow the coarsening of the cation-ordered domains and the elimination of domain boundaries for these samples and correlate the changes in microstructures with the changes in magnetic properties.

References

Ishikawa, Y. and Syono, Y., 1963. J. Phys. Chem. Solids, 24, 517-528.

Lawson, C.A., Nord, G.L., Dowty, E., and Hargraves, R.B., 1981. Science, 213, 1372-1374.

HYDROTHERMALLY GROWN Mg- AND Fe-TOURMALINES

LEBEDEV A.S., KARGAL'TSEV S.V., PAVLYUCHENKO V.S., Institute of Geology and Geophysics, Novosibirsk-90, 630090, USSR

Tourmalines (T) $X_{1-n}Y_3Z_6\ Si_6O_{18}\ BO_3\ _3\ (O_{3-n}OH_{1+n})_4$, where X = Na,□; Y = Mg(Fe) and Z = Al, were grown at 600°C and 1 kbar in Al_2O_3-MgO(FeO)-$2SiO_2$-$45H_2O$-aH_3BO_3--bNaOH-cHCl system where a+b+c=5 (Fig.1)

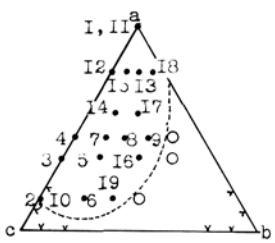

Fig.1. The synthesis field of Fe(Mg)T

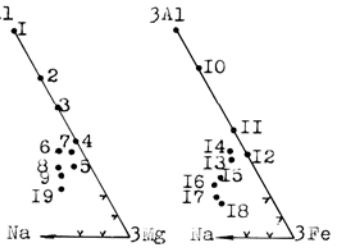

Fig.2. Composition of grown tourmalines

Microanalysis of T was carried out on Al, Si, Fe, Mg, Na with further recalculation of percent contents of Al_2O_3, SiO_2, MgO, FeO per 15 cations (Fig.2). Parameters of a T unit cell were determined along the reflections (212) and (051) on a "DRON 1.5" instrument (CuK_α-radiation, V = 0.25°/min). The synthesis of Mg(Fe)-T is shown in Fig.1. When Na/Cl increased in systems with Mg a change of the association was observed: T + talc → T + talc + vermiculite → T + paragonite (albite) → nepheline (sodalite); in the systems with Fe: T + fayalite → T + Fe_3O_4 + paragonite (albite) → nepheline + Fe_2FeBO_5 + Fe_3O_4. With the increase in Na/Cl Fe content in T grew and colour varied from blue (green) to black. In systems without Mg(Fe) and with Mg(Fe) contents less than 0.1 T grew only on a seed and $Al_4B_2O_6$ appeared among the synthesis products.

When Na was absent and Mg(Fe) increased in the system up to 1.0, the content of Mg(Fe) in crystals increased up to 1.7 (2.0) f.u., Al content being decreased proportionally. In similar systems with Na the content of Mg(Fe) in T increases up to 2.2 (2.3) f.u. The latter confirms a possibility of isomorphous substitution $Al^{3+} \rightarrow Mg,Fe^{2+} + Na^+$. Tourmalines without Mg(Fe) in which X sites were vacant (□) were grown onto a seed even in the presence of Na in the system.

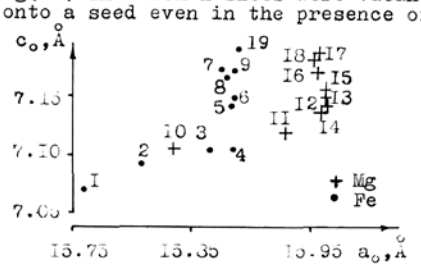

Fig.3. Relationship between a_o and c_o parameters of a T unit cell

Spontaneous crystallization of T terminated also with f_{O_2} increased above the magnetite-hematite equilibrium, T of brown colour being grown on a seed of elbaite.

As data from Figs 2 and 3 show, the first parameter increased with Mg(Fe) content in the grown T is a_o and only then c_o increases. It seems to be connected with the character of Mg(Fe) distribution in T among Y and Z sites that will be the subject of a further investigation.

APPLICATION OF COMPUTER-CONTROLLED MICROSCOPY IN APPLIED MINERALOGY

LEE, R. J., and WALKER, J. S., Energy Technology Consultants , 350 Hochberg Road, Monroeville, PA 15146, USA

Microscopy has a fundamental role in applied mineralogy. There is no substitute for the ability to directly identify an individual grain or particle, or to directly describe mineral habit and association. In recent past, the electron microprobe has played an invaluable role in obtaining detailed compositional information that has use in mineral processing as well as fundamental research. Electron microscopy in general has played a major role in furthering the science of mineralogy.

Computer controlled electron microscopy (CCEM), an emerging technology has the potential to dramatically affect the ability of the applied mineralogist to quantify observations. A CCEM system is basically a sophisticated extension of the type of image analysis system used in optical microscopy. CCEM technology takes advantage of modern digital techniques to capture, analyze, and classify the multitude of signals produced when a finely focused electron beam interacts with a solid.

Using CCEM, the distribution of sizes of particles or grains, the abundance of individual mineral species, and the percentages of locked and liberated minerals can be quantified. Algorithms permitting selected grains to be located and analyzed in detail have been developed, thus linking the traditional benefit of the interpretive ability of the human eye with the quantitative, numerical data produced by an automated system.

In many respects, this technology redefines the role of the mineralogist, removing the person from the tedious manual analysis, thereby permitting greater involvement in the interpretive aspects of the problem.

This paper will present an overview of CCEM technology and applications in environmental and process control problems.

OPALS OF GEMOLOGICAL INTEREST IN THE NEOGENE BASIN OF MADRID.

LEGUEY, S., Gª GIMENEZ, R., MORANTE, M. and MEDINA, J.A.: Dept. of Geology and Geochemistry. University Autonoma of Madrid, 28049 Madrid, SPAIN.

The Neogene basin of Madrid contains numerous outcrops of siliceous rocks associated with carbonate containing layers and with clayey rocks containing sepiolite and/or palygorskite, Bustillo (1976). Among these rocks there are scattered layers in which opal A and opal C-T predominate. Worthy of mention, from a gemological point of view, are the varieties of black opals, biogenic in origin, appearing as inserts 5-10 cm thick, between clacretes with palygorskite. Varieties of white opal appear as filling fissures (veins) of up to 1 cm, in massive silcrete inserts between sepiolite layers.

Black opals are characterized by their silky shine and soft dispersion. Their refraction index varies from 1.42 - 1.428 ± 0.005 and their density from 1.898 - 2.054 ± 0.002. Detection of trace elements revealed Mg, Al, Ti, Cu, Pb and Be. Laminose in texture, they are composed of silicified vegetable remains, with gramineous stalks and diatoms, impregnated with organic matter. Degradation of the organic matter, on the one hand, produces a progressive loss in colour, giving rise to banded structures in brown, grey and white tones. This degradation also causes a reordering of the silica which goes from opal A to opal C-T, and fibrous and cryptocrystalline quartz, Berner (1980).

White opals are translucent and highly fluorescent. Their refraction index varies from 1.436 - 1.449 ± 0.005 and their density ranges between 1.886 - 1.891 ± 0.002. Mg, Al and Cu are the trace elements detected. They are globular in texture, containing lepispheres of 2 - 5 mμ in an amorphous silica matrix. They display luminiscence, with absorption bands at 505, 526.5 and 549 nm, for an excitation wavelength of 422 nm. These three bands give very similar excitation spectra around 390:440 nm. According to Marfunin (1979), these bands correspond to a coexistence of O^- - Al and O^- - Al/H^+ aluminun centers.

BERNER, R.A. (1980) Early diagenesis. Princeton U. Press. 148.

BUSTILLO, M.A. (1976) Estudio petrológico de las áreas silíceas miocenas de la cuenca del Tajo. Est. Geol. 32, 451-497 Madrid.

MARFUNIN, A.J. (1979) Spectroscopy Luminescence and Radiation Centers in Minerals. Springer Verlag, 352.

• ULLMANNITE IN A GOLD-BEARING QUARTZ VEIN

LEI Yunfen, LIN Yeuying and YANG Mingming, Institute of Mineral Deposits, Chinese Academy of Geological Sciences, Beijing, People's Republic of China

Ullmannite is a fairly rare mineral. In China, it was first found in the gold-bearing quartz veins in the Triassic crystalline schist zone on the western side of Ailao Mountain, Southeast Yunnan Province. The ullmannite occurs as small crystal grains disseminated in the quartz. It is idiomorphic but with a distinctly corroded affect. Grain size is 0.01-0.05 mm; occasionally, the coarse ones may reach 0.25-0.3 mm. Ullmannite is associated with freibergite, stibnite and other Sb-minerals; obviously, native gold is the principal ore mineral in the vein.

The chemical formula of ullmannite $(Ni_{1.08}EE_{0.001}Co_{0.001}Cu_{0.08})_{1.09}(Sb_{0.97}As_{0.09})_{1.06}(S_{0.96}Se_{0.04})$ is calculated from the composition determined with an electron probe. The unit-cell parameter a = 5.934 Å is rather larger than that (5.91 Å) on the ASTM card. It is probably due to the As and Se contents.

The color of reflection is whitish, with a faint tint of blue. Reflectivities from 405-700 nm were determined serially with an MPV-1 microscope. The data are as follows:

λ nm	405	436	480	526	546	589	644	656	700
R%	50.52	50.22	47.34	47.29	45.83	45.12	46.07	45.78	42.23

The color indexes (SE) calculated from the dispersion curve of reflectivities are: Rvis = 45.64, x = 0.3281, y = 0.3262, λd = 468, and Pe = 0.025.

It is known that ullmannite commonly occurs in carbonate veins. Nevertheless, the present mineral is present in a quartz vein and associated with native gold. The authors suggest that the ore-bearing hydrothermal solution might originally derive from the ultrabasic rocks in a nearby region.

RESIDENCE OF SILVER, THUNDER MOUNTAIN CALDERA COMPLEX, IDAHO

LEONARD, B. F., and CHRISTIAN, RALPH P., U.S. Geological Survey, MS 905, Box 25046, Federal Center, Denver, Colorado 80225, USA

Silver is an accessory element in gold, antimony, and tungsten deposits of the caldera complex. Gold deposits are replacements of Eocene rhyolitic ash-flow tuffs and volcaniclastic rocks at the center of the complex of nested calderas. Gold, antimony, and tungsten deposits are replacements within and close to silicified zones and stockworks related to ring fractures in the pre-Eocene rocks. Most of the deposits are economically of low grade and genetically of xenothermal or epithermal character. Their gold- and silver-bearing minerals are usually disseminated, fine grained, and difficult to study. Sparsely disseminated pyrite and arsenopyrite are common associates.

Identified silver minerals are: native silver and electrum; the sulfides acanthite, argentite (the latter always inverted to acanthite), and members of the Silberkies group; the sulfosalts matildite, miargyrite, pyrargyrite, argentian tetrahedrite, and unnamed Ag-Sb-S and Ag-Fe-Sb-S minerals; the telluride hessite and the selenide naumannite; halides of the cerargyrite group; and the antimonate stetefeldtite*. Suspected silver minerals include the sulfide uytenbogaardtite and the sulfosalts andorite, diaphorite, and polybasite. Electrum, acanthite, and argentian tetrahedrite are common, though nowhere abundant. The other silver minerals are rare.

Electrum ranges in composition from $(Au_{0.315}Ag_{0.685})$ to $(Au_{0.914}Ag_{0.086})$, or from 456 to 951 fine. A common composition is $(Au_{0.41}Ag_{0.59})$, or 560 fine. Electrum occurs as the sole ore mineral in parts of some deposits; as grains isolated in quartz in deposits containing a trace of disseminated base-metal sulfides, or containing acanthite, argentian tetrahedrite, and base-metal sulfides; as inclusions in stibnite in a high-grade antimony deposit; and as inclusions with native silver, acanthite after argentite, argentopyrite(?), pyrrhotite, and arsenopyrite in the early-formed pyrite crystals of a scheelite-huebnerite deposit.

Acanthite is mostly stoichiometric Ag_2S. Rarely, a little Cu or Se is present in solid solution. Acanthite is ubiquitous, occurring typically as rims on base-metal sulfides and argentian tetrahedrite but also as clusters of radiating fibers in quartz and as pseudomorphs after argentite.

Argentian tetrahedrite varies in composition within limits that are not precisely known for samples from this region. Representative grains from one gold-silver deposit (Trigold) are homogeneous, ranging in composition from $(Cu_{5.99}Ag_{3.55}Fe_{1.71}Zn_{0.24})(Sb_{3.81}As_{0.24})S_{13.00}$ to $(Cu_{5.69}Ag_{3.92}Fe_{1.76}Zn_{0.25})(Sb_{3.90}As_{0.23})S_{13.00}$. Though electrum, acanthite, and other silver minerals are present, most of the silver value in the Trigold deposit is in argentian tetrahedrite. In the B and B antimony-mercury deposit 2 km distant, some tetrahedrite is argentian, some is mercurian, and some contains both Ag and Hg (example: ~3 wt % Ag, ~10 Hg). No other Ag-bearing mineral has been identified from the B and B. Argentian tetrahedrite in various deposits occurs as intergrowths with other ore minerals, especially with base-metal sulfides, and as irregular grains separated from the quartz gangue by thin rims of acanthite and other silver minerals.

Silver is present as a minor element in the structure of some varieties of other minerals. These include arsenopyrite (1-2 ppm Ag*), chalcopyrite (maximum 1500 ppm Ag), chalcostibite (0.04 Ag atom in the formula unit*), covellite (minor Ag), digenite (minor Ag), galena (trace to 0.6 wt % Ag), sphalerite (0.6-1 ppm Ag*), and stibnite (1 ppm to 0.15 wt % Ag*). The search for adventitious Ag in most of these minerals has been cursory. The results merely indicate that elemental silver is not confined to discrete silver minerals and is, therefore, an additional complication for the recovery of silver-bearing material from some deposits.

Silver occurs cryptically in some plants of the region. At Red Mountain, for example, the ashed sapwood of douglas-fir (Pseudotsuga menziesii) contains 2 to 300 ppm Ag. Silver in the ashed wood is roughly 100 times as abundant as it is in soil. The phenomenon, useful in biogeochemical exploration, deserves the attention of mineralogists.

*Unpublished data from non-USGS sources.

DEHYDRATION KINETICS OF CORDIERITES

LEPEZIN G.G.,OSORGIN N.U. Institute of Geology and Geophysics of Siberian Branch Academy of Sciences of the USSR, Novosibirsk-90, USSR

Dehydration kinetics of cordierites has been studied using chromatograph and mass spectrometer. Four specimens were investigated by chromatograph (Table 1).

Table 1
Microprobe analyses for cordierites

No	1	2	3	4
SiO_2	49.92	49.03	48.40	48.45
TiO_2	0.00	0.00	0.00	0.00
Al_2O_3	33.42	33.03	32.41	30.88
FeO	0.34	4.86	9.73	18.81
MnO	0.04	0.73	0.00	1.05
MgO	13.27	10.38	7.11	0.58
CaO	0.00	0.00	0.00	0.00
Na_2O	0.38	0.35	0.10	1.08
K_2O	0.03	0.05	0.00	0.00
Sum	97.35	98.47	97.45	97.85
F	1.5	24.0	43.6	95.3
Δ	0.223	0.234	0.260	0.139
H_2O	2.33	1.34	n/d	1.95

The experiments were carried out under isothermal conditions at temperatures 600,700, 750,800,900,1000 and1100°C. The results were treated by an equation,describing diffusion from sphere

$$\frac{M_t}{M_\infty} = 1 - \frac{6}{\pi^2}\sum_{n=1}^{\infty}\frac{1}{n^2}\exp\left(-\frac{Dn^2\pi^2 t}{r_0^2}\right) \quad (1)$$

where M_∞ is the initial H_2O content; M_t is water content left after annealing; t is time, r_0 - mean size of particles in a fraction.

The dependence of water diffusion coefficients for each specimens is given by Arenius' equation.

$$D_1 = 2{,}083\cdot10^{-3}\left(^{+5{,}920\cdot10^{-5}}_{-4{,}874\cdot10^{-5}}\right)\exp\left(-\frac{27000\pm100}{RT}\right)$$

$$D_2 = 1{,}061\cdot10^{0}\left(^{+0{,}330}_{-0{,}250}\right)\exp\left(-\frac{40300\pm500}{RT}\right)$$

$$D_3 = 2{,}332\cdot10^{1}\left(^{+2{,}808}_{-2{,}507}\right)\exp\left(-\frac{47400\pm250}{RT}\right)$$

$$D_4 = 3{,}600\cdot10^{3}\left(^{+0{,}200}_{-0{,}200}\right)\exp\left(-\frac{56000\pm150}{RT}\right)$$

Here, D_0 is given in cm^2/sec, E -in cal/mole, R in cal/mole K^{-1}.

A linear dependence was established between $\ell n\, D_0$ and E

$$\ell n\, D_0 = 4.848\cdot10^{-4}E - 19.448 \quad (2)$$

with a correlation coefficient r=0.999. This is due to the so-called cancelling effect.

More than 30 specimens were studied by mass spectrometer under non-isothermal regime. In this case the results were treated by an equation

$$\ell n\left(\frac{1}{f(\alpha)}\cdot\frac{d\alpha}{dT}\right) = \ell n\,\frac{A}{dT/dt} - \frac{E}{RT} \quad (3)$$

When the reaction rate is determined by diffusion,the parabolic law $\alpha^2 = kt$ is valid, hence $f(\alpha)=1/2$.From the data obtained a dependence of activation energy on Fe/Mg values and distortion index is derived

$$E = 1106 + \Delta(64486 + 60583\ \ell nF) \quad (4)$$

Reproducibility of the equation is found to be 8.5%.

By substituting (2) and (3) into Arenius' equation we obtain the dependence of water diffusion coefficients in cordierites on T, Δ and F

$$D = 3{,}580\cdot10^{-9}\left\{[1106+\Delta(64486+60583\,\ell nF)]\cdot(4{,}848\cdot10^{-4}-\frac{1}{RT})\right\} \quad (5)$$

It permits one to plan the time of an experiment on saturation and dehydration of cordierites considering r_0, T,F and Δ .

• SOME NEW SPECTROSCOPIC ASPECTS OF SPHALERITE FROM CHINA AND THEIR SIGNIFICANCE

LI Dien and PENG Mingsheng, Department of Geology, Central South Polytechnic University, Changsha, Hunan, People's Republic of China

We have carried out spectroscopic studies on more than 100 sphalerite samples from more than 10 deposits of different genetic types in China. In this paper, we only present and discuss some interesting results. It is generally thought that the color of sphalerite is varied from yellow, through brown, to black with the increase of iron content, while red or green sphalerite is very rare in nature. But we have collected and studied some red and green sphalerite from some lead-zinc deposits in China. The green sphalerite contains less iron and relatively higher cobalt. An absorption band at about 700 nm can be seen in its optical absorption spectrum that is assigned to the spin-allowed $^4A_2 \rightarrow {}^4T_1$ electron transition of Co^{2+} ion in the Td crystal field of the sphalerite structure. In fact, the band is split into two hyperfine peaks at 715 nm and 690 nm. It is the crystal field transition of Co^{2+} ion that causes sphalerite to be green in color.

Other sphalerite samples have inhomogeneous color with trace amounts of iron and relatively higher contents of Hg and Ga. UV-visible absorption spectra have been measured on a micro-spectrophotometer. The results show that an absorption edge at 365 nm and an absorption band at 450 nm can be seen for the red area, but only an absorption edge at 345 nm for the colorless area. Therefore, we have proposed a new energy band model for such red sphalerite (see Fig. 1) in which Hg^+ is at 0.3 ev above the valence band as an acceptor level. The red color of sphalerite is caused by the transition between the acceptor level Hg^+ and donor level Ga^{3+}. The study on the EPR spectra of sphalerite shows that there are two types of Mn^{2+} paramagnetic centers (see Fig. 2). One is Mn(I) center with g = 1.996-1.9998 and A = $64.3\cdot10^{-4}cm^{-1}$, which is assigned to Mn^{2+} substituting for Zn^{2+} in tetrahedral sites. The other is Mn (II) center with g = 2.0016-2.0027 and A = $86.6\cdot10^{-4}cm^{-1}$, which has never been reported in the literature. We think such Mn^{2+} ion occur in the interstitial octahedra of the sphalerite structure. This is based on the fact that its EPR spectrum is anisotropic with the hyperfine structure parameter similar to that of Mn^{2+} ion in cubic field of fluorite (A = $88.7\cdot10^{-4}cm^{-1}$) and in six-coordinated polyhedra of dolomite (A = $87.7\cdot10^{-4}cm^{-1}$) and the covalent parameter calculated (C = 0.51) being much less than that of Mn(I) center (0.732). The thermodynamic calculation shows that the Mn(II) center is formed and stable in the sphalerite structure at higher temperatures and less oxidation. Based on the EPR spectra of sphalerite, the distribution of manganese in sphalerite from the same deposit has been shown to increase from the early stage to the late stage. Besides, the spectroscopic studies of sphalerite can provide some information for the genesis and geochemical processes of deposits. One or two cathodoluminescence bands can be seen for sphalerite from stratibound deposits, while no cathodoluminescence pattern for sphalerite from hydrothermal deposits related to granite. In particular, based on all spectroscopic characteristics of sphalerite, the reproductio period of some deposits can be divided into four mineralized stages. Furthermore, the stability field of sphalerite and the evolution of ore-forming fluid during the mineralization can be discussed by the thermo- dynamic calculation.

Reference

[1] Li Dien and Peng Mingsheng (1985) The EPR study of sphalerite and its significance. Acta of Central South Institute of Mining and Metallurgy, No. 4 (suppl.).

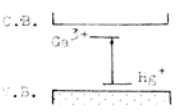

Figure 1. Energy band model for red sphalerite.

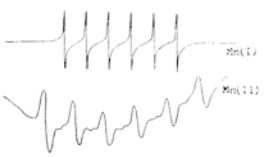

Figure 2. EPR spectra of sphalerite.

•THE RECENT DEVELOPMENT AND FUTURE PROSPECTS OF THE RESEARCH OF MINERALS FOR MEDICAL APPLICATIONS

LI Hongchao, Changchun College of Geology, Jilin, People's Republic of China

The research of minerals for medical applications has entered into a new phase since the beginning of the 1980s with the aim of furthering the exploitation of mineral resources, and development methods are being introduced in the research (combined with the polarizing microscope and supplemented by X-ray and infra-red spectrometers as well as multi-instrumental means of thermal analysis and trace element analysis). Cooperations have begun between mineralogists and traditional Chinese medicine scholars in their studies of mineral drugs. Yet, most of their activities still remain at the stage of identification and discussion of species. There seem to be many difficulties in confirming the samples and putting them into clinical applications due to the lack of source investigations.

In the applied mineralogical research sector, the author believes, first of all, a general survey should be carried out on those single mineral drugs which have been proposed by the community of traditional Chinese medicine with specific requirements. At the same time, comparative studies of samples should be conducted, thus paving the way for the standardization and systematization of each single mineral drug. Then, from the remaining uncertainties put forward by the community of traditional Chinese medicine, select and make further investigations on some ancient mineral drugs of their localities or origins of species, mineral compositions and variations of chemical constituents, so that these minerals' medical applications can be restored or developed.

In the theoretical research sector, however, the most urgent task is to find out the soluble constituents and their physical and chemical functions when used at different dosages (including the minerals themselves or their soluble constituents as well as their derivatives or compounds). It should be emphasized here that these studies must be linked with pharmacology of traditional Chinese medicine. Research projects should cover studies of single mineral drugs themselves, specific prescriptions and even some proved old recipes. Obviously, these researches are also the aspiration of the environmental geologists.

•THE STUDY ON THE SPECTROSCOPY AND THE COLOR NATURE OF SOME GEM MINERALS

LI Ping and PENG Mingsheng, Department of Geology, Central South University of Technology, Changsha, Hunan, People's Republic of China

Optical absorption spectra, combined with LPR spectra and Mossbauer spectra, are the most effective methods for studying the nature of color in gem minerals. The occurrences, spectroscopy, and color of some gem minerals are discussed.

Aquamarine. Aquamarine occurs in the Altai granitic pegmatite and is associated with colored tourmaline, lepidolite, etc. An absorption band at 810 nm is seen in its polarized absorption spectra. EPR spectra show that three lines in the C||H direction with g = 2.048 and a single line in the C-H direction with g = 1.9894, being assigned to Fe^{3+} in octahedral sites as confirmed by Mossbauer spectra. But Fe^{2+} is located in the channel structure of aquamarine whose double peaks in Mossbauer spectra are asymmetric, differing from Fe^{2+} in tetrahedral or octahedral sites. It is shown that water is in the channel structure of aquamarine by IR and NMR spectra. Therefore, we think that Fe^{2+} is combined with water in the channel to form hydrated ferrous ion $Fe^{2+}\cdot H_2O$, causing its blue color in which the water stabilizes the smaller Fe^{2+} in the structure and reduces the difference between 3d electron levels in Fe^{2+}.

Sapphire. Sapphire occurring in Hailand, Guangtong, is associated with spinel, zircon and olivine, all these being used as gem minerals. The sapphire is pale blue with 0.73% iron and 0.03% titanium. We have measured the optical absorption spectra (400-800) for the natural sapphire at room temperature, in which two absorption bands at 440 and 540 nm can be seen. Besides, there may be absorption bands in the near-infrared and near-ultraviolet regions. The EPR spectra of the same sample at room temperature show essentially three isotropic lines, assigned to Fe^{3+} in octahedral sites of the structure. In this way, it is reasonable that the nature of color in the sapphire is due to electron transitions in Fe^{3+} in octahedral sites, but does not exclude the charge-transfer transition of Fe^{3+}-Fe^{3+} or Fe^{3+}-Fe^{2+}pairs.

Lazurite. The lazurite has higher content of sulfur, its color being blue. It is observed that the EPR spectra of lazurite is a single line with g = 2.027, assigned to an S_3^- paramagnetic center in the structure. A strong absorption band at 600 nm and a weak band at 400 nm can be seen in its optical absorption spectra. The former is assigned to the electron transition between the ground state $^2B_1$ and the excited state $^2A_1$ of S_3^- causing the blue color of lazurite, but the latter is attributed to the electron transitions $1e \rightarrow 2a$ in SO_4^{2-} and $\sigma_{2Px} \rightarrow \pi_{2Py}$ in S^{2-}. Except for colored transition metal ions, therefore, sulfur elements of different valence are colored ions. The sulfur ions of different valence (S^{2-}-S_3^--SO_4^{2-}) coexist in lazurite structure only in the system containing an appropriate amount of sulfur and chlorine as a buffer, and with increased acidity and reduced oxygen fugacity, which has important significance in the synthesis of lazurite.

References

Peng, Mingsheng et al., Spectroscopic studies of aquamarine from Altai (in Chinese), Acta of Mineralogy, 1985, No. 2, p. 140.
Peng, Mingsheng et al., A study on spectroscopy of lazurite and its significance (in Chinese), Acta of Central South Institute of Mining and Metallurgy, 1983, No. 2, p. 90.

KYANITE GROUP MINERALS -- HIGH ALUMINA REFRACTORY MATERIALS IN CHINA

LI Shuzi

[By title only. No address given.]

THE CRYSTAL STRUCTURE OF A NEW FERRIC SULFATE MINERAL

LI Wanmao, Department of Geology, WANG Qiguang, Analysis & Testing Center, CHEN Guoying and SUN Shurun, Department of Geology, Lanzhou University, Lanzhou, Gansu Province, People's Republic of China

[By title only.]

COMPOSITIONS OF INCLUSIONS IN CHONDRITE MINERALS IN CHINA

LI ZHAOLIN, Department of Geology, Nanjing University, Nanjing, P.R. of China

Belong to iron-rich group, the chondrites studied are made up of chondrules and matrix, with SiO_2 content in the range of 36-37%, SiO_2/MgO ratio 1.6. Olivine and pyroxene are the predominant minerals, kamacite and troilite minor ones. There are different kinds of inclusions found in these minerals, including solid inclusion, melt inclusion, gas inclusion and liquid inclusion. Of these inclusions, melt inclusion is the most common type of inclusion to be found and can be subdivided into three groups: amorphous melt inclusion (composed of Asi+G, or just Asi)*; crystalline melt inclusion (Cfe+G, Csi+G, Cfe)*; and multi-crystalline-phase melt inclusion (nCsi+Cfe+G, nCsi+G)*. Measuring 5x2-20x40 um, these inclusions are generally in the shape of ellipse, tube or square. With 5-25% of gas phase, their homogenizing temperatures range from 1120 to 1250°C, or higher. Testified by electron microprobe, chromic oxide, greenish grain melting at 1020°C, is a new species of minerals found in melt inclusion by this study. Also found in melt inclusion is troilite, melting at 1240°C, and carbon dioxide-rich gas inclusions, homogenizing at 35°C.

In this study, five sections containing different types of melt inclusions were selected for electron microprobe study. According to the data of 37 detected points, inclusions contain mainly glass, chromite, troilite, kamacite and chromic oxide etc. These are the solids formed in the process of differentiation and cooling of original melton nebula materials trapped in the chondrite minerals. Their chemical composition is characterized by:

a. Ununiformity, different inclusion has different composition, varying by a factor of 0.03-27 with one to another. Even within the same melt inclusion, as show by different detected points, compositional variation is sometimes conspecuous, with basic componants higher in the center of the inclusion. This means that the composition of primary meteorite material were not homogeneous.
b. Glass phase normally make up to 60-80 vol.% of melt inclusion, with the composition of 64-71% SiO_2; 17.9-21.5% Al_2O_3; plus a small amount of Cr_2O_3, Fe, TiO_2, Na_2O, K_2O, MnO etc. Within the composition, three pairs of elements: Si/Al, Na/K, Fe/Cr vary in direct proportion, two other pairs: Na/Cr, Fe/Si in inverse proportion. Compared with the bulk composition of chondrite, the glass phase in melt inclusions enriches in SiO_2, Al_2O_3, K_2O, Na_2O and CaO, and depletes in MgO, FeO etc. This tells us that differentiation has

COMPOSITIONS OF INCLUSIONS IN CHONDRITE MINERALS IN CHINA

LI ZHAOLIN

taken place during the process of cooling of the original nebula material after being trapped.

c. Chromite: Cr_2O_3 57-58%, FeO 31-32%; troilite: Fe 64-63%, S 35-36%, kamacite: Fe 93.05-93.25%.
d. Measuring less than 10 um in size and 5-10% the whole volume of melt inclusion, chromic oxide is composed of Cr_2O_3 80.1-96.8%, Fe 1.31-2.23%, and some amount of Na, Si, Mg, Al, Ca, Ti, Mn etc.
e. As indicated by the mass spectrometric analyses, the gas phase of melt inclusion, with 55% CO and 31.4% H_2, is composed of CO, H_2, CO_2, N_2, CH_4, C_iH_i, H_2O, etc. in the relative abundance order, which is similar to the composition of the atmosphere of outer planets in the solar system.

The results in this paper show that composition study of melt inclusion in chondrite minerals is a new way leading us to the understanding of the formation and evolution of meteorites.

* A refers to amorphous phase; C to crystalline phase; G gas phase; Csi siliceous cryst.; and Cfe ferrous cryst.

THE IMPORTANCE OF THE PACKING OF THE STRUCTURAL UNITS ON THE STRUCTURAL CLASSIFICATION OF MINERALS

LIMA-DE-FARIA, J., Centro de Cristalografia e Mineralogia, Instituto de Investigação Científica Tropical, Alameda D.Afonso Henriques 41-4ºEsq., 1000 Lisboa, Portugal

Any structural classification of minerals (Lima-de-Faria, 1983, Hawthorne, 1984 and 1985) should derive from a general classification of inorganic crystal structures, because minerals are a part of the domain of inorganic structures. Several attempts have been made in the past to work out general classifications of inorganic crystal structures, and practically all of them are based on the concept of structural unit which is defined direct or indirectly by the bond strength distribution. If the bond strength distribution is homogeneous the structural units are large isolated atoms, and if it is heterogeneous the structural units are the assemblages of atoms more tightly linked than any others in the structure. The main categories of structural units which have been considered are isolated atoms, finite groups, infinite chains, infinite sheets, and infinite frameworks, but certain authors only admit part of these categories, and others subdivide some of them.

The formation of the structural units seems to be related to the satisfaction of the anion bond-valence requirements, involving coordination polyhedra with higher bond-valence (Hawthorne, 1985), and many structural units are interrelated through a general polymerization process (Lima-de-Faria and Figueiredo, 1976 and 1978, Hawthorne, 1984 and 1985) which consists of the condensation of isolated atoms into groups, of groups into chains, of chains into sheets, and of sheets into frameworks.

Among the principles of stability of crystal structures one of the more important is the so called space principle (Laves, 1956) which corresponds to the tendency to good space filling. As a consequence the structural units tend to pack together as close as possible giving rise to a structure with a minimum volume. The packing of the structural units is therefore an important structural factor, and depends mainly on their constitution and shape. Well known examples are the packing of the silicate chains in pyroxenes and amphiboles.

This tendency for close packing of the structural units is so strong and important in the domain of mineral structures that most of them can be considered as distortions of other structures based on ideal close packings, the so called packing analogues. In this respect Belov said in 1947: "Nevertheless the variety of the mineral crystalline world, the whole mineralogical game, just reduces to various modes of filling gaps in uniform close packings to various corresponding patterns". Examples are the pyroxenes, the amphiboles and the phyllosilicates, but many other structures could be mentioned such as tourmaline, which is a group structure built of silica rings and whose packing analogue is formed by the cubic closest packing of the oxygens with the other atoms occupying the interstices of this packing. In this work an analysis of the packing of the structural units is made, and certain relationships between them and the corresponding packing analogues are established.

References: Belov, N.V. - 1947. In Structure of ionic crystals and metallic phases (in Russian). Izd. Akad. Nauk SSSR, Moscow; Hawthorne, F.C. - 1984. Poster presented at the XIII International Cryst. Congress, Hamburg; Hawthorne, F.C. - 1985. Amer. Miner., 70, 455-473; Laves, F. - 1956. In Theory of alloy phases, American Society of Metals, Cleveland, Ohio; Lima-de-Faria, J. - 1983. Garcia de Orta, Série de Geologia, 6, 1-14; Lima-de-Faria, J. and Figueiredo, M.O. - 1976. J. Solid State Chem., 16, 7-20; Lima-de-Faria, J. and Figueiredo, M.O. - 1978. Garcia de Orta, Série de Geologia, 2, 69-76.

AN EHMO STUDY ON THE CRYSTAL-FIELD SPECTRUM AND g-TENSOR OF Cu^{2+} ION IN TURQUOISE

LIN CHUANYI, Institute of Geochemistry, Academia Sinica, Guiyang, Guizhou, The People's Republic of China

It has been found that both the crystal-field spectrum and g-tensor of Cu^{2+} in turquoise can be well explained in terms of the ligand-field(LF) theory.[1] In the interpretation of the g-tensor, it is important to take account of the covalency effect. However, in LF calculations this can be done only in a phenomenological manner. In order to take the covalency effect into account in a more natural way, we have made an iterative calculation on a CuO_6^{10-} cluster.

As in the LF calculation, the symmetry of the CuO_6^{10-} unit is also assumed to be D_{2h}. Since H_{ii}, the diagonal elements of the one electron Hamiltonian, are highly charge dependent, an iterative procedure is adopted:

$$H_{ii} = -\alpha_i - k\beta_i q_A \qquad (i \in A)$$

where q_A is the net charge on atom A. The input parameters α_i and β_i are taken from refs. 2 and 3 for Cu and for O respectively, and the damping factor k is taken to be 0.1. The off-diagonal elements are estimated from:

$$H_{ij} = -KG_{ij}\sqrt{H_{ii}H_{jj}},$$

and a value of 2.0 is used for K.

The crystal field transition frequencies are approximated as the energy differences between the filled molecular orbitals $3b_{3g}$, $3b_{2g}$, $3b_{1g}$, $7a_g$ and the half-filled orbital $8a_g$, which are all mainly of Cu3d character. The ordering of the crystal field energy levels predicted by the EHMO calculation is the same as that by the LF calculation.

The principal values of the g-tensor are given by

$$g_x \approx 2\{1-\lambda(\sqrt{3}a+b)^2\gamma^2/|E(^2B_{3g})-E(^2A_g)|\}$$
$$g_y \approx 2\{1-\lambda(\sqrt{3}a-b)^2\beta^2/|E(^2B_{2g})-E(^2A_g)|\}$$
$$g_z \approx 2\{1-4\lambda b^2\alpha^2/|E(^2B_{1g})-E(^2A_g)|\}$$

where λ is the spin-orbit coupling constant of the

AN EHMO STUDY ON THE CRYSTAL-FIELD SPECTRUM AND g-TENSOR OF Cu^{2+} ION IN TURQUOISE

LIN CHUANYI

free Cu^{2+} ion and a, b, α, β, and γ are appropriate LCAO coefficients of MOs. The g_x, g_y and g_z values thus obtained are 2.032, 2.135 and 2.368 respectively, which are in very good agreement with those observed (2.043, 2.135 and 2.373).[4] Compared with the previous LF results (2.021, 2.184 and 2.373)[1], obvious improvement has been achieved with the EHMO method.

1. Lin Chuanyi et al., J. Mol. Sci., 3(3), 77 (1983) (in Chinese)
2. M. Zerner and M. Gouterman, Theoret. chim. Acta (Berl.), 4, 44 (1966)
3. R. Rein et al., J. Chem. Phys., 45, 4743 (1966)
4. J. Diaz et al., Am. Mineral., 56, 773 (1971)

•A PRELIMINARY DISCUSSION ON PROBLEMS OF THE STUDY OF GENETICAL MINERALOGY

LING Wentong, Department of Geology, Hefei Polytechnical University, Hefei, Anhui Province, People's Republic of China.

There are four methods of studying the genesis of minerals:

(1) Mineralogy method: including the way of formation and the change in minerals, gas-liquid inclusions in minerals, typomorphic peculiarities of minerals, typomorphic minerals, mineral parageneses, etc.

(2) Geology method: utilizing the features of varied geological processes of minerals, formation-magmatic processes, sedimentation processes, metamorphic processes, etc.

(3) Geochemistry method: studies the condition of the collection of chemical elements in the earth's crust on the process of varied geological processes, such as temperature, pressure, acidity, alkalinity, etc. It explains the physico-chemical environment of mineral formation, the origin of minerogenetic matter, and the genesis of minerogenetic fused masses and solutions.

(4) Physico-chemistry method: examines the physico-chemical conditions of mineral genesis.

PARAGENESES OF Ca-Na PYROXENES AND AMPHIBOLES FROM FRANCISCAN BLUESCHISTS, CAZADERO, CALIFORNIA

LIOU, J. G. and MARUYAMA, S. Department of Geology, Stanford University, Stanford, CA 94305, USA

Ca-Na pyroxenes and amphiboles are common in both Type II and III Franciscan metabasites from Ward Creek. Their textural evolution and compositional variation with increasing grade were determined. With increasing grade, pyroxenes change their habit from bundles of fine-grained aggregates through fan-shaped prisms of intermediate-grained to blocky, coarse crystals. Their color varies from green and dark green, through colorless and pale-green to pale brown, roughly corresponding to the compositional change from aegirine-augite and aegirine-jadeite through impure jadeite and chloromelanite to omphacite. Characteristic features of metamorphic pyroxenes include (1) common occurrences of coexisting pyroxenes in Type II metabasites; (2) large compositional variations within a single specimen; and (3) progressive compositional trends in single specimens and in 3 metamorphic zones. Large compositional variations are believed due to combination of small-scale domain equilibrium, crystallization within a considerable large P-T range, and metastable equilibrium. Coexistence of two clinopyrosenes was used to establish compositional gaps between C2/c and P2/n.

Sodic amphiboles occur as (1) vein-fillings, (2) overgrowth on relict augites, (3) discrete tiny crystals in groundmass, and (4) composite crystals with metamorphic Ca-Na pyroxenes in low-grade rocks. They become coarse-grained and show strong preferred orientation in schistose high-grade rocks. As shown in Fig. 1, in the lowest grade, only riebeckite to crossite appears; with increasing grade, sodic amphibole first enriches in glaucophane component, later coexists with actinolite to define a compositional gap, and finally becomes winchite. Ca-amphibole first appears in foliated blueschists of the upper pumpellyite zone. It occurs (1) as interlayered on a millimeter scale with glaucophane prisms and (2) as segments of composite amphibole crystals. Both Ca- and Na-amphiboles possess similar optical orientation, but exhibit slightly different pleochroic color. Detailed analyses delineate a compositional gap for the coexisting sodic and calcic amphiboles. Three distinct amphiboles were identified in the upper epidote zone. Winchite appears between actinolite and glaucophane crystals or forms as discrete grains along foliation. Textural relationships suggest that winchite forms at the expense of the actinolite - glaucophane pair at the highest grade.

Common occurrence of Ca-Na pyroxene together with albite + quartz and both sodic and calcic amphiboles in the Ward Creek metabasites and their compositional trends are characteristics for the jadeite-glaucophane type facies series. In New Caledonia blueschist, Ca-Na pyroxenes are also common; but actinolite appears earlier than crossite-glaucophane in the progressive sequence. However, for metabasites of the intermediate pressure facies sereis such as those in Sanbagawa, Japan and New Zealand, Ca-Na pyroxene and glaucophane are not common; most sodic amphiboles are restricted to crossite and riebeckite in composition. Such differences in assemblage and compositional trends are consistent with P-T variations for sliding equilibria involving Ca-Na pyroxenes (e.g., Holland, 1983) and sodic amphiboles (e.g., Maruyama et al., in press).

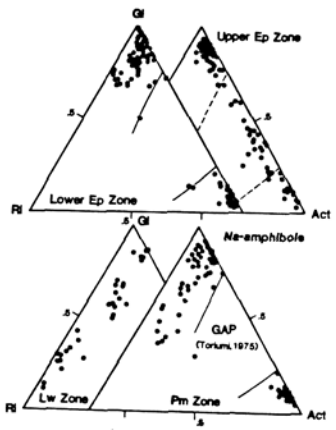

Fig. 1. Compositional variations of both sodic and calcic amphiboles from 3 zone metabasites from Ward Creek. Our data support the occurrence of a compositional gap in the pumpellyite and lower epidote zones.

REFERENCES

Holland, T. (1983) The experimental determination of activities in disordered and short-range ordered jadeitic pyroxenes. Contrib. Min. Petrol., 82, 214-220.

Maruyama, S., Cho, M. and Liou, J. G. (in press) Experimental investigations of blueschist-greenschist transition equilibria: Pressure dependence of Al_2O_3 contents in sodic amphiboles - a new geobarometer. Geol. Soc. Amer. Memoir 164.

Toriumi, M. (1975) Actinolite-alkali amphibole miscibility gap in an amphibole composite-grain in glaucophane schist facies, Kanto Mountains, Japan. Jour. Geol. Soc. Japan, 80, 75-80.

"MAGIC ANGLE SPINNING (MAS) HIGH RESOLUTION NMR SPECTROSCOPY AS A TOOL FOR STUDYING SHORT RANGE ORDER IN LAYER SILICATES"

LIPSICAS, M., Schlumberger-Doll Research, Old Quarry Road, Ridgefield, CT 06877-4108, USA

The position and width of the nuclear magnetic resonance (NMR) line in a solid is largely determined by the interaction of the nucleus with the near neighbor environment. In phyllosilicates, the relevant nuclear species with non-zero spin suitable for NMR experiments are ^{29}Si, ^{27}Al and ^{1}H (the proton). NMR studies of cation ordering in phyllosilicates are based on observations of the ^{29}Si and ^{27}Al spectra. The dominant nuclear interactions are:-

1. The "chemical shift" interaction which describes the electronic shielding of the nucleus by the surrounding electrons.
2. The nuclear dipole-dipole interaction with the neighboring nuclei.
3. The nuclear electric quadrupole interaction with the gradient of the local electric field. (This applies only to the case of ^{27}Al).

All these interactions are anisotropic and are greatly reduced by the Magic Angle Spinning (MAS) technique so that the observed ^{29}Si and ^{27}Al NMR lines are narrow enough to yield high resolution (parts per million) spectra. At this level of resolution it becomes possible to study the (remaining) isotropic chemical shift. Chemical shift data can be correlated with details of the chemical bonding and the near neighbor environment of the cation.

The conditions required to obtain adequate spectral resolution in ^{29}Si and ^{27}Al MASNMR will be discussed. The application of the technique to the study of short range cation ordering in mica - like minerals will be reviewed.

MULTIPHASE INCLUSIONS IN PLAGIOCLASE FROM THE STILLWATER ANORTHOSITES: IMPLICATIONS FOR REE GEOCHEMISTRY

LOFERSKI, P.J., U.S. Geological Survey, M.S. 954, Reston, VA 22092

Interpretation of rare earth element (REE) analytical data for samples from the two extensive anorthosite sheets of the Middle Banded Series of the Stillwater Complex, Montana, has proven to be complex. This and previous studies have documented low total REE abundances, seemingly random fluctuations with stratigraphic height, and a negative correlation with the amount of intercumulus pyroxene.

Mineralogical control on the anorthosite REE geochemistry is indicated by the presence of ubiquitous multiphase inclusions within cumulus plagioclase (Pl) grains. Individual multiphase inclusions consist of about 85% clinopyroxene (Cpx), 10% ilmenite (Ilm), and 5% Cl-apatite (Ap), a phase known to concentrate REE. The inclusions are commonly rounded, average from 10-50 μm, but locally vary up to several hundred μm across, and they generally occur closer to cores than rims of Pl grains, either singly, or in clusters. They are randomly distributed within and between samples. Microprobe analyses show that Cpx compositions range from Mg/Mg+Fe = 0.75 to 0.50 compared with 0.75 to 0.69 for the intercumulus Cpx. Furthermore, calcic Pl (An 90 to 95) forms 10 to 15 μm-wide rims around the inclusions, in contrast to Pl of An 75 to 85 throughout the rest of the grains.

Despite its low modal abundance (< 0.1%), the Ap inclusions may significantly affect the REE patterns for both whole rocks and mineral separates because of its affinity for REE and the general low concentration of REE in the anorthosites. Preliminary microprobe analyses show that the Ap contains about 1500 ppm Ce. Therefore, only 0.1% Ap is required to account for all of the Ce in the Pl mineral separates (an average of about 2 ppm) . The REE patterns clearly have Pl signatures (negative slopes and large positive Eu anomalies); however, the distribution of Ap within Pl may account for the erratic REE abundances and ratios in the anorthosites and the higher REE abundances in the Pl-rich as opposed to the pyroxene-rich samples.

The multiphase nature and constant modal composition of the inclusions imply that they were trapped as liquid globules that were enriched in Ca, P, Ti, and Fe relative to the liquid crystallizing the bulk of the Pl. Liquid immiscibility has been documented experimentally between Fe-rich liquids, similar in composition to the multiphase inclusions, and Si+alkali-rich melts in the system K_2O-Al_2O_3-FeO-SiO_2. Furthermore, Pl crystallization drives liquids toward the miscibility gap, and the Fe-rich melt fraction is enriched in REE. This suggests that a miscibility gap was intersected during the anorthosite crystallization, and that the multiphase inclusions were trapped as small immiscible globules that formed, possibly by boundary layer effects, at the margins of crystallizing Pl grains. The calcic Pl rimming the inclusions probably also crystallized from this liquid, as suggested by abrupt compositional breaks. Boundary-layer liquid immiscibility implies that the crystallization of Pl in the Stillwater anorthosites was rapid enough, and/or diffusion rates were slow enough for the Fe-rich globules to form. Interestingly, the inclusions are similar to nelsonites, Ilm + Ap -rich rocks, associated with massif-type anorthosites, and which are also attributed by some workers to liquid immiscibility. In both cases, the immiscibility is associated with the crystallization of abundant Pl.

Regardless of their origin, the fact remains that Ap-bearing inclusions occur within cumulus Pl grains in the anorthosites. They may occur in other areas of the Stillwater as well. Therefore, caution must be exercised when attempting to use REE abundances and ratios in order to model liquid fractionation trends, or when evaluating the possibility of multiple parental liquids in the Stillwater Complex.

THE ROLE OF HETEROGENEOUS NUCLEATION IN THE DEVELOPMENT OF IGNEOUS ROCK TEXTURES

LOFGREN, G.E., SN-4, NASA Johnson Space Center, Houston, TX 77058, USA

Heterogeneous nucleation (nucleation on a preexisting crystalline substrate) is an important factor in the development of igneous rock textures. In contrast, homogeneous nucleation is a rare event even in plutonic magmas. Nucleation in melts becomes increasingly difficult with the increasing complexity of the crystal structure of the precipitating phase. For a given driving force (e.g. supercooling) the mineral embryos (subcritical size nuclei) which can most readily add atoms or polymerized units from the melt, will nucleate at the expense of even more thermodynamically stable phases. Experimental observations verify that oxides nucleate more readily than olivine which nucleates more readily than pyroxene which in turn nucleates more readily than feldspar. This is true whether unmelted crystal remnants or a foreign substrate serve as the embryo. Crystal remnants, however, are energetically more favorable nucleation sites than a foreign substrate.

Heterogeneous nucleation behavior in response to the degree of supercooling is also an important variable. The most significant variable in heterogeneous nucleation is the size of the critical radius at which an embryo becomes a viable nucleus. In general, this radius decreases with increasing supercooling such that a slowly cooling melt with subcritical embryos may remain a glass while the same melt cooling more rapidly will crystallize, albeit with a texture representative of growth at a high degree of supercooling. A slowly cooled melt could also reach a sufficiently high degree of supercooling for embryos to become nuclei, and would also produce textures representative of growth at a high degree of supercooling. The ability of the slowly cooled melt to crystallize depends even more on the degree of recalescence (melting of the embryos during the early stages of the slow cooling) and whether the

melt becomes too viscous to crystallize before the embryos reach critical size.

Without heterogeneous nucleation most volcanic rocks would contain much more glass and many plutonic rocks would lack feldspar and quartz. All magmas are in continuous contact with crystalline material and most have originated by partial melting of such material. Either or both circumstances could introduce heterogeneous nuclei; nuclei free magmas are, no doubt, rare. The kind, size, and distribution patterns of these nuclei, which are the factors that control textures in rocks, will depend on the thermal and mechanical history of the magma prior to the final cooling event.

Most plutonic magmas are partial melts containing numerous crystals (crystal mush) and nucleation is not a problem. Relatively nuclei-free magmas in slowly cooled plutonic environments may become significantly supercooled before growth from the few nuclei begins and produces unusual textures such as comb-layering.

In basaltic rocks, experiments have shown that plagioclase would crystallize with radiate or spherulitic crystal forms unless heterogeneous nuclei for feldspar are present. The spinifex textures in the central portions of komatiitic flows can develop only if all nuclei are removed from the spinifex zone. This is accomplished by crystal settling. The magma in this zone can then supercool sufficiently to support the relatively rapid growth rates necessary to produce the spinifex textures in spite of the slow cooling rates present in this zone.

In more silicic rocks, feldspar is often present only as phenocrysts which represent a subsurface event. Feldspar microlites may represent embryos which become nuclei at moderate degrees of supercooling perhaps associated with movement of the magma in conduits to the surface. Obsidian represents essentially nuclei-free, granitic magmas which could have cooled relatively slowly and remained glassy. The spherulites often present in obsidians represent embryos which became nuclei at very high degrees of supercooling.

PETROGENESIS OF RARE-ELEMENT PEGMATITES: EVIDENCE FROM FLUID INCLUSIONS AND PHASE EQUILIBRIUM EXPERIMENTS

LONDON, DAVID, School of Geology and Geophysics, University of Oklahoma, Norman, OK 73019

Pegmatites represent the ultimate products of fractionation in plutonic silicic magma systems. Highly fractionated rare-element pegmatites are enriched in a number of incompatible lithophile elements (e.g., Li, Rb, Cs, Be, Ga, Sn, W, Nb, Ta) and volatile components (e.g., H_2O, B, F, P) by 10^4 - 10^6 above their average abundances in typical granitic plutons. Such pegmatites constitute an important link between magmatic and hydrothermal processes, and they hold a wealth of information on the geochemical behavior of these economically and petrologically important lithophile components.

Rare-element pegmatites are typically lithium-rich and contain one or more of the lithium aluminosilicates petalite ($LiAlSi_4O_{10}$), spodumene ($LiAlSi_2O_6$), and eucryptite ($LiAlSiO_4$). Experimental calibration of the phase relations among these and other lithium minerals has yielded a petrogenetic grid by which the P-T conditions of pegmatite consolidation can be ascertained. Primary crystallization of lithium-rich rare-element pegmatites occurs between 450°-650°C and pressures of 250-450 MPa. Spodumene-bearing pegmatites form at higher pressures than those that contain only petalite. Subsolidus recrystallization (e.g., formation of eucryptite + quartz assemblages) is operative to approximately 300°C, 160 MPa or lower. Retrograde alteration involves alkali metasomatism, followed by acidic metasomatism.

Lithium aluminosilicate stability relations can be combined with fluid inclusion analysis to assess fluid compositions and crystallization sequences with decreasing P-T conditions. Rare-element-rich hydrous silicate fluids may exist down to temperatures of 450°C at fluid pressures of 250 - 450 MPa. Although H_2O is an important component of these late-stage fluids, boron and fluorine play especially important roles in promoting solidus depression, enhanced silicate liquid - H_2O miscibility, decreased viscosity, and concentration of lithophile rare elements through melt depolymerization. Chlorine is a negligible component of most fractionated pegmatitic fluids. In principle, the transition from magmatic to hydrothermal conditions may be continuous (i.e., supercritical), partly because the instability of tourmaline promotes concentration of boron in fractionated liquids. The accumulation of boron enhances H_2O and lithophile element solubilities in residual fluids. A major cause of discontinuous fluid behavior (i.e., silicate fluid - H_2O unmixing) is the loss of the components B and F from late-stage fluids when tourmaline and micas crystallize. As a consequence, rare-element-rich aluminosilicates and oxides are deposited along with feldspars and quartz, and low-density, solute-poor aqueous fluids are exsolved. This process contributes to the generation of gem-bearing miarolitic cavities.

Preliminary phase equilibrium experiments with the rare-element-rich Macusani rhyolite as starting material corroborate many of the above observations on crystallization and fractionation within lithium-rich pegmatites. At 200 MPa H_2O, the liquidus of the Macusani rhyolite occurs at about 650°C, and the solidus lies below 500°C. The naturally high contents of boron and fluorine increase melt depolymerization and crystal growth rates, and decrease nucleation densities. In H_2O-saturated runs of short duration, both quartz and (subsolvus) feldspars grown by supercooling of 100°C below liquidus saturation temperatures form large (200 microns), sharply euhedral crystals. Muscovite saturation is driven in part by the speciation of Na with F and B(?), and the creation of peralkaline residual fluids. Additional details of this experimental research will be presented at the meeting.

QUANTUM MECHANICAL CALCULATIONS OF STRUCTURAL PROPERTIES OF MATERIALS*

LOUIE, STEVEN G. and COHEN, MARVIN L., Dept. of Physics, University of California, and Materials and Molecular Research Division, Lawrence Berkeley Laboratory, Berkeley, CA 94720, USA.

Because of recent advances in condensed matter theory, it is now possible to explain and predict the structures and properties of materials with only information about the constituent atoms. Using ab initio pseudopotentials and total energy schemes, calculations have been performed for the electronic, structural, vibrational, and superconducting properties of a number of crystals. Results for some prototype materials will be presented to illustrate the applicability of the method to metals, semiconductors, and insulators.

Recent theoretical studies on the properties of solid-solid structural phase transitions will be highlighted. Calculated transition volumes, pressures, and the structural properties of the low and high pressure phases are shown to be in excellent agreement with experiment. In addition, some predictions of new structural phases have been verified.

*This work was supported by National Science Foundation grant No. DMR83-19024 and by the Director, Office of Energy Research, Office of Basic Energy Sciences, Materials Sciences Division of the U.S. Department of Enerty under Contract No. DE-AC03-76SF00098.

•SERIES AND CHARACTER OF VOLCANIC ROCKS IN NEGARI, TIBET, CHINA

LU Fengxiang, Department of Geology, Wuhan College of Geology, Wuhan and ZHAO Chonghe, Beijing Graduate School, Wuhan College of Geology, Beijing, People's Republic of China

The Negari region can be divided into four tectonic zones: The Kelakunlun zone, the Gangdisi zone, the north Himalayan zone, and the high Himalayan zone from north to south. The earliest volcanic suite (Premo-Triassic) is represented by the Duoma basic volcanics which are exposed in the Kelakunlun zone. It is a tholeiitic-alkali basalt and a type of relatively stable environment. The second suite is most extensive and is represented by two areas in Gangdisi zone, Bangong Lake-Ritu and Lameila-Shiqianhe areas. The age of these volcanics has been considered to be lower Cretaceous. This suite consists of lava (meta-basalts, olivine basalts, diabases, dolerites, andesites, dacites), hypabyssal equivalents, and a few pyroclastic rocks. These volcanic rocks are accompanied by peridotites, serpentines, cumulates, clastic sedimentary rocks, limestone, and radiolarites; therefore, this suite constitutes the major geological unit within the Ritu, Lameila and Shiqianhe ophiolite belts. The third suite in the eastern part of Gangdisi zone is called the Shiduo volcanics in which andesites, dacites, rhyolites, and ignimbrites are predominant over basalts. This volcanism took place from upper Cretaceous to Tertiary time. The fourth suite, including altered basalts and diabases, is very limited in the north Himalayan zone. Its age is Triassic.

In the second suite a few metabasalts yield the lowest K_2O (0.19, 0.040) and a flat REE pattern. However, K_2O, Na_2O, FeO, TiO_2, and P_2O_5 of most of these basalts are higher than those of typical oceanic ridge basalts and similar to those between island arc tholeiites and continental tholeiites. On the other hand, most of the basalts are enriched in Rb (up to 59 ppm), Ba (up to 401 ppm), and LREE (La/Yb 4-18.2). All the data (the plots in ACF, SiO_2-K_2O+Na_2O, FeO/MgO-SiO, etc. diagrams) support the fact that the second suite belongs to an orogenic tholeiite series (TH) and could represent the production of a tensional environment.

The evolution of this magma series was mainly controlled by crystal fractionation involving olivine, pyroxene, and not many iron ores. As a result, a few andesites and dacites were produced. The lowest evolved basalts which have higher MgO (9.14) Cr_2O_3NiO content, Mg/(Mg+Fe)=0.65-0.69 and relatively lower ΣREE (38.13) have been discovered. In the Harker and ACF diagrams, the fractional lines of descent are very clear.

In contrast, the diagrams as mentioned above show the third suite belongs to the calc-alkali series (CA). ΣREE and LIL are higher than those in TH with the same SiO_2 content; Ni is also higher with the same MgO; FeO/MgO is lower than that in TH, fO_2 estimated in basalts of CA are higher (-3.96, -9.47) than that (-13.2) in basalts of TH.

Magma mixing and asimilation are more important petrogenetic processes in the CA series rocks. The xenolithic crystals of quartz have been observed in basalts and andesites very commonly. In olivine andesites there are phenocrysts of olivines and two kinds of plagioclases: euhedral labradorite (An_{53}, 0.5-0.7mm) and andesine (An_{47}, 1-2mm) including a lot of glass inclusions and with sieve texture. The olivine + labradorite and rounded andesine represent the phenocrystal assemblages of basalt and andesite, respectively. According to the calculation of a magma mixing model, these olivine andesites were made up of 35% basalts (lowest evolved basalt) and 75% higher silica andesite (the product of differentiation). This process can be called mixing- fractionation or insidious mixing of consanguineous magma (D.Walker, 1983).

A large number of dacites and rhyolites in CA imply that there was another source of magma in the crust besides the mantle. The evidences of mixing between two magmas from two sources are also observed; for example, basaltic inclusions with plastic form are retained in dacites and rhyolites. It seems quite possible that the processes of magma formation in CA were more complicated than that in TH.

We consider that the Ca series was generated in a compressional environment when the collision took place between India and Tibet platforms in the upper Cretacious to Tertiary.

•THE DISCOVERY OF PENTLANDITE IN DEEP-SEA COSMIC SPHERULES

LU Kang and PENG Hanchang, First Institute of Oceanography of State Oceanic Administration, Qingdao, P.O. Box 98, LIU Zhenkun, Institude of Hunan Metallurgical Industry, Changsha, ZHIFANG Chai, Institute of High Eenrgy Physics, Academia Sinica, Beijing, ZHUANG Shijie, China National Nonferrous Metals Industry Corp., Research Institute of Geology for Mineral Resources, Guilin, YU Zhong, Institute of Petroleum Exploration and Planning, Beijing, People's Republic of China

Recently, we found a few silicate spherules with golden inclusion in deep-sea sediments from the Northern Pacific (lat 7°-11°N, long 158°-178°W). The inclusions have unique surface features. For example, they are round spherules, golden in color, have strong metallic luster, and there are many parallel canals on the surfaces. Due to hardness of inclusions higher than crusts (olivine), inclusions were often broken away from the crusts (Fig. 1-A), the Ni elements being highly concentrated in the inclusion (Fig. 1-B). The results of electron probing analysis showed a primary chemical composition of pentlandite.

The discovery of pentlandite in deep-sea cosmic spherules is of significance for further investigation of the origin and formation of marine processing of cosmic spherules.

References

Brownlee, D.E., 1981, Extraterrestrial components. The Sea, 7, 733-762.

Millard, H.T. and Finkelman, R.B., 1970, Chemical and mineralogical compositions of cosmic and terrestrial spherules from marine sediment. J. Geophys. Res., 75, 2125-2133.

Figure 1. Photograph of silicate spherule with golden inclusion (A) and its NiKα planar distribution (B). [Not reproducible]

Figure 2. Distribution of Fe, Ni and S in pentlandite. [Not reproducible]

METHODS FOR COMPARING MAJOR-ELEMENT CHEMISTRY OF IGNEOUS ROCKS

LUDINGTON, STEVE, U. S. Geological Survey, Reston, VA 22092

The most widely available chemical data for igneous rocks are analyses of Si, Al, Fe, Mg, Ca, K, and Na. These data have been compared graphically in many ways, though entire provinces have seldom been portrayed. Petrologists seeking comparison with the suites that they study have been hampered by the lack of readily available and manageable data sets. The availability of microcomputers and computer-readable data has made the job easier.

This paper presents the first results of an attempt to provide a readily accessible group of diagrams for comparison and to determine which common variation diagrams are most useful. A microcomputer and a published database were used to study data from seven petrologic provinces in North America, the Cascades volcanic field (CAS), Sierra Nevada Batholith (SRN), Boulder Batholith (BLB), Idaho Batholith (IDB), San Juan volcanic field (SAJ), Davis Mountains (Trans-Pecos) volcanic field (DAV), and Pikes Peak Batholith (PPG). Tectonic environments range from a compressional continental margin subduction zone (CAS) to an extensional anorogenic stable craton (PPG) and the analyses should represent much of the range of composition found in continental igneous rocks. The data are taken from PETROS (Mutschler and others, 1978), a compilation of more than 34,000 major element analyses.

For plotting, all analyses were recalculated to total 100% volatile-free. A small percentage of analyses was culled from the database using the following criteria: 1) volatile-free (not normalized) summations <96% or >102%, 2) SiO_2>82%, 3) outliers on a plot of SiO_2 vs. K_2O+Na_2O, and 4) assorted extreme outliers on other plots. Trends were extracted from the data using moving averages, after initial attempts to fit regression lines yielded poor results.

Smoothed Harker plots (individual oxides vs. SiO_2) were prepared for each province, and the trends for each element were then evaluated separately. The Al_2O_3 curves for all provinces are very similar to each other, and show either no change or a slight increase with respect to silica until 65-70% SiO_2, after which they all decrease continuously. IDB has the highest values over most of the range, though DAV, which has the lowest values at SiO_2>66%, has the highest values near SiO_2= 60%. Total iron decreases continuously and shows little difference between provinces. DAV is lowest in iron at 56%<SiO_2<60%, but highest at SiO_2>66%. Both iron and aluminum show much greater differences among samples within provinces than between provinces and, for the provinces studied, would serve as well as silica for an index. The shapes of CaO and MgO curves are very similar to each other. Both decrease continuously with silica for all provinces. DAV and PPG show distinctly lower values of CaO and MgO than the

other provinces; SAJ is generally the lowest of the other five. Na_2O shows relatively little change with silica within suites, though differences between suites are quite pronounced. DAV and PPG contain 5-6% Na_2O whereas IDB analyses are near 2%. SAJ is lower in Na_2O than SRN, BLB, and CAS. The greatest distinction between suites is shown by K_2O. DAV and PPG have the highest values for most silica compositions, and show a distinctive decrease in K_2O at SiO_2>70%. SAJ is the highest of the remaining five provinces, and at high silica contents, K_2O in SAJ continues to increase and is higher than DAV or PPG. In decreasing order of potassium content, the remaining suites are BLB, SRN, IDB, and CAS. K_2O content at SiO_2=57.5% ranges from 1.3% for CAS to 4.7% for DAV.

On plots of K_2O+Na_2O and CaO vs. SiO_2 (Peacock diagram), CAS, SRN, BLB, and IDB all yielded intersections near SiO_2=61% and K_2O+Na_2O=CaO=6%, very near the calc-alkalic/calcic boundary. Only CAS plots in the calcic field. DAV and PPG intersect near 50,7, distinctly in the alkalic field. SAJ again appears to be transitional, plotting near the calc-alkali/alkali-calcic boundary, at 56,6.5.

The alkalis-iron-magnesium (AFM) ternary diagram, often used to distinguish calc-alkaline trends from tholeiitic trends, shows surprisingly small differences between provinces, and is of little use in distinguishing them. CAS, SAJ, SRN, BLB, and IDB plot virtually on top of each other, barely within the calc-alkaline field, whereas DAV and PPG plot only a few percentage points distant, just along the calc-alkaline/tholeiitic boundary.

A calcium-iron-magnesium (CFM) ternary was plotted for each province because detailed variations in these elements on Harker diagrams suggested that distinctions between provinces might be thus accentuated. This is not the case. Though outliers are more common, the results are closely analagous to those for AFM. Except for the most felsic compositions, which trend toward the iron corner, CAS, SAJ, SRN, BLB, and IDB trends remain largely within C35-45-F40-50-M5-25. DAV and PPG trends exceed F70, but are otherwise not distinguishable from those for other provinces.

It is unfortunate that the constituents most useful in distinguishing rock suites (K and Na) are the very constitutents that are most amenable to alteration and that show the most variation within provinces. The decrease in K_2O shown by anorogenic suites and the absolute values of K_2O are the most distinctive features of the diagrams examined so far.

In general, the differences in major element chemistry are larger between igneous rocks within a given petrologic province than they are between provinces, and many commonly used variation diagrams do not show clear-cut differences between provinces. Extreme care must be used in distinguishing tectonic environments based on these diagrams. Meaningful distinctions cannot be made without an appreciation of the variability of a rock suite, and to attempt distinctions on the basis of a handful of samples will often lead to unsupportable conclusions.

ELECTRON MICROPROBE ANALYSIS OF FELDSPARS AND MICAS FROM THE HARDING PEGMATITE, TAOS COUNTY, NEW MEXICO

LUMPKIN, Gregory R., Department of Geology, University of New Mexico, Albuquerque, NM 87131

Feldspars and micas from several lithologic units of the Harding pegmatite have been analyzed for major and minor elements using a JEOL 733 operated at 15 keV, 20 nA, and 10 µm beam diameter. In the feldspars, MgO, MnO, FeO, SrO, BaO, and PbO were not detected at the 0.02 wt.% level. Rb_2O is present at 0.3-0.7 wt.% in K-feldspar but was not detected at the 0.03 wt.% level in albite. Average end-member compositions (200 analyses) are given for four lithologic units in Table 1. K-feldspars in the quartz-lath spodumene zone and the microcline-spodumene zone ("spotted rock") have the highest Ab and Rb contents. Maximum values of 10 mole % Ab and 2 mole % Rb were found for these two lithologic units. Lower Ab and Rb values were found for K-feldspars from the cleavelandite replacement unit. Albites from the quartz-lath spodumene and microcline spodumene zones have higher Or and An contents than those of the cleavelandite unit. Albites have a maximum An content of 5 mole % in the quartz-lath spodumene zone and a maximum Or content of 1 mole % in the microcline-spodumene zone. Two-feldspar pairs in apparent textural equilibrium were used to calculate temperatures assuming a pressure of 3-4 kb. The quartz-lath spodumene zone gives a temperature of 365-390°C with a few values near 460-485°C. Limited data suggest a bimodal temperature distribution of 345-370°C and 435-460°C for the microcline-spodumene zone. The cleavelandite unit gives temperatures of 350-375°C in the beryl zone and 325-350°C in the core of the pegmatite. Two-feldspar temperatures are currently interpreted to reflect primary equilibration of feldspars at ∿450°C followed by re-equilibration at ∿350°C during pervasive albitization.

Average compositions of micas (210 analyses) are given by lithologic unit in Table 2. CaO, SrO, BaO, and PbO were not detected at the 0.02 wt.% level. H_2O was estimated by calculating the amount of OH necessary to give F + OH = 2.00 in the structural formula and Li_2O was estimated by difference. Results indicate that the inferred Li_2O contents show a good 1:1 correlation with observed F content. Muscovites contain 0.2 -1.0 wt.% MnO, 0.0-1.3 wt.% FeO, 0.2-0.7 wt.% Na_2O, 0.3-0.7 wt.% Rb_2O, and 0.0-2.0 wt.% F. Lepidolites contain 0.7-2.1 wt.% MnO, 0.3-2.1 wt.% FeO, 0.1-0.4 wt.% Na_2O, 0.7-1.1 wt.% Rb_2O, and 3.0-6.5 wt.% F. The major difference in composition between micas from different lithologic units is an elevated FeO/MnO ratio in samples from the cleavelandite replacement unit. Typically <0.3 in other lithologic units, FeO/MnO approaches 2.0 in muscovite and 1.0 in lepidolite in the cleavelandite unit. These values are much like the FeO/MnO ratios in crystal rims and altered areas of microlite from the cleavelandite unit. Low FeO/MnO ratios are found in microlites from other lithologic units. Structural formulas of the micas range from near end-member muscovite to near end-member trilithionite with 10-20 mole % polylithionite in intermediate compositions. A few analyses lie near the trilithionite-polylithionite join, approaching 60 mole % polylithionite. Interlayer cation totals range from 0.92 to 0.98 atoms per formula unit.

Table 1. Average microprobe analyses of feldspars (mole %).

	K-Feldspar			Albite		
Lithologic Unit	Or	Ab	Rb	Or	Ab	An
Quartz-Lath Spodumene	93.5	4.6	1.9	0.6	97.4	2.0
Microcline-Spodumene	93.1	5.4	1.5	0.8	98.6	0.6
Cleavelandite/Beryl Zone	94.4	4.3	1.3	0.4	99.1	0.5
Cleavelandite/Core	95.4	3.4	1.2	0.4	99.1	0.5

Table 2. Average microprobe analyses of micas (weight %).

Lithologic Unit	MnO	FeO	Na_2O	Rb_2O	F	(Li_2O)	*
Quartz-Lath Spodumene	0.98	0.41	0.16	0.91	5.3	4.8	L
	0.41	0.17	0.34	0.54	0.48	0.4	M
Microcline-Spodumene	0.33	0.12	0.31	0.43	0.28	0.2	M
Lepidolite-Cleavelandite	1.50	0.43	0.27	0.85	4.9	4.4	L
	0.28	0.13	0.59	0.49	1.0	1.2	M
Cleavelandite/Beryl Zone	0.63	0.22	0.33	0.48	0.58	0.6	M
Cleavelandite/Core	1.68	1.63	0.15	0.88	5.0	5.8	L
	0.39	0.61	0.32	0.44	0.52	0.6	M

* L = Lepidolite, M = Muscovite

•THE TELLURIDES IN THE GOLD DEPOSITS OF CHINA

LUO Zheng-Kuan, Tianjin Geological Academy, 42 Youyi Road, Tianjin, People's Republic of China

There are minor tellurides in most primary gold deposits in China, but only in some deposits are these important ore minerals. Boyle (1979) discussed the occurrence of tellurides, pointing out that they often occur in the gold deposits related with volcanic rocks, such as the well known Archean greenstone-gold deposits of Kirkland Lake, Ontario, and Flin Flon, Manitoba, Canada; Kalgoorlie, Australia; and in some deposits related with younger volcanic rocks (Tertiary), such as Cripple Creek, Colorado, Brad and Nagyag, Romania, Vatukola, Fiji, and others.

The gold deposits in which tellurides are found in China are of three types:

(1) Quartz-vein type gold deposits, occurring in metamorphic rocks of the Archean; for example, Yangzaiyu deposits, Henan Province.

(2) Altered-fragmented zone-type gold deposits, occuring in intermediate-basic rocks of the Proterozoic; for example, Shang Gong gold deposit, Henan Province.

(3) Epithermal gold-silver deposits, related to younger (generally Jurassic) volcanic rocks, for example, Yinkengshan gold-silver deposits, Zhejiang Province.

The tellurides found in the gold deposits are calaverite, petzite, sylvanite, hessite, altaite, tellurobismuthite, tetradymite, volynskite, melonite, coloradoite, and rickardite. Tellurides occur as the interstitial fill of pyrite and in the fractures of pyrite as intergrowth and secondary inclusions, and are often found associated with native gold.

In the Yinkengshan deposit, it seems that silver is first combined with tellurium as hessite, then with gold as petzite and calaverite, and native gold is formed when tellurium is exhausted. Tellurides and selenides are found in the same deposits but they are not associated with each other, due to being formed in different mineralization stages.

THE CONSTITUTION AND GENETIC MARKS OF RARE-EARTH MINERALS IN THE WESTERN ORE AREA OF BAIYUN EBO

MA Fengjun and SUN Weijun, Tianjin Geological Academy of the Ministry of Mettallurgical Industry, 42 Youyi Road, Tianjin, People's Republic of China

[By title only.]

• FABRIC CHARACTERISTICS AND MINEROGENESIS OF COPPER AND NICKEL SULFIDE ORES IN A DEPOSIT OF XINJIANG

MA Xinxing, Bureau of Geology and Mnieral Resourses, Xinjiang, People's Republic of China

The ore-bearing rock bodies are small in scale but with higher Cu-Ni content, and they are slightly differentiated. They occur chiefly in olivine norite and gabbro-norite. The ore bodies can be separated into three types:

I Liquation, II Injected, III Metasomatized.

The ore can be separated into nine types: massive, brecciated, seemingly striped, impregnation, spongy and meteoritic iron formation, taxite, star point, veinlet-stockwork, and cloudy-fog form. There are various ore textures, with the most common ones those formed by differentiation of soild solution. The characteristic textures are emulsive drop, nodular, chain form, flame form, plumose, foliaccous, grating, skeleton texture, interstitial texture, replacement-graphic texture, porodine texture and griddle texture.

The composition of the ore is very complicated, with more than fifty minerals present. Besides the Cu-Ni-minerals, there are noble metals, Co, Te, Se, Bi, and Pb. The ore contains djerfisherite, a rare mineral, along with various transitional types of polydimite and violarite.

There are three metallogenic periods (magmatic, hydrothermal, and hypergene) and four stages (early stage of liquidation, later stage of magma injection, hydrothermal metasomatic of high to middle temperature, and hypergene stage).

Conclusions: (1) Dissemination of the ore body is related to magma liquidation. (2) The injected ore body is controlled by the fractures within the rock body and related to the injection of deep liquidational mineralized magma. (3) The last metallogenic stage entered into the hydrothermal stage. (4) The metasomatic-type ore body not only occurs in the rock body but also in the country rock. (5) The temperature of mineralization is thought to be about 600-425°C.

ELECTRON PROBE MICROANALYSIS OF SUBSURFACE PHASES: AN EMPIRICAL APPROACH

MAASKANT, P., Institute of Earth Sciences, De Boelelaan 1085, 1081 HV Amsterdam, The Netherlands

Petrographic studies may reveal phases which, by their very nature, are never found at the surface in thin sections (eg. fluid inclusions). Moreover, grinding and polishing procedures easily destroy solid phases and brines, which can be present in these inclusions. A laser Raman-microprobe identifies solid, subsurface phases with a molecular bond, but does not provide direct chemical information. A scanning electron microscope, with an energy-dispersive detection system, gives a chemical analysis when the inclusion has been opened. In the present study experiments were carried out to investigate the possibilities of (semi-) quantifying electron microprobe data from subsurface phases.

Crystal fragments of biotite, spinel, almandine and pyrope garnet, jadeite, sylvite, and synthetic CdS were adjacently mounted in an epoxy resin block. This was sawn into several pieces, each then remounted in a brass ring of one cm diameter, ground and polished.

A Leybold-Heraeus HV25 electron gun was thence used to coat the various samples with SiO_2 layers of varying thickness by evaporation of quartz glass (ρ = 2.20 g/cm^3). Before coating, each sample was dried at 90° C for about 4 hours in order to disperse any adsorbed water vapour. Vacuum pressure during coating was about 5.10^{-6} Torr, target temperature was 20° C and evaporating velocity about 50 Å/sec. Thickness was determined with an Inficon-XTM quartz thickness monitor with an estimated accuracy of 3%. Density of the SiO_2 layer was checked by measuring the refractive index using immersion liquids, while the chemical composition was monitored with the electron microprobe. Despite of precautions taken, the adherence of SiO_2 layers to the various phases proved quite variable: none for sylvite, poor for CdS and jadeite, moderate to good for the other minerals. Mineral inclusions in quartz were thus simulated, situated at known depths below the surface: 0.9, 1.9, 2.9, 3.7, 4.5, and 7.9 µm, recalculated on a ρ = 2.65 g/cm^3 basis. All samples were subsequently coated with approximately 200 Å of carbon.

The analyses were carried out using a Cambridge Instruments Cy Microscan 9, with two crystal spectrometers and a take-off angle of 75°; probe currents varied from 20 to 50 nA dependent on the kV used. Six samples at a time could be placed in the holder and analysed for the major elements at accelerating voltages which varied from 15 to 40 kV in steps of 5 kV, using a non-SiO_2-coated sample as reference standard. The 7.9 µm sample was analysed separately.

Ratios of background-corrected values for coated vs. non-coated samples were plotted against depth. The figure for 40 kV is given below: it shows that when the Si ratio is - for example - 80%, analysed Fe and Mg contents should be multiplied by 1/0.32 and 1/0.08, respectively.

This study shows the possibility to estimate elemental compositions in fluid inclusions in a non-destructive way to a depth of 5-7 µm.

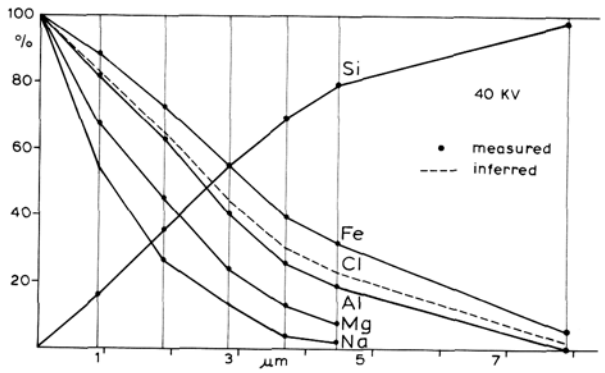

DETERMINATION OF MOLECULAR COMPOSITION OF 5-COMPONENT GARNETS BY GRAPHICAL PROCEDURES

MADUREIRA Fº, J.B. & CAMARGO, W.G.R. de; Dept. of Mineralogy & Petrology, Institute of Geosciences, University of São Paulo, São Paulo, SP, C.Px. 20.899, Brazil.

The physical properties may convey to the determination of composition of mineral solid solutions through 2-, 3-, 4-, or 5-component diagrams.

The 5-component diagram, here presented for the garnet group, is a regular pentagon, whose vertices indicate 100% of end-member of almandine (Alm), andradite (And), spessartite (Sp), grossular (Gr) and pyrope (Py), whose compositions and respective physical constants are according to Table 1:

Table 1*

	D	n	Δd(A)	composition
A-almandine	4.318	1.830	0.766	$Fe_3Al_2Si_3O_{12}$
B-andradite	3.859	1.887	0.649	$Ca_3Fe_2Si_3O_{12}$
C-spessartite	4.190	1.800	0.745	$Mn_3Al_2Si_3O_{12}$
D-grossular	3.594	1.734	0.693	$Ca_3Al_2Si_3O_{12}$
E-pyrope	3.582	1.714	0.781	$Mg_3Al_2Si_3O_{12}$

In a given diagram of any kind, a composition should correspond to one point in the diagram (entry), and this same point should turn back to the original composition (return).

The entries are necessary in order to draw in the graph, the contour lines of the physical property variations (D, n, Δd), and the returns are needed for the determination of molecular compositions, from the known sample physical constants.

In order to enter into a pentagon diagram, the following steps should be pursued for a given composition: 1) the pentagon is divided into 10 interpenetrated isosceles triangles; 2) the proposed 5-component composition should be separated into 10 ternary compositions, which are adjusted to 100% (Tab. 2); 3) the 3-component compositions are plotted in the respective triangles, selecting however only the points located simultaneously in the same group of triangles (2, 3, or more points) (the experience shows that the remaining points are of no significance); 4) the center G of the figure formed by the chosen points is the point representing the 5-component proposed molecular composition.

Table 2

	A	B	C	D	E		A	B	C	D	E
ABC	68.7	20.5	10.8	-	-	ADE	77.0	-	-	8.1	14.9
ABD	71.3	21.2	-	7.5	-	BCD	-	53.1	28.1	18.8	-
ABE	67.1	20.0	-	-	12.9	BCE	-	46.0	24.3	-	29.7
ACD	79.2	-	12.5	8.3	-	BDE	-	50.0	-	17.6	32.4
ACE	74.0	-	11.7	-	14.3	CDE	-	-	34.6	23.1	42.3

The reverse route, that is, from the point G (as determined by the sample physical constants) to the molecular composition, is given by only two steps: 1) ternary compositions, related to G, should be determined in the triangles to which G belong simultaneously ; 2) such ternary compositions indicate the 5-component composition according to computation on Table 3. The Table 3 indicate the results for a garnet sample, whose physical constants are D= 4.130 ; n= 1.811 and Δd= 0.749A.

The composition obtained graphically (line 1 - Table 3) compared with the original proposed molecular composition (line 2 - Table 3), gives a good idea of viability of the presented graphical method.

Table 3 - 5-component composition according to G

	A	B	C	D	E	
ABC	79.3	8.7	12.0	-	-	
ABD	70.3	22.0	-	7.7	-	
ABE	57.7	29.6	-	-	12.7	
No readjusted comp.	69.1	20.1	12.0	7.7	12.7	
Readjusted comp. 100%	56.8	16.5	9.9	6.3	10.5	(1)
Original proposed comp.	57.0	17.0	9.0	6.0	11.0	(2)

* Definitions of constants mentioned in Table 1
D= specific gravity; n= index of refraction;
Δd= d(10$\bar{1}$1) quartz - d(420) garnet

WAXING AND WANING MAGMA CHAMBERS: A COMPARISON OF ZONING IN IGNIMBRITES AND PLUTONS

MAHOOD, G., Geology Dept., Stanford Univ., Stanford CA 94305 USA

Nearly all voluminous ignimbrites are compositionally and mineralogically zoned from silicic bases to more mafic tops, indicating that, at the time they are tapped by eruptions, silicic to intermediate magma chambers are zoned with cooler, more felsic, volatile-rich, and phenocryst-poor magma near the roof. Vertically zoned plutons--those with the most felsic material at the roof, grading downward to more mafic material--record the same zonation inferred from ignimbrites. Eruptions from chambers in which felsic magma occurs at all margins and passes into mafic material coreward could also produce ignimbrite zonations. Many mafic coreward plutons, however, probably represent rearrangement of a vertical pattern during emplacement. Felsic magma beneath more mafic magma in lower contacts of sill-like lobes is gravitationally unstable; such felsic margins must have quenched in place. Nearly all mafic coreward and many vertically zoned plutons form central intrusions of calderas. Thus these magmas were emplaced at high levels into crust fractured by caldera collapse, which allowed rapid cooling by hydrothermal circulation. Additionally, synresurgence volcanism associated with emplacement of these bodies may pressure-quench them by loss of magmatic volatiles, causing them to "freeze" in place.

In contrast to high-level plutons, plutons emplaced at sufficiently great depths that associated volcanic rocks are lacking and roofs are rarely preserved are commonly zoned from mafic walls to felsic cores. The sense of zoning in these felsic coreward plutons is not analogous to that in most ignimbrites. (A few ignimbrites are "reversely zoned", i.e., the most mafic material erupted first, but it has not been established whether the mafic magmas were wall cumulates or were tapped first when a conduit intersected a vertically zoned chamber beneath its apex.) Zonation in felsic coreward plutons probably results from early-formed crystals adhering to walls, while differentiated liquids rise as boundary layers or are absorbed by a central convecting body. In some cases, the felsic phenocryst-poor core may detach from the crystallizing carapace to rise en masse, imparting a foliation to partially crystallized magma and producing internal contacts and sawtooth patterns of element abundances in horizontal slices through the pluton. If a mobilized core were to escape to higher levels, it might form a mafic coreward pluton.

Development of the contrasting zoning patterns--vertical versus felsic coreward--is a function of both depth and time. The waxing stage of a magmatic system is characterized by vigorous addition of heat by mafic magmas. Convection maintains a near-adiabatic gradient within a chamber and, together perhaps with migration of volatiles to the roof, suppresses crystallization there. Crystallization along the walls at deeper levels produces differentiated magmas that rise to form a vertically zoned cap. Ignimbrite-forming eruptions tap this cap but rarely draw down to cumulate magma. Hybridization of the felsic layers in the cap is inhibited by their high viscosities. It can occur if pluton cooling times are long (i.e., deep and/or large chambers) or if mechanical mixing is promoted by venting of a part of a chamber, stoping of large wallrock blocks, or collapse of a chamber roof during caldera formation. Strong thermal contrasts with wallrocks may promote liquid-state diffusion. Contamination is likely during this waxing stage due to the relatively large heat content of undifferentiated magmas. As a system wanes thermally, the zone of marginal accretion of crystals expands horizontally and vertically, overprinting a previously established vertical zonation. This crystalline carapace protects the magma from further interaction with wallrocks. Magmas produced during the waning stage are poorly represented in the volcanic record, as crystal-rich magmas are mechanically inhibited from eruption. Products of the waxing stage, on the other hand, commonly erupt as zoned ignimbrites, but are preserved in plutons only if chambers cool quickly.

Only high-level plutons are likely to contain rocks that reflect liquid compositions. Most plutonic rocks formed at greater depths are to some extent cumulates and therefore cannot be used to define a liquid line of descent. Straight lines on variation diagrams for plutonic suites may reflect mixtures of cumulate phases with variable proportions of differentiated liquids, rather than mixing between magmas. The more felsic rocks in a felsic coreward pluton probably resemble liquid compositions more closely than the mafic and intermediate rocks because separation of liquids from crystals will become less efficient as the silica content of the liquids increases.

CATION ORDER-DISORDER IN OCTAHEDRAL SITES (M1,M2 AND M3) OF HORNBLENDES

MAKINO,K.,Dept. of Geology and Mineralogy,Kyoto University,Kyoto 606,Japan;TOMITA,K.,Dept. of Geology and Mineralogy,Kyoto University,Kyoto 606 ,Japan

Ca-amphiboles have simillar octahedral sites,designated M1,M2 and M3. In hornlendes, the octahedral sites are mainly occupied by Mg,Fe2+,Fe3+,Al and Ti. From view point of order-disorder characterization of cation distribution in octahedral sites, the site occupancies and crystal structures of five hornblendes crystallized under different conditions were refined. Mg ,Fe ,Al and Fe3+ disordering in the octahedral sites was discovered in volcanic hornblendes.

Five examined hornblendes are as follows. 1)ferrohastingsite (Obira Mine,Japan) crystallized at hydrothermal stage (Matsumoto; 1974). 2)pargasite(Iratsu epidote amphibolite mass in Sambagawa belt,Japan) formed under metamorphic condition(epidote amphibolite facies). 3) K-pargasite(Einstodogain Island, Antarctica) formed under metamorphic condition(granulite facies) (Matsubara and Motoyoshi ;1984). 4)pargasite(Parao Island) from aggromerate in volcanic tuff. 5)hornblende(Kawabe,Japan) from andesite rock. Judging from occurrences, it is obvious that Obira-ferrohastingsite,Iratsu-pargasite and Antartica-pargasite crystallized at lower temparature than Parao-pargasite and Kawabe-hornblende.

Site occupancy refinements were made with the sum of the site chemistries constrained to equal the bulk chemistry of the crystals and with Mg*=Mg+Al and Fe*=Fe2++Fe3+ for difficulty of distingwishing X-ray powers between Mg and Al, and between Fe2+ and Fe3+. Ti was assigned to M2 site.

Distribution of Al ,Fe3+ in the octahedral sites

Hawthorne(1983) found that the variations in the mean octahedral bond lengths in C2/m amphiboles were linear functions of the variations in mean radious of constituent cations. Therefore, it is useful in deriving complete site occupancy in cases of where the result of a site occupancy refinement do not give a unique solution.

The observed grand <M-O> bond lengths of five hornblendes coincide with the grand <M-O> bond lengths calculated using the equation of Hawthorne(1983). When Al,Fe3+ and Ti were assined to

CATION ORDER-DISORDER IN OCTAHEDRAL SITES (M1,M2 AND M3) OF HORNBLENDES

MAKINO,K.,TOMITA,K.

M2 sites, the observed <M2-O> of Obira-ferrohastingsite, Iratsu-pargasite and Antarctica-pargasite are in good agreement with the calculated <M2-O> from the curve of hawthorne(1983).It is confirmed that Al Fe3+ and Ti are concentrated to M2 site of hornblendes formed at lower temparature. But on Parao-pargasite and Kawabe-hornblende the observed <M2-O> are larger, and the obserbed <M1-O> and <M3-O> are smaller than those of Hawthorne's curves. These relations indicate that for hormblendes crystallized at higher temparature Al and Fe3+ are excess in M2 and lacking for M1 and M3. And so,Al and Fe3+ can be assigned to the octahedral sites to agree with the curves of Hawthorne(1983),retaining the same Mg* and Fe* values.

Cation order-disorder in the octahdral sites

In five hornblendes M1 contains the same Mg/Fe2+ ratio as M3. It is shown in Fig.1 that M2 site enriches Mg over M1 and that Al and Fe3+ are strongly ordered to M2 at low temparature. At high temparature ,however, Al and Fe3+ are distributed randamly over the octahedral sites. Al and Fe3+ disordering in the octahedral sites takes place with random distributions of Mg and Fe2+ in volcanic hornblendes.(Fig.2)

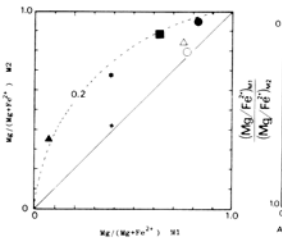

Fig.1

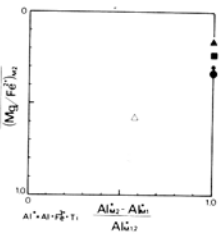

Fig.2

▲ Obira-ferro-fastingsite
■ Iratsu-pargasite
● Antarctica-pargasite
○ Prao-pargasite
△ Kawabe-hornblende
* Ferro-tshermakite (Hawthorne & Glundy;1973)

Hawthorne,F.C.,1983;Can.Min. 21,174-353
Hawthorne,F.C.,Glundy,H.D.,1973;Min.Mag. 39,36-48
Matsubara,S.,Motoyoshi,Y.,1984;Annu.Meeting Abs.Min.Soc.Japan 84
Matsumoto,Y.,1974;Memoirs Geol.Soc.Japan 11,36-48

ARCHETYPES, STRUCTURE-BUILDING PRINCIPLES AND CLASSIFICATION OF THE SULFOSALTS OF As, Sb AND Bi

MAKOVICKY, E., Inst. of Mineralogy, University of Copenhagen, Ostervoldgade 10, DK-1350 Copenhagen K, Denmark

Sulfosalts are complex sulfides (and selenides) of As^{III}, Sb^{III} or Bi^{III} with Pb, Cu, Ag, Hg, Fe, Tl and other metals. The synthetic complex sulfides and selenides with alkali metals, Ca, Sr, Ba and REE belong here as well.

Crystal structures of many sulfosalts are composed of blocks of simple, archetypal structures joined in various ways by the structure-building operators such as chemical (unit-cell) twinning, unit-cell intergrowths, out-of-phase boundaries, crystallographic shear or non-commensurate interfaces (see Makovicky 1981, 1985 for references). Formation and distribution of (direct or inverted) lone electron pair micelles (Makovicky & Mumme 1983) in which the lone electron pairs of (primarily) As, Sb and Bi are collectively accommodated, is equally important.

In the structures with weakly to moderately expressed lone electron pair character (mostly those with Bi), the building blocks can be compared with the blocks of PbS structure. For stereochemically active lone electron pairs (As-, Sb- and some Bi-containing structures), this archetype is frequently replaced by the SnS archetype, often copied in detail in sulfosalts. The two archetypes can occur as blocks in the same structure; the (fragments of) 2 atomic planes thick layers parallel to (100) of PbS belong to either archetype. If chemical elements with coordinations other than octahedral and prismatic prevail, other archetypes have to be used (e.g. for the sulfosalts rich in Cu or Ag).

Many sulfosalts represent members of homologous series, i.e. of the series of structures in which the type(s) of building blocks, and the structure-building principles that define their mutual relationships, remain preserved but the size of the blocks varies incrementally by varying the number of coordination polyhedra in them. Every member of the homologous series can itself represent a single compound or it can be a continuous or a discontinuous solid solution series with ordered members.

Mirror twinning of (131)/PbS/layers gives the lillianite and the pavonite series; that of (111)/PbS/slabs the jordanite series; glide-plane twinning of (h01)/SnS/layers yields the emplectite, sartorite, meneghinite and berthierite series; that of (hk1)/SnS/defines the plagionite and parapierrotite series. Unit-cell intergrowths based on (133)/PbS/give the cuprobismutite series; cyclic twinning of PbS-based rods the zinckenite and the Ba-Bi sulfide series. They all are element-multiplication series. The series based on non-commensurate combination of 2 kinds of layers (the cannizzarite and cylindrite series) or of their fragments (the galenobismutite series and the layered sulfosalt structures with crystallographic shear) represent variable-fit series. The sulfosalt structures based on layers/rods of (mostly) SnS archetype parallel to [001]/SnS/e.g. jamesonite, dadsonite, boulangerite and cosalite, are interconnected by complex relationships. Combinations of blocks of PbS and SnS archetypes give the kobellite series and chabournéite.

Homologous series and similar families (e.g. the sheared layer structures) are suited for sulfosalt classification because they include all the properties of the classified structures. Certain structural changes which take place from one homologue to another (e.g., inversion of lone electron pair micelles) must be allowed for. Homologous series also show which members are still missing. Among the members of the same series the composition changes regularly and by increments. Therefore, the microprobe data for such phases can be used to determine the mineral phase from chemical data alone.

E. Makovicky (1981), Fortschr.Min., 59, 137-190,
E. Makovicky & W.G. Mumme (1983), N.Jb.Miner.Abh., 147, 58-79,
E. Makovicky (1985), Fortschr.Miner., 63, 45-89,
in which original works and structure determinations are quoted.

X-RAY ABSORPTION STUDY OF CO AND NI CRYSTAL CHEMISTRY IN LITHIOPHORITE AND ASBOLANE

MANCEAU, A., Laboratoire de Minéralogie-Cristallographie, Universités Paris 6 et 7, 4 place Jussieu, 75252 PARIS Cedex 05; LLORCA, S., Laboratoire de Minéralogie-Cristallographie, 39 allée J. Guesde, 31400 TOULOUSE; CALAS, G., Laboratoire de Minéralogie-Cristallographie, Universités Paris 6 et 7, 4 place Jussieu, 75252 PARIS Cedex.

The chemical structure of Ni- and Co-bearing lithiophorites and asbolanes, coming from the lateritic weathering profiles of New Caledonia, has been investigated by X-ray absorption spectroscopy. EXAFS spectra at the Mn, Co and Ni K-thresholds are displayed in Fig. 1. Of significance in these spectra is their overall shape which is nearly identical for all samples at the Co as well as at the Mn thresholds. That means that the local order around Co atoms is maintained whatever the Co-bearing phase and is close to that of Mn atoms. The EXAFS structure of asbolane at the Ni K-edge is quite identical to that known for $Ni(OH)_2$ (Manceau and Calas, 1986) suggesting a similar short range order. The EXAFS spectrum of lithiophorite does not look like to any other one seen up to now which indicates a different structural environment. It is thus concluded that the Ni atoms are not in the same site in asbolane and lithiophorite and that their site location is clearly distinct fom that of Co atoms. Additional informations are provided by Fourier filtering. The similitude of the radial distribution functions around Co and Mn atoms (Fig. 2) confirms previous assumptions concerning the short range order around both atoms. The radial structure of asbolane at the Ni K-edge presents a second peak with the same intensity and at the same location than that of $Ni(OH)_2$. The partial RDF of lithiophorite presents a second peak of weaker intensity and shifted towards shorter R values and as a consequence partly overlapped by the main Ni-(O,OH) peak. This latter structure corresponds to a second atomic shell filled with light atoms like Al at a short distance from the X-ray absorbing atom (Manceau and Calas, 1986). Structural parameters of each atomic shell were then determined by fitting the corresponding Fourier filtered wave function.

The Co-(O,OH) distance of 1.95Å is characteristic of an octahedral coordination for trivalent cobalt. This finding is

also supported by the pre-edge and the main edge analysis which both show a chemical shift consistent with this oxidation state. The similarity of the Mn-O and Co-(O,OH) distances found by EXAFS militates for close values between the ionic radii of Mn^{4+} and Co^{3+} and, hence, a low spin configuration of Co^{3+} ions. The Co-(Co,Mn) distance is equal to 2.84Å which rules out the possibility of an adsorption of Co atoms on MnO_2 layers. Structural data strongly support a Co for Mn substitution although a discrete pure Co-phase (like CoOOH) cannot be completely rejected because Mn^{4+} and Co^{3+} atoms are too similar to be distinguished by X-ray methods.

In asbolane, Ni atoms build $Ni(OH)_2$ layers. Ni-OH distances are lowered as compared to the free Ni hydroxide because of the formation of hydrogen bonds between $Ni(OH)_2$ and MnO_2. In lithiophorite Ni is located in the brucitic layer. Both chemical composition and ionic radii considerations support a Ni for Li substitution. Finally evidence is also given for the existence of a mixed-layering between lithiophorite and asbolane and the chemical variations generally observed in these Mn-oxides are interpreted as a variable proportion of $(Mn,Co)O_2$, $Ni(OH)_2$ and $(Al,Li,Ni)OH_3$ layers.

Manceau A. and Calas G. (1986) Clay Miner. (under press).

Fig. 1

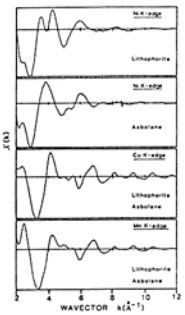

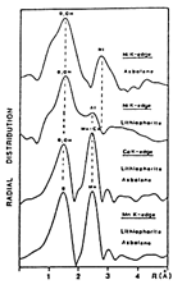

Fig. 2

THE PROCEDURE FOR OBTAINING APPROVAL OF A NEW MINERAL SPECIES FROM THE COMMISSION ON NEW MINERALS AND MINERAL NAMES, I. M. A.

MANDARINO, J. A., Chairman of the Commission on New Minerals and Mineral Names, c/o Department of Mineralogy and Geology, Royal Ontario Museum, 100 Queen's Park, Toronto, Ontario, M5S 2C6, CANADA

The Commission on New Minerals and Mineral Names (CNMMN) is responsible for many matters involving nomenclature: establishment of new mineral species, discreditation of species, clarification of mineral groups and numerous other general problems. This paper deals only with new mineral species.

The number of valid mineral species is about 3300 at the present time. Over one-third of these have been approved by the I. M. A.'s Commission on New Minerals and Mineral Names since it began its work about 20 years ago. This population explosion in the Mineral Kingdom is further attested to by the approximately 100 proposals for new minerals which are submitted to the Chairman of the CNMMN each year. In spite of this, there seems to exist a great deal of misinformation with respect to the approval process; proposals vary from a letter requesting approval (without any data) to the submission of manuscripts of over 100 pages!

In order to facilitate the processing of proposals and to maintain a high degree of quality of new data, the Chairman of the CNMMN now requires that a check-list be submitted for every proposed new mineral. In addition to the physical, chemical, crystallographical, optical and paragenetical data requested on the check-list, proposers are also requested to supply details on the new name and the museums in which type specimens are deposited. The authors may supply any additional information which they think will help to clarify their proposals. Check-lists are available from the Chairman or members of the CNMMN.

The Chairman carries out chemical and X-ray powder diffraction searches and, where required, optical and single-crystal searches. Once he is satisfied that the mineral is new, he checks all numerical data such as the derivation of the chemical formula, crystallographic parameters, optical data, density, etc. Any discrepancies among these or the other data presented by the proposers are brought to their attention. After corrections and/or additional data are received, the Chairman prepares an abstract (usually about two pages long) which is sent to each member of the CNMMN for assessment and voting. Two months are allowed for this. In the case of ore minerals, abstracts also are sent to four advisors from the Commission on Ore Microscopy. Members and advisors are asked to comment on the completeness of the data and the appropriateness of the name. If a member has a serious question about the validity of a proposed new mineral, he or she may suggest that voting be suspended. The Chairman can suspend voting on his own initiative if he considers that the comments made by members warrant such action. In cases of suspension, the authors are asked to resolve any problems. Occasionally, the Chairman may ask the members to vote a second time on a proposal after they have seen the comments of all members.

Proposers are notified of the outcome of voting as soon as possible after the voting deadline. A mineral is considered approved if at least 2/3 of the voting members vote yes; a name is approved if at least 1/2 of the voting members vote yes. The authors of non-approved minerals may submit new or corrected data for another vote.

ELASTICITY OF CoO AS A FUNCTION OF PRESSURE AND TEMPERATURE: COMPARISON WITH TRANSITION METAL OXIDES

MANGHNANI, Murli H., WEBB, Sharon L., University of Hawaii, Hawaii Institute of Geophysics, Honolulu, HI 96822

Using ultrasonic interferometry, the single-crystal elastic constants C_{ij} of CoO have been measured to 4 kbar at 25° and 75°C (Fig. 1), and in the temperature range from -50° to 250°C at ambient pressure (Fig. 2).

With decreasing temperature, CoO undergoes the paramagnetic (B_1) ⇄ antiferromagnetic (distorted B_1) phase change at $T_N \sim 17°C$. This phase change is accompanied by a dramatic decrease in C_{44}. This is in marked contrast with MnO and FeO.

The temperature dependence of $(\partial C_{ij}/\partial P)_T$ is positive for all the C_{ij}'s except C_{12}.

At 25°C, (dC_{44}/dP) for CoO is negative (-0.27) as in the case of MnO. This softening is characteristic of all B1 structures at high pressures. With increasing temperature, all (dC_{ij}/dP) except (dC_{12}/dP) increase, with (dC_{44}/dP) being positive (0.04) at 75°C.

With decreasing temperature C' decreases markedly, and a tetragonal distortion accompanies the magnetic transition. This behavior of C_{44} and C' in CoO indicates a different transition mechanism from that in MnO. The latter shows a rhombohedral distrotion of the B1 structure accompanying the magnetic transition, and exhibits C_{44} softening with increasing pressure and decreasing temperature.

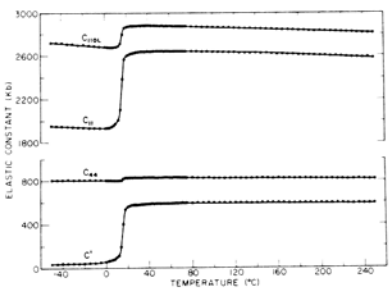

Fig. 1. Temperature dependences of C_{ij} for CoO.

ELASTICITY OF CoO AS A FUNCTION OF PRESSURE AND TEMPERATURE: COMPARISON WITH TRANSITION METAL OXIDES

MANGHNANI, Murli, et al.

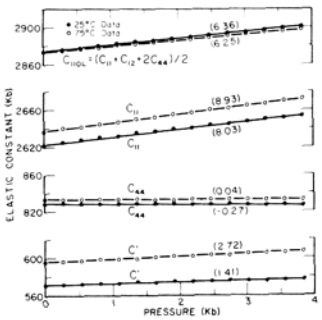

Fig. 2. Pressure dependences of C_{ij} for CoO at 25° and 75°C.

A COMPARATIVE STUDY OF MONAZITE SPECIMENS FROM THE ALPINE REGION

MANNUCCI,G.,DIELLA,V.,GRAMACCIOLI,C.M.,Earth Science Dept.,University of Milan;PILATI,T.,C.N.R.Centre c/o Dept.of Physical Chemistry,University of Milan,I-20133 Milan,Italy

Eleven specimens of monazite from different occurrences in fissures and pegmatites in the Alps have been analyzed by electron microprobe,and for some of them also unit-cell data have been obtained,from single crystal X-ray diffraction.Fissure monazite is poorer in nonessential elements (Si,Ca,Y,Th,U) than pegmatite monazite;the latter specimens can be at times extraordinarily enriched in U and Th.

In all the samples,the REE distribution shows a low Nd and high Sm content relative to the averages given in literature.Appreciable variation of such distribution can be noticed,especially when large quantities of nonessential elements are present;however,such variations are irregular. In view of the constancy of the unit-cell volume,even for large substitution of the REE by U and Th,the monazite crystals behave as ideal solutions,and the REE distribution is practically independent of temperature and pressure,or of the presence of other components in the solid state.Therefore if some correlations are found,these only depend on processes of fractionation which occurred during the evolution of the melt or solution before the monazite crystals were formed.

In all cases,the substitution of the REE by U and Th is accompanied by the presence of enough Ca or Si to maintain the charge balance,with no need to call in other possible causes (defects,etc.),which are very improbable to occur in large amounts,at least in the fresh crystals.The Y content seems to be greater than usual,especially for pegmatite samples. The Y-REE fractionation does not depend exclusively on differences in ionic radii.

GARNET IDENTIFICATION BY REFLECTIVE I.R. SPECTROMETRY

F. MARTIN; P. ZECCHINI; H. MERIGOUX, Laboratoire de Cristallographie et Synthèses Minérales ; Université de Fanche-Comté - 25030 Besançon Cédex - FRANCE

There are several physicochemical methods to distinguish the different types of garnet (i.e. color, reflective index,specific gravity, X-ray diffraction).

The stone is often removed from the mounting for the analysis.

We present, in this paper, a very quick and non destructive method which allows the differenciation of all varieties of garnet used in jewellery.

Natural garnets are silicate with the general formula $M_3^{2+}\ M'_2^{3+}(SiO_4)_3$. Among the possible isomorphs are generaly distinguished the following seven types :

- Pyrope $Mg_3Al_2(SiO_4)_3$
- Almandine $Fe_3Al_2(SiO_4)_3$
- Spessartine $Mn_3Al_2(SiO_4)_3$
- Uvarovite $Ca_3Cr_2(SiO_4)_3$
- Grossular $Ca_3Al_2(SiO_4)_3$
- Andradite $Ca_3Fe_2(SiO_4)_3$
- Hydrogrossular $Ca_3Al_2Si_2O_8(SiO_4)_{1-m}(OH)_{4m}$

The garnet name is also given to some synthetic rare earth oxydes used in imitation of diamond. The best known are YAG, YIG and GGG.

Using reflective I.R. spectrometry, we obtain very rapidly spectra showing differencies between the specific atomic vibrations in the observed garnet. These spectra are employed as "finger prints" for the mineral recognition. During the observation, the stone is placed in the focus of an elliptical device in the I.R. spectrometer, reducing the energy loss produced by the numerous facets.

Some results are shown below:

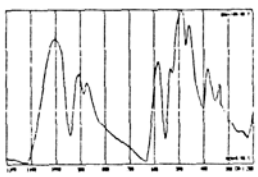

Pyrope

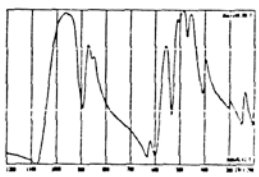

Grossular

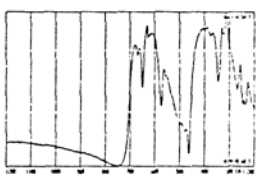

YIG

FELDSPAR MINERALOGY OF GRANITIC PEGMATITES

MARTIN, R.F., Dept. of Geological Sciences, McGill University, Montreal, Quebec H3A 2A7, Canada.

Granitic pegmatites crystallize, as a rule, from evolved H_2O-saturated melts in a mesozonal environment. The tendency for the aqueous phase to remain in the pegmatite body during its cooling is reflected in the feldspar assemblage achieved. Typical are low microcline and low albite in a subsolvus assemblage. The microcline is coarsely grid-twinned according to the albite and pericline laws, indicating that the structural conversion from a monoclinic feldspar was efficiently catalyzed. In peralkaline systems, the conversion is virtually assured. If the bulk composition of the system is subalkaline, or if water left the pegmatite during a subsolidus event, the K-feldspar may be structurally stranded in a disordered state (orthoclase). Sudden evacuation of the system can result in the nucleation of high sanidine whose survival, in some instances even since Archean times, must indicate the absence of water until the temperature was so low that the reaction was kinetically impeded. Compositional equilibrium typically is achieved, but structural equilibrium may not have been achieved after decompression.

Granitic pegmatites that are highly evolved contain Rb- and Cs-enriched K-feldspar. Granitic pegmatites of alkaline affinity that are emplaced in a boron-enriched host rock may contain B-bearing albite and microcline as well as coexisting reedmergnerite. Granitic pegmatites formed from melts 1) derived by desulfurization of a galena-bearing quartzofeldspathic sequence, or 2) depleted in sulfur owing to earlier crystallization of sulfides in a less evolved igneous product, may well contain amazonitic and non-amazonitic K-feldspar that contains many thousands of ppm Pb. Ordering of the magmatic Pb-bearing K-feldspar leads to a progressive removal of Pb from the feldspar structure, and characteristically gives as product a late generation of galena if sulfur is available in the aqueous fluid that must necessarily catalyze the ordering reaction.

PETROGENESES AND MINERAL COMPOSITIONS OF FRANCISCAN BLUESCHISTS FROM CAZADERO, CALIFORNIA

MARUYAMA, S. and LIOU, J. G. Department of Geology, Stanford University, Stanford, CA 94305, USA

The Cazadero blueschist allochthon lies within the Central Melange Belt of the Franciscan assemblage in the northern Coast Range of California. Mineral compositions and assemblages of more than 200 blueschists from Ward Creek were investigated. The results delineate lawsonite-, pumpellyite-, and epidote-zones. Both lawsonite and pumpellyite zones are equivalent to the Type II metabasites of Coleman & Lee (1963) and are characterized by well-preserved textures, relict augites, and pillow structures, whereas epidote zone rocks are equivalent to the Type III strongly deformed and schistose metabasites. Chlorite, phengite, aragonite, sphene, and minor quartz and albite are ubiquitous. Compositional variations and representative assemblages for three different zones are presented in the chlorite-projection diagrams of Fig. 1.

The lawsonite zone metabasites contain lawsonite (3 wt% Fe_2O_3), riebeckite-crossite, Ca-Na pyroxenes; some rocks have two distinct clinopyroxenes separated by a compositional gap. The clinopyroxene of the lowest grade metabasites contains very low X_{Jd}. As shown in Fig. 1, tie line of Lw + crossitic amphibole is stable and common metabasites contain 3-phase assemblage Lw + Cpx + Crossite together with other excess phases. In pumpellyite-zone metabasites, the most common assemblages contain Pm + Cpx + Gl and some samples with higher Al_2O_3 and/or Fe_2O_3 have Pm + Lw + Cpx. Actinolite joins the above assemblage in the upper pumpellyite zone where the actinolite-glaucophane compositional gap is well defined.

The epidote zone metabasites are characterized by assemblages Ep + Cpx + two amphiboles, and Lw + Pm + Act, and Ep + Pm + two amphiboles depending on the Fe_2O_3 content of the rock. In upper epidote zone, winchite appears, Fe-free lawsonite is stable, pumpellyite disappears and omphacite contains very low Ac component. Therefore, common assemblages are Ep + winchite + Lw, and Lw + Omp + winchite. With further increase in metamorphic grade, epidote becomes Al-rich and lawsonite is no longer stable. Hence epidote + - omphacite + winchite + - garnet is characteristic. These assemblages were not found in the Ward Creek metabasites, but are common elsewhere in Franciscan knockers such as the Laytonville quarry (Liou et al., in press).

Mineral assemblages and paragenetic sequences delineate three discontinuous reactions: (1) pumpellyite-in, (2) actinolite-in, and (3) epidote-in reactions. Using the temperatures estimated by Taylor and Coleman (1968) and phase equilibria for Ca- Na pyroxenes, the P-T positions of these reactions and the metamorphic gradient are located. All three zone metabasites occur within the aragonite stability field and are bounded by the maximum pressure curve of Ab = Jd + Qz and the maxmium stabilities of pumpellyite and lawsonite. The lawsonite zone appears to be stable at T below 200°C with large pressure range of 4 to 6.5 kb; the pumpellyite zone in beween 200 and 290°C and the epidote zone above 290°C with less pressure variation between 6.5 and 8 kb. Metamorphic field gradient appears to have an inflection point at about 20 km which reflects the possible depth for underplating of oceanic crust in a subduction zone. Below P and T of the inflection point, metamorphism proceeds under predominantly pressure increases from 4 to 7 kb at nearly constant T about 150-200°C. Whereas at higher grade recrystallization above the inflection point, metamorphic T increases from 200 to 350°C at nearly constant P (7-8 kb).

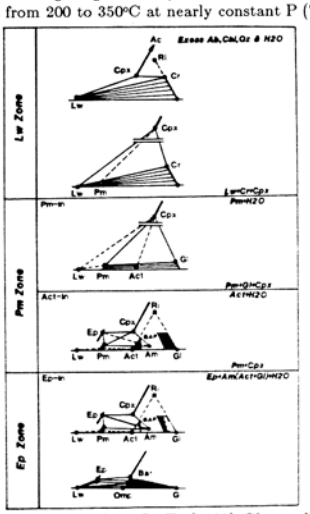

Fig. 1. Paragenetic relations of amphiboles, clinopyroxene, and Ca-Al silicates in the 3-zone metabasites to illustrate the Pm-in, Act-in and Ep-in reactions. Abbreviations of minerals are: Ab: albite, Act: actinolite, Am: amphibole, Bar: barroisite, Chl: chlorite, Qz: quartz, Cpx: clinopyroxene, Cr: crossite, Ep: epidote, Gl: glaucophane, Lw: lawsonite, Omp: omphacite Pm: pumpellyite, Ri: riebeckite,

REFERENCES

Coleman, R. G. & Lee, D. E. (1963) Glaucophane-bearing metamorphic rock types of the Cazadero area, California. J. Petrol. 4, 260-301.

Liou, J. G., Maruyama, S., Coleman, R. G., & Gilbert, M. C. (1986) Field trip guide book to Franciscan blueschists and eclogites in northern California.

Taylor, H. P., Jr. & Coleman, R. G. (1968) O^{18}/O^{16} ratios of coexisting minerals in glaucophane-bearing metamorphic rocks. Geol. Soc. Am. Bull., 79, 1727-56.

EVIDENCE AGAINST THE COMAGMATIC CHARACTER OF THE DEVONIAN GRANODIORITE-GRANITE SUITE OF SW NOVA SCOTIA FROM THE CHEMICAL VARIABILITY OF THEIR BIOTITES

MASSONNE, H.-J., Institut für Mineralogie, Ruhr-Universität, Postfach 102148, 4630 Bochum 1, FRG

The Meguma terrane of SW Nova Scotia consists of folded Cambro-Ordovician flysch, which was intruded in Devonian times by huge masses of acidic melts. By means of fractional crystallization of biotite and plagioclase these melts may have formed a comagmatic suite ranging from biotite granodiorite to alaskite as the highest differentiation product. McKenzie & Clarke (1975, Can.J. Earth Sci. 12, 1209) believed to have found evidence for this by demonstrating clear chemical trends for the intrusion of the South Mountain batholith outcropping over about 10.000 km² like the continuous decrease of Ti, Mg, and Fe with rising SiO_2 content of the comagmatic rocks.

About 1500 microprobe analyses of biotite from 90 samples of rocks as a representative spectrum of the Devonian granodiorites and granites of SW Nova Scotia were achieved to clarify the following aspects: (1) zonation of single biotite grains, (2) chemical variability of biotite both within one rock sample and over the whole rock suite.

With rising degree of differentiation, the mean biotite compositions of the rock samples show increasing ratios of (Fe+Mn) = F to (Fe+Mn+Mg) = FM, which range between 0.6 to 1.0. Ti contents of biotite decrease clearly, whereas Mn contents increase slightly with rising F/FM values. Si contents per formula unit lie at 5.35 (Table 1) if biotites from highly differentiated rocks are neglected, which may contain considerable amounts of Li. It is important to note that the Ti and Mn contents scatter strongly at fixed F/FM values around the correlation curves, which cannot only be due to analytical errors (Table 1). On the other hand, correlations considering regional or mineralogical aspects like the presence of magmatic cordierite fail.

More importantly, it was found that biotite compositions vary within one rock sample. However, in contrast to the trend observed for the whole rock suite, here falling Ti contents correlate with decreasing F/FM values (Figure 1). In each case, the smaller Ti contents were found to be in rims of zoned biotite grains, which occur frequently in highly differentiated rocks, as well as in small biotite grains enclosed in the late phases of crystallization, muscovite and cordierite.

It is concluded that during biotite crystallization the melt is depleted in Ti but enriched in Mg relative to Fe+Mn, which is in contrast to the assumed continuous development of granodioritic to alaskitic melts becoming enriched in Fe+Mn relative to Mg. In the author's opinion, the so called comagmatic suite of SW Nova Scotia is the product of a continuous melting of lower crustal material leading first to granodiorites and then to granites. This could also rather explain, why granitic rocks similar in mode and position show biotites differing clearly in Ti and Mn contents.

Table 1: Average cation contents of biotite from a granodiorite (M72-80) and a two-mica granite (M72-159) of the South Mountain batholith (cf. McKenzie & Clarke, 1975) calculated on the basis of 42 valencies neglecting the valencies of interlayer cations.

Sample No.	M72-80 (N=18)	M72-159 (N=21)
Si	5.327 (6)	5.384 (8)
Al	3.279	3.757
Mg	1.452	0.632
Mn	0.035 (1)	0.047 (2)
Fe	3.036	3.268
Ti	0.452(12)	0.325(15)
K+Na	1.889	1.862

N = Number of analyzed biotites. Numbers in parentheses concern calculated 1σ standard deviation. Fe was calculated as Fe^{2+}.

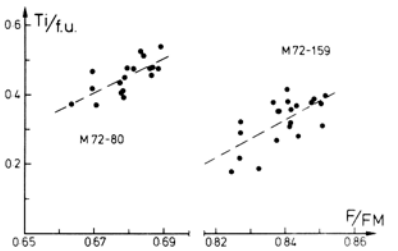

Figure 1: Correlation of Ti contents and F/FM values of biotites from the two samples of Table 1.

STRUCTURAL AND ELASTIC PROPERTIES OF THE ILMENITE AND PEROVSKITE PHASES OF $MgSiO_3$, OBTAINED FROM A COMPUTATIONAL MODEL

MATSUI, M., Chemical Laboratory, Kanazawa Medical University; AKAOGI, M. and MATSUMOTO, T., Department of Earth Sciences, Faculty of Science, Kanazawa University, Japan

Magnesium-rich silicate pyroxenes are major constituents of the upper mantle. At very high pressures characteristic of the deep mantle, they transform to the ilmenite and subsequently to the distorted (orthorhombic) perovskite phases (e.g. Ito and Yamada, 1982); the perovskite phase is generally accepted to be the most abundant mineral in the lower mantle.

The purposes of this investigation are to develop a realistic potential model of the ilmenite and perovskite phases of $MgSiO_3$, and, further, to apply the model to the prediction of the elastic constants of the perovskite phase, as well as to the simulation how the structural and elastic properties change with pressure.

The techniques employed are based on the energy-minimization method under external forces (Busing and Matsui, 1984). The potential energy of the crystal is approximated by the sum of Coulomb, van der Waals attraction and repulsion terms between atoms. Required energy parameters were determined to reproduce not only the observed crystal structures of the ilmenite (Horiuchi et al., 1982) and perovskite (Ito and Y. Matsui, 1978) phases of $MgSiO_3$, but also the measured elastic constants of the ilmenite phase (Weidner and Ito, 1985) as closely as possible, in which some energy parameters were fixed at values obtained for α- and β-Mg_2SiO_4 (Matsui and Matsumoto, 1985). The potential model thus obtained was used to calculate the elastic constants of the perovskite phase. The calculated bulk, K, and shear, μ, moduli of the perovskite phase are 2.6 and 1.4 Mbar, respectively, in close agreement with the value of 2.6(2) Mbar for K obtained by a volume-compression experiment (Yagi et al., 1982), and also in good agreement with the values estimated from empirical elasticity systematics of perovskite-type compounds (K=2.5(3) and μ=1.5(2) Mbar; Liebermann et al., 1977, and K=2.6(2) and μ=1.4(3) Mbar; Bass, 1984). The potential model was then used to simulate the pressure dependence of the crystal structures and elastic constants of the ilmenite and perovskite phases.

EXPERIMENTAL DETERMINATION OF Fe_3O_4 ACTIVITY IN COMPLEX SPINELS: IMPLICATIONS FOR UPPER MANTLE fO_2

GLEN S. MATTIOLI and **BERNARD J. WOOD** (both at Department of Geological Sciences, Northwestern University, Evanston, IL 60201, USA)

Spinels are important as accessory minerals in terrestrial igneous rocks and as the characteristic phase of the spinel-lherzolite facies in the Earth's upper mantle. The magnetite (Fe_3O_4) component in this mineral exerts a major control of its magnetic, electronic, and transport properties. In addition, Fe_3O_4 is the main ferric iron component in the Earth's upper mantle, and hence its concentration may be used to estimate the equilibrium oxygen fugacity recorded by spinel-bearing, mantle-derived xenoliths. We have experimentally determined Fe_3O_4 activities on the pseudobinary spinel join Fe_3O_4-$MgAl_2O_4$ using a zirconia solid electrolyte at 1 atm total pressure. Results of these experiments, performed in the temperature range 800°-1000°C and the composition range 0.05-0.15 mole fraction Fe_3O_4 in $MgAl_2O_4$-rich spinel, are summarized by the following equation

$$A_{Fe_3O_4} = (\xi + \phi T) X_{Fe_3O_4} \qquad (1)$$

where $X_{Fe_3O_4}$ and $A_{Fe_3O_4}$ are the mole fraction and activity of magnetite in spinel, respectively, $\xi = -6.5 \pm 0.5$, $\phi = 8.5 \pm 0.5 \times 10^{-3}$, and T is in °C.

Additional activity experiments were conducted at 900° & 1000°C in the composition range 0.05-0.80 mole fraction Fe_3O_4 component, in order to constrain the solution properties of the complex spinel more precisely. These data provide an excellent test of the O'Neill & Navrotsky (1983, 1984) cation distribution model and the available thermodynamic data on order-disorder relations of the end-members. The unusual behavior of increasing Fe_3O_4 activity with increasing temperature at constant Fe_3O_4 content may be modelled quantitatively by applying the O'Neill/Navrotsky formalism to the following cation distribution reactions

$$Fe^{2+} + (Fe^{3+}) = (Fe^{2+}) + Fe^{3+} \qquad \Delta H_D = 7.76\chi - 6.15\chi^2 \qquad (2)$$
$$Fe^{2+} + (Al^{3+}) = (Fe^{2+}) + Al^{3+} \qquad \Delta H_D = 14.20\chi - 7.24\chi^2 \qquad (3)$$
$$Mg^{2+} + (Al^{3+}) = (Mg^{2+}) + Al^{3+} \qquad \Delta H_D = 9.84\chi - 6.63\chi^2 \qquad (4)$$
$$Mg^{2+} + (Fe^{3+}) = (Mg^{2+}) + Fe^{3+} \qquad \Delta H_D = 3.40\chi - 5.54\chi^2 \qquad (5)$$

where the species in the ( ) resides on the octahedral sublattice, χ is the degree of inversion, and ΔH_D is in kcal. Of the four possible cation distribution reactions above, only three are linearly independent, such that (5) = (2) + (4) - (3). The values of α and β for reactions (2), (3), & (4) used to calculate the cation distribution were determined from data of Wu & Mason (1981), Mason (1985), and Wood et al. (1986), respectively. Our derived values for reaction (5) are in good agreement with the values of Trestman-Matts et al. (1984), assuming an uncertainty of ± 1 kcal. These values for α & β yield equilibrium cation distributions at 800°, 900°, & 1000°C, which result in increasing Fe_3O_4 activity with increasing temperature. Additional excess free energy terms are necessary to describe completely the polythermal activity-composition relations along the Fe_3O_4 - $MgAl_2O_4$ join and to generate the observed asymmetric miscibility gap between 0.20 and 0.60 mole fraction Fe_3O_4 at 900°C (see figure). Our activity data indicate that the crest of the solvus is between 900° & 1000°C.

Thermobarometric oxygen fugacities recorded by spinel-lherzolite xenoliths may be estimated using our Fe_3O_4 activity data (eqn. (1)) and available thermodynamic data for olivine ($X_{Fa} = 0.10$) and orthopyroxene ($X_{Fs} = 0.10$). Results for spinel compositions ranging between 0.01 and 0.05 mole fraction Fe_3O_4 component, the approximate limits observed by electron microprobe, wet chemistry, and Mössbauer spectroscopy for mantle derived spinels from Type 1 xenoliths, yield fO_2's close to the synthetic QFM buffer at 15 kbar total pressure. Magnetite concentrations would have to be significantly below $X_{Fe_3O_4} = 0.01$ in order to stabilize sp-opx-ol assemblages near IW, as suggested by published intrinsic fO_2 measurements.

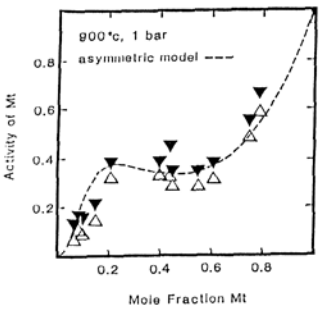

Preliminary magnetite activity measurements of synthetic Cr-bearing spinel, as well as published data for Fe-Al-Cr mixing in spinel, indicate that Cr-substitution does not alter this conclusion.

APPLICATION OF THE 1986 JCPDS-ICDD MINERAL POWDER DIFFRACTION FILE COMPUTER DATABASE TO MINERALOGICAL PROBLEMS

McCARTHY, G.J., Depts. of Chemistry and Geology, GARVEY, R.G, Dept. of Chemistry, North Dakota State University, Fargo, ND 58105, and the MINERAL SUBCOMMITTEE of the JCPDS-International Centre for Diffraction Data, 1601 Park Lane, Swarthmore, PA 19081, USA.

The 1986 update of the Mineral Powder Diffraction File (MPDF), described earlier in this symposium by Professor Bayliss, is available for lease in computer readable form. Because it contains all of the information on the PDF card, queries of this database can include crystallographic and crystal chemical attributes, specific gravity, optical properties, etc., in addition to d-I data. Thus, the range of mineralogical problems that can be solved through application of the MPDF is greatly enlarged.

The database supplied by the JCPDS-ICDD adheres to a fixed format and is 10.5 Mb (132,000 80-column "cards") in size. For efficient use it should be converted into a more compressed format, preferably through a data management system. Implementation of this database using the SAS Institute's Statistical Analysis System on an IBM 3081 mainframe will be described. SAS INPUT statements provide conversion of the database fields to an internal storage format. The resulting SAS FILE is then searched on user-specified fields for desired ranges of values using logical relationships ranging from simple to sophisticated. Records matching the selection criteria become available to various SAS statistical and report PROCedures.

Examples of utilization of the MPDF database will include: (1) alphabetized sorts of minerals based on combinations of crystallographic properties and physical properties (optical, density, etc.); (2) mineral identification using fragments of diffraction data, crystallography and physical properties; (3) creation of subfiles based on chemical, crystallographic and physical property data; (4) evaluation of mineral XRD data based on figures of merit.

Recent developments of any commercial or public domain software that is available at the time of the General Meeting will be noted.

GEOTHERMOMETRY AND GEOBAROMETRY FOR KYANITE ECLOGITES FROM BELLSBANK AND ROBERTS VICTOR KIMBERLITES

MCCORMICK, T. C.; SMYTH, J. R., Dept. of Geological Sciences, University of Colorado, Boulder CO 80309-0250

Equilibration conditions have been determined for ten kyanite eclogites from Bellsbank and four kyanite eclogites from Roberts Victor kimberlites. The geothermometer is based on Ellis and Green (1979) and the geobarometer is based on Lappin's (1978) method. A problem arises for aluminous eclogites that have substantial non-stoichiometry of their pyroxenes. The distribution of Ca and Al between pyroxene and garnet then becomes more complex than the simple equilibrium:

Diopside + Ca-Tschermak's molecule = Garnet,

since the Al content of the pyroxene is related to the Ca-Eskola molecule as well as Ca-Tschermak's and jadeite components. Of the fourteen eclogites described here, only two have stoichiometric pyroxenes, and these have exsolution lamellae of kyanite and garnet in their pyroxenes. Ca-Eskola contents for the pyroxenes range from 2.5 mol% in a corundum-kyanite eclogite to 17 mol% in a coesite-kyanite eclogite.

Calculations of pressure were done first assuming X_{cpx}^{CaTs} = (Al-Na)/2, and secondly, with $X_{cpx}^{CaTs} = Al^{IV}$. Differences between these two methods are greatest in the most non-stoichiometric pyroxenes. Figure 1 shows P-T estimates based on the second set of calculations (i.e. $X_{cpx}^{CaTs} = Al^{IV} = 2.00-Si$). These are more consistent with other estimates of the continental geotherm; the first set of calculations give pressure estimates that are 5-15 kbar lower for similar temperatures.

Also shown in Figure 1 are data for kyanite eclogites from Carswell et al. (1981), calculated by this method, and the linear and kinked paleogeotherm for this area as estimated by Carswell et al. (1981). The aluminous eclogites reported here in general plot 50-100°C above this paleogeotherm. Continental geotherms of Harte (1978) and Mercier and Carter (1975) essentially provide good fit to the P-T estimates in Figure 1. There is no evidence here for a kinked geotherm in this region. The results show that calculations for pressure and temperature for highly aluminous eclogites, based on the method of Lappin (1978) and using the geothermometer of Ellis and Green (1979), appear to be consistent with other estimates of geotherms, despite the presence of substantial vacancy in their pyroxenes.

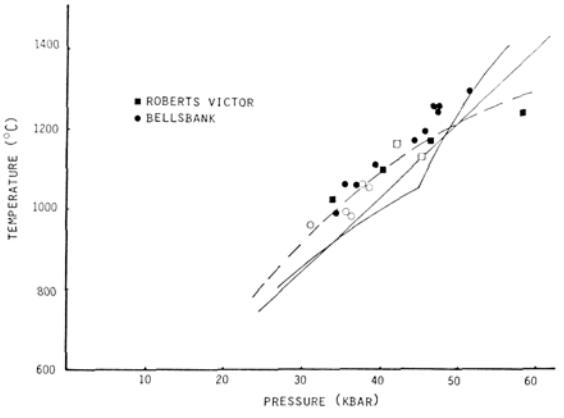

Figure 1: Estimated pressures and temperatures of equilibration for kyanite eclogites from Roberts Victor and Bellsbank kimberlites. Open symbols are data from Carswell et al. (1981). Solid curves are linear and kinked geotherms from Carswell et al. (1981) and dashed curve is geotherm from Mercier and Carter (1975).

References:

Carswell, D. A., Dawson, J. B., Gibb, F. G. F. (1981) Mineral. Mag., 44, 79-89.
Ellis, D. J., Green, D. H. (1979) Contrib. Mineral. Petrol., 71, 13-22.
Harte, B. (1978) Phil. Trans. R. Soc. Lond., A288, 487-500.
Lappin, M. A. (1978) Contrib. Mineral. Petrol., 66, 221-241.
Mercier, J.-C., Carter, N. L. (1975) J. Geophys. Res., 80, 3349-3362.

RAMAN SPECTROSCOPY OF ALUMINOSILICATE GLASSES

McMILLAN, PAUL, Dept. of Chemistry, Arizona State University, Tempe, AZ 85287

There have been a large number of studies using vibrational spectroscopy, especially Raman scattering, to investigate the structures of silicate and related glasses and melts. These studies have had some success in identifying molecular species within the glass, and in following their relative concentrations as a function of glass composition. However many of the interpretations of the Raman spectra of silicate glasses remain highly subjective, and it is often difficult to ascertain the validity of structural models based on these interpretations. Silicates in general form complex solid state structures whose dynamics are poorly understood. In order to interpret a vibrational spectrum in terms of molecular structure, it is necessary to know the atomic displacements associated with each vibrational mode. This is only possible when the magnitudes of the various force constants and interaction terms are known reliably. This is not yet the case for silicates, although recent advances in quantum mechanical calculations should make this possible in the near future. At present the interpretation of silicate vibrational spectra is largely phenomenological.

The spectrum of vitreous silica is similar to all of its crystalline tetrahedral polymorphs, consistent with the generally accepted opinion that SiO_2 glass has a fully-polymerized network structure. On adding alkali or alkaline earth metal oxide component to SiO_2, the silicate glass specta show features similar to the major peaks of crystalline ortho-, pyro-, meta-, and disilicates. These features appear at successively lower silica contents, suggesting progressive depolymerization of the silica network. At any given silica content, there is a superposition of several band systems, consistent with the coexistence of several polymer types. One of the major unanswered questions is whether the spectra are indicative of long range silicate polymer units, such as sheets, chains or rings, or reflect differing degrees of polymerization on possibly neighbouring tetrahedra. This question is of interest for the discussion of bulk properties, such as glass and melt density, or melt viscosity, as well as thermodynamic modelling.

The spectra of aluminosilicate glasses are less well understood. SiO_2-Al_2O_3 and CaO-Al_2O_3 glasses show a loss of spectral structure at high alumina content. This has been interpreted in terms of a loss of local structure about Al to give highly distorted aluminate polyhedra with some range in average coordination number; however, this interpretation remains untested by any independent structural studies. The spectra of glasses along joins SiO_2-$MAlO_2$ may be interpreted assuming that Al remains tetrahedrally coordinated to oxygen. The spectra are dominated by bands in the 400-600 cm^{-1} region, and bear some similarity to the spectrum of vitreous silica. This has been used to suggest that the aluminosilicates have the same type of framework structure as SiO_2 glass. There has been some controversy over the detailed interpretation of the high frequency region, which contains a number of poorly resolved bands. Differences of opinion have arisen as to the validity of individual band deconvolution schemes, which are often heavily dependent on particular interpretations of the aluminosilicate glass structure. The low frequency bands are generally assigned to motions of oxygen within intertetrahedral linkages TOT, but again, there is some discussion as to the best interpretation of particular features.

In summary, the Raman spectra of silicate and aluminosilicate glasses have been well studied. There is agreement on the general interpretation of the spectra of binary silicate glasses, and the remaining questions will require a better understanding of the dynamics of the glasses to be resolved. In contrast, the spectra of the aluminosilicate glasses are more complex, and even first order band assignments have not been reliably made. This presentation will attempt to summarize the field, to present opposing interpretations of particular features of interest, and discuss future methods to resolve the remaining problems.

THE T-O LAYER OF LIZARDITE: NEW STRUCTURE REFINEMENTS

MELLINI, M., CS Geologia Strutturale Dinamica Appennino, Pisa, and ZANAZZI, P.F., Dip. Scienze della Terra, Perugia, ITALY.

Lizardite, $Mg_3Si_2O_5(OH)_4$, is the flat-layer serpentine polymorph. The detailed knowledge of the bond geometry within the tetrahedral-octahedral layer has been largely hampered by the low degree of three-dimensional order and, up to now, only one satisfactory structure refinement was reported (lizardite 1T from Val Sissone, A.M. 67, 1982). The high crystal order of that specimen was explained as due to the favourable composition

$$(Mg_{2.79}Fe_{0.14}Al_{0.07})(Si_{1.83}Al_{0.17})O_5(OH)_4 .$$

In particular, the substitution of trivalent atoms for magnesium and silicon led to stronger hydrogen bonds, thus promoting the formation of flat-layer structure.

A new finding of lizardite 1T and 2H1 from Val Trebbia, with approximate chemical compositions

$$(Mg_{2.80}Fe_{0.11}Al_{0.07})(Si_{1.93}Al_{0.07})O_5(OH)_4$$

offers the way to further analyze the role of chemical substitutions on the geometry of the T-O layer. Furthermore, the comparison between the isochemical 1T and 2H1 polytypes from Val Trebbia shows the different effects of the different interlayer interactions. For instance, whereas negative ditrigonalization occurs in the 1T polytypes, positive value is found in the 2H1 polytype. The most important data are

	1T Val Sissone	1T Val Trebbia	2H1 Val Trebbia	
a	5.332	5.325	5.318	Å
c	7.233	7.259	7.270x2	
Sp. gr.	P31m	P31m	$P6_3cm$	
R factor	0.031	0.074	0.024	
Si-O1	1.616	1.588	1.602	
Si-O2	1.646x3	1.650x3	1.648x3	
average Mg-O	2.067	2.070	2.067	
α	-3.5	-1.7	+6.4°	

CORRELATIONS BETWEEN OPTICAL PROPERTIES AND CRYSTAL STRUCTURES OF URANYL CARBONATE MINERALS

MEREITER, K. & PREISINGER, A., Institut für Mineralogie, Kristallographie und Strukturchemie, Technische Universität Wien, Getreidemarkt 9, A-1060 Vienna, Austria

We examined recently the optical properties and crystal structures of a series of uranyl carbonate minerals and analogous synthetic tricarbonatodioxouranates(VI), and found them to be nice examples for correlations between crystal optics and crystal structures. The compounds studied were: bayleyite, $Mg_2[UO_2(CO_3)_3].18H_2O$, monoclinic, $n\alpha$=1.453, $n\beta$=1.498, $n\gamma$=1.499, 2Vx=16°; swartzite, $CaMg[UO_2(CO_3)_3].12H_2O$, monoclinic, $n\alpha$=1.468, $n\beta$=1.530, $n\gamma$=1.538, 2Vx=40° and its Sr analogue, $SrMg[UO_2(CO_3)_3].12H_2O$, $n\alpha$=1.463, $n\beta$=1.525, $n\gamma$=1.532, 2Vx=35°; liebigite, $Ca_2[UO_2(CO_3)_3].11H_2O$, orthorhombic, $n\alpha$=1.495, $n\beta$=1.501, $n\gamma$=1.541, 2Vz=41°; $Sr_2[UO_2(CO_3)_3].8H_2O$, monoclinic, $n\alpha$=1.511, $n\beta$=1.594, $n\gamma$=1.598, 2Vx=24°; schröckingerite, $NaCa_3[UO_2(CO_3)_3](SO_4)F.10H_2O$, triclinic, $n\alpha$=1.489, $n\beta$=1.539, $n\gamma$=1.541, 2Vx=25°; albrechtschraufite, $MgCa_4F_2[UO_2(CO_3)_3]_2.17H_2O$, triclinic, $n\alpha$=1.511, $n\beta$=1.549, $n\gamma$=1.566, 2Vx=63°; andersonite, $Na_2Ca[UO_2(CO_3)_3].\sim 6H_2O$, trigonal, $n\omega$=1.527, $n\varepsilon$=1.541 ("anomalous" biaxial with low 2Vz); and grimselite, $K_3Na[UO_2(CO_3)_3].H_2O$, hexagonal, $n\omega$=1.601, $n\varepsilon$=1.478 (all data for λ=589 nm with estimated errors of $\leq$0.001 for refractive indices and $\sim$1° for 2V).

The crystal structures of all these compounds contain the complex anion $[UO_2(CO_3)_3]^{4-}$ which consists of a linear uranyl group and three chelating bidentate CO_3 groups in equatorial geometry. This complex anion governs the optical anisotropy of the compounds and does this in two ways: Firstly, by means of the various orientations which the anions adopt in the crystal lattice; secondly, by deformations of the anion from ideal C_{3h}-$\bar{6}$m2 to lower symmetry, mainly by out-of-plane bending of individual CO_3 groups from the equatorial plane of the anion. In six of the compounds all $[UO_2(CO_3)_3]$ anions with their equatorial planes are oriented parallel to subparallel throughout the lattice. These crystals behave uniaxial negative (grimselite) to biaxial negative with low 2V (e.g. schröckingerite). In the three remaining minerals the $[UO_2(CO_3)_3]$ anions adopt differing orientations which leads from biaxial negative character with larger 2V (albrechtschraufite) via biaxial positive character (liebigite) to uniaxial positive character (andersonite). Comparable relations exists, moreover, for the absorption colors which vary between colorless, when light vibrates parallel to all uranyl groups, and different hues of yellow for perpendicular vibration directions. Thus pleochroism of the type $n\alpha$--colorless and $n\beta/n\gamma$--yellow is observed for one uniaxial negative and five biaxial negative crystals with low 2V, while pleochroism for albrechtschraufite, liebigite and andersonite is represented by different hues of yellow. Calculations, which are currently in progress, show that the refractive indices, 2V and optic orientation can be predicted quite well by a tensor expansion of the Gladstone-Dale relation with anisotropic coefficients for the CO_3 groups and isotropic ones for the remaining constituents.

OBSERVATION OF INHOMOGENITY IN CULTURED QUARTZ BY I.R. SPECTROMETRY

H. MERIGOUX ; F. MARTIN ; P. ZECCHINI ; Laboratoire de Cristallographie et Synthèses Minérales ; Université de Franche-Comté - 25030 Besançon Cédex - FRANCE

Systematic studies of cultured quartz by I.R. spectrometry were undertaken in order to know the quality of quartz.

We have found, of course, the different growth zones observed by X-ray topography. Using either OH absorption bands or the Q_{IR} quality factor, we may observe the purity in a quartz block. The growth influence or the place in the autoclave is observed this way.

At room temperature or at liquid nitrogen temperature, we have noted in the Z-zone, the purest zone, a variation of quality and particularly an unexpected difference between the two Z-zones of a same block despite the two fold axis connection.

We have also seen, in some cases, a surprising electrical twinning in a cultured quartz.

These studies are being carried out on several cultured quartz before and after irradiation or sweeping.

The different behaviors of quartz will be presented showing the effect of the ion mobility in the crystal lattice.

This research has practical applications in the quartz resonator industry where there is a need for the largest possible volume of high purity quartz.

Mg-Mn AND Mg-Fe OLIVINES: USE OF DIFFRACTION PEAK INTENSITIES, *d*-SPACINGS AND LATTICE PARAMETERS IN DETERMINING COMPOSITION AND INTRACRYSTALLINE CATION DISTRIBUTION

MILLER, Mark L. and RIBBE, Paul H., Department of Geological Sciences, Virginia Polytechnic Institute & State University, Blacksburg, VA 24061, USA

Multiple linear regression analysis on five data sets from structure analyses (Fig. 1) has been used to determine the relationship between the unit cell parameters and the average radii, *r*, of the *M1* and *M2* octahedral cations in the forsterite-tephroite (Fo-Te) binary system. The equations are:

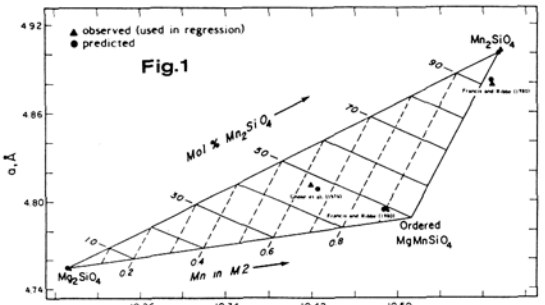

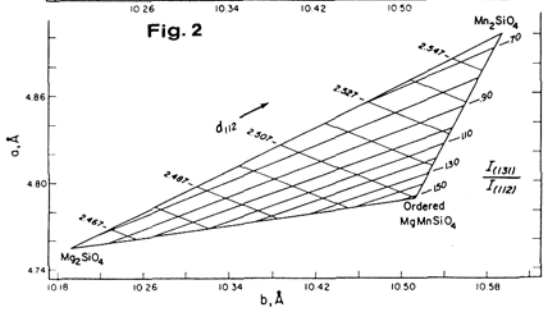

$$\mathbf{a} = 3.798_{(28)} + 1.014_{(44)} rM1 + 0.314_{(46)} rM2 \qquad [R^2 = 0.9987],$$
$$\mathbf{b} = 7.552_{(46)} + 0.745_{(73)} rM1 + 2.922_{(78)} rM2 \qquad [R^2 = 0.9995].$$

Because the **a** cell edge is mainly dependent on *rM1* and **b** on *rM2*, these equations are used to construct an **a** *vs* **b** diagram which may be contoured for bulk composition (in mol fraction or % Te, and X_{M2}, the Mn content of the *M2* octahedral sites (see Fig. 1; $X_{M1} = 2\text{Te} - X_{M2}$). To obviate lattice parameter refinement, the intensity ratios of the prominent and order-disorder-sensitive 131 and 112 peaks in a powder pattern (Cu$K\alpha$ radiation) may be used together with the *d*-spacing of the 112 peak (sensitive only to bulk composition) to locate a point on the **a**-**b** grid (Fig. 2). This is transferred to Figure 1 to estimate Fo-Te composition and Mg-Mn distribution.

A construction similar to Figure 2 has been made for the forsterite-fayalite (Fo-Fa) binary system. However, because the range of Mg-Fe order-disorder is so slight in both natural and synthetic specimens and because there is a disconcertingly large measure of inconsistency in the results of the many crystal structure and Mossbauer analyses of Mg-Fe distribution in these olivines, regressions on cell parameters are of questionable utility. This may be due in part to ambiguous site assignments of the minor impurities in natural specimens.

Figure 3 is an **a**-**b** plot of data from three variously synthesized series of Mg-Fe olivines. With the exception of two Fa specimens whose cell parameters have large estimated errors, all these data fall on a smooth curve. Using the best of the regression equations obtained from Fo-Fa structural data, we estimate that these specimens have Fe preferentially ordered into the *M1* site with $K_D \equiv 0.80 \pm 0.05$, where $K_D = [\, X_{M1}(1 - X_{M2}) \,] / [\, X_{M2}(1 - X_{M1}) \,]$.

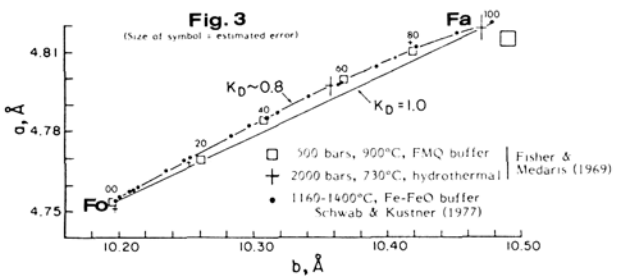

MOISSANITE, SiC: YES OR NO?

MILTON, CHARLES, Dept. of Geology, The George Washington University, Washington, D. C. 20052, USA; VITALIANO, DOROTHY B., U. S. Geological Survey, Bloomington, Indiana 47401, USA.

For the first half of this century, silicon carbide--moissanite--first described as a minor accessory mineral in the Canyon Diable (Arizona) meteorite (Moissan, 1904, 1905) was of little interest to geologists. Noted in the Limburg Loess (Netherlands), it was traced to carborundum contamination (Druif, 1927). Its appearance in numerous North American well cuttings (Ohrenschall and Milton, 1931) was attributed to a meteoritic source in the light of Moissan's discovery, because SiC is extremely resistant chemically and physically. However, this was challenged (Edelman, 1932) and laboratory contamination by carborundum indicated. In the USSR, SiC had been noted in crushed geological samples, but viewed as a contaminant (Popov, 1952). And Moissan's report, already questioned (Merrill, 1930), was finally discredited--carborundum again (Yudin, 1970).

In 1958 authigenic SiC was reported in the Eocene Green River oil shale of Wyoming, USA (Regis and Sand, 1958), and in kimberlite in the USSR (Bobrievich et al., 1958). Since then, over 150 articles, in a dozen languages, have described finds of moissanite, practically all of them in heavy mineral concentrates from igneous, sedimentary, and metamorphic rocks or natural alluvium; many authors cite Regis and Sand and Bobrievich et al. as pioneer discoverers. By far, most such reports are from Eastern Europe and Siberia.

Not one of the hundreds of geologists who have studied the Green River shale has confirmed Regis and Sand's discovery. As for other occurrences, simple calculations from readily available data show that enough SiC has been manufactured, ground to powder and discarded all over the world, then to be dispersed by wind and water, to provide a hundred dust-sized particles for every square meter of the earth's surface!

In 1979 the late eminent Russian geologist V. S. Sobolev vigorously questioned moissanite findings, stressing (carborundum) contamination of samples. He proposed that only a large rock sample showing indisputable SiC mineralization--not isolated microscopic grains--should be acceptable evidence of moissanite's existence in nature. Additional criteria would be SiC included in or including any known magmatic (especially hydrothermal) mineral; eutectic or sutured intergrowth with a magmatic mineral; completely euhedral and unbroken single crystals; and fluid (not solid!) inclusions. Has any reported moissanite met even one of these criteria? Sobolev called for an All-Union committee to examine the moissanite problem; the International Mineralogical Association, recognizing that the problem is not only Soviet, but world-wide, has authorized a USSR-USA committee to study the matter and reports its conclusions. As Sobolev stated, "spurious mineralogical data" can lead to theoretical considerations with far-reaching implications, and to false practical conclusions that can do serious damage to the national economy (using SiC as a guide-mineral in diamond prospecting being a case in point).

Therefore in view of the ever-present possibility of carborundum contamination of geological samples, either in the field, or despite all reasonable precautions, in the laboratory, it is necessary to verify beyond doubt that reported occurrences of SiC are actually of natural terrestrial origin. Meeting stated and accepted criteria of authenticity is the essential means of verification. The I.M.A. Committee will seek to evaluate, using such criteria, the validity of all published moissanite reports.

HIGH PRESSURE-HIGH TEMPERATURE STUDIES WITH SYNCHROTRON RADIATION

MING, L. C., and MANGHNANI, M. H., University of Hawaii, Hawaii Institute of Geophysics, 2525 Correa Road, Honolulu, HI 96822, USA

Diamond anvil pressure cell (DAC) is capable of generating pressures up to 300 GPa at room temperature; it can be heated internally to 5000-6000 K (by means of a high power laser) as well as externally to ∿1000°C with a resistance-wire heater. However, measurements at simultaneously high pressure and high temperature x-ray diffraction, using conventional x-ray sources, are not feasible. The major problem is the long duration of data aquisition (e.g., 20-300 hours for one data point) because of the extremely small sample size (e.g., 10^{-5} cm^3) and weak x-ray source. At high temperatures above 600°C, diamond is gradually graphitized and metal parts in the DAC tend to creep, thereby losing high strength properties needed to sustain pressure. This difficulty can now be overcome by using synchrotron radiation.

In past years, we have successfully interfaced DAC with the synchrotron radiation at the Stanford Synchrotron Radiation Laboratory (SSRL), and carried out x-ray diffraction experiments at simultaneously high pressure-high temperature conditions up to 30 GPa and 600°C using an energy dispersive system. The extremely intense and brilliant synchrotron radiation has enabled us to obtain a high quality x-ray diffraction spectrum in 5-20 minutes.

Experimental data for Fe, FeF_2, Fe_3O_4, MgO, (Fe,Mg)O, and γ-$(Mg,Fe)_2SiO_4$ are presented and discussed in light of high temperature equations of state and the observed phase transitions (i.e., in Fe and FeF_2).

Mn-BEARING MINERALS FROM TRIKORFO METAMORPHIC ROCKS, THASSOS, GREECE.

MITSAKI-HAFNER V., Institute of Geology and Mineral Exploration, Messoghion 70, Athens 11527, Greece.

Trikorfo rocks belong to Maries Schist Unit of Thassos. The rocks of this small area are characterized by a wide range of mineral assemblages : (1) qtz + phl ± mus ± zo/czo/piemt ± garn ± chl + fld, (2) qtz + Mn-and ± Ky + mus + phl + piemt + plg, (3) qtz + ky + sill + mus + phl + plg, (4) qtz + staur + ky + sill + mus + phl + garn + chl + fld, (5) qtz + diops + tr + epd + mus ± chl + fld, (6) horn + epd + biot + chl + fld.

Minerals from theses assemblages have been studied by optical and electron microprobe techniques. It is the first time that Mn-andalusite is found in Greece. It occurs in green crystals and contains up to 8.4 Mol% Mn_2SiO_4 and 2.40 Mol% Fe_2SiO_4. Kyanite coexisting with Mn-andalusite contains 2.73 Mol% Mn_2SiO_4 and 0.77 Mol% Fe_2SiO_4, whereas kyanite coexisting with sillimanite contains 0.11 Mol% Mn_2SiO_4 and 0.94 Mol% Fe_2SiO_4. Garnet from the assembage mus + garn + piemt has the composition $spess_{78.9}$ $py_{3.4}$ $gross_{12.6}$ $andra_{5.1}$. Piemontite from the same assemblage contains from 4.36 to 12.84 wt% Mn_2O_3 and from 3.84 to 7.47 wt% Fe_2O_3. Piemontite coexisting with Mn-andalusite contains from 3.05 to 7.31 wt% Mn_2O_3 and from 9.54 to 12.82 wt% Fe_2O_3. Thulite occurs as pink crystals in a thin layer in the assemblage (5) and in some phlogopite schists. Phlogopite from the assemblage (2) contains up to 1.26 wt% MnO. Diopside, tremolite and epidote from assemblage (5) contain 0.84 wt%, 0.64 wt% MnO and 0.62 Wt% Mn_2O_3 respectively. Abundant hematite occurs in all the assemblages. Ti-Mn hematite was found in the assemblage (2) and braunite in the assemblage mus + garn + piemt.

The conditions of metamorphism are discussed. The origin of the Mn-bearing minerals is assumed to be a very thin, high oxidized, Mn rich layer in a pelitic sediment.

SERPENTINE-GROUP MINERALS WITH AND WITHOUT CHLORINE IN TERRESTRIAL AND EXTRATERRESTRIAL MATERIALS

Miúra, Y., Department of Mineralogical Sciences and Geology, Faculty of Science, Yamaguchi University, Yoshida, Yamaguchi, 753, Japan.

Serpentine-group minerals have been found among in the terrestrial rocks [1], carbonaceous chondritic meteorites [2] and interplanetary dust particles (IPDs) [3]. The details of classification of the serpentine-group minerals, however, have not been reported so far. The purposes of this study are to classify the these serpentines based on electron microprobe (EPMA) data, and to determine the structural site of chlorine ions in the fine-grained serpentines from terrestrial ultramafic dunites by applying the transmission electron microscopy (TEM) with EDS analytical aids.

The terrestrial serpentine-group minerals with minor Fe content are classified as lizardite (OC/TC=1.70∿1.95), chrysotile (OC/TC=1.52∿1.70) and antigorite (1.4∿1.52) by EPMA and TEM data, where the OC and TC means octahedral and tetrahedral cations, respectively. The lizardite with the chlorine is, therefore, the first serpentine phase from olivine (OC/TC=1.95∿2.00) under hydrous condition [4].

The chlorine sites in the Dumont fine-grained serpentines [1] are found by the TEM-EDS data. The irregular grain boundaries, stacking-faults, and wavy lattice images are observed mainly in the lizardite crystals. The most probable site for the chlorine is considered to be the grain boundary and OH atomic site.

The reaction process among the serpentines is assumed to be from lizardite, chrysotile to antigorite, because of the OC/TC ratios of these phases are changed gradually in the Si-Mg-Fe diagram.

The ferrous serpentine [5] (FeO≒17wt%, Fe/Si<1) and cronstedtite (FeO≒54wt%, Fe/Si>1) as 7Å aqueous phyllosilicates are found in carbonaceous chondrites. The difference in compositional ratios of OC/TC (1.21-1.71 in Allende; 1.22-1.38 in ALH-77307,85-1) and Fe/Si(<1) is essential in the Fe-serpentine, because there are few differences in TEM-ED data of the Fe-serpentine and cronstedtite. The trace amount of chlorine in the Fe-serpentine is found only in the Allende chondrite. The Fe-serpentine is assumed to be formed in aqueous parent body, but the occurrence in the Fe-serpentine is completely at random in the matrix, compared with that of the terrestrial serpentine.

The study is supported by the Grant for Fundamental Scientific Research (The Monbusho) of 1985 of the author.

REFERENCES:

[1] Miúra, Y., Rucklidge, J. and Nord,G.(1981): Contrib. Mineral. Petrol, 76, 17-23.
[2] Miúra, Y. (1986): Proc. Symposium of Antarctic Meteorites XI (Tokyo), 11, 21-22.
[3] Tomeoka, K. and Buseck, P.R. (1984): Earth and Planetary Science Letters, 69, 243-254.
[4] Miúra, Y. et al. (1986): Technical report of the Fundamental Scientific Research of 1985. 112-115.
[5] Tomeoka, K. and Buseck, P.R. (1985): Geochimica Cosmochimica Acta, 49, 2149-2163.

STRUCTURAL STUDIES THROUGH PAIR POTENTIALS

MIYAMOTO, M., Coll. of Arts and Sci., Univ. of Tokyo, Komaba, Tokyo 153, JAPAN; TAKEDA, H., Mineral. Inst., Faculty. of Sci., Univ. of Tokyo, Hongo, Tokyo 113, JAPAN

We have applied lattice energy calculations (WMIN, 1) of some silicates to predicting their structures under high pressure. We assume the total energy (W) of a crystal consisting of both the coulomb energy and repulsive energy.

$$W = 1/2 \cdot \Sigma\Sigma_{ij}[Q_i \cdot Q_j/r_{ij} + f_0 \cdot (B_i+B_j) \cdot \exp((A_i+A_j-r_{ij})/(B_i+B_j))] \quad (1)$$

where r_{ij} is the distance between two ions; Q_i is the ionic charge; f_0 is a constant. The Born-Mayer type repulsive force is calculated by ionic radius A and ionic compressibility B, which are defined as characteristics of each ion. This expression may give more information about physico-chemical interpretation on mantle mineral structures than that obtained by briefly describing crystal structures of minerals on the basis of the 'ionic radii' data alone (2), because it includes a term of the softness of ions in addition to the radii.

We have shown that high pressure structures of some Mg-silicates can be predicted by using the repulsive parameters obtained by the forsterite (Mg_2SiO_4) structure under the constraint that the cell dimensions are fixed at the observed values at high pressure (3,4). Our calculations are satisfactory to deduce the general principles of the changes of bond distances with increase of pressure. For example, degrees of shortening of larger bonds are larger than those of shorter bonds (e.g., 5). However, we had to assume that the A and B terms will be unchanged at high pressure.

In order to examine pressure dependence of repulsive parameters, repulsive parameters of Ti have been calculated in high pressure structures of rutile (6) and those of Fe in high pressure structures of fayalite (6,7). The results do not show much changes of repulsive parameters in high pressure structures of mantle minerals. We also obtained similar repulsive parameters of octahedrally coordinated Si in stishovite as those tetrahedrally coordinated Si in forsterite.

In order to elucidate the crystal chemical aspect of repulsive parameters defined in eq. (1), we have calculated the repulsive parameters of transition metals (Mn, Fe, Co, and Ni) in the olivine structures (8), rare earth elements except for La and Ce in the perovskite structures (7), and Si, Ge, Sn, Mn, and Ru ions in the rutile structures. These results show that ionic radii (A) usually have strong correlation with traditional ionic radii (2) and that ionic compressibilities (B) seem to reflect electron density distributions of ions. In the rutile structures ionic compressibilities may influence interionic distances, because the B values of these ions are relatively large. These results may lead us to interpret crystal structures or crystal-chemical properties of minerals on the basis of repulsive parameters.

Formal charges of ions in eq. (1) are used in our calculations, although true charges of ions in a crystal may be different (9). In order to examine this, we have refined charges of Mg, Si, and O ions in forsterite together with all repulsive parameters under the constraint of electrical neutral. Although the repulsive parameters do not change much, the charges of Mg, Si, and O ions are 1.46, 1.68, and -1.15, respectively. These results are consistent with those obtained by X ray diffraction study (9) (they are 1.75, 2.11, and -1.40, respectively).

Our simple model can predict the frameworks of structures of mantle minerals, as an extension of traditional ionic radii. Although we often meet the divergence of the nonlinear least-squares method to determine repulsive parameters, more precise X ray structure data sometimes lead to convergence. Namely, the least-squares method is sensitive to the quality of structure data. We need precise structure data at high pressure to obtain repulsive parameters as well as better expression for repulsive forces of ions in minerals.

References: (1) Busing, W. R. (1981) ORNL-5747, Oak Ridge. (2) Shannon, R. D. and Prewitt, C. T. (1969) Acta Cryst., B25, 925. (3) Miyamoto, M. and Takeda, H. (1980) Geochem. J., 14, 243. (4) Miyamoto, M. and Takeda, H. (1984) Amer. Mineral., 69, 711. (5) Hazen, R. M. and Prewitt, C. T. (1977) Amer. Mineral., 62, 309. (6) Kudoh, Y. and Takeda, H. (1986) Proc. 10th AIRAPT Conf. (in press). (7) Yamada, N. and Takeda, H. (1986) unpublished data. (8) Miyamoto, M., Takeda, H., Fujino, K., and Takeuchi, Y. (1982) Mineral. J., 11, 172. (9) Fujino, K., Sasaki, S., Takeuchi, Y. and Sadanaga, R. (1981) Acta Cryst., B37, 513.

CRYSTAL CHEMISTRY OF HYDROUS RARE EARTH CARBONATE MINERALS — THE CRYSTAL STRUCTURE OF TENGERITE —

MIYAWAKI, R., TAKASE, J. and NAKAI, I., Dept. of Chemistry, The University of Tsukuba, Ibaraki, 305 Japan.

1. Introduction The crystal structures of hydrous rare earth carbonates have been known only for lanthanite and ancyrite. It seems likely that the formation of these minerals are related with kinds of rare earths (RE), and that structures of $RE_2(CO_3)_3 \cdot nH_2O$ depend on the number of water molecules, n. Since lacking of the structural data for the other minerals makes it difficult to understand these problems, the authors have initiated synthetic investigation of the RE_2O_3-CO_2-H_2O and RE_2O_3-CaO-CO_2-H_2O systems.

2. Synthesis Effects of pH and temperature conditions and kinds of the RE on the phase formations were examined by the gel method, and hydrothermal methods using a stellite bomb of the test tube type and using a pyrex glass tube. The products were characterized by the X-ray diffraction, IR spectrum and chemical analysis (ICP-AES for RE and C.N.H. elementary analysis). Tengerite, lanthanite, ancyrite, hydroxyl-bastnaesite and four unknown hydrous rare earth carbonates have been synthesized.

3. Crystal structure of tengerite The structure of tengerite has been determined using a single crystal synthesized by the hydrothermal method[1]. Crystal data: $Y_2(CO_3)_3 \cdot 2H_2O$, $Bb2_1m$, a=6.078(4), b=9.157(2), c=15.114(6)Å, Z=4; intensity data: $\sin\theta/\lambda \leq 0.904$, 765($|F_o| \geq 3\sigma$) reflections, corrected for absorption effect. The structure was determined by a combination of direct method and Patterson method and refined by full-matrix least-squares program RFINE2 to final R (R_w) of 0.045 (0.050).

4. Description and discussion The crystal structure of tengerite can be described in terms of a sheet structure built up from 9-coordinated Y-polyhedra and CO_3 triangles (Fig.1). The corrugated sheets are connected to each other by CO_3 triangles to form a three-dimensional framework (Fig.2). The chemical formula thus found is $Y_2(CO_3)_3 \cdot 2H_2O$. The difference of the number of H_2O, n=2, from the values determined by our chemical analysis ($2<n<3$) suggests the presence of zeolitic water in tengerite, as estimated by Nagashima and Wakita[2]. On the other hand, crystal structure of lanthanite[3] is built up from free H_2O and platy-sheets of 10-coordinated RE polyhedra and CO_3 triangles, and their sheets are connected by hydrogen bonds. The difference of C.N. of RE atoms reflects on the results of the syntheses. Y-group RE with smaller ionic radii crystallized in tengerite structure (C.N.=9) and Ce-group RE with larger ones in lanthanite structure (C.N.=10). Tengerite, kimuraite[4] and lokkaite[4] show an interesting correlation among the cell dimensions and the number of cations (Table 1), suggesting a structural relation in these minerals. Such a correlation is also found between lanthanite and calkinsite.

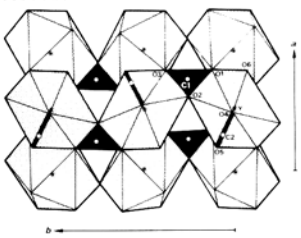

Fig.1. Crystal structure of tengerite, showing the corrugated sheet parallel to the (001) plane.

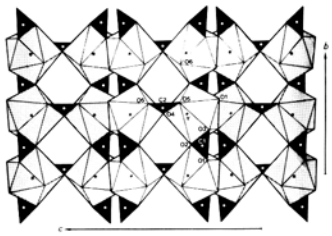

Fig.2. The corrugated sheets (Fig.1) are connected by CO_3 triangles of C2.

Table 1. Relationship among crystal data.

	tengerite $RE_2(CO_3)_3 \cdot 2H_2O$	kimuraite[4] $CaRE_2(CO_3)_4 \cdot 6H_2O$	lokkaite[4] $CaRE_4(CO_3)_7 \cdot 9H_2O$
Cell dimensions	a= 6.078(4) Å b= 9.157(2) c=15.114(6)	c= 6.0433(7) Å a= 9.2545(8) b=23.976(4)	b= 6.104(4) Å c= 9.26(1) a=39.35(2)
ratio	[c:1.92]	[b:3.05]	[a:5]
No. of cations	2	3	5

1. Tareen, J. A. K., et al. (1980) J. Cryst. Growth, 49, 761.
2. Nagashima, K. & Wakita, H. (1968) Nippon Kagaku Zasshi, 89, 856.
3. Dal Negro, A., et al. (1977) Am. Mineral., 62, 142.
4. Nagashima, K., et al. (1986) Am. Mineral., 71, in press.

A SMALL SCALE ADIABATIC CALORIMETER FOR HEAT CAPACITY MEASUREMENT OF MINERALS

MIZOTA, T., Dept. of Mining and Mineral Engineering, Faculty of Engineering, Yamaguchi University, Ube 755, JAPAN

Heat capacity and transition enthalpy are essential parameters for thermodynamic consideration of materials. Adiabatic calorimetry is the most reliable method for heat capacity measurement and has been used extensively, but the method requires commonly large amount of sample as much as 10-100g. Such amount of a mineral is not easy to accumulate in a pure state from natural specimens, so that the application of the method has been limited to a few minerals obtainable in a considerable amount or to synthetic minerals. Because of the difficulty to collect such amount of a sample, the DSC method has been developed recently for heat capacity measurement of minerals using some 10mgs of the sample. As DSC is a kind of relative methods like DTA, base line drift may be fatal for a precisely quantitative measurement and fine spectral features in a heat capacity curve around higher order transition, for example, may remain doutful. For a lower temperature calorimetry, a small scale adiabatic calorimeter having a sample cell of 0.6cm^3 was made and used successfully (Matsuo and Suga,1985). As geoscientists, however, have strong interest in thermodynamic properties of minerals at higher temperature, an adiabatic calorimeter having a relatively small sample container has been made by Mizota et al. (1983) to measure heat capacity and transition enthalpy of cubanite (Mizota et al. 1985). In the present investigation the calorimeter has been improved so as to measure up to higher temperature, 800°C. The central part of the calorimeter including sample container and the 1st adiabatic shield is made of Pt-Rh10% alloy. The maximum sample volume available is 2.6cm^3. Most part of the calorimeter was made of metals so as not only to reduce the heat capacity but also to increase the thermal conductivity in order to homogenize temperature distribution during measurement. The miniaturization of the calorimeter contributed effectively to the rapid attainment of thermal equilibration in the calorimeter. This enables us to make relatively quick temperature elevation saving measuring time. The sample can be exchanged as easily as in the case of DTA or DSC method. The calorimeter system is equipped with an analog PID circuit for the adiabatic control. Data acquisition and data processing are automated by using a microcomputer system. Totally, the calorimeter system is compatible with easy handling which is effective to utilize in the field of geoscience.

The figure shows an example of a heat capacity measurement of quartz from Brasil between 40°C and 600°C . Quartz powder, -48+100mesh, 2.17513g, was used in the measurement. The solid line indicates the heat capacity curve of quartz reported by Moser(1936) who used a cylindrically formed crystal of quartz from Brasil of about 32.6g.

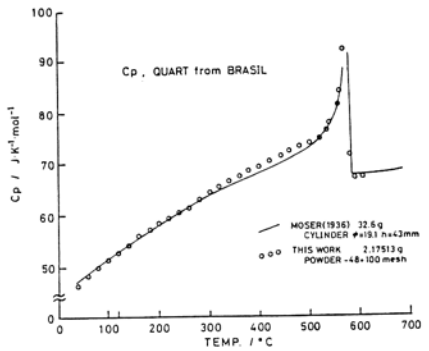

MATSUO, T. and SUGA, H.(1985) Thermochim. Acta, 88, 149-158.
MIZOTA, T., TANAKA, H., FUJII, Y. and KOTO, K.(1985) Canad. Mineral., 23, 77-82.
MIZOTA, T., TANAKA, H., FUJII, Y. and SHIMA, H.(1983) J. Mineral. Soc. Japan, 16, Special issue 1, 39-47.
MOSER, H.(1936) Physik. Zeit., 37, 737-753.

LEAD-SULFOSALT MINERALOGY : THE STATE OF THE ART.

MOËLO, Y., CNRS-CSCM, 45071 Orléans Cedex 2, France.

Among the 150 sulfosalts known, more than ninety are lead sulfosalts. Half of them were defined during the last two decades, which corresponds to the discovery of about two new species per year. This explosive development of lead-sulfosalt mineralogy is principally due to the use of electron microprobe, which facilitates largely metallographic studies.

In the seventies, the crystal structure determination underwent a strong development, and today two thirds of structures are solved. They permitted, during the last five years, the elaboration of a detailed crystal-chemical classification of these compounds (for instance, see Makovicky, 1985). Simultaneously, the majority of lead sulfosalts were synthetized by experimental studies on pseudo-binary, -ternary and -quaternary systems.

The increasing interaction between microprobe analyses, structure determination and experimental studies led to understand better the crystal-chemical role of major constituents, and opened new exploration for the integration of minor elements (Cu,Mn,Cl,Se,Cd...) within specific structures.

Lead-sulfosalt mineralogy left now the field of pure systematic approach, becoming an integral part of mineralogical and petrological studies on hydrothermal sulfide ores (vein or stratiform deposits, and their metamorphic equivalents). Despite the fact that quantitative thermochemistry data are still scarce at the present time, the lead-sulfosalt mineralogy contributes to the knowledge on the genesis and evolution of sulfide ores. This type of approach was applied to the comparative paragenetic study of numerous deposits from french hercynian ore-fields.

MAKOVICKY, E. (1985) - The building principles and classification of sulphosalts based on the SnS archetype. - Fortschr. Miner. 63, 45-89.

LILLIANITE HOMOLOGUES (GUSTAVITE, VIKINGITE, Ag-Bi RICH HEYROVSKYITE ...) FROM THE W-As-(Pb,Bi,Ag) OCCURRENCE OF LA ROCHE-BALUE (LOIRE-ATLANTIQUE, FRANCE).

MOËLO, Y., CNRS-CSCM, 45071 Orléans Cedex 2, France ; MARCOUX, E. et LEGENDRE, O., BRGM, 45060 Orléans Cedex, France ; MAKOVICKY, E., Institut for Mineralogi, 1350 København K, Danemark ; KARUP-MØLLER, S., Institute of Mineral Industry, 2800 Lyngby, Danemark.

In the gneiss quarry of La Roche-Balue (West of Nantes, France), a quartz vein is principally mineralized with scheelite, arsenopyrite and galena, with numerous Pb-Bi-Ag sulfosalts. Three stages of deposition have been observed :

- stage 1 : pneumatolytic, with quartz and orthoclase ;
- stage 2 : hypothermal (350 - 400°C), with quartz, scheelite, arsenopyrite (+ pyrrhotite and molybdenite), gustavite I + vikingite + Ag-Bi rich heyrovskyite + eskimoite (+ gold), galena ;
- late stage 3 : epithermal, with pyrite, marcasite, chalcopyrite, argentiferous cosalite, gustative II, bismuth and tetrahedrite.

Between crossed polars, gustative I and II show ubiquitous complex twinning. In gustavite I, numerous exsolution lamellae of an Ag-Bi poor member of the gustavite-lillianite series are always present. On the contrary, the smaller crystals of gustavite II are pure members of the series. Vikingite is polysynthetically twinned, with another twinning, analogous to that of gustavite, visible on a smaller scale. Ag-Bi rich heyrovskyite is untwinned. These three sulfosalts frequently form epitactic associations. Weak anisotropy of galena reveals polysynthetic twinning of mechanical origin.

Microprobe analyses show 3.1 % Bi and 1.6 % Ag in anisotropic galena. Pb sulfosalts contain 0.02 - 0.05 % Se, 0.04 - 0.14 % Sb and 0.10 - 0.80 % Cd. In the lillianite homologues, Cd increases with Ag-Bi content. Cosalite contains 1 % Cu and 2.6 % Ag. In stage 2, the sulfosalts show a composition trend subparallel to the Bi_2S_3-Pb_2S_2 join in the Pb_2S_2-Bi_2S_3-Ag_2S system.

X-ray study of lillianite homologues permitted to characterize the five sulfosalts included in galena, specially the two members of the gustative-lillianite series, and the minor eskimoite in epitactic association with heyrovskyite.

During the final epithermal stage, primary Pb sulfosalts dissolved to give (gustavite II + cosalite + galena) association. Decomposition of these lillianite homologues may be due to their instability at low temperature, or to the presence of copper wich favours the crystallization of cosalite.

Cd content of Pb-Bi-Ag sulfosalts is similar to Cd content frequently observed in the andorite series. Apparently, Cd enrichment is typical for ore solutions mobilized in post-magmatic processes generated by granitic intrusions.

MINERALOGICAL INVESTIGATIONS ON FRANCKEITE-CYLINDRITE INTERGROWTHS

MOH, G.H., Mineralogisch-Petrographisches Institut der Universität, 6900 Heidelberg, Germany

Among numerous naturally occurring sulfosalts the franckeite group and the crystalchemically related cylindrites are the most complex ones. They can be understood as thio-antimonates and thiostannates of various cations. Due to contradicting literature data about these minerals, a research program was initiated coordinating ore microscopy, X-ray and microprobe studies, experimentation and Mössbauer analyses.

Concerning franckeite, the now available results show iron as a structurally essential element, while lead can be substituted by bivalent tin, producing a solid solution series. Tin occurs in two valency states. Silver may or may not be present. Of the well established silver-free formula the ideal lead-rich endmember is potosiite $Pb_6Fe^{2+}Sb_2^{3+}Sn_2^{4+}S_{14}$. Most natural franckeites, however, reveal a partial lead-tin replacement up to about $Pb/Sn^{+2} = 2/1$ which corresponds to incaite. Though the tin-rich and lead-free endmember $Sn_5^{2+}Fe^{2+}Sb_2^{3+}Sn_2^{4+}S_{14}$ has been synthesized at elevated temperatures, its natural occurrence is doubtful. Valencies of the elements concerned are proved by Mössbauer spectroscopy of the isotopes ^{57}Fe, ^{121}Sb, and ^{119}Sn. The structure of franckeites is yet unknown. Positions of 4-5 thousand atoms in the large monoclinic unit cell are assumed to be involved in the structure analysis.

Franckeites may contain traces of Zn, In and Ge, all together less than 1%; the partial substitution of Sn^{4+} by Ge^{4+} has been experimentally confirmed.

In some Bolivian occurrences intergrowths of typical cylindrites with franckeite or incaite, respectively, are known. Experiments and subsequent microprobe analyses on ores demonstrate also the direct replacement of incaite by cylindrite producing pseudomorphic lamellae but no cylinders. The formation of cylindrite requires increased sulfur activity. Thus in a simplified reaction, starting with incaite, most or all bivalent tin oxidizes to tetra-valent and cylindrite $Pb_4FeSb_2Sn_4^{4+}S_{16}$ forms. Numerous microprobed cylindrites indicate a restricted solid solution series with slight Pb/Sn^{+2} variations.

The research project on complex sulfosalts with G. Amthauer, H.-J. Bernhardt, Li Jiuling, and N. Wang is being continued.

CRYSTAL-CHEMISTRY OF MAGMATIC C2/c CLINOPYROXENES OF LOW AND HIGH PRESSURE ORIGIN: STRUCTURAL DISTINCTIONS

MOLIN G.M.,SECCO L.,DAL NEGRO A.,Ist. Mineralogia e Petrologia Università di Padova,Italy;CUNDARI A.,Dept. of Geology University of Melbourne,Australia;PICCIRILLO E.M.,Ist. Mineralogia e Petrografia Università di Trieste,Italy.

An extensive research program on C2/c clinopyroxene (cpx) belonging to volcanic and mantle materials has been under way since 1978 (Universities of Padova, Melbourne and Trieste). The main goals concern: a) Relationships between site geometry variations over a wide range of cpx compositions and the influence of single site geometry on the structural framework; b) Relationships between cpx site geometry and host-rock compositions at low and high pressure regimes; c) Applications to petrology in terms of crystallization-melting process(es), and intracrystalline cation site partitioning.

The investigated products are: 1) Tholeiitic, Transitional and Alkaline Basalts;2) Quartz to Nepheline normative Trachytes; 3) Lamproites; 4) Basalt-Andesite-Dacite suite; 5) Transitional Basalt-Comendite-Pantellerite suite; 6) Basanite-Phonolite suite; 7) Leucitite-Phonolite suite; 8) Spinel Lherzolite to Harzburgite nodules.

Results are based on ca. 250 single crystals both X-ray refined and Electron Probe analysed;(Ca^{θ}=Ca+Na; $R^{3+}=Al^{VI}+Cr^{3+}+Fe^{3+}+Ti^{4+}$).

Low-pressure clinopyroxene (LPC)

LPC is characterized by a larger cell volume than that of high-pressure clinopyroxene (HPC), namely: LPC=437-449 $Å^3$, HPC=433-437 $Å^3$. This larger cell volume for LPC is mainly due to the larger volume of M1 site for LPC than that of HPC.

Site geometry variations

1) V(M2) (i.e. Ca^{θ}) increase is obtained by shortening of the longest bond lengths (M2-O1, M2-O2), and lengthening of the shortest bond distances (M2-O1, M2-O2), allowing more regular M2 site geometry. This opposite behaviour of M2-O bond lengths causes lengthening of T-O3 and shortening of M1-O1 and M1-O2 bond lengths which favour the entry of Al^{IV} and R^{3+} into T and M1 sites, respectively. V(M2) increase is responsible for increasing of O3-O3-O3 angle and tetrahedron angle distortion, both emphasized by V(T) decrease.

2) V(M1) (in general Fe^{2+}) increase is obtained by the lengthening of M1-O bond lengths, allowing more regular M1 site geometry. Such lengthening causes shortening of $T\text{-}O_{non\ brg.}$ bond lengths which favours high Si content in T site.

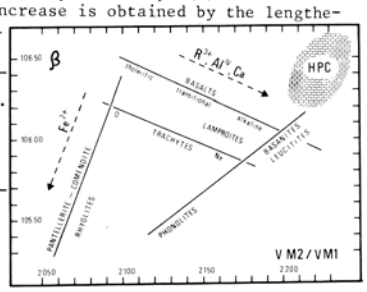

Site geometry and magma composition

1) The site geometry variation described as 'V(M2) increase' (see point 1 above) mainly explains the mineral chemistry of cpx in basaltic rock-types with alkaline (high Ca^{θ}, Al^{IV} and R^{3+}) to tholeiitic (low Ca^{θ}, Al^{IV} and R^{3+}) affinity.

2) The site geometry variation described as 'V(M1) increase' (see point 2 above) mainly explains the mineral chemistry of cpx in evolved rock-types (e.g. trachytes, phonolites, etc.). It is to be noted in this case that the high Si content of cpx must be found not only for oversaturated but also for undersaturated evolved melts.

3) The relationships between relevant site geometry variations and magma composition are illustred in the figure by the variations between V(M2)/V(M1) ratios and the β angle, which is mainly negatively correlated to V(M1).

High-pressure clinopyroxene (HPC) (spinel peridotite nodules)

The small volumes of M1 and T sites (11.40-11.68 $Å^3$ and 2.23-2.25 $Å^3$ respectively) cause large reduction of HPC cell volume relative to that of LPC. Notably, V(M2) of HPC and LPC are comparable. The small volume of T site is ensured by a large quantity of Si (ca. ≥1.90 a.f.u.), while the small volume of M1 site is obtained either by high content of Al^{VI} (ca. 0.20 a.f.u.) or Cr^{3+} and Fe^{3+} (ca. 0.10 a.f.u.).

The cpx response to increasing $Mg/(Mg+Fe^{2+})$ (i.e. temperature) is achieved by progressive depletion of Fe^{2+}(M1), Al^{VI} and Ti^{4+}, and enrichment in Mg, Cr^{3+} and Fe^{3+} in M1 site. Depletion of Fe^{2+}(M2) occurs at the highest thermal levels and after Fe^{2+}(M1) has been strongly depleted or exhausted, depending on the total pressure.

ELEMENT FRACTIONATION AND DIFFERENTIATION OF THE GRANITES OF NE-BAVARIA, FEDERAL REPUBLIC OF GERMANY

MÖLLER, P., Geochemical Group, Hahn-Meitner-Institut für Kernforschung GmbH, Berlin, F. R. G.;
MORTEANI, G., Institut für Angewandte Mineralogie und Geochemie, University of Munich, F. R. G.

The Fichtelgebirge (NE-Bavaria) is the western extension of the Erzgebirge with its well-known tin mineralizations. The Oberpfalz Mountains are the southern annex of the Fichtelgebirge. In both areas intensive granitic magmatism at the end of the Sudetic (Early Variscan) orogenesis started. According to STETTNER (1972) and RICHTER and STETTNER (1979) the Variscan granites intruded in two series at about 315 Ma and 285 Ma. The porphyric granites (G1) solidified at deeper levels than the later granites G2, G3, and the so-called tin granite (G4). The time hiatus between the two series is about 30 Ma.

The whole rock samples of the granites display nearly no (G1) to large (G4) Eu-anomalies. The amount of the Eu anomalies are negatively correlated with the content of Ba, Sr, and Ca in the granites. This set of elements is typical for plagioclase. Their concerted decrease is due to plagioclase segregation. In the sequence G1 to G4 the rare alkalis, Nb, Ta, and U increase, the REE decrease from Lu to La. Mg, Ti, Zr, and Hf decrease together with Th. The geochemical behaviour of the cited elements will be discussed as the result of Lewis acid-base reactions of the various oxides in granitoid melts of increasing acidity. Postmagmatic alteration is negligible in general. Only locally REE redistribution between feldspar and biotite is observed (Möller et al., 1985).

In literature the question of one or two magmatic sources for the granites of the two intrusion episodes is discussed controversively. One of the reasons to state two independent magma chambers is the difference in the initial Sr ratios. They are 0.708 and 0.717 in both areas (BESANG et al., 1976; KÖHLER et al., 1974). Supported by the chemical results according to which Sr has been greatly reduced in the melt by plagioclase segregation it can be delineated that the Rb/Sr ratio of the residual melt shifted continuously to higher values. Modelling the changes of Sr content, Sr initials and Rb/Sr ratios as well as considering the time hiatus between the first and second intrusion sequence it can be demonstrated that all granites could stem from the same magma reservoir. This implies that the magma cooled very slowly. A rather dry magma as the initial melt would serve such a model best. Based on this model the grade of solidification of the magma in the reservoir and segregation rate of plagioclase between the intrusion episodes are estimated.

The combination of geochemical and geochronological work leads to a rather vivid picture of the history of the granite differentiation in the area studied.

BESANG, C., HARRE, W., KREUZER, H., LENZ, H., MÜLLER, P., and WENDT, I., 1976. Radiometrische Datierung, geochemische und petrographische Untersuchungen der Fichtelgebirgsgranite: Geol. Jb., Ser. E, v. 8, pp. 3-71.

KÖHLER, H., MÜLLER-SOHNIUS, D., and CAMMAN, K., 1974. Rb-Sr-Altersbestimmungen an Mineral- und Gesamtgesteinsproben des Leuchtenberger und des Flossenbürger Granits, NE Bayern: N. Jb. Mineral. Abh., v. 123, pp. 63-85.

MÖLLER, P., MORTEANI, G., and HOEFS, J., 1985. REE and $^{18}O/^{16}O$ distributions in altered Variscan granites of the Western Harz, Germany, and southern Sardinia, Italy. In: High heat production (HHP) granites, hydrothermal circulation and ore genesis. London. The Institute of Mining and Metallurgy, pp. 213-220.

RICHTER, P. and STETTNER, G., 1979. Geochemische und petrographische Untersuchungen der Fichtelgebirgsgranite: Geol. bavar., v. 78, pp. 1-144.

STETTNER, G., 1972. Zur geotektonischen Entwicklung im Westteil der Böhmischen Masse bei Berücksichtigung des Deformationsstils im orogenen Bewegungssystem: Z. dtsch. geol. Ges., v. 123, pp. 291-326.

EARLY GREENSCHIST-AMPHIBOLITE FACIES METAMORPHISM IDENTIFIED IN BLUESCHIST AND ECLOGITE EXOTIC BLOCKS OF THE FRANCISCAN COMPLEX, CALIFORNIA

MOORE, D. E., and BLAKE, M. C., JR., U.S. Geological Survey, Menlo Park, CA 94025

The high-grade blueschists, eclogites and amphibolites that occur as exotic blocks in the Franciscan Complex of California have long been considered to have formed contemporaneously from unmetamorphosed oceanic lithosphere under slightly varying temperature-pressure (± composition) conditions. However, recent studies suggest that the eclogite and high-grade blueschist assemblages in numerous blocks have instead developed from greenschist- to amphibolite-facies precursors. At least some of the amphibolite blocks appear to be well-preserved remnants of this earlier metamorphism, rather than higher temperature equivalents of the eclogites and high-grade blueschists.

The degree of preservation of the relict assemblages is correlated to their calcic amphibole compositions. Most commonly, the relics are simply cores of blue-green amphibole within glaucophane crystals in blueschist blocks. These amphibole cores are actinolites, magnesio-hornblendes and barroisites with Si = 7.2-7.9 and Na_{total} = 0.25-0.8 atoms in their structural formula. Better preserved amphibolite assemblages in eclogite and blueschist blocks contain magnesio-hornblende with Si = 6.6-7.1, and Na_{total} = 0.8-1.1. Relict hornblendes in eclogite and interlayered eclogite/blueschist blocks have the highest Mg contents (Mg = 3.0-3.5), suggesting a possible chemical control of the formation of eclogite. The overall range of Mg in the relict amphiboles is Mg = 2.0-3.5.

To adequately describe these mineral relationships, the mineral chemistry of an eclogite/amphibolite block from the Diablo Range of central California is being exmained in detail. The initial amphibolite assemblage consists of a greenish-brown magnesio-hornblende (Si = 7.1; Na_{total} = 0.75; Mg = 3.5), garnet ($Alm_{50}Pyr_{18}$ rims), sodic augite ($Jd_{22}Di_{70}Ac_8$), rutile, and apatite. Thoroughly eclogitized areas in the block contain omphacite ($Jd_{40}Di_{48}Ac_{12}$), garnet ($Alm_{60}Pyr_{10}$ rims), blue-green actinolite (Si = 7.6; Na_{total} = 0.6; Mg 3.3), rutile, sphene, phengite, and small amounts of interstitial quartz. Core compositions of the eclogite garnet correspond to the compositions of garnet in the relict amphibolite assemblages, which suggests that the eclogite garnet is a slightly altered relict mineral. Transitional areas in this block are marked by the growth of omphacite and eclogitic actinolite along the outer edges of hornblende porphyroblasts. In hand specimen, the transitional zones have a mottled appearance, with lozenge-shaped areas of dark-colored amphibolite surrounded by greenish-colored, omphacite-rich matrix. Both the eclogite and relict amphibolite assemblages were affected by a subsequent retrograde metamorphism characterized by the growth of glaucophane within the block and development of an outer alteration rind rich in pale-green tremolitic actinolite (Si = 7.9; Na_{total} = 0.25; Mg = 3.95).

Many of the blocks identifiable in the field as amphibolite are identical in appearance to the relict amphibolite assemblages, although the calcic amphiboles analyzed thus far from the amphibolite blocks have slightly lower Si contents (Si = 6.2-6.6) than the clearly relict amphiboles. Some of these amphibolite blocks show incipient alteration to high-grade blueschist and eclogite minerals, similar to that described above for the transitional zone in the eclogite/amphibolite block. Such blocks may also be relict amphibolites.

The complex history recorded in these blocks is still difficult to assess; however, some important relationships seem to be fairly well established. The blocks are largely of basaltic or gabbroic composition (a few were clearly chert). Metamorphic ages of hornblende, white mica, and sphene tend to cluster around 160 m.y. whereas many glaucophane and actinolite ages are appreciably younger. Nearly all of the blocks were once embedded in serpentinite as recorded in their actinolite-chlorite rinds. Taking all of these data into account it would appear that the early greenschist-amphibolite facies metamorphism might have occurred during obduction of the Coast Range ophiolite during the Nevadan orogeny. The succeeding high-pressure metamorphism may also have been part of the Nevadan orogeny, which immediately preceded the beginning of the Franciscan deposition.

CATIONS WITH LONE PAIRS IN MINERAL CHEMISTRY

MOORE, PAUL BRIAN, Dept. of Geophysical Sciences, The University of Chicago, Chicago, IL 60637, USA

Each chemical element from Group IIIA through VIIA possesses an electronic package consisting of a closed core of electrons ([ ]) and the valence electrons. For ordinary geochemical reactions, maximum valence states from 3+ for IIIA to 7+ for VIIA elements have been recorded. Consulting tables of ionization potentials, one notes a substantial increment between ionized states with two valence electrons remaining and the fully ionized state where all valence electrons are stripped away. I will refer to these two remaining valence electrons as $[...(n-1)d^{10}]ns^2$ electrons, where n = row in the Periodic Table or the principal quantum number. For example, I denote fully ionized lead as Pb^{4+}, but lead with two valence electrons remaining I denote $6s^2$ Pb^{2+}. The ns^2 pair of electrons is variously called the chemically inert pair, the stereochemically inert pair, the nonbonding pair or the lone pair. In a crystal, the environs about a cation can be considered as a collection of lone pairs (symbolized Ψ) and bond pairs (symbolized φ).

Cations which possess at least one lone pair of electrons are found in over 15% of the mineral species. These are among the most perplexing compounds in Nature's store. They pervade the phrenotropic alkaloids which by definition contain N^{3+} in a heterocycle, most of the so-called heavy metal poisons (especially Hg°, Tl^{1+}, Pb^{2+}, As^{3+}, Se^{4+}) and nearly all the sulfosalts. The biggest problem facing the chemical crystallographer is rationalizing their anionic coordination polyhedra, the distortions of these polyhedra and the realization that much of the "matter" is missing in the crystal structure. Lone pairs are rarely defined in crystal structure analysis.

It is now recognized that lone pairs on cations in crystal structures have fixed centroids in space and crystallographically play a role much like anions about a cation. Although they perturb the environment through Ψ-φ electrostatic repulsions, their volumetric contribution can be calculated. Defining V_E as the packing efficiency of anions (volume per anion, obtained by dividing the unit cell volume by total anions in that cell) and $V_{E+\Psi}$ as packing efficiency of anions plus lone pairs on cations in the unit cell, their sphere of influence or umhüllungsraum has an effective radius which approximates the O^{2-} anion (r=1.40 A) but is demonstrably smaller than the S^{2-} anion (r = 1.82 A).

Three principal types of lone pair geometry have been discerned. In the first, the lone pair is spherically distributed within the coordination polyhedron about the cation. This leads to a polyhedral expansion. The famous example is galena, $Pb^{2+}S\Psi$. It can be appreciated by studying the pair $Pb^{2+}S\Psi$-$Pb^{4+}S_2$. The second type exhibits a lone pair-bond pair interaction such that the polyhedron is seriously distorted away from regularity. Most Pb^{2+} oxysalts fall into this category. In the third type, the lone pair is emerged and plays the role of the missing anion at a vertex of the coordination polyhedron. Lone pair cations of low principal quantum number and of high charge usually display this property: $N^{3+}\Psi$, $P^{3+}\Psi$, $As^{3+}\Psi$, $S^{4+}\Psi$, $Se^{4+}\Psi$, $Cl^{5+}\Psi$. In one structure, more space is occupied by lone pairs than anions: about two-thirds of the packing efficiency is taken up by lone pairs in carlinite, $Tl_2^{1+}S\Psi_2$.

The sulfosalts have been largely rationalized by including lone pairs in the calculations. For some fifty structure types, over 40% ($100xV_{\Psi}/V_{E+\Psi}$) of the anion packing space is accommodated by lone pairs. Most structures can be idealized, based on perfect dense packing where the lone pairs occupy the "voids" in anion space. In such structures, the deviations of ideal atom coordinates from real atom coordinates are within 0.6 A of each other.

Finally, let me remark that even solid solutions between a lone pair cation (such as Pb^{2+}) and an inert gas configuration cation (such as K^{1+}) have been studied. Here, both ions are "under one roof" of enveloping coordinating anions. The distortion of the envelope is minor, but the Pb^{2+} is displaced ca. 0.6 A from the K^{1+}. This suggests that distortion of a coordination polyhedron in most cases is due to an off-centered central cation with a lone pair. Experiments with lone pair cations over a range of temperature and pressure should be interesting, and the classic problem of morphological hemihedry in wulfenite should be attacked. The deleterious effects of the "heavy metals" on living organisms may be better understood through this reasoning, involving (K^{+}-Pb^{2+}) pathways.

Chemical crystallographic studies in progress include the system $PbO-PbCl_2$ and the series $X^{1+}ClO_4$-$X^{1+}ClO_3\Psi$-$X^{1+}ClO_2\Psi_2$-$X^{1+}ClO\Psi_3$.

DIFFUSION COEFFICIENT OF SILICA IN SUPERCRITICAL WATER

Nobuo MORIMOTO, Kenzi SAKANAKA and Masao KITAMURA
Department of Geology and Mineralogy,
Faculty of Science, Kyoto University,
Sakyo, 606, Japan.

Diffusion coefficient of silica in supercritical water and its dependency upon temperature and pressure have been determined. The pairs of quartz-brucite, quartz-periclase, quartz-portlandite, quartz-lime, and quartz-calcite were hydrothermally heated at temperatures 400-700°C and pressures 500-1250 bars for 3-93 hours. The reaction product zone and the void zone grew from the initial contact towards the Ca or Mg compound zone and quartz zone, respectively. In most cases, the length of the reaction product zone was proportional to the square root of the run duration. This suggests that silica was dissolved into supercritical water, diffused towards the Ca or Mg compound zone, and formed the reaction product zone.

The diffusion coefficient of silica in supercritical water was calculated from the growth rate of the reaction product zone of each run. The dependence of the diffusion coefficients on temperature and pressure was determined from the data in the system quartz-brucite as follows; $D = D_o\{-(E+PV^*)/RT\}$, where D_o = 0.55(+0.57,-0.28) cm^2/sec, E = 48±5 kJ/mol, V^*= 81±12 cm^3/mol.

The width of metasomatic zone has been estimated from this result. Forsterite zone of a few meters in width would be formed between quartz and brucite zones with porosity of 1% for 1 m.y. under the experimental P-T conditions.

The distance of diffusion, ($\sqrt{Dt}$), has been estimated to be a few kilometers for 1 m.y. under the experimental P-T conditions. This suggests that the equilibrium can be maintained during the regional metamorphism.

CRYSTAL-CHEMICAL EVOLUTION AND RELIABILITY OF GARNET ANALYSES

Annibale MOTTANA

Dipartimento di Scienze della Terra, Sezione Mineralogico-Cristallografica, Università di Roma "La Sapienza", 00185 Roma, Italy

The reliability of a mineral analysis depends, in primis, on the precision and accuracy of the analytical method used, but also to a certain extent on the criteria used when screening the raw analytical data for accidental or/and systematic errors.

To assess the quality of garnet analyses, the recasting method of Rickwood (1968) is commonly used. Analyses are considered to be acceptable when at least 95% of the 12 cations considered can be allocated to as many as 19 end-members. However this method, and its later improvements (e.g. Coombs et al., 1977), is not specifically designed for electron microprobe analysis, and therefore overlooks the problem of valence state for Fe and Mn. It also fails to account for a number of substitutional possibilities which were discovered in recent years, while it considers others that clearly result from contamination.

Mottana (1985) devised reliability tests based on rigorous crystal-chemical constraints which were deduced from the latest garnet crystal structure refinements. These tests were initially devised for anhydrous garnets in eclogitic rocks. Cations in the formula are calculated on the basis of a total number of 8 and the valence states of Fe, Mn are determined by the charge balance equation 8-2Si-2Ti-2.5P-Al-Cr+Na=M(3+), modified after Ryburn et al., 1976. Deviations in the occupations of the X, Y, Z sites are permitted to a maximum of ±2%.

This testing method is now extended to a variety of garnet com-

CRYSTAL CHEMICAL EVOLUTION AND RELIABILITY OF GARNET ANALYSES

MOTTANA, A., et al.

positions previously disregarded as improbable in eclogites, so as to account for a total of 16 possible cations. It is also devised for the broadest possible range of garnet compositions and crystallization conditions.

The significance of the proposed reliability tests has been tested statistically using two sets of samples: garnets in eclogitic rocks (804 EMP analyses performed from 1964 to 1984), and garnets in metasomatic rocks in geothermal areas (138 EMP analyses performed from 1971 to 1985). The acceptance rates are very low in both cases (36 and 22% respectively). Comparative considerations with similar tests carried out on eclogitic pyroxenes (Mottana, 1985) and evaluations on the error distribution in samples performed in the same laboratory under homogeneous conditions of analysis do, however, indicate that the low acceptance rates are not due to defects inherent in the testing method, but they reflect real analytical errors in the EMP analyses.

Coombs, D.S. et al. (1977) - Contrib.Mineral.Petrol., 63, 229.

Mottana, A. (1985) - Second Int. Eclogite Conference, Vienna, August 28-31, 1985 (in press, Lithos, vol.19).

Rickwood, P.C. (1968) - Contrib.Mineral.Petrol., 18, 175.

Ryburn, R.J. et al. (1976) - Lithos, 9, 161.

PARAMAGNETIC DEFECT CENTERS IN NATURAL KAOLINITES.

MULLER, J.P., ORSTOM, Centre de Recherches, BONDY and Lab. Minéralogie-Cristallographie, UA CNRS 09, Universités de Paris 6 et 7, 75230 PARIS CEDEX 05, France; CALAS G., Lab. Minéralogie-Cristallographie, UA CNRS 09, Universités de Paris 6 et 7, 75230 PARIS CEDEX 05, France.

Electron Spin Resonance (ESR) spectra of natural kaolinites exhibit two signals usually superimposed on the broad magnetic spectrum of the associated iron oxides. The former is characteristic of substitutional trivalent Fe in various kinds of sites giving rise to a complex signal centered near g=4.3. The latter is an anisotropic signal centered at values just above g=2, characteristic of a single anisotropic site. It has a smaller width and has been interpreted as arising from a trapped hole, although its relationships to the geochemical surrounding are still unknown. This axially distorted site is attributed to a trapped hole nearby a silicon atom, favoured by the presence of impurities or vacancies located in the vicinity of the silicon atom.

We present data concerning kaolinites sampled in a lateritic weathering profile, developed at the expense of a gneissic basement from Goyoum, East Cameroon. Various generations of kaolinites can be separated on the basis of their mutual relationships and correspond to distinct particle sizes, structural order and substitutional-Fe content. This material is closely associated to haematite and goethite, which both exhibit variable Al content. X- and Q-band ESR spectra were studied on carefully selected samples.

The parameters obtained concerning the anisotropic defect signal are the following: $g_{//} = 2.049$ and $g_{\perp} = 2.006$. The broadening of this signal arises from a site distribution but the possibility of the coexistence of various discrete centers cannot be excluded: Q-band spectra show some evidence of another site which gives a nearly isotropic signal. These distinct sites might be accounted for by the variety of possibilities to create vacancies in this type of material, probably associated with minor components of the kaolinite.

The specific behaviour of this defect signal was found in its relations with the other crystal chemical parameters measured in the same kaolinites: there is no relation with the Fe-content of the kaolinite lattice or with the crystallinity of the mineral. On the contrary there exists a linear relationships between the integrated intensity and the total Fe-content of the samples, including the associated oxides whatever their mineralogical nature. By taking into account the efficient chemisorption of uranium (and its desintegration products) on poorly crystallized iron oxides, these defects can be attributed to an inherited irradiation of the kaolinites during the first stages of the weathering and their subsequent crystallization. The evolution of the iron oxides towards a better crystallinity leads to an evacuation of the radioactive elements, and the irradiation defects are thus the memory of the uranium transit. This defect signal allows at the same time an efficient fingerprint determination of the successive generations of kaolinites during the weathering processes.

APPLIED MINERAL SCIENCE--ALIVE AND WELL IN MODERN TECHNOLOGY

MUMPTON, FREDERICK A., Department of the Earth Sciences, SUNY-College at Brockport, Brockport, New York 14420, U.S.A.

For decades the forgotten stepchild of pure mineralogy and geology, applied mineral science is currently a highly visible and sought-after branch of technology that contributes far beyond its geological heritage to almost every field of modern technology. Applied mineral science is, by definition, the application of mineralogical principles, concepts, and techniques to industrial, agricultural, environmental, and bio-medical problems. It is not a narrowly defined field, but ranges from the use of the petrographic microscope for examining the texture of Alka-Seltzer pellets to propping apart the 14-Å layers of smectite with metal organics to form catalyst supports. It includes such widely different investigations as the delineation of the cation-exchange properties of clinoptilolite tuffs which will possibly be used to store radioactive wastes, the characterization of micrometer-size particles of gold in Nevada shales to guide metallurgical operations, the development of hydrothermal techniques to grow bigger and better synthetic emeralds, the forensic identification of airborne fission products to characterize nuclear explosions, and the monitering of the hemolytic activity of mineral particles in the human body.

Applied mineralogical investigations require varying degrees of intellectual sophistication; hence, the people who do the work differ widely in their training and experience. Some studies make use of little more than routine microscopic or X-ray diffraction examinations; others may require delving into the basic crystal structure and chemistry of a particular mineral phase. The common denominator is that all of the studies are applied, that is, directed towards solving a specific problem of importance to society. This is not to say that fundamental scientific discoveries are not forthcoming from applied mineral science; far from it, our current ideas about shale and clay diagenesis are in large part the result of applied mineralogical studies in petroleum company laboratories aimed at finding and producing more hydrocarbons from deep-seated reservoirs. What we know today about the phases and reactions in the system CaO-Al_2O_3-SiO_2-H_2O has resulted chiefly from mineralogical studies of industrially important cement systems.

Because of its problem-solving approach, applied mineral science is often more closely associated with "other" disciplines than with its parent mineralogy or geology, and its technical reports are generally published in non-geological journals. It is erroneous described by many "pure" mineralogists as "blue collar" mineralogy, and hence applied papers are not commonly featured at mineralogical meetings. The present I.M.A. meeting is an exception. This state of affairs is most unfortunate because the lifeblood of an applied mineral scientist is and will always be the new findings of "pure" mineral science. Moreover, by rubbing shoulders with his applied cousin, the "ivory tower" mineralogist may often benefit (and probably be more readily funded for his next research project) by seeing how his efforts ultimately can be used to serve people.

Although small technical societies have been formed from time to time, each distinguished in its own right, that focus on a specific mineral or mineral group (e.g., clays, zeolites, asbestos), no one organization currently speaks for all of applied mineral science, and no one journal covers all aspects of this diverse subject, despite the fact that each area of applied mineral science utilizes the same basic mineralogical approaches and information. The lack of a spokesman society may possibly

be solved by existing mineralogical organizations expanding their scope to include and highlight the applied area of the subject. The absence of a periodical, however, dedicated to applied studies of all mineral materials--metallic and nonmetallic alike--from occurrence to end use, should be rectified if applied mineral science is to be fully recognized as a contributing branch of technology and if mineral science as a whole is to be of the greatest benefit to all.

NON-ISOTHERMAL CRYSTAL GROWTH KINETICS IN THE SYSTEM ALBITE-ANORTHITE-H_2O AT P_{H_2O} = 2 KBAR

MUNCILL, G.E., Geophysical Laboratory, 2801 Upton St., N.W., Wash. D.C. 20008, USA

Isothermal experiments had been performed previously in a gas-media apparatus at 2 kbar confining pressure for plagioclase crystal growth from An_{30} and An_{20} bulk compositions under H_2O-saturated conditions. Resulting crystals were found to be unzoned in composition. Furthermore, the compositions of the crystals corresponded to the equilibrium composition at the temperature of growth. Significantly, no evidence was found for reverse or oscillatory zoning in any of the isothermal runs.

New experiments consist of inducing crystal growth upon natural anorthite seed crystals (An_{95}) during computer-controlled cooling of the run from hyperliquidus to subliquidus (but hypersolidus) temperatures. Initial experiments were conducted with linear cooling. Microprobe analysis of a seed crystal, plagioclase overgrowth and surrounding glass (quenched melt) is shown in Figure 1 for crystal growth in an An_{30} bulk composition with a linear cooling rate of 0.5°C per minute. The initial and final compositions of the plagioclase overgrowth correspond to the equilibrium compositions at the liquidus and

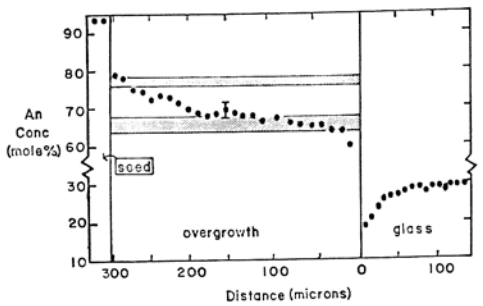

quench temperatures, respectively, as indicated by the shaded regions of the figure.

In all of the runs involving linear cooling the composition of the resulting plagioclase overgrowths appear to "track" along the solidus for the system. The plagioclase crystals are normally zoned in a manner that would be expected for fractional crystallization, but the zoning is clearly the result of the coupling of crystal growth kinetics and diffusive mass transfer through the melt phase and not fractional crystallization in the charge during the experiment. The production of normal zoning by coupled crystal growth and mass transfer kinetics with local equilibrium at the crystal-melt interface represents an irreversible, time-dependent mechanism for generating compositional zoning in crystals. The viability of such a mechanism will have serious consequences for application of "equilibrium" models of fractionation and geothermometry, such as one- and two-feldspar geothermometers.

Probe traverses were performed along each of the crystal growth directions, and severe constraints could be placed upon the possible mechanisms for crystal growth. Mass balance is not preserved for models involving simple, static diffusive boundary layer surrounding the crystal. Convective mixing must, therefore, have taken place in the melt. Thus, the concentration gradient around the plagioclase grains represents a coupled diffusive-convective boundary layer.

Another important feature is the absence of observed oscillatory zoning in any of the crystals from the linear cooling experiments. As in the isothermal crystal-growth experiments, no oscillatory or reverse zoning was observed in any of the plagioclase crystals, including runs with relatively fast cooling rates (0.5°C/minute). Additional experiments were performed with an oscillatory temperature versus time profile superimposed upon the linear cooling curve. The resulting plagioclase crystals were normally zoned with oscillatory compositional zoning superimposed. A natural corollary to the experiments may be either oscillatory temperature variations during convective overturn or cyclic pressure release during eruption.

HIGH RESOLUTION ELECTRON MICROSCOPY OF CRYSTALLINE, PARTIALLY METAMICT AND METAMICT ZIRCONS

MURAKAMI, T.*, CHAKOUMAKOS, B. C. and EWING, R.C., Dept. of Geology, Univ. of New Mexico, Albuquerque, NM 87131, USA. *On leave from the Dept. of Environmental Safety Research, Japan Atomic Energy Research Institute, Tokai, Ibaraki 319-11, Japan

Gem-quality zircons from Sri Lanka showing the full range of damage (caused by alpha-decay events) from fully-crystalline to the fully-damaged metamict state were examined by x-ray diffraction and high resolution transmission electron microscopy (HRTEM). Concentrations of U and Th were determined by instrumental neutron activation analysis and the calculated doses (based on an age of 570 ± 20 million years [Holland and Gottfried, 1955]) range between 0.8 - 4.5 x 10^{15} alpha-decays/mg. These doses are equivalent to a range of displacements per atom (dpa) of 0.4-2.1.

Significant changes occur in the x-ray diffraction patterns of the seven zircons examined as a function of increasing alpha-decay dose: [1] Peaks shift to lower values of two theta corresponding to an expansion of the unit cell (a = 0.661 to 0.667 nm and c = 0.598 to 0.616 nm). Diffraction maxima were deconvoluted into a Bragg and diffuse scattering component, and unit cell parameters were calculated using only the Bragg component. [2] There is a regular decrease in the intensity of the Bragg diffraction maxima and an increase in the intensity of the diffuse scattering component (on the high two-theta side of the Bragg peak). [3] Diffraction maxima broaden and are asymmetric, skewed to higher values of two theta (the maximum change occurring at doses > 2.2 X 10^{15} alpha-decays/mg). The skewed peaks are due to the increasing intensity of the diffuse scattering component. At even higher doses the intensity of the diffuse scattering component decreases. [4] At intermediate doses, split peaks are observed. [5] At doses greater than 4.5 X 10^{15} alpha-decays/mg, zircon is x-ray diffraction amorphous.

The specimens for HRTEM were examined (JEOL 2000FX TEM operated at 200 kV) as crushed fragments and in an ion-milled (at liquid nitrogen temperature) section parallel to (101). The following microstructural changes were observed as a function of increasing dose: [1] Lattice fringe images are complete with clear electron diffraction patterns. [2] There is a mottled contrast in the bright-field image with isolated aperiodic domains (2-10 nm) in which lattice fringes are almost absent. Some lattice fringes are bent and discontinuous. In some areas, lattice fringes are distorted parallel to the c axis, and this may correspond to the split x-ray diffraction maxima. [3] Amorphous areas are more abundant than in the previous stage, and lattice fringe distortion and discontinuities are more apparent. Crystalline domains up to 10 nm in size form high angle grain boundaries. Although the diffraction pattern is still that of zircon, the intensities of diffraction maxima have changed. [4] Misoriented domains 2 to 10 nm in size exist with areas of distorted and discontinuous lattice fringes in narrow regions which are up to 20 nm wide. Powder diffraction rings and a diffuse halo from the aperiodic domains are apparent in the diffraction pattern. [5] No lattice fringes are evident, and the diffraction pattern consists only of diffuse rings. It should be noted that the distribution of U and Th is heterogenous on the scale of the TEM; therefore, individual samples show some variation in the microstructural damage.

Holland, H.D. and Gottfried, D. (1955) The effect of nuclear radiation on the structure of zircon. Acta Crystallographica, 8, 291-300.

This work was supported by the U.S. Department of Energy, Office of Basic Energy Sciences under grant #DE-FG04-84ER45099(RCE).

THE MÖSSBAUER SPECTRUM OF ALMANDINE

MURAD, E., Lehrstuhl für Bodenkunde, T.U. München, D-8050 Freising-Weihenstephan, Federal Republic of Germany; WAGNER, F.E., Physik Department E15, T.U. München, D-8046 Garching, Federal Republic of Germany

The Mössbauer parameters of Fe^{2+} in the eightfold-coordinated 24c position of paramagnetic garnets are virtually independent of the garnet composition. Subordinate amounts of Fe^{2+} in the 24c position of pyrope or spessartine, for example, have parameters similar to those of almandine (at 77K quadrupole splitting ΔE_Q = -3.65 mm/s; isomer shift relative to metallic Fe δ/Fe = 1.43 mm/s; Amthauer et al., 1976). Mössbauer spectra taken in the paramagnetic state therefore do not provide features diagnostic for the characterization of Fe^{2+}-bearing garnets.

Even minor replacement of Fe^{2+} in an almandine by ions with a different electronic configuration (e.g. Mg^{2+} or Mn^{2+}) should, however, cause magnetic perturbations and consequently change magnetic properties like the Néel temperature and the magnetic hyperfine field noticeably. Such changes can be observed by Mössbauer spectroscopy at sufficiently low temperatures.

For the interpretation of Mössbauer spectra of magnetically ordered garnets it is necessary to know the parameters of the garnet end-members to begin with. To determine the Néel temperature and hyperfine field of pure almandine, Mössbauer spectra of a synthetic almandine (Alm_{100}, cf. Bohlen et al., 1984) were run at different temperatures between 295 and 4.2K. For comparison, spectra of an almandine-rich natural garnet (Alm_{86}; USNM #107105, Novak & Gibbs, 1971) were also run at selected temperatures.

At 78K the Mössbauer spectrum of Alm_{100} consists mainly of a doublet with ΔE_Q = -3.668(1) mm/s, δ/Fe = 1.421(1) mm/s and an average line width at half height W of 0.264(1) mm/s. A minor, unresolved component with δ/Fe = 0.42(1) mm/s, W = 0.75(4) mm/s and a relative area of 2.8(2)% is attributable to Fe^{3+}.

At 11.0K Alm_{100} is still completely paramagnetic. Mössbauer parameters are essentially the same as at 78K except for a narrowing of the Fe^{2+} band to 0.46(6) mm/s. At 10.4K, however, wings (which become particularly apparent when the spectrum is fitted with just three Lorentzians) have developed on the sides of the Fe^{2+} lines, indicating incipient magnetic order.

The contribution of a magnetically ordered component to the Mössbauer spectra of Alm_{100} becomes more pronounced as temperatures decrease below 10.0K, the high-velocity line (m_I = ½ ⟶ ± ½ transition) broadening more rapidly than the low-velocity line. At 9.6K 50% of the total spectral area can be assigned to an antiferromagnetic phase. At 9.0K no indication of a paramagnetic phase remains, but the spectrum has lines of different widths – some rather high – suggesting the existence of hyperfine field distributions. A tentative fit indicates an average magnetic hyperfine field B_{hf} of about 12.5 T at 9.0K.

At 4.2K the spectral lines have narrowed significantly, facilitating analysis of the spectra. These are more complex than that of a natural garnet containing 79% of the almandine molecule described by Prandl & Wagner (1971). The spectra of both Alm_{100} and Alm_{86} can be fitted by two eight-line magnetic hyperfine patterns of equal intensities. Thus, although Fe^{2+} ions occupy only one lattice position in almandine, **two** non-equivalent Mössbauer sites exist in the magnetically ordered state. Alternate, qualitatively equally good fits of the spectrum of Alm_{100} indicate the development of two subspectra to be attributable to either:
— 1) the existence of two different polar angles θ of 73 and 90° between the directions of B_{hf} and the principal axis of the electric field gradient V_{zz} (both components having similar quadrupole splittings $\frac{1}{4}eQV_{zz}$ that average -3.71 mm/s), or
— 2) two distinctly different quadrupole splittings of -3.25 and -4.11 mm/s, but similar polar angles θ of 80°.

The asymmetry parameter η (0.06) is quite low, indicating the electric field gradient at the 24c sites to be almost axially symmetric. Because of the low value of η, the azimuthal angle ϕ between V_{xx} and the projection of B_{hf} on the V_{xx}-V_{yy} plane is of no significance; ϕ was therefore fixed at zero during the fitting procedure. Other parameters for Alm_{100} at 4.2K are similar hyperfine fields B_{hf} averaging 25.3 T and an average line width of 0.34 mm/s. Alm_{86} has slightly lower hyperfine fields of 22.8 T and line widths of 0.44 mm/s.

References

G. Amthauer, H. Annersten & S.S. Hafner (1976) Z. Krist. **143**, 14.
S.R. Bohlen, V.J. Hall & A.L. Boettcher (1983) Am. Min. **68**, 1049.
G.A. Novak & G.V. Gibbs (1971) Am. Min. **56**, 791.
W. Prandl & F. Wagner (1971) Z. Krist. **134**, 344.

SULFIDE AND OXIDE MINERALS FROM S-TYPE AND I-TYPE GRANITIC ROCKS

MURATA,M., Rigaku Industrial Corporation, 14-8, Akaoji-cho, Takatsuki-shi, Osaka 569, Japan
ITAYA.T., Hiruzen Research Institute, Okayama University of Science, 1-1 Ridai-cho, Okayama 700, Japan

The Ohmine granitic rocks of Miocene age, 11 to 16 Ma in the Kii Peninsula, central Japan consist of fine-grained porphyritic granodiorite and granite, granite porphyry and quartz porphyry. On the basis of mineral assemblage, alumina saturation and isotopic ratios for strontium, oxygen and sulfur, these granitic rocks fall into two distinct types; I-type of 11.6 to 14.2 Ma and S-type of 12.6 to 15.6 Ma. The Ohmine I-type rocks are lower in Strontium initial ratio(0.7049 to 0.7058) and $d^{18}O$ values(7.2 to 7.6 per mill), and higher in $d^{34}S$ values(-2.7 to -3.6 per mill) than the S-type rocks(Sr I.R.=0.7083 to 0.7086, $d^{18}O$=9.8 to 11.5 per mill and $d^{34}S$= about -16.2 per mill), respectively. Chemical compositions of biotite and pyrrhotite of the two types of rocks are different from each other, i.e., biotite from the I-type is higher in Si content and lower in Al content than that from the S-type, and Ni-bearing pyrrhotite is common in the I-type but is rare in the S-type. The K-Ar age data and the differentiation systematics of the Ohmine granitic rocks showed that the S-type rocks were never due to the large scale interaction between the I-type magma and crust as well as the mixing between I- and S-type magmas.

The S-type rocks having non-minimum melting compositions in the granite and granodiorite system commonly contain mineral clots such as biotite + sillimanite + quartz + orthoclase + cordierite + garnet and biotite + garnet + quartz + orthoclase + cordierite + orthopyroxene, which are occasionally included in quartz and plagioclase phenocrysts. The mineral assemblages and the Fe-Mg distribution systematics of garnet-cordierite and garnet-biotite pairs suggest that the S-type rocks were in the conditions of granulite facies, 5kb and 700°C. The country rocks around the Ohmine mass have no sillimanite + garnet bearing assemblage. These facts suggest that the S-type magma was generated by the partial melting of sedimentary and/or metasedimentary rocks under the above mentioned conditions, and that the mineral clots could be the residues, i.e., "restite". The I-type magma could be partial melting products from intermediate igneous and/or metaigneous rocks as suggested from the isotopic studies of two types of rocks.

In the Ohmine I-type and S-type granitic rocks, ilmenite, rutile, pyrrhotite, pyrite and chalcopyrite are common, but no magnetite is present. Their primary paragenetic relations were confirmed by the examination of their mode of occurrences as inclusion species in major silicate minerals such as plagioclase, orthoclase, quartz, Ca-amphibole and biotite though their parageneses changed in cooling of the rocks. This makes it possible to estimate the fugacities of oxygen and sulfur in the granitic rocks on the basis of their paragenetic relations, and to discuss the nature of volatiles in rocks. The mineral paragenetic relations in the Fe-Ti-O-S system at 5 kb and 700°C showed that both I- and S-type rocks with ilmenite + rutile + pyrrhotite + pyrite were $10^{-14.6}$ in fO_2 and $10^{-0.7}$ in $fS_2$and the rocks with two or three sulfide and oxide phases, around the fugacites of oxygen and sulfur. This suggests that the Ohmine granitic rocks were in the graphite unstable condition, and that the possible graphite in the S-type rocks was relic as inclusion particles in phenocrysts.

Significant subsolidus reactions for sulfide minerals continued until the rocks cooled below 300°C and took place in two types of mineral grains, in groundmass and as inclusions. The removal of sulfur and copper through the silicate crystals was too easy to preserve the chemistry of sulfides included in silicates. However, the removal of nickel through silicate crystals as well as along grain boundary of minerals was restricted as suggested from the facts that the distribution freqency of nickel-bearing pyrrhotite was higher for inclusion species than interstitial ones, and significantly higher in the cognate enclave than the host I-type rocks.

STRUCTURE AND PROPERTIES OF IRON-BEARING SILICATE MELTS

MYSEN, B. O.; Geophysical Laboratory, 2801 Upton St., N.W., Washington, D. C., 20008, USA

Ferrous and ferric iron may occupy structurally different positions in silicate melts. The overall melt structure depends, therefore, on ferric/ferrous, and melt properties that depend on structure are functions of $Fe^{3+}/\Sigma Fe$. The structural roles of Fe^{3+} and Fe^{2+} also must be ascertained because ferric/ferrous of magmatic liquids may be employed to calculate pressure, temperature, oxygen fugacity paths of magma.

Spectroscopic data are generally consistent with ferrous iron in a network-modifying position in silicate liquids, whereas that of ferric iron is a complex function of $Fe^{3+}/\Sigma Fe$. Mossbauer and Raman spectra of melts on binary $MO-SiO_2$ and M_2O-SiO_2 and more complex $M_2O-Al_2O_3-SiO_2$ and $MO-Al_2O_3-SiO_2$ joins (where M denotes network-modifying metal cation) indicate a systematic correlation between $Fe^{3+}/\Sigma Fe$ and the number of oxygens in its coordination polyhedron. With $Fe^{3+}/\Sigma Fe>0.6$ ferric iron occurs in tetrahedral coordination, with most likely, alkali metals or alkaline earths for electrical charge-balance. Tetrahedrally and octahedrally coordinated Fe^{3+} coexist in melts with $Fe^{3+}/\Sigma Fe=0.6-0.3$, whereas Fe^{3+} in more reduced systems exists only in octahedral coordination. From Mossbauer spectroscopy, the $IS_{Fe^{3+}}$ increases by about 0.05 mm/sec and $QS_{Fe^{3+}}$ by 0.6-0.8 mm/sec as a function of increasing Z/r^2 of the metal cation with the lowest values obtained for K^+-charge-balanced and the highest values for Mg^{2+}-charge-balanced Fe^{3+}, suggesting perhaps increasing distortion of the $Fe^{3+}-O$ tetrahedra.

The $Fe^{3+}/\Sigma Fe$ is silicate melts is a systematic function of degree of melt polymerization, type of metal cation, Al/(Al+Si), temperature, pressure and oxygen fugacity. The relationship between melt structure and $Fe^{3+}/\Sigma Fe$ can be illustrated with expressions such as;

$$6Si_2O_5^{2-}+4Fe^{2+}+O_2=12SiO_2+4FeO_2^-, \quad (1)$$

where SiO_2 and $Si_2O_5^{2-}$ are coexisting structural units in the melts. Raman spectra of these melts are consistent with tetrahedrally-coordinated Fe^{3+} in simple complexes such as FeO_2^-. From the equilibrium constant;

$$K_1=(FeO_2^-/Fe^{2+})^4((SiO_2^2/Si_2O_5^{2-})^6 1/f_{O_2}, \quad (2)$$

a systematic increase in $Fe^{3+}/\Sigma Fe$ with increasing NBO/T (increasing degree of depolymerization) of the melt is observed. Analogous expressions may be written for aluminosilicate melts.

Under the assumption that the activity coefficient for Fe^{2+}-complexes does not vary with melt composition, $Fe^{3+}/\Sigma Fe$ vs. f_{O_2} relationships suggest that $\gamma_{Fe^{3+}}$ increases systematically with increasing Z/r^2 of the metal cations. The ΔG° of reduction of Fe^{3+} to Fe^{2+} in binary metal oxide melts is positively correlated with increasng Z/r^2 of the metal cation. In ternary metal oxide-alumina-silica melts, the ΔG° is positively correlated with decreasing Al/(Al+Si).

From an experimental data base of 460 analyses of $Fe^{3+}/\Sigma Fe$ of both complex natural magmatic liquids as well as liquids in binary, ternary and quarternary systems, step-wise, linear regression of an expression of the form;

$$\ln(Fe^{3+}/Fe^{2+})=a+b/T+c\ln f_{O_2}+d[Al/(Al+Si)]$$
$$+e[Fe^{3+}/(Fe^{3+}+Si)]+\Sigma f_i(NBO/T)_i, \quad (3)$$

where a-f are regression coefficients and $(NBO/T)_i$ is the proportion of nonbridging oxygens associated with individual network-modifying cations, yields coefficients that reproduces 85% of the oxygen fugacity values to within 1 log unit. Both experimentally-determined partial molar volume data and direct experimental observation indicate a strong pressure effect on the $Fe^{3+}/\Sigma Fe$, but this relationship has not yet been quantified.

CHEMICAL CHANGES DURING CONTACT METAMORPHISM OF THE WEEKS FORMATION AT THE NOTCH PEAK COMPLEX, UTAH.

NABELEK, P.I., Dept. of Geology, Univ. of Missouri-Columbia, Columbia, MO 65211; LABOTKA, T.C., Dept. of Geological Sci., Univ. of Tennessee, Knoxville, TN 37996; GLASCOCK, M.G., Research Reactor, Univ. of Missouri, Columbia, MO 65211, USA

Introduction

The Upper Cambrian Weeks Formation was intruded 165 My ago by the granitic Notch Peak Stock at a depth between 4 and 6 km. The Weeks Formation consists mostly of thin-bedded argillaceous limestones and forms most of the roof of the stock. We employed mass-balance calculations to examine the geochemical changes in the Weeks during contact metamorphism by the stock. The aim is to quantify the loss or gain of major and trace elements relative to metamorphic grade and mineral assemblages.

The unmetamorphosed samples contain a mixture of calcite, muscovite, quartz; with increasing grade, diopside and wollastonite isograds are observed (1). Idocrase, scapolite, sphene, and feldspars are other important metamorphic phases. In addition, calc-silicate reactions (1) resulted in a systematic loss of CO2 with grade.

Methodology

Given the multicomponent sedimentary mixture, which made up the rocks prior to metamorphism, and the loss of mass as CO2, several steps were used to calculate the composition of each sample prior to metamorphism. First, the composition of each sample was "corrected" for the loss of CO2. Since in the unmetamorphosed rocks essentially all calcium is contained in calcite, we assumed that CaO - CO2 (molar) yields the amount of CO2 lost from each sample. Second, because the samples are multicomponent sedimentary mixtures, the variation of each examined element was defined by a linear multiple regression with "corrected" concentrations of the most correlated (or inversely correlated) immobile elements in the lowest-grade samples with the least loss of CO2. We initially considered Ti, Mg, Al, and Ca as immobile conserved elements. Thus defined, the pre-metamorphic "initial" concentration of each examined element in the high-grade samples was calculated. The difference between the "corrected" and "initial" concentrations of the element in a sample yields the gain or loss of the element during metamorphism. Only values falling outside the residuals of the regressions are considered significant. In this manner we found insignificant loss or gain of silica with grade. Therefore, silica was also used to define the "initial" concentrations of some elements.

Results

The results suggest lack of loss or gain of Fe, Co, other transition metals, Cs, and U. The variation of Na is unsystematic with grade, although several high-grade samples may have lost while others may have gained Na. This suggests that Na was mobile in the system and its apparent loss or gain may be related to the amount of feldspar, scapolite, or fluid inclusions in a given sample. As much as 150 ppm Rb was lost from the highest- grade samples, probably due to lack of formation of phases which could accept Rb, which was mostly in muscovite prior to metamorphism. As much as 1500 ppm Sr was lost and 1500 ppm Ba was gained by the high - grade samples (Fig.). The loss of Sr and gain of Ba appear to be related to the disappearance and appearance of calcite and alkali feldspar, respectively. Only one sample appears to have gained Sr. It contains a substantial amount of feldspar. The loss or gain of elements during contact metamorphism therefore appears to be controlled primarily by the availability of appropriate crystal sites in a given sample.

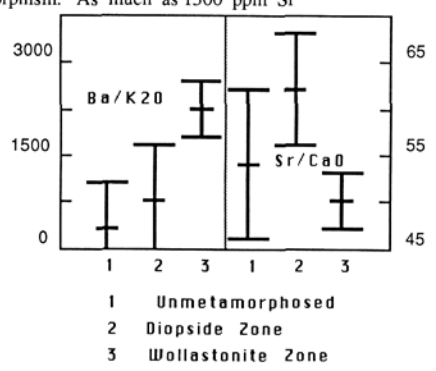

(1) Labotka and Nabelek, This volume.

NEW EXPERIMENTAL DATA ON BIOTITE SOLID SOLUTIONS IN HYDROTHERMAL CONDITIONS . APPLICATION TO THE TYPOLOGY OF GRANITOIDS .

NACHIT H.,Lab. de Pétrologie,Univ. de Bretagne Occ.,29287 Brest Cedex,France.MONIER G.,CREGU,B.P. 23,54501 Vandoeuvre lès Nancy, Cedex,France.ROBERT J.-L.,CRSCM-CNRS,1A rue de la Férollerie 45071 Orléans Cedex,France.

Following previous works on Mg-biotite solid solutions,we have investigated the solid solution domain of Fe-biotites,as a function of T and fO_2 (MW,NNO and HM buffers) under 2 kbar P_{H_2O}.

One must distinguish two domains:un aluminous domain,with $(Al/Al+Si)^{IV} \geq 1/4$ ([1],Fig.1) and a low aluminum domain with $(Al/Al+Si)^{IV} < 1/4$ ([2],Fig.1).

In the aluminous domain,the extent of the solid solutions of Fe-biotites is maximum for T<600°C,with the buffer NNO.This situation is similar to that of Mg-biotites.With the buffer MW,this domain slightly reduces and it is limited to a very narrow range,close to the Fe-eastonite composition with the buffer HM (Fig. 1).At 720°C, with the buffer NNO,annite and compositions close to annite are no longer stable.The extent of the solid solution domain is reduced, towards the join Fe-eastonite - Siderophyllite (Fig. 1);this behavior is at the opposite of that of Mg-biotites whose compositions stable at high temperatures belong to the join phlogopite-muscovite. The reduction of the solid solution domain of Fe-biotites is accentuated with the buffer MW and no mica is stable with the buffer HM. At 800°C,no mica is stable whatever the buffer may be.In this aluminous domain,all micas have a d_{060} inferior to the d_{060} of annite.

In the low aluminum domain,there are stable micas for starting compositions located inside the triangle Annite (Ann) - Montdorite (Md) - Y (Y is a hypothetical mica having tetrahedrally coordinated ferrous iron) (Fig. 1).In this domain [2],the maximum extent of the solid solution is also for T≤600°C,with the buffer NNO and is more reduced with the buffer MW;no mica is stable in this domain,with the buffer HM.At T≥600°C,with the buffers MW and NNO,the two domains [1] and [2] are connected,which indicates that the biotite compositions can move continuously from one domain to the other one. At 720°C,the extent of the solid solution range in the low aluminum domain is very reduced with the buffer NNO;under these conditions of temperature and fO_2,one have two different biotites susceptible to coexist : one of aluminous-type and another one of low aluminum-type.

Two hypothesis,which are not conflicting,can be proposed to explain these low-aluminum biotite compositions : either the ferriannite molecule in solid solution or a molecule of mica having tetrahedrally coordinated Fe^{2+} in solid solution (Y , Fig. 1).An intermediate situation is observed for $0<X_{Fe}<1$.

The solid solution ranges determined experimentally for $X_{Fe} \simeq 1$, under fO_2 conditions corresponding to the buffer NNO closely correspond to the repartition areas of biotites of granitic origin (Fig. 2).In the projection M^{2+}-Al-Si,biotites from granitoids belong to distinct domains,according to their origin.Three domains can be distinguished in Fig. 2 : the alkaline domain (a);the calc-alkaline domain (lato sensu) (b) and the peraluminous domain (c).

In these different lineages,the most evolved terms converge towards the ternary granitic minimum and neither their chemical nor their modal compositions permit an easy determination of these lineages.

The composition of their biotites,which reflects the increasingly aluminous character of the host lineages,from (a) to (c),can provide a precious aid for this purpose.

References.

. ROBERT J.-L.,Chem. Geol.,17,195-212,(1976).
. SEIFERT F. and SCHREYER W.,Contr. Mineral. Petrol.,196-215,(1971
. WONES D.,Amer. Mineral.,57,316-317,(1972).

Fig.1

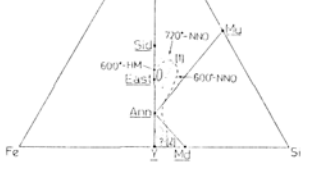

Fig.2

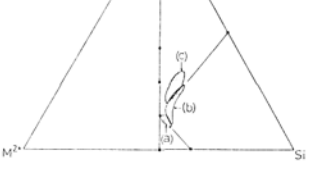

CRYSTAL CHEMISTRY OF THE As-Sb-S SYSTEM
—SYNTHESIS OF WAKABAYASHILITE AND STUDY OF SOLID SOLUTIONS BY X-RAY CRYSTAL STRUCTURE ANALYSIS AND EXAFS

NAKAI,I., YOKOI,H., IMAFUKU,M., AND MIYAWAKI,R. Dept. of Chemistry The University of Tsukuba, Ibaraki 305 JAPAN

Introduction As and Sb exhibit different chemical behaviors in their sulfides, though they are analogous elements of Group V. So far, four minerals are known near the As_2S_3-Sb_2S_3 join: i.e. orpiment, wakabayashilite, getchellite and stibnite. Dickson et al., reported solid solution ranges of orpiment, stibnite, and realgar[1]. The purpose of our study is to reveal the crystallochemical behaviors of As and Sb in sulfides. We report a complete information about the solid solution ranges among the four minerals including the first success in synthesis of wakabayashilite, X-ray structure analysis of As-rich stibnite, and getchellite. EXAFS analysis has been made to reveal local structure around the As atoms in the solid solutions.

Synthetic Study Synthesis was made by hydrothermal treatment of $(As_{1-x},Sb_x)_2S_3$ glass ($0 \leq x \leq 1$) with solvent of Na_2S soln. at 250-400°C, and 1000kg/cm² pressure. The products were analyzed by electron microprobe to clarify their solid solution ranges. The results are summarized in Fig. 1. Substitution of As for Sb in

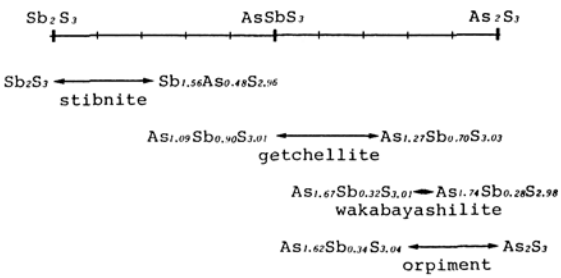

Fig.1. Solid solution ranges of the phases in As_2S_3-Sb_2S_3 system

stibnite caused lengthening of the a axis and shortening of the b and c axes. Single crystals of wakabayashilite up to 1.8mm long have been successfully synthesized. The color and appearance closely resemble natural wakabayashilite.

Structure Analysis The structures of synthetic stibnite containing 25mol% As and As-rich getchellite were determined using diffractometer data. Crystal data : $Sb_{1.5}As_{0.5}S_3$, Pbnm, a=11.282(3), b=11.279(4), c=3.786(1)Å, Z=4, final R=0.047(984 obs.refl.); $As_{1.3}Sb_{0.7}S_3$, $P2_1/a$, a=11.850(14), b=9.040(7), c=10.197(13)Å, β=116.15(11)°, Z=8, final R=0.063(2646 obs.refl.)

The structures of the solid solutions are basically the same as those of natural stibnite[2] and orpiment[3] previously reported, respectively. The site occupancy refinements have indicated that the distribution of As and Sb at the metal sites are disorder in both structures. The substitution of As for Sb in stibnite caused shrinking of the double chain structure like pantograph. This result accounts for the lattice parameter changes described above.

EXAFS analysis EXAFS measurements were made with synchrotron radiation at BL-10B in Photon Factory, Tskuba, Japan. As K-absorption spectra of the synthetic stibnite, getchellite and natural orpiment, getchellite, and realgar were measured and Fourier transforms of $k^3\chi(k)$ were calculated. The result indicates that local structure of As in getchellite and stibnite is very close to that in orpiment. Consequently, all As atoms are found to be in trigonal pyramidal coordination by S even in stibnite.

Conclusion Half the Sb in stibnite show trigonal pyramidal 3-coordination by S, and the other half, as well as many Sb in sulfosalts, exhibit square-pyramidal 5-coordination by S using the sp^3d^2 hybridization, which As could not utilize, as confirmed by the result of our EXAFS analysis. Moreover, As-S distance is much (about 0.2 Å) shorter than Sb-S. These two factors could account for structural discontinuity and observed limit of solid solution ranges in the As_2S_3-Sb_2S_3 system to some extent.

1) Dickson,F.W.,Radtke,A.S.,Weissberg,B.G. & Heropoulos,C.(1975) Econ. Geol.,70,591.
2) Bayliss,P. & Nowacki,W.(1972) Z. Kristallogr.,136,308.
3) Guillermo,T.R. & Wuensch,B.J.(1973)Acta Cryst., B29,2536.

ORE MICROSCOPY AND OTHER METHODS ADOPTED IN ORE MINERALOGY

NAKHLA , F. M. , Dept. of Mining , Faculty of Engineering, Cairo University , Giza-Cairo , EGYPT

Ore Mineralogy has made remarkable progress during the past three decades by adopting new quantitative methods and modern techniques for the determination of ore minerals and their intergrowths from their polished surfaces. Moreover, Ore Mineralogy has become an indispensable tool for exploitation of low-grade deposits and solving wide variety of problems in various phases of mineral industry inculding the domains of exploration , mineral dressing and extractive metallurgy.

Methods commonly used in Ore Mineralogy are divided into four principal groups as follows :

Group 1. Optical and physical methods which comprise :

i. Identification of physical and optical characters of ore minerals from their polished surfaces by qualitative observations under reflected polarised light with the ore microscope.

ii. Quantitative determination of spectral reflectance electronically with highly sensitive photomultiplier tubes besides other reflectance parameters such as bireflectance , $\underline{\Delta}R\%$ ($R\%_{470}-R\%_{650}$ nm) and $\underline{\Delta}R'$ ($R\%_{650}-R\%_{470}$ nm).

iii. The investigation of textures and microstructures such as mineral intergrowths, inclusions and solid solutions.

The optical, textural and structural characteristics of the polished metallic mineral surfaces represent the fundamental domain of the fascinating field of Ore Microscopy which is an important branch of the field of Ore Mineralogy .

Group 2. Chemical methods that are generally divided into two main subgroups as follows :

i. Qualitative methods include simple, easy and quick methods that are quite helpful for the detection of most common and minor metallic constituents of ore minerals by the aid of highly sensitive and specific organic reagents. Among these methods may be mentioned the following :
(iA). Methods applied on polished surfaces for example :
(a) Chromographic Contact Print Method.
(b) Etch Reactions. and (c) Staining Tests.

iB. Methods applied on mineral powder such as microchemical tests and paper chromatography.

ii. Quantitative or semi-quantitative methods which comprise two main categories as follows :

iiA. Methods applied on polished ore mineral surfaces which include electron probe microanalysis and the laser or Raman Probe Microanalysis.

iiB. Methods applied on mineral powder of the ore mineral, these include Mössbauer Spectroscopy and X-ray fluorescence analysis.

Group 3. Structural method by X-ray diffraction analysis and it is the most reliable method for the determination of crystalline substances including ore minerals. There are two main techniques as follows:

i. Powder method is the most simple and commonly used method for mineral identification by X-ray diffraction method.

ii. Methods applied in the case of crystal fragments or oriented well-developed crystals by using more complicated techniques such as rotation and oscillation method , Weissenberg method and the precision method .

Group 4. Other special methods among which are the following:
a. micro-radiography , b. cathodoluminescence microscopy ,
c. electron microscopy, d. acoustic microscopy ,
e. Vickers micro-indentation hardness ,
f. DTA and similar methods,
g. several specific methods among which are studying the thin sections by the petrographic microscope, separation of minerals by heavy liquids, electromagnetic or flotation methods, IR absorption spectroscopy, atomic absorption , mass spectroscopy for the age determination and studying gas or fluid inclusions trapped in vacuoles within certain ore minerals for the determination of the probable temperature of formation.

ORE MINERALS DETERMINATION BY THEIR REFLECTANCE PARAMETERS AND CHEMICAL COMPOSITION

NAKHLA, F. M., Dept. of Mining, Faculty of Engineering , Cairo University , Giza-Cairo , EGYPT

Reflectance values at wavelengths of 470, 546 and 650 nm in air from polished metallic ore mineral surfaces are dependent upon chemical , physical and crystal structure parameters. An important and reliable coefficient of reflectance property is the difference between R% at 470 and 650 nm , $\underline{\Delta}R$, or between R% at 650 and 470 nm , $\underline{\Delta}R'$, as shown in Fig.1. Accordingly, ore minerals can be classified into two principal groups :

i. The First Group includes minerals having R% at 470 nm more than R% at 650nm while difference in R% is expressed as $\underline{\Delta}R$. In this group, essential metals that form the minerals are one or more of the following elements: Cu, Ag, Pb, Zn, As, Sb, Bi, U, Th, Sn, W, Ta-Nb, Cr, Mn and rare earths. These minerals usually exhibit white , bluish and various shades of grey colours. Moreover, minerals composed of oxides and hydrated oxides are invariably belonging to this group.

ii. The Second Group contains minerals having R% at 470nm less than R% at 650 nm while variation in R% is designated as $\underline{\Delta}R'$. In this category predominant metals constituting the minerals include Fe (either alone or associated with other metals such as Cu , Ag or Ti) , Co, Ni, Pd, Ir, Au, Au+Ag, and Te. Minerals of this group have idiochromatic colours ranging from pale or deep yellow to reddish and brownish tones.

In present study, 4 determinative Tables for the systematic identification of about 170 ore mineral species have been established on the basis of their reflectanoe parameters as well as chemical composition. Tables 1 and 2 , include the plots of R% at 470 nm against $\underline{\Delta}R$ together with some optical characters and essential metals forming the ore minerals . Tables 3 and 4 include the plots of R% at 650 nm against $\underline{\Delta}R'$ in association with certain optical properties as well the chemical composition of ore minerals included in these Tables.

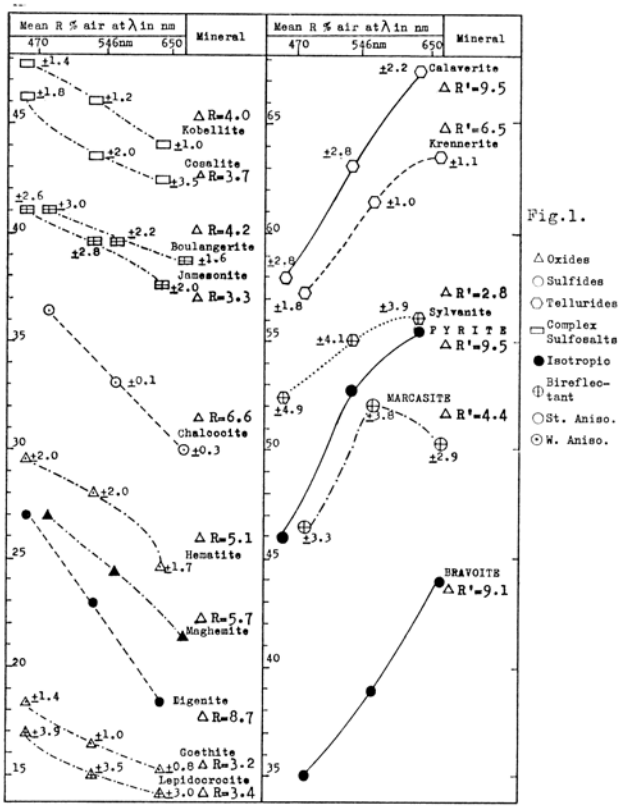

Fig.1.

ESTIMATION OF THE TRAPPED LIQUID COMPOSITION IN THE BASISTOPPEN SILL, EAST GREENLAND

NASLUND, H.R., Dept. of Earth Sciences, Dartmouth College, Hanover, NH 03755; CHALOKWU, C.I., Dept. of Geology, Auburn University, Auburn, AL 36849

The Basistoppen sill is a differentiated tholeiitic sill that has intruded the upper part of the Skaergaard complex (Douglas,1964; Naslund, 1984). The sill varies from a Mg-rich gabbro precipitating olivine Fo_{79} at its base to a Fe-rich diorite precipitating olivine Fo_{02} at its top, and can be divided into four units based on the distribution of cumulus minerals: a gabbro picrite zone (GPZ = cumulus olivine and Fe-Cr spinel); a bronzite gabbro zone (BGZ = cumulus augite, plagioclase, and orthopyroxene); a pigeonite gabbro zone (PGZ = cumulus augite, plagioclase, pigeonite, and Fe-Ti spinel); and a fayalite diorite zone (FDZ = cumulus ferroaugite, plagioclase, olivine, Fe-Ti spinel, and apatite). A ferrohedenbergite granophyre overlies the FDZ, and may represent a final differentiate. The extreme differentiation developed in the 600 M thick Basistoppen sill is the result of its emplacement into the upper part of the Skaergaard intrusion before the Skaergaard had cooled much below its solidus (Naslund, 1986).

Texturally the rocks of the sill are orthocumulates, and hence their composition should represent a mixture of cumulus minerals and trapped liquid. The composition of the trapped liquid, which ideally should record the composition of the differentiating Basistoppen magma, has been estimated by two different methods: (1) A bulk composition for the sill can be calculated from the estimated composition and volume of each unit. Such a calculation using 23 elements yields a bulk composition similar to that of the Basistoppen chilled margin. If it is assumed that the sill crystallized from the bottom upwards, the composition of the differentiating magma at any point in the sill, and hence the theoretical composition of the trapped liquid, can be calculated from the compositions of the overlying units. (2) Alternatively, the composition of the trapped liquid for any sample can be calculated from its bulk composition, and the relative proportions and compositions of its cumulus minerals. Plagioclase in these samples preserves an inner core of uniform composition surrounded by outer zones of variable composition. If these inner cores are assumed to be cumulus and the outer zones are assumed to be intercumulus, the relative abundances of cumulus and intercumulus plagioclase can be determined. Pyroxene, olivine, spinel, and apatite in these samples do not preserve visible zoning, so as a result, the relative abundances of cumulus and intercumulus material for these minerals must be estimated. The ratio (% intercumulus/% cumulus) determined for plagioclase was used as an approximation of this ratio for the other cumulus phases. Modal abundances determined by point counting have been corrected for the differences in the densities of the minerals.

A comparison of the trapped liquid compositions calculated by the two methods (Figure 1) provides an indication of how the crystallization of the Basistoppen sill differed from the crystallization assumed for an ideal orthocumulate. Trapped liquid compositions calculated by procedure (2) are generally richer in Si and Mg and poorer in Al, Fe, and Na than those calculated by procedure (1). The low Si values for (1) may indicate that a small granophyre component should be added to the model. The low Na and Al values calculated by (2) suggest that some of

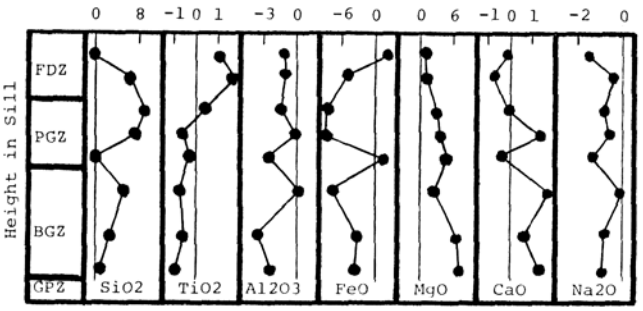

Figure 1 - Comparison of the trapped liquid compositions determined by models 1 and 2.

the plagioclase that appears to be cumulus is actually adcumulus in origin, and grew in situ as a result of diffusion or convection within the intercumulus liquid. The high Mg and low Fe values calculated by (2) suggest that the compositions measured for cumulus pyroxene and olivine are more Fe-rich and Mg-poor than the true cumulus compositions. Reequilibration between cumulus minerals and the intercumulus liquid could produce such an effect. The lack of zoning in the pyroxenes and olivines of the sill indicate that some reequilibration has occurred. The relative Ti and Ca contents of the calculated trapped liquids change with height in the sill. The upward increase in Ti in model (2) relative to model (1) may indicate that ilmenite, which is an intercumulus phase throughout the sill, becomes a cumulus phase in the upper part. The Ca content calculated by model (2) is affected by the abundances of both plagioclase and augite. The upward decrease in Ca may indicate that cumulus augite is underestimated in the lower part of the sill or that cumulus plagioclase is overestimated in the upper part.

References

Douglas, J. A. V., 1964. Geological investigations in East Greenland: VII The Basistoppen sheet, a differentiated basic intrusion into the upper part of the Skaergaard complex, East Greenland. Medd. om Grønland, 164, 1-66.

Naslund, H.R., 1984. Mineralogical and compositional trends in the Basistoppen sill, East Greenland. Geol. Soc. Amer. Abst. with Prog., 16, 608.

Naslund, H.R., 1986. Disequilibrium partial melting and rheomorphic layer formation in the contact aureole of the Basistoppen sill. Contr. Mineral. Petrol., in press.

THE PHYSICS AND CHEMISTRY OF THE THIRTEEN CAUSES OF COLOR IN MINERALS

NASSAU, K., Materials Research Laboratory, AT&T Bell Laboratories, Murray Hill, NJ 07974

No less than thirteen of the fifteen causes of color (see The Physics and Chemistry of Color, K. Nassau, John Wiley and Sons, New York, 1983) apply in one way or another to minerals. Five distinct formalisms are required to provide the most direct insight into these causes: Vibrations and simple excitations; ligand fields; molecular orbitals; energy bands; and geometrical and physical optics. All fifteen causes are outlined.

Incandescence (resulting in the color sequence black, red, orange, yellow, white, bluish white) is produced by any hot substance; gas excitations (as in neon tubes and the aurora) involve electronic excitations in individual gas or vapor atoms. These are the only two mechanisms which do not apply, not even indirectly, to minerals.

Vibrations and rotations within individual molecules or within liquids or solids lead to excited energy levels and the absorption of light. This explains the pale blue color seen in pure water and in glacial ice.

Ligand field (earlier crystal field) effects involve unpaired electrons in a transition metal ion; the energy levels are controlled by number, symmetry, and bond strengths of the surrounding atoms. This mechanism applies to idiochromatic transition metal compounds, such as Mn in rhodochrosite, Fe in hematite, and Cu in malachite, as well as to allochromatic transition metal impurities, such as Cr in ruby and emerald, and Fe in citrine.

Molecular orbitals explain the color of organic compounds, including dyes, with excited states of electrons involved in orbitals spread out over conjugated systems of single and double bonds, often with electron donor and acceptor groups attached. This accounts for the colors of amber, lignite, petroleum, and related minerals.

Electron orbitals in charge transfer (CT) are spread out over two or more atoms. Variable valence transition elements can be involved, as in the blue sapphire color derived from Fe + Ti, and the blue of vivianite, the black of magnetite, or the brown to red color of many rocks derived from the CT interaction of the two valence states of Fe. Not involving transition elements are ligand-ligand CT in groups of three S atoms in blue lazurite (lapis lazuli), and metal-ligand CT as in crocoite, wulfenite, and hematite.

Band theory covers systems where electrons from individual atoms can move over the whole specimen. This explains the color as well as the electrical and thermal properties of metals and alloys such as copper, silver, gold, and cuprouaride. When applied to pure semiconductors, the presence of an energy gap between the valence and the conduction bands leads to the color sequence (with decreasing band gap energy) of colorless, (diamond), yellow (sulfur, greenockite), orange (realgar), red (cinnabar), black (metacinnabar, galena). Doped semiconductors contain impurities in the band gap, as in B-containing blue diamonds (where these shallow acceptors conduct electricity) and N-containing yellow diamonds.

Color centers can be explained by band theory. These involve an electron displaced (usually by irradiation) from an impurity or defect, forming a hole center, with the electron trapped elsewhere, forming an electron center; either center can absorb light and produce color. Examples are smoky quartz, amethyst, blue topaz, red tourmaline, and F-centers in fluorite.

Dispersive refraction produces the play of fire in a faceted gemstone. Scattering can be of various types: Rayleigh scattering with very fine particles produces blues as in butterfly wings, sky, and eyes, while the Mie scattering of larger particles produces mostly white, as in moonstone and silver-sheen obsidian. Yet larger particles lead to asterism as in star corundum.

Interference of light from reflections in a thin film produces iridescent color, the color depending on the thickness of the film and its refractive index. This leads to the iridescence of tarnish films, as in bornite, and to the luster on pearls. Diffraction is a special case of interference in the light scattered from a regular grating and produces spectrally pure colors. A three-dimensional example occurs in the play of color in opal.

THERMOCHEMISTRY OF HIGH PRESSURE $MSiO_3$ AND $MGeO_3$ PHASES

NAVROTSKY, A., Dept. of Geological and Geophysical Sciences, Princeton University, Princeton, NJ 08544 USA

Thermochemical studies by high temperature calorimetry have been performed on the high pressure polymorphs of $CaGeO_3$, $CdGeO_3$, $MgGeO_3$, $MnSiO_3$ and on $MgSiO_3$ ilmenite. The enthalpies of transition show systematic trends. The enthalpies of transition among pyroxene and pyroxenoid polymorphs are uniformly small. The pyroxenoid (or pyroxene) to garnet transition has a ΔH° of less than 10 kJ mol^{-1} in magnitude for $CaGeO_3$ and $CdGeO_3$, 36 kJ mol^{-1} in $MnSiO_3$ and (estimated) 50-60 kJ mol^{-1} in $MgSiO_3$. The entropies of these transitions, obtained both by combining calorimetry and phase studies and from lattice vibrational modelling using Kieffer's approach, are small and negative, confirming shallow positive P-T slopes. The transition from pyroxene to ilmenite occurs stably in $MgGeO_3$, with ΔH° = 6 kJ and metastably (with β + stishovite or γ + stishovite as intervening phases) in $MgSiO_3$ with ΔH° = 70 kJ. It has small negative ΔS° values but $MgSiO_3$ ilmenite may have a slightly higher entropy than a mixture of spinel and stishovite. The transition pyroxenoid (or pyroxene) to perovskite has ΔH° near 40 kJ mol^{-1} for $CaGeO_3$, $CdGeO_3$ and $MgGeO_3$. The garnet to perovskite transition has a positive ΔS° for $CaGeO_3$ and $CdGeO_3$ as probably also does the ilmenite to perovskite transition in $MgSiO_3$. The vibrational modelling supports this conclusion and the idea that perovskite-forming transitions have negative P-T slopes. The table shows the energetics of these transitions.

Thermodynamics of ABO_3 Phase Transitions

	ΔH°(kJ mol^{-1})	ΔS(J $mol^{-1}K^{-1}$)	ΔV°(cm^3 mol^{-1})
pyroxene or pyroxenoid → garnet			
$CaGeO_3$	-4.9 ± 4.2	-5.9 ± 1.5	-5.97
$CdGeO_3$	+0.5 ± 2.7	-8.4 ± 2.0	-5.30
$MnSiO_3$	+34.6 ± 2.5	-6.7 ± 2.1	-4.00
$MgSiO_3$	+37.0 ± 3.0		
garnet → perovskite			
$CaGeO_3$	+43.3 ± 5.0	+10.9 ± 3.8	-5.35
$CdGeO_3$	+43.1 ± 5.0	-1.7 ± 3.0	-4.88
$MgSiO_3$	(83)		
pyroxene → ilmenite			
$MgGeO_3$	+7.5 ± 0.6	-6.3 (or -20?)	-5.11
$MgSiO_3$	+71.8 ± 6.3	-10.9 ± 4.0	-4.94
ilmenite → perovskite			
$CdTiO_3$	+15.0 ± 0.8	+14.2	-2.94
$CdGeO_3$	+34.3 ± 4.0	+2.6 ± 2.0	-3.00
$MgSiO_3$	(48.2)	positive	-1.90

GEOCHEMISTRY OF THE GRANITIC ROCKS AND THEIR MINERALS FROM SERRA DA ESTRELA, CENTRAL PORTUGAL

NEIVA, A. M. R., Dept. of Mineralogy and Geology, Coimbra University, 3 000 Coimbra, PORTUGAL

Different types of Hercynian granitic rocks occur in the horst of Serra da Estrela, the highest Portuguese mountain. The main outcrops are of coarse grained porphyritic biotite-muscovite granite, which intruded granodiorite and the medium to fine grained biotite-muscovite granite with some and small phenocrysts of microcline and plagioclase. Both granites contain xenoliths of micaschists. The granodiorite also occurs in small outcrops. There are also a later medium grained muscovite granite and some aplite and pegmatite veins. Next to faults the coarse grained porphyritic biotite-muscovite granite was transformed into coarse grained porphyritic pink and reddish biotite-muscovite granites.

The plagioclase in the granodiorite has composition of andesine to albite, it is oligoclase to albite in both two mica granites and albite (An=0) in the muscovite granite. The molecular $(Al_2O_3/CaO+Na_2O+K_2O)$ ratio is 1.09 to 1.11 in the granodiorite and greater than 1.1 in all the granites.

Both two mica granites have more SiO_2, K_2O, Rb, U, less TiO_2, Al_2O_3, FeO, MgO, CaO, Na_2O, Zr, Sr, Cr, Ce, Nd, La, Ba, Sc, Th and smaller La/Sm, Ce_N/Yb_N ratios than the granodiorite. All of them have negative Eu anomalie, but the size is not significantly different. The coarse grained granite has more TiO_2, FeO, MgO, CaO, Li, Zr, Zn, Ce, Nd, U, Th, less K_2O, Sr, a larger negative Eu anomalie and higher Ce_N/Yb_N ratio than the fine grained granite. The granodiorite and both two mica granites correspond to three different pulses of magma probably originated by partial refusion of country rock (phyllite, metagraywacke and intercalated marbles).

The muscovite granite is differentiated from the coarse grained granite and has more Al_2O_3, Na_2O, Nb, Li, Rb, U, less TiO_2, Fe_2O_3, FeO, MgO, CaO, Zr, Ce, Nd, La, Ba, Sc, Th, larger negative Eu anomalie and smaller La/Sm ratio.

The distribution of major and trace elements of magmatic Fe^{2+}-biotite and muscovite from granodiorite and granites confirm the suggested origin.

f_{O_2} is lower than 10^{-17} in the granodioritic magma and lower than 10^{-18} in both two mica granite magmas. Log (f_{H_2O}/f_{HF}) is not significantly different in these three magmas, but has a lower value in the muscovite granite magma. Log (f_{H_2O}/f_{HCl}) is greater in both two mica granite magmas than in the granodioritic magma and the highest value was found in the fine to medium grained biotite-muscovite granite magma.

The coarse grained porphyritic pink and reddish biotite-muscovite granites occurring next to faults with quartz veins were originated by reaction of fluids with the coarse grained porphyritic grey biotite-muscovite granite at great depth. The plagioclase lost anorthite content and became albite, potash feldspar became pink or reddish, biotite disappeared, the amount of magmatic muscovite decreased strongly, but chlorite, muscovite and some epidote were newly formed. The chlorite is ripidolite in the pink granite and brunsvigite in the reddish granite. This transformation is accompanied by increase in Fe_2O_3t, Na_2O, Nd, La and decrease in CaO, F, Zn, Cu, Li, Rb. In the reddish granite SiO_2 and Eu/Eu* decrease, while Al_2O_3 increases.

The chlorite of the reddish granite has more Si, Fe^{3+}, Mg, H_2O+, Zr, Zn and less Al, Fe^{2+}, Li, Cr, V than the chlorite of the pink granite. The muscovite of the pink and reddish granites has more Si, less Al^{IV}, Ti, K, F, Zn, Li, Ba and smaller f_{H_2O}/f_{HF} than the muscovite of the parental granite.

THERMOCHEMISTRY OF BINARY AND TERNARY GARNET SOLID SOLUTIONS

NEWTON, R.C., GEIGER, C.A., KLEPPA, O.J. and BROUSSE, C., Dept. of the Geophysical Sciences, Univ. of Chicago, Chicago, IL 60637

Enthalpies of solution of synthetic garnet solid solutions on the binary joins pyrope (Py: $Mg_3Al_2Si_3O_{12}$)-grossular (Gr: $Ca_3Al_2Si_3O_{12}$), grossular-almandine (Al: $Fe_3Al_2Si_3O_{12}$) and pyrope-almandine have been measured with high temperature oxide melt calorimetry. Binary subregular interaction parameters for pyrope-grossular are $W_{Py-Gr} = 3000$ cal/gfw and $W_{Gr-Py} = 12140$ cal/gfw, where the excess enthalpy of mixing is $\Delta H^{ex} = X_{Gr}X_{Py}W_{Gr-Py} + X_{Py}X_{Gr}W_{Py-Gr}$, X = mol fraction. Similarly, $W_{Py-Al} = 7230$ and $W_{Al-Py} = -4610$, which predicts considerable positive deviation from ideality near the almandine end of Py-Al, and $W_{Gr-Al} \cong W_{Al-Gr} \cong 0$, indicating a nearly ideal almandine-grossular join.

Enthalpy of solution measurements on two ternary garnets rich in almandine, $Al_{.6}Py_{.2}Gr_{.2}$ and $Al_{.8}Py_{.1}Gr_{.1}$, indicate that mixing obeys the ternary subregular approximation without need for a ternary mixing constant.

Assymetric non-ideal mixing in pyrope-almandine and near-ideal mixing in grossular-almandine are not readily explainable in terms of cation size considerations, which would predict the opposite relations. Crystal-field energies or quasi-ordering producing superlattice structures may be necessary to explain the near-ideality of grossular-almandine, despite a significant excess volume of mixing.

Recent theoretical discussions of garnet mixing properties in terms of experimental phase equilibria have discounted the necessity of excess entropy of mixing in Fe- and Mg-dominated garnets. Lack of excess entropy may be related to anomalously small partial molar volumes of grossular in pyrope-almandine-rich garnets. If Ca in relatively dilute concentration behaves as site-defects, an excess entropy of mixing may not be anticipated. Thus, the measured enthalpies of mixing may provide a reasonably accurate account of Gibbs energies of mixing for ternary garnets of granulites, eclogites and peridotites.

THERMODYNAMICS OF ORTHOPYROXENE, PLAGIOCLASE AND GARNET: UNCERTAINTIES AFFECTING GEOBAROMETRY

NEWTON, R.C., Department of the Geophysical Sciences, University of Chicago, Chicago, IL 60637

Orthopyroxene, plagioclase and garnet are the most useful assemblage in the geobarometry of quartzofeldspathic granulites. Published calibrations give nearly concordant paleopressures although they require different assumptions about thermodynamic properties of the minerals.

Orthopyroxene is variously regarded as having either somewhat positive or somewhat negative excess free energy of mixing at temperatures below 1000°C, and may be an asymmetric solid solution. Calculations based on M1-M2 partitioning of Mg and Fe yield large temperature dependence of non-ideality and are somewhat suspect in the lack of reversed experimental data.

A possible disordering entropy of anorthite accounts for an uncertainty of ± 1.5 kbar in the thermodynamically-based calibrations. Various experimental determinations of the reaction to grossular, Al_2SiO_5 and quartz show some uncertainty in extrapolation to the temperature range of 600°-800°C. The best thermodynamic measurements available require a disorder entropy of 0.5-1.0 cal/K-mol to explain the phase equilibrium data. Plagioclase solid solution models based on thermodynamic measurements yield deviations from non-ideality at 600°-800°C which are too small in the Na-rich range to be consistent with phase equilibrium measurements and natural parageneses, probably because of inadequate account of Al,Si ordering.

Discussions of the geobarometry of natural assemblages infer an asymmetric excess enthalpy of mixing in Fe^{2+},Mg garnets, greatest near almandine. This deduction, though not explainable by ionic size arguments, is supported by enthalpy of solution measurements. A ternary enthalpy of mixing constant may be non-negligible. Excess entropy of mixing in Ca,Mg garnets revealed by adiabatic calorimetry are probably not important in Fe-dominated garnets. For these reasons many natural garnets are somewhat less stable than some models imply.

The total maximum uncertainty of garnet granulites in geobarometry from all sources may be 3-4 kbar. It is very probable that existing calibrations are actually subject to much smaller errors.

MINFIND

NICKEL,E.H. and FLETCHER,A.B., Division of Minerals & Geochemistry, CSIRO, Private Bag PO, Wembley, W.A., Australia 6014

This microcomputer program consists of data files that contain data on all valid mineral species and of search programs that enable information to be extracted from the data files.

The data files consist of eleven files on seven floppy disks, with each file restricted to one category. The categories are: 1)Elements, 2)Sulfides), 3)Halides, 4)Oxides, 5)Carbonates, 6)Borates, 7)Nitrates, 8)Sulfates, 9)Phosphates, 10)Silicates, and 11)Organic Minerals. The data for each mineral include name, group, chemical formula, symmetry, space group, unit-cell parameters, Z, and up to three literature references.

The search programs are on a separate disk, and enable the data to be searched for a number of descriptors including name, group, chemical composition and references.

HYDROTHERMAL DETERMINATION OF INTERFACIAL ENERGIES AT ELEVATED TEMPERATURES AND PRESSURES

NITKIEWICZ, A. M., AND KERRICK, D. M., Geochemistry and Mineralogy Program, Department of Geosciences, The Pennsylvania State University, University Park, Pa. 16802, USA

"Equilibrium" bracketing studies of heterogeneous reactions under hydrothermal conditions have been used to quantify the surface free energy of bulk powders for selected silicates at elevated temperatures and pressures. This approach offers the distinct advantage over other techniques for determining surface energies in that it allows for the direct measurement of solid-fluid interfacial energies under supercritical conditions and is therefore of direct geological significance. With this method, isobaric shifts in the apparent equilibrium temperature of a heterogeneous reaction are measured as a function of the surface area of the phase in question. This is accomplished by monitoring reaction direction for experiments of sufficiently short duration such that recrystallization, and thus, true equilibrium with coarse-grained solids, is not achieved. Knowing the temperature shift, it is possible to calculate the excess energy for the reacting system and translate this into a surface energy. The observed temperature shift is transient and is expected to decrease as run duration becomes sufficiently long for recrystallization to coarsen the fine powder. The sensitivity of this technique is dependent upon the sensitivity of the reaction monitor, the kinetics and entropy change of the heterogeneous reaction, and the surface area of the powders. Excess energies as small as 50 J/mole, or surface energies as small as 20 mJ/m^2, are feasibly determined with this technique.

This method has been used to determine the solid-fluid interfacial energy for bulk powders of sillimanite and tremolite using the following reactions:

(1) Sillimanite = Andalusite

(2) 5 Talc + 6 Calcite + Quartz = 3 Tremolite

(3) Tremolite = 2 Diopside + 3 Enstatite + Quartz + H_2O

Experiments were performed in hydrothermal cold-seal apparatus using sealed noble metal capsules containing fluid and a single crystal of one phase surrounded by a powder mixture of the other components. The surface area of one of the phases, either sillimanite or tremolite, was allowed to vary. The point of zero weight change of the single crystal marked the apparent equilibrium temperature for each powder size-fraction studied.

The surface energy of a fibrolitic sillimanite from Lewiston, Idaho ($Al_{1.97}Si_{1.02}Fe^{3+}_{0.003}K_{0.006}O_5$) in a pure H_2O fluid was determined from isobaric temperature shifts in the polymorphic transformation of andalusite to sillimanite. Experiments of two weeks duration at 200 MPa and temperatures ranging between 825 and 1100 K generated an isobaric temperature shift of 142±48 K using

HYDROTHERMAL DETERMINATION OF INTERFACIAL ENERGIES AT ELEVATED TEMPERATURES AND PRESSURES

NITKIEWICZ, A. M., and Kerrick, D. M.

fibrolite powders with surface areas of 16 and 810 m^2/mole respectively. This temperature shift results from an excess free energy of only ~390 J/mole of sillimanite, and corresponds to an interfacial energy between fibrolite and H_2O of 490±230 mJ/m^2 at 200 MPa in the vicinity of 1000 K. Similar equilibrium temperatures for two equivalent coarse powders, one monocrystalline and the other a polycrystalline aggregate of ~1 micron wide fibers, suggest that internal grain boundaries (up to 700 m^2/mole) do not contribute to the observed isobaric shift. TEM examinations of defect populations in the powders confirm that lattice defects cannot account for the observed excess energy.

The surface energy of tremolite was studied using a natural tremolite from St. Gotthard, Switzerland ($Ca_2Mg_{4.94}Fe_{0.03}Si_{7.92}Al_{0.01}O_{22}(OH)_2F_{0.03}$) which was sized into a coarse fraction (10-20 micron) and a fine fraction (<10 micron) having BET surface areas of 338 and 24,800 m^2/mole respectively. Tremolite was chosen for study on the basis of 1) its high molar surface area relative to equivalently sized phases, and 2) the common use of sub-micron synthetic tremolites in phase equilibrium studies. Initial experiments on reaction (2) in an equimolar H_2O:CO_2 fluid at 200 MPa between 700 and 800 K produced a small, but discernible temperature shift of 11±7 K. This is the result of an excess energy of 1.5 kJ/mole of tremolite and corresponds to an interfacial energy of only 63±58 mJ/m^2 for tremolite in the binary fluid. Although the observed isobaric temperature shift is only 11 K, this a much larger net excess energy than that associated with the 142 K shift in the sillimanite reaction. The large uncertainty is a consequence of the relatively large entropy of this devolatilization reaction, thus, this reaction is relatively insensitive to large excess energies. In contrast to this entropy effect, the relatively large uncertainty in the sillimanite interfacial energy results primarily from the sluggish kinetics of the andalusite = sillimanite reaction in the coarse-grained powders.

Isobaric experiments on reaction (3), at 75 MPa in pure H_2O between 1000 and 1150 K resulted in a 36±7 K shift in the apparent equilibrium temperature. The observed temperature shift results from a net excess energy of ~3.3 kJ/mole of tremolite and corresponds to an interfacial energy of 135±28 mJ/m^2, a factor of two greater than for tremolite in the equimolar H_2O:CO_2 fluid under the conditions of reaction (2). The lower uncertainty in this determination reflects not only a larger surface energy contribution, but also the smaller entropy of reaction (3). Additional experiments are currently underway in order to differentiate between the relative contributions of pressure, temperature and fluid composition on the magnitude of these interfacial energies.

PHOTOMETRIC STUDY OF UV-LUMINISCENCE OF CUT DIAMONDS, AND ITS RELATIONSHIP WITH THERE COLOUR CLASSIFICATION

Nogués-Carulla,J.Mª*, Vendrell-Saz,M.*, Arbunies,M.* and López-Soler,A.**

* Escola de Gemmologia. Universitat de Barcelona.
** Instº de Invest.Geológicas "Jaime Almera" C.S.I.C.

Measurements of UV-luminiscence emission of 55 brilliant cut diamonds have been made in the visible range. The data are treated in order to obtein the colour coordinates.

The points displaying a linear distribution correspond to a dominant wavelength of 484 mm.

The transmission curves of these diamonds were obtained between 400 and 700 mm. The colour coordinates and colour saturation were calculated, and the points of x, and y are adjusted to a straight line, whose dominant wavelenght corresponds to 578 mm.

The comparation of the two photometric results shows that the observed colour is the addition of both, transmission and visible range emission luminiscence.

In addition, several examples of uncorrect colour classification originated by a strong emission of luminiscence superimposed to the transmission colour are given.

THE ORDER-DISORDER TRANSITION AND TRANSFORMATION-INDUCED DOMAINS IN ILMEMITE-HEMATITE

NORD JR., GORDON L. and LAWSON, CHARLES A., 959 National Center, U. S. Geological Survey, Reston, VA 22092 USA

The solid solution between hematite (Fe_2O_3) and ilmenite ($FeTiO_3$) is characterized by an $R\bar{3}c$ to $R\bar{3}$ order-disorder transition and a solvus (Fig.). The transition arises from Fe and Ti ordering on alternate layers parallel to (0001) resulting in the loss of the c-glide and the appearance of superlattice reflections of the type $hh\bar{2}l$, l=2n+1, in the ordered $R\bar{3}$ phase. Upon cooling through the transition, transformation-induced domains are formed. Domain boundaries have been imaged by dark-field transmission electron microscopy using superlattice reflections.

The transformation-induced domain boundaries are important microstructures for several reasons. (1) Boundaries indicate that a crystal has passed through the transition and thus can be used to locate the transition curve. (2) Boundaries represent strips of cation-disordered phase within ordered ilmenite-hematite. A crystal with domain boundaries can be considered a mixture of two phases, the proportions of which change as the domains coarsen within the ordered field. (3) Statistically, a portion of the disordered boundaries will be hematite-rich; this is an important control for magnetic properties (see companion abstract, Lawson and Nord) as the domains coarsen and the boundary area is reduced. (4) Disordered boundaries provide nucleation sites for hematite precipitation within the solvus.

Ilmenite-hematite grown at 1300°C in a gas mixing furnace and at 900°C in vacuo, in silica tubes have been examined by transmission electron microscopy. (1) Ilm_{60}, Ilm_{70}, and Ilm_{80} grown at 1300°C and Ilm_{60} grown at 900°C all have a domain microstructure, indicating that they crystallized as the disordered phase and that the transition curve lies below their crystallization temperature. Ilm_{90} and Ilm_{100} grown at 1300°C and Ilm_{70} grown at 900°C do not contain any domain boundaries indicating that they crystallized as the ordered phase and the transition curve lies above their crystallization temperature. The transition as determined by the presence or absence of domains lies at a lower temperature than that determined by Ishikawa (1958). Ishikawa used the change in magnetization measured at room temperature of ilmenite-hematite that was annealed above and below the transition. (2) The transition was reversed for Ilm_{70} by taking samples synthesized at one temperature and annealing them at another. Domains present in the 1300°C quenched sample coarsened at 900°C indicating that the transition is above 900°C. The 900°C sample with no domain boundaries was found to have domains after it was annealed at 1300°C and quenched, indicating that the transition lies below 1300°C for Ilm_{70}. (3) The transformation-induced domains decrease in size as the transition temperature decreases with increasing hematite component. The domain size for samples quenched from 1300°C is approximately 1.0 um for Ilm_{80}, 0.1 um for Ilm_{70} and 0.05 um for Ilm_{60}. The size change is due to decreasing diffusion rates at lower transition temperatures.

REFERENCES Ishikawa, Y., 1958, J. Phys. Soc. Japan, 13, 828-837.
Burton, B. P., 1982, PhD Thesis, SUNY Stony Brook, NY.

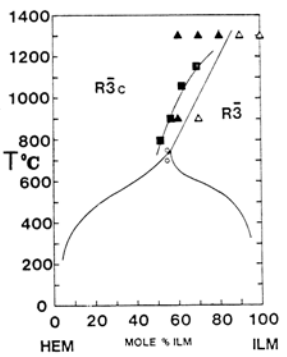

HEM-ILM PHASE DIAGRAM. Filled triangles show the composition and crystallization temperature of samples containing domain boundaries after quenching and open triangles show samples that do not contain domain boundaries after quenching. Open circles represent appearance and disappearance of superlattice reflections by in situ-heating on a single crystal x-ray diffractometer (Burton, 1982). Filled squares are from Ishikawa, 1958. The solvus is after Burton, 1982, and is constrained to fit our experimentally determined order-disorder curve.

NATIVE METALS, CARBIDES AND CARBON IN METACOMATIC ROCKS.

NOVGORODOVA M.I., Institute of ore deposits, mineralogy and geochemistry, Academy of Science of the USSR, 109017 MOSCOW, Staromonetny 35, USSR.

In the last years widespreading of native metals and intermetallic compounds in the various geologocal objects was to be proved. The stable association native metals with carbides and carbon (graphite, dispersed rentgeno-amorphic carbon matter, rare diamond) have been ascertained in the rock that was altered by metasomatic processes (postmagmatic fluid, volcanic exhalant, mantle metasomatic fluid).

The associations of native metals in deposits were formed at the early stages of ore processes. Its are intermediate ore forms to be oxidated, dissolved and reprecipitated as oxides, sulfides and other mineral forms at the later stages of ore-forming procrsses.

The associations of native metals are indicators of restored fluids containing volatile phases of system C-O-H-N. Carbon-containing compounds and its fragments have been discovered on surface of some grains of native cupper, lead and aluminium by SIMS method.

Some aspects of crystallochemical features of native metals and intermetallic compounds are discussed. Native source of native metals and carbides are discussed too.

THE EXTENT OF COMPOSITIONAL GAP BETWEEN ACTINOLITE AND HORNBLENDE AGAINST THE EFFECT OF Fe^{2+} CONTENT

OBA,T., Inst. Earth Sci., Fac. Sci., Kagoshima Univ., Kagoshima, 890 Japan; YAGI,K., Hokusei Gakuen College, Sapporo, 004 Japan

Many investigators have discussed the existence of a miscibility gap between actinolite and hornblende (SHIDO and MIYASHIRO 1959, KLEIN 1969, TAGIRI 1977, GRAPES and GRAHAM 1978). OBA(1980) concluded on the basis of experimental study at 1 kbar that there is a compositional gap between tremolite and pargasite.

GRAHAM(1974) and TAGIRI(1977) suggested that extent of the compositional gap between coexisting amphiboles depends on the Fe^{2+}/Mg ratio. In spite of the importance of this join to define the genetic conditions of metamorphic amphiboles, so far no experimental data have been given for the solid solution series of actinolite-pargasite(hastingsite). In this study, experiment on Fe-bearing tremolite-pargasite join has been performed with special emphasis on the compositional gap between coexisting amphiboles against the effect of Fe^{2+} content.

Actinolite and hornblende are separated by a solvus and the field of actinolite+hornblende+vapor is present in the region between Ac85Pa15 and Ac55Pa45 at 680 °C, P_{H2O}=1 kbar and the oxygen fugacities defined by the iron-wustite(IW) buffer (Fig. 1). Complete miscibility is achieved at 720 °C. At higher temperatures than solvus there is a continuous solid solution series between the two end members. The stability field of amphibole solid solution gradually increases with increasing pargasite content in actinolite.

In the iron-free system the tremolite-pargasite miscibility gap is between Tr90Pa10 and Tr10Pa90 at 800 °C and persists to higher temperatures(OBA 1980). The extent of the miscibility gap decreases with increase in the Fe^{2+} content, as compared with Fe-free system.

Compositional gaps in the calcic amphibole series should be explained by the existence of a miscibility gap.

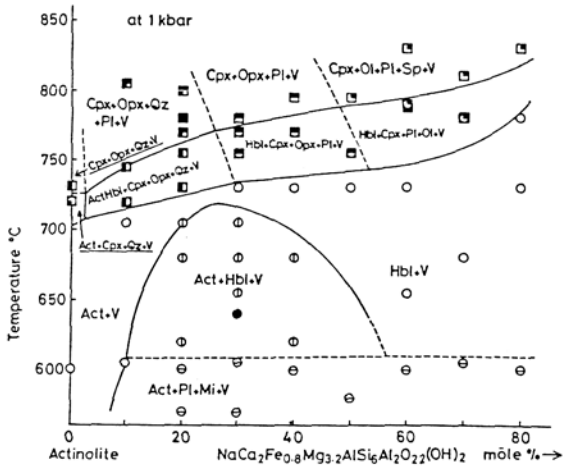

Fig.1. T-X section in the join actinolite-pargasite at 1 kbar under Fe-FeO buffer

References
GRAHAM,C.M., 1974. Contr.Miner.Petrol. 47, 165-185.
GRAPES,R.H. and GRAHAM,C.M., 1978. Lithos 11, 85-97.
KLEIN,C.J., 1969. Am.Miner. 54, 212-237.
OBA,T., 1980. Contr.Miner.Petrol. 71,247-256.
SHIDO,F. and MIYASHIRO,A., 1959. J.Fac.Sci.Univ.Tokyo Ser.2, 12, 85-102.
TAGIRI,M., 1977. Contr.Miner.Petrol. 62, 271-281.

APPLICATIONS OF HIGH RESOLUTION NMR TO ALUMINOSILICATE GLASS STRUCTURE

OESTRIKE, R., Dept. of Geol. & Geophys. Sci., Princeton Univ., Princeton, NJ 08544, USA; YANG, W. H., Dept. of Geology, Univ. of Ilinois, Urbana, IL 61801, USA; MONTEZ, B., TURNER, G. L., both at: School of Chemical Sci., Univ. of Illinois, Urbana, IL 61801, USA; NAVROTSKY, A., Dept. of Geol. & Geophys. Sci., Princeton Univ., Princeton, NJ 08544, USA.

The coordination state of Al,Si and B have been determined for a variety of geologically significant glasses prepared at one atmosphere pressure. All of the aluminum is in tetrahedral coordination for aluminosilicate framework-stoichiometry glasses and the systems Cats-Di and An-Di-(0-20%)Fo. However, based on three systems containing boron, it is tentatively concluded that the presence of boron stabilizes some octahedral aluminum in glasses prepared at one atmosphere. In all of our glass systems studied silicon is tetrahedrally coordinated to oxygen. Boron in glasses exists both in tetrahedral and trigonal coordination with oxygen. In the glass system $NaAlSi_3O_8$-$NaBSi_3O_8$ (albite-reedmergnerite) boron coordination changes from dominantly trigonal to dominantly tetrahedral as total boron increases.

For a variety of framework-stoichiometry glasses there is a simple linear relationship between ^{27}Al peak position measured at 11.7 Tesla and Si/(Al+Si) ratio, as follows,

$$\delta^{27}Al = -21.6[Si/(Al+Si)] + 70.5 \qquad (1)$$

with $r^2 = 0.96$. This linear distribution falls in the empirically defined region of aluminum in Q^4 sites of framework minerals. More surprisingly, the aluminum-27 peak positions for glasses in the systems An-Di-Fo and Cats-Di fall in the region for framework minerals (Q^4 sites). This strongly suggests that most, if not all, of the Al in these systems is in fully polymerized sites. Models for polymerization state along the join An-Di suggest that the glasses consist of Q^4 sites with Si/(Al+Si) ratios of 0.55±0.1 and Al poor sites with an average polymerization of Q^2. Similar models for the join Cats-Di suggest that those glasses are composed of Q^4 sites and sites with an average polymerization of $Q^{1.7}$ (fig. 1),

with the Q^4 sites having variable Si/(Al+Si) ratios from ~0.3 to ~0.7 for Cats 100 and Cats 10 respectively.

Empirical correlations from the literature for structural parameters of crystals with ^{29}Si chemical shift can be used to obtain useful estimates of the average $\overline{Si-O-T}$ bond angle and the average $\overline{Si-O}$ bond length for a variety of aluminosilicate glasses. Using this technique yields average $\overline{Si-O-T}$ angles varying from 151°±2.7 for SiO_2 glass to 135°±2.0 for Cats glass and average $\overline{Si-O}$ lengths vary from 1.60Å±0.008 to 1.62Å±0.004 for SiO_2 and Cats glasses respectively.

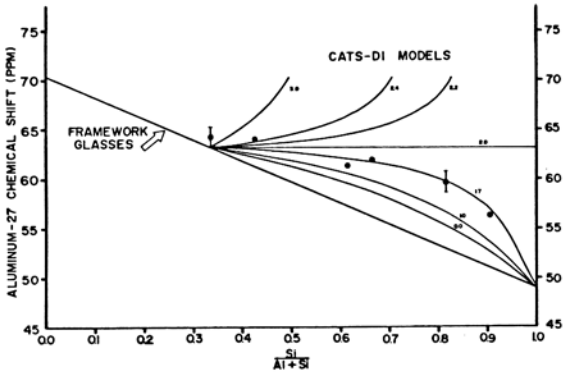

Figure 1. ^{27}Al peak positions for glasses along the join Cats-Di (dots) compared to predicted ^{27}Al peak positions for a variety of structural models (curved lines). Each model consists of Al rich Q^4 sites and Al poor Q^n sites, with the value of n adjacent to each curve (i.e. 3.0, 2.4, 2.2 etc.).

A SEMI-QUANTITATIVE METHOD FOR DISTINQUISHING ASBESTIFORM AND NON-ASBESTIFORM, ACICULAR CRYSTALS: DATA FOR TREMOLITE.

David S. O'Hanley and Tibor Zoltai. Department of Geology and Geophysics University of Minnesota. Minneapolis, Minnesota 55455

A simple, rapid microscopic test was designed to obtain semi-quantitative measurements of the bending strength of acicular or fibrous crystals. A small-diameter rod is pushed against the horizontally mounted crystals and the distance between the contact and fracture points is measured for the calculation of the bending strength. The gauge length is 0.202mm.

The instrument was tested on samples of asbestiform tremolite from Baltimore, Maryland, and non-asbestiform tremolite from the Warren Head mine in New Hampshire. The samples ranged in size from 0.3 to 0.8 mm in length and 0.9 to 15 μm in diameter. The asbestiform tremolite was stronger than the non-asbestiform tremolite at every diameter, with an order of magnitude higher strength at small diameters. This indicates that asbestiform tremolite behaves as a whisker, whereas non-asbestiform tremolite does not.

DEHYDRATION OF BRUCITE TO PERICLASE

OHMASA M. and SATO A., Inst. of Materials Science, University of Tsukuba, Sakura-mura, Niihari-gun, Ibaraki 305, Japan

Although a large number of investigations on the dehydration of brucite to periclase have been reported, many problems remain unsolved. The mechanism of the dehydration is also one of such problems. Some models have been proposed for the mechanism of the dehydration of the precursor and the formation of the product, but non of them was accepted as the valid one. The present studies have therefore been carried out to elucidate the mechanism of the dehydration.

The analyses of the dehydration process are difficult usually, because the processes are affected by various factors: pressure, temperature, heating rate etc. The present studies were made under the following conditions.

(1) The brucite crystals used were synthesized from very pure chemicals by a hydrothermal method, because it was necessary to avoid effects of impurities of metals.
(2) All samples were dehydrated at 400°C in the air.
(3) A quenching method was employed, since diffracted beam was too weak to make in situ observation.

The synthesized crystals were platy and the maximum diameter is 1.5mm and the thickness 30 m. They showed very sharp spots in the X-ray diffraction patterns. No impurity was detected by EPMA analyses. The crystals were heated at 400°C and heating period was varied from 3 minutes to 12 hours. The change of the sample was examined by X-ray diffraction and by microscopic observation. The sample heated for 12 hours and converted completely to periclase was cut perpendicular to (001) of brucite, and the cross section was observed by SEM. The results are as follows.

(1) The rate of shrinkage of the precursor is about 3% in the direction parallel to (001) and also in that normal to (001), though the expected volume change is more than 50%.
(2) New orientatio relationship between the precursor and the product was found, that is, $(001)_b$ $(111)_p$.
(3) The mechanism of the dehydration in the surface of the precursor is probably different from that in the inside.

EXAFS ANALYSIS UNDER HIGH PRESSURE USING DIAMOND ANVIL CELL

OHSUMI, K.[1], SUENO, S.[2], NAKAI, I.[3], IMAFUKU, M.[3], MORIKAWA, H.[4], KIMATA, M.[2], NOMURA, M.[1] and SHMOMURA, O.[5]
1) Photon Factory, National Laboratory for High Energy Physics, Ibaraki 305, Japan. 2) Institute of Geoscience, University of Tsukuba, Ibaraki 305, Japan. 4) Research Laboratory of Engineering Materials, Tokyo Institute of Technology, Yokohama 227, Japan. 5) National Institute for Research in Inorganic Materials, Ibaraki 305, Japan.

In spite of serious need to get crystal chemical information of the bond distances or coordination numbers of the specific atom in a material under high pressure, the usual X-ray diffraction method has still had some problems to perform the purpose.

EXAFS technique has been made widely available to investigate the local structure of the materials whether they are crystalline or not, owing to the utilization of synchrotron radiation and development of the analytical treatment of the EXAFS spectra.

The present study was carried out to find the way for the purpose, the diamond anvil technique was applied to EXAFS measurement at EXAFS station of Photon Factory, KEK. The preliminary result was obtained by the examination on the materials including several elements such as Fe, Co, Ni, Cu and Ge atom.

Synchrotron radiation was monochromated by Si(311) channel-cut crystal to provide an X-ray beam with the desired wave length. And then the beam was made fine less than 300 μm in diameter by the aperture and then driven through the hole of the gasket between diamonds. This was achieved by the newly developed goniometer stage with the remote controlled motor to drive X-Y-Z axes. It should be emphasized that an X-ray beam does not hit the gasket. The examination on several elements revealed that Co and Ni atoms were suitable for the present study on the standpoint of absorption and diffraction by the diamond anvils. The longer wave length than K-edge of Co was seriously affected by the absorption through the 1/8 carets diamond anvil and the shorter than Ni by Bragg diffraction. In case of the wave length corresponding K-edge of Co and Ni atom, the diffraction by the diamond anvils can be easily avoided by slightly moving the arc of the goniometer stage.

Ni-dmg molecules (Fig. 1) extended in a plane are connected with each other by one dimensional Ni-Ni bonding to form a crystal. It is also known that the compound is changed easily in its Ni-Ni bond distance in accordance with pressure. The absorption spectra were measured at 1 atm., 34 Kb and 56 Kb. The Fourier transform of the spectra at various pressures are shown in Fig. 1. The peak at around 1.54 Å corresponding intramolecular Ni-4N bonds shows slightly shorter by the effect of high pressure, while Ni-Ni intermolecular distance expected to be clearly shorter could not be apparent.

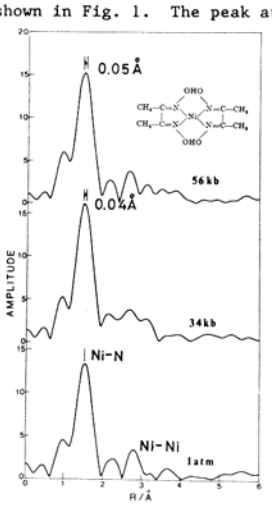

Fig. 1 Fourier transform of $k^3\chi(k)$ EXAFS for Ni-dmg at various pressures.

The present study revealed that EXAFS measurement under high pressure using the diamond anvil cell can be performed on the materials including Co and Ni atom. In the further study, the diamond with minimum allowable thickness combined with strong synchrotron radiation such as obtained from wiggler line or accumulation ring of KEK may make possible to measure the absorption spectra of the materials having Fe, Mn, Cr, V or Ti atom.

NORMAL AND INVERSE ZONING IN TOURMALINES FROM PEGMATITES OF NORTH VICTORIA LAND, ANTARCTICA

OLESCH, M., Inst. f. Mineralogie, Univ. Würzburg, Am Hubland, 8700 Würzburg, Fed.Rep.Germany

The medium-grade to high-grade metamorphic rocks of the Wilson Group in North Victoria Land, Antarctica, are intruded by Cambro - Ordovician granitoids, the Granite Harbour Intrusives (490 - 470 Ma K-Ar age). The post-tectonic plutonism is connected with a subsequent emplacement of numerous pegmatites in the granitoid batholiths as well as in the surrounding schists and gneisses. The medium-grained pegmatites show a monotonous modal composition of quartz, albite, K feldspar, and muscovite or biotite as accessories. Part of the biotite-free pegmatites contain tourmalines that can be enriched in nests or schlieren. The tourmaline crystals reach about 1 cm in diameter and some cm in length. The tourmalines are macroscopically homogeneous black, the colour in thin section is light brown to olive. The colour variation in individual crystals is related to a chemical zoning that was investigated in detail. The core - rim compositions of tourmalines from pegmatites intruded in granitoids and biotite-sillimanite schists are plotted in the diagram of HENRY & GUIDOTTI (1985) in Fig. 1a and b, respectively. The core - rim relations of tourmaline solid solution from pegmatites in a granitic environment exhibit a trend of continuous chemical zoning from schorl-rich, uvite-poor core compositions to rim compositions richer in dravite and uvite components. A minor tsilaite component remains nearly constant. Mean values of core and rim compositions are: schorl (Sh) 0.473(esd 7), dravite (Dr) 0.372(24), tsilaite (Ts) 0.005(2), uvite (Uv) 0.150(29), and Sh 0.357(17), Dr 0.389(24), Ts 0.004(1), Uv 0.251(38), respectively. This trend is typical not only for pegmatites but also for zoned tourmalines from aplitic and granitic intrusives. It is defined as n o r m a l zoning and caused probably by decreasing crystallisation temperature and by differentiation of the fluid phase composition. The core - rim relations of tourmaline solid solution from pegmatites intruded in schists show an opposite trend. The cores are richer in dravite and uvite components than the rims. Mean values of core and rim compositions are: Sh 0.431(24), Dr 0.356(28), Ts 0.006(1), Uv 0.207(16), and Sh 0.455(57), Dr 0.323(77), Ts 0.022(21), Uv 0.182(24), respectively. The zoning is less regular with a tendency to discontinuous gradients. This i n v e r s e zoning characterizes tourmalines influenced metasomatically (cf. SHEARER et al. 1984) by a fluid altered in composition by reaction with the surrounding schists. The zoning pattern of tourmaline solid solution may serve as an indicator for metasomatic alteration of pegmatites.

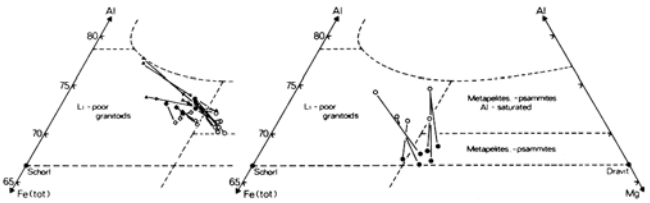

Fig. 1. Al - Fe(tot) - Mg diagram for tourmaline core (filled symbols) and rim (open symbols) compositions. a) Tourmalines from pegmatites intruded in granitoids: normal zoning, b) in schists: inverse zoning.

References

HENRY, D. J., GUIDOTTI, C. V. (1985) Amer. Mineral. 64, 788 - 798.
SHEARER, C. K., PAPIKE, J. J., SIMON, S. B. (1984) Geochim. Cosmochim. Acta 48, 2563 - 2579.

AN EXPERIMENTAL APPROACH TO THE CONDITIONS REQUIRED FOR BIOTITE-CHLORITE INTERLAYERING

ONRUBIA, Y., AMOURIC, M. and BARONNET, A., CRMC2, Campus Luminy, case 913, 13288 Marseille cedex 09, France.

A number of TEM investigations of the topology of the terminations and related possible "solid-state" mechanisms involved for interlayering during the chloritization of the biotite have been reported recently [1-4] from altered granite and metamorphic rocks. Two different, and sometimes complementary, mechanisms were proposed for the production of unit chlorite layers inside a biotite matrix : 1/ insertion of an extra brucite-like layer into the biotite interlayer after removal of potassium, a volume increasing mechanism [1,3] ; 2/ loss of K from the mica interlayer followed by stripping of tetrahedral sheets from half the biotite talc-like layers, a volume reducing mechanism [2,4]. Chemical exchanges during the transformation were established by AEM [2-4].

Since in these works, chloritization of biotite was a part of complex reactions involving minerals other than phyllosilicates, we decided to chloritize experimentally synthetic phlogopite and biotite under various T, P_{H_2O} and solution compositions. In such simpler systems, we attempted to delineate the chemical and charge-balance constraints, if any ,attached to solution-mediated recrystallization of biotite into chlorite and more specifically to the "solid-state" intermediate interlayering of the two phases during the transformation.

All runs were performed under P_{H_2O} = 1 kb, 300 ≤ T ≤ 600°C, for two days in one molar hydrothermal solutions.

The treatment of pure synthetic phlogopite into chloride solutions with varying Mg/K led to an increasing chloritization with T and Mg/K ratio with subordinate production of talc. HRTEM showed clearly that phlogopite, 14 Å chlorite and talc occured as separate, very rarely interlayered, crystals [5]. Lateral dissolution of phlogopite, and growth of chlorite and talc did indicate a fully solution-mediated process of recrystallization. IR spectra of the chlorite combined with its easy reversal to phlogopite in the solid state via a disordered mixed-layered phase did indicate that Al was more likely replacing Mg in the brucite-like sheet than in octahedra of talc-like sheet. In chloride solution where Al was introduced so that Al/Mg = 1/2, easy disordered interstratification, with occasional 1/1 chlorite-phlogopite ordering, was observed. Phlogopite crystals were splitting into slabs during interlayering, which took place mostly in the "solid-state".

Using the same Al-free solutions as above and buffered close to NNO but on an $Ann._{50}$ $Phl._{50}$ biotite, significant solid-state interstratification was obtained, contrasting with the former results on pure phlogopite.

In the rare cases where chlorite-phlogopite (biotite) terminations could be seen, they were consistent with mechanism 1/, which seems likely when hydrostatic pressure and no volume constraint apply on the system. As a whole, these results suggest that solid-state interlayering of chlorite into a biotite matrix may occur when the electric charge of the brucite-like sheet to be inserted is increased by the Al-Mg substitution if Al is available in solution, and/or by a decrease of the charge of the talc-like sheet by an in situ Fe^{2+}-Fe^{3+} oxydation. Whatever the case, attainment of charge balance between the two sub-units of resulting chlorite must take place without solid-state diffusion affecting the initial mica talc-like sheet

[1] OLIVES-BANOS, J., AMOURIC, M., DE FOUQUET, C. and BARONNET, A. Amer. Mineral. (1983) 68, 754-758
[2] VEBLEN, D.R. and FERRY, J.M.. Amer. Mineral. (1983), 68, 1160-1168
[3] YAU, Y.C., ANOVITZ, L.M., ESSENE, E.J. and PEACOR, D.R.. Contrib. Mineral. Petrol. (1984) 88, 299-306
[4] EGGLETON, R.A. and BANFIELD, J.F.. Amer. Mineral. (1985) 70, 902-910
[5] ONRUBIA, Y., AMOURIC, M., BARONNET, A. and BAUMER, A. (1986). Int. Symp. Exp. Mineral. Geochem. (Nancy), abstract.

MINERALOGICAL FACTORS THAT INFLUENCE THE STRENGTH OF MOULDS MADE FROM CHROMITE FOUNDRY SAND

OOSTHUYZEN, E.J. Council for Mineral Technology, Private Bag X3015, Randburg 2125, REPUBLIC OF SOUTH AFRICA

High-grade chromite sand mixed with a small amount of binder is an excellent medium in which foundries can make metal castings. Large quantities of chromite sand are therefore used by foundries all over the world to produce moulds for special purposes and refractory linings. The specifications for foundry sand usually relate to chemical purity, slurry content, and particle size, while the results of standardized flexion-resistance tests (conducted in the laboratory on moulded test pieces) provide a measure of the ability of a particular sand to produce moulds of the required strength. These flexion-strength values are therefore important criteria in the final evaluation of chromite foundry sands.

However, it has been found that, although different chromite sands may conform to specifications and appear to be very similar, their flexion-strength values can differ widely. In an attempt to resolve this problem, a detailed mineralogical investigation of five specially selected samples of chromite sand was undertaken at the request of a large South African supplier and exporter of chromite foundry sand.

Flexion-strength tests carried out in an industrial laboratory formed a basis for the comparison and ranking of the sands in terms of mould strength. The factors that could possibly affect mould strength were examined by a combination of mineralogical techniques, as follows: (a) the purity of the chromite concentrate (chemical analysis, X-ray diffraction, and microscopy), (b) the nature of the particle surfaces, i.e. roughness, coatings, etc. (optical and scanning electron microscopy, surface-area measurement, and X-ray analysis of fines after scrubbing, (c) binding mechanisms and the relationship between the resin (binder) and the chromite particles (optical and scanning electron microscopy), (d) packing density and interrelationship between chromite particles within moulds (test pieces) (automatic image analysis for which special software incorporating interesting image transformations according to the concepts of mathematical morphology was developed for the automatic measurement of porosity, mean intercept length, $\bar{L}$, mean free path, $\bar{\lambda}$, the number of possible adhesion points between chromite particles per unit area of mould and also per unit area of chromite, the percentage of total chromite that forms a continuous framework in the mould, and $\bar{L}$ and $\bar{\lambda}$ of the 'framework' chromite), (e) size and size distribution (screening and automatic image analysis), and (f) the shape of the chromite particles (automatic image analysis, four dimensionless 'shape parameters' being measured on specially prepared polished sections).

The following conclusions were drawn.

(1) Resin (binder) in the test pieces is to be found only at contact points between chromite particles. (2) Small amounts of impurities (e.g. talc and chlorite) are not detrimental to mould strength. (3) According to Spearman's correlation test, significant correlations are indicated between mould strength on the one hand, and the porosity of the mould, the mean intercept length (a shape-related size parameter), the proportion of the chromite that forms a continuous framework, the mean free path of this 'framework chromite', and the shape of the particles, on the other. The particles in high-strength sands have shape factors approaching that of the natural grain shape of chromite. A tail in the size distribution towards the finer sizes correlates negatively with strength. (4) For maximum strength, the sand should contain a high proportion of idiomorphic chromite particles of uniform shape and size, which should then produce a mould with a low porosity (< 50%) and with the particles arranged in such a way that they form a continuous framework having small openings.

The work was sponsored by Rand Mines Ltd (Chrome Division) and their permission to present this paper is acknowledged, as is the permission of the Council for Mineral Technology (Mintek).

THE ORIGIN OF SODIUM-CALCIUM SULFATE DEPOSITS OF MADRID BASIN (SPAIN).

ORDOÑEZ,S., Dep. de Petrología, Facultad de Geología, U.C.M., Ciudad Universitaria, 28040 Madrid, Spain; GARCIA DEL CURA, M.A. Instituto de Geología Económica. C.S.I.C., Facultad de Geología, Ciudad Universitaria, 28040 Madrid, Spain.

Saline Unity of the Madrid Basin in located in the lower part of refill basin outcroping; the thickness of saline deposits are more than a thousand of meters.

Couplets of anhydrite-magnesite or silty magnesite are the mainly mineralogical features of saline unity. The maximun thickness of a couplet never exceeded 10 mm with an average of 4,3 $\pm$ 0,3 mm, and 3,2 $\pm$ 0,3 mm for magnesite and anhydrite, respectively. Micritic magnesite (<2 μ) is always present, but anhydrite crystals appear with different habits like idioblastic, fascicular, bundle and bow-tie.

Glauberite, is also a common mineral, with idiomorphic and subidiomorphic lenticular crystals. These crystals are clean of inclusions and their long axis lie commonly parallel to bedding. Indeed glauberite forms irregular couplets with magnesite or anhydrite.

The "Roca Negra", a mining local name, is a glauberite bearing rock. This contains alotriomorphic glauberite crystals, with many solid inclusions of magnesite, quartz and also micas. This glauberite crystals appear with diffuse and wavy rims.

Thenardite is scarcely present mineral, and it is related to the cementation process. However, glauberite crystals are "floating" on the thenarditic cement. Both, mosaic-like thenardite, and palisade-like thenardite are rarely found. Thenardite layers are located in the upper part of Saline Unity, locally some layers may exceed 8 meters of thickness. The down part of thenardite layers is commonly occupied by "Piedra Negra" layer underlying it. The later is at once underlayed by an homogeneous red halitic silt layer.

There are also many layers with couplet of halite-anhydrite, halite polyhalite and also halite-glauberite. Halite crystals commonly belong to the chevron type.

Polyhalite crystals either masive or in polyhalite-magnesite and polyhalite (magnesite)- halite couplets is usually found within the Saline Unity preferently at its lower part. These crystals of polyhalite show both felty and spherulitic aggregates of microlites. An intercrystalline relation among the polyhalite and halite crystals is often seen. When polyhalite is associated to anhydrite the former shows a clear felty texture.

Weathering of this Saline Unity lead to genesis of gypsum and calcite secondary minerals. Gypsum shows some pseudoforms like that of glauberite crystals and chevron halite pseudoforms are scarcely present. Weathering is often intense at the surface and decrease downward, but commonly a layer of hydrated sodium sulfate (mirabilite) is located in the weathered - unweathered surface.

Sedimentogenetic interpretation is supported by the following $\delta^{34}S$ $\delta^{13}C$ and $\delta^{18}O$ isotopic data ($\bar{x} \pm \sigma$).

YUST - Secondary Gypsum, TT - Thenardite, PT - Polyhalite, AT - Anhydrite, GT - Glauberite.
MT - Magnesite.

$\delta^{34}S$ isotopic data from triassic evaporites (BIRBAUM et al 1979) and paleogene evaporites (ORDOÑEZ et al 1983) allow us support a mixing model to sulfate genesis.

Evaporites from Saline Unity may be interpreted as deep saline lake sediments. The brine is genetically related with weathering of paleogene and triassic evaporites. Contribution of sulfide deposits or atmospheric precipitation, as sources of lighter sulfur, may be neglected.

BIRNBAUM,S.J. and COLEMAN,M. Chemical Geology 25 (1979) 163-168.
ORDOÑEZ,S., FONTES,J.Ch. and GARCIA DEL CURA, M.A. Comunicaciones X Congreso de Sedimentología. Menorca 1983. 49-52

DETERMINATION OF ATOMIC CHARGE OF MG AND SITE IONICITIES IN FORSTERITE AND ENSTATITE BY USING THE MOLECULAR ORBITAL METHOD

Osamu Tamada* and Kazuyoshi Tanaka**

*College of Liberal Arts, Kyoto University, Kyoto 606, Japan
**Department of Hydrocarbon Chemistry, Faculty of Engineering, Kyoto University, Kyoto 606, Japan

Recently the net atomic charges of olivines and orthopyroxenes were determined by the precise X-ray analyses (Fujino et al., 1981, Sasaki et al., 1982 and Tamada et al., 1983). The results showed a characteristic feature of net charges in octahedral cations. The M(2) cation tended to have larger value than the M(1) cation in each olivine endmember and orthopyroxenes showed the reverse relation in octahedral cations. Tamada (1984) proposed from electrostatic energies of the minerals that these charge relations resulted from stabilizing energy of the minerals, and that the site ionicity of the minerals and the net atomic charges gave the qualitative explanation for the unusual intracrystalline cation distributions in olivines.

To confirm the site ionicities of the minerals the calculations by molecular orbital method were performed for forsterite and enstatite. The Pople type CNDO/2 approximation was used for the study. The convergence was achieved for fairly large clusters of atoms, $(Mg(1)_3Mg(2)_2Si_2O_{22}H_{26})$ cluster for Mg(1) and Mg(2) of forsterite, and $(Mg(1)_3Mg(2)_3O_{22}H_{32})$ for Mg(1) and $(Mg(1)_3Mg(2)SiO_{18}H_{24})$ for Mg(2) of enstatite. These clusters included all the polyhedra which shared edges with the central $Mg(1)O_6$ or $Mg(2)O_6$ octahedron. The atomic positions were taken from the data of Fujino et al.(1981) for forsterite and from Sasaki et al.(1982) for enstatite. H atoms were attached to the outer oxygens of cluster at the distance of 0.96A for keeping the local charge neutrality around the cluster.

The charges of Mg(1) and Mg(2) atoms were obtained to be 0.68 and 0.80e for forsterite, and 0.73 and 0.69e for enstatite. The charge of Mg(2) is larger than Mg(1) in forsterite, while Mg(1) charge is larger in enstatite

The approximation is rather rough, it may concluded that the site ionicity of M(2) is higher than M(1) in olivine and the reverse relation is found in orthopyroxene. The result is consistent with the result from X-ray analyses and electrostatic calculations.

References

Fujino et al.(1981) Acta Cryst., B37, 513-518.
Sasaki et al.(1982) Z. Krist., 158, 279-297.
Tamada et al.(1983) Acta Cryst., B39, 692-697.
Tamada(1984) Miner. J., 12, 137-141.

CHARACTERISTICS AND ORIGIN OF THE MUZO EMERALD DEPOSIT, COLOMBIA

OTTAWAY, T.L. and WICKS, F.J., Dept. of Mineralogy and Geology, Royal Ontario Museum, 100 Queen's Park, Toronto, Ontario, M5S 2C6; BRYNDZIA, L.T., and SPOONER, E.T.C., Dept. of Geology, University of Toronto, Ontario, M5S 1A1

Emeralds occur in a stockwork of albite + calcite-dolomite ± barite veins cross-cutting Cretaceous shales and limestones. Fluorite and parisite occur in association with emerald mineralization and pyrite and quartz are locally abundant. There is no direct evidence of igneous activity either at Muzo or at other localities in the emerald belt of the Cordillera Oriental, and thermal metamorphism has not been seen in the region of the vein systems. Fluid inclusions in Muzo emeralds contain ~40 wt % NaCl, ±KCl, and homogenize by NaCl dissolution at 324 ±10°C (1σ; n=154). Emeralds and intergrowths of albite/emerald or shale/emerald both known as trapiche are found in the vicinity of bleached zones locally called the Cenicero. The Cenicero is an irregular, extensively brecciated formation containing native sulphur. It is interpreted to be the remains of an evaporite which conducted hydrothermal fluids into the Muzo deposit through the development of solution porosity, and may have been the source, or partial source, of the hypersaline fluids found in the fluid inclusions in emeralds, quartz and parisite. It is suggested that evaporite dissolution either regionally and/or locally mobilized other elements such as Be^{2+}, Mg^{2+}, Ca^{2+}, Ba^{2+}, F^- and LREE. Evaporitic sulphates were reduced to sulphur. Hydrothermal fluids exceeding 300°C were not restricted to fractures but permeated the deposit, carbonizing palynomorphs and "cracking" the organic matter, to produce a well-ordered *pyrobitumen, impsonite. The resultant* N_2 and CH_4 are detected in the fluid inclusions in the emerald, and N_2 is detected in the fluid inclusions in the parisite. Pyrobitumen reflectance measurements indicate diagenetic/metamorphic temperature levels in the range of metagenesis to middle greenschist facies. Beryl precipitation is related to fluctuations in both pH, as indicated by replacement of plagioclase in the wall rock by a Na-rich muscovite ($2M_1$), and in the activity ratio of Be^{2+}/Na^+ as indicated by beryl overgrowths on albite and albite overgrowths on beryl in the vein centre. The organic-rich shales are likely the source of Cr which imparts the characteristic green colour to the emeralds. Experimentally determined beryl solubilities show that low concentrations of beryllium will precipitate the emeralds seen at Muzo. Large volumes of Be-dilute hydrothermal fluids would favour fewer nucleation sites and, given sufficient time for diffusion, would result in large, clean crystals. Evidence of crystallization occurring during deformation of the host rock includes fractures transecting internal but not external growth zones in emeralds, brecciated veins, fibrous calcite and pyrite and a range in density of CO_2 in emerald fluid inclusions. The latter suggests a significant pressure interval over which crystallization occurred. This was produced by cycles of increased pressure up to lithostatic values followed by partial release through fracture propagation. Tectonism can be related to the Cordilleran orogeny of the Miocene.

TEM DETERMINATION OF SITE OCCUPANCIES IN PYROPE GARNET

OTTEN, Max T. and BUSECK, Peter R., Departments of Geology and Chemistry, Arizona State University, Tempe, AZ 85287

ALCHEMI (Atom Location by CHannelling-Enhanced MIcroanalysis), a transmission-electron microscope technique, has been used to determine site occupancies in pyrope garnet, which has a composition (as determined by thin-film TEM analysis) of $(Mg_{2.32}Fe_{0.55}Mn_{0.02}Ca_{0.33})(Al_{1.74}Ti_{0.04}Cr_{0.07})Si_{2.99}O_{12}$.

The ALCHEMI technique employs the channelling of electrons that occurs along specific crystallographic planes for certain directions of the incident beam. The channelling produces a maximum in electron intensity on these planes, causing increased emission of X rays from the atoms on the planes. With the incident beam inside the Bragg angle for the 444 diffraction, the emission from atoms on the X (dodecahedral: Mg,Fe,Mn,Ca) and Z (tetrahedral: Si) sites is enhanced, while the emission of atoms from the Y (octahedral: Al,Cr,Ti) site is enhanced with the beam outside the Bragg angle (Fig. 1).

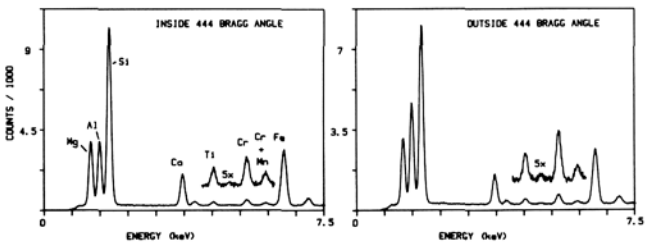

Fig. 1. EDS X-ray spectra for pyrope with the incident beam oriented inside and outside the 444 Bragg diffraction. Note the differences in height of the Al, Cr and Ti peaks.

Although garnet has three cation sites, the X and Z sites are taken together because they lie on the same (444) plane. Si is used as the reference element for the combined X and Z sites. Since Si almost fills the Z site, Al must be confined nearly completely to the Y site and can be used as reference element there. The fraction of unknown element E on the X + Z sites is: $C = [1-(E/Al)_1/(E/Al)_2] / [(E/Si)_1/(E/Si)_2-(E/Al)_1/(E/Al)_2]$, where the subscripts 1 and 2 refer to the two different channelling directions and E, Al and Si are X-ray counts.

Ten channelling experiments were performed on the pyrope. Representative results are shown in Table 1. The magnitude of the channelling effect can be seen from the Al-Si ratios. The most interesting results were obtained for Mg and Fe. From the thin-film analysis it is apparent that there is an excess of cations on the X site, while the Y site has a deficiency. Conventionally one would presume that this deficiency is filled by ferric iron. From the element ratios and the calculated occupancies in Table 1, it is apparent that actually a large part of the deficiency of the Y site is filled by Mg (on average nine percent on Y) and to a lesser degree by Fe (on average three percent). The experiments show further that Ca occurs only on the X site, while Ti and Cr are confined to the Y site. The results for Mn are meaningless because of the high analytical error, which results from its low abundance and the overlap of its Kα peak by the Cr Kβ.

Acknowledgements. This study was supported by NSF grant EAR-8408168; microscopy was performed at the ASU HREM facility which is supported by NSF and ASU. Pyrope samples were kindly provided by Dr. J.R. Smyth (Univ. Colorado, Boulder).

Table 1. Elemental ratios for channelling inside (I) and outside (O) the Bragg angle and the fraction (C) of Mg and Fe on the X site.

$\frac{(Al/Si)_I}{(Al/Si)_O}$	$\frac{(Mg/Al)_I}{(Mg/Al)_O}$	$\frac{(Mg/Si)_I}{(Mg/Si)_O}$	C_{Mg}	$\frac{(Fe/Al)_I}{(Fe/Al)_O}$	$\frac{(Fe/Si)_I}{(Fe/Si)_O}$	C_{Fe}
0.67	1.42	0.96	0.91	1.50	1.01	1.02
0.64	1.49	0.95	0.90	1.56	0.99	0.98
0.67	1.43	0.96	0.92	1.48	0.99	0.99
0.69	1.41	0.97	0.93	1.46	1.00	1.00
0.66	1.44	0.95	0.90	1.46	0.97	0.94

A HYDROUS MANGANESE PHYLLOSILICATE WITH 12 Å BASAL SPACING

OZAWA,T.*, TAKAHATA,T.**, BUSECK,P.R***, *, *** Departments of Geology and Chemistry, Arizona State University, Tempe, AZ85287, USA; ** Mineralogical Institute, Faculty of Science, University of Tokyo, 7-3-1 Hongo, Bunkyo, Tokyo-113, Japan.

A hydrous manganese phyllosilicate was described from Alps Val d'Err, Graubünden, Switzerland and named parsettensite (Jacob,1923). It has generally been accepted as the stoichiometrical equivalent of stilpnomelane (Dunn et al.,1984), although its X-ray powder diagram (JCPDS 25-8) does not correspond closely with that of stilpnomelane. We have used electron diffraction and high-resolution imaging to examine a fine-grained specimen labeled parsettensite from the type locality. It has different structural characteristics from known phyllosilicates including stilpnomelane. Only the hydrous manganese phyllosilicate that we reported from the Kumahata Mine, Shiga Prefecture, Japan (Takahata et al.,1984) has the same characteristics as those of the present specimen. The probable symmetry of specimens from both localities is monoclinic, and the unit cell dimensions are reported for the Kumahata specimen as $a=\sqrt{3}b=39.1$, $b=22.6$, $d_{001}=12.6$Å. A pseudo-trigonal cell with $\vec{a}_1=(\vec{a}_m-\vec{b}_m)/2$ and $\vec{a}_2=\vec{b}_m$ ($a_1=a_2=22.6$Å) and a subcell with $a_1/7$ and $a_2/7$ are recognized for both specimens from hk0 electron-diffraction patterns, indicating that 7x7 manganese octahedra are arranged in a trigonal cell. When we interpret the results of electron-microprobe analysis for the Kumahata specimen (Table 1) based on these 7x7 octahedra, the ratio of silicon to manganese atoms is 72:49. This value resembles 72:48 of stilpnomelane (Eggleton and Bailey,1965; Eggleton,1972), which has similar cell dimensions. However, the orientation relation of their unit cells with the octahedral sheet is different, as shown in Fig.1, and thus their tetrahedral sheets must differ. Superstructure reflections appear in the patterns of both stilpnomelane and the present phase, but they are markedly different. Since the superstructure reflections are mainly produced by contributions from the tetrahedral sheets, this difference is to be expected.

It is probable that our specimens from both localities are parsettensite. Our phase is not stoichiometrically equivalent to stilpnomelane, but it does have many characteristics in common with parsettensite. Therefore, if our phase is indeed parsettensite, which we believe, then parsettensite is not stoichiometrically equivalent to stilpnomelane.

Electron-microscopy studies show frequent stacking disorder, producing the diffuse streaks along the c* axis. This disorder closely resembles that in the pyrosmalite group (Ozawa et al.,1983; Takeuchi et al.,1983). In addition to this stacking disorder, however, some defects that vary the basal spacing and that result from disorder in the tetrahedral sheet, have also been observed.

The authors (TO and TT) are grateful to Dr.M.Shimizu of the University Museum, University of Tokyo for assistance in electron-microprobe analysis. Partial financial support was provided (to PRB) by grant EAR-8408168 from the US National Science Foundation.

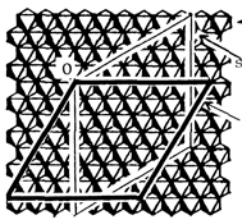

← Figure 1.

	Wt.%	atomic ratio	
SiO_2	45.80	63.89	71.3
Al_2O_3	4.43	7.28	
TiO_2	0.02	0.02	49.0
FeO	0.68	0.79	
MnO	36.20	42.83	
MgO	2.58	5.36	
CaO	0.22	0.33	
K_2O	0.77	1.37	
H_2O	(9.30)		
total	(100.00)		

Table 1. →

REFERENCES

[1] Dunn,P.J.,Peacor,D.R.& Simmons,W.B.(1984) Can.Mineral. 22, 259-263. [2] Eggleton,R.A.(1972) Mineral.Mag. 38,693-711. [3] Eggleton,R.A.& Bailey,S.W.(1965) Clays and Clay Minerals 13,49-63. [4] Jacob,J.(1923) Schweiz.Min.Petr.Mitt. 3,227-237. [5] Ozawa,T.,Takeuchi,Y.,Takahata,T., Donnay,G.& Donnay,J.D.H. (1983) Can.Mineral. 21,7-17. [6] Takahata,T., Ozawa,T.& Takeuchi,Y.(1984) Coll.Abst.Annual Meet.Min.Soc.Japan p.68. [7] Takeuchi,Y.,Ozawa,T.& Takahata,T.(1983) Can.Mineral. 21,19-27.

* On leave from the Mineralogical Institute, Faculty of Science, University of Tokyo, 7-3-1 Hongo, Bunkyo, Tokyo-113, Japan.
**Present address: Toyo Soda Mfg.Co.Ltd., Tokyo Research Center, 2743-1 Hayakawa, Ayase-shi, Kanagawa-252, Japan.

THE MINERALOGY AND PARAGENESIS OF HUMAN RENAL CALCULII

Liberto de Pablo-Galán
Instituto de Geología
Universidad Nacional Autónoma de México
04510 México, D. F. - México

A population of 1214 renal calculii, 825 from male patients and 389 from female ones, from Mexico City (81.28%) and from the rest of the country (18.72%) was studied mineralogically, determining their composition and content of minerals, texture, trace elements, and size, and correlated to the anthropological type, nutritional habits, metabolic disorders, infections, clinical data, location of the urolithes, and other pertinent data from the patients. The distribution of the calculii is, for males and females, (1) weddellite 13.46% and 4.11, (2) whewellite 12.61%, 9.77, (3) weddellite-whewellite 20.11%, 17.74, (4)weddellite - whewellite -apatite 25.21%, 22.35, (5) whewellite-weddellite-apatite-struvite-uric acid 5.10%, 2.31, (6) apatite 2.18%, 10.28, (7) apatite-weddellite-whewellite 1.57%, 7.71, (8) apatite-weddellite-whewellite-struvite 4.25%, 10.28, (9) apatite-weddellite-whewellite-struvite-uricite 1.21%, 4.37, (10) struvite 0.85%, 3.34, (11) struvite-apatite 1.58%, 0.51, (12) struvite-apatite-weddellite-whewellite 0.36%, 1.80, (13) uricite 7.40%, 2.83, and (14) uric acid-weddellite-whewellite-apatite-sodium acid urate-ammonium acid urate 4.48%, 2.57. The trace elements contents of pure weddellite stones is 297 ppm Fe and 214 ppm Zn, whewellites 766 and 255, apatites 1297 and 703, struvites 248 and 264, and uricites 1218 and 320. The composition of the urolithes is represented in the system weddellite-whewellite-apatite-struvite where the stripped area in the base weddellite-whewellite-apatite represents the most common compositions and from which a volume rises towards the struvite apex. The absence of stones in the weddellite-apatite and the whewellite-apatite systems points exsolution between oxalate and phosphate; struvite does not associate with weddellite or with whewellite.

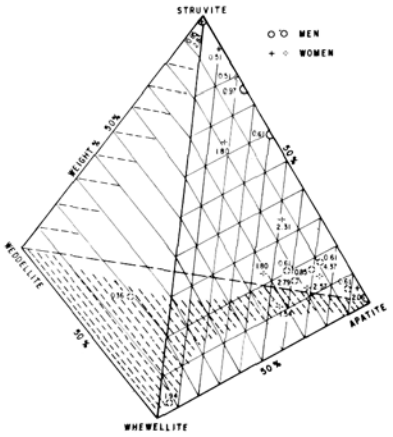

Weddellite-whewellite calculii crystallize from mildly alkaline solutions high in oxalate, possibly resulting from poor metabolism of lipids and carbohydrates; they are common to mesomorphic and obese individuals with minor disorders of excessive calcium, uric acid, diabetes, and gout. Apatite precipitates from stronger alkaline solutions, in men under diets rich in proteins and in mineral matter, and with high incidence of hyperparathyroidism, dissolution of bone apatite, and disruption of the phosphorus and calcium regimenes. Weddellite-whewellite-apatite stones, with variable concentrations of either oxalates or phosphate and textural differences would correspond to conditions intermediate or successive between the two cases. Struvite stones are linked to chronic infections, poor nutritional habits, strong alteration of the phosphorus metabolism and the osmotic level, with development of renal acidosis and production of ammonium by the kidneys or from bacterial activity. They are monomineral stones or the struvite is associated with apatite, never with oxalates or with uricite; two textures are common, one is hard, dry odorless urolithes, others are soft, wet, bad odor, suggestive of NH_4^+ from bacterial origin. Uricites crystallize or precipitate from concentrated acid solutions where calcium remains soluble and the formation of the urolithes is attributed to enzimatic activity, changes in the acidity-alkalinity and phosphate ratios in the renal tract, and poor metabolism of lipids, proteins, and carbohydrates resulting in high uric acid and urates

PROTEROZOIC GRANITE/PEGMATITE SYSTEMS OF THE BLACK HILLS, S.D.

PAPIKE, J.J., SHEARER, C.K., JOLLIFF, B.L., DUKE, E.F., REDDEN, J.A., Inst. for the Study of Mineral Deposits, S.D. Sch. of Mines & Tech., Rapid City, SD 57701, USA; WALKER, R.J., National Bureau of Standards, Gaithersburg, MD 20899, USA; LAUL, J.C., Battelle, Richland, WA 99352, USA

The Proterozoic (~1.7 b.y.) S-type Harney Peak Granite is located in the south-central portion of the Precambrian core of the Black Hills, South Dakota. The Harney Peak is a complex of thousands of dikes and sills which grades outward to a pegmatite field with evolved pegmatites prevalent at increasing distances from the granites (C.K. Shearer, et al., this volume). At least two Archean granites also crop out in the region. The Black Hills provide a critical link between the Wyoming and Superior Archean Provinces and the Black Hills granite systems are potentially powerful probes of the nature of the lower crust and Proterozoic crust building processes. Because of the importance of this granitic terrane, the Institute for the Study of Mineral Deposits launched a geochemical program of study (1982) building on the excellent previous field structural research in the region. I. SOURCE REGION: Nd, O, and Sr isotope characteristics indicate that the Harney Peak Granite was not derived from any sampled Proterozoic metasedimentary rock exposure in the region. The granite and the pegmatite were either derived from a single source whose average precursor became LREE-enriched during late-Archean, or they were derived from at least two sources with at least one endmember of the source having a late Archean or older mantle extraction age. II. THE HARNEY PEAK GRANITE-PEGMATITE CONNECTION: We considered four models in our geochemical modeling: (1) Crystallization from a silicate melt derived from a one-stage anatexis event; (2) crystallization from a fluid produced by exsolution from the granite or by metamorphic dehydration of metasediments; (3) a model which concerns melt scavenging of the elements enriched in pegmatites (e.g. Li, Rb, Cs) from fluids or rocks with which it comes in contact; (4) crystallization from a melt derived through some fractionation of the Harney Peak Granite. Our favored model is a variation of (4) which involves a crystal-melt fractionation process requiring periodic removal of melt from its restite. III. EMPLACEMENT MECHANISM: The Calamity Peak layered complex is a satellitic composite pluton (~1 km^2) with many structural, textural, and chemical features mimicking the larger (~100 km^2) Harney Peak dome. The Calamity Peak dome (and by inference parts of the Harney Peak dome) grew by repeated conformable intrusions of granitic layers on the hanging-wall side of the initial intrusion (E.F. Duke, et al., this volume). Plastic deformation of the roof rocks resulted in induced quasi-concordancy, whereas discordancy was maintained at the footwall contact. IV. PEGMATITE INTERNAL EVOLUTION: Major, minor, trace elements, and oxygen isotope compositions have been evaluated to delineate the sequence of crystallization in the zoned and highly fractionated Tin Mountain pegmatite. Oxygen isotope geothermometry, rare earth element patterns, low concentrations of Rb, Cs and Li, and high concentrations of Ba and Sr in the wall zone indicate that it crystallized first. Cooling trends indicated by two-feldspar geothermometry, the presence of positive Eu anomalies in feldspars, and low concentrations of Rb and Cs in the uppermost inner zone suggest that it crystallized next. The three remaining lower zones then crystallized simultaneously. It is suggested that an aqueous fluid film connected all crystallization fronts in the body. This aqueous fluid vertically redistributed Si, Al, K, Na, and possibly Rb and Cs in such a manner that the melt retained a ternary minimum melt composition throughout crystallization. A different approach was taken to characterize the internal evolution of the Bob Ingersoll No. 1 pegmatite which involves the use of mineral recorders (e.g. tourmaline, apatite, feldspar, mica, columbite-tantalite; B.L. Jolliff, et al., this volume). In brief, tourmaline compositional trends in this pegmatite, coupled with textural features and mineral associations, provide evidence of an inward, generally sequential crystallization of the border zone, wall zone, intermediate zones, and finally the core, but with overlap between the inner wall zone and intermediate zones. The pegmatite melt was probably saturated at the onset of crystallization; however, fluid exsolution may have temporarily stopped during the initial crystallization of the third intermediate zone and a period of tourmaline instability, but then resumed, along with tourmaline crystallization, during the formation of the pegmatite core.

POWDER CRYSTAL STRUCTURE REFINEMENT: AN EXAMPLE OF THE ADVANTAGES OF SYNCHROTRON X-RAYS

PARRISH, W., WILL, G.* and MASCIOCCHI, N. IBM Almaden Research Center, San Jose, CA, 95120**

There are several important advantages of storage ring X-rays over conventional X-ray tube focusing methods (1-3). Any wavelength in the range from about 0.5 to 2.5 Å can be easily selected to maximize peak-to-background, and for anomalous dispersion measurements. A single wavelength (with very small spread determined by the monochromator) produces single profile reflections instead of the $K\alpha$ doublets. The parallel beam eliminates a number of the geometrical aberrations. The reflections are virtually symmetrical Gaussian type profiles whose shape is constant over a wide 2Θ range, the width increasing slightly at higher 2Θ values. This simplifies the profile fitting procedure (5) and the determination of the specimen contribution to the profile broadening caused by small particle size, strain, stacking faults, etc., for Warren-type profile analysis. High precision determination of lattice parameters can be obtained with weighted least squares refinement. The primary beam intensity is approximately uniform over a wide range of wavelengths and can be orders of magnitude higher than X-ray tubes. The instrumentation is similar to conventional diffractometry with a few important exceptions: a channel monochromator is used to select the wavelength from the white beam source. It has the important property that the direction and position of the monochromatic beam remains fixed making it unnecessary to realign or recalibrate over a wide range of wavelengths. The diffracted beam can be defined by a crystal analyzer (1), receiving slit (2) or horizontal parallel slits (3). A vertical scanning powder diffractometer (4) avoids problems with the highly polarized beam in the horizontal plane.

The section of the quartz pattern shown in the Figure is typical of the synchrotron powder data. It shows the digital data (not a strip-chart recording) collected with a computer-controlled diffractometer using 0.02°(2Θ) 2:1 step-scanning, 0.17° FWHM resolution, and 1 Å X-rays, covering the range d = 1.37 to 0.54 Å. Profile fitting results shown by the dashed line curves in the insert was done with a sum of two Gaussians curves and revealed 161 resolved reflections in the full pattern (12° – 135°2Θ corresponding to sin Θ/λ = 0.105 – 0.942 $Å^{-1}$). The differences between observed points (triangles) and profile fitted intensities are shown at half height. Using Cu $K\alpha$ the limit is d = 0.79 Å with 65 reflections. The overlaps can be resolved by profile fitting. The integrated intensities derived from the profile fitting were used in the powder least squares refinement program POWLS to determine the structure (5). The structure of quartz is being refined to high precision using anisotropic temperature factors which is made possible by the large number of reflections resolved by profile fitting. Typical crystallographic R(Bragg) values are 0.5 to 0.9 % for various inorganic structures (Si, CeO_2, Yb_2O_3). The resolution can be increased (with some loss of intensity) and the wavelength also increased to increase the dispersion for recording more complex overlapping patterns of orthorhombic and lower symmetry.

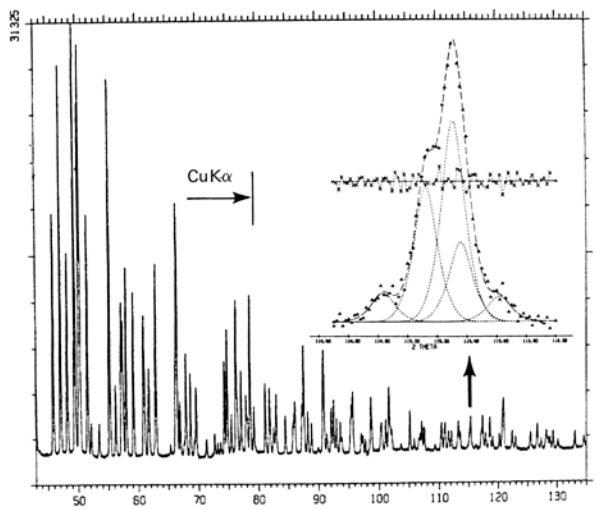

References:

(1) J.B.Hastings, W.Thomlinson and D.E.Cox, J.Appl.Cryst.,17, 611, 1983
(2) W.Parrish, M.Hart and T.C.Huang, J.Appl.Cryst.,19, in press,1986
(3) W.Parrish amd M.Hart, Trans.Am.Cryst.Assoc., 21, in press,1985
(4) W.Parrish, X-ray Analysis Papers, Centrex Pub.Co., Eindhoven, 1965
(5) G.Will, W.Parrish and T.C.Huang, J.Appl.Cryst., 16, 611, 1983

THE GOLDEN Ni-Fe CORE IN DEEP-SEA COSMIC SPHERULE

PENG HANCHANG AND CHEN SUITIAN, First Institute of Oceanography of State Oceanic Administration, Qingdao, P.O.Box 98, People's Republic of China; ZHUANG SHIJIE, China National Nonferrous Metals Industry Corporation, Research Institute of Geology for Mineral Resources, Guilin, People's Republic of China; CHAI ZHIFANG, Institute of High Energy Physics, Academia Sinica, Beijing, People's Republic of China; YU ZHONG, Institute of Petroleum Exploration and Planning, Beijing, People's Republic of China; LIU ZHENKUN, Institute of HUNAN Metallurgical Industry, Changsha, People's Republic of China

Recently, we collected several thousand cosmic spherules in deep-sea sediments from the Northern Pacific (lat 7° - 11° N, long 158° - 178° W). Many of golden Ni-Fe cores were found in naturally broken iron spherules. Under stereoscope the core can be seen clearly as golden round spherule with rough surfaces, they have strong metallic luster, their size about ⅛-¼ of a iron spherule (Fig.1). The results of electron probing analysis showed that major elemental compositions of core are Fe(20-70 %), Ni(28-80 %), Co(0.5-2.0 %), also contains small amount of Cu, Au, Cr, etc. The results of X-ray powder crystal photography showed that iron spherules with golden Ni-Fe core contains magnetite (Fe_3O_4, a_o=8.394±0.008 Å) and Wüstite($Fe_{1-x}O$, a_o=4.279±0.0018 Å).

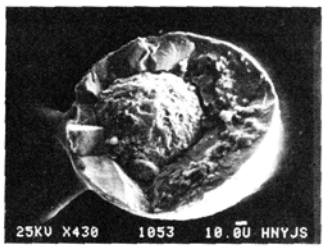

Fig.1 Photograph of iron spherule with golden Ni-Fe core

The discovery of golden Ni-Fe core in deep-sea iron spherule is of significance for further investigate the origin and formatived machine-process of cosmic spherules.

References: Brownlee D.E., 1981, Extraterrestrial Components, The Sea, Vol.7, 733-762; Bruun A.F., et al, 1955, Magnetic particles found by raking the deep sea bottom, Deep-Sea Res., 2, 230-246; Kazuo Yamakoshi, 1985, Further Studies on Size Distribution of Siderophile Element Concentrations in Black Magnetic Spherules from Deep Sea Sediments.

THE SYSTEMMATICAL STUDY OF QUANTUM MINERALOGY OF PIEMONTITE FROM HAILAND

PENG Mingsheng, ZHENG Chusheng, and LI Dien, Department of Geology, Central South Polytechnic University, Changsha, Hunan, People's Republic of China

Quantum mineralogy is a new marginal science. Based on the chemical bonding theories (crystal field theory, molecular orbital theory, energy band theory), the studies of natural minerals are carried out in composition, structure, physical properties, material and process property genesis, electron structure and their relationships with the help of spectroscopic methods. Since 1980, many studies have been carried out in the framework of quantum mineralogy. A case study on piemontite from the Hailand Iron Mine, China, is given in which piemontite occurred during regional metamorphism, contact metamorphism and hydrothermal processes.

Piemontite is a Mn^{3+}-bearing nesosilicate with space group P2/m. The linear variation of the refractive indices of piemontite as a function of the ratio $(Fe^{3+} + Mn^{3+})(Al^{3+} + Fe^{3+} + Mn^{3+})$ was determined before and after the ratio is equal to 33%. The piemontite shows strong pleochroism, with α = yellow, ß = pink, γ = red. Based on an X-ray study the site M(3) is occupied by Mn^{3+} ion in preference to M(1) and M(2) sites. Mossbauer spectra show that Fe^{3+} occurs in the M(3) site of piemontite. EPR spectra show that Mn^{2+} probably exist in the M(2) and M(1) sites. We measured the polarized absorption spectra of piemontite on a refitted micro-spectrophotometer. The spectral pattern (see Fig. 1) is basically in agreement with that given by Burns (1967) and is attributed to Mn^{3+} in the M(3) site of piemontite, but the band at 21,500 cm^{-1} in the γ spectral pattern is assigned to Fe^{3+} in the M(3) site. Furthermore, based on the spectral pattern and structural data of Dollase (1969), the crystal field potential and the energy levels of the Mn^{3+} ion in the M(3) site have been calculated theoretically. The results of our calculation are in keeping with the experimental spectral bands (see Table 1), which is also confirmed by our results according to the method of calculating the energy equation of d-orbitals proposed by Ballhusen. Meanwhile, the crystal field stabilization energy (CFSE) of Mn^{3+} in the distorted M(3) site of piemontite is calculated to be 40.5 Kc/mole, the 17 Kc/mole of which is an additional energy caused by the Jahn-Teller effect. In this way, the nature of strong pleochroism and color in piemontite and the stability of the Mn^{3+} ion in the piemontite structure have been explained.

The thermodynamic calculation shows that piemontite may be formed and stable in a wider range of temperature and pressure. Therefore, the stability field of piemontite is governed by higher oxygen fugacity in the alkaline condition (external cause) and the acquisition of CFSE by Mn^{3+} ion in piemontite structure (internal cause). The ordered distribution of cations in the piemontite structure also indicates that the lower temperature is more favorable to the formation of piemontite. The mentioned studies on piemontite from Hailand, China, on the other hand, have confirmed that the Hailand Iron Mine is a polygenetic deposit characterized by sedimentary processes, metamorphic processes and hydrothermal processes.

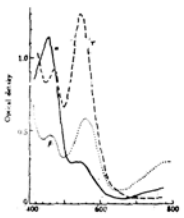

Fig. 1. Polarized absorption spectra of piemontite.

Energy (cm^{-1})		polariz.	assignment
Cal.	Exp.		
22518	22222	α, β	$x^2-y^2 \rightarrow z^2$
18401	18519	γ	$xz \rightarrow z^2$
17676	18018 19492	β	$yz \rightarrow z^2$
12301	12000	β, α	$xy \rightarrow z^2$
13.382	13.586		Δ (cm^{-1})
40.5	40.5		CFSE(Kc/Mo)

Table 1. The assignment of spectral bands

REFERENCES: [1] Peng Mingsheng et al. (1980) Quantum mineralogy. Acta of Central South Inst. Mining and Metallurgy, No. 2, 110. [2] Peng Minsheng et al. (1982) A study of crystal field theory on piemontite. Molecular Sciences and Chemical Study, No. 2, 81. [3] Xu Zitu et al. (1982) Calculation of crystal field theory of Mn^{3+} in piemontite. Kexue Tongbao, Vol. 27, No. 11, 1999. [4] Peng Mingsheng et al. (1984) A study on the stability field of Hailand piemontite. Acta Geologica Sinica, Vol. 58, No. 1, 63.

THE DEDUCTION OF QUASICRYSTAL LATTICE AND THE FRACTAL STRUCTURE MODEL OF QUASICRYSTAL

PENG Zhizhong, Beijing Graduate School, Wuhan College of Geology, Beijing, People's Republic of China

Two principles dominate the quasicrystal structure, i.e., the icosahedron principle and the golden mean principle. The former indicates that the icosahedron ligand is favored in energy when the atoms similar in size form isolated ligands with 12 coordination; the latter means that the arrangement of atoms in quasicrystal with five-fold symmetry follows the Fibonacci series:

n = 0	1	2	3	4	5	6	7	8
	a / b /	a /	ab /	aba /	abaab /	abaababa /	abaabbabaabaa /	
F_n = 1	1	2	3	5	8	13	21	33

Two distances (a,b) between the lattice points in the quasilattice row, a/b = 1.618, each step's increase is 0.618, the relations in Fibonacci numbers are: $F_0 = F_1 = 1$, $F_n = F_{n-2} + F_{n-1}$ (n = 2). Thus, the quasilattice deduced in the isometric, pentagonal, decagonal system is orthopentagonal dodecahedron and icosahedron, pentagonal, decagonal, respectively. The deduced quasilattice is characteristic of fractal structure, i.e., has the self-similarity, no translational symmetry. The lattice points are distributed heterogeneously.

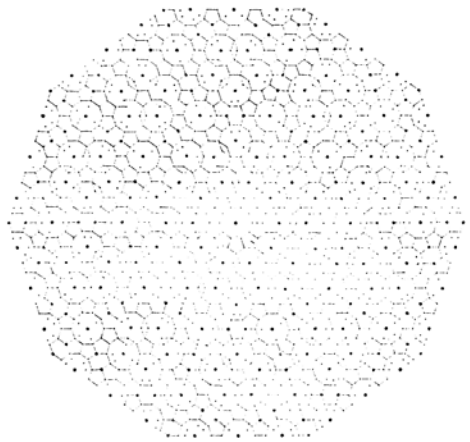

Ideal quasicrystal lattice deduced from five-fold axis.

Peng Zhizhong (1985) Building principles of quasicrystal and the fractal structural model. Earth Science, 10, 159-174. Peng Zhizhong (1986) The deduction of quasicrystal lattice and the fractal structure model of quasicrystal. Earth Science (in press).

THE PROBLEMS OF MINERAL EQUILIBRIA IN MAGMATIC AND METAMORPHIC SYSTEMS

PERCHUK, L.L., Institute of Experimental Mineralogy, USSR Academy of Sciences, Chernogolovka, Moscow distr., 142432, USSR

Magmatic systems. At the present moment thermodynamic treatment of phase diagrams and direct thermochemical data on some systems enable estimation of P-T conditions of generation and crystallization of magmas. The geological literature includes a number of approximations concerned with such results (e.g. Roeder and Emslie, 1970; Carmichael et al., 1977; Perchuk and Vaganov, 1977; Langmuir and Hanson, 1981; Nicholls, 1977). One of the recently modified approximations, for example, that of Perchuk (1983) allows for the experimental data on melting of natural basalts up to 10 kbar: $t°C = 1039.62 + 0.437368x + 353.86y + + 0.001182x^2 + 0.125186x^2y - 3.1 \cdot 10^{-5}x^3y + 0.004P$, where x is the mole fraction of forsterite (Fo) in the olivine at liquidi, y is that of the oxygen bound in a melt with Mg, Fe and Mn ($y = (Mg + Fe + Mn)/O^{\Sigma}$). For K-and Na-bearing systems, one should introduce activity coefficients for Mg and Fe in the melts. Binary and multi-component systems may be described by the Shreder equation. Specifically, for Fo on the liquidus of any potassium-poor systems, P/T = 4.77 cal/bar and $\Delta H = 13.5 \pm 2.6$ kcal/mol. The value $\Delta H_{Di} = 18.5 \pm 1$ kcal/mol (Robie et al., 1978) describes adequately the system $CaMg_2Si_2O_6$-H_2O at $V_{Di} = 0.14025 - 0.10955 \cdot 10^{-5}P - 0.25498P^2$ cal/bar. This was estimated experimentally at a pressure up to 30 kbar. An increase in pressure and concentration of alkalis involves an essential decrease in activity of SiO_2 in melts (near the liquidus). This effect may be calibrated in order to estimate pressure of basic magma generation. In addition, there still exist problems of kinetics of crystallization of water-saturated basalt magmas at $P \geqslant 10$ kbar. Al-and Fe-rich clinopyroxene on the liquidus crystallizes very sluggishly, commonly at a temperature that is by 100-150°C lower than that of liquidus.

Metamorphic systems. Thermodynamics of solid solutions and a series of mineral equilibria are well understood in these systems. The K-Na-Ca system has used effectively experimental data on exchange equilibria involving aqueous solutions and alkali chloride melts The same approach is applicable to the systems with the $Fe^{3+} \rightleftarrows Al$ isomorphism. These data have served as a good basis for calibrating the mineralogical thermometers and barometers involving feldspars, epidotes, garnets, scapolites etc. In fact, ion exchange between Fe-Mg silicates does not take place, particularly in the garnet-bearing systems. The determination of diffusion coefficients for Fe and Mg in a number of silicates has shown that just the garnets feature the lowest values. As is well known, this is the most possible explanation of a well-developed zoning in natural garnets. At the same time, our experiments on biotite-cordierite-garnet equilibria (Perchuk and Lavrent'eva, 1983) have indicated a recrystallization of garnet in aqueous solutions with a high-rate development of equilibrium compositions. The two factors, i.e. low diffusion rates, on the one hand, and high recrystallization rates, on the other, are the cause of re-equilibration of garnets in each infinitely small volume of metamorphic rocks at given P and T. Such a basis makes it possible not only to estimate P-T conditions at the final stages of metamorphism but also to follow their evolution. This is illustrated by examples typical of shields and fold belts. Thermodynamics of fluid-mineral equilibria is of paramount importance and viewed in terms of the gas component mixture fugacities as part of metamorphic evolution.

APPLICATIONS OF AUGER AND COMBINED AUGER/X-RAY PHOTOELECTRON SPECTROSCOPY TO THE CHARACTERIZATION OF MINERALS AND THEIR SURFACES

PERRY, DALE L., Lawrence Berkeley Laboratory, University of California, Berkeley, CA 94720, USA

One of the most powerful experimental techniques for studying the surface chemistry of minerals is that of x-ray photoelectron spectroscopy. The chemical and electronic states of elements both inherent to the sample bulk and the surface of the sample can be studied, and changes in the surface species resulting from subsequent chemical reactions can be observed. Frequently overlooked, however, is the fact that the x-ray source that is responsible for creating the x-ray photoelectron spectrum can also simultaneously create an Auger spectrum for some or all of the same elements of interest. This x-ray induced Auger spectrum can be used to derive information about the mineral surface chemistry, information that complements those bonding data derived from the x-ray photoelectron spectrum.

This presentation describes the research in this area to date and its applications to the study of mineral surface chemistry. Topics that are included are line shape analysis, Auger kinetic energies, differences in kinetic energies of photoelectron and Auger lines for the same element, and the Auger parameter. Examples are given to show how combined Auger/x-ray photoelectron spectroscopy can be used to differentiate between various forms of minerals and to study chemical species found on the mineral surfaces.

DEVELOPMENT OF AN AUTOMATED SEM-IPS-IA IMAGE ANALYSIS SYSTEM

PETRUK, W., CANMET, Department of Energy, Mines and Resources, 555 Booth St., Ottawa, Ontario, Canada K1A OG1

An automated microprobe-SEM-IPS-IA Image Analysis System was developed at CANMET by interfacing a Jeol 733 superprobe and a Tracor Northern 2000 energy dispersive X-ray analyser (EDXA) with a SEM-IPS image analyser in such a manner that two-way communication is obtained between all units. The system is referred to as the SEM-IPS-IA Image Analysis System to differentiate it from the SEM-IPS image analyser. The system has combined the capabilities of a full-sized stand-alone image analyser and the beam steering and mineral classification capabilities of the EDXA. The three units are interfaced in such a manner that the electron beam can be steered to scan particles displayed in a stored image of the image analyser, and it is possible to selectively scan only those particles that cannot be identified on the basis of their grey level. This capability is extremely important because it saves image analysis time, since the slowest step is X-ray analysis of particles.

The image analysis system was designed to incorporate the following features:

(1) Capability of performing image analysis routines that will solve the problem at hand;
(2) ability to collect an image that is a faithful reproduction of the image under study, and to accurately discriminate all phases in the image, and
(3) to operate without intereactive editing.

The SEM-IPS-IA Image Analysis System is used at CANMET to characterize the minerals and phases in ores and in products that are produced during such processes as mineral dressing, extraction metallurgy, pyrometallurgy, weathering etc.. The mineral or phase properties that must be determined are quantities, size distributions, liberation characteristics and grain shapes. Only a full-sized stand alone image analyser has the capability of determining all of these properties, and it can do this only when a precise image has been obtained and when the phases displayed in it have been accurately differentiated. Unfortunately many minerals cannot be discriminated from each other in an image obtained with an optical microscope. On the other hand, most minerals and phases can be discriminated in the backscattered electron (BSE) image obtained with a scanning electron microscope (SEM) or microprobe. The grey levels of the phases in the BSE image are dependent upon their average atomic number, with the lowest atomic number phase being darkest grey, and the highest atomic number phase being white. Since many fields need to be analysed to obtain statistically valid data, the detection of each mineral must be reproduced as the sample is moved from field to field. This reproducibility is possible only with a SEM or microprobe equipped with a beam stabilizer and a meter that reads the beam current on the Faraday cup in order to ensure that no beam current drift, and hence no variation in grey level discrimination, has occurred during the period of analysis which may be several hours.

During set-up for analysis a BSE image is obtained on the microprobe and transferred to the image analyser via an interface. Each mineral or phase is differentiated on the basis of its grey level in the image, and identified off-line with the EDXA. If it is found that several minerals or phases have the same grey level, they are identified during analysis by scanning the particles of that grey level with the electron beam. In this manner the speed of identifying the minerals on the basis of their grey level is combined with the accuracy of X-ray analysis of the particles that cannot be differentiated by their grey level. During analysis the images of the identified minerals or phases are saved in separate image memories. The particles in each image memory are then analysed to determine the required properties, i.e. quantities, size distributions, mineral liberation characteristics and grain shapes. In addition, a series of special table formats and graphs for data output has been developed.

CHEMICAL COMPOSITION OF ZWIESELITE

PFAFFL, F. A., Pfarrer Fuerst Strasse 10, D-8372 Zwiesel/Bay W-Germany

This new primary phosphate mineral was first described by BREITHAUPT in the year 1841 and it was named zwieselite after the place where it was found. Before that time this mineral was named iron-apatite, pitch-ironore, pseudotriplite. LAUBMANN & STEINMETZ described this mineral from the pegmatite of Hagendorf-North (Eastern Bavaria) as triplite. Zwieselite $(Fe^2,Mn)_2(F/PO_4)$ is different from triplite. It has a chemical distinction to triplite $(Mn, Fe^2)_2(F/PO_4)$ only through the prevail of Fe^2 contrary to Mn^2. The chemical analysis of zwieselite from Zwiesel gave CaO 0.50, FeO 38.52, MnO 24.20, P_2O_5 32.65, F 6.02, H_2O 0.62 (OTTO, 1935). The colour-luster is clove brown; brownish black to black on alteration. Zwieselite is changeable from a primary phosphate mineral to the secondary phosphate minerals hureaulite, purpurite, rockbridgeite.

The paragenesis of the granite pegmatite Birkhöhe near Zwiesel (Bavarian Forest, South Germany) shows quartz, microcline, muscovite, biotite, tourmaline (schorl), columbite, zwieselite and some uran minerals. Further occurrences are Hühnerkobel, Hörlberg, Döfering, Hagendorf-North/South (Eastern Bavaria), Kimoto (Finland), Limoges (France), Sierra de Cordoba (Argentina), Black Hills (South Dakota), Fremont and El Paso (Colorado) USA and some highthermals tinveins in Siberia.

References:

NRIAGU, J.O. & MOORE, P.B. (Edit.)(1984) Phosphate Minerals. p. 136, Springer Verlag Berlin-Heidelberg-New York-Tokyo
OTTO, H. (1936) Die Rolle des Mangans in den Mineralien (mit Analysen von Triphylin vom Hühnerkobel und Zwieselit von Zwiesel. Min. Petrogr. Mitt., 47, 89-140
PFAFFL, F. (1973) Der Pegmatit auf der Birkhöhe in Zwiesel und seine Mineralparagenese. Der Aufschluß, 24, 38-42
STRUNZ, H. (1971) Mineralien und Lagerstätten des Bayer. Waldes. 21. Sonderheft, Aufschluß, 8-91.

INCREASED RESOLUTION FOR SOLID-STATE ^{27}Al NMR

PHILLIPS, BRIAN L., and KIRKPATRICK, R. J., Dept. of Geology, University of Illinois, Urbana, IL 61801, USA.

Recent advances in experimental technique, aided by new theoretical calculations, have significantly increased the resolution of ^{27}Al MASS NMR spectra. Previously, ^{27}Al NMR has found but limited use in studies of solids, whereas ^{29}Si MASS NMR has become increasingly important, especially for problems concerning short range order/disorder. The problem with ^{27}Al NMR is that the moderate to large quadrupolar interactions in minerals are not completely averaged by rapid sample spinning at the magic angle. The non-averaged (second order) portion of the interaction produces a residual line width that normally precludes resolution of signals from non-equivalent sites of like coordination in the prominent peak for the central transition. It is now known (Samoson, Chemical Physics Letters, 119, 24-32, 1985) that this second order line width can be up to a factor of three smaller in the spinning sidebands of the satellite transitions. These appear in the spectra (Figs. 1 - 3) as a set of near-equal-intensity lines spaced at the spinning speed (ω_r) and symmetric about a center of gravity that is slightly shifted from the isotropic chemical shift, which can then be calculated.

Figure 1 is an ^{27}Al MASS spectrum of a microcline perthite, illustrating the gain in resolution available in the satellite lines. The isotropic chemical shifts obtained agree well with published values for Al(4) in microcline and albite. Figure 2 shows three resolved Al(4) peaks in leucite, from which the isotropic chemcial shifts can be calculated with a precision of $\pm$ .1 PPM. Figure 3, a low Fe vesuvianite, shows a resonance centered at about -2 PPM, a typical value for Al(6) in aluminosilicates. Separate peaks for two Al(6) sites are nearly resolved in the satellite sidebands. It also shows a peak at about 40 PPM due to pentahedrally coordinated Al, that is slightly deshielded from the value for Al(5) in andalusite but more shielded than any known Al(4) signal in aluminosilicates.

INCREASED RESOLUTION FOR SOLID STATE ^{27} Al NMR

PHILLIPS, Brian L., and KIRKPATRICK, R. J., et al.

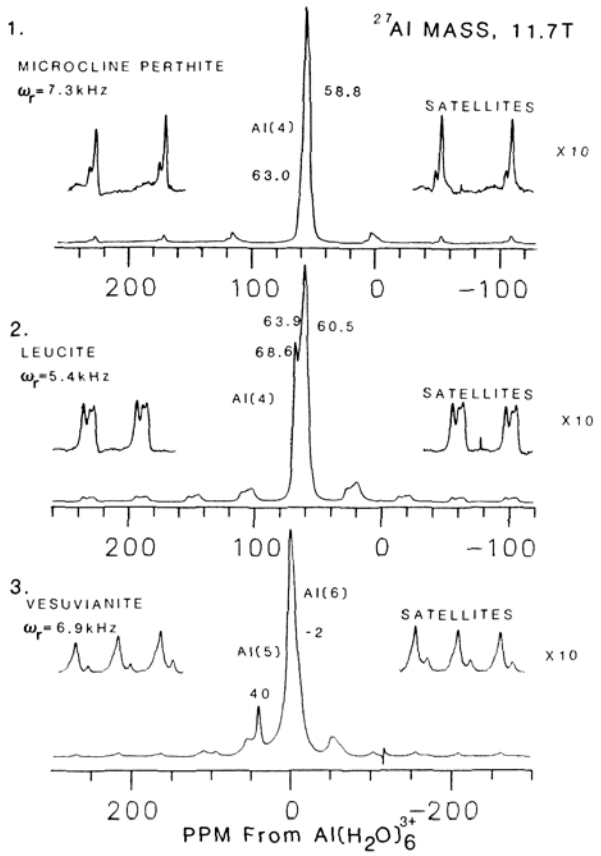

PROGRAM SEARCH: A METHOD FOR EXTRACTING EXCHANGE VECTORS FROM MINERAL COMPOSITION DATA

PHILLIPS, W. S., M. S. J979, Los Alamos National Laboratory, P. O. Box 1663, Los Alamos, NM, 87545; and DYAR, M. D., 170-25, Division of Geological and Planetary Sciences, California Institute of Technology, Pasadena, CA, 91125, USA.

Program SEARCH performs multiple regression/correlation analysis on all possible pairs of all possible combinations of components in a data base. It is especially well suited for application to large data bases of mineral analyses, where it is desirable to extract combinations of variables (e.g. cations) which correlate, such as in the Tschermak exchange $Al_{iv} + Al_{vi} = Mg + Si$. Use of this program may often result in the discovery of previously unnoticed substitutions, since there is no bias in the selection of combinations of variables.

The program compiles a list of all possible combinations of "N" components taken in "M" combinations of up to 10 at a time. The N components represent analyses which have been run on a suite of samples. Once the list of combinations has been generated, each list element can be matched up with any other element without duplication, in order to generate a set of ordered pairs upon which regression can be performed. The method described here is much quicker than simply looping through all the possible combinations; duplicate calculations are skipped in the code to be presented.

In order to make a list of N components taken at most M at a time (M=1-10), we must first see how to take N components exactly M at a time (with replacement). From the theory of homogeneous products, tne number of elements in such a list is

$$n = \frac{(M + N - 1)!}{M!\ (N - 1)}$$

where "!" represents the factorial operator:

$$N! = N\ (N - 1)\ (N - 2)\ \ldots\ (2)$$

A list of all possible unique combinations can then be generated in the following way. Consider a list of vectors each containing M elements, where each element represents a component index. Restrict this set of vectors to those in which the M elements are written in non-descending order (i.e. each element is greater than or equal to the element on its left). Starting with all elements equal to one, increment the right-most element by one until its value reaches N (the number of components), then increment the element to its left while rewinding the right-most, taking care that its value is never less than any of its neighbors to the left. Continue the procedure until n (as calculated above) non-decreasing vectors are found.

In order to find all combinations taken at most M at a time, we simply concatenate lists as described above for all positive integers less than or equal to M. The number of elements in the final list is

$$n = \sum_{i=1}^{M} \frac{(i + N - 1)!}{i!\ (N - 1)!}$$

In practice we start with the 0 vector and increment as described above until n vectors are formed. Matching each element of this list with all others will result in n!/(n-2)!2! possibilities to which regression may be applied. However, some duplication will be encountered since the correlation coefficient of $\bar{x}$ vs $\bar{y}$ is equal to that of $a\bar{x}$ vs $b\bar{y}$, where $\bar{x}$ and $\bar{y}$ are vectors and a and b are scalars (integers in our case). Duplications are caught by the subroutine CHECK and are skipped to eliminate confusion.

Program operation is simple. Although this program was developed and tested on both Cray and MicroVAX computers (which perform such lengthy calculations readily), the code will run (albeit slowly) on any computer with a Fortran-77 compiler. An input file is set up to contain the number of components, the number of samples, component labels, and the data for each sample. Null data are indicated by negative values. The operator chooses the number of combinations (M) desired and a minimum absolute value for the correlation coefficient. Intercepts, slopes, and standard errors are output to a result file, along with the correlation coefficient if its absolute value exceeds the cutoff. Meaningful interpretation of the results is left the user!

F, B, AND H_2O: EFFECTS ON PHASE EQUILIBRIA IN GRANITIC SYSTEMS

PICHAVANT, M., C.R.P.G., B.P. 20, 54501, Vandoeuvre Cedex, France, and MANNING, D.A.C., Department of Geology, The University, Newcastle-upon-Tyne, England

Phase relations concerning the effects of the addition of F, B (and also Li) to the H_2O-saturated granite system Qz-Ab-Or are now available at 1 kbar. The results can be used to infer crystallization paths in felsic magmas becoming progressively enriched in these components by crystal fractionation. In all cases, the minimum liquidus temperatures are markedly reduced. The addition of F and B progressively shifts the minumum composition towards the albite corner, whereas with Li there is no significant change in the phase relations except a small migration of the minimum liquidus composition towards the Qz-Ab binary. Although the three additional components interact with the melt structure by different mechanisms, the observed change in phase relations (particularly for F and B) is consistent with a reduction in the activity of the Ab-forming components within the melt. The interpretation of the results in the B-bearing system is complicated by the concomitant increase of the melt H_2O content compared to a B-free system.

Phase relations in the same system (B_2O_3 = 4.5 wt % in the melt) and at the same pressure but with $aH_2O < 1$ allow the effect of both B and pressure to be separated from those of increasing aH_2O. With decreasing aH_2O, the minimum composition changes from $Qz_{31}Ab_{46}Or_{23}$ (6.5 wt % H_2O) to $Qz_{31}Ab_{34}Or_{35}$ (2.4-3.2 wt % H_2O) and its temperature increases from 630 to 760°C. There is no large displacement of the quartz-feldspar field boundary. The observed displacement of the minimum composition with variable aH_2O is transverse to that of the H_2O-saturated minima and eutectics at increasing P in the B-free system. This suggests that H_2O also lowers the activity of the Ab-forming components. Thus, H_2O and the other granophile elements studied behave similarly to form complexes with the Ab-forming components in the melt, although by different mechanisms. There is indirect evidence of the nature of these complexes.

F, B, AND H_2O : EFFECTS ON PHASE EQUILIBRIA IN GRANITIC SYSTEMS

PICHAVANT, et al.

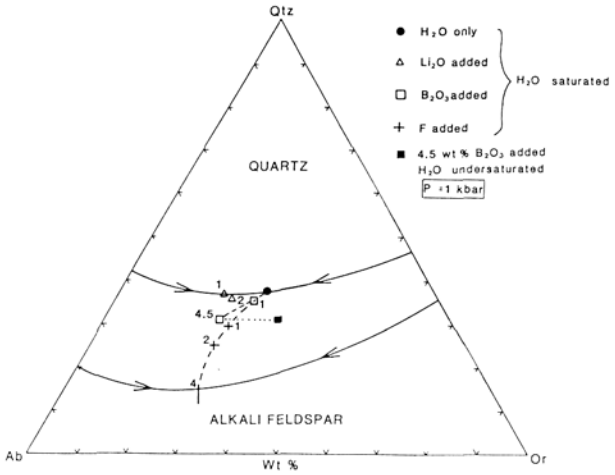

REFLECTED LIGHT MICROSCOPY OF PYROMETALLURGICAL PRODUCTS

Susanne Pignolet-Brandom, Richard D. Hagni, Robert T. Brandom, and Christopher B. Vierrether, Department of Geology and Geophysics, University of Missouri-Rolla, Rolla, Missouri 65401, USA; Daniel T. Kremser, Department of Earth and Planetary Science, Box 1169, Washington University, St. Louis, Missouri 63130, USA

The complex nature of pyrometallurgical products presents a challenge to their study. The phases are often fine-grained, intimately intergrown and the optical properties of artifical compounds often are poorly documented. To identify the phases present in pyrometallurgical products we utilize a combination of techniques, including reflected light microscopy, scanning electron microscope - energy dispersive spectrometry (SEM-EDS) and backscatter analysis, and electron microprobe analysis. Reflected light microscopy is used for initial identification of phases for which optical properties are known. Other phases are grouped into metals, sulfides, oxides and silicates. SEM-EDS standardless analysis is employed to determine the major elements in unknown phases and the minor elements in all phases. Although these data are semiquantitative, they are very useful to indicate which elements should be sought and analyzed with the microprobe. SEM study in the backscatter mode is especially useful to study intergrowths that are difficult to distinguish or even irresolvable by ore microscopy. Furthermore, the backscatter image is helpful to insure that the phases analyzed are homogeneous. Electron microprobe analysis is used to determine the quantitative abundances of major and minor elements. Reliable differentiation between some elements, such as lead and sulfur, require this technique. In addition, the microprobe is used to determine element ratios that are essential for distinguishing phases such as the lead silicates.

Several examples of the pyrometallurgical problems to be discussed include metal losses to slag, identification of phases containing deleterious constituents, investigation of reactions with furnace liners, study of the extent of phase conversions, comparison of phases present with thermodynamically predicted phases, comparison between products with desirable and undesirable physical properties, and determination of the physical mechanism of separation of slag and matte phases. Samples studied thus far include lead sinter, lead blast furnace slag, copper dross formed during the cooling of lead boullion, reverberatory dross furnace product, experimental copper flash furnace samples, samples from operating flash furnaces, dust particles collected from emitted gases and direct reduction iron pellets.

These studies have shown that microscopy provides invaluable information to the metallurgist that can aid in the prevention of metal losses and in optimizing processes for the most efficient operation.

Future work on these samples includes the application of transmitted light microscopy, X-ray diffraction, and cathodoluminescence microscopy.

UNUSUAL OCCURRENCES OF COBALT AND NICKEL MINERALS IN THE SOUTHEAST MISSOURI LEAD DISTRICT.

Susanne Pignolet-Brandom, Richard D. Hagni, and Robert T. Brandom, Department of Geology and Geophysics, University of Missouri-Rolla, Rolla, Missouri 65401, USA

Cobalt and nickel are present throughout the Southeast Missouri Lead District as the thiospinel siegenite and the nickel-cobalt pyrite-type mineral, bravoite. Both minerals are associated with the lead-zinc-copper mineralization. In contrast, cobalt and nickel sulfides, nickel sulfides, nickel sulfosalts and rare cobalt-nickel-copper thiospinels are present in rare paragenetically early chalcopyrite-bornite lenses and colloform ores.

The massive chalcopyrite-bornite lenses are present at the Fletcher, Milliken, Brushy Creek and Casteel mines. All of these lenses are small, commonly about three meters wide and one-half meter or less thick. The chalcopyrite and bornite exhibit exsolution, colloform, and replacement intergrowths. Chalcocite-group minerals occur as late replacement patches, small vug fillings, and veinlets within the massive bornite and chalcopyrite. Cobalt and nickel minerals have been detected only in the lenses at the Milliken mine and Fletcher mine, but the Casteel ores have not yet been studied by ore microscopy. The cobalt-nickel minerals include fletcherite, nickelean carrollite, cobaltian pyrite gersdorffite, vaesite, and a cobalt-nickel-iron sulfide.

Gersdorffite occurs as euhedral pyritohedral crystals that are disseminated or form stringers. Gersdorffite commonly forms overgrowths and partial replacements of earlier deposited tennantite and enargite.

Vaesite occurs as disseminated euhedral octahedral, cubo-octahedral and mosaic crystals. Vaesite occurs as overgrowths on enargite and fletcherite.

Cobaltian pyrite exhibits a pinkish yellow color, distinct growth zoning, and partial replacement by gerdorffite, chalcopyrite, and bornite. Electron microprobe analysis indicates that the pyrite contains an average of 8% cobalt.

Fletcherite, a copper-cobalt-nickel thiospinel, has been detected only from the ores at the Fletcher mine. It occurs as cubic and octahedral crystals that are disseminated in chalcopyrite. Nickelean carrollite, a copper-nickel-cobalt thiospinel, is present at the Milliken mine. Typically it is highly fractured with chalcopyrite, bornite, and vaesite filling the fractures.

A distinctly pink thiospinel that is highly fractured with chalcopyrite and a white sulfide filling the fractures is present at the Milliken mine. Preliminary semi-quantitive analyses indicate that it contains approximately equal amounts of cobalt, iron, and nickel.

In addition to the thiospinels present in the bornite-chalcopyrite lenses, siegenite is present within the chalcopyrite at the margins of the lenses. Siegenite of this generation, in contrast to that which occurs later in the paragenetic sequence, contains up to 17% copper, and its cobalt content is greater than that of nickel.

Rare colloform nickel ores that are present in the Magmont West orebody show a crustified sequence that provides an excellent opportunity to study their paragenetic sequence. In these ores, crystals of millerite, two to four milimeters across, are almost completely replaced by polydymite and vaesite. These crystals are coated and replaced along their borders by tennantite and enargite. The latter two minerals are coated by a one millimeter thick deposit of colloform gersdorffite or vaseite and gersdorffite. Gersdorffite of this generation veins and replaces the millerite-polydymite and vaesite crystals. As many as five bands of gersdorffite, including three bands of 200 um crystals, were subsequently deposited. A final generation of gersdorffite formed euhedral pyritohedrons that are coated by tennantite enargite, sphalerite and chalcopyrite. Chalcopyrite of this generation veins the banded gersdorffite and replaces and veins the earlier millerite, polydymite, and vaesite crystals.

These two types of ores represent a paragenically early influx of nickel-cobalt mineralization that was significantly more nickel- and arsenic-rich than later periods of cobalt-

nickel mineralization. Both types are much less pervasive than the later cobalt-nickel mineralization associated with the typical copper-lead-zinc ores. Exsolution textures in the chalcopyrite-bornite lenses indicate that those ores were deposited at higher temperatures than the lead-zinc ores.

• APPLICATION OF MINERAL SPECTROSCOPY IN GEOLOGY -- A CASE STUDY OF TIN DEPOSITS

PING Xing and LI Dien, Department of Geology, Central South Polytechnic University, Changsha, Hunan, People's Republic of China

Mineral spectroscopy can provide some information on the geneses and geochemical processes of deposits, which is an important aspect of modern genetic mineralogy and quantum mineralogy. In this paper, an investigation has been carried out on the infrared (IR) and Raman spectrum, absorption spectrum (UV-Vis-NI), EPR spectrum and cathodoluminescence spectrum of cassiterite from different genetic types such as granitic magmatic deposit, hydrothermal cassiterite-sulfide deposits related to granite or volcanism-subvolcanism and magmatization granite tin deposits in China, as well as hydrothermal synthesis.

Based on the correlation analysis of factor group and site group, the calculation on harmonic vibration model, and the selection rules, as well as the IR and Raman measurements, we have obtained the four IR and Raman active models of cassiterite: $\Gamma_{IR} = A_{2u} + 3E_u$ and $\Gamma_R = A_{2g} + B_{1g} + B_{2g} + E_g$, respectively, whose absorption frequencies (cm^{-1}) are:

IR v(Eu) = 630-680, v(Eu) = 310-325, v(Eu) = 268-270, $v(A_{2u})$ = 525-550
Raman $v(B_{1g})$ = 111, $v(E_g)$ = 475, $V(A_{1g})$ = 633, $v(B_{2g})$ = 777

Furthermore, according to the spectral shape and symmetry, IR spectra of cassiterite can be divided into three types: standard spectra (type I) in synthetic cassiterite, deformation spectra (type II) of cassiterite from hydrothermal deposits, and distorted spectra (type III) of cassiterite from granite magmatic deposits (see Fig. 1). It is also to be noted that type III and type II can be seen in cassiterite samples from the early stage and late stage of magmatization granite tin deposit, respectively. Therefore, the characteristics in the IR spectra of cassiterite is of significance in studying its geneses. The UV absorption spectra show that cassiterite is a semiconductive mineral with a wide energy gap. Impurity ions Nb^{5+}, Ta^{5+} and Fe^{3+} as a donor or acceptor level deepen its color and decrease E_g. Two strong peaks at 410 and 460 nm and two weaker peaks at 730 and 780 nm can be seen in the visible absorption spectra of cassiterite from hydrothermal deposits. The former are attributed to spin-forbidden $^6A_{1g} \rightarrow {}^4A_{1g}$ or ^4E_g electron transition of Fe^{3+} ion in D_{2h5} field; the latter are assigned to spin-allowed $^5B_{2g} \rightarrow {}^5B_{1g}$ and $^5B_{1g} \rightarrow {}^5A_{1g}$ electron transitions of Fe^{2+} in the same field, which show that the cassiterite was formed in a more oxidizing condition. But in absorption spectra of cassiterite from magmatization granite tin deposit, other peaks at 625 and 760 nm can be seen besides the peak at 410 nm. The EPR spectra of the same sample show that V^{4+} ion exist in the D_{2h} field of the structure with g = 1.9296 and A = 42.4610^{-4} cm^{-1}. Therefore, according to the calculation results of crystal field theory, the peaks at 625 and 769 nm can be assigned to $^2B_{1g} \rightarrow {}^2B_{3g}$ and $^2B_{2g} \rightarrow 2B_{3g}$ electron transitions, respectively, which indicates the cassiterite was crystallized in a more reducing condition. In addition, the cathodoluminescence spectra of cassiterite can also provide some information for the existing state of the impurity ion and the genesis of deposits.

As mentioned above, the cassiterites from different genetic deposits are different from each other in the spectral characteristics, which can also provide some information about the formation conditions and the geochemical processes of tin deposits.

References

[1] Peng Mingsheng et al. (1985) A spectroscopic study of cassiterite of different geneses, Kexue Tongbao, 30, 600.

[2] Peng Mingsheng et al. (1985) A spectroscopic study on the geneses of cassiterite. The collected papers of International Symposium on Geology of Tin Deposits.

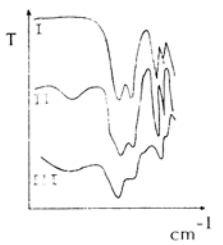

Figure 1. Infrared spectra of cassiterite.

LATTICE DEFECTS IN PEROVSKITES - TEM EXAMINATION AND CREEP EXPERIMENTS

J.P. POIRIER, J. PEYRONNEAU, S. BEAUCHESNE, M. MADON, F. GUYOT
Institut de Physique du Globe de Paris, 4 place Jussieu, 75252 Paris Cedex 05 (France)

Silicate $MgSiO_3$ perovskite and analogue germanates ($MnGeO_3$ and $CaGeO_3$) have been synthetized in diamond anvil cell and examined in transmission electron microscopy. With the exception of $MnGeO_3$, these perovskite become amorphous under the electron beam and can be examined for a short time only at low beam intensity.

$MgSiO_3$ and $CaGeO_3$ perovskites produced from the corresponding olivines exhibit no dislocations. $MgSiO_3$ shows the $GdFeO_3$ distortion and appears as twinned domains with boundaries parallel to {100} planes in the pseudo-cubic lattice. The rather equant shape of the domains and the sometimes sinuous boundaries suggest that the distortion was present at high temperature and pressure (rather than appearing during the quench).

Dislocations were observed in $MnGeO_3$ (prepared from pyroxene) ; they were straight edge dislocations with <100> Burgers vector (pseudo cubic indices). Similar dislocations were observed in $BaTiO_3$ deformed at high temperatures, whereas at lower temperatures the dislocations generally have a Burgers vectors of the <110> type (as already observed in $KNbO_3$, $KTaO_3$ and $CaTiO_3$ by other authors). This conforts the approach that consists in studying high temperature plastic properties of analogue perovskites in the hope of getting information on the mantle perovskite. High temperature creep experiments on $BaTiO_3$ single crystals have yielded a creep law with a stress dependent activation energy.

X-RAY ABSORPTION STUDY OF YTTERBIUM IN QUENCHED ALUMINOSILICATE MELTS

PONADER, C.W., BROWN, G.E., JR., Department of Geology, Stanford University, Stanford, CA 94305, USA

Studies of trace element contents of igneous rocks and of trace element partitioning between melts and crystal have provided important constraints on the evolution of magmatic systems. While something is known about the sites occupied by trace elements in minerals, little is known about the structural environment of these elements in melts. There appears to be a connection between melt structure (and composition) and the partitioning behavior of trace elements (*e.g.* Mysen and Virgo, 1980, Mahood and Hildreth, 1983), implying that there may be important variations in the local environment about certain trace elements in melts of different compositions. Additionally, analytical studies on many silicic volcanic centers have shown that certain trace elements are concentrated near the top of the magma chamber, while other elements are concentrated toward the bottom. It has been suggested that volatile components may play a key role in effecting this segregation (Mahood, 1981).

In order to to test the validity of this last hypothesis and to determine the effect of melt structure on the trace element environment we have begun a structural study of selected trace-element/melt systems and report here the first EXAFS and NEXAFS studies on trace levels (2000ppm) of ytterbium in silicic glasses of various compositions: albite ($NaAlSi_3O_8$), sodium trisilicate ($Na_2Si_3O_7$) and a peralkaline glass on the join between albite and sodium trisilicate ($Na_{3.3}AlSi_7O_{17}$). The glasses were made with and without fluorine to examine the possibility of volatile complexes with the trace elements and to determine the effect of volatiles on the local structure. These compositions were chosen because they are compositionally simple, synthetic analogues of high-silica framework-type melts (albite composition) that grossly approximate natural granitic melts and less polymerized melts (sodium trisilicate and peralkaline compositions) which approximate lower silica content melts such as basalts and andesites.

Fluorescence EXAFS and NEXAFS spectra were collected at the Stanford Synchrotron Radiation Laboratory on wiggler-magnet line IV-3 using Si(111) monochromator crystals. The data were analyzed, using YbO_3 and YbF_3 as model compounds, by least-squares fitting of the fourier-filtered, back-transformed and k^3-weighted chi function. The bond lengths and coordination numbers of Yb showed a large difference in local structure between the strongly polymerized melt, albite, and the less polymerized peralkaline and trisilicate melts; however, no difference was detected in the local Yb structure between the two depolymerized melts. Yb in albite glass is coordinated by an average of 7.7 oxygen atoms at 2.14 A. In the less polymerized melts the average coordination is approximately 10 oxygens at 2.22 A. The estimated accuracies of the coordination numbers and distances are $\pm$ 20% and $\pm$ 0.05 A respectively. Despite the uncertainty in the coordination numbers, the increase in bond length suggests that the increased coordination in the depolymerized glasses relative to albite glass is real. The Yb environment in the albite plus fluorine melt was determined to be nearly identical to that in the trisilicate melt. (Fig. 1) There is no evidence for Yb-F complexes in the melt, suggesting that the change in Yb environment between the fluorine-containing albite glass and the fluorine-free albite glass is due to the depolymerizing effect of fluorine on the tetrahedral network. This initial EXAFS study of Yb demonstrates the high sensitivity of the trace element environment to changes in melt composition and melt structure. It also shows that F is not an important complexing anion for Yb in the melt compositions considered in this study.

Study supported by NSF Grant EAR-8513488

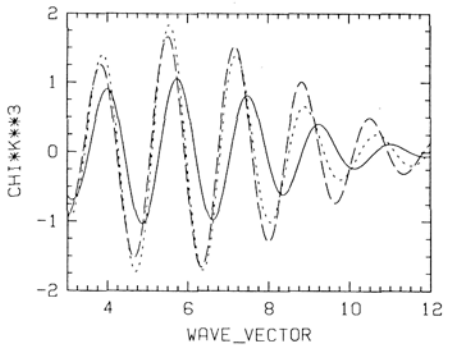

Fig. 1. Back-transformed chi functions for albite (solid), sodium trisilicate (dashed), and fluorine-containing albite (dotted) glasses. The large differences in phase and amplitude between the curve for albite glass and the curves for the trisilicate and fluorine-containing glasses demonstrate the differences in the local Yb structure between the polymerized and depolymerized glasses.

REFERENCES

Mahood, G. (1981) Contrib. Mineral. Petrol. 77, 129-149.
Mahood, G. and Hildreth, W. (1983) Geochim. Cosmochim. Acta 47, 11-30.
Mysen, B.O. and Virgo, D. (1980) Geochim. Cosmochim. Acta 44, 1917-1930.

EXPERIMENTAL STUDY OF RODINGITIZATION AND SERPENTINIZATION

PONADER, H.B. and LIOU, J.G., Dept. of Geology, Stanford University, Stanford, CA 94305, USA.

A matrix of flow-through experiments and thermodynamic calculations have been performed in order to test the concurrency of rodingitization and serpentinization as well as to characterize the compositon of the fluids responsible for the formation of the minerals that characterize these assemblages.

Rodingites are widespread but are commonly restricted by their association with serpentinites. The Ca-rich rodingites develop as reaction zones at the contact between the serpentinites and the adjacent rock or tectonic inclusion. Often sandwiched between them is a narrow Mg-rich aureole called a black wall. Based on these common field relationships and some experimental observations *(e.g.,* Yale *et al.,* 1984; Ponader, 1986), these alteration assemblages are thought to form as a result of localized Ca- and Mg-metasomatism due to the infiltration of serpentinizing fluids; however, little is known about the exact conditions of formation of rodingites and serpentinites and of the behavior of the chemically active aqueous species during their formation.

The flow-through apparatus (Potter *et al.,* 1985) can be set up to be a direct experimental analog of metasomatic reactions. In an open system, solutions are infiltrated through a core of powdered material. In the present study, the flow rate (10 ml/day), temperature (300°C), and pressure (300 bars, $P_{fluid}=P_{total}$) are kept constant while the initial solution composition (deionized water and $Ca(OH)_2$ solutions), starting materials (lherzolite, labradorite, and lherzolite in series with labradorite), and duration (8 to 60 days) are varied. The lherzolite consists of a mixture of powdered (105-149 μm) 70% $forsterite_{90}$, 20% $enstatite_{85}$, and 10% diopside; the labradorite (An_{50}) is a powdered (105-149 μm) single crystal, free of inclusions. The textures of the starting materials and the solid run products were characterized by SEM. The initial crystals showed few ultrafine particles on their surfaces and little evidence of surficial disruption due to sample preparation. The effluent is sampled daily, measured for pH and analyzed for major element chemistry. The cores are sectioned based on the degree of lithification and zones of color changes. The techniques of XRD, SEM/EDAX, Auger spectroscopy (Hochella, in press), and electron microprobe are used to identify secondary phases.

All phases of the lherzolite serpentinized to chrysotile and lizardite; the chrysotile is concentrated at the inlet end, decreasing in relative proportion with the lizardite further from the inlet. Other phases within the lherzolite include goethite and iron oxide. Brucite was not detected in the x-ray patterns and not observed by SEM. At the contact between the lherzolite and labradorite, a multi-colored zone was produced, but the clay-like particles have not yet been identified conclusively. Within the labradorite, the grains exhibit dissolution textures varying from etch pits to extensive corrosion, depending on the duration of the experiment. The labradorite grains have been leached of their alkalis, and the new phases include diaspore and hydrous calcsilicates. The secondary phases are all less than 5 microns in size and are in relatively small proportion to the primary phases; hence, their identification is difficult.

Thermodynamic relations are used to interpret and predict the phase equilibria of rodingite and serpentinite minerals in the presence of metasomatic fluids. Using analyzed fluid compositions, EQ3 (Wolery, 1979) calculates activities and the relative saturation states of the primary and secondary minerals. Activity-activity relations within the $CaO\text{-}MgO\text{-}Al_2O_3\text{-}SiO_2\text{-}H_2O$ (CMASH) system at 300°C were generated using the program SUPCRT (see Helgeson *et al.,* 1978, and references therein), and on them the path of the sequential reactant fluids with relative mineral saturation states has been traced to evaluate the changes in species distribution during each experiment.

When affinity ($\underline{A}$) is plotted against time for each experiment, all of the primary phases of the lherzolite begin within the undersaturated region and trend toward a steady state as equilibrium ($\underline{A} = 0$) is approached. The calculated behavior of the secondary phases is different for each experiment according to the initial fluid composition and core material; however, some phases are supersaturated within the solutions but are not precipitated phases within the experimental core. These calculations determine which mineral assemblage is capable of being formed from each experimental solution.

References:

Helgeson H.C., Delaney J.M., Nesbitt H.W., and Bird, D.K. (1978). Am. Jour. Sci. *278-A,* 1-200.
Hochella M.F., Harris D.W., and Turner A.M. (in press). Am Min. *71.*
Ponader, H.B. (1986). EOS, *67.*
Potter J.M., Pohl D.C., Guillemette R.N., Ponader H.B., and Liou J.G. (1985). N. Jb. Min. Mh., *7,* 329-335.
Wolery T.J. (1979). UCRL-52658, Law. Liv. Nat. Lab., Livermore, CA.
Yale L.B., Ponader H.B., and Liou J.G. (1984) GSA Abstr. Progr. *16* (6), 702.

STRUCTURE REFINEMENT OF ROMANECHITE; SUBCELL AND SUPERCELL

POST, J.E. and TURNER, S.
Department of Mineral Sciences, Smithsonian Institution, Washington D.C. 20560

Romanechite is a manganese oxide mineral that occurs in widespread geologic deposits. It has an ideal formula of $(Ba,H_2O)_2Mn_5O_{10}$ and a 2x3 tunnel structure closely related to that of 2x2 hollandite and 3x3 todorokite. The structure of romanechite was solved and refined in two dimensions to R =0.16 by Wadsley(1953). Wadsley suggested the possibility of a superstructure arising from ordering of the tunnel Ba and water, and recently, Chukhrov et al. (1983) using electron diffraction confirmed the existence of a superstructure.

A single crystal x-ray refinement was carried out on a romanechite crystal from Schneeberg, Germany. Microprobe analysis yields a formula of $Ba_{.66}Mg_{.02}Ca_{.03}Na_{.01}(Si_{.05}Al_{.01}Mn^{4+}_{4.81}R_{.08})O_{10}\cdot nH_2O$ (where R= W,Cu,Zn,Ni,Co). Unit cell parameters were determined from x-ray powder diffraction analysis giving $\underline{a}$ = 13.929(1)A, $\underline{b}$ = 2.8459(4)A, $\underline{c}$ = 9.678(1)A, β =92.39(1). Long exposure precession photographs reveal a superstructure with a tripling of $\underline{b}$ as reported by Chukhrov et al. Additionally, we found that precession patterns of the superstructure layers at 1/3 and 2/3 along b^* show streaking in the $[20\bar{1}]$ direction. These streaks are modulated perpendicular to c^*.

The subcell was refined in space group C2/m using 653 reflections to R=0.065 using isotropic temperature factors and 0.041 using anisotropic temperature factors. In general our structure agrees well with that of Wadsley, although there are signigicantly different atom positions and bond lengths. Our average octahedral Mn-O bond distances are 1.909A for Mn(1)-O, 1.962A for Mn(2)-O and 1.902A for Mn(3)-O. The larger Mn(2) octahedron indicates that the lower valence octahedral cations preferentially occupy the Mn2 site. Further, the Mn(2) octahedron is Jahn-Teller distorted (<apical Mn-O>= 2.056A and <equatorial Mn-O>= 1.916A) consistent with Mn^{+3}, rather than Mn^{+4} as has been generally assumed in the past, being the primary lower valence octahedral cation.

The structure was then refined using the subcell and 60 supercell reflections. A simplest supercell was chosen with $\underline{a}$ and $\underline{c}$ the same as for the subcell, with $\underline{b}$ tripled and with a space group of C2/m. The framework atom positions were held fixed to values determined in the subcell refinement, and the positions, temperature factors and occupancies for the two Ba sites were refined to R=.068. The results indicate that 55% of the Ba occupies the Ba1 site (or special position). The remainder of the Ba and water go on the Ba2 site (or the general position). The assumption that water occupies the Ba2 site is supported by a larger Ba2 temperature factor (U = 0.022) relative to that of Ba1 (U =0.01).

Chukhrov, F.V., A.I. Gorshkov, M.t. Dmitrieva and A.V. Sivtsov(1983) Izvest. Akad. Nauk, Ser. Geol. 83, no. 3, 68-75.

Wadsley, A.D. (1953) Acta Cryst., 6, 433-438.

THE SPIN GLASS STATE IN GARNET MIXED CRYSTALS : NEW EVIDENCE FROM NEUTRON SCATTERING AND MACROSCOPIC MEASUREMENTS.

PRANDL, W., Universität Tübingen, Institut für Kristallographie, Charlottenstr. 33, D-7400 Tübingen, West-Germany

Garnets of the composition $Fe_2Ca_3(GeO_4)_3$ and $Cr_2Ca_3(GeO_4)_3$ order antiferromagnetically at T_N = 14 and 12 K, respectively. The magnetic structures have the magnetic space groups I_P4_122 in the Fe-, and $I'4_1/ac'd$ in the Cr-garnet. We find from neutron diffraction powder data /1/ in a continuous series of mixed crystals $(Fe_xCr_{1-x})_2Ca_3(GeO_4)_3$ the coexistence of the two types of magnetic long range order. The magnetic reflections do not show any broading with respect to the nuclear ones. Any clusters, if present, must be larger than 200 Å, the resolution limit of the diffractometer.

Starting from the composition x = 0 the Cr-type saturation sublattice magnetisation dimimishes smoothly with increasing Fe-concentration without any discontinuity. The same thing happens with the Fe-type reflections when Cr is added. At x = .50 both sublattice magnetisations are reduced to about 40 % of their end member values, respectively. At this composition the magnetic Bragg reflections become time dependent: depending on the kind of thermal treatment of the sample (in the region of $4 \leq T \leq 15$ K) the relaxation time for reaching the antiferromagnetic saturation is several hours. A strong component of diffuse magnetic scattering occurs at $T \leq 15$ K the largest part of which is quasielastic.

The magnetic susceptibility χ /2/ measured in a Faraday balance with a field of .5 T shows for x = 1 the behaviour typical for an antiferromagnet: Curie-Weiß law at $T > T_N$, temperature independent for $T < T_N$. In the mixed phases the change of slope at T_N is gradually washed out. For x = 0.5 χ increases monotonically with decreasing temperature without any noticable change at the T_N known from the neutron measurements. In a SQUID magnetometer the x = 0.5 sample shows a maximum of χ' (real part) at 3.8 K. For $T \leq 2.9$ K the zero field cooled susceptibility is smaller than the field cooled susceptibility: an observation typical for spin glasses. Losses in the sample in oscillatory fields are given by the imaginary part χ''. $\chi''(\nu)$, measured at the very low frequencies $0.01 \leq \nu \leq 0.25$ Hz, increases strongly at $T \leq 4$ K ($\leq T_N$ (x)) for samples with $0.40 < x < 0.6$.

We conclude from this observation by using the fluctuation-dissipation theorem that very low frequency fluctuations set in at temperatures well below the Neel temperature. Combining the neutron results and the data from macroscopic measurements we find that only a small fraction of the magnetic moments contributes to the long range order, in particular in mixed crystals with x = 0.5. Fluctuations in space and time persist down to very low temperatures.

/1/ Th. Brückel, W. Prandl, to be published
/2/ Th. Brückel, U. Köbler, W. Prandl, R. Weinmann, submitted to Sol. State Communic.

A MODEL FOR POLYTYPISM AND POLYSOMATISM

PRICE, G.D., Department of Geological Sciences, University College London, Gower St, London WC1E 6BT, England, and YEOMANS, J., Department of Theoretical Physics, University of Oxford, Oxford, England.

Crystal structures can be analysed at many levels, howerver, it is becoming increasingly apparent that many families of structures can be usefully described in terms of larger basic structural units or modules. If such an approach to the description of crystal structures is adopted, many complex solids may be systematised in terms of series of stacking varients of the simple subunits. Variations in the stacking of structurally compatible, isochemical modules give rise to polytypic families, epitomized by the classic polytypes such as SiC, ZnS and CdI_2. A more general case exists, however, in which the constitutent modules are structurally compatible yet chemically distinct. Under these circumstances, a series of structures with a range of chemical compositions can be produced by changes in the proportion of the two kinds of module. The resulting structures form what is known as a polysomatic series. Well known examples of polysomatic series include the biopyribole minerals (pyroxenes, amphiboles and sheet silicates), the humite group, pyroxenoids and phases in the $CeFCO_3$-$CaCO_3$ system. In principle there is an infinite number of structures that can be constructed from combinations of two modules. However, in practice it is found that certain stacking sequences occur much more frequently than others.

In this paper, a theory is outlined in which the observed equilibrium behaviour of many polytypic and polysomatic families is explained in terms of the Axial Next Nearest Neighbour Ising or ANNNI model. This statistical mechanical model was originally developed to describe magnetic systems. To relate the polytypic compounds to the ANNNI model it is proposed that the basic polytypic structual units can be mapped onto a magnetic spin variable. The interactions between units are then represented by a Hamiltonian with competing first and second neighbour interactions. The resulting ANNNI model provides a simple equilibrium description of polytypism as the temperature and interaction parameters are varied. In particular short-range couplings can lead to the existence of polytypes with very long period stacking sequences. Other important features of polytypism are also explained by this model: notably that only a specific set of polytypes are stable for a given compound, that reversible phase transitions can occur, and that polytypes with short stacking sequences occur most frequently. This approach can also be successfully used to explain the behaviour of polysomatic phases. As in the case of polytypes, there is in theory an infinite number of members of a given polysomatic family, but in fact, in any one series, only a limited number of phases are found. These systems are successfully modelled by mapping the two chemically distinct units which are involved in a polysomatic sequence onto magnetic spins with orientations 1 and 1 respectively. A Hamiltonian is then constructed which includes the interactions between the modules, together with a chemical potential term which controls the relative abundance of the two species. The resulting model is shown to be equivalent to the ANNNI model in a magnetic field.

PLATINUM GROUP MINERALS FROM TWO PGE-RICH LOCALITIES IN THE SHETLAND OPHIOLITE COMPLEX

PRICHARD, H.M., Dept of Earth Sciences, The Open University, Walton Hall, Milton Keynes, MK7 6AA, England. TARKIAN, M., Institute of Mineralogy and Petrology, Hamburg University, Federal Republic of Germany.

Chromite-rich rocks from the Shetland ophiolite complex contain a very varied assemblage of platinum group minerals (PGM's). The larger minerals have been quantitatively analysed and smaller (less than 5μ) and composite PGM's have been examined optically and qualitatively using single element scans. The samples were collected from two disused chromite quarries newly discovered to be unusually platinum group element (PGE)-rich, (Prichard et al. in press). They are situated in dunite lenses in mantle harzburgite which forms the lower part of the Caledonian ophiolite complex in the Shetland Islands, NE of Scotland.

The assemblage includes in order of abundance sperrylite, mertieite/stibiopalladinite, laurite, irarsite, hollingworthite, genkinite, hongshiite, native osmium, Rh-Sb-S, Ir-Sb-S, Rh-Ni-Sb, Pt-Pd-Au-Cu alloys, potarite and a Pd telluride with a new composition. The latter ten minerals are to the authors' knowledge new to ophiolite complexes. Included amongst these are the first descriptions of PGM's with Rh as the major PGE in ophiolite complexes. The PGM's occur within chromite grains, in the altered chromite rims and in the chloritised and serpentinised interstitial silicate matrix. The PGM's often form composite grains and detailed investigations of the textural relationships with other PGM and their host minerals enables a paragenetic sequence for the PGM's to be determined. The following paragraphs describe the different PGM's in order of their formatioin.

Laurite the most common mineral described from ophiolite complexes and present in Shetland,occurs as an early Os-rich phase (≤ 20% Os) entirely enclosed by chromite , as an Os- poor laurite associated with tiny (2 μ) inclusions of native Os and as a late pure, inclusion free, phase present in the silicate, interstitial to chromite grains. This last type of laurite is, in some cases, surrounded by pentlandite containing approximately 10% Ru.

In composite PGM grains, associated with silicate inclusions in the chromite, irarsite frequently surrounds laurite. Irarsite also contains antimony-rich inclusions for example, Rh-Ni-Sb, Pd antimonide and breithauptite (Ni Sb). Irarsite is commonly rimmed by hollingworthite and analyses show the existance of a solid solution series between the two pure end members IrAsS and RhAsS. Although only qualitatively analysed, pure Ir-Sb-S and Rh-Sb-S are also present, surrounded by irarsite and hollingworthite which may have superseded them with the substitution of As for Sb. This subsequent formation of irarsite indicates the introduction of a more arsenic-rich environment.

The Pd-bearing PGM's are only present in altered chromite rims and the interstitial silicate matrix. Mertieite/stibiopalladinite is the most abundant mineral. However, these two are difficult to distinguish because their composition and optical properties are rather similar. Potarite and the Pd bearing Au alloys are present as tiny (less than 5 μ) grains in the chromite rims. Two grains of Pd telluride occur in the silicate matrix. This is a complex intergrowth of $(Pd,Ni)_3 (Te,Sb,Bi)_2$ and $(Pd,Ni)_3 (Sb,Te,Bi)_2$ with substitution of Sb for Te. These are new compounds probably corresponding to the synthetic Pd_3Te_2.

The most common PGM is sperrylite which marks the introduction of Pt as the last PGE to become available for mineral formation. The sperrylite is restricted to the interstitial silicate matrix and it occasionally encloses hollingworthite and Pd antimonide. Genkinite, $(Pt, Pd, Ni)_4 Sb_3$ previously only described from Driekop, Onverwacht and Yubdo in Ethiopia, is present in two chromite-rich samples. Other Pt-bearing phases are present as alloys, for example, Pt-Pd-Cu (Pt>Pd>Cu).

The final phase of PGM formation recorded in the samples studied corresponds to a late stage hydrothermal alteration. Sperrylite is observed breaking down with the removal of As to form a net textured growth of hongshiite with Ni-Cu filled meshes associated with a cross-cutting silicate-filled vein. Pt-Pd-Au-Cu alloys associated with native copper may also be produced in this late reducing environment.

Hence the sequence of crystallisation of the PGE's was Os and Ru followed by Ir, Rh, Pd and Pt. Os/Ir alloys commonly described from ophiolite complexes are absent in these samples but the assemblage shows an extremely unusual diversity of PGM's compared with that so far described from ophiolite complexes.

Prichard, H.M., Neary, C.R. and Potts, P.J. (in press), Platinum Group Minerals in the Shetland Ophiolite. In the Metallogenesis of Basic and Ultrabasic Rocks, IMM Symposium volume, Edinburgh 1985, Ed.Gallagher, M.J., Ixer, R.A., Neary, C.R. and Prichard, H.M.

PART OF SCIENTIFIC HISTORY IN THE SCIENTIFIC TEACHING.

PROUVOST Jean, Dept. of Mineralogy, U.S.T.L. 59655 Villeneuve d'Ascq Cédex - FRANCE.

First is there such a part ? The problem claims our attention because within the commission on History and Teaching, somes are supportèrs of the separation of these two terms, while others think they are undissociable.

We will show it is not pedagogically convenient to make the history of a Science into a separate chapter because it would not be in that case properly teaching the discipline but bare history.

History must take a part in the very pedagogy by indicating to the student as naturally as possible on which grounds the discipline has arisen and by showing him its developments in a clear and logic manner up to the point of it newest attainments.

This means of transmitting knowledge appears to contrast with the axiomatic pedagogy which was attempted some years ago. By making one takes for granted concepts that are fairly long to acquire, time was saved. Conversely the mind was formed to conditioning. It is a rather comfortable state of mind driving to the use of paradigms instead of a concern for acute research (1).

For one who looks superficially at these questions the historical approach may be considered to be turned toward the past but do not forget that the one who said "most people are looking back and are going backwards" was not less than a founder of conservatory (films archives) (2).

Finally we will take for example of the contribution of the historic knowledge in mineralogy, with enlargement to connex sciences, the comparison of the Romé de l'Isle law (1772) with that of Proust (1801) and the Haüy law (1781) with that of Dalton (1808) (3).

REFERENCES :

(1) KUHN T.S. (1970) The structure of scientific revolution. The University of Chicago Press.

(2) LANGLOIS H. † - Founder of the French films archives - Oscar 1974 for his special devotion for films keeping (sponsors Groucho Marx and Gene Kelly).

(3) GAY R. (1958) - Cristallographie géométrique. Gauthier-Villars, Paris.

A STUDY OF THE DEVELOPMENT OF SHORT-RANGE Aℓ,Si ORDER IN ANNEALED CORDIERITE USING MAGIC ANGLE SPINNING NMR.

PUTNIS, A., Dept. of Earth Sciences, University of Cambridge, Cambridge, CB2 3EQ, England; FYFE, C. A., Dept. of Chemistry, University of Guelph, Ontario, Canada, NIG 2W1.

Silicon-29 magic angle spinning nuclear magnetic resonance (NMR) spectroscopy has been used to study the changes in local Si environment during Aℓ,Si ordering in synthetic cordierite, $Mg_2Aℓ_4Si_5O_{18}$. The basis of the method is the empirical observation that in framework structures, Si-29 chemical shifts depend on whether a given SiO_4 tetrahedron is linked to four, three, two, one or no $AℓO_4$ tetrahedra (Lippmaa et al. 1980, J. Am. Chem. Soc. 102, 4889-4893). These environments are denoted Si(nAℓ). Each environment is identified by a peak in the Si-29 NMR spectrum, the area under the peak being proportional to the populations of these environments in the sample.

In the most disordered cordierite, crystallized from a glass, eight distinct tetrahedral environments for silicon can be identified and assigned. These correspond to peaks for Si(4Aℓ), Si(3Aℓ), Si(2Aℓ) and Si(1Aℓ) in each of the two crystallographically distinct sites, T_1 and T_2 of the hexagonal polymorph. In fully ordered cordierite only two Si sites are distinguishable and these may be assigned as Si(4Aℓ) and Si(3Aℓ) in the T_1 and T_2 sites respecively. Changes in the Si site environments have been studied as a function of annealing time and temperature for the transformation from the "disordered" to the ordered form. The degree of partitioning of Si between T_1 and T_2 sites in the "disordered" form is in good agreement with the structure determination of Meagher and Gibbs (Can. Miner. 15, 43-49, 1977).

The Si site population data is used to calculate the number of Aℓ-O-Aℓ bonds per unit cell, and this order parameter varies linearly with the logarithm of the annealing time. The slope of this plot may be correlated with heat of solution data on similar samples (Carpenter et al. 1983, Geochim. Cosmochim. Acta 47, 899-906) to determine that the enthalpy change associated with a single Aℓ ⇌ Si interchange is 8 kcal/mole.

NMR data on samples annealed at a number of temperatures may be used to determine directly the activation energy for an Si-Aℓ interchange in the sample. Arrhenius plots from NMR data on cordierites annealed at 1185°C, 1290°C and 1400°C reveal that the mechanism and kinetics of ordering at 1185°C is different from that at 1400°C. Transmission electron microscopy also shows a different type of microstructure associated with the development of long range Aℓ,Si order at high temperatures.

The NMR data may be used to discriminate between various possible models for the short-range ordered cordierite, and this is currently the only technique that can provide quantitative data on these earliest stages of ordering. An ordering model derived from group theoretical constraints on possible Aℓ,Si distributions within hexagonal cordierite (McConnell, 1985, Reviews in Mineralogy, Vol. 14, M.S.A.) provides a good fit to the NMR data.

CHARACTERISTICS OF DEPOSITIONAL FERROMANGANESE MINERALS IN THE SOUTH CHINA SEA

Qiu Chuanzhu, Senior Researcher, Marine Sedimentation Section, South China Sea Institute of Oceanology, Academia Sinica, Guangzhou, People's Republic of China

Depositions of ferromanganese minerals are important components on the continental slope and on the central oceanic basin in the South China Sea. So many variety of shapes in the depositions of ferromanganese minerals have been found, such as little lump, microspheric, biologic (as foraminifera, radiolaria), membranous, nodular and crusted shape.

The observation of scanning electron microscope shows the little lump and membrane which are of microlite scaly texture. Microspheric and biodetritus are of microlite scaly texture or geltexture. Noudle and crust are of geltexture. According to the data of X-ray powder photography analysis and the curve of X-ray diffraction of ferromanganese minerals in South China Sea, the minerals components are 7Å and 10Å manganite, pyrolusite, leptonematite, adlerstein, lepidocokite and hydroadlerstein etc.

The highest retio of component of manganese in the microspheric texture is in the range of 43.82 - 60.94%. The second in the biologic, little lump and crusted texture are from 30.44 to 51.29%. The membranous texture is in the lowest range of 24 - 38.23%. It is enriched by titanium, copper, cohalt and nickel. The combination, shape and structure of the ferromanganese minerals, indicate that it is formed by the main compounds of ferromanganese oxides and hydroxides with geltexture and metageltexture, and small amounts of clay minerals, silt and micromicrobes in the South China Sea.

In the central oceanic basin of the South China Sea, mainly in the northern part the ferromanganese mineral is more concentrated than continental slope. Most of the ferromanganese minerals with nodular texture have been found in the continental slope, little lump, microspheric, biologic and membranous texture are located in the continental slope and in the soft mud of central oceanic basin. The ferromanganese minerals with crusted texture cover over the sea mountains which are made by basalt in the central oceanic basin of the South China Sea. Two kind of reason for formation of ferromanganese minerals were suggested: A. The genesis of gelatinous chemical sediment. B. The genesis of biochemistry. The major genesis of the deposition of ferromangese minerals in this regain is chemical sediment and the organisms canonly support the formation of ferromanganese sediment. This is the opinion presented by writer.

LATTICE DYNAMICS OF FORSTERITE, Mg_2SiO_4: PHONON DISPERSION RELATIONS, ELASTIC AND THERMODYNAMIC PROPERTIES

RAO, K. R., CHAPLOT, S. L., CHAUDHURY N., Nuclear Physics Division, Bhabha Atomic Research Centre, Trombay, Bombay 400 085, India; GHOSE, SUBRATA, Department of Geological Sciences, University of Washington, Seattle, WA 98195, U.S.A.; PRICE, D. L., Argonne National Laboratory, 9700 South Cass Ave., Argonne, IL 60439, U.S.A.; HASTINGS, J. M., Chemistry Department, Brookhaven National Laboratory, Upton, NY 11973, U.S.A.

Lattice dynamics of forsterite at room temperature has been studied by the external mode formalism assuming [SiO_4] to be a rigid group. Phonon dispersion relations along three high symmetry directions in the Brillouin zone were calculated using a realistic atom-atom potential consisting of Coulombic and short range terms. The parameters of the potential function, namely effective ionic charges and radii were refined from initial values taken from an x-ray determination by Fujino et al. (1980). The elastic constants determined from the slopes of the acoustic branches are in fair agreement with the measured values. The range of calculated optic modes covered the measured range of infra-red and Raman frequencies. The eigen frequencies and eigen vectors of the normal modes were used to calculate one phonon dynamic structure factors as a preliminary to inelastic neutron scattering experiments. The total and partial density states of the system corresponding to translational and rotational degrees of fredom corresponding to individual magnesium atoms and the rigid tetrahedral [SiO_4] groups were computed. The calculated low temperature specific heat within the range 0-100 K shows excellent agreement with measured values (Robie and Hemingway, 1982). The phonon density of states (weighted by neutron cross sections) was determined on a 45 gm powder sample by inelastic neutron scattering (INS) at IPNS, Argonne National Labortory, which shows good agreement with theoretical expectations. All the acoustic and a number of optic phonon branches measured by INS on a large single crystal at HFBR, Brookhaven National Laboratory agree with calculated frequencies within 10%. A full scale rigid-ion model calculation is currently in progress.

ELECTRON ENERGY-LOSS SPECTROSCOPY OF MN COMPOUNDS

RASK, James H., MINER, Barbara A., and BUSECK, Peter R., Departments of Geology and Chemistry, Arizona State University, Tempe, AZ 85287

Determination of the oxidation state of elements in small particles can be problematic. We have found that electron energy-loss spectroscopy (EELS) performed in a transmission electron microscope (TEM) is sensitive to changes in the formal oxidation state of Mn and can be used to approximately determine the oxidation state of Mn in small particles. We have obtained and analyzed EELS spectra of MnO, Mn_3O_4 (hausmannite), α-Mn_2O_3, γ-MnOOH (manganite), β-MnO_2 (pyrolusite), $BaFeMn_7O_{16}$ (hollandite), MnO_2 (ramsdellite), $MnCO_3$ (rhodochrosite), $MnSiO_3$ (rhodonite), $MnSO_4$, and Mn metal. Two regions of these energy-loss spectra are relevant: the high-loss region, which includes the Mn $L_{2,3}$ and oxygen K peaks, and the low-loss region.

The Mn $L_{2,3}$ feature represents energy losses incurred by excitations of electrons in Mn $2p_{1/2}$ and $2p_{3/2}$ states to unfilled molecular orbitals with metallic d-like character. This feature appears as two sharp peaks in the region from 635 to 675 eV. The intensity ratios between the L_3 and L_2 peaks increase from 2.1 for MnO_2 to 5.3 for MnO. The peaks shift slightly in energy with change in Mn oxidation state.

The oxygen K feature represents excitations from oxygen 1s states to molecular states with 2p character. In energy-loss spectra of MnO_2 this feature consists of two distinct peaks in the region from 525 to 565 eV. These peaks move closer with decreasing Mn oxidation state; they appear as a single, broad peak in spectra of MnO. The energy of the lower energy peak increases with decreasing Mn oxidation state. The different chemical environments of oxygen atoms in divalent Mn compounds ($MnSiO_3$, $MnSO_4$, $MnCO_3$, and MnO) result in distinctive oxygen K edges for each of these compounds.

There are several features in the low-loss region (0 to 100 eV) of these spectra that change with Mn oxidation state. The apex of the lowest energy peak varies from c. 9 eV in MnO_2 to c. 11 eV in MnO. This feature is absent in EELS spectra of Mn metal. The collective excitation peak is broad and centered on about 26 eV in MnO_2. It becomes sharper and moves to lower energies with decreases in Mn oxidation state. There is an unexplained shoulder at c. 32 eV that becomes more pronounced as the Mn oxidation state decreases; however, it is not present in spectra of Mn metal. Finally, the Mn $M_{2,3}$ excitation from Mn $3p_{1/2}$ and $3p_{3/2}$ states to molecular orbitals with 3d character is represented by a feature between 45 and 65 eV. In MnO_2 this feature appears as two peaks of approximately equal intensity. With decreases in Mn oxidation state, the lower energy peak decreases in intensity relative to the higher energy peak and both peaks shift to lower energies.

No differences have been detected among the energy-loss spectra of crystalline compounds whose Mn is exclusively tetravalent (pyrolusite, ramsdellite, and hollandite). Also, the Mn peaks in energy-loss spectra of compounds containing only divalent Mn (MnO, $MnSiO_3$, $MnSO_4$, $MnCO_3$) are indistinguishable. These observations suggest that EELS is not as sensitive to structural changes as it is to oxidation state.

With the information from the energy-loss spectra of these standards, we can determine the oxidation state of Mn in any phase observed in a TEM equipped with an EELS detector. This ability has been used in two interesting instances.

1) Todorokite, a mineral identified in marine Mn nodules, contains primarily Mn^{4+}. There is a question whether Mn^{2+} is a significant component of all todorokites. Low-loss regions in energy-loss spectra of terrestrial and nodule todorokites indicate Mn oxidation states slightly less than 4+.

2) Poorly crystalline layer manganates (buserite, birnessite, vernadite) are a major component of Mn nodules and are easily synthesized. Chemical analysis of these phases typically give stoichiometries of MnO_2 to $MnO_{1.9}$. However, EELS of synthetic and Mn-nodule layer manganates indicates lower Mn oxidation states. Further work is needed to determine why supposedly tetravalent layer manganates produce spectra characteristic of compounds containing divalent Mn.

This research was supported by NSF grants EAR 8408169 and OCE 8401107.

BIOTITE OXIDATION IN HYDROTHERMAL SYSTEMS : AN EXPERIMENTAL STUDY

REBBERT, Carolyn R., and HEWITT, David A., Dept. of Geological Sciences, Virginia Polytechnic Institute and State University, Blacksburg, VA 24061, USA

It has commonly been assumed that oxidation of ferruginous biotites proceeds by the oxybiotite substitution:

$$Fe^{2+} + OH^- = Fe^{3+} + O^{2-} + 0.5H_2$$

The role of this mechanism as an equilibrium process in hydrothermal systems was studied for two compositions, annite, $K_2Fe_6Al_2Si_6O_{20}(OH)_4$, and an annite with one Tschermak's substitution, $K_2Fe_5Al_4Si_5O_{20}(OH)_4$. The biotites were synthesized from oxide mixes and then annealed in Shaw-type bombs under controlled hydrogen fugacities. Run conditions were chosen near the maximum thermal stability limit and within the biotite stability field along lines of constant hydrogen fugacity. Run yields range from 93-96% for annite and 95-98% for the aluminous biotite. Sanidine was the major impurity identified along with minor amounts of fayalite or magnetite. The ferrous iron content of the run products was determined by the wet chemical technique developed by Whipple (1974). Total iron as FeO, as well as K_2O, Al_2O_3, and SiO_2 were obtained by means of the electron microprobe and the biotite compositions were found to be close to the stoichiometry of their ideal counterparts. Ferric iron was then determined by difference. Hydrogen contents were measured by heating the sample *in vacuo*, reducing all hydrogen species released, and determining the moles of H_2 volumetrically.

The hydrogen contents of the biotites are low(<3% H_2O) and do not vary with hydrogen fugacity for a given composition. The ratio of ferrous to total iron was found to be directly proportional to the hydrogen fugacity regardless of temperature. For hydrogen fugacities of 1 to 100 bars, this ratio varied from 0.76 to 0.90 for the annites and from 0.86 to 0.96 for the more aluminous biotites. The amounts of ferrous iron and the nearly constant difference in ferrous iron content between the two compositions is consistent with the proposed instability of a completely reduced annite due to structural misfit between the octahedral and tetrahedral layers (Hazen and Wones, 1972).

The annite stability field as presented by Eugster and Wones (1962) can thus be contoured with lines of constant ferrous iron content. The curves mimic the trends of the solid oxygen buffers which suggests that the mechanism of oxidation is similar for both. Moreover, when mineral formulas are calculated on the basis of 12 anions there is an excess of atoms in the octahedral sites. This excess varies directly with the hydrogen fugacity of the runs. Recalculation of the analyses on the basis of seven octahedral and tetrahedral cations results in a variable number of anions(11.6-12.0) that is positively correlated with the amount of ferrous iron. This, together with the lack of variation of the hydrogen contents in response to changing oxidation state, suggests that the oxybiotite substitution is not the controlling mechanism in hydrothermal biotite oxidation. The data support the following as an alternative reaction:

$$Fe^{2+} + 0.25O_2 = Fe^{3+} + 0.5O^{2-}$$

In this model the reduced biotites have anion vacancies that are filled as oxidation proceeds without changing the hydrogen content. The data also suggest that other anion vacancy producing reactions may be occurring in addition to the reaction above. Additional data are needed to substantiate or disprove the model, but if supportive it will lead to important changes in our ideas on the crystal chemistry of the micas.

REFERENCES:

Eugster, H.P. and Wones, D.R. (1962) Stability relations of the ferruginous biotite, annite. Journal of Petrology, 3, 82-125.

Hazen, R.M. and Wones, D.R. (1972) The effect of cation substitution on the physical properties of trioctahedral micas. American Mineralogist, 57, 103-129.

Whipple, E.R. (1974) A study of Wilson's determination of ferrous iron in silicates. Chemical Geology, 14, 223-238.

THE $I\bar{1}\Leftrightarrow P\bar{1}$ STRUCTURAL PHASE TRANSITION IN ANORTHITE: TEMPERATURE EVOLUTION OF THE SPONTANEOUS STRAIN

REDFERN, S.A.T.; SALJE, E., Dept. of Earth Sciences, University of Cambridge, Downing Street, Cambridge, CB2 3EQ, England.

The $I\bar{1}\Leftrightarrow P\bar{1}$ phase transition in anorthite ($T_c \approx 240°C$) has been studied both experimentally by X-ray diffraction and theoretically within the scope of Landau theory. The phase transition is reversible and continuous. It is described by a zone boundary instability of the $I\bar{1}$ phase. The temperature evolution of the lattice parameters results from the order parameter - strain coupling. The symmetry conditions of this coupling are different from those of Na and K feldspar, due to the fact that the spontaneous strain does not depend linearly on the order parameter. Furthermore, all components of the spontaneous strain, $x_1 \ldots x_6$, couple non-linearly with the order parameter, as opposed to albite, where linear coupling involves x_4 and x_6 only.

The experimental results suggest a tricritical behaviour in the case of pure anorthite from the Val Pasmeda locality. However, strong variations of the critical behaviour occur due to Al/Si disorder and Na-content in the samples. This result is in agreement with calorimetric observations of Wruck [1]. Earlier investigations of the temperature dependence of neutron scattering intensities by Adlhart *et al.* [2] can also be understood within the scheme of the present theory.

The Al/Si disorder was found to have a systematic influence on the strain parameters x_4 and x_6, as indicated by linear coupling theory (analogous to the behaviour of albite). It is therefore possible to distinguish between the strain contributions due to the structural phase transition $I\bar{1}\Leftrightarrow P\bar{1}$ and the 'parasitic' Al/Si disorder, which acts as a secondary order parameter.

[1] B.Wruck, Ph.D. Thesis, University of Hannover (1986).
[2] W.Adlhart, F.Frey and H.Jagodzinski, Acta Cryst. A36, 450-460 (1980).

MAGNETISM OF PYROXENES

REGNARD, J.R., DRF/Service de Physique/MDIH, CEN Grenoble, 85 X - F38041 Grenoble cedex ; WIEDENMANN A., DRF/Service de Physique/MDN, CEN Grenoble, 85 X - F38041 Grenoble cedex ; FILLION G., Laboratoire Louis Néel, CNRS, 166X - F38042 Grenoble cedex

Ferrous chain silicates with composition $(Fe_xM_{1-x})_2Si_2O_6$ (with M = Mg or Ca) belonging to the pyroxene group crystallise either in an orthorhombic structure (space group Pbca) or in a monoclinic structure (space group C2/c) according to the nature of the cation M and the iron concentration x. In orthopyroxenes, the divalent cations Fe^{2+} and M^{2+} occupy two different octahedral sites M1 and M2 (M2 has the more distorted oxygen octahedron). The M1 and M2 octahedra share edges and form infinite ribbons parallel to the c axis. These ribbons are made up of a central zig-zag chain of M1 sites with isolated M2 sites on the outside, and they are separated by corner-sharing chains of SiO_4 tetrahedra. The cation structure, specifically the large difference in the Fe^{2+} - Fe^{2+} distances within a ribbon ($\approx$ 3.1 Å) and between ribbons ($\approx$ 4.9 Å) is the reason for the quasi one-dimensional magnetic behavior of the ferrous ions.

Measurements of susceptibility and magnetization have been carried out on a synthetic sample $FeSiO_3$ and on a natural sample $Fe_{0.87}Mg_{0.13}SiO_3$ [1]. The inverse susceptibility of both samples follows a Curie-Weiss law above 200 K. Values of the paramagnetic Curie temperature θ_p are 27 K and 34 K for the samples with x = 1 and x = 0.87 respectively, indicating that exchange interactions are predominantly positive. The antiferromagnetic ordering temperature T_N is 38 K for x = 1 and 26 K for x = 0.87. The susceptibility of $Fe_{0.87}Mg_{0.13}SiO_3$ measured along the three axes of the orthorhombic cell reflects the strong anisotropy which results from the crystal field splitting of the ^5D level of Fe^{2+} and shows that the b axis is the easy magnetization direction. Magnetization measured as a function of applied field (up to 15 T) shows an inflection point at a critical field B_c of 5 T and 3.5 T for x = 1 and x = 0.87 respectively, as well as some hysteresis. This behaviour is characteristic of a metamagnetic transition from an antiferromagnetic to a ferromagnetic state [1].

Neutron diffraction measurements indicate that the same type of collinear antiferromagnetic order sets in at T_N for both the natural and synthetic samples [2]. It is characterized by a vector k = [010] and by the alignment of moments $\vec{m}_1$ and $\vec{m}_2$ on the two sites along the b axis. From the analysis of the diagrams, the couplings between

MAGNETISM OF PYROXENES
REGNARD, J.R., et al.

the 16 Bravais lattices have been determined, as well as the moments on the two sites, $m_1 = 4.25 \pm 0.15 \mu_B$ and $m_2 = 3.25 \pm 0.15 \mu_B$.
It is found that, in agreement with magnetic measurements, the moments within each ribbon are aligned parallel among themselves and lie along the b axis whereas the moments of the adjacent ribbons are aligned antiparallel, giving rise to the overall antiferromagnetic structure.

The Mössbauer spectrum of $FeSiO_3$ taken at 4.2 K is fitted by two ferrous magnetic hyperfine patterns with different hyperfine fields [3]; the one with B_{hf} = 6.9 T is attributed to M1 sites and the other with B_{hf} = 31.8 T to M2 sites. The 4.2 K Mössbauer spectrum for $Fe_{0.87}Mg_{0.13}SiO_3$ is more complex ; there is line broadening due to a distribution of hyperfine fields which results from the different configurations of Fe^{2+} and Mg^{2+} nearest neighbours surrounding the $^{57}Fe^{2+}$ probe in M1 or M2 sites [1].

The magnetic properties of monoclinic $CaFe_{0.8}Mg_{0.2}Si_2O_6$ (Θ_p = 21 K, T_N = 23 K, B_c = 4 T) are similar to those observed above for the orthorhombic pyroxenes, but neutron diffraction indicates that the iron moments within a zig-zag chain of M1 sites are aligned among themselves and lie in the a-c plane along a direction which makes an angle of 45° with a [2].

All these results on pyroxenes containing only ferrous ion indicate (1) that magnetic ordering takes place only at low temperature (T_N < 45 K) in these materials, in contrast to iron oxides (2) there is fairly strong ferromagnetic coupling of moments within each ribbon or chain, and a weaker antiferromagnetic coupling between adjacent ribbons or chains. The ratio of magnetic exchange integrals between and within ribbons or chains, $J'/J \approx 0.2$ reflects the quasi one - dimensional character of the magnetic interactions in ferrous pyroxenes and (3) the magnetic properties depend sensitively on the concentration of iron, the nature of the other cations present in M1 and M2 sites, the cation distribution and the distances between magnetic ribbons or chains.

[1] A. Wiedenmann, J.R. Regnard, G. Fillion , S.S. Hafner, to be published in J. Phys. C (1986).
[2] A. Wiedenmann and J.R. Regnard, Solid State Commun. 57, 499-504 (1986).
[3] J.R. Regnard, R. Guillen, A. Wiedenmann, G. Fillion, S. Hafner and K. Langer, to be published in Hyperfine Interactions (1986).

Solubility and electrokinetic properties of bassetite.

REMAUT, G., and VOCHTEN, R., Laboratory of Physical and Chemical mineralogy.
State University Antwerpen, Middelheimlaan 1,
2020 Antwerpen, Belgium, Europe.

The variation of the zeta potential as function of the ph of the suspension is correlated with the solubility of bassetite.
The solubility of oxidized bassetite is much lower than for non oxidized bassetite.
The kinetic of the oxidation of bassetite is reflected in the variation of the zeta potential with time.
Regarding the zeta potential and its relation with the pH, we may conclude that bassetite oxidizes very easily in an aqueous medium, even in the absence of oxidants.
From surface conductivity measurements in KCl, we conclude that the surface structure of bassetite remains unaltered upon oxidation.
A very simple model is proposed for the effect of the pH on the zeta potential both for bassetite and its oxidized phase.

X-RAY SPECTROMETRY INDUCED BY ELECTRON (EPMA) AND PROTON BOMBARDMENT (MICRO-PIXE) APPLIED TO TRACE ELEMENT ANALYSIS IN SULFIDES: PROBLEMS AND PROSPECTS.

REMOND,G.,Bureau de Recherches Géologiques et Minières,Orléans, FRANCE;CESBRON,F.,Université P. et M. Curie,Paris, FRANCE;CAMPBELL,I.L.,Dept. of Physics,Guelph,Ontario N1G 2W1,CANADA;TRAXEL, K.,Physikalisches Institut der Universität,Heidelberg,FRG;CABRI, L.J.,Canmet,Ottawa,Ontario K1A 0G1,CANADA.

EPMA and micro-PIXE complementarity for minor and trace element localization in sulfides has been evaluated. Chalcopyrite and sphalerite from various deposits have been analyzed emphasizing on Ag, Cd, In, Se, Ga, Ge and Hg. Reproducibility, statistical precision and accuracy are discussed.

Chalcopyrite. For Ag-bearing chalcopyrites, an excellent agreement between data was obtained by comparing successively EPMA analyses carried out by different laboratories and micro-PIXE data from two independent analytical runs. For micro-PIXE, the statistical detection limit is improved by a factor of ≈10 as compared to the EPMA limit (300 ppm for the experimental conditions).

The accuracy of EPMA data is influenced by the presence of surface contamination thin films containing elements assumed to be present as bulk impurities. The respective sensitivity of EPMA and micro-PIXE to surface thin films has been evaluated in studying polished sulfide minerals coated with ≈10 and 20 nm thick silver films. Comparisons between experimental and calculated data showed that thin films of a few tenths of nm led to a X-ray intensity, measured by means of the EPMA, equivalent to that which should be measured in the case of a ≈400 ppm Ag concentration in volume. By the use of micro-PIXE, the measured intensity should be equivalent to an apparent Ag concentration of ≈10 to 20 ppm.

Thus, although micro-PIXE analysis is also sensitive to the presence of surface films, their influence on the reliability of micro-PIXE data may be neglected for concentrations above a few hundreds of ppm.

Sphalerite. Micro-PIXE analysis of (Zn,Fe)S matrices are much more complex than for chalcopyrite because of large variations in composition. Depending upon the energy of the analyzed X-ray photons, the X-ray intensities and X-ray yields may be more or less influenced by Fe concentration variations and, in a less extent, by the presence of other impurities such as Cu, Ga... We used concentration data derived from EPMA analyses of the major and minor constituents to process the micro-PIXE data characteristic of the trace elements of interest.

Experimental and calculated data showed that Cd Kα, Ag Kα, In Kα, Hg Kα X-ray emission may be processed by using an average composition of the (Zn,Fe)S matrix whereas data manipulation for Ge Kα and more particularly Ga Kα required an accurate knowledge of the matrix composition.

For Cd analysis with concentrations ranging from ≈1000 to 7000 ppm, the percent difference between EPMA and micro-PIXE was ≈25 %. A percent difference of about 25 % was also obtained in the case of Ga (0.1 to 1.3 %) with Cu concentrations ranging from 0.2 to 2 % and thus creating a large matrix effect for the Ga Kα X-ray emission.

The comparison of EPMA and micro-PIXE data demonstrated the credibility of the models used for data processing with the micro-PIXE and the validity of both techniques for quantitative analysis of a few hundreds to thousands of ppm.

Some trace elements such as In, Se, Hg were detected by means of the micro-PIXE but were not detected by EPMA analysis. However, owing to instrumental factors, some minor elements (Fe, Cu) in the sphalerite specimens were not analyzed by the use of the micro-PIXE. The comparisons demonstrated the complementarity of EPMA and micro-PIXE for studying the localization of trace elements in sulfide minerals.

•X-RAY STUDIES OF COARSE-GRAINED KAOLINITE FROM TONSTEIN IN PU-BEI AREA, SHAANXI, CHINA

REN Da-Wei, CHEN Yiang-Jie, Department of Geology, Xi'an Mining Institute, Xi'an, Shaanxi; and **HE Rui-Lin,** Laboratory of Shaanxi Bureau of Geology and Mineral Resources, Xi'an, Shaanxi, The People's Republic of China

Coarse-grained kaolinite crystals found in Carboniferous-Permian coal-bearing measures in Pu-Bei area, Shaanxi Province, China, were studied using single crystal X-ray diffraction methods.

Oscillation photographs of *a*-, *b*- and *c*- axis and (*0kl*), (*1kl*), (*h0l*) and (*hk0*) Weissenburg photographs showed that the kaolinite studied is pseudo-monoclinic with cell parameters a = 5.144(3) Å, b = 8.949(5) Å, c = 7.551(5) Å, $\alpha = 90°$, $\beta = 104°30'$ and $\gamma = 90°$. The space group was determined to be C1.

The lines on oscillation photographs are similar to those characteristic of polycrystals and diffraction spots on both oscillation and Weissenburg photographs show bar-like streaks, indicating the structural irregularities in kaolinite. As the triclinic angle of kaolinite changes from 91°5′ with a partially-order structure to 90° with a disordered structure, its structure becomes pseudo-monoclinic. The asymmetrical features of diffraction spots on oscillation photographs were interpreted as the results of the disordered collection-layer state along the *b*-axis. It was concluded that the kaolinite studied is *b*-axis disordered and less well crystallized. Apparently, the crystals are not pure kaolinite, but polytype modifications of kaolinite-dickite with kaolinite being the predominant phase.

This kind of kaolinite-dickite polytype occurring in tonsteins of coal beds can be used as an ideal geothermometer for coal metamorphism.

•TELLUROBISMUTHINIDES FROM PANGUSHAN, CHINA

REN Ying-Chen, Geological Academy Ministry of Metallurgical Industry, 42 Youyi Road, Tianjin, People's Republic of China

In a study of wolfrobismuth vein deposits at Pangushan, a group of tellurobismuthinides was identified. They are unusually good in both size and crystallinity and can be separated from the host rocks without much difficulty. Therefore, a mineralogical study on their physical and chemical properties was made.

1. *Joesite.* Joseite is the most abundant tellurobismuthinide in the vein deposits. From chemical compositions analyzed, based on a formula of $Bi_4(Te,S)_3$, they are joesite A $Bi_4TeS_{1.8}\square_{0.2}$ (its chemical composition is 77.78% Bi, 2.49% Pb, 12.50% Te, 5.81% S.) Joseite A $Bi_4Te_{0.75}\square_{0.24}S_2$ (82.04% Bi, 0.61% Pb. 9.33% Te, 6.59% S) and joseite B $Bi_4Te_{1.8}\square_{0.2}S$ (75.25% Bi, 0.024% Pb, 20.92% Te, 3.61% S).

2. *Ingodite.* Ingodite was first reported in USSR by E.N. Zavyalov (1981, 1984); it has a composition close to Bi_2TeS. In the occurrence at Pangushan, ingodite has an approximate formula of $Bi_2Te_{2.1}S_{1.9}$ (its composition is 71.75% Bi, 22.79% Te, 1.06% Pb, 5.11% S). Major X-ray powder diffraction lines deduced from samples of both joseite B and ingodite are 3.10(10), 2.28(6), 2.14(6), and 1.98(4) Å.

4. *Tetradymite.* Tetradymite found at Pangushan has grain size up to 1 cm. Its chemical composition is 60.69% Bi, 2.80% Pb, 32.16% Te, 5.23% S, and gives an approximate formula of $Be_2Te_{1.8}S_{1.1}$ close to theoretical Bi_2Te_2S.

4. *Unnamed tellurobismuthinide.* This mineral occurs in close association with joseite at Pangushan. It has a hardness of 62 kg/mm^2(VHN) and a density of 8.037 g/cm^3. In polished section, it is gray with a slight yellow-brownish tinge. Chemical analysis of this mineral shows that it has 74.52% Bi, 12.92% Te, and 6.65% S. Its formula is $Be_3Te_{1.26}S_{1.74}$. Major X-ray powder diffraction lines are 3.08(10), 2.24(8), 1.88(6), 1.66(6), 1.41(5), 1.35(5), and 1.212(9) Å. Zarigalov (1982) reported a $Bi_3(Te,S)_3$ phase, sulphosumoite, with a Te/S ratio of 2/1 in contrast to this unnamed mineral with a Te/S ratio of approximately one-half. An examination of X-ray powder data shows that sulphosumoite matches better with joseite B, whereas the unnamed mineral and joseite A are closer. Except for tetradymite, this group of tellurobismuthinides represents the metal excess and non-stoichiometric type. Tetradymite is enriched in the upper part of this deposit. Joseite B, on the other hand, is concentrated in the lower part. Joseite A and ingodite occur at the middle level. On the basis of textural relationships, the sequence of formation can be analyzed as $Bi_3Te_{1+x}S_{2-x}$ → tetradymite → joseite A → ingodite.

AN OCCURRENCE OF MOOIHOEKITE AND HAYCOCKITE IN THE TOWNLANDS IRON-RICH ULTRAMAFIC PIPE, RUSTENBURG, SOUTH AFRICA.

REYNOLDS, I.M. and PHILLIPS, D., Department of Geology, Rhodes University, Grahamstown, 6140, South Africa.

The Townlands iron-rich ultramafic pegmatite is a large pipe-like body that transgresses the noritic layered sequence of the upper critical zone of the Bushveld Complex. Surface exposures are very poor, but underground development and borehole intersections have shown that it consists essentially of a dunitic core (olivine Fo_{30}-Fo_{52}) Surrounded by a wherlitic marginal zone (clinopyroxene $Wo_{45}En_{30}Fs_{25}$-$Wo_{45}En_{37}Fs_{18}$). Accessory phases include ilmenite, Ti-magnetite, apatite, amphibole, chlorite-group minerals, biotite, ilvaite and a variety of sulphide phases.

Sulphide minerals are ubiquitous minor accessory phases that are disseminated throughout the body, but rarely exceed one percent by volume. Primary sulphide mineral assemblages consist predominantly of troilite with subordinate pentlandite, chalcopyrite and cubanite, and are confined to the marginal areas of the pipe. The core of the pipe is extensively fractured and is cut by numerous late-stage veinlets consisting of serpentine and minor magnetite. All minerals of the primary sulphide assemblage show varying degrees of alteration and replacement by Mooihoekite and Haycockite which seems to have been accomplished by the introduction of Cu-bearing solutions. Evidence for these solutions is afforded by the presence of native copper in the centres of late-stage serpentine-filled veinlets. The textural features and relationships involved are illustrated. Simplified equations for the replacement can be written as follows:

a) Troilite: (i) $16FeS + 9Cu^{2+} \longrightarrow Cu_9Fe_9S_{16} + 7Fe^{2+}$

(ii) $8FeS + 4Cu^{2+} \longrightarrow Cu_4Fe_5S_8 + 3Fe^{2+}$

b) Pentlandite:

(i) $2(Fe,Ni)_9S_8 + 9Cu^{2+} \longrightarrow Cu_9Fe_9S_{16} + 9Fe^{2+} + 18Ni^{2+}$

(ii) $(Fe,Ni)_9 + 4Cu^{2+} \longrightarrow Cu_4Fe_5S_8 + 4Fe^{2+} + 9Ni^{2+}$

c) Cubanite: (iii) $6CuFe_2S_3 + 3Cu^{2+} \longrightarrow Cu_9Fe_9S_{16} + 2FeS + Fe^{2+}$

$3CuFe_2S_3 + Cu^{2+} \longrightarrow Cu_4Fe_5S_8 + FeS$

d) Chalcopyrite: (i) $8CuFeS_2 + Cu^{2+} + Fe^{2+} \longrightarrow Cu_9Fe_9S_{16}$

$4CuFeS_2 + Fe^{2+} \longrightarrow Cu_4Fe_5S_8$

The Fe^{2+} released during the replacement of troilite may be reprecipitated to form magnetite that is always associated with the mooihoekite and haycockite. Pentalandite is a minor component of the sulphide assemblage and any Ni^{2+} that is released may be incorporated in the associated magnetite. The FeS components that are released during the replacement of cubanite may be reprecipitated as mackinawite which is also found intergrown with mooihoekite and haycockite. The Cu required for the alteration of the sulphide assemblage was probably introduced by the late-stage or deuteric hydrothermal solutions that caused extensive serpentinization of the dunitic core of the pipe.

CALCULATED X-RAY DIFFRACTION PATTERNS OF MIXED LAYER ILLITE-SMECTITES INCORPORATING THE EFFECTS OF DIFFERENT REACTION MECHANISMS

REYNOLDS, R.C., Dept. of Earth Sciences, Dartmouth College, Hanover, NH 03755

The mechanism of formation of clay-sized mica (illite) in sedimentary rocks is controversial. Illite may form, wholly or in part, by (1) comminution of coarse-grained muscovite, (2) crystal growth, either at the expense of pre-existing smectite, or *de novo*, and (3) layer-by-layer replacement of smectite. Studies of the shapes of the peaks of the basal diffraction series can be used to evaluate the likely importances of these mechanisms.

Basal intensities have been calculated as a continuous function of diffraction angle by means of computer methods that use the Laue interference function expressed as a Fourier series. These are compared to experimental profiles.

Diffraction patterns of illite show broad peaks, consistent with coherent scattering domain sizes of 120 to 140Å. Line shape indicates the presence of a range of domain sizes which may be a distribution of domain sizes in large crystals or a range of particle sizes whose mean is small. Ergun, in a series of papers, has shown that defect broadening, caused by the statistical distribution of stacking defects along the Z direction, produces a special kind of particle size distribution that leads to line shapes with Cauchy or Lorentzian forms. Experimental profiles fit this model, suggesting that illite crystals are larger than supposed, but are broken into smaller diffracting units by defects whose mean separation is 60 to 100Å. The results are probably inconsistent with an origin that involves only the cleavage of coarse grained muscovite.

Fine particle sizes or small domain units produce diffraction line shapes that are sensitive to the structure and composition of the ends of the diffracting arrays. Intuition suggests that illite crystallites formed by the cleavage of large particles, or perhaps by layer-by-layer transformation, should terminate on the oxygen plane of the tetrahedral sheet. Termination on a partial octahedral sheet may imply crystal growth effects. Modeling of the illite diffraction pattern, particularly the 001, discloses that agreement between calculated and observed line shapes requires the incorporation of about half of the terminations of each kind. These findings, together with the strong component of defect broadening observed, lead to the conclusion that most illites are not derived from detrital muscovite, and that the mode of formation may have involved some *de novo* crystal growth.

GMELINITE GEOCHEMISTRY AND PHASE RELATIONSHIPS

RICE,S.B. and VAUGHAN,D.E.W.,Corporate Research Science Laboratory Exxon Research and Engineering Co., Annandale, NJ 08801

A geochemical investigation of a suite of natural gmelinites revealed a wide range of Na/Ca ratios and a fairly narrow range of Si/Al ratios, consistent with previous work (Passaglia et al 1978). The structural similarity with chabazite makes intergrowth possible, and this has often been proposed to explain the poor sorption properties of gmelinite (Barrer, 1944; Kokotailo and Lawton, 1964). Chabazite was identified by X-ray diffraction as a coexisting phase in several specimens and could be observed macroscopically in most cases. Direct imaging by high resolution electron microscopy has thus far failed to reveal chabazite intergrowths in analyzed gmelinite crystals.

A suite of basaltic vug gmelinites was obtained primarily from the Smithsonian Institution. Locations included Springfield, OR(1); Flinders Is., Australia(2); Secaucus, NJ(3); Bergen Hill, NJ(4); W. Paterson, NJ(5); Prospect Park, NJ(6); Antrim, N. Ireland(7); Vicenza, Italy(8); and two from Nova Scotia, Canada(9 and 10). Phase identifications were made initially by Debye-Scherrer techniques. Gmelinites were further analyzed by electron probe (EDS) and HREM.

With some exceptions, microprobe Si/Al ratios were closely clustered around 2.2-2.3. ^{29}Si-MAS NMR of #10 gave a clean 4 peak spectrum indicating an Si/Al = 2.39, with Si(3Al) = -91.2; Si(2Al) = -97.2, Si(Al) = -102.5 and Si(0Al) = -108.1 ppm vs. TMS. The Springfield specimen was unique in that there was an obvious intergrowth in the probe cross-section, consisting of a sodic lath composition and a more calcic blade composition. This may be a case of chabazite (calcic) intergrown or overgrown on a relatively large scale (2-10um) with gmelinite (sodic). In addition to chabazite, major impurity phases were quartz and bakerite. Figure 1 illustrates relative Na, Ca, and K contents of analyzed spots from representative crystals. The fresh specimens span the Na-Ca join, and several display significant variation from one spot to another within the same crystal. This may be caused by sequential growth (zoning) of the same phase from a changing crystallization medium (a well known phenomenon in both natural and synthetic zeolites), or phase intergrowths that show different cation selectivities which occur on a scale smaller than the electron probe's excitation volume (1-2um^3). One specimen was unique in containing an appreciable amount of K cation (10), but lattice imaging results show it to be the most defect-free specimen among those we have examined.

The spread of values toward the K apex represents edge pieces separated from the bulk crystals by fractures. The compositions and morphologies of these edge pieces strongly suggest the substitution of K for Na and Ca in a post-crystallization alteration or exchange process.

Gmelinite and chabazite are members of a family of zeolites related by stacking of sheets of corner-linked tetrahedra. Fig. 2 shows the c-axis projections. Gmelinite has AABB stacking (Hex., c=10Å); chabazite has AABBCC stacking (Rhomb, c=15Å). If enough chabazite-like stacking faults occurred, there would be a perturbation in c* and the actual intergrowths ought to be directly observable in a correctly oriented crystal. Preliminary HREM data obtained for Nova Scotia(10), Antrim, and Springfield has uncovered only very minor defects, and these are attributable to dislocations rather than stacking faults.

We wish to thank the Smithsonian Institution, Washington, D.C., for the loan of 8 gmelinites, and M. H. Sherwood for assitance in sample preparation.

Barrer, R.M., 1944, Trans. Faraday Soc. 40, 555-564.
Kokotailo, G.T. and Lawton, S.L., 1964. Nature 203, 621-623.
Passaglia, E., Pongiluppi, D., and Vezzalini, G., 1978. N. Jahr. Miner 1978, 310-324.

Figure 1

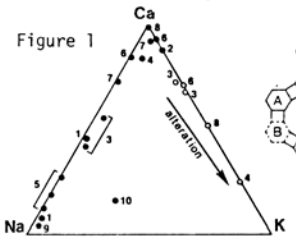

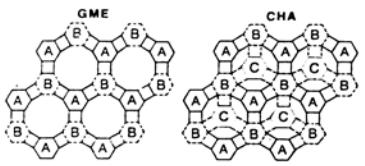

Figure 2

•THERMOCHEMICAL ASPECTS OF THE RHEOLOGY OF VISCOUS LIQUIDS

RICHET, P., Institut de Physique du Globe, 4 Place Jussieu, 75005 Paris, France

A major feature of the rheology of silicates and other viscous liquids is the non-Arrhenian behavior, i.e., a non-linear variation of the log viscosity vs. reciprocal temperature. These deviations from Arrhenius law are generally large and depend specifically on the composition of the liquid, increasing with decreasing SiO_2 contents. The theory of relaxation processes of Adam and Gibbs (1965) provides a quantitative explanation for these facts through a simple relationship between the viscosity and the configurational entropy. To use this theory, one needs to know accurately the configurational entropy of the liquid, which requires extensive thermochemical measurements on the liquid, glassy, and crystalline phases of the material considered. In turn, however, the validity of the theory would imply that simple, rapid viscosity measurements could be used to determine the configurational entropies of liquids and, particularly, the entropies of mixing in multicomponent systems. The available thermochemical and rheological data for silicates will be reviewed from this point of view, and new data will be presented for aluminosilicate and germanate compositions.

OBLIQUE - TEXTURE X - RAY PHOTOGRAPHS - A NEW MODIFICATION OF THE POWDER METHOD

RIEDER, M., Inst. Geol. Sciences, Charles University, Albertov 6, 12843 Praha 2, Czechoslovakia; WEISS, Z., Coal Research Institute, 71607 Ostrava - Radvanice, Czechoslovakia

In diffraction experiments on materials prone to preferred orientation, intensities are distorted depending on the orientation of diffracting planes to the cleavage. One way of handling the problem is to suppress or eliminate preferred orientation, the other is to accentuate it and take advantage of its predictable effects. Closely related to its electron counterpart (Zvyagin, 1967), the oblique - texture X - ray technique is based on the second approach.

For phases with one system of cleavage planes, the reciprocal lattice corresponding to a mount with perfect preferred orientation appears as a system of coaxial rings whose axis is the normal to the cleavage. Coordinates of rings follow from coordinates of reciprocal - lattice nodes and so do positions of diffraction spots on film. To model various tilts of the mount and different film arrangements program OBLITEXT (FORTRAN IV) can be used (Fig.1). The theory is analogous to that of the single - crystal rotation method except that the axis is a reciprocal-lattice vector, not direct - lattice.

Oblique - texture X - ray patterns can be taken on any instrument permitting a controlled tilting of the mount, such as precession or Weissenberg. Unlike electron diffraction, no evacuation is needed (hence no danger to hydrated phases). Good oblique - texture X - ray patterns are obtained only on samples with very good preferred orientation. The less perfect the preferred orientation, the more smeared the diffraction spots become. However, compared to electron diffraction, the smearing runs more perpendicular to the "ellipses", thus generally permitting a better separation of spots (Fig.1).

The technique permits an easy recording of diffraction intensities of $hk\underline{\ell}$ families that are very difficult to obtain by other powder techniques or cannot be recorded at all. An obvious application is the investigation of layer silicates (polytypism), but other uses are under study.

Zvyagin, B.B.(1967) Electron - Diffraction Analysis of Clay Mineral Structures. Plenum Press, New York.

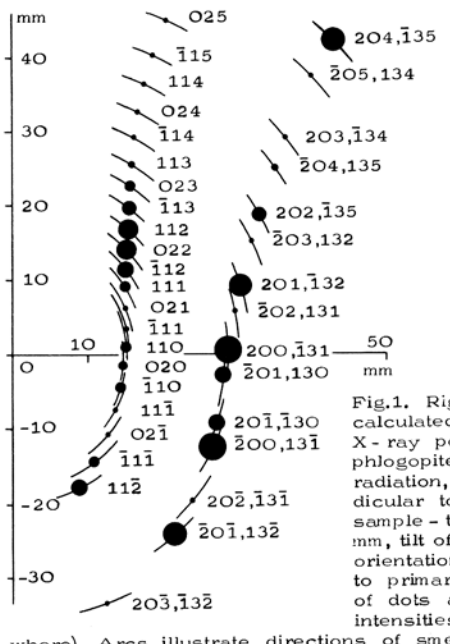

Fig.1. Right half of a calculated oblique - texture X - ray powder pattern of phlogopite - 1M : CuK alpha radiation, flat film perpendicular to primary beam, sample - to - film distance 60 mm, tilt of axis of preferred orientation relative to a normal to primary beam 35°. Sizes of dots are proportional to intensities (obtained elsewhere). Arcs illustrate directions of smearing of spots due to imperfectness of preferred orientation in the mount.

TRACE ELEMENT MICROANALYSIS BY SYNCHROTRON X-RAY FLUORESCENCE

RIVERS, M.L., SUTTON, S.R., SMITH, J.V., Dept. of the Geophysical Sciences, University of Chicago, Chicago, IL 60637, USA; JONES, K.W., Dept. of Applied Science, Brookhaven National Laboratory, Upton, NY 11973, USA

Synchrotron radiation has a number of features which make it an attractive x-ray source for trace element microanalysis:

a) The radiation is naturally collimated in the vertical direction, enabling the use of small spot sizes.
b) The source is very bright, and can thus be focussed to yield even smaller spot sizes.
c) The spectrum is continuous, so one can choose the optimum excitation energy for a particular element.
d) The radiation is highly polarized in the plane of the electron orbit, which minimizes backgrounds from scattered radiation.

SXRF is also non-destructive, has a low energy deposition for a given sensitivity, and can be readily quantified. Some potential problems include the rather large beam penetration depths and interferences from diffraction when using white light.

We have made measurements at the NSLS using an unfocussed beam, filtered white radiation and a Si(Li) detector. With spot sizes of 30-50μm and 5 minute collection times, the minimum detectable limits for silicate glasses are 300-500 ppb (Fig. 1) and 3-5 ppm for sulfide minerals (Fig. 2) [1].

In a study of the trace element composition of common sulfide minerals from ore deposits, we have found 150-200 ppm Pd in pentlandites from Merensky Reef and Stillwater, and < 5 ppm in those from Sudbury[1]. Both pyrrhotite and pentlandite from Merensky also contain detectable Ru (10-25 ppm). These results compare well with previous analyses using micro-PIXE[2].

We are studying the trace element chemistry of cosmic particles extracted magnetically from deep sea sediments [3] or mechanically from melt lakes of the Greenland Icecap [4]. Preliminary results on the Greenland particles (Fig. 3) show that 1) Ni, Zn, Cu, Ga, Ge, Pb, Se and Br are detected with minimum detectable limts of about 10 ppm, 2) Composition varies dramatically, especially in Ni content, 3) High concentrations of Pb (tens of ppm) are detected in some particles, presumably from terrestrial contamination.

A fluorescence microprobe which uses an 8:1 grazing incidence ellipsoidal mirror to focus the x-ray beam is being constructed at BNL. This device will produce a much greater photon flux at the target, and permit the use of monochromators to select a particular excitation energy. Spot sizes will range from 1-100μm with use of appropriate pinholes. Detectors will include Si(Li) and curved crystal spectrometers. Calculated sensitivities for this device are 10-100 ppb for elements from S to Pb in a basaltic matrix.

Fig. 1 NBS standard glass 612

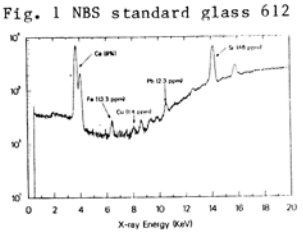

Fig. 2 Synthetic Pyrrhotite

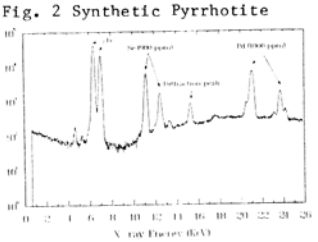

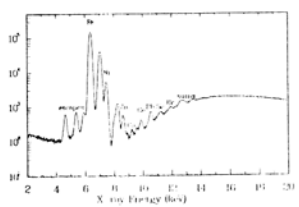

Fig. 3 Greenland particle

[1] Cabri,L., Rivers,M.L., Smith,J.V., Jones,K.W. (1985) Eos 66, 1150.
[2] Cabri,L., Blank,H., El Goresy,A., LaFlamme,J.H.G., Nobiling,R., Sizgoric,M., Traxel,K. Canadian Mineralogist, 22, 521-542.
[3] Brownlee,D.E., (1985) Ann. Rev. Earth Planet. Sci. 13, 147-173.
[4] Maurette,M., and Hammer,C. (1985) Le Recherche 168, 851.
[5] Sutton,S.R., Delaney,J., Smith,J.V., and Prinz,M. (1986) Lunar Planet Sci XVII, 853-854.

GENERALIZATION OF THE CORRELATIONS BETWEEN HYDROXYL STRETCHING FREQUENCIES AND COMPOSITION OF MICAS : A SINGLE MODEL FOR BIOTITES, MUSCOVITE, PHENGITES AND LEPIDOLITES.

ROBERT J.-L.,CRSCM-CNRS,1A rue de la Férollerie,45071 Orléans Cedex 2,France.

A systematic measurement of ν_{OH} of synthetic mica solid solutions has been performed in order to establish correlations between OH stretching frequencies and mica compositions.

Biotites belong to the series TMM (tetrasilicic magnesian mica) : $K_2(Mg_5\square)Si_8O_{20}(OH)_4$ - phlogopite : $K_2Mg_6(Si_6Al_2)O_{20}(OH)_4$ - eastonite $K_2(Mg_5Al)(Si_5Al_3)O_{20}(OH)_4$ and more aluminous and vacancy-rich solid solutions investigated by ROBERT (1976),and to their synthetic equivalents (ROBERT,1981).Data on the phengitic series are from VELDE (1978).

Fig. 1 shows the observed correlations,in Mg-micas,between ν_{OH} and the variable ($Al^{IV}+Al^{VI}$) which has been chosen as an indicator of the variation of compositions in the solid solutions studied. Full lines correspond to measurements,dotted lines correspond to calculated extrapolations.Four lines are remarkable in Fig. 1 :

- lines A+B correspond to OH groups of N-type (nomenclature proposed by VEDDER ,1964),i.e. to OH groups bonded to 3Mg , with the OH dipole //c*.Data represented by these lines A and B are from the biotitic series indicated above;
- line C represents OH groups of I-type,i.e. OH groups bonded to 2Mg,1Al , with the OH dipole tilted away from the c* direction;
- line D represents the phengitic series,i.e. OH groups of type V,bonded to 2M cations (divalent or trivalent) and adjacent to one octahedral vacant site.In that case,the OH dipole lies inside or close to a plane parallel to (00l).The intersection of line D with the ordinate axis is at 3595 cm^{-1},which is the ν_V-OH value observed in the tetrasilicic potassium mica (KODAMA et al.,1974).

The equations of these four remarkable lines are :

. A : ν = -5.6 Al + 3735 (r = 0.995)
. B : ν = -11.28Al + 3748 (r = 0.976)
. C : ν = -18.65Al + 3732 (r = 0.991)
. D : ν = 5.72Al + 3595 (r = 0.960) with Al = $Al^{IV}+Al^{VI}$.

Several important facts merit attention :

- the break between lines A and B corresponds to the change in the coordination of potassium : twelve-fold for $0 \leqslant Al < 2$,and six-fold for $Al \geqslant 2$ (ROBERT,1981);
- the slopes of lines A and D are similar,with opposite signs;
- muscovite is located at the intersection of lines C and D;
- lines A and C have the same origin (see Fig. 1);
- the calculated intersection of the two extreme lines,A and C, is for $Al^{IV}+Al^{VI}$ = 12.63,close to the maximum Al content conceivable in a mica structure (i.e. 14),corresponding to the hypothetical formula $K_2Al_6Al_8O_{20}(OH)_4$.The intersection is noted by an asterisk in Fig. 1.

The interpretation of this set of data rests on local charge balance considerations which control the OH...O interactions by plus or minus strong hydrogen bondings.This interaction OH...O is weak in the case of N-type OH and it increases regularly with increasing total Al (lines A and B);it is stronger for I-type OH (line C),due to the tilting of the OH dipole which shortens the OH...O distances.At the opposite,V-type OH are in strong interaction with the underbonded apical O(3),adjacent to the vacant M(1) site.The underbonded character of O(3) decreases with increasing total Al,explaining the unique positive slope of line D.

Fig. 1

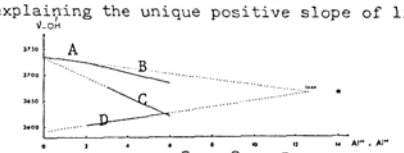

The same facts exist in Fe^{2+},Co^{2+},Ni^{2+} series,with some differences among which the negative slope of line A in the Co^{2+} series, indicating the progressive passage of some Co^{2+} in the tetrahedral layer,with decreasing total Al;this can be predicted from layer dimensional constraints.The salient fact observed in lepidolites is the presence of high frequency bands ($\nu \geqslant 3760$ cm^{-1}),due to OH groups bonded to 2Mg,1Li;such high frequencies can be interpreted from the same model;they reflect the charge balance on oxygens.

REFERENCES.

KODAMA et al.,Amer. Mineral.,59,491-495,(1974).
ROBERT J.-L.,Chem. Geol.,195-212,(1976).
ROBERT J.-L.,Thèse d'Etat,Université Paris XI,(1981).
VEDDER W.,Amer Mineral,49,736-768,(1964).
VELDE B.,Amer. Mineral.,63,343-349,(1978).

MONTROYALITE, A NEW HYDRATED SR-AL CARBONATE FROM THE FRANCON QUARRY, MONTREAL, QUEBEC

ROBERTS, A.C., SABINA, A.P., BONARDI, M., Geological Survey of Canada, 601 Booth St., Ottawa, Ontario, K1A 0E8, Canada; JAMBOR, J.L., CANMET, 555 Booth St., Ottawa, Ontario, K1A 0G1, Canada; RAMIK, R.A., STURMAN, B.D., Dept. of Mineralogy and Geology, Royal Ontario Museum, 100 Queen's Park, Toronto, Ontario, M5S 2C6, Canada; CARR, M.J., Sandia National Laboratories, Albuquerque, New Mexico 87185, U.S.A.

Montroyalite, ideally $Sr_4Al_8(CO_3)_3[(OH),F]_{26}\cdot 10\text{-}11\ H_2O$, occurs as translucent white 1mm-sized hemispheres in cavities in a silicocarbonatite sill exposed at the Francon quarry, Montreal, Quebec. Major associated minerals are albite, quartz, strontiodresserite, calcite, dawsonite, ankerite and fluorite. Montroyalite hemispheres have a dull surface and an interior that is porcelaneous with a waxy lustre. Indistinct fibres radiate from the core and produce rough to botryoidal exterior surfaces. Individual grains are irregular to lens-shaped, up to 0.02mm long and 0.005mm thick. The mineral is brittle, has a white streak, Mohs hardness of 3 1/2, uneven to splintery fracture, no observable cleavage, is soluble in 1:1 HCl at room temperature, and fluoresces white under both long- and short-wave ultraviolet light. D(meas.) 2.677g/cm^3. Montroyalite is biaxial negative, α 1.515(5), β 1.530(5), γ 1.545(5), -2V(meas.) 80(10)°, 2V(calc.) - 89°; Y is parallel or nearly parallel to the elongation and X and Z are at angles of about 45° to the elongation. Microprobe analyses and TGA/EGA gave Al_2O_3 28.8, SrO 27.7, CaO1.1, $CO_2$9.2, H_2O 24.6, F 11.5, total 102.9, less O=F 4.84, total 98.06 weight %. The material is not suitable for X-ray single-crystal studies. The strongest eight lines in the X-ray powder diffraction pattern [d in Å(I)] are: 6.57(100), 4.00(50), 3.283(55), 3.190(50), 2.862(40), 2.551(40b), 2.481(40) and 2.356(45b). Transmission electron microscopy studies revealed the presence of 50Å twins parallel to a 6.55Å plane and a net with axial translations of 7.14 and 6.55Å and an inter-axial angle of approximately 77.5°. The name is derived from Mont Royal, the Monteregian hill that is a prominent landmark in Montreal, and from which the name Montreal is derived. An updated listing of Francon minerals that have been identified since 1979 will also be presented.

ORIGIN OF RHYTHMIC LAYERING IN THE CALAMITY PEAK SATELITE PLUTON OF THE HARNEY PEAK GRANITE, BLACK HILLS, SOUTH DAKOTA: THE ROLE OF BORON IN PETROGENESIS

ROCKHOLD, J.R., NABELEK, P.I., Department of Geology, GLASCOCK, M.D., Research Reactor. University of Missouri, Columbia, MO 65211, USA

The Calamity Peak complex, a small satelite pluton on the southern flanks of the Harney Peak Granite, South Dakota, displays prominent mineral and textural layering. Textural layering is defined by alternating layers of fine-grained and pegmatitic granite. Superimposed on the fine-grained layers is a unique fine-scale (0.1-5 cm) rhythmic layering defined by modal differences in light and dark minerals. The light layers average 62% plagioclase (Ab_{96}), 31% quartz, 3% microcline (Or_{94}), 3.5% muscovite, 0.5% tourmaline ($schorl_{54}$, $dravite_{23}$, $elbaite_{23}$). The dark layers average 46% plagioclase (Ab_{96}), 29% quartz, 18% microcline (Or_{95}), 1% muscovite, 5% tourmaline ($schorl_{53}$, $dravite_{20}$, $elbaite_{27}$), and 0.5% garnet (alm_{78}, sp_{18}, pyr_{3}). Such small-scale layering is rare in granites and in this case is defined by tourmaline. Thus, it appears that boron plays a fundamental role in the petrogenesis of the layering. Redden (1) proposed repetitive changes in volatile pressure to account for the rhythmic layers.

There is essentially no variation in mineral compositions between like layers in the whole complex and variation between differently colored layers is minimal. Tourmaline is slightly enriched in elbaite (Al,Li endmember) and microcline in potassium in the dark relative to the light layers.

Analyses of B in mineral separates by Prompt-Gamma Neutron Activation (2) reveal 1.1% less B_2O_3 in tourmaline and 133 ppm more B in the combined other phases in the light relative to the dark layers. Whole rock B_2O_3 content is 0.07% in the light layers and 0.65% in the dark layers. These relative amounts are essentially proportional to tourmaline abundance in each layer.

Pichavant (3) has shown that the addition of B to the granitic system depresses the solidus and enhances the solubility of H_2O in the melt. Therefore, removal of B from melt tends to result in saturation of the melt with H_2O. We suggest that the textural and mineralogic layering can be explained by the interplay of crystallization and exsolution of H_2O-rich fluid. As tourmaline crystallized, B was depleted in the melt next to the crystallization front, resulting in saturation of the melt with H_2O. The increase in the activity of H_2O stabilized muscovite + albite relative to microcline (Fig.). The amount of muscovite in the light layers was limited by the amount of excess alumina available in the peraluminous melt. Furthermore, the removal of B from the crystallization front may have been enhanced by removal in the exsolved fluid because the melt/fluid partition coefficient for boron is about 0.33 (3). The pegmatitic layers, some of which crosscut previously formed rhythmic layers and occasionally have tourmaline along their borders, may have crystallized from the exsolved fluid phase. The depletion of B in the melt significantly lowered the ability of tourmaline to nucleate and grow, resulting in the light layers. However, once the crystallization front caught-up with melt rich in boron, the cycle began to repeat.

This suggested process, similar to one proposed for the origin of rhythmic layers in gabbroic bodies (e.g. 4) requires that tourmaline nucleated at a faster rate than at which B can diffuse in the magma. This is reasonable, since B probably behaves in the melt similarly to Al which has a relatively slow diffusion rate (5).

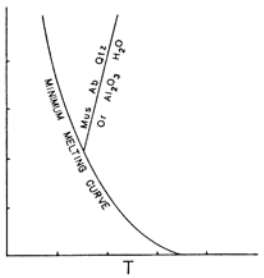

1. Redden, J.A. (1963) USGS Prof Pap, 297-D: 199-291
2. Glascock, M.D. et al. (1981) Nucl. Inst. Meth. Phys. Res. 1042-1046.
3. Pichavant, M. (1981) Contrib Mineral Petrol: 430-439
4. McBirney, A.R., Noyes R.M. (1979) J. Petrol, 20: 487-554
5. Hofmann, A.W. (1980) Physics of Magmatic Process: 385-417

GEM VARIETIES OF BERYL, CHRYSOBERYL AND PHENAKITE GROWN BY CHEMICAL VAPOUR TRANSPORT

RODIONOV A,Ya., SOLNTSEV V.P., Institute of Geology and Geophysics, Siberian Branch of the Academy of Sciences of the USSR, Novosibirsk-90, USSR

Colored varieties of beryl, chrysoberyl and phenakite are grown by chemical vapour transport in closed halogen-bearing systems. Crystallization was carried out in heat-resistant containers and ampules made of quartz glass of 20-40 mm in diameter and 100-120 mm in length at 950-1150°C under ΔT conditions[1]. Fe, Cu, and Ni sealed tubes make the regulation of redox conditions during crystal growth possible. Beryl, chrysoberyl, phenakite, oxides of Be, Al, Si and chromophorous elements as well as halogenides of some metals are used as charge. The process of growth takes 20-30 days. Colored beryls, chrysoberyls and phenakites are formed in the upper part of containers as spontaneous crystals of 5x5x5 mm and on seed crystals of some square cm in size.

Dark blue Co-bearing (up to 0.1wt % of CoO) and blue V-bearing (up to 0.1wt % of V_2O_3) phenakite were grown. Phenakite dark blue color is attained due to Co^{2+} ions in Be^{2+} sites and the blue color of phenakite is conditioned by V^{4+} ions in Si^{4+}_{IV} sites.

The following chrysoberyl varieties were obtained: alexandrite(15 wt% of Cr_2O_3), cymophane(4-5 wt% of Fe_2O_3), orange Mn-bearing chrysoberyl(0.3-0.5 wt% of MnO), green V-bearing chrysoberyl(4-6 wt% of V_2O_3), dark blue Ti-bearing chrysoberyl(4-8 wt% of Ti_2O_3), green Ni-bearing chrysoberyl(0.5-1 wt% of Ni_2O_3), brown Co-bearing chrysoberyl(0.2-0.5 wt% of CoO). According to EPR data the color of Cr, N, Ti, Fe-bearing chrysoberyls is conditioned by trivalent ions of these elements in Al^{3+}_S sites. The color of Co, Ni, Mn-bearing chrysoberyls depends on bi-and trivalent ions in Al^{3+}_S sites.

FLUID INCLUSION STUDY OF THE TAOLIN Zn-Pb-FLUORITE DEPOSIT, PRC

ROEDDER, EDWIN and HOWARD, KEVIN, W., 959 U.S.G.S., Reston, VA 22092

The Taolin Zn-Pb-fluorite deposit, near Linxiang in NE Hunan Prov., PRC, has been known for 28 years. Its genetic affiliation, however, remains uncertain: Is it Mississippi Valley-type (MVT), or epithermal hydrothermal? Ore production is ~10^6 t/yr averaging ~13 wt.% CaF_2 and 3% (ZnS + PbS). Cu is low (~0.1%); Ag (~10 g/t) is present in galena (gn) at ~400 g/t; Au is <1 g/t in sulfide concentrate. Sphalerite (sp), particularly the late yellow sp, is high enough in Cd, Ge, and In for their commercial recovery. Gangue is quartz (cherty to coarsely crystalline), + barite (ba) and minor chlorite, pyrite (py), and calcite. The ore occurs in a major fault zone (dip 30-45°N) between a 136-Ma granite (to the S) and metasediments; average ore thickness is 20-30 m. The Taolin mine is one of six similar deposits along 10 km of outcrop of the fault, which has some mineralization along most of its length. "Alteration" is limited mainly to silicification and chloritization but, as with the ore minerals, appears to occur only as open space filling, not replacement. Ore minerals are coarsely crystalline, with rare vugs; ba blades ≤20 cm in length were seen.

Following early, barren, preore quartz + minor py near the footwall (termed "Stage 0"), three stages of ore deposition are recognized at the mine: I) high-Fe dark sp (≤4% Fe) + amethystine quartz, closest to the footwall, II) dark sp, fluorite (fl) + minor gn and ba, and III) ba, yellow sp (≤0.1 Fe) + "gel" quartz. With increasing depth, the ore still has Cu + fl, but (Zn + Pb) decreases, and py increases.

Ding and Rees (1984, Geochim. Cosmo. Acta), on the basis of $\delta^{34}S$ studies, proposed a closed-system model operating at 325-250°C for Taolin. They also presented unpublished fluid inclusion data "from Wei." These include 3 data pairs of homogenization temperature (Th, °C) and salinity (wt.% NaCl, here converted to temperature of melting of ice, Tm ice, °C) for Stage I, as follows: 285, -10.9; 300, -13.8; and 305, -12.5. Also, one pair from Stage II showed 245, -8.2.

The results of our studies on mainly primary and possibly pseudo-secondary inclusions in a small suite of samples personally collected in 1985 from the -200 m level, ~800 m west of the main shaft, are (at present) inexplicably different from the previous data. With two possibly spurious exceptions, the highest Th value found among 190 inclusions from fl, quartz, and sp was 204°C, well below the lowest value previously reported, and our mean (153°C) is far below (Fig. 1). Only 81 Tm ice determinations were made. The values were -7 to -9°C (with major Ca) for Stages 0 and I and were strongly bimodal between saline and essentially fresh water for Stage II (Fig. 2).

The major differences between our data and the earlier data may stem from sampling different parts of the paragenetic sequence or in the specific mine locations sampled and may eventually be clarified, but the available data do not fit well with either proposed genetic affiliation. The lack of recognized alteration is difficult to explain if the fluids and rock have been ~300°C. Many of our Th values are higher than those from most MVT deposits, and even our highest salinities (i.e., lowest Tm ice values) are less than those from most MVT deposits. Our very low salinities (for fl) are completely atypical of MVT deposits. In fact, these values are even much lower than most ordinary epithermal deposits. If the relative paragenetic assignments for our samples are correct, some of the large and enigmatic intra- and interstage Th differences found raise the question of how extensive was the natural decrepitation of earlier, lower Th inclusions by later, hotter fluids. A few large primary inclusions in Stage III fl do show clear decrepitation halos. Obviously, a more detailed sampling of the entire paragenetic sequence will be needed to clarify these problems.

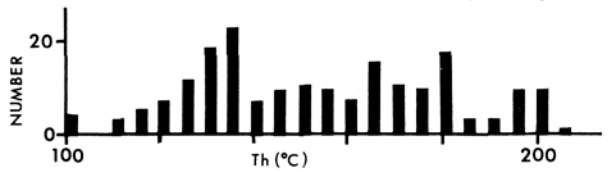

FIG. 1

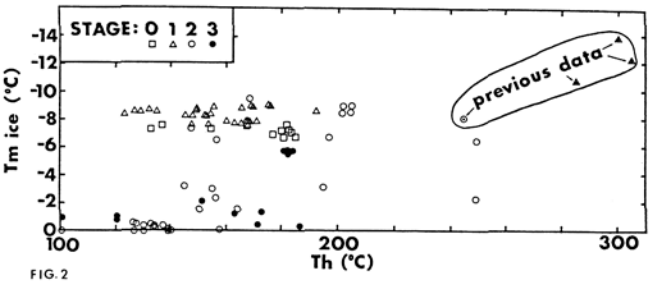

FIG. 2

PETROLOGY AND GEOCHEMISTRY OF ARCHEAN STEATITES FROM CENTRAL BRAZIL

Hubert ROESER*, Ursula ROESER*, Heinz Juergen TOBSCHALL**, Burkhard SCHULZ-DOBRICK** (*Ouro Preto, Brazil and **Mainz, West Germany)

Onde-hundred total rock analysis and about 200 microprobe analysis of selected minerals of Archean steatites from the area of the Iron Quadrangle, State of Minas Gerais, Central Brazil were carried out.

The rocks are part of the serpentinitic belt from Eastern-Central Brazil and are bearers of Ni- and Cr- ores in the Diamantina district.

Most of the steatite bodies occur in the Archean gneissic basement of the Iron Quadrangle and the base of the Archean Rio das Velhas greenstone belt (2.7 b.a.) and show a zonal arrangement of various minerals with irregular boundaries between each zone. From the center of a steatite body to the contact with the host rocks (schists, gneisses) the following zones were observed:

massive steatite - carbonate talc rock - amphibole rock - chlorite rock.

The transition of the zones are gradual except the chlorite rocks, which envelop the bodies and show neat boudaries.

The steatites are orthosteatites, derived from ultramafic/ ultrabasic rocks from the upper mantle. The trace element compositions is:

Ni up to 2500 ppm, Cr up to 3500 ppm, Co up to 120 ppm with the following element ratios: Ti/Zr = 238, Y/Zr = 1.7, Ti/Y = 296, Nb/Zr = 5.3, ratios comparable to peridotites and chondrites.

The quantitatively most important minerals are talc, Mg chlorite, amphiboles and carbonates. The principal bearers of Cr are the chlorites with up to 1.52 % Cr_2O_3. The amphiboles only have up to 0.06 % and talc up to 0.03 % Cr_2O_3. The Ni contents are highest in the talc (0.44% NiO) followed by the chlorites (0.22 % NiO) and the amphiboles (0.12 % NiO).

Two types of amphiboles were distinguished: members of the series: actinolite - tremolite and orthoamphiboles of the series: anthophyllite - gedrite. The latter show Al_2O_3 contents up to 1.12% which characterize the minerals as anthophyllites.

The carbonates were indentified as dolomites with Ca/Mg ratios of about 1.45 and contents of MnO up to 0.54 % and FeO up to 4.75 %.

Acessory minerals are pyrite, ilmenite, hematite, magnetite, apatite and relicts of serpentine minerals.

The originally ultramafic rocks were transformed during at least two different metamorphic events, both of PT conditions of the greenschist facies. In the first metamorphism the transformation from the lherzolite to serpentine took place. Later a second metamorphism, probably the 2.0 b.a. old Minas metamorphism (Transamazonic cycle), caused a remarkable metamorphic differentiation (in the sense of Escola) of the serpentinites where the fluid phase (H_2O + CO_2) caused the migration of the elements. The result were the typical formation of steatites and their mineral zones, described above.

Especially in the exo - contact area the host rocks were strongly transformed by hydrothermal processes.

The steatites received an addition of Si from the host rocks (schists and gneisses) while they were impoverished in Mg and alkali elements. The trace elements Cr, Ni, Co, Ti, Zr, Y and Nb were very immobile and changed only very little.

Most of the mineral paragenesis such as: talc - dolomite - serpentine - pyrite or: talc - actinolite - chlorite - dolomite indicate PT conditions of low grade metmaorphism (greenschist facies). During the second metamorphism locally higher metamorphic conditions were reached.

This is shown by the paragensis: talc - carbonate-anthophyllite in some rocks, which suggests about 520° C and 2 kb under X-CO_2 greater than 80 %.

As derivates from the upper mantle, the rocks were transported during an orogenetic cycle into higher levels of the crust and then were injected tectonicaly in the host rocks where they were then transformed metamorphically.

This work was supported by the German foundation STIFTUNG VOLKSWAGENWERK.

RARE EARTH ELEMENT ENRICHMENT IN APATITE FROM PERALKALINE UNDERSATURATED ROCKS

RØNSBO, J.G., Inst. of Mineralogy, University of Copenhagen, Ostervoldgade 10, DK-1350 Copenhagen K, Denmark

The Ilímaussaq intrusion belongs to the late Precambrian Gardar province of South Greenland. The intrusion consists of three major units: the early outer shell of augite syenite, sheets of alkali acid rocks emplaced in the upper part of the augite syenite, and the layered series of agpaitic nepheline syenites.

The most evolved nepheline syenites, the lujavrites, and also the pegmatites and hydrothermal veins are characterized by a number of rare earth element (RE)-rich minerals: steenstrupine, britholite, semenovite, vitusite, tundrite, etc. Data given by Larsen (1979) indicate that accessory apatite is one of major RE-bearing minerals in the pulaskite, foyaite, sodalite foyaite and naujaite, representing the agpaitic roof sequence.

Combined electron microprobe analysis and scanning electron microscopy investigations of the apatites revealed a complex evolution. Primary apatites are oscillatory and sector zoned having a RE content between c. 5 and 17% RE_2O_3. The $Ca^{2+} \ddagger RE^{3+}$ substitution is primarily stoichiometric being balanced by a coupled $P^{5+} \ddagger Si^{4+}$ substitution. The Na content is low. The primary apatite thus represents part of a solid solution series from apatite towards lessingite ($Ca_2RE_3(SiO_4)_3(OH,F)$). The highest RE content in the primary apatite is observed in the sodalite foyaite and corresponds to the composition $Ap_{75}Les_{25}$.

The primary apatites show an extensive alteration with increasing peralkalinity and in the sodalite foyaite and naujaite reequilibrated apatites are dominant. The secondary apatites are characterized by an increase in the Na content and a relative enrichment in the light RE.

In the sodalite foyaite, at least two generations of secondary apatite can be observed. One is only slightly enriched in Na, whereas the latest formed is strongly Na-enriched and almost Si-free. For these apatite the RE enrichment follows the substitution scheme $2Ca^{2+} \ddagger Na^{+} + RE^{3+}$. Secondary apatite in the foyaite contains up to 40% of the theoretical endmember $Na_5RE_5(PO_4)_6(OH,F)_2$. These apatites provide evidence for post-magmatic Na-metasomatism in the sodalite foyaite.

Larsen, L.M. (1979): Distribution of REE and other trace elements between phenocrysts and peralkaline undersaturated magmas, exemplified by rocks from the Gardar igneous province, south Greenland, Lithos 12, 303-315.

THE DANGERS OF ASBESTOS IN OUR ENVIRONMENT: FACT AND FICTION

ROSS, MALCOLM, U.S. Geological Survey, MS 959, Reston, VA 22092

Of the six forms of asbestos, only three (chrysotile, amosite, and crocidolite) have been used to any significant extent in commerce. Between 1870 and 1980 approximately 100 million tonnes of asbestos was mined worldwide, of which more than 90 million tonnes was chrysotile.

The three principal diseases related to asbestos exposure are (1) lung cancer, (2) cancer of the pleural and peritoneal membranes (mesothelioma), and (3) asbestosis. These diseases, however, are not equally prevalent in the various groups of asbestos workers that have been studied: the amount and type of disease depends on the duration of exposure, on the intensity of exposure, and, particularly, on the type or types of asbestos to which the individual has been exposed. Lung cancer is linked to exposure to chrysotile, amosite, and crocidolite asbestos; amosite and crocidolite are far more dangerous than chrysotile. Moreoever, significantly increased risk from chrysotile is found only in those who smoke and who were heavily exposed for many years. Asbestosis is caused by prolonged exposure to all forms of asbestos, whereas mesothelioma is caused principally by exposure to crocidolite asbestos. Chrysotile asbestos does not cause significant mesothelioma mortality. The common non-asbestiform amphibole minerals cummingtonite, grunerite, tremolite, anthophyllite, and actinolite, which are often defined as "asbestos" for regulatory purposes, have not been shown to cause disease.

The possible health effects of exposure to rock dust containing one or more of the many amphibole minerals is an important issue. Amphiboles are contained within the gangue of many hard-rock mines - gold, vermiculite, talc, iron ore, crushed stone and aggregate, copper, etc. Unusually tight controls of amphibole mineral particles, such as those proposed by NIOSH in 1976 for asbestos fibers (0.1 fibers per cm^3) could stop major mining in the United States - with no health benefit.

Chrysotile asbestos, which accounts for about 95% of the asbestos used in the U.S., has been shown by extensive Canadian studies to be safe where the air exposures do not exceed 1 fiber per cm^3 for the working lifetime of the asbestos miners. The lack of risk from non-occupational exposure to chrysotile asbestos has been well documented by various studies concerning the mortality of the women of the Quebec chrysotile asbestos mining towns, women who did not work in the asbestos industry but who were exposed to very high levels of ambient chrysotile dusts from the local mines and mills throughout their lives (Ross, ASTM STP 834, p. 82-86, Ref. 70, 71, 72, 73, 81, 86, 1984; see also J. Siemiatycki, Proc. World Symp. Asbestos, Montreal, May 25-27, p. 337-348, 1982). Chrysotile dust levels found in buildings rarely exceed 0.001 fibers per cm^3. Such dust concentration will have no measurable health effect on the building occupants.

Notwithstanding, the presence of asbestos in schools, homes, and other buildings is generating a national crisis of such proportions that the U.S. economy could be very adversely affected; full ripout of asbestos is the only option if the public believes "one fiber" can induce cancer. Building owners, school systems, and local and state governments are suing many businesses for costs and damages related to asbestos removal, insurance companies are dropping liability coverage on workers removing asbestos, and occupants of buildings are suing over health effects or potential effects alleged to be caused by exposure to asbestos during renovation.

With the newly proposed limit of 7.1 asbestos fibers per liter of drinking water (EPA, Nov. 13, 1985), fear of asbestos in natural waters and of asbestos-cement water pipe (200,000 miles in the U.S.A.) may lead to additonal costly remedial measures despite the fact that no evidence from the many human and animal studies indicates that ingestion of asbestos causes disease. This proposed water standard could particularly affect the state of California because of its numerous large areas of chrysotile-bearing rocks and soils and its asbestos-laden rivers (up to 290 billion fibers/l).

The time has come to take a hard look at the theory of "zero threshold" with respect to cancer induction - the "one fiber or one molecule can kill you" concept. The risk associated with exposure to small amounts of a disease-causing agent, whether to chrysotile asbestos, coal dust, or certain pesticides, is extremely low, but the risk of severe economic and social dislocations through asbestos ripout in buildings, removal of asbestos-cement water pipe, abandoning the use of pesticides, etc. is high.

RESIDUAL ELECTRON DENSITY AT THE M2 SITE IN C2/c CLINOPYROXENES: RELATIONSHIPS WITH BULK CHEMISTRY AND SUB-SOLIDUS EVOLUTION.

ROSSI, G., OBERTI, R., Centro Studio Cristallografia Strutturale C.N.R., Pavia; DAL NEGRO, A., MOLIN, M., Centro Studio Orogeno Alpi Orientali C.N.R., Padova; MELLINI, M., Centro Studio Geologia Strutturale Dinamica Appennino C.N.R., Pisa, Italy.

During the systematic study of the C2/c clinopyroxenes (cpx's) by X-ray structure analysis, a significant asymmetric broadening of the electron density at the M2 site (Fig. 1) has been often observed. This broadening results in a peak in the difference Fourier map located on the diad axis and away from the M2 site towards the positions occupied by Mg in clinoenstatite.

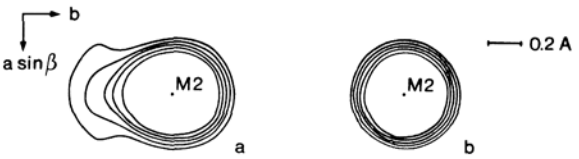

Fig. 1. The observed electron density at the M2 site of a low-Ca augite (a) and of diopside (b). Resolution $\underline{d}$ = 0.4 A. Contours at arbitrary equal intervals.

Previous reports described this residual electron density (labelled M2') as due to the splitting of the M2 site.

X-ray structure refinements carried out at different resolutions ($\underline{d}$ from 0.7 to 0.4 A) has shown that the height of the residual maximum M2' and its apparent position depend on the resolution: as resolution increases the height increases and the distance from M2 decreases. Therefore the location and the occupancy of the M2' site can be determined only if the resolution $\underline{d}$ is smaller than the real M2-M2' distance, which should be less than 0.4 A.

The height of the M2' peak (at constant resolution) varies broadly in the examined samples:fassaites, omphacites, synthetic diopside show no residual peak, whereas some low-Ca augites display the largest ones. In general, the residual electron density tends to vanish as the sum Ca+Na approaches one atom p.f.u., and, in samples of similar composition, it is larger in cpx's which underwent metamorphic equilibration than in those from volcanic rocks.

As split sites and residual electron density may indicate exsolution or twinning, the most significant specimens were submitted to complete microstructural analysis, which revealed a non-ubiquitous occurrence of spinodal decomposition. This is not strictly related to the broadening of the M2 electron density: synthetic cpx's are completely homogeneous and yet show significant broadening, whereas metamorphically equilibrated cpx's with comparable broadening display marked spinodal decomposition. In the latter case the chemical composition does not vary largely along the modulation, as it is indicated by the absence of satellite spots in the electron diffraction pattern.

It has been concluded that the asymmetric electron density at the M2 site is a real feature of the crystal structure of cpx's dependent mainly on composition and also on the thermal history of the host rock. That feature of the M2 site can be seen as an off-center displacement of some small cations. Whereas the larger cations (Ca, Na) actually occupy the eight coordinated M2 site, the smaller ones (Fe,Mg) tend to move away from that site and towards the walls of the cavity in order to achieve a better coordination and to provide more positive charges to the underbonded O1 and O2 oxygen atoms. The extreme situation occurs in the synthetic $Zn_2Si_2O_6$ pyroxene where M2 has coordinates similar to those of M2' in common cpx's and a distorted tetrahedral coordination. A similar trend can be observed in orthopyroxenes where the M2 coordination is not actually octahedral, but can be described as a 4+2 coordination, with the four short distances accounting for 80 per cent of the total cationic bond strength. The overall distribution of cations along the diad axis may be completely disordered (high T cpx's) or may undergo ordering phenomena by spinodal decomposition (metamorphically annealed cpx's).

THE HYDROUS COMPONENT IN GARNETS

ROSSMAN, G.R., Division of Geological and Planetary Sciences, California Institute of Technology, Pasadena, CA 91125, USA

The concept of the hydrogarnet substitution ($SiO_4 = O_4H_4$) is generally accepted as the mode of incorporation of H into the garnet structure and is proposed to be the mode of incorporation of H in a variety of other silicates. Most identifications of hydrogarnets have been based upon cell parameters determined by powder diffraction. In an attempt to directly observe the hydrous component, Aines and Rossman examined the infrared spectra in the OH region of more than one hundred garnets. The spectra revealed that nearly all of them contained OH. The OH signal is most intense for grossulars, spessartites, uvarovite, and andradites.

The infrared spectra of grossulars are highly variable (Fig. 1). This variation suggests that a single mode of OH incorporation does not occur in these garnets. The spectra of our garnets are different from the spectra of both the plazolite of Woodford et al. (1941) and synthetic $Ca_3Al_2(SiO_4)_2(O_4H_4)$. The concept of a hydrogrossular substitution common to all grossulars is not supported by either the infrared or proton NMR data.

The highest infrared intensities which we observed in a well-characterized garnet were from the melanite variety of andradite. These have about twice the intensity of the highest OH absorption for a grossular. Nearly the same intensity was observed for the interior regions of uvarovite. Many garnets are zoned in OH content, but seldom as spectacularly as the uvarovites (Fig 2).

Pyrope-almandines generally had the lowest content of a hydrous component. However, the infrared spectra of the pyrope-almandine garnets were the most consistent from crystal to crystal and varied the most systematically with chemical composition. A hydrous component was observed in chromian-pyropes of mantle origin as well as in the spectra of the other various colored pyropes from kimberlites.

Absolute calibration of the OH content has been attempted by weight loss on heating, hydrogen manometry, evolved water coulometry, and hydrogen-specific nuclear reactions. The total H concentration expressed as wt% H_2O seldom exceeds 0.25%. Most garnets contain 0.0x%. Among the samples we have directly analyzed, the highest contents were observed in the grossulars. The formula of the most water-rich grossular we have directly analyzed was $Ca_3Al_2(SiO_4)_{2.967}(O_4H_4)_{0.033}$ assuming that $SiO_4 + (O_4H_4) = 3.00$ and ignoring minor Fe and Mn substitution. A grossular too small to analyze directly had the most intense infrared OH band. It is about four times as intense as the most hydrous grossular with a direct analysis, but still even less intense than some melanites.

Our results suggest that a "hydro" substitution in garnets is commonplace, but that the amount of H_2O is usually low; most garnets have 1/100 the hydro content of the classical hydrogarnets.

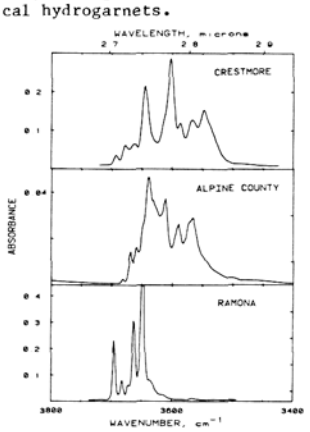

Figure 1. Infrared spectra of three grossulars presented for 100 μm thickness.

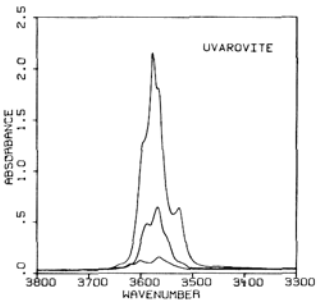

Figure 2. Infrared spectra of uvarovite from Jacksonville, Calif. Top = interior of first crystal; middle = interior of second crystal; bottom = rim of second crystal. Plotted for 40 μm thickness.

OPTICAL SPECTROSCOPY OF MINERALS

Rossman, G.R., Division of Geological and Planetary Sciences, California Institute of Technology, Pasadena, Cal., USA

The optical absorption spectra of minerals should provide information about cation oxidation state, site occupancy and concentration. The quantitative intensity of absorption bands, however, is strongly influenced by geometric aspects of the cation site and by interactions between cations. Attempts to obtain cation concentrations from optical spectra can be subject to large errors due to non-linearities in the intensity vs concentration relationship which arise from cation interactions.

Antiferromagnetic interactions between Fe^{3+} cations can cause the intrinsically weak Fe^{3+} absorption bands to become 50 times more intense than those of non-interacting Fe^{3+}. The deep red and brown colors of hematite and hydrous iron oxides are a common manifestation of these interactions. Strong absorption anisotropy will result if the interacting cation pairs are similarly aligned in the crystal structure.

Intervalance charge transfer is one the most promimant cation interactions in minerals. It has strong absorption anisotropy if the interacting units are aligned. Recent works by Amthauer, Mattson and Rossman have determined the intensity of Fe^{2+}-Fe^{3+} and Fe^{2+}-Ti^{4+} interactions in a variety of minerals (Table 1). Although the intense color of many minerals is commonly attributed to a small amount of Fe^{2+}-Fe^{3+} intervalence charge transfer, the results of Table 1 suggest that the color in many such minerals is due more to the high concentration of the Fe^{2+}-Fe^{3+} pairs rather than their intrinsic intensity. On the other hand, the Fe^{2+}-Ti^{4+} pair has a much higher intensity and can be the dominant cause of color in Fe^{2+} minerals with relatively low titanium concentrations. The reddish-brown color of titanian amphiboles, pyroxenes and micas is commonly due to the Fe^{2+}-Ti^{4+} interaction.

The intrinsic Fe^{2+} bands can be intensified when Fe^{2+} ions are adjacent to Fe^{3+}. This process is distinct from intervalence charge transfer because a new band does not appear at a different wavelength (the IVCT band). The enhanced Fe^{2+} bands are strongly anisotropic with maximum intensity along the direction of the Fe^{2+}-Fe^{3+} direction. In this respect, they are the same as Fe^{2+}-Fe^{3+} intervalence bands. The enhanced Fe^{2+} bands are a major cause of color in black micas and tourmalines. Their high absorption intensity means that they will usually be a dominant cause of color. They are frequently simultaneously present with Fe^{2+}-Fe^{3+} and Fe^{2+}-Ti^{4+} intervalence bands which also contribute to the color.

Criteria to distinguish among the different types of interactions are useful, but imperfect. The full-width at half-height of the absorption band is one of the most useful. Intervalence bands are generally much broader than single ion bands. The wavelengths of intervalence charge transfer bands vary in response to the nature of the coordination polyhedra of the interacting ions and also to the number of ions involved in the intervalence interaction. This variability makes it difficult to confidently assign a particular band in the absence of other criteria.

Table 1
Typical absorption band intensities and wavelengths for Fe^{2+} and Fe^{3+}

ion	environment	epsilon	wavelength
Fe^{2+}	regular sites, non-interacting	3	1000 nm
	large, distorted sites	100	1000 nm
Fe^{3+}	$^4T_{1g}$ band isolated ions	0.2	860 nm
	magnetically coupled ions	10	860 nm
	($^4A_{1g}$,^4E_g) band isolated ions	1	440 nm
	magnetically coupled ions	50	440 nm
Fe^{2+}-Fe^{3+} pair	IVCT band (per Fe^{2+})	150	680 nm
Fe^{2+}-Ti^{4+} pair	IVCT band (per Fe^{2+})	2000	460 nm
Fe^{2+}-Fe^{3+} pair	enhanced Fe^{2+} band	1000	1000 nm

Intensity values are the epsilon coefficient
Absorbance = epsilon x thickness (cm) x concentration (M/l)

THE ROLE OF MINERALOGY IN CEMENT CHEMISTRY

ROY, D.M., Materials Research Laboratory, The Pennsylvania State University, University Park, PA 16802, USA

The manufacture of portland cement involves the reaction of limestone and siliceous rocks (clays, shales, etc.), through a complex sequence of steps as the temperature is increased: dehydration, dehydroxylation, and solid state reactions, to form dicalcium silicate (usually the larnite, β-Ca_2SiO_4 form), calcium aluminate, CaO, residual amorphous material, and other minor phases. As the temperature is increased above ~1300°C, tricalcium silicate, the most important cementitious phase, is formed by reaction of Ca_2SiO_4 and CaO in the presence of liquid. On subsequent cooling to ambient to produce 'cement clinker', the major phases present are Ca_3SiO_5 (hatrurite), Ca_2SiO_4 (larnite or bredegite), $Ca_3Al_2O_6$ and $Ca_2Al_{2-x}Fe_xO_7$ (brownmillerite), along with minor amounts of other components, such as periclase (MgO). Each of the major phases exists in several polymorphic forms, as the result of incorporating different amounts of substituent ions, including alkalis, in its crystal structure; the calcium aluminoferrite phase is in itself part of an extensive solid solution series, and excess sulfate may be present as anhydrite, K_2SO_4 or other complex sulfates. Minor variations in composition can result in changes in the properties of the resulting cement during hydration.

The cement clinker is intermixed with a small percentage of gypsum ($CaSO_4 \cdot 2H_2O$) ground to a high fineness with average particle size ~15 μm, and is thereafter sold as 'cement'. When mixed with water, metastable cement undergoes a complex series of exothermic hydration reactions, as each mineral phase has its own hydration/hydrolysis characteristics, but these are synergistic when the several phases are present together. Tricalcium silicate and dicalcium silicate release calcium ions and form an amorphous calcium silicate hydrate, 'C-S-H' which is the major phase of hardened cement paste. Part of this calcium reacts with the calcium aluminate and aluminoferrite phases, and the gypsum, to form crystalline calcium alumino(ferrite) sulfate hydrates. The tricalcium silicate and tricalcium aluminate hydrate rapidly, the other two phases more slowly. Remarkably, cement paste hydration is essentially a constant volume process, as much fine microporosity is entrapped within the C-S-H, compensating for volume inequities, and allowing a material to be cast in a particular shape with very little shrinkage.

Another series of reactions takes place with cement hydration at elevated temperatures, where better defined mineralogical entities such as the hydrous calcium silicates, plombierite, tacharanite, tobermorite, xonotlite, gyrolite or truscottite may appear, generally forming a strong coherent structure, albeit slightly more porous as the high temperature phases contain less structural water and are crystalline, rather than more nearly colloidal in behavior. Other crystalline phases such as ettringite, $Ca_3Al_2O_6 \cdot 3CaSO_4 \cdot 32H_2O$, lose water of hydration at elevated temperatures, and convert to other phases. A number of these phase changes have been investigated, both in commercial application of autoclaved building materials, and in nuclear waste management applications where they would be exposed to higher temperatures.

AN EXPERIMENTAL/TEM STUDY OF THE OLIVINE → SPINEL TRANSFORMATION WITH IMPLICATIONS FOR TRANSFORMATIONAL PLASTICITY

RUBIE, D.C., and CHAMPNESS, P.E., Dept. of Geology, Manchester University, Manchester M13 9PL, U.K.

The olivine → spinel transformation in Mg_2GeO_4 has been studied at high pressure in a piston-cylinder apparatus using NaCl as the pressure medium. The starting material consisted of a previously hot-pressed Mg_2GeO_4 olivine aggregate with a grain size of 30-50 μm. The microstructure of samples run at 20 kbar/900°C for times varying from 0.5 to 70 hrs has been studied in detail using optical and transmission electron microscopy. These conditions overstep the equilibrium boundary by ~17 kbar.

An absence of crystallographic orientation relationships between olivine and spinel in partially reacted samples shows that the reaction is not martensitic under these conditions (see also Vaughan et al., 1984). During the early stages of transformation (<5 hr at 900°C/20 kbar), olivine undergoes dynamic recrystallization which results in a pronounced grain-size decrease (from ~40 μm to ≤12 μm). This recrystallization occurs by the development of a high dislocation density and the subsequent arrangement of these dislocations into low angle subgrain boundaries. Spinel nucleates on grain boundaries and on the newly-formed subgrain boundaries in the olivine and develops as fine-grained aggregates. These aggregates consist of subgrains (~1 μm diam.) which are separated by low-angle grain boundaries consisting of arrays of dislocations. Our observations suggest that, following nucleation and growth, the spinel has also undergone dynamic recrystallization and that it is this process which is responsible for the extremely small grain size of the product phase.

Our main conclusions from these observations are:

(1) The dependence of overall transformation rates on P and T must be complex. This is because the recrystallization of olivine creates new nucleation sites during the transformation and the rate of this process, involving the climb of dislocations, must itself be dependent on P and T. The derivation of a rate equation to describe the kinetics of the transformation must take into account the creation of new nucleation sites.

(2) Recrystallization and the development of a subgrain structure in both olivine and spinel must be the result of differential stress. According to data of Vaughan and Coe (1981), a differential stress exceeding 3 kbar is required to produce a recrystallized grain size of 12 μm in Mg_2GeO_4 olivine. Such stress is unlikely to be caused by the high-pressure apparatus because, at 900°C/20 kbar, the NaCl pressure medium is fairly close to its melting temperature and therefore should not be capable of supporting a significant shear stress. It is more likely that localized differential stresses are set up in the reacting aggregate as a result of the large volume change (-9%). Such stresses must be of great importance for deformation for two reasons. Firstly the small grain size of the recrystallized spinel favours deformation by structural superplasticity with a likely reduction in flow stress as a consequence of the transformation (Vaughan and Coe, 1981; Rubie, 1984). Secondly, according to theories of transformational plasticity, internal stresses due to volume change are thought to reduce the magnitude of the externally-applied shear stress required for deformation (Greenwood and Johnson, 1965). The combination of these two phenomena should have a pronounced effect on rheology during the olivine → spinel transformation by significantly reducing the flow stress.

Greenwood, G.W., and Johnson, R.H., 1965. Proc. Roy. Soc. 283A, 403.
Rubie, D.C., 1984. Nature 308, 505.
Vaughan, P.J., and Coe, R.S., 1981. J. Geophys. Res. 86, 389.
Vaughan, P.J., Green, H.W., and Coe, R.S., 1984. Tectonophysics 108, 299.

ACCELERATOR MASS SPECTROMETRY IN GEOLOGY

RUCKLIDGE, J.C., Dept. of Geology, University of Toronto, Toronto, Canada, M5S 1A1

A tandem accelerator in conjunction with a sputter ion source yields an instrument which can combine high spatial resolution with very low detection levels for a wide range of elements and isotopes. Ions with MeV energies can be charge-changed in such a way that molecular ions can be eliminated from the analyzed beam and hence an overwhelming source of background is removed. Isotope ratios as low as 10^{-15} can be measured, thus making posssible determinations of rare radioisotopes whose decays are too infrequent to be measured by conventional decay counting. Carbon-14 ages as old as 50,000 years are now made routinely on milligram size samples of extracted carbon, and other cosmogenetic isotopes such as Be-10, Al-26, Cl-36 and I-129 can also be measured in a wide range of geological materials. Ages range from hundreds of years to tens of millions, depending on the systematics used. Dating of certain sediments, ice cores, groundwaters, meteorite falls and even landform features can be tackled using these isotopes. The rollover time for sediments subducted and remobilized in island arc volcanoes has been measured using Be-10, and new data showing that Al-26 is being generated from Si in the top few meters of exposed surface rocks will be discussed.

The method requires negative ions for injection into the accelerator so the yields are best for those elements with high electron affinities, such as C, O, S, Cl, Cu, Sn, Au and most platinum group elements. These latter can be detected at sub-ppb levels using a primary microbeam of caesium directly on a polished rock section, though difficulties arise in quantitative interpretation of the data, partly because of the paucity of standards. Graphites from Sri Lanka, Stillwater and Bushveld have yielded trace element spectra where intensities range over 11 orders of magnitude. The prospect of using the method for microprobe measurement of stable isotope ratios will also be considered.

POLYMETAMORPHISM OF PELITIC ROCKS IN THE HEADQUARTERS REGION, NORTHERN IDAHO

RUENDAL, Aime P., Department of Geology, University of Oregon, Eugene, OR 97503, USA; RICE, Jack M., Department of Geology, University of Oregon, Eugene, OR 97403, USA

Metapelitic Beltian rocks in the Headquarters area, northern Idaho show evidence for two metamorphic events which can be correlated with the M2 and M3 events observed by Lang and Rice (1985) and Carey (1985). During the earlier event (M2) the metapelitic rocks were metamorphosed to sillimanite- muscovite-quartz grade and locally to sillimanite - K-feldspar grade. The foliation is defined by parallel alignment of biotite, sillimanite, plagioclase, ± muscovite, and separation of mafic and felsic components to form schistose to gneissic layers. Sillimanite has several modes of occurrence: 1. as fibrous aggregates which form lenses and schlieren (i.e. fibrolite), 2. as small prismatic crystals intergrown with biotite, and 3. as pods of prismatic crystals which are possibly pseudomorphs of M2 kyanite. Locally, muscovite and K-feldspar are intergrown in the presence of quartz and sillimanite, indicating the onset of the second sillimanite isograd defined by the reaction muscovite + quartz = K-feldspar + sillmanite + H_2O.

The later event (M3) is associated with a separate deformation event (D2) which produced low-amplitude folds and a crenulation cleavage at a high angle to the foliation. This event resulted in partial transposition of micaceous layers, rotation of garnet porphyroblasts and strain effects such as undulatory extinction in quartz, feldspars, micas, and kinking of micas. Secondary muscovite crystallized syn- to post-tectonic relative to the crenulation and in places it separates K-feldspar from sillimanite. Idioblastic helicitic andalusite porphyroblasts developed locally and include aligned sillimanite needles. Andalusite grew post-tectonically across the crenulated foliation.

POLYMETAMORPHISM OF PELITIC ROCKS IN THE HEADQUARTERS REGION, NORTHERN IDAHO

RUENDAL, A.P., and RICE, J.M.

The observations made to date in the Headquarters area are consitent with the polymetamorphic history of this region developed by Lang and Rice (1985) and Carey (1985). M2 metamorphism was typically Barrovian in character with pressure ranging from 4500 bars to as much as 7000 bars. The presence of M3 andalusite and cordierite(?) indicates low pressures relative to M2. If the development of the crenulation cleavage is related to uplift of the Idaho batholith as suggested by Carey (1985), the uplift path in P-T space may be reflected and preserved by the transition from M2 to M3 mineral parageneses.

Carey, J.W. (1985) Petrology and metamorphic history of the metapelites in the Boehls Butte quadrangle, northern Idaho. M.S. Thesis, University of Oregon, Eugene.

Lang, H., and Rice, J.M. (1985) Metamorphism of pelitic rocks in the Snow Peak area, northern Idaho: Sequence of events and regional implications. *GSA Bulletin*, 96, 731-736.

THE CRYSTAL STRUCTURE OF HYDROCALUMITE FROM MONTALTO DI CASTRO, VITERBO, ITALY.

SACERDOTI, M. and PASSAGLIA, E., Istituto di Mineralogia, Università di Ferrara, Ferrara, Italia.

Hydrocalumite is the natural counterpart of a series of synthetic hydrated calcium aluminates with schematical formula $Ca_4M_2^{3+}(OH)_{12}(X \cdot nH_2O) \cdot 4H_2O$, where M^{3+} is normally Al but also Fe, Cr and Ga, X is $2Cl^-$, $2Br^-$, $2I^-$, $2(OH)$, $2(NO_3)^-$, or $(CO_3)^{2-}$, $(SO_4)^{2-}$, and n ranges from 0 to 2.

The structures of synthetic crystals were approximately solved by Ahmed and Taylor (1967) (X = 2(OH); n ≅ 1), Allmann (1968) (X =(SO_4); n = 2), Le Bel and Grasland (1969) (X =2Br; n = 0), Kuzel (1969) (X = 2Cl; n = 0). Respect to the synthetic compounds, the natural hydrocalumites described to date show a narrower range in chemical composition, M being always Al and X admistures, in different ratios, of $2Cl^-$, $2(OH)^-$ and $(CO_3)^{2-}$.

The first complete single crystal structure refinement of a natural hydrocalumite is now presented. The sample, found at Montalto di Castro, Viterbo, Italy, has chemical composition $Ca_4Al_2(OH)_{12}\{Cl_{0.65}(CO_3)_{0.65}(OH)_{0.05}(H_2O)_{1.13}\} \cdot 4H_2O$, obtained by microprobe and TG analyses. The structure (space group C 2/c, a = 10.020(1), b = 5.751(1), c = 16.286(3) Å, β = 104.22(4)°, Z = 2), was solved by direct methods and refined to R = 0.022.

Portlandite-like layers containing an ordered arrangement of Ca and Al cations in a 2:1 ratio alternate with intermediate layers containing water molecules and anions. The Al cations are coordinate by six (OH), the Ca ones by six (OH) and one H_2O. The layers are linked by the interlayer anions through hydrogen bonds of water molecules. Due to the ordening of interlayer atoms, the crystal present a superstructure with b = 11.501 Å and space group P 2/c. This superstructure is now under investigation.

References

AHMED, S.J. and TAYLOR, H.F. (1967). Nature, 215, 622-623.
ALLMANN, R. (1968). N. Jb. Miner. Mh., 1968, 140-144.
LE BEL, F. and GRASLAND, G. (1969). Proc. 5th Int. Symp. Chem. Cement, Tokyo, 1968, 2, 79-83.
KUZEL, H.J. (1969). Proc. 5th Int. Symp. Chem. Cement, Tokyo, 1968, 2, 93-97.

APPLICATION OF ORDER PARAMETER THEORY TO THE THERMODYNAMIC PROPERTIES OF PHASE TRANSITIONS.

SALJE,E., Dept. of Earth Sciences, University of Cambridge, Downing Street, Cambridge, CB2 3EQ, U.K.

Transformations between two polymorphic minerals are related to changes in their respective Gibbs energies. The relevant energy difference and its fluctuation is described by a thermodynamic quantity, called the "order parameter", which may represent a variety of physical features depending on the transformation mechanism. Typical quantities described by the order parameter are atomic movements (displacive phase transitions if a dynamical soft mode occurs), occupation numbers and clustering (order-disorder transitions), Jahn Teller distortions, percolation paths, positions of mobility edges with respect to Fermi levels and many others.

In many cases, the thermodynamic behaviour of the mineral depends only on the order parameter, irrespective of its physical meaning, and universal rules can be applied to understand the transformation behaviour without any further consideration of the particular structural behaviour. This concept has proven to be highly successful for the elucidation of phase transitions in ferroelectric and ferroelastic materials, superconductors and complex mineral structures. Examples are discussed including feldspars, langbeinite and palmierites.

The concept of thermodynamic order parameters is extended to phase transitions with more than one ordering scheme involved in the transition mechanism. In particular, phase transitions with strain-induced coupling between several order parameters occur in framework structures undergoing Al-Si ordering (e.g. its influence on the $I\bar{1}$-$P\bar{1}$ transition in anorthite or the high albite-low albite thermal crossover). It is shown that displacive phase transitions are often most sensitive to such non-critical ordering processes. They can, therefore, be used as highly sensitive detectors of Al-Si disorder in framework silicates.

PHLOGOPITE: A PETROGENETIC INDICATOR DURING KIMBERLITE MAGMATISM

SALPAS, Peter A. and TAYLOR, Lawrence A., Dept. of Geological Sciences, Univ. of Tennessee, Knoxville, TN 37996, USA.

Mineralogical studies of kimberlites provide valuable insights into the nature of the upper mantle and lower crust. For the most part, such studies focus on included xenoliths and megacrysts which represent samples brought up from depth. Mineralogical studies of kimberlites per se generally are of a classificatory nature, e.g., to distinguish between kimberlite and lamprophyre. Yet kimberlite is generated in the upper mantle/lower crust, and their minerals should offer clues to mantle conditions and to processes operating at depth and during the ascent of the kimberlitic magma. In this context, we have focussed our studies on the nature of phases which crystallized directly from the kimberlite melt. In particular, this report deals with the chemistry of phlogopites from the micaceous kimberlite at Blue Ball, Arkansas (1), 100 km. north of Murfreesboro.

Phlogopite occurs as both groundmass and phenocryst phases in the Blue Ball kimberlite. One aspect of these micas that holds important petrogenetic information is their pleochroism. Phenocryst micas are characterized by normally pleochroic cores with patches and rare rims that display reverse pleochroism. The patches are a replacement texture and are associated with resorption features such as holes, embayments, and fritted edges. In contrast, groundmass micas are either wholly reversely pleochroic or are made up of normally pleochroic cores overgrown by distinct reversely pleochroic rims. Domains of normal pleochroism in both occurrences of mica are compositionally identical, whereas domains of reverse pleochroism are heterogeneous, negating comparison between groundmass versus phenocryst phases.

Reverse pleochroism in phlogopite is a product of tetrahedrally coordinated Fe^{3+} (2,3). In these micas, Si^{4+} and Al^{3+} occupy the tetrahedral sites so that reverse pleochroism signals a deficiency in one or both of these ions. Furthermore, it has been suggested that Ti^{4+} shows a greater tetrahedral site preference than Fe^{3+} (4). Regardless of which ion Fe^{3+} substitutes for, the presence of reverse pleochroism in association with normal pleochroism is evidence for a significant change in intensive properties of the magma, with particular regard to the chemical potential of Fe^{3+}.

PHLOGOPITE: A PETROGENETIC INDICATOR DURING KIMBERLITE MAGMATISM
SALPAS, P.A. and TAYLOR, L.A.

A combination of the textural and compositional observations outlined above allows us to make inferences regarding the history of crystallization of Blue Ball phlogopites and the petrogenesis of the kimberlite. Phlogopite crystallization was initiated at depth with growth of the normally pleochroic phenocrysts. This period of crystallization was interupted by rapid injection of the magma into upper crustal levels. The curvature of the kimberlite solidus implies that in this event the magma might attain high degrees of superheat. Resorption of the early-crystallized phenocrysts occurred until magma temperatures adjusted to ambient conditions, at which time a second period of phlogopite crystallization began. Initially, this second period saw growth of normally pleochroic micas. However, an increase in fO_2 during the later stages of crystallization increased $a_{Fe^{3+}}$ which brought about an increase in tetrahedrally coordinated Fe^{3+}. The resulting growth of reversely pleochroic phlogopite mantled the groundmass grains and invaded the phenocryst phases. Such an increase in fO_2 is typically well-documented in the oxide phases, particularly ilmenite (5). This replacement of normally pleochroic mica is a type of **autometasomatism.**

REFERENCES: (1) Salpas and Taylor (1986) Jour. Geol., in press; (2) Wones (1963) Am. Jour. Sci. 261, 581-596; (3) Faye and Hogarth (1969) Can. Mineral. 10, 25-34; (4) Farmer and Boettcher (1981) Am. Mineral. 66, 1154-1163; (5) Hunter and Taylor (1984), Am. Mineral. 69, 16-29.

TETRAHEDRAL CATION DISTRIBUTION IN PHYLLOSILICATES 2:1 BY ^{29}Si NMR SPECTROSCOPY.

Jesus Sanz, Carlos P. Herrero and Jose M. Serratosa.
Instituto de Fisico-Quimica Mineral CSIC, Serrano 115 28006 Madrid (Spain).

NMR spectroscopy affords a valuable adjunct to diffraction methods in crystalline structure analysis permitting in certain cases, the identification of different crystalline environments of ions and the determination of short range order in crystalline solids.

The ^{29}Si NMR spectra of phyllosilicates 2:1 (1-3) consists of several components which correspond to the different possible environments of Si in the tetrahedral sheet, i.e. Si surrounded by 3Si, 2Si1Al, 1Si2Al and 3Al. The analysis of the Si,Al distribution can be made using two different approaches: a)by the use of certain parameters deduced from the NMR spectra that give information about the nature of neighboring cations of Al and b)by comparison between the experimental and model generated Si NMR intensities.

From the relative intensities of the ^{29}Si NMR components it has been possible to determine tetrahedral Si/Al ratios and to show that Loewenstein's rule is obeyed (avoidance of tetrahedral Al-O-Al linkages). Information about second neighbor cations of Al can be obtained from the parameter P_2

$$P_2 = \frac{I_2 + 3I_3}{I_1 + 2I_2 + 3I_3}$$

which gives the probability that the second neighbor of Al be also an Al. In this expression I_1, I_2 and I_3 are the intensities of NMR components associated to Si surrounded by 1, 2 or 3 Al. The comparison of experimental and calculated values for a random model in which the Loewenstein's rule has been introduced indicates that the Al ions are more dispersed that what is required by this rule (4).

A more complete information on Si,Al distribution is obtained when all the experimental intensities are compared with those corresponding to different models of tetrahedral cation distribution generated by a computer following a Montecarlo procedure. For all the layer silicates analyzed,with a range of Al fractional content of $0.12 < x < 0.29$, the model that best fits the experimental NMR results is one in which the number of Al per hexagonal ring is maintained as close as possible to the average value corresponding to each composition (4,5).

This study proves that tetrahedral cation distribution is mainly controlled by a requirement of homogeneous dispersion of charges in order to minimize the electrostatic energy. This requirement includes as a partial aspect the Loewenstein's rule.

References:

1.Sanz,J. and Serratosa,J.M., J.Amer.Chem.Soc., 106, 4790 (1984).
2.Mägi,M.,Lippmaa,E.,Samoson,A.,Engelhardt,G. and Grimmer,A.R., J.Phys.Chem., 88, 1518 (1984).
3.Kinsey,R.A.,Kirkpatrick,R.J.,Hower,J.,Smith,K.A. and Oldfield,E., American Mineralogist, 70, 537 (1985).
4.Herrero,C.P.,Sanz,J. and Serratosa,J.M., Solid State Comm., 53, 151 (1985).
5.Herrero,C.P.,Sanz,J. and Serratosa,J.M., J.Phys.C: Solid State Phys. 18, 13 (1985).

APPLICATION OF APD 3600 IN QUANTITATIVE MINERALOGICAL PHASE ANALYSIS

Shondeep L. Sarkar
Faculty of Applied Sciences
University of Sherbrooke, Canada

The APD 3600 automated X-ray powder diffractometer system comprising the diffractometer unit, a minicomputer with its peripherals and the software appears to have taken a major step forward in the direction of quantitative mineralogical phase analysis. In order to test the versatility of the software and the high degree of automation of the system, the author used mixtures of cement minerals of known proportions. Cement minerals were deliberately chosen (as an extreme), because solid solution in most of these phases, and thus their variable diffraction patterns, coupled with overlaps of several important peaks, render quantitative analysis extremely difficult.

Of the several routines available in the package program, the two used were QUALSYS and QUANTSYS, the former for data collection and peak identification, and the latter for quantitative phase analysis. Each peak is identified by the top of a three point parabola fit through the smoothed data points, which gives very accurate peak positions. Using the MATCH subroutine enables one to compare the diffraction pattern with the known JCPDS pattern, and in the case of an unknown mineral the application of the SANDMAN program, which lists the possible JCPDS fits and the corresponding reliability factors, proves highly effective in the identification process.

The QUANTSYS program supports four different correction models, namely linear, internal standard, emperical and pseudo-binary. In case of cement minerals the linear model proved most appropriate. The internal standard method can be successful only if sufficient homogeneity in the mix is obtained. The emperical method created a major difficulty in optimizing a set of interphase correction coefficients, whereas the pseudo-binary which assumes that the phases (other than the analyte) do not change significantly in relative concentrations, had to be rejected considering the wide compositional variations that are possible in cement. The program also calculates interphase absorption effects and the maximum penetration depth, thus predicting the possible sources of errors in the quantification process.

The program performs regression analysis on each phase until the iterated solutions have converged or until 48 iterations have been completed. The progress of the regression can be monitored by the value of the weighted sum of squares printed at the end of each regression. The resultant fits can also be printed for inspection. Finally, the program calculates the concentration for each phase after taking into consideration the corrected coefficients obtained from the regression analysis.

The application of QUALSYS and QUANTSYS proved successful in quantifying the cement phases within reasonable degree of confidence, and is anticipated to be useful for routine quantitative analysis of mineralogical phases.

CHEMICAL COMPOSITION OF ORTHOPYROXENE IN THE BRONZITE ANDESITE OF GOSHIKIDAI, NORTHEAST SHIKOKU, JAPAN

SATO, H., Dept. Integrated Arts & Sciences, Hiroshima University Hiroshima, 730 Japan

The volcanic rocks of Goshikidai plateau (ca. 10 km^3) belongs to the middle Miocene Setouchi volcanic province of southwest Japan (Tatsumi & Ishizaka 1982, EPSL 60). They are composed of pyroclastic deposits of garnet-biotite rhyolite and hornblende dacite, and four lava flows of bronzite andesites, in the ascending order. SiO_2 content of the bronzite andesite varies from 55 to 67 wt.%. The glassy variety of the most silicic bronzite andesite has been named "sanukite" by Weinschenk (1891). The bronzite andesite may carry phenocrysts of orthopyroxene, olivine, hornblende, augite and plagioclase. The highest Mg/(Mg+Fe) ratio of orthopyroxene in each rock specimen ranges from 0.87 to 0.92, and does not correlate with the Mg/(Mg+Fe) ratio of the host rocks (Figure 1). The low values of the calculated ferric iron content of the orthopyroxene (Figure 2) suggest that the magma was not oxidized when the magnesian orthopyroxene crystallized. The Cr_2O_3 content of the magnesian orthopyroxene is 0.5-1.0 wt.%, similar to or even higher than those of orthopyroxenes in mantle-derived peridotites. Because

Figure 1

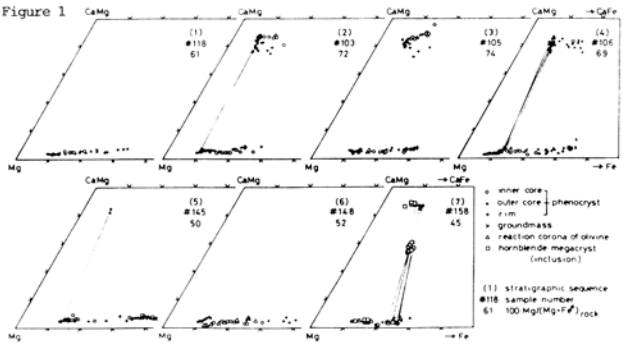

Cr content of the andesites rapidly decreases as fractionation proceeds, the Cr-rich magnesian orthopyroxene may have crystallized from rather primitive andesitic magmas. On the other hand, the magnesian orthopyroxene phenocryst often shows reverse or oscillatory zonings in the core, and normal zoning at the rim. The inner core of the reversely-zoned orthopyroxene phenocrysts have low Ca and high Al contents, and show wide range of Mg/(Mg+Fe) ratio (Figure 3). These compositional characteristics of orthopyroxene, as well as the linear increase of $^{87}Sr/^{86}Sr$ ratio against the increase of SiO_2 content of the host andesites suggest that the magnesian orthopyroxene phenocrysts have crystallized during ascent and mixing of high-magnesian andesite and acid andesite or dacite magmas.

Figure 3

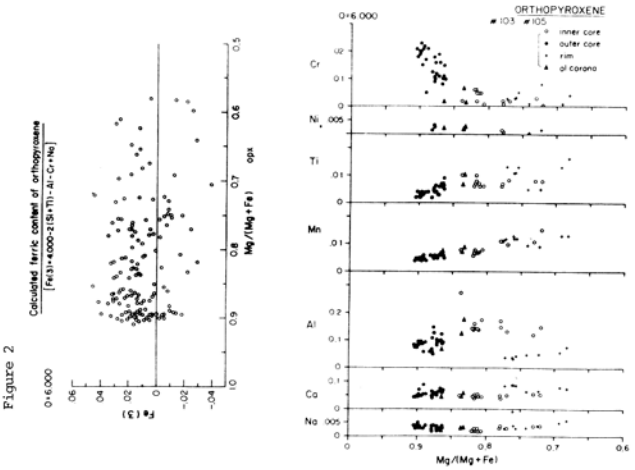

Figure 2

PHASE EQUILIBRIA AT HIGH PRESSURE AND TEMPERATURE

S.K.SAXENA, Y.FEI, Department of Geology and Graduate Center, City University of New York, Brooklyn College, Brooklyn, N.Y. 11210

Phase equilibrium calculations on chemical systems appropriate to upper and lower mantle (with pressure not exceeding one Mbar) require thermochemical data on phases at low to high pressures and at low to high temperatures (ca. 4000 K). The thermochemical and physical data on solids and fluids usually measured over narrow pressure/temperature ranges must be extrapolated to natural conditions using empirical expressions (e.g. Maier-Kelley expression for heat capacity). The applicability of such expressions over an extended range of temperature must be thoroughly understood for mineralogical phases and fluids. Based on a large set of heat capacity data; on silicates, the following expression has been found to be compatible both with the Debye formulation at high temperatures and the measured low-temperature heat capacity data:

$$C_p = 3Rn(1 + k_1T^{-1} + k_2T^{-2} + k_3T^{-3}) + A(T)T$$

where R is gas constant, n is the number of atoms in the chemical formula, k's are the coefficients determined usually from low temperature heat capacity data and

$$A(T) = \alpha^2(T)\, V(T)\, K(T)$$

where α is the isobaric coefficient of thermal expansion and K the isothermal bulk modulus.

The pressure-temperature dependence of molar volume is best modeled through the use of the Birch-Murnaghan equation:

$$P = (3/2)K[(V_o/V)^{7/3}-(V_o/V)^{5/3}]$$

$$[1-(3/4)(4-K')\{(V_o/V)^{2/3}-1\}+\ldots]$$

where K'is the first derivative of the bulk modulus, V_o the volume at zero pressure.

The simpler Murnaghan formulation may be used at pressures upto 300 kbar in phase equilibrium computations, but at higher pressures the Murnaghan formulation becomes progressively worse.

For many fluids, the high pressure shock-wave data supports the use of a form of corresponding states equation. For the gases H_2, O_2, N_2, Ar and CH_4, the equation in reduced temperature and reduced pressure for Z (=PV/RT) is

$$Z = -.668058$$
$$+(3.220261E\text{-}2T_r^{-1}+6.06913E\text{-}2T_r^{-2})P_r$$
$$-(9.1551E\text{-}8+2.83256E\text{-}10T_r)P_r^2+2.51846E\text{-}12P_r^3$$
$$-(0.365207T_r-1.004771nT_r)-(6.547011E\text{-}2T_r)P_r^{-1}$$
$$+(4.97216E\text{-}1T_r+.59568T_r^{-.5})P^{-.5}$$
$$+(3.37461E\text{-}3T_r+4.8713E\text{-}3T_r^{.5})P^{.5}+.508744lnP_r.$$

We prefer the use of Kohler formulation for multicomponent systems:

$$\Delta Z^{ex}_{12\ldots N} = \Sigma^N_{i=1}\Sigma^N_{j>i}\,(X_i+X_j)(f_i+f_j)\,(\Delta Z^{ex}_{ij})^*$$

in which the last term is the molar excess property (enthalpy, entropy, volume, free energy etc.) of the binary system with components at the same molar ratio as the multicomponent system and f_i and f_j are weighted mole fractions using weighting factors based on the excess properties of the binary systems. X is used as the mole fraction in the multicomponent system.

All the formulations considered above have now been incorporated in the Gibbs free energy minimization program and many phase equilibrium computations relevent to upper and lower mantle have been performed with interesting results.

STRUCTURE REFINEMENT OF A NATURAL HIGH SANIDINE OF UPPER MANTLE ORIGIN

SCAMBOS, T. A.; SMYTH, J. R.; MCCORMICK, T. C., Dept. of Geological Sciences, University of Colorado, Boulder, CO 80309

The crystal structure of sanidine from a coesite-sanidine grospydite nodule from the Roberts Victor kimberlite (Smyth and Hatton, 1977) has been refined using x-ray techniques. Microprobe analyses yield an $Or_{98}Ab_1An_0Cn_1$ composition (Ba content is approximately 4000 ppm). The coexistence of coesite with high sanidine in the nodule indicates an equilibration pressure of at least 29 kbar (Boyd and England, 1960), and temperatures in excess of 900°C (Smith, 1974). Additional minerals found in the nodule (omphacitic pyroxene, grossular, and kyanite) further constrain the equilibration conditions to about 48-50 kbar and 1050-1125°C (Wohletz and Smyth, 1984; McCormick and Smyth, 1986). Quenching was sufficiently rapid to preserve large crystals of coesite.

Cell parameters (and errors) determined by least-squares refinement of setting angles from 25 strong reflections with $2\theta > 45°$ (Mo Kα) are: a = 5.595(3) Å; b = 13.028(5) Å; c = 7.175(2) Å; β = 115.94(2)°. The space group is C2/m. These cell parameters indicate very high Al-Si disorder, as shown by a b-c plot (figure 1). Refinement of the structure is based on 6927 measured reflections with a maximum 2θ of 80°. Equivalent measured reflections were combined into a set of 2332 reflections with an R for averaging (after applying an absorption correction) of 0.020. After removal of weak ($F_{obs} < 3\sigma$) and seven anomalous data points, least squares refinement of positional and anisotropic thermal parameters on 2150 reflections gave an R value of 0.055 and an R_{wt} of 0.047.

Applying techniques outlined by Kroll and Ribbe (1983), T_1 site Al occupancy was calculated to be 0.266 to 0.291, depending on method used. Within statistical error, the structure is completely disordered, and may represent a more disordered state than previous synthetic high alkali feldspars (Al in T_1 0.27-0.28). A comparison of individual T-O distances with Phillips and Ribbe (1973, figure 2) shows close agreement with synthetic high-disorder feldspars. Further refinements of the structural parameters are in progress.

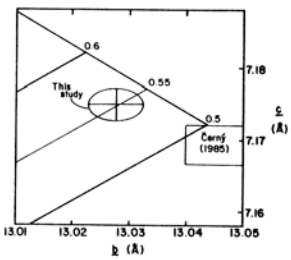

Figure 1. Plot of b-c cell edges.

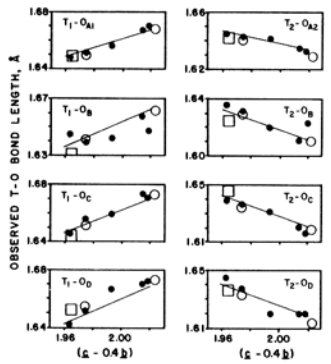

Figure 2. T-O distances vs. b-0.4c. Square represents this study; other data are from Phillips and Ribbe, 1973.

This unusual mantle occurrence of alkali feldspar and its long-term exposure to high P and T conditions followed by rapid quenching is consistent with the very high disorder of the mineral. The only other natural end-member sanidines of similar structural state are pegmatitic adularia reported by Černý (1985), which are shown in figure 1 for comparison.

Boyd, F.R., England, J.R. (1960) Jour. Geoph. Res., 65, 749-756.
Černý, P. (1985) Eos, 66, 1117.
Kroll, H., Ribbe, P.H. (1983) MSA Rev. of Mineral., Vol. 2, 2nd ed., 57-99.
McCormick, T.C., Smyth, J.R. (1986) this volume.
Phillips, M.W., Ribbe, P.H. (1973) Am. Mineral., 58, 263-270.
Smith, J.V. (1974) Feldspar Minerals I, Springer-Verlag, 627 p.
Smyth, J.R., Hatton, C.J. (1977) Earth and Planet. Sci. Lett., 34, 284-290.
Wohletz, K.H., Smyth, J.R. (1984) in Kimberlites II: The Mantle and Crust-Mantle Relationships, J. Kornprobst, ed., 33-42.

ON SATELLIC TYPE OF BRAZIL TWINS IN NATURAL QUARTZ.

SCANDALE, E. and STASI, F., Dipartimento Geomineralogico, Università di Bari, Via G. Salvemini, 70124 Bari, Italy.

Several natural quartz crystals have been studied by X-ray topography to identify the nature of some defects that appeared as small inserts in the shape of right and equilateral triangles, when basal slices were studied with symmetrical reflections $10\bar{1}0$. Optical tests in polarized light and chemical etching of basal plates suggested the inserts would be satellic types of Brazil twins.

Analysis of the topographic contrasts should that the observed defects could not be worked out as common surface defects and that care must be taken for unambigous correlation between morphological crystal axes and those utilized in X-ray diffraction indexing. Extinction examination confirmed the optical tests and it was possible to state that the triangular shaped contrasts are due to growth twins - Brazil law - in the form of small inserts. Tacking into account that the structure factors F_L and F_R, for the left-handed and right-handed structures respectively, are related by $F_L = F_R \cdot \exp(i\varphi)$ and that the two parts of the Brazil twin are displaced relative to one another by a vector $\underline{R}$ so as to introduce an additional phase angle $2\pi\underline{g}\cdot\underline{R}$, the total phase angle is $\alpha = 2\pi\underline{g}\cdot\underline{R} + \varphi$.

It follows that the boundary of the Brazil twin will not be visible as diffraction contrast when $\alpha = \pm 2\pi n$, then composition planes and displacement vectors can be determined.

The results of the present work are in agreement with those obtained by other authors in the case of thin lamellae and confirm that X-ray topography is a powerful tool for the study of growth defects. In fact Brazil twins are difficult to recognize by classical mineralogical and crystallographic tools when they are thin plates or bodies of restricted sizes inserted in a large crystal.

SUPERPARAMAGNETIC CRYSTALLINE PRECIPITATES IN VOLCANIC GLASSES OF THE KBS TUFF: MINERALOGY, MAGNETISM AND RELATIONSHIP TO VOLCANISM

SCHLINGER, C.M., Dept. of Geology & Geophysics, Univ. of Utah, Salt Lake City, Utah 84112, USA

Volcanic glasses from the water-lain KBS tuff of the Turkana basin of northern Kenya exhibit marked variability in magnetic susceptibility and color. We have examined both free shards of glass and pumice. The glasses vary in color from clear (colorless or 'light') to dark brown, with magnetic susceptibility increasing with opacity. The shards can be isolated by color using magnetic separation; the light and dark shards are equivalent in composition. The darker shards are superparamagnetic at room temperature (Fig. a); at 7°K magnetic hystersis is present (Fig. b). The origin of this superparamagnetism, established using TEM, is a group of inclusions of Fe-rich spinel. In any shard this population has a remarkably uniform spatial distribution and narrow size distribution, with a maximum grain size (darkest glass) of ~10 nm. The light glass is free of inclusions.

Similar inclusions are known in synthetic glasses (e.g., O'Horo & O'Neill 1977; Beall & Rittler, 1976) and form due to high-temperature precipitation in quenched iron-bearing homogeneous glass. Our theory is that the precipitate formed in quenched KBS glass during eruption, c. 1.9 m.y. ago, at temperatures of 1000-1300 °K. Experiments support this idea: heating light KBS shards results in an increase in their magnetic susceptibility and darkening (1000 °K for 17 hours or 1250 °K for 5 minutes). The thermally-activated precipitation in quenched glasses affects the optical properties of the glass with both absorption and Rayleigh scattering playing a role. The variable optical properties in this suite of shards result then from variable cooling histories, rather than compositional variations.

Rare pumices of the KBS tuff include conspicuous 'banded' pumice, which is a composite of light and dark glass of differing compositions. This banding is thought to present a snapshot of magma mixing (e.g., Macdonald and Katsura, 1965). The dark glass of the banded pumice is Fe-enriched relative to the light glass of the pumice (about twice as much iron). The pumice is age-equivalent to the KBS tuff and the light pumice is isocompositional with the KBS glass shards. The dark pumice has higher susceptibility than the light pumice and contains a

precipitate similar to that of the dark KBS shards. The cooling history of the pumice was such that precipitation occurred in the 'mafic' endmember (dark pumice) but not in the 'silicic' endmember (light pumice). Banded pumices appear so due to thermally-activated precipitation and darkening in the 'mafic' portions. The optical properties of banded pumices are thus a function of both thermal history and composition, in contrast to the KBS shards.

These conclusions can presumably be generalized to color variations that are observed in volcanic glasses elsewhere. Because light and dark shards of the KBS tuff are isocompositional it appears as though magma mixing did not occur on a grand scale during the eruption of the KBS parental magma. Had such occurred the dark shard composition would be skewed towards that of the 'mafic' endmember (dark pumice) which it is not.

Finally, the KBS Shards present us with a natural sample of spinel crystals at the lower end of attainable dimension, ~3 to ~10 nm. A desired size distribution can be attained by standard magnetic separation methods.

References: Beall, G. H. and Rittler, H. L. (1976) Ceram. Bull. 55, 579-582; MacDonald, G. A. and Katsura, T. (1965) Geol. Soc. Am. Bull. 76, 475-482; O'Horo, M. P. and O'Neill, J. F. (1977) in Levy, R. A. and Hasegawa, R, Eds., Amorphous Magnetism II, Plenum Press, pp 651-662.

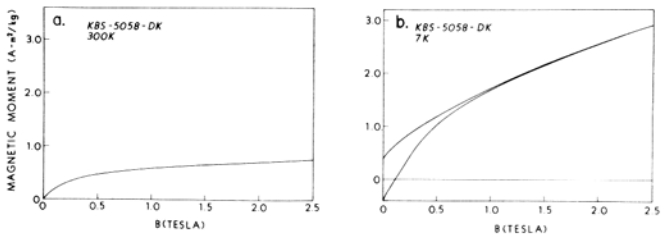

• THE ROLE OF POINT DEFECTS IN SOLID PHASES

SCHMALZRIED, H., Institut für Physikalische Chemie und Elektrochemie und SFB 173 der Universität Hannover, Hannover, West Germany

The role that point defects play in determining the physical and chemical properities of crystals is discussed systematically. Two basic aspects are treated in detail:

(1) Point defect thermodynamics. This statistically oriented branch of solid state thermodynamics has been developed in order to answer the following question: In which way do the concentrations of defects (structural elements) depend on the complete set of intensive thermodynamic variables (P, T, chemical potentials μ_k of crystal components k). The conceptual difficulty arises from the fact point defects are structural elements of the crystal lattice, but not thermodynamic components. A consistent thermodynamic treatment of components, building elements and structural elements is presented. Theoretical predictions on the concentration dependence of defects are verified for a number of oxide systems, such as CoO, Fe_3O_4, (Ni,Fe)O, Fe_2SiO_4 [1,2,3,4].

(2) Reactivity of solids due to point defects. At sufficiently high temperatures (in local thermodynamic equilibrium) it is essentially the point defects that render the regular lattice constituents (atom, ion) mobile. From the balance of elementary jumps it follows for small defect concentrations that the mobility of regular structural elements is directly proportional to the respective defect concentrations. Examples (Fe_3O_4, Fe_2SiO_4) are presented [5,6]. The applications of this concept to a number of situations in the field of solid state reactions are worked out:

a) The behavior of oxide solid solutions and compounds in oxygen potential gradients, kinetic demixing and decomposition [7,8].

b) Internal oxidation (reduction) of oxide solid solutions [9,10].

c) The build-up of internal pressures in reacting systems [11].

d) Defect relaxation processes in reacting systems.

[1] U. Hölscher, H. Schmalzried, Z. phys. Chem. NF. 139, 69 (1984). [2] R. Dieckmann, Ber. Bunsenges. Phys. Chem. 86, 112 (1982). [3] F. Schneider, Doctoral Thesis, University of Hannover, 1986 [4] A. Nakamura, H. Schmalzried, Phys. Chem. Minerals 10, 27 (1983) [5] R. Dieckmann, H. Schmalzried, Ber. Bunsenges. Phys. Chem. 81, 415 (1977) [6] J. Hermeling, H. Schmalzried, Phys. Chem. Minerals 11, 161 (1984) [7] H. Schmalzried et al., Z. Naturf. 34a, 192 (1979) [8] U. Brinkmann, W. Laqua, Phys. Chem. Minerals 12, 283 (1985) [9] H. Schmalzried, Ber. Bunsenges. Phys. Chem. 87, 551 (1983) [10] K. Ostyn et al., J. Am. Ceram. Soc. 67, 679 (1984) [11] H. Pfeiffer, H. Schmalzried, Z. phys. Chem. NF. (1986) in print.

MINERALS AND MINERAL ASSEMBLAGES OF HIGH-PRESSURE METAMORPHIC CRUSTAL ROCKS

SCHREYER, W., Institut für Mineralogie, Ruhr-Universität Bochum, D-4630 Bochum 1, Fed. Rep. of Germany

Since the discovery of the pyrope-coesite rock in the Alps (Chopin 1984) it is clear that parts of the continental crust may be subducted to mantle depths of as much as about 100 km. The geotectonic regimes of deep crustal subduction are continent/continent collision zones such as the Mediterranean between the European and African plates during the Mesozoic. However, such processes probably took also place in older orogenies. In addition, it has long been recognized that especially the predominantly basic materials of the oceanic crust may be subducted to considerable depths.

Eclogites with their characteristic assemblage omphacite+garnet are formed by deep subduction of basic rocks, but they may also represent primary crystallization products of basic melts within the mantle. Therefore, unless eclogites show typical crustal textures (pillows etc.), they cannot be unequivocally regarded as of crustal origin. Such origin is clearly demonstrated, however, for all those high-pressure rocks that have unambiguously sedimentary bulk chemistry such as ironstones or metapelites.

In the last two decades a number of high-pressure minerals and mineral assemblages were identified in nature and for most of them the approximate minimum pressures required for stability were determined by experiment. These minerals may be Na-bearing like jadeite and glaucophane, Ca-bearing (lawsonite, aragonite), Fe-rich (deerite, howieite, zussmanite, ferrosilite), or dominantly magnesian like pyrope. This paper will deal mainly with the latter ones, which were detected recently in metapelitic high-pressure rocks of varying metamorphic grade. Some of them are simply Mg-rich members of common rock-forming Fe- or Mn-minerals that are stable at lower pressures as well. The minerals are listed in the following, together with crude information on their chemical composition in nature as well as on the necessary minimum pressure ($P_{fl}=P_{tot}$ unless otherwise noted) of the synthetic end members. Only phases requiring more than 5 kbar are given.

High-Pressure Minerals: Mg-carpholite (up to 95 mol% end member; 6 kbar at 370°C); yoderite (always with some Fe^{3+}; 9 kbar at 750°C); Mg-staurolite (up to 95 % end member recently found by Chopin, pers.comm.; 12 kbar at 750°C); pyrope (up to 98 % end member; 15 kbar at 800°C); Mg-chloritoid (up to 74 % end member; 18 kbar at 600°C); high-silica phengite (up to 3.8 Si atoms per formula unit; for this composition 20 kbar at 600°C); ellenbergerite (for the pure MgTiAl silicate some 37 kbar at 750°C; incorporation of P for Si lowers this minimum pressure considerably).

In addition, the following high-pressure mineral assemblages may be enumerated: Talc+kyanite (6 kbar at 625°C); talc+corundum (7 kbar at 700°C); talc+phengite (11 kbar at 600°C); enstatite+Al_2SiO_5 (6 kbar, 700°C, in the absence of water); sapphirine+quartz (8 kbar, 900°C, water deficiency required); pyrope+coesite (29 kbar at 825°C). The assemblages talc+chloritoid and talc+garnet containing considerable Fe in the respective second phases have not been calibrated experimentally as yet. For details see Schreyer (1985).

Whether or not the above high-pressure minerals and assemblages are preserved in natural rocks depends entirely on their retrograde pressure-temperature-time paths during uplift or tectonic transport. Unlike many eclogites the more acidic and aluminous rocks show favorable reaction kinetics for low-pressure-reequilibration, so that, unfortunately, the preexisting high-pressure mineralogy is often no longer there and can perhaps only be reconstructed on textural grounds.

CHOPIN, D. (1984) Coesite and pure pyrope of the Western Alps: a first record and some consequences. - Contrib.Miner.Petrol. 86,107-118.
SCHREYER, W. (1985) Metamorphism of crustal rocks at mantle depths: High-pressure minerals and mineral assemblages in metapelites. - Fortschr.Miner. 83,277-261.

INTERGROWTHS AND REACTIONS INVOLVING ORTHO- AND CLINO-PYRIBOLES FROM ORIJÄRVI, SOUTHWEST FINLAND

SCHUMACHER, J. C., Mineralogishes Institut, Olshausenstr. 40 Christian-Albrechts-Universität, Kiel, F. R. Germany

The PYRiboles have been found in two assemblages: 1) PYR + PHLogopite + Zn-rich SPinel and 2) PYR + PHL + Mg-CHLorite. Characteristic (010) lamellae (Veblen and Burnham, 1978) are observed optically in both samples, and high resolution transmission electron microscopy (HRTEM) confirms the presence of triple chains in assemblage 1. The HRTEM study of assemblage 1 PYR shows that large double-chain areas on the order of thousands of Å s and triple-chain lamellae (jimthompsonite, JT) as wide as 311 Å exist but that no intermediate ordered sequences of double and triple chains (e. g. chesterite) are present. Some double-chain areas are composed of lamellae of ANTHophyllite and CUMMingtonite. Qualitative energy dispersive analyses indicate only traces of Ca are present in ANTH but significant amounts in the CUMM. This unmixing may result from the accomodation of the Ca in the double-chain part. No analogous unmixing in the JT has yet been detected. The a*-c* diffraction photographs confirm the presence of CUMM and ANTH.

Differences in cation totals between the double- and triple-chain parts (23 oxygen basis) give a rough estimate of the proportions of the two structures present at an analytical point. This criterion indicates that Si, Al, and Na increase and Fe and Ca decrease in the triple-chain structure relative to the double-chain structure, and are explained by the differences in the proportions of A-site, octahedral sites, and tetrahedral sites between the two structures. Representative formulae of JT (provisionally) from assemblages 1 and 2 are:
$Na_{.092}(Na_{.022}Ca_{.076}Mn_{.027}Fe_{1.550}Zn_{.037}Mg_{8.165}Ti_{.006}Al_{.117})(Si_{11.797}Al_{.203})$
$Na_{.080}(Na_{.002}Ca_{.063}Mn_{.020}Fe_{1.490}Zn_{.024}Mg_{8.283}Ti_{.006}Al_{.119})(Si_{11.800}Al_{.200})$
both with $O_{32}(OH)_4$, and of ANTH from assemblages 1 and 2 are:
$(Na_{.034}K_{.002})(Na_{.001}Ca_{.077}Mn_{.024}Fe_{1.349}Zn_{.053}Mg_{5.429}Al_{.067})(Si_{7.898}Al_{.102})$
$Na_{.032}(Na_{.002}Ca_{.054}Mn_{.021}Fe_{1.313}Zn_{.018}Mg_{5.518}Ti_{.002}Al_{.071})(Si_{7.892}Al_{.108})$
both with $O_{22}(OH)_2$. In assemblage 1 SP is $(Mg_{.281}Fe_{.148}Zn_{.570})Al_2O_4$ and the Mg/(Mg+Fe)(X_{Mg}) of the PHL = 0.921. In assemblage 2, X_{Mg} of PHL = 0.913 and CHL = 0.891. The ANTH-JT pair coexisting with SP (assemblage 1) is richer in Fe than the pair coexisting with CHL (assemblage 2). Zn is likely to stabilize SP in assemblage 1.

Assuming that Fe^{2+} and Mg are partitioned similarly between the distorted octahedral (dM) and regular octahedral (rM) sites of the ANTH and the JT the differing proportions of dM and rM in the two structures allows the estimation of site occupancies and calculation of an intersite distribution coefficient for Fe-Mg. For assemblage 1 $\ln(Kd^{dM-rM}_{Fe-Mg}) = 2.630$ and for assemblage 2 it = 2.714. The Kd^{dM-rM}_{Fe-Mg} is extremely T dependent (Seifert, 1977) and the values obtained here suggest equilibration at about 600°C, which is consistent with metamorphic T estimates of 550 to 630°C (Schreurs, 1985). The Kd^{dM-rM}_{Fe-Mg} estimated in this way should represent the last T of equilibration between the double- and triple-chain structures, but given the strong T dependence, later intersite Fe-Mg redistribution is likely to have occurred within both phases.

The high variance of these assemblages, their inferred T of equilibration, and lack of talc as a product of triple-chain formation suggest that the JT (assemblage 1) is not simply an intermediate step in the transformation of ANTH to talc but that it actually has a stability field. The textures suggest that unmixing of the ANTH and CUMM followed the JT formation, and using the remaining phases, the following continuous Fe-Mg reactions are possible mechanisms of JT formation via hydration of ANTH. For assemblage 1:

MgFe-ANTH + MgFe-fTC + H_2O = MgFe-JT + MgFe-SP,

and for assemblage 2:

MgFe-ANTH + MgFe-fTC + H_2O = MgFe-JT + MgFe-CHL

(where fTC is talc component in PHL, double chains and triple chains are treated as ANTH and JT).

References

Schreurs, J. (1985) Lithos, 18, 69-80.
Seifert, F. A. (1977) Amer. Jour. Sci., 278, 1323-1333.
Veblen, D. R., & Burnham, C. W. (1978) Amer. Min., 63, 1000-1009.

PROGRADE METAMORPHISM OF HORNBLENDE- AND EPIDOTE-BEARING ROCKS, LOWER TO UPPER AMPHIBOLITE FACIES, CENTRAL MASSACHUSETTS, USA

SCHUMACHER, Renate, Mineralogisch-Petrographisches Institut, Poppelsdorfer Schloß, 5300 Bonn, F. R. Germany

Hornblende- and epidote-bearing rocks that underwent Acadian (Devonian) metamorphism were studied in areas with estimated peak metamorphic conditions ranging from about 580°C, 6.2 kbar to 720°C, 6.3 kbar, which correspond to the kyanite-staurolite to garnet-cordierite zones in pelitic rocks (zones I to VI, Tracy et al., 1976; Robinson et al., 1982). Hornblende (HBL) coexisting with plagioclase (PLAG), epidote (EP), and/or clinopyroxene (CPX), ± quartz (QZ) ± garnet (GT) shows systematic changes with increasing grade of metamorphism.

Since site assignments in HBL are highly dependent on the Fe^{2+}-Fe^{3+} ratio, an accurate estimate of Fe^{3+} in microprobe analyses is crucial. An empirical ferric iron correction was derived using gravimetrically analyzed hornblendes (Leake, 1968), which are from metamorphic assemblages containing PLAG, CPX, or EP and which give the linear relationship:

$$Ca\ (M4) = -1.497\ Na\ (M4) + 1.998$$

for Na and Ca assigned to the M4 site. Since Na (M4) is highly dependent on Fe^{3+}, the above relation can be used to obtain cation sums used for the Fe^{3+} corrections. The Fe^{3+} contents of five hornblendes have been determined by Mössbauer and wet chemical analyses and the results are in reasonable agreement with the calculated values.

With increasing metamorphic grade the HBL's display the following changes in composition: increasing Ti content, increasing $(Na+K)^A$ (in A site, edenite-like substitution), increasing Al^{IV}-$(Na+K)^A$ (tschermakite-like substitution) up to Zone IV, and increasing $Fe^{2+}/(Fe^{2+}+Mg)$ ratio.

PLAG compositions range from An20 to An100. The ratio X_{Ab}/X_{Ed}, where X_{Ab} = Na/(Na+Ca) in PLAG and X_{Ed} = Na in the HBL A-site (23 oxygen basis), increases with increasing metamorphic grade.

Epidote group minerals have $Fe^{3+}/(Fe^{3+}+Al)$ that range from 0.028 (zoisite, ZO) to 0.311 (EP). ZO and clinozoisite (CLZ) are abundant in the metamorphic zones I and II, but nearly absent from these bulk compositions at higher grades, where only one sample consisting of CLZ + HBL + CPX + PLAG + minor calcite has been found (Zone IV). EP is still abundant at the metamorphic conditions of zone IV. Within zones V and VI the assemblage HBL + CPX + PLAG (without QZ) occurs in rocks with similar bulk compositions to those that contain the assemblage HBL + EP ± CPX ± GT ± PLAG ± QZ at lower metamorphic grades. The breakdown of the epidote group minerals, the disappearence of QZ, as well as the changes in mineral composition of the HBL and PLAG suggest that with increasing metamorphic grade the Fe-Mg continuous reaction:

$$HBL + EP + QZ = CPX + PLAG + H_2O, \quad (1)$$

takes place and that the $Fe^{2+}/(Fe^{2+}+Mg)$ of the minerals increases at higher metamorphic grades. When QZ has been consumed or is absent from reaction 1, the SiO_2 balance of reaction 1 can be maintained via:

$$1\ AB = 1\ (NaAl\square_{-1}Si_{-1})^{in\ HBL} + 4\ SiO_2. \quad (2)$$

Combining reactions 1 and 2 yields:

$$HBL + EP + AB^{in\ PLAG} = CPX + AN^{in\ PLAG} + (NaAl\square_{-1}Si_{-1})^{in\ HBL} + H_2O. \quad (3)$$

This reaction accounts for the observed increases in edenite content and Fe-Mg ratio of the HBL and higher An content of PLAG at higher metamorphic grades in these bulk compositions.

References

Leake, B. E. (1968) Geol. Soc. Amer. Sp. Paper 98, 200p.
Robinson, Peter et al., (1982) Guidebook for fieldtrips in Connecticut and south-central Massachusetts, 74th Ann. Meeting, New Eng. Intercoll. Geol. Conf., 289-339.
Tracy et al., (1976) Am. Min., 61, 762-775.

ENVIRONMENTAL EFFECTS ON IRON OXIDE FORMATION IN TWO FINNISH LAKES

SCHWERTMANN, U., Lehrstuhl für Bodenkunde, T.U. München, D-8050 Freising-Weihenstephan, Federal Republic of Germany; CARLSON, L., Department of Geology, University of Helsinki, SF-00171 Helsinki, Finland; MURAD, E., Lehrstuhl für Bodenkunde, T.U. München, D-8050 Freising-Weihenstephan, Federal Republic of Germany

Iron oxide accumulations at the bottom of two Finnish lakes (lake ores) contain up to 50 % Fe. DXRD (differential X-ray diffraction) and differential dissolution show these to be made up of associations of poorly crystalline goethite and ferrihydrite in various proportions. On heating under hydrothermal conditions (180°C), ferrihydrite turns into hematite, whereas goethite remains unchanged. The goethites of the oxalate treated samples were characterized by unit cell parameters, MCD ("crystallinity"), OH-bending characteristics, dehydroxylation temperature, dissolution kinetics and Mössbauer spectroscopy. The following Table shows the goethites of the two lakes to differ significantly in their properties:

Average values for goethite properties of the two lakes

	cell volume nm^3	Al subst. mole %	δ_{OH}-γ_{OH} cm^{-1}	DTA °C	k^A h^{-1}
Murto	0.13915(12)	0.07(4)	92.8(2.1)	249(6)	0.068(29)
Eno	0.13798(15)	7.9(5)	97.7(1.5)	260(4)	0.016(8)

[A] Dissolution rate constant

The difference in Al substitution is attributed to the difference in the lake bottom environment: The gravelly-sandy sediment in Lake Murto has a much lower Al supply than the silty-clayey sediment in Lake Eno, which may supply more Al during goethite formation. The difference in Al substitution explains the difference in the distance of the two OH-bending modes (δ_{OH}-γ_{OH}), in dehydroxylation temperature, and rate of dissolution in agreement with studies of synthetic goethites.

Al substitution was determined chemically from Al_s and by XRD line shift. The use of c dimension of the unit cell obtained from computer fitted XRD line profiles disagreed with the chemically determined value. Instead, agreement was obtained by using the unit cell volume. This indicates that a reduction in the c-dimension is not necessarily caused by Al substitution.

Mössbauer spectra taken at 77 K showed a gradual disappearance of (superparamagnetic) ferrihydrite present in the samples with increasing number of oxalate extractions. Goethite has magnetic hyperfine field distributions with a field of maximum probability of 48.4 T. The magnetic hyperfine field distributions of goethite do not change significantly in the course of the oxalate treatments, indicating that goethite is not fractionated by this reagent.

SIGNIFICANCE OF IRON OXIDE MINERALS IN SOIL ENVIRONMENTS

SCHWERTMANN, U., Lehrstuhl für Bodenkunde, T.U. München, D-8050 Freising-Weihenstephan, Federal Republic of Germany.

Iron oxide and hydroxides are ubiquitous minerals in soils. Generally they form by an oxidative hydrolytic decomposition of Fe(II) in silicates, which are the most important primary sources of Fe in the parent rocks from which soils form. All soil iron oxides consist simply of octahedrally coordinated Fe(III), the ligands being O^{2-} and OH^-. Five to six forms occur in soils, which differ only in the way in which the $Fe(O,OH)_6$-octahedra are arranged in space. Their color varies between red and yellow.

Besides in mineral form (goethite, hematite, lepidocrocite, maghemite, ferrihydrite, feroxyhite), Fe oxides vary both widely in crystal size and disorder (crystallinity) and in the degree of substitution of Fe(III) by Al in the octahedral position. Besides Al, Mn(III) may also substitute for Fe(III). These variations are of interest in soil science and weathering studies because they reflect the physical (water activity, temperature) and chemical (pH, Eh, composition) environment in which the Fe oxides are formed, and thereby the weathering environment. Past environments may thus also be occasionally traced back.

Mineral form: Geographically, hematite (α-Fe_2O_3) and goethite (α-FeOOH), the two most common Fe-oxides, are distributed zonally: Goethitic, yellow-brown soils free of hematite dominate in temperate zones, whereas red, hematitic soils are widespread in the subtropics and tropics. Within the tropics, the proportion of hematite increases with increasing soil dryness and temperature. Lepidocrocite (γ-FeOOH) indicates anoxic conditions in soils, leading to microbial formation of Fe^{2+}, which is then oxidized to form lepidocrocite. Maghemite (γ-Fe_2O_3) occurs in many tropical soils. In soils of temperate regions it appears to have formed on heating (fire) other Fe oxides in the presence of organic matter. Ferrihydrite ($5\ Fe_2O_3 \cdot 9\ H_2O$), a poorly crystalline form, occurs as a young Fe oxide predominantly where Fe^{2+}-bearing underground waters oxidize rapidly on exposure to oxygen.

Crystallinity: All Fe oxides are of extremely low solubility in the pH range of most soils. They crystallize at high supersaturations, where high nucleation rates lead to very small crystals (10-50 nm). Additionally, the aqueous phase of soils usually contains numerous other soluble compounds, many of which interfere with crystal growth, leading to defect, high surface area crystals.

Al-substitution: The substitution of Al for Fe varies with the mineral form, but more so with the availability of Al in the environment of formation. Goethite and hematite of highly weathered soils often have the highest possible Al substitution, whereas less weathered materials and hydromorphic environments lead to lower substitutions. The substitution may be quantified by XRD line shift or Mössbauer spectroscopy, because Al reduces unit cell size and lowers the magnetic hyperfine field.

Mode of formation: Field observations can indicate the mechanisms of formation of the various Fe oxides. More precise results can be obtained from synthesis experiments in which the conditions of natural environments are approximated. Such syntheses are easy to carry out and have produced a large amount of information on the mode of Fe oxide formation. Generally, Fe oxides form via solution through nucleation and crystal growth from small entities (monomers, dimers) supplied by the dissolution of a solid Fe compound. The formation via solution facilitates the incorporation of foreign ions, such as Al, into the structure.

HIGH-PRESSURE METAMORPHISM AND UPLIFT OF BLUESCHIST AND ECLOGITE IN THE CEDROS COMPLEX, CENTRAL BAJA CALIFORNIA

SEDLOCK, R.L., Dept. of Geology, Stanford University, Stanford, CA 94305, USA

The Cedros Complex of Cedros Island, central Baja California, Mexico is an exhumed subduction complex similar in many respects to parts of the Franciscan Complex of California. Three fault-bounded subterranes have been identified within the Complex; each consists of an originally intact stratigraphic sequence of interbedded turbidites, volcanic rocks, chert, and limestone that has been regionally metamorphosed at high pressures and very low temperatures and disrupted by a complex network of faults. Volumetrically insignificant block-in-matrix "melange" is present only along small small fault zones.

All three subterranes have experienced only a single metamorphic event, a high-pressure, low-temperature metamorphism inflicted during subduction. Subterrane 1 is more or less completely recrystallized, with rare relict clinopyroxene phenocrysts and partial preservation of relict clastic textures in some metasedimentary rocks. Metavolcanic rocks contain abundant groundmass sodic amphibole (crossite-glaucophane), lawsonite, and sodic clinopyroxene (Jd60-75); augite phenocrysts are partially altered to crossite and rarer aegerine-jadeite (Jd30-70). Metasedimentary rocks consist mainly of jadeitic clinopyroxene (Jd75-90) and quartz, with minor lawsonite and sodic amphibole (crossite-glaucophane) and only trace amounts of albite.

Subterrane 2 is only weakly recrystallized; good relict textures are preserved in sedimentary and subordinate volcanic rocks. In thin-bedded turbidites, plagioclase is partially altered to fine-grained bladed lawsonite and fine sprays of nearly pure incipient jadeite with quartz. Conglomerates contain not only coarser and more widespread lawsonite but also sodic amphibole (crossite-glaucophane), apparently because of the abundance of mafic protoliths among the clast population. Volcanic rocks contain groundmass sodic amphibole and lawsonite and aragonite (partially inverted to calcite) in veins and amygdules. Aragonite is also locally present in veins in conglomerate.

In subterrane 3 metamorphic minerals are generally present only in veins and amygdules, sites where reaction kinetics were enhanced by increased fluid flow. Volcanic rocks contain blocky aragonite partially inverted to calcite along internal cracks and grain boundaries. Most volcanic rocks also contain iron-rich sodic clinopyroxene (Jd20-30) in both veins and groundmass. In some porphyritic volcanic rocks, aegirine or aegirine-jadeite (Jd25) also occurs as a topotactic alteration product of relict augite. Sodic amphibole is a very rare product of the breakdown of relict augite. Coarse, fibrous lawsonite is locally present in veins with aragonite and sodic clinopyroxene. Sedimentary rocks very rarely contain fine-grained lawsonite.

The P-T paths followed by the three subterranes are tightly limited by jadeite content of Na cpx, vitrinite reflectance, the presence of aragonite, and the absence of a higher-T (e.g., greenschist) overprint. Conditions at the peak of metamorphism are as follows:

subterrane 1: T = 230 to ~ 300° C, P > 8 kb;
subterrane 2: T = 170-220° C, P = ~ 8 kb;
subterrane 3: T = 170-200° C, P = ~ 5 kb.

Geothermal gradients for both burial *and* uplift curves range from 7-12°/km. These low values, similar to those calculated for parts of the Franciscan Complex of California, attest to rapid uplift from subduction-related depths. Shallowly-dipping faults that bound the Cedros Complex are interpreted as low-angle normal faults along which deep-level, high-pressure metamorphic rocks of the Cedros Comlex have been elevated to shallow crustal depths. Irregular bands of sheared serpentinite along these faults suggests that serpentinite diapirism played a role in the uplift. The presence of eclogite and very-coarse grained blueschist in the serpentinite indicates the presence of a higher-grade subduction complex terrane at depth.

HIGH TEMPERATURE RAMAN SPECTRA OF QUARTZ POLYMORPHS OF GeO_2 AND SiO_2

SHARMA, SHIV K., Hawaii Institute of Geophysics, University of Hawaii, Honolulu, Hawaii 96822, USA

Raman spectra of crystalline quartz polymorphs of GeO_2 and SiO_2 have been measured at high temperatures. With the 488.0 nm line of a CW Ar^+ ion laser as an excitation source, the Stokes-Raman spectra of crystalline GeO_2 could be measured easily up to 1293 ±4K (see Fig. 1). The antiStokes-Raman spectra of crystalline GeO_2 was studied close to the melting temperature (1388 ±4K). Frequencies of the Raman bands in the spectrum of α-quartz polymorph of GeO_2 decrease linearly with increasing temperature. However, no soft mode, similar to the one observed in the spectrum of α-quartz form of SiO_2, is observed in the spectra of GeO_2 crystal. The temperature coefficients of the Raman bands of GeO_2 lie in the range -2.965×10^{-2} cm^{-1}/K to $-.802 \times 10^{-2}$ cm^{-1}/K. The ν_s(Ge-O-Ge) band, that appears as a strong band at 441 cm^{-1} shifts at -0.01805 cm^{-1}/K and broadens considerably at high temperature (Fig. 1). Both the $\partial\nu/\partial T$ and broadening of the ν_s(Ge-O-Ge) band with temperature are ound to be higher for the GeO_2 crystal than the corresponding quantities for the ν_s(Si-O-Si) band of α-quartz form of SiO_2.

In contrast to observed linear temperature dependencies of the frequencies of Raman active modes of the GeO_2 (quartz) crystal, the frequencies of the quartz-form of SiO_2 varies nonlinearly with temperature even before the temperature for α-β quartz phase transition is reached. The nonlinear variations in the phonon frequencies of α-quartz form of SiO_2 probably arise from the structural instability of the crystal at higher temperature.

The present high temperature Raman data of GeO_2 and SiO_2 will be combined with previously published high pressure Raman data of GeO_2 and SiO_2 (Mammone and Sharma, 1979; Asell and Nicol, 1968). The lattice dynamics of quartz-form of GeO_2 and SiO_2 at high temperatures will be discussed.

References

Asell, J. F. and M. Nicol (1968) Raman spectra of α-quartz at high pressures. J. Chem. Phys. 49, 5395-5399.

Mammone, J. F. and S. K. Sharma (1979) A Raman study of GeO_2 in crystalline and glassy states at high pressures. Carnegie Inst. Washington Year Book 78, 640-645.

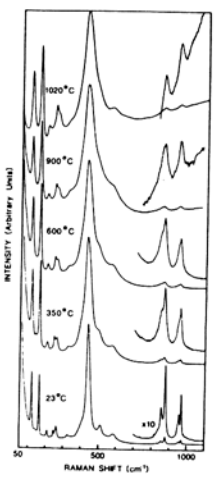

Fig. 1. Stokes-Raman spectra of quartz-form of GeO_2 at high temperatures.

EXSOLUTION STRUCTURES IN PYROXENES FROM METAMORPHIC ROCKS OF KOKCHETAV MASSIF (NORTHERN KAZAKHSTAN)

SHATSKY V.S., SOBOLEV N.V., STENINA N.G., Institute of Geology and Geophysics, Novosibirsk-630090, USSR

Clinopyroxenes (CPx) from eclogites (Ec) and associated garnet pyroxenites of the Kokchetav Massif have been investigated.

Two types of structural-chemical transformations were observed in omphacite (Omp) from Ec (Table): decomposition into diopside-plagioclase symplectite and formation of SiO_2 needles of quartz(Qz)-amphibole(Amp) intergrowth and discrete lamellae of Amp [1]. The *former transformation* is rather common in Ec of metamorphic complexes [2]. Communications on Px contained oriented needles of SiO_2 are scarce [3]. The study by the Raman spectroscopy has shown that they have Qz structure [4]. By *methods of transmission electron* microscopy (TEM) we have stated that SiO_2 needles form an amorphous matrix in some cases where cut single crystals of Qz structure are present according to the microdiffraction data. They are located in periodical layers oriented at 45° to the defect axis and vary in size from tenths to hundredths of a micron. These peculiarities of the internal structure suggest that initially the SiO_2 needles could be of coesite structure. The Amp lamellae oriented parallel to (100) differ in chemical composition from Px-replacing Amp, which is not bound orientationally with the matrix according to the TEM data.

Table

Microprobe analyses of minerals

Oxides	K 82/03			K 83/20	
	1	2	3	4	5
SiO_2	54.3	45.6	43.9	52.1	62.1
TiO_2	0.18	0.27	1.15	0.06	-
Al_2O_3	7.97	11.7	15.0	1.52	17.6
MnO	0.03	0.02	0.03	0.11	0.03
FeO	8.32	11.8	13.3	5.68	0.13
MgO	8.46	12.5	11.7	14.7	0.04
CaO	15.2	11.4	10.4	23.8	0.19
Na_2O	5.45	2.93	3.51	0.36	1.04
K_2O		0.03	0.07		15.9
Total	99.91	96.25	99.06	98.33	97.03

1 - Omp with SiO_2 needles; 2 - Amp lamellae; 3 - Amp developing over Omp; 4 - P_x with PFS lamellae; 5 - PFS lamellae

Lamellae corresponding in composition to potassium feldspar are found in garnet pyroxenites in Px. They have a complicated domain construction and orthoclase structure according to the X-ray analysis.

The appearance of SiO needles in Omp is a result of discarding of extra silica which enters CPx as a minal $Ca_{0.5}AlSi_2O_6$. The solubility of this minal grows with pressure [5]. At high pressures, K may enter Px as a structural impurity, its maximum amounts being stated in Px of a facies of diamondiferous Ec 6 . The presence of PFS lamellae suggests that K was a structural impurity in the Px composition of garnet pyroxenites.

Thus, we can conclude from the study of exsolution structures that Ec of the area Kumdy-Kul and associated garnet pyroxenites have been formed at pressures above 20 kbar.

1. Shatsky V.S., Sobolev N.V., Stenina N.G. 1985. Structural peculiarities of pyroxenes from eclogites. Terra Cognita, v.5, p.436-437. 2. Boland J.N., Roermund U.L.M.van, 1983. Mechanism of exsolution in omphacites from high temperature, type B, eclogites. Phys.Chem.Miner. v.9, p.30-32. 3. Smith D.C., Cheeney R.F. 1980. Oriented needles of quartz in clinopyroxene: evidence for exsolution of SiO from a non-stoichiometric supersilicic "clinopyroxene". 26th Intern. Geol.Cong., Paris, Abstracts 02.3.1:145. 4. Boyer H., Smith D.C. 1984. Petrological applications of the Raman microprobe (RMP): examples of the characterization of micron-sized minerals in eclogites. Microbeam Analysis, 107-110. 5. Zharikov V.A., Itbulatov R.A., Chudinovskikh L.T. 1984. Eclogite barrier and high pressure clinopyroxenes. Geologia i geofizika, N 12, p.54-63. 6. Sobolev N.V. 1974. Deep inclusions in kimberlites and the problem of upper mantle composition. Novosibirsk, "Nauka".

OPTICAL ABSORPTION SPECTRA OF MINERALS AND GLASSES AT HIGH TEMPERATURE

SHANKLAND, T. J., Geophysics Group, MS C335, Los Alamos National Laboratory, Los Alamos, NM 87545, USA

Although it is common practice to measure optical spectra at low temperature because of the consequent enhanced sharpness of absorption bands, we have examined mineral spectra at high temperatures (up to 1400°C in an atmosphere controlled to maintain the minerals' chemical stability). We have looked at olivine, magnesiowüstite, rhyolitic obsidian, and a nuclear waste isolation glass. The principal application has been evaluation of the radiative contribution to heat transport, but we have observed several features of general interest.

In olivine, absorption significantly increases with increasing temperature due to thermal broadening of both crystal field and multi-phonon lattice vibrational absorption bands--the principal absorption bands occurring in the spectral region involved in radiative heat transfer. In particular, in the "window" region between these bands the absorption coefficient increases from near zero at 20°C to about 10-15 cm^{-1} at 1400°C. The radiative thermal conductivity (K_R) under mantle conditions, calculated from the olivine single crystal spectra, increases from near zero at 20°C to about 5×10^{-3} cal/cm-sec-K (2 W/m-K) at 1400°C. The potentially strong temperature dependence of K_R beyond 800°C is largely offset by the marked decrease in the photon mean free path as temperature rises.

The spectra of obsidian samples show that the radiative spectral window is limited by a charge transfer band in the UV (400 nm) and Si-O stretching overtone in the IR (4500 nm). In order of decreasing importance, the main obstacles to radiative transfer within this window are background scattering, an OH-band centered at 2800 nm, and an Fe^{2+} crystal field band at 1100 nm. Unlike crystalline silicates such as olivine, absorption bands in obsidian do not broaden significantly as temperature increases; indeed, the OH-band appears to narrow slightly. As a result, the temperature dependence of the calculated radiative thermal conductivity K_R is dominated by the T^3 term theoretically predicted for a "gray body." Actual values of K_R increase from 9×10^{-5} to 6×10^{-3} cal/cm-sec-deg between 300 and 900°C, making this one of the most highly conductive terrestrial materials.

MINERALOGICAL AND CHEMICAL EVOLUTION OF A RARE-ELEMENT GRANITE-PEGMATITE SYSTEM: HARNEY PEAK GRANITE, BLACK HILLS, SOUTH DAKOTA

SHEARER, C.K., PAPIKE, J.J., SCOFIELD, N., Inst. for the Study of Mineral Deposits, S.D. Sch. of Mines & Tech., Rapid City, SD 57701, USA; WALKER, R.J., National Bureau of Standards, Gaithersburg, MD 20899, USA; LAUL, J.C., Battelle, Richland, WA 99352, USA

Central granitic plutons are spatially associated with most rare-element pegmatite districts. The genetic relationships that exist between the central granite and the surrounding, compositionally complex pegmatite district are not well defined. Understanding the growth and mineralogical-chemical evolution of the central "parental" granites may provide valuable insight into conditions and processes that were instrumental in the evolution of the complete granite-pegmatite system.

The Harney Peak Granite (1.7 b.y.) in the Black Hills, South Dakota, is a well-exposed granite complex surrounded by a rare-element pegmatite district (barren to Nb-, Ta-, Be-, Li-enriched pegmatites). The granite consists of a multitude of large and small sills and dikes which exhibit great variation in texture, mineralogy and geochemistry. Nd and Sr isotopic characteristics of the granite suggest it was derived by partial melting of a heterogeneous source. The texture of the granite ranges from a fine- to coarse-grained granite to a fine- to medium-grained pegmatite and typically exhibits compositional layering. The granite appears to be situated within a complex structural dome. By analogy to other less complex granite dome structures in the immediate area, the Harney Peak Granite complex appears to have generally grown outward (Duke et al., this volume).

The granite is strongly peraluminous with the following mineralogy: plagioclase (An_1-An_{22}) + microcline (Or_{70-96}) + quartz + muscovite ± apatite ± biotite [Fe/(Fe + Mg) = .66 - .73, $Fe^{3+}/(Fe^{3+} + Fe^{2+})$ = 0.20 - 0.45] ± garnet ($Al_{.62-.84}$, $Sp_{.10-.37}$, $Py_{.00-.09}$, $Gr_{.01-.02}$) ± sillimanite ± tourmaline [Fe/(Fe + Mg) = 0.58 - 0.85]. The granitic intrusions in the interior of the complex have similar K/Rb ratios (250), whereas this ratio decreases and is more variable for intrusions along the perimeter of the complex (Figure 1). The intrusions along the perimeter of the complex are commonly enriched in Be, Nb, Ta, and/or Sn compared to the granitic intrusions in the interior of the complex. Although anomalously high Cs, Li, and B concentrations are observed in some of the perimeter granites, overall, for the entire granite complex Cs, Li, and B concentrations overlap. Mineral chemistry variations from the interior to the perimeter of the granite complex are as follows: garnet: increase in Mn and decrease in Mg; tourmaline: increase in Fe/(Fe + Mg); muscovite: increase in the celadonite component and a decrease in Ti (Figure 2).

The mineralogical and chemical characteristics of the Harney Peak Granite suggest (1) partial melting of a heterogeneous source and fractional crystallization were important processes; (2) the peak granite-producing phase is represented by the sills and dikes of the interior of the complex; (3) this phase of granite production is characterized by high degrees of partial melting and/or efficient mixing of granitic melts; and (4) the granites along the perimeter of the complex represent low degrees of partial melting and/or inefficient mixing of granitic melts.

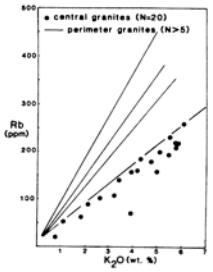

Fig. 1. Lines represent individual intrusions or groups of intrusions along the perimeter of the granite. Each line is defined by at least 6 samples and has a correlation coefficient of >0.80.

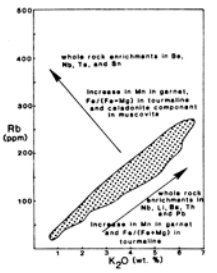

Fig. 2. Chemical variations in granite and minerals with constant and decreasing K/Rb ratio in the granite. Shaded area represents the interior granites.

CROCIDOLITE FIBER DIMENSIONS FROM MINING REGIONS IN WESTERN AUSTRALIA, SOUTH AFRICA, AND BOLIVIA

SHEDD, K. B., U.S. Bureau of Mines, Avondale Research Center, Avondale, MD 20782, USA

Mineral particle characterizations are essential to help answer some of the health-related questions regarding occupational and environmental exposure to fibrous minerals. The Bureau of Mines examined the fiber morphology of crocidolite samples from four locations where it has been produced commercially (1). The objective of the study (2) was to determine whether there are measurable differences in fiber dimensions that correlate with the high reported incidence of mesothelioma in mining and mill employees in the Cape Province of South Africa and Western Australia, as compared with little or no incidence of this cancer in the Transvaal Province of South Africa or Bolivia (1, 3).

Ten samples were obtained from the four regions. Fiber received in rock form was milled to minus 20 mesh in a rotating knife mill. Fiber lengths and widths on each sample were measured by scanning transmission electron microscopy. Detailed descriptions of samples, sample preparation, and fiber measurement are reported elsewhere (2).

Crocidolites from Western Australia and the Cape Province have more short and more thin fibers than crocidolites from the Transvaal Province and Bolivia. When lengths and widths of individual fibers are considered, an important distinction between the regions becomes evident: longer fibers from the Cape Province and Western Australia tend to be thinner than longer fibers from the Transvaal Province or Bolivia. This division based on fiber morphology correlates with the reported incidence of mesothelioma. Crocidolites from areas of high reported incidence of mesothelioma are characterized by thin fiber widths that are relatively independent of fiber length. A high percent of the long fibers in crocidolites from these regions meet the length and width dimensions proposed by health scientists as having a high correlation with carcinogenicity (4,5). In contrast, longer fibers in crocidolites from the Transvaal Province and Bolivia tend to be wider, so fewer long fibers meet the proposed length and width categories.

References

1. Ross, M. The Geologic Occurrences and Health Hazards of Amphibole and Serpentine Asbestos. Ch. in Amphiboles and Other Hydrous Pyriboles - Mineralogy, ed. by D. R. Veblen. Mineral. Soc. America, Rev. in Mineral., v. 9A, 1981, pp. 279-323.

2. Shedd, K.B. Fiber Dimensions of Crocidolites from Western Australia, Bolivia, and the Cape and Transvaal Provinces of South Africa. Bureau of Mines Report of Investigations 8998, 1985, 33 pp.

3. Harington, J. S., J. C. Gilson, and J. C. Wagner. Asbestos and Mesothelioma in Man. Nature, v. 232, 1971, pp. 54-55.

4. Stanton, M. F., M. Layard, A. Tegeris, E. Miller, M. May, E. Morgan, and A. Smith. Relation of Particle Dimension to Carcinogenicity in Amphibole Asbestoses and Other Fibrous Minerals. J. Nat. Cancer Inst., v. 67, No. 5, 1981, pp. 965-975.

5. Harington, J. S. Fiber Carcinogenesis: Epidemiologic Observations and the Stanton Hypothesis. J. Nat. Cancer Inst., v. 67, No. 5, 1981, pp. 977-989.

MOLECULAR ORBITAL CALCULATIONS APPLIED TO THE HIGH PRESSURE ELECTRONIC TRANSITIONS OF FE(II) MINERALS IN THE EARTH'S MANTLE

SHERMAN, D.M., U.S. Geological Survey, Reston VA 22092

Owing to their partially occupied d-orbitals, iron(II) oxides and silicates can undergo several low energy electronic transitions which are of geophysical relevance. Understanding how the energies of such transitions change with pressure is necessary for predicting the physical properties of the Earth's interior.

The $^5T_{2g} \rightarrow {}^5E_g$ ligand field transition of Fe^{2+} which, at low pressures, occurs in the near infrared can block heat transport via radiative conduction. At the high pressures of the lower mantle, however, the energy of the $^5T_{2g} \rightarrow {}^5E_g$ transition may increase enough to provide a window for radiative heat transport.

At high pressure, Fe^{2+} cations will undergo a high-spin to low-spin transition. Such a transition will result in a decrease in the ionic radius of Fe^{2+} and, hence, may give rise to a volume discontinuity with depth. Not previously considered, however, is that the HS → LS transition will prevent the possibility of a high pressure semiconductor-to-metal transition in iron(II) oxides and silicates since the Fe(t_{2g}) d-band will be completely full. In fact, the increased splitting of the d-orbitals by the crystal field together with an increase in the O(2p)-Fe(3d) and Fe(3d)-O(2p) band gaps should force all iron(II) oxides and silicates to become electrical insulators at sufficiently high pressures. In short, if all of the iron were in the low-spin state, the physics of the lower mantle might be greatly simplified.

To address these problems, the electronic structures of $Fe^{2+}O_6$ clusters as a function of Fe-O bond length were calculated using the SCF-Xα-SW molecular orbital method. The energies of the $^5T_{2g} \rightarrow {}^5E_g$ and the HS → LS transitions were evaluated and the results are given in Table 1. (Experience to date suggests that the accuracy of such calculated energies is within 15% of the experimental results.) The pressure corresponding to a given Fe-O bond length can be estimated by extrapolating the P-V results for wustite (Hazen et al., 1981).

The calculated shift of the $^5T_{2g} \rightarrow {}^5E_g$ transition of Fe^{2+} over the pressure interval 0 to 28.6 GPa is in excellent agreement with that found by Shankland et al. (1974). Over the whole pressure range investigated, the shift of the transition energy is within 10% of that predicted by electrostatic crystal field theory. The shift of the $^5T_{2g} \rightarrow {}^5E_g$ band out of the near infrared is greater than the shift of the mantle black body radiation curve. Hence, iron(II) minerals might allow radiative heat transport in the lower mantle. However, other electronic transitions, such as $Fe^{2+} \rightarrow Fe^{3+}$ charge transfer, may prevent radiative heat transport and should be considered.

Depth(km)[1]	0	775	1584	2638
P(GPa)	0	28.6	66.3	121.3
T(K)[2]	298	2000	2400	2800
R(Fe-O)	2.16	2.05	1.95	1.85
ΔU(kJ/mole)[3]	173.6	94.4	-8.3	-31.3
K_{eq}(HS → LS)	7.5×10^{-32}	9.3×10^{-4}	0.54	1.92
$^5T_{2g} \rightarrow {}^5E_g$(cm^{-1})	11,131	14,826	18,040	23,520

[1]Depth corresponding to a given pressure derived from Earth models of Dziewonski et al. (1975). [2]Approximate temperature at a given depth derived assuming adiabatic gradient, γ= 1, and T=3000K at the core-mantle boundary. [3]Internal energy change for the HS → LS transition.

The free energy, and hence the equilibrium constant, K_{eq} for the HS → LS transition of FeO can be estimated by assuming a molar volume change of -1.77 cm^3 and a molar entropy change of -Rln(5). Only the electronic entropy contribution is considered. From the calculated equilibrium constants, it can be seen that low spin Fe^{2+} is not a significant component of total iron at depths less than 1400 km. At the high temperatures of the lower mantle, however, high-spin Fe^{2+} persists even at depths greater than 2600 km (i.e., near the core-mantle boundary). Hence, both spin states must be considered when modeling the electronic properties of the lower mantle iron(II) mineralogy. Because of the thermal excitation to the high-spin state, the HS → LS transition will not give rise to a sharp volume discontinuity with depth.

Si-Al ORDERING OF SCAPOLITES FROM ^{29}Si, AND ^{27}Al, MAS NMR

SHERRIFF, B.L., GRUNDY, H.D., Department of Geology, McMaster University, Hamilton, Ontario L8S 4M1. HARTMAN, J.S., Department of Chemistry, Brock University, St. Catharines, Ontario L2S 3A1.

Scapolites are framework alumino-silicates forming a solid solution series with end members marialite $Na_4Al_3Si_9O_{24}Cl$ and meionite $Ca_4Al_6Si_6O_{24}CO_3$. The three T sites form two types of 4-membered rings joined parallel to the C axis to form 5-membered rings. Large voids contain four sodium or calcium cations and one chloride, carbonate or sulphate ion.

^{29}Si MAS nmr spectra of scapolites from 21% meionite to 91% meionite vary considerably with meionite content and type of ordering (Fig.). Peaks were allocated from calculations based on the empirical formulae of Radeglia and Engelhardt (1985) and Janes and Oldfield (1985) using T-O-T angles. A modification to the latter formula allowing for the effect of varying the Si-O-Al angles gives chemical shift values which correlate closely with those measured. The measured and calculated values of chemical shift for T1(3Si1Al) site diverge in the spectra of scapolites above 34% meionite. The x-ray data are an average of aluminum and silicon containing sites whereas the nmr relates only to the silicon sites. Therefore the distortion of the T-O-T angles which causes the variation in calculated values must be confined to aluminum containing sites.

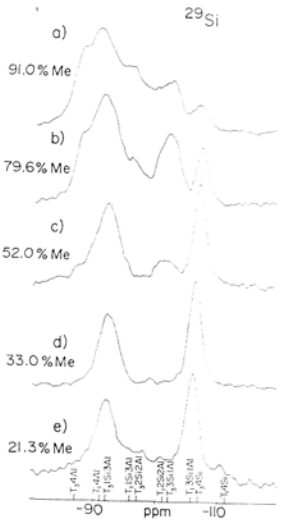

^{27}Al MAS nmr spectra of scapolite consist of one broad assymmetric peak at 58.0±0.5 ppm with a peak-width which increases steadily with meionite content but with an additional increase of 200 Hz when aluminum enters the T1 site.

Scapolites with a composition of 37% meionite are completely ordered with aluminum only in the T2 site (Lin 1971). The peak at -106 ppm in the ^{29}Si MAS nmr spectrum (Fig.) is allocated to the T1(3Si1Al) site and the low field peak at -92 ppm to T1(1Si3Al) site. The peak at -100 ppm in more meionitic scapolites is due to T1(2Si2Al) configurations and increases initially as one aluminum enters the T1 rings but diminishes past 75% meionite as two aluminums replace silicon in these four membered rings and the peak due to T1(1Si3Al) at -96 ppm increases. The low field peak at -88 ppm due to T2(4Al) and T3(4Al) increases steadily from 37% to 91% meionite. In compositions of less than 37% meionite the number of silicon configurations increase as extra silicon enters the T2 and T3 rings and as aluminum becomes equally distributed between the T2 and T3 sites. These extra sites cause the raising of the base line between -92 and -110 ppm in the spectrum of ON8 21% meionite.

The nmr spectra indicate the Al-Si environment of silicon and can be used together with x-ray data to produce a model for Si-Al ordering scheme for each composition of the scapolite series.

References

Lin, S.B., (1971): The crystal structure and crystal chemistry of scapolites. Ph.D. thesis, McMaster University, Hamilton, Ont.

Janes, N., & Oldfield, E., (1985): Rediction of silicon-29 nmr chemical shift using a group electronegativity approach. Applications to silicate and aluminosilicate structures. J. Am. Chem. Soc., 107, 6769-6775.

Radeglia, R., & Engelhardt, G., (1985): Correlation of Si-O-T (T=Si or Al) angles and ^{29}Si nmr chemical shifts in silicates and aluminosilicates. Interpretation by semiempirical quantum chemical considerations. Chem. Phys. Letters, 114, 28-30.

SECONDARY ION MASS SPECTROMETRY (SIMS) IN ANALYTICAL MINERALOGY

SHIMIZU, N., Dept. of Earth, Atmospheric and Planetary Sciences, Massachusetts Institute of Technology, Cambridge, MA 02139, USA

Sputtering of solid material with focused ion beam of keV energy produces ion (secondary ions) from the surface of the sample. Mass spectrometry of the secondary ions provides isotopic compositions and abundances of elements in a small area of the sample surface. Although the SIMS techniques have been extensively used in materials science and in semi-conductor industry, applications to mineralogy-geochemistry have been hampered by the complexity of secondary ion mass spectra of geologic materials due to: (1) the presence of molecular ion species (oxides, hydroxides, dimers, etc.) resulting in mass interferences, (2) isotopic fractionation during sputtering/ionization process, and (3) matrix effects, i.e., the secondary ion intensity of an element is dependent on concentration not only of the element but also of other elements. Systematic studies of isotopic compositions and ion intensities of various elements as a function of kinetic energy and matrix have provided a technique (energy filtering technique) by which (1) molecular ion interferences are sufficiently suppressed, (2) isotopic fractionation is minimized, and (3) matrix effects are reduced and simplified. Using the energy filtering technique, coupled with well-documented standards, accurate and precise data can be obtained for the major and trace elements in various silicate minerals including rare earth elements in Ca-rich pyroxenes and garnets at sub-ppm concentration levels. The capability of performing in-situ trace element analysis with this technique has been used to study zoned crystals in natural rocks (e.g., metamorphic garnets, augite phenocrysts in basalts etc.) in detail. The results show that incorporation of trace elements into growing crystals is controlled more significantly by kinetics of interface processes than by transport in the medium. The in-situ isotope analysis capability has been utilized in studying isotopically zoned PbS crystals from the Mississippi Valley-type Pb-Zn ores, and in determining self-diffusion coefficients of various elements in silicate melts using diffusion couples with enriched isotopes. The results of the diffusion study provide information not only of the diffusivity itself but also of the relationship between the mobility of elements and the structure of silicate melts. The surface analysis capability has been applied to obtain diffusivity data in solids by in-depth profiling techniques.

CURRENT ACTIVITY OF MAX80 AT PHOTON FACTORY

SHIMOMURA,O., National Institute for Research in Inorganic Materials, Namiki 1-1, Sakura-mura, Niihari-gun, Ibaraki 305, Japan

A high temperature and high pressure X-ray apparatus dedicated to synchrotron radiation (SR) X-ray source, named MAX80, has been successfully operated since Jan. 1983 at Photon Factory (PF) in Japan. The maximum generated pressure is 13 GPa and the temperature is raised to 1700 C with DIA-10 type cubic anvil apparatus.

Combination of SR and MAX80 reveals that the accuracy in determination of lattice constant becomes better by one order of magnitude compared to the conventional high pressure X-ray system and the measuring time with an energy dispersive method can be shortened to 10 sec. Corresponding to the high quality data by SR under pressure, techniques of pressure calibration and temperature measurements have been also improved.

Because the Photon Factory is an Institute for cooperative researches, the MAX80 system is widely open not only for high pressure investigators but also to the general user. More than 30 proposals have been offered to use the MAX80. Their subjects extend over solid state physics, material sciences, earth science and high pressure techniques.

Through these experiments, phase boundaries can be determined precisely and easily (P, Ge, ZrO_2, Fe_2SiO_4, $CaGeO_3$,...). Information on the kinetics of the transition are accumulated (BaS, KF, HgI_2,...). Magnetic anisotropy is detected by precise measurement of linear compressibility ($NiMnO_3$, $CoMnO_3$, ...). Transformations from graphite to diamond and hexagonal BN to cubic BN are directly observed for the first time by X-ray diffraction method. Trials to establish a new pressure scale instead of NaCl is continued. EXAFS experiments were successfully carried out for normal simiconducting and high preesure metallic phases of Ge.

These features are strongly enhanced by the use of X-ray from the wiggler, whose X-ray energy is more than 100keV. Structural behavior of liquid and amorphous materials under pressure and temperature are investigated (Se, Na_2SiO_4,Ge, ...). Hallow

CURRENT ACTIVITY OF MAX80 AT PHOTON FACTORY
SHIMOMURA, O.

Diffraction patterns can be observed up to Q=10, then the radial distribution function can be obtained by Fourier transformation of the hallow pattern. The certification of high pressure generation using sintered diamond anvils are performed. A pair of tapered anvils made of sintered diamond were set inside the Boron pressure transmitting medium as a second stage of the pressure cell. With this assembly, pressure generation of more than 60 GPa was confirmed based on Au pressure scale.

Accumulation Ring, which is an intermediate accelerator ring for Tristan (an electron-positron collider ring) and is operated at 6GeV, has also SR facility and becomes open just recently. The MAX80 was puicked up for the first apparatus to use SR from Accumulation Ring. Preliminary experiments shows the energy range is over 120 keV and the intensity is stronger than the SR from wiggler line of PF by about 5 times.

These activities using MAX80 will be reported together with further program.

EFFECT OF SYNTHETIC CONDITIONS OF HIGH-SILICA ZSM-5 TYPE ZEOLITE ON ITS CATALYTIC LIFE IN METHANOL CONVERSION TO LOWER OLEFINS

SHIN,S., Energy Chemistry Division, National Chemical Laboratory for Industry, Tsukuba Research Center, 305 Japan; SUZUKI,K., Energy Chemistry Division, National Chemical Laboratory for Industry, Tsukuba Research Center, 305 Japan; KIYOZUMI,Y., Energy Chemistry Division, Tsukuba Research Center, 305 Japan; OKADO,H., Maruzen Petrochemical Co. Ltd., Tokyo, 104 Japan; NOGUCHI,K., Idemitsu Petrochemical Co. Ltd., Tokyo, 100 Japan

High-silica ZSM-5 type zeolite has been recently known as a hopeful industrial catalyst which converts methanol not only to high-quality gasoline but to lower olefins, i.e., ethylene and propylene. High reaction temperature over ca. 800 K is desirable to increase the yield of lower olefins, but it so often deteorates the zeolite catalyst within several hours, depending on its synthetic conditions. Life of the catalyst is one of the most important problems to evaluate its catalytic properties from the view of industrial catalyst. Therefore, we investigated the relationship between the synthetic conditions and the catalytic properties of high-silica ZSM-5 type zeolite in order to improve its catalytic life in the conversion of methanol to lower olefins at high temperatures.

A series of ZSM-5 type zeolites were hydrothermally synthesized at 373 K with tetrapropylammonium bromide(TPABr) as a template reagent, by varying one of the synthetic conditions, i.e., the molar ratio of H_2O/SiO_2 or the hydrothermal treatment time of the starting sodium aluminosilicate gels but keeping the other synthetic conditions constant. Crystallinity of the products was checked by both X-ray diffractometry(XRD) and thermogravimetry(TG), whereas their mophology and texture were observed by scanning electron microscopy(SEM). The as-made zeolites were then transformed to the hydrogen form by a 0.6-N HCl solution, and the H-ZSM-5 type zeolites were subjected to the measurement of their BET surface area, acid property, adsorption property of hexane isomers, bulk and surface molar ratios of SiO_2/Al_2O_3. The catalytic lives in methanol conversion of the various H-ZSM-5 type zeolites thus obtained were measured by gas chromatography, using an ordinary fixed-bed reactor at 0.1 MPa and 573-873 K. Methanol was fed at the velocity of LHSV=2/h together with Ar as

EFFECT OF SYNTHETIC CONDITIONS OF HIGH-SILICA ZSM-5 TYPE ZEOLITE ON ITS CATALYTIC LIFE IN METHANOL CONVERSION TO LOWER OLEFINS
SHIN,S., et al.

a diluent gas(MeOH/Ar=1). The spent catalysts were to undergo TG analysis so as to clarify the thermal properties of their coke deposits.

The following results were obtained:

1. Perfect crystallization of ZSM-5 type zeolites took place when the starting gels with the molar compositions of SiO_2/Al_2O_3=350-800, H_2O/SiO_2=8-120, $NaOH/SiO_2$=0.322 and $TPABr/SiO_2$=0.0513 were heated more than 8 days.

2. As the H_2O/SiO_2 ratio decreased from 120 to 8, the mean particle size of ZSM-5 type zeolite crystals decreased from several micrometer to 0.3 micrometer.

3. As the mean particle size decreased, the observed molar ratio of SiO_2/Al_2O_3 increased at the surface of H-ZSM-5 crystals while that of the bulk crystals was kept nearly constant.

4. As the crystallization period was prolonged from 8 to 20 days, the coagulated ZSM-5 particles were dispersed homogeneously while both crystallinity and mean particle size of ZSM-5 was kept nearly constant.

5. Smaller mean particle size and shorter crystallization period of the zeolite resulted in the decrease in coke deposition which strikingly improved the catlytic life of H-ZSM-5 type zeolites in the conversion of methanol to lower olefins at higher temperatures ranging from 813 to 873 K.

6. The most favorable H-ZSM-5 type zeolite catalyst for the production of lower olefins from methanol at 813 K was obtained refluxing the starting materials with the composition of SiO_2/Al_2O_3=800, $NaOH/SiO_2$=0.322, $TPABr/SiO_2$=0.0513 and H_2O/SiO_2=8 for 8 days at 373 K with a continuous stirring, and the catalytic life, which was defined as to the time on stream required to the appearance of dimethyl ether as one of the reaction products, was improved up to 160 h.

This work is a part of "C1 Chemistry Project", a National Research and Development Program of Agency of Industrial Science and Technology, Ministry of International Trade and Industry (M.I.T.I.), Japan.

THREE TYPES OF PHOTO-LUMINESCENCE IN NATURAL ZIRCON

SHINNO, I., Institute of Earth Science, College of General Education, Kyushu University 01, Fukuoka 810, Japan

A microcomputer processed spectrophotometer mounted on a polarizing microscope has been constructed. It consists of (1) optical, (2) electrical, and (3) data processing systems. In the optical system, the light that passed through one of three body tubes of the microscope is first led to a photo-modulator and next to a monochromator. The chopped and monochromized light is introduced to the electric system, in which the beam is converted to amplified alternative current by a photo-detector and a lockin-amplifier or a Boxcar averager. The amplified signals are finally digitized by ADC in the microcomputer. The method using the system has such advantages that both of absorption and luminescence spectra can be obtained using the identical light path without any rearrangement of apparatuses. The life time(τ) of the photo-luminescence larger than several microseconds is also obtainable. However, the spectral measurement is restricted in the visible region.

Photo-luminescence spectra of synthetic zircons doped with each one of the elements such as REE, the first transition elements, B, Mg, Al and others (42 elements as a total), and those of fifty natural zircons have been examined. The fundamental data such as luminescence band positions and those relative intensities were obtained.

Three types of luminescent centers in natural zircons are distinguished from the luminescence spectra: (1) type I which consists of line spectra is due to the transition within 4f electrons of REE (Dy^{3+}, Eu^{3+}, $Sm^{3+}$and Tm^{3+}can be detected); (τ= 400 μs), (2) type II with broad bands may be originated from radiation centers of U and Th which may be closely related to the geologic age of the formation of zircon; (τ= 500 μs), (3) type III is formed by the activators of Mn, Ni, Nb and V with the transition of 3d - 3d electrons, and of Ca, Zn, Ba, Sc and P with electron - hole centers, where P acts as a sensitizer ; (τ= 580 μs).

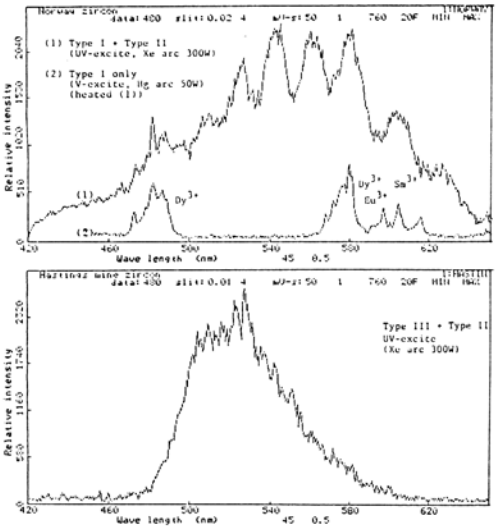

Typical spectra are shown in the figure at the right.

Natural zircons have usually the type II together with varying proportions of the type I or the type III luminescences. The type II spectra show remarkable extinction- restoration phenomena against the heat-treatment, and show the displacement of those band positions as the crystallographic direction changes (pleochroism). There exists an quantitaive relation between the intensity of Eu- luminescence and Eu content(ppm) : Eu(ppm) = -173 + 36.6 ln(Ic), where Ic is the relative intensity of Eu -luminescence band at 592 nm position and at constant crystal thickness(mm). This relation would enables us to determine the Eu content in natural zircon under the microscope.

The photo-luminescence spectra can be more easily and sensitively detectable rather than the absorption spectra for characterizing the optical properties of natural zircon.

BINOCULAR SCANNING ELECTRON MICROSCOPE FOR SIMULTANEOUS STEREOGRAPHY

SHOJI,T., Dept. of Mineral Development Eng., Univ. Tokyo, Tokyo 113, Japan; OKAYA,K., Eng. Res. Inst., Univ. Tokyo, Tokyo 113, Japan; GOTO,K., Sanyu-Denshi Co. Ltd., Hyakunin-cho, Tokyo 160, Japan; OTSUKA,S., Eng. Res. Inst., Univ. Tokyo, Tokyo 113, Japan

The stereographic image of a material is recognized by a pair of figures which are observed from different visual points. The most common is the stereography of aerial photographs. The binocular microscope has been developed for the stereography of fine materials. The minimum size to be observable is a few tens μm. It is not applicable for the finer materials, because of its small depth of focus. On the other hand, the scanning electron microscope (SEM) has a large depth of focus.

When we cannot observe a three-dimensional (3-D) shape in real time, we must decide on the two dimensional image whether to take a stereophoto pair or not. Unless by chance, we may fail to find such an interest 3-D pattern that is recognizable only by the stereography. The binocular SEM has been developed in order to keep out this failure.

The electron beam irradiates a specimen from the direction approximately parallel to the optical axis in the ordinary SEM (Fig. 1). On the other hand, the incident direction of the binocular SEM should be oblique to the optical axis (Fig. 2). A pair of coils, named as leaning coils, is set between the objective lens and a specimen (Fig. 2). The upper coil (L_1) deflects the electron beam outward. The lower coil (L_2) reflects again the beam to go to the original focus. For this detour of the path, the beam irradiates a specimen from the direction oblique to the optical axis. The binocular SEM has double scanning lines, as compared with the ordinary one. The beam leans leftward at odd scans, while rightward at even scans. The odd scanning image is displayed on the left CRT, while the even image on the right CRT. We see both images using a stereoscope. We can observe, therefore, 3-D shape of an object in real time. However, it is unfortunately impossible to demonstrate the simultaneous stereography using the binocular SEM in this paper.

The stereography of SEM images has been applied in many fields of science and engineering, such as mineralogy, biology, mechanics, and so on. In all of the previous studies, the stereographic observation was carried out not in real time, but after taking stereophoto pairs. We belive that the binocular SEM contributes to give more interest informations to the research works using the SEM.

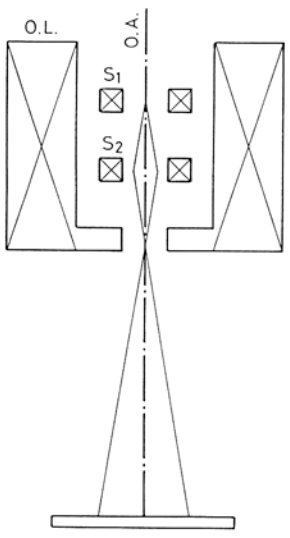

Fig. 1. Ordinary SEM. S_1 and S_2 are scanning coils.

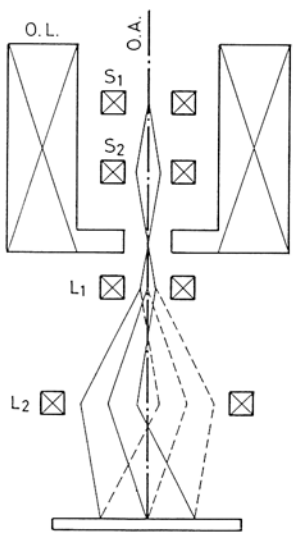

Fig. 2. Binocular SEM. L_1 and L_2 are leaning coils. Solid and dashed lines represent the path of electron beam at odd and even scans, respectively.

CHEMICAL FRACTIONATION AND EVOLUTION OF THE SOUTH PLATTE PEGMATITE SUITE, JEFFERSON COUNTY, COLORADO

SIMMONS, WM.B.; LEE, M.T.; BREWSTER, R.H., Dept of Geology and Geophysics, University of New Orleans, LA 70148, USA; WAYNE D.M., Dept. of Geological Sciences, Virginia Polytechnic Institute, Blacksburg, VA 24061, USA

The South Platte pegmatite district is well known for its strong enrichment in rare earth elements, yttrium, niobium, fluorine, and for the exceptionally well-developed internal zonation of the complex pegmatites which are located wholly within a reversely zoned portion of the Pikes Peak batholith. A reexamination of this district has revealed a number of previously unknown chemical trends and zonal patterns, both within and between pegmatites. These relationships help define the behavior of these elements and the role of fluorine in the fractionation of the granitic magma and pegmatitic fluids and suggest a new model for the evolution of the granite-pegmatite system.

Whole-rock XRF and INAA analyses of the host Pikes Peak granite and quartz monzonite and pegmatite wall zones provide strong evidence that all three are genetically related by some process of differentiation. Variation diagrams of major and trace elements show regular trends from quartz monzonite to pegmatite. With increasing SiO_2, there is systematic enrichment in K_2O, Na_2O, and Rb, and depletion in CaO, MgO, FeO*, TiO_2, P_2O_5, Al_2O_3, Ba, Sr, and Sc. These results imply that fractional crystallization played an important role in the generation of the quartz monzonite and granite which is contrary to the previous interpretation that these rock units were subsolvus-hypersolvus equivalents that resulted mainly from differences in water pressure (Simmons and Heinrich, 1980).

Strong depletions of REE, Y, Zr, and Th in the pegmatite wall zones indicate that there are dramatic changes in the behavior of certain trace elements in the pegmatitic melts relative to the granitic melt. Within the pegmatitic melts, these elements are strongly partitioned out of the wall zone into the final residual fluids where they may be concentrated up to an order of magnitude over their levels in the granite.

Extreme concentration of fluorine occurs in the late-stage replacement bodies in a number of South Platte pegmatites. In the White Cloud pegmatite, fluorite is the dominant mineral of the replacement units. Its composition ranges from nearly pure CaF_2 to yttrofluorite containing up to 25 wt.% total Y + REE. Microprobe analyses of the associated REE-silicate assemblages reveal a pronounced differentiation of LREE, HREE, Y, and (Be); with the assemblage allanite - gadolinite-Ce crystallizing early and the assemblage thalenite - allanite - gadolinite-Y forming later in the sequence of crystallization. Complexing of HREE, Y, and Be with fluorine is believed to be the most likely cause of this effect.

Within the district, there is also chemical zonation of F, Nb, Th, U, and REE between groups of pegmatites, which correlates strongly with the type of internal structure that the pegmatites exhibit. The poly-zonal quartz-core types typically contain more fluorite, samarskite, HREE-zircon, and yttrian-fluorite than their bi-zonal composite-core counterparts, which contain only sparse fluorite and allanite.

Preliminary two-feldspar thermometry using integrated perthite compositions yields temperatures ranging from 650 to 700 degrees for the quartz monzonite, with the highest values from the cores of zoned plagioclase. Temperatures for the granite range from 575 to 650 degrees and the pegmatite wall zones give temperatures of about 550 degrees. Pressure estimates of 5 Kb for the quartz monzonite and 2 Kb for the granite were obtained from the Q-Or-Ab-An-(H_2O) plot of Simmons and Heinrich, (1980).

The proposed sequence of magmatic evolution of the Buffalo Park pluton which led to the compositional zonation of the district involved: (1) a process of diffusive differentiation and fractional crystallization, which produced a chemically stratified magma chamber with a hotter more mafic quartz monzonitic base and a more felsic, granitic top enriched in H_2O, F, HREE, Nb, and Y; (2) resurgence of the more mafic lower level crystal mush into the upper more felsic part of the pluton, accounting for the reversed zonation; and (3) separation of pegmatitic fluids from the juxtaposed magmas giving rise to the two compositionally distinct groups of pegmatites. The poly-zonal, quartz-core pegmatites were generated from the volatile enriched felsic magma whereas the bi-zonal composite-core pegmatites developed from the quartz monzonitic magma.

ULTRA-HIGH TEMPERATURE DAC STUDIES USING SYNCHROTRON RADIATION

SKELTON, E. F., ELAM, W. T., and WEBB, A. W., Naval Research Laboratory, Washington, D.C. 20375-5000, USA; SCHAEFER, M. W., National Research Council Postdoctoral Associate, Naval Research Laboratory, Washington, D. C. 20375-5000, USA; QADRI, S. B., Sachs/Freeman Assoc., Inc., Bowie, MD. 20715, USA; SCHIFERL, D., Los Alamos National Laboratory, Los Alamos, NM, 87545, USA

A resistively heated diamond-anvil cell (DAC) capable of achieving uniform, well characterized pressures and temperatures to 1300°C has been constructed and tested.

High pressure research above 600°C is frequently complicated by materials problems: diamonds oxidize in air and graphitize more rapidly at elevated temperatures; many load bearing alloys melt or are subject to rapid creep deformation below 1300°C. This DAC is designed to achieve the highest possible temperatures and pressures permitted by the properties of diamond for durations of about one hour. Because of this limited holding time, intense synchrotron radiation is needed in order to obtain diffraction data quickly. Preliminary tests were carried out at the Stanford Synchrotron Radiation Laboratory, Stanford University and more recent studies were performed at the National Synchrotron Light Source, Brookhaven National Laboratory.

Initial research with this cell is being directed toward cross-calibration of prospective high pressure/high temperature standards, specifically Au and W. Energy dispersive diffraction spectra are recorded at different load settings as a function of temperature. Data recorded at three different P/T-settings are shown in the figure below.

Temperatures in the cell are measured with W-5% Re/W-26% Re thermocouples. The thermocouple calibrations were checked against the melting of Pb, Al, and Au at zero load. Diamond anvils with culet diameters of 600 μm are used; gaskets are prepared from Mo-13% Re sheet 250 μm thick, prepressed to 50 μm, and drilled with a 180 μm hole.

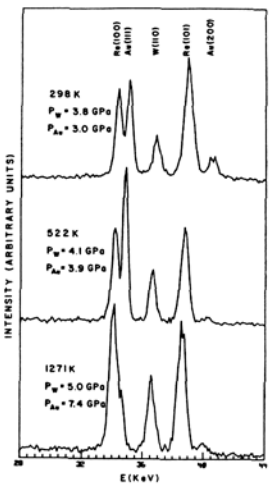

Pressures are determined separately from the measured shift in the Au-(111) and the W-(110) diffraction peaks using existing equation of state calculations [1, 2]. There appears to be a variance between the two pressure determinations which increases with increasing temperature; at 1271°K, the pressure from the Au-peak is 7.4 GPa, whereas that from the W-peak is only 5.0 GPa. Further commentary on this apparent discrepancy will be given.

Work is also in progress on detailed measurements of the equation-of-state of Au in reference to that of NaCl, at pressures and temperatures up to the melting curve of NaCl. These data will be compared to the calculated values so that extensions beyond this P/T-range may be carried out with increased confidence.

[1] J. C. Jamieson, J. N. Fritz, and M. H. Manghnani, in High Pressure Research in Geophysics, S. Akimoto and and M. H. Manghnani, eds., Center for Academic Publishing, Tokyo (1982), pp. 27-48.

[2] D. Schiferl, J. N. Fritz, A. I. Katz, M. Schaefer, E. F. Skelton, S. B. Qadri, L. C. Ming, and M. H. Manghnani, in Proc. U.S.-Japan Seminar: High Pressure Research-Applications in Geophysics and Geochemistry, 13-16 Jan. 1986, Honolulu, HI.

KINETICS OF INTRACRYSTALLINE FE-MG DISTRIBUTION IN TREMOLITE

SKOGBY,H. and ANNERSTEN,H. Department of Mineralogy and Petrology University of Uppsala, Box 555, S-751 22 Uppsala, Sweden

Kinetics of order-disorder reactions in ferromagnesian silicates can be used in order to estimate rock cooling rates. Hydrothermal technique and Mössbauer spectroscopy are here applied to investigate the intracrystalline Fe-Mg exchange in a tremolite from Zillertal, Austria. The crystal structure of tremolite contains four non-equivalent octahedral cation positions suitable for divalent ions; the small M2-position, the regular M1- and M3-positions and the large distorted M4-position. The M4-position is in the ideal formula occupied by Ca only, but has in reality been shown to contain smaller amounts of Fe(2+) and Mg. A relative site preference of Fe(2+) in the order M4>M1,M3>M2 has been observed, with Fe(2+) strongly ordering into the M4-position in natural samples (Skogby & Annersten 1985).

The results of 18 hydrothermal ordering and disordering experients at temperatures between 600 and 700 °C, show that the cation exchange is restricted to Fe-Mg partitioning between the M2 and M4 positions only, with a disordering reaction as:

$$Fe(2+)(M4) + Mg(M2) = Mg(M4) + Fe(2+)(M2)$$

The experimental site occupancy data were fitted according to the second order kinetic model of Mueller (1969). The rate constants were shown to be strongly temperature dependent, giving an activation energy of 290 kcal/mole in an Arrhenius plot.

In the beginning of the natural cooling process of the rock, the Fe-Mg distribution in the tremolite orders under equilibrium. At lower temperatures the distribution starts to deviate from equilibrium, and is finally frozen in at the apparent equilibrium temperature (Tae). Extrapolation of experimental data suggests a Tae of (411±42) °C for the Fe-Mg distribution of the natural sample. Assuming an asymptotic cooling model for the rock, this would suggest a cooling rate of 0.02 deg/year at the kinetic cut off temperature of 405 °C, where the exchange reaction stops.

References

Mueller,R.F.(1969): Kinetics and thermodynamics of intracrystalline distribution. Miner.Soc.Amer., Special Paper 2. 83-93.

Skogby & Annersten(1985): Temperature dependent Mg-Fe-cation distribution in actinolite-tremolite. N.Jb.Miner.Mh.1985, 193-203.

THE MINIDENT DATA BASE - EXAMPLES OF APPLICATIONS TO THE THOR LAKE RARE METAL DEPOSITS

SMITH, D.G.W. and de ST. JORRE, L., Department of Geology, University of Alberta, Edmonton, Alberta, Canada, T6G 2E3.

MINIDENT is an interactive mineral identification and mineral data base management program, now written in FORTRAN 77 (Smith & Leibovitz, 1986). The program accesses a data base currently containing information for nearly 4000 minerals. These data are divided into 26 categories including parameters such as composition, optical properties in transmitted or reflected light, hardness, d-values and cell dimensions.

Many applications of MINIDENT are envisaged in the fields of mineralogy, petrology, geochemistry, etc., but perhaps particularly important are applications to the identification of the components of mineral deposits which, by their very nature, often contain the rarer elements and their mineral phases. Excellent examples of such applications are provided by the Thor Lake rare-metal deposits which contain significant concentrations of Be, Li, Y, REE, Ga, Ta, Nb and Zr. The general features of parts of these deposits have been described by Trueman et al. (1985) and de St. Jorre (1986). The deposits occur within a series of alteration zones in the Thor Lake Syenite and the Grace Lake Granite which are the peralkaline phases of the Blatchford Lake Intrusive Suite (Davidson, 1978).

The mineralogy of the deposits is complex with as many as 70 different mineral species having already been recognised in the two principal areas of mineralisation - the T-zone and the Lake-zone. Although many different techniques have been used to aid in recognising the minerals present, determining their genetic relationships and assessing their economic potential, microbeam techniques (SEM & EMPA), and the compositional data they provide, have been particularly important. However, such techniques, whilst providing vital clues to mineral identities, do not always permit the analyst to make prompt and unequivocal identifications. In such cases MINIDENT can be used in one or more of several different ways to assist in identification.

In the simplest procedure, the program generates lists of minerals that meet certain input criteria. For example, the user could obtain a list of Be-bearing minerals by entering the condition that Be must be present in amounts greater than say, 0.1%. This will certainly include all Be minerals as well as a few others where Be is a non-essential constituent. If the user wanted hydrous Be minerals only, the additional qualifier that H_2O should be greater than, say, 0.5% could be added.

THE MINIDENT DATA BASE - EXAMPLES OF APPLICATIONS TO THE THOR LAKE RARE METAL DEPOSITS

SMITH, D.G.W. & de ST. JORRE, L.

The most direct and incisive procedure for identification is called MATCH. This is simply an extension of the procedure just described, in which more complete information about an unidentified mineral is normally entered. The additional data might be qualitative, semi-quantitative or quantitative analyses, refractive indices, d-values, reflectances, etc. All minerals for which the range of values in the data base includes those for the unidentified mineral, will then be listed. However, if the data for any one parameter do not match, then that mineral is rejected and will not appear in the list of possibilities. In some contrast to this procedure is another called IDENTIFY. In this case no minerals are rejected from further consideration because of a mismatch. Rather demerit points are assigned according to the extent of the mismatch. Eventually, when all minerals in the data base have been compared in this way, the twenty most likely identities are listed.

The TABLE procedure of MINIDENT tabulates selected data for any minerals of interest. The DISPLAY procedure may be used to display all the information available for particular minerals - either in summary form ("compiled data") or sample by sample ("sample data").

MINIDENT has proved useful in unravelling the mineralogy of the Thor Lake deposits, using the various procedures mentioned above. The application of these procedures will be illustrated using optical, X-ray and backscattered electron imaging techniques.

REFERENCES:

DAVIDSON, A. (1978): The Blachford Lake Intrusive Suite: An Aphebian alkaline plutonic complex in the Slave Province, Northwest Territories. Geol. Surv. Can., Pap. 78-1A, p. 119-127.

de ST.JORRE, L. (1986): Economic mineralogy of the Thor Lake, N.W.T. rare metal deposits: north T-zone. M.Sc. Thesis, Univ. of Alberta, (in prep.).

SMITH, D.G.W. and LEIBOVITZ, D.P. (1986): MINIDENT - A data base for minerals and a computer program for their identification. Can. Mineral. (in press).

TRUEMAN, D.L., PEDERSEN, J.C., de ST.JORRE, L. and SMITH, D.G.W. (1985): The Thor Lake, N.W.T. rare-metal deposits. In: Granite-related Mineral Deposits, R.P. Taylor & D.F. Strong, eds.; Ext. Abstr. of papers, CIM Conf. Halifax, N.S., Sept. 1985, p. 279-284.

POWD - MODELING CRYSTAL STRUCTURES FOR X-RAY POWDER DIFFRACTION STUDIES. VERSION FOR THE IBM PC MICROCOMPUTER

K. L. Smith and D. K. Smith
The Pennsylvania State University
University Park, Pennsylvania 16802, U. S. A.

The POWD program for calculating x-ray powder diffraction patterns from the crystallographic information describing a crystal structure has been adapted to the IBM PC microcomputer. This program simulates the diffractometer trace that would be produced by a sample of material with the described structure. It can be used to produce reference diffraction patterns for minerals whose crystal structures have been determined accurately or to examine models of structural changes such as cation ordering and substitution. Such calculations provide the basis for the interpretation of experimental data.

The program package includes data files for the atomic scattering factors and the symmetry positions of the space groups. An interactive dialog guides the user in the setup of the input file. The DINT program allows the user to calculate bond distances and angles for the crystal structure as a test of the input parameters. The POWD routine then is used to calculate the diffraction data. Both d-I tables and graphical outputs are provided. Another routine, COMBIN, is part of the package which will add individual patterns and background effects to simulate a mixture.

The software requires a minimum configuration of 320K RAM and 2 disc drives under MS-DOS 2.0 or higher. Additionally, a graphics card, hard disc and graphics printer are highly recommended.

IDENTIFICATION AND QUANTIFICATION OF CLAY MINERALS IN SEDIMENTS: THE PENN STATE CLAY MINERALS XRPD DATABASE

D. K. Smith, G. G. Johnson, Jr., and C. O. Ruud
The Pennsylvania State University
University Park, Pennsylvania 16802, U. S. A.

A database of x-ray powder diffraction patterns for over 40 clay minerals has been set up on a microVAX-II computer system. This database is unique in that the basis is the whole diffraction trace from 2 - 70° 2θ in digital form in 2θ intervals of 0.02°. Samples are selected to represent the major clay species with variations in crystallinity. Standard techniques employing size fractionation were used to concentrate the main specie in each sample. Each concentrate was used to produce 5 reference patterns: 1. Randomly oriented, 2. Air-dried oriented, 3. Glycol-saturated oriented, 4-5. Oriented heated to 375°C and 550°C. Calculated diffraction traces are included for hypothetical mixed-layer clays.

Identification is accomplished by one of several approaches. Peak positions are analyzed graphically or numerically for clay mineral families and treatments. The d-I pairs of each reference are compared with the d-I set of the unknown and a figure-of-merit determined. Families may be determined on the basis of the first line or the strongest line. Alternatively, Patterns of the unknown and the reference are compared directly, and a figure-of-merit based on the possible presence of the reference is established. In each case the user makes a selection which is subtracted and the process is repeated.

Quantification is done by reconstructing the unknown pattern as a weighted sum of selected reference patterns using a least-squares procedure. The selection is based on the identification step or on a preconceived knowledge of the minerals present. The best-fit weights are converted to weight fractions using experimentally determined reference intensity ratios. Quantification is usually done with the random sample or the glycolated sample. Errors in weight fraction estimates are around 2% absolute.

ROCK-FORMING GARNETS OF THE UPPER MANTLE

SOBOLEV N.V., Institute of Geology and Geophysics, Novosibirsk, 630090, USSR

Garnet is one of the major rock-forming minerals of the upper mantle within the garnet peridotite and eclogite stability field of both principal types of the mantle silicate environment: ultramafic (type I) and eclogitic (type II). Mantle fragments extracted to the surface by kimberlites and lamproites include also rocks and assemblages from the diamond stability field represented diamond-pyrope facies of the upper mantle to a depth of 200-250 km (2). The Cr-rich Mg-garnets from type I rocks contain a variable admixture of CaO and all these garnets in respect of both Ca- and Cr-contents make up a continuous series (Fig. 1a). The variability in the Ca-content is caused by a difference in paragenesis. Garnets from rocks containing both ortho- and clinopyroxene (lherzolite-websteritic) is characterized by moderate calcium contents and form a clearly outlined field 2 plotted in Fig.1a, so called "lherzolitic trend" (3). The left part of this field with low chromium garnets (5 wt% Cr O) is most widely represented in lherzolites, websterites, megacrysts from alkaline basalts, kimberlites and lamproites. More than 90% of 10000 garnet analyses from kimberlite concentrates of Yakutia might be plotted in this part of Fig.1a. The Cr-rich garnets (5 wt% of Cr O) are more rare but rather typical of the field 2.

Ca-poor garnets are related to the paragenesis without clinopyroxene as a phase (harzburgite-dunitic), their compositions might be plotted within the field 1, Fig.1a. All these are rich in Cr. More than 400 garnets from diamonds and 500 garnets from about 40 kimberlitic pipes of Yakutia might be plotted within the field 1. Ca-rich garnets are related to the paragenesis without enstatite as a phase (wehrlitic).

ROCK-FORMING GARNETS OF THE UPPER MANTLE
SOBOLEV, N.V.

Garnets from type II rocks are mainly free of chromium and form a pyrope-grossular-almandine continuous series with the Fe/Fe+Mg ratio no more than 70%. Cr-bearing garnets from type I rocks are plotted in Fig. 1b within the left part, field 1. A wide field approaching pure grossular end member is occupied by garnets from grospydites (2), kyanite and corundum eclogites and grospytes (5). Garnets with moderate and low calcium contents are typical of Mg-Fe eclogites without kyanite. The most magnesian garnet containing 26.0 wt% of MgO and 0.64 wt% of CaO is known from garnet--spinel rock (alkremite) of Udachnaya pipe (4).

Thus, as opposed to the classification (1) where deep seated garnets are divided into 12 groups, a subdivision of the garnets from type I rocks into 3 main groups according to their parageneses (see Fig.1a) is proposed with the groups 1 and 2 divided into Cr-poor and Cr-rich subgroups. Type II garnets are proposed to be divided into 2 main groups: Ca-rich corresponding to the field 2 (Fig.1b) and Ca-poor with a wide range of the Fe/Fe+Mg ratios (field 3 of Fig.1b).

1. Dawson J.B., Stephens W.E., 1975. J. Geol., v.83, 589-607. 2. Sobolev N.V., 1977. Deep-seated inclusions in kimberlites and problem of the composition of the Upper Mantle (Transl. D.A.Brown) (Ed. F.R.Boyd) Am. Geophys. Union, Wash. 3. Sobolev N.V. et al., 1973. Contrib. Miner. Petrol., v.40, 39-52. 4. Sobolev et al., 1977. in: Extended Abstr. 2nd Intern. Kimberlite Conf., Santa Fe, unpaged. 5. Sobolev N.V. et al., 1984. Doklady Akadem. Nauk SSSR, v.274, 172-178.

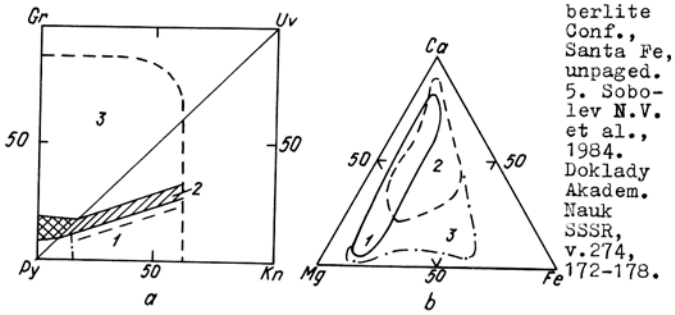

•THREE-LAYER BIOTITE 3Tc FROM THE KHIBINI ALKALINE MASSIF

SOBOLEVA, S.V. and BOROUTZKY, B. E., Institute of Ore Deposits, Mineralogy and Geochemistry, Academy of Science USSR, Moscow 109017, Staromonetny 35, USSR

Trioctahedral micas of biotite-phlogopite series crystallize mostly in polytype 1M. Infrequently among the metamorphic or igneous micas there is the polytype $2M_1$, appearing as a rule in close association with 1M. Besides the short period basic structures, the X-ray single crystal and electron microscopy (high resolution lattice image) studies reveal the long period non-uniform structures, such as 4M, 8Tc, 11M, etc. In contrast to the basic uniform polytypes, formed from the layers rotated at angles 0°, ±120° and 120° for polytypes 1M, $2M_1$ and 3T, respectively, these non-uniform polytypes reveal the arbitrary orientation of layers within the definite periodicity.

During the long period of time we have used the electron diffraction oblique texture patterns, we never observed the non-uniform polytypes. It can be explained by the nature of the specimen, represented by the textured polycrystal in which thin crystalline flakes are parallel by (001) faces to the substrate plane. The separate flakes of the non-uniform polytypes, even if present in polycrystal specimens, could not change significantly the diffraction pattern of the main polytype 1M. For the first time the non-uniform polytype 3Tc in massive and homogeneous segregation was discovered in the samples from the Khibini alkaline massif in thread veinlet (20 cm) of an alkaline trachyte. The composition of the biotite studies is

$$(K_{.97}Na_{.06})(Fe^{2+}_{1.42}Mg_{.66}Mn_{.11}Al_{.30}Fe^{3+}_{.11}Ti_{.40})(Si_{2.73}Al_{1.27})O_{10.83}(OH)_{.96}F_{.21}$$

(on the basis of the electron microprobe analysis for four separate flakes combined with the chemical analysis).

The second ellipsis (reflections 20*l*, 20*l*, 13*l*, 13*l*) of the electron diffraction oblique texture pattern from the biotite studied is completely equivalent to the second ellipsis of the pattern from 1M, $2M_1$ polytypes that indicate the alternation of the mica layers with rotation in 0° and ±120°. The minimum distance between the reflections 11*l*, 11*l* and 02*l* on the first ellipsis corresponds to the 9-layer orthogonal cell, the reflections with l = 3n being omitted. The analysis of the calculated intensity distribution for the first ellipsis reflections corresponding to the possible orthogonal 9-layer and monoclinic 6- and 3-layer polytypes ambiguously reveal the polytype 3Tc with the layer sequence $s_1s_1s_3$ (in Zvyagin notation) or [022] (in Ross, Takeda and Wones notation). The unit-cell parameters are: a = 9.27, b = 5.35, c = 30.17 Å, ß = 95.84°, space group C1.

This modification can be considered as a combination on the unit-cell scale of the polytypes 1M and $2M_1$ and formed by the introduction of the regular stacking faults in 1M layer sequence. The polytype 3Tc is a member of the most probable series of structures for mica resulting from screw dislocation ledges containing a single low energy fault configuration [1].

[1] D. Pandey and P. Krishna (1983) The origin of polytype structures. In Crystal Growth and Characterization of Polytype Structures. Pergamon Press.

CRYSTAL CHEMICAL TRENDS IN MOSSBAUER SPECTRA OF ^{57}Fe-BEARING OXIDE, SILICATE, AND ALUMINOSILICATE MINERALS

SOLBERG, T.C., and BURNS, R.G., Dept. of Earth, Atmospheric & Planetary Sciences, Massachusetts Institute of Technology, Cambridge, MA 02139, USA.

Mossbauer spectroscopy has proven to be useful for characterizing the valencies, coordination numbers, electronic configurations, and magnetic states of Fe cations in rock-forming minerals. Over the years, many attempts have been made to assist the interpretation of mineral Mossbauer spectra by outlining trends and correlations between isomer shift (I.S.), quadrupole splitting (Q.S.), and various distortion and bonding parameters. In particular, correlations between valence, coordination number, and bond length with I.S. have been proposed; correlations between bond angle variation and bond length distortion (quadratic elongation) with Q.S. have also been sought. Correlations between Fe^{+2} I.S. and Fe^{+3} I.S. in the same mineral, as well as between Q.S. and I.S., have been more successful.

Data are presented which confirm the absence of any statistical correlation of I.S. with average bond length, $\overline{R}$, or polyhedral volume. The absence of these correlations may come as a surprise to many researchers, since a theoretical basis supports their existence. In response, it is demonstrated that, if such relations exist, they are for all practical purposes obscured and modified by other effects to such an extent that trends within a coordination number cannot be used for site occupancy determinations. However, volumes are sufficiently different between coordination numbers that a variation in I.S. may be seen between octahedral and tetrahedral sites (Figure 1).

It becomes apparent that factors beyond the immediate Fe coordination polyhedra influence the I.S. parameter. One such factor is the inductive effect of next-nearest neighbor cations, M, which share oxygens at vertices, edges, or faces of Fe coordination sites [Menil, F., J. Phys. Chem. Solids, 46, 736 (1985)]. The more covalent the M-O bond, the more ionic the $\overline{Fe}$-O bond, leading to a higher I.S. Thus, oxygens shared with Si result in higher I.S. than those shared with Al or Mg. This factor explains the apparent anomalously low I.S. of octahedral Fe^{+3} in sapphirine, chloritoid and other aluminosilicates.

The Q.S. parameter, dependent upon non-spherical distributions of electrons in 3d orbitals and asymmetry of coordination polyhedra, has been correlated in the past with the bond-length distortion (Δ) and bond-angle variation (σ^2) parameters. Data are presented which demonstrate that, for a wide range of coordination polyhedra, a poor correlation exists in plots of Q.S. versus Δ, as well as Q.S. versus (σ^2). The deficiencies of these parameters are discussed, recognizing their inability to distinguish in some cases, between widely varying structures which would be expected to have very different Q.S.'s. It is shown that next-nearest neighbor effects also have a major influence on the Q.S.; this effect is highlighted by the chromite series, as well as others presented in this study.

CRYSTAL CHEMICAL TRENDS IN MOSSBAUER SPECTRA

SOLBERG, T.C., et al.

ISOMER SHIFT FERRIC vs MEAN METAL-OXYGEN DISTANCE

FIGURE 1

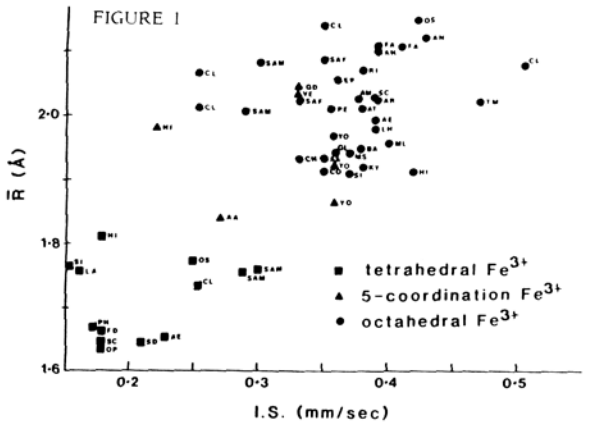

TUNGSTEN-, TIN-, AND BORON-BEARING SKARNS AT EL HAMMAM, MOROCCO.

SONNET, Ph. and VERKAEREN, J., Laboratoire de Minéralogie et de Géologie Appliquée, Bâtiment Mercator, 3, Place Louis Pasteur, 1348, Louvain-La-Neuve, Belgium.

The El Hammam region is situated in a Variscan massif referred to as the central Morocco. This massif is made up of folded epimetamorphic Paleozoic series intruded by several post-tectonic calco-alcaline granites (290 M.Y.).

In the vicinity of the El Hammam fluorite mine, a 6 x 13 Km^2 spotted slate aureole reveals the presence of a still buried granite. Carbonate beds made up of limestone-shale alternations were transformed in banded calc-silicate rocks.

Aside from scheelite-bearing skarns, which are common elsewhere in Central Morocco, an unusual skarn deposition sequence developed in the metamorphic calc-silicate bands. These are, chronologically :

1. Scheelite-bearing pyroxene (ferro-salite) skarns.
2. Garnet (andradite with up to 5.6 wt.% SnO_2), pyroxene (hedenbergite) and malayaite ($CaSnSiO_5$) skarns.
3. B-bearing skarns containing datolite and axinite.

Maximal size recorded for Sn-bearing skarns is about 150m x 6m in outcrop with a variable tin content up to 10 wt.% SnO_2. The skarns form in calc-silicate bands (excluding carbonated bands) or in previously formed scheelite-bearing skarn. Two different metasomatic colums occur depending on the presence, or absence, of wollastonite in the replaced rock :

1. Wollastonite / wollastonite + Sn-rich andradite / Sn-rich andradite + malayaite / hedenbergite + malayaite.
2. Pyroxene + feldspar or grossular ± diopside or W-bearing pyroxenite / pyroxene + Ti-rich malayaite / hedenbergite + malayaite .

Mineralogical assemblages suggest low fCO_2 and high T conditions. The development of Sn-rich andradite instead of the association wollastonite + malayaite in the second zone of column 1 indicates iron-rich moderably reduced conditions. In the second column malayaite form first by replacement of sphene. Ti-content in malayaite (up to 4.6 wt.% TiO_2) suggests T above 480°C at 1 kb. Compared with W-bearing skarns, Mn content in the fluids was high as pyroxene compositions lie along a trend which is richer in Mn than the pyroxene trend in scheelite-bearing skarns.

Alteration of Sn-bearing skarns may involve one or several of the following features (in chronological order) :

1. superimposition of B-bearing skarn : axinite, usually a ferroaxinite, becomes a manganaxinite with up to 1.7 wt.% SnO_2 when it forms in Sn-bearing skarns.
2. sulfidation with formation of stannite- and cassiterite-bearing pyrrhotite ore.
3. hydroxylation at very low f CO_2 with formation of the late tin minerals stokesite, burtite, wickmanite and varlamoffite.
4. recarbonatation with formation of cassiterite owing to the decomposition reaction of malayaite : $CaSnSiO_5 + CO_2 = CaCO_3 + SnO_2 + SiO_2$.

ZONED METAMORPHIC GARNETS AND METAMORPHIC P-T PATHS

SPEAR, F. S. Dept of Geology, Rensselaer Polytechnic Institute, Troy, NY 12181

Compositionally zoned minerals such as garnet have potential value in determining the evolutionary history of a metamorphic rock. For garnets growing via continuous reaction, changes in P and T produce unique changes in mineral chemistry, provided that local equlibrium prevails.

The Gibbs' Method (Spear, *et al.*, 1982, MSA Rev. in Mineralogy, 10, 105-152) is an algebraic formulation that specifies the thermodynamic constraints among all of the intensive variables of a heterogeneous system at equlibrium. Application of Duhem's Theorem to the Gibbs' Method results in additional mass balance constraints of the form

$$0 = \sum_k dM_k \sum_j \nu_{k,j,i}\, X_{k,j} + \sum_k M_k \sum_j (\nu_{k,j,i} - \nu_{k,1,j})\, dX_{k,j}$$

where M_k, and $X_{k,j}$ are the mole fractions of the k^{th} phase and the j^{th} phase component in the k^{th} phase and $\nu_{k,j,i}$ is the stoichiometric coefficient of the i^{th} system component in the j^{th} phase component in the k^{th} phase. Collectively, these equations permit calculation of changes in all dependent intensive and extensive variables in systems undergoing equilibrium or fractional crystallization from specified changes in only two independent variables. By specifying P and T as the independent variables, changes in mineral composition and modes for any metamorphic P-T path can be calculated.

Examples from low- and medium-grade pelitic schist assemblages in the system CNMnKFMASH are presented. For the assemblage garnet(G) + biotite(B) + chlorite(C) + plagioclase(P) + quartz(Q) + muscovite(M) + H_2O(W), (dP/dT) isopleths for almandine (Alm) and spessartine (Spes) are near vertical and isopleths for grossular (Gros) are steep (70 bar/deg). For clockwise P-T paths, Alm increases with increasing T then decreases, resulting in a zoning profile with a maximum in Alm at X_{Spes}=.07-.15. Spes, Gros and Fe/(Fe+Mg) decrease monotonically. Fractional crystallization results in more rapid decreases in Spes and Gros than equilibrium crystallization. With continued reaction on cooling (and decompression), Alm increases, but Spes and Gros remain relatively constant, resulting in a "dog leg" in the zoning pattern.

For the assemblage G+B+staurolite(S)+P+Q+M+W, isopleths for Alm and Spes are negative (-60 bar/deg) and those for Gros are positive (30-40 bar/deg). Gros decreases monotonically following a clockwise P-T path whereas Alm and Spes change little. For the assemblage G+B+Kyanite+P+Q+M+W, isopleths for Gros, Alm and Spes are shallow and positive (15, 14, and 2 bar/deg) whereas for Fe/(Fe+Mg) they are negative. Clockwise P-T paths result in decreases in Gros and Alm, increases in Spes and little change in Fe/(Fe+Mg).

Many low- and medium-grade metamorphic garnets display zoning patterns characterized by core-rim decreases in Mn and Ca and increases in Fe/(Fe+Mg). The results of this study show that for the assemblages G+B+C+P+Q+M+W and G+B+S+P+Q+M+W, decreases in Mn accompanied by increases in Fe/(Fe+Mg) are characteristic of increasing T, but contain no information about pressure changes. Decreases in Ca can be accomplished by increasing T *or* decreasing P. For the assemblage G+B+K+P+Q+M+W, decreasing Mn implies increasing pressure, whereas decreasing Fe/(Fe+Mg) suggests increasing T or P and decreasing Ca implies increasing T or decreasing P.

ZONED METAMORPHIC GARNETS AND METAMORPHIC P-T PATHS

Comparison of the computed isopleths with published garnet zoning profiles from Barrovian terranes such as west-central New England, the Alps and the Dalradian, reveals that the zoning profiles exhibited by many low and medium-grade Barrovian garnets are consistent with the rocks having crystallized along clockwise P-T paths.

ATOMIC MOTION IN MOLTEN SILICATES: NMR RESULTS

STEBBINS,J.F., Dept. of Geology, Stanford University, Stanford, CA 94305, USA

Liquids are distinguished from crystalline and amorphous solids by the motion of atoms and "molecules" at distance scales many orders of magnitude greater than, and on times scales many orders of magnitude less than normal interatomic vibrations. Such motion in molten silicates is generally appreciated as bulk transport phenomena such as viscous flow, diffusion, and electrical conduction, but is equally important in causing the often major increases in heat capacity, thermal expansivity, and compressibility that occur on transition from glass to liquid. The link between viscosity and the rate of increase in configurational entropy with temperature has been made particularly clear in recent publications in the geochemical literature by Richet and others.

Background in crystal chemistry leads to the conception of configurational change as a static effect similar to the disordering of cations in minerals at high temperature. This viewpoint may have some applicability in the structure of very viscous melts, but consideration of the time dimension is crucial to complete understanding. The rate at which structures interchange among various configurations is the key, but difficult to determine, variable.

NMR spectroscopy holds considerable promise for relatively direct observation of motion and structural change in silicate melts. Several basic conclusions can be drawn from our recent ^{23}Na and ^{29}Si NMR studies of melts at high temperature. The first is the observation of "motional narrowing" in all compositions studied in the soda-alumina-silica systems, at temperatures beginning as little as about one hundred degrees above glass transition temperatures. The wide and sometimes multipeaked lines observed in ^{29}Si MAS spectra of glasses rapidly become narrow and single in the liquid, implying that interchange of Si cations among different sites is occurring at at least the ms time scale. Much of this exchange involves the rapid breaking and reforming of strong Si-O bonds, even in liquids as depolymerized as Na_2SiO_3. Silicate "molecules" in melts are therefore ephemeral at even high viscosities.

A second general finding, although still somewhat tentative, is that the apparent activation energies for NMR spin-lattice relaxation in melts are close to the values expected from the appropriate bulk transport properties: conductivity and diffusivity for Na, and viscosity for Si. This suggests that the atomic motions responsible for relaxation are those which are interesting from the standpoint of melt chemical and physical properties. Direct study of these motions by NMR is thus possible.

MINERAL GLASS THIN FILM STANDARDS FOR ANALYTICAL ELECTRON MICROSCOPY

Eric B. Steel
National Bureau of Standards
Gaithersburg MD 20899

Quantitative chemical analysis is performed on the Analytical Electron Microscope (AEM) with sensitivity factors derived from thin film or particle standards. The AEM needs standards that have characterized homogeneity, chemical composition, and mass-thickness. This is often difficult to achieve with mineral specimens. NBS has achieved these results using ion beam sputtered thin film glasses.

These films are created by bombarding a bulk mineral glass target with Argon ions. The sputtered glass is collected on 3 mm AEM specimen support grids with carbon films. To minimize matrix corrections, the glasses are sputter deposited to a thickness of approximately 0.1 μm.

Each sputtered film is characterized for several properties for use as primary research standards. Chemical composition is measured by several independent techniques. Thickness and uniformity is measured by profilometry and interferometry. Chemical homogeneity is measured on the electron probe and the AEM. The glass film density is calculated from the measured mass and thickness. And chemical and physical stability of the films under electron beam bombardment at typical electron doses and accelerating voltages of 100 and 200 kV is measured on the AEM.

The first two films offered for sale as standard reference materials are composed of major Mg, Si, Ca, Fe and Al, Si, Ca, Ti, Mn, Zn respectively. These elements cover many of the major elements of importance to the geologic community. Future plans include films that contain certified concentrations of light elements such as O, C, or B as well as a series of heavy element glasses.

CRYSTAL CHEMISTRY OF PHASE TRANSITIONS IN OMPHACITES FROM ECLOGITES OF NORTHERN KAZAKHSTAN (USSR)

STENINA N.G., SHATSKY V.S., Institute of Geology and Geophysics, Siberian Branch of the Academy of Sciences of the USSR, Novosibirsk-90, 630090, USSR

Genetical information contained in phase transition defects in silicate solid solutions has been used to clear up the mechanism of the regressive stage transformation of eclogites from Northern Kazakhstan (USSR).

Optically homogeneous omphacites have been investigated by means of high voltage (HVEM) and high resolution (HRTEM) electron microscopy to solve the problem.

A large variety of microstructural features was revealed by HVEM in the samples investigated. The grains are badly deformed, the low-angle dislocation boundaries are established and complicated aggregations of dislocations are observed. The structural-chemical transitions of omphacite matrix arise on the deformation substructures. The corresponding defects have a complicated diffraction contrast which is not solvable by means of the conventional methods of analysis. The largest defects are microlamellae of domain structure of micron tenths in width, some domains being amorphous.

Lattice images of (010) planes show that breaks and displacements of silicium-oxygen chains occur. These defects form lines normal to the C-axis and distributed periodically (with a period distance about 80 Å) in omphacite matrix. They represent a type of structural imperfections earlier unknown and unusual for the chain silicates. High magnification lattice images of the imperfect microareas show a rotation and bending of chains, new structural arrangements of the cation polyhedra.

These data suggest a new stepped mechanism of the structural-chemical transitions in clinopyroxenes caused by a transformation of eclogites during one of the stages of its geological history. The mechanism of displacive transitions stimulated by a deformation of matrix acts at the first stage, the secondary chemical bonds being broken during these transitions. This process triggers the reconstructive mechanism breaking the primary bonds. This leads to the diffusion and ordering of Si and Al followed by the stabilization of the "weakened" zones by Ca and Na. Such a process results in the formation of new phase microdomains periodically distributed in matrix, feldspar or plagioclase being the most probable.

Mn-ENRICHMENT IN ARFVEDSONITES, BIOTITES AND ILMENITES FROM THE GRANITES OF HINCHINBROOK ISLAND, QUEENSLAND, AUSTRALIA.

P.J. Stephensen[1], M.T. Frost* and G. Tsambourakis*

[1]Geology Department, James Cook University, University of North Queensland, Queensland, 4811.
*CSIRO Division of Mineral Chemistry, PO Box 124, Port Melbourne, Victoria 3207.

Permian arfvedsonite or biotite granites, surrounded by older granites, granodiorites and acid volcanics, extend over an area of 150 km^2 of the eastern part of the island (1). A detailed study of the geology and mineralogy of the peralkaline granites has begun. Field work suggests widespread near horizontal layering that involves variation in grain size from aplitic to pegmatitic with variations in amphibole colouration.

The mineralogy of twenty-five samples has been studied in detail. Average bulk composition gave: SiO_2 74.86, TiO_2 0.06, Al_2O_3 13.79, Fe_2O_3 0.99, FeO 0.34, MnO 0.05, MgO 0.04, CaO 0.05, Na_2O 3.85, K_2O 4.41, Li_2O 0.01, Rb_2O 0.06, SrO 5ppm, SnO_2 8 ppm, H_2O^+ 0.72, H_2O^- 0.36 = 99.23. Arfvedsonite granites with minor biotite, biotite (annite) granites and arfvedsonite-biotite granites are all common. Granites containing aegirine and arfvedsonite are rare.

The unusual feature of the ferro-magnesian minerals is their high Mn-content relative to those found in similar granites from other localities. Typical compositions are shown in the following Table. These analyses suggest a series from arfvedsonite to a Mn-rich grunerite with Fe^{2+} and Mn^{2-} entering the M4 site. Work is in progress to ascertain whether these compositions represent true single phases or whether they are very fine grained mixtures.

Electron microprobe analyses of arfvedsonites (1-4), annite (5) and two ilmenites (6,7), (wt.%).

	1	2	3	4	5	6	7
SiO_2	49.98	49.03	49.37	47.90	37.81	0.03	0.02
TiO_2	0.92	0.24	0.12	0.83	2.39	52.77	53.03
Al_2O_3	1.55	0.69	0.29	1.93	12.71		
FeO	32.97	39.95	42.94	32.78	29.68	17.02	2.39
MnO	2.17	4.07	4.04	2.63	2.53	30.81	43.10
MgO	0.16	0.33	0.22	1.16	1.98		
CaO	0.61	0.19	0.53	5.09	0.00		
Na_2O	9.02	3.90	1.02	5.59	0.26		
K_2O	0.93	0.12	0.01	0.90	9.22		
F^-	0.98	0.47	0.00	0.39	1.34		
Total	99.29	98.99	98.54	99.20	97.92	100.63	98.56
Formulae							
Si	8.00	7.99	8.08	7.69	6.04	0.00	0.00
Al(iv)	-	0.01	-	0.31	1.96		
Al(vi)	0.29	0.13	0.12	0.05	0.43		
Ti	0.11	0.03	0.02	0.10	0.29	0.99	1.01
Fe	4.41	5.45	5.42	4.40	3.96	0.35	0.05
Mg	0.04	0.08	0.08	0.28	0.47		
Mn	0.29	0.56	0.56	0.36	0.34	0.65	0.93
Ca	0.10	0.03	0.04	0.88	0.00		
Na	2.80	1.23	1.02	1.74	0.08		
K	0.19	0.03	0.02	0.18	1.88		
F	0.50	0.03	0.22	0.20	0.68		
Y	5.15	6.24	6.19	5.19	5.49	1.00	0.98
X	3.09	1.29	1.08	2.80	1.96		

Formulae calculated on 23 O-atoms for analyses 1-4; 22 O-atoms for analysis 5 and 3 O-atoms for analyses 6 and 7.

(1) Ewart, A., 1978. Some aspects of the geology of Hinchinbrook Island. Qd. Nat. 22, 25-30.

POCKET MINERALOGY AND CALCULATED PHASE RELATIONS OF A LAYERED PEGMATITE-APLITE INTRUSIVE; THE LITTLE THREE MINE, RAMONA, CA

STERN, L.A.*, BROWN, G.E.,Jr., BIRD,D.K., JAHNS, R.H.**, Department of Geology, Stanford University, Stanford, CA 94305, USA; FOORD, E.E., Branch of Central Mineral Resources, U. S. Geological Survey, Mail Stop 905, Box 25046, Denver,CO 80225, USA; SHIGLEY, J.E., Research Department, Gemological Institute of America, 1660 Stewart Street, Santa Monica, CA 90404, USA; SPAULDING, L.B.,Jr., P.O. Box 807, Ramona, CA 92065, USA

Several layered pegmatite-aplite intrusives exposed at the Little Three mine, Ramona, California, USA, display closely associated fine-grained to giant-textured mineral assemblages which are believed to have co-evolved from a hydrous aluminosilicate residual melt with an exsolved supercritical vapor phase. The asymmetrically zoned intrusive known as the Little Three main dike consists of a basal sodic aplite with overlying quartz-albite-perthite pegmatite and quartz-perthite graphic pegmatite. Muscovite, spessartine, and schorl are subordinate but stable phases distributed through both the aplitic footwall and pegmatitic hanging wall. Although the bulk composition of the intrusive lies near the haplogranite minimum, centrally located pockets concentrate the rarer alkalis (Li, Rb, Cs) and metals (Mn, Nb, Ta, Bi, Ti) of the system, and commonly host a giant-textured suite of minerals including quartz, alkali feldspars, muscovite or F-rich lepidolite, moderately F-rich topaz, and Mn-rich elbaite. Less commonly, pockets contain apatite, microlite-uranmicrolite, stibiobismuto-columbite-tantalite, and columbite. Several of the larger and more richly mineralized pockets of the intrusive, which yield particularly high concentrations of F, B, and Li within the pocket mineral assemblages, display a marked internal mineral segregation and major alkali partitioning which is curiously inconsistent with the overall alkali partitioning of the system.

Calculations of phase relations between the major pegmatite-aplite mineral assemblages and supercritical aqueous fluid were made assuming equilibrium and closed-system behavior as a first-order model. These relations are assessed through the generation of isobaric phase diagrams which constrain the observed mineral assemblages in the system K_2O-Na_2O-Al_2O_3-SiO_2-H_2O as a function of temperature and cation activity ratios of the coexisting fluid phase. Log activity - temperature plots of the stoichiometric assemblage microcline-albite-quartz-muscovite at 2 kb show that log $a_{(K^+/H^+)}$ of the fluid phase remains essentially constant throughout crystallization, while log $a_{(Na^+/H^+)}$ rises slightly with falling temperatures. Modelling muscovite nonstoichiometry by decreasing activity of the pure component from unity to 0.5 markedly shifts the upper thermal stability limit of the assemblage microcline-albite-quartz-muscovite from approximately 630°C upward to 710°C. In the pegmatite-aplite system exposed at the Little Three main dike, crystallization temperatures are thought to have ranged from approximately 700°C downward towards 540°C at the central pocket zone; muscovite nonstoichiometry caused by extensive F, Li, and Mn substitution may contribute to the stability of this assemblage at the outer zones of the system where stoichiometric muscovite is not predicted to be stable.

* current address: U. S. Geological Survey, 345 Middlefield Road, Mail Stop 977, Menlo Park, CA 94025

** deceased December 31, 1983

Synchrotron radiation: an application to the oceanic hydrothermal oxides.

STOUFF Pierre and BOULEGUE Jacques
Lab. de Géochimie et Métallogénie - CNRS UA196 - Univ. Pierre et Marie Curie - 4, place Jussieu - 75252 PARIS CEDEX 05 - FRANCE

Mixed Iron and Manganese hydrothermal oxides in association with sulfides have been dredged on the East Pacific Rise near 7°N. They present a very important enrichment in Copper (as far as 30% in weight of oxide). Lead isotopic measurements indicate an hydrothermal origin (Fig.1).

Sample	CO	OX	Fes2	Basalt
206Pb/204Pb	18.243	18.185	18.289	18.293
207Pb/204Pb	15.495	15.503	15.488	15.508
208Pb/204Pb	37.77	37.73	37.79	37.811

Fig.1: Lead isotopic ratios for hydrothermal deposits and basalt at the 7°N E.P.R. site. CO is Cu-poor and OX is Cu-rich mixed Mn-Fe oxides.

Copper is mainly under the Cu(I) oxidation state (ESCA measurement confirmed by X-ray absorption) and exclusively situated in the Manganese phase. X-ray diffraction (in spite of poorly resolved diffractogram), reflected and transmitted light microscopy, have shown the presence of buserite (10Å phase) and birnessite (7Å phase).We noticed an evolution during the storage of the samples: all the 10Å phase slowly transformed into 7 Å phase. To acquire data pertinent to the conditions of hydrothermal events in oceanic ridges, we have performed laboratory experiments of synthesis of Manganese oxides. The products are studied by X-ray absorption using synchrotron radiation (X-ray Absorption Edge and EXAFS).

Experiments:

X-ray absorption experiments were done at LURE(Lab. pour l'Utilisation du Rayonnement Electromagnétique) using the DCI storage ring of ORSAY(FRANCE) with an energy of 1.72 GeV. Spectra were enregistred in the air at room temperature. The monochromator was a channel cut single crystal of Silicium using the 220 reflection.

Low temperature and pressure chemical experiments consist in Cu-buserite and Cu-birnessite synthesis. High temperature and pressure experiments were done using one liter Teflon bottles. Hydrothermal conditions at 350°C, for which concerns ion speciations of Mn and Cu, have been obtained by the use of highly concentrated chloride solutions at 150°C.

Preliminary results:

In both natural and synthetic Manganese oxides Cu was neither in substitution with Mn(IV) nor with Mn(II) or Mn(III) near the Mn(IV) vacancies. Cu(I) and Cu(II) are situated inside the water sheets of the manganese oxide(Fig.2).

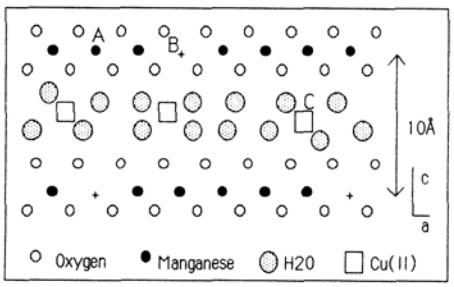

Fig.2: Schematic hypothetical structure of Cu-buserite or Cu hydrothermal oxide. Cu is neither in A (MnIV) or B(vacancies) sites but probably in C sites.

Cu(II) is in octaedral coordination and surrounded by 6 Oxygen atoms or OH molecules. The Cu(OH)6 octahedra presents a Jahn-Teller distortion in the case of the Cu(II)-buserite but not in the case of Cu(I) natural Manganese oxide.

Only low pressure and temperature synthesis have been successful. Cu(II)-buserite and birnessite were obtained: Cu(I) was not founded to enter the water sheets or Cu(I) oxide was unstable in the conditions of the synthesis.

Further experiments:

High temperature and pressure experiments are presently done to reach conditions in which Cu(I) should be incorporated in the oxides.

THE CHEMICAL AND SPECTRAL CHARACTERISTICS OF GEM GARNETS FROM EAST AFRICA

STOCKTON, C.M., and MANSON, D.V., Gemological Institute of America, Santa Monica, CA 90404, U.S.A.

The recent development of gem mining in East Africa (especially Kenya and Tanzania) revealed new types of garnets that do not fit the existing classification systems. In order to characterize and classify these new garnets, and to resolve some ambiguities in the gemological classification and identification of other garnet types, a study was done that included 140 gem-quality garnets that belong to the compositional space primarily defined by the end members pyrope, almandine, and spessartine. 70 of these are known to be from East Africa, 52 are of uncertain origin (although at least 16 are believed to be East African), and 18 come from other known localities (e.g., the USA, Brazil, and Sri Lanka). Refractive index, specific gravity, optical absorption spectrum, CIE chromaticity coordinates, and chemical composition (microprobe) were determined for each sample.

Many of the garnets from East Africa have unusual properties that have not previously been encountered among garnets from other localities. We found that 73 of the specimens occupy a new range for naturally-occurring garnets along the compositional join pyrope-spessartine (29-59 wt.% pyrope and 21-56 wt.% spessartine; fig.1). Many of these garnets contain appreciable Fe (up to 5.7 wt.% FeO or 11.6 wt.% almandine) and, interestingly, Ca (0.9-8.9 wt.% CaO or up to 23.3 wt.% as grossular). These 73 garnets can be subdivided into three categories, the first of which includes 33 stones of pinkish orange to orange color that are of a type called "malaia" in the gem trade. We propose this term be adopted and a new variety be defined for these garnets on the basis of distinctive chemistry and color. Their refractive index range (1.742-1.779) and density range (3.75-3.99) overlap with those for garnets along the pyrope-almandine join. The optical absorption spectra of the "malaia" specimens all exhibit strong absorption features that suggest Mn2+ is the primary coloring agent, although less prominent Fe2+-associated bands also appear in some of the spectra.

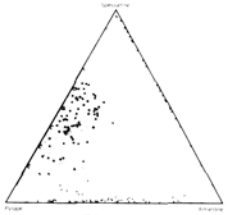

Figure 1

The second category includes 7 specimens high enough in pyrope content that we suggest they be classified as such; all are notably lighter in color than the "malaias," and their properties ($n<1.742$ and $D\leq3.80$) approach those of end-member pyrope. The remaining 33 garnets in the third category are notable in that they exhibit a distinct color change between daylight and incandescent light. The only type of garnet previously known to show this phenomenon is chrome pyrope. While Cr3+ alone is the cause of the behavior in pyropes, color change in pyrope-spessartine garnets was observed to correlate with minor amounts of V3+ and/or Cr3+ present in conjunction with Mn2+. Optical absorption spectra of these color-change garnets exhibit the two broad absorption regions typical of most color-change minerals (fig.2). Otherwise, these color-change garnets are similar to "malaia" garnets in chemical composition, refractive index ranges, and densities.

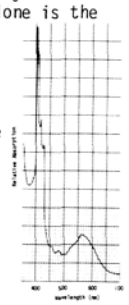

Figure 2

The 67 garnets not belonging to the new pyrope-spessartine range are representative of more well-known garnet types: pyrope, pyrope-almandine, almandine, almandine-spessartine, and spessartine. However, previous data available on these types are inadequate to enable us to make the correlations among chemistry, spectra, color, etc. that are necessary to answer gemological problems. Comparison of the interrelationships among the properties obtained for all 140 specimens enabled us to devise a classification system consistent with mineralogic practice but with characteristic properties defined such that gemologists can classify garnets with the methods available to them on a routine basis. We defined eight species for gem garnets: pyrope, pyrope-almandine, almandine, almandine-spessartine, spessartine, pyrope-spessartine, grossular, and andradite. A garnet can be identified by a gemologist as a member of one of these categories on the basis of just three properties: refractive index, optical absorption spectrum (as seen in a hand spectroscope), and color.

ON THE CLASSIFICATION OF THE SILICATES

STRUNZ, H., Institut für Mineralogie, Technische Universität, D-1000 Berlin 12, West Germany

The Chemical-Structural Mineral Classification includes twelf Classes: I.Elements, II.Sulfides, III.Halides, IV.Oxides and Hydroxides, V.Sulfites (arsenites, selenites, tellurites), VI.Nitrates, VII.Carbonates, VIII.Borates, IX.Sulfates (chromates, molybdates, wolframates), X.Phosphates (arsenates, vanadates), XI.Silicates, XII.Organic compounds.

XI.SILICATES. Five divisions (with subdivisions α,ß,γ etc.):

A.Nesosilicates. (α) only insular SiO_4 anions, groups 1-7. (ß) SiO_4 and nonsilicate anions O,OH,F and/or H_2O, groups 1-18. (γ) SiO_4 and complex nonsilicate anions CO_3, SO_4, BO_3, BO_4, etc. or complex cations UO_2, groups 1-12.
B.Sorosilicates. (α) only Si_2O_7 anions, groups 1-9. (ß) Si_2O_7 and nonsilicate anions O,OH,F and/or H_2O, groups 1-12. (γ) anions Si_3O_{10}, Si_4O_{13}, etc., groups 1-8. (δ) mixed silicate anions SiO_4+Si_2O_7, SiO_4+Si_3O_{10}, etc., groups 1-7.
C.Cyclosilicates. (α) rings Si_3O_9. (ß) rings Si_4O_{12}, double rings Si_8O_{20}, branched tetragonal rings. (γ) rings Si_6O_{18}, double rings $Si_{12}O_{30}$, branched hexagonal rings. (δ) rings Si_8O_{24}, Si_9O_{27}, $Si_{12}O_{30}$,etc., also mixed silicate anions.
D.Inosilicates. (α) two-tetrahedron repeat, single, double, triple chains. (ß) three-,five-,seven-tetrahedra repeat, single, double branched chains. (γ) four-,six-,twelf-tetrahedra repeat, single double chains. (δ) loop chains, tubular chains. (ε) transitional structures ino-phyllo-silicates.
E.Phyllosilicates. (α) tetragonal and pseudotetragonal layers. (ß) mica-type layers, also with regular interstratification. (γ) kaolinite-type layers. (δ) pyrosmalite-, palygorskite-type layers, etc. (ε) hybride layers, double-sheet layers, etc.
F.Tectosilicates. (α) without nonsilicate anions: nepheline-, leucite-,feldspar-type structures, etc. (ß) with nonsilicate anions: cancrinite-, sodalite-, scapolite-type structures, etc. (γ) zeolites.

The sequence in the subdivisions of A and B is with increasing cation radii (Mineralogische Tabellen 1941), now with increasing coordination number. A complete classification of A and B was circulated in the IMA Commission on Mineral Data and Classification (1986). It gives a basis for further considerations.

Structural-Geometrical Consideration. In the first groups of the subdivisions α,ß, etc., we find. Polymict Tetrahedral Networks: (Aα1) liberite, with one oxygen sharing for cations (Li_2BeSi), phenakite (Be_2Si); (Aα2) trimerite (BeSi), larsenite ($Zn_2Si)_2$(ZnSi)(Si); (Bα5) barylite (Be_2Si)(BeSi); (Bß1) bertrandite (Be_2Si)$(Si)_2$, hemimorphite (Zn_2Si)(Si_2). Polymict Tetrahedral Sheets: (Aß2) hodgkinsonite, clinohedrite; (Aß4) yeatmanite; (Aγ9) cappelenite; (Bα3) melilite. Polymict Tetrahedral Chains: (Aß2) euclase; (Aß3) surinamite, one-side open-branched, sapphirine, two-side open-branched, topologically related to aenigmatite; (Aß6) sillimanite, double-chains; (Bδ1) davreuxite single- and double-chains; (Bδ2) queitite, chains of four- and five-membered rings. Polymict Tetrahedral Clusters: (Bß3) axinite $Be_2Si_8O_{30}$.

Corner-sharing Octahedral Chains: (Aß14) titanite. Edge-sharing Octahedral Chains: (Aα3) olivine, (Aß6) sillimanite, andalusite, kyanite; (Aß8) topaz; (Aß9) norbergite, chondrodite, etc.; (Bδ3) epidote, etc.; (Bδ4) zoisite; (Bδ5) pumpellyite, etc.; (Bδ6) sursassite, etc.; (Bδ9) ardennite.
Edge-sharing Octahedral Sheets: (Bα3) thortveitite, etc.
Edge-sharing Octahedral Networks: ?

Polyhedral-Octahedral Chains, Sheets, Networks: (Bß6) cuspidine, wöhlerite, etc.; (Bß7) mosandrite, rosenbuschite, etc.; (Bß8) seidozerite, lamprophyllite, etc.; (Bß11) tilleyite, killalaite; etc. etc. - Belov (1961) discovered the close relation of the Ca-sorosilicates, etc. - Moore, Shen, Araki (1985) found related structural principles in lawsonite (Bß5), orientite (Bγ3), ruzite (Bγ5), pumpellyite (Bδ5), sursassite, macfallite (Bδ6) and ardennite (Bδ9) (Am.Min.70.171).

Structural-Geochemical Considerations are emphasized by I.Kostov (1975) etc.).

A Historical Review on Modern Mineral Classifications was given by H.Strunz (1984) Proceedings of the 27th International Geological Congress, Vol.10, pp.65-112, VNU Science Press, Utrecht, The Netherlands. - In Russian by Academia Nauk CCCP, Moscow (1984). - In Chinese by Academia Sinica, Beijing (1985).

OPTICAL PROPERTIES OF ALKALI FELDSPARS

SU, Shu-Chun, RIBBE, Paul H., and BLOSS, F. Donald, Dept. of Geological Sciences, Virginia Polytechnic Institute & State University, Blacksburg, VA 24061 USA

In an earlier study it was found that labelling the principal refractive indices of the low microcline-high sanidine [LM-HS] series of K-rich alkali feldspars -- not conventionally according to magnitude (i.e., nα, nß, nγ) but as na, nb, nc, according to which crystallographic axis their vibration direction most nearly parallels -- permitted us to model the variation of indices and 2Vx with structural state. The latter is expressed as $\Sigma t1 \equiv 2t1$ for monoclinic and $\Sigma t1 \equiv (t1o + t1m)$ for triclinic feldspars, where t is the Al content of the T1, T10 and T1m tetrahedral sites. We found that na, nb, nc varied inversely with the lengths of the **a**, **b**, **c** cell parameters. If linearity is assumed, 2Vx varies sigmoidally with Σt1, and observed values fit the calculated curve with remarkable precision. Both **a** and na vary little, but **b** decreases twice as much as **c** increases with Σt1, **b** varying linearly with [2 - Σt1] and **c** with [(1 + Σt1)/ 2]. Partly as a consequence, nb and nc cross at $\Sigma t1 \equiv 0.67$ (see figure below). At this point 2Vx = 0° and the optic axial plane (OAP) changes from OAP ⊥ (010) in low sanidine to OAP = (010) in HS. The quantity $\sin^2 Vx$ varies linearly with Σt1, based on regression analysis of data from more than 50 K-rich feldspars whose lattice parameters and/or structure analyses gave independent estimates of Σt1.

Refractive indices, 2Vx and optic orientations have been measured on a series of heat-treated single crystals in the series low albite-high albite [LA-HA] whose structural states were determined by measurement of reciprocal lattice angles α* and γ* from *x*-ray precession photographs. The same principles of structurally interpreting these results apply to Na- as to K-rich order-disorder series, but in the case of albites, na = nα, nb = nγ, nc = nß, and although their slopes are predictably opposite, nb and nc do not cross (see figure). 2Vx is curvilinear, and regression analysis shows $\sin^2 Vx$ to be linear with Σt1, as well as $\Delta t1 \equiv (t1o - t1m)$.

In the solid solution series high albite (analbite)-high sanidine [HA(AA)-HS], it was impossible to select a set of specimens which were (1) free from minor constituents (anorthite, celsian, Sr- and Rb-feldspar, and Fe), (2) totally free of evidences of exsolution, and (3) all of precisely the same structural state. So data were gathered for 31 feldspars whose range of structural states was $0.52 \le \Sigma t1 \le 0.65$ (average, 0.60). Only specimens thought to be at least 95% homogeneous were used, and corrections to the refractive indices (many from Spencer (1937, *Mineral. Mag.*) and Hewlett (1959, *J. Geology*)) were made for non-binary constituents. The resulting na,b,c vs. mol % Or curves were found to change slope at Or~60, and each was conveniently represented by two linear segments (see figure). The segments and inflection point correspond very closely to those representing the plot of density versus mol % Or. As in the case of LM-HS, the nb and nc curves cross; 2Vx = 0° at Or~73 for $\Sigma t1 \equiv 0.6$, with composition of the crossing point (in-) decreasing with (in-) decreasing Σt1.

No index data are available for the LA-LM solid solution series, except for the end members. So using those plus the density versus mol % Or curves (which closely resemble those for HA(AA)-HS), segmented curves of na,b,c versus composition were constructed (see figure). The 2Vx values calculated from these curves match rather well 2Vx measured by Rankin (1967, *Am. Mineral.*) on cation-exchanged specimens of Orville (1967, *Am. Mineral.*).

From these studies a set of reference refractive indices and 2Vx values have been carefully selected to represent hypothetical members [minus sign indicates OAP = (010)]:

Hyp'l member	mol % Or	Σt1	na	nc	nb	2Vx
Low albite	0	1.0	1.5289	1.5329	1.5393	103.0°
High albite	0	0.5	1.5273	1.5348	1.5361	45.0°
Na-high sanidine	60	0.5	1.5185	1.5242	1.5240	-44.1°
High sanidine	100	0.5	1.5174	1.5229	1.5214	-64.0°
Low microcline	100	1.0	1.5183	1.5217	1.5243	82.2°
Na-low microcline	60	1.0	1.5194	1.5226	1.5257	89.2°

Using these reference points, it is possible to calculate 2Vx values and to construct a plot of 2Vx versus mol % Or contoured for Σt1. This in turn permits us to estimate structural state to within ±0.02 for 83% and ±0.04 for 97% of a suite of 109 homogeneous alkali feldspars for which Σt1 had been determined independently from lattice parameters and/or crystal structure analyses.

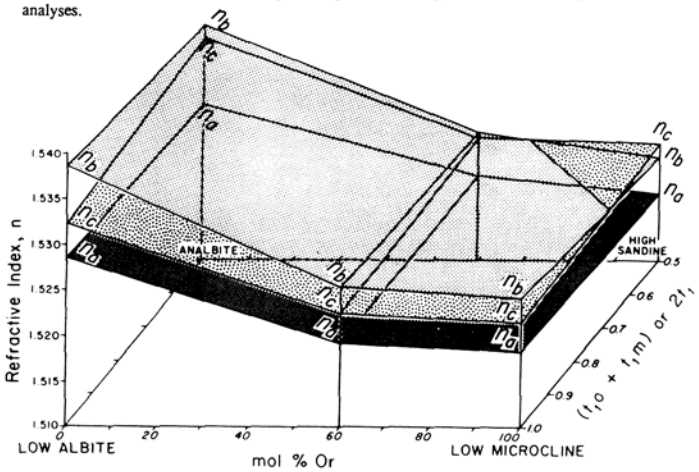

A MINERALOGICAL STUDY ON TWO NATURAL PROTO AMPHIBOLES

SUENO, S. and MATSUURA, S., Institute of Geoscience, University of Tsukuba, Ibaraki, 305 JAPAN

The basic structural unit of amphibole can be represented by a tetrahedral-octahedral-tetrahedral unit. Due to different octahedral stacking sequence of this unit which can de defined by whether the apices of the octahedra point to +a or -a, different amphibole polymorphs are generated. It has long been believed that the natural amphiboles have only two stacking sequences, (++) or (--) for clino-amphibole and (+-+-) for ortho-amphibole. Gibbs et al.(1960) have reported a synthetic amphibole which has (+-) stacking and named it "proto amphibole". Recently, Matsuura & Sueno (1984) and Matsuura et al.(1985) found two chemically different proto amphiboles from different natural occurrences. The amphiboles were termed "proto ferro-anthophyllite" (PFA) and "proto manganese-anthophyllite" (PMA) and these names were recommended to the Commission on New Minerals and Mineral Names of IMA. These amphiboles are the first mineral with proto type stacking sequence (+-) in the biopyribole species found in nature.

(1) Occurrence: [PFA], brownish-yellow acicular crystals (up to 3mm) in sheaf like aggregates, occurs in pegmatite and granite in "vugs" of dark brown masses found at Gifu, Japan and Colorado, U.S.A.. Associated minerals are fayalite, laihunite, magnetite, and quartz. [PMA], light brownish-yellow acicular crystals forming sheaf-like aggregates, occurs in bedded manganese deposit at Asio mountainland area in Japan in large amphibole blocks (40cm in diameter) associated with pyroxmangite and rhodonite.

(2) Optical data (PFA for Colorado sample):

	α	β	γ	2V	Orientation	Pleochroism
PFA	1.690	1.710	1.726	86°-88°(-)	X=a,Y=b,Z=c	X,Y,Z=pale yellow
PMA	1.695	1.714	1.731	76°(-)	X=a,Y=b,Z=c	X,Y,Z=pale yellow

(3) chemical data (PFA for Colorado sample)

	SiO_2	Al_2O_3	FeO	MnO	MgO	CaO	Total
PFA	46.27	---	46.39	2.51	0.12	0.09	95.38
PMA	48.99	0.17	34.44	9.98	3.69	0.16	97.43

PFA; $Fe_{6.65}Mn_{0.35}Si_8O_{22}(OH)_2$, PMA; $Fe_{4.69}Mn_{1.38}Mg_{0.9}Si_8O_{22}(OH)_2$

(4) Lattice parameters (PFA for Colorado sample):

	a(Å)	b(Å)	c(Å)	α	β	γ	V(Å^3)
PFA	9.382(2)	18.390(4)	5.343(2)	90.0	90.0	90.0	921.9(7)
PMA	9.425(2)	18.303(4)	5.345(1)	90.0	90.0	90.0	922.0(3)

(5) Crystal chemical properties:

Structure refinements for PFA and PMA were carried out using the intensity data measured by a Rigaku four circle diffractometer.

	Specimen(μm)	Radiation	Abs.Correct.	No. of Fo	R-factor
PFA	35 X 65 X 115	MoKα	No	1493	0.035
PMA	50 X 100 X 200	MoKα	No	1520	0.05

The results are listed on Table 1 with the results of protoamphibole (Gibbs,1969). The tetrahedral chain angles for both PFA and PMA are close to 180° (E-chain), and this minimize the parity rule violation, therefore, M(1)-M(3) octahedra become close to regular in shape. This may be related to the large contents of the Fe ion in these sites although the mean M(1)-O, M(2)-O, M(3)-O distances of PMA are slightly smaller than those of PFA because of the occupancy of the smaller Mg ion. In PMA, the larger Mn ion can be assigned to the M(4)-site, however, the mean M(4)-O distance is shorter than that of PFA. The M(4)-O(2) and M(4)-O(4) in PMA is longer than those in PFA, that is, the shrinkage of the M(4)-O(6) is a cause of the shorter mean M(4)-O in PMA. This short M(4)-O(6) has the effect of straightening the tetrahedral chain in PMA. The mean ionic radii of M-site cations both in PFA and PMA are 0.782Å. For stabilizing the Fe-Mn-Mg proto amphibole structure, it is conceivable that the M(1)-M(3) sites must be occupied mostly by Fe ion and the mean ionic radii of the M-site cations must be equal to or a little larger than 0.782Å because these conditions are necessary for giving rise to the E-chain in the amphibole structure.

Table 1. Comparison of Interatmic Distances and Interatmic Angles of Proto Amphiboles

atoms	Proto ferro-anthophyllite	Proto manganese-anthophyllite	Protoamphibole (Gibbs,1969)
Si(1)-O	1.620(Å)	1.619(Å)	1.614(Å)
Si(2)-O	1.627	1.627	1.620
M(1)-O	2.126	2.121	2.070
M(2)-O	2.132	2.122	2.084
M(2)-O(1)	2.173	2.167	2.179
M(2)-O(2)	2.148	2.138	2.084
M(2)-O(4)	2.075	2.060	1.989
M(3)-O	2.114	2.113	2.048
M(4)-O	2.264	2.256	2.196
M(4)-O(2)	2.141	2.155	2.107
M(4)-O(4)	1.980	2.032	2.029
M(4)-O(6)	2.671	2.582	2.453
O(5)-O(6)-O(5)	177.2°	178.6°	172.5°

(1)Gibbs,G.V., F.D. Bloss, and H.R. Shell(1960) Amer. Mineral. 45, 974-989. (2)Gibbs,G.V.(1969) Mineral. Soc. Amer. Spec. Pap., 2, 101-109.

•THE COMPARATIVE STUDY OF ß-FERGUSONITE IN TWO DIFFERENT GENETIC DEPOSIT TYPES IN THE BAIYUN-EBO MINING DISTRICT, CHINA

SUN Weijun, Tianjin Geological Academy, Ministry of Metallurgical Industry, 42 Youyi Road, Tianjin and MU Shengjie, Chengde Region Gold Industry Company, Hebei Province, People's Republic of China

Fine mineral grains with brown-red and yellow-red color were discovered in the skarn-type deposit of eastern contact and the western sedimentary-metamorphic deposit [1] during the research work for mineral composition of REE iron deposit in Baiyun-Ebo mining district. After the mineral separation, they are thought to be a ß-fergusonite, rich in ΣCe_2O_3. Physical property determination, X-ray powder analysis and electron microprobe analysis indicate that the ΣCe_2O_3 contents of this mineral are the highest of any such groups (the average ΣCe_2O_3 of three samples is 53.9). After the discovery of ß-fergusonite (ΣCe_2O_3 = 50.31) by A.I. Chaska in some carbonatite in the Soviet Union [2], its content was near the theoretical value (55.26) of total contents of Ce_2O_3 in synthetic $CeNbO_4$ [3].

The major results of a comparative study of ß-fergusonite in two different genetic deposit types are as follows:

(1) The X-ray powder analysis (no heating) showed that the strongest lines are similar and comparable with the same mineral occurring in carbonatites (after being heated at 700°C) of other countries.

(2) The chemical composition and REE of ß-fergusonite of different occurrences are similar, and no distinct difference is seen from the same mineral derived from carbonatite, indicating that ß-fergusonite rich in ΣCe_2O_3 has a stability that does not change with temperature and pressure. But there are differences in the ratios of REE, such as in the western contact Nd is obviously high in ß-fergusonite and La and Ce are relatively low. This characteristic shows that the mineral was formed during the later mineralization period, while the mineral occurred in the eastern contact was formed earlier.

(3) It is generally considered that crystallized fergusonite should be heated to over 800°C to produce ß-fergusonite; thus, ß-fergusonite was thought to be the modification of fergusonite. However, ß-fergusonite that occurred in the western Baiyun-Ebo mining district is not related to the contact, so it might be related to extensive alkaline hydrothermal metasomatism genetically. The metallogenetic temperature might not exceed 500°C; it is concluded that ß-fergusonite in this study area is an isometric modification rather than a variant formed at high temperature.

(4) ß-fergusonite rich in Ce_2O_3 in this area contains very little radioactive Th and U. That can explain the main reason for incomplete crystallization.

[1] Sun Weijun et al. (1983) Scientia Geol. Sinica, 78-80. [2] Chaska, A.I. et al. (1977) Am. Mineral., 62, 3-4. [3] A.S.T.M. (1972) Index to the Powder Diffraction File, "Inorganic."

IN-SITU OBSERVATION OF GROWTH AND DISSOLUTION PROCESSES OF SILICATE CRYSTALS AT ELEVATED TEMPERATURES

SUNAGAWA, I., TSUKAMOTO, K., ABE, T.*, NAKAMURA, H., KAWASAKI, M. Faculty of Science, Tohoku University, Sendai, JAPAN; *Faculty of Science, Yamaguchi University., Yamaguchi, JAPAN

The most direct way to understand kinetic processes of crystallization is in-situ observation of the process, provided that the growth parameters could be controlled and measured precisely and the processes could be observed with high visibility. We have developed a series of instruments with which these requirements were fulfilled at elevated temperatures relevant to magmatic crystallization.

The instrument consists essentially of (1) transmission type optical microscope with phase contrast, interference contrast and polarization equipments, (2) high temperature furnace workable on the microscope stage, (3) temperature controlling system consisting of a stabilizer, a digital voltmeter and a microcomputer, and (4) imaging and recording system by TV camera and video recorder. High temperature liquid is hold by its surface tension, in a form of thin film on a loop heater in the furnace. This enables observation by transmitted light. Necessary ΔT is given through a thin thermocouple inserted in the film. To improve visibility, IR ray is cut off by a couple of filter, a newly designed aberration corrected objective lens is used, and the image is electrically processed. By these combinations, temperature fluctuation within the liquid film could be stabilized down to $\pm 0.3^{\circ}C$ at $1600^{\circ}C$; the visibility could be improved to such an extent as growth layers thinner than 100Å in height became observable; and growth rates became easily and precisely measurable on TV image on which temperature and time are superimposed. In addition, the mass flow and diffusion boundary layer around a growing or dissolving crystal are visualized by means of Schlieren technique or Mach-Zehnder interferometer. Thus it is now possible to observe in-situ how crystals grow or dissolve and to measure their rates under precisely controlled growth conditions and known environmental movement, in a magma which is prepared under the microscope.

Various unexpected and exciting phenomena have been observed. A few examples will be shown by a cine film converted from video image. Out of these phenomena, problem of metastable nucleation will be selected for discussion.

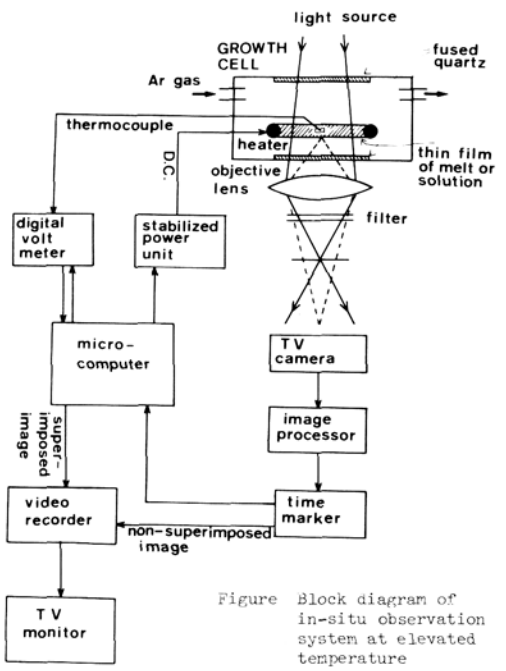

Figure Block diagram of in-situ observation system at elevated temperature

THE SPINEL TO GARNET LHERZOLITE MANTLE TRANSITION BENEATH EASTERN AUSTRALIA, IN RELATION TO A HOT TASMANIAN GEOTHERM.

SUTHERLAND, F.L., Div. Earth Sciences, The Australian Museum, Sydney, NSW. 2000; RAYNOR, L.R., Dept. Geology & Geophysics, University of Sydney, NSW. 2006.

Garnet ± spinel lherzolites and related pyroxenites occur rarely in Eastern Australia from:

a) Mesozoic-Cainozoic basalts erupted through Palaeozoic fold belts (Jugiong-Murrumburrah, New South Wales; Meredith, Victoria; Bow Hill, Tasmania; Boowinda Creek, Queensland)

b) Mesozoic kimberlites intruding Precambrian cratons just west of the Palaeozoic fold belts (Terowie, South Australia).

c) a Permian 'melilititic' pipe intruding near the margin between the Precambrian craton and Palaeozoic fold belts (Kayrunnera, W. New South Wales).

Co-existing gnt, spl and two pyroxenes in these mantle xenoliths enable various geothermometers and barometers to be used to estimate geotherms and the depth range of the spinel to garnet lherzolite transition zone. These geotherms can be checked using their intersection with experimentally determined stability fields for gnt-spl-lherzolites (e.g., O'Neil, 1981).

Most of the P,T determinations indicate 'hot' geotherms, with the Tasmanian Tertiary geotherm being the hottest. For comparative estimates, the Cr-corrected barometer of Nickel and Green (1985) was applied to mainland and Tasmanian xenoliths. With the 2 pryoxene thermometer of Wells (1974), pressures at depth to the spl-gnt lherzolite transition zone range from 18-21 kb for Tasmania (mid-Tertiary) to >14 kb for Boowinda Creek (late Oligocene), 17-20 kb for Jugiong-Murrumburrah (lower Jurassic?) and 16 kb for Terowie, South Aust. (Jurassic?) The hotter Tasmanian Tertiary geotherm is unexpected since Tasmanian volcanism is more limited in time (13-47 Ma) than many mainland regions. A few geotherms related to the youngest mainland volcanism (<1 Ma) approach or exceed Tasmanian gradients, but these may still be cooling towards ambient geotherms.

Tasmanian basalts also show unusual features from mainland basalts, including lherzolite-bearing olivine tholeiite, garnet-lherzolite bearing nepheline hawaiite and unusually mafic fractionation series, including one based on olivine nephelinite. The basalts also show particularly low $^{87}Sr:^{86}Sr$ (0.7026-0.7034) and E Nd values (+7.5 to 5.8) suggesting an isotopically anomalous mantle source compared to that of South East Australian basalts. This contrasts with Tasmanian Jurassic dolerites (≡ Ferrar Antarctic dolerites), which show relatively enriched K,U,Th,Sr and high $^{87}Sr:^{86}Sr$ ratios.

These facts suggest that Tasmania's geotherm may be augmented by a more radiogenically enriched mesosphere (old subducted slab?) which initiated basaltic melting to incorporate xenoliths from slightly greater depths than usual in East Australia.

References:

Nickel, K.G. and Green, D.H., 1985. Empiracal geothermobarometry for garnet peridotites and implications for the lithosphere, kimberlites and diamonds. Earth Planet. Sci. Lett., 73, 158-170.
O'Neill, H.St.C., 1981. The Transition between spinel lherzolite and garnet lherzolite, and its use as a geobarometer. Contrib. Mineral Petrol, 77, 185-194.
Wells, P.R.A., 1977. Pyroxene thermometry in simple & complex systems. Contrib. Mineral. Petrol, 62, p. 129-139.

TEXTURAL AND MINERALOGIC ZONING IN THE ROCKLIN PLUTON, WESTERN SIERRA NEVADA, CALIFORNIA, U.S.A.

Samuel E. Swanson, Department of Geology and Geophysics, University of Alaska, Fairbanks, AK 99775-0760, U.S.A.

The Rocklin pluton is a texturally and mineralogically zoned tonalite pluton of early Cretaceous age located in the western foothills of the Sierra Nevada of California. Rocks are all equigranular, but an assymetric pattern of textural and mineralogic zoning is progressively displayed across the pluton. All of the zones appear to be in gradational contact with each other and include (in inferred order of crystallization) a medium-grained biotite hornblende zone, a coarse-grained hornblende biotite zone, a coarse-grained biotite zone, a coarse-grained muscovite biotite zone and a fine-grained alltriomorphic muscovite biotite zone. All of the zones are composed of tonalite, except the late-stage muscovite-biotite zone which is a granodiorite. Dikes with pegmatite/aplite textures are associated with the late stage zone and intrude all of the earlier zones.

Patterns of major element variation in the Rocklin pluton follow the same trends as the textural zoning. Hornblende-bearing rocks are lowest in silica (SiO_2=52-68%), coarse-grained muscovite-bearing rocks are higher in silica (SiO_2=69-74%) and the late-stage aplitic rocks are highest in silica (75-77% SiO_2). Aluminum content of the rocks changes from metaluminous to peraluminous with increasing silica, while Na/K and Feo/Fe_2O_3 decrease.

Mineral composition variation in the Rocklin pluton is variable, depending on the phase. Hornbelende (Fe/Fe+Mg=0.32-0.36, Na+K=0.34-0.49), muscovite (Na/Na+K=0.04-0.17), alkali feldspar (Ab=4-13%) and magnetite (essentially pure) show little, if any, compositional variation while other phases, such as plagioclase (rims Ab64-87) and biotite (Fe/Fe+Mg=0.35-0.60) vary reflecting fractionation. Textural relations suggest a reaction relationship between hornblende and melt to produce biotite.

Fractional crystallization of early phases (plagioclase and hornblende) and subsequent reaction of the evolved silicate liquid with these phases is responsible for the mineralogic and geochemical variation within the Rocklin pluton. Development of textural and mineralogic zoning in the Rocklin pluton was promoted by the retention of volatiles until the late stages of crystallization.

STRUCTURAL VARIATIONS IN ORTHOPYROXENES

SYKES, JULIA, Dept. of Geology, Brooklyn College, Brooklyn, NY 11210 and Dept. of Earth and Environmental Sciences, Graduate School, CUNY, New York, NY 10036. USA; MOLIN, G.M., Istituto di Mineralogia e Petrologia, 37 Corso Garibaldi, Padova, ITALY.

The structure of the Pbca orthopyroxene consists of alternating tetrahedral and octahedral layers. Tetrahedral layer A (TA) is smaller and more distorted than TB. The octahedral layer consists of zig-zag chains of regular M1 octahedra parallel to **c** and joined by larger, distorted M2 polyhedra. Mg and Fe^{2+} prefer M1 and M2 respectively and the partitioning between M1 and M2 depends on the Fe/Mg ratio and on temperature.

Structural refinements of natural and heated orthopyroxene crystals with high Fe/(Fe+Mg) ratios have been used to augment a systematic analysis of structural variations as a function of chemical composition and ordering degree. The X-ray data collection was carried out using a Siemens four circle diffractometer. First, data was collected for the natural crystal, then a series of heating experiments were conducted on the same crystal until a close approximation to equilibrium was attained. Structural refinements were carried out in space group Pbca without chemical constraints. The choice of scattering factors was Mg^{2+} and Fe^{2+} for both M1 and M2 sites. All structural sites were considered fully occupied. Finally, each crystal was analyzed by microprobe.

This study reconfirms that Al^{IV} only substitutes in the TB site with an elongation in [TB-O] bridging and non-bridging bond lengths. [TA-O] bonds show no real changes with either increasing Fe content or Al content. Unit cell volume increases systematically with increasing Fe-content.

Figure 1a shows the regularity of the variation of the mean M1-O bond lengths compared to Fe in M1. These bond lengths all increase with Fe-content. Heating of the crystal, causing Fe to move to the M1 site, leads to an increase in this bond length showing the same trend as the natural series.

Figure 1b shows variation in M2-O3A with Fe content in the M2 site (lower curve) and the M1 site (upper curve). Again the fit is highly regular. With heating, Fe moves into the M1 site and these bond lengths show little change. This is due to these bond lengths being related to the positions of the oxygens O3A and O3B as the chains straighten and not affected by the cation in M2.

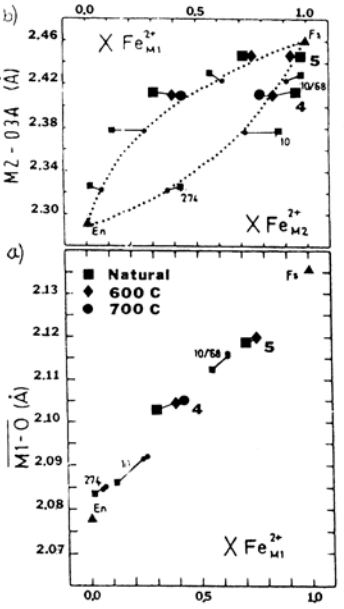

The only exception to the regularity is the M2-O3B bond length, especially the iron-rich crystals, which can show either lengthening or shortening with heating. This bond has a very long length and low strength and thus is affected greatly by framework changes. This result could be attributed to either the thermal history of the rock, the high Fe content or a pressure effect that disappears on heating at one atmosphere.

Figure 1. Variation in bond lengths with Fe content. Opx 4 and 5, this study (Fe/Fe+Mg = 0.62 and 0.82 resp.). Opx 274, 10, 10/68 (Fe/Fe+Mg = 0.18, 0.46 and 0.76 resp.) from Domeneghetti, M.C., Molin, G.M. and Tazzoli, V. Am. Mineral., 1985, 987-995.

NON-DIFFUSIVE MECHANISM FOR THE SHOCK-INDUCED PHASE TRANSITION IN SILICATES AND OXIDES

SYONO, Yasuhiko, The Research Institute for Iron, Steel and Other Metals, Tohoku University, Katahira, Sendai 980, Japan

The phase transition due to non-diffusive mechanism is typical to be completed within a microsecond time scale of shock loading experiments. Numerous phase transitions due to displacive mechanism, not to speak of the electronic origin, have been found to be induced rather easily under shock condition by means of in-situ measurements of shock compression curve and observation of residual effects in shock recovered materials. B1-B2 transition in CaO[1] and rutile-fluorite-like transition in TiO_2[2] were observed to occur instantly under shock compression, accompanying a large volume contraction. Complete conversion of zircon, $ZrSiO_4$, to the scheelite structure was confirmed in shock recovery experiments.[3] Diaplectic glass of quartz and feldspar is believed to be formed in the solid state by shock loading.[4] A series phase transformations revealed by electron microscopic study of shocked Nb_2O_5 should also be interpreted by some non-diffusive mechanism.[5]

Considering from these results, it is noteworthy to mention that no evidence has been obtained for the olivine-spinel transformation by shock experiments, in spite of the martensitic mechanism proposed by Poirier.[6] Careful Hugoniot measurements of forsterite single crystals showed no indication of abrupt volume decrease well above the transition pressure to spinel determined at static condition.[7] The phase transition started around 50 GPa showed a very broad mixed phase region before entering the high pressure regime above about 100 GPa, suggesting very sluggish character. Shock recovered products showed only an evidence for disproportionation reaction to MgO plus $MgSiO_3$ glass, instead of formation of the spinel phase.[8]

Structural transformations induced in silicate minerals by shock waves seem to be achieved by rearrangements of SiO_4 tetrahedra without breaking Si-O bonds.

NON-DIFFUSIVE MECHANISM FOR THE SHOCK-INDUCED PHASE TRANSITION IN SILICATES AND OXIDES
SYONO, Yasuhiko

For example, the zircon-scheelite transition can be explained by coherent rotation of SiO_4 tetrahedra under shock loading.[9] High density diaplectic glass of the framework silicates may be caused by incoherent rotation of SiO_4 tetrahedra, achieving more efficient packing than the corresponding fused glass.[10] The reason why potential martensitic mechanism for the olivine-spinel transformation cannot apparently be activated under shock loading is probably found in especially strong Si-O bonds, which may prevent the slipping process of oxygen layers in olivine. Ringwoodite, natural silicate spinel reported in meteorites[11], might be formed under prolonged shock duration in natural impact events compared with the artificial condition.

[1]R. Jeanloz, T. J. Ahrens, H. K. Mao and P. M. Bell, Science, 206, 829 (1979).
[2]Y. Syono, K. Kusaba, M. Kikuchi, K. Fukuoka and T. Goto, Proc. US-Japan Seminar on High Pressure Research Application in Geophysics and Geochemistry, Honolulu, Jan. 1986, to be published.
[3]K. Kusaba, Y. Syono, M. Kikuchi and K. Fukuoka, Earth Planet. Sci. Lett., 72, 433 (1985).
[4]J. Arndt, in Shock Waves in Condensed Matter-1983, Eds J. R. Asay et al., Elsevier, Amsterdam (1984), p. 473.
[5]M. Kikuchi, K. Kusaba, E. Bannai, K. Fukuoka, Y. Syono and K. Hiraga, Jpn. J. Appl. Phys., 24, 1600 (1985).
[6]J. P. Poirier, Phys. Earth Planet. Interiors, 26, 179 (1981).
[7]Y. Syono, T. Goto, J. Sato and H. Takei, J. Geophys. Res., 86, 6181 (1981).
[8]Y. Syono, T. Goto, H. Takei, M. Tokonami and K. Nobugai, Science, 214, 177 (1981).
[9]K. Kusaba, T. Yagi, M. Kikuchi and Y. Syono, J. Phys. Chem. Solids, in press.
[10]M. Okuno, F. Marumo and Y. Syono, Miner. J.(Japan), 12, 197 (1985).
[11]L. C. Coleman, Canad. J. Miner., 15, 97 (1977).

•MINERALOGY: AN INTERDISCIPLINARY SCIENCE FROM ELECTRONIC TECHNOLOGY TO BIOGEOCHEMISTRY

SZYMANSKI, A., Scientific Secretary, Institute of Electronic Materials Technology, UNITRA-ITME, 01-919 Warszawa, Wolczynska Street, 133, TX 815386 cnpme pl, Poland

Modern electronic and biomedical microtechnologies have derived from neither mineralogy nor geochemistry. However, further progress in these spheres requires precise interference in crystalline structures. For millions of years Nature, obeying the physical laws, has been producing such effects. Physicists mostly describe scientifically new electronic technologies calling them "crystal engineering"; biologists dealing with living structures name their work "molecular engineering." In both cases inorganic, organic or mixed structures created by Nature are imitated or modified. The specific diamond structure is a pattern for telementary semiconductor technology (Ge and Sl). The spinel and garnet structures are imitated in ferrites, laser crystals and bubble memories. The isotypic quartz and berlinite structures are used as resonators, and the apatite and ß-whitlockite structures to make bearing frame of the human body. The DNA structures contain cods of hereditary properties of living organisms. We may, therefore, state that Nature is the best teacher for modern technologists.

The schematic diagram presents the range of the typical mineralogical sciences activity which usually ends in raw materials processing (Area I). Mineralogists seldom can be found at the stage of technology projection (Area II). Such a situation is disadvantageous: it slows down penetration of genetic mineralogy knowledge into technological processes modification (e.g., ceramic technology) and does not help to define permissible range of metals and ceramics interference by implantation into the human body.

Impetuous growth of microelectronics was initiated in 1947 with the manufacture of the first transistor. By the 1960s MOS and bipolar types of transistors had achieved a size of 250 µm, i.e., about 1000 atoms in electronic element. During the 1970s bubble domains store achieved a size of 50 µm, i.e., about 200 atoms in the electronic element. Ballistic transistors were prepared for manufacture in 1986/87. According to the L.F. Estman concept, based on signal transmittance by electron breakdown through super-thin-film semiconductor, one should be able to form structure one atom after the other. The diameter of such transistors based on GaAs monocrystal will be near 0.3 µm. Miniaturization and operation speed of the third generation computers with ballistic transistors will perhaps even supersede the imagination of electronic engineers.

Transformation of n-type to p-type conductance or invertedly, in such miniaturized semiconductor elements, can be obtained by: (1) controlled thermal diffusional doping with cations precisely situated in the crystal structure fragments; (2) nuclear transmutation of Si to P atoms with thermic neutrons stream irradiation of Si crystal in reactor (Eu ~ 0.025 eV); or (3) ion implantation. In the process of ion implantation dopant atoms are ionized and accelerated in electric field up to high energy (30 ÷ 350 keV). These techniques may be considered as geochemically controlled isomorphical, isotypical or morphotropical structure reconstruction and conscious forming of defected vacancy structures with exactly specified technically useful parameters.

In the second half of the 20th century we observe new methods in medicine activity, especially in two directions: (1) implantation of inorganic and organic parts into bone and soft tissue; (2) uses of some basic for living system bioelements as stimulators of elements cycle in the human body. Implantation frequently creates phase changes on the boarder implant-bone or implant-soft tissue as *in situ* (e.g., in bone) growth of new mineralization, e.g., topotactic transformation of ß-whitlockite, closely connected with some elements concentration. This concentration is dependent with food structure, changes with geographical regions and the age of patient and may be stimulated. The same elements may have cancerous or therapeutic properties according to their concentration in a living system. Magnetic elements, especially in blood, are sensitive to the magnetic field. Thus, there are many frailness problems for which closed cooperation of mineralogists and geochemists with physicians and technologists must be realized. Mineralogists are predisposed, on the basis of paleontological analysis of earth history, compared with natural environment -- its geochemical and genetic modifications -- to indicate possible boundary ranges of technological ingerention into the human body. Therefore, mineralogists must understand that medical circles are very closed and traditionally disinclined for cooperation with other sciences.

The paper gives a review of actual situations in both fields seen by the mineralogist who dealt with the aforementioned technologies.

References

Brodie, I. and Murray, J.J. (1982) The Physics of Microfabrication. Plenum Press, New York.
Dorfman, V.F. (1978) Micrometallurgy in Microelectronics. Mietalurgija, Moscov (in Russian).
Meese, J.M., editor (1978) Neutron Transmutation Doping in Semiconductors. Plenum Press, New York.
Szymanski, A. (1986) Technical Mineralogy and Petrography. Elsevier/PWN, Amsterdam-Warsaw.
Vincenzini, P., editor (1983) Ceramics in Surgery. Proc. 2nd BIOSIMP, Material Science Monographs, 17. Elsevier, Amsterdam.

PARENT BODIES OF DIFFERENTIATED METEORITES

TAKEDA, H., Mineralogical Institute, Faculty of Science, University of Tokyo, Hongo, Tokyo 113, JAPAN

The parent bodies of differentiated meteorites preserve the texture and mineral assemblages of the most primitive planetary materials generated by igneous processes in early solar system. Ten major classes of differentiated stony and stony-iron meteorites may be grouped into at least five different parent bodies on the basis of the inter-element relationships, mineralogy, petrology, oxygen isotope data, isotopic chronology and others. Mars and lunar origin has been proposed for the SNC meteorites and anorthositic regolith breccias, respectively.

Three major groups of achondrites, the howardites, eucrites, and diogenites (HED meteorites), are believed to have formed by igneous processes on the same parent body. The partial melting model of Stolper (1), a layered crust model (2), and a primitive crust formation model by crystal fractionation (3, 4) have been proposed to account for crystallization and thermal history of the HED meteorites. Because of the special bulk chemical composition of the HED magma, the crystallization of pyroxene changes from orthopyroxene to low-Ca pigeonite, and to Pig. + plagioclase during crystal fractionation. This trend provides us with information on a general principle of crust formation of terrestrial planets.

The discovery of an intermediate lithology between diogenite and eucrite, such as Yamato 75032, from Antarctica helped us to trace the differentiation trend. The pyroxene data of the Yamato 75032-type achondrites and the relation between the anorthite content (An) of plagioclase and the Mg/(Mg + Fe) = (mg) number of the coexisting pyroxene in the lithic clasts revealed two crystallization trends. One trend has a steep decrease in the An content, while the mg of pyroxene remains effectively constant. The characteristic exsolution and shock textures and the low-Ca compositions of pigeonite have been useful in finding similar components in brecciated polymict HED achondrites. We found a clast 1 x 3 mm in size, composed of plagioclase and inverted pigeonite known in cumulate eucrites, and another clast similar to the Y75032-type pyroxene-rich material and minor plagioclase in the Yamato 791960 polymict eucrites. Such components have not been found in the polymict breccias as a lithic clast. The finding that many components of the HED crust are found both as an individual meteorite and a clast in the polymict breccias, suggests their close genitic link.

The ureilite parent body (5) shows no systematic pyroxene crystallization trends. The most Mg-rich ureilite, ALH82106 has a mineral assemblage, olivine + pigeonite + augite, the second Mg-rich members, Y74659 and ALH77257 have Ol. + Pig. + minor orthopyroxene assemblage. Y74130, one of the Fe-rich member has Ol. + Opx. + Aug. and Pig. + Aug. assemblages. A weak anticorrelation between MnO and FeO delineated by these pyroxenes suggests that a reduction reaction involving metal and carbon is responsible for the chemical variations. A heat source of ureilite formation may be a planetesimal scale collision, which might have facilitated a compaction and recrystallization of mafic silicate. During the high temperature episodes, Fe-Ni-S euctectic melt and a minor partial melt rich in Ca, Al and Fe might have been carried away through grain boundaries from a carbonaceous-chondrite-like source material. This model offers that the olivine and pyroxene crystals were grown and homogenized without destroying the carbonaceous veins at the grain boundaries and that moderately volatile siderofilic and chalcophilic elements and Rb, Cs, Ga were drained away by a partial melt.

The aubrite parent body was formed under heavily reducing condition, so that all iron was segregated into core and the crust is composed of nearly pure enstatite. Nysa and Hertha have been proposed to be asteroids with such materials (6).

I thank National Inst. of Polar Res. and the Meteorite Working Group for meteorite samples.

References: (1) Stolper E., Geochim. Cosmochim. Acta, 41, 587, 1977. (2) Takeda H., Icarus, 40, 455, 1979. (3) Ikeda Y. and Takeda H., Proc. Lunar Planet. Sci. Conf. 15th, in J. Geophys. Res., 90, C649, 1985. (4) Warren P. H., Geochim. Cosmochim. Acta, 49, 577-586, 1985. (5) Berkley J. L. et al., Geochim. Cosmochim. Acta, 44, 1579, 1980. (6) Zellner B. et al., Geochim. Cosmochim. Acta, 41, 1759-1767, 1977.

DEVIATIONS OF GARNETS FROM CUBIC SYMMETRY

TAKÉUCHI, Y., College of Humanities and Sciences, Nihon University, 3-25-40 Sakurajosui, Tokyo 156, Japan

Cases have been covered of the structural distortions of garnet $A_3B_2[XO_4]_3$, Ia3d, resulting from ordering of cations at the octahedral sites. The garnet structure type may be looked upon as consisting of a packing of columns [1] (or rods [2]), parallel to <111>, which are composed of alternating octahedra about the B cations and polyhedral voids, the latter being surrounded by triplets of dodecahedra about the A cations. Non-cubic derivatives of the garnet structure type may then be well represented and studied in terms of such a column-packing model. They may be classified into two categories.

Those of the first category have structures consisting of such a column in which two kinds of atoms, one is divalent and the other quadrivalent, take a perfect ordered arrangement at the octahedral sites, yielding a tetragonal symmetry $I4_1/a$ (Fig. 1, viewed down [111], the ordering in each column being shown by the difference in shading). Examples of silicates are high-pressure phases of $Mn_3(Mn, Si)[SiO_4]_3$, or $MnSiO_3$, (c/a = 0.9883)[3], and $MgSiO_3$ (c/a = 0.9935) [4]. Distortions from the cubic symmetry may readily be identified by powder diffraction.

Those of the second category are represented by non-cubic grandite garnet. The basic structure type consists of two kinds of columns: one is relatively rich in Fe^{3+} and the other in Al.

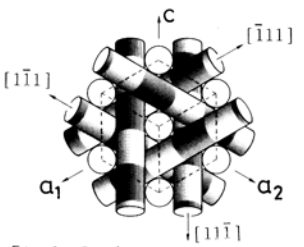

Fig.1. $I4_1/a$.

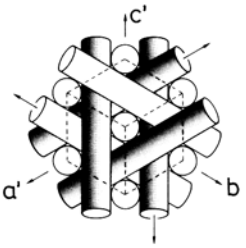

Fig.2. Fddd.

Such a partial ordering distorts the cubic structure to orthorhombic with symmetry Fddd. The pseudocubic cell of this type, having the orthorhombic cell edge a, b, c, is shown in Fig. 2 (viewed down [111]) and Fig. 3 (down b), where **a'**=(**a**+**c**)/2 and **c'**=(-**a**+**c**)/2 and Al-rich columns are shaded. Maximum possible deviation of the angle between a' and c' from 90° is predicted to be about 0.8% for $Gr_{60}An_{40}$ at which maximum birefringence was observed [5]. Extra reflections, which are consistent with Fddd but in general undetectable, have been observed for a garnet from a specific locality [6]. If the octahedral cations are ordered in each kind of column, the structure may further be distorted to I2/c or I$\bar{1}$ depending upon mode of the ordering. Other features of non-cubic grandite include: (i) They may be synthesized at 500°C under 1 kbar [7]. (ii) Fe^{3+}/Al ordering takes place during crystal growth [8]. (iii) Iridescent varieties show a peculiar lamellar texture consisting of isotropic and anisotropic parts [9, 10, 11]; iridescence arises only in the latter.

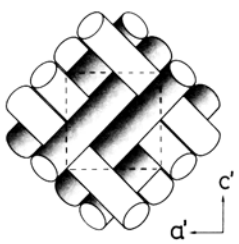

Fig.3. Fddd.

[1] Takéuchi, Y., Haga, N., Umizu, S., Sato, G.: Z. Krist. 158, 53 (1982). [2] O'Keeffe, M., Anderson, S.: Acta Cryst. A33, 914 (1977). [3] Fujino, K., Momoi, H., Sawamoto, H., Kumazawa, M.: Am. Mineral. (1986)(in press). [4] Sawamoto, H., Kanzaki, M.: Seismological Soc. Jpn Annual Meeting, Abstr. B49 (1984). [5] Mariko, T., Nagai, Y.: Mineral. J.: 4, 181 (1980). [6] Hirai, H., Nakazawa, H.: Am. Mineral. (1986) (in press). [7] Mariko, T., Shoji, T., Kinouchi, S.: Bull. Sci. Engi. Res. Lab., Waseda Univ. 106, 1, (1984). [8] Akizuki, M.: Am. Mineral. 69, 328 (1984). [9] Hirai, H., Nakazawa, H.: Phys. Chem. Minerals, 8, 25 (1982). [10] Hirai, H., Sueno, S., Nakazawa, H.: Am. Mineral. 67, 1242 (1982). [11] Akizuki, M.: Am. Mineral. 69, 896 (1984).

ON THE MANGANESE MINERAL COMPOSITION OF TYPICAL SEDIMENTARY MANGANESE CARBONATE ORE IN CHINA

Tang Xing Ming and Zhan Zhe Ming, Changsha Research Institute of Mining and Metallurgy, P.O. Box 67, Changsha, Hunan, China

Manganese carbonate ores of sedimentary origin are very plentiful in China. Notable characteristics of this kind ore include the following: 1) intimate interlocking of manganese carbonate minerals with different compositions. 2) the size of constituent grains is very small, generally from 5 to 35 microns. The samples we studied are the manganese ores from three typical Chinese sedimentary deposits of different minerogenetic epochs: Taojiang manganese Mine (Middle Ordovician), Xiangtan Manganese Mine (Lower Sinian) and Zunyi Manganese Mine (Upper Permian). Using x-ray spectroscopy has furthered research into the compositions of manganese minerals. Measurement of the elemental composition was completed entirely on a JSM-35$_C$ equipped with an EDAX 9100 using the following settings: 1) exciting voltage of 20 KV 2) sample current of 2×10^{-9}A 3) 3000-5000 CPS 4) analysis time of 180 seconds 5) manual substraction of background 6) quantitative analysis with all standards 7) standards: calcium-vilnite: manganese, iron, magnesium-pure metals. After selecting some typically determined data and checked them with WDS method, the margin of discrepancy did not, in most cases, exceed 5%. Because of this, we believe that the results achieved completely satisfy the requirements for investigating the composition of manganese carbonate mineral and its solid solution relationships. The samples (polished sections) were moved at pre-determined intervals in perpendicular direction while spectrographic measurements were performed. With each sample producing 35-40 data points, the 30 polished sections produced a total of more than 1000 points. To ensure that the determined micro areas (points) originated within single crystals of minerals during the measuremints, we conducted backscatter image to check, and using the energy dispersive spectrum plot avoided the interference of any noncarbonate minerals. Data which were obtained showed that the compositions approach the ternary system of $CaCO_3$-$MgCO_3$-$MnCO_3$. For this reason, we present the data in a triangular composition chart (Fig.1). The chart shows that the content of $MnCO_3$ in manganese carbonate minerals, in the range

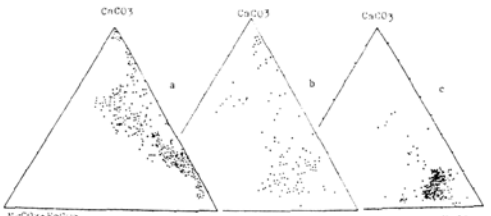

Fig.1 Compositions of manganese carbonate minerals (small amount of $FeCO_3$ is combined with $MgCO_3$ in this plot) a. Taojiang Mine b. Xiangtan Mine c. Zunyi Mine

of 0%-90%, is completly continuous. Approximately 40% of the data points are located in the 50%-80% range for $MnCO_3$.

The laboratory discoveries of J.R.Goldsmith et al (1,2) concerning subsolid relations in the systems $CaCO_3$-$MnCO_3$ and $CaCO_3$-$MgCO_3$-$MnCO_3$, state that below 550°C, the solid solution series is not continuous between $CaCO_3$ and $MnCO_3$, that a solubility gap is observed in the Mn-rich side of the series, and that when Mg is present, the range of this solubility gap is increased slightly. On the basis of this experimental result, and the confirmation of kutnohorite as an ordered or partially ordered compound of the dolomite group, it has been thought that naturally occurring minerals do not exist in the isomorphous series between 50 and 80 mol per cent $MnCO_3$, though if they did, it would be because they had crystallyzed at above about 550 C and they could exist metastably as a disordered solid solution (3). Because of this, some have estimated minerogenetic temperatures for a deposit on the basis of the copmositional characteristics of coexisting Ca-Mn carbonates, calling the process "carbonate thermometry" (4).

The data presented by this paper do not reveal this kind of solubility gap. It had been established that the minerogenetic temperatures of the three typical chinese sedimentary deposits were very far below 550°C. What this proves without a doubt, therefore, is that a complete solid solution series can be formed between calcite and rhodochrosite under lower minerogenetic temperatures conditions in nature. The same is true when the considerable substitution of magnesium in the series exists.

ON A NEW ULTRAMICRO TEXTURE FOUND IN THE WALL GRANITE OF THE GRANITIC PEGMATITE FROM HANAZONO QUARRY, KOSEICHO, SHIGA PREFECTURE, JAPAN

TATEKAWA,M., Dept. of Liter., Bukkyo University, Kyoto, 604, Japan.

The texture of granite and granitic pegmatite is very important to study the origine of them. one new ultramicro texture contributing to that study was found in the wall granite of the granitic pegmatite from Hanazono quarry.

Fig. 1 shows that texture electronmicroscopically found in the macroperthite(4 / 5 / 8 mm in size and subhedral). In this figure, we can see a stripe in the sodium rich phase of the perthite, which is ultramicroscopecally twined after albite law. Judging from the limitted electron diffraction pattern on the stripe,the stripe is the sodium rich plagioclase twined periodically after albite law. The width of each individual of the periodic twinningis about 5 nm which corresponds about four times of the b-axis length in the unit cell of a albite. Therefore each individual is consist of four unit cells along the direction of b-axis. And we can see the imperfection in the twined plagioclase similar to the edge dislocation in a single crystal, as shown in fig. 2.

The new texture mentioned above might be produced by the process that a water-rich fluid derived from magma during magamtic fractuation resolved the part of the preexisting alkali-feldspar crystals and then the resulting fluid rich in Al constituent crystallized secondarily the sodium rich plagioclase which is periodically twined after albite law under strain condition.

Fig. 1

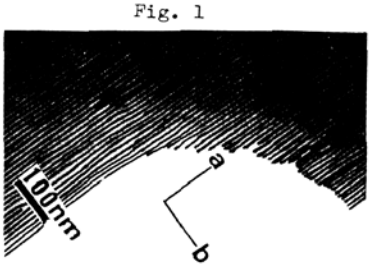

Fig. 2

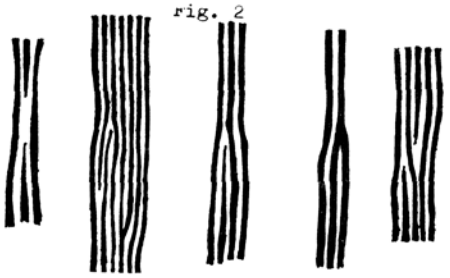

COMPOSITIONAL VARIATIONS AND REFLECTANCE OF THE PLATINUM GROUP MINERALS

TARKIAN, M., Institute of Mineralogy and Petrology,
Hamburg University, Federal Republic of Germany

Microprobe studies during the past twenty years have revealed the complexity of the platinum group minerals (PGM). Over 80 named PGM are now well known.Most of the available data have been compiled by Cabri (1981). For the optical diagnosis of the PGM a R-VHN key diagram has been developed (Tarkian & Bernhardt, 1984). In our Hamburg laboratory 35 different PGM have been optically and chemically investigated from Driekop, Merensky Reef, Stillwater, Shetland and from placers from Japan, Borneo and the Urals. At present over 150 reflectance spectra of these PGM are available in our data bank.

The same types of PGM occur in many of the deposits studied. But the chemical compositions of the minerals show variations between deposits dependant on their different ore genesis. Some of PGM form solid-solution series, whereas in others there may be considerable substitution between elements. Some examples of recently investigated PGE-alloys, -sulfides, sulfarsenides and tellurides are summarized:

1. Os-Ir-Ru alloys from placers in Borneo, Japan and the Urals show significantly different compositions. Those from the Urals are mostly Ru-rich, while those from Borneo almost only contain Os-Ir alloys with a range of different Os/Ir ratios. On the basis of six reflectance spectra increasing reflectance with increasing Ir content is illustrated. Moreover natve Os, iridosmine and osmiridium have different shaped reflectance curves with distinct divergence between 560 and 680 nm.

2. Pt-Fe alloys are common PGM in most of the deposits. Their compositions range between Pt(Fe), Pt3Fe and PtFe. Six reflectance spectra suggest a distinct decraese of reflectance with increasing Fe content without affecting the shape of the curves (Tarkian, 1981).

3. Solid-solution series (Pd,Pt)S:Analyses of the members of the (Pd,Pt)S from the Merensky Reef and Stillwater plotted in the PtS-PdS-NiS system show that cooperite and Pt-rich braggite are common in the Merensky Reef; vysotskite is lacking. In contrast vysotskite and Pd-rich braggite are the most abundant PGE sulfides in Stillwater. Their widespread occurrence together with Pd tellurides, -arsenides, antimonides and Pd-bearing pentlandite document the very high Pd:Pt ratio of about 3.5:1 in bulk analyses compared with those of 0.4:1 in the Merensky Reef. Reflectance spectra measured on Pd-free cooperite, Pt-free vysotskite and on braggite of intermediate composition indicate similar shaped curves for the latter two and a distinct divergence from the cooperite curve. Moreover the reflectance of vysotskite is about 2% higher than braggite of intermediate composition.

4. Ru-Os-Ir sulfides: No mineral corresponding to IrS2 has so far been discovered. Chemical data available for laurite and erlichmanite suggest substitution of Os for Ru which appears to be continuous between Os-free RuS2 and the intermediate member (Ru.5 Os.5)S2, whereas substitution of Ir does not exceed 10% of Ru. Reflectance spectra measured on laurite of ideal composition, RuS2, Os-bearing and Os-rich laurite are not affected by compositional variations.

5. Rh-Ir-Pt sulfarsenides: Analysis of the hollingworthite-irarsite series from the shetland ophiolites (Tarkian & Prichard, 1986) reveals for the first time the ideal end-member IrAsS and RhAsS and intermediate members free of all other PGE. It is very likely that a complete isomorphous solid-solution series (Ir,Rh)AsS exists. Their reflectance continuously increases with increasing Rh content. For the first time also a Rh-poor variety of platarsite was discovered in the Merensky Reef (Tarkian, 1986). In contrast to the platarsite from the type locality (Cabri et al., 1977) it is remarkably Ir-rich(Ir:15-18 wt.%) and contains only minor Rh (Ir>>Rh; Ir≥ Ru). Consequently this platarsite belongs to the PtAsS-IrAsS-RhAsS system, in which the ideal end-member PtAsS has so far not been found. Considering that Rh need not necessarily be a major PGE in platarsite and that there are now available new compositions in the hollingworthite-irarsite series, a new definition of these minerals is necessary.

6. Pd-Pt tellurides: Spectral reflectance curves of kotulskite, merenskyite and monchiite with different chemical composition have been checked for correlation. Bi-poor kotulskite has significantly higher reflectance than the Bi-rich one. In this context it is worth mentioning the fist discovery of a mineral with the composition (Pd.99 Pt.04)Σ1.03 (Bi.85 Te.12)Σ0.97 from the Merensky Reef (Tarkian, 1986). X-ray data will decide if it is Pb-free polarite or sobolevskite. However, its reflectance is distinctly lower than that of Bi-rich kotulskite. Consequently the reflectance of the Pt-free minerals in the Pd-Bi-Te system continuously decreases with incraesing Bi content. Merenskyite behaves in the same way. Additionally the substitution of Pt for Pd in merenskyite affects its reflectance. This is also the case for monchiite by substitution of Pd and Bi for Pt and Te, respectively. High Pd together with high Bi contents affect the curve shape and bireflection, but at present no useful correlation is possible.

References

Cabri, L.J. et al. (1977): Can.Mineral., 15, 385-388.
Cabri, L.J. (1981): CIM Special Colume 23, 267 pp.
Tarkian, M. (1981): N. Jb. Miner. Abh. 142, 124-138.
Tarkian, M. and Bernhardt, H.J. (1984): TMPM 33, 121-129
Tarkian, M. and Prichard, H. (1986): Submitted Miner. Dep.
Tarkian, M. (in preparation): Mineral. Deposita.

ORIGIN OF SUBDUCTION ZONE MAGMAS: EXPERIMENTAL APPROACH

TATSUMI,Y., Dept. of Geology & Mineralogy, Kyoto University, Kyoto 606, Japan; KUSHIRO,I., Geological Inst., Univ. of Tokyo, Tokyo 113, Japan

At least four types of primary magmas are produced in the mantle wedge in subduction zones: high-magnesian andesite (HMA), olivine tholeiite (OTH), high-alumina basalt (HAB), and alkali olivine basalt (AOB). P-T-H_2O conditions of segregation of those magmas and role of the subducted slab and the mantle wedge are highlighted on the basis of recent experimental data.

Conditions of Magma Segregation: Melting experiments on natural and synthetic compositions of the above four types of magmas suggest the following points;(1) HMA magmas are formed at relatively shallow levels (near the crust-mantle boundary) under H_2O-undersaturated conditions, (2)opx-HMA including boninite is generated by higher degree of partial melting than cpx-HMA, (3)three types of basalt magmas are segregated from mantle sources at nearly constant temperatures (1300°C) and at different depths (OTH<HAB<AOB) with different degrees of partial melting (OTH>HAB>AOB), and (4) the high temperature conditions would be attained in the diapirs which ascend from the hot (>1400°C), less dense zone in the mantle wedge.

Role of the Slab: The dehydration of subducted oceanic crust is not a direct trigger of production of initial magmas in the mantle wedge; the slab can supply H_2O only beneath the fore-arc region. The slab-derived fluid phase is more enriched in incompatible elements with larger ionic radii, and it migrates into the mantle wedge to form amphibole peridotite (the "island-arc magma (IAM) source") which determines the geochemical characteristics of subduction zone magmas.

Formation of the Volcanic Front: The "IAM source" migrates down-dip above the slab by the induced convection in the mantle wedge; amphibole in the peridotite source is decomposed at around 30 kbar. The within-wedge dehydration of amphibole causes partial melting of wedge peridotite at shallower levels to produce initial magmas for volcanic rocks on the volcanic front.

Origin of Lateral Variation: The across-arc lateral variation of isotope and trace element ratios in arc magmas are caused by the difference in degree of partial melting and their source compositions formed through the process of along-slab migration; the "island-arc source" is mixed with "non-polluted" peridotite in the mantle wedge which would have compositions similar to the "MORB source"; the ratio of "IAM source" and "MORB source" decreases toward the back-arc side in the source of arc magmas.

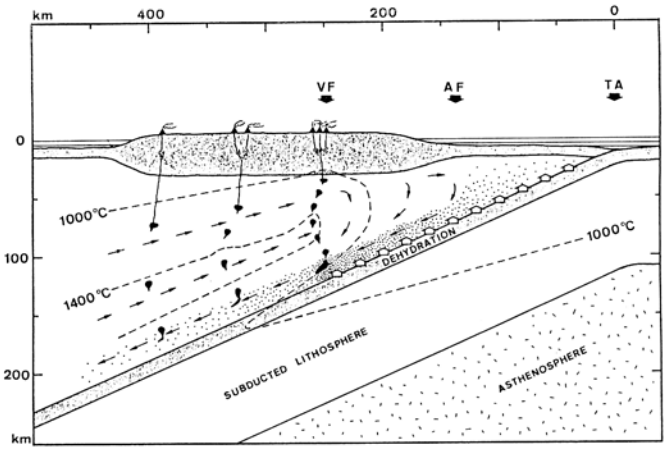

Plausible cross-section of a subduction zone

ALUMINUM IN ORTHOPYROXENES: ITS ORDERING IN NATURAL AND HEATED CRYSTALS

TAZZOLI, V. and DOMENEGHETTI, M.C., C.N.R. Centro di Studio per la Cristallografia Strutturale - Dipartimento di Scienze della Terra, Università di Pavia, Via Bassi 4, 27100 Pavia, Italy.

X-ray single crystal diffraction data of natural and heated Al-rich orthopyroxenes have been used to follow the structural changes induced by the substitution $Si + R^{2+} = Al^{IV} + R^{3+}$.

The samples examined come from high-grade metamorphic basic rocks and have already been studied by Mössbauer spectroscopy (Seifert, 1983). In this series the Al^{IV} content ranges from 0.05 to 0.20 a.p.f.u. and the $Fe^{2+}/Fe^{2+}+Mg$ ratio from 0.37 to 0.50. For each sample the crystal-chemical formula was deduced from structure refinement and microprobe analysis, carried out on the same crystal.

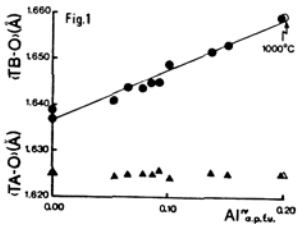

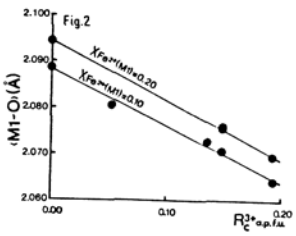

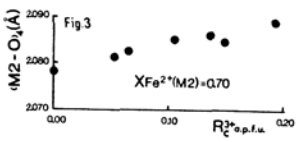

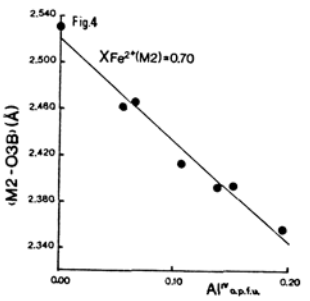

The main results, which fully agree with previous observations (Domeneghetti et al., 1985), may be summarized as follows:

i) Tetrahedra. The mean TB-O distance increases linearly with Al^{IV} content, whereas the mean TA-O distance remains unchanged (Fig. 1); both mean distances are not affected by the $Fe^{2+}/Fe^{2+}+Mg$ ratio of the sample. Al^{IV} is fully ordered at the TB site also in samples equilibrated at 1000°C by heating experiments. The amount of Al^{IV} may be deduced from the equation:

$$Al^{IV} = 9.044\langle TB\text{-}O\rangle - 14.801$$

ii) M1 and M2 polyhedra. In order to compare samples with different amounts of trivalent cations (Al^{3+},Fe^{3+}) in the bulk composition but with the same Fe^{2+} content in M1 or in M2 site, structure refinements have been carried out both in natural and in heated (700°C) crystals. For a given amount of Fe^{2+} in the M1 site, the mean M1-O distance shows a fairly linear negative correlation with R_c^{3+} (Fig. 2, $R_c^{3+} = Al^{VI} + c\ Fe^{3+}$ where $c = \langle Al^{VI}\text{-}O\rangle / \langle Fe^{3+}\text{-}O\rangle = 0.95$). The complete ordering of trivalent cations at M1, which is maintained also in samples heated at 1000°C, is supported by the analysis of the M2 polyhedron. For a given amount of Fe^{2+} in M2, the mean of the four M2-O shortest bond lengths ($\langle M2\text{-}O\rangle_4$ in Fig. 3) does not decrease but actually increases with R_c^{3+} ; therefore the contraction of the mean M2-O distance is only due to the relevant shortening of the M2-O3B bond length (Fig. 4), induced by Al^{IV} entering the TB site.

References

SEIFERT, F. (1983). Mössbauer line broadening in aluminous orthopyroxenes: evidence for next nearest neighbors interactions and short-range order. Neues Jahrbuch Miner. Abh., 148, 2, 141-162.

DOMENEGHETTI, M.C., MOLIN, G.M. and TAZZOLI, V. (1985) Crystal-chemical implications of the Mg^{2+}-Fe^{2+} distribution in orthopyroxenes. Am. Mineral., 70, 987-995.

FELDSPAR PHENOCRYSTS IN GRANITIC ROCKS:A TEXTURAL REVIEW.

THELIN Ph.,Inst.de Minéralogie, Collège Propédeutique University of Lausanne,1015 Dorigny,Switzerland.

It is generally considered that the formation of alkali feldspar megacrysts in granitoids is the product of three processes which,altough clearly distinct,are in many case complementary,and even successive:

1)Early crystallization(orthomagmatic) in a melt(about 650-900°C,depending on X_{H2O}) leading to the genesis of macro-phenocrysts.

2)Late-magmatic crystallization,under supercritical conditions,or even deuteric,with important marginal autometasomatic growth,in a subsolidus environment strongly impregnated with interstitial fluids (at about 450-500°C). This may lead to the growth of a number of small early crystals of alkali feldspar,which coalesce,recrystallize and grow in the form of an apparently single idiomorphic endoblast,which may itself be formed of small sub-grains.

3)Metasomatic or blastic growth at a post-magmatic stage through the hydrothermal percolation of alkaline solutions.

The three processes can,at a certain level of analysis,give rise to textural convergence and therefore to controversy stemming from this ambiguity. Certain considerations may clarify the problem:

a)Experimental data(Swanson,1977;Chesney,1981;Winkler & Schultes,1982) on growth simulation and on fusion in granitic system have established a fundamental fact,i.e. alkali feldspar megacrysts grow best at a late stage,near the solidus,or even below the solidus if an important part of the rock (about 25%) is finely impregnated with fluids. Consequently,a very considerable portion of a porphyric granite (about 40% in modal terms) may crystallize in a very small temperature interval, of the order of 20-40°C. This is due to the fact that alkali feldspars,as opposed to quartz and plagioclase,is characterized in the presence of H2O,by a high rate of crystallization growth and a very small rate of nucleation.

b)Geochemical considerations(Mehnert & Büsch,1981; Thélin,1983;Schüler,1983) on the distribution of Ba and quasi point isotopic Rb-Sr determinations in K-mega feldspars(Albtal Granite,W-Germany) have demonstrated that the development of such a porphyric structure is a continuous process,in several stages, from the orthomagmatic to the subsolidus-strongly dependant on local conditions(ΔT°,Δviscosity,state of magmatic turbulence,rate of injection of supercritical fluids,etc.)

c)Particular emphasis is laid on textural considerations,which occasionally have not been given enough attention,as they are descriptive and not easy quantifiable,in particular concerning the refractory inclusions(quartz,plagioclase,biotite) of the alkali feldspar megacryst. Analysis of their frequency,distribution,orientation,morphology,mode of assemblage,composition and alteration allows their use as significant markers of the multi-stage growth of their host mineral. Attention will also be given to criteria indicating presence or absence of plagioclase synneusis on one hand,and to assess the petrogenetic meaning of so-called mantled feldspars on the other,leading to a better understanding of the contrasted morphologies(rectangular or oval) of the megafeldspars in granites.

Chesney,M(1981):Phd Thesis,Univ.Paul Sabatier,Toulouse,France.
Mehnert,K.R.& Büsch,W(1981):Neu.Jb.Min.Abh.140/3
Schüler,Ch.(1983):Phd Thesis,no.7356,ETH,Zürich
Swanson,S(1977):Am.Mineral.64,514-518.
Thélin,Ph.(1983):Phd Thesis.Univ.Lausanne
Winkler,H.G.F.& Schultes,H.(1982):Neu.Jb.Min.Abh. 15,558-564.

GENESIS AND FORMATION OF OCEANIC CRUST: EVIDENCE FROM THE CYPRUS CRUSTAL STUDY PROJECT DRILLING IN THE PLUTONIC SEQUENCES OF THE TROODOS OPHIOLITE

THY, P.[1,2] and MOORES, E.M.[1], 1. Department of Geology, University of California, Davis, CA 95616, U.S.A. 2. Department of Geology, University of Aarhus, DK-8000 Aarhus C, Denmark.

The CY-4 drillhole of the Cyprus Crustal Study Project sampled the lower sheeted dike complex, gabbros and ultramafic cumulates of the Troodos ophiolite. Major petrographical and compositional breaks occur in the igneous stratigraphy at approximately 600, 1300 and 1750 meters depth in the core. The lowermost 514 meters (1750-2264) are coarse grained ultramafic cumulates containing augite, enstatite, olivine and interstitial plagioclase. From 1300 to 1750 the rocks are coarse grained gabbroic cumulates with augite, enstatite, plagioclase and from 1600 meters also olivine. From 1300 to 600 meters the rocks are medium grained olivine-free, two-pyroxene gabbros. Fe-Ti oxides appear as cumulus phases at 1200-1220 meters depth. The core above 1265 meters contains two petrographically distinct components. The most abundant is a medium grained gabbroic rock. The less abundant is fine grained, granular two-pyroxene dikes containing augite, orthopyroxene, plagioclase, Fe-Ti oxides and sulphides. The amount of dikes increases upwards and above 600 meters the Fe-Ti oxide-free gabbroic rocks disappear.

The petrography can be linked to the mineral chemistry. The lower gabbroic to ultramafic cumulates contain anorthitic (An>95) plagioclase and the pyroxenes are characterized by very low Ti and high Cr. The dike rocks contain labradoritic to bytownitic plagioclases (An60-80) and the pyroxenes have relatively higher Ti and low Cr. The upper gabbroic cumulates contain anorthitic plagioclases (An86-95) and pyroxenes with Ti-contents comparable to that found in the dike rocks but with higher Mg#s. The cumulates show a complex chemical pattern with in general decreasing Fo, An, and Mg#s of cumulus phases going upwards in the core. A recurrence to more primitive compositions occurs at 1500. Above 1300 the cumulates show an intricate patttern of complex phase and cryptic layering indicative of crystal fractionation and magma chamber replenishments.

The plagioclase of the gabbros and ultramafic cumulates have unusually high-An content, unknown or rare from present day oceanic spreading centers. Numerical and experimental simulation of the expected one atmosphere crystallization show that the Troodos plagioclases cannot be reproduced from known spreading or subduction related glasses. Mineralogical evidence indicate that the extrusives and the cumulate sequences are genetically related. Glasses from the extrusives, nevertheless, also fails to reproduce the mineral compositions. Attempts to model high PH2O crystallization produced results more consistent with those observed in the cumulates.

The upper pillow lavas of the extrusives contain high-Si and low-Ti basaltic andesite glasses bearing olivine and diopside phenocrysts chemically comparable to cumulus phases in the lower gabbros and ultramafics. The lower pillow lavas range from andesites to rhyodacites and compare mineralogically with the main part of the sheeted dike complex. This suggest that the upper level gabbros of the plutonic sequences are not represented among the extrusives. These may constitute a basaltic parent to the sheeted dike complex.

The petrology and chemistry of the Troodos suggest that the ophiolite formed in an early island arc setting. On the other hand, the extensive sheeted dike complex and graben structures points to a spreading related origin. It may be significant that spreading related oceanic lavas occur in major ocean basins which show mineralogical and chemical patterns comparable to the Troodos upper pillow lavas. The andesitic sheeted dike complex and the lower extrusives have, however, no known modern analog in major spreading or back-arc basins. The implications are that either 1) significant extensional tectonics may be important during the early formation of an arc or 2) silicic magmatism may play a significant role during incipient rifting and formation of spreading basins. The apparent conflict between a spreading related origin and the arc petrology for the Troodos ophiolite may be an artifact of lack of detailed studies of the geology and chemistry of early oceanic rifting environments.

A MINERALOGICAL COMPARISON OF FOUR HYDRATED INTERPLANETARY DUST PARTICLES

TOMEOKA, K. and BUSECK, P.R., Departments of Geology and Chemistry, Arizona State University, Tempe, Arizona 85287, USA

Interplanetary dust particles (IDP's) are unique forms of extraterrestrial material that contain records of the early solar system and possibly even of events that predate it. A significant fraction of IDP's contain hydrated silicates. Of particular interest are the mineralogical relationships between hydrated IDP's and carbonaceous chondrite meteorites. We present here a summary of transmission electron microscope studies of four IDP's (NASA nos. u21-M2-1, r21-M3-5A, r21-M1-9A1, r21-M1-9A2) that belong to the "hydrated silicate" class.

All of these IDP's mainly consist of phyllosilicates, and these contain major Fe and Mg and minor Al and have interlayer spacings between 10 and 12 Å. They occur in fluffy aggregates of poorly crystallized, fine fibers. The phyllosilicates are probably Fe-, Mg-rich smectites or micas (smectite/mica). The Fe/Mg ratios are relatively consistent within individual particles, but they vary considerably among particles. When the compositions are plotted on an Fe/Si vs. Mg/Si diagram, they scatter along a straight line connecting nontronite and saponite, suggesting the phyllosilicates are intermediate between nontronite and saponite. IDP r21-M3-5A contains phyllosilicate having unusually high Fe contents (Fe/Si=0.79, Mg/Si=0.21) and so may differ from smectite/mica.

Mg-Fe carbonates, primarily breunnerite and magnesian siderite, occur in all four IDP's; they are not known from other IDP's. Carbonates are particularly abundant in r21-M1-9A1 and r21-M1-9A2, where they occur as rhombohedral and rounded crystals (from 100 to 3000 Å in diameter). They show a wide range of Mg and Fe contents (from 20 to 90 mole % $MgCO_3$) and contain small amounts of Ca and Mn. Similarities between infrared spectra of some dust-rich interstellar regions and a carbonate-rich IDP suggest that carbonate may be an interstellar constituent (Sandford and Walker, 1985).

Rounded and subhedral grains (~0.1 μm in diameter) of pyrrhotite and pentlandite are abundant throughout the particles. In u21-M2-1, we identified a low-Ni pentlandite (<3 at. % Ni) that is unknown from terrestrial and meteoritic samples, although it has been synthesized.

Forsterite and enstatite are ubiquitous in r21-M3-5A, while they are rare in other IDP's. They occur as platelets (0.1-3 μm in diameter) and spherical grains (<0.1 μm). Enstatite platelets commonly display a disordered stacking of clino- and ortho-enstatite, resembling those in non-hydrated IDP's. Fassaite, $[Ca_{0.7}Mg_{0.8}Al_{0.4}](Si_{1.8}Al_{0.2})O_6$, occurs in r21-M3-5A and is of special interest because it is common in and thus reminiscent of the refractory Ca-, Al-rich inclusions in the carbonaceous chondrites.

The phyllosilicates in the CI and CM carbonaceous chondrite meteorites are mainly serpentines. Smectite and mica occur in some CV meteorites, but they differ chemically from the IDP smectite/mica in that they are rich in Al and alkalis and depleted in Fe. The mineralogy of the characterized hydrated IDP's is considerably different in detail from the carbonaceous chondrites, suggesting they may have different formation histories or environments. Furthermore, serpentine and a variety of other phyllosilicates have been reported from other IDP's. It seems evident that there are mineralogically distinct particles in the hydrated class.

REACTION AND DIGESTION OF XENOLITHS IN THE LIGHT OF MELTING/DISSOLUTION EXPERIMENTS

TSUCHIYAMA,A., Dept. of Geology and Mineralogy, Kyoto University, Sakyo-ku, Kyoto 606, JAPAN

Reaction and digestion of xenoliths in magmas are discussed in the light of recent experimental works on melting and dissolution kinetics [1-8]. Two types of processes are taken into consideration in this paper; (case-1) partial melting of xenoliths above the solidus temperatures, and (case-2) dissolution of xenoliths into host magmas above the liquidus temperatures.

If minerals forming solid solutions are included in xenoliths, specific textures composed of fine mixtures of minerals and melts (e.g., dusty zone, spongy texture, etc.) can be formed due to mineral-melt reaction. This reaction called "partial dissolution" [1] takes place when the mineral is less refractory than the crystal in equilibrium with the melt [1,2]. Case-1. If xenoliths receive partial melting, partial dissolution should occur between minerals and partial melts [3]. Examples are spongy crystals of augite usually found in ultramafic xenoliths. Case-2. Reaction of minerals in xenoliths with host magmas is expected to take place only when the minerals are less refractory than the equilibrium minerals. Dusty crystals of plagioclase, orthoclase and pyroxene are formed by partial dissolution [1]. (It is noted that the same textures are also formed due to this reaction during mixing of magmas [1,2].)

The rates of xenolith digestion in magmas are calculated for a simple system (diopside-plagioclase). The calculations are made for the two cases-1 and -2 independently to simplify the problem although the processes can take place simultaneously. In the case-1 (partial melting), square-root time kinetics are considered [3,4]. In the case-2 (dissolution), linear kinetics and square-root kinetics are taken into consideration for simple dissolution of end members [5-8,9] and for partial dissolution [1], respectively. Results are follows; (1) partial melting is important as well as dissolution for the digestion, (2) the xenolith is easily digested into the magma within a week to 10^3 years depending on temperature, and (3) diffusion of elements in partial melt of the xenolith toward the host magma is much slower than the digestion process (in another word, contamination due to the diffusion can be ignored).

The above results strongly suggest that many xenoliths are easily digested into basaltic magmas for a geologically long period of time, and many xenoliths found in basaltic rocks could be incorporated into the basalts just prior to eruptions. The results may also suggest that basalts are easily contaminated by wall rocks if magma reservoirs are stable for a long period.

REFERENCES: [1]Tsuchiyama,A. (1985) Contrib. Mineral. Petrol., 89, 1-16. [2]Lofgren,G.E. & P.N.Norris (1981) G.S.A. Abstr. [3]Tsuchiyama,A. (1985) Contrib. Mineral. Petrol., 91, 12-23. [4]Marvin,U.B. & D.Walker (1985) Proc. Lunar Planet. Sci. Conf. 15th, C421-429. [5]Watson,E.B. (1982) Contrib. Mineral. Petrol., 80, 73-87. [6]Harrison,T.M. & E.B.Watson (1983) Contrib. Mineral. Petrol., 84, 66-72. [7]Kuo,L.C. & R.J.Kirkpatrick (1985) Am. J. Sci., 285, 51-90. [8]Donaldson,C.H. (1984) in "Progress in Experimental Petrology" 6th. 174-175. N.E.R.C. [9]Cooper,A.R.Jr. (1962) in "Advances in Glass Technology", 6, I.C.G. Am. Ceram. Soc., 217-229.

OBSERVATION OF POSITIONAL SHIFTS AMONG TRANSITION-METAL ATOMS IN ORTHOPYROXENE BY SYNCHROTRON X-RAY RESONANT SCATTERING

TSUKIMURA, Katsuhiro, Geological Survey of Japan, Yatabe, Ibaraki 305, Japan; SASAKI, Satoshi, The Photon Factory, National Laboratory for High-Energy Physics, Oho-machi, Ibaraki 305, Japan; OHASHI, Haruo, National Institute for Research in Inorganic Materials, Sakura-mura, Ibaraki 305, Japan

X-ray crystallographic data for $(Co,Ni,Zn)SiO_3$ orthopyroxene (Co:Ni:Zn = 1:1:1) were collected on the 0.01 Å longer wavelength sides of the K-absorption edges of Co, Ni, and Zn atoms, using synchrotron radiation from the Photon Factory (BL10A station). By calculating Shell Structure Factor on the resonant scattering, positional shifts and asphericity in the distribution were detected among transition-metal atoms occupying crystallographically-unique sites.

The use of synchrotron radiation on the resonant scattering effect (or anomalous dispersion) is of great advantage to determine the degree of ordering between atoms of closely similar atomic number in crystals and to detect the positional shift of a particular atom from the averaged atomic position when several atoms overlappedly occupy an unique site.

The orthopyroxene has orthorhombic symmetry (Pbca) with cell dimensions a = 18.209(1), b = 8.915(1), and c = 5.2182(4) Å. The crystal structure of orthopyroxene has a pair of unique sites, M1 and M2, which are simultaneously occupied by Co, Ni, and Zn atoms.

We have determined the site-occupancy parameters as 0.53:0.20:0.27 (M1) and 0.14:0.46:0.39 (M2) in the order of Ni, Zn, and Co atoms. The triangle diagram in Fig. 1 shows that the difference between observed and calculated structure factors becomes the smallest at the intersection of two solid lines. Ni atoms prefer the smaller M1 sites, while Co atoms show strong preference for the smaller sites than do the Zn atoms, although the ionic radii for the two atoms are almost identical.

Atomic coordinates from the K-shell electrons belonging to an atom in the M1 and M2 sites can be obtained from Shell Structure Factors by means of the least-squares method. Because the positional shift on the ab plane in the M2 site is dominant, the distributions have been schematically drawn in Fig. 2. The Ni atoms in the M2 sites were found to have a deviation of 0.16 Å from the averaged position in the negative direction of the a axis. The second largest deviation is for the Zn atoms in the M1 sites, where they deviate by 0.1 Å in the positive a direction. Such atoms occupy the respective sites with the smallest contents. The maximum shifts of atomic coordinates of the Co, Ni, and Zn atoms are (0.08, 0.04, 0.03) and (0.17, 0.08, 0.03 Å) for the M1 and M2 sites, respectively. These characteristics are consistent with the crystal structure. Namely, the direction along the a axis may be the most flexible because it is perpendicular to the layers of MO_6 polyhedra. The metal-metal distances between the nearest two sites vary within 0.12 Å (0.4 %) when the constituent atoms are exchanged.

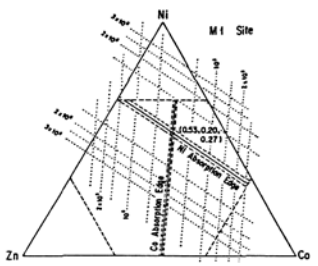

Fig. 1

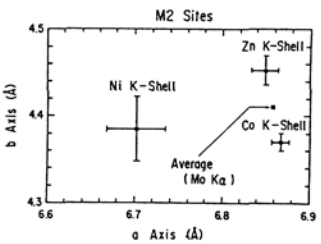

Fig. 2

THE USE OF ELECTRICAL MEASUREMENTS TO DETERMINE POINT DEFECTS AND THEIR BEHAVIOR

TULLER, Harry L., Crystal Physics and Optical Electronics Laboratory, Department of Materials Science and Engineering, Massachusetts Institute of Technology, Cambridge, Massachusetts 02139

The nature and concentration of charged defects in ionic solids are generally sensitive functions of crystal structure, temperature, atmosphere and purity, whereas carrier mobilities depend primarily on structure (atomic and electronic) and temperature. Since these factors are combined in the electrical conductivity, its measurement and interpretation can provide important insight into both the thermodynamic and kinetic factors characterizing defect generation and transport.

This presentation begins by summarizing the versatility of electrical conductivity and related techniques in probing the defect properties of solids, as well as some of the limitations. Both bulk and interfacial phenomena are examined. Next, examples are provided which illustrate how electrical measurements combined with a defect chemical approach can be utilized to extract specific thermodynamic and kinetic data such as defect formation and ionization energies, ion diffusivities, electron mobilities, and phase stability boundaries. Some of the materials systems to be considered include $Y_3Al_5O_{12}$, (Mn, Zn)Fe_2O_4, $SrTiO_3$, ZnO and others.

THE EFFECT OF MAJOR AND TRACE ELEMENT CHEMISTRY ON THE LUMINESCENCE SPECTRA OF THE SCHEELITE-POWELLITE SERIES

TYSON, R. M., HEMPHILL, W. R., and THEISEN, A. F., U.S. Geological Survey, Flagstaff, AZ 86001, U.S.A.

Using a fluorescence spectrometer, we analyzed 21 synthetic members and 85 natural samples in the scheelite-powellite series to characterize their luminescence and to determine if they could be excited by solar radiation. Previous investigations had used an excitation wavelength of 253.7 nm to produce a single emission peak which shifted regularly from 425 nm for pure scheelite to 530 nm for scheelite containing 10 mole percent $CaMoO_4$. From 10 to 100 mole percent $CaMoO_4$, the emission peak remained at 530 nm. The apparent shift of the emission peak was interpreted as resulting from the wavelength dependence on composition (See Shoji and Sasaki, 1978). We collected emission spectra from 410 to 830 nm for excitation wavelengths every 10 nm from 240 to 400 nm. The emission spectra produced by excitations at 240, 250, and 260 nm exhibit a shift of the emission peak similar to that observed by previous workers. However, at excitations from 280 to 320 nm, emission spectra for samples containing molybdenum exhibit a peak at 530 nm whose only response to an increase in molybdenum content is an increase in intensity. The same data were used to construct three-dimensional perspective plots of excitation, emission, and relative intensity that show two separate emission peaks, one at 425 nm and the other at 530 nm. Their maximum excitations are at 243 nm and 280 nm, respectively. The emission peak at 425 nm is seen only in those samples containing less than 10 mole percent $CaMoO_4$; the peak at 530 nm is seen in all samples containing molybdenum but is not present in pure scheelite. The two emission peaks seen in the perspective plots are characteristic of scheelite and powellite, respectively, and result from electronic transitions in the molecular orbitals of the anionic tungstate and molybdate complexes (Blasse, 1980). With the addition of $CaMoO_4$, the tungstate emission shows a marked decrease in intensity that is not proportional to the W:Mo ratio. One explanation for the apparently irregular behavior of the tungstate peak is that the excitation has been non-radiatively transferred from the higher energy tungstate to the lower energy molybdate. The energy cannot be transferred back to the tungstate and is trapped in the molybdate. With as little as 10 mole percent $CaMoO_4$ present, all excitation is transferred to the molybdate and only the luminescence characteristic of the molybdate (530 nm) is seen.

Our laboratory measurements of synthetic specimens indicate that scheelites containing at least 8 mole percent $CaMoO_4$ exhibit significant luminescence when excited at wavelengths greater than 300 nm. Such luminescence can result from solar excitation and should be detectable by the Fraunhofer line discriminator, a passive airborne instrument that measures solar stimulated luminescence at an optically isolated Fraunhofer line. Although 78 of the natural scheelites contain less than 8 mole percent $CaMoO_4$ and would not be expected to exhibit detectable levels of solar-stimulated luminescence, 43 of these specimens exhibit intensities above the predicted values and would be detectable with a FLD. Thirty-three of these same 43 exhibit sharp emission peaks (20 nm wide) which are narrower and have lower intensities than the tungstate and molybdate peaks. These sharp peaks are close to some Fraunhofer lines and are correlated to rare earth elements (REE). This suggests that the higher intensity of these 33 specimens is due to emission from REE replacing calcium in the scheelite structure. The higher intensity of the other 10 natural scheelites could result from non-stoichiometry (an excess of calcium), structural strains, or imperfections in the crystal lattice.

REFERENCES CITED

Blasse, G., 1980, The luminescence of closed-shell transition-metal complexes--New developments, in Luminescence and energy transfer, volume 42 of Structure and bonding: New York, Springer-Verlag, York, p. 1-42.

Shoji, T. and Sasaki, N., 1978, Fluorescent color and x-ray powder data of synthesized scheelite-powellite series as guides to determine its composition: Mining Geology, v. 28, p. 397-404.

ABOUT THE CORRELATIONS OF THE CONTENT OF THE ELEMENTS IN TETRAHEDRITE-TENNANTITE SERIES

TZEPIN A.I., IGEM AN SSSR, Starom.per. 35, 109017 Moskva, USSR; BRESKOVSKA V.V., Sofia University, 1000 Sofia, 15 Ruski blvd. PRB; BORODAEV Y.S., Moscow State University, USSR; MOZGOVA N.N., IGEM AN SSSR, Moskva

The statistical processing of microprobe analyses /1000/ of tetrahedrite-tennantite series, $Me_{12}SMe_4S_{13}$ of various types of ore deposits has confirmed the earlier established qualitatively /Mozgova, Tzepin, 1983/ varied correlations between mineral forming elements.

1.Standard negative /between elements taking equal positions in the structure/. In the group of SMe: As-Sb/Fig.1A/, in the group of Me: Zn-Fe/Fig.2,2A/.

2.Non-standard /between Me and SMe elements taking different positions in the structure/. Most often positive: Sb-Ag/Fig.4/, Sb-Zn/Fig.5/, As-Fe. These correlations are usually mutually connected with the standard; only in the case of zonal tetrahedrite-tennantite series the thin zonation of As and Sb is superimposed on wide zones of Fe and Zn distribution. Sometimes there is no correlation Sb-Zn.

3.In the group of Me: the opposite Hg-Zn, Hg-Fe and the absence of connections between the indicated elements /Fig.6/.

4.In the group of SMe: the negative Te-Sb at the absence of connections Te-As/Fig.7/ and As-Sb/Fig.1B/.

5.The opposite between Me^{2+} and Me^{+} - in Te containing /Fig.8/ and rich in copper /Fig.9/ tetrahedrite-tennantite series. Usually Me^{2+} is close to 2 and the connection to Me^{+} is absent.

The determined dependence is visualized when scanning microheterogeneous /in particular zonal/ tetrahedrite-tennantite series.

The standard dependencies are explained by isomorphs, non-standard are probably connected with the specific character of the geochemical behaviour of the elements in the process of mineral formation.

Note: the numbers on the co-ordinate axes graphs are formula coefficients.

Mozgova N.N., Tzepin A.I., 1983, Tetrahedrite-Tennantite Series, M., "Nauka"

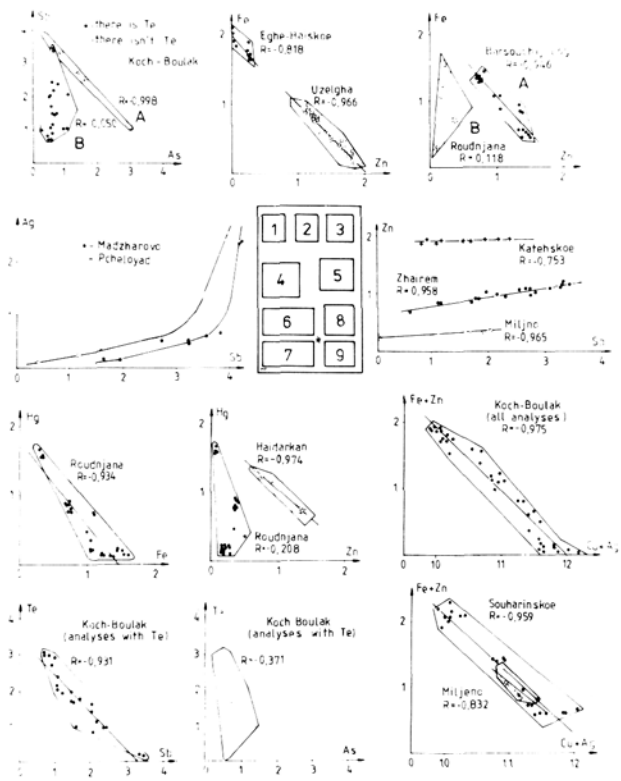

DISCRIMINANT ANALYSIS (DA) OF 400 X-RAY REFINED CLINOAMPHIBOLES

UNGARETTI, L., OBERTI, R., CANNILLO, E., Centro Studio Cristallografia Strutturale del CNR, 27100-Pavia, Italy; SMITH, D.C., Muséum National d'Histoire Naturelle, 75005-Paris, France.

400 natural C2/m amphiboles, from rocks of diverse origins and compositions, have now been studied by single-crystal X-ray diffractometry (XRef), following an updated version of the CORANF procedures described by Ungaretti et al. (Bull. Minéral., 1981, 104, 400-412 and 1983, 106, 645-672). Crystal-chemical parameters (cell dimensions, angles, distances, mean atomic number per site) have been so determined with high confidence levels which permit reliable statistical treatments.

To start the DA treatments, 276 amphiboles of known origin were selected for defining three groups I, L and H :

I = igneous rocks (intrusive + effusive), including kimberlites and other diatremes and their nodules, but excluding any sample with indications of post-igneous metamorphic re-adjustments;

L = low-pressure metamorphic rocks with no indications of pressure exceeding 10 kbar, i.e. amphibolites and greenschists, but excluding blueschists;

H = high-pressure metamorphic rocks (blueschists + eclogites), including their retrograde amphiboles which grew along with plagioclase during decreasing P and/or increasing T, i.e. highest-pressure amphibolites at P exceeding 10 kbar.

124 amphiboles of different or uncertain origin were excluded.

The first DA treatment was allowed to use only the crystal-chemical parameters (n = 114) directly derived from XRef.

To set the chemical context, however, the compositions may be indicated here by the IMA-approved names of the magnesio-alumino- nearest end-member in multi-component space as follows:

Group I (121 crystals) = pargasites, edenites, hornblendes;
Group L (70 crystals) = tschermakite, hornblendes, tremolites;
Group H (85 crystals) = glaucophanes, nyböites, taramites, barroisites, winchites.

This DA treatment found 32 variables sufficient to distinguish the three groups with 99.6% efficiency (Wilks' Λ = 0.003), as is displayed in Fig. 1 plotting the scores of the two orthogonal canonical discriminant functions obtained.

The second DA treatment was made with the same 276 crystals but with only the chemical compositional variables (n = 11) derived from XRef. 7 variables (K, Na(A), Na(M4), Ca, Ti, Al(VI), Al(IV)) sufficed to distinguish the 3 groups (Fig. 2) with 92.0% efficiency.

Since the chemical variation of the host rock composition is large within each group, but similar between the groups, then the distinction of the groups according to the crystal-chemical parameters is believed to represent the different physical conditions of formation. In particular, the wide separation of the H amphiboles from the others (Fig.1) may be attributed to the P difference ($P < \text{or} > 10$ kbar), whereas the difference between the I and L amphiboles may be attributed to the higher T of the igneous amphiboles. Hence the mineral chemical differences evident in Fig. 2 are due to the same P,T differences and not to the host rock chemistry.

Most of the amphiboles not used in the group definitions plot in positions compatible with their observed petrological evolution; e.g. those from some amphibolite-facies metamorphosed intrusive rocks plot between groups I and L, whereas some eclogite-facies metamorphosed igneous rocks plot between groups I and H.

Other DA treatments with sub-divided groups (e.g. effusive and intrusive rocks separated, Fig. 3) or with additional groups (e.g. hydrothermal rocks = richterites and arfvedsonites) yielded discriminations with 100% efficiency.

Hence amphibole crystals of geologically-uncertain origins (e.g. those lacking independent mineral-chemical, rock-chemical, or even petrographic analysis) may be genetically classified with measured confidence on the basis of XRef alone.

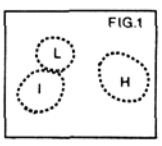

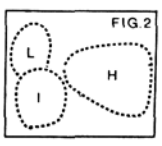

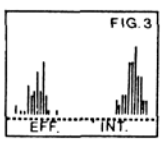

THE CONUNDRUM AT CASCADE SLIDE: A PETROLOGIC/STABLE ISOTOPIC ANSWER

VALLEY, JOHN W., Department of Geology and Geophysics, University of Wisconsin, Madison, Wisconsin 53706, U.S.A.

The xenolith of marble and calc-silicate at Cascade Slide in the Adirondack Mountains, New York contains exotic mineralogy that is normally thought to be characteristic of sanidinite facies, contact metamorphism, yet the xenolith and its anorthositic country rock were regionally metamorphosed to granulite facies during the Grenville Orogeny (1.0-1.1by.). This riddle is central to many classic problems of Adirondack geology.

The zoned body measures about 30x200m in outcrop and contains metamorphic mineral assemblages which include: akermanite(Ak), monticellite(Mo), wollastonite(Wo), Mg-spinel(Sp), vesuvianite, forsterite(Fo), cuspidine, harkerite, wilkeite, grossular(Gr), quartz(Qz), tremolite, diopside(Di), sphene, calcite(Cc), scapolite, magnetite, sphalerite, and pyrrhotite (1).

Coexisting Ak_{90}+Mo_{92}+Wo_{99} and Gr_{84}+Qz restrict the conditions of last equilibration in the xenolith to 750±30°C, $5.0<P<7.4$kbar (1), consistent with numerous estimates of 750±30°C, 7.6±0.5kbar for granulite facies metamorphism of associated gneisses (4). Assemblages of Cc+Qz located within 100m of Ak indicate gradients in $\log f\,CO_2$ with values ranging from >4.3 to <2.5 within the xenolith during metamorphism (3). Thus, fluid flow was not sufficient to exhaust buffering assemblages. In the core of the xenolith Mo+Fo+Di+Cc+Sp are only stable if $(P\,CO_2 + P\,H_2O)<0.5$kbar, indicating fluid-absent granulite facies conditions.

Values of $\delta^{18}O(Cc)=26.1$ to 17.6 in the xenolith while $\delta^{18}O(\text{feldspar})=7.2$ to 11.6 in adjacent anorthosite (2). The highest $\delta^{18}O$ values are in the core of the xenolith. Limited exchange is seen near the margin, but the overall gradient in $\delta^{18}O$ is very steep: 18‰ per 15m across the contact. The high $\delta^{18}O$ in calcite (>25) can only have formed at low T in sediments where fractionation is large. No known igneous or metamorphic process could have elevated $\delta^{18}O$ to this level. Metamorphic volatilization to form the assemblage Mo+Fo+Di+Cc in the core of the xenolith (mode: 15-25%Mo, 75-85%Cc) would have decreased $\delta^{18}O$ by approximately 1‰ due to ^{18}O fractionation into escaping CO_2. Large amounts of externally derived fluids cannot have infiltrated the xenolith core as they would have further depleted ^{18}O. If fluid/rock had been >0.1 then the present value of 26.1 requires that initial limestones had $\delta^{18}O>28.0$ for which there is no evidence among pre-Grenvillian sediments.

Taken together these results prove a polymetamorphic history where the anorthosite intruded shallowly ($P<3$kbar), perhaps at 1.3by. Metamorphic minerals formed near the contacts of the crystallizing anorthosite ($T>750$°C) and volatilization proceeded at high $X\,CO_2$. Oxygen isotope exchange occurred along the margins of the xenolith, but the core was never infiltrated by fluids. No volatilization or infiltration occurred during the subsequent granulite event which thus was fluid-absent. However, reequilibration of minerals recorded the granulite P, T, $f\,CO_2$, and $f\,H_2O$ such that Ak, Mo, and Wo may be regarded as "granulite-facies minerals" stabilized by low $f\,CO_2$.

An alternate theory where granulite metamorphism occurred during isobaric cooling following deep (20-30km) intrusion of anorthosite cannot be reconciled with these results. The formation of 25 mode% Mo at 750°C, 7.5kbar could only proceed at $X\,CO_2<0.02$ while at the same time pure CO_2 was being liberated. Such a process would require large amounts of H_2O infiltration (water/rock>2.25) to dilute all evolved CO_2, however such infiltration is ruled out by the preserved sedimentary $\delta^{18}O$ values which would have been exchanged to lower values. Thus, the anorthosite must have intruded shallowly where decarbonation could proceed at high $X\,CO_2$. Crystallization of anorthosite was unrelated to granulite facies metamorphism and could not have been the "heat source" that caused the onset of the granulite conditions.

(1) Valley,J.W. and Essene,E.J. (1980) Akermanite in the Cascade Slide xenolith and its significance for regional metamorphism in the Adirondacks. Contrib. Mineral. Petrol. 74, 143-152.
(2) Valley,J.W. and O'Neil,J.R. (1984) Fluid heterogeneity during granulite facies metamorphism in the Adirondacks: stable isotope evidence. Contrib. Mineral. Petrol. 85, 158-173.
(3) Valley,J.W. (1985) Polymetamorphism in the Adirondacks: wollastonite at contacts of shallowly intruded anorthosite. In: The Deep Proterozoic Crust in the North Atlantic Provinces, A.C. Tobi and J.L.R. Touret (eds.), 217-236.
(4) Bohlen,S.R., Valley,J.W., and Essene,E.J. (1985) Metamorphism in the Adirondacks. I. Petrology, Pressure and Temperature. J. Petrol. 26, 4, 971-992.

ELECTRON PARAMAGNETIC RESONANCE POWDER SPECTRA OF NATURAL QUARTZES, ESPECIALLY IN RELATION TO GOLD MINERALISATION.

VAN MOORT, J. C., Geology Department, University of Tasmania, Hobart (Tas.), 7001, Australia.

A systematic study of EPR spectra of about 1200 natural vein quartzes revealed particular intensities and shapes for various geological environments. Because of lack of good crystals this study is restricted to powder spectra. Distinction can be made between quartzes of igneous, metamorphic and diagenetic origin.

Particular attention was paid to various phases of quartz in gold deposits. While miners develop a subjective ability to recognise kindly quartz there is no commonly used quantitative method other than assay, to identify auriferous quartz. Studies of EPR spectra of quartz from core at Beaconsfield, Tasmania, suggest a cost effective technique which could be used to discriminate between auriferous and barren quartz. Both shoulder angle and peak height of the EPR powder spectra may be used. See figure below. A further study of 130 gold-bearing museum specimens from gold mines in Victoria and New Zealand corroborates this observation. Detailed study of quartzes at Stawell (Vic.), where there is a good geological control, indicates seven phases of quartz formation.

Metamorphism and shear destroys the ERR signals from the quartzes.

Correlation with spectra of quartz intergrown with minerals containing larger amounts of P, As, Sb, Bi and also Mo indicates that these elements in particular are responsible for the typical paramagnetic behaviour of the auriferous quartzes. Study of the spectra of quartzes intergrown with minerals rich in Ca, Ag, Ge, Ti, Fe, Al, V and U did not reveal anomalies of the same magnitude.

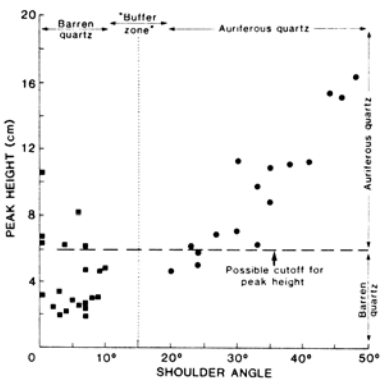

Discrimination of quartz at Beaconsfield gold mine(Tas.).

The cutoff between auriferous and barren quartz used for this figure was an assay value of 0.3 ppm Au for any particular section of core from which the sample was taken.

SULFIDE ORE MINERALS: SURFACE PROPERTIES AND ELECTRONIC STRUCTURE

VAUGHAN, D.J., Dept. of Geological Sciences, Aston University, Aston Triangle, Birmingham B4 7ET, England

Spectroscopic studies, in combination with quantum mechanical calculations, have enabled models to be developed for the electronic structures of many sulfide ore minerals.[1] Attention is now being focused on the surfaces of these materials, and the extent to which the electronic structure at the surface differs from the bulk material. This aspect of sulfide mineralogy is of great importance as regards problems of extraction and of understanding the alteration and replacement reactions studied by ore microcopists.

Contrasting examples of surface chemical behaviour are provided by major sulfide minerals such as galena and bornite. In our work, surfaces of the "pure" minerals and surfaces exposed to oxidation in air and in aqueous media are being studied using techniques including X-ray photoelectron and Auger spectroscopy, conversion electron Mössbauer spectroscopy, and spectral reflectance and quantitative color determinations. In addition, we are undertaking calculations on "molecular" cluster units aimed at modelling surface sites.

In galena, the surface most likely to be exposed is the (100) cleavage surface. The simplest models indicate that surface cations are 5-coordinate and experimental evidence suggests little or no relaxation of the surface atoms. Studies by UV photoemission spectroscopy[2] have suggested a reduction in the band gap from 0.4eV in the bulk to less than 0.1eV at the (100) surface in PbS. Calculations using the SCF-X_α method[3,4] indicate that this would involve a lowering in energy of the empty conduction band antibonding levels which are dominantly Pb 6s and 6p in character relative to the top of the valence band comprised of S3p nonbonding orbitals. Calculations also show that Pb or S vacant sites may produce holes in the valence band and bound states below the conduction band edge respectively.

Studies of galena oxidation in air and aqueous solution suggest oxygen chemisorption on to the galena surface, and spectroscopic evidence shows that oxygen at the surface behaves very similarly to sulfur.[2] The transfer of electrons associated with oxygen chemisorption should generate positive holes in the valence band and calculations[3] suggest that these holes are delocalized and would enhance conductivities and reaction rates. Hence also the more rapid reaction rate for S-rich galenas observed experimentally.[5] Sulfur vacancies present at the surface of the Pb-rich galenas apparently produce localized electron states[3] not conducive to rapid reaction rates. Vacant sites may also become occupied by chemisorbed oxygen and thereby approach a more stable quasi-stoichiometric condition (and the least reactive state).

In bornite, metal atoms occurring in tetrahedral interstices in the sulfur sublattice are in essentially tetrahedral or trigonal coordination. Low energy electron diffraction work on related compounds such as ZnS[6] shows that displacements of the cation and anion from their bulk positions by ~0.5Å occur in the surface layer. Thus on the (110) surface of ZnS for which both Zn and S are 3-coordinate, a reconstruction occurs with movement of Zn atoms inwards and S atoms outwards. Theoretical arguments[7] suggest that electronegativity differences between cation and anion influence the degree of distortion and since Cu and Fe are of similar electronegativity to Zn, we expect CuS_3 and FeS_3 groups on the surface of bornite will be distorted towards a planar coordination.

Bornite rapidly tarnishes on exposure to the atmosphere, exhibiting color changes that we have monitored by reflectance measurements and derivation of quantitative color values.[8] There is an increase of reflectance with duration of tarnish at ~400nm and a decrease at ~700nm. A plot of R% at 600nm against time shows an approximately logarithmic rate for this reaction. However, examination of several specimens showed markedly different overall rates, apparently related particularly to Cu:Fe ratio and stoichiometry. Spectroscopic studies of tarnished and untarnished samples suggest development of a hydrated Fe^{3+} oxide at the surface with possibly a copper sulfide layer immediately beneath.

A preliminary model to explain these reactions may be proposed using the data from SCF-X_α calculations on appropriate clusters[1]. Cu^{+1} is stable in triangular coordination whereas trigonal planar Fe^{3+} is apparently unstable. Thus, surface reconstruction may lead to the relative destabilization of Fe^{3+} and its reaction to form the hydrated oxide in which Fe^{3+} is again stabilized in tetrahedral coordination. The rapid tarnish rate of bornite compared to other copper-iron sulfides may be a consequence of more rapid diffusion of iron towards the surface. This diffusion rate should also be influenced by stoichiometry, offering an explanation for major differences in tarnish rate between specimens.

(1) Vaughan D.J. and J.A. Tossell, Phys. Chem. Min. 9, 253 (1983); (2) Grandke, T. and M. Cardona, Surf. Sci. 92, 385 (1980); (3) Hemstreet L.A., Phys. Rev. B11, 2260 (1975); (4) Tossell J.A. and D.J. Vaughan, in prep; (5) Eadington P. and A. Prosser, Trans. I.M.M. C.78, 74 (1969); (6) Duke, C.B., J. Vac. Sci. Tech. B1 732, (1983); (7) Harrison W. Electronic structure and the Properties of Solids, Freeman (1980); (8) Vaughan D.J., Tossell J.A. and C.J. Stanley, Min. Mag.,submitted.

CALCULATION OF ELASTIC CONSTANTS FROM BRILLOUIN SCATTERING DATA

VAUGHAN, Michael T., Department of Geological Sciences, University of Illinois at Chicago, Chicago, Illinois 60680, U.S.A.

Brillouin scattering is a phenomenon whereby light is scattered from the thermally generated acoustic waves always present in a crystal. The crystal is mounted on a Eulerian cradle and has a known orientation; this orientation may be altered by adjusting the Eulerian angles in analogy to a 4-circle diffractometer. See Vaughan and Guggenheim [*1986*] and references therein for a description of the method. The determination of single-crystal elastic moduli involves collection of the raw Brillouin scattering spectrum on a multichannel scalar, digital transmission of this data to a microcomputer, processing this data with one program to get a filtered spectrum, calculation of acoustic velocities using another program, plotting the acoustic velocities using a third program, and finally, inverting the acoustic velocity data set to get the elastic constants using a fourth program.

The first program, BS11, is written in compiled BASIC. The data is transmitted over a serial line to an IBM PC at 9600 Baud to the PC where it is stored on a RAM-disk. The program then re-formats the data and smoothes it using a 9-point polynomial smoothing routine. The spectrum is plotted on the screen and the location of the peaks is determined by the user, usually to a precision of 1/10 channel. Finally the complete spectrum is plotted and the locations of the peaks are printed out. The equipment requirements to run this program are about 320 kbytes of RAM which allows the use of a small RAM disk; an 8087 co-processor, and an IBM color graphics card and monitor or its equivalent.

The second program, VELOC3, calculates the acoustic velocity and direction of propagation for each mode in each Brillouin spectrum. It takes into account the polarization of both the indicent and scattered light, the orientation of the faces through which the light enters the crystal, the orientation of the optical indicatrix, and the refractive index corresponding to the polarization of the light. These optical calculations are described in Vaughan and Bass [*1983*]. All of this requires knowledge of the orientation of the crystal. Its orientation matrix has been previously determined on the 4-circle diffractometer. The simplest part of the program is the calculation of the acoustic velocities once the above optical and orientation parameters are determined. The program is written in FORTRAN 77 and was originally run on an Univac 1110 mainframe. Although it is a rather large program, it has been successfully ported to the IBM PC and compiled using the Microsoft FORTRAN compiler, so it can now be considered as a microcomputer program. This program requires as input the peak location for each spectrum; these are obtained from BS11. There may be anywhere from 25 to 150 separate spectra for as many different orientations of the crystal. The Eulerian angles for the crystal for each spectrum, and the orientation matrix for each mounting of the crystal and the appropriate crystallographic and optical parameters are also required. The hardware requirements are modest; the program needs 256 kbytes of RAM. The availability of an 8087 co-processor and a RAM disk increases the speed, but are not essential.

The third program, VELPLOT, is actually a pair of programs. The first of the pair of programs involves calculation of theoretical acoustic velocities, which is an eigenvalue problem. It was most easily written in FORTRAN. As FORTRAN does not have any built-in graphics, VELPLOT creates a file of data points to be plotted, and another program, also called VELPLOT makes use of the screen graphics facilities of BASIC to actually plot the results. This makes possible very speedy plots of theoretical and experimental results.

The fourth program, ORTHO, makes the final calculations to determine the elastic constant model which best fits the acoustic data. This program has not yet been converted to a microcomputer version and will not be further discussed here.

Vaughan, M. T., and S. Guggenheim, Elasticity of muscovite and its relationship to crystal structure, *J. Geophys. Res.* (in press, 1986)

Vaughan, M. T., and J. D. Bass, Single crystal elastic properties of protoenstatite: a comparison with orthoenstatute, *Phys. Chem. Minerals, 10*, 62-68, 1983.

MECHANISMS AND CHEMISTRY OF SHEET SILICATE REACTIONS IN METAMORPHIC ROCKS

VEBLEN, D. R., Department of Earth and Planetary Sciences, The Johns Hopkins University, Baltimore, Maryland 21218, USA

Many reactions in metamorphic rocks involve growth of new crystals along grain boundaries, typically with no rigorous orientation relationship between the new and surrounding crystals. In some reactions, however, one mineral is replaced directly by another, with a strict orientation relationship determined by the two crystal structures. In topotactic reactions of this type, the reactant and product structures impose strict controls on the reaction, and there is a close relationship between the detailed structural mechanisms of reaction, the overall reaction chemistry, and the physical consequences of the reaction.

Reactions of the latter type are common among sheet silicates. These include prograde reactions, such as the growth of muscovite from clay minerals in pelites (Lee et al., 1984), and retrograde reactions, such as the replacement of biotite by chlorite (e.g., Chayes, 1955). This latter reaction has been studied extensively with high-resolution transmission electron microscopy during the past several years. This paper discusses some of these results, which suggest that the submicroscopic details of reaction can vary from occurrence to occurrence, presumably as a function of the detailed physical and chemical environment.

Different mechanisms for the biotite-chlorite reaction can entail very different physical and chemical effects. Two end-member reaction mechanisms (Veblen and Ferry, 1983) are shown in the figure. Mechanism 1 involves a major volume increase; consumes major amounts of octahedrally-coordinated cations and H_2O; and releases H^+ and potassium. Mechanism 2 entails a major volume decrease; consumes both H_2O and H^+; and releases silica and potassium. Because the chemical reactions characteristic of these two mechanisms are different, the chemical environment can be expected to determine which occurs. For example, mechanism 2 requires H^+ and can be expected to occur in low-pH environments.

The first mechanism of biotite-chlorite reaction has been inferred for biotites from deformed gneisses by Olives et al. (1983). The second mechanism has been observed by Veblen and Ferry (1983) in an altered granitic rock, and it was shown that the chemical consequences of this mechanism matched closely the analysis now make it possible to measure a structural width for grain boundaries from their diffraction patterns (e.g., Ricoult and Kohlstedt, 1983). In addition, recent results on structurally well-constrained grain boundaries show that HRTEM combined with computer simulation by periodic continuation can be a powerful approach to interface structure determination, even for complex crystal structures. Unlike some other approaches, HRTEM is applicable to heterophase boundaries. Examples of grain boundaries between different chain silicates and between chain silicates and oxides show that they can be very "tight," with boundary widths measured in tenths of nanometers.

Extended defects play an important role in many transformation processes in minerals. Reconstructive transformations can occur by migration of the reactant/product grain boundary through the structure, but they may also occur by the formation of planar defects produced by propagation of dislocations or other linear defects through the structure (e.g., Coe and Kirby, 1975). Higher-order phase transformations typically involve a change in space group symmetry, and they can proceed by the formation and coarsening of domains separated by planar defects corresponding to the symmetry elements lost in the transformation (e.g., Van Tendeloo et al., 1976). The dynamics of these processes can be studied using in situ heating techniques in the transmission electron microscope.

References: Buseck, P. R. and Iijima, S. (1974) Am. Mineral., 59, 1-21; Coe, R. S. and Kirby, S. H. (1975) Contrib. Mineral. Petrol., 52, 29-55; Cowley, J. M. and Moodie, A. F. (1957) Acta Crystallogr., 10, 609-619; Kröger, F. A. (1974) Chemistry of Imperfect Crystals, North-Holland, Amsterdam; Ricoult, D. L. and Kohlstedt, D. L. (1973) Phys. Chem. Minerals, 9, 133-138; Van Tendeloo, G., Van Landuyt, J., and Amelinckx, S. (1976) Phys. Stat. Solidi, A33, 723-735; Veblen, D. R. (1985) Ann. Revs. Earth Planet. Sci., 13, 119-146.

DIRECT ELECTRON IMAGING OF EXTENDED DEFECTS IN MINERALS

VEBLEN, D. R., Department of Earth and Planetary Sciences, The Johns Hopkins University, Baltimore, Maryland 21218, USA

The chemistry of point defects in crystals is commonly treated in a thermodynamic framework, since point defects can be equilibrium phenomena (e.g., Kröger, 1974). Extended defects such as dislocations and planar faults, on the other hand, are inherently non-equilibrium phenomena. Therefore, understanding their distribution, structure, chemistry, and mode of formation generally requires experimental approaches. Due to the improved point-to-point resolutions of modern instruments, high-resolution transmission electron microscopy (HRTEM) in recent years has become an important tool for studying extended defects in minerals (e.g., Buseck and Iijima, 1974; Veblen, 1985). In the present paper, recent applications of TEM to two problems will be discussed: (1) the structure of grain boundaries and (2) the role of extended defects associated with various types of phase transformations.

With point resolutions of approximately 0.3nm, it is possible to image structural detail below the scale of the unit cells of most minerals. Under carefully controlled experimental conditions, it is possible to obtain contrast that allows determination of the structures of defects and grain boundaries. However, reliable interpretation of structure from HRTEM images requires computer simulation of images from model structures. For defects, such simulations are problematical, because the necessary dynamical electron diffraction calculation is performed with a set of discrete complex structure amplitudes in Fourier space (Cowley and Moodie, 1957); this formulation requires that the simulated structure be periodic, but defects are inherently non-periodic features. Therefore, defect simulations are performed using the method of periodic continuation, in which defects are embedded in a block of normal structure in a very large, artificial unit cell.

There are several electron microscopic approaches to grain boundary structure determination. For example, low-angle boundaries between crystals of the same structure commonly consist of arrays of dislocations, which can be studied with conventional TEM techniques. Advances in electron diffraction reaction chemistry inferred by Ferry (1979) on the basis of more standard petrologic techniques. Both mechanisms have been observed in the phlogopite-chlorite reaction in a marble by Yau et al. (1984), as well as a more complex, volume-preserving reaction involving replacement of 14 phlogopite layers by 10 chlorite layers. Eggleton and Banfield (1985) showed that both mechanisms operated in biotites from two granitic rocks and demonstrated that the mechanisms are consistent with the bulk reaction chemistry. Eggleton and Banfield (1985) and Ferrow and Veblen (in prep.) also have recognized the complexity and importance of other reaction products finely intergrown with the sheet silicates, such as oxides and epidote. The reverse reaction, from chlorite to phlogopite, has also been examined by Maresch et al., who showed that the reverse of mechanism 2 was the predominant means of transformation.

Taken together, these studies of replacement reactions involving biotite and chlorite show that there is an intimate link between the submicroscopic crystallography of reaction and the bulk chemical and physical effects. Full understanding of such reactions requires characterization on both scales.

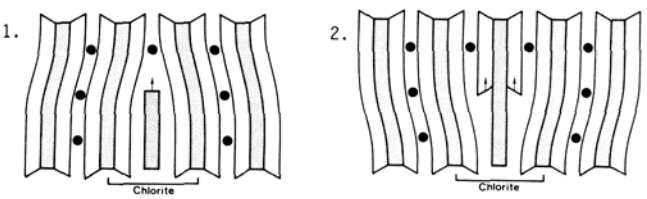

References: Chayes, F. (1955) J. Geol., 63, 75-82; Eggleton, R. A. and Banfield, J. F. (1985) Am. Mineral., 70, 902-910; Ferry, J. M. (1979) Contrib. Mineral. Petrol., 68, 125-139; Lee, J. H., et al. (1984) Contrib. Mineral. Petrol., 88, 372-385; Maresch, W. V., et al. (1985) N. Jb. Mineral. Abh., 152, 79-100; Olives, J., et al. (1983) Am. Mineral., 68, 754-758; Veblen, D. R. and Ferry, J. M. (1983) Am. Mineral., 68, 1160-1168; Yau, Yu-C., et al. (1984) Contrib. Mineral. Petrol., 88, 299-306.

CHEMISTRY AND CRYSTALLOGRAPHY OF DEEP CRUSTAL PYROXENES

VEBLEN, D. R., Dept. of Earth and Planetary Sciences, The Johns Hopkins University, Baltimore, MD 21218, USA; BISH, D. L., Los Alamos National Laboratory, Earth and Space Sciences Division, MS J978, Los Alamos, NM 87545, USA; SCHLINGER, C. M., Dept. of Geology and Geophysics, University of Utah, Salt Lake City, UT 84112, USA

Microstructures and chemical variations resulting from subsolidus reactions in quadrilateral pyroxenes have been studied intensively for several decades (e.g., Poldervaart and Hess, 1951). During the past 15 years, TEM studies have contributed much to our understanding of the processes and kinetics of exsolution, coarsening, and phase transformations in pyroxenes from basalts and basic intrusions (e.g., Nord et al., 1976; Nobugai and Morimoto, 1979; Kitamura et al., 1981; Rietmeijer and Champness, 1982). However, less attention has been devoted to quadrilateral pyroxenes from other petrologic settings. The present study of deep crustal pyroxenes with complex and extended thermal histories reveals many features that are not observed in typical rocks of basaltic composition, even from large, slowly cooled basic intrusions. Results of HRTEM and AEM studies of two different types of deep crustal pyroxene are considered: aluminous orthopyroxene megacrysts from Precambrian anorthosites and augites from granulite facies gneisses.

It has been recognized that orthopyroxene megacrysts characteristic of some anorthosites commonly contain (100) lamellae of calcic plagioclase, clinopyroxene, and oxides (Emslie, 1975; Morse, 1975; Dymek and Gromet, 1984). Single-crystal X-ray study of orthopyroxene megacrysts from several localities shows, however, that clinoamphibole also can be an important component of these megacrysts, perhaps having been identified as pyroxene in previous investigations. To clarify the nature of these pyroxenes, a TEM study of a megacryst from the Nain, Labrador, anorthosite massif was undertaken. The megacryst contains at least nine distinct types of lamellae parallel or subparallel to (100) of orthopyroxene: (1) host orthopyroxene; (2) clinopyroxene; (3) clinoamphibole; (4) complex hybrid lamellae of clinopyroxene and clinoamphibole intergrown on (010); (5) calcic plagioclase; (6) chromian magnetite; (7) hercynite; (8) ilmenite; and (9) hybrid lamellae of clinopyroxene, clinoamphibole, or plagioclase intergrown on (100) with an oxide. Textures within the amphibole and hybrid pyroxene-amphibole lamellae indicate that amphibole forms by replacement of earlier (100) clinopyroxene lamellae.

TEM methods also have been applied to augites in granulite facies gneisses from Lofoten, Norway (Schlinger, 1986). Three types of chain silicate lamellae occur in the augite: (1) orthopyroxene, (2) pigeonite, and (3) grunerite. The orthopyroxene lamellae have coarsened out of the (100) boundary orientation that invariably is observed between host augite and orthopyroxene and now have irregular, nonplanar interfaces. Lamellae of "001" grunerite are unusual, because low-Ca clinoamphibole typically does not occur with high-Ca pyroxene; these lamellae may have formed metastably by alteration of some of the "001" pigeonite lamellae. Many of the exsolution lamellae have been decorated with precipitates of Fe-Ti oxides. In addition to the chain silicates and oxides, numerous other precipitates in the 10nm size range occur in the augite, including some rare-earth-rich inclusions.

Thus, these deep crustal pyroxenes display many features that are not observed in pyroxenes previously studied with TEM methods, presumably as a result of their long and complex thermal and alteration histories. These results have important implications for the geochemical behavior of pyroxene-bearing rocks of the deep crust. During processes such as partial melting, these complex, multiphase "crystals" probably do not behave as pure chain silicate assemblages, and the use of K_d values for pyroxene would be inappropriate for modelling the chemistry of melting.

References: Dymek, R. F. and Gromet, L. P. (1984) Canad. Min., 22, 297-326; Emslie, R. F. (1975) Canad. Min., 13, 138-145; Kitamura et al. (1981) Bull. Min., 104, 278-284; Morse, S. A. (1975) Earth Planet. Sci. Lett., 26, 331-336; Nobugai, K. and Morimoto, N. (1979) Phys. Chem. Min., 4, 361-371; Nord, G. L. et al. (1976) in Wenk et al., Eds., Electron Microscopy in Mineral., Springer-Verlag, pp. 220-227; Poldervaart, A. and Hess, H. H. (1951) J. Geol., 59, 472-489; Rietmeijer, F. J. M. and Champness, P. E. (1982) Min. Mag., 45, 11-24; Schlinger, C. M. (1986) J. Geophys. Res., in press.

Transformation of uranite into different hydrated uranium oxides.

VOCHTEN, R.F., Laboratory of Physical and Chemical mineralogy.
State University Antwerpen, Middelheimlaan 1, 2020 Antwerpen, Belgium, Europe.

In nature the formation of secondary uranium minerals is mainly controlled by the alteration of the primary mineral uraninite into different uranium oxide minerals. In a contineous system, uraninite or synthetic uraniumdioxide, reacts in an acqueous medium with a mixture of CO_2 and O_2.
The system consists of a three stage reactor and a concentration vessel, working at 100°C and 25°C respectively. If the reaction is carried out at 100°C with uraninite, the mineral fourmarierite ($PbO.4UO_3.4H_2O$) is formed, while starting the reaction with synthetic uraniumdioxide a complex mixture of different hydrates of UO_3 was obtained.
It was observed that the reaction being realized at 25°C, meta schoepite ($(UO_3(2-x)H_2O$) was formed.
The identifications of the obtained phases are realized by Guinier X-ray powder diffraction, chemical and thermal analyses.
Since the adsorption energy of O_2 for UO_2 is very low, chemisorption takes place and the $^{+4}$active U places on the surface become saturated with oxygen. As a consequence the surface is inactivated for further oxidation.
The kinetic of the reaction decreases markedly with time and the surface becomes completely inactive after $\pm$ 9 hours.
The kinetic, governed by the chemisorption of oxygen on the uraninite surface, is studied by zeta potential measurements.

PHASE TRANSITIONS IN THE MEGABAR PRESSURE RANGE USING THE CORNELL SYNCHROTRON SOURCE

VOHRA, Y.K., BRISTER, K.E., WEIR, S.T., DESGRENIERS, S. , DUCLOS, S.J., RUOFF, A.L., Dept. of Materials Science and Engineering, Cornell University, Ithaca, NY 14853, USA

Energy dispersive x-ray diffraction techniques[1] at the Cornell High Energy Synchrotron Source have been modified to perform x-ray diffraction from small sample areas (10 μm in diameter) in the diamond anvil cell. The essential improvement is in the collimator system, where a stainless steel tube with a lead pinhole is located close to the table of the diamond (about 15 mm from the sample) and is adjusted with motor driven motion in the two directions perpendicular to the beam. The collimator movement is controlled by a computer and can be moved with a precision of 0.2 μm. The adjustment and alignment procedures allow rapid optimization of the sample signal. The small sample areas ensure more homogeneous pressure conditions. The new collimator system also offers the possibility of measurements of pressure gradients across the diamond anvil face by x-ray techniques.

Some of the specific examples of the highest known phase transitions near and above one megabar using this technique will be presented. The studies include BaO to 60 GPa and Ge to 125 GPa (1.25 Mbar).

For BaO three structure phases[2,3] were found between 0 GPa and the highest pressure of 60.5 GPa. BaO(I) is in the rocksalt phase between 0 and 10 GPa, BaO(II) is in the hexagonal NiAs phase between 10 and 15 GPa, and BaO(III) is in the tetragonal PH_4I phase from 15 GPa up to the highest pressure of 60.5 GPa. From the variation in the intensities of the diffraction line for BaO(III) with pressure, we conclude that this tetragonal PH_4I phase is continuously approaching a cesium-chloride type structure as the pressure increases. Extrapolation of c/a plot suggests that BaO may adopt the undistorted cesium chloride phase only above 100 GPa (1 Mbar) in the absence of any intervening first order transition. This behavior of BaO(III) is a new phenemenon in the study of barium chalcogenides and alkaline earth oxides.

There is considerable interest in the phase transitions induced by application of high pressures in the covalent group IV

PHASE TRANSITIONS IN THE MEGABAR PRESSURE RANGE USING THE CORNELL SYNCHROTRON SOURCE
VOHRA, Y.K., et al.

elements C, Si and Ge. For pressures up to 50 GPa[4,5] Si was found to have a structural transition sequence: cubic diamond to tetragonal to sh to an intermediate structure[4] and finally to hexagonal close packed (hcp) above 40 GPa. Ge studied in the same pressure range showed only one transition from the cubic diamond structure to the β-Sn structure around 11 GPa[4]. Two separate high pressure experiments were made on Ge samples. One high pressure run was made to 90 GPa with ruby as a pressure marker with 300 μm flat diamonds. In another ultra high pressure experiment Ge-20 wt.% Pt mixture was placed in the 25 μm hole of the spring steel gasket and the pressure was measured from the Pt marker and gasket material via its isothermal equation of state. Beveled diamonds with 300 μm tips with 5° bevel and flats of 100 μm were used in the latter experiment. X-ray diffraction measurements were made to pressures of 1.25 Mbar and were terminated only because scheduled time on CHESS ended. A transformation from the tetragonal β-Sn to the simple hexagonal phase is found at 75±3 GPa in good agreement with the total-energy pseudopotential prediction of 84±10 GPa[5]. Another phase transition was observed from the simple hexagonal structure to a double hexagonal close packed structure (dhcp) at a pressure of 102±5 GPa. This is the highest pressure for which a crystalline structure change has been directly observed in any material by x-ray diffraction. The theory[6] predicts a transformation to the hexagonal close packed structure at 105±2 GPa. The dhcp phase of Ge is stable to 125 GPa. The eventual transition of Ge into hcp structure may occur at higher pressures. It would be interesting to extend the high pressure studies on Ge to pressures of 2 Mbar.

1. M. Baublitz, Jr., V. Arnold and A.L. Ruoff, Rev. Sci. Instrum. 52, 1616 (1981).
2. L. Liu, J. Appl. Phys. 42, 3702 (1971).
3. L. Liu and W.A. Bassett, J. Geophys. Res. 77, 4934 (1972).
4. H. Olijnyk, S.K. Sikka and W.B. Holzapfel, Phys. Lett. 103A, 137 (1984).
5. J.Z. Hu and I.L. Spain, Solid State Comun. 51, 263 (1984).
6. Y.K. Vohra, K.E. Brister, S. Desgreniers, A.L. Ruoff, K.J. Chang and M.L. Cohen (submitted to Phys. Rev. Lett).

QUESTIONS ABOUT HIGH CHLORINE MICAS AND AMPHIBOLES.

VOLFINGER M. and ROBERT J.-L.,CRSCM-CNRS,1A rue de la Férollerie 45071 Orléans Cedex 2,France.

Chlorine is systematically involved in metallogenic processes,in magmatic as well as hydrothermal conditions.In natural environments chlorine is present in numerous minerals : sodalite (up to 7 wt%), apatite (up to 4 wt%),scapolites (up to 3 wt%),clinoamphiboles (up to 1.5 wt%),trioctahedral micas (up to 1 wt %).

Micas and amphiboles are quite ubiquitous and their compositions are highly variable,due to complex solid solutions able to influence the local site properties controlling the possible replacement of OH^- by Cl^-.Previous experiments have shown that high X_{Fe} favors higher storage in biotites [1],[2].The same phemenon is known in natural tremolite-actinolite series [3].In the series phlogopite-annite,the annite end member traps ≈30 times more chlorine than the magnesian end member phlogopite;a similar increase is observed in that natural tremolite-actinolite series [3].

A statistical crystal-chemical study shows that phlogopite is representative of most natural biotites.For this Mg-end member,the Cl content is only 10 ppm when it is in equilibrium with a 0.5M KCl hydrothermal solution,at 600°C,2 kbar.Increasing the Cl content of the mica needs an increase in the solution molarity,but,at 600°C, the maximum Cl content that could be reached in the phlogopite end member is no more than 150 ppm,even with a 10M KCl solution;this Cl content is around 60 times smaller than the maximum Cl content known in natural biotites.

Two additional factors can play an important role on the storage of chlorine in OH-silicates:acidity of the solution and temperature Experiments made on phlogopite with 0.5M HCl solutions,at 600°C, permitted to reach 40 ppm of Cl in the mica phase.The genesis of Cl-rich phlogopites,at 600°C,could be exemplified by the reaction of high chloride fluids (10M KCl) on the oxide mixture $6MgO-1Al_2O_3-6SiO_2$.In that case,HCl is a reaction product and the generated mica contains up to 1000 ppm of Cl.A similar Cl content of the mica phase could be reached with a 0.5M HCl solution,at 800°C,2 kbar.

The question is about the discrepancy between the highest Cl content of some natural biotites and the maximum Cl content obtained experimentally for HCl molarity and temperature conditions compatible with the stability of the mica phase.

Experiments on clinoamphiboles belonging to the series tremolite-Fe-tremolite indicate that these amphiboles can store much more Cl at 500°C than phlogopite : 120 ppm for the amphibole in equilibrium with a 1M salt solution,compared to around 20 ppm in phlogopite in the same experimental conditions.However,even in the most favourable conditions for the storage of Cl in these amphiboles (high HCl content of the hydrothermal solution),compatible with their stability, the maximum Cl content that could be reached is no more than 1000 ppm,far from the highest Cl content known in nature.

The possible fixation of molecular HCl in the alkaline site of micas and amphiboles was proposed to explain the discrepancy between experimental results and natural data [2].This hypothesis was tested by Raman and mass spectrometries;no detectable molecular HCl is present in our samples.

The crystal-chemical control of the Cl content of OH-bearing silicates is well established [2] but the experimentally observed variations of this Cl content with temperature and with the nature of the Cl-bearing species in the fluid phase in equilibrium indicate that the properties of the solution are fundamental.

These properties of solutions strongly depend on T and P conditions.The role of pressure can be fundamental and should be considered in future works.

References.

[1] . MUNOZ J.L. and SWENSON A.,Econ. Geol.,76,2212-2221,(1981).
[2] . VIELZEUF D.,Bull. Minéral.,105,681-690,(1982).
[3] . VOLFINGER M.,ROBERT J.-L.,VIELZEUF D. and NEIVA A.M.R.,Geoch. Cosmochim. Acta,49,37-48,(1985).

APPLICATION OF HIGH-GRADIENT MAGNETIC SEPARATION TO STRUCTURAL AND COMPOSITIONAL STUDIES OF LAYER SILICATES IN FINE GRAINED ROCKS

WALKER, J. R., Dept. of Earth Sciences, Dartmouth College, Hanover, NH 03755, USA

A difficulty common to many studies of layer silicates in fine grained sedimentary and low-grade metamorphic rocks is separation of the minerals for structural and compositional analysis. The mineral grains are typically too fine to be clearly distinguished in thin section, so optical studies and microprobe analyses are difficult. In addition, the minerals are too fine to be hand picked, and tend to flocculate if separation using heavy liquids is attempted. The most commonly implemented separation techniques are: particle size separation by timed centrifugation, which is effective only if the minerals to be separated have sufficiently different settling characteristics; and dissolution or transformation of one of the interfering phases. The latter technique can be effective if the mineral to be studied is resistant to the chemicals employed. If, however, one wishes to study a mineral which is easily altered or destroyed, a more specialized technique, such as differential X-ray diffraction, must be used. This method has two problems, however, which make it difficult to use. First of all, it destroys the mineral of interest, so measurements cannot be made a second time on the same sample. In addition, intersample variations due to sample preparation, resulting in significant differences in preferred orientation and/or sample thickness, may cause differences in the resulting diffraction pattern which are not related to the mineral under study.

High-gradient magnetic separation (HGMS) is an easily applied, nondestructive technique which separates fine-grained minerals on the basis of their magnetic susceptibilities. In this investigation of the effectiveness of HGMS at separating minerals for structural and compositional study, the technique obtained a separation of chlorite from muscovite in slates and shales pure enough to allow polytype analysis of the chlorite (<20% mica) in one sample, and separated two compositionally distinct chlorites in another.

The equipment used is a Franz L-1CN separator with pole pieces specially modified to accomodate a stainless steel canister. The canister is filled with stainless steel wool, which acts as a filter material by carrying the magnetic field applied by the Franz. It also provides the high gradients necessary for separation since lines of magnetic flux converge at the sharp edges and corners of the steel wool fibers. The sample is pumped through

APPLICATION OF HIGH-GRADIENT MAGNETIC SEPARATION TO STRUCTURAL AND COMPOSITIONAL STUDIES OF LAYER SILICATES IN FINE GRAINED ROCKS

WALKER, J. R.

the filter as a clay/water suspension. After the suspension has passed the filter, the magnet is turned off and the magnetic fraction is flushed out. In order to optimize the separation, several paramters may be varied. The strength of the magnetic field, and the velocity of the sample suspension can be easily adjusted by controlling the current on the electromagnet and the speed of the pump respectively. Viscosity of the sample suspension is controlled by the ratio of clay to water. For minerals with very similar magnetic susceptibilities (e.g. illite and mixed layered illite/smectite) an expandible phase can be made more susceptible by saturating it with a suitable cation (such as Fe^{2+}, Mn^{2+}, or Cr^{2+}).

The enclosed figure shows the results of a separation performed on a slate. The original mineralogy of the rock, as shown in the top pattern, is chlorite, mica (presumably muscovite), quartz, and feldspar. With decreasing magnetic field strength (represented by decreasing current, measured in amps), the filter retained increasingly higher percentages of chlorite relative to the other minerals. At 0.1 amps, quartz and feldspar are almost totally removed, and mica is down to approximately 20%. The magnetic fraction was analyzed using a powder camera, and the chlorite was determined to be of the II*b* polytype.

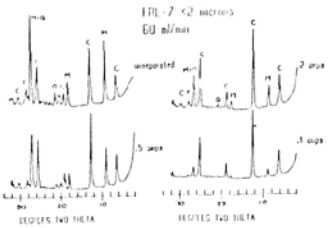

COMPUTER MODELLING OF MAGNESIUM SILICATE PEROVSKITES

WALL, A. and PRICE, G.D., Department of Geological Sciences, University College London, Gower St., London WC1E 6BT, England.

The aim of much recent research within Earth Sciences has been to determine the fundamental processes and mechanisms involved in mantle dynamics, lithospheric motion and plate tectonics. Many of the models, however, which have been advanced in an attempt to describe these vital processes rest upon unconfirmed assumptions concerning the response of rock-forming minerals to changes in their physical and chemical environment. Thus, although it is now widely accepted that approximately 70% of the lower mantle and 40% of the entire earth is composed of $(Mg,Fe)SiO_3$-perovskite, virtually nothing is known of the rheological or physical properties of this phase. The direct measurements of the majority of these properties for $MgSiO_3$-perovskite is currently beyond the limits of technology, because of the high pressures and temperatures (>250 kbars and 1500°C) required to enter the perovskite stability field. As an alternative to direct study therefore, theoretical and computer-based techniques of lattice simulation and molecular dynamics have been employed to obtain an understanding of perovskite behaviour. Several sets of pair-wise additive interatomic potentials have been developed to describe the forces within the structure of the silicate perovskite enabling the properties of perfect perovskite crystals, and their elastic and spectroscopic characteristics to be investigated. In addition, the energetics of defects, the activation energy for diffusional processes, the effects of pressure on the distortions within the perovskite structure, and the suggested high temperature superionic conductivity of perovskites are being studied. The results of these investigations and the use of a recently developed three-body potential will be discussed

• THE CHARACTERISTICS OF MINERAL CHEMISTRY AND THE GENESIS OF ROCK-FORMING MINERALS IN THE KAINOZOIC BASALTS FROM EASTERN CHINA

WANG Fangzheng and WANG Rnjieng, Department of Geology, Wuhan College, Yujiashan, Wuhan 430074, Hubei, People's Republic of China

The Kainozoic basalts are abundant in Eastern China. The regions under study include Wudalianchi, Heilongjiang province, Shanwang, Shandong province and Xilinhote, Inner Mongolia, Niutoshan, Fujian province and Hainan Island, Guangdong province, Chenxian-Xinchang, Chekiang province, etc. Basalts are classified into quartz tholeiite and olivine tholeiite, olivine alkali basalt, basanite and potassium-rich basalt. Some 251 samples of plagioclase and 58 samples of alkali feldspars, 108 samples of olivine and 328 samples of pyroxenes, 22 samples of Fe-Ti oxide, etc. have been studied by electron probe microanalysis. Aside from this, textural and optical properties of minerals mentioned before have been studied. Different degrees of Al-Si ordering of feldspars have been detected by optical and X-ray powder methods.

PLAGIOCLASE. Both in pheocrysts and groundmass, various types of zonal structures are found: normal 58.06%, abnormal 12.9%, cyclical 16.13%, irregular 12.90%. The Pil end members from various kinds of basalts: in quartz tholeiite P1 phenocrysts, An 53.0-72.7 Ab 26.7-34.6 Or 0.5-1.1 and groundmass An 42.1-75.1 Ab 24.1-55.4 Or 0.6-2.5, in olivine tholeiite P1 phenocrysts An 46.7-67.9 Ab 31.1-53.3 Or 0.50 and groundmass An 34.5-66.2 Ab 32.7-60.5 Or 0-5, in olivine alkali basalt P1 phenocrysts An 45.3-59.6 Ab 37.3-53.3 Or 0-3.6 and groundmass An 34.2-77.1 Ab 22.1-60.2 Or 0.6-5.6, in basanite P1 pheocrysts An 22.7-58.3 Ab 40.5-77.3 Or 0-1.5 and groundmass An 42.1-50.0 Ab 45.9-50.4 Or 3.4-4.1. Degrees of A1-Si ordering (S) of phenocrysts show that S = 0.0-0.2 49%, S = 0.2-0.4 31%, S = 0.4-0.5 14%, S = 0.5-0.73 6%.

OLIVINE. Both phenocrysts and the groundmass of olivine show zonal structure. The compositional zoning from core to rim is increasingly higher in FeO content. The end member constituent olivine from various rock types show: in quartz tholeiite phenocrysts, Fo 66.4-70.5; in olivine tholeiite phenocrysts, Fe 49.9-89.9 and groundmass Fo 40.1-66.6; in olivine alkali basalts phenocrysts, Fo 71.1-91.4 and groundmass Fo 82.0; in basanite phenocrysts Fo 74.5-91.0 and groundmass Fo 70.0-85.0; in K-rich basalts phenocryst Fo 76.5-85.5 and groundmass Fo 65.0-80.8. The minor constituents of olivine are different from various regions. CaO content of olivine in South China > 0.18 wt %, in Northeastern China 0.06-0.13 wt %, in North China < 0.06 wt %. It depends upon the chemical composition of basalts from various regions.

PYROXENE. The compositional range of phenocrysts and groundmass pyroxene is rather large. All of them show zonal structure. The compositional zoning from core to rim shows an increase in Ca and Fe. The end-member constituent of pyroxenes from various rock types show that: in quartz tholeiite phenocrysts of orthopyroxene: En 72.6-77.0, Fs 16.0-23.9, Wo 4.1-4.6; phenocrysts of clinopyroxene En 45.2-57.9 Fs 16.0-23.9 Wo 18.5-34.9, in affinity with subcalcic augite and augite, in groundmass clinopyroxene are also subcalcic augites and augites with a compositional range of En 30.3-64.1, Fs 14.0-36.2, Wo 5.0-15.4; in addition, there are magnesium pigeonite or Cpx En 59.5-78.6, Fs 17.6-28.6, Wo 3.8-12.2, with TiO_2 0.53-0.95, Na_2O 0.01-0.36. In olivine tholeiite the majority of Cpx phenocrysts are augites, with a few phenocrysts of salite, En 38.6-47.5, Fs 10.7-20.1, Wo 35.5-49.1. Groundmass Cpx are titaniferous augite and salite: En 30.8-51.2, Fs 11.8-29.1, Wo 29.7-52.2. In olivine alkali basalts large amounts of phenocrysts Cpx are titansalite, but a few are titanaugite: En 36.2-48.0, Fs 6.8-17.0, Wo 38.7-50.2. The majority of groundmass Cpx are Ca-rich salites, while augites are very rare: En 36.2-48.0, Fs 6.8-17.0, Wo 42.0-47.0. Most of them can be designated as titanaugite. In basanite, both phenocrysts and groundmass Cpx are mainly Ca-rich salite. Phenocrysts are of En 28.2-52.0, Fs 4.7-16.3, Wo 38.1-55.7. The end member constituent Cpx in K-rich basalts are similar to pyroxenes in alkali basalts, phenocryst Cpx are: En 38.9-59.2, Fs 8.0-16.3, Wo 38.1-47.5; groundmass: En 34.8-48.2, Fs 10.0-17.1, Wo 41.8-49.4.

DISCOVERY OF 1T-LIZARDITE WITH CYCLICAL TWINING IN KIMBERLITE

WANG Gongqing, Changchun College of Geology, Jili; HUANG Yuzhu, 3rd Institute of Nuclear Industry Ministry, P.O. Box 764, Beijing; LIU Wei, Beijing Institute of Physics, Academy of Sciences, Beijing, People's Republic of China

In kimberlite, lizardite of this kind is an accessory mineral. They are often in stout prismatic habit and elongated parallel to a-axis with grain size ranging from 0.1 to 0.4mm. This mineral frequently makes twins after the following laws: 1) with (034) as twin plane in result of pseudohexagonal star-like cyclical twin; 2) simple contact twin with (001) as twin plane; 3) polysynthetic twins with a-axis as twinaxis and (001) as composition plane (fig.1.).

Chemical composition is determined at 11 points from 3 grains and 3 sets of x-ray image for each major element by microprobe analysis. The chemical formula for its average composition is: $(Mg_{5.39}Fe_{0.26}Al_{0.35})_{6.0}[(Si_{3.84}Al_{0.17})_{4.01}O_{10}](OH)_{7.1}$. Here, the amount of OH was estimated according to the data of thermo-analysis. The center of lizardite crystal contains more Mg, Al, and outer zone—more Fe, Si.

The indentation hardness of them is 81.8-97.5 Kg/mm². And its refractive index is Ng≈Nm= 1.5732, Np=1.5685. They are usually characterized by obvious zonal structure (fig.1) and more uniform, not undulatory extinction. The center of crystal shows uniaxial negative with gray to black interference color; while middle and outer-zone of them is biaxial positive ($-2V=0-6^{\circ}$), with light yelloish to white interference color. From middle zone to outer zone, the extinction angle

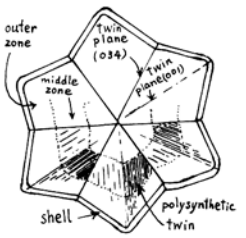

Fig.1. Twin and zonal structure of Lizardite. (Cross section).

A MINERALOGICAL STUDY OF AMBER IN THE XIXIA REGION OF HENAN, P.R.C.

Wang Huishu
Deputy Director of Geology Department
Xi'an Mining Institute, P.R.C.

Abstract

The ambers occur in the red sand-conglomerate formation of the upper section of Mesozoic group (K_2^3) in the Xixia region of Henan province are lenticular, striped or irregular. Their volume is about several dozen cubic centimeters, ranging from several cubic metres to several cubic millimetres. the rocks associated with them are quartzite, siliceous rocks and gravels of metamorphic rock.

They are white, yellow, orange, red and reddish brown in colour. The refractive index is N = 1.5426 - 1.5549 and the reflectance is $\bar{R}m$ = 0.2%. The ambers irradiated with ultraviolet light can show light blue, dark blue or grey fluorescent light. The microhardness is H = 22.96 - 31.27 and the specific gravity is d_{20}^{20} = 1.113. Both N、H、d and fluorescence colour will rise with the darkening of the ambers.

When the amber is magnified by an electron micro - scope 3,000 - 4,000 times, it shows honeycomb structure. When magnified 15,000 to 55,000 times, it consisted of a group of gel grain, like a pistil. When it was 60,000 times, it changes into an aggregate consisting of pisolitic gel-grain.

The infra-red spectra of amber shows that the main framework of the amber is of fatty compound structure and it includes a large number of carboxyl and a small number of ester, alcohol, ether and other oxygenated structures besides hydroxyl. According to the results from the TLC and LC method, element analysis, measuring of melting point and molecular weight the main composition of the amber is succinic resin acid (47.3 - 87.3%) succinic eseralcohol (1.2 -17.0%), succinic abietic acid (10.4 - 25.3%), succinic oil (1.6 - 6.7%).

From element analysis and X-fluorescence spectrum analysis the carbon content of amber is 75.32 - 84.00%, hydrogen 9.92 - 11.38%, oxygen 2.69 - 6.28%, nitrogen 0.067 - 1.80% , sulphur 0.24 - 0.44%. The chemical molecular formulas of various ambers have been deter - mined. The proportion of C:H:O in the experiment formula is about 2n:3n:m ('n' and 'm' are differential constants). Among them the oxygen content has a greater change. If m = 1 then the simplified chem - ical formula is $C_{2n}H_{3n}O$. This formula should be the general chemical formula for amber.

It has been found that amber in sand-conglomerate in the Xixia region is rich in C, H, and S. It is poor in O, N, and Fe. Amber however in coal in Fushun, Liaoning province, indicates contrary data.

According to the proximate analysis of the amber, both the water content (0.36 - 0.38%) and the ash content (0.12 - 0.22%) of light colour amber are lower; but, the volatile matter (99.06 - 99.08%) is greater and has no residue. On the contrary, both the water content (1.16 - 1.78%) and the ash content (1.34 - 9.16%) of dark colour amber are greater, but the volatile matter (85.54 - 95.36%) is relatively lower. The reason which causes the above mentioned slight difference is the diversity in the original material, plant community, forming process and the metamorphic grade, etc.

In order to ascertain the origin of amber, we subjected them to infra-red analysis and find that abietyl has close relevance to amber. We hold that it is the oxidization which makes the carbon chain in abietic resin acid shorten, even break and transform abietic resin into petrified amber acid. So, abietyl acid is the original substance in the formation of amber.

The amber in the Xixia region was transported in company with the sand and gravels. The sediment which contains the amber is the river facies. The amber found here is of a rare genetic type.

• GENETIC MINERALOGY STUDY OF PYRITE

WANG Kuiren and YANG Haitao, Department of Earth and Space Sciences, University of Science and Technology of China, Hefei, People's Republic of China

Pyrite is one of the most common minerals which exhibit wide variation of properties depending on the different modes of occurrences, so it is a very important mineral to direct the genesis of ore deposits and rocks. Having collected 115 samples of pyrite from different provenances, such as gold ore, Pb-Zn sulfide deposits, volcanic Cu-Pb-Zn deposits, sedimentary rocks and metamorphic rocks, we made some analyses of pyrite including trace element chemical analysis, electron microprobe analysis, unit cell parameter, mid-far infrared absorption spectra, Mossbauer spectra, reflectance spectra, and scanning electron microscope analysis of morphology and surface microtopography. The main results are as follows.

The contents and distribution of trace elements in pyrite are very important geochemical directors to solve the problems of the genesis of ore deposits and can tell the conditions of physical-chemistry and the background of geochemistry. The distribution of trace elements in pyrite has relation to the degree of metamorphism. It can be found that the contents and distribution of trace elements are different in pyrite from different parts of the same ore body. This may be related to the history of the ore deposit. The value of the unit cell parameter of pyrite increases with Co, Ni and As contents. The results of mid-far infrared absorption spectra suggest that one of the characteristic absorption bands is related to the lattice vibration. In a few samples of pyrite, the absorption band showed a double peak. The parameters of Mossbauer spectra of pyrite showed characteristic variation. They are related to Co and As contents. In a few samples, the reflecting anisotropy has been found. It may be related to the following parameters: temperature of mineral formation; pressure which the mineral suffered; composition of the mineral, etc. Scanning electron microscope analysis of surface microtopography of pyrite gives much information about the crystal growth procedures. The results of SEM analysis suggest that the mechanism of crystal growth of pyrite is two-dimensional nucleation and layer-by-layer growth. This is consistent with the theoretical analysis of crystal growth. Therefore, the morphology of pyrite and its variation with crystal growth procedure can also be explained using the above suggestion. Recently, the variation of crystal habits of pyrite and its features of microtopography have been noted by many mineralogists.

In summary, through studying the properties of pyrite and its variation, much information about the genesis of minerals, ore deposits and rocks can be obtained; therefore, many mineralogists and geochemists have paid more attention to this important sulfide mineral, pyrite.

AN INTRODUCTION TO A HANDBOOK OF "SYSTEMATIC MINERALOGY" IN CHINA

Wang Pu, Pan Zhao-lu, Wong Ling-bao, Chen Dai-zhang, et al, Research Gr. of Mineralogy, Beijing Graduate School of Wuhan College of Geology, 29 Xueyuan Road, Beijing, China

In writing this handbook of "Systematic Mineralogy" the primary aim has been to provide a work of reference useful to advanced students and research workers in mineralogy and related sciences. This book consists mainly of two parts, general mineralogy and systematic mineralogy. The former includes an elementary knowledge of chemistry, crystal structure, morphology, physical properties and genesis of minerals and the latter is the main body including the descriptions of all of the minerals systematically in this book.

Based on the redefinding concepts of mineral, mineral species, subspecies and variety, we collected almost all of the mineral species which were known at the end of the year 1979, and described them in several aspects, such as chemical composition, crystal structure, morphology, physical properties, characteristics under microscope, diagnosis, occurrence and uses of minerals. There are about 2740 minerals of independent species together with subspecies which belong to the end member of isomorphic series, meteorite and lunar minerals, amorphous minerals and organic minerals.

The classification used in this book is essentially based on the system of crystal chemical classification by Povarennykh, in which we have made some revisions and supplements.

This book is divided into three volumes. The first volume includes an introduction, general mineralogy and a part of systematic mineralogy including native element, sulfide, oxide, and hydroxide minerals. The silicates are gathered in the second volume. The third one includes all of the oxysalts except silicates, and halides. In addition, there are appendices of new minerals approved in 1977 to 1979 by IMA commission on New Minerals and Mineral Names, meteorite and lunar minerals, amorphous minerals and organic minerals, and Chinese, English and Russian indices of mineral species and a chemical formula index at the end of this volume. The first two volumes was published successively in 1982 and1984 by Chinese Geological Publishing House and the third one will be published soon.

The completion of this book would have been impossible without the great achievements of very many workers in the world and the help and encouragements of many friends and publishers. Although they can not be mentioned here, they are none in the less remembered and thanked for their kindness. We would thank also the many authors whose diagrams and pictures have served as a basis for the illustrations and thus facilitated our task.

THE ASSEMBLAGE AND ENVIRONMENT OF AUTHIGENIC IRON MINERALS

WANG Qi and ZHU Erqin, Shandong College of Oceanology, Qingdao, People's Republic of China

[By title only.]

• ON THE SIMILARITIES BETWEEN ANISOTROPIC ROTATION AND REFLECTION ROTATION FOR OPAQUE MINERALS

WANG Shu, Geological Publishing House, Beijing, The People's Republic of China

A series of theoretical formulae for the anisotropic rotation and reflection rotation are systematically derived and discussed. They are

1. Equations of the reflectivities R_ψ and R_φ;
2. Equations of the anisotropic rotation angle $A_{r\beta}$ and the reflection rotation angle $R_{r\beta}$;
3. Equations relating the maximum values of $A_{r\beta}$ and $R_{r\beta}$ and the angles ψ and φ, respectively;
4. Equations of the apparent angle of anisotropic rotation A_r and the apparent angle of reflection rotation R_r;
5. Equations of the ellipticities $2\theta_\psi$ and $2\theta_\varphi$;
6. Equations of the reflectivities between crossed polars R_+ and r_+;
7. Equations of the reflectivities between uncrossed polars R_{+A} and r_{+A}.

The similarities between the anisotropic rotation and reflection rotation are demonstrated. The formulas of one type of rotation can be readily transformed into those of another type of rotation simply by exchanges between the related symbols. Whenever a new formula or a new application is proposed for one type of rotation, it can be immediately extended to another type because of the similarities between them. However, the formulas of the two types of rotation, though identical in their forms, are essentially different in their physical significances.

Optical phenomena in polarization figures can be quantitatively interpreted by these formulas of the reflection rotation introduced and demonstrated for the first time by the author.

• ON THE TYPOMORPHIC PECULIARITIES OF WOLFRAMITE

WANG Shunjin, Department of Geology, Wuhan College of Geology, Wuhan, Hubei, 430074, People's Republic of China

The typomorphic peculiarities of wolframite and other associated minerals (such as scheelite, cassiterite, beryl, arsenopyrite, muscovite, feldspar, quartz) of many tungsten mineral deposits from the Nanling Mt. range of S. China have been studied in detail by means of chemical analysis, scanning electron microscope, atomic absorption spectrometry, X-ray analysis, infrared spectra, etc.

The existence state of Fe, Mn and minor elements in the wolframite of Dajishan and Yaoganxian tungsten deposits is discussed. Some elements are homogeneously distributed (Nb, Ta, Y, Sc, Mo, Co, Zn) as shown in a photograph of the scanning electron microscope, but a few elements (Ca, Al) are distributed heterogeneously. By combination of X-ray powder diffractometry and EMP, inclusions of plagioclase (Ca and Al) and scheelite (Ca) in wolframite have been found. Ca and Al are homogeneously distributed in the area other than the inclusions. Many kinds of elements in wolframite (Nb, Ta, Mg, Sc, Mo, Co, Zn) are parts of solid solution; for example, W is replaced by Nb, Ta and Mo. Fe and Mn are replaced by Mg, Y, Sc, Co and Zn. A few elements (Ca and Al) are contained in inclusions and/or in wolframite (Fe and Mn are replaced by Ca and Al).

The zonal structure in wolframite from vein #6 of Dajinshan was found in 1983 by the author. The crystal of wolframite has nine zones, and its content of iron is respectively as follows: 100, 21.28, 46.81, 8.51, 91.49, 6.38, 66.38, 17.02, 31.91. Wolframite of Yaoganxian has zonal structure, too, which was revealed by electron probe microanalysis (see the figure).

The variations of value of Mn/Fe and the contents of Nb, Ta, Sc in wolframite are caused by the genetic types, the formation temperatures, the chemical compositions of the intrusive bodies, the wall rocks and the associated minerals, the distance from the ore body to the intrusive.

The wolframite of porphyric type is mainly ferberite, and the wolframite relating to granitic rocks ranges from huberite to ferberite. The intermediate members of $FeWO_4$-$MnWO_4$ solid solution have a wide-ranging distribution. It is bound up with the chemical composition of granitic rocks. Generally speaking, the value of Mn/Fe of wolframite is inversely proportional to formation temperature. This conclusion has been proved by geochemistry, crystallochemistry, crystal field theory, and thermodynamics.

When the wolframite is associated with iron-sulfide, its value of Mn/Fe will rise. For instance, the value of Mn/Fe of wolframite is 0.62 for W-type, 0.72 for W-Mo type, 1.10 for W-Sn-S type, and 1.61 for W-S type.

The paragenetic association of minerals exerts tremendous influence on the content of Nb,Ta in wolframite. For example, the value of Nb/Ta rises when the wolframite is associated with cassiterite.

The relations between specific gravity and chemical composition of wolframite from Nanling could be summarized as follows:

(1) The value of Mn/Fe of wolframite is inversely proportional to the specific gravity.
(2) The value of WO_3 in wolframite is directly proportional to the specific gravity.
(3) The other elements (such as Nb, Ta and Sc) affect the specific gravity of wolframite.

In addition, the hardness of wolframite is related to the content of $MnWO_4$. X-ray powder diffraction analysis shows that the MnO/FeO has positive correlation with d(400) of wolframite. The d(111) is related to Ca.

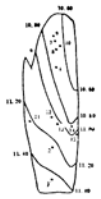

Figure. Zonal structure of wolframite from Yaoganxian, single crystal. The number shows the content of FeO in wolframite.

•THE CRYSTAL STRUCTURE OF QITIANLINGITE, $Fe_2Nb_2WO_{10}$

WANG Su, PENG Zhizhong, and MA Zhesheng, Beijing Graduate School, Wuhan College of Geology, Wuhan, People's Republic of China

Qitianlingite, $Fe_2Nb_2WO_{10}$, from Mount Qitianling, Hunan province, China, is orthorhombic, Pbcn, with a = 23.706, b = 5.723, C = 5.045 Å and Z = 4. The structure was solved by the direct method and refined by the full-matrix least-squares method using anisotropic temperature parameters. The final residual R is 11.09% for 531 reflections collected on a four-circle diffractometer. The structure type is α-PbO_2. There are three kinds of octahedra (Fe-O, Nb-O, W-O) in the structure. Each kind of octahedra shares two edges to form staggered chains parallel to the c-axis. The chains are ordered, being combined by shared corners. Mean octahedral cation-oxygen distances are Fe-O = 2.122, Nb-O = 2.013, W-O = 1.954 Å, respectively.

The structure of qitianlingite can be looked upon as a superstructure of ixiolite. The three kinds of octahedra are ordered in the direction of the a-axis. The relationship of the unit cells between qitianlingite, columbite-tantalite, wodginite and ixiolite is shown as follows:

axis (Å)	Ixiolite	Columbite	Qitianlingite	Wodginite
a	4.74	3 x 4.75	5 x 4.74	2 x 4.76
b	5.73	5.73	5.723	2 x 5.73
c	5.16	5.08	5.045	5.10
ß	90°	90°	90°	90.3°
S.G.	Pbcn	Pbcn	Pbcn	P2/c

References

J. Graham and M.R. Thornber (1974) The crystal chemistry of complex niobium and tantalium oxides. American Mineralogist, 59, 1026-1044.

Peng Zhizhong (1985) New achievement in structural mineralogy. Part 8. Cuptal structure of oxide minerals in view of close packing of oxygen anion. "Scientific and Technical Information of Geology," No. 2, 55-63.

GLAUCONITES IN THE NORTHERN SOUTH CHINA SEA

WANG Tianxin and SU Guangqing, South China Sea Institute of Oceanology, Academica Sinica, Guangzhou, People's Republic of China

[By title only.]

A STUDY ON THE EQUILIBRIUM GROSSULAR + CLINOCHLORE = 3 DIOPSIDE + 2 SPINEL + 4 H_2O

Wang, X and Greenwood, H.J., Department of Geological Sciences, University of British Columbia, Vancouver, British Columbia, Canada V6T 2B4

The equilibrium grossular + clinochlore = 3 diopside + 2 spinel + 4 H_2O was investigated using cold seal pressure vessels from 500°C to 700°C at 0.5 kilobar to 4.0 kilobars. All phases used in the experiments were synthesized from oxides. Good brackets with assemblages diopside + spinel or grossular + clinochlore were made at conditions far from the equilibrium. Unusual assemblages diopside + clinochlore were found at conditions close to the equilibrium over the entire pressure range. The only possible solid solution phase is diopside. X-ray refinement demonstrates that the cell parameters of the diopside are well within the range for pure diopside and Ca-Tschermak pyroxene. Scanning electron microscope and electron microprobe analyses showed that these diopsides contain aluminum interpreted as substitution of both Ca-Tschermak and Mg-Tschermak pyroxene. This interpretation satisfies the mass-balance requirements of these assemblages. Thermodynamic calculation using reduced diopside activity in clinopyroxene showes significant shift in the equilibrium curve. Comparison of experimental results with natural minerals results in contradiction. Natural diopsides (clinopyroxene) found in similar assemblages at similar conditions contain much less aluminum.

EVOLUTION OF K-FELDSPAR IN THE RED CROSS LAKE PEGMATITIC GRANITE AND ITS PEGMATITE AUREOLE, NORTHEASTERN MANITOBA, CANADA

WANG,X.J., ČERNÝ,P., CHACKOWSKY,L.E. and EBY,R. Department of Geological Sciences, University of Manitoba, Winnipeg, MB R3T 2N2 Canada

The Red Cross Lake pegmatite field is located in the Oxford Lake greenstone belt of the Sachigo Subprovince, in the northeastern part of the Archean Superior Province of the Canadian Shield. A granite-pegmatite suite was emplaced into an early expression of an ESE-trending shear zone coaxial with the greenstone belt, close to an offsetting N-S fault. The suite consists of a highly fractionated and moderately to strongly sheared pegmatitic granite (PGG) adjoined by non-sheared, barren tourmaline-bearing pegmatites (TPG) and extremely sheared to mylonitized complex pegmatites of the lepidolite type (LPG). This latter pegmatite type also carries spodumene (probably secondary after petalite), schorl to rubellite, pollucite, beryl, amblygonite, manganotantalite, wodginite and microlite.

Potassium feldspar shows a more or less continuous geochemical evolution from PGG to LPG, with K, Rb and Cs increasing and Na, Ba decreasing (Figure 1; averages of the 3 groups in Table 1). Fractionation of Rb and Cs in LPG K-feldspar reaches the most extreme levels ever encountered (K/Rb 1.90, K/Cs 22.4, Rb/Cs 2.55).

Structural state of the K-feldspar is highly ordered, with 0.95 Al in T_{1o}. In the PGG and in part also in the LPG that were affected by shearing, ordering of Al in the K-feldspar seems to follow the direct single-step path from(T_{1m}, T_{2m}, T_{2o}) to T_{1o}. In the non-sheared TPG and in part also in the sheared LPG, the two-step ordering process is indicated: from (T_{2m}+T_{2o}) to (T_{1m}+T_{1o}) and subsequently to T_{1o} alone (Figure 2).

The data suggest that moderate Rb,Cs contents (1 wt.%; e.g., in the TPG feldspars) do not retard ordering, particularly in the first step. However, high Rb,Cs contents (1 wt.%; e.g., in the LPG feldspars) may retard the ordering, particularly during the second stage. The data support the conclusion that high Rb,Cs contents may retard ordering in K-feldspar but are not a primary controlling factor.

The only exception to the above relationships is a late sanidine-type adularia, which replaces augen of pollucite and contains only minor substituents.

Table 1

	PGG	TPG	LPG
Or(%)	75.4	80.9	85.8
Ab(%)	23.6	18.6	13.4
An(%)	1.0	0.5	0.8
K(wt%)	8.58	9.34	8.56
Na(wt%)	1.58	1.28	0.79
Rb(ppm)	903	5089	20255
Cs(ppm)	52	340	3512
K/Rb	95.0	18.4	4.3
Ca(ppm)	1186	619	867
Sr(ppm)	82	52	167
Ba(ppm)	862	339	174
Sr/Ba	0.10	0.15	0.96

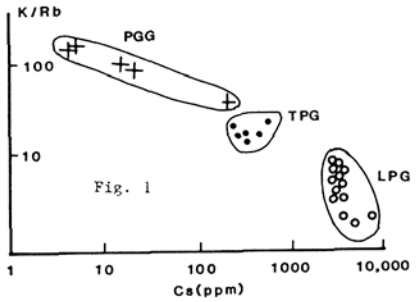

Fig. 1

Fig. 2

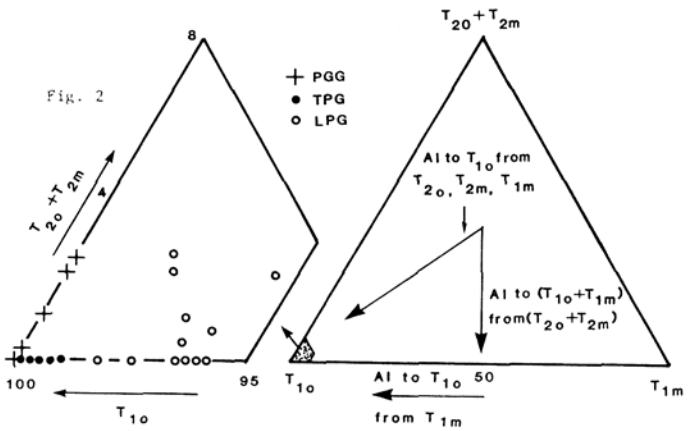

•THE CHARACTERISTICS OF GALENA FROM THE MENG'EN Ag-Pb-Zn DEPOSIT AND ITS SIGNIFICANCE IN THE STUDY OF ORE GENESIS

WANG Yinxiang, Institute of Mineral Deposits, Chinese Academy of Geological Sciences, Baiwangzhuang, Beijing, People's Republic of China

Galena is known as a major economic mineral in Ag-Pb-Zn deposits as well as in Pb-Zn deposits. Quite a number of minor elements it contains can find their application not only in comprehensive utilization but also in the study of ore genesis. The properties of galena in Ag-Pb-Zn deposits and its significance in ore genesis are discussed. They are exemplified by the Meng'en Ag-Pb-Zn deposit in comparison with the data acquired from several Pb-Zn deposits, such as the Shuicaoping deposit in Fankou County, the Dabaoshan deposit in Shaoguan County, Guangdong Province, the Taolin deposit in Hunan Province, and the Zhongsai deposit in Anyuan County, Jiangxi Province, as well as some other mesothermal deposits occurring in siliceous rocks.

The Meng'en Ag-Pb-Zn deposit is confined to a nearly E-W trending brush structure with the ore bodies occurring in clusters in the middle of Late Hercynian biotite plagioclase, granite and muscovite grandiorite. It has sphalerite, galena and seven silver-bearing minerals, namely, pyrargyrite, canfieldite, freibergite, native silver, argentite, pyrostilpnite and miargyrite, as the major economic minerals associated with certain amounts of chalcopyrite, pyrite, magnetite, stannite, arsenopyrite, cassiterite, etc.

The specific gravity (7.6), hardness (54-67 kg/mm^2 by loading 10, 20, 50 and 100 g respectively) and reflectivity (43.76 at 480 nm, 41.01 at 546 nm, 41.69 at 589 nm and 40.46 at 656 nm) of galena in this deposit are lower than those of an ordinary galena. The content of minor elements has been obtained through the bulk analysis of some selected representative samples of galena. Of these elements, Ag = 0.75, Sb = 0.50, Ti = 0.01, In = 0.003 and Sn = 0.72 (wt %), which are apparently high compared with their concentrations in galenas from the above-mentioned well-known Pb-Zn deposits in China.

A great variety of silver minerals exists in large quantities in this galena. Of the seven silver-bearing minerals, the first five were recognized by the author under reflected light while the last two were identified by microprobe analysis (Guilin Institute of Rock and Mineral Analysis and Beijing Institute No. 3).

To sum up, galena in the Meng'en Ag-Pb-Zn deposit differs from those in ordinary Pb-Zn deposits not only in physical and optical properties but also in its obviously high content of some minor elements, especially silver, which is present in large amounts as various silver-bearing minerals mosaicked in the galena. All the characteristics peculiar to Ag-Pb-Zn deposits may be of some help in the search for silver deposits.

To understand the genesis of the deposit, the Cd contents in the associated galena and sphalerite collected from orebody No. 4 of this deposit were first determined through chemical analysis to be 0.002% and 0.21% respectively, then the ore-forming temperature was calculated by the empirical formula of W.E. Rose to be 235±20°C. This temperature, in combination with the occurrence pattern, has led the author to believe that this deposit is of a mesothermal, fissure-filling, Ag-Pb-Zn polymetallic type.

EVOLUTION OF THE SOLAR SYSTEM: FROM DUST TO PLANETS.

WÄNKE, H., Max-Planck-Institut für Chemie, Mainz, F.R.Germany.

The chemical and isotopic composition of the solar nebula from which Sun and planets have been formed is well known from spectroscopic measurements of the Sun and from the analyses of the most primitive meteorites, the carbonaceous chondrites type 1 (C 1) which contain all condensable elements in solar abundances. The solar nebula was heated during its collapse. However the temperatures reached in various parts are highly uncertain.

Compaction of the dust led to larger and larger planetesimals as intermediate bodies between dust and planets. The different densities of the inner planets are evidence for differencies in their composition (uncompressed densities: Mercury=5.3;Venus=3.96 Earth=4.07 and Mars=3.73). Venus, Earth and Mars can be modelled by assuming a C 1-composition except for the most volatile elements. Varying abundances of oxygen, leading to different Fe(metal)/FeO ratios can explain the density differences. However the density of Mercury seems to require a drastic increase of the Fe/Si ratio relative to the C 1-value.

The K/U ratio remaining unchanged during crust - mantle fractionations of the Earth, Venus and Mars (known from measurements of lander missions) indicates severe depletion of the moderately volatile element K relative to U and the C 1-ratio. The only plausible explanation is depletion of K due to its higher volatility; the temperature required is about 1000 K. Much higher temperatures are reached during the accretion of planets, however it seems likely that this depletion took place either in the solar nebula or in planetesimals from which the planets formed.

The depletion of all more volatile elements which in the Earth's mantle have in fact similar abundances as the moderately siderophile elements led to the two component model for the formation of the Earth (1). The striking depletion of Mn, Cr and V not to be explained by volatility and the high abundance of Ni and Co indicates that the Earth's mantle was never in equilibrium with a pure metal phase (core). Hence, inhomogeneous accretion of the Earth is suggested (2). Accretion of the Earth started with highly reduced material free of all elements more volatile than Na, but all other elements in C 1-abundance ratios. Iron and all siderophile elements as metals, Si partly as metal, Cr, Mn and V as metals or sulfides. Component A.

After accretion of about 2/3 of the Earth - segregation of the metal phase, simultaneous to accretion - more and more oxidized material (Fe, Ni, Co, etc. as well as all other siderophile and lithophile elements as oxides) was added containing all elements (including volatiles) in C 1-abundances. Component B.

The same highly peculiar composition as observed for the Earth mantle - unexpected high abundances of Ni and Co and depletion of Mn, Cr and V - was found for the Moon. Hence, a close genetic link between Earth and Moon is the unavoidable consequence. The most plausible origin of the Moon is impact-induced evaporation of the Earth's mantle material (3). After recondensation the Moon can be formed in orbit around the Earth in a time scale fast enough to account for the lunar magma ocean.

Aside the samples from the Apollo and Luna missions, we have lunar samples also in form of a number of meteorites recently discovered in Antarctica. Even more exciting are the SNC-meteorites which with almost certainty are samples from Mars. Their young crystallization ages and the trapped Martian atmosphere (4) being the most decisive evidences. Hence, it is possible to estimate the bulk composition of Mars to a high degree of certainty. From these data it became evident that Mars was formed from the same two components as the Earth. While for the Earth the mixing ratio of component A/component B was 85:15, a ratio of 60:40 was found for Mars. Contrary to the inhomogeneous accretion of the Earth, Mars accreted homogeneously (5).

Component A obviously formed mainly at and inside the orbit of the Earth, while component B was formed in the region of the asteroidal belt. Mars located just at the transition of the region dominated by component A and the region dominated by component B was fed from both components simultaneously and in approximately equal proportions. In the case of the Earth and Venus material of component B was added only at a late phase of the accretion as the transfer of material from the region outside of Mars' orbit required additional time.

(1) Ringwood AE (1979) Origin of the Earth and Moon. Springer.(2) Wänke H (1981) Phil.Trans.R.Soc.Lond.A303,287. (3) Hartman WK & Davis DR (1975) Icarus 24,504.(4) Pepin RO (1985) Nature 317, 473 (5) Dreibus G. & Wänke H. (1984) Proc.27th Int. Geol. Con.,11,1.

X-RAY METHODS FOR STRUCTURE DETERMINATION IN NON-CRYSTALLINE MATERIALS

WAYCHUNAS, G. A., Centet for Materials Research, Stanford University, Stanford, CA 94305, USA

Large angle X-ray scattering (LAX) studies have provided much of the information on the atomic arrangements in non-crystalline materials. This derives from the relative ease of application and the excellent results obtained with standard laboratory X-ray sources. However, new X-ray techniques may offer advantages over LAX work, either because of their larger sampling in k-space, or their greater selectivity for the local structure about particular atoms. A hypothetical example of a Fe-silicate glass which illustrates the k-space sampling differences between these methods is shown in the figure.

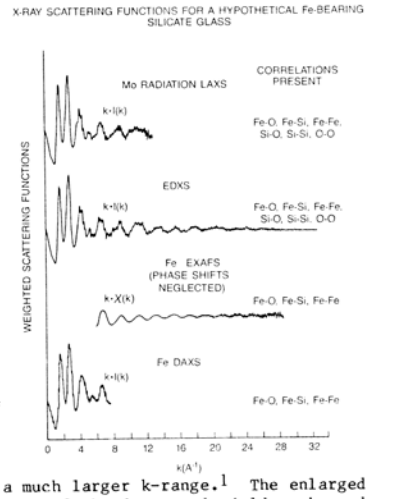

In the standard LAX method, the scattering interference function contains the information for all pair correlations and is thus quite complex. For a low-Fe glass, the Fe-X correlations make only small contributions to the total scattering, and are thus partially obscured by the other atom-atom correlations. Also, k-space oscillations continue up to the limit in k, possibly creating termination difficulties during Fourier analysis.

In contrast, the use of energy dispersive X-ray scattering (EDXS) allows the same scattering function to be collected over a much larger k-range.[1] The enlarged k-range can improve processing of the data, and yields enhanced resolution in the resulting transform (RDF). This method is also useful for applications where a diffractometer cannot be used, e.g., with a high temperature or diamond anvil cell, since only a few scattering angles are needed.

Analysis of the individual atom extended X-ray absorption fine structure (EXAFS) spectra can also provide an interference function.[2] The function contains only effects of pair correlations of the absorber atom with its neighbors. Hence, Fe EXAFS for the glass would only contain Fe-X correlation information. Particularly for nearest neighbors, this greatly simplifies the resulting RDF over that obtained from LAX or EDXS methods. The k-range of EXAFS is also excellent, yielding high resolution of interatomic distances, but small k-values are unobtainable. This low k truncation has serious effects on the analysis of disordered materials. For example, the longer bond distances in a non-Gaussian distribution of bond lengths may be partially lost from the EXAFS, creating apparently "contracted" bonds and reduced coordination numbers. However, EXAFS can be collected for any atom, so that Si and O environments can also be directly explored in glasses, although synchrotron radiation sources are usually necessary.

The newest method is that of differential anomalous X-ray scattering (DAXS). It involves collecting LAX data at X-ray energies both near and far from an absorption edge of one of the constituent atoms. The difference between the interference functions, properly normalized, contains only scattering information involving the particular atom.[3] The DAXS interference function is thus like the EXAFS function, but samples only the lower k range. The upper k value is limited by the specific atom's absorption edge energy. The low k data gives DAXS more sensitivity to long range correlations than EXAFS, but the short k-range decreases resolution in r-space. The methods are thus complementary.

Because of their selectivity, DAXS and EXAFS can be applied to study the environments of dilute species in non-crystalline matter. Due to its ability to sense long range correlations, DAXS should be of special importance for the study of complexes in aqueous solutions.

1. Egami, T., J. Appl. Phys., 1979, 50(3), 1564-1569.
2. Waychunas, G. A., Brown, G. E., Jr., and Apted, M. J., Phys. Chem. Minerals, 1986, 13, 31-47.
3. Fuoss, P. H., Eisenberger, P., Warburton, W. K., and Bienenstock, A., 1981, Phys. Rev. Lett. 46, 1537.

ALUMINUM-27 AND SILICON-29 NMR SPECTROSCOPY OF MIXED-LAYERED ILLITE/SMECTITES

WEISS, C.A., JR.; KIRKPATRICK, R. J., Dept of Geology, University of Illinois at Urbana-Champaign, Urbana, IL 61801, USA.

Silicon-29 and Aluminum-27 solid state MASS NMR Spectroscopy of natural and synthetic mixed-layered Illite/Smectites provides local structural information not obtainable by diffraction methods. The silicon-29 spectra contain resolvable peaks for smectite-like sites and muscovite-like sites. The smectite-like sites in these mixed-layered phases are dominantly Q^3(0Al) and resonate at ∿-94 PPM relative to TMS. This chemical shift is essentially the same as that of tetrahedral aluminum-poor smectites (montmorillonites) and is significantly more shielded than that of the Q^3 (0Al) sites of more tetrahedral aluminum-rich smectites such as beidellites (∿-92 PPM). Muscovite-like sites include Q^3 (0Al), Q^3 (1Al), and Q^3 (2Al) sites with resonances of ∿-89.5, -86.5, and -83.0 PPM. There is a well defined negative correlation between the % illite as determined by X-ray diffraction and the relative area of the peak fit for smectite Q^3 (0Al) site (Figure 1).

Aluminum-27 MASS and Static NMR at high field (11.7 T) resolves peaks for both tetrahedral aluminum (∿70 PPM relative to $AlCl_3$) and octahedral aluminum (∿0 PPM), but does not distinguish between aluminum in smectite layers and in illite layers. There is a correlation between the % illite layers determined by X-ray diffraction and the relative amount of tetrahedral aluminum, and at this field, quantitative Al(4)/Al(6) ratios can apparently be obtained (Figure 2).

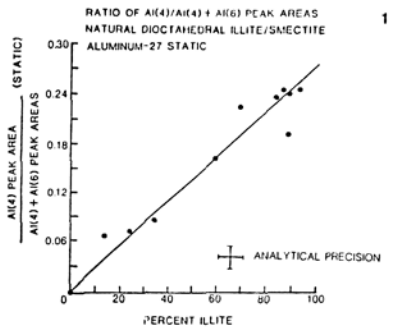

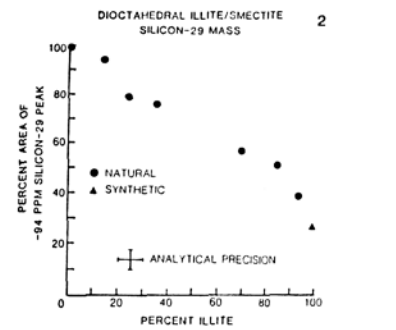

CATION DISTRIBUTION AND OXIDATION STATE OF IRON IN GLAUCOPHANE

Wirth, R., Werkstoffwissenschaften, Fachbereich 12.1/Bau 2, Universität des Saarlandes, D-6600 Saarbrücken, FRG;
Ying,Y., Institut für Kristallographie und Mineralogie, Universität Marburg, Lahnberge, D-3550 Marburg, FRG.

Glaucophane crystals from China and Europe have been investigated by microprobe analysis and Mössbauer spectroscopy. The two european samples have been separated from glaucophanites and eclogites from the Sesia-Lanzo Zone (Italian Alps). The Sesia-Zone is a tectonic and petrographic unit in the Western Alps bordered to the SE by the Ivrea Zone and to the NW by the Piemonte Zone. During an Early Alpine event, the Sesia unit was overprinted by high-pressure metamorphisme owing to a subduction process. Despite of the geochemical differences of the glaucophanites and Eclogites the glaucophane crystals of both rocks exhibit no different cation distribution and no change of the oxidation state of the amphiboles.

Alkali amphiboles of the glaucophane type usually contain between 5 and 15 wt% FeO and between 1 and 6 wt% Fe_2O_3. In principle, Fe^{2+} is expected to occupy the octahedrally coordinated M positions, while Fe^{3+} may occur at M and at the tetrahedral T positions in the crystal structure of amphibole, but the detailed cation distributions are often not known. The occupancy of M and T sites may be determined approximately from a combination of accurate microprobe analysis and Mössbauer spectroscopy of ^{57}Fe. For this, it is assumed that among the M positions, the trivalent cations Al^{3+} and Fe^{3+}, and the quadruvalent cations Ti^{4+}, can enter only M2. At M1 and M3, only bivalent cations occur.

We have studies samples of glaucophane from localities in Europe and China using microprobe analysis and Mössbauer spectroscopy of ^{57}Fe at 295 and 78 K. From a review of previously published and new data, the following conlusions are reached:

(i) The resolution of the Mössbauer spectra at 295 and 78 K is somewhat different. Independent evaluation of spectra taken at both temperatures allows to obtain an estimate of the error in the site occupancies.

(ii) There is no indication in our spectra for Fe^{3+} at T sites.

(iii) Fe^{3+} apparently occurs only at M2. It may be at that site in various proportions.

(iv) It is the M2 position which reflects the oxidation state of the amphibole. M2 may be completely filled by Al^{3+},Fe^{3+} and Ti^{4+} thus representing a maximum degree of oxidation. However, in certain glaucophanes, as much as 25% of M2 may be occupied by Fe^{2+}, thus representing a low oxidation state of the mineral. It would be of interest to study the relationship between the site occupancy of M2 and the amount of Iron at M1, M2, M3, and M4, as well as the relationship to the oxidation state of coexisting minerals in the glaucophane bearing rocks.

THE STATUS OF IXIOLITE

WISE,M.A. and ČERNÝ,P., Dept. of Geological Sciences, University of Manitoba, Winnipeg, MB R3T 2N2, Canada.

Since the formal recognition of ixiolite as a mineral species in 1963, this name has been applied to quite a few phases with widely variable chemical composition and, apparently, somewhat variable structural state. At first glance, all these phases have an orthorhombic unit cell corresponding to the basic columbite subcell Pbcn with a ~4.74, b ~5.73, and c ~5.15 Å, and a chemical composition derived from $(Fe,Mn)_{1.33}(Nb,Ta)_{2.67}O_8$ by appreciable R^{3+}, R^{4+} and/or R^{6+} substitution, yielding a general formula of $(Fe^{2+}, Mn^{2+}, Fe^{3+}, Sc^{3+}, Sn^{4+}, Ti^{4+}, Nb^{5+}, Ta^{5+}, W^{6+})_4O_8$. Upon closer examination, minerals collectively hiding under the term ixiolite reveal individual characteristics that contradict their assignation to one and the same species.

Graham and Thornber (1974) proposed to apply the name ixiolite to minerals close to the $(Fe,Mn)_{1.33}(Nb,Ta)_{2.67}O_8$ composition, which were termed "pseudo-ixiolite" by Nickel et al. (1963). These phases should be classified as disordered columbite-tantalites, as they correspond to columbite-tantalite in chemistry and convert to ordered columbite-tantalite on heating (with Pbcn unit cell dimensions equal to 3a, b, c of the columbite subcell).

The stannian ixiolite described by Nickel et al. (1963) seems to be the most common variety, with the dominant substitution of $3Sn^{4+}$ for $(Fe,Mn)^{2+} + 2(Nb,Ta)^{5+}$. However, all the 11 specimens from 5 localities we have recently examined (including the holotype from Skogböle, Finland) show slight monoclinic distortion in geometry as well as distribution of single-crystal XRD intensities. The XRD patterns can be interpreted on the basis of the monoclinic cell of wodginite (with C2/c cell dimensions equal to 2a, 2b, c of the columbite subcell; see Table 1 for examples). The monoclinic distortion is enhanced by heating which produces XRD patterns typical of more or less ordered wodginite (Ercit et al. 1984). This behavior of stannian ixiolite confirms the suspicion expressed by Nickel et al. (1963), Gorzhevskaya and Sidorenko (1974) and Černý (1975) that it may represent a disordered counterpart of wodginite.

No single-crystal XRD data are available at present for titanian ixiolite, which is a common exsolution product in niobian rutile and coexists with other Ti-saturated phases. In view of the existence of titanowodginite it could be expected that the structural and compositional features of titanian ixiolite may be analogous to those of the stannian variety.

Table 1.

	a	b	c	β
Skogböle (holotype)	9.481(3)	11.494(5)	5.158(2)	90°08'(2)
Skogböle "	9.475(4)	11.470(4)	5.157(1)	90°04'(2)
Yellowknife	9.489(3)	11.469(3)	5.154(2)	90°18'(2)
Lower Tanco	9.471(3)	11.426(3)	5.122(2)	90°17'(2)
Sweden	9.496(3)	11.432(4)	5.164(2)	90°47'(2)

Scandian ixiolite has Sc^{3+} and Fe^{3+} as major substituents, and it also contains some Zr and REE's. No rigorous single-crystal XRD data are available at present, and heating produces XRD powder patterns of the $Fe^{3+}NbO_4$-type wolframite structure. No ordered monoclinic analogs seem to be known that would approach the scandian ixiolite compositionally.

Wolframoixiolite typically shows W as the dominant substituting cation, and subordinate Ca and Zr. On XRD, some specimens clearly represent mechanical mixtures of columbite- and wolframite-type phases but others produce either columbite or wolframite patterns. The scarce heating experiments show a breakdown to an ordered columbite phase and a UTa_2O_8-type compound. It seems probable that most minerals currently lumped under the term wolframoixiolite correspond to different members, or assemblages, of the discontinuous columbite-wolframite series.

It is evident that the different types of "ixiolite" require further crystallochemical study and a review of nomenclature, coordinated with the systematics of the whole AB_2O_6-type family of Nb,Ta-bearing minerals. The examination of scandian, titanian and tungstenian ixiolites is currently in progress.

APPLICATION OF XPS TO WEATHERING IN MINERALS AND GLASSES

WHITE A. F., Geochemistry Group, Lawrence Berkeley Laboratory, University of California, Berkeley, CA 94720

X-ray photoelectron spectroscopy (XPS) is an important tool for characterizing natural and experimental weathering at ambient temperatures where reactions occur within tens to hundreds of Å of mineral and glass surfaces. Of particular importance has been recent advances in coupling aqueous weathering and dissolution data to surface chemistry using XPS. Studies of both experimentally and naturally reacted surface have discounted the previous held concept that weathering of crystalline silicates is controlled by diffusion transport through precipitated layers of Al or Fe hydroxide. (Holdren and Berner, 1979, Schott and Berner, 1983).

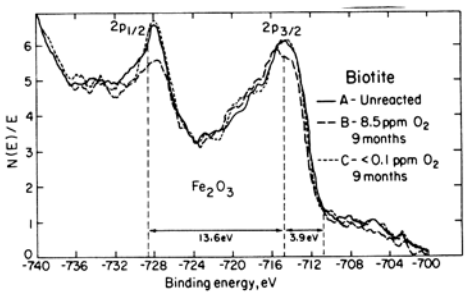

The similar Fe $2P_{1/2}$ - $2P_{3/2}$ XPS peak intensities for unreacted biotite and biotite that weathered under oxic and anoxic conditions in the above figure confirm a lack of a protective iron oxyhydroxide layer and support the general observation, based on XPS data, that silicate minerals weather principally by congruent dissolution. XPS can also furnish important data on redox processes during weathering of silicates. The electron bonding energies, indicating surface Fe(III) in the above spectra, can be contrasted to predominant Fe(II) release to the aqueous solution from biotite. Such a redox reaction can be explained by a coupled cation-electron transfer model (White and Yee, 1985) of the form

$$[Fe^{+2},K^{+}]_{silicate} + Fe^{+3} \rightarrow [Fe^{+3}]_{silicate} + Fe^{+2} + K^{+}$$

XPS studies involving the weathering of natural silicate glasses document greater near-surface cation mobility and solid state diffusion relative to crystalline silicates. Significant losses for example of cations from the surface of the glass fraction of the Mount St. Helens ash were demonstrated over a two year period following the eruption as shown in the figure below for Na.

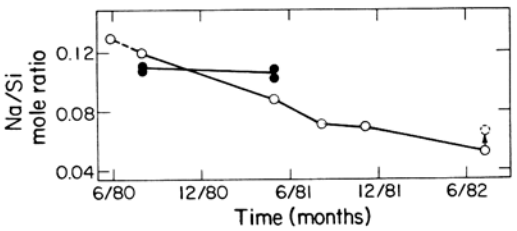

The solid points indicate a lack of Na loss from the bulk glass. Sputtering of the surface by an Ar^+ beam indicated that leaching occurred from depths > 100 Å.

The mobility of surface cations during weathering in glasses relative to crystalline silicates is a function of lower diffusion activation energies. Such energies calculated from Na diffusion obtained by XPS profiling in silicate glasses at 25 °C range from 75 to 100 K J. $mole^{-1}$ compared to reported energies in excess of 250 K J. $mole^{-1}$ for crystalline silicates such as albite.

Holdren, G. R. and Berner, R. A. (1979) Geochim. Cosmochim 43, 1164-1171.

Schott, J. and Berner, R. A. (1983) Geochim. Cosmochim 47, 2233-2240.

White, A. F. and Yee, A. (1985) Geochim. Cosmochim 49, 1263-1275.

RAMAN SPECTRA OF SILICATE MINERALS

WHITE, WILLIAM B., Materials Research Laboratory and Department of Geosciences, The Pennsylvania State University, University Park, PA 16802, USA

Raman spectroscopy is an inelastic light scattering experiment that permits the observation of specific vibrational modes on oriented single crystals or on bulk mineral grains. Systematic measurements have been made, for the most part on oriented single crystals, on many of the silicate structure types. Although much detail appears in individual mineral spectra and individual structure types, the most persistent features of the silicate spectra are a set of intense modes near 1000 cm^{-1} due to O-Si-O stretching motions and one or more bands in the range of 450 to 600 cm^{-1} due to Si-O-Si motions across the tetrahedral bridging bonds. Raman spectra of ordered silicates are sharp with band widths of only a few wavenumbers. Disorder due to defects or to random cation substitution such as Al/Si disorder tends to broaden the main Raman lines.

The wavenumbers of the O-Si-O bands shift from 850 cm^{-1} in orthosilicates to progressively higher values in ring silicates, chain silicates, sheet silicates, and framework silicates. This effect may be modeled by normal coordinate analysis of structural fragments that contain complete information on the polymerization of silicate tetrahedra but which are smaller than the full content of the unit cell. The intensities of the O-Si-O bands fall off with decreasing numbers of non-bridging oxygens in the structure and the most intense polarized component is lost in framework structures. The intensity shift can also be accounted for with structural fragment models. The Si-O-Si bridging bond modes shift to lower wavenumbers with increasing polymerization of the silica tetrahedra but the band retains its intensity. In sheet and framework silicates this is the most intense feature in the Raman spectrum. For poorly understood reasons, the sheet silicates, both clay minerals and micas, are extremely poor Raman scatterers although crystalline alkali metal disilicates which also have sheet structures give strong Raman scattering.

Substitution of AlO_4 tetrahedra into silicate structures produces mixed mode spectra rather than new bands specific to alumina tetrahedra. Bands shift to lower wavenumbers due to longer Al-O distances and therefore weaker force constants. Aluminum-silicon disorder produces a temperature-independent line broadening that scales with degree of disorder.

The Study of Time - Dependant Phenomena shown on the Kinetics of the Pressure induced Olivine - Spinel Phase Transition in Mg_2GeO_4

WILL, G. and LAUTERJUNG, J.
Mineralogical Institute of the University of Bonn, Bonn, West Germany

Synchrotron radiation combines high energies with high intensities. Using energy dispersive diffraction techniques this allows one to measure diffraction spectra in rapid sequence as fast as 1 second and thereby study the dynamics and kinetics of phase transitions in solids. We have developed two different modes of operation: one where we record the fully accessible spectra every minimum 45 seconds, and the other, the socalled window method, where we stay within a preselected energy window containing one reflection and pass along the channels in the multi channel analyzer with time. The minimal recording time here is 0.1 - 0.5 seconds.

We work at the DESY in Hamburg and we have applied these techniques the kinetics of the pressure induced phase transformation in Mg_2GeO_4 as a compound homologue to the mantle relevant mineral forsterite Mg_2SiO_4 of the olivine series. The experimental range in this case was 0 - 20 kbar and 800 - 1200 degree C. We have run 7 cycles through the olivine to spinel phase transformation at different p - T conditions with a total of 109 spectra. When we plott the observed intensities of the new spinel phase vs. time, the data can be fitted to the Avrami equation and from the coefficients in that equation the growth mechanism and thermodynamic quantities can be deduced. (Fig. 1)

Since we record the full spectra at every step with sufficient lines we can also attempt a structure factor calculation. Hereby analysis is done by profile fitting the diffraction lines and then to calculate or refine the crystal structure with our powder least squares program POWLS. With this method we can follow quantitatively the growth of the spinel phase with time. In the present study this method proved to be of sufficient accuracy to follow the cation distribution for Ge and Mg as they migrate into the oxygen frame with time.

The transformation, e.g. the crystallization of the spinel phase begins with the formation of a cubic close packed oxygen arrangement. After about 15 minutes reflection with contributions from the A- and B- sites can be observed.

In the course of this investigation we have also measured the thermal expansion of the olivine phase and the compressibility of both phases. The values obtained are: $K_0 = 746$ (7) kbar for the olivine phase and 1455 (20) kbar for spinel phase. The phase transition is accompanied by a density increase of 8.7 %.

With the window method the phase transformation of KCl from a fcc NaCl - type structure to the B2 CsCl - type structure was studied. This transformation occurs much faster within a few seconds.

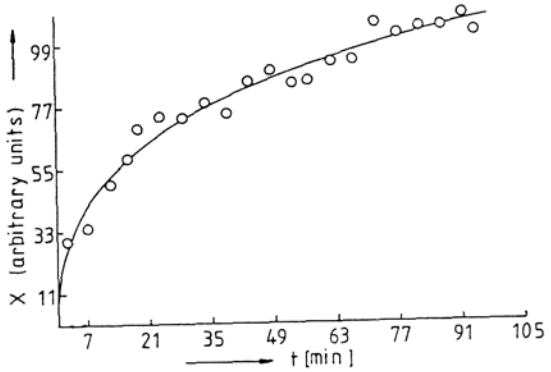

Kinetics of the phase transformation of Mg_2GeO_4 from the olivine to the spinel type phase. CONDITIONS: p = 28.7 kbar; T = 774 K. The solid line is calculated with the Avrami equation; coefficients are n = 1; k = 2.06

This work was supported by the Bundesminister fuer Forschung und Technolgie, Bonn, which is gratefully acknowledged.

OPTICAL, X-RAY AND MICROPROBE STUDY OF LOW PLAGIOCLASE SINGLE CRYSTALS: DISCRIMINANT ANALYSES OF DISCONTINUITIES

WOLFE, H. Edward, SU, Shu-Chun, RIBBE, Paul H. and BLOSS, F. Donald, Dept. Geol. Sci., Virginia Polytechnic Inst. & State Univ., Blacksburg, VA, USA

We have measured the refractive indices, optic axial angle $2V_z$, and optic orientation (by spindle stage methods), the chemical composition (by electron microprobe), the reciprocal lattice angle γ^* and, where available, the separation δc of the non-Bragg type 'e' diffraction maxima (using *x*-ray precession photographs), all on one and the same grain chosen from each of thirty plagioclase specimens whose geologic origins were considered to be "low temperature." Our intent was to gain further insight into the nature and composition of the discontinuities in physical properties and lattice parameters in low plagioclases.

Flexures in refractive index versus mol % An curves could be seen in the data of J.R. Smith (1960, *Geol. Soc. Am. Mem. 80*), and discontinuities were observed near An33, An50 and An90-95 by Doman et al. (1965, *Am. Mineral.*) in plots of refractive indices, $n\alpha$, $n\beta$, and $n\gamma$ versus γ^*, and γ^* and δc versus mol % An (as deduced from $n\alpha$ measured on the same grain). Although Burri et al. (1967, *book*) do not call attention to it, they show breaks near An30 and An50 in trends of optical migration curves, i.e., Euler angles Ψ, R, LA, Lα, and N, optical indicatrix axis Y, the X' direction in the plane perpendicular to [110], crystallographic directions [010], [001], $\perp$[001]/(010) and $\perp$(010), and normals to the planes (001), (021), (0$\bar{2}$1) and (110). Pronounced discontinuities near An33 and An50 are also very evident if unit cell edge lengths (especially **b** and **c**), angles (especially γ and γ^*), and such γ^*-related parameters as $2\theta_{131} - 2\theta_{1\bar{3}1}$, are plotted as a function of composition (Bambauer et al., 1967, *Schweiz. Min. Petr. Mitt.*; Kroll, 1983, *Rev. Mineral. 2-II*).

Not surprisingly, our optical and *x*-ray observations confirm these (see Figure A), and despite the additional effort to gather all data on each individual crystal, we seem only to have added to the data base. However, Figure B shows new $2V_z$ versus mol % An curves (those of Burri et al. are shown as dashed lines). We undertook discriminant analysis using the software packages of SAS Institute (1982) on our data and various combinations of these and other data sets from the aforementioned. Conclusions are as follows:

(i) Our data alone indicate that An30 and An45 are adequate points of discontinuity; however, the results of discriminant analyses on the various data sets show that there is no significant difference between An30 and An33 as the lower boundary. The migration curves of Burri et al. (1967) rather strongly suggest that An30 is the more preferred value, but their lack of precise chemical control leaves the matter still undecided.

(ii) For the upper boundary, An45 gives either no "misclassified" points or many less than are found if An50 is selected as the boundary, especially if $n\alpha$ and $2V_z$ are included in the discriminant analyses. However, if only lattice parameters and related quantities are included, no distinction can be made between An45 and An50.

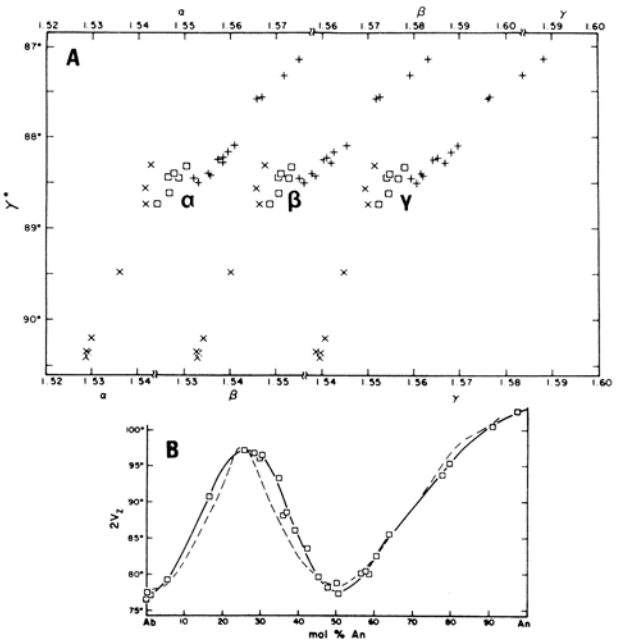

MINERALOGY OF FANKOU LEAD-ZINC DEPOSIT IN NORTHERN GUANGDONG PROVINCE, CHINA

Wong Ling-bao, Chen Dai-zhang & Wang Pu, Research Gr. of Mineralogy, Beijing Graduate School of Wuhan College of Geology, 29 Xueyuan Road, Beijing, China

The Fankou lead-zinc deposit is a famous and huge mine in China. It regionally lies between the Nanling granite belt and Quren basin in the northern Guangdong province, southern China , and locally occurs in the hanging wall, composed of Devonian --Carboniferous strata with drag syncline structure, of a major shear fault in NNW trending in the northern boundary of Quren basin.

The ore bodies controlled by a series of faults parallel to the major fault, their derivative fractures and bedding openings are in the shapes of stocks, layers, lenses and veins. Most of the ores possess deformation fabrics, we named them "tectonic ores". The main minerals such as sphalerite, galena, quartz and calcite except pyrite in the tectonic ores have their own preferred orientations.

The chemical characteristics of the main minerals in Fankou lead-zinc deposit are as follows: 1. The chemical compositions of pyrite, sphalerite and galena exhibit non-stoichiometry. There are sulfur deficiencies in most pyrite, and metal atoms deficiencies in sphalerite and galena. 2. The contents of Co, Ni, Se, Sb and Co/Ni ratio in pyrite are similar with that of the deposits of magmatic hydrothermal origin, but the contents of Au, Ag, Te and Bi are evidently higher than that of the related deposits. The high contents of Fe, Au, Ag, Te and Cd/Fe ratio in sphalerite may be used as its chemical characteristics. And in galena the content of Ag is the highest in ore sulfides. 3. The chemical characteristic in calcite is rich in Mn.

Mineralizations, having relation to the structure movements, may be divided into four structure--mineralization stages. There are specific mineral assemblage and mineralized zoning in each stage. Wall rock alterations associated with sulfide mineralizations mainly include silicification, sericitization and carbonatization.

The geological, mineralogical and geochemical studies of ore bodies and the studies of mineralizations, wall rock alterations and their mutual relations, and of fluid inclusions and carbon, oxygen, sulfur and lead isotope compositions of minerals indicate that the Fankou lead-zinc deposit is one special type of hydrothermal metasomatic deposit formed from a series of carbonate rocks replaced by an ascending polygenetic hydrothermal fluid and associated with dynamic forces in the course of formation of the mineral deposit.

U, Th, Pb AND REE MINERALOGY OF GRANITES FROM THE SOUTHWESTERN U.S.

WOODHEAD, J. A., Dept. Geology, Occidental College, Los Angeles, CA 90041, USA; SILVER, Leon T., Div. of Geological and Planetary Sciences, California Institute of Technology, Pasadena, CA 91125, USA

Studies of uraniferous and thoriferous anorogenic granites from the southwestern U.S., (Lawler Peak Granite, Bagdad AZ; Dells Granite, Prescott, AZ; Ruin Granite, Gila County, AZ; and Marble Mountains Granite, San Bernardino County, CA) show them to contain complex and diverse assemblages of trace accessory minerals. Up to 30 accessory minerals and 20 radioactive minerals have been identified in some of the rocks. The granites are all ~1400 m.y. old, siliceous (SiO_2 > 69%), leucocratic and highly differentiated. Texturally, their radioactive trace minerals occur as inclusions in, or in association with, biotite, muscovite, and Fe-, Nb- and Ti-oxides in aggregates interstitial to the major minerals. Mineralogical, textural and compositional evidence suggests that, in some instances, this may be the result of late stage magmatic separation of an Fe-Mn-Ti-rich melt enriched in the incompatible elements (U, Th, REE, Nb, Ta, P, F).

Trace minerals stoichiometric for U, Th, and the REE's occurring at the 1 to 10 ppm level are invariably the major sites for these elements. Strong similarities in accessory assemblages such as the ubiquity of Zircon group members (zircon, thorite, uranothorite, coffinite, and xenotime) and Monazite group members (monazite and cheralite) in close association suggest that the conditions of formation of the rocks were very similar. Differences in whole-rock Th/U, Nb/Ti, P/Si and heavy-/light-REE ratios cause complex differences in the radioactive mineral suites. For instance, the Lawler Peak and Dells granites are extremely similar in their major element compositions but differ by an order of magnitude in Ti, P, Ce, and Y contents. Nb-rutile ($Fe^{+3}Nb^{+5}Ti_2O_8$), brannerite (UTi_2O_6), monazite ($[REE,Ca,Th]PO_4$) and xenotime (YPO_4) are the major sites for Nb, U, Th and the heavy-REE's, respectively, in the relatively Ti-, P- and Ce-rich, Y-poor, Lawler Peak, but a number of niobates and thorite are the major sites for Nb, U, Th and the heavy-REE's in the Dells. Monazite is the major light-REE site in each, but its scarcity in the Dells reflects the low light-REE content of the rock.

The various U- and Th-bearing minerals, including silicates, phosphates, titanates and niobates, have diverse susceptibilities to radiation damage, annealing, alteration, and U- Th- and Pb-leaching or fixation. Thus whole-rock U, Th and Pb mobilities depend more on the identity of the species which are the major U and Th sites than on U and Th endowments alone. The accessory mineral suite therefore controls the whole-rock response to secondary geochemical processes affecting behavior of U, Th and Pb.

Trace accessory minerals may be more useful in analysis of crystallization and subsolidus histories of granites than are the major minerals because they initiate crystallization over a greater range of conditions and have a wider range of responses to secondary and hydrothermal processes. Radioactive accessories exhibit several primary disequilibrium textural and compositional features. Strong, sharp zonation in zircons and monazites, nearly adjacent monazites of significantly different compositions, and inclusions of both thorite and uranothorite in the same host all suggest severe local disequilibrium in the final stages of magma crystallization and may result from separation of immiscible melts with strongly different compositions and mineral-melt distribution coefficients. Complex secondary textures including reaction rims on thorite, monazite and niobates; pseudomorphous replacements of one niobate by others, irregular replacements of biotite by allanite and epidote, "biotization" of muscovites, exsolution intergrowths of apatite and thorite or cheralite in monazites, and Fe-Nb-Pb-U-rich haloes around most radioactive grains reveal the scale and extent of secondary and hydrothermal alteration of the rock and the resultant U- and Pb-loss.

The ubiquity and unusual composition of the interstitial aggregates of oxides and radioactive accessory minerals suggests the possibility of immiscible separation of an Fe-Mn-Ti-P-rich melt from a late-stage siliceous magma in these highly differentiated granites. If their sub-solidus phase diagrams were better known, the degree of crystalline solution among related radioactive minerals such as monazite-apatite-thorite(huttonite)-cheralite, zircon-xenotime-thorite-coffinite or the many niobates could be a powerful tool to unravel the post-crystallization histories of the granites. Both of these problems are amenable to experimental petrological testing.

TEM STUDIES OF THE PYROMETAMORPHIC BREAKDOWN OF PHENGITE AND CHLORITE

WORDEN, R.H., DROOP, G.T.R., and CHAMPNESS, P.E., Dept. of Geology, Manchester University, Manchester M13 9PL, U.K.

Dalradian greenschists, from the Cowal peninsula in Scotland, whose original mineralogy was quartz, albite, chlorite and phengite with minor biotite and garnet, were metamorphosed at very low pressures (0.5 kb) and high temperatures (800°C+). Much of the original texture and mineralogy still remain, although albite and quartz have undergone partial melting. The phyllosilicate reaction products are not resolvable by light optical or microprobe techniques.

TEM investigation of phengite reveals the assemblage:

phengite + phlogopite + hercynite + mullite + sanidine.

Grain sizes are very small, about 0.25 microns on average, and all phases are intimately mixed. Phengite compositions are the same as those of fresh, unaltered phengites, implying the discontinuous reaction:

phengite → phlogopite + hercynite + mullite + sandine.

Projection of reactant and product phases from 3:2 mullite sanidine and water onto the phengite plane in the system K_2O-Al_2O_3-FeO-MgO-SiO_2-H_2O indicates that there has been input of SiO_2 to account for the absence of corundum. This SiO_2, and the Na_2O in the sanidine have their sources in the partial melt.

Pronounced crystallographic orientation relationships are observed: $(001)_{pheng}//(001)_{biot}//(001)_{mull}//(010)_{san}//(1\bar{1}1)_{herc}$
$[010]_{pheng}//[010]_{biot}//[410]_{mull}//[102]_{san}//[110]_{herc}$.

The reaction products have clearly inherited their parent's closest packed planes as this leads to a minimal surface energy term and minimum disruption of the structure during the reaction.

TEM investigations of chlorite also reveal an intimate mixture of very fine-grained phases. The assemblage:

chlorite + phlogopite + hercynite + orthopyroxene + cordierte

was observed. The chlorite composition is the same as in unaltered rocks implying the discontinuous reaction:

chlorite → phlogopite + hercynite + pyroxene + cordierite.

Phase diagram analysis indicates that K_2O must be added to the system. Protecting from hercynite onto the SFM plane reveals that SiO_2 must also have been added to produce this assemblage. The source of K_2O will have been the phengite decomposition while the SiO_2 came from the partial melting of the quartz and the albite.

The pyroxene and phlogopite have a crystallographic relationship:

$(010)_{pyx}//(001)_{phlog}$
$[100]_{pyx}//[010]_{phlog}$.

These are the closest packed planes, indicating a similar mechanism for reaction as proposed for phengite.

The reactions, assumed by Smith (1969) to be isochemical, require external input of material and proceed by a mechanism of minimum disturbance to the crystal structure of the parent material.

Smith, D.G.W. 1969. Pyrometamorphism of phyllites by a dolerite plug. J. Pet. 10, 20-55.

STRUCTURAL STUDIES OF GLASSES USING NEUTRON DIFFRACTION TECHNIQUES

WRIGHT, Adrian C., *J.J. Thomson Physical Laboratory, Whiteknights, Reading RG6 2AF, U.K.*

As with crystalline materials diffraction is the major probe for investigating the structure of the vitreous state. There is, however, an important difference between crystalline and glassy solids in that, whereas the structure of the former may be specified by relatively few parameters (unit cell + translational symmetry) and can be determined absolutely, the fact that glasses are isotropic and non-periodic means that the maximum that can be obtained for the latter from a diffraction experiment is a one-dimensional real-space correlation function, from which the regeneration of the underlying three-dimensional structure can never be unique. As a result structural modelling plays an important role in the analysis of diffraction data from glasses and complementary structural information is obtained from a wide range of other techniques such as vibrational and magnetic resonance spectroscopy. On the other hand modern diffraction techniques are capable of providing accurate structural data with high real space resolution which are a very stringent test for any proposed structural model.

An account is given of neutron diffraction techniques for the study of glasses using both steady state reactor and pulsed accelerator sources together with the associated data analysis and modelling techniques. Illustrations are drawn from a wide range of glasses including oxides (silica, germania and boron oxide) halides (zinc chloride and fluoroberyllates, including beryllium fluoride) and chalcogenides (arsenic sulphide and germanium selenide). The requirement for the comparison between model and experiment to be carried out using the appropriate functions in both real and intensity space is emphasised, as is the need to correctly include the effects of experimental resolution and thermal vibration. It is concluded that the greatest barrier to progress in understanding the structure of glasses lies not with the diffraction experiments themselves, but in the development of adequate modelling techniques which will allow model parameters to be varied in a systemmatic way.

MOSSBAUER STUDY OF MANGANESE BIOTITE FROM KUIQI, CHINA

Wu Gongbao and Chen Shurong
(Chinese Academy of Geological Sciences)

A sample of Mn-biotite from riebeckite miarolitic granite in Kuiqi region of Nanling was studied by means of Mossbauer spectrum, XRD, IR and chemical analyses. The chemical composition of the sample obtained by wet chemical analysis is given in Table 1.

Table 1. Chamical composition of Mn-biotite

Si	Na	Ti	Fe3+	Fe2+	Mn2+	Mg
3.168	0.522	0.144	0.467	1.264	0.564	0.254
Li	K	Na	Ca	Rb	OH	F
0.389	0.938	0.049	0.017	0.020	0.753	1.251

The 57Fe Mossbauer spectrum of Mn-biotite at 295K is shown in Figure 1.The spectrum consists of five doublets. The obtained Mossbauer parameters are given in Table 2. The value of MISFIT is $M\pm\Delta M=0.122\%\pm0.021\%$. Four of the doublets, like those of normal biotite, can be assigned to Fe2+(M2), Fe2+(M1), Fe3+(M1) and Fe3+(M2), respectively. The fifth doublet of the sample can be judged to correspond to Fe3+(IV), since its IS value is small enough to fall into the typical numerical range of four-fold coordinated high spin ferric ion.

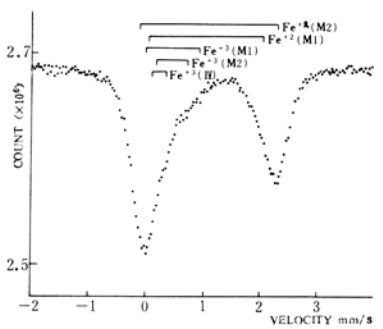

Fig. 1. Mossbauer spectrum

It is noticed that the sums of positive and negative valency charges in the chemical formula corrected by the Mossbauer method are 21.850 and 22.004, respectively(all Mn ions were regarded as Mn2+ in the calculation). Such discrepancy may be caused by Mn3+. From the difference the content of Mn3+ was calculated. The crystal chemical formula of Kuiqi Mn-biotite is determined as

Table 2. Mossbauer parameters of Mn-biotite

Assign-ment	IS (mms-1)	QS (mms-1)	Γ (mms-1)	Area (%)	Number of ion
Fe2+(M2)	1.134	2.437	0.38	49.78	0.862
Fe2+(M1)	1.088	2.012	0.38	21.02	0.364
Fe3+(M1)	0.488	0.974	0.38	3.15	0.055
Fe3+(M2)	0.497	0.526	0.38	8.40	0.145
Fe3+(IV)	0.257	0.287	0.38	17.66	0.306

$$(K_{0.938}Na_{0.049}Rb_{0.020}Ca_{0.017})_{1.024}\ (Fe^{2+}_{1.226}Mn^{2+}_{0.410}$$

$$Li_{0.389}Mg_{0.254}Fe^{3+}_{0.200}Mn^{3+}_{0.154}Ti_{0.140})_{2.773}\ (Si_{3.168}$$

$$Al_{0.522}Fe^{3+}_{0.306}Ti_{0.004})_{4.000}O_{10}(OH_{0.753}F_{1.251})_{2.004}.$$

The site occupancy data show the relative enrichment at site Z of the Mn-biotite to be Fe3+>Ti4+. Our result is consistent with the condition of schorlomite. It seems to be a universal rule for silicate minerals. It is concerned with that Fe3+ has greater electronegativity than Ti4+ does, especially in meca, this preference order becomes more obvious becauce of its structure feature (Si: Al≅3:1).

Our research shows that presence of Fe3+(1V) in Kuiqi Mn-biotite is caused by lack of Al, and has no direct relation to a great amount Mn ions entering biotite structure. As compared with other types of granites of Nanling, the riebeckite miarolitic granite has much less Al_2O_3. Kuiqi Mn-biotite is the crystalline product of later stage. Its above structure feature reflects the composition character of host-rock. Kuiqi Mn-biotite has a strong pleochroism, especially there is a very strong absorption paralled to X-axis. The strong absortion paralled to X is mainly caused by a charge transter Fe3+(IV)→O2- and the d-d transitions of Fe3+(IV) (they have more effective absorption paralled to X). In addition, the d-d transitions of Mn2+(VI) and Mn3+(VI) may make some contribution to it.

POINT DEFECTS AND DIFFUSION

WUENSCH, Bernhardt J., Department of Materials Science and Engineering, Massachusetts Institute of Technology, Cambridge, MA 02139, USA

Direct measurement of diffusion coefficients is based on analysis of the distribution of solute produced by an annealing for specified time at elevated temperature. Boundary and initial conditions for the sample are selected and controlled such that a simple solution to Fick's second law obtains--usually one in which some function of solute concentration varies linearly with a function of solute penetration into the sample. Simple in concept, many unsuspected sources of artifact exist in such experiments. These will be illustrated for oxides with examples from work in our laboratory and from the literature. Preparation of an initial surface on the host crystal may introduce mechanical damage, increasing dislocation densities by three orders of magnitude for relatively plastic materials such as periclase, MgO. The damage extends to 100 μm from the surface, a distance which exceeds the depth of most diffusion zones produced by experiment. Preannealing at elevated temperatures to 1850°C polygonizes the dislocation array but effects a reduction in dislocation density by factors of only two to three. In less plastic materials (corundum, for example) damage may be confined to shallower depths on the order of 1 μm and may be successfully eliminated by annealing.

Materials of high melting point are strongly bonded and have high energies for defect formation and migration. These materials have low intrinsic defect concentrations and their transport properties are likely to be controlled by accidental impurities. Chemical analysis of the impurity content of the host crystal is thus an essential part of sample characterization but is commonly slighted in comparison with the care lavished on other aspects of the experiment. Anion impurity levels, in particular, usually remain unexamined. Impurities may be introduced, however, to a nominally pure sample in the course of specimen preparation. Tracer isotopes carry copious amounts of impurities, including daughter elements and the precursor element for those radiotracers produced by irradiation. These impurities have been shown to influence the measured diffusion coefficient. Impurities may also be derived from furnace elements in annealing at

POINT DEFECTS AND DIFFUSION
WUENSCH, Bernhardt J.

high temperature. Silicate glass droplets, for example, have been observed to condense on samples and produce Si^{4+} gradients in the diffusion zone. Moreover, many materials have high vapor pressure at elevated temperature. Thermal etching has been found to cause spurious results in gas-exchange experiments and, in extreme cases, the rate of vaporization of the host crystal may be significant relative to the rate of diffusion into the surface.

The results of self-diffusion measurements will be examined for selected stoichiometric oxides with simple close-packed structures. Data obtained by separate workers are usually not in good agreement due to influences such as those mentioned above. Arrhenius plots of the diffusion coefficient usually lack the definitive break which would clearly distinguish regions of intrinsic and extrinsic mass transport. In periclase, MgO, a close agreement between theoretical and experimental values for the enthalpy of migration, as well as agreement between activation energies derived from diffusion and ionic conductivity measurements, suggests that cation self-diffusion occurs by an extrinsic vacancy mechanism at all temperatures up to the melting point. The mechanism of anion self-diffusion remains unclear. The defect structures of other alkaline earth oxides is also unclear. Concentration profiles are anomalous in that two different diffusion coefficients with similar activation enthalpies are obtained from the near surface region and from the bulk of a crystal. There is no consensus on which represents lattice diffusion. Self-diffusion in corundum occurs by a vacancy mechanism and may be intrinsic. The results for self-diffusion coefficients in zincite, ZnO, vary over a wide range, but data are in close accord for experiments in which vaporization of the sample is prevented. Cation self-diffusion in ZnO is isotropic and independent of Zn partial pressure. A Frenkel defect mechanism thus seems unlikely and diffusion probably occurs via an extrinsic vacancy mechanism as appears to be the case for the majority of close-packed oxides.

PHASE TRANSFORMATION AND CATION DISTRIBUTIONS IN FAST-ION CONDUCTORS

WUENSCH, Bernhardt J., Department of Materials Science and Engineering, Massachusetts Institute of Technology, Cambridge, MA 02139, USA

A number of halides and chalcogenides of Ag and Cu have structures with simple anion packings (bcc, fcc or hcp) and phase transformations which occur at modest temperatues (90°-200°C). The phases at elevated temperatures have disordered and delocalized cations which are extraordinarily mobile. Ionic electrical conductivities are as large as 6 reciprocal ohm-cm, placing these phases within the class of materials known as fast-ion conductors. Although this interesting transport behavior has long been known, the nature of the phase transformations and the details of the cation distribution in the high-temperature phases have not been established to satisfaction until recently, despite the simplicity of the anion arrays. The reason is that the phase transformation usually destroys a single-crystal. All early studies were accordingly confined to powder samples and the delocalization of the cations causes the diffraction intensities to be limited in number and extremely weak. Procedures for preparing single-crystals of several of these phases have been developed and single-crystal studies performed over a range of temperatures with neutron diffraction.

Miersite, AgI, has the wurtzite structure at low temperature (β-AgI) and transforms to a fast-ion conducting body-centered cubic form (α-AgI) at 147°C. The transformation in the anion array corresponds to the martensitic phase transformation found in many metals with these packings. Peculiar aspects of the transformation in AgI (such as a "memory effect") may be explained in terms of well-known aspects of this type of transformation. The Ag ion in bcc α-AgI is found to undergo highly anharmonic thermal vibration and is disordered among the tetrahedral interstices. The probability distribution suggests a hop between face-shared tetrahedra as the diffusion mechanism. Use of the experimental Ag densities in a Boltzmann ratio provides an activation energy for Ag migration which agrees with the directly-measured value to within a few percent.

Acanthite (low-temperature Ag_2S) is a monoclinic superstructure based upon ordering of Ag ions among the tetrahedral and octahedral interstices of a bcc sulfur ion array. Acanthite transforms to the body-centered argentite structure (β-Ag_2S) at 177°C. Neutron studies (2) show the Ag ions to be completely delocalized in bands along <100> even though the activation energy for Ag migration, twice that for α-AgI, should require greater localization. The distribution is thus interpreted as a position average over closely-spaced sites, rather than a time average of dynamic vibration. The different behaviors of α-AgI and β-Ag_2S may be explained in terms of the concentration of mobile cations and the bonding characteristics evidenced by the structures of the low-temperature phases.

The high temperature phase of Ag_3SI, intermediate to AgI and Ag_2S, has disordered S and I arranged in a statistical bcc arrangement. The Ag distribution is delocalized, as in β-Ag_2S, but displays fine structure which may be interpreted as an average over positional disorder of the equilibrium position within the tetrahedral interstice, the location depending upon the short-range configuration of anions about the site(3). The Cu distribution(4) among the hcp sulfur atom arrangement in high-chalcocite (β-Cu_2S) will also be discussed.

(1) R. J. Cava, F. Reidinger and B. J. Wuensch, Solid State Comm. 24, 411 (1977).
(2) R. J. Cava, F. Reidinger and B. J. Wuensch, J. Sol. State Chem. 31, 69 (1980).
(3) J.-J. Didisheim, R. K. McMullan and B. J. Wuensch, Solid State Ionics (1986) in press.
(4) R. J. Cava, F. Reidinger and B. J. Wuensch, Solid State Ionics 5, 501 (1981).

PROGRESS IN EXPERIMENTAL PETROLOGY OF GRANITE

WYLLIE, PETER J., Division of Geological and Planetary Sciences, California Institute of Technology, Pasadena, CA 91125, USA

Experimental petrology of granite, in a restricted sense, involves determination of the phase fields for the granite bulk composition as a function of pressure, temperature, and activities of volatile components, including measurement of the compositions of all phases, solid, liquid, and vapor, and their variations throughout the range of the phase diagram. These data are fundamental properties that should be known for all igneous rocks. They permit evaluation both of the paths of equilibrium and fractional crystallization of liquids and of the process of progressive partial melting. In a broader sense, experimental petrology of granite involves use of phase diagrams for granitoid rocks to place constraints on their petrogenesis, which involves geophysical processes producing conditions suitable for generation of magma and intrusion of granitic magma bodies, as well as eruption of rhyolite lavas and ash flows. Experimental petrology of granites and of source rocks for granitic magmas calibrates geophysical and petrologic processes fundamental to the origin and evolution of continents.

Experimental petrology of granites advanced rapidly after 1950, when O.F. Tuttle and N.L. Bowen designed simple apparatus to study mineral and rock melting reactions in the presence of water under pressure. With the realization that many granitoid rocks represent the near-surface expression of processes initiated perhaps 100 km deep in subducted oceanic crust, phase relationships of appropriate materials were extended from crustal pressures to 35 kb.

Projections from, and sections through, the complete P-T-X(water) diagrams for biotite-granite and muscovite-granite from 1 bar to 35 kb, from dry to conditions with excess water, illustrate the distribution of significant phase volumes for minerals, minerals + vapor, minerals + liquid, minerals + liquid + vapor, liquid, liquid + vapor, and vapor, along with the solubility of water in granitic melt as a function of pressure and temperature. Variations in oxygen fugacity influence the stability ranges of femic minerals.

The phase diagram for a granite represents an isopleth through the multicomponent rock system. Phase equilibrium studies in

PROGRESS IN EXPERIMENTAL PETROLOGY OF GRANITE
WYLLIE, PETER J.

selected synthetic systems provide the geometric framework for interpreting paths of crystallization or fusion within complex rock systems. Knowledge of all parts of the feldspar-quartz system is fundamental for understanding granitoid rocks. The phase fields intersected by a fixed bulk composition within a synthetic system correspond to the phase diagram for a whole rock.

The forward experimental approach determines compositions of liquids formed from possible source rocks under various conditions, and relates these to granitoid rocks; the inverse approach seeks a source rock for a possible primary granitic magma by determining liquidus minerals for the granite under a variety of conditions, and relating these to possible residual minerals in partially fused source. Both these approaches neglect dynamic conditions of formation, migration, and emplacement of granitic magmas, but the phase relationships do provide limits for conditions of origin. Recent experiments deal with processes of contamination of magmas, and of reaction products at contacts between dissimilar magmas and rocks at various positions from subducted slab source through the mantle and crust.

The natural processes occurring in silicic magmas are dynamic, commonly involving nonequilibrium conditions. Furthermore, it is difficult to achieve stable, reversible equilibrium in experimental studies on granitic compositions. Nevertheless, the best approach to stable phase equilibrium diagrams provides the best point of departure for interpreting the petrogenesis of granitoid rocks, by locating the polybaric, polythermal field boundaries which control melt and mineral compositions not only under equilibrium conditions, but also for fractional processes and those involving assimilation and magma contamination.

•STUDY OF THE OMPHACITES IN ECLOGITES IN THE DABEI MOUNTAINS, CHINA

XIE Douke and GUO Kunyi, Nanjing Institute of Geology and Mineral Resources, Nanjing, People's Republic of China

Omphacite was found in the boundary of the paleoceanic plate in the Dabei Mt. It is the characteristic clinopyroxene occurring in eclogites typical of group C. According to the generally established usage, which means the rock is mainly composed of omphacite and almandine-pyrope-grossular garnet [*sic*].

(1) *Crystal structure.*

Single-crystal studies of the Dabei Mt. omphacite show that the symmetry of the whole structure decreases due to the disorder replacement probability of the cation site. The space group is P2/c, and the unit cell parameters are: a = 9.473 Å, b = 8.756 Å, c = 5.254 Å, ß = 105.07°, V = 420.8 Å^3, D = 3.348 g/cm^3, Z = 4, (R = 0.047). The a axis is in conformity with diopside, but b and c axes were obviously shortened 0.14 Å and 0.24 Å. The cations in the crystal body, in the analysis of the structure, were replaced by Al atomic sites, occupancy rate: Al_1 = 0.57, Al_2 = 0.59, Al_3 = 0.59, Al_4 = 0.47, as well in M2 and M2(1) sites are mainly replaced by Ca and Na. There is in a great measure Na in M2 site, and the M1 and M1(1) sites are for the greater part Mg, and probably are occupied by Al, with only a little Fe.

The bond lengths: Si_1-01,02,05,06: 1.583-1.647 Å. Si_2-01,02,03,04: 1.588-1.666 Å. Al_1-03,04,06: 1.894-2.002 Å. Al_2-04,05,06: 2.001-2.128 Å. Al_3-02,05,06: 2.389-2.459 Å. Al_4-01,03,04: 2.361-2.446 Å. Bond angles: O-Si-O are between 104.9-118.2°, O-Al-O are between 88.9-174.3°.

Si-O tetrahedral chains in the omphacite cell are formed by two different kinds of Si-O tetrahedra linked to each other. In every Si-O tetrahedra, there are two oxygens, O1-O2, as bridging oxygens, shared by a pair of tetrahedra to link two tetrahedra. The length of bridging-oxygen chain is 0.025-0.078 Å longer than the nonbridging oxygen bonds, and both of them joined by the larger positive ion are longer than those in the M1-O chain; they increase with Ca content.

Using the same method, we obtained positional and thermal parameters and their estimated deviations, and general temperature factor expresseed as -β's and -U's.

We also used Mossbauer spectra to study P2/c omphacites. The doublets are characterized by C.S values of 1.169, 1.19, 1.15, 1.36 and Q.S values of 2.88 mm/sec, 2.25 mm/sec, 1.95 mm/sec, 1.8 mm/sec. The occupancies studied by X-ray suggest that nearly all of the Fe^{2+} in P2/c omphacites appears in the M1 positions and the Fe^{2+} content of the M2 positions is negligible. The Mossbauer results are consistent with this suggestion.

(2) *Chemistry.*

The crystal-chemical formula is:

$$(CaO_{.4189}Na_{.5060})(Mg_{.3930}Fe^{2+}_{.1086}Fe^{3+}_{.1159}Al_{0.41}Ti_{.0056})(Si_{1.9870}Al_{.013})O_6.$$

We analyzed seven omphacites, which in the system Di-Hd-Jd-Ac-Cats are between the boundary planes: Na/(Na+Ca) ≤ 0.55, and limited to the ratio is $(Al^{IV}+Fe^{3+}) \geq 0.78$. The single crystals of Shi 4 omphacite from Dabei Mt. have been studied and the empirical formulas are: Si 2, Al 1, Na 1, oxygen 6, and the oxide wt % compositions are Si: 27.79, Al: 13.35, Na: 11.37, O: 47.49. The distribution of Fe and Mg between the omphacites and garnets of ecologists were examined, and the distribution coefficient is $K_D^{cpx\text{-}gt} = 11.4$. We can uniquely obtain the temperature = 290°C and pressure estimate = 10 kbar, when the K_D value is known.

ON THE BEHAVIOR OF MINERALS DURING THERMAL AND SHOCK METAMORPHISM OF METEORITES

XIE XIANDE, Institute of Geochemistry, Academia Sinica, Guiyang, The People's Republic of China

The behavior of opaque and silicate minerals in Jilin H5 chondrite(JHC) and Qingzhen enstatite chondrite(QEC) during thermal and shock metamorphism has been studied by optical, SEM, EMA, and HRTEM techniques, and by high temperature and high pressure experiments as well as by shock-loading experiments.

Ni-Fe metal and troilite(FeO) in chondrites are relatively mobile during thermal metamorphism. Fine metal grains in JHC are able to migrate easily and aggegate into metal nodules about 5-10mm long, and the largest ones are 30mm in size. The formation of eutectic melts of Ni-Fe metal together with FeS in veinlets was observed. EMA analyses were made on opaque minerals of different sizes. No major variation in composition was found.

Similar phenomena were also noticed during HT-HP experiments(10-58kb, 700°-1300°C) on JHC. When the temperature reached 1,000°C, Ni-Fe metal grains gradually moved and aggregated into rather coarse grains or spheres by thermal diffusion and partial melting, or through the formation of eutectic melts together with FeS, and futher when the temperature reached about 1,300°C, the immiscibility and gravitational differentiation of metal-silicate melts took place[1]. No obvious variation in composition of aggregated opaque mineral grains was noticed. EMA analyses of recrystalized olivine from silicate melt show that its Fe content decreases (from Fa=18.57 to Fa=14.79). However, during shock-loading experiments, Ni-Fe metal grains in JHC exhibited no remarkable change when the shock pressure was as high as or less then 220kb, and only a few of them become elongated when shock pressure reached 300kb.

The above facts indicate a close temperature-dependence of Ni-Fe metal and troilite in the meteorites. Shock-induced fractures may provide additional passage ways for metal migration during thermal metamorphism.

The main feature of thermometamorphism in JHC is shown by the homogenization of olivine and pyroxene in their chemical composition. As the results of shock, olivine and pyroxene grains in JHC are broken down with well developed fractures and the pyroxene grains show distinctly undulatory extinction and free cleavages can be seen even in pyroxene crystals.

Thermometamorphism of minerals in QEC is unremarkable, but enstatite and clinoenstatite in QEC show the characteristics of plastic deformation by shock events, commonly with undulatory or uneven extinction. Deformed twinning lamellation or lamellae in some grains were subjected to contorsion and dislocation; in some cases kink bands are viewed and the inversion of enstatite to clinoenstatite under the shock process is recognized as well.

HRTEM investigations of enstatite from both the JHC and QEC show the following shock effects: (1) dislocation gliding (up to 18 Å) along [100]; (2) gliding of Si-O chains along [001] of clinoenstatite; (3) curving of Si-O chains (<5°); and (4) twinning in clinoenstatite with the composition plane of (100).

It is revealed from lattice imaging that the content of clinoenstatite in QEC is much higher than that in JHC, indicating that the influence of thermometamorphism of QEC is much weaker than that of JHC. This is consistent with the above mentioned facts of optical observations.

The plastic deformation of mineral olivine in JHC submitted to experimental shock-pressures of 40, 70, 105, 132, 156, 220 and 300kb was investigated. It is found that with increasing shock intensity, the olivine crystal grains are internally broken down into more and more "mosaic blocks" of progressively smaller size(from ~150 μ at 132kb to ~10 μ at 300kb) and of progressively larger subgrain misorientation angle (from 3° at 132 kb to 7-10° at 300 kb).

1) Wang Daode and Xie Xiande: Chinese Journal of Space Sciences, vol. 1, No.2, 1981, 85-92.

•A NEW METHOD FOR SIMPLE IDENTIFICATION OF ZEOLITES

XU Bangliang, Nanjing Geological School, Nanjing, People's Republic of China

[By title only.]

•THE DISCOVERY OF IRON-BEARING TENNANTITE FROM A CERTAIN LOCALITY IN SHANXI PROVINCE, CHINA, AND ITS SIGNIFICANCE

XU Guofeng, Department of Mineral Resources, and SHAO Jielian, Department of Geology, Wuhan College of Geology, Yujiashan, Wuhan, Hubei, People's Republic of China

A large amount of iron-bearing tennantites occur from a certain gold deposit in Shanxi Province, China. They not only occur as an independent copper ore but also contain more than 10 g of gold per ton, so they have industrial importance. The gold deposits make their appearance in the carbonate rock formation of the middle Devonian system.

In this paper, systematic data on morphological characteristics, chemical composition, unit cell dimensions, reflectance, reflection color indices, infrared absorption spectrum, coefficient of thermoelectricity, specific gravity, decrepitation temperature and sulfur isotopes are given for iron-bearing tennantite from this gold deposit. The tennantite is characterized by high iron content, 8.82 wt %, but in the "pure" end member, it is 0.4 wt %. Its reflectance data are as follows: 480 nm, R = 31.14%; 546 nm, 30.53%; 589 nm, 29.46%; 656 nm, 27.46%. Its quantitative color data are given below: the visual reflectance of reflection color Rv is 29.4064%; chromaticity coordinates: x = 0.3290, y = 0.3335, dominant wave length d = 492 nm, and purity Pe = 0.0151. These lines of evidence support the "transmissive hot brine" genesis of the gold deposit and provide further prospecting indicators for gold.

A NEW VIEW ABOUT THE ORIGIN OF DISPERSION OF BIAXIAL NON-OPAQUE MINERALS

Zhiping Xu

East China Geological College. Fuzhou, Jiangxi.

The theory now used to explain the origin of dispersion of biaxial non-opaque minerals was formulated by Professor E.S. Larson and E.E. Wahlstron in University of Colorado fifty years ago. The principle of dispersion of the optic axes on some given section of the thin biaxial crystal plate is used to show the forms, character, and origin of dispersion in the interference figure. However, this theory does not hold water because it is difficult to show why the feature and the origins of dispersion within the interference figure of the biaxial minerals is present.

The interference figure is usually seen under the conoscope in white light illumination between crossed polars within the thin biaxial non-opaque crystal plate in some sections. For example, it may be perpendicular to Bxa or OA or the sections near them. As a result of the function of dispersion and the color coincidence of the transmission light of dispersion spectrum, none of the dispersion of the light appear in most of the interference color in the field of the microscope. For example, this is true of the thin section of the isotropic and the uniaxial minerals.

In both sides of the dark hyperbolic segments near the points of the melatopes, various wavelengths of light moving along these regions may be removed because of the different covering action of the hyperbolic segments of the isogyres. The other different wavelengths of the light will be refracted off the dark hyperbolic segments and form interference color of various wavelengths of the lights. Therefore, different light fringes of the dispersion resulted by isogyres included by the optic axes may appear in both sides near the dark hyperbolic segments.

For these reasons, the light borders of dispersion with the shape of crescent moon or semi-moon are always close to the dark hyperbolic segments and turning around while the dark hyperbolic segments are turning. When the dark hyperbolic segments is turning into the dark cross, the dispersion light borders are parallel to it. Therefore, the dispersion light fringes are removed.

In order not to change the habits of using the forms and the procedures of the dispersion formula, they can also be applied continually.

•INVESTIGATION OF THE INDEX MINERALOGY OF CHINA'S HIMALAYAS: THE METAMORPHIC SILICATES OF THE WESTERN ALI REGION

XUE Junzhi, CHEN Shengping, ZHAO Yanming, GE Yingya, REN Yingxin, REN Yingxin, ZHANG Hankai, HO Yong, and PAN Tiehong, Department of Geology, Wuhan College of Geology, Yujiashan, Wuhan, Hubei, People's Republic of China

Metamorphic silicates are widely distributed over the western Ali region. The main metamorphic rock-forming minerals of this region have distinct chemical features. The arithmetic means of the chemical coefficients M(=Mg/Fe+Al), A(=Al/Si), and N(=Na+K/Ca+Mg) of the Ali metabasite Ca-amphiboles are 1.875±0.818, 0.216±0.111, and 0.099±0.052 respectively; the means for the para-metamorphic Ca-amphiboles are 2.148±0.852, 0.079±0.058, and 0.035 ±0.025, respectively. The 0.95 probability confidence intervals of M and A of metabasite Ca-amphiboles are 1.454-2.296 and 0.159-0.270, respectively; those of the para-metamorphic Ca-amphiboles are 1.089-3.207 and 0.007-0.151, respectively.

The 0.95 confidence intervals of Mg/Fe, Al/Si, and Ti/Si for ortho-metamorphic biotite are -0.019-2.109, 0.439-0.817, and 0.039-0.065, respectively, while those of para-metamorphic biotites are 0.747-1.541, 0.474-0.632, and 0.036-0.060, respectively.

The component $Ca(Mg,Fe)Si_2O_6$ percentage of regional metamorphic clinopyroxenes ranges from 96 to 99 which indicates the metamorphic characteristics of mafic rock. The percentages of the component $Ca_3(Al,Fe,Cr)_2Si_3O_{12}$, $(Fe, Mn)_3Al_2Si_3O_{12}$ and $Mg_3Al_2Si_3O_{12}$ of metamorphic garnet are 2.0-40.2, 46.6-91.0, and 6.0-29.0, respectively, which indicate mainly amphibolite facies metamorphism.

In westerm Ali, the ranges of metamorphic temperature and pressure are 201° to 770°C and 200 to 939 MPa on the bases of the Ca-amphibole-plagioclase, biotite-garnet, garnet-plagioclase, garnet-hornblende, garnet-clinopyroxene, and clinopyroxene-plagioclase mineral geothermobarometry.

At the Ayila mountain fault zone, the metmorphic T-P intervals belong to the low-, and almost high-pressure facies series; in the Qusong-Xiangquanhe fault zone 1 are parts of the low-, medium-, and high-pressure facies series; at the Gurang-Bolin fault zone and Xierwa of Pulan county, the metamorphic T-P intervals belong to low-, medium-, and medium-high-pressure series. The 0.95 confidence intervals of regional metamorphic T-P of the low-pressure series are 413-527°C and 205-335 MPa, while those of the high- or approximately high-pressure series are 483-627°C and 667-855 MPa. The contact metamorphic temperatures of this region are 195-580°C; their pressures are below 200 MPa.

STRUCTURE DETERMINATION OF GeO_2 POWDER SAMPLE AT HIGH PRESSURE AND TEMPERATURE BY SYNCHROTRON RADIATION

YAMANAKA,T., OGATA,K., SUGIYAMA,K. and TOKONAMI,M.
Mineralogical Institute, Faculty of Science, Univ. of Tokyo
7-3-1 Hongo Tokyo, Japan 113

A new X-ray powder diffractometer was designed for a multiple use of synchrotron radiation (SR) source (2.5 GeV, 200 mA) at Photon Factory, KEK (Yamanaka et al., 1983). Structure analyses of powder samples by Rietveld method enabled the diffractometer to give highly reliable results (Ogata et al., 1985).

Structure analyses of GeO_2, isostructures to α-quartz and rutile, have been undertaken at high pressures and temperatures by angular and energy-dispersive powder diffraction using SR.

1) Structure Refinement by Rietveld Method

Powder diffraction intensities were measured by using monochromatized radiation, while samples were rotated. An ionization chamber monitored X-ray source decay. Rietveld analyses were executed by the least-squreas refinement program "RIETAN" (Izumi, 1985) modified for SR. Variables of 19 parameters were refined, indicating R_F = 6.73 % for data by SSD and 3.85 % by scintillation counter (Fig. 1). Profile shape observed from SR was determined to have about 95 % of Gaussian fraction based on a pseudoVoigt function, i.e. the sum of Gaussian and Lorentzian function, whereas the shape from the ordinary X-ray source had about 40 % of the fraction.

Fig. 1

Rietveld Analysis
The calculated and observed patterns are shown by solid line and dots, respectively.
The diffrence between these is presented at the lower portion.

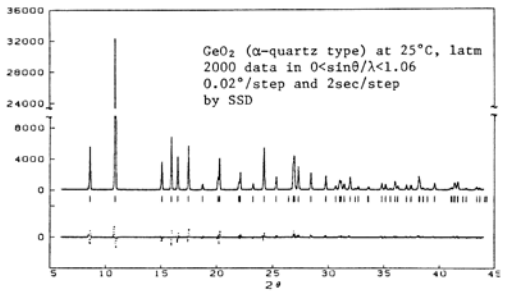

2) Structure Analyses using High Temperature Diamond Anvil Cell

A newly devised diamond anvil cell with a ring heater interposed between two diamonds was employed for diffraction intensity measurements up to 20 GPa and 550°C. The pressure cell mounted on the goniometer was rotated along the incident beam for lessening effects of the preferred orientation and of grain growth. Pressure was estimated by an internal standard of NaCl and temperature was measured by thermocouple. Energy-dispersive diffraction intensity was measured up to 50 KeV by an intrinsic Ge detector and multichannel analyzer (MCA).

Pattern fitting to the diffraction profiles was applied after the intensity correction regarding energy distribution of incident SR beam, absorption effect from diamond and pressure media and compton scattering in back-ground intensity. The calculated and observed energy-dispersive patterns of GeO_2 and NaCl at 4.0 GPa is shown in Fig. 2. The profile fitting elucidated variations of the cell parameters and volume of GeO_2 with pressure and temperature. An inverse relationship of the variations in temperature and pressure is presented in Fig. 3. The compressibility and thermal expansion coefficient were calculated.

Fig.2 Energy-Dispersive Diffraction Pattern and Profile Fitting

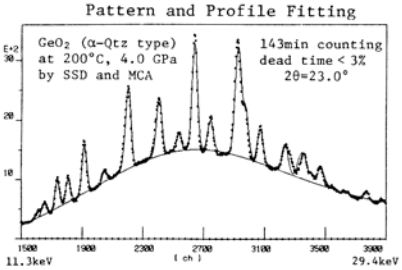

Fig.3 Cell Parameter variation with T and P

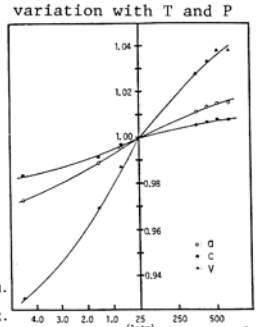

Izumi,F. Jour. Cryst.Soc. Japan. 27, 23 (1985)
Ogata,K. Yamanaka,T. Sugiyama,K. Tokonami,M. & Morikawa,H. Photon Factory Activity Report 1984/1985
Yamanaka,T. Takeuchi,Y. Tokonami,M. Matsumoto,T. & Koto,K. Photon Factory Activity Report 1983/1984 VI-12

•THE GEOCHEMISTRY OF THE EVOLUTION SERIES OF AMAZONITE GRANITES AND AMAZONITE MINERALS IN GANSU PROVINCE, CHINA

YANG, Minzhi, Tianjin Geological Academy, Ministry of Metallurgical Industry, 42 Youyi Road, Tianjin, People's Republic of China

[By title only.]

^{29}Si, ^{27}Al, ^{23}Na MASS AND ^{29}Si CP/MASS NMR SPECTROSCOPIC STUDIES OF THE REACTION OF ROCK-FORMING SILICATE MINERALS AND GLASSES WITH AQUEOUS SOLUTION

YANG, WANG-HONG, Dept. of Geology, University of Illinois, Urbana, IL 61801, USA.

I have reacted Amelia albite, synthetic fluorophlogopite, and albite glass individually with aqueous solutions having different pH values at 250°C, 80°C, and 25°C for various lengths of time at water/rock ratio of 100ml/1.5g and 20ml/1g and examined the initial reactants and final products of each dissolution experiment with XRD and ^{29}Si, ^{27}Al, ^{23}Na (if necessary) MASS and ^{29}Si CP/MASS NMR spectroscopy.

X-ray amorphous phases are the common initial precipitates occurring as metastable phases from supersaturated solutions during dissolution reactions. The structures and compositions of these amorphous precipitates can be explicitly examined using the high-resolution solid-state NMR spectroscopy. The hydrated silica gels which initially precipitate during dissolution of Amelia albite and synthetic fluorophlogopite in highly acidic environments show a three-dimensional tetrahedral framework structure which is partially depolymerized by an appreciable amount of protons. The proton concentration in these silica gels increases with increasing reaction temperatures. No aluminum signal from the aqueous alteration product of synthetic fluorophlogopite in highly acidic environment is observed, implying that all aluminum cations released from the primary phase remain in solution. The amorphous phase which precipitates during dissolution of albite glass is sodium (potassium) aluminosilicate gel with zeolite-like framework structure containing molecular water (see Figure). This sodium (potassium) aluminosilicate gel may be a precursor of analcime. Kaolinite is the common thermodynamically stable precipitate during dissolution of Amelia albite and albite glass. The amorphous phases continue to precipitate during the formation of kaolinite. Analcime often occurs as a final alteration product when aqueous solution becomes alkaline due to the dissolution of albite glass.

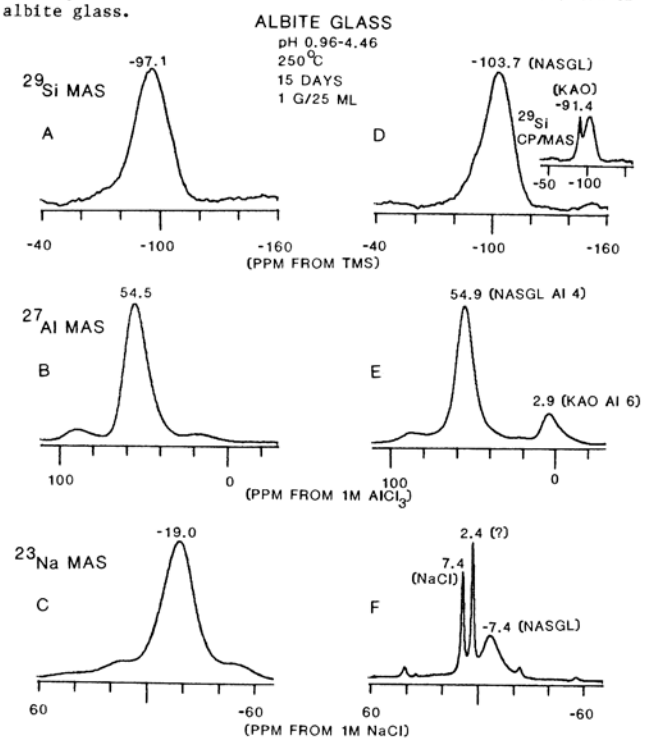

KAO: KAOLINITE
A, B, C: BEFORE REACTION

NASGL: SODIUM ALUMINOSILICATE GEL
D, E, F: AFTER REACTION

KULANITE FIRST FOUND IN CHINA

Yang Yueqing, Ni Yunxiang, Guo Yongquan
(Institute of Mineral Deposits, Chinese Academy of Geological Sciences)

(Abstract)

Xiyantou muscovite-albite-spodumene pegmatite of Nanping pegmatite field, Fujian province is the third place in the world and first in China where kulanite is discovered. Xiyantou kulanite replaces montebrasite partly as disseminated and irregular aggregate or occurs in the fractures of quartz-montebrasite assemblage in interior zone of the pegmatite. The associated minerals include triphylite, augenite, palermoite, goyazite, lazulite, apatite, quartz and so on. The quantity of kulanite is more than other two sites: one is in Yukon, Canada, another in Whitepicacho, U.S.A., so the sample available is enough for detailed mineralogical study.

kulanite chiefly occurs as irregular fine grains, and some as tablets. Grain diameter usually is 0.5--3 mm. Yellow-green or dark-green in color. The lustre is vitreous. Conchoidal fracture. Hardness(vickers):810.5 Kg/mm². Specific gravity: 3.973--3.997(obs.), 4.01 (calc.). Biaxial(+), 2V(means)=34°. Weak pleochroism, Ng=1.722—brownish green, Nm=1.705—blue-green, Np=1.701—yellowish green. Absorption: Ng > Nm > Np. Nm=b, cΛNg=11°.

X-ray single crystal study for Xiyantou kulanite shows it is monoclinic, not triclinic reported by J. A.Mandarino et.al(1976) in JCPDS cards. The space group is $P2_1$ or $P2_1/m$, the optical features also support authors' opinion. Unit cell: a_o=9.024Å, b_o=12.079 Å, c_o=4.924Å, β=100.462°, V=527.76Å³, and Z=2. The result of chemical analysis are given in the table, and are compared with those of analogues: penikisite and bjarebyite (see the figure). Perhaps these three minerals can be concluded in a (Fe,Mn,Mg) isomorphous series. The chemical formula of Xiyantou kulanite is follows:

$$Ba_{1.04}(Fe^{++}_{0.97}Mn_{0.54}Mg_{0.28}Ca_{0.08})_{1.87}(Al_{2.04}Fe^{+++}_{0.03})_{2.07}$$
$$(P_{2.90}Si_{0.13})_{3.03}O_{12}(OH_{2.96}F_{0.01})_{2.97}$$

Table. Chemical analysis of kulanite and analogues

No.	1	2	3*	4	5	6
site	Xiyantou, China			Yukon, Canada		Rwanda
mineral	kulanite dark-green	kulanite yellowish green		kulanite	penikisite	bjarebyite
Na_2O	0.12	0.02		0.02		
K_2O	0.14					
CaO	0.67	0.46	0.1	0.77	0.55	
MgO	1.78	0.80	0.69	3.08	5.81	
MnO	6.1	8.34	6.09	6.32	0.30	15.84
BaO	25.40	24.02	25.68	23.66	24.42	23.35
FeO	11.03	10.40	12.25	10.50	12.55	5.54
Fe_2O_3	0.36	1.20		2.14		3.74
Al_2O_3	16.37	17.37	15.34	14.30	17.04	13.33
SiO	1.23	0.84	0.17	0.19		
P_2O_5	32.65	32.13	33.76	33.28	36.66	33.74
Cl^-	0.005	0.012				
F^-	0.042	0.14				
H_2O	4.23	4.37		3.83	3.90	4.81
total	100.05	100.19		98.09	101.23	99.62
report	the author			J.A.Mandarino etal		O.Knorring

* Analysis by microprobe JCXA-733.

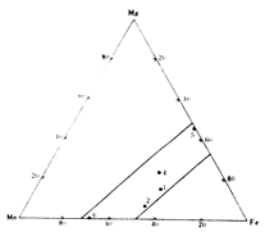

Figure. Site of kulanite, penikisite and bjarebyite in the Fe-Mg-Mn diagram (see the table for No. of samples).

IR absorption curve of Xiyantou kulanite includes three principal absorption zones at 3200—3600 cm^{-1}, 1193—833 cm^{-1} and 660—431.5 cm^{-1}. DTA curve has one strong peak at 700 °C.

• RELATION BETWEEN THE OPTICAL ANISOTROPY INDEX AND THE ORIENTATION OF ATOM GROUPS IN MINERALS

YE, D.N., Institute of Geology, Academia Sinica, P.O. Box 634, Beijing, People's Republic of China

A new concept, the refractivity indicatrix (RI), has been adopted by the author of this paper (Ye, 1982), which is defined by the equation of ellipsoid,

$$\frac{X^2}{(\alpha-1)^2}+\frac{Y^2}{(\beta-1)^2}+\frac{Z^2}{(\gamma-1)^2}=1$$

Another new concept, the optical anisoptropy index (OAI), is derived from the RI. The OAI of crystal in a given direction is equal to the ratio of the radius of RI in the direction to mean radius of the ellipsoid section which is perpendicular to the direction. For example,

$$\alpha-\mathrm{OAI}=\frac{2(\alpha-1)}{(\beta-1)+(\gamma-1)}\ ,\qquad \omega-\mathrm{OAI}=\frac{2(\omega-1)}{(\omega-1)+(\varepsilon-1)}\ ,$$

$$\gamma-\mathrm{OAI}=\frac{2(\gamma-1)}{(\alpha-1)+(\beta-1)}\ ,\qquad \varepsilon-\mathrm{OAI}=\frac{\varepsilon-1}{\omega-1}\ \ldots$$

The concept of OAI is very useful in studying structural-optical mineralogy (Zeng and Ye, 1980; Ye, 1982, 1983a,b, 1985). If the crystal structure has been determined, the OAI value in any direction of a mineral may be calculated theoretically. Birefringence of minerals, such as carbonate, nitrate, borate, chlorate, bromate, iodate, sulphite and isothicyanate, does not depend mainly on the kind of cations in it, but only on the kind of radical and its orientation. If the polarizability ellipsoid of radical and its orientation in the crystal are known, the relative value of polarizability in any direction of crystal may be calculated, too. The polarizability ellipsoid is a revolution ellipsoid in which the rotation axis is the line normal to the radical plane (for CO_3, BO_3 and NO_3) or radical base plane (for ClO_3, BrO_3, IO_3 and SO_3), or the axis line for linear atomic groups. The ratio of the two principal radii of the polarizability ellipsoid just equals the OAI value of mineral or compound in which there is only one orientation of the radical. The relative values of principal radii of the ellipsoid for some radicals are

Table 1. Relative values of principal radii of polarizability ellipsoid for some radicals.

radical	R_ε	R_ω	radical	R_ε	R_ω
CO_3	0.75	1	ClO_3	0.79	1
BO_3	0.85	1	BrO_3	0.79	1
NO_3	0.63	1	IO_3	0.84	1
CNS	1.53	1	SO_3	0.91	1

The OAI of mineral in any direction may be calculated using the following equations:

$$\mathrm{A}-\mathrm{OAI}=\frac{2P_A}{P_B+P_C}\ . \qquad (1)$$

where P_A, P_B and P_C are the relative values of polarizability of the mineral in directions A, B and C perpendicular to each other, and

$$P_A=\sum_1^n\sqrt{R_\varepsilon^2\cos^2\theta_A+R_\omega^2\sin^2\theta_A}$$
$$P_B=\sum_1^n\sqrt{R_\varepsilon^2\cos^2\theta_B+R_\omega^2\sin^2\theta_B} \qquad (2)$$
$$P_C=\sum_1^n\sqrt{R_\varepsilon^2\cos^2\theta_C+R_\omega^2\sin^2\theta_C}$$

where R_ε and R_ω are the two principal radii of the polarizability ellipsoid of the radical, and θ_A, θ_B and θ_C are three direction angles of the rotation axis against the coodination axes A, B and C, respectively.

The calculation method of OAI in a given direction of mineral on the basis of data collected from the structure analysis is as follows:

(1) To select three axes perpendicular to each other, as coordination axes, including the one given.
(2) To transform the fractional parameters of atom positions against the crystallographic axes into absolute parameters against the fixed coordination axes.
(3) To calculate the direction angles of the normal line of the radical plane or that of the axis line for the linear atom group against coordination axes.
(4) To calculate the OAI value in the given direction on the basis of equations (1) and (2).

The calculated values of OAI are in very good agreement with the experimental values.

REFERENCES: Ye, D.N. (1982) Earth science. Journal of Wuhan College of Geology, 3, 75-86. Ye, D.N. (1983a) Acta Mineralogica (China), 2, 92-97. Ye, D.N. (1983b) Acta Petrologica Mineralogica et Analyica (China), 2, 25-34. Zeng, R.S. and Ye, D.N. (1980) Scientia Geologica Sinica, 1, 43-51.

^{1}H HIGH SPEED MAS NMR STUDIES OF MINERALS

YESINOWSKI, JAMES P.; ECKERT, HELLMUT, Division of Chemistry and Chemical Engineering, California Institute of Technology, Pasadena, CA 91125; ROSSMAN, GEORGE R., Divison of Geological and Planetary Sciences, California Institute of Technology, Pasadena, CA 91125.

The structural behavior of protons in minerals provides key information relating to both physical and chemical characteristics. The application of high-resolution proton solid state nuclear magnetic resonance (NMR) spectroscopy at 200 and 500 MHz permits discrimination of different chemical species and bonding environments. At the low hydrogen levels of interest, the hydrogen-containing species tend to be structurally isolated, therefore significant line-narrowing is achievable by magic angle sample spinning (MAS) with spinning speeds between 4 and 8 kHz. Since the NMR experiment is inherently quantitative, and MAS results in a considerable increase of detection sensitivity, we anticipate that this method will become a valuable tool in the quantitative analysis of hydrogen contents down to ca. 10-100 ppm H_2O. We have used this technique to distinguish quantitatively between OH groups and molecular water in feldspar from Elizabeth R Mine with 0.12 wt% H_2O (see Fig. 1). The chemical shifts are, respectively, 2.0 and 5.4 ppm downfield from tetramethylsilane. The chemical shift observed in the ammonium feldspar buddingtonite is 6.7 ppm, close to the value measured in synthetic ammonium salts. The static linewidth of 11.2 kHz at 200 MHz indicates that at ambient temperature the NH_4^+ group is mobile on the NMR timescale (c.a. 10^{-5}s). In studies of various grossular garnets, the existence of multiple sites for the OH group as suggested by IR spectroscopy has been confirmed. Spectra obtained for a grossular garnet from Transvaal containing 5 wt% H_2O and a grossular garnet from Asbestos, Canada (H_2O content 0.12 wt%) closely resemble each other. MAS above 4 kHz also effects substantial line-narrowing in the minerals pyrophyllite and datolite (see Fig. 4). The ^{1}H NMR chemical shifts for these minerals which represent model compounds for isolated Al-OH and B-OH groups are 2.4 and 4.4 ppm, respectively. In contrast, homogeneous dipolar interactions in other interesting model systems such as lawsonite, pectolite, and colemanite are too strong to permit line-narrowing at achievable spinning speeds.

Fig. 1: ^{1}H MAS NMR spectrum of microcline from Elizabeth R mine at 200.27 MHz. Spinning speed: 6.85 kHz.

Fig. 2: ^{1}H NMR spectrum of buddingtonite at 200.27 MHz: a) static, b) magic angle spinning at 4.6 kHz.

Fig. 3: ^{1}H MAS NMR spectrum at 500.13 MHz of grossular garnet from Asbestos, Canada (0.12 wt% H_2O), spinning speed 7.75 kHz.

Fig. 4: ^{1}H MAS NMR spectra at 500.13 MHz of a) pyrophyllite, spinning speed 8.00 kHz. b) datolite, spinning speed 7.09 kHz.

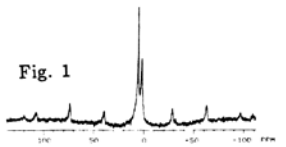

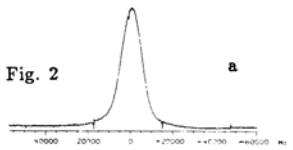

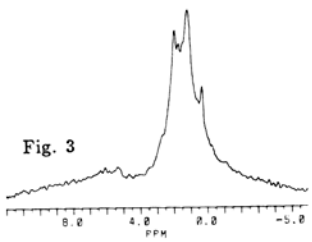

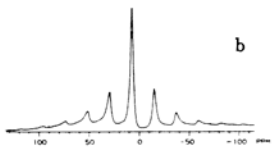

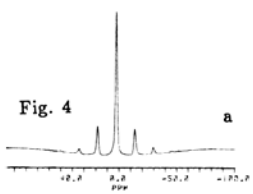

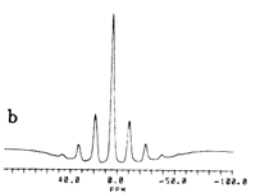

Hornblende-cummingtonite and hornblende-actinolite unmixing in late magmatic stage of Koyama calc-alkaline intrusive, Susa, southwest Japan.

Yoshiaki Yamaguchi Department of Geology, Shimane University, Matsue 690, Japan

The Koyama calc-alkaline intrusive is a small elliptical body (2.0 x 2.4 Km), and intrudes sedimentary rocks of Miocene age, converting them to pyroxene hornfels facies on the contact (Yamaguchi, 1985). The intrusion has a biotite K-Ar age of 11 m.y.. The solidification of the intrusive is considered to have taken place at a shallow level (< 1.5 Kbar) and it consists of olivine gabbro, anorthositic gabbro, quartz gabbro, quartz diorite and aplite with gradational transition. The solidification process was strongly controlled by the primary hydrous nature of the magma. The various rock types in the intrusive evolved according to different degrees of accumulation of olivine, pyroxene, and calcic plagioclase in the magma chamber. The quartz diorite occurs at the top of the intrusive.

In the quartz diorite, amphiboles crystallized interstitially replacing pyroxene in the late magmatic stage. Back-scattered electron scanning observation and microprobe analysis shows that the hornblende began to form by reaction between pyroxene and residual liquid and intergrew with cummingtonite under a condition at which the solidus extended into the hornblende-cummingtonite solvus (Ross et al., 1969; Cameron,1975); then, during cooling of the residual magma, hornblende changed in composition toward actinolite with the decrease of cummingtonite component. With further decrease in temperature, hornblende finally had $Al^{IV} \simeq 0.5$ and began to intergrow with relatively Fe-rich hornblende. The hornblende-actinolite miscibility gap (Shido and Miyashiro,1959; Oba, 1980; Yamaguchi et al., 1983) is here very small. Back-scattered electron scanning shows exsolution texture between hornblende and cummingtonite and between hornblende and actinolite.

Equilibration temperature (< 600°C) derived from the coexisting interstitial feldspars, texturally associated with the hornblende-actinolite intergrowth, may be slightly lower than the minimum solidus temperature. The hornblende-actinolite intergrowth may have occurred under the influence of a fluid associated with the crystallizing magma.

References

Cameron, K.L. (1975) Amer. Mineral., 60, 375-390.
Oba, T. (1980) Contrib. Mineral. Petrol., 71,247-256.
Ross et al. (1969) Mineral. Soc. Amer. Special Publication, 2,275-299.
Shido, F and Miyashiro, A (1959) J. Fac. Sci. Univ. Tokyo, Sec. 2, 12, 85-102.
Yamaguchi, Y. (1983) Nature, 304, No. 5923, 257-259.
Yamaguchi, Y. (1985) Amer. Mineral., 70, 980-986.

SAPONITE FROM THE COASTAL RANGE OF TAIWAN

Yu, S. C. and Jiang, W. D.
Department of Earth Sciences
National Cheng Kung University
Tainan, Taiwan, Republic of China

Saponite, a variety of montmorillonite in which the octahedral Al was replaced by Mg, occurred in the cavities and veinlets of the basaltic rocks at the Wu-shih-pi area in the Coastal Range has been identified. Two types of occurrence were found for saponite. In the first type, white colored saponite was found in association with phillipsite in the basalt cavities, and in the second type, green colored saponite was found in the basalt cavities without any zeolite association. Chemical composition analysis indicates that saponite has a chemical formula of $(Ca_{0.34}{}^{Na}{}_{0.06}{}^{K}{}_{0.01})(Mg_{6.28}{}^{Fe}{}_{0.07}{}^{Mn}{}_{0.01})(Si_{6.44}{}^{Al}{}_{1.41}{}^{Fe}{}_{0.14}{}^{Ti}{}_{0.01})O_{20}(OH)_4 \cdot nH_2O$.

X-ray diffraction measurements were carried out at room temperature and at 250°C, 500°C, 800°C and 1000°C. The results indicate that the saponite structure remains stable up to about 800°C, and at this temperature saponite decomposes and transforms into orthoenstatite following the hydroxyl groups being driven out of the saponite structure. At temperature between ambient condition and 800°C, the contraction of the saponite structure was not observed with increasing temperature in contrast with montmorillonite which displays a significant reduction in the inter-layer spacing with increasing temperature due to the loss of the molecular water adsorbed between the silicate layers.

The phase transition (decomposition) of saponite into orthoenstatite observed in the present study is supported by a DTA analysis that an endothermic peak was detected at 842°C. The chemical composition of orthoenstatite has been calculated to be $Fs_{11.4}En_{83.2}Wo_{5.4}$ from the saponite composition excluding all the molecular water and the hydroxyl ions.

•THE OCCURRENCE OF SOME NEW MINERALS IN PLATINUM-BEARING BASIC AND ULTRABASIC ROCKS FROM THE YAN-SHAN REGION, CHINA

YU Zuxiang, Institute of Geology, Chinese Academy of Geological Sciences, Baiwanzhang Road, Beijing, People's Republic of China

There are 5 platinum mineralization types in the Yan-shan minerogenetic province:

1. *Magmatic genesis of platinum-bearing diopsidite, with monomineralization (except platinum group, without other useful elements).* An example of this is the Hong district. The rock bodies are intruded in gneiss, 3 km long, 200 m wide, along the stratified strike. They are mainly hornblende diopsidite with some differentiated facies. These are the zone of diopside hornblendite which is situated in both sides of the rock body, and the hornblende diopsidite or diopsidite which is situated in the central part. The ore bodies lie on the upper part of diopsidite. It is lenticular in form and is composed of small lenses. Near ore bodies, the country rock is strongly actinolized. The platinum mineral aggregates form oil pearl, globule, crust and crescent shapes. Except for some magnetite and apatite, the ore consists of platinum minerals only including cooperite, sperrylite, hongshiite, fengluanite, etc. The hongshiite is coarse, interstitial in pyroxenes, and encloses many microcrystalline fengluanite inclusions.

2. *Genesis of platinum-bearing pyroxenite by hydrothermal process with Cu-mineralization.* An example of this is the Ma district where the rock bodies always have an ultrabasic core and are bigger than type (1) deposits. Mineralization is restricted by a system of cracks. The ore consists of minute disseminated specks, and the ore minerals are bornite, chalcopyrite, limonite, carrolite, pyrite, sperrylite, cooperite, moncheite, daomanite, and ferrous platinum. Platic idiomorphic daomanite is enclosed in Cu-sulfide and replaced bornite.

3. *Genesis of platinum-bearing garnet pyroxenite by contact metasomatism with Cu,Co-mineralization.* An example of this is the Dao district. The pyroxenite is intruded into plagioclasite. With an adjoining angular unconformity, it is 2 km long and 300 m wide. Rock bodies are differentiated weakly. It consists of hornblende diopsidite, garnet hornblende diopsidite and garnet plagioclasite. The ore bodies are localized in the garnet hornblende diopsidite. It occurs as pockets (nest-shaped); the country rocks have experienced chloritization, tremolitization, and epidotization. The ore consists of chalcopyrite, bornite, digenite, carrollite, geothite, cooperite, sperrylite, moncheite, co-malanite, fengluanite, daomanite, yixunite, braggite. Yixunite is enclosed in Cu-sulfide in pearl shapes.

4. *Genesis of platinum-bearing olivine pyroxenite by magmatic immiscibility with Cu,Ni-mineralization.* An example of this is the Lan district. The rock bodies are >1000 m long, and < 100 m wide, but the platinum mineralization is localized in a small range. The ore consists of pyrrhotite, pentlandite and bornite and it is different from the typical magmatic immiscible Cu-Ni deposit. The platinum minerals are moncheite, cooperite, malanite and native platinum.

5. *Late magmatic genesis of platinum-bearing dunite with Cr-mineralization.* An example of this is the Gao district. The rock body is up to 9 km long and 1.14 km wide, obviously is differentiated and consists of an outer rim of diopsidite, a narrow transition zone of fine or medium grain dunite, and a platinum-bearing coarse dunite in the inner zone. The ore bodies occur as monoclinic lenses, chambers, stockworks and magmatic segregation. The ores are disseminated and contemporaneously brecciated. The type platinum minerals are native osmite, ferrous platinum, xingzhongite, iridisite, yinhelite, wuhelite, liuhelite and sperrylite. The platinum mineral aggregates formed interstitial fillings, automorphic, emulsion colloid, sieve, oil pearl, crust, and band structures.

•d-d TRANSITION OF Fe^{2+} IONS IN DIOPSIDE

YUAN Yunmei and QUI Xianjun, Guizhou Institute of Technology, and GUO Yensong, Institute of Chemical Engineering, Guizhou Province, Guiyang, People's Republic of China

The optical absorption spectrum of the Fe^{2+} ion in natural diopside has been observed (see Fig. 1). Ten bands are observed between 300 and 2500 nm, which are two more than all the bands observed by previous investigators (Refs. 1 to 6). The experimental frequencies and the distinguish and calculation for frequencies are presented in Table 1. The bands at 21276, 21413 cm^{-1} are characteristic peaks of ferric iron. The chemical composition of the specimen is referred to data 1.

In diopside, there are two sites, M1 and M2 (Ref. 7 or 1). M1 sites have been occupied by an amount of Fe^{2+} ions, and Fe^{2+} ion is surrounded by six O^{2-} ions. Under the O_h approximation, we adopt the 3d-orbit of Fe^{2+} ion proposed by Zhao (Ref. 8). The orbit is given by

$$R_d(r) = 0.5192\left[\frac{11.03806^7}{6!}\right]^{\frac{1}{2}} r^2 \exp(-5.51903\gamma) + 0.6500\left[\frac{3.54794^7}{6!}\right]^{\frac{1}{2}} r^2 \exp(-1.77397\gamma) \ .$$

According to the point-charge model, we can obtain $(r^2) = 2.2949$ a.u., $(r^4) = 14$ a.u., A = 160830 cm^{-1}, B = 947 cm^{-1}, C = 3375 cm^{-1}. Considering the M1 structure, we have $D_q = -981$ cm^{-1}.

(1) The comparison of the theoretical calculations and experiment is quite good. We reasonably interpreted the spin-allowed and spin-forbidden spectra of Fe^{2+} ions in M1 sites. The theory has also predicated the existence of another spin-forbidden transition.

(2) In the calculation, we did not use any fitting parameters; therefore, we have avoided the difficulties in experimental fitting of many parameters and the arbitrary character of fitting.

(3) Whether the band 4420 cm^{-1} observed by W.B. White et al. belongs to M1 or M2 was not resolved in the previous work. According to Ref. 6, every M1 site has CN = 8. The sites are occupied mainly by Ca^{+2} ions and a small amount of Fe^{2+} ions. The bond lengths are about R1 = 2.30 Å to R2 = 2.70 Å. Under the approximation of two four-ligands spherical shells, and by using T_α, we have

$$D_q(T_\alpha) = -\frac{4}{9} D_q(O_h) \ .$$

We obtain

$$\Delta = \frac{4}{9}\left[10e^2\frac{<r^4>}{3R_1^5} + 10e^2\frac{<r^4>}{3R_2^5}\right] = 4250 \text{ cm}^{-1} \ .$$

Band 4250 cm^{-1} is in quite good agreement with the 4201 cm^{-1} observed by us. Now, we have obtained the conclusion: It is the spin-allowed band produced by d-d transition of Fe^{2+} ions of the M2 sites.

References

1. 袁先梅、邓贤俊、郭汉松, 矿物学报, 第2期, 1985年, 154－157页.
2. White, [illegible]
3. [illegible]
4. [illegible]
5. Платонов, А.Н., Природа Окрасок Минералов, Изд. «Наукова Думка», Киев, 1976, стр. 148.
6. [illegible]
7. [illegible]
8. [illegible]

d-d TRANSITION OF Fe^{2+} IONS IN DIOPSIDE

YUAN, Y., et al.

TABLE 1. d-d transition in diopside(cm^{-1})

Transition	Theoretical frequency	experimental frequency
T(D)	9,610	8,333
E (D)		9,615
		10,309
T (H)	9,706	
T (H)	12,747	13,700
T (G)	18,170	18,000
T (br)	20,353	19,000
E (H)	21,467	20,740
T (G)	21,601	21,000
T (G)	23,019	23,360
T(ar)	26,067	
T (br)	28,019	
E (D)	28,962	
A (G)	31,853	
T (D)	34,481	
T(br)	35,244	
E (G)	37,154	
A (br)	50,572	
T (ar)	50,841	
T (ar)	52,622	
T(ar)	56,695	
		4,201

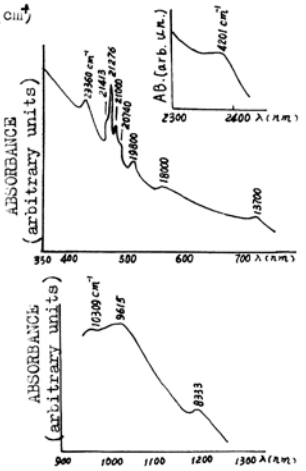

Fig.1 Optical absorption spectra of Fe ions in diopside

•Ag - BEARING TALNAKHITE AND ITS GEOLOGICAL SIGNIFICANCE

YUE Shuqin, Institute of Mineral Deposits, Chinese Academy of Geological Sciences, Beijing, People's Republic of China

The talnakhite occurs in the gold-silver-bearing quartz vein deposits related to volcanism in Zhejiang Province, China. They are generally situated in the region of biotite-plagioclase gneiss, lower Paleozoic. The most common veins are present dominantly as open fillings along the flat structures formed by faults. In rare cases, veins are metasomatic.

The mineral assemblages are varied. We have found about 40 species. Pyrite is most common, and the other minerals are sphalerite, galena, chalcopyrite, marcasite and gold-silver alloys. Occasionally one can find a little silver-teluride, -sulfide and -selenide, as well as gold sulfide (uytenbogaardite).

The Ag-bearing talnakhite is usually present as compact aggregates and irregular shaped intergrowths with native silver and acanthite, occasionally in veinlets along bedding planes of gneiss.

Under reflected light, the Ag-bearing talnakhite is colored chalcopyrite-like. It tarnishes very rapidly in air, changing from the chalcopyrite color to hues of pink and brown, and eventually becoming iridescent shades which are dark orange, dull brown-orange and dull pinkish brown. It is optically isotropic, without internal reflection. The values of reflectivity are (%): 405 nm 20.5, 436 nm 25.4, 480 nm 35.7, 526 nm 42.7, 546 nm 43.8, 589 nm 46.9, 644 nm 47.1, 700 nm 43.6. VHN(20) ranges from 155-149. Electron microprobe analysis of six grains give: Cu 35.99-38.41, Fe 27.82-29.03, S 31.29-33.83, Ag 0.58-4.22, Au 0-0.07, Pb 0-0.31, Te 0-0.08, with totals 99.47-100.87. The first four average corresponds to $(Cu_{18.46}Ag_{0.24})_{18.70}Fe_{15.92}S_{32}$; the average of the latter two gives $(Cu_{18.4}Ag_{1.26})_{19.66}Fe_{16.2}S_{32}$.

From the data presented it is certain that we are dealing with a mineral whose composition, physical and optical properties bear a resemblance to talnakhite of Noril'sk, but the reflectances of our talnakhite are certainly higher than those of the Noril'sk specimen. Electron microprobe analysis proved its composition is Ag-bearing (up to 4.22 wt %).

It is interesting that, as Ni-bearing talnakhite occurs in the Noril'sk Cu-Ni sulfide deposit, our Ag-bearing talnakhite is located in the Au-Ag-bearing deposit. It seems that the small amount of Ni or Ag in talnakhite is specific to its related deposits, and can be used as a type indicator for search and exploration of Ni or Ag deposits.

MINERAL/GROUNDMASS PARTITION COEFFICIENTS FOR MINERALS

YURIMOTO,H. and SUENO,S., Inst. of Geoscience, The Univ. of Tsukuba, Ibaraki 305, JAPAN

A large number of partition coefficients between mineral and magma have been accumulated previously for the purpose of explaining the origin and history of igneous activity. Recently YURIMOTO and SUENO (1984) have developed a new method for obtaining a set of coherent partition coefficients for trace elements by ion micro-probe, so that partition coefficients of anions and tri- and tetra-valent cations constrained in four coordinated sites in minerals as well as other cations are also readily available. This study presents new partition coefficient vs. ionic radius diagrams or ONUMA diagrams (originally prepared by ONUMA et al., 1968) for minerals using secondary ion mass stectrometry (SIMS).

The instrument used is the CAMECA IMS-3F ion micro-probe mass analyzer. A beam of O^- ions with net energy of 14 keV at secondary positive or 7.5 keV at secondary negative detection mode, was focused to a spot about 10 μm in diameter on the gold-coated surface of a polished rock thin section, and the beam current was several tens nano-ampere. The secondary ion intensities were measured by an electron multiplier coupled with pulse-counting circuitry and mass resolution of about 5000. (+)secondary ion intensity ratios relative to Si were measured for Li,Na,K,Mg,Ca,Mn,Fe,Co,Cu,Zn,Sr,Cd,Ba,B,Al,Sc,V,Cr,Ga,Y,La,Ce,C,Ti,Zr,P,As,H,F,S and N. (-)ion intensities relative to Si were measured for H,F,Cl and S. For these secondary ions, the high mass resolution adjusted in this study was enough to separate interference peaks (e.g. molecular ions, dimmer ions etc.) from the objective peak. The relative ion intensity ratios using this SIMS method were compatible with partition coefficients within 30% errors. This method is suitable for obtaining a set of coherent data for partitioning from the micro area of a given sample.

The characteristic of partition patterns on ONUMA diagram may derive the following summary as an extension of the crystal structure control mechanism reviewed by Matsui et al., (1977):
(1) On crystal-magma partitioning, each crystallographically distinct site has one parabola-shaped curve for homovalent ions on ONUMA diagram. The curves between homovalent ions tend to parallel one another.
(2) The deviation from the curve is observed in cases of ions with strong field stabilization energies and in cases of ions which prefer an unusual coordination number.
(3) The peak position for homovalent cations is decided by the size of anion polyhedron around the cation site. The peak position for anions may be decided by the size of coordinated anion polyhedron around anion site. The peak position is insensitive to the chemical composition and physical condition of the system.
(4) The peak shift on ONUMA diagram is ascribed to the coordination change around the crystallographic site.
(5) The sharpness of a peak corresponds to geometrical flexibility of the coordination polyhedron in the crystal structure.
(6) The relative height between partition curves for homovalent ions is mainly controlled by electrical charge balancing between sites in the crystal structure.
(7) Generally, the partition coefficients between A and B phases may be defined by relative internal energy change provided by the substitution of an ion of the main component (j) by an ion of a trace component (i) between the phases as shown in below:

$$\ln K_D^{A/B}(i/j) = -(kT)^{-1}[(\partial E^A/\partial N_i^A)_p - (\partial E^B/\partial N_i^B)_p]$$

where k is Boltzman's constant, T and p are the temperature and the pressure, respectively, and E and N denote the internal energy and the number of ions, respectively.

References

Matsui,Y.,Onuma,N.,Nagasawa,H.,Higuchi,H. and Banno,S. (1977) Bull. Soc. fr. Mineral. Crystallogr. **100**, 315.
Onuma,N.,Higuchi,H.,Wakita,H. and Nagasawa,H. (1968) Earth Planet. Sci. Lett. **5**, 47.
Yurimoto,H. and Sueno,S. (1984) Geochem. J. **18**, 85.

STUDIES OF TRANSITIONS OF QUARTZ BY SYNCHROTRON RADIATION

ZARKA A., and CAPELLE B., Laboratoire de Minéralogie-Cristallographie, Universités P. et M. Curie et Paris VII, associé CNRS, 4 Place Jussieu, 75252 PARIS CEDEX 05 (France)

Evidence for a new phase between the classical α and β phases of quartz has been obtained recently by measurements of thermal expansion and heat capacity (1). Its incommensurate character was revealed by neutron diffraction, electron microscopy (2) and X-ray measurements (3).

Using a high temperature furnace (4) designed for in situ synthrotron-radiation X-ray topography, the α-β transition was investigated in Z-cut synthetic (5) and natural samples.

Dynamical observations of the different α,β and i (incommensurate) phases and the α_1-α_2 twinning were followed with a TV camera and the information was stored in a video recording system (Laue topography). Static observations were also obtained on films.

Diffraction spots and satellite reflections due to the incommensurate phase were also observed and their evolution during the heating and the cooling of the sample were studied. The role of extended defects like growth bands seems to be important either for the α_1-α_2 domain nucleation or for the behavior of the incommensurate phase. The modulation vectors and the structure of the satellite spots will be presented.

REFERENCES

(1) G. DOLINO, J.P. BACHHEIMER & C.M.E. ZEYEN (1983) Sol. State Commun. 45, 295-299
(2) G. DOLINO, J.P. BACHHEIMER, B. BERGE, C.M.E. ZEYEN, G. Van TENDELOO, T. Van LANDUYT & S. AMELINCKX (1984) J. Phys. 45 125-136
(3) K. GOUHARA, Y.H. LI & N. KATO (1983) J. Phys. Jap. 52,3697-99
(4) J. GASTALDI, C. JOURDAN, P. MARZO, C. ALLASIA & J.N. JULLIEN (1982) J. Appl. Cryst. 15, 391-395
(5) A. ZARKA (1983) J. Appl. Cryst. 16, 354-356

Fig. 1 X-ray topograph of Z cut natural sample. 301 reflection. Temperature about 846.5K. Coexistence of the i (incommensurate) and α phases due to the temperature gradient. The α_1 and α_2 domains correspond to the Dauphiné twinning

Fig. 2 Diffraction spots given by a collimated beam. 220 reflection. Temperature about 846.5K. Note the satellite spots around the central Bragg spot.

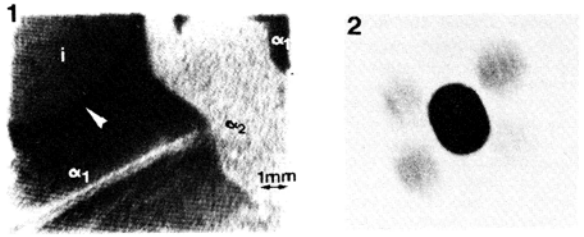

NON DESTRUCTIVE IDENTIFICATION OF GEMS AND MAN-MADE STONES BY I.R.SPECTROMETRY

P. ZECCHINI ; H. MERIGOUX ; F. MARTIN , Laboratoire de Cristallographie et Synthèses Minérales ; Université de Franche-Comté - 25030 Besançon Cédex - FRANCE.

The relatively important number of gems and man-made stones used in jewellery causes problems of identification, particularly if the stone is cut and mounted.

The I.R. spectrometry allows this identification, presenting the following important advantages

- non destructive observations
- rapidity
- numerical or graphical criteria.

This method permits an immediate characterisation of the origin, natural or synthetic.

Using this technic, it is possible to establish a classification of certain varieties of a given stone without taking into account the coloration. We can detect by this mean the physicochemical treatments employed to improve the monetary value of some inferior quality gems.

The development of the application will include

- beryl
- corundum
- spinel
- garnet
- diamond substitutes
- different fine stones.

• STRUCTURAL CLASSIFICATION OF CARBONATES

ZEMANN, J., Institute for Mineralogy and Crystallography, University of Vienna, A-1010 Vienna, Austria

In general the structural classification of carbonates meets with the same problems as known also from other classes of compounds. The choice of the adopted classification depends on what is considered to be of prime importance for the purpose. Items worth consideration are: point symmetry of the carbonate groups, distortion of the carbonate groups with several ways to define the distortion, consideration of possible hydrocarbonate groups and their interconnection via hydrogen bonds, coordination numbers and coordination polyhedra of the cations, topology of the structure, lattice complexes, relationships by non-characteristic orbits, consideration of disorder phenomena and of incommensurate structures.

These principles will be exemplified mainly on carbonate minerals. Special consideration will be given to the geometrical relationships between the structure types of calcite, dolomite, norsethite, eitelite, buetschliite and benstonite.

MAGMATIC-EPIDOTE-BEARING TONALITIC PLUTONS IN THE WESTERN CORDILLERA AND THEIR TECTONIC SIGNIFICANCE

ZEN, E-an, U.S. Geol. Survey, 959 National Ctr., Reston VA 22092, U.S.A.

Late-stage magmatic epidote (ps content 20) occurs in numerous Cretaceous (93-110 Ma) tonalitic plutons within the western Cordillera, extending from western Idaho, through northern Washington, into the area west of the Work Channel lineament-Coast Range megalineament of British Columbia and southeast Alaska, as far as Haines Point (fig. 1).

Petrographic criteria for the magmatic origin of epidote follow: (1) euhedral epidote against xenomorphic magmatic biotite, (2) wormy to myrmekitic intergrowth of epidote with plagioclase, including epidote crystals showing relation (1) above, (3) epidote overgrowing embayed, partly resorbed unaltered high-Al hornblende in rocks where similar hornblende also is surrounded by magmatic plagioclase, and (4) epidote not associated with veins and fractures and not in saussuritic relation with magmatic feldspars; absence of hydrothermal rock alteration.

Tonalite and granodiorite containing epidote plus two feldspars, hornblende, biotite, sphene, quartz (± magnetite or ilmenite, apatite) formed at total pressure of not less than ~6 kbar (20-km depth). This conclusion is based on: (1) the intersection of tonalitic solidus (H_2O-saturated) with quartz-epidote (ps ~25, nickel-bunsenite buffer) assemblage is about 6 kbar; this pressure would be increased with lower activity of H_2O in magma and with additional reactive phases but could decrease with higher fO_2. (2) The only systematic laboratory experimental data (Naney, 1983, AJS) reporting magmatic epidote was at 8 kbar (NB buffer); Naney's mineral compositions closely resemble those from natural samples. (3) The Ecstall pluton in British Columbia was synmetamorphic; the metamorphic assemblages near the pluton yielded 8±1 kbar at 625±25°C (Crawford and others, in press).

The plutons gauge minimum pressure at the depth of intrusion, leading to estimates of the paleogeothermal gradient down to the level of the plutons if temperature can be independently estimated. For the four plutons studied, estimated dT/dZ at the time of intrusion is given below:

	Round Valley ID	Tenpeak WA	Ecstall BC (N end)	Moth Bay AK
dT/dZ (°C/km)	30	30	25	20
Depth: initial-final (km)	25- 0	20- 1	25-10	20- 5
Age: initial-final (Ma)	110-17	93-30	98-72	96-24
dZ/dt (mm/yr)	0.3	0.3	0.6	0.2

The exposure of these plutons indicates that 20-25 km of sialic crust has been removed by erosion or tectonic denudation. The country rocks are sedimentary and volcanic rocks metamorphosed to greenschist and amphibolite facies, T ~450- 650°C. The temperatures do not correspond to lower crustal conditions. The present thickness of the crust above the Moho at the four areas, about 30-35 km, may not correspond to the remnant crust below the level of the plutons in late Cretaceous time. However, even if as much as 10 km of crust was added during the Tertiary, thick (40- 50 km) and average to cool sialic paleocrusts are indicated at the time of plutonism, perhaps resulting from rapid accumulation of thrust sheets of supracrustal material. Magma was produced by anatexis of the depressed lower crust.

Uplift rates can be estimated if younger bracketing events of known depth can be obtained. These estimates, given in the table, are 0.2-0.6 mm/year for the four studied plutons. High uplift rates of 0.1-1 mm/yr are characteristic of active orogens today, and these high rates may have prevailed over much of the Mesozoic accreted terrane of the northern North American Cordillera as a result of crustal thickening during accretion.

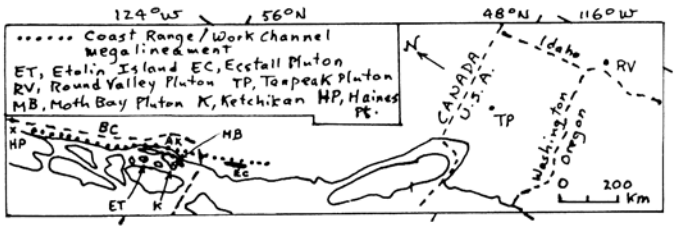

A STUDY OF THE EXISTING FORMS OF IRON IN RUTILE

ZHANG HUIFEN AND XIE XIANDE, Institute of Geochemistry, Academia Sinica, Guiyang, People's Republic of China

A detailed mineralogical study has been conducted of rutile samples from various types of ore deposit in different localities of China. The occurrences and chemical analyses of representative rutile samples are presented in Table 1. It can be seen from the table that the content of Fe (converted to Fe_2O_3) in natural rutile varies from 0.17 to 2.58 %.

In reflected light these rutile samples are greyish white in color. Their reflection spectra are almost the same, and the absorption spectra are so simple that only absorption deges at 3.2-3.43eV are observed. Table 1 shows that the most significant difference among these rutiles lies in whether there is exsolution of solid solutions and to what extent the exsolution occurs.

Table 1. Characteristics of rutile samples

Sample No.	Occurrence	TiO_2	Fe_2O_3	Exsolution
5	Metamorphic rock	98.08	0.17	No
7	Metamorphic rock	97.76	0.21	No
16-2	Intrusive rock	97.19	0.88	No
16-1	Intrusive rock	97.19	0.88	Minor
1	Pegmatite	98.03	0.91	Minor
6	Intrusive rock	97.82	1.00	Obvious
4	Valley placer	97.69	1.78	Obvious
2	Eclogite	97.91	1.91	Extensive
3	Eclogite	97.54	2.51	More ext.
9-1	Placer	96.65	2.58	No

Two types of exsolution mineral are recognized. One is white in reflected light and its reflection spectrum is similar to that of pure hematite. Containing 90.68 % Fe_2O_3 and 9.11% TiO_2, it is named titano-hematite. The other is brownish grey and its reflection spectrum is the same as that of ilmenite. Bearing 48.00% FeO and 51.43% TiO_2, it is named ilmenite.

Titano-hematite normally occurs in the form of acicular exsolution lamellae arranged in two parallel groups with an angle range of 90°-140°. Titano-hematite is often associated with ilmenite to form veinlets(1-3 μ) in rutile grains. Sometimes, these two types of exsolution mineral are concentrated locally, and sometimes they occur as aggregates in the veinlets.

Typical exsolution of titano-hematite is also observed in exsolved ilmenite grains. It is mostly vermicular in form, and occasionally it is around ilmenite grains to form a bright ring, and then extends as acicular crystals in a certain direction.

EPR measurements of single rutile crystals have shown ;(1)No matter whether there occurs exsolution or not, all the rutile samples show extremely strong Fe^{3+} spectra with a line width of about n x 10 Gauss in general. In addition, the spectra are characteristic of tetragonal crystals, indicating a replacement of Ti^{4+} by Fe^{3+}. (2) In rutile with relatively high Fe_2O_3 a wide spectrum is also observed in addition to the narrow Fe^{3+} peak mentioned above, whose line width $\Delta H > 500$ Gauss and $g \simeq 2$, indicating another existing form of Fe^{3+} in rutile, i.e. in the form of inclusions of an Fe-rich independent mineral.

Heating experiment showed that when the temperature rised to 500°C, acicular exsolution crystals became coarser, and when the temperature continued rising to 600°C, the exsolution crystals disappeared, and only two groups of coarser cleavages were left behind. The above phenomenon can be well accounted for in terms of phase diagrams of the corresponding components.

Our conclusions are presented as follows :

1. The extent of exsolution depends mainly on the content of Fe in rutile. 0.88% Fe_2O_3 is regarded as the lower limit of Fe content for the occurence of exsolution in ferro-minerals. With increasing Fe content, exsolution will tend to become more and more obvious.

2. Iron in rutile exists mainly in the form of Fe^{3+}, which is isomorphously substituted for Ti^{4+}, and exsolution minerals --titano-hematite and ilmenite.

3. In individual samples, for example in sample 9-1, no exsolution phase is observed, though the content of Fe is relatively high and its distribution is not homogenous. This seems to be related to the conditions of formation of rutile.

RARE ELEMENT MINERALS OF GRANITIC PEGMATITE IN CHINA

Zhang Jing
Institute of Geochemistry, Academia Sinica
Guiyang, Guizhou Province, People's Republic of China

The granitic pegmatite formed mainly at Precambrian, Caledonian, Hercynian and Yanshanian and by metamorphism or magmatic differentiation respectively in genesis. About 56 categories of rare element minerals (Li 11, Be 4, Cs 1, Zr 4, Nb 21 and REE 14) distributed in them.

Precambrian and Caledonian granitic pegmatites appear weak autometasomatism and product the minerals only rare earth, niobium and beryllium but no lithium and tantalum. The Hercynian granitic pegmatites are great in scale and complete in differentiation, they developed with autometasomatism and producted many categories of rare element minerals.

The granitic pegmatites mentioned above are regarded as metamorphic genesis and it was seen that the rare element minerals present the evolution in category and in quantity with ages. A regular variation is seen in the properties of the same mineral from older age to younger age.

However, Yashanian granitic pegmatites are formed by the differentiation of granitic magma. They are small in scale and not complete in differentiation, the categories of rare element minerals are simple.

•CHARACTERISTICS OF THE FERGUSONITE AND AESCHYNITE MINERAL GROUPS IN CHINA

ZHANG Pei-Shan and TAO Ke-Jie, Institute of Geology, Academia Sinica, Beijing, People's Republic of China

In recent years many new mineral species or new variety members of the fergusonite group and the aeschynite group are being found in China. The results enlarge the name list of the numbers of these two groups of minerals.

In mineralogy there is classification of fergusonite-formanite series and aeschynite-priorite series. However, according to the variation of their crystal structure and to the fact that they do not form a continuous isomorphous series in nature, it is suitable to classify these minerals as fergusonites and aeschynites.

The mineral species of the fergusonite group in China are as follows: (1) Fergusonite occurring in marginal facies of the Gu-Po-shan granite, Guang Xi province, has the ideal formula $(Y,\Sigma Y),NbO_4$. (2) Ce-fergusonite occurring in the magnesium skarn of the outer contact zone of eastern granite of Beiyan-Obo has the ideal formula $(Ce,La,RE,Th)(Nb,Fe)O_4$. (3) Nd-fergusonite occurring in veinlets in aegirine-type ores of the Beiyan-Obo ore deposits has the ideal formula $(Nd,Ce,RE,Fe)(Nb,Ti)(O,OH)_4$. (4) ß-fergusonite occurring in natro-amphibolized dolomite of the Beiyan-Obo ore deposits has the ideal formula $(Y,\Sigma Y,\Sigma Ce)NbO_4$. (5) ß-Ce-fergusonite occurring in magnesium skarn of the outer contact zone of the eastern granite of Beiyan-Obo has the ideal formula $(Ce,RE)(Nb,Al)(O,OH)_4$. (6) ß-Nd-fergusonite occurring in natro-amphibolized dolomite of Beiyan-Obo ore deposits has the ideal formula $(Nd,Ce)NbO_4$. (7) Formanite occurring in albitized granites of Jiang Xi province has the ideal formula $(Y,\Sigma Y,\Sigma Ce,Ca)(Ta,Nb,Fe)O_4$.

Mineral species of the aeschynite group in China are as follows: (1) Ce-aeschynite occurring in aegirine-fluorite veinlets of Beiyan-Obo ore deposits has the ideal formula $(Ce,Nd,\Sigma Ce)(Ti,Nb,Al)_2(O,OH)_6$. (2) Nd-aeschynite occurring in aegirine-type ore of the Beiyan-Obo ore deposits has the ideal formula $(Nd,Ce,\Sigma Ce,Ca,Th,Mg)(Ti,Nb,Fe)_2(O,OH)_6$. (3) Ce-nioboeschynite occurring in natro-amphibole aegirine type ore of the Beiyan-Obo ore deposits has the ideal formula $(Ce,Nd,\Sigma Ce,Ca)(Nb,Ti,Fe)_2(O,OH)_6$. (4) Nd-nioboeschynite occurring in natro-amphibole aegirine ore of Beiyan-Obo ore deposits has the ideal formula $(Nd,Ce,\Sigma Ce,Ca)(Nb,Ti,Al,Fe)_2(O,OH)_6$. (5) Y-aeschynite (priorite) occurring in the weathered crust of a quartz-porphyry in Shichuan province has the ideal formula $(Y,\Sigma Y,Ca)(Ti,Nb,Fe)_2(O,OH)_6$. Y-aeschynite occurring in alkaline granite of Jilin province has the ideal formula $(Y,\Sigma Y)(Ti,Nb,Al)_2(O,OH)_6$. Y-aeschynite occurring in muscovite granite in Jang Xi province has much higher titanium and may be called Ti-Y-aeschynite (titanian priorite or blomstrandinite). Its ideal formula is $(Y,\Sigma Y,)(Ti,Nb,Al)_2(O,OH)_6$. (6) Y-tantalaeschynite $(Y,Ce,Ca)(Ta,Ti,Nb)_2O_6$ has not yet been found in China; however, Ta-Ce-aeschynite occurs in a placer of Guang Xi province. Its ideal formula is $(Ce,Nd,\Sigma Ce,\Sigma Y,Ca)(Ti,Nb,Ta,Fe)_2O_6$. (7) Rynersonite, $Ca(Ta,Nb)_2O_6$, has not been found in China.

The diadochic substitution of elements in the two group minerals is described. The metamict state is observed in REE- and radioactive element-bearing minerals. The previous two mineral groups have a metamict state as their common characteristic. However, the degree of metamictness of each mineral is quite different. According to the optical properties and X-ray diffraction condition, the classification of degree of metamictness of the fergusonite and aeschynite group minerals in China have been determined.

The main factors influencing the metamict state in minerals are the stability of the crystal lattice, the concentration contents of radioactive elements, and the date of formation of minerals.

•THE FIRST FIND OF CUBIC SYSTEM NATIVE SILICON IN CHINA

ZHANG Ru-Bo, Department of Geology, Chengdu College of Geology, Sichuan, Chengdu 610059, DU Chong-Liang, Chengdu Institute of Geology and Mineral Resources, Sichuan, Chengdu 610061, and WANG Yi-Gen, Anhui 324 Geological Team, Anhui province, People's Republic of China

Native silicon was found in natural heavy placer deposits of Anhui province, China. It occurs as small crystals and rimming aggregates are around ferdisilicite ($FeSi_2$). It was only discovered in collected ferdisilicite, and very little, its size being from 0.07 to 0.015 mm in diameter. But not all ferdisilicite grains contain intergrowths of native silicon. Cassiterite, zircon, sphene, rutile, magnetite, etc. are also found in the heavy placer.

The native silicon powder was obtained from broken ferdisilicite by means of flotation. Its color is black-gray, and it has metallic lustre. In polished sections, the reflective color of the native silicon is sky-bluish. The microhardness is 1018.8 kg/mm^2 (50 load), calculated density = 2.32 g/cm^3. The reflectance value was determined by MPV-3 microphotometer in air (standard: SiC): 410 nm 48.03%, 470 nm 43.70%, 510 nm 40.24%, 550 nm 38.02%, 650 nm 35.04%-, 700 nm 34.46%.

The chemical composition of native silicon was determined with a JEOL Superprobe 733, under the following conditions: 20kv, beam current 2×10^{-8}A, probediameter 10 µm, computer union ZAF correction, and using standard pure single crystal Si (for Si), pure Fe (for Fe), pure Al (for Al), given are: Si 98.91, 100.093, 99.185, 99.608, 99.577, 97.260, Fe 0.118, 0.1, 0.116, 0.091, 0.134, 0.27, Al 0.044, 0.028, 0.035, 0.035, 0.03, n.d., Sn n.d., n.d., n.d., n.d., n.d., 0.016, total 99.072, 100.221, 99.336, 99.734, 99.742, 97.546.

Major strongest X-ray lines: 3.12(10,111), 1.91(8,220), 1.653(8,311), 1.245(6,331), 1.105(7,422): cell parameters a = 5.43 Å, V = 160.103Å^3, Z = 8.

No X-ray single-crystal study of native silicon could be made, because no crystals were found that would be suitable in size. Consequently, only X-ray powder data could be recorded. Photographs of BEL and X-ray scanning for Si, Fe, of native silicon have also been taken.

THE LITHUIM MINERALS OF CHINA'S Li-PEGMATITES

ZHANG Ru-Bo, Department of Geology, Chengdu College of Geology, Sichuan, Chengdu 610059, People's Republic of China

China's lithium minerals from Li-pegmatites include spodumene, holmquistite, cookite, lepidolite, petalite, elbaite, lithiophilite, amblygonite, Mn-sicklerite, etc. Characteristic associated minerals and the physical properites of these minerals are discussed, as are compositions, DTA, IR, and X-ray data.

•THE PRINCIPLE OF THE MULTI-USE DOUBLE VARIABLE REFRACTOMETER AND ITS APPLICATION IN MINERAL REFRACTIVE INDEX MEASUREMENTS

ZHANG Shu-ye, KANG We-kuo, CHANG Le-hua, WEN Ming-ju, Department of Geology, Changchun College of Geology, Changchun, People's Republic of China

This instrument is based on the principle of the Double Variable Immersion Method. It comprehends the main essence of the principle of the V-Prism Refractometer, Rotation Needle, Federov Rotation Stage and other related instruments, which can measure the refraction of liquids and crystals. When combined with a polarized light microscope, monochromat or thermostat, it can measure the refraction of any small form of isotropic and non-isotropic fragments (within the diameter of 0.5-0.1 mm). It can also measure the dispersion index and temperature coefficients of liquids and minerals. The main features of the instrument are:

1. Wide range of measurement: It can measure liquids and all kinds of crystals and also N, No, Ne, or Ng, Nm, Np.
2. Large stage of measurement: It can determine the refractive index within the range of N = 1.3000 to 2.1000. The original designed precision is 2×10^{-4}.
3. When it is measured with Double Variable Immersion Method, it may remove the influence from other elements because it is at the same place (in one prism), under the same condition and with the same factor.
4. Size small, operation easy.

An example from Fig. 3: small V type of refractometer according to the following formula:

$N_d + N_{dv}{}^2 + \sin\theta\,(N_{dv}{}^2 - \sin\theta^2)$, where N_d = refractive index (Na-light).
N_d = refractive index of the prism
θ = the angle of specimen.

Fig. 1. (not reproducible)
a. parallel light tube
b. small sleep V prism [sic]
c. observing telescope
d. reading system
e. four axis rotation stage
f. rotation needle
g. temperature control box

Fig. 2. (not reproducible)
Multi-use double variation refractometer on the polarizing microscope stage.

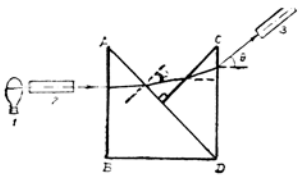

Fig. 3. Diagram of the light path.
a. light source
b. parallel light tube
c. observing telescope

CHARACTERISTICS OF INCLUSIONS IN SOME TYPES OF ORE DEPOSITS: THEIR APPLICATION TO THE GENESIS OF ORE DEPOSITS

ZHAO Xicheng, Laboratory of Rock-forming and Ore-forming, Department of Geology, Changchun College of Geology, People's Republic of China

Lately, studies of inclusions in minerals have provided a lot of information of many aspects for studying ore genesis. The present paper collects results of inclusion studies of ore deposits all over the world and by analyzing these data suggests the characteristics and rules of inclusions in deposits including magmatic Nb-Ta, hydrothermal W, gold, porphyry Cu(Mo), masive sulphide, and stratabound and strataform. It is also proposed in the paper that according to the types and shapes of inclusions, abundances of each type, genesis of non-mixing inclusions, kinds and abundances of daughter minerals in poly-phase inclusion, development of CO_2-bearing inclusions, and those got from inclusions such as temperature, salinity, density, chemical composition, and isotopic composition of H, O, S and C, the genesis of deposits and origin of ore elements, especially the origin of ore-forming hydrothermal solution, can be identified and that the sign of prospecting and the criterion of evaluating of mineralization can be based on the data of inclusions.

FORMATION OF GRANITES IN THE ACTIVE MARGIN OF ALDAN-STANOVOY SHIELD

ZHARIKOV, V.A., GAVRIKOVA, S.N., Institute of Experimental Mineralogy USSR Acad. Sci., 142432 Chernogolovka, Moscow district, USSR

Based on geologic position and petrological-geochemical data, two different processes of granite formation are recognized. One of these represents granitization, the other includes the interaction of the crustal substance with arising mantle melts and subsequent magmatic differentiation.

1. Granitization is a single process in terms of petrochemical and geochemical parameters which involves metasomatic alteration (feldspatization) of the metamorphic substrate, generation of leucogranite melts which replace the country rocks (magmatic replacement). In the process, the rocks being replaced undergo debasification, and the water molar fraction (or partial pressure) in the reaction fluid increases.

2. The earliest granitization (1.96-1.87 b.y.) in the south margin of the Aldan-Stanovoy shield occurs et two depth levels: in the conditions of the granulitic (22-25 km depth) and amphibolic (10-12 km) facies. At all depth levels there occurs an increase in Rb and a loss of Sr (by debasification). their intensity varying with the activity of alkalies. The REE distribution reflects the evolution of the granitization process : the zones of metasomatisms of the substrate (the feldspatization zone) mark the growth of the REE contents and their differentiation, LREE prevailing over HREE; the appearance of leucogranitic melts (the zone of generation and impregnation of the melt, the magmatite zone) enhances the REE differentiation and gives rise to a positive Eu-anomaly; the formation of large veins and granitic massifs (the zone of massifs) reduces slightly the REE differentiation, cancels the Eu anomaly.

3. Repeat granitization (in late Prz) produced large masses of granites which moved into the higher crustal levels. The first to intrude were biotite granites (identical in all geochemical properties with granites at the granitization stage); the second stage of intrusion gave leucogranites often associated with garnet. The latter are characterized by very low (first p.p.m.) Sr contents, slight REE differentiation complicated by negative Eu-anomalies. Such granites are believed to form from the action of high-acid fluids on residual granite melts (metamagmatism).

4. The second mechanism involves the interaction between mantle basalt melts and the crustal substance followed by the differentiation of the resulting magma chambers. Six age groups are recognized for granites intruded in the early Proterozoic, late Paleozoic and Mesozoic. By their geological position and petrological-geochemical characteristics (allowing for REE, Rb/Sr, Bc/Rb, K/Rb indicators and Sr content), intrusive rocks can be classed with the gabbro-monzonite-syenite formation (granites in the continental margins) and with the calc-alkaline granitoid magmas.

The observed diversity of granitoids stems from: a) varied composition and alkalinity of arising mantle melts and fluids; b) varied composition of the crustal substance being replaced; c) different direction and degree of magmatic differentiation; d) different depth of formation, responsible in particular for the oxygen fugecity control and the behaviour of petrogenic, volatile and rare-earth elements during crystallization.

Cs-GEYSERITE AT TARGAJA GEOTHERMAL FIELD,TIBET

Zheng Mianping Kuo Tsungshan
Institute of Mineral Deposits Chinese Academy of Geological Sciences, Beijing, China

Targaja Geothermal Field is situated at Ngamring County, Tibet, elevation 4970-5060m, annual average temperature<0°C and atmosphere pressure 577mm Hg. There outcrop strata of Cretaceous and Tertiary purple aglomerate with intercalated beds of volcanic rocks. The geyserits, 15m in thickness, are of two types: 1) The old type is distributed in larger area, forming terraces with 2 abandoned spring vents of diameter 50-70m and consisted, in section, mainly of chalcedony with lower Cs-content and 2) the new geyserite occurs along the narrow western faulted region of the old geyserite, is a deposit formed under temperature of 86°C of local boiling point of water, erupted intermittently 2-3 minutes with the H_2O geyser plume about 10m high. The thermal H_2O contains Cs 6.45 mg/l, SiO_2, 12 mg/l and has PH7.4-9.5.

The new geyserite contains Cs 0.32-1.55%, SiO_2 75-86% & H_2O 7.5-9.9% with minor amount of Al_2O_3, K_2O, CaO, Fe_2O_3, Co_2 totally 5-10%. The main mineral is the Cs-bearing opal, $SiO_2 \cdot nH_2O$, n 1.4685, D2.06 and X-ray diffraction with 2θ=23 30' shows a low broad diffused peak. Other minerals are hydromica and calcite. The old geyserite contains Cs 0.065 0.25%, SiO_2 77-99%, H_2O 1.05-5.15% and 4-7% of $Al_2O_3+K_2O+Fe_2O_3$. The main minerals are Cs-chalcedony, α-Quartz, minor Cs-opal, hydromica and igneous debris.

The Targaja Geyserite forms a part of the Tethyan Geothermal Belt with δD and $\delta^{18}O$ being -149~-153.43 &-18.38~18.63 respectively; its $\delta^{18}O$-(Cl) trending is similar to that at Yangbajain Thermal water. The geyserite field is located at the intersection of 3 systems of faults trending NW, NE, NS; The heat energy and Cs may be derived from magma cells and in part leached from country rocks. The Cs (Rb, Li) content is directly proportional to the content of H_2O and inversely proportional to that of SiO_2% and to time scale (i.e. opal--chalcedony). There may be H-bonding between the SiO_4^{4-} clusters and Cs^+ ions. The higher the H_2O content and finer the SiO_4^{4-} cluster size, the more the H-bonds and the higher the Cs-content. The first author carried out a colloidal-synthetic model experiment of Cs-bearing $SiO_2 \cdot nH_2O$ and proved the condition of formation mentioned aforehand.

REFERENCE

1. Чухров, Ф.В., 1955, Коллоиды в земной коре. Изд. АН СССР, Москва.
2. FRONDEL, C 1962, SILICA MINERALS. THE SYSTEM OF MINERALOGY, Vol III. HAVARD UNIVERSITY.
3. TON WEI ET AL.,1981,GEOTHERMALS IN DATA XIZANG PLATU. S.P.B.

STUDING OF FINE TEXTURES OF FERRIFAYALITE AND DISSCUSING OF OXIDATION OF FAYALITE

ZHOU JIANXIONG
Institute of Mineral Deposits, CAGS, 26 Baiwanzhuang Road, Beijing, China

Z. JOHAN
Centre de Recherches Synthèse et la Chimie des Mineraux, CNRS, 45045 Orleans Cedex, France

After ferrifayalite (or laihunite) was discovered in one of metamorphic iron ore deposits of north-east China (Ferr. Res. Group, 1976; Lai. Res. Group, 1976), a few detailed studies on this mineral have been made by many mineralogists at home and abroad (Shen B et al. 1981; Zhang R et al. 1981; Martha et al., 1985; Kan X et al. 1985). Although there were different points of view, almost all mineralogists identify that ferrifayalite is a new mineral or a distorted olivine type mineral.

In this study, many SEM, EPM, TEM, XRD and LARAM work on this mineral have been done. First of all, SEM, EPM was used to check the homogeneity of more than 100 grain ferrifayalites. It is provided that the called ferrifayalite was very heterogeneous from BE, AE, SE and XR images. Two phases can be distinguished at least, in addtion to eulite, magnetite and quartz. One is fayalite. The other is oxidative fayalite. Electron probe microanalyses of fayalite matrix give a formular $Fe^{2+}_{1.94}Mg_{0.05}Si_{1.01}O_4$ without Fe^{3+} (according to fine structure of Fe L X-ray spectra). But when oxidative fayalite was put under the electron beam, the point, line and area quantitative analysis reaults are significant different one point by one point. Especially the variation in FeO content is from 57.72% to 65.45% without evident concentration in area analysis (46 x 46 = 2116 points). The EPM total values of a few oxidative fayalites are as low as about 92%. It means all of Fe^{2+} were oxidized to Fe^{3+}. The lamellaes of glass matter are also discovered in oxidative fayalite by TEM and LARAM. The orientation of lamellaes with respect to the fayalite mainly parallel to (001), but often heterogeneously on small cracks or dislocation.

In short, the present SEM, EPM, TEM, XRD and LARAM data give the following new points:

1. After froming of fayalite, it was suffered two alteration at least. At first fayalite was altered by oxidation to form intergrowth of eulite, magnetite and quartz. Secondly oxidative fayalite occured as no stoichimetric alteration product under the high temperature (about 400°C). It is different from oxidation of other olivine(Haggerty et al. 1967; Kohlstedt et al. 1975; Naslund et al. 1983; Putnis, 1979; Wenk et al. 1973).

2. Ferrifayalite discovered in China is not a homogeneouse phase. Its chemical and physical properties are different even within every individual grain. Originally called ferrifayalite actually is a mixture of fayalite, oxidative fayalite and a little glass, magnetite, hematite, quartz and so on. The glass matter must be final product of altered fayalite.

3. Oxidative fayalite as transitional phase between fayalite and glass, even on a micon scale it varies widely in chemical and physical properties with oxidation degree. It seems that a continous suite between fayalite and glass.

4. Lamellaes discovered in called ferrifayalite in this study is very important.

Which one is a new phase? How does the substitution of Fe^{2+} by Fe^{3+} dispread in fayalite? It is needed to do more work by TEM and XRD.

References

1. Ferrifa. Research Group, 1976, Acta Geol. Sinica, 2, 160-175.
2. Haggerty S. E et al., 1967, Contr. Miner. Petrol., 16, 233-257.
3. Kohlstedt S. E et al., 1975, Contr. Miner. Petrol., 53, 13-24.
4. Kan Xuemin et al., 1985, Am. Miner., 70, 576-580.
5. Laihunite Research Group, 1976, Geochimica, 2, 95-103.
6. Martha W. S., 1985, Am. Miner., 70, 729-735.
7. Naslund H. R. et al. 1983, Am. Miner. 68, 1004-1008.
8. Putnis A, 1979, Miner. Mag., 43, 293-296.
9. Shen B. et al, 1981, Ann. Meet. Miner. Soc. Japan. A36, 66.
10. Wenk H. R. et al., 1973, Z. Kristallogr., 137, 86-105.
11. Zhang R. et al., 1981, TMPM Tscher. Min. Petr., 28, 167-187.

•THE MINERALOGIC FEATURES OF CALCIC BIOGENIC DETRITUS IN THE CHINA SEA

ZHU Erqin and LI Jianhua, Shandong College of Oceanology, Qingdao, People's Republic of China

The skeletal mineralogy of foraminifera, gastropods, bivalve, bryzoan, coral, echinozoan and polychaeta in the sediments of the East China Sea has been researched. The foram tests dominantly consist of low-Mg calcite, with high-Mg calcite in much less amounts, and exhibit a triple-layer structure. Based on their chemical components the foram tests may be divided into two types: homogeneous and heterogeneous. The former could also be distinguished into the subtypes of high-Mg internal layer and high-Mg external layer. The strontium contents of the foram tests in the East China Sea are quite low, ranging from 0.05% to 0.10%. Some gastropod shells are composed of aragonite, but the pteropod contains 29% calcite and higher strongium concentration. The mineralogical components of coral studied are variable, consisting of aragonite containing Sr 0.85-0.93T and that of high-Mg calcite with Sr quite low. Obviously, the mineralogical, chemical and isotopic components of the biogenic detritus in the sediments of the East China SEa are related to the species of organism. In addition, the skeletal minerals display some relationship to the ecological environments. The biogenic species of the middle shelf in the East China Sea are made up of low-Mg calcite with low abundance of Mg and Sr; those of the outer shelf consist of high-Mg calcite with Mg,Sr relatively high.

TEXTURAL ASSOCIATION OF PLATINUM-GROUP MINERALS, STILLWATER COMPLEX, MONTANA

ZIENTEK, M. L., and OSCARSON, R. L., U.S. Geological Survey, Menlo Park, CA 94025, USA

Mineralogy, grain size, and textural associations of platinum-group element (PGE) minerals have been determined for samples collected from the Stillwater Complex, Montana by back-scattered electron microscopy combined with qualitative and semi-quantitative energy dispersive x-ray analysis. The samples come from the platinum-enriched horizon in the complex (J-M Reef), the Basal series, and one of the Stillwater-associated sills and dikes (gabbronoritic diabase).

Approximately 160 PGE mineral grains were observed in a 5 cm^2 area from a J-M Reef sample containing 37 ppm Pd and 55 ppm Pt. At least 14 minerals are present: moncheite, Pd-tellurides, and isoferroplatinum are the most common; michinerite, plumbopalladinite, and potarite, which have not been previously reported from the Stillwater Complex, are also present. There are distinct textural occurrences of these minerals, each characterized by differing proportions of minerals and grain size. PGE minerals may occur as inclusions in base-metal sulfide (BMS), either totally surrounded by BMS or, more commonly, directly against the BMS-gangue contact. This is the textural occurrence most commonly described from the Merensky Reef, Bushveld Complex, South Africa. Fourteen percent of the observed grains fall in this category; moncheite and isoferro-platinum are most common in this group. The maximum dimension of all grains in this group averages 41 microns. Associated with many PGE-mineral inclusions in BMS are PGE minerals included in the adjacent silicate gangue. This occurrence accounts for 10% of the grains and is dominated by moncheite. The grain size is much finer, averaging 4 microns. Approximately 6% of the PGE minerals occur in chalcopyrite, which occurs in irregularly shaped clusters of grains included within bronzite. Pd-tellurides dominate this occurrence, with an average grain size of 1.5 microns. Most grains (70%) occurred in discontinuous stringers or veinlets with or without BMS. Their mineralogy is dominated by Pd-tellurides and a very high proportion of the phases observed other than moncheite. Au-alloys, vysotskite, palladian pentlandite, and potarite are all characteristic of these veinlets. Grain size is quite fine, averaging 4 microns. These veinlets probably represent the end product of the crystallization of a PGE-enriched immiscible sulfide liquid; serpentinization and associated veining post-date these veinlets.

Eight samples collected from the Basal series and the Stillwater-associated sills and dikes, with a total surface area of 45 cm^2 and Pd+Pt contents ranging between .13 and 1.01 ppm, were examined for PGE-minerals. In one sample, 3 grain clusters of Pd-Bi tellurides associated with hessite and altaite were found near pyrrhotite/gangue contacts. In most samples, Ag, Bi, and Pb, rather than PGE, form tellurides and alloys. Bismuth, hedleyite, altaite, Pb-Ag/Bi-Pb/Ag-Pb tellurides, bismuthian silver, and argentian pentlandite were found in a textural context comparable to the PGE minerals in the J-M Reef. In addition, Cd-sphalerite, sphalerite, galena, clausthalite (?), niccolite, and molybdenite were also observed.

TOCHILINITE IN C2 CARBONACEOUS CHONDRITES: A COMPARISON WITH TERRESTRIAL MATERIAL

ZOLENSKY, M.E., Planetary Materials Branch, NASA, SN2, Johnson Space Center, Houston, TX 77058, USA

The so called "poorly characterized phases" (PCP's) are common constituents of C2 carbonaceous chondrites [1&2]. A dominant form of PCP has been demonstrated to be tochilinite [3&4]. Tochilinite may be an important indicator of paragenesis for carbonaceous chondrites [5], and thus compositional and structural comparisons with terrestrial material have been made.

Tochilinites within the Mighei, Murray, Murchison, and Jodzie meteorites display massive, layered, rolled, and cylindrical forms [3]. Terrestrial tochilinite from Cornwall and Morgantown, PA, and Jacupiranga, Brazil can show all of these diverse morphologies within a single specimen [4]. Meteoritic tochilinites are therefore morphologically identical to their terrestrial relatives.

Tochilinite is predominantly a coherently interstratified iron sulfide - magnesium/iron hydroxide phase. The sulfide layer is similar to mackinawite, and the hydroxide layer is similar to brucite. Comprehensive reviews have demonstrated the existence of a homologous series of tochilinites [4&6]. The general formula for the observed terrestrial tochilinite homologous series may be written as:

$$2[(Fe,Mg,Cu,\square)S]\cdot 1.57\text{-}1.85[(Mg,Fe,Al,Ca)(OH)_2] \quad (1)$$

Due to the fine-grained nature of meteoritic tochilinite, only two accurate analyses of this material have been reported [1&2] which, when recast into formulas compatable with the general tochilinite formula (1), are, respectively:

$$2[Fe_9S]\cdot 1.67[(Fe_{.55}Ni_{.29}Cr_{.10}Mg_{.04}Al_{.02})(OH)_2] \quad (2)$$

and $$2[Fe_{.82}S]\cdot 1.67[(Fe_{.57}Mg_{.19}Al_{.13}Ni_{.12})(OH)_2] \quad (3)$$

Figure 1a has tochilinite compositions plotted onto the system Al-Mg-total siderophiles, while Figure 1b shows where these same analyses plot within the subsystem Fe-Ni-Cr. Terrestrial tochilinite compositions are plotted as filled circles. The meteoritic tochilinite analyses are plotted as open circles. For comparison, two tochilinite-type phases, the extremely iron-rich Phase 2 of Organova [6] and Ni-rich haapalaite [6] are plotted as filled and open diamonds, respectively.

The compositional range of the meteoritic tochilinites falls within that delineated by the terrestrial material, if the iron-rich Phase 2 is a tochilinite, however the meteoritic compositions are markedly magnesium-poor. This is an interesting result since altering forsterite grains should have supplied ample magnesium to the growing tochilinite crystals in the carbonaceous chondrites. The aluminum contents of both terrestrial and extraterrestrial tochilinites are of the same order. In Figure 1b all of the terrestrial tochilinites as well as Phase 2 plot at the iron corner. The meteoritic tochilinites contain nickel and chrome, unlike the typical terrestrial tochilinites. However, the meteoritic tochilinites lie intermediate in nickel composition between tochilinite and haapalaite, which is itself probably a tochilinite-type phase.

Major differences between the terrestrial and meteoritic tochilinites are therefore 1) the presence of nickel and chrome coupled with 2) a deficiency of magnesium in the extraterrestrial material. The presence of nickel and chrome can probably be ascribed to their availability within the host meteorite. The deficiency of magnesium in these tochilinites is an intriguing problem which deserves further consideration.

REFERENCES: [1] Bunch and Chang, Geochim. Cosmochim. Acta, 44, 1543-1577, 1980; [2] Tomeoka and Buseck, Geochim. Cosmochim. Acta, 49, 2149-2164, 1985; [5] Mackinnon and Zolensky, Nature, 309, 240-242, 1984; [6] Zolensky and Mackinnon, Am. Miner., in press; [7] Zolensky, Meteoritics, 19, 346-347, 1984; [8] Makovicky and Hyde, Structure and Bonding, 46, 101-170, 1981.

Figure 1 Plotted Compositions of Tochilinites

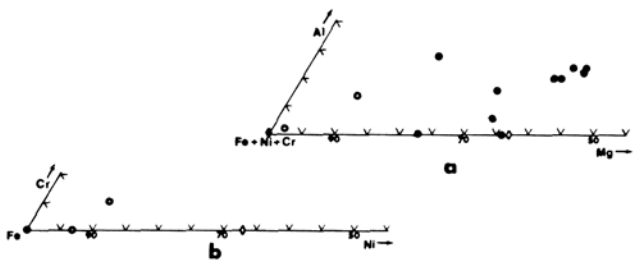

•PALYGORSKITE POLYTYPES AND THEIR SYMBOLIC DESCRIPTION

ZVYAGIN, B.B. and LYGINA, T.Z., Institute of Ore Mineralogy (IGEM), Ac.Sc. USSR, 109017 Moscow, USSR

Two kinds of palygorskite T-sheets with strips of tetrahedra pointing up (·) and down (x) (Fig. 1a,b) are displaced against connecting them to O-bands by the same vectors as describing intralayer displacements of phyllosilicates (Fig. 2). The origins are in the centers of the middle octahedra (Fig. 3) and nearest T-hexagons, all displacements 1-6 being possible in case (a), 1,2,4,5 in case (b) (Fig. 4). Any polytype as a sequence of storeys along a may be described by the sequence of displacements mn.pq-rs... (mn, pq or rs of the same parity), signs ., - marking T-sheets (a) or (b) and implying intrasheet displacements of respective hexagon centers t_1 = [1/4,1/2], t_2 = [2/4,0], t_3 = [3/4,1/2] (Fig. 1). The relative displacements of any sheets and/or bands in the normal projection on bc, in particular the components y_n,z_n of the normal projection a_n of the axis a on the plane bc defining ß,γ (α = π/2) may be calculated as a sum of consecutive displacements 1-6, $t_{1,2,3}$. Considering the symbols, one may deduce4 the cells and symmetry. Thus, polytypes with equivalent mn-units are the following.

A	I	1	33•33	0,4/3;0,1/3	C2/m; I2/m
		2	33•66	0,0	Pbmn
	II	1	55•55	1/3,2̄/3;1̄/3,1/3	C1̄; I1̄
		2	55•11	0,-2/3;0,1/3	P2/a; P2/n
		3	55•22	0,0	$P2_1/b$, $2_1 \parallel [100]$
		4	55•44	-1/3,0	P2/n, $2 \parallel [001]$
	III	1	51•51	0,-2/3;0,1/3	C2; I2
		2	51•15	0,-2/3;0,1/3	P2/a; P2/n
		3	51•24	0,0	$P2_1$, $2_1 \parallel [100]$
		4	51•42	0,0	Pm2n
	IV	1	31•31	1/6,1/3	C1
		2	31•13	1/6,1/3	P1̄
		3	31•35	0,1/3	Pc
		4	31•53	0,1/3	$P2_1$
A	IV	5	31•62	1/6,0	Pn, $n \parallel (001)$
		6	31•26	1/6,0	P2, $2 \parallel [001]$
		7	31•64	0,0	$P2_1$, $2_1 \parallel [100]$
		8	31•46	0,0	Pb, $b \parallel (100)$
B	I	1	55-55	1/6,-2/3;0,1/3	C1̄; I1̄
		2	55-11	0,-2/3;0,1/3	P2/a; P2/n
		3	55-22	0,0	$P2_1/b$, $2_1 \parallel [100]$
		4	55-44	1/6,0	P2/n, $2 \parallel [001]$
	II	1	51-51	0,-2/3;0,1/3	C2; I2
		2	51-15	0,-2/3;0,1/3	P2/a; P2/n
		3	51-24	0,0	$P2_1$, $2_1 \parallel [100]$
		4	51-42	0,0	Pm2n

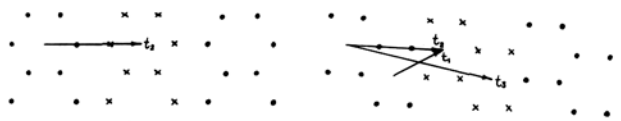

(a) (b)

Fig. 1

Fig. 2

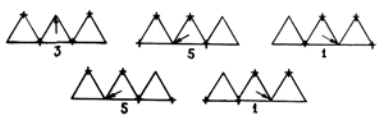

Fig 3.

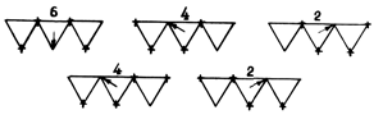

Fig.4

Organizing Committee

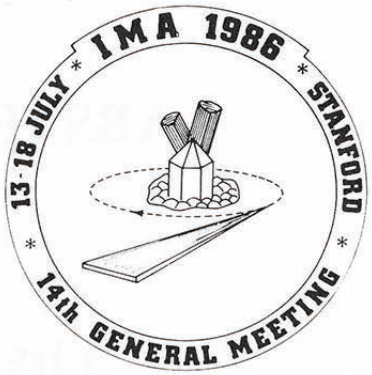

General Chairman C. T. Prewitt
First Vice President, IMA P. J. Wyllie
MSA Representative to IMA L. W. Finger
Subcommittees:
Registration: C. T. Prewitt (Chair), G. E. Brown, Jr.
Finance: J. S. Huebner (Chair), G. E. Brown, Jr., C. T. Prewitt, P. J. Wyllie, P. Parton, G. Nord
Program: R. J. Kirkpatrick (Chair), J. D. Bass, G. E. Brown, Jr., R. C. Ewing, L. W. Finger
Publications: P. H. Ribbe (Chair), F. D. Bloss, S. Ghose, J. L. Munoz
Local Arrangements: G. E. Brown (Chair), Jr., J. F. DeMouthe, G. A. Waychunas
Field Trips: H. O. A. Meyer (Chair), G. E. Brown, Jr., R. G. Coleman, M. C. Gilbert
Publicity: L. W. Finger (Chair)

ACKNOWLEDGMENTS

The Mineralogical Society of America sponsored and subsidized this meeting, with partial financial support from the National Science Foundation, Grant No. EAR-8519299. This volume was compiled at the University of Illinois (Program Chairman, R. James Kirkpatrick) and at Virginia Polytechnic Institute and State University (Publications Chairman, Paul H. Ribbe), with assistance from Ada Simmons, Wendy Smith and Margie Strickler. The Executive Secretary of the Mineralogical Society of America, Barbara Minich, contributed a great effort behind the scenes to the success of this volume, and it is she who is responsible for soliciting the advertisements. [See disclaimer on page 39.]

For additional copies of this volume, write or telephone --

MINERALOGICAL SOCIETY OF AMERICA
1625 I Street N.W., Suite 414 Washington, D.C. 20006 (202) 775-4344

Organizing Committee

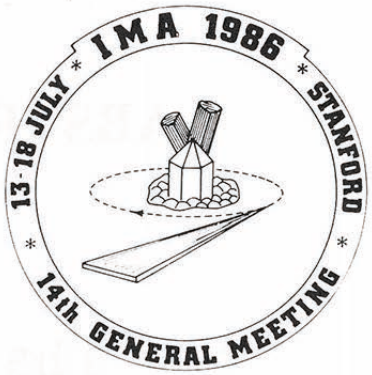

General Chairman C. T. Prewitt
First Vice President, IMA P. J. Wyllie
MSA Representative to IMA L. W. Finger
Subcommittees:
Registration: C. T. Prewitt (Chair), G. E. Brown, Jr.
Finance: J. S. Huebner (Chair), G. E. Brown, Jr., C. T. Prewitt, P. J. Wyllie, P. Parton, G. Nord
Program: R. J. Kirkpatrick (Chair), J. D. Bass, G. E. Brown, Jr., R. C. Ewing, L. W. Finger
Publications: P. H. Ribbe (Chair), F. D. Bloss, S. Ghose, J. L. Munoz
Local Arrangements: G. E. Brown (Chair), Jr., J. F. DeMouthe, G. A. Waychunas
Field Trips: H. O. A. Meyer (Chair), G. E. Brown, Jr., R. G. Coleman, M. C. Gilbert
Publicity: L. W. Finger (Chair)

ACKNOWLEDGMENTS

The Mineralogical Society of America sponsored and subsidized this meeting, with partial financial support from the National Science Foundation, Grant No. EAR-8519299. This volume was compiled at the University of Illinois (Program Chairman, R. James Kirkpatrick) and at Virginia Polytechnic Institute and State University (Publications Chairman, Paul H. Ribbe), with assistance from Ada Simmons, Wendy Smith and Margie Strickler. The Executive Secretary of the Mineralogical Society of America, Barbara Minich, contributed a great effort behind the scenes to the success of this volume, and it is she who is responsible for soliciting the advertisements. [See disclaimer on page 39.]

For additional copies of this volume, write or telephone --

MINERALOGICAL SOCIETY OF AMERICA
1625 I Street N.W., Suite 414 Washington, D.C. 20006 (202) 775-4344